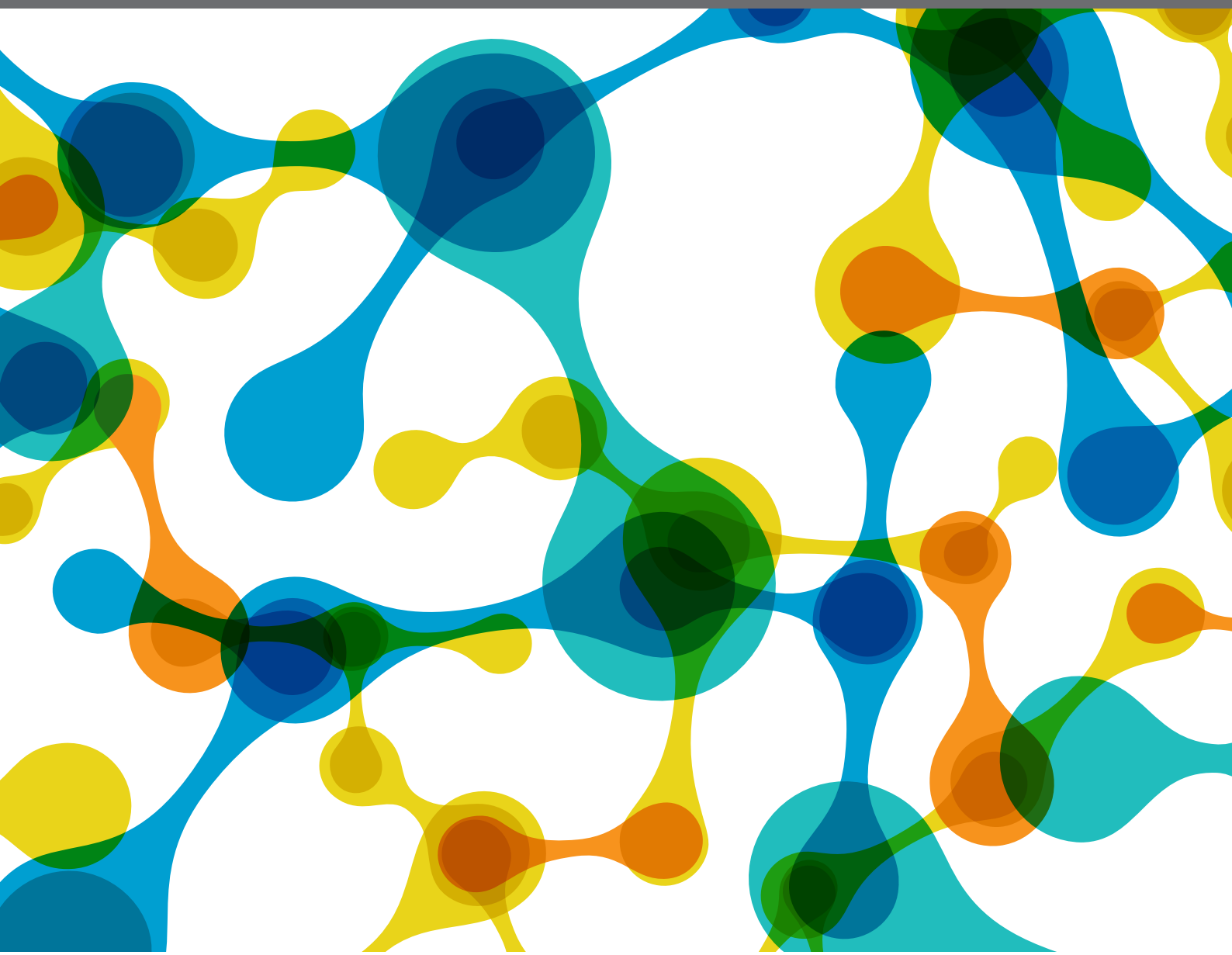
TRADITIONAL CHINESE MEDICINE: ORGAN VASCULAR INJURY - VOLUME II,
2nd Edition

EDITED BY: Jing-Yan Han, Qiaobing Huang, Jincai Luo and Gerald A. Meininger
PUBLISHED IN: Frontiers in Physiology and Frontiers in Pharmacology



frontiers Research Topics

Frontiers eBook Copyright Statement

The copyright in the text of individual articles in this eBook is the property of their respective authors or their respective institutions or funders. The copyright in graphics and images within each article may be subject to copyright of other parties. In both cases this is subject to a license granted to Frontiers.

The compilation of articles constituting this eBook is the property of Frontiers.

Each article within this eBook, and the eBook itself, are published under the most recent version of the Creative Commons CC-BY licence. The version current at the date of publication of this eBook is CC-BY 4.0. If the CC-BY licence is updated, the licence granted by Frontiers is automatically updated to the new version.

When exercising any right under the CC-BY licence, Frontiers must be attributed as the original publisher of the article or eBook, as applicable.

Authors have the responsibility of ensuring that any graphics or other materials which are the property of others may be included in the CC-BY licence, but this should be checked before relying on the CC-BY licence to reproduce those materials. Any copyright notices relating to those materials must be complied with.

Copyright and source acknowledgement notices may not be removed and must be displayed in any copy, derivative work or partial copy which includes the elements in question.

All copyright, and all rights therein, are protected by national and international copyright laws. The above represents a summary only. For further information please read Frontiers' Conditions for Website Use and Copyright Statement, and the applicable CC-BY licence.

ISSN 1664-8714
ISBN 978-2-8325-5205-6
DOI 10.3389/978-2-8325-5205-6

About Frontiers

Frontiers is more than just an open-access publisher of scholarly articles: it is a pioneering approach to the world of academia, radically improving the way scholarly research is managed. The grand vision of Frontiers is a world where all people have an equal opportunity to seek, share and generate knowledge. Frontiers provides immediate and permanent online open access to all its publications, but this alone is not enough to realize our grand goals.

Frontiers Journal Series

The Frontiers Journal Series is a multi-tier and interdisciplinary set of open-access, online journals, promising a paradigm shift from the current review, selection and dissemination processes in academic publishing. All Frontiers journals are driven by researchers for researchers; therefore, they constitute a service to the scholarly community. At the same time, the Frontiers Journal Series operates on a revolutionary invention, the tiered publishing system, initially addressing specific communities of scholars, and gradually climbing up to broader public understanding, thus serving the interests of the lay society, too.

Dedication to Quality

Each Frontiers article is a landmark of the highest quality, thanks to genuinely collaborative interactions between authors and review editors, who include some of the world's best academicians. Research must be certified by peers before entering a stream of knowledge that may eventually reach the public - and shape society; therefore, Frontiers only applies the most rigorous and unbiased reviews.
Frontiers revolutionizes research publishing by freely delivering the most outstanding research, evaluated with no bias from both the academic and social point of view. By applying the most advanced information technologies, Frontiers is catapulting scholarly publishing into a new generation.

What are Frontiers Research Topics?

Frontiers Research Topics are very popular trademarks of the Frontiers Journals Series: they are collections of at least ten articles, all centered on a particular subject. With their unique mix of varied contributions from Original Research to Review Articles, Frontiers Research Topics unify the most influential researchers, the latest key findings and historical advances in a hot research area! Find out more on how to host your own Frontiers Research Topic or contribute to one as an author by contacting the Frontiers Editorial Office: frontiersin.org/about/contact

TRADITIONAL CHINESE MEDICINE: ORGAN VASCULAR INJURY - VOLUME II, 2nd Edition

Topic Editors:
Jing-Yan Han, Peking University, China
Qiaobing Huang, Southern Medical University, China
Jincai Luo, Peking University, China
Gerald A. Meininger, University of Missouri, United States

Publisher's note: This is a 2nd edition due to an article retraction.

Citation: Han, J.-Y., Huang, Q., Luo, J., Meininger, G. A., eds. (2024). Traditional Chinese Medicine: Organ Vascular Injury - Volume II, 2nd Edition. Lausanne: Frontiers Media SA. doi: 10.3389/978-2-8325-5205-6

Table of Contents

06 ***Editorial: Traditional Chinese Medicine: Organ Vascular Injury - Volume II***
Jing-Yan Han, Gerald Meininger, Jin-Cai Luo and Qiao-Bing Huang

14 ***NMR Metabolomics and Random Forests Models to Identify Potential Plasma Biomarkers of Blood Stasis Syndrome With Coronary Heart Disease Patients***
Lin-Lin Zhao, Xin-Jian Qiu, Wen-Bo Wang, Ruo-Meng Li and Dong-Sheng Wang

24 ***Herbal Compatibility of Ginseng and Rhubarb Exerts Synergistic Neuroprotection in Cerebral Ischemia/Reperfusion Injury of Rats***
Wen-Ting Yang, Yong Wang, Yi-Hua Shi, Huan Fu, Zhen Xu, Qing-Qing Xu and Guo-Qing Zheng

37 ***Integrating Pharmacokinetics Study, Network Analysis, and Experimental Validation to Uncover the Mechanism of Qiliqiangxin Capsule Against Chronic Heart Failure***
Yu Zhang, Mingdan Zhu, Fugeng Zhang, Shaoqiang Zhang, Wuxun Du and Xuefeng Xiao

52 ***YangXue QingNao Wan, a Compound Chinese Medicine, Attenuates Cerebrovascular Hyperpermeability and Neuron Injury in Spontaneously Hypertensive Rat: Effect and Mechanism***
Ying-Qian Jiao, Ping Huang, Li Yan, Kai Sun, Chun-Shui Pan, Quan Li, Jing-Yu Fan, Zhi-Zhong Ma and Jing-Yan Han

65 ***Ginkgolide B for Myocardial Ischemia/Reperfusion Injury: A Preclinical Systematic Review and Meta-Analysis***
Peng-Chong Zhu, Qiang Tong, Zhuang Zhuang, Zi-Hao Wang, Li-Hui Deng, Guo-qing Zheng and Yan Wang

81 ***Screening for Potential Active Components of Fangji Huangqi Tang on the Treatment of Nephrotic Syndrome by Using Integrated Metabolomics Based on "Correlations Between Chemical and Metabolic Profiles"***
Xiao Liu, Qi-Gang Zhou, Xiao-Chai Zhu, Li Xie and Bao-Chang Cai

93 ***Post-treatment With Qing-Ying-Tang, a Compound Chinese Medicine Relives Lipopolysaccharide-Induced Cerebral Microcirculation Disturbance in Mice***
Hao-Min Wang, Ping Huang, Quan Li, Lu-Lu Yan, Kai Sun, Li Yan, Chun-Shui Pan, Xiao-Hong Wei, Yu-Ying Liu, Bai-He Hu, Chuan-She Wang, Jing-Yu Fan and Jing-Yan Han

108 ***Efficacy and Safety of Ginkgo Leaf Extract and Dipyridamole Injection for Ischemic Stroke: A Systematic Review and Meta Analysis***
Ping Xue, Zhuoya Ma and Shuguang Liu

120 ***MRI Evaluation of Axonal Remodeling After Combination Treatment With Xiaoshuan Enteric-Coated Capsule and Enriched Environment in Rats After Ischemic Stroke***
Man-Zhong Li, Yu Zhan, Le Yang, Xue-Feng Feng, Hai-Yan Zou, Jian-Feng Lei, Ting Zhao, Lei Wang and Hui Zhao

138 ***Saussureae Involucratae Herba (Snow Lotus): Review of Chemical Compositions and Pharmacological Properties***
Guowei Gong, Jing Huang, Yang Yang, Baohui Qi, Guangyi Han, Yuzhong Zheng, Huan He, Kelvin Chan, Karl WK Tsim and Tina TX Dong

149 ***Comparative Pharmacokinetics of Hydrophilic Components in* Salvia miltiorrhiza Bge. *and* Carthamus tinctorius L. *in Rats That Underwent Cerebral Ischemia Reperfusion Using an HPLC-DAD Method***
Xixi Zhao, Li Yu, Yulin Chen, Yu Wang, Haitong Wan and Jiehong Yang

158 ***Total Glycosides of* Cistanche deserticola *Promote Neurological Function Recovery by Inducing Neurovascular Regeneration* via *Nrf-2/Keap-1 Pathway in MCAO/R Rats***
Fujiang Wang, Ruiyan Li, Pengfei Tu, Jianping Chen, Kewu Zeng and Yong Jiang

174 ***Different Processed Products of Curcumae Radix Regulate Pain-Related Substances in a Rat Model of Qi Stagnation and Blood Stasis***
Zhimin Chen, Lin Hu, Yujiao Liao, Xi Zhang, Zhuo Yang, Changjiang Hu and Lingying Yu

182 **HuangqiGuizhiWuwu *Decoction Prevents Vascular Dysfunction in Diabetes via Inhibition of Endothelial Arginase 1***
Hong Cheng, Tian Lu, Jingya Wang, Yucen Xia, Xiaoshu Chai, Minyi Zhang, Yutong Yao, Na Zhou, Sisi Zhou, Xinyi Chen, Weiwei Su, Cunzhi Liu, Wei Yi, Yongjun Chen and Lin Yao

192 ***Erratum:* HuangqiGuizhiWuwu *Decoction Prevents Vascular Dysfunction in Diabetes via Inhibition of Endothelial Arginase 1***
Frontiers Production Office

194 ***Zi Shen Huo Luo Formula Enhances the Therapeutic Effects of Angiotensin-Converting Enzyme Inhibitors on Hypertensive Left Ventricular Hypertrophy by Interfering With Aldosterone Breakthrough and Affecting Caveolin-1/Mineralocorticoid Receptor Colocalization and Downstream Extracellular Signal-Regulated Kinase Signaling***
Xiaotong Song, Yue Zhao, Shijun Wang, Yuan Wang, Qian Chen, Haijun Zhao, Hua Wang, Sheng Tian, Huayun Yu and Zhichun Wu

206 ***Danqi Pill Protects Against Heart Failure Post-Acute Myocardial Infarction* via *HIF-1α/PGC-1α Mediated Glucose Metabolism Pathway***
Qian Zhang, Dongqing Guo, Yuanyuan Wang, Xiaoping Wang, Qiyan Wang, Yan Wu, Chun Li, Wei Wang and Yong Wang

217 ***Non-Targeted Metabolomic Profiling of Coronary Heart Disease Patients With Taohong Siwu Decoction Treatment***
Tianqi Tao, Tao He, Huimin Mao, Xudong Wu and Xiuhua Liu

231 ***Targeting Myeloperoxidase (MPO) Mediated Oxidative Stress and Inflammation for Reducing Brain Ischemia Injury: Potential Application of Natural Compounds***
Shuang Chen, Hansen Chen, Qiaohui Du and Jiangang Shen

247 ***Clinical and Economic Evaluation of Salvianolate Injection for Coronary Heart Disease: A Retrospective Study Based on National Health Insurance Data in China***
Lisong Yang, Xiaolan Chen, Carolina Oi Lam Ung, He Zhu, Hao Hu and Sheng Han

259 ***Shexiang Baoxin Pill, a Traditional Chinese Herbal Formula, Rescues the Cognitive Impairments in APP/PS1 Transgenic Mice***
Wei-Hui Hu, Shing-Hung Mak, Zhong-Yu Zheng, Ying-Jie Xia, Miranda Li Xu, Ran Duan, Tina Ting-Xia Dong, Shao-Ping Li, Chang-Sen Zhan, Xiao-Hui Shang and Karl Wah-Keung Tsim

271 ***Qiliqiangxin Capsules Optimize Cardiac Metabolism Flexibility in Rats With Heart Failure After Myocardial Infarction***
Wenkun Cheng, Lei Wang, Tao Yang, Aiming Wu, Baofu Wang, Tong Li, Ziwen Lu, Jingjing Yang, Yang Li, Yangyang Jiang, Xiaoxiao Wu, Hui Meng and Mingjing Zhao

286 ***Evaluation of Long-Time Decoction-Detoxicated* Hei-Shun-Pian *(Processed* Aconitum carmichaeli *Debeaux Lateral Root With Peel) for Its Acute Toxicity and Therapeutic Effect on Mono-Iodoacetate Induced Osteoarthritis***
Lei Zhang, Ting Li, Rongrong Wang, Jiaan Xu, Li Zhou, Li Yan, Zhengyan Hu, Hongwen Li, Fucun Liu, Wenxi Du, Peijian Tong, Huiling Wu, Shanxing Zhang, Letian Shan and Thomas Efferth

298 ***Antihypertensive and Antifibrosis Effects of Acupuncture at PC6 Acupoints in Spontaneously Hypertensive Rats and the Underlying Mechanisms***
Juan-Juan Xin, Qiu-Fu Dai, Feng-Yan Lu, Yu-Xue Zhao, Qun Liu, Jing-Jing Cui, Dong-Sheng Xu, Wan-Zhu Bai, Xiang-Hong Jing, Jun-Hong Gao and Xiao-Chun Yu

310 ***Astragaloside IV Derivative (LS-102) Alleviated Myocardial Ischemia Reperfusion Injury by Inhibiting Drp1^{Ser616} Phosphorylation-Mediated Mitochondrial Fission***
Li Chen, Xiao-Yi Chen, Qian-Long Wang, Si-Jin Yang, Hua Zhou, Li-Sheng Ding, Lin-Sen Qing and Pei Luo

327 ***The Ameliorating Effects of Bushen Huatan Granules and Kunling Wan on Polycystic Ovary Syndrome Induced by Dehydroepiandrosterone in Rats***
Yang Xu, Chun-Shui Pan, Quan Li, Hao-Lin Zhang, Li Yan, Gulinigaer Anwaier, Xiao-Yi Wang, Lu-Lu Yan, Jing-Yu Fan, Dong Li and Jing-Yan Han

frontiers in Physiology

EDITORIAL
published: 11 June 2021
doi: 10.3389/fphys.2021.677858

Editorial: Traditional Chinese Medicine: Organ Vascular Injury - Volume II

Jing-Yan Han[1]*, *Gerald Meininger*[2]*, *Jin-Cai Luo*[3] and *Qiao-Bing Huang*[4]

[1] Department of Integration of Chinese and Western Medicine, Peking University Health Science Center, Beijing, China, [2] Department of Medical Pharmacology and Physiology, Dalton Cardiovascular Research Center, University of Missouri-Columbia, Columbia, MO, United States, [3] Beijing Key Laboratory of Cardiometabolic Molecular Medicine, Institute of Molecular Medicine, Peking University, Beijing, China, [4] Guangdong Provincial Key Lab of Shock and Microcirculation, Department of Pathophysiology, School of Basic Medical Sciences, Southern Medical University, Guangzhou, China

Keywords: cardiovascular disease, inflammation, organ injury, hyperlipidemia, hyperglycemia, cerebrovascular, microcirculation

Editorial on the Research Topic

Traditional Chinese Medicine: Organ Vascular Injury - Volume II

Hypertension, hyperlipidemia, diabetes, cardiovascular disease, cerebrovascular disease, kidney damage, chronic stress, inflammatory responses, and diseases caused by endotoxin, etc. are all major diseases that seriously threaten people's health and increase medical financial burdens worldwide. These diseases are characterized by an interacting network of abnormalities, resulting from genetic factors, unhealthy lifestyle, stress, immunological factors, environmental factors etc. It is increasingly important to recognize that these diseases are frequently conditions that involve multi-gene, multi-protein, and multi-cellular and tissue involvement. Thus, the pathways leading to and maintaining complex diseases are frequently multi-pathway. Currently, a host of single-component medicines are available to deal with these diseases, respectively, e.g., antihypertensive drugs for hypertension, lipid-lowering drugs for hyperlipidemia, and hypoglycemic agents for diabetes, which are effective. However, they a range of pathologically related manifestations linked to these conditions remain unresolved, including, for example, the reperfusion injury caused by recanalization after cardiac infarct and stroke, and the combination of microvascular and large vessel injuries caused by hypertension, hyperlipidemia, and diabetes.

Traditional Chinese Medicine (TCM) is a medical system with an extensive history spanning more than 2,000 years. Fundamental to TCM is an underlying philosophy of using a multi-target approach to complex disease. Over the long period of TCM evolution an abundance of clinical wisdom and effective compound preparations have been developed and accumulated that aid in the prevention and treatment of diseases related to vascular and organ damage. This has been of great advantage in China for combating complex diseases as in prevention and treatment of hypertension, hyperlipidemia, diabetes, cardiovascular, cerebrovascular diseases, chronic stress, and diseases caused by endotoxin. The TCM approach has also been of societal benefit in reducing the financial costs of medical treatments.

Professor G. A. Meininger and I organized a Research Topic for Frontiers in Physiology—Vascular Physiology, and received 76 manuscripts from 2017–January 5, 2018, of these 29 were accepted and published after peer review. In addition, Professors Meininger, Qiaobing Huang, Jincai Luo, and I organized an extension of This Research Topic for Frontiers in Physiology-Vascular Physiology to address the topic of "Traditional Chinese Medicine and Organ Vascular Injury," and received 67 manuscripts from

OPEN ACCESS

Edited and reviewed by:
Vincenzo Lionetti, Sant'Anna School of Advanced Studies, Italy

***Correspondence:**
Jing-Yan Han
hanjingyan@bjmu.edu.cn
Gerald Meininger
meiningerg@missouri.edu

Specialty section:
This article was submitted to Vascular Physiology, a section of the journal Frontiers in Physiology

Received: *08 March 2021*
Accepted: *17 May 2021*
Published: *11 June 2021*

Citation:
Han J-Y, Meininger G, Luo J-C and Huang Q-B (2021) Editorial: Traditional Chinese Medicine: Organ Vascular Injury - Volume II. Front. Physiol. 12:677858. doi: 10.3389/fphys.2021.677858

2018 to 2020, among which 26 were accepted and published after peer review. This Research Topic also is cross-listed with the Ethnopharmacology section of Frontiers in Pharmacology, in which 10 were finally accepted and published after peer review. Here we compile these collected articles into an ebook to help scientists in the field learn and gain insight into TCM and its applications to complex diseases as well as TCM and organ vascular injury.

THE EFFECTS AND MECHANISMS OF TCM ON IMPROVING TREATMENT OF HYPERTENSION AND RELATED ORGAN INJURY

Among the papers included in this ebook, there are 4 papers regarding the mechanisms of TCM to improve treatment of hypertension. Xin et al. from the team of professors Xiao-Chun Xu and Xiang-Hong Jing demonstrated that electroacupuncture at PC6 for 30 min per day, for a period of 8 weeks, could inhibit the myocardial fibrosis in spontaneously hypertensive rats (SHRs), which might be mediated by downregulation of the activity of the AngII-TGF-β-CTGF/TNFα pathway, and upregulation of the diminished expression of MMP-9. Jiao et al. from the team of professors Jing-Yan Han and Zhi-Zhong Ma found that SHR rats manifested not only insufficient cerebral perfusion. This was accompanied by high expression of caveolin-1 in extracted proteins from brain tissues, low expression of tight junction proteins such as Claudin-5, Occludin, JAM-1, ZO-1, disarrangement and discontinuity of claudin-5 and ZO-1, albumin leakage from cerebral microvessels, Evans blue extravasation and increased cerebral edema. Enalapril plus nifedipine can lower blood pressure and improve cerebral perfusion, but have no effect on the cerebral microvascular effusion. YangXue QingNao Wan, a compound Chinese medicine for treating headaches and dizziness in China, can not only lower blood pressure and improve cerebral perfusion, but also inhibited the high expression of cerebral caveolin-1 and the low expression of tight junction proteins such as Claudin-5, Occludin, JAM-1, ZO-1, inhibited the disordered and discontinuous arrangement of Claudin-5 and ZO-1, and attenuated plasma albumin leakage from cerebral microvessels. There was also reduced Evans blue extravasation and cerebral edema, upregulation of ATPα and ATP5D, the two subunits of mitochondrial complex V, in extracted protein from brain tissue, elevation of the ratio of ATP/ADP and ATP/AMP, and inhibition of the damage of hippocampal neurons (Jiao et al.). Hao et al. from the team of professor Jing-Yan Han also demonstrated that Rhynchophylline, one of the main components of YangXue QingNao Wan, was capable of activating Src-PI3K/Akt-eNOS cascade and improving endothelium-dependent relaxation in the renal arteries from SHRs (Hao et al., 2017). Song et al. from the team of Professors Huayun Yu and Zhichun Wu demonstrated that Zi Shen Huo Luo formula could enhance the efficacy of angiotensin-converting enzyme inhibitors in left ventricular hypertrophy after hypertension by improving aldosterone activity and affecting mineralocorticoid receptor and Caveolin-1 colocalization and the downstream EGFR signaling pathway.

THE EFFECTS AND MECHANISMS OF TCM ON IMPROVING TREATMENT OF HYPERLIPIDEMIA AND RELATED ORGANS INJURY

There are 4 papers regarding the improvement effects of TCM on hyperlipidemia and related cognitive dysfunction and arteriosclerosis. Gao et al. from the team of professors Yuan-Lu Cui and Chun-Quan Yu demonstrated that Dan-Lou prescription effectively attenuated macrophage foam cell formation induced by ox-LDL via the TLR4/NF-κB and PPARγ signaling pathways (Gao et al., 2018). Yi et al. from the team of professors Fei Ye and Xiaolin Zhang demonstrated that Rho, a extract from *Rhodiola crenulate*, could ameliorate hepatic steatosis in high-fat diet (HFD)-induced obesity mice, KKAy mice, and HFD combined with tetracycline stimulated Model-T mice, respectively. The mechanism was related to enhancing insulin sensitivity, suppressing fatty acid uptake and inhibiting *de novo* lipogenesis in liver (Yi et al., 2018). Gu et al. from the team of professors Jing-Yan Han and Zhi-Zhong Ma demonstrated that YangXue Qing Nao Wan and Silibinin Capsules could improve cognitive impairment of aged LDLR (+/–) golden Syrian hamsters, which was associated with attenuated albumin leakage from middle cerebral artery and neuronal damage in hippocampus, concomitant with an increase in cerebral blood flow, a decrease of perivascular edema and an up-regulated expression of claudin-5, occludin and ZO-1 (Gu et al., 2018). Deng et al. from the team of professor Jing-Yan Han also demonstrated that combination of Cardiotonic Pills, a compound Chinese medicine for coronary heart disease and angina pectoris, and recombinant human prourokinase, a thrombolytic drug, effectively attenuated atherosclerosis plaque in $LDLR^{-/-}$mice plus high fat diet, which is associated with normalizing the lipid metabolism in the liver and aorta, reducing phagocytosis of receptor-mediated modified-LDL uptake and inhibiting systemic inflammation (Deng et al., 2019).

THE EFFECTS AND MECHANISMS OF TCM ON IMPROVING TREATMENT OF HYPERGLYCEMIA AND RELATED ORGANS INJURY

We have included 5 papers reporting the effect of TCM on diabetes, especially the vascular comorbidity and related organ injury. Li et al. from the team of professors Qiaobing Huang and Xiaohua Gao showed that Src plays a pivotal role in advanced glycation end products-promoted HUVECs angiogenesis by phosphorylating ERK, and very likely through RAGE-Src-ERK pathway (Li et al., 2018b). Zhu et al. from the team of professors Ximing Liu and Xiaobo Sun found that Dai-Zong-Fang, a traditional Chinese herbal formula containing berberine, naringin, and other components,

exhibits a prominent effect in improving insulin sensitivity, hepatic steatosis, and skeletal muscle energy metabolism in db/db mice (Zhu et al., 2018a). Cheng et al. from the team of professors Lin Yao and YongJun Chen reported that HuangqiGuizhiWuwu Decoction improved streptozocin-induced vascular dysfunction by targeting endothelial arginase 1. Chen et al. from the team of professors Jianxun Liu and Junguo Ren discovered the therapeutic potential of Tang Wang Ming Mu Granule, a compound Chinese medicine, for prevention of diabetic retinopathy in Type 2 diabetes rats, which may be attributable to anti-inflammation, anti-oxidation, upregulation of SOCS3 expression, and inhibition of the JAK/STAT/VEGF signaling pathway (Chen et al., 2017). Li et al. from the team of professors Jing-Yan Han and Xue-Mei Wang reported that Bushen Huoxue (BSHX), a compound Chinese medicine, significantly ameliorated the type 2 diabetes mellitus related insults in diabetic KKAy mice, including the increased blood glucose, the impaired spatial memory, decreased cerebral blood flow, occurrence of albumin leakage, leukocyte adhesion and opening capillary rarefaction. Meanwhile, the downregulation of the tight junction proteins claudin-5, occludin, zonula occluden-1 and JAM-1 between endothelial cells, the amyloid-β accumulation in hippocampus, increased advanced glycation end-products and RAGE, and expression of RhoA/ROCK/moesin signaling pathway and phosphorylation of Src kinase were significantly protected by BSHX treatment. These results indicate that the protective effect of BSHX on type 2 diabetes mellitus-induced cognitive impairment involves regulation of RhoA/ROCK1/moesin signaling pathway and phosphorylation of Src kinase (Li et al., 2018c).

THE EFFECTS AND MECHANISMS OF TCM ON IMPROVING TREATMENT OF CARDIAC INJURY, MYOCARDIAL FIBROSIS AND HEART FAILURE

We have included 22 papers regarding the improvement effects of TCM on cardiovascular injury, including 1 paper investigating the role of TCM in myocardial injury caused by homocysteine, 6 papers about the improvement of ischemic myocardial injury by TCM, 5 papers about the improvement of myocardial ischemia-reperfusion injury by TCM, 4 papers reporting the protective effect of TCM on heart failure, 3 papers regarding the systematic biological characteristics of cardiovascular disease with different syndromes of TCM, 3 papers regarding the effect of TCM on coronary heart disease in clinic.

The Effects of TCM on Improving Treatment of Homocysteine-Induced Cardiac Injury

The work of Fan et al. from the team of professors Bao-liang Sun and Xiao-yan Fu showed the suppressed effect of astaxanthin on homocysteine-induced cardiotoxicity *in vitro* and *in vivo* by inhibiting mitochondrial dysfunction and oxidative damage (Fan et al., 2017).

The Effects and Mechanisms of TCM on Improving Treatment of Ischemic Myocardial Injury

Zhang et al. from the team of professors Pengfei Tu and Yong Wang revealed the anti-apoptotic effects of Baoyuan Decoction both *in vivo* and *in vitro*, is mediated by regulation of the P38 mitogen-activated protein kinase-αB-crystallin signaling pathway (Zhang et al., 2018b). Cheng et al. from the team of professor Mingjing Zhao reported that 1 day after left anterior descending coronary artery ligation, continuous administration of Qiliqiangxin Capsules (QLQX) by intragastric administration for 8 weeks can reduce the area of myocardial infarction, improve cardiac function and myocardial blood flow. The role of QLQX is attributable to inhibition of cardiac glycolysis and promotion of glucose oxidation and fatty acid metabolism (Cheng et al.). Chen et al. from the team of professors Xiumei Gao and Guanwei Fan revealed that Danhong Injection combined with mesenchymal stem cells intervention can significantly improve cardiac function and inhibit ventricular remodeling in murine myocardial infarction model. This benefit may be due to the regulation of the SDF-1/CXCR4 axis and promote angiogenesis (Chen et al., 2018). Sun et al. from the team of professors Xiaohui Ma and Feng Yu demonstrated the protective effect of compound danshen dripping pills on isoproterenol-induced myocardial ischemia in rat and the acute myocardial infarction rat induced by ligation of the left anterior descending (LAD) coronary artery, whereas the circulating microRNA-1 was only ameliorated in the LAD rat model (Sun et al., 2018b). Cui et al. from the team of professor Jing-Yan Han found that treatment with QiShenYiQi Pills (QSYQ) significantly inhibited ischemia-induced rat myocardial injury, as demonstrated by the improvement of myocardial morphology and heart function and decline in cardiac cTnI release. QSYQ also relieved myocardial energy disorders manifested by the increase in ATP production, ATP 5D protein expression, and ATP synthase activity. AS-IV and Rb1, but not Rg1, R1, and DLA, had similar effect as QSYQ in regulation of energy metabolism (Cui et al., 2018). Fu et al. from the team of professor Qi-Tao Zhao demonstrated that Trichosanthes pericarpium aqueous extract displays protective effect on acute myocardial infarction by promoting the mobilization of endothelial progenitor cells and up-regulating the expression level of VEGF, eNOS, NO, and MMP-9 in myocardium and their plasma content in acute myocardial ischemic rats (Fu et al., 2018).

The Effects and Mechanisms of TCM on Improving Treatment of Myocardial Ischemia and Reperfusion Injury

Yan et al. from the team of professors Jing-Yan Han and Xin-Sheng Yao revealed that Gualou Xiebai Decoction, a compound Chinese medicine, significantly protected the myocardium from I/R injury in hyperlipidemia rat, as shown by the decreased level of CK, CK-MB, LDH, cTnI, cTnT, and IL-6, improved cardiac function, and mitigated myocardium damage, possibly via regulating energy metabolism involving inactivation of RhoA/ROCK signaling pathway (Yan et al., 2018). Zuo

et al. from the team of professors Hua Zhou and Pei Luo demonstrated that an acid polysaccharides fraction of *Panax ginseng* exerted a protective effect in H9c2 cardiomyocytes underwent hypoxia/reoxygenation on mitochondrial pathway apoptosis via elevating the expressions of glucocorticoid receptor and estrogen receptor and activating eNOS increasing NO production (Zuo et al., 2018). Li et al. from the team of professors Jing-Yan Han and Li Huang demonstrated that ginsenoside Rg1, a major ingredient of *Radix ginseng*, protected heart from I/R-induced myocardial impairment, as shown by the decrease of myocardial infarction size, the increase in myocardial blood flow, and amelioration of cardiomyocyte structure and function. The cardiac protection afforded by ginsenoside Rg1 may be attributed to its ability to adjust energy metabolism via regulating the expression of energy metabolism related proteins (HIF1, ENOα, ALDO, ECH1), increasing the activity of mitochondria respiratory complexes and the expression of ATP5D, all of which may at least partially be mediated through its binding to RhoA to inactivate the RhoA/ROCK pathway (Li et al., 2018a). Zheng et al. from the team of professors Yan Wang and Guo-Qing Zheng conducted a preclinical systematic review to evaluate the effectiveness and the mechanisms of Astragaloside IV for myocardial I/R injury, and the findings indicate that Astragaloside IV exerted potential cardioprotective function in acute myocardial I/R injury largely through promoting angiogenesis, improvement of the circulation, antioxidant, anti-apoptosis, and anti-inflammatory (Zheng et al., 2018). Zhu et al. from the team of professors Yan Wang and Guo-Qing Zheng performed a systematic review over the available preclinical evidence and possible mechanisms of Ginkgolide B in treating myocardial I/R injury, finding that the possible mechanisms via which Ginkgolide B exerts cardioprotective effects are mainly associated with anti-oxidation, anti-inflammation, anti-apoptosis, and improvement of energy metabolism (**Figure 1**).

The Effects and Mechanisms of TCM on Improving Treatment of Heart Failure

Zhang et al. from the team of professors Yong Wang, Wei Wang, and Chun Li demonstrated that Danqi Pill could improve myocardial glucose metabolism, mitochondrial oxidative phosphorylation and biogenesis by regulating HIF-1α/PGC-1α signaling pathway in heart failure post-acute myocardial infarction. Mao et al. from the team of professor Minzhou Zhang reported that Tongguan Capsule improves cardiac remodeling in a murine model of myocardial infarction by preventing cardiomyocyte inflammation and apoptosis while enhancing autophagy through Sirt1 activation (Mao et al., 2018). Ruan et al. from the team of professor Liyue Wang showed that treatment with QiShenYiQi Dripping Pills could protect against transverse aortic constriction-induced cardiac dysfunction, disrupted myocardial fiber structure and heart failure. The mechanism may be associated with the improvement in impaired cardiac angiogenesis (Ruan et al., 2018). Zhao et al. from the team of professors Yi Wang and Guanwei Fan found that Yiqifumai Injection could alleviate cardiac hypertrophy and apoptosis, and reduce cardiac fibrosis and heart failure caused by ligation of the left anterior descending coronary artery in rats, which is associated with the upregulation of MiR-21-3p and miR-542-3p (Zhao et al., 2018).

Systematic Biological Characteristics of Different Syndromes of TCM in Cardiovascular Disease

Zhao et al. from the team of professor Dong-Sheng Wang proposed a metabolomics method based on ^{1}H-NMR and random forest models to elucidate the underlying biological basis of blood stasis syndrome in coronary heart disease (CHD). Choline, β-glucose, α-glucose, and tyrosine were considered as potential biomarkers of CHD-blood stasis syndrome (Zhao et al.). Zhu et al. from the team of professor Wuxun Du investigated the metabolic profiles of plasma samples from myocardial infarction (MI) patients with phlegm stasis syndrome to identify potential disease biomarkers. Significant difference in the plasma levels of the following 10 metabolites was observed in the MI patients compared with the controls: phosphatidylserine, C16-sphingosine, N-methyl arachidonic amide, N-(2-methoxyethyl) arachidonic amide, linoleamidoglycerophosphate choline, lysoPC (C18:2), lyso-PC (C16:0), lyso-PC (C18:1), arachidonic acid, and linoleic acid (Zhu et al., 2018b). Xu et al. from the team of professors Xue-Zhong Zhou and Jing-Qing Hu proposed a network medicine-based approach to identify the characteristic of proteins in ischemic heart disease patients with phlegm-stasis syndrome, which could be used for interpreting the pharmacological mechanisms of well-established Chinese herbal formulas (e.g., Tao Hong Si Wu Decoction, Dan Shen Yin Decoction, Hunag Lian Wen Dan Decoction, and Gua Lou Xie Bai Ban Xia Decoction) (Xu et al., 2018).

The Effects of TCM on Coronary Heart Disease Patients

Tao et al. from the team of professor Xiuhua Liu investigated the metabolic profiles of the serum in CHD patients after treatment of Taohong Siwu Decoction (THSWD) using non-targeted ultra-performance liquid chromatography with tandem mass spectrometry-base metabolomics. The results indicated that THSWD promoted energy generation by upregulating fatty acid metabolism and downregulating tricarboxylic acid cycle and pentose phosphate pathway. THSWD also downregulated glycerophospholipid metabolism and arachidonic acid metabolism and involved amino acid metabolism. They showed that small molecular metabolites such as glycerophosphocholine, 8,9-DiHETrE, 5′-MTA, hippurate, indoxyl sulfate, and 3-UPA may be the potential targets of THSWD for anticoagulation and lipid reduction, and the material foundation of the "blood" to promote blood circulation in CHD treatment (Tao et al.). Following a systematical review, Yang et al. from the team of professor Ya-Hong Wang claims an effect of Tai Chi on cardiorespiratory fitness and coronary heart disease rehabilitation (Yang et al., 2018b). Based on a retrospective study on the National Health Insurance Data, Yang et al. from the team of professors Sheng Han and Hao Hu

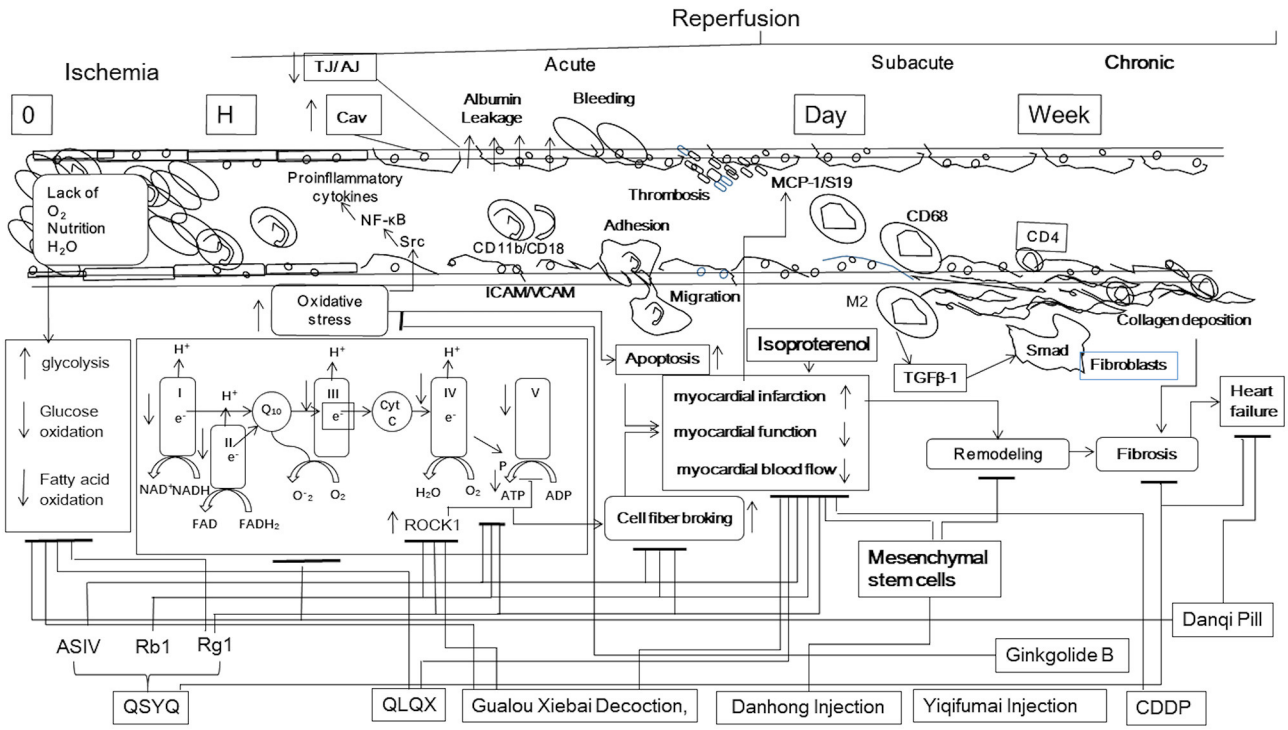


FIGURE 1 | I/R-induced microcirculatory disturbance and tissue injury stepwise progress involving the ischemia, acute, subacute, and chronic phases after reperfusion. Some TCM showing attenuation effect on I/R-induced microcirculatory dysfunction and tissue injury at various phases. I, mitochondrial complex I; II, mitochondrial complex II; III, mitochondrial complex III; IV, mitochondrial complex IV; V, mitochondrial complex V; ADP, adenosine diphosphate; AJ, adhesion junction; ASIV, astragaloside IV; ATP, adenosine triphosphate; Cav, caveolae; CDDP, compound danshen dripping pills; Cyt C, cytochrome c; FAD, flavin adenine dinucleotide; ICAM, intercellular adhesion molecule; M2, M2 macrophages; MCP-1, monocyte chemotactic protein 1; NAD, nicotinamide adenine dinucleotide; NF-κB, nuclear factor kappa-B; Q10, Coenzyme Q10; QLQX, QiLiQiangXin capsule; QSYQ, QiShenYiQi; Rb1, Ginsenoside Rb1; Rg1, Ginsenoside Rg1; ROCK, Rho-associated kinase; S19, ribosomal protein S19; TGF-β1, transforming growth factor-β1; TJ, tight junction; VCAM, vascular cell adhesion molecule. ↑, increase; ↓, decrease; ⊥, inhibition.

evaluated the clinical efficiency and economics of salvianolate injection for patients with CHD in comparison to Danhong injection and alprostadil injection. The result indicated the advantage of Salvianolate injection in reducing hospitalization duration for inpatients with CHD (Yang et al.).

THE EFFECTS AND MECHANISMS OF TCM ON CEREBROVASCULAR DISEASES

In cerebrovascular disease, 8 articles are included, of which 3 are studies on improving effects of TCM on cerebral ischemic injury and 5 on cerebral ischemia and reperfusion injury.

The Effects of TCM on Improving Treatment of Cerebral Ischemic Injury

Zhang et al. from the team of professors Yan Wang, Guo-Qing Zheng, and Jie Liu using a mouse cerebral ischemic model evaluated the effect of borneol, finding that mesenchymal stem cells (MSCs) plus borneol was more effective in attenuation of neurological deficits, infarct volume, cell death, and neurogenesis than MSCs alone (Zhang et al., 2018a). Li et al. from the team of professor Hui Zhao reported that Xiaoshuan enteric-coated capsule along with enriched environment exerted synergistic effects on alleviating atrophy and encouraging axonal reorganization partially by promoting oligodendrogenesis and overcoming intrinsic growth-inhibitory signaling, thereby facilitating higher cognitive recovery. Xue et al. from the team of professors Zhuoya Ma and Shuguang Liu based on a review and meta-analysis suggested that the combination of conventional treatments and Ginkgo leaf extract and dipyridamole injection is safe and more effective in treating ischemic stroke than conventional treatments alone.

The Effects of TCM on Improving Treatment of Cerebral Ischemia and Reperfusion Injury

Zhao et al. from the team of professors Jiehong Yang and Haitong Wan showed that many influencing factors could affect the compatibility of components contained in two formulas (CG4 and CG6), such as the metabolism by CYP450 enzymes, plasma protein binding rates, and effects related to the blood-brain barrier. This study provided new insights for choosing appropriate dosages of active components of TCM to aid in prevention and treatment of

cerebral ischemic diseases (Zhao et al.). Yang et al. from the team of professor Guo-Qing Zheng reported that the herbal compatibility of Ginseng and Rhubarb synergistically exerted neuroprotective function during acute cerebral I/R injury, mainly through reducing the expression of connexin-43 and aquaporin-4. Fu et al. from the team of professor Guo-Qing Zheng investigated the neuroprotective effects of Sanhua Decoction, a classic Chinese herbal prescription, on cerebral I/R injury in rat model, showing that Sanhua Decoction exerted neuroprotection probably by regulating p-tau level and promoting the proliferation, migration, and differentiation of endogenous neural stem cells, accompanying with neurobehavioral recovery. Wang et al. from the team of professors Yong Jiang and Kewu Zeng demonstrated that as the main active components of *Cistanche deserticola,* total Glycosides have porential to protect against I/R-induced cerebral injury, and the protection was mainly via the Nrf-2/Keap-1 pathway. Chen et al. from the team of professor Jiangang Shen discuss the important roles of myeloperoxidase (MPO) in mediating oxidative stress and neuroinflammation during cerebral I/R injury and summarize the active compounds from medicinal herbs with potential as MPO inhibitors for anti-oxidative stress and anti-inflammation to attenuate cerebral I/R injury, and as adjunct therapeutic agents for extending the window of thrombolytic treatment.

THE EFFECTS AND MECHANISMS OF TCM ON IMPROVING TREATMENT OF KIDNEY INJURY

Two research papers and 1 review article are included with respect to the improvement of kidney injury by TCM. An et al. from the team of professor Lin Yao and Yongjun Chen demonstrated that the protective effect of Xiao-Shen-Formula on kidney injury might be related with vascular prevention, anti-inflammation and anti-oxidation through intervening with multi-targets including glomerular endothelial arginase-heparanase signaling pathway in diabetic nephropathy model (An et al., 2018). Zhou et al. from the team of professor Jing-Yan Han demonstrated that pretreatment with QiShenYiQi Pills (QSYQ), a compound Chinese medicine with potential of tonifying Qi and activating blood, significantly attenuated the cisplatin induced insults, including the increase in plasma urea and creatinine, histological damage, and the renal microcirculation disturbance. These effects were ascribed to its ability to upregulate mitochondrial respiratory chain Complex I, II, and IV thus containing the production of peroxides and apoptosis, and elevate the expression of the complex V increasing ATP yield (Zhou et al., 2017). Lv et al. from the team of professor Richard J. Roman in a review article concerning oxidative stress and renal fibrosis revealed that a spectrum of TCM were reported effective in attenuation of renal injury, including compound Chinese medicines Liu-Wei-Di-Huang-Wan, Ba-Wei-Di-Huang-Wan, Fufang Xue Shuan Tong, Hu-Lu-Ba-Wan, Chinese material medica Dan-Shen, Xuan-Shen, Huang-Qi, San-Qi, Chuan-Xiong, Shan-Zha, Ge-gen, bioactive ingredients magnesium lithospermate B, caffeic acid, Icariin, Berberine, Curcumin, Paeoniflorin, Ferulate, Triptolide, Total flavonoids, Taxol, etc. (Lv et al., 2018).

THE EFFECTS AND MECHANISMS OF TCM ON ORGAN INJURY CAUSED BY CHRONIC STRESS

Two papers are included that addressed the effect of TCM on organ injury caused by chronic stress. Sun et al. from the team of professor Jing-Yan Han demonstrated the potential of Xiao-Yao-San, a classic Chinese medicine formula, to ameliorate follicle development abnormalities in a polycystic ovary syndrome rat model caused by chronic stress. The study revealed that the beneficial role of Xiao-Yao-San was correlated with the inhibition of elevated beta hydroxylase in locus coeruleus, noradrenaline release, β2R expression and apoptosis and autophagy of granulosa cells (Sun et al., 2017). Chen et al. from the team of professor Changjiang Hu reported that Huangsiyujin and its processed products may alleviate pain by regulating the release of 5-hydroxytryptamine, increasing the content of β-endorphin and inhibiting the expression of c-fos in a rat model of Qi stagnation and blood stasis.

AMELIORATING EFFECTS OF TCM ON MICROCIRCULATION DISORDERS AND ORGAN INJURY CAUSED BY ENDOTOXIN

Three papers are included that are devoted to identify effects of TCM on microcirculation disorder and organ injury caused by endotoxin. Wang et al. from the team of professor Jing-Yan Han demonstrated that post-treatment with Qing-Ying-Tang (QYT), a classic compound Chinese medicine, significantly ameliorated LPS-induced leukocyte adhesion to microvascular wall, albumin leakage from cerebral venules and brain tissue edema. The compound also attenuated the increase of MCP-1, MIP-1α, IL-1α, IL-6, and VCAM-1 in brain tissue and the activation of NF-κB and expression of MMP-9 in brain. QYT ameliorated the downregulation of claudin-5, occludin, JAM-1, ZO-1, collagen IV as well as the expression and phosphorylation of VE-cadherin in mouse brain. QYT protected cerebral microvascular barrier from disruption after LPS involving both transcellular pathway and paracellular pathway (Wang et al.). Sun et al. from the team of professors Jing-Yan Han and Xian Wang demonstrated that schisandrin (Sch), an ingredient of *Schisandra chinensis*, alleviated leukocyte adhesion to pulmonary venules and infiltration into lung tissue after LPS stimulation, which is attributable to inhibition of the increase in the expression of TLR-4, phosphorylation of I-κB, nuclear translocation of NF-κB, the expression of leukocyte adhesion molecules CD11b/CD18 and endothelial adhesion molecules ICAM-1 and VCAM-1. Sch ameliorated the downregulation of claudin-5, occludin, JAM-1, ZO-1, and lung endothelium and epithelium injury, attributable to the regulation of Akt/FoxO1 signaling pathway (Sun et al., 2018a). Wang et al. from the team of professors Chun-Yu Niu and Zi-Gang Zhao reported that resveratrol treatment partly

reduced the whole blood viscosity and regional blood flow, and increase white blood cell content in peripheral blood following the LPS challenge, suggesting a favorable role in expanding the quasi-sympathetic effects of LPS in blood viscosity at early stages (Wang et al., 2018).

MULTI-COMPONENT PHARMACOLOGICAL EFFECTS OF COMPOUND CHINESE MEDICINE

There are 4 papers regarding the multi-link pharmacological effects of compound Chinese medicine. Gong et al. from the team of professors Tina TX Dong and Kelvin Chan reviewed the chemical compositions and pharmacological effects of "Snow lotus" in treating various disorders. Yang et al. from the team of professors Ping Li and Xuezhong Zhou using network pharmacological methods revealed that G-protein coupled receptor signaling pathway and cellular protein metabolic process are the key pathways for LianXia NingXin formula. This formula was used to treat coronary heart disease phenotypes with corticotropin releasing hormone and natriuretic peptide precursor A being the two key drug targets. Further evidences from Chinese herb pharmacological databases indicate that *Pinellia ternata* (Banxia) has relatively strong adjustive effect on the two key targets (Yang et al., 2018a). Liu et al. from the team of professors Xuan Liu, Ben He, and Xianting Ding proposed that feedback system control optimization technique could be used in optimization of anti-platelet drug combinations and might be helpful in designing personal anti-platelet therapy strategy. Furthermore, feedback system control analysis could also identify interactions between different drugs which might provide useful information for research of signal cascades in platelet (Liu et al., 2018). Zhang et al. from the team of professors Xuefeng Xiao and Wuxun Du provided a strategy for understanding the mechanism where by Qiliqiangxin capsule (QLQX) protected against chronic heart failure, which included pharmacokinetics study, network pharmacology, and experimental validation. A total of 29 ingredients were determined by pharmacokinetics study, instead of herb databases, and used for network pharmacology analysis. Through experimental validation of the hub targets (VEGFA, IL-6, p-STAT3, and p-JAK2), the JAK/STAT signaling pathway were identified as the mechanism by which QLQX attenuated inflammatory process in chronic heart failure (Zhang et al.).

AUTHOR CONTRIBUTIONS

J-YH and GM have contributed to the writing of this editorial. All authors contributed to the article and approved the submitted version.

REFERENCES

An, X., Zhang, M., Zhou, S., Lu, T., Chen, Y., and Yao, L. (2018). Xiao-Shen-Formula, a traditional Chinese medicine, improves glomerular hyper-filtration in diabetic nephropathy via inhibiting arginase activation and heparanase expression. *Front. Physiol.* 9:1195. doi: 10.3389/fphys.2018.01195

Chen, J., Wei, J., Huang, Y., Ma, Y., Ni, J., Li, M., et al. (2018). Danhong injection enhances the therapeutic efficacy of mesenchymal stem cells in myocardial infarction by promoting angiogenesis. *Front. Physiol.* 9:991. doi: 10.3389/fphys.2018.00991

Chen, M., Lv, H., Gan, J., Ren, J., and Liu, J. (2017). Tang Wang Ming Mu granule attenuates diabetic retinopathy in type 2 diabetes rats. *Front. Physiol.* 8:1065. doi: 10.3389/fphys.2017.01065

Cui, Y. C., Yan, L., Pan, C. S., Hu, B. H., Chang, X., Fan, J. Y., et al. (2018). The contribution of different components in QiShenYiQi Pills® to its potential to modulate energy metabolism in protection of ischemic myocardial injury. *Front. Physiol.* 9:389. doi: 10.3389/fphys.2018.00389

Deng, J. N., Li, Q., Sun, K., Pan, C. S., Li, H., Fan, J. Y., et al. (2019). Cardiotonic pills plus recombinant human prourokinase ameliorates atherosclerotic lesions in LDLR-/- Mice. *Front. Physiol.* 10:1128. doi: 10.3389/fphys.2019.01128

Fan, C. D., Sun, J. Y., Fu, X. T., Hou, Y. J., Li, Y., Yang, M. F., et al. (2017). Astaxanthin attenuates homocysteine-induced cardiotoxicity *in vitro* and *in vivo* by inhibiting mitochondrial dysfunction and oxidative damage. *Front. Physiol.* 8:1041. doi: 10.3389/fphys.2017.01041

Fu, N., Li, H., Sun, J., Xun, L., Gao, D., and Zhao, Q. (2018). Trichosanthes pericarpium aqueous extract enhances the mobilization of endothelial progenitor cells and up-regulates the expression of VEGF, eNOS, NO, and MMP-9 in acute myocardial ischemic rats. *Front. Physiol.* 8:1132. doi: 10.3389/fphys.2017.01132

Gao, L. N., Zhou, X., Lu, Y. R., Li, K., Gao, S., Yu, C. Q., et al. (2018). Dan-Lou prescription inhibits foam cell formation induced by ox-LDL via the TLR4/NF-κB and PPARγ signaling pathways. *Front. Physiol.* 9:590. doi: 10.3389/fphys.2018.00590

Gu, Y. Y., Huang, P., Li, Q., Liu, Y. Y., Liu, G., Wang, Y. H., et al. (2018). YangXue QingNao Wan and Silibinin capsules, the two chinese medicines, attenuate cognitive impairment in aged LDLR (+/-) golden syrian hamsters involving protection of blood brain barrier. *Front. Physiol.* 9:658. doi: 10.3389/fphys.2018.00658

Hao, H. F., Liu, L. M., Pan, C. S., Wang, C. S., Gao, Y. S., Fan, J. Y., et al. (2017). Rhynchophylline ameliorates endothelial dysfunction via Src-PI3K/Akt-eNOS cascade in the cultured intrarenal arteries of spontaneous hypertensive rats. *Front. Physiol.* 8:928. doi: 10.3389/fphys.2017.00928

Li, L., Pan, C. S., Yan, L., Cui, Y. C., Liu, Y. Y., Mu, H. N., et al. (2018a). Ginsenoside Rg1 ameliorates rat myocardial ischemia-reperfusion injury by modulating energy metabolism pathways. *Front. Physiol.* 9:78. doi: 10.3389/fphys.2018.00078

Li, P., Chen, D., Cui, Y., Zhang, W., Weng, J., Yu, L., et al. (2018b). Src plays an important role in AGE-induced endothelial cell proliferation, migration, and tubulogenesis. *Front. Physiol.* 9:765. doi: 10.3389/fphys.2018.00765

Li, Y., Li, Q., Pan, C. S., Yan, L., Hu, B. H., Liu, Y. Y., et al. (2018c). Bushen Huoxue attenuates diabetes-induced cognitive impairment by improvement of cerebral microcirculation: involvement of RhoA/ROCK/moesin and Src signaling pathways. *Front. Physiol.* 9:527. doi: 10.3389/fphys.2018.00527

Liu, W., Li, Y. L., Feng, M. T., Zhao, Y. W., Ding, X., He, B., et al. (2018). Application of feedback system control optimization technique in combined use of dual antiplatelet therapy and herbal medicines. *Front. Physiol.* 9:491. doi: 10.3389/fphys.2018.00491

Lv, W., Booz, G. W., Fan, F., Wang, Y., and Roman, R. J. (2018). Oxidative stress and renal fibrosis: recent insights for the development of novel therapeutic strategies. *Front. Physiol.* 9:105. doi: 10.3389/fphys.2018.00105

Mao, S., Chen, P., Li, T., Guo, L., and Zhang, M. (2018). Tongguan capsule mitigates post-myocardial infarction remodeling by promoting autophagy and inhibiting apoptosis: role of Sirt1. *Front. Physiol.* 9:589. doi: 10.3389/fphys.2018.00589

Ruan, G., Ren, H., Zhang, C., Zhu, X., Xu, C., and Wang, L. (2018). Cardioprotective effects of QiShenYiQi dripping pills on transverse aortic constriction-induced heart failure in mice. *Front. Physiol.* 9:324. doi: 10.3389/fphys.2018.00324

Sun, H. Y., Li, Q., Liu, Y. Y., Wei, X. H., Pan, C. S., Fan, J. Y., et al. (2017). Xiao-Yao-San, a Chinese medicine formula, ameliorates chronic unpredictable mild stress induced polycystic ovary in rat. *Front. Physiol.* 8:729. doi: 10.3389/fphys.2017.00729

Sun, K., Huang, R., Yan, L., Li, D. T., Liu, Y. Y., Wei, X. H., et al. (2018a). Schisandrin attenuates lipopolysaccharide-induced lung injury by regulating TLR-4 and Akt/FoxO1 signaling pathways. *Front. Physiol.* 9:1104. doi: 10.3389/fphys.2018.01104

Sun, T., Zhang, L., Li, X., Chen, F., Li, Y., Ma, X., et al. (2018b). MicroRNA-1 and circulating microvesicles mediate the protective effects of dantonic in acute myocardial infarction rat models. *Front. Physiol.* 9:664. doi: 10.3389/fphys.2018.00664

Wang, Y., Cui, H., Niu, F., Liu, S. L., Li, Y., Zhang, L. M., et al. (2018). Effect of resveratrol on blood rheological properties in LPS-challenged rats. *Front. Physiol.* 9:1202. doi: 10.3389/fphys.2018.01202

Xu, W. M., Yang, K., Jiang, L. J., Hu, J. Q., and Zhou, X. Z. (2018). Integrated modules analysis to explore the molecular mechanisms of phlegm-stasis cementation syndrome with ischemic heart disease. *Front. Physiol.* 9:7. doi: 10.3389/fphys.2018.00007

Yan, L. L., Zhang, W. Y., Wei, X. H., Yan, L., Pan, C. S., Yu, Y., et al. (2018). Gualou Xiebai Decoction, a traditional chinese medicine, prevents cardiac reperfusion injury of hyperlipidemia rat via energy modulation. *Front. Physiol.* 9:296. doi: 10.3389/fphys.2018.00296

Yang, Y., Yang, K., Hao, T., Zhu, G., Ling, R., Zhou, X., et al. (2018a). Prediction of molecular mechanisms for Lianxia Ningxin formula: a network pharmacology study. *Front. Physiol.* 9:489. doi: 10.3389/fphys.2018.00489

Yang, Y. L., Wang, Y. H., Wang, S. R., Shi, P. S., and Wang, C. (2018b). The effect of tai chi on cardiorespiratory fitness for coronary disease rehabilitation: a systematic review and meta-analysis. *Front. Physiol.* 8:1091. doi: 10.3389/fphys.2017.01091

Yi, Q., Sun, P., Li, J., Kong, S., Tian, J., Li, X., et al. (2018). Rho, a fraction from rhodiola crenulate, ameliorates hepatic steatosis in mice models. *Front. Physiol.* 9:222. doi: 10.3389/fphys.2018.00222

Zhang, X. G., Shan, C., Zhu, J. Z., Bao, X. Y., Tong, Q., Wu, X. F., et al. (2018a). Additive neuroprotective effect of borneol with mesenchymal stem cells on ischemic stroke in mice. *Front. Physiol.* 8:1133. doi: 10.3389/fphys.2017.01133

Zhang, Y., Li, C., Meng, H., Guo, D., Zhang, Q., Lu, W., et al. (2018b). BYD ameliorates oxidative stress-induced myocardial apoptosis in heart failure post-acute myocardial infarction via the P38 MAPK-CRYAB signaling pathway. *Front. Physiol.* 9:505. doi: 10.3389/fphys.2018.00505

Zhao, Y., Li, Y., Tong, L., Liang, X., Zhang, H., Li, L., et al. (2018). Analysis of microRNA expression profiles induced by yiqifumai injection in rats with chronic heart failure. *Front. Physiol.* 9:48. doi: 10.3389/fphys.2018.00048

Zheng, Q., Zhu, J. Z., Bao, X. Y., Zhu, P. C., Tong, Q., Huang, Y. Y., et al. (2018). A Preclinical systematic review and meta-analysis of astragaloside iv for myocardial ischemia/reperfusion injury. *Front. Physiol.* 9:795. doi: 10.3389/fphys.2018.00795

Zhou, L., Wei, X. H., Pan, C. S., Yan, L., Gu, Y. Y., Sun, K., et al. (2017). QiShenYiQi Pills, a compound chinese medicine, prevented cisplatin induced acute kidney injury via regulating mitochondrial function. *Front. Physiol.* 8:1090. doi: 10.3389/fphys.2017.01090

Zhu, L., Zhu, X., Sun, G., Meng, X., Wang, M., Cui, H., et al. (2018a). Dai-Zong-Fang, a traditional chinese herbal formula, ameliorates insulin resistance in db/db mice. *Front. Physiol.* 9:224. doi: 10.3389/fphys.2018.00224

Zhu, M., Han, Y., Zhang, Y., Zhang, S., Wei, C., Cong, Z., et al. (2018b). Metabolomics study of the biochemical changes in the plasma of myocardial infarction patients. *Front. Physiol.* 9:1017. doi: 10.3389/fphys.2018.01017

Zuo, Y. H., Han, Q. B., Dong, G. T., Yue, R. Q., Ren, X. C., Liu, J. X., et al. (2018). Panax ginseng polysaccharide protected H9c2 cardiomyocyte from hypoxia/reoxygenation injury through regulating mitochondrial metabolism and RISK pathway. *Front. Physiol.* 9:699. doi: 10.3389/fphys.2018.00699

Conflict of Interest: The authors declare that the research was conducted in the absence of any commercial or financial relationships that could be construed as a potential conflict of interest.

Copyright © 2021 Han, Meininger, Luo and Huang. This is an open-access article distributed under the terms of the Creative Commons Attribution License (CC BY). The use, distribution or reproduction in other forums is permitted, provided the original author(s) and the copyright owner(s) are credited and that the original publication in this journal is cited, in accordance with accepted academic practice. No use, distribution or reproduction is permitted which does not comply with these terms.

frontiers in Physiology

ORIGINAL RESEARCH
published: 04 September 2019
doi: 10.3389/fphys.2019.01109

NMR Metabolomics and Random Forests Models to Identify Potential Plasma Biomarkers of Blood Stasis Syndrome With Coronary Heart Disease Patients

*Lin-Lin Zhao[1], Xin-Jian Qiu[2], Wen-Bo Wang[2], Ruo-Meng Li[3] and Dong-Sheng Wang[2]**

[1] Health Management Department, The Third Xiangya Hospital, Central South University, Changsha, China, [2] Institute of Integrated Traditional Chinese and Western Medicine, Xiangya Hospital, Central South University, Changsha, China, [3] Traditional Chinese Medicine Department, The Third Xiangya Hospital, Central South University, Changsha, China

OPEN ACCESS

Edited by:
Jing-Yan Han,
Peking University, China

Reviewed by:
Xuemei Qin,
Shanxi University, China
Jie Wang,
Guang'anmen Hospital, Academy of Chinese Medical Sciences, China

***Correspondence:**
Dong-Sheng Wang
wdsh666@126.com

Specialty section:
This article was submitted to Vascular Physiology, a section of the journal Frontiers in Physiology

Received: 10 April 2019
Accepted: 12 August 2019
Published: 04 September 2019

Citation:
Zhao L-L, Qiu X-J, Wang W-B, Li R-M and Wang D-S (2019) NMR Metabolomics and Random Forests Models to Identify Potential Plasma Biomarkers of Blood Stasis Syndrome With Coronary Heart Disease Patients. Front. Physiol. 10:1109. doi: 10.3389/fphys.2019.01109

Background: Coronary heart disease (CHD) remains highly prevalent and is one of the largest causes of death worldwide. Blood stasis syndrome (BSS) is the main syndrome associated with CHD. However, the underlying biological basis of BSS with CHD is not yet been fully understood.

Materials and Methods: We proposed a metabolomics method based on ^{1}H-NMR and random forest (RF) models to elucidate the underlying biological basis of BSS with CHD. Firstly, 58 cases of CHD patients, including 27 BSS and 31 phlegm syndrome (PS), and 26 volunteers were recruited from Xiangya Hospital affiliated to Central South University. A 1 mL venous blood sample was collected for NMR analysis. Secondly, principal component analysis (PCA), partial least squares discrimination analysis (PLS-DA) and RF was applied to observe the classification of each group, respectively. Finally, RF and multidimensional scaling (MDS) were utilized to discover the plasma potential biomarkers in CHD patients and CHD–BSS patients.

Results: The models constructed by RF could visually discriminate BSS from PS in CHD patients. Simultaneously, we obtained 12 characteristic metabolites, including lysine, glutamine, taurine, tyrosine, phenylalanine, histidine, lipid, citrate, choline, lactate, α-glucose, β-glucose related to the CHD patients, and Choline, β-glucose, α-glucose and tyrosine were considered as potential biomarkers of CHD–BSS.

Conclusion: The combining of ^{1}H-NMR profiling with RF models was a useful approach to analyze complex metabolomics data (should be deleted). Choline, β-glucose, α-glucose and tyrosine were considered as potential biomarkers of CHD–BSS.

Keywords: coronary heart disease, blood stasis syndrome, metabolomics, random forests, ZHENG types, Systems Biology

BACKGROUND

Coronary heart disease (CHD) is always associated with metabolic disorder, and the metabolic risk factors, such as hyperlipidemia and diabetes, powerfully predict the cardiac events (Lacoste et al., 1995; Ansar et al., 2011). CHD remains highly prevalent and is one of the largest causes of death worldwide. Specific and sensitive diagnostic methods are critical both for early detection and treatment of CHD (Rubin, 2013). Metabonomics technologies have been studied to diagnose the presence and severity of CHD (Brindle et al., 2002). It is a newly developed platform of systems biology that allows holistic, quantitative and qualitative determination of low molecular endogenous metabolites in biofluids or tissues (Lindon et al., 2004). It concerns the dynamic multivariate metabolic changes in response to pathophysiological stimuli, genetic modification, environmental influences or drug perturbations (Nicholson and Lindon, 2008). Analysis of differential metabolites enables us to obtain novel biomarkers discovery and disturbed metabolic pathways (Sabatine et al., 2005).

Nowadays, Traditional Chinese Medicine (TCM) has become popular worldwide. Systematic, holistic and dynamic characteristics of TCM theory are perfectly coincident with metabonomics (Wang et al., 2005; Sun et al., 2012). Metabonomics technologies have been applied in study on the essence of the syndrome (ZHENG type or pattern in TCM) and shown the superiority and advanced nature. According to TCM theory, a syndrome is a combination of clinical manifestations including symptoms, signs, tongue appearances and pulse feelings. Syndrome is not only the core of TCM theory, but also the base of definite diagnosis and effective therapies (Xu and Chen, 2008). It will not only improve the validity and reliability of "syndrome differentiation" through syndrome model established based on metabonomics, but also help to establish the clinical curative criteria.

Blood stasis syndrome (BSS) is the most common syndrome associated with CHD. Our previous study has shown that the metabonomics approach based on liquid chromatography/quadrupole time-of-flight mass spectrometry (LC-Q-TOF/MS) was useful for interpreting the differentiation of syndrome [phlegm syndrome (PS) and BSS] in TCM (Zhao et al., 2014). There were 18 differential metabolites mainly involved in amino acid metabolism, purine metabolism and pyrimidine metabolism contributing to the clustering and discrimination between PS and BSS in CHD patients. However, it is clear that the two metabonomics technologies are complementary, giving information on different sets of biomarkers and providing more comprehensive classification and biomarker information.

Random forests (RFs) is machine learning algorithm which uses an ensemble of classification trees and is an ideal method for classification and feature selection. Spectral buckets are employed as input variables. RF could be employed for both supervised (outcome labels are used) and unsupervised (outcome labels are not used) learning (Breiman, 2001). In this study, we proposed a metabolomics method based on ^{1}H-NMR and RF models to validate the separated trend between BSS and PS in CHD patients and acquire more potential biomarkers of BSS in CHD patients.

MATERIALS AND METHODS

Subjects Collection

A total of 58 cases CHD patients (27 BSS and 31 PS) and 26 volunteers were derived from the Xiangya Hospital affiliated to the Central South University in Hunan Province, China (June 1, 2013 to April 30, 2014). All selected CHD patients were diagnosed and confirmed by coronary angiography. Diagnosis standard of CHD refers to "nomenclature and diagnosis criteria of ischemic heart disease" which is established by the Joint International Society and Federation of Cardiology/World Health Organization Task Force on Standardization of Clinical Nomenclature (Nomenclature and criteria for diagnosis of ischemic heart disease, 1979). The syndrome was identified by three chief physicians, according to "criteria for TCM syndrome differentiation of patients with coronary heart disease" (Subcommittee of Cardiovascular Diseases of China Society of Integrated Traditional Chinese, and Western Medicine, 1991).

Patients who suffered from diabetic cardiomyopathy, hyperthyroid heart disease, hypertensive heart disease, pulmonary heart disease, anemic heart disease, systemics scleroderma heart disease, inborn coronary abnormity and rheumatic heart disease, who suffered from severe hypertension, malignant tumor, renal failure, thyroid disease, pulmonary infection, who suffered from infectious diseases, who suffered from invigorative system disease and women in pregnant or in lactation were excluded.

All patients aged from 45 to 75 were eligible for enrollment. The age and sex of volunteers in control group were group-matched with the cases group. The study was approved by the hospital ethics committee and all subjects provided written informed consent.

Chemicals and Reagents

NaCl, $K_2HPO_4 \cdot 3H_2O$, and $NaH_2PO_4 \cdot 2H_2O$ (all in analytical-grade) were obtained from Sinopharm Chemical Reagent Co., Ltd. (Shanghai, China); NaN_3 (in analytical-grade, used for anticorrosion) was provided by the Tianjin Fu Chen Chemical Reagent Factory. D_2O (in analytical-grade) was produced from Cambridge Isotope Laboratories Inc., United States.

Plasma Collection and Preparation

A 1 mL venous blood sample was collected in a vacutainer tubes with ethylenediaminetetraacetic acid (EDTA) at 7 o' clock in the morning after 12 h of overnight fasting and then centrifuged at 10,000 rpm for 10 min at 4°C. The supernatant was stored at −80°C until NMR analysis.

A total of 200 μL plasma was mixed with 400 μL of K_2HPO_4/NaH_2PO_4 buffer (45 mM, pH 7.4) containing 50% D_2O and 0.9% NaCl in a centrifuge tube (1.5 mL), after centrifugation (12,000 rpm) for 10 min, a total of 550 μL of the supernatant was placed into a 5 mm NMR tubes directly for NMR analysis.

NMR Analysis

All ^{1}H NMR spectra were measured at 298 K on a Bruker AVIII 600 spectrometer (Bruker Biospin, Germany) equipped with Ultra cryogenic probe operating at 600.13 MHz for ^{1}H.

A standard one-dimensional (1D) ^{1}H-NMR spectra were recorded using a NOESYPR1D pulse sequence [recycle delay (RD)-90°-t_1-90°-t_m-90°-acquire] (Nicholson et al., 1995) to obtain all observed metabolites signals, CPMG pulse sequence [RD-90°-(τ-180°-τ)$_n$-acquire] (Meiboom and Gill, 1958) to obtain small molecule metabolites signals and DIFFUSIONEDIT [RD-90°-G_1-τ-180°-G_2-τ-90°-△-90°-G_3-τ-180°-G_4-τ-90°-Te-90°-acquire] to obtain macromolecules metabolites. The following parameters were set for NMR detection in the experiments: 90° pulse length (P_1) was 11.2 μs, PLW_1 was 10, −10 [W, −dBW], spectral width was 20 ppm, the sampling point was 32 k, the acquisition time was 1.64 s. 64 scans, 8 dummy scans. In the NOESYPR1D experiments, t_1 was 4 μs, mixing time (D_8) was 100 ms, relaxation decay time (D_1) was 2 s, In the CPMG experiments, total echo time: 80 ms, Echo evolution time (d20): 350 μs, Echo cycle (L_4): 100. In the DIFFUSIONEDIT experiments, gradient recovery (D_{16}): 150 μs, diffusion time (D_{20}): 0.2 s; Gradient strength (GPZ6) 85%, gradient pulse length (P_{30}): 1100 μs.

For resonance assignment, a range of two-dimensional (2D) NMR spectra were acquired including ^{1}H-^{1}H correlation spectroscopy (COSY), ^{1}H-^{1}H total correlation spectroscopy (TOCSY) NMR spectra,^{1}H-^{1}H J-Resolved Spectroscopy (JRES), ^{1}H-^{13}C heteronuclear single quantum correlation (HSQC) and ^{1}H-^{13}C heteronuclear multiple bond correlation spectra (HMBC). Briefly, in COSY and TOCSY experiments, the sampling point of 160 (F_1) and 2048 (F_2), spectral width of 10.5 ppm (F_1) and 10.5 ppm (F_2), 90°pulse length (P_1) of 11.87 s. TOCSY 2D NMR spectra were acquired with MLEV as the spin lock pulse and the spin-lock time of 80 ms. ^{1}H-^{1}H JRES were acquired with the sampling point of 64 (F_1) and 2048 (F_2) the spectral widths were 0.1 ppm in the F_1 dimension and 10.5 ppm in the F_2 dimension. ^{1}H-^{13}C HSQC 2D NMR spectra were acquired using composite pulse broad band decoupling (globally alternating optimized rectangular pulses, GARP), the sampling points were 128 (F_1) and 2048 (F_2), with the spectral widths of 220 ppm (F_1) and 10.5 ppm (F_2). ^{1}H-^{13}C HMBC 2D NMR spectra were acquired into 128 data points (F_1) and 2048 data points (F_2), the spectral widths were 220 ppm (F_1) and 10.5 ppm (F_2).

Data Pre-processing of NMR Spectra and Multivariate Data Analysis

Baseline and phase corrections for the NMR spectra were manually achieved using mestrenova (version 9.0.1, Mestrelab Research, Santiago de Compostela, Spain). The peak of L-lactate with a chemical shift at δ1.33 was used as a spectral reference for plasma. The spectral region of δ0.5–9.5 was segmented into 0.002 ppm (He et al., 2009) chemical shift buckets, the region at δ4.70–5.00 and δ 5.6–6.0 were discarded to eliminate the effects of imperfect water suppression and urea signal, respectively. The regions of EDTA-Ca resonance (δ2.55–2.58, δ3.07–3.17), EDTA-Mg resonance (δ2.68–2.70, δ3.23–3.26), Free-EDTA resonance (δ3.6–3.63) were removed. The integral value of each spectrum was used as input variables for the subsequent statistical analysis.

Principal component analysis (PCA) and partial least squares discrimination analysis (PLS-DA) were performed to examine intrinsic variation of the NMR spectral data using SIMCA-P 14.0 (Umetrics, Sweden). Each point on the scores plot is defined by the spectrum of an individual sample. Then, RFs in software MATLAB (2010b, The MathWorks Inc., Natick, MA, United States) were applied to uncover the underlying structure of this data, multidimensional scaling (MDS) was employed to map the proximity into a lower-dimensional space.

A one-way analyses of variance (ANOVA) with a Bonferroni correction of the SPSS 17.0 for Windows (SPSS Inc., Chicago, IL, United States) was used for significance analysis. *P*-values less than 0.05 were considered significant.

Random Forest

There are two powerful machine learning techniques advantages with RF: bagging and random feature selection. In bagging, each tree is trained on a bootstrap sample of the training data, and predictions are made by majority vote of trees. Instead of using all features, RF randomly selects a subset of features to split at each node when growing a tree. To assess the prediction performance of the RF algorithm, it performs a type of cross-validation in parallel with the training step by using the so-called out-of-bag (OOB) samples. On average, each tree is grown using about 2/3 of the training data, leaving about 1/3 as OOB. The RF algorithm can be stated as follows (Huang et al., 2013):

Draw n_{tree} bootstrap samples from the original data, n_{tree} is the number of ensemble tree in RF. The n_{tree} is equal to 2000 in this study.

For all bootstrap samples, grow an un-pruned classification or regression tree, with the following modification: at each node, rather than choosing the best split among all variables, randomly sample mtry of the variables and choose the best split from among those variables (bagging can be thought of as the special case of RFs obtained when mtry = *p*, the number of variables). In general, mtry is simply a number (positive integer) between 1 and *p*.

Predict new data by aggregating the predictions of n_{tree} (i.e., majority votes for classification).

Variable Importance

Random forest algorithm has the ability to estimate feature importance. A measure of how each feature contributes to the prediction performance of RF algorithm can be calculated in the course of the training. The important scores can be used to identify biomarkers. The frequently used type of RF algorithm to measure feature importance is the mean decrease in classification based on permutation. The prediction accuracy after permutation is subtracted from the prediction accuracy before permutation and averaged over all trees in the forest to give the permutation importance value. In the current research, the mean decrease in classification accuracy was accepted to measure variable importance.

Proximity Measure

Proximity matrix is the important feature of RF algorithm which can be used to identify structure in the data. RF algorithm not only generates variable-related information such as variable

importance measures, but also calculates the proximities between samples. All samples in the original data set are classified by the forest. The proximity between two samples is calculated as the number of times the two samples end up in the same terminal node of a tree, divided by the number of trees in the forest. The resulting matrix is symmetric with diagonal element equal to 1 and off-diagonal elements ranging from 0 to 1. The proximities between similar samples are always high. Proximity scores may also be used to construct MDS plots. MDS plots aim to visualize the similarity or dissimilarity (calculated as 1 proximity) between samples.

RESULTS

Demographic and Clinical Characteristics of the Samples

Demographic and clinical data of the subjects were summarized in **Table 1**. There was no significant difference in age, gender ratio, body mass index and other clinical feature between the three groups ($P > 0.05$), as assessed by Friedman's ANOVA.

^{1}H NMR Spectrum of Plasma Samples

A typical 1D ^{1}H NMR CMPG spectrum of plasma samples from (A) control and (B) CHD group were shown in **Figure 1**. Resonance assignments of metabolites were made according to the literature and confirmed by 2D NMR spectra. 69 metabolites were identified, covering amino acids, organic acids, lipids, glucose, salts, choline and urea. In addition, Tricarboxylic acid (TCA) cycle metabolites, such as succinate and citrate were included. Visual inspection of the 1D ^{1}H NMR CMPG spectra showed clear differences in overall composition between CHD patients and control (**Figure 1**). However, these qualitative observations were all by visual inspection, multivariate data analysis of NMR spectra were performed to recover the characteristics of metabolic patterns of CHD (included BSS and PS) and control.

Classification Using PCA, PLS-DA, and RF

Principal component analysis on plasma CPMG spectra were applied to observe the classification of CHD patients and controls. The first two principal components were plotted to present the distribution of the three groups (**Figure 2**).

As visually observed, the three groups were totally overlapped in the PCA scores plot, suggesting that the unsupervised PCA method could not extract useful information in the NMR CMPG data. PLS-DA was also used to show the classification of the three groups, as presented in **Figure 2**, and only the differences between the CHD and control groups could be observed. As for BSS and PS of CHD patients, they were completely overlapped, and had no separation trend. PCA and PLS-DA on plasma NOESY and BPP-LED spectra, and model verification of PLS-DA on plasma CMPG spectra, BPP-LED spectra and NOESY spectra were shown in **Supplemetary Figures S1–S5**.

Then, RF method was used to explore the underlying characteristics of this NMR data. 2000 trees were grown, during the trees growing, proximities were computed for the cases. Similar cases may fall into the same terminal node or derive from the same parent. In order to better present the differences of the samples, MDS was employed to map the proximity into a lower dimensional space. OOB estimate of error rate and fivefold cross validation were used to evaluate the stability of the forest tree model. It could be seen from **Figure 3**, the OOB error rate did not decrease with the number of trees constructed, the RF algorithm could avoid overfitting to a certain extent, and the area under the curve of ROC was 0.96. As shown in **Figure 3A**, the controls were far away from other two groups. Furthermore, an obvious distinction between CHD–BSS and CHD–PS was observed in the MDS plot. **Figure 3B** showed the OOB error rate.

It can be seen from **Figure 3**, the OOB error rate did not decrease with the number of trees constructed, the RF algorithm could avoid overfitting to a certain extent.

TABLE 1 | Demographic and clinical characteristics of the samples.

	HC (n = 26)	CHD–BSS (n = 27)	CHD–PS (n = 31)	P-value
Age, mean ± SD, years	53.73 ± 11.39	53.70 ± 13.20	54.97 ± 10.88	0.896
Male, n (%)	20 (76.92)	19 (70.37)	18 (58.06)	0.298
Body mass index, mean ± SD (kg/m^2)	24.42 ± 2.57	25.59 ± 3.89	23.61 ± 2.58	0.054
Active smoking, n (%)	10 (38.46)	11 (40.74)	10 (32.26)	0.785
Diabetes mellitus, n (%)	5 (19.23)	9 (33.33)	10 (32.26)	0.445
Hypertension, n (%)	8 (30.77)	9 (33.33)	11 (35.48)	0.932
Dyslipidemia, n (%)	7 (26.92)	14 (51.85)	16 (51.61)	0.106

Discovery of Plasma ^{1}H-NMR Potential Biomarkers in CHD Patients and CHD–BSS Patients

Metabolic biomarker discovery is an important aim of metabolomics studies. In model construction, the purpose of variable selection is to find the best combination of variables, which provide the best classification result (Huang et al., 2013). A measure of how each feature contributes to the prediction performance of RF can be calculated in the course of training, and its importance score (VIM) was obtained. VIM was used to measure the contribution of the variable to the classification. **Figure 4** showed MDS plots and the variable importance. The feature importance was set to 0.1, from the bar plot of variable importance, we found that some metabolites make a contribution to the classification of controls and CHD samples (**Figure 4a**), the peak area quantitative of each spectrum were manually achieved by segmenting into 0.002 ppm in mestrenova, then t-test was implemented to test the significant of these metabolites and the result was summarized in **Table 2** ($P < 0.05$). Finally, we obtained 12 characteristic metabolites, including lysine (1.40 ppm), glutamine (2.45 ppm), taurine (3.28 ppm), tyrosine (3.93 ppm), phenylalanine (3.96 ppm), histidine (4.0 ppm), lipid (2.0 ppm), citrate (2.55 ppm), choline (3.20 ppm, 4.05 ppm), lactate (4.11 ppm), α-Glucose (5.23 ppm, 3.39 ppm, 3.56 ppm,

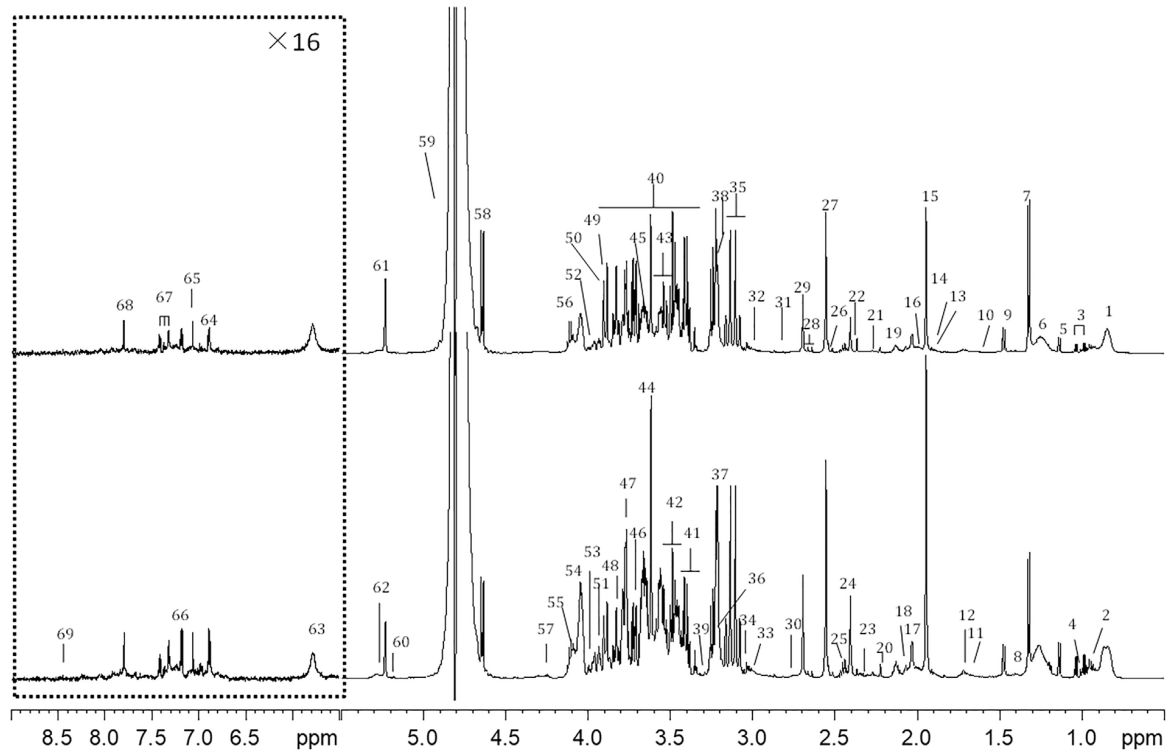


FIGURE 1 | Typical cpmgpr1d spectra (600 MHz) of **(A)** CHD patient, **(B)** control from plasma samples (the region at δ5.5–9.0 was expanded for 16 times). Key: 1, lipid (CH_3); 2, leucine and isoleucine; 3, valine; 4. isoleucine; 5, 3-hydroxybutyrate; 6, lipid (CH_2); 7, lactate; 8, lysine; 9, alanine; 10, lipid (CH_2CH_2CO); 11, lysine and arginine; 12, leucine; 13, lysine and arginine; 14, acetate; 15, acetic acid (CH_3COOH); 16, lipid ($CH_2C=C$); 17, N-acetyl glycoproteins (NAG) 18, glutamate; 19, glutamine; 20, acetoacetate; 21, lipid ($CH_2C=O$); 22, pyruvate; 23, glutamate; 24, succinate; 25, glutamine; 26, citrate; 27, Ca-EDTA; 28, citrate; 29, Mg-EDTA; 30, lipid ($C=CCH_2C=C$); 31, trimethylamine; 32, lysine; 33, creatine; 34, creatinine; 35, Ca-EDTA; 36, choline and GPC, glycerophosphocholine (GPC) and phosphocholine (PC); 37, free-EDTA; 38, Mg-EDTA; 39, taurine; 40, glucose and amino acid; 41, α-glucose and taurine; 42, β-glucose; 43, α-glucose; 44, free-EDTA; 45, choline; 46, α-glucose; 47, β-glucose; 48, α-glucose; 49, α-glucose; 50, β-glucose; 51, tyrosine; 52, phenylalanine; 53, histidine; 54, choline; 55, TG; 56, lactate; 57, TG; 58, β-glucose; 59, H_2O; 60, TG; 61, α-glucose; 62, lipid (CH = CH); 63, urea; 64, tyrosine; 65, histidine; 66, tyrosine; 67, phenylalanine; 68, histidine; 69, formate.

3.71 ppm,3.83 ppm, 3.89 ppm), and β-Glucose (3.47 ppm, 3.72 ppm) related to the CHD patients. These metabolites involved in the key metabolic pathways are shown in **Figure 5**.

The variable importance measures of samples obtained by RF models revealed that in the plasma of CHD patients contained significantly higher levels of some amino acids, including lysine, glutamine, taurine, tyrosine, phenylalanine and histidine compared to the controls. Plasma lipid, lactate, α-glucose and β-glucose in CHD patients were higher when compared with controls ($P < 0.01$). However, citrate and choline of plasma from CHD patients were lower than those from angiography normal (controls) ($P < 0.01$).

In order to explore potential metabolite biomarkers of CHD–BSS patients, RF methodology was applied to extract important variables of the control group and CHD group. The feature importance was enhanced to 0.2 to obtain the most important variables. The variable importance measures of each two groups obtained by RF models were shown in **Figure 4**. The important variables ($P < 0.01$) of the each two groups were shown in **Table 3**, we found that 72/choline, 73/β-glucose, 74/α-glucose, 75/α-glucose, 77/α-glucose, 78/tyrosine could be the potential metabolite biomarkers of CHD–BSS patients.

DISCUSSION

The use of the analytical techniques, ^{1}H-NMR, was feasible to study the metabonomic differences between angiography normal and CHD patients. ^{1}H-NMR analysis enabled the identification of a total of 12 metabolites as contributors to the discrimination of controls and CHD patients. We found that the potential biomarkers were principally correlated to lipid metabolism dysfunction, energy metabolism dysfunction, amino acid dysfunction and glucose metabolism dysfunction in the pathological development of CHD. In our previous studies using LC-MS, we found 27 potential biomarkers which were principally involved in arachidonic acid metabolism, amino acid metabolism, purine metabolism, pyrimidine metabolism, steroid biosynthesis and linoleic acid metabolism that discriminated CHD patients from healthy controls. In those potential biomarkers, citric acid and phenylalanine were found in the current research with NMR technology. Integration of several metabonomics technologies could provide more comprehensive biomarker information.

Choline is an important methyl donor, precursor of acetylcholine, and it is needed for lipid metabolism (Ueland, 2011).

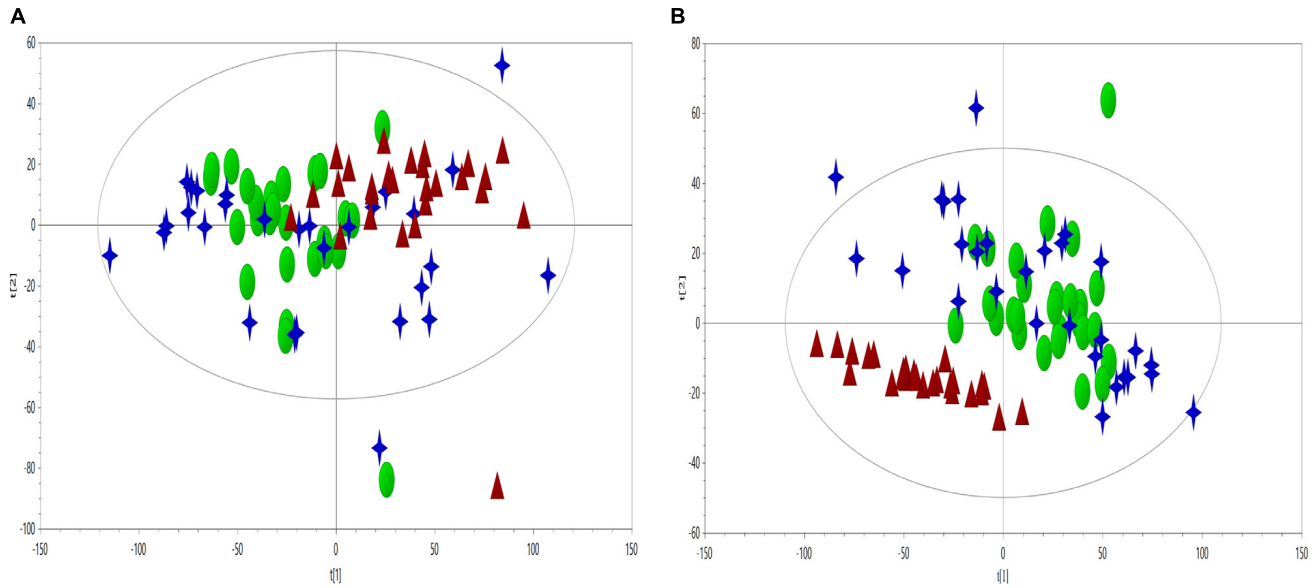


FIGURE 2 | PCA scores plot (**A**, R^2X = 0.636, Q^2 = 0.560) and PLS-DA scores plot (**B**, R^2X = 0.599, Q^2 = 0.318, R^2Y = 0.37) derived from NMR data to compare the metabolome of the control (triangles, red), CHD–BSS (circles, green) and CHD–PS (stars, blue).

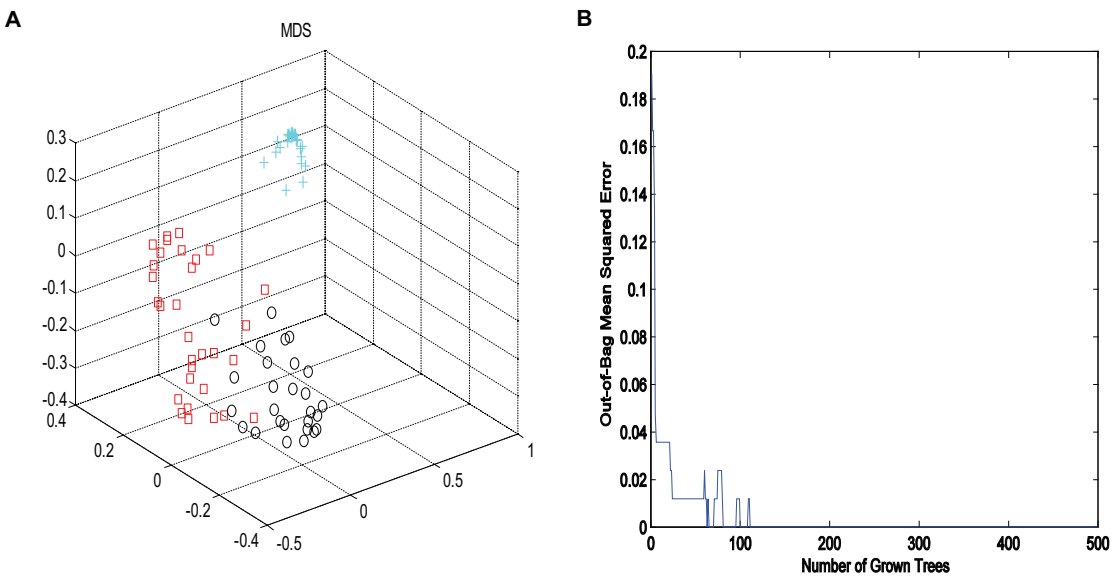


FIGURE 3 | The MDS plot **(A)** for plasma profiles derived from NMR data for control (cross, blue), CHD–BSS (circles, black) and CHD–PS (squares, red). Plot of OOB error for RF classification of the three groups **(B)**.

Choline can be converted to betaine in a two-step enzymatic reaction occurring mainly in the mitochondria of liver cells. Choline or betaine may be important for lowering plasma homocysteine concentrations (Steenge et al., 2003), which is associated with increased risk of cardiovascular disease (CVD) (Homocysteine Studies Collaboration, 2002). LC-HRMS method was applied to measure the plasma concentrations of choline in a cohort of 339 patients undergoing coronary angiography for the evaluation of suspected coronary artery disease, the results show plasma levels of choline are significantly lower in patients with a history of acute myocardial infarction as compared to those without such history (Mueller et al., 2015). Brindle et al. (2002) have shown that choline contributed most strongly to the discrimination of the CHD and control group. Choline (Oliver and Martin, 2010) are emerging biomarkers in acute coronary syndrome. Our study

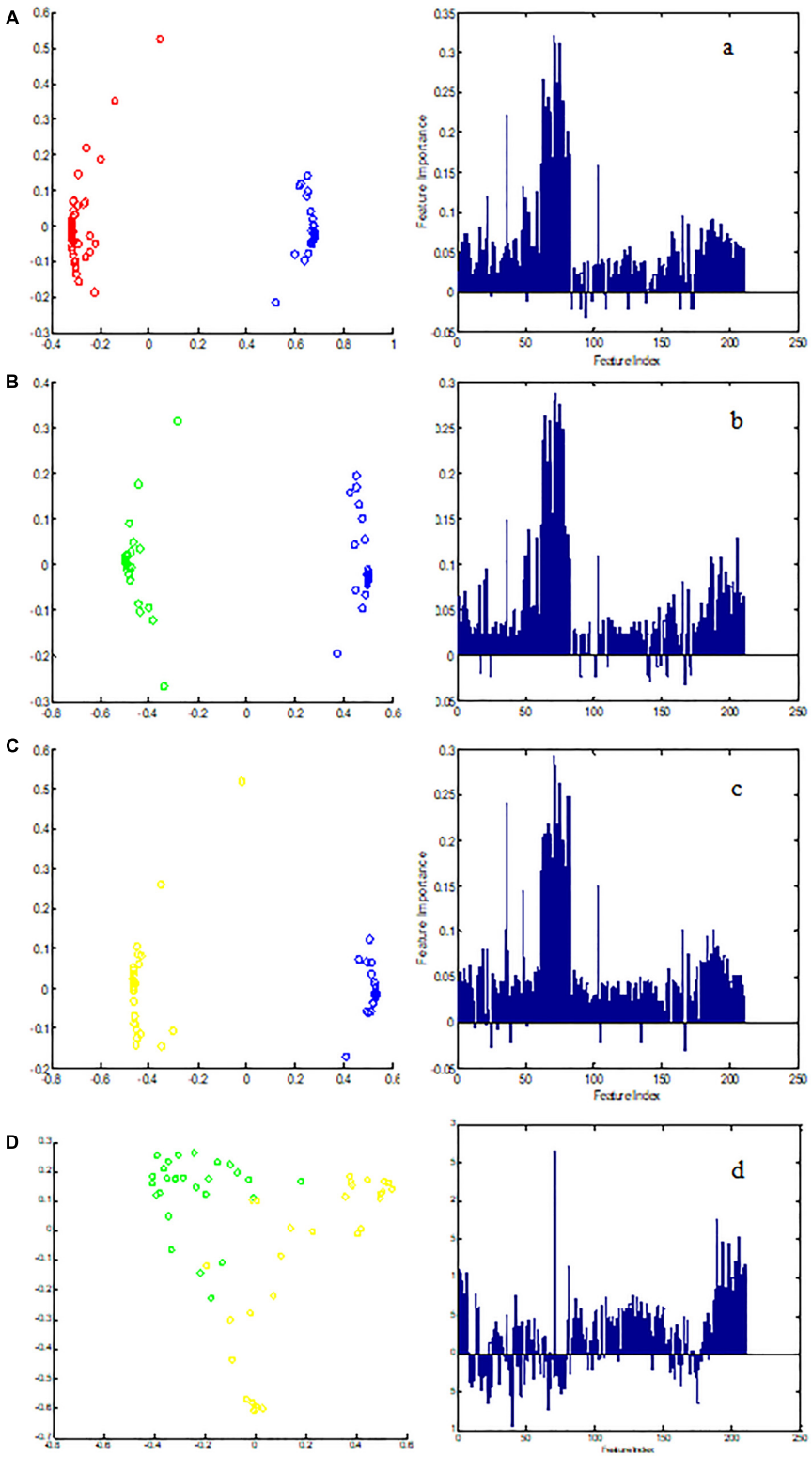


FIGURE 4 | The MDS plot of **(A)** control (blue) and CHD (red), **(B)** control and CHD–BSS (green), **(C)** control and CHD–NBSS (yellow), and **(D)** CHD–BSS and CHD–NBSS. The VIM plot of **(a)** control and CHD, **(b)** control and CHD–BSS, **(c)** control and CHD–NBSS, and **(d)** CHD–BSS and CHD–NBSS obtained by random forest were shown in the right.

TABLE 2 | The summaries of the metabolites that contributed to the clustering of CHD patients and angiography normal (controls) ($P < 0.01$).

Important variables	Chemical shift (ppm)	Potential biomarker	Peak area in controls	Peak area in CHD patients	*P*
22	1.403	Lysine	12.31 ± 9.82	39.60 ± 35.78	0.000
36	1.963	Lipid ($CH_2C=C$)	59.58 ± 8.84	546.19 ± 440.76	0.000
48	2.443	Glutamine	69.39 ± 10.88	164.45 ± 99.36	0.000
50	2.523	Citrate	55.25 ± 10.79	35.83 ± 11.83	0.000
62	3.203	Choline	337.94 ± 55.40	208.86 ± 72.96	0.000
63	3.283	Taurine	61.80 ± 18.77	140.70 ± 38.35	0.000
64	3.323	α-glucose	8.26 ± 7.97	45.48 ± 19.54	0.000
66	3.403	α-glucose	85.09 ± 19.24	236.05 ± 126.66	0.000
67	3.443	β-glucose	111.78 ± 19.55	387.09 ± 201.84	0.000
68	3.483	β-glucose	134.09 ± 28.85	513.31 ± 292.54	0.000
69	3.523	α-glucose	132.77 ± 26.66	368.55 ± 210.79	0.000
70	3.563	α-glucose	180.07 ± 30.66	572.60 ± 332.92	0.000
71	3.643	Choline	3044.12 ± 833.95	537.74 ± 335.80	0.000
72	3.683	α-glucose	58.88 ± 41.69	709.10 ± 486.93	0.000
73	3.723	β-glucose	48.88 ± 25.24	290.72 ± 137.02	0.000
74	3.763	α-glucose	79.92 ± 17.81	260.75 ± 112.37	0.000
75	3.803	α-glucose	73.26 ± 14.69	652.03 ± 417.20	0.000
76	3.843	α-glucose	89.50 ± 20.28	241.12 ± 117.13	0.000
77	3.883	α-glucose	77.35 ± 14.27	197.34 ± 247.43	0.016
78	3.923	Tyrosine	107.86 ± 18.32	274.94 ± 117.29	0.000
79	3.963	phenylalanine	44.95 ± 14.34	143.55 ± 82.69	0.000
80	4.003	histidine	54.72 ± 14.74	106.16 ± 44.69	0.000
81	4.043	Choline	34.25 ± 15.40	253.45 ± 174.81	0.000
82	4.083	Lactate	58.42 ± 17.47	395.31 ± 295.24	0.000
103	5.243	α-glucose	−33.66 ± 29.03	58.58 ± 90.43	0.000

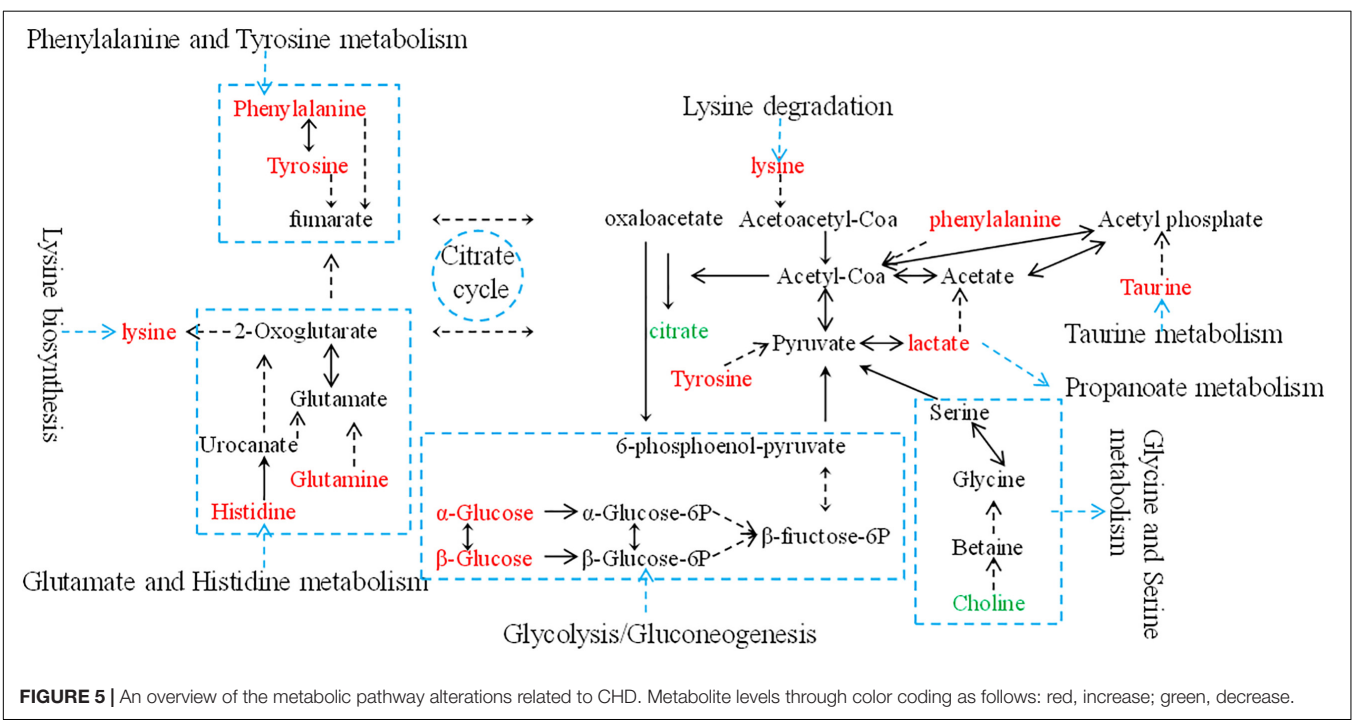


FIGURE 5 | An overview of the metabolic pathway alterations related to CHD. Metabolite levels through color coding as follows: red, increase; green, decrease.

TABLE 3 | The important variables ($P < 0.01$) of the each two groups.

Group	Important variables/metabolites
Control-CHD	36/lipid, 63/taurine, 64/α-glucose, 67/β-glucose, 68/β-glucose, 71/choline, 72/choline, 73/β-glucose, 74/α-glucose, 75/α-glucose, 77/α-glucose, 78/tyrosine, 81/choline
Control-BSS	63/taurine, 64/α-glucose, 67/β-glucose, 68/β-glucose, 71/choline, 72/choline, 73/β-glucose, 74/α-glucose, 75/α-glucose, 77/α-glucose, 78/tyrosine
Control-PS	36/lipid, 64/α-glucose, 67/β-glucose, 68/β-glucose, 71/choline, 72/choline, 73/β-glucose, 75/α-glucose, 81/choline, 82/lactate
BSS–PS	71/choline

demonstrated that plasma choline levels in patients with CHD remarkably decreased, suggesting the relationship between choline and CHD risk.

Abnormal metabolism of the lactate and citrate were the indications of energy metabolism abnormality. Lactate, which is an end product of glucose anaerobic glycolysis, is reportedly a useful indicator for ischemia according to the clinical and scientific studies. It has been found that lactate was remarkably increased in plasma of patients with CHD in this study which suggested that glycolysis was activated by myocardial ischemia and hypoxia. Previous studies (Barderas et al., 2011; Rowland et al., 2013) have shown an obvious lactate increased in CHD patients. The citric acid cycle plays a central role in oxidative phosphorylation in the myocardium. In the setting of acute ischemia, preservation of citric acid cycle intermediates becomes of paramount importance to defend ATP production. Sabatine et al. (2005) have demonstrated highly statistically significant changes in circulating levels of metabolites belonging to the citric acid pathway, including citrate. In our study, the citrate level was also found lower in the CHD group than in the control group.

In the metabolic processes of the amino acids, plasma lysine, glutamine, taurine, tyrosine, phenylalanine and histidine of the CHD patients had increased significantly in this study, especially taurine and tyrosine. It has been found in several metabolic studies that amino acid metabolism is frequently abnormal in patients with CHD. The surplus amino acids provided adequate raw materials for the synthesis of lipid, thus abnormal lipid metabolism of CHD patients had been aggravated at the same time.

Our study found that the level of α-glucose, β-glucose in the plasma of CHD patients was higher than that in the control group. Glucose, as a short-term marker for glycemic control (Dungan, 2008), could indicate that significant disorders of glucose metabolism were happened in CHD patients, and CHD individuals at higher risk for developing diabetes or insulin resistance.

Furthermore, this study showed a clear metabonomic difference between CHD–BSS group and CHD–PS group (**Figure 4**), indicating CHD–BSS and CHD–PS were different metabolism patterns. Choline, β-glucose, α-glucose and tyrosine were considered as potential biomarkers of CHD–BSS in this study. Choline can prevent CVD by preventing the deposition of TC in the inner wall of blood vessels and improving the absorption and utilization of fat. A proteome study (Zhao et al., 2008) found that there was lipid metabolism disorder in patients with CHD–BSS. Apolipoproteins in plasma of patients with CHD–BSS decreased. Apolipoproteins A IV is involved in the reverse transport of cholesterol. In our previous studies, amino acids, fatty acids, purine and so on were selected as a panel of candidate biomarkers of CHD–BSS based on GC-MS (Wei et al., 2013) and LC-MS (Zhao et al., 2014) technology, integration of several technologies could provide more comprehensive classification and biomarker information. It suggested that the potential biomarkers revealed by the three techniques were supplementary. In addition, PCA and PLS-DA method could not extract useful information in the NMR CMPG data for pattern-recognition analyses of biological samples. The RF method could be used to explore more the underlying characteristics of biological samples in this study. Therefore, it is important to develop more efficient pattern recognition approach for the analysis of complex metabolomics data. CHD–BSS is not exist alone in the clinics, so one limitation is that CHD–BSS group included in the study is also mixed with other syndromes, such as qi deficiency, yin deficiency, etc., we will enroll patients of BSS with different diseases and adopt targeted LC-MS/MS analysis to verify the potential markers of BSS in future studies.

CONCLUSION

Our study demonstrated a clear metabonomic difference between CHD–BSS group and CHD–PS group, indicating CHD–BSS and CHD–PS were different metabolism patterns. Choline, β-glucose, α-glucose and tyrosine were considered as potential biomarkers of CHD–BSS. It is also worth noting that RF and MDS could be used to explore more the underlying characteristics of biological samples in this study, and RF could effectively mine the pattern information hidden in the complex metabolomics data.

DATA AVAILABILITY

All datasets generated for this study are included in the manuscript and the **Supplementary Files**.

ETHICS STATEMENT

This study was carried out in accordance with the recommendations of "The IRB of Xiangya Hospital, Central South University" with written informed consent from all subjects. All subjects gave written informed consent in accordance with the Declaration of Helsinki. The protocol was approved by the "The IRB of Xiangya Hospital, Central South University."

AUTHOR CONTRIBUTIONS

D-SW conceived and designed the research. L-LZ and W-BW performed the following research projects. X-JQ, R-ML, and D-SW contributed toward the identification of disease and

ZHENG types. L-LZ conducted data pre-processing of the NMR spectra, data analysis, and drafted the manuscript. W-BW and D-SW contributed toward the results validation. All authors revised the manuscript.

FUNDING

This research was supported by the National Natural Science Foundation of China, China (No. 81173198, 81373553, and 81703963).

ACKNOWLEDGMENTS

We thank Jian-Hua Huang (Hunan Academy of Chinese Medicine) for useful discussions and suggestions.

SUPPLEMENTARY MATERIAL

The Supplementary Material for this article can be found online at: https://www.frontiersin.org/articles/10.3389/fphys.2019.01109/full#supplementary-material

REFERENCES

Ansar, S., Koska, J., and Reaven, P. D. (2011). Postprandial hyperlipidemia, endothelial dysfunction and cardiovascular risk: focus on incretins. *Cardiovasc. Diabetol.* 10:61. doi: 10.1186/1475-2840-10-61

Barderas, M. G., Laborde, C. M., Posada, M., Cuesta, F., Zubiri, I., Vivanco, F., et al. (2011). Metabolomic profiling for identification of novel potential biomarkers in cardiovascular diseases. *J. Biomed Biotechnol.* 2011:790132. doi: 10.1155/2011/790132

Breiman, L. (2001). Random forests. *Mach. Learn.* 45, 5–21.

Brindle, J. T., Antti, H., Holmes, E., Tranter, G., Nicholson, J. K., Bethell, H. W., et al. (2002). Rapid and noninvasive diagnosis of the presence and severity of coronary heart disease using 1H-NMR-based metabonomics. *Nat. Med.* 8, 1439–1444.

Dungan, K. M. (2008). 1,5-anhydroglucitol (GlycoMark) as a marker of shortterm glycemic control and glycemic excursions. *Expert Rev. Mol. Diagn.* 8, 9–19. doi: 10.1586/14737159.8.1.9

He, Q., Kong, X., Wu, G., Ren, P., Tang, H., Hao, F., et al.(2009). Metabolomic analysis of the response of growing pigs to dietary L-arginine supplementation. *Amino Acids* 37, 199–208. doi: 10.1007/s00726-008-0192-9

Homocysteine Studies Collaboration (2002). Homocysteine and risk of ischemic heart disease and stroke: a meta-analysis. *JAMA* 288:2015. doi: 10.1001/jama.288.16.2015

Huang, J. H., Xie, H. L., Yan, J., Cao, D. S., Lu, H. M., Xu, Q. S., et al. (2013). Interpretation of type 2 diabetes mellitus relevant GC-MS metabolomics fingerprints by using random forests. *Anal. Methods* 5, 4883–4889. doi: 10.1039/c3ay40379c

Lacoste, L., Lam, J. Y., Hung, J., Letchacovski, G., Solymoss, C. B., and Waters, D. (1995). Hyperlipidemia and coronary disease correction of the increased thrombogenic potential with cholesterol reduction. *Circulation* 92, 3172–3177. doi: 10.1161/01.cir.92.11.3172

Lindon, J. C., Holmes, E., Bollard, M. E., and Stanley, E. G. (2004). Metabonomics technologies and their applications in physiological monitoring, drug safety assessment and disease diagnosis. *Biomarkers* 9, 1–31. doi: 10.1080/13547500410001668379

Meiboom, S., and Gill, D. (1958). Modified spin-echo method for measuring nuclear relaxation times. *Rev. Sci. Instrum.* 29, 688–691. doi: 10.1063/1.1716296

Mueller, D. M., Allenspach, M., Othman, A., Saely, C. H., Muendlein, A., Vonbank, A., et al. (2015). Plasma levels of trimethylamine- N-oxide are confounded by impaired kidney function and poor metabolic control. *Atherosclerosis* 243, 638–644. doi: 10.1016/j.atherosclerosis.2015.10.091

Nicholson, J. K., Foxall, P. J., Spraul, M., Farrant, R. D., and Lindon, J. C. (1995). 750 MHz 1H and 1H-13C NMR spectroscopy of human blood plasma. *Anal. Chem.* 67, 793–811. doi: 10.1021/ac00101a004

Nicholson, J. K., and Lindon, J. C. (2008). Systems biology: metabonomics. *Nature* 455, 1054–1056.

Nomenclature and criteria for diagnosis of ischemic heart disease (1979). Report of the Joint international society and federation of cardiology/World Health Organization task force on standardization of clinical nomenclature. *Circulation* 59, 606–609

Oliver, O., and Martin, M. (2010). Choline in acute coronary syndrome: an emerging biomarker with implications for the integrated assessment of plaque vulnerability. *Expert Rev. Mol. Diagn.* 10, 159–171. doi: 10.1586/erm.10.2

Rowland, A., Miners, J. O., and Mackenzie, P. I. (2013). The UDP-glucuronosyltransferases: their role in drug metabolism and detoxification. *Int. J. Biochem. Cell Biol.* 45, 1121–1132. doi: 10.1016/j.biocel.2013.02.019

Rubin, G. D. (2013). Emerging and evolving roles for CT in screening for coronary heart disease. *J. Am. Coll. Radiol.* 10, 943–948. doi: 10.1016/j.jacr.2013.09.018

Sabatine, M. S., Liu, E., Morrow, D. A., Heller, E., McCarroll, R., Wiegand, R., et al. (2005). Metabolomic identification of novel biomarkers of myocardial ischemia. *Circulation* 112, 3868–3875. doi: 10.1161/circulationaha.105.569137

Steenge, G. R., Verhoef, P., and Katan, M. B. (2003). Betaine supplementation lowers plasma homocysteine in healthy men and women. *J. Nutr.* 133, 1291–1295. doi: 10.1093/jn/133.5.1291

Subcommittee of Cardiovascular Diseases of China Society of Integrated Traditional Chinese, and Western Medicine (1991). Criteria for TCM syndrome differentiation of patients with coronary heart disease. *Chin. J. Integr. Trad. West Med.* 11, 257–258. doi: 10.1155/2018/7356546

Sun, S. J., Dai, J. Y., Wang, W. Y., Cao, H. J., Fang, J. W., Hu, Y. Y., et al. (2012). Metabonomic evaluation of ZHENG differentiation and treatment by fuzhenghuayu tablet in hepatitis-b-caused cirrhosis. *Evid. Based Complement. Alternat. Med.* 2012:453503. doi: 10.1155/2012/453503

Ueland, P. M. (2011). Choline and betaine in health and disease. *J. Inherit. Metab. Dis.* 2011, 3–15. doi: 10.1007/s10545-010-9088-4

Wang, M., Lamers, R. J., Korthout, H. A., van Nesselrooij, J. H., Witkamp, R. F., van der Heijden, R., et al. (2005). Metabolomics in the context of systems biology: bridging traditional Chinese medicine and molecular pharmacology. *Phytother Res.* 19, 173–182. doi: 10.1002/ptr.1624

Wei, X., Wan, L., Liu, S. M., Xia, J. D., Yi, L. Z., and Wang, D. S. (2013). Study on Plasma Metabolism of coronary heart disease with blood stasis syndrome. *J. Tradit. Chin. Med.* 54, 587–591.

Xu, H., and Chen, K. J. (2008). Integrative medicine: the experience from China. *J. Altern. Complement. Med.* 14, 3–7. doi: 10.1089/acm.2006.6329

Zhao, H. H., Wang, W., and Guo, S. Z. (2008). Proteomics Study on Unstable Angina Pectoris Patients with Blood Stasis Syndrome. *Chin. J. Arterioscler.* 16, 545–548.

Zhao, L. L., Wan, L., Qiu, X., Li, R. M., and Wang, D. S. (2014). A metabonomics profiling study on phlegm syndrome and blood-stasis syndrome in coronary heart disease patients using liquid chromatography/quadrupole time-of-flight mass spectrometry. *Evid. Based Complement. Alternat. Med.* 2014:385102. doi: 10.1155/2014/385102

Conflict of Interest Statement: The authors declare that the research was conducted in the absence of any commercial or financial relationships that could be construed as a potential conflict of interest.

Copyright © 2019 Zhao, Qiu, Wang, Li and Wang. This is an open-access article distributed under the terms of the Creative Commons Attribution License (CC BY). The use, distribution or reproduction in other forums is permitted, provided the original author(s) and the copyright owner(s) are credited and that the original publication in this journal is cited, in accordance with accepted academic practice. No use, distribution or reproduction is permitted which does not comply with these terms.

frontiers in Physiology

ORIGINAL RESEARCH
published: 13 September 2019
doi: 10.3389/fphys.2019.01174

Herbal Compatibility of Ginseng and Rhubarb Exerts Synergistic Neuroprotection in Cerebral Ischemia/Reperfusion Injury of Rats

*Wen-Ting Yang†, Yong Wang†, Yi-Hua Shi†, Huan Fu, Zhen Xu, Qing-Qing Xu and Guo-Qing Zheng**

Department of Neurology, The Second Affiliated Hospital and Yuying Children's Hospital of Wenzhou Medical University, Wenzhou, China

OPEN ACCESS

Edited by:
Jing-Yan Han,
Peking University, China

Reviewed by:
Yumin Luo,
Xuanwu Hospital, Capital Medical University, China
Teresa Pasqua,
University of Calabria, Italy

****Correspondence:***
Guo-Qing Zheng
gq_zheng@sohu.com

† These authors have contributed equally to this work

Specialty section:
This article was submitted to Vascular Physiology, a section of the journal Frontiers in Physiology

Received: *07 June 2019*
Accepted: *30 August 2019*
Published: *13 September 2019*

Citation:
Yang W-T, Wang Y, Shi Y-H, Fu H, Xu Z, Xu Q-Q and Zheng G-Q (2019) Herbal Compatibility of Ginseng and Rhubarb Exerts Synergistic Neuroprotection in Cerebral Ischemia/Reperfusion Injury of Rats. Front. Physiol. 10:1174. doi: 10.3389/fphys.2019.01174

Objective: Ischemic stroke is a complex multifactorial disease caused by interactions among polygenetic, environmental, and lifestyle factors with limited effective treatments. Multi-herbal formulae have long been used for stroke through herbal compatibility in traditional Chinese medicine (TCM); however, there is still a lack of evidence due to their unimaginable complexity. Herbal pairs represent the simplest and basic features of multi-herbal formulae, which are of great significance in clarifying herbal compatibility. Here, we aim to investigate the neuroprotective effects of the herbal compatibility of Ginseng and Rhubarb on a cerebral ischemia/reperfusion (I/R) injury model of rats.

Methods: Male adult SD rats were randomly divided into a sham group, a normal saline (NS) group, a Ginseng group, a Rhubarb group, and a Ginseng + Rhubarb (GR) group, a Carbenoxolone [CBX, gap junction (GJ) specific inhibitor] group, and a GR + CBX group. Each group was further assigned into four subgroups according to ischemic time (6 h, 1 day, 3 days, and 7 days). The cerebral I/R injury model was established according to the modified Zea Longa method. The Neurological Deficiency Score (NDS) was assessed by the Zea-Longa scale; the cerebral infarction area was detected by TTC (2,3,5-triphenyltetrazolium chloride) staining; and the expression of connexin-43 (Cx43) and aquaporin-4 (AQP4) were detected based on an immunofluorescence technique and quantitative real-time-PCR.

Results: Compared to the I/R group, both the independent and combined use of Ginseng and Rhubarb can significantly improve NDS ($P < 0.05$), decrease the percentage of the cerebral infarction area around the infarction penumbra ($P < 0.05$) and down-regulate the expression of Cx43 and AQP4 after I/R injury ($P < 0.05$). The GR had more significant effects than that of Ginseng and Rhubarb ($P < 0.05$). Compared with the GR group, the GR + CBX group significantly improved in NDS ($P < 0.05$), and decreased the percentage of the cerebral infarction area ($P < 0.05$) and expression of Cx43 and AQP4 protein ($P < 0.05$).

Conclusion: The herbal compatibility of Ginseng and Rhubarb synergistically exerts neuroprotective function during acute cerebral I/R injury, mainly through reducing the expression of Cx43 and AQP4.

Keywords: Ginseng, Rhubarb, cerebral ischemia/reperfusion, connexin-43, aquaporin-4, neuroprotection

INTRODUCTION

Stroke is an acute cerebrovascular disease caused by local cerebral blood circulation disorder, which is the second cause of global human deaths (GBD 2016 Causes of Death Collaborators, 2017). According to the report published by the World Health Organization in 2017, about 6.24 million people die of stroke every year (World Health Organization, 2017). Stroke has a more serious impact in China (Gao et al., 2018). There are 1596.0 per 100,000 people suffering from stroke in China, and the incidence and mortality of stroke are 246.8/100,000 and 114.8/100,000, respectively, which causes a heavy medical and social burden (Wang et al., 2017). The incidence of stroke in China is increasing at an annual rate of 8.7% and the age of onset is becoming younger and younger (Wang et al., 2019). Stroke includes ischemic and hemorrhagic stroke, and the former is the most common subtype, accounting for 87% of all cerebrovascular accidents (Benjamin et al., 2017). Currently, intravenous alteplase and/or mechanical thrombectomy, recommended by the 2018 American Heart Association/American Stroke Association (AHA/ASA) guidelines, are effective treatments for patients with acute ischemic stroke (Powers et al., 2018). However, thrombolysis has a narrow time window and associates with lethal complications such as an intracerebral hemorrhage (Shobha et al., 2011; Wołoszyńska and Stępień, 2017). Mechanical thrombectomy requires rapid cerebral angiography in experienced stroke centers and qualified neurointerventional doctors. These factors largely limit their clinical use. Thus, it is necessary to find alternative therapeutics for patients with acute ischemic stroke.

Traditional Chinese medicine (TCM) has been applied in the treatment of stroke for thousands of years (Wang et al., 2011). Herbal formulas are the most common approach of TCM intervention, which is usually formed with more than two herbs to produce synergistic effects and/or reduce potentially adverse reactions (Cheng et al., 2017). Herbal pairs are the most fundamental and simplest unit of complex herbal formulae without altering their basic therapeutic characteristics (Deng et al., 2008), which represent the cornerstone of herbal compatibility (Wang et al., 2012; Jin et al., 2016). Ginseng and Rhubarb are two frequently prescribed herbs in TCM intervention for acute stroke, guided by TCM principles. Ginseng is the root and rhizome of *Panax ginseng* C. A. Meyer, which has been used as a representative tonic remedy in China and elsewhere for over 2000 years (Nah et al., 2007), and remains one of the most commonly used healing herbs for stroke (Zheng et al., 2011). The main pharmacologically active ingredients of Ginseng are Ginsenosides, responsible for most of the activities of Ginseng (Lü et al., 2009). Rhubarb is listed as the dry root and rhizome of *Rheum officinale* Baill., *Rheum palmatum* L., and *Rheum tanguticum* Maxim in the current Chinese Pharmacopeia. Extensive phytochemical research on Rhubarb has isolated and identified about 200 chemical compounds (Wang et al., 2013), such as anthraquinones, dianthrones, stilbenes, anthocyanins, flavonoids, tannins, organic acids, and chromones (Huang et al., 2007). Ginseng functions to strengthen vital Qi for brain protection aimed at its root causes, while the latter has Tongfu functions (Lu et al., 2014) for pathogenic factors aimed at manifestation. This herbal pairing thus serves to treat both the manifestation and root cause of acute stroke, according to TCM principles of treatment. Based on modern pharmacological studies, Ginseng and its active ingredients are potential neuroprotective agents in the treatment of stroke (Rastogi et al., 2015), which have multi-leveled, multi-channeled, and multi-targeted protective effects (Kim et al., 2013; Ong et al., 2015; Rokot et al., 2016). In modern pharmacological research, Ginseng and total ginsenosides could improve neurological function, reduce the volume of cerebral infarction, promote angiogenesis, and nerve regeneration in cerebral ischemia/reperfusion (I/R) injury rats (Zheng et al., 2011). *In vitro* experiments indicated that ginsenoside had anti-inflammatory, anti-oxidative stress and anti-apoptotic effects, promoting cell survival (Zhang et al., 2016; Dong et al., 2017). Our previous study showed that ginsenoside Rg1 could improve neurological injury and alleviate blood brain barrier disruption in cerebral I/R rats, and the mechanism may be related to the down-regulation of aquaporin 4 (AQP4) expression (Zhou et al., 2014). Rhubarb compound prescription can promote cerebral vascular recanalization, improve brain tissue injury, and alleviate brain cell damage caused by cerebral ischemia (Yan and Fu, 2011). Active compounds of Rhubarb root and rhizome can alleviate focal cerebral ischemia injury and have neuroprotective effects in rats (Liu et al., 2015). Our previous study indicated that Sanhua Decoction, with Rhubarb as its main component, has a significant protective effect on the neurovascular unit (NVU) in cerebral I/R injury rats, and the mechanism is mainly related to the regulation of AQP4 expression (Lu et al., 2015). However, there is lack of studies on the mechanisms of herbal compatibility in Ginseng and Rhubarb.

Brain edema is one of the most common complications of ischemic stroke, which can cause neurological deterioration and even death. Preventing and treating brain edema effectively is a key measure in reducing the mortality and disability rate (Kimberly et al., 2018). AQP4 is the most abundant and important aquaporin expressed in the nervous system (Papadopoulos and Verkman, 2013; Maugeri et al., 2016). Brain edema is closely related to the increased expression of AQP4 at the early stage of ischemic cerebral infarction. The result of studies on cerebral I/R mice with AQP4 gene knockout showed that the deletion of AQP4 gene could alleviate cytotoxic edema (Yao et al., 2015), and improve the long-term

prognosis (Hirt et al., 2017) and the survival rate (Akdemir et al., 2014). Gap junction (GJ) channels span two plasma membranes to allow cells to exchange messages and material (Hervé and Derangeon, 2013). Connexin (Cx) is a family of membrane proteins that constitute the basic structure of GJ between cells. Up to now, more than 20 types of Cx have been found in mammals (Nielsen et al., 2012). Cx43 is the most common connexin in the nervous system. When it comes to ischemic necrosis, the expression of Cx43 in reactive astrocytes increases and the half-channels in the neurons open (Thompson et al., 2006; Le et al., 2014). Apoptotic information is then transmitted causing "bystander death" of adjacent cells. At the same time, adenine nucleoside triphosphate, calcium ion, cyclic adenosine phosphate, and inositol triphosphate can exchange between cells through half-channels causing further neuronal damage (Orellana et al., 2011; Gilleron et al., 2018). Inhibiting the expression of Cx43 and the opening of half-channels can therefore play a neuroprotective role. Cx43 and AQP4 are interrelated in water balance and GJ communication. The high expression of Cx43 would be decreased with the silencing of the AQP4 gene (Kong et al., 2008). In addition, the absence of Cx43 may also lead to partial loss of AQP4 (Ezan et al., 2012; Li et al., 2015). In the present study, we aim to investigate the synergistic effects of the herbal pairing of Ginseng and Rhubarb on Cx43 and AQP4 expression in cerebral I/R injured rats.

MATERIALS AND METHODS

Ethics Statement

All experimental animals were obtained from the Shanghai Laboratory Animal Center (License number: SCXK (Hu), 2010-0002). The animal experiment protocol was approved by the local ethics committee of the Wenzhou Medical University (Approval number: wydw2015-0148) and was performed in strict accordance with its guidelines. Anesthesia was used to sacrifice the animals at the end of the experiment. The utmost efforts were made to reduce the number of experimental animals and to minimize animal suffering.

Animals and Groups

Adult male Sprague-Dawley (SD) rats weighing between 250 and 280 g were housed at 23 ± 2°C in relative humidity of 50 ± 10% with a 12 h light/dark cycle, and with free access to food and water.

Healthy SD rats were randomly divided into seven groups: sham group, normal saline (NS) group, Ginseng group, Rhubarb group, Ginseng + Rhubarb (GR) group, Carbenoxolone (CBX, GJ specific inhibitor) group, and GR + CBX group. The sham group, NS group, Ginseng group, Rhubarb group, and GR group were further assigned into four subgroups according to 6 h, 1 day, 3 days, and 7 days the time points after I/R injury, respectively. There was only one subgroup (1 day after I/R) in CBX group and GR + CBX group. There were 15 rats in the subgroup of each time point.

Drug Administration

Ginseng (Guangdong Yifang Pharmaceutical Co., Ltd., approval number: country medicine accurate character 7032361) and Rhubarb (Guangdong Yifang Pharmaceutical Co., Ltd., approval number: country medicine accurate character 6112271) were granules and were dissolved in distilled water at 100°C. Carbenoxolone (Abcam (Shanghai) Trading Co., Ltd.) was dissolved in NS at a concentration of 10 μg/μl. After conversing human doses to rat equivalent doses based on body surface area (Food and Drug Administration, 2005; Chen, 2011; State Pharmacopoeia Commission, 2015), a Ginseng dose of 0.7 g/kg was administered intragastrically to the rats in the Ginseng group. A Rhubarb dose of 0.2 g/kg was administered intragastrically to the rats in the Rhubarb group. Ginseng and Rhubarb (2:1) doses of 0.7 g/kg:0.2 g/kg were administered intragastrically to rats in the GR and GR + CBX group. The same of NS volume was administered intragastrically to rats in the sham group, NS group, and the CBX group instead. Administration of Ginseng, Rhubarb, GR, or NS was performed once a day starting at 3 days before the operation until the rats were sacrificed. Intracerebroventricular injection of CBX at a dose of 25 μg/kg was performed on rats in the GR + CBX group and CBX group at 0.5 h before the operation (Zhang et al., 2013; Wang et al., 2015).

Ischemia/Reperfusion Model

Rats were anesthetized with 4% chloral hydrate (3 ml/kg) intraperitoneally and then received an operation according to the modified Zea Longa method (Longa et al., 1989). In brief, the left common carotid artery (CCA), internal carotid artery (ICA), and external carotid artery (ECA) of the rats were isolated *via* the midline incision of the neck. A 0.26 mm diameter monofilament nylon suture with a rounded tip (Beijing Cinontech Co., Ltd., Beijing, China) was introduced into ECA lumen and then gently advanced into the ICA in order to block the origin of the middle cerebral artery (MCA). For the rats in the sham group, the nylon suture was inserted into ECA lumen but not advanced into the ICA. After 2 h of occlusion, the nylon suture was withdrawn to establish reperfusion. After arousal from anesthesia, the rats were returned to cages with free food and water.

Neurological Deficiency Score

Rats were examined for a neurological deficiency score (NDS) at 6 h, 1 day, 3 days, and 7 days after I/R using a five-tiered grading system according to Longa et al. (1989) as follows: 0, no deficit; 1, failure to extend contralateral forepaw; 2, spin longitudinally; 3, falling to the contralateral side; 4, unable to walk spontaneously. Rats with a score between 1 and 3 were selected for the study.

Triphenyltetrazolium Chloride Staining and Infarction Area Assessments

Rats were anesthetized with 4% chloral hydrate (3 ml/kg) intraperitoneally at 6 h, 1 day, 3 days, and 7 days after I/R, and the brains were removed after profusion with NS. A brain slicer was used to coronally section the brains

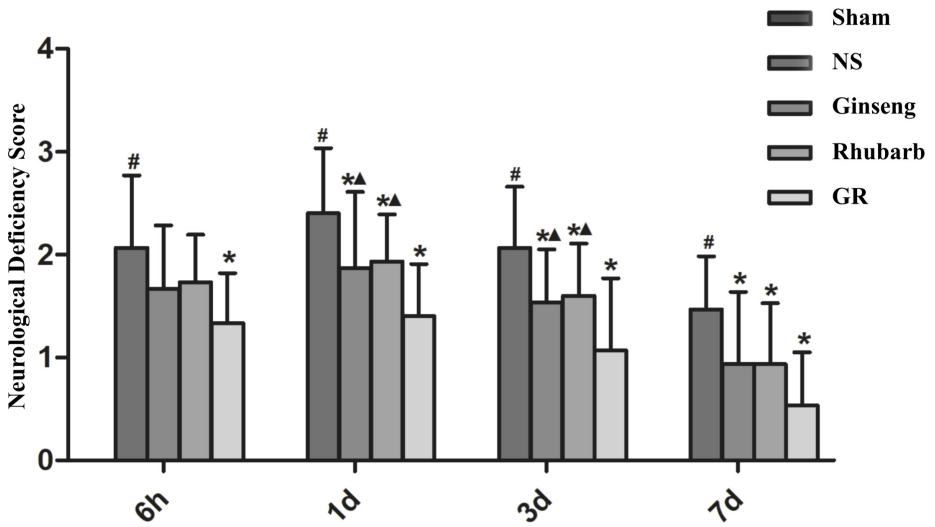


FIGURE 1 | The Neurological deficiency score (NDS) in the sham group, normal saline (NS), Ginseng, Rhubarb, and the Ginseng + Rhubarb (GR) group at 6 h, 1 day, 3 days, and 7 days after I/R in rats ($n = 5$). $^{\#}P < 0.05$, compared to the Sham group; $^{*}P < 0.05$, compared to the NS group; $^{\blacktriangle}P < 0.05$, compared to the GR group.

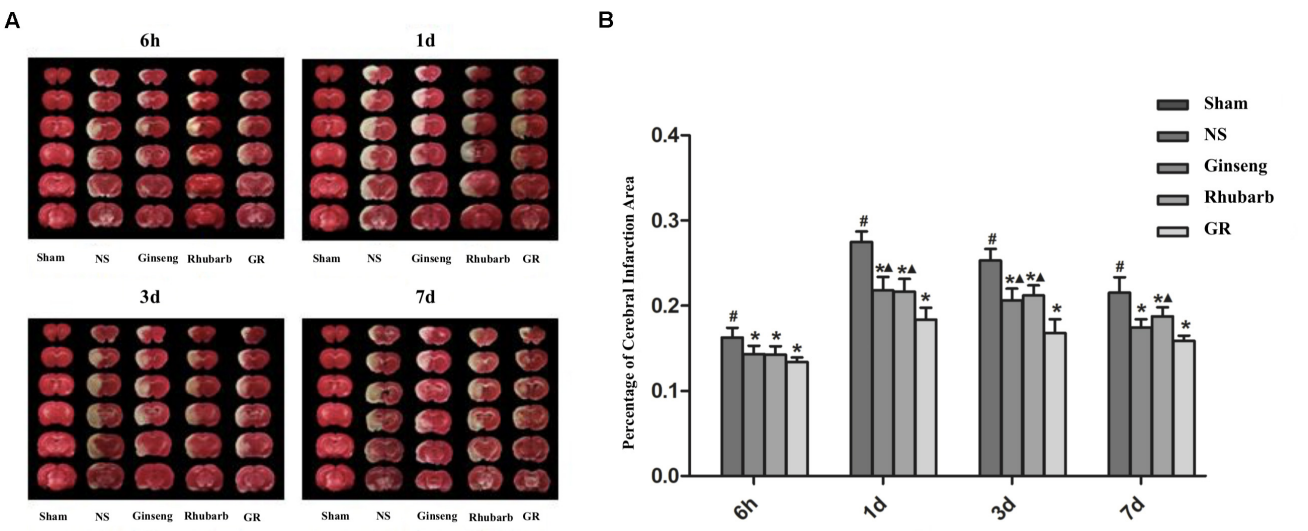


FIGURE 2 | Infarction area assessments in the sham group, normal saline (NS), Ginseng, Rhubarb, and the Ginseng + Rhubarb (GR) group at 6 h, 1 day, 3 days, and 7 days after I/R in rats. **(A)** Triphenyltetrazolium chloride (TTC) staining. **(B)** Quantitative analysis for the percentage of the cerebral infarction area ($n = 5$). $^{\#}P < 0.05$, compared with the Sham group; $^{*}P < 0.05$, compared with the NS group; $^{\blacktriangle}P < 0.05$, compared with the GR group.

at 2 mm intervals from the frontal pole. The slices were incubated with 1% triphenyltetrazolium chloride (TTC) solution for 15 min at 37°C in the dark, and then immersed with 4% paraformaldehyde. The infarct areas and total area on each slice were calculated using Image-Pro Plus 6.0 software, and then expressed as the percentage of infarction in the total area.

Immunofluorescence Staining

The rats were anesthetized at 6 h, 1 day, 3 days, and 7 days after I/R, and their brains were removed after perfusion with 4% paraformaldehyde. After gradient elution with sucrose, the brains were imbedded with OCT (Sakura Finetek, United States) and quickly frozen, and then coronally cut into 6 μm thick sections. The sections were permeabilized with 0.3% Triton X-100 for 15 min, retrieved with retrieval buffers for 10 min, and then blocked with 10% donkey serum for 1 h at 37°C. Next, the sections were incubated with Connexin43 antibody (1:200, Abcam, United States) or Aquaporin 4 Antibody (1:200, Abcam, United States) overnight at 4°C. The sections were then briefly washed with PBST and incubated with donkey anti-mouse secondary antibody (1:400, Abcam, United States) for 1 h at 37°C in the dark. After counterstaining with 4,6-diamidino-2-phenylindole

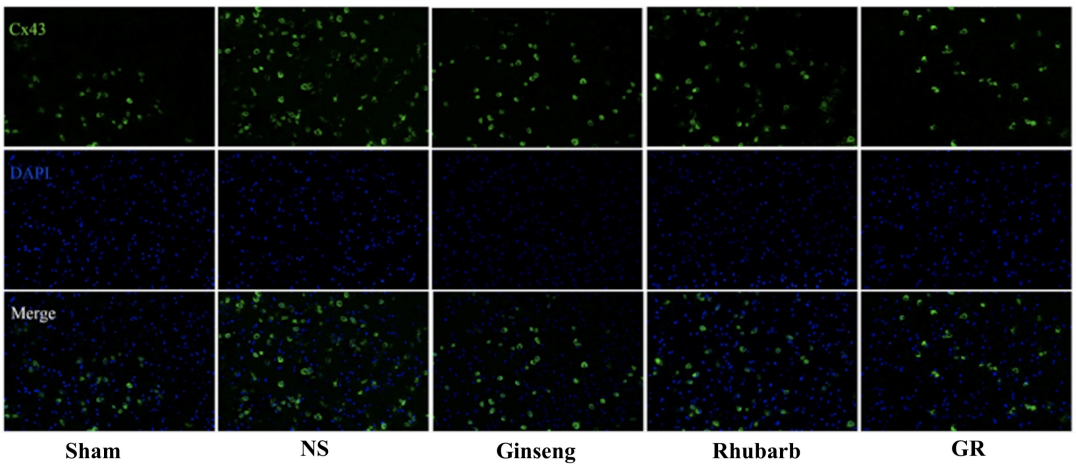


FIGURE 3 | Immunofluorescence staining of the Cx43 protein around the infarction in the Sham, NS, Ginseng, Rhubarb, and the GR group at 1 day after I/R (n = 5).

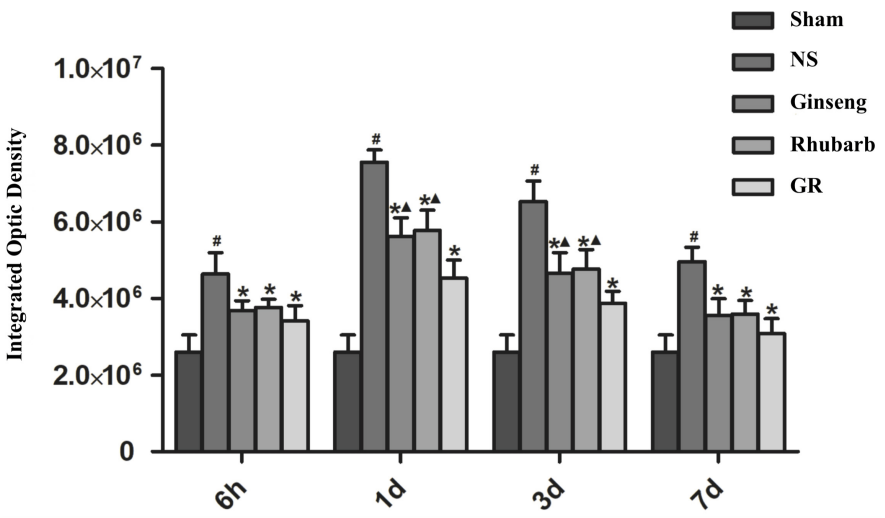


FIGURE 4 | Quantitative analysis for the results of immunofluorescence staining of the Cx43 protein around the infarction in the Sham, NS, Ginseng, Rhubarb, and the GR group at 6 h, 1 day, 3 days, and 7 days after I/R (n = 5). $^{\#}P < 0.05$, compared to the Sham group; $^{*}P < 0.05$, compared to the NS group; $^{\blacktriangle}P < 0.05$, compared to the GR group.

(DAPI; Solarbio, Beijing, China), the sections were observed and photographed with fluorescent microscopy. Semi-quantitative analysis of the sections was conducted with the Image-J software.

Real-Time Quantitative Reverse Transcription Polymerase Chain Reaction (RT-qPCR)

Total RNA was extracted by Trizol reagent (Invitrogen, United States). The RNA was then transcripted reversely into complementary deoxyribonucleic acid (cDNA) using a PrimeScript^{TM} RT reagent Kit (TAKARA, Japan), used as the template for polymerase chain reaction amplification. Quantitative RT-qPCR was conducted on a Light Cycler thermal cycler system (Bio-Rad, United States) using SYBR® Premix Ex Taq^{TM} II (TAKARA, Japan). Gene-specific primers were used as follows: Cx43: The upstream primer: 5′−GGAAAGTACCAAACAGCAGCAG−3′, the downstream primer: 5′−CTGGGCACCTCTCTTTCACTT−3′, the amplified fragment was 152 bp; AQP4: The upstream primer: 5′−CATGGAGGTGGAGGACAACC−3′, the downstream primer: 5′−GCAGGAAATCTGAGGCCAGT−3′, the amplified fragment was 200 bp; GAPDH: The upstream primer: 5′−TGAAGAACAGGGAAGCAGCAA−3′, the downstream primer: 5′−ATCCAGTCCATTTTCCACCACA−3′, the amplified fragment was 200 bp. Amplification system: SYBR® Premix Ex Taq^{TM} II 12.5 μl, Forward Primer (10 μm) 1 μl, Reverse Primer (10 μm) 1 μl, cDNA Template 2 μl, RNase FreedH_2O 8.5 μl, and the final volume was 25 μl; amplification

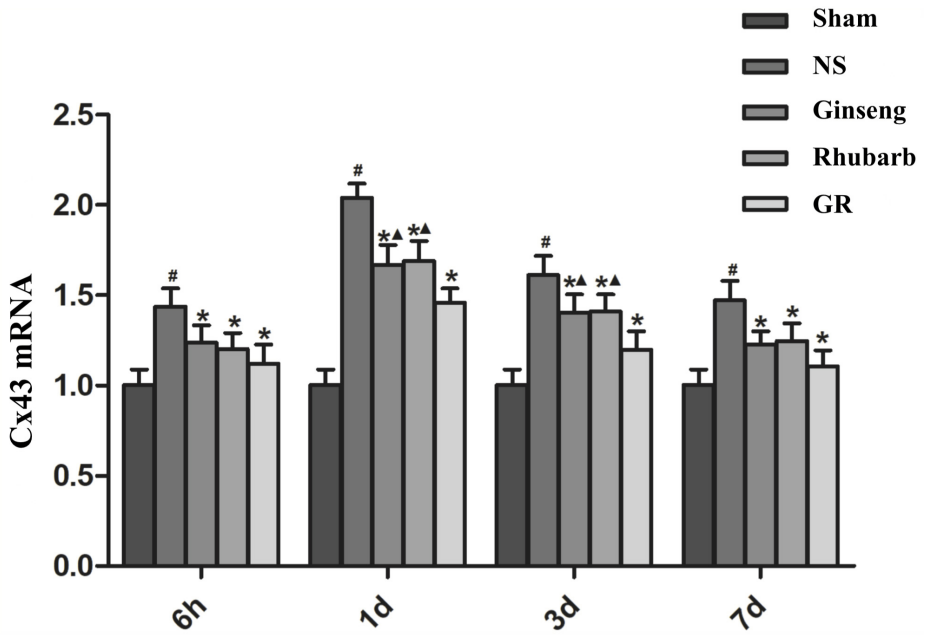


FIGURE 5 | The Cx43 mRNA expression in the Sham, NS, Ginseng, Rhubarb, and the GR group at 6 h, 1 day, 3 days, and 7 days after I/R ($n = 5$). $^{\#}P < 0.05$, compared to the Sham group; $^{*}P < 0.05$, compared to the NS group; $^{\blacktriangle}P < 0.05$, compared to the GR group.

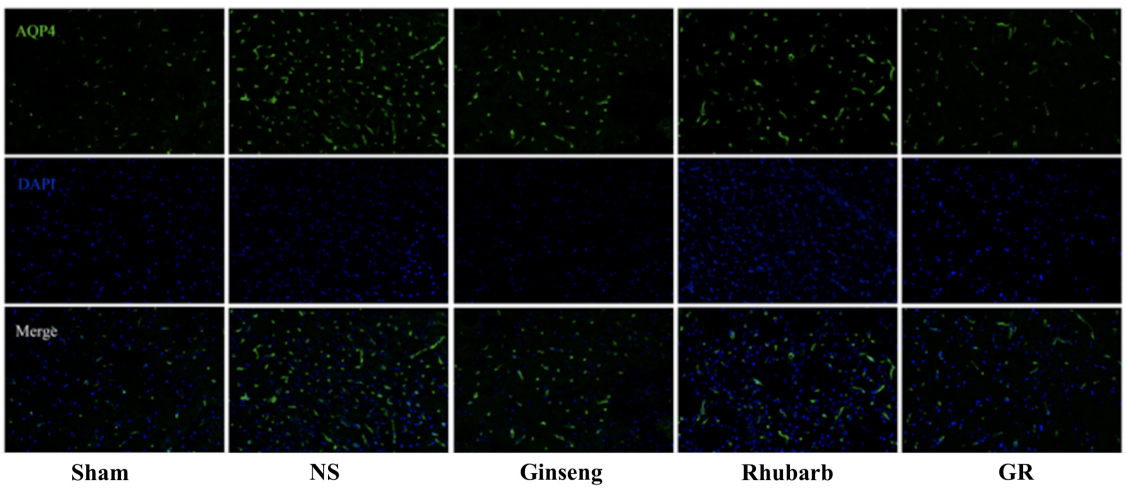


FIGURE 6 | Immunofluorescence staining of the AQP4 protein around the infarction in the Sham, NS, Ginseng, Rhubarb, and the GR group at 1 day after I/R ($n = 5$).

conditions: step 1: 95°C for 30 s, 1 cycle; step 2: 95°C for 5 s and 60°C for 30 s, 40 cycles; step 3: 95°C for 15 s, 60°C for 15 s, and 95°C for 15 s.

Statistical Analysis

SPSS software (version 20.0) was used for data analyses; all data were expressed as mean ± standard deviation (SD). Differences between multiple groups were analyzed by One-way analysis of variance (ANOVA), while differences between two groups were analyzed by a *t*-test. Values of $P < 0.05$, are considered statistically significant.

RESULTS

Neurological Deficits

The sham group showed no neurological deficiency symptom, the NDS of the NS group was significantly increased from 6 h after I/R, and peaked at 1 day, then declined gradually. Compared with the NS group, the Ginseng and Rhubarb groups showed significantly lower NDS at 1 day, 3 days, and 7 days after I/R ($P < 0.05$). The GR group showed a significantly lower NDS at 6 h, 1 day, 3 days, and 7 days after I/R compared with the NS group ($P < 0.05$). Compared with the Ginseng and Rhubarb

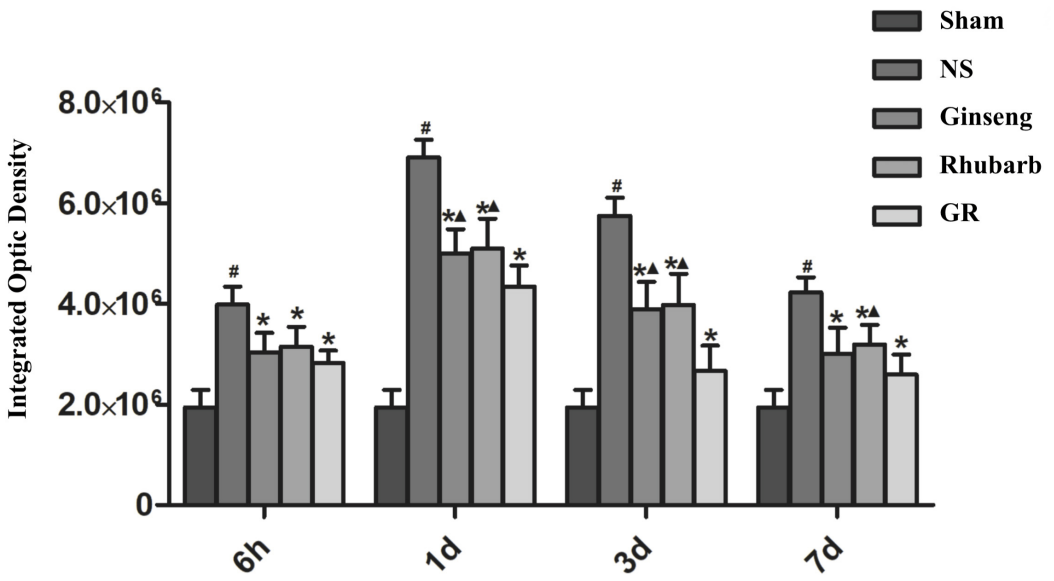


FIGURE 7 | Quantitative analysis for the results of immunofluorescence staining of the AQP4 protein around the infarction in the Sham, NS, Ginseng, Rhubarb, and the GR group at 6 h, 1 day, 3 days, and 7 days after I/R ($n = 5$). $^{\#}P < 0.05$, compared to the Sham group; $^{*}P < 0.05$, compared to the NS group; $^{\blacktriangle}P < 0.05$, compared to the GR group.

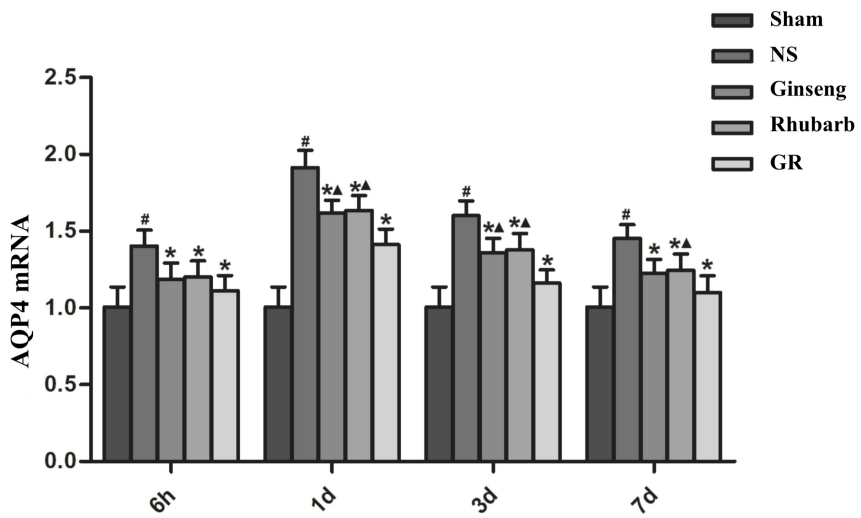


FIGURE 8 | The AQP4 mRNA expression in the Sham, NS, Ginseng, Rhubarb, and the GR group at 6 h, 1 day, 3 days, and 7 days after I/R ($n = 5$). $^{\#}P < 0.05$, compared to the Sham group; $^{*}P < 0.05$, compared to the NS group; $^{\blacktriangle}P < 0.05$, compared to the GR group.

group, The GR group showed a significantly lower NDS at 1 day and 3 days after I/R ($P < 0.05$) (**Figure 1**).

The Percentage of Cerebral Infarction Area

The sham group showed no infarction area, the infarction area of the NS group was significantly increased from 6 h after I/R, and peaked at 1 day, then declined gradually. Compared with the NS group, all intervention groups showed significantly smaller infarction areas at 6 h, 1 day, 3 days, and 7 days after I/R ($P < 0.05$). Compared with the GR group, the Ginseng group showed a statistical difference at 1 days and 3 days after I/R, and the Rhubarb group showed a statistical difference at 1 day, 3 days and 7 days after I/R ($P < 0.05$) (**Figures 2A,B**).

Expression of Cx43 Around Infarction Penumbra

Immunofluorescence and RT-q PCR showed that the expression of the Cx43 protein and mRNA was low in the sham group.

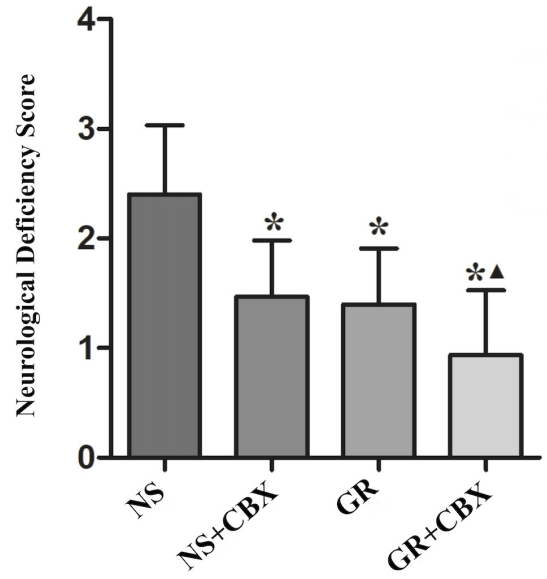


FIGURE 9 | The NDS in the NS, Carbenoxolone (CBX), GR, and GR + CBX group at 1 day after I/R in rats ($n = 5$). *$P < 0.05$, compared to the NS group; ▲$P < 0.05$, compared to the GR group.

The expression of the Cx43 protein and mRNA in the NS group increased at 6 h after I/R and peaked at 1 day, then declined gradually. Compared to the NS group, the intervention groups showed significantly lower expression of the Cx43 protein and mRNA at 6 h, 1 days, 3 days, and 7 days after I/R ($P < 0.05$). Compared with the Ginseng and Rhubarb group, the Cx43 protein and mRNA showed a statistically lower expression in the GR group at 1 day and 3 days after I/R ($P < 0.05$) (**Figures 3–5**).

Expression of AQP4 Around Infarction Penumbra

Immunofluorescence and RT-q PCR showed that the expression of the AQP4 protein and mRNA was low in the sham group. The expression of the AQP4 protein and mRNA in the NS group increased at 6 h after I/R and peaked at 1 day, then declined gradually. Compared with the NS group, the intervention groups showed a significantly lower expression of the AQP4 protein and mRNA at 6 h, 1 day, 3 days, and 7 days after I/R ($P < 0.05$). Compared with the Ginseng group, the AQP4 protein and mRNA showed a statistically lower expression in the GR group at 1 day and 3 days after I/R ($P < 0.05$). Compared with the Rhubarb group, the AQP4 protein and mRNA showed a statistically lower expression in the GR group at 1 day, 3 days, and 7 days after I/R ($P < 0.05$) (**Figures 6–8**).

Inhibitor CBX Reduce the NDS After I/R Injury

Compared to the NS group, the CBX group showed a significantly lower NDS 1 day after I/R ($P < 0.05$). Compared with the GR group, the GR + CBX group showed lower NDS 1 d after I/R ($P < 0.05$) (**Figure 9**).

Inhibitor CBX Reduce the Infarction Area After I/R Injury

Compared to the NS group, the CBX group showed a significantly smaller infarction area 1 day after I/R ($P < 0.05$). Compared to the GR group, the GR + CBX group showed a smaller infarction area 1 day after I/R ($P < 0.05$) (**Figures 10A,B**).

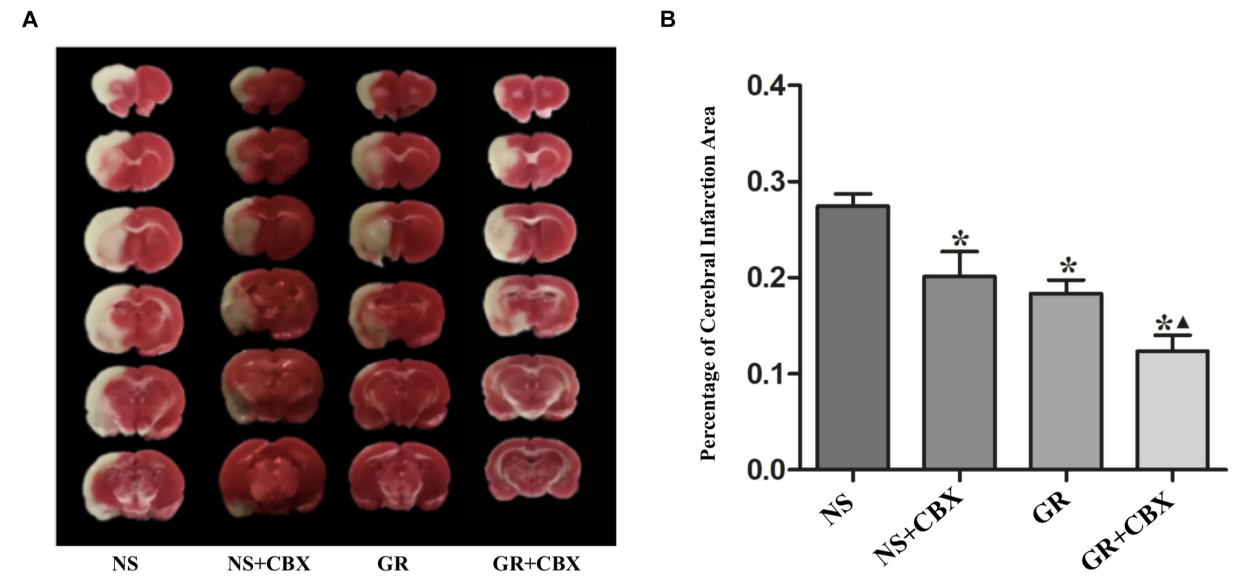


FIGURE 10 | Infarction area assessments in the NS, CBX, GR, and GR + CBX group at 1 day after I/R in rats. **(A)** Triphenyltetrazolium chloride (TTC) staining. **(B)** Quantitative analysis for the percentage of the cerebral infarction area ($n = 5$). *$P < 0.05$, compared to the NS group; ▲$P < 0.05$, compared to the GR group.

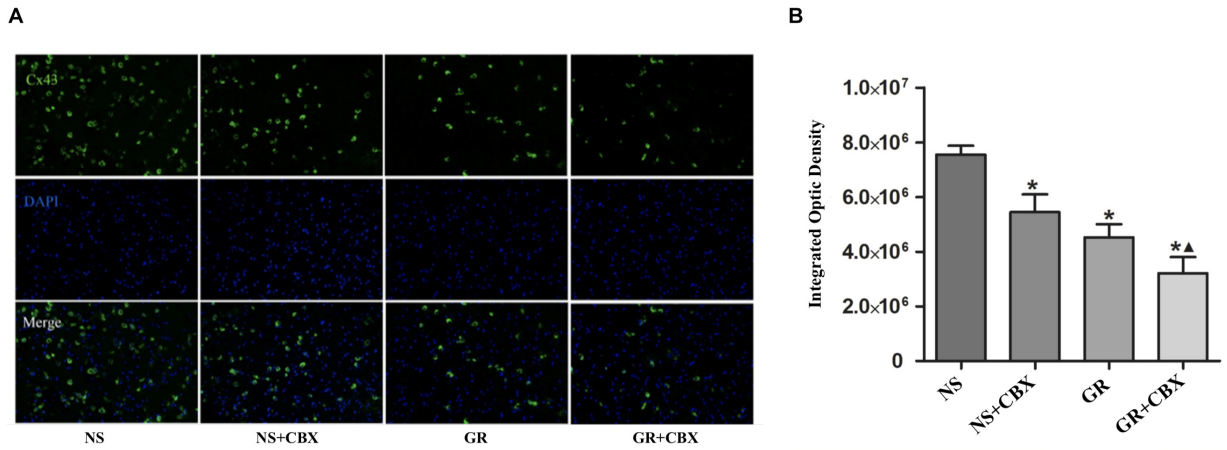


FIGURE 11 | The expression of the Cx43 protein around the infarction in the NS, CBX, GR, and GR + CBX group at 1 day after I/R. **(A)** Immunofluorescence staining of the Cx43 protein. **(B)** Quantitative analysis for the results of immunofluorescence staining of the Cx43 protein ($n = 5$); $^*P < 0.05$, compared to the NS group; $^▲P < 0.05$, compared to the GR group.

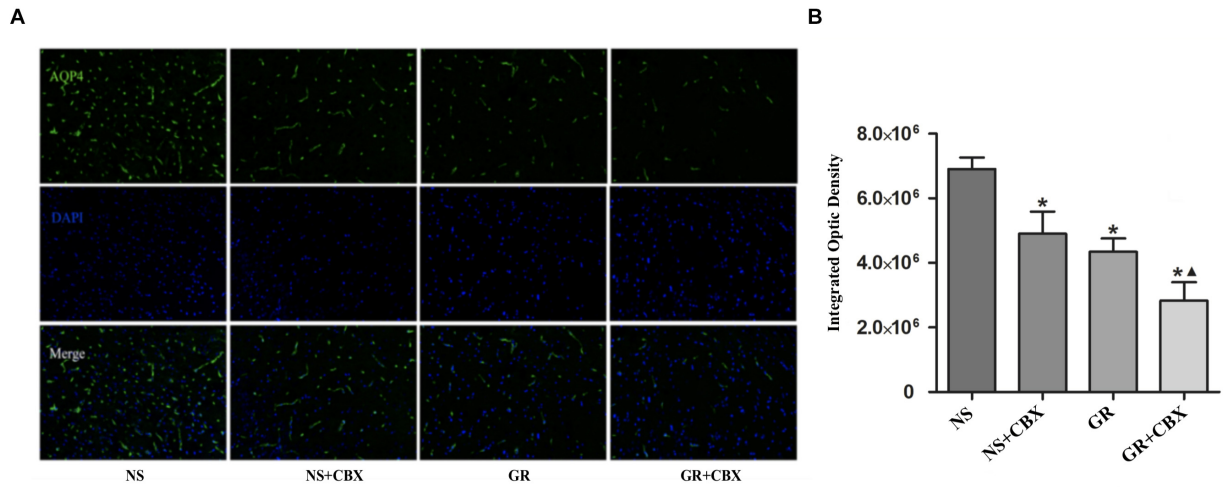


FIGURE 12 | The expression of the AQP4 protein around the infarction in the NS, CBX, GR, and GR + CBX group at 1 day after I/R. **(A)** Immunofluorescence staining of the AQP4 protein. **(B)** Quantitative analysis of the results of immunofluorescence staining of the AQP4 protein ($n = 5$); $^*P < 0.05$, compared to the NS group; $^▲P < 0.05$, compared to the GR group.

Inhibitor CBX Down-Regulates the Expression of Cx43 and AQP4 After I/R Injury

Immunofluorescence showed that compared to the NS group, the CBX group showed a significantly lower expression of the Cx43 and AQP4 protein 1 days after I/R ($P < 0.05$). Compared to the CBX group, the GR + CBX group showed a significantly lower expression of the Cx43 and AQP4 protein 1 day after I/R ($P < 0.05$). Compared to the GR group, the expression of the Cx43 and AQP4 protein was significantly lower in the GR + CBX group ($P < 0.05$) (**Figures 11A,B**, **12A,B**).

RT-q PCR showed that compared to the NS group, the GR and GR + CBX group showed a significantly lower expression of the Cx43 and AQP4 mRNA 1 day after I/R ($P < 0.05$), while the CBX group showed no significant difference ($P > 0.05$); there was no significant difference in the expression of the Cx43 and AQP4 mRNA between the GR group and the GR + CBX group ($P > 0.05$) (**Figures 13**, **14**).

DISCUSSION

Multi-herbal compatibility of formulas is the main function of TCM intervention, which uses two or more Chinese medicinal substances in combination, as per the pharmaceutical principle of TCM, according to patients' pattern, herbal properties, and their interactions. The applications of herbal medicines through adequate compatibility can exert synergistic effects and reduce side effects and drug resistance (Zhou et al., 2017). Herbal

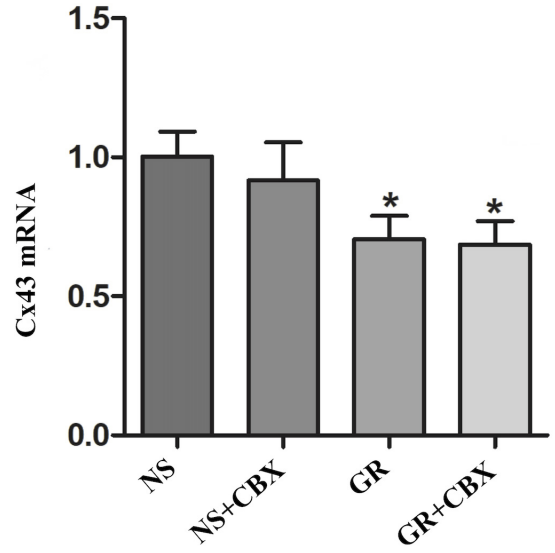


FIGURE 13 | The Cx43 mRNA expression in the NS, CBX, GR, and GR + CBX at 1 day after I/R ($n = 5$). *$P < 0.05$, compared to the NS group; ▲$P < 0.05$, compared to the GR group.

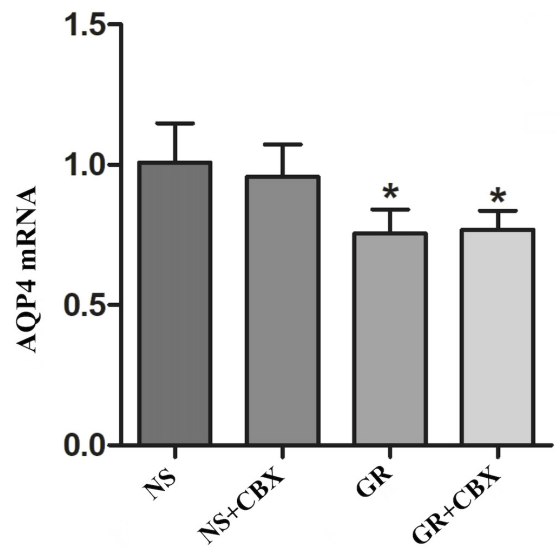


FIGURE 14 | The AQP4 mRNA expression in the NS, CBX, GR, and GR + CBX at 1 day after I/R ($n = 5$). *$P < 0.05$, compared to the NS group; ▲$P < 0.05$, compared to the GR group.

pairings refer to the unique combination of two compatible herbs guided by the TCM principle, which is the most basic and the simplest form of multi-herbal formulas. It thus plays a fundamental and important role in the exploration of herbal compatibility (Wang et al., 2012). The present study showed the herbal compatibility of Ginseng and Rhubarb which has a synergistically neuroprotective effect in cerebral I/R rats, providing preclinical evidence of the herbal pairing in the treatment of ischemic stroke.

During cerebral ischemia and cerebral I/R injury, a series of pathological changes, such as oxidative stress injury, brain cell edema, inflammatory reaction and glutamate overload, will cause neuronal cell death and NVU damage (Jin et al., 2010; Chen et al., 2011), leading to further neurological impairment and increasing the infarction area (Mizuma and Yenari, 2017). After that, self-defense and self-repair will occur in the brain, attributing to angiogenesis, axon regeneration, and neural stem cell proliferation and differentiation. Neurological function will gradually improve, but will not be capable of completely returning to normal due to irreversible damage of the brain tissue. In this study, the five-point neurologic grading scale using Zea-Longa criteria (Longa et al., 1989) and the percentage of the infarction area were assessed in cerebral I/R rats, showing that the percentage of the infarction area and NDS increased at 6 h after I/R and peaked at 1 days, then decreased gradually but remained higher than that of the NS group at 7 days. The change trend of the cerebral infarction area percentage was basically consistent with the change of NDS, indicating that both the percentage of the cerebral infarction area and NDS could accurately reflect the severity and overall change trend of cerebral I/R injury. The present study indicates that the herbal compatibility of Ginseng and Rhubarb exerts synergistic effects on the functional recovery in rats with cerebral I/R injury.

A cerebral edema is a common pathological phenomenon in ischemic stroke, which may cause intracranial hypertension or even a cerebral hernia, leading to the death of patients (Walberer et al., 2008). AQP4 plays an important role in the formation and dissipation of a cerebral edema (Papadopoulos and Verkman, 2007), and has become a potential target for the treatment of cerebral edemas (Tang and Yang, 2016; Verkman et al., 2017). AQP4 is mainly distributed in brain parenchyma and between the fluid compartments (Papadopoulos and Verkman, 2013). During cerebral ischemic injury, AQPs regulate the permeability of the cell membrane mainly through the mitogen activated protein kinase pathway (Yang et al., 2013). When the permeability of blood vessels changes and the ion concentration gradient inside and outside the vessels and cell increases, AQP4's own osmoreceptor can actively participate in water regulation after it is activated. Nito et al. (2012) found that the expression of AQP4 increased in cerebral I/R injured rats. Aoki et al. (2003) found that the expression of AQP4 mRNA was significantly increased around cerebral infarction. It can therefore be speculated that cerebral edema caused by cerebral ischemia may be related to the water transport involved in AQP4, which may be achieved by the upregulation of the AQP4 expression in astrocytes and the rapid transfer of water from the extracellular and mesenchymal to the intracellular. The knockout mouse model further verified that the deletion of the AQP4 gene can alleviate cerebral edema and blood–brain barrier (BBB) damage after cerebral ischemia, as well as reduce endothelial cell edema and cytotoxicity after saccharide and oxygen deprivation in brain tissue sections, indicating that AQP4 is involved in the formation of cytotoxic edema and BBB injury after cerebral ischemia (Katada et al., 2014). The present study indicates that monotherapy and combination therapy of

Ginseng and Rhubarb have neuroprotective effects through the down-regulation of AQP4, while the combined use of Ginseng and Rhubarb could play a better protective role, which may be associated with the reduction of cerebral edema caused by ischemic stroke.

The function of GJ is related to the following aspects: (1) the expression of Cx protein; (2) the conformational change of Cx, opening or closing of the central aperture; (3) the changes of Cx distribution. During cerebral I/R injury, the transcription and expression of Cx43 in reactive astrocytes around the cerebral infarction can be increased (Haupt et al., 2007; Freitas-Andrade et al., 2017), and the conformation can be changed. Meanwhile, the gap connected half-channel can maintain an open state (Cotrina et al., 1998), and Cx43 can redistribute on the endfoot of astrocytes in the ischemic penumbra (Kondo et al., 1996). Some research found that the application of the GJ inhibitor can inhibit the function of Cx43 and alleviate cerebral I/R injury (Deng et al., 2014; Fan et al., 2015). The present study indicates that the change in Cx43 expression is consistent with the improvement of NDS and the decrease in the cerebral infarction area, suggesting that the monotherapy and combination therapy of Ginseng and Rhubarb have a neuroprotective effect via the down-regulation of Cx43; while the combined use of Ginseng and Rhubarb could play a better protective role.

Cx43 and AQP4 can interact in both structure and function. It has been demonstrated that Cx43 and AQP4 co-locate in the endfoot of astrocytes in the central nervous system and jointly participate in the transport of K+ from astrocytes to blood vessels, indicating that Cx43 and AQP4 are correlated at the level of water balance and GJ communication (Kong et al., 2008). AQP4 may be integrated with the astrocyte surface protein Cx43 and potassium channel Kir4.1 to eliminate excess fluid (Wu et al., 2013). Nicchia et al. (2005) found that astrocytes of AQP4 gene knockout mice significantly down-regulated Cx43, decreased cell coupling and cytoskeletal remodeling, suggesting that AQP4 and Cx43 on astrocytes may have a functional association. In addition, the absence of Cx43 also results in partial loss of AQP4 (Ezan et al., 2012; Li et al., 2015). Zhang et al. (2013) found that a intracerebroventricular injection of CBX can reduce the production of reactive oxygen species (ROS) and inhibit the activation of astrocytes and microglia, further reducing the cerebral infarction area in rats. It was found in an *in vitro* PC12 cell experiment that CBX can partially inhibit the opening of GJ and improve cell viability. The present experimental results found that CBX can inhibit GJ, reduce the expression of both the Cx43 and AQP4 protein, improve the NDS and reduce the percentage of the cerebral infarction area. However, this study mainly investigated the combined effect of Ginseng and Rhubarb on neuroprotection in I/R injury, without further research into the concentration-response relationship between AQP4 and Cx43, which is the limitation in this study as well as our future research directions.

CONCLUSION

The herbal compatibility of Ginseng and Rhubarb has a synergistically neuroprotective effect during acute cerebral I/R injury, mainly by reducing the expression of Cx43 and AQP4.

DATA AVAILABILITY

All datasets generated for this study are included in the manuscript/supplementary files.

AUTHOR CONTRIBUTIONS

W-TY and G-QZ designed the study. W-TY, YW, Y-HS, HF, ZX, and Q-QX performed the experiments and analyzed the data. W-TY and YW supervised the study and wrote the manuscript. All authors participated in the final approval of the version to be published.

FUNDING

This project was supported by a grant from the National Natural Science Foundation of China (81573750/81473491/81173395/H2902), The Young and Middle-Aged University Discipline Leaders of Zhejiang Province, China (2013277), and the Zhejiang Provincial Program for the Cultivation of High-level Health Talents (2015).

REFERENCES

Akdemir, G., Ratelade, J., Asavapanumas, N., and Verkman, A. S. (2014). Neuroprotective effect of aquaporin-4 deficiency in a mouse model of severe global cerebral ischemia produced by transient 4-vessel occlusion. *Neurosci. Lett.* 574, 70–75. doi: 10.1016/j.neulet.2014.03.073

Aoki, K., Uchihara, T., Tsuchiya, K., Nakamura, A., Ikeda, K., and Wakayama, Y. (2003). Enhanced expression of aquaporin 4 in human brain with infarction. *Acta Neuropathol.* 106, 121–124. doi: 10.1007/s00401-003-0709-y

Benjamin, E. J., Blaha, M. J., Chiuve, S. E., Cushman, M., Das, S. R., Deo, R., et al. (2017). Heart disease and stroke statistics-2017 update: a report from the american heart association. *Circulation* 135, e146–e603. doi: 10.1161/CIR.0000000000000485

Chen, H., Yoshioka, H., Kim, G. S., Jung, J. E., Okami, N., Sakata, H., et al. (2011). Oxidative stress in ischemic brain damage: mechanisms of cell death and potential molecular targets for neuroprotection. *Antioxid. Redox Signal.* 14, 1505–1517. doi: 10.1089/ars.2010.3576

Chen, Q. (2011). *Methodology of Pharmacological Research of Traditional Chinese Medicine*. Beijing: People's Medical Publishing House.

Cheng, C. W., Wu, T. X., Shang, H. C., Li, Y. P., Altman, D. G., Moher, D., et al. (2017). CONSORT extension for chinese herbal medicine formulas 2017: recommendations, explanation, and elaboration (Simplified Chinese Version). *Ann. Intern. Med.* 167, W21–W34. doi: 10.7326/IsTranslatedFrom_M17-2977_2

Cotrina, M. L., Kang, J., Lin, J. H., Bueno, E., Hansen, T. W., He, L., et al. (1998). Astrocytic gap junctions remain open during ischemic conditions. *J. Neurosci.* 18, 2520–2537. doi: 10.1523/jneurosci.18-07-02520.1998

Deng, Y., Liao, Q., Li, S., Bi, K., Pan, B., and Xie, Z. (2008). Simultaneous determination of berberine, palmatine and jatrorrhizine by liquid chromatography-tandem mass spectrometry in rat plasma and its application

in a pharmacokinetic study after oral administration of coptis-evodia herb couple. *J. Chromatogr. B Analyt. Technol. Biomed. Life Sci.* 863, 195–205. doi: 10.1016/j.jchromb

Deng, Z. H., Liao, J., Zhang, J. Y., Liang, C., Song, C. H., Han, M., et al. (2014). Inhibition of the connexin 43 elevation may be involved in the neuroprotective activity of leptin against brain ischemic injury. *Cell Mol. Neurobiol.* 34, 871–879. doi: 10.1007/s10571-014-0066-5

Dong, X., Zheng, L., Lu, S., and Yang, Y. (2017). Neuroprotective effects of pretreatment of ginsenoside Rb1 on severe cerebral ischemia-induced injuries in aged mice: involvement of anti-oxidant signaling. *Geriatr. Gerontol. Int.* 17, 338–345. doi: 10.1111/ggi.12699

Ezan, P., André, P., Cisternino, S., Saubaméa, B., Boulay, A. C., Doutremer, S., et al. (2012). Deletion of astroglial connexins weakens the blood-brain barrier. *J. Cereb. Blood Flow Metab.* 32, 1457–1467. doi: 10.1038/jcbfm.2012.45

Fan, Z., Tong, X., Li, Y., Yu, L., Chen, Y., Liu, H., et al. (2015). Protective effect of propofol against cerebral ischemic/reperfusion injury may involve inhibition of gap junction. *Nan Fang Yi Ke Da Xue Xue Bao* 35, 1678–1682.

Food and Drug Administration (2005). *Guidance for Industry on Estimating the Maximum Safe Starting Dose in Initial Clinical Trials for Therapeutics in Adult Healthy Volunteers*. Maryland, MD: Food and Drug Administration.

Freitas-Andrade, M., She, J., Bechberger, J., Naus, C. C., and Sin, W. C. (2017). Acute connexin43 temporal and spatial expression in response to ischemic stroke. *J. Cell Commun. Signal.* 12, 193–204. doi: 10.1007/s12079-017-0430-6

Gao, Y., Jiang, B., Sun, H., Ru, X., Sun, D., Wang, L., et al. (2018). The burden of stroke in China: results from a nationwide population-based epidemiological survey. *PLoS One* 13:e0208398. doi: 10.1371/journal.pone.0208398

GBD 2016 Causes of Death Collaborators (2017). Global, regional, and national age-sex specific mortality for 264 causes of death, 1980-2016: a systematic analysis for the global burden of Disease Study 2016. *Lancet* 390, 1151–1210. doi: 10.1016/S0140-6736(17)32152-9

Gilleron, J., Carette, D., Segretain, D., and Pointis, G. (2018). Multiple and complex influencesof connexins and pannexins on cell death. *Biochim. Biophys. Acta* 1860, 182–191. doi: 10.1016/j.bbamem.2017.06.004

Haupt, C., Witte, O. W., and Frahm, C. (2007). Up-regulation of connexin43 in the glial scar following photothrombotic ischemic injury. *Mol. Cell Neurosci.* 35, 89–99. doi: 10.1016/j.mcn.2007.02.005

Hervé, J. C., and Derangeon, M. (2013). Gap-junction-mediated cell-to-cell communication. *Cell Tissue Res.* 352, 21–31. doi: 10.1007/s00441-012-1485-6

Hirt, L., Fukuda, A. M., Ambadipudi, K., Rashid, F., Binder, D., Verkman, A., et al. (2017). Improved long-term outcome after transient cerebral ischemia in aquaporin-4 knockout mice. *J. Cereb. Blood Flow Metab.* 37, 277–290. doi: 10.1177/0271678X15623290

Huang, Q., Lu, G., Shen, H. M., Chung, M. C., and Ong, C. N. (2007). Anti-cancer properties of anthraquinones from rhubarb. *Med. Res. Rev.* 27, 609–630. doi: 10.1002/med.20094

Jin, R., Yang, G., and Li, G. (2010). Inflammatory mechanisms in ischemic stroke: role of inflammatory cells. *J. Leukocyte Biol.* 87, 779–789. doi: 10.1189/jlb.1109766

Jin, Y., Qu, C., Tang, Y., Pang, H., Liu, L., Zhu, Z., et al. (2016). Herb pairs containing angelicae sinensis radix (Danggui): a review of bio-active constituents and compatibility effects. *J. Ethnopharmacol.* 181, 158–171. doi: 10.1016/j.jep.2016.01.033

Katada, R., Akdemir, G., Asavapanumas, N., Ratelade, J., Zhang, H., and Verkman, A. S. (2014). Greatly improved survival and neuroprotection in aquaporin-4-knockout mice following global cerebral ischemia. *FASEB J.* 28, 705–714. doi: 10.1096/fj.13-231274

Kim, H. J., Kim, P., and Shin, C. Y. (2013). Comprehensive review of the therapeutic and pharmacological effects of ginseng and ginsenosides in central nervous system. *J. Ginseng Res.* 37, 8–29. doi: 10.5142/jgr.2013.37.8

Kimberly, W. T., Dutra, B. G., Boers, A. M. M., Alves, H. C. B. R., Berkhemer, O. A., van den Berg, L., et al. (2018). Association of reperfusion with brain edema in patients with acute ischemic stroke: a secondary analysis of the MR CLEAN Trial. *JAMA Neurol.* 75, 453–461. doi: 10.1001/jamaneurol.2017.5162

Kondo, T., Kinouchi, H., Kawase, M., and Yoshimoto, T. (1996). Astroglial cells inhibit the increasing permeability of brain endothelial cell monolayer following Hypoxia Preoxygenation. *Neurosci. Lett.* 208, 101–104. doi: 10.1016/0304-3940(96)12555-6

Kong, H., Fan, Y., Xie, J., Ding, J., Sha, L., Shi, X., et al. (2008). AQP4 knockout impairs proliferation, migration and neuronal differentiation of adult neural stem cells. *J. Cell Sci.* 121, 4029–4036. doi: 10.1242/jcs.035758

Le, H. T., Sin, W. C., Lozinsky, S., Bechberger, J., Vega, J. L., Guo, X. Q., et al. (2014). Gap junction intercellular communication mediated by connexin43 in astrocytes is essential for their resistance to oxidative stress. *J. Biol. Chem.* 289, 1345–1354. doi: 10.1074/jbc.M113.508390

Li, G., Liu, X., Liu, Z., and Su, Z. (2015). Interactions of connexin 43 and aquaporin-4 in the formation of glioma-induced brain edema. *Mol. Med. Rep.* 11, 1188–1194. doi: 10.3892/mmr.2014.2867

Liu, A. J., Song, L., Li, Y., Zhang, X. G., Chen, Z. X., Huang, L. B., et al. (2015). Active compounds of rhubarb root and rhizome in animal model experiments of focal cerebral ischemia. *Evid. Based Complement. Alternat. Med.* 2015, 210546. doi: 10.1155/2015/210546

Longa, E. Z., Weinstein, P. R., Carlson, S., and Cummins, R. (1989). Reversible middle cerebral artery occlusion without craniectomy in rats. *Stroke* 20, 84–89.

Lü, J. M., Yao, Q., and Chen, C. (2009). Ginseng compounds: an update on their molecular mechanisms and medical applications. *Curr. Vasc. Pharmacol.* 7, 293–302. doi: 10.2174/157016109788340767

Lu, L., Li, H. Q., Fu, D. L., Zheng, G. Q., and Fan, J. P. (2014). Rhubarb root and rhizome-based Chinese herbal prescriptions for acute ischemic stroke: a systematic review and meta-analysis. *Complement. Ther. Med.* 22, 1060–1070. doi: 10.1016/j.ctim.2014.10.002

Lu, L., Li, H. Q., Li, J. H., Liu, A. J., and Zheng, G. Q. (2015). Neuroprotection of sanhua decoction against focal cerebral ischemia/reperfusion injury in rats through a mechanism targeting aquaporin 4. *Evid. Based Complement. Alternat. Med.* 2015:584245. doi: 10.1155/2015/584245

Maugeri, R., Schiera, G., Di Liegro, C. M., Fricano, A., Iacopino, D. G., and Di Liegro, I. (2016). Aquaporins and brain tumors. *Int. J. Mol. Sci.* 17:E1029. doi: 10.3390/ijms17071029

Mizuma, A., and Yenari, M. A. (2017). Anti-Inflammatory targets for the treatment of reperfusion injury in stroke. *Front. Neurol.* 8:467. doi: 10.3389/fneur.2017.00467

Nah, S. Y., Kim, D. H., and Rhim, H. (2007). Ginsenosides: are any of them candidates for drugs acting on the central nervous system? *CNS Drug Rev.* 13, 381–404. doi: 10.1111/j.1527-3458.2007.00023.x

Nicchia, G. P., Srinivas, M., Li, W., Brosnan, C. F., Frigeri, A., and Spray, D. C. (2005). New possible roles for aquaporin-4 in astrocytes: cell cytoskeleton and functional relationship with connexin43. *FASEB J.* 19, 1674–1676. doi: 10.1096/fj.04-3281fje

Nielsen, M. S., Axelsen, L. N., Sorgen, P. L., Verma, V., Delmar, M., and Holstein-Rathlou, N. H. (2012). Gap junctions. *Compr. Physiol.* 2, 48–56. doi: 10.1002/cphy.c110051

Nito, C., Kamada, H., Endo, H., Narasimhan, P., Lee, Y. S., and Chan, P. H. (2012). Involvement of mitogen-activated protein kinasepathways in expression of the water channel protein aquaporin-4 after ischemiain rat cortical astrocytes. *J. Neurotrauma* 29, 2404–2412. doi: 10.1089/neu.2012.2430

Ong, W. Y., Farooqui, T., Koh, H. L., Farooqui, A. A., and Ling, E. A. (2015). Protective effects of ginseng on neurological disorders. *Front. Aging Neurosci.* 7:129. doi: 10.3389/fnagi.2015.00129

Orellana, J. A., Froger, N., Ezan, P., Jiang, J. X., Bennett, M. V., and Naus, C. C. (2011). ATP and glutamate released via astroglial connexin 43 hemichannels mediate neuronal death through activation of pannexin 1 hemichannels. *J. Neurochem.* 118, 826–840. doi: 10.1111/j.1471-4159.2011.07210.x

Papadopoulos, M. C., and Verkman, A. S. (2007). Aquaporin-4 and brain edema. *Pediatr. Nephrol.* 22, 778–784. doi: 10.1007/s00467-006-0411-0

Papadopoulos, M. C., and Verkman, A. S. (2013). Aquaporin water channels in the nervous system. *Nat. Rev. Neurosci.* 14, 265–277. doi: 10.1038/nrn3468

Powers, W. J., Rabinstein, A. A., Ackerson, T., Adeoye, O. M., Bambakidis, N. C., Becker, K., et al. (2018). 2018 guidelines for the early management of patients with acute ischemic stroke: a guideline for healthcare professionals from the American Heart Association/American Stroke Association. *Stroke* 49, e46–e110. doi: 10.1161/STR.0000000000000158

Rastogi, V., Santiago-Moreno, J., and Doré, S. (2015). Ginseng: a promising neuroprotective strategy in stroke. *Front. Cell Neurosci.* 8:457. doi: 10.3389/fncel.2014.00457

Rokot, N. T., Kairupan, T. S., Cheng, K. C., Runtuwene, J., Kapantow, N. H., Amitani, M., et al. (2016). A role of ginseng and its constituents in the treatment of central nervous system disorders. *Evid. Based Complement. Alternat. Med.* 2016, 1–7. doi: 10.1155/2016/2614742

Shobha, N., Buchan, A. M., and Hill, M. D. (2011). Canadian alteplase for stroke effectiveness study (CASES). Thrombolysis at 3-4.5 hours after acute ischemic stroke onset–evidence from the Canadian alteplase for stroke effectiveness study (CASES) registry. *Cerebrovasc. Dis.* 31, 223–228. doi: 10.1159/000321893

State Pharmacopoeia Commission (2015). *Pharmacopoeia of the People's Republic of China, Part I*. Beijing: China Pharmacopoeia Science and Technology Press.

Tang, G., and Yang, G. Y. (2016). Aquaporin-4: a potential therapeutic target for cerebral edama. *Int. J. Mol. Sci.* 17:1413. doi: 10.3390/ijms17101413

Thompson, R. J., Zhou, N., and MacVicar, B. A. (2006). Ischemia opens neuronal gap junction hemichannels. *Science* 312, 924–927. doi: 10.1126/science.1126241

Verkman, A. S., Smith, A. J., Phuan, P. W., Tradtrantip, L., and Anderson, M. O. (2017). The aquaporin-4 water channel as a potential drug target in neurological disorders. *Expert Opin. Ther. Targets* 21, 1161–1170. doi: 10.1080/14728222.2017.1398236

Walberer, M., Ritschel, N., Nedelmann, M., Volk, K., Mueller, C., Tschernatsch, M., et al. (2008). Aggravation of infarct formation by brain swelling in a large territorial stroke: a target for neuroprotection? *J. Neurosurg.* 109, 287–293. doi: 10.3171/JNS/2008/109/8/0287

Wang, S., Davis, S., Dong, Q., Wang, Y., Liu, L., Liang, H., et al. (2019). Advanced clinical education for stroke physicians in China: The ACTION and SCA models. *Int. J. Stroke* 14, 215–219. doi: 10.1177/1747493018816515

Wang, S., Hu, Y., Tan, W., Wu, X., Chen, R., Cao, J., et al. (2012). Compatibility art of traditional Chinese medicine: from the perspective of herb pairs. *J. Ethnopharmacol.* 143, 412–423. doi: 10.1016/j.jep.2012.07.033

Wang, W., Jiang, B., Sun, H., Ru, X., Sun, D., Wang, L., et al. (2017). NESS-China investigators. prevalence, incidence, and mortality of stroke in china: results from a nationwide population-based survey of 480–687 adults. *Circulation* 135, 759–771. doi: 10.1161/CIRCULATIONAHA.116.025250

Wang, Y., Fan, Y. C., Xie, C. L., and Zheng, G. Q. (2011). History of post-stroke epilepsy in ancient China. *J. Neurol.* 258, 1555–1558. doi: 10.1007/s00415-011-5959-3

Wang, Y. K., Deng, F., Miao, J., Xie, H., and Feng, J. C. (2015). Neuroprotection by carbenoxolone against ischemia injury involves PI3K/Akt pathway. *Clin. Lab.* 2015, 1561–1568.

Wang, Z., Ma, P., Xu, L., He, C., Peng, Y., and Xiao, P. (2013). Evaluation of the content variation of anthraquinone glycosides in rhubarb by UPLC-PDA. *Chem. Cent. J.* 7:170. doi: 10.1186/1752-153X-7-170

Wołoszyńska, I., and Stępień, A. (2017). Risk factors of rt-PA therapy in patients with ischemic stroke. *Acta Pol. Pharm.* 74, 293–298.

World Health Organization (2017). *The Top 10 Causes of Death*. Geneva: WHO.

Wu, Z., Xu, H., He, Y., Yang, G., Liao, C., Gao, W., et al. (2013). Antisense oligodeoxynucleotides targeting connexin43 reduce cerebral astrocytosis and edema in a rat model of traumatic brain injury. *Neurol. Res.* 35, 255–262. doi: 10.1179/1743132813Y.0000000165

Yan, H., and Fu, M. F. (2011). The development of research in the treatment of ruhbarb for acute stroke. *Chin. Pharm. J.* 36, 655–657.

Yang, M., Gao, F., Liu, H., Yu, W. H., Zhuo, F., Qiu, G. P., et al. (2013). Hyperosmotic induction of aquaporin expression in rat astrocytes through a different MAPK pathway. *J. Cell Biochem.* 114, 111–119. doi: 10.1002/jcb.24308

Yao, X., Uchida, K., Papadopoulos, M. C., Zador, Z., Manley, G. T., and Verkman, A. S. (2015). Mildly reduced brain swelling and improved neurological outcome in aquaporin-4 knockout mice following controlled cortical impact brain injury. *J. Neurotrauma* 32, 1458–1464. doi: 10.1089/neu.2014.3675

Zhang, G., Xia, F., Zhang, Y., Zhang, X., Cao, Y., Wang, L., et al. (2016). Ginsenoside Rd is efficacious against acute ischemic stroke by suppressing microglial proteasome-mediated inflammation. *Mol. Neurobiol.* 53, 2529–2540. doi: 10.1007/s12035-015-9261-8

Zhang, L., Li, Y. M., Jing, Y. H., Wang, S. Y., Song, Y. F., and Yin, J. (2013). Protective effects of carbenoxolone are associated with attenuation of oxidative stress in ischemic brain injury. *Neurosci. Bull.* 29, 311–320. doi: 10.1007/s12264-013-1342-y

Zheng, G. Q., Cheng, W., Wang, Y., Wang, X. M., Zhao, S. Z., Zhou, Y., et al. (2011). Ginseng total saponins enhance neurogenesis after focal cerebral ischemia. *J. Ethnopharmacol.* 133, 724–728. doi: 10.1016/j.jep.2010.01.064

Zhou, M., Hong, Y., Lin, X., Shen, L., and Feng, Y. (2017). Recent pharmaceutical evidence on the compatibility rationality of traditional Chinese medicine. *J. Ethnopharmacol.* 12, 363–375. doi: 10.1016/j.jep.2017.06.007

Zhou, Y., Li, H. Q., Lu, L., Fu, D. L., Liu, A. J., Li, J. H., et al. (2014). Ginsenoside Rg1 provides neuroprotection against blood brain barrier disruption and neurological injury ina rat model of cerebral ischemia/reperfusion through downregulation of aquaporin 4 expression. *Phytomedicine* 21, 998–1003. doi: 10.1016/j.phymed.2013.12.005

Conflict of Interest Statement: The authors declare that the research was conducted in the absence of any commercial or financial relationships that could be construed as a potential conflict of interest.

Copyright © 2019 Yang, Wang, Shi, Fu, Xu, Xu and Zheng. This is an open-access article distributed under the terms of the Creative Commons Attribution License (CC BY). The use, distribution or reproduction in other forums is permitted, provided the original author(s) and the copyright owner(s) are credited and that the original publication in this journal is cited, in accordance with accepted academic practice. No use, distribution or reproduction is permitted which does not comply with these terms.

frontiers in Pharmacology

ORIGINAL RESEARCH
published: 18 September 2019
doi: 10.3389/fphar.2019.01046

Integrating Pharmacokinetics Study, Network Analysis, and Experimental Validation to Uncover the Mechanism of Qiliqiangxin Capsule Against Chronic Heart Failure

Yu Zhang[1,2†], Mingdan Zhu[2†], Fugeng Zhang[3], Shaoqiang Zhang[2], Wuxun Du[2] and Xuefeng Xiao[1*]*

[1] School of Graduate, Tianjin University of Traditional Chinese Medicine, Tianjin, China, [2] The Second Affiliated Hospital, Tianjin University of Traditional Chinese Medicine, Tianjin, China,[3] Department of Pharmacy, Tianjin Huanhu Hospital, Tianjin, China

OPEN ACCESS

Edited by:
Jincai Luo,
Peking University, China

Reviewed by:
Rongli Zhang,
Case Western Reserve University, United States
Ren Jun Guo,
Xiyuan Hospital,China

***Correspondence:**
Wuxun Du
cnduwux@163.com
Xuefeng Xiao
kai1219@163.com

†These authors have contributed equally to this work

Specialty section:
This article was submitted to Ethnopharmacology, a section of the journal Frontiers in Pharmacology

Received: 23 May 2019
Accepted: 19 August 2019
Published: 18 September 2019

Citation:
Zhang Y, Zhu M, Zhang F, Zhang S, Du W and Xiao X (2019) Integrating Pharmacokinetics Study, Network Analysis, and Experimental Validation to Uncover the Mechanism of Qiliqiangxin Capsule Against Chronic Heart Failure. Front. Pharmacol. 10:1046. doi: 10.3389/fphar.2019.01046

Objectives: The purpose of this study was to propose an integrated strategy for investigating the mechanism of Qiliqiangxin capsule (QLQX) to treat chronic heart failure (CHF).

Methods: Pharmacokinetics analysis was performed to screen the active components of QLQX using high-performance liquid chromatography–tandem mass spectrometry techniques. We then constructed the component–target network between the targets of active components in QLQX and CHF using Cytoscape. A network analysis, including topological parameters, clustering, and pathway enrichment, was established to identify the hub targets and pathways. Finally, some of the predicted hub targets were validated experimentally in human cardiac microvascular endothelial cell (HCMEC).

Results: We identified 29 active components in QLQX, and 120 consensus potential targets were determined by the pharmacokinetics analysis and network pharmacology approach. Further network analysis indicated that 6 target genes, namely, *VEGFA*, *CYP1A1*, *CYP2B6*, *ATP1A1*, *STAT3*, and *STAT4*, and 10 predicted functional genes, namely, *KDR*, *FLT1*, *NRP2*, *JAK2*, *EGFR*, *IL-6*, *AHR*, *ATP1B1*, *JAK1*, and *HIF1A*, may be the primary targets regulated by QLQX for the treatment of CHF. Among these targets, *VEGFA*, *IL-6*, *p-STAT3*, and *p-JAK2* were selected for validation in the HCMEC. The results indicated that QLQX may inhibit inflammatory processes and promote angiogenesis in CHF *via* the JAK/STAT signaling pathway.

Conclusions: This study provides a strategy for understanding the mechanism of QLQX against CHF by combining pharmacokinetics study, network pharmacology, and experimental validation.

Keywords: pharmacokinetics, network pharmacology, Qiliqiangxin capsule, chronic heart failure, HCMEC

INTRODUCTION

Traditional Chinese medicine, characterized by a holistic approach, has attracted increasing attention worldwide because of its satisfactory clinical efficacy (Fung and Linn, 2015; Zhang et al., 2015; Chao et al., 2017). Chinese herbal medicine, as the mainstay and principal form of traditional Chinese medicine practice, is composed of multiple herbal ingredients and hundreds of chemical compounds (Zhou et al., 2019). Hence, it is difficult to fully understand their effective ingredients and the mechanism of action which depends on the overall interactions among all the ingredients.

Qiliqiangxin capsule (QLQX), comprising 11 crude herbs, has been clinically used for treating chronic heart failure (CHF) in China, providing an effective alternative for treatments of CHF (Li et al., 2013; Tang and Huang, 2013; Sun J. et al., 2016). Chemically, flavonoids, saponins, cardiac glycosides, diterpene quinones, phenolic acids, diterpene alkaloids, and triterpenoids have been identified as the main constituents of QLQX (Yun et al., 2018). Recent pharmacological studies showed that QLQX performs various activities, including attenuating atrial structural remodeling (Tingting et al., 2019), improving endothelial cell function (Chen et al., 2015), and protecting cardiac myocytes and mitochondrial function (Zhang et al., 2013). However, the active compounds, potential targets, and pathways involved in these effects have not been systematically investigated.

Recently, integrated strategies based on bioinformatics, system biology, and high-throughput analytical techniques have emerged as a holistic and efficient tool to solve this issue (Ning et al., 2018; Xing et al., 2018; Huang et al., 2019). Network pharmacology gives us helpful tools to screen potential bioactive ingredients and understand the molecular mechanisms underlying the therapeutic effects by constructing component–target and target–disease networks (Li and Zhang, 2013; Yuan et al., 2017). In recent years, the network pharmacology-based method has been used to analyze the system-level mechanisms of mono- and poly-pharmacology, manifesting "multicompound, multitarget" characteristics (Engin et al., 2014; Park et al., 2018). However, there exist limitations in the insufficient accumulation and poor quality of traditional Chinese medicine-related data, and the nonreproducible nature of the existing data (Zhang R. et al., 2019). The information on the active constituents of Chinese herbal medicine is critical for accurate assessments of the network. Thus, the greater the reliability and correlation of the information on the active constituents, the more convincing will be the results of network research. It has also been accepted that the components absorbed into the blood that attain a certain blood concentration can produce pharmacodynamics effects and are considered pharmacologically active substances (Li et al., 2015; Mi et al., 2019). Therefore, pharmacokinetics study provides powerful evidence for determining the main active compounds absorbed into the blood and deciphering their process *in vivo*.

In the current study, a comprehensive method focusing on the main active compounds was used to illustrate the molecular mechanisms of QLQX by adopting pharmacokinetics study, network pharmacological analysis, and experimental validation. The flowchart is illustrated in **Figure 1**. Briefly, (1) a pharmacokinetics study was employed to determine the main active components of QLQX; (2) a component–target (C–T) network was established to visualize the synergistic interactions between the targets of the main active components and CHF; (3) topological parameters of the C–T network, clustering, and pathway enrichment analysis of major hubs of QLQX against CHF were used to pinpoint the hub targets and pathways; (4) the hub targets determined by topological parameters and clustering analysis were used to construct the protein–protein interaction (PPI) network; (5) some hub targets in the PPI network were experimentally validated in the human cardiac microvascular endothelial cell (HCMEC).

MATERIALS AND METHODS

Reagents and Materials

The powder of QLQX was provided by Yiling Pharmaceutical Co. Ltd. (Shijiazhuang, China). Astragaloside, calycosin-7-glucoside, sinapine bisulfate, ginsenoside Rb_1, Rb_2, Rg_1, Rg_3, Rd, Re, Rf, and F_2, salvianolic acid A, salvianolic acid B, danshensu, rosmarinic acid, protocatechuic acid, hydroxysafflor yellow A, formononetin, hesperidin, rutin, quercetin, mesaconitine, hypaconitine, benzoylaconine, benzoylmesaconine, and benzoylhypaconine were obtained from the National Institutes for Food and Drug Control (Beijing, China), and ginsenoside Rc, lithospermic acid, and aconitine were obtained from Shanghai Yuanye Biotechnology Co. Ltd. (Shanghai, China). High-performance liquid chromatography (HPLC)-grade methanol, acetonitrile, and ammonium acetate were obtained from Fisher Scientific International Inc. (Fair Lawn, NJ), and formic acid was obtained from CNW Technologies GmbH (Duesseldorf, Germany). HCMEC and complete growth medium [containing 90% high Dulbecco's modified Eagle medium (H-DMEM), 10% fetal bovine serum (FBS), and penicillin/streptomycin] were purchased from BeNa Culture Collection (Beijing, China). Methylthiazolyldiphenyl-tetrazolium bromide (MTT) and bicinchoninic acid assay (BCA) protein assay kit were obtained from Beyotime (Shanghai, China). Rabbit antihuman monoclonal antibodies (*JAK2*, *phosphorylated-JAK2*, *STAT3*, *phosphorylated-STAT3*, *VEGFA*, and *β-actin*) and mouse antihuman monoclonal antibodies (*IL-6*) were provided by Beyotime (Shanghai, China). Rabbit antihuman monoclonal antibodies (*ADRB1*, *ADRB2*) were provided by Guidechem (Hangzhou, China).

HPLC-MS/MS Method for Pharmacokinetics Study

High-performance liquid chromatography–tandem mass spectrometry (HPLC-MS/MS) analysis (Shimadzu Co., Japan) was performed to assess the pharmacokinetic properties of 29 components in QLQX according to the method described in our

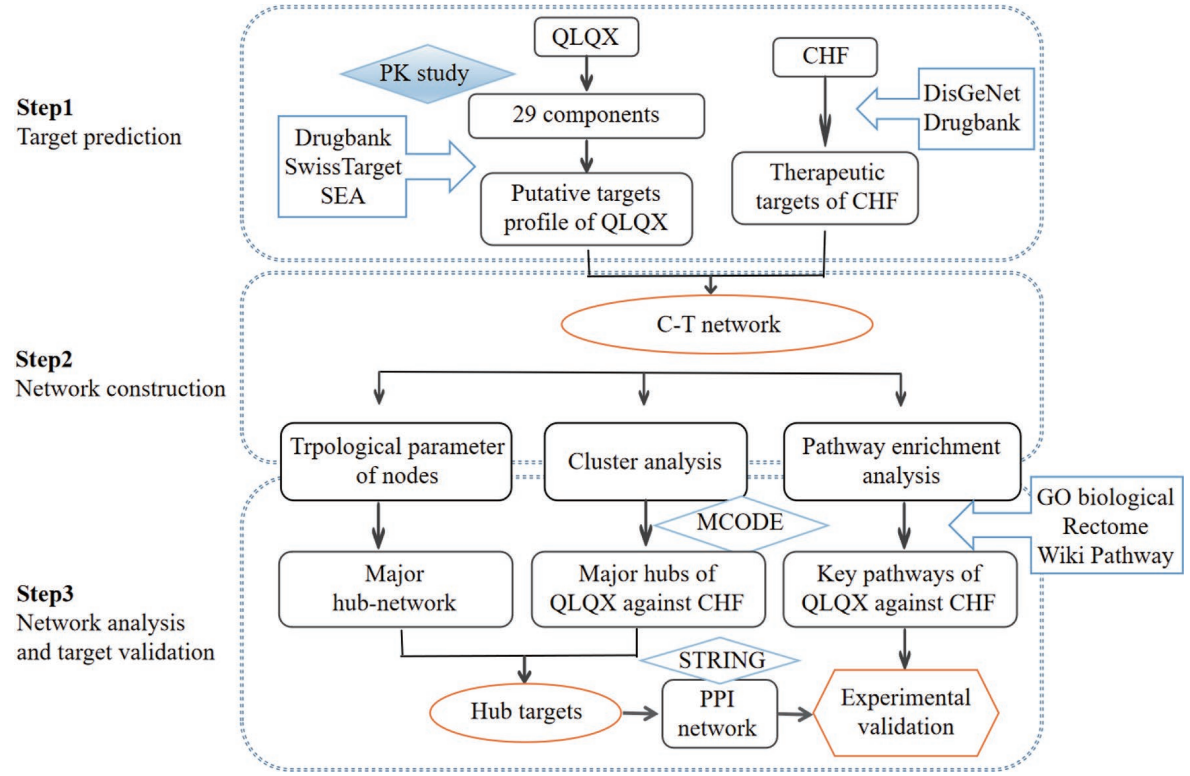


FIGURE 1 | Flowchart of the study.

previous study (Zhang et al., 2018). Briefly, chromatographic separation was achieved on an Agilent ZOBRAX XDB-C_{18} column (4.6 mm × 50 mm, 3.5 μm) maintained at 40°C. The mobile phase consisted of water (A) and methanol (B) both containing 0.1% (*v*/*v*) formic acid for astragaloside, calycosin-7-glucoside, sinapine bisulfate, and ginsenoside Rb_1, Rb_2, Rg_1, Rg_3, Rc, Rd, Re, Rf, and F_2 detection with a gradient elution. The mobile phase consisted of water (A) and acetonitrile (B) both containing 0.1% (*v*/*v*) formic acid for salvianolic acid A, salvianolic acid B, danshensu, lithospermic acid, rosmarinic acid, protocatechuic acid, hydroxysafflor yellow A, formononetin, hesperidin, rutin, and quercetin detection with a gradient elution. The mobile phase consisted of water containing 5 mM ammonium acetate (A) and methanol containing 0.1% formic acid (B) for aconitine, mesaconitine, hypaconitine, benzoylaconine, benzoylmesaconine, and benzoylhypaconine detection with a gradient elution. The flowrate was set at 0.45 ml/min, and the injection volume was 10 μl. The quantitative analysis was performed with multiple reaction monitoring in positive and negative ion modes.

Plasma Sample Preparation

The powder of QLQX was diluted with 0.5% sodium carboxymethyl cellulose yielding a concentration of 0.13 g/ml suspension. Sprague–Dawley rats were intragastrically administered with QLQX suspension at 1.3 g/kg, and the blood samples were collected into a heparinized centrifuge tube at 5, 10, 20, 40, 60, 90, 120, 180, 240, 360, 480, 720, and 1,440 min after dosing *via* the postorbital venous plexus. Then, the whole blood was centrifuged at 12,000 rpm for 10 min, the supernatant was obtained, and stored at −80°C until analysis. The preparation of blood samples was conducted according to our previous research (Zhang et al., 2018). This study was carried out in accordance with the principles of the Basel Declaration and recommendations of guidelines of the National Institutes of Health. The protocol was approved by the Ethics Committee of Tianjin University of Traditional Chinese Medicine (Tianjin, China).

Targets Fishing

The targets of active components in QLQX determined by pharmacokinetics analysis were obtained from three databases: DrugBank,[1] Swiss Target Prediction,[2] and Similarity Ensemble Approach (SEA).[3] Known therapeutic targets of CHF were collected from the DrugBank database[1] and DisGeNet database[4]. The keywords "chronic heart failure" and "congestive heart failure" were used, and the targets were human genes/proteins enrolled in this study.

[1] https://www.drugbank.ca/
[2] http://www.swisstargetprediction.ch/
[3] http://sea.bkslab.org/
[4] http://www.disgenet.org/web/DisGeNET/menu/home

Network Construction and Topological Analysis

The C–T network was constructed using Cytoscape (Version 3.2.1) (Smoot et al., 2011). Four topological features (degree, betweenness centrality, average shortest path length, and closeness centrality) were analyzed using Network Analyzer (Assenov et al., 2008). The major hub network comprising putative major components and major targets was extracted by defining nodes with degrees higher than the average number of neighbors.

Clustering Analysis

MCODE (Version 1.4.2) (Bader and Hogue, 2003) was employed to identify the major hubs of QLQX against CHF. MCODE analyzes the network based on the given parameter, and it assigns the weight to the vertex in local neighborhoods from the dense regions using vertex weighting, cluster prediction, and optimal postprocessing. Finally, we defined the hub targets by considering the results of the topological analysis and clustering analysis. To obtain the proteins interacting with the hub targets, the STRING[5] database was used, and the association score ≥0.9 was considered the highest confidence.

Pathway Enrichment Analysis

ClueGO (Version 2.3.2) (Rubinov and Sporns, 2010) was utilized to analyze the representative biological processes and pathways associated with QLQX against CHF. All targets obtained from the C–T network were imported. GO biological process, Reactome pathway, and Wiki pathway were selected from the ClueGO setting panel, and a two-sided hypergeometric test with $p \leq 0.01$ significance level for biological process analysis and a $p \leq 0.05$ significance level for pathway analysis was used.

Cell Culture and Treatments

HCMECs were maintained in complete growth medium (90% H-DMEM, 10% FBS, and penicillin/streptomycin). All cells were cultured at 37°C in a humidified atmosphere containing 5% CO_2. After three or four passages, the HCMECs were digested with 0.25% trypsin and adjusted to a density of 5×10^4 cells/ml and 1×10^5 cells/ml for cell viability assay and Western blot analysis, respectively. The powder of QLQX was accurately weighed and dissolved in complete growth medium to various concentrations (0.15 and 0.3 mg/ml). The cells used for cell viability assay were seeded on 96-well plates in 100 µl of complete growth medium (0.15 or 0.3 mg/ml QLQX were added) for 24, 48, or 72 h and were then treated with 10 mM Hcy for another 24 h. The cells used for Western blot analysis were divided into the following groups: control, model, positive-captopril (CA), QLQX-low (-L), and QLQX-high (-H). Cells in the control group were cultured without any treatments. In the model group, the HCMECs (1×10^5/ml) were cultured in 3 ml complete growth medium (10 mM Hcy was added) for 24 h. In the CA, -L, and -H groups, cells were pretreated with 0.075 mg/ml captopril, 0.15 mg/ml QLQX, and 0.3 mg/ml QLQX for 48 h, respectively, and then cultured in complete growth medium (10 mM Hcy was added) for a further 24 h.

[5]https://string-db.org/

Cell Viability Assay

Cell viability of the HCMECs was evaluated using the MTT assay. Cells were seeded on 96-well plates with a density of 5×10^4 cells/ml in 100 µl of complete growth medium (0.15 or 0.3 mg/ml QLQX were added) for 24, 48, or 72 h and were then treated with 10 mM Hcy for 24 h. Following treatment, 10 µl of MTT (5 mg/ml) was added to each well. After 4 h, the culture medium was removed, and 100 µl of dimethyl sulfoxide (Beyotime, Shanghai, China) was added. The absorbance was measured at 570 nm using a microplate reader (Infinite M200 Pro, Tecan, Switzerland), and the cell viability was expressed as a percentage of the value of the untreated group.

Western Blot Analysis

HCMECs (1×10^5 cells/ml) were seeded on 60 × 20-mm dishes in 3 ml of complete growth medium for 24 h. After treatment, the HCMECs were scraped off and washed twice with cold phosphate-buffered saline. The cells were solubilized by radioimmunoprecipitation assay lysis buffer (Beyotime, China) containing 1% phenylmethylsulphonyl fluoride (Beyotime, China) and 1% phosphatase inhibitor for 20 min on ice. Whole-cell lysates were clarified by centrifuging at 12,000 rpm for 10 min at 4°C, and the supernatants were collected. Protein concentrations were determined by the BCA protein assay. The protein samples were mixed with sodium dodecyl sulfate polyacrylamide gel electrophoresis sample loading buffer (Beyotime, China) and boiled at 100°C for 5 min. Equal concentrations of protein (2 mg/ml) were separated by electrophoresis on 10% sodium dodecyl sulphate polyacrylamide gels and were transferred onto polyvinylidene difluoride membranes. These membranes were soaked in 5% skimmed milk, and dissolved with TBST buffer (Tris Buffer Saline supplemented with 0.1% Tween-20) 5 times (15 min each time) to block nonspecific binding sites. The membranes were then incubated overnight at 4°C with the primary antibodies (*VEGFA*, *STAT3*, *p-STAT3*, *JAK2*, *p-JAK2*, *IL-6*, *ADRB1*, and *ADRB2*). After washing with TBST, the membranes were incubated for 2 h at room temperature with horseradish peroxidase-labeled secondary antibodies. After rewashing with TBST, the membranes were scanned using a fluorescent scanner (Odyssey CLX, Gene Company Limited, USA). Band intensity was analyzed using ImageJ software (National Institutes of Health, Bethesda, MD, USA).

Statistical Analysis

Data were presented as mean ± SD and analyzed using GraphPad Prism 6 (GraphPad Software, Inc., La Jolla, CA, USA). One-way analysis of variance (ANOVA) was used, and p-value < 0.05 was considered statistically significant.

RESULTS

Pharmacokinetics Study of 29 Components in QLQX by HPLC-MS/MS

Pharmacokinetic properties of 29 components in QLQX (astragaloside, calycosin-7-glucoside, sinapine bisulfate, ginsenoside Rb_1, Rb_2, Rg_1, Rg_3, Rc, Rd, Re, Rf, F_2, salvianolic acid A, salvianolic acid B, danshensu, lithospermic acid, rosmarinic

acid, protocatechuic acid, hydroxysafflor yellow A, formononetin, hesperidin, rutin, quercetin, aconitine, mesaconitine, hypaconitine, benzoylaconine, benzoylmesaconine, and benzoylhypaconine) were studied using the HPLC-MS/MS method according to the method in our previous study (Zhang et al., 2018). The pharmacokinetic properties of 29 components are shown in **Table 1**, and the mean concentration–time curves are shown in **Figure 2**. These 29 components of QLQX detected in the blood of the rats and with appropriate pharmacokinetic properties were determined to be the main active components and used to construct the C–T network.

Compound–Target Network Construction

Totally, 1,288 targets were found for the 29 components using Drugbank, Swiss Target Prediction, and SEA databases. The detailed target information for the 29 components in QLQX is shown in **Supplementary Table S1**. A total of 812 candidate targets of CHF were obtained from DisGeNet and Drugbank databases after removing redundant entries (**Supplementary Table S2**). Taking the intersection of the 1,288 putative targets of the 29 components in QLQX and the 812 candidate targets associated with CHF, a total of 120 consensus targets were collected as potential therapeutic targets of QLQX against CHF and used to establish the C–T network. As a result, a C–T network comprising 29 components and 120 consensus targets was constructed using Cytoscape. As shown in **Figure 3A**, the network comprised 149 nodes (29 components and 120 targets) and 446 edges.

Network Topological Analysis

Network analyzer was used to calculate four topological features (degree, betweenness centrality, average shortest path length, and closeness centrality) of the nodes of the C–T network. Nodes with degrees higher than the average number of neighbors (5.830) were identified and extracted as the major hub networks (**Figure 3B**). Among these, 32 major targets with higher degree, closeness centrality, betweenness centrality, and lower average shortest path length were recognized as the major putative targets, and the results are shown in **Table 2**. Twenty-eight components were identified as the main active components (**Table 3**), and quercetin had the highest degree and betweenness centrality of 46 and 0.35, respectively, thereby indicating that quercetin has the most important position in the network.

Clustering Analysis

MCODE was used to identify the major hubs of QLQX against CHF, which generated a well-organized cluster containing 17 nodes (*SLC22A8*, *SLCO1B3*, QLQX-9, QLQX-11, QLQX-5, QLQX-8, *CYP1A1*, QLQX-12, QLQX-6, *ATP1A1*, *VEGFA*,

TABLE 1 | Pharmacokinetic properties of 29 components in QLQX determined by HPLC-MS/MS.

No.	Compounds	Polarity	Parent (m/z)	Daughter (m/z)	Pharmacokinetic parameters				
					C_{max}	T_{max}	$t_{1/2}$	AUC_{0-t}	$AUC_{0-\infty}$
1	Astragaloside	Positive	807.5	627.3	120.46 ± 45.03	0.67 ± 0.00	5.74 ± 0.78	320.92 ± 79.10	369.14 ± 103.83
2	Calycosin-7-glucoside	Positive	447.2	285.2	31.49 ± 12.00	0.67 ± 0.06	6.05 ± 3.34	103.26 ± 47.63	120.71 ± 50.71
3	Sinapine bisulfate	Positive	310.2	251.2	1.35 ± 0.62	1.50 ± 0.00	3.52 ± 0.17	3.98 ± 1.21	8.76 ± 2.85
4	Ginsenoside Rb_1	Positive	1,131.7	365.2	323.00 ± 91.00	0.67 ± 0.00	9.16 ± 3.18	590.15 ± 257.83	713.49 ± 270.66
5	Ginsenoside Rb_2	Positive	1,107.8	335.0	31.25 ± 9.89	1.50 ± 0.06	10.11 ± 4.53	143.73 ± 35.67	307.99 ± 79.92
6	Ginsenoside Rg_1	Positive	823.5	643.5	113.44 ± 48.22	0.67 ± 0.00	8.69 ± 3.17	362.17 ± 118.25	422.31 ± 180.63
7	Ginsenoside Rg_3	Positive	807.6	364.9	20.49 ± 7.16	0.67 ± 0.24	5.03 ± 2.02	67.13 ± 27.93	89.81 ± 34.43
8	Ginsenoside Rc	Positive	1,101.6	789.5	180.00 ± 70.00	0.67 ± 0.00	4.32 ± 2.10	432.71 ± 178.66	493.04 ± 233.70
9	Ginsenoside Rd	Positive	969.5	789.6	97.49 ± 31.00	0.67 ± 0.00	5.90 ± 1.14	204.66 ± 87.30	257.92 ± 101.52
10	Ginsenoside Re	Positive	969.6	789.6	118.94 ± 52.82	0.67 ± 0.06	7.33 ± 3.45	268.84 ± 103.24	310.95 ± 147.36
11	Ginsenoside Rf	Positive	823.5	365.2	43.03 ± 12.49	0.67 ± 0.00	6.12 ± 3.53	130.27 ± 27.91	177.68 ± 68.95
12	Ginsenoside F_2	Positive	807.5	627.7	3.83 ± 1.23	0.67 ± 0.00	6.23 ± 2.89	12.73 ± 3.62	18.64 ± 5.28
13	Salvianolic acid A	Negative	493.1	294.9	8.96 ± 2.90	0.17 ± 0.00	7.50 ± 4.92	18.59 ± 7.91	21.40 ± 7.36
14	Salvianolic acid B	Negative	717.3	519.2	502.00 ± 68.43	0.33 ± 0.14	5.32 ± 1.32	818.47 ± 249.00	980.47 ± 112.07
15	Danshensu	Negative	196.9	134.8	98.60 ± 23.66	0.67 ± 0.00	3.52 ± 0.42	290.92 ± 68.38	390.90 ± 66.50
16	Lithospermic acid	Negative	537.4	493.2	77.25 ± 19.90	0.67 ± 0.00	4.80 ± 0.89	173.49 ± 38.57	216.94 ± 27.39
17	Rosmarinic acid	Negative	358.9	160.9	52.16 ± 5.96	0.67 ± 0.00	5.28 ± 1.35	78.65 ± 35.72	96.69 ± 24.81
18	Protocatechuic acid	Negative	152.9	108.8	17.00 ± 7.26	0.67 ± 0.00	8.38 ± 1.02	44.15 ± 18.02	61.03 ± 10.51
19	Hydroxysafflor yellow A	Negative	611.2	491.0	8.62 ± 3.51	0.17 ± 0.00	5.03 ± 2.00	15.63 ± 4.42	21.99 ± 6.25
20	Formononetin	Negative	266.9	251.7	5.17 ± 1.13	0.17 ± 0.00	5.07 ± 2.13	14.70 ± 5.48	18.04 ± 6.69
21	Hesperidin	Negative	609.2	300.9	64.63 ± 23.49	0.67 ± 0.00	3.34 ± 0.42	154.32 ± 66.50	187.77 ± 34.98
22	Rutin	Negative	609.2	299.6	3.63 ± 1.25	0.33 ± 0.00	5.33 ± 1.27	12.29 ± 2.47	16.92 ± 5.21
23	Quercetin	Negative	301.1	150.7	3.23 ± 1.26	0.67 ± 0.00	5.04 ± 0.98	10.96 ± 3.42	15.03 ± 5.28
24	Aconitine	Positive	646.4	586.4	1.44 ± 0.68	0.33 ± 0.00	18.35 ± 5.44	7.03 ± 2.31	18.16 ± 6.87
25	Mesaconitine	Positive	632.3	572.3	0.52 ± 0.16	0.17 ± 0.06	6.23 ± 1.23	3.95 ± 1.02	5.13 ± 2.32
26	Hypaconitine	Positive	616.3	556.3	1.97 ± 0.33	0.33 ± 0.00	8.01 ± 2.39	7.89 ± 2.57	13.85 ± 6.67
27	Benzoylaconine	Positive	604.2	554.3	1.83 ± 0.33	1.00 ± 0.00	18.63 ± 7.20	8.63 ± 2.39	25.94 ± 9.03
28	Benzoylmesaconine	Positive	590.2	540.3	5.84 ± 0.61	0.67 ± 0.11	8.23 ± 2.02	20.13 ± 6.27	35.34 ± 11.22
29	Benzoylhypaconine	Positive	574.2	542.3	0.67 ± 0.32	0.67 ± 0.00	12.88 ± 3.47	4.03 ± 1.03	7.80 ± 3.84

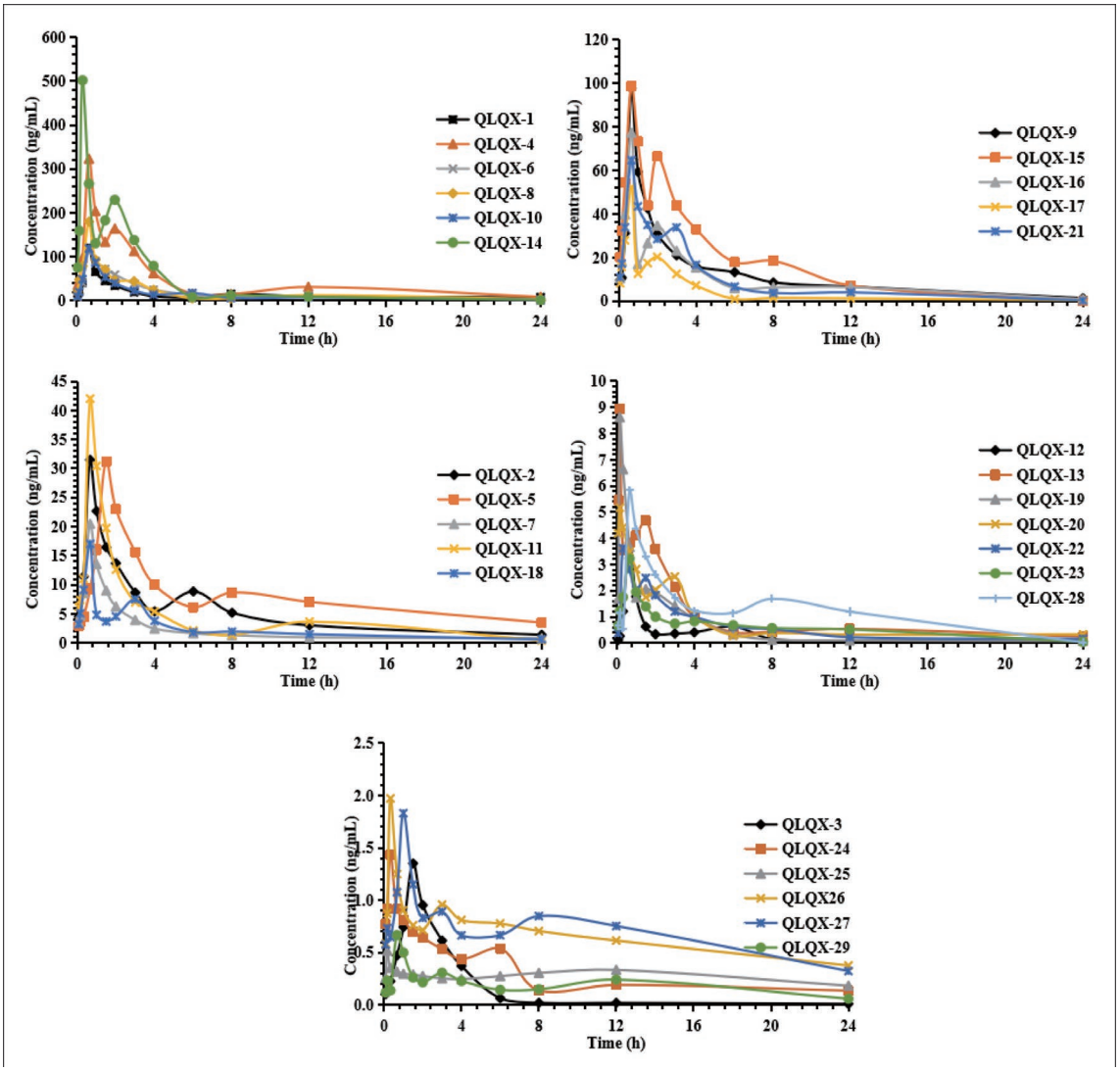


FIGURE 2 | Mean concentration-time profiles of astragaloside (QLQX-1), calycosin-7-glucoside (QLQX-2), sinapine bisulfate (QLQX-3), ginsenoside Rb_1 (QLQX-4), Rb_2 (QLQX-5), Rg_1 (QLQX-6), Rg_3 (QLQX-7), Rc (QLQX-8), Rd (QLQX-9), Re (QLQX-10), Rf (QLQX-11), F_2 (QLQX-12), salvianolic acid A (QLQX-13), salvianolic acid B (QLQX-14), danshensu (QLQX-15), lithospermic acid (QLQX-16), rosmarinic acid (QLQX-17), protocatechuic acid (QLQX-18), hydroxysafflor yellow A (QLQX-19), formononetin (QLQX-20), hesperidin (QLQX-21), rutin (QLQX-22), quercetin (QLQX-23), aconitine (QLQX-24), mesaconitine (QLQX-25), hypaconitine (QLQX-26), benzoylaconine (QLQX-27), benzoylmesaconine (QLQX-28), benzoylhypaconine (QLQX-29).

CYP2B6, *STAT3*, *SLCO1A2*, QLQX-10, QLQX-4, and *STAT4*). Taking the intersection of the topological analysis and clustering analysis results, a total of nine consensus targets were collected to be hub targets of QLQX against CHF, namely, *SLC22A8*, *SLCO1B3*, *CYP1A1*, *ATP1A1*, *VEGFA*, *CYP2B6*, *STAT3*, *SLCO1A2*, and *STAT4*. Then, the nine consensus targets were used as hub targets and submitted to STRING to generate the proteins interacting with these hub targets. The STRING database provides both experimental and predicted interaction information and provides a probabilistic association confidence score by calculation. As shown in **Table 4**, six target genes, namely, *VEGFA*, *CYP1A1*, *CYP2B6*, *ATP1A1*, *STAT3*, and *STAT4*, and 10 predicted functional genes, namely, *KDR*, *FLT1*, *NRP2*, *JAK2*, *EGFR*, *IL-6*, *AHR*, *ATP1B1*, *JAK1*, and *HIF1A*, having the highest confidence with an association score ≥0.9 were imported into Cytoscape 3.2.1 (**Figure 3C**). The network analysis tool was used to analyze the PPI network and targets with a higher degree played an important role in central correlation. The results are shown in **Table 5**.

Pathway Enrichment Analysis

To analyze the representative biological processes and pathways associated with the 120 targets of the C–T network, GO biological, Reactome, and Wiki pathway analysis were used to explore the potential biological processes and pathways affected by QLQX through analysis of the 120 targets. The biological

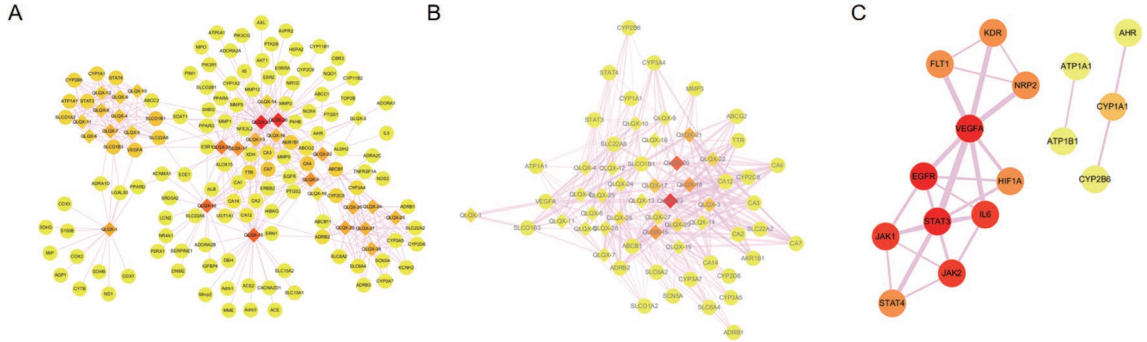


FIGURE 3 | The networks associating with QLQX in the treatment of CHF. **(A)** The component-target network consisted of 149 nodes and 446 edges. **(B)** The major hub network define by nodes with degree higher the average number of neighbors (5.830). **(C)** The PPI network of hub targets obtained from STRING database and constructed by Cytoscape. The ellipse nodes represent targets, and the diamond nodes represent active components in QLQX, the widths of the edges represent the order of the edge betweenness and the colors of the nodes are illustrated from red to yellow in descending order of degree values.

processes were ranked by their nominal *P* values with a cutoff at 0.01, and 120 targets were enriched to 26 biological processes; the top 10 are shown in **Supplementary Table S3** and **Figure 4A**. The pathways were ranked by their nominal *p* values with a cutoff at 0.05, and the top 10 pathways included interleukin-4 and 13 signaling, phase I functionalization of compounds, drug induction of bile acid pathway, xenobiotics, tamoxifen metabolism, reversible hydration of carbon dioxide, electron transport chain, adrenoceptors, adenosine P1 receptors, and angiotensin-converting enzyme inhibitor pathway (**Figure 4B**). The functional targets involved in each pathway are illustrated in **Supplementary Table S4**. The C–T pathway/biological process network (C–T–P) was constructed using Cytoscape (**Figure 5**) based on the interactions among the 29 components, 120 consensus targets, and top 10 biological processes and pathways.

Experimental Validation of Key Targets and Pathway

MTT assays showed that 0.15 (-L) and 0.3 mg/ml (-H) QLQX dramatically inhibited Hcy-induced injury in the HCMEC at 48 and 72 h in a time-dependent manner (**Figure 6**). To determine the mechanisms of QLQX in the treatment of CHF, some of the key proteins with a higher degree in the PPI network were experimentally validated in the HCMEC. Besides, considering that *ADRB1* and *ADRB2* play an essential role in heart failure (Doughty and Sharpe, 1997; Spadari et al., 2018), *ADRB1* and *ADRB2* were used as a control to validate the effect of QLQX. As shown in **Figure 6**, QLQX significantly increased the ratio between *ADRB1* and *ADRB2*. Meanwhile, QLQX significantly increased the expression level of *VEGFA* and inhibited the expression levels of *p-STAT3*, *p-JAK2*, and *IL-6* in a dose-dependent manner.

DISCUSSION

As a multicomponent drug, QLQX has been used for several years to treat CHF in China and has been demonstrated as effective in lowering the NT-proBNP level in CHF patients (Li et al., 2013). However, its "multicompound, multitarget" characteristics make it difficult to decipher the active ingredients and mechanisms of QLQX in the treatment against CHF.

Integrated strategies based on network pharmacology provide a useful approach to investigate the active components and molecular mechanisms. For instance, Gao et al. (2018) proposed a "main active compound-based network pharmacology" based on quantitative analysis of components to explore the anticancer mechanism of CKI. They selected herbs used in the clinical therapy of hepatoma to ascertain molecular targets and antitumor mechanisms, emphasizing the combination of clinical study and network pharmacology. However, in previous studies, all herbal ingredients were collected from herb databases and filtered according to absorption, distribution, metabolism, and excretion properties or drug-likeness value, which may be inconsistent with the ingredients present in the blood (Gao et al., 2016). Here, we proposed an integrated strategy *via* pharmacokinetics study, network analysis, and experimental validation to achieve an accurate and systematic exploration of the mechanisms of QLQX against CHF.

In this study, the 29 components of QLQX showing proper pharmacokinetics behavior in rats were determined to be the active ingredients of QLQX. These compounds were mainly categorized as triterpenoid saponins, phenolic acids, flavonoids, and alkaloids. Particularly, astragaloside, ginsenoside Rb_1, Rb_2, Rg_1, Rg_3, Rc, Rd, Re, Rf, and ginsenoside F_2, as triterpenoid saponins, are known for their anti-inflammatory property during the period of ventricular remodeling (Sun Y. et al., 2016; Qi et al., 2017); salvianolic acid A, salvianolic acid B, danshensu, lithospermic acid, rosmarinic acid, and protocatechuic acid, as phenolic acids, exert cardioprotection through promoting angiogenesis in animal models (Yu et al., 2017); calycosin-7-glucoside, hydroxysafflor yellow A, formononetin, hesperidin, rutin, and quercetin, as flavonoids, can reduce cardiomyocytes damage and apoptosis and improve cardiac function by decreasing oxidative stress (Mattera et al., 2017); and aconitine, mesaconitine, hypaconitine, benzoylaconine,

TABLE 2 | The topological parameters of 32 major targets.

Swiss prot	Genes/ proteins	Description	Degree	Betweenness centrality	Average shortest path length	Closeness centrality
Q9Y6L6	SLCO1B1	Solute carrier organic anion transporter family member 1B1	12	0.09496758	2.69078947	0.37163814
Q9NPD5	SLCO1B3	Solute carrier organic anion transporter family member 1B3	11	0.04862563	3.28289474	0.30460922
P43166	CA7	Carbonic anhydrase 7	11	0.04690937	2.40131579	0.41643836
P22748	CA4	Carbonic anhydrase 4	11	0.04164377	2.45394737	0.4075067
P15692	VEGFA	Vascular endothelial growth factor A	11	0.11260667	2.79605263	0.35764706
Q8TCC7	SLC22A8	Solute carrier family 22 member 8	10	0.03755913	3.23026316	0.3095723
P15121	AKR1B1	Aldo-keto reductase family 1 member B	10	0.02861805	2.70394737	0.36982968
P08183	ABCB1	Multidrug resistance protein 1	10	0.06692038	2.67763158	0.37346437
Q14765	STAT4	Signal transducer and activator of transcription 4	9	4.74E–04	4.08552632	0.24476651
P46721	SLCO1A2	Solute carrier organic anion transporter family member 1A2	9	4.74E–04	4.08552632	0.24476651
P40763	STAT3	Signal transducer and activator of transcription 3	9	4.74E–04	4.08552632	0.24476651
P20813	CYP2B6	Cytochrome P450 2B6	9	4.74E–04	4.08552632	0.24476651
P10632	CYP2C8	Cytochrome P450 2C8	9	0.05421697	2.75657895	0.3627685
P05023	ATP1A1	Sodium/potassium-transporting ATPase subunit alpha-1	9	4.74E–04	4.08552632	0.24476651
P04798	CYP1A1	Cytochrome P450 1A1	9	4.74E–04	4.08552632	0.24476651
P02766	TTR	Transthyretin	9	0.02882135	2.53289474	0.39480519
P08684	CYP3A4	Cytochrome P450 3A4	8	0.01906502	3.15131579	0.31732777
P07550	ADRB2	Beta-2 adrenergic receptor	8	0.04366511	3.20394737	0.31211499
P07451	CA3	Carbonic anhydrase 3	8	0.03416389	2.45394737	0.4075067
Q9UNQ0	ABCG2	ATP binding cassette subfamily G member 2 (Junior blood group)	7	0.0203742	2.74342105	0.36450839
Q9ULX7	CA14	Carbonic anhydrase 14	7	0.02057174	2.625	0.38095238
P31645	SLC6A4	Solute carrier family 6 member 4	7	0.0021531	3.83552632	0.26072041
P23975	SLC6A2	Solute carrier family 6 member 2	7	0.0021531	3.83552632	0.26072041
O43570	CA12	Carbonic anhydrase 12	7	0.01886671	2.66447368	0.37530864
Q14524	SCN5A	Sodium voltage-gated channel alpha subunit 5	6	1.51E–04	4.09868421	0.24398074
P24462	CYP3A7	Cytochrome P450 3A7	6	1.51E–04	4.09868421	0.24398074
P20815	CYP3A5	Cytochrome P450 3A5	6	1.51E–04	4.09868421	0.24398074
P10635	CYP2D6	Cytochrome P450 2D6	6	1.51E–04	4.09868421	0.24398074
P08588	ADRB1	Adrenoceptor beta 1	6	1.51E–04	4.09868421	0.24398074
P08254	MMP3	Matrix metallopeptidase 3	6	0.00514916	2.95394737	0.33853007
P00918	CA2	Carbonic anhydrase 2	6	0.01628126	2.67763158	0.37346437
O15244	SLC22A2	Solute carrier family 22 member 2	6	1.51E–04	4.09868421	0.24398074

benzoylmesaconine, benzoylhypaconine, and sinapine bisulfate, as alkaloids, can improve left ventricular systolic and diastolic function (Liu et al., 2012). Moreover, the hub targets of these active ingredients were determined *via* combining network topological parameters with clustering and PPI network analysis. In total, 6 targets, namely, *VEGFA*, *CYP1A1*, *CYP2B6*, *ATP1A1*, *STAT3*, and *STAT4*, and 10 predicted functional targets, namely, *KDR*, *FLT1*, *NRP2*, *JAK2*, *EGFR*, *IL-6*, *AHR*, *ATP1B1*, *JAK1*, and *HIF1A* were collected as hub targets of QLQX against CHF.

As the leading cause of cardiovascular mortality, CHF is associated with many pathogenic factors, such as increased hemodynamic overload, ventricular remodeling, neurohormonal activation, and energy metabolism disorder (Gedela et al., 2015; Tanai and Frantz, 2015). In recent years, increasing evidence has shown that cardiac microvascular and microcirculation functions are closely related, in that, proper cardiac function requires myocardial oxygen balance. Furthermore, the perturbations in microcirculation caused by the interplay of neurohumoral, metabolic, and endothelium-derived factors lead to cardiac microvascular dysfunction and further result in cardiac insufficiency or heart failure (Den Uil et al., 2008; Heinonen et al., 2015).

It is thought that the presence of endothelial dysfunction, which induced by impairment of endothelium-dependent relaxation of

TABLE 3 | The topological parameters of 28 main active components.

No.	Compounds	Degree	Betweenness centrality	Average shortest path length	Closeness centrality
QLQX-23	Quercetin	46	0.34943416	2.21052632	0.45238095
QLQX-20	Formononetin	37	0.20139204	2.47368421	0.40425532
QLQX-15	Danshensu	27	0.14738861	2.85526316	0.35023041
QLQX-18	Protocatechuic acid	25	0.14911094	2.65789474	0.37623762
QLQX-21	Hesperidin	22	0.10590127	2.71052632	0.36893204
QLQX-3	Sinapine bisulfate	18	0.06332468	2.94736842	0.33928571
QLQX-17	Rosmarinic acid	18	0.05489072	2.96052632	0.33777778
QLQX-22	Rutin	15	0.03964651	2.98684211	0.33480176
QLQX-1	Astragaloside	15	0.13507408	3.44736842	0.29007634
QLQX-29	Benzoylhypaconine	15	0.02499921	3.17105263	0.3153527
QLQX-27	Benzoylaconine	14	0.0210363	3.18421053	0.31404959
QLQX-26	Hypaconitine	14	0.0210363	3.18421053	0.31404959
QLQX-7	Ginsenoside Rg_3	13	0.03221083	3.19736842	0.3127572
QLQX-13	Salvianolic acid A	13	0.0102585	3.19736842	0.3127572
QLQX-28	Benzoylmesaconine	13	0.01850138	3.19736842	0.3127572
QLQX-25	Mesaconitine	13	0.01786266	3.19736842	0.3127572
QLQX-24	Aconitine	13	0.01786266	3.19736842	0.3127572
QLQX-16	Lithospermic acid	12	0.00961587	3.21052632	0.31147541
QLQX-8	Ginsenoside Rc	11	0.01141274	3.22368421	0.31020408
QLQX-4	Ginsenoside Rb_1	11	0.01141274	3.22368421	0.31020408
QLQX-9	Ginsenoside Rd	10	0.0092025	3.23684211	0.30894309
QLQX-6	Ginsenoside Rg_1	10	0.0092025	3.23684211	0.30894309
QLQX-5	Ginsenoside Rb_2	10	0.0092025	3.23684211	0.30894309
QLQX-12	Ginsenoside F_2	10	0.0092025	3.23684211	0.30894309
QLQX-11	Ginsenoside Rf	10	0.0092025	3.23684211	0.30894309
QLQX-10	Ginsenoside Re	10	0.0092025	3.23684211	0.30894309
QLQX-14	Salvianolic acid b	9	0.0045723	3.25	0.30769231
QLQX-19	Hydroxysafflor yellow a	7	0.01639755	3.09210526	0.32340426

blood vessels, might contributed to the pathogenesis of heart failure (Kishimoto et al., 2017). Previous study have suggested that Hcy could initiate mitochondrial dysfunction, which contributes to the cell apoptosis and chronic inflammation, thereby resulting in endothelial dysfunction (Han et al., 2015; Zhang et al., 2017). In this manuscript, the Hcy-induced HCMECs injury was used as the model to explore the role of QLQX in endothelial dysfunction of damaged microvascular endothelial cell. It has been shown that, captopril, as a positive control drug to treat HCMEC in our study, improves endothelium-dependent vasodilatation in patients with CHF (Drexler et al., 1995). Meanwhile, captopril can increase vascular endothelial growth factor (VEGFA) expression during the period of pathological angiogenesis and rarefaction and inhibit proinflammatory cytokine expression (IL-1β, IL-6, and IL-8) in cultured human coronary artery endothelial cells (Greene and Amaral, 2002; Haas et al., 2019). Studies have also reported that captopril exerted a cardioprotective effect on heart failure by inhibiting phosphorylation of JAK2/STAT3 (Zhang Y. et al., 2019).

We have shown that QLQX dramatically inhibited Hcy-induced injury on the HCMEC in a time-dependent manner as observed through MTT assays. Western blotting confirmed that QLQX significantly increased the ratio between *ADRB1* and *ADRB2*, upregulated the expression level of *VEGFA*, and downregulated the expression levels of *p-STAT3*, *p-JAK2*, and *IL-6* in Hcy-induced HCMEC. Evidence has shown that a reduction in the *ADRB1*/*ADRB2* ratio has been observed in heart failure, and the use of adrenoceptor beta blockers is a cornerstone of current heart failure therapy (Baker, 2014; Woo et al., 2015). Consistent with prior study, we validated the effect of QLQX on the expression of adrenoceptor beta, which showed the prediction power in network pharmacological analysis of our study. On this basis, CHF is defined by cardiac dysfunction associated with ventricular remodeling, and, more recently, an imbalance between angiogenesis and cardiac hypertrophy has increasingly been acknowledged as an additional contributing mechanism (Taimeh et al., 2013). Accordingly, the therapeutic effect of myocardial angiogenesis is emerging as a promising approach for the prevention and treatment of CHF (Vila et al., 2008; Oka et al., 2014). VEGFA, a cornerstone cytokine of angiogenesis, participates in the process of vascular remodeling and myocardial angiogenesis in CHF through maintenance and repair of luminal endothelium (Morine et al., 2016). Besides, increased expression of VEGFA levels has been associated with the process of angiogenesis, and it may be adopted as an indicator of revascularization (Kucukardali et al., 2008; Wang et al., 2017; Yan et al., 2019).

As shown in the present study, QLQX exerts a protective effect against IL-6 secretion induced by Hcy in the HCMEC, which may be associated with negative regulation of the Janus kinase signal transducer and signal transduction activator of transcription (JAK-STAT) signaling. Recent evidence has revealed that inflammation is a critical pathological process of CHF (Dick and Epelman, 2016; Ayoub et al., 2017; Cocco

TABLE 4 | The proteins interacting of hub targets.

Node 1	Interaction	Node 2	Score
VEGFA	pp	KDR	0.999
VEGFA	pp	FLT1	0.999
VEGFA	pp	NRP2	0.998
JAK2	pp	STAT3	0.998
EGFR	pp	STAT3	0.998
CYP1A1	pp	AHR	0.997
JAK1	pp	STAT3	0.997
ATP1A1	pp	ATP1B1	0.997
IL6	pp	STAT3	0.997
VEGFA	pp	HIF1A	0.996
VEGFA	pp	STAT3	0.994
NRP2	pp	FLT1	0.988
FLT1	pp	KDR	0.988
HIF1A	pp	STAT3	0.986
STAT4	pp	JAK2	0.984
NRP2	pp	KDR	0.983
STAT4	pp	JAK1	0.983
VEGFA	pp	EGFR	0.979
IL6	pp	JAK2	0.975
HIF1A	pp	EGFR	0.973
IL6	pp	JAK1	0.968
JAK1	pp	EGFR	0.966
VEGFA	pp	IL6	0.959
JAK2	pp	JAK1	0.943
STAT4	pp	STAT3	0.938
JAK2	pp	EGFR	0.928
CYP1A1	pp	CYP2B6	0.928
IL6	pp	EGFR	0.921

et al., 2017) and high levels of IL-6, a proinflammatory cytokine, have been reported to be an important mediator in chronic inflammatory and cardiovascular disorders (Smart et al., 2006; Bacchiega et al., 2017). Moreover, IL-6 exerts its action through a specific IL-6R and a soluble IL-6 receptor, whereby the IL-6/IL-6R complex binds to the membrane glycoprotein 130 to induce intracellular signaling pathways (Hirota et al., 2004; Ptaszynska-Kopczynska et al., 2017). The JAK-STAT pathway is a characteristic signal transduction pathway that plays a crucial role in this process (Mohri et al., 2012). Specifically, the activated JAK2, a key member of the Janus family of kinases, leads to phosphorylation and activation of a group of transcription factors collectively called STATs. Among them, STAT3 also appears to be involved in a broad range of cytoprotection activities, such as inflammation, angiogenesis, extracellular matrix composition, and apoptosis in the heart (Shen-Orr et al., 2016). Previous study has implicated astragaloside could improve vascular endothelial dysfunction induced by hyperglycemia by increasing eNOS expression and decreasing the content of IL-6 (Leng et al., 2018). Evidence provided by Jiang et al. (2015) showed calycosin protected vascular endothelial from LPS-induced endothelial injury through suppression of ROS and VEGFA level. Furthermore, it has been reported that salvianolic acid A inhibited endothelial dysfunction and vascular remodeling in spontaneously hypertensive rats (Teng et al., 2016). All these mentioned above suggest that some compounds in QLQX exerts a protective effect on vascular endothelial, which in another way could support the results in our study.

Therefore, we focused on the inflammation in the HCMEC, as we were interested in the role of the JAK/STAT signaling in the pathogenesis of QLQX against CHF. Inflammatory processes and angiogenesis may be interrelated during the process of CHF, and the angiogenesis factor promotes angiogenesis mainly through signaling pathways, of which JAK2-STAT3 is one of the important ones (Fujio et al., 2011). It was reported that inflammation and neovascularization in atheromatous plaques might be mediated by VEGFA (Moulton et al., 2003), and the antihuman IL-6 receptor monoclonal antibody was shown to improve endothelial function in patients with acute coronary syndromes (Holte et al., 2017). Thus, QLQX can rectify the injury of microvascular endothelial cells induced by Hcy while significantly decreasing the levels of *IL-6*, *p-JAK2*, and *p-STAT3*, which suggests that QLQX may inhibit inflammatory processes and promote angiogenesis in CHF *via* the JAK/STAT signaling pathway.

TABLE 5 | The topological parameters of PPI network.

Genes/proteins	Degree	Betweenness centrality	Average shortest path length	Closeness centrality
VEGFA	7	0.47407407	1.3	0.76923077
STAT3	7	0.21481481	1.3	0.76923077
EGFR	6	0.08888889	1.4	0.71428571
JAK2	5	0.01481481	1.8	0.55555556
JAK1	5	0.01481481	1.8	0.55555556
IL6	5	0.05925926	1.5	0.66666667
KDR	3	0	2	0.5
FLT1	3	0	2	0.5
NRP2	3	0	2	0.5
HIF1A	3	0	1.7	0.58823529
STAT4	3	0	2	0.5
CYP1A1	2	1	1	1
AHR	1	0	1.5	0.66666667
ATP1A1	1	0	1	1
ATP1B1	1	0	1	1
CYP2B6	1	0	1.5	0.66666667

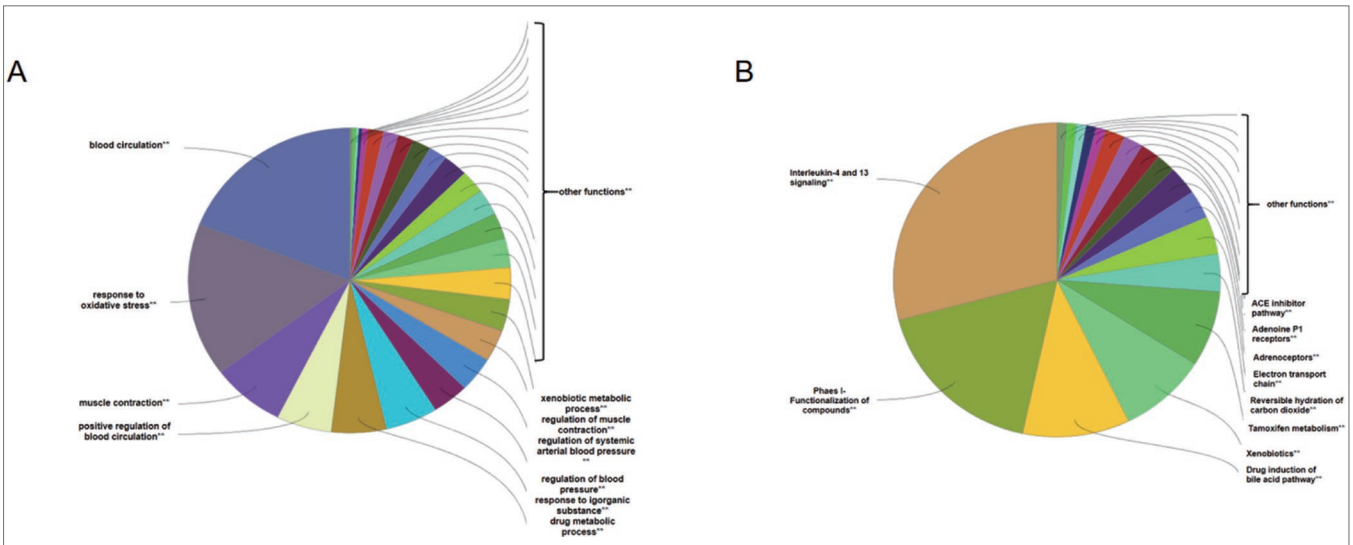


FIGURE 4 | ClueGO analysis of the candidate targets. **(A)** Representative biological process among 120 candidate targets. **(B)** Representative reactome and Wiki pathway analysis amng 120 candidate targets. Only top ten concerned biological processes and pathways were shown in figures.

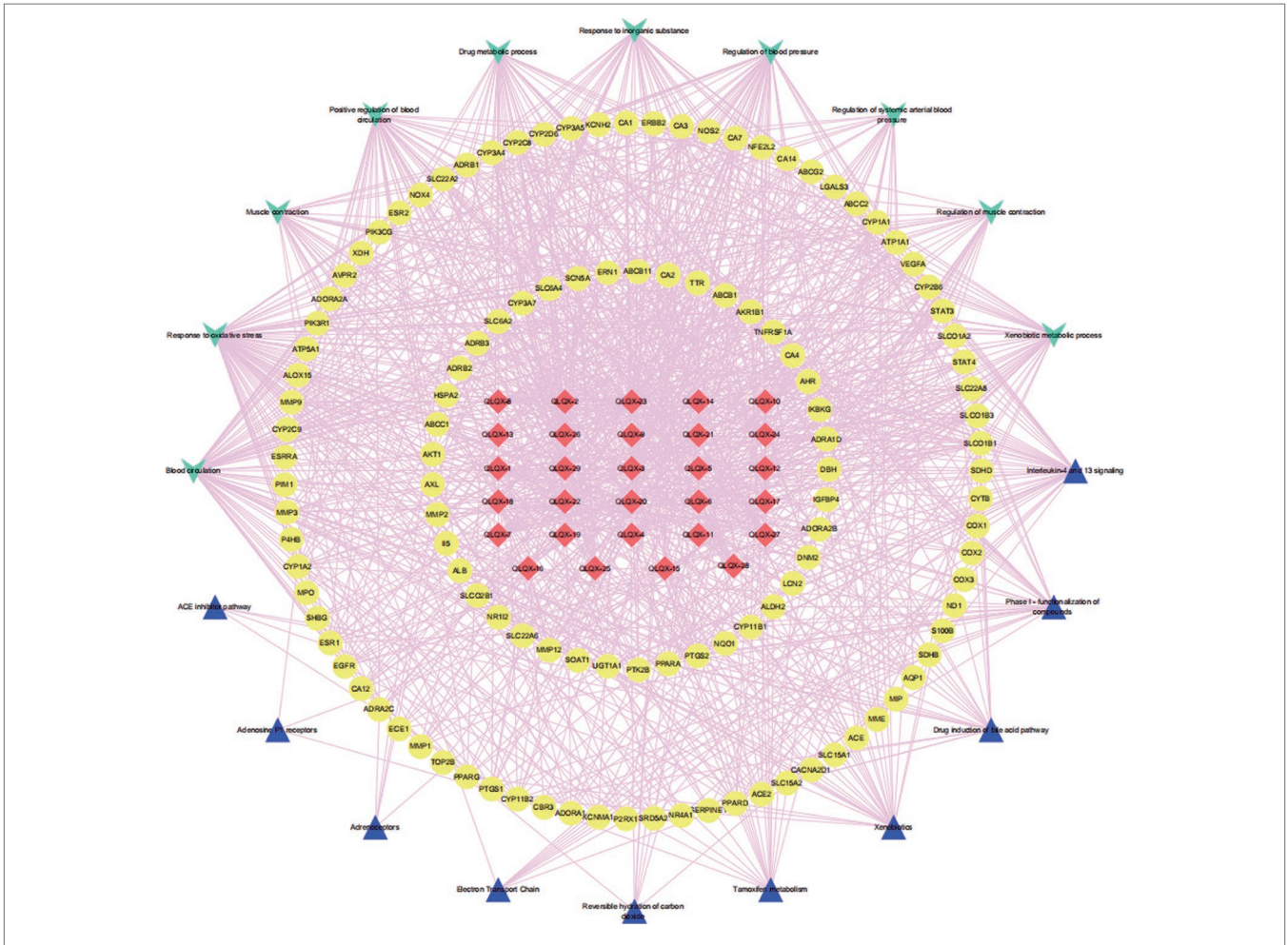


FIGURE 5 | The component-target-pathway/biological process network. The red diamond nodes represent the 29 active components in QLQX, the yellow ellipse nodes represent 120 putative targets associated with QLQX in the treatment of CHF, the wathet V nodes represent top ten biological processes and the mazarine triangle nodes represent top ten pathways related the 20 putative.

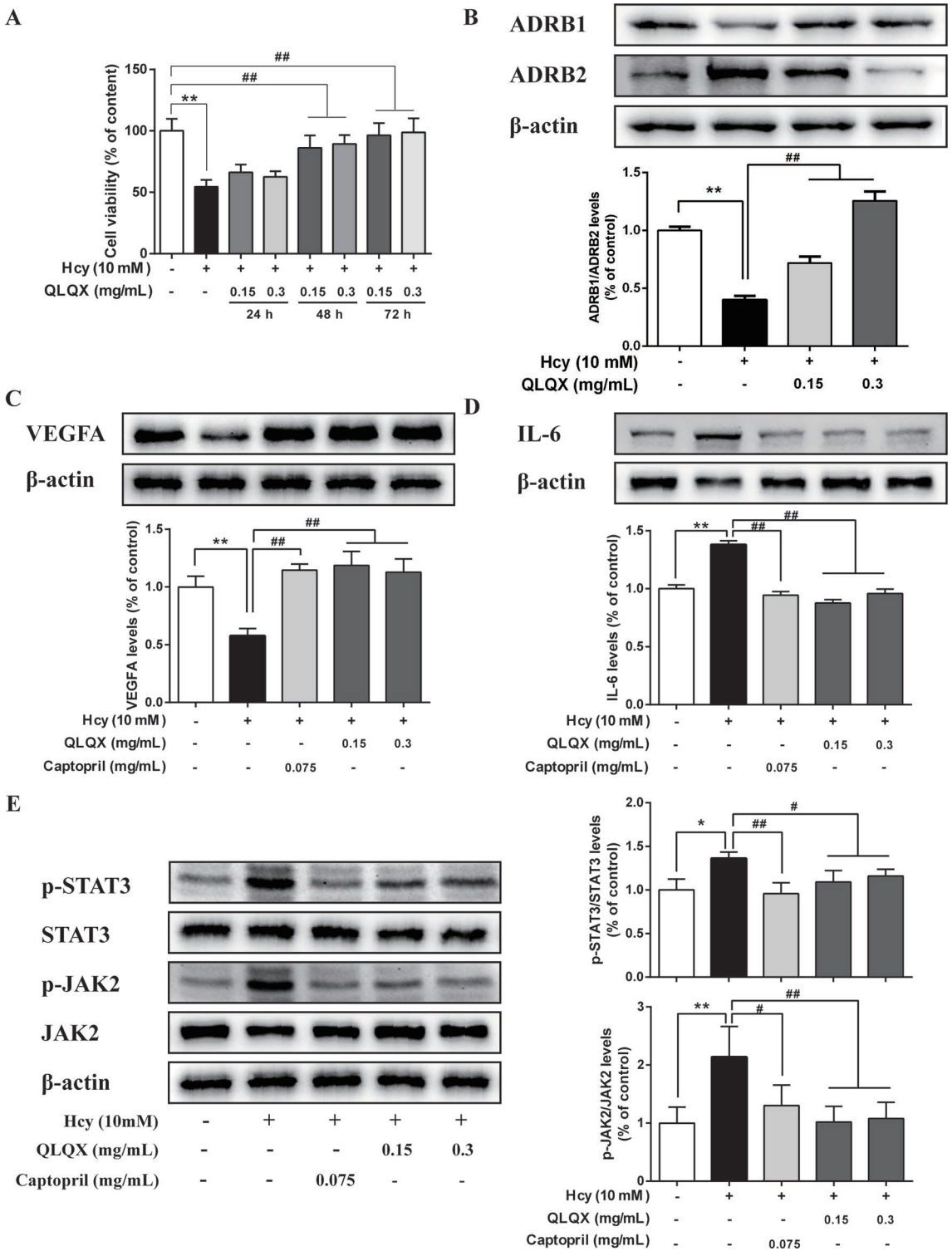


FIGURE 6 | Experimental validation of key targets and pathway in HCMEC. **(A)** Effect of QLQX treatment on Hcy-induced HCMEC cell viability. HCMECs were treated with 0.15 mg/mL and 0.3 mg/mL QLQX for 24, 48, and 72 h, after then cells were treated with Hcy for 24 h. The cell viability was determined using the MTT assay. **(B)** Effect of QLQX treatment on Hcy-induced *ADRB1/Anti-ADRB2* ratio in HCMEC. **(C)** Effect of QLQX and captopril treatment on Hcy-induced *VEGFA* expression in HCMEC. **(D)** Effect of QLQX and captopril treatment on Hcy-induced *IL-6* expression in HCMEC. **(E)** Effect of QLQX and captopril treatment on Hcy-induced phosphorylation of STAT3/JAK2 signaling pathway. HCMECs were treated with 0.075 mg/mL, 0.3 mg/mL QLQX for 48 h and exposed to 10 mM Hcy for a further 24 h. The levels of *VEGFA, IL-6, p-STAT3,* and *p-JAK2* expression were determined by western blot. Data were presented as mean SD of three independent experiments. $^{*}p < 0.05$ or $^{**}p < 0.01$ compared with the Hcy-untreated control. $^{\#}p < 0.05$ or $^{\#\#}p < 0.01$ compared with the Hcy-treated control.

CONCLUSION

In the current study, an integrated strategy was used to illustrate the active ingredients and molecular mechanisms of QLQX in the treatment of CHF by adopting pharmacokinetics study, network pharmacological analysis, and experimental validation. In total, 29 ingredients determined by pharmacokinetics study, instead of herb databases, were used for network pharmacology analysis. Through experimental validation of the hub targets (*VEGFA*, *IL-6*, *p-STAT3*, and *p-JAK2*), the JAK/STAT signaling pathway was identified as the mechanism of QLQX against inflammatory process in CHF. Additionally, the established C–T–P network remained a characteristic of multilink and multilevel comprehensive effects of QLQX. These results provided an efficient way to understand the pharmacological mechanisms of traditional Chinese medicine prescriptions.

DATA AVAILABILITY

The data used to support the findings of this study are available from the corresponding author upon request.

ETHICS STATEMENT

The animal study was reviewed and approved by the Ethics Committee of Tianjin University of Traditional Chinese Medicine (Tianjin, China). This study was carried out in accordance with the principles of the Basel Declaration and recommendations of guidelines of the National Institutes of Health.

AUTHOR CONTRIBUTIONS

YZ is the first author and performed all the experiments and drafted the manuscript. MZ revised the manuscript. FZ and SZ helped the first author and prepared the materials of this paper. WD and XX contributed toward study design, experimental setup, results supervision, and manuscript correction.

FUNDING

This work was supported by the National Natural Science Foundation of China (81774227), Natural Science Fund of Tianjin City (17JCZDJC34600), Project of TCM and combining TCM and western medicine of Tianjin Health and Family Planning Committee (2015050), and Technology program in key areas of Tianjin (20190101).

ACKNOWLEDGMENTS

The authors would like to acknowledge the technical supports to Yan Wang from Tianjin University of Traditional Chinese Medicine.

SUPPLEMENTARY MATERIAL

The Supplementary Material for this article can be found online at: https://www.frontiersin.org/articles/10.3389/fphar.2019.01046/full#supplementary-material

REFERENCES

Assenov, Y., Ramirez, F., Schelhorn, S. E., Lengauer, T., and Albrecht, M. (2008). Computing topological parameters of biological networks. *Bioinformatics* 24, 282–284. doi: 10.1093/bioinformatics/btm554

Ayoub, K. F., Pothineni, N., Rutland, J., Ding, Z., and Mehta, J. L. (2017). Immunity, inflammation, and oxidative stress in heart failure: emerging molecular targets. *Cardiovasc. Drugs Ther.* 31, 593–608. doi: 10.1007/s10557-017-6752-z

Bacchiega, B. C., Bacchiega, A. B., Usnayo, M. J., Bedirian, R., Singh, G., and Pinheiro, G. D. (2017). Interleukin 6 inhibition and coronary artery disease in a high-risk population: a prospective community-based clinical study. *J. Am. Heart Assoc.* 6, e005038. doi: 10.1161/JAHA.116.005038

Bader, G. D., and Hogue, C. W. (2003). An automated method for finding molecular complexes in large protein interaction networks. *BMC Bioinf.* 4, 2. doi: 10.1186/1471-2105-4-2

Baker, A. J. (2014). Adrenergic signaling in heart failure: a balance of toxic and protective effects. *Pflugers Arch.* 466, 1139–1150. doi: 10.1007/s00424-014-1491-5

Chao, J., Dai, Y., Verpoorte, R., Lam, W., Cheng, Y. C., Pao, L. H., et al. (2017). Major achievements of evidence-based traditional Chinese medicine in treating major diseases. *Biochem. Pharmacol.* 139, 94–104. doi: 10.1016/j.bcp.2017.06.123

Chen, F., Wu, J. L., Fu, G. S., Mou, Y., and Hu, S. J. (2015). Chronic treatment with Qiliqiangxin ameliorates aortic endothelial cell dysfunction in diabetic rats. *J. Cardiovasc. Pharmacol. Ther.* 20, 230–240. doi: 10.1177/1074248414537705

Cocco, G., Jerie, P., Amiet, P., and Pandolfi, S. (2017). Inflammation in heart failure: known knowns and unknown unknowns. *Expert Opin. Pharmacother.* 18, 1225–1233. doi: 10.1080/14656566.2017.1351948

Den Uil, C. A., Klijn, E., Lagrand, W. K., Brugts, J. J., Ince, C., Spronk, P. E., et al. (2008). The microcirculation in health and critical disease. *Prog. Cardiovasc. Dis.* 51, 161–170. doi: 10.1016/j.pcad.2008.07.002

Dick, S. A., and Epelman, S. (2016). Chronic heart failure and inflammation: what do we really know? *Circ. Res.* 119, 159–176. doi: 10.1161/CIRCRESAHA.116.308030

Doughty, R. N., and Sharpe, N. (1997). Beta-adrenergic blocking agents in the treatment of congestive heart failure: mechanisms and clinical results. *Annu. Rev. Med.* 48, 103–114. doi: 10.1146/annurev.med.48.1.103

Drexler, H., Kurz, S., Jeserich, M., Munzel, T., and Hornig, B. (1995). Effect of chronic angiotensin-converting enzyme inhibition on endothelial function in patients with chronic heart failure. *Am. J. Cardiol.* 76, 13E–18E. doi: 10.1016/S0002-9149(99)80497-4

Engin, H. B., Gursoy, A., Nussinov, R., and Keskin, O. (2014). Network-based strategies can help mono- and poly-pharmacology drug discovery: a systems biology view. *Curr. Pharm. Des.* 20, 1201–1207. doi: 10.2174/13816128113199990066

Fujio, Y., Maeda, M., Mohri, T., Obana, M., Iwakura, T., Hayama, A., et al. (2011). Glycoprotein 130 cytokine signal as a therapeutic target against cardiovascular diseases. *J. Pharmacol. Sci.* 117, 213–222. doi: 10.1254/jphs.11R05CR

Fung, F. Y., and Linn, Y. C. (2015). Developing traditional Chinese medicine in the era of evidence-based medicine: current evidences and challenges. *Evid. Based Complement Altern. Med.* 2015, 425037. doi: 10.1155/2015/425037

Gao, L., Wang, K. X., Zhou, Y. Z., Fang, J. S., Qin, X. M., and Du, G. H. (2018). Uncovering the anticancer mechanism of compound Kushen injection against HCC by integrating quantitative analysis, network analysis and experimental validation. *Sci. Rep.* 8, 624. doi: 10.1038/s41598-017-18325-7

Gao, L., Wang, X. D., Niu, Y. Y., Duan, D. D., Yang, X., Hao, J., et al. (2016). Molecular targets of Chinese herbs: a clinical study of hepatoma based on network pharmacology. *Sci. Rep.* 6, 24944. doi: 10.1038/srep24944

Gedela, M., Khan, M., and Jonsson, O. (2015). Heart Failure. *S D Med* 68, 403-405, 407-409. doi: 10.1056/NEJMra021498

Greene, A. S., and Amaral, S. L. (2002). Microvascular angiogenesis and the renin–angiotensin system. *Curr. Hypertens. Rep.* 4, 56–62. doi: 10.1007/s11906-002-0054-x

Haas, M. J., Jurado-Flores, M., Hammoud, R., Feng, V., Gonzales, K., Onstead-Haas, L., et al. (2019). The effects of known cardioprotective drugs on proinflammatory cytokine secretion from human coronary artery endothelial cells. *Am. J. Ther.* 26, e321–e332. doi: 10.1097/MJT.0000000000000648

Han, S., Wu, H., Li, W., and Gao, P. (2015). Protective effects of genistein in homocysteine-induced endothelial cell inflammatory injury. *Mol. Cell. Biochem.* 403, 43–49. doi: 10.1007/s11010-015-2335-0

Heinonen, I., Sorop, O., de Beer, V. J., Duncker, D. J., and Merkus, D. (2015). What can we learn about treating heart failure from the heart's response to acute exercise? Focus on the coronary microcirculation. *J. Appl. Physiol. (1985)* 119, 934–943. doi: 10.1152/japplphysiol.00053.2015

Hirota, H., Izumi, M., Hamaguchi, T., Sugiyama, S., Murakami, E., Kunisada, K., et al. (2004). Circulating interleukin-6 family cytokines and their receptors in patients with congestive heart failure. *Heart Vessels* 19, 237–241. doi: 10.1007/s00380-004-0770-z

Holte, E., Kleveland, O., Ueland, T., Kunszt, G., Bratlie, M., Broch, K., et al. (2017). Effect of interleukin-6 inhibition on coronary microvascular and endothelial function in myocardial infarction. *Heart* 103, 1521–1527. doi: 10.1136/heartjnl-2016-310875

Huang, P., Ke, H., Qiu, Y., Cai, M., Qu, J., and Leng, A. (2019). Systematically characterizing chemical profile and potential mechanisms of Qingre Lidan decoction acting on cholelithiasis by integrating UHPLC-QTOF-MS and network target analysis. *Evid. Based Complement Altern. Med.* 2019, 2675287. doi: 10.1155/2019/2675287

Jiang, Y. H., Sun, W., Li, W., Hu, H. Z., Zhou, L., Jiang, H. H., et al. (2015). Calycosin-7-O-beta-D-glucoside promotes oxidative stress-induced cytoskeleton reorganization through integrin-linked kinase signaling pathway in vascular endothelial cells. *BMC Complement Altern. Med.* 15, 315. doi: 10.1186/s12906-015-0839-5

Kishimoto, S., Kajikawa, M., Maruhashi, T., Iwamoto, Y., Matsumoto, T., Iwamoto, A., et al. (2017). Endothelial dysfunction and abnormal vascular structure are simultaneously present in patients with heart failure with preserved ejection fraction. *Int. J. Cardiol.* 231, 181–187. doi: 10.1016/j.ijcard.2017.01.024

Kucukardali, Y., Aydogdu, S., Ozmen, N., Yonem, A., Solmazgul, E., Ozyurt, M., et al. (2008). The relationship between severity of coronary artery disease and plasma level of vascular endothelial growth factor. *Cardiovasc. Revasc. Med.* 9, 66–70. doi: 10.1016/j.carrev.2007.11.005

Leng, B., Tang, F., Lu, M., Zhang, Z., Wang, H., and Zhang, Y. (2018). Astragaloside IV improves vascular endothelial dysfunction by inhibiting the TLR4/NF-kappaB signaling pathway. *Life Sci.* 209, 111–121. doi: 10.1016/j.lfs.2018.07.053

Li, S., and Zhang, B. (2013). Traditional Chinese medicine network pharmacology: theory, methodology and application. *Chin. J. Nat. Med.* 11, 110–120. doi: 10.1016/S1875-5364(13)60037-0

Li, X., Zhang, J., Huang, J., Ma, A., Yang, J., Li, W., et al. (2013). A multicenter, randomized, double-blind, parallel-group, placebo-controlled study of the effects of qili qiangxin capsules in patients with chronic heart failure. *J. Am. Coll. Cardiol.* 62, 1065–1072. doi: 10.1016/j.jacc.2013.05.035

Li, Y., Wang, Y., Tai, W., Yang, L., Chen, Y., Chen, C., et al. (2015). Challenges and solutions of pharmacokinetics for efficacy and safety of traditional Chinese medicine. *Curr. Drug Metab.* 16, 765–776. doi: 10.2174/1389200216091512011114223

Liu, X. X., Jian, X. X., Cai, X. F., Chao, R. B., Chen, Q. H., Chen, D. L., et al. (2012). Cardioactive C(1)(9)-diterpenoid alkaloids from the lateral roots of *Aconitum carmichaeli* "Fu Zi". *Chem. Pharm. Bull. (Tokyo)* 60, 144–149. doi: 10.1248/cpb.60.144

Mattera, R., Benvenuto, M., Giganti, M.G., Tresoldi, I., Pluchinotta, F.R., Bergante, S., et al. (2017). Effects of polyphenols on oxidative stress-mediated injury in cardiomyocytes. *Nutrients* 9, 523. doi: 10.3390/nu9050523

Mi, N., Cheng, T., Li, H., Yang, P., Mu, X., Wang, X., et al. (2019). Metabolite profiling of traditional Chinese medicine formula Dan Zhi Tablet: an integrated strategy based on UPLC-QTOF/MS combined with multivariate statistical analysis. *J. Pharm. Biomed. Anal.* 164, 70–85. doi: 10.1016/j.jpba.2018.10.024

Mohri, T., Iwakura, T., Nakayama, H., and Fujio, Y. (2012). JAK-STAT signaling in cardiomyogenesis of cardiac stem cells. *JAKSTAT* 1, 125–130. doi: 10.4161/jkst.20296

Morine, K. J., Paruchuri, V., Qiao, X., Mohammad, N., Mcgraw, A., Yunis, A., et al. (2016). Circulating multimarker profile of patients with symptomatic heart failure supports enhanced fibrotic degradation and decreased angiogenesis. *Biomarkers* 21, 91–97. doi: 10.3109/1354750X.2015.1118539

Moulton, K. S., Vakili, K., Zurakowski, D., Soliman, M., Butterfield, C., Sylvin, E., et al. (2003). Inhibition of plaque neovascularization reduces macrophage accumulation and progression of advanced atherosclerosis. *Proc. Natl. Acad. Sci. U. S. A.* 100, 4736–4741. doi: 10.1073/pnas.0730843100

Ning, Z., Wang, C., Liu, Y., Song, Z., Ma, X., Liang, D., et al. (2018). Integrating strategies of herbal metabolomics, network pharmacology, and experiment validation to investigate frankincense processing effects. *Front. Pharmacol.* 9, 1482. doi: 10.3389/fphar.2018.01482

Oka, T., Akazawa, H., Naito, A. T., and Komuro, I. (2014). Angiogenesis and cardiac hypertrophy: maintenance of cardiac function and causative roles in heart failure. *Circ. Res.* 114, 565–571. doi: 10.1161/CIRCRESAHA.114.300507

Park, S. Y., Park, J. H., Kim, H. S., Lee, C. Y., Lee, H. J., Kang, K. S., et al. (2018). Systems-level mechanisms of action of *Panax ginseng*: a network pharmacological approach. *J. Ginseng Res.* 42, 98–106. doi: 10.1016/j.jgr.2017.09.001

Ptaszynska-Kopczynska, K., Szpakowicz, A., Marcinkiewicz-Siemion, M., Lisowska, A., Waszkiewicz, E., Witkowski, M., et al. (2017). Interleukin-6 signaling in patients with chronic heart failure treated with cardiac resynchronization therapy. *Arch. Med. Sci.* 13, 1069–1077. doi: 10.5114/aoms.2016.58635

Qi, Y., Gao, F., Hou, L., and Wan, C. (2017). Anti-inflammatory and immunostimulatory activities of astragalosides. *Am. J. Chin. Med.* 45, 1157–1167. doi: 10.1142/S0192415X1750063X

Rubinov, M., and Sporns, O. (2010). Complex network measures of brain connectivity: uses and interpretations. *Neuroimage* 52, 1059–1069. doi: 10.1016/j.neuroimage.2009.10.003

Shen-Orr, S. S., Furman, D., Kidd, B. A., Hadad, F., Lovelace, P., Huang, Y. W., et al. (2016). Defective signaling in the JAK-STAT pathway tracks with chronic inflammation and cardiovascular risk in aging humans. *Cell Syst.* 3, 374–384. e4. doi: 10.1016/j.cels.2016.09.009

Smart, N., Mojet, M. H., Latchman, D. S., Marber, M. S., Duchen, M. R., and Heads, R. J. (2006). IL-6 induces PI3-kinase and nitric oxide-dependent protection and preserves mitochondrial function in cardiomyocytes. *Cardiovasc. Res.* 69, 164–177. doi: 10.1016/j.cardiores.2005.08.017

Smoot, M. E., Ono, K., Ruscheinski, J., Wang, P. L., and Ideker, T. (2011). Cytoscape 2.8: new features for data integration and network visualization. *Bioinformatics* 27, 431–432. doi: 10.1093/bioinformatics/btq675

Spadari, R. C., Cavadas, C., de Carvalho, A., Ortolani, D., de Moura, A. L., and Vassalo, P. F. (2018). Role of beta-adrenergic receptors and sirtuin signaling in the heart during aging, heart failure, and adaptation to stress. *Cell. Mol. Neurobiol.* 38, 109–120. doi: 10.1007/s10571-017-0557-2

Sun, J., Zhang, K., Xiong, W. J., Yang, G. Y., Zhang, Y. J., Wang, C. C., et al. (2016). Clinical effects of a standardized Chinese herbal remedy, Qili Qiangxin, as an adjuvant treatment in heart failure: systematic review and meta-analysis. *BMC Complement Altern. Med.* 16, 201. doi: 10.1186/s12906-016-1174-1

Sun, Y., Liu, Y., and Chen, K. (2016). Roles and mechanisms of ginsenoside in cardiovascular diseases: progress and perspectives. *Sci. China Life Sci.* 59, 292–298. doi: 10.1007/s11427-016-5007-8

Taimeh, Z., Loughran, J., Birks, E.J., and Bolli, R. (2013). Vascular endothelial growth factor in heart failure. *Nat. Rev. Cardiol.* 10, 519-530. doi: 10.1038/nrcardio.2013.94

Tanai, E., and Frantz, S. (2015). Pathophysiology of heart failure. Compr. Physiol. 6, 187–214. doi: 10.1002/cphy.c140055

Tang, W., and Huang, Y. (2013). Cardiotonic modulation in heart failure: insights from traditional Chinese medicine. *J. Am. Coll. Cardiol.* 62, 1073–1074. doi: 10.1016/j.jacc.2013.05.028

Teng, F., Yin, Y., Cui, Y., Deng, Y., Li, D., Cho, K., et al. (2016). Salvianolic acid A inhibits endothelial dysfunction and vascular remodeling in spontaneously hypertensive rats. *Life Sci.* 144, 86–93. doi: 10.1016/j.lfs.2015.06.010

Tingting, H., Guangzhong, L., Yanxiang, Z., DongDong, Y., Li, S., and Li, W. (2019). Qiliqiangxin attenuates atrial structural remodeling in prolonged pacing-induced atrial fibrillation in rabbits. *Naunyn. Schmiedebergs Arch. Pharmacol.* 392, 585-592. doi: 10.1007/s00210-018-01611-0

Vila, V., Martinez-Sales, V., Almenar, L., Lazaro, I. S., Villa, P., and Reganon, E. (2008). Inflammation, endothelial dysfunction and angiogenesis markers in chronic heart failure patients. *Int. J. Cardiol.* 130, 276–277. doi: 10.1016/j.ijcard.2007.07.010

Wang, Y., Huang, Q., Liu, J., Wang, Y., Zheng, G., Lin, L., et al. (2017). Vascular endothelial growth factor A polymorphisms are associated with increased risk of coronary heart disease: a meta-analysis. *Oncotarget* 8, 30539–30551. doi: 10.18632/oncotarget.15546

Woo, A. Y., Song, Y., Xiao, R. P., and Zhu, W. (2015). Biased beta2-adrenoceptor signalling in heart failure: pathophysiology and drug discovery. *Br. J. Pharmacol.* 172, 5444–5456. doi: 10.1111/bph.12965

Xing, X., Chen, S., Li, L., Cao, Y., Chen, L., Wang, X., et al. (2018). The active components of Fuzheng Huayu Formula and their potential mechanism of action in inhibiting the hepatic stellate cells viability—a network pharmacology and transcriptomics approach. *Front. Pharmacol.* 9, 525. doi: 10.3389/fphar.2018.00525

Yan, P., Sun, C., Ma, J., Jin, Z., Guo, R., and Yang, B. (2019). MicroRNA-128 confers protection against cardiac microvascular endothelial cell injury in coronary heart disease via negative regulation of IRS1. *J. Cell. Physiol.* 8, 13452-13463. doi: 10.1002/jcp.28025

Yu, L. J., Zhang, K. J., Zhu, J. Z., Zheng, Q., Bao, X. Y., Thapa, S., et al. (2017). Salvianolic acid exerts cardioprotection through promoting angiogenesis in animal models of acute myocardial infarction: preclinical evidence. *Oxid. Med. Cell. Longev.* 2017, 8192383. doi: 10.1155/2017/8192383

Yuan, H., Ma, Q., Cui, H., Liu, G., Zhao, X., Li, W., et al. (2017). How can synergism of traditional medicines benefit from network pharmacology? *Molecules* 22, 1135. doi: 10.3390/molecules22071135

Yun, W. J., Yao, Z. H., Fan, C. L., Qin, Z. F., Tang, X. Y., Gao, M. X., et al. (2018). Systematic screening and characterization of Qi-Li-Qiang-Xin capsule-related xenobiotics in rats by ultra-performance liquid chromatography coupled with quadrupole time-of-flight tandem mass spectrometry. *J. Chromatogr. B. Analyt. Technol. Biomed. Life Sci.* 1090, 56–64. doi: 10.1016/j.jchromb.2018.05.014

Zhang, F., Zhang, Y., Li, X., Zhang, S., Zhu, M., Du, W., et al. (2018). Research on Q-markers of Qiliqiangxin capsule for chronic heart failure treatment based on pharmacokinetics and pharmacodynamics association. *Phytomedicine* 44, 220–230. doi: 10.1016/j.phymed.2018.03.003

Zhang, J., Wei, C., Wang, H., Tang, S., Jia, Z., Wang, L., et al. (2013). Protective effect of Qiliqiangxin capsule on energy metabolism and myocardial mitochondria in pressure overload heart failure rats. *Evid. Based Complement Altern. Med.* 2013, 378298. doi: 10.1155/2013/378298

Zhang, J. H., Zhu, Y., Fan, X. H., and Zhang, B. L. (2015). Efficacy-oriented compatibility for component-based Chinese medicine. *Acta Pharmacol. Sin.* 36, 654–658. doi: 10.1038/aps.2015.8

Zhang, R., Zhu, X., Bai, H., and Ning, K. (2019). Network pharmacology databases for traditional Chinese medicine: review and assessment. *Front. Pharmacol.* 10, 123. doi: 10.3389/fphar.2019.00123

Zhang, Y., Zhang, L., Fan, X., Yang, W., Yu, B., Kou, J., et al. (2019). Captopril attenuates TAC-induced heart failure *via* inhibiting wnt3a/beta-catenin and Jak2/Stat3 pathways. *Biomed. Pharmacother.* 113, 108780. doi: 10.1016/j. biopha.2019.108780

Zhang, Z., Wei, C., Zhou, Y., Yan, T., Wang, Z., Li, W., et al. (2017). Homocysteine induces apoptosis of human umbilical vein endothelial cells *via* mitochondrial dysfunction and endoplasmic reticulum stress. *Oxid. Med. Cell. Longev.* 2017, 5736506. doi: 10.1155/2017/5736506

Zhou, X., Li, C.G., Chang, D., and Bensoussan, A. (2019). Current status and major challenges to the safety and efficacy presented by Chinese herbal medicine. *Medicines (Basel)* 6, 14. doi: 10.3390/medicines6010014

Conflict of Interest Statement: The authors declare that the research was conducted in the absence of any commercial or financial relationships that could be construed as a potential conflict of interest.

Copyright © 2019 Zhang, Zhu, Zhang, Zhang, Du and Xiao. This is an open-access article distributed under the terms of the Creative Commons Attribution License (CC BY). The use, distribution or reproduction in other forums is permitted, provided the original author(s) and the copyright owner(s) are credited and that the original publication in this journal is cited, in accordance with accepted academic practice. No use, distribution or reproduction is permitted which does not comply with these terms.

frontiers in Physiology

ORIGINAL RESEARCH
published: 01 October 2019
doi: 10.3389/fphys.2019.01246

YangXue QingNao Wan, a Compound Chinese Medicine, Attenuates Cerebrovascular Hyperpermeability and Neuron Injury in Spontaneously Hypertensive Rat: Effect and Mechanism

Ying-Qian Jiao[1,2,3,4,5,6], Ping Huang[2,3,4,5,6], Li Yan[2,3,4,5,6], Kai Sun[2,3,4,5,6], Chun-Shui Pan[2,3,4,5,6], Quan Li[2,3,4,5,6], Jing-Yu Fan[2,6], Zhi-Zhong Ma[1,3,4,5,6] and Jing-Yan Han[1,2,3,4,5,6]**

[1] Department of Integration of Chinese and Western Medicine, School of Basic Medical Sciences, Peking University, Beijing, China, [2] Tasly Microcirculation Research Center, Peking University Health Science Center, Beijing, China, [3] Key Laboratory of Stasis and Phlegm, State Administration of Traditional Chinese Medicine of the People's Republic of China, Beijing, China, [4] Academy of Integration of Chinese and Western Medicine, Peking University Health Science Center, Beijing, China, [5] Key Laboratory of Microcirculation, State Administration of Traditional Chinese Medicine of the People's Republic of China, Beijing, China, [6] State Key Laboratory of Core Technology in Innovative Chinese Medicine, Beijing, China

OPEN ACCESS

Edited by:
Antonio Colantuoni,
University of Naples Federico II, Italy

Reviewed by:
Giovanna Zoccoli,
University of Bologna, Italy
Andrea Moriondo,
University of Insubria, Italy
Dominga Lapi,
University of Pisa, Italy

***Correspondence:**
Zhi-Zhong Ma
zhma@bjmu.edu.cn
Jing-Yan Han
hanjingyan@bjmu.edu.cn

Specialty section:
This article was submitted to Vascular Physiology, a section of the journal Frontiers in Physiology

Received: 28 May 2019
Accepted: 12 September 2019
Published: 01 October 2019

Citation:
Jiao Y-Q, Huang P, Yan L, Sun K, Pan C-S, Li Q, Fan J-Y, Ma Z-Z and Han J-Y (2019) YangXue QingNao Wan, a Compound Chinese Medicine, Attenuates Cerebrovascular Hyperpermeability and Neuron Injury in Spontaneously Hypertensive Rat: Effect and Mechanism. Front. Physiol. 10:1246. doi: 10.3389/fphys.2019.01246

Objective: The purpose of the study was to explore the effect of YangXue QingNao Wan (YXQNW), a compound Chinese medicine, on cerebrovascular hyperpermeability, neuronal injury, and related mechanisms in spontaneously hypertensive rat (SHR).

Methods: Fourteen-week-old male SHR were used, with Wistar Kyoto (WKY) rats as control. YXQNW (0.5 g/kg/day), enalapril (EN, 8 mg/kg/day), and nifedipine (NF, 7.1 mg/kg/day) were administrated orally for 4 weeks. To assess the effects of the YXQNW on blood pressure, the systolic blood pressure (SBP), diastolic blood pressure (DBP), and mean blood pressure (MBP) were measured. After administering the drugs for 4 weeks, the cerebral blood flow (CBF), albumin leakage from microvessels in middle cerebral artery (MCA)-dominated area, and the number and morphology of microvessels were assessed in the hippocampus area and cortex. Neuronal damage and apoptosis were assessed by Nissl staining and TUNEL staining. To assess the mechanisms of cerebrovascular hyperpermeability, we performed immunofluorescence and Western blot to assess the expression and integrity of cerebral microvascular tight junction (TJ) and caveolin-1 (Cav-1) in cortex. Energy metabolism and Src-MLC-MLCK pathway in cortex were assessed then for elucidating the underlying mechanism of the observed effect of YXQNW.

Results: Spontaneously hypertensive rat exhibited higher blood pressure, Evans blue (EB) extravasation, albumin leakage, increased brain water content, decreased CBF, perivascular edema, and neuronal apoptosis in the hippocampus and cortex, all of which were attenuated by YXQNW treatment. YXQNW inhibited the downregulation of TJ proteins, mitochondrial Complex I, Complex II, and Complex V, and upregulation

of caveolin-1, inhibiting Src/MLCK/MLC signaling in SHR. YXQNW combined with EN + NF revealed a better effect for some outcomes compared with either YXQNW or EN + NF alone.

Conclusion: The overall result shows the potential of YXQNW to attenuate blood–brain barrier (BBB) breakdown in SHR, which involves regulation of energy metabolism and Src/MLCK/MLC signaling. This result provides evidence supporting the application of YXQNW as an adjuvant management for hypertensive patients to prevent hypertensive encephalopathy.

Keywords: hypertension, tight junction, caveolin-1, blood–brain barrier, ATP, microvessel

INTRODUCTION

Hypertension affects approximately 1.0 billion people in the world, with an incidence close to 30% (Marwick et al., 2015), which is a major risk factor for vascular diseases including coronary artery disease, congestive heart failure, stroke, end-stage renal disease, and peripheral vascular disease (Go et al., 2014).

The constriction or sclerosis of arteriole blood vessel can not only cause hypertension, but also impairs the microvascular integrity leading to plasma albumin leakage from cerebral vessels (Fan et al., 2015; Wang et al., 2018). Blood–brain barrier (BBB) disruption during acute and chronic hypertension has been noticed in animal models, which may contribute to hypertensive encephalopathy observed in human (Heistad, 1984). Although antihypertensive drugs can dilate arterioles and lower blood pressure (Chrysant, 2007), the effect of these drugs on BBB disruption during hypertension is largely unknown. On the other hand, at least some antihypertensive drugs have been reported as ineffective for prevention of BBB dysfunction (Mamo et al., 2017). Therefore, it is appealing to search for a management that possesses the potential to protect BBB dysfunction during hypertension thus benefits patients at risk of hypertensive encephalopathy.

YangXue QingNao Wan (YXQNW) is a compound Chinese medicine that contains the same herbs as Cerebralcare Granule (CG) does, but in different dosage form. Chinese herbs in YXQNW include Dang Gui (*Radix angelicae sinensis*), Bai Shao (*Radix paeoniae alba*), Chuan Xiong (*Rhizoma chuanxiong*), Ji Xue Teng (*Caulis spatholobi*), Di Huang (*Radix rehmanniae preparata*), Gou Teng (*Ramulus uncariae cum uncis*), Xia Ku Cao (*Spica prunellae*), Jue Ming Zi (*Semen cassiae*), Zhen Zhu Mu (*Concha margaritifera usta*), Yan Hu Suo (*Rhizoma corydalis yanhusuo*), and Xi Xin (*Herba asari*). YXQNW and CG have been used for the treatment of headache, dizziness, irritability, insomnia, and dreaminess in clinic (Huang et al., 2012). Previous studies confirmed the protective effect of CG on cerebrovascular hyperpermeability and neuron injury in rats and hamsters caused by ischemia and reperfusion (I/R) (Sun et al., 2010; Huang et al., 2012; Xu et al., 2015). However, it is not clear whether YXQNW can attenuate cerebrovascular hyperpermeability and neuron damage caused by hypertension. The present study aimed to explore the effect of YXQNW on BBB dysfunction during hypertension, and underlying mechanism in spontaneously hypertensive rats (SHRs).

MATERIALS AND METHODS

Animals and Groups

The animals used in the study were SHR weighing 230–250 g with male Wistar Kyoto (WKY) rats weighing 220–240 g as control. The animals were housed in cages at 22 ± 2°C and a humidity of 40 ± 5% under a 12 h light/dark cycle, and received a standard diet and water *ad libitum*. The rats were fasted for 12 h before the experiment but allowed free access to water. The experimental procedures were carried out in accordance with the European commission guidelines (2010/63/EU). All rats were purchased from the Animal Center of Peking University Health Science Center. All animals were handled according to the guidelines of the Peking University Animal Research Committee. Experiment handling was approved by the Committee on the Ethics of Animal Experiments of Peking University Health Science Center (LA2017214).

Thirty WKY rats with mean blood pressure (MBP) of 90 ± 10 mm Hg were used in WKY + deionized water group (WKY + DW) as control; a total of 120 SHR (MBP, 140 ± 10 mm Hg) were included and randomly divided into four groups: SHR + deionized water group (SHR + DW), SHR + enalapril + nifedipine group (SHR + EN + NF), SHR + YXQNW group (SHR + YXQNW), and SHR + enalapril + nifedipine + YXQNW group (SHR + EN + NF + YXQNW).

The number of animals used in each group for determination of each parameter is detailed in **Table 1**.

Drugs

YangXue QingNao Wan (batch number 160345) was provided by the Tasly Pharmaceutical Co. Ltd. (Tianjin, China). Enalapril (EN, batch number E6888) and nifedipine (NF, batch number N7634) were provided by the Sigma Chemical Company (St. Louis, MO, United States). YXQNW, EN, and NF were dissolved in DW to a concentration of 100, 1.6, and 1.4 mg/ml, respectively, before use.

Drug Administration

The animals received each drug daily by gavage for 4 weeks at following doses: YXQNW at 500 mg/kg/day, EN at 8 mg/kg/day, and NF at 7.1 mg/kg/day. The animals in WKY + DW and SHR + DW groups were given an equal amount of deionized

TABLE 1 | The number of animals for different experimental groups and various parameters.

Group	Blood pressure					
	CBF and albumin leakage	Evans blue	Water content	Nissl stain, immunochemistry and immunofluorescence	Western blot	Total
WKY + DW	8	6	6	4	6	30
SHR + DW	8	6	6	4	6	30
SHR + EN + NF	8	6	6	4	6	30
SHR + YXQNW	8	6	6	4	6	30
SHR + EN + NF + YXQNW	8	6	6	4	6	30
Total	40	30	30	20	30	150

The same animals were used for detection of CBF and albumin leakage. The same animals were used for immunochemistry and immunofluorescence. The same animals were used for Western blot and ELISA. The 30 animals in each group were all subjected to evaluation of blood pressure. SHR + YXQNW: post-treatment with YXQNW at 500 mg/kg/day group. SHR + EN + NF: post-treatment with enalapril at 8 mg/kg/day + nifedipine at 7.1 mg/kg/day. WKY + DW: WKY given an equal amount of deionized water per day group; SHR + DW: SHR given an equal amount of deionized water per day group.

water. The dose of YXQNW used in the present study was determined based on our previous works (Xu et al., 2009; Sun et al., 2010). The doses of EN and NF were derived from the clinical use of human doses in the hypertension guidelines.

Evaluation of Blood Pressure

Systolic blood pressure (SBP), diastolic blood pressure (DBP), and MBP of the rats were measured between 9 and 12 am on the day before administration, and 1, 2, 3, and 4 weeks after administration, respectively (n = 30). For this purpose, the rats were fixed in a net insulation cover under quiet and awake state for habituation with the temperature being preheated for 10 min at 37°C. SBP, DBP, and MBP were measured by intelligent non-invasive sphygmomanometer (U0130163, Softron Company, Japan), respectively, for three times, taking the average as the value at the time point (Tian et al., 2013).

Cerebral Blood Flow Measurement

Cerebral blood flow (CBF) (n = 8) was measured using laser speckle perfusion image system (PeriScan PIM3 System; PERIMED, Stockholm, Sweden). In short, rats were anesthetized with pentobarbital sodium (0.1 g/kg body weight, i.p.), with an incision made through the scalp, and the skin was retracted to expose the skull. The periosteal connective tissue adherent to the skull was removed with a sterile cotton swab. A parietal bone window of 3 × 5 mm^2 was opened with a hand-held drill on the right side 1 mm behind the coronal suture, and 1 mm lateral to sagittal suture as per described protocol (Xu et al., 2009). A low-powered He/Ne laser beam over the exposed parietal bone was directed by a computer-controlled optical scanner. The distance between the scanner head and cerebral cortex was 18.5 cm, with the scanner head parallel to the cerebral cortex surface. At each measuring site, the beam illuminated the tissue to a depth of 0.5 mm, as set in the instrument (Gu et al., 2018), and images were acquired after 10 min of basic observation. A color-coded image to denote specific relative perfusion level was displayed on a video monitor, and all images were evaluated with the software LDPI win 3.1 (PeriScan PIM3 System; PERIMED, Stockholm, Sweden), by which the number of perfusion unit for each image was calculated automatically.

Observation of Microcirculation

Assessment of albumin leakage from cerebral venules was undertaken after 4 weeks of treatment. For this, rat was secured in a stereotactic frame and anesthetized with pentobarbital sodium (0.1 g/kg body weight, i.p.). A 3 × 5 mm^2 cranial window was prepared as above at the same location, which corresponds to the margin of the middle cerebral artery (MCA) territory. The dura was removed and the pia mater was superfused continuously with 37°C warm physiological saline. The cerebral venules ranging from 35 to 45 μm in diameter and 200 μm in length were selected under a fluorescence microscope (X51WI, Olympus, Tokyo, Japan). Ten minutes before observation, the rat was intravenously infused with 50 mg/kg fluorescein isothiocyanate (FITC)-albumin (Sigma–Aldrich, St. Louis, MO, United States) through the femoral vein. Fluorescence signal (excitation wave length at 420–490 nm, emission wave length at 520 nm) was acquired using a super-sensitive CCD camera (USS-301, UNIQ Vision Inc., Santa Clara, CA, United States). The fluorescence intensities of FITC-albumin in the venules (v) and the perivenular interstitial area (i) were assessed with ImageJ (Bethesda, MD, United States) software. Albumin leakage was presented as i/v.

The adherent leukocytes were identified as cells that attached to the venular walls for > 30 s. The fluorescence tracer Rhodamine 6G (Sigma, St. Louis, MO, United States) was administrated (5 mg/kg body weight) through femoral vein. After craniotomy, the cerebral cortex venules were observed under an upright intravital fluorescent microscopy (BX51WT; Olympus, Tokyo, Japan), illuminated with an argon laser beam with a wavelength of 543 nm (Wang et al., 2012).

Evans Blue Leakage and Brain Water Content

Evans blue (EB) leakage was assessed as previously described (Wang et al., 2012) with some modifications (n = 6). In short, rats were anesthetized with pentobarbital sodium (0.1 g/kg body weight, i.p.), and EB dye (Sigma–Aldrich, St. Louis, MO, United States; 4%, 3 ml/kg) in saline was injected within 2 min into the left femoral vein and allowed to circulate for 3 h. Rats were transcardially perfused with phosphate-buffered saline (PBS) until colorless perfusion fluid drained from the

right atrium. The amount of extravasated EB in the brain was determined by spectroflurophotometry at an excitation wavelength of 620 nm.

Brains (n = 6) were removed and quickly separated into the left and right cerebral hemispheres and weighed (wet weight). Brain specimens were then dried in an oven at 120°C for 48 h and weighed for determination of dry weight. The percentage of water content was presented as per [(wet weight−dry weight)/wet weight] × 100% (Wang et al., 2012).

Nissl Staining and TUNEL Assay

Continuous sections starting from the optic chiasma were selected, and each section was 10 μm thick.

For Nissl staining (n = 4 for each group), the sections were stained with cresyl violet acetate (Sigma–Aldrich, St. Louis, MO, United States) and examined with light microscope (BX512DP70, Olympus, Tokyo, Japan) according to the standard procedure.

Transferase-mediated deoxyuridine triphosphate-biotin nick end labeling (TUNEL) assay was applied to assess the apoptotic neurons in CA1 region of hippocampus and cortex of rats, using the *in situ* cell death detection kit (Roche, United States), and conducted according to the instruction of the manufacturer. The number of total nuclei and TUNEL-positive nuclei in each field of CA1 region was scored with Image-Pro Plus 5.0 software, using laser confocal microscope (Axiovert200, Zeiss, Germany) with a 63× objective, and five fields of CA1 and cortex region were examined for each animal. As a control, a consecutive section was prepared and processed by the same procedure but without addition of TdT enzyme (Gu et al., 2018).

Immunohistochemistry

For immunohistochemistry (n = 4 for each group), coronal fresh frozen sections were sliced starting from the optic chiasma in 10 μm thick using a cryostat (CM1800, Leica, Bensheim, Germany). The slicing method was the same as above. The sections were incubated with mouse anti-CD31 (1:50, Thermo Fisher Scientific, MA1-80069, Waltham, MA, United States) diluted in PBS overnight at 4°C after blocking with bovine serum albumin. Then the samples were incubated with a biotinylated secondary antibody followed by avidin–biotin–peroxidase complex. Positive staining was visualized with diaminobenzidine. The images were captured by a digital camera connected to a microscope (BX512DP70, Olympus, Tokyo, Japan). Five fields were randomly selected for each rat. The number of open microvessels and microvessels with perivascular edema was analyzed with Image-Pro plus 5.0 software (IPP, Media Cybernetic, Bethesda, MD, United States). Five fields of the hippocampus and cortex region were randomly selected and examined separately for each animal (Gu et al., 2018). The microvessels that had the CD31-positive endothelium sticking together without any lumen were defined as closed microvessels. The percentage of microvessels with perivascular edema and closed microvessels in each field was calculated.

Immunofluorescence

For evaluation of the expression of tight junction (TJ) proteins claudin-5 and ZO-1 in cerebral microvessels, immunofluorescence staining was performed. The tissue preparation and staining was performed as per described protocol (Li et al., 2018), and the primary antibodies applied included: mouse anti-claudin-5 and anti-ZO-1 (1:50, Invitrogen, Camarillo, CA, United States), and rabbit anti-vWF (1:100, Millipore, Temecula, CA, United States). The brain sections were mounted, coverslipped, and photographed under a laser scanning confocal microscope (TCS SP5, Leica, Mannheim, Germany), as described previously (Li et al., 2018).

Western Blot

Western blot analysis was conducted as described previously (Huang et al., 2012), using the tissue from the right neocortex of rats. Protein concentrations were estimated by the Bradford method, and an equal amount of protein (100 μg/lane) was diluted in 10× sample buffer, boiled, and loaded onto 12% SDS-PAGE gels and transferred to a nitrocellulose membrane (Hybond-C, Amersham Biosciences, United States) after separation by electrophoresis. Then, the membranes were incubated overnight at 4°C with the primary antibodies against GAPDH, occludin, ZO-1, myosin light chain (MLC), MLC kinase (MLCK), phospho-MLC (P-MLC) (Abcam, Cambridge, United Kingdom), claudin-5 (Santa Cruz Biotechnology, Santa Cruz, CA, United States), caveolin-1, Src, and P-Src (Tyr416) (Cell Signaling Technology, Beverly, MA, United States), ATP synthase-α subunit (ATP-α), ATP synthase-β subunit (ATP-β) (Thermo Fisher Scientific, Waltham, MA, United States), and ATP-5D (Abcam, Cambridge, United Kingdom). The membranes were washed with tris-buffered saline and tween20 (TBST) and incubated with the respective horseradish peroxidase-conjugated secondary antibodies at a 1:5000 dilution for 60 min at room temperature. The protein bands were detected by enhanced chemiluminescence, and the band intensities were quantified by densitometry and expressed as mean area density using the ImageJ (Bethesda, MD, United States) software.

ELISA

The rats were perfused with NS, and a tissue block of about 2 mm^3 was removed from the cortex for the assessment of the concentrations of Complex I, Complex II, Complex IV, Complex V, ATP, AMP, and ADP by ELISA kits (Abcam, Cambridge, United Kingdom) according to the manufacturer's protocol. OD values were determined by enzyme microplate reader (Thermo Multiskan Mk3, Thermo Fisher Scientific Inc., Barrington, IL, United States). The concentrations of Complex I, Complex II, Complex IV, Complex V, ATP, AMP, ATP/ADP, and ATP/AMP were calculated based on the standard curves (Chen et al., 2018).

Statistical Analysis

The data of all groups were expressed as means ± SEM. Meanwhile, statistical analysis was conducted by one-way or two-way analysis of variance, followed by Bonferroni test. A value of $P < 0.05$ was considered statistically significant.

RESULTS

YXQNW Attenuates the Blood Pressure and Cerebral Blood Flow Decrease in SHR

The blood pressure of animals was recorded over time. As shown in **Figures 1A–C**, before administration, MBP, DBP, and SBP in the SHR groups were significantly higher than that in the control group. Treatment with either EN + NF or YXQNW or EN + NF + YXQNW reduced the MBP, DBP, and SBP in SHR gradually with time, reaching a value close to WKY group at 4 weeks with YXQNW alone treatment being less effective.

Cerebral blood flow was determined at the end of experiment and the representative images of the five groups are shown in **Figure 1E**, while the quantification of the results is presented in **Figure 1D**. Compared with control group (573.7 ± 37.64), CBF in SHR + DW group decreased significantly (391.8 ± 6.213), while EN + NF, YXQNW, and EN + NF + YXQNW administration markedly relieved CBF of SHR (515.3 ± 20.38 in EN + NF group, 488.3 ± 16.74 in YXQNW group, 599.5 ± 33.99 in EN + NF + YXQNW group, $P < 0.05$).

YXQNW Increases the Number of Closed Capillaries, Inhibits Perivascular Edema in the Hippocampus and Cortex of SHR

Displayed in **Figure 2A** are the representative images of hippocampus and cortex region acquired by immunohistochemistry staining for CD31 in all the groups, with the statistic result for the number of closed microvessels (dotted arrows) and the microvessels with perivascular edema (solid arrows) in each group presenting in **Figures 2B–E**. Apparently, in the hippocampus, compared to control group, the percentage of closed capillaries in SHR + DW group was significantly higher (60.00 ± 6.12 vs. 0.00 ± 0.00, $P < 0.05$). Interestingly, YXQNW and EN + NF + YXQNW treatment attenuated this alteration (10.67 ± 6.86 and 3.33 ± 3.33, $P < 0.05$), while treatment with EN + NF did not show significant effect (51.60 ± 8.60) (**Figure 2C**). Similar results were observed in the cortex ($P < 0.05$), as presented in **Figure 2E**. The quantitative evaluation of the percentage of microvessels with perivascular edema in hippocampus (**Figure 2B**) and cortex (**Figure 2D**) revealed similar results ($P < 0.05$). These results offered morphological evidence for the ability of the drugs to protect microvessels from collapsing in SHR.

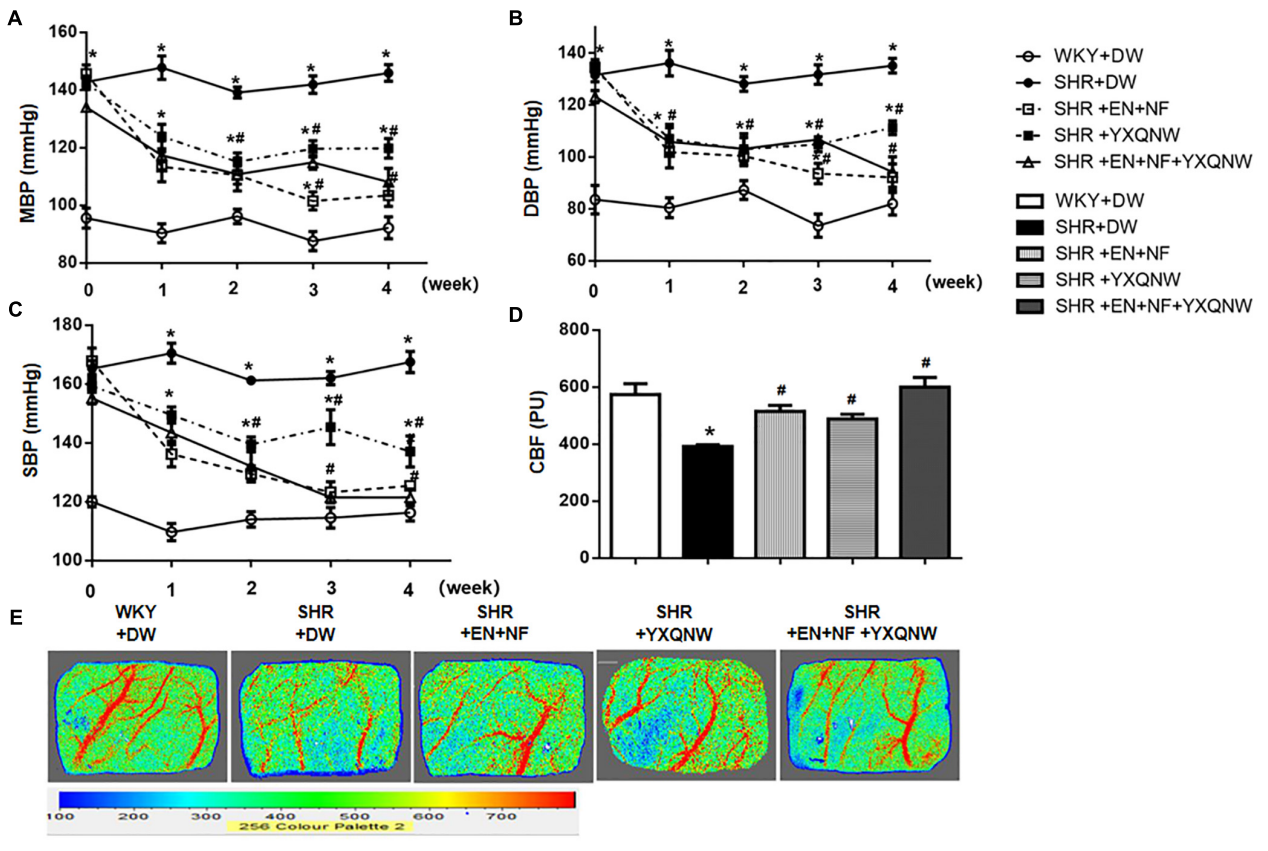


FIGURE 1 | YXQNW attenuates the blood pressure and cerebral blood flow decrease in SHR. Panels **(A–C)** show the change of MBP, DBP, and SBP with time, respectively, before (0 week) and after (1, 2, 3, and 4 week) drug administration in each group. $n = 30$. **(D)** Quantitative analysis of CBF in different groups. The unit of *Y*-axis is perfusion unit (PU). **(E)** The representative images of CBF of ipsilateral cortex in different groups. The magnitude of CBF is represented by different colors, with blue to red denoting low to high. Values are the mean ± SEM. $^{*}P < 0.05$ vs. control group, $^{\#}P < 0.05$ vs. SHR + DW group.

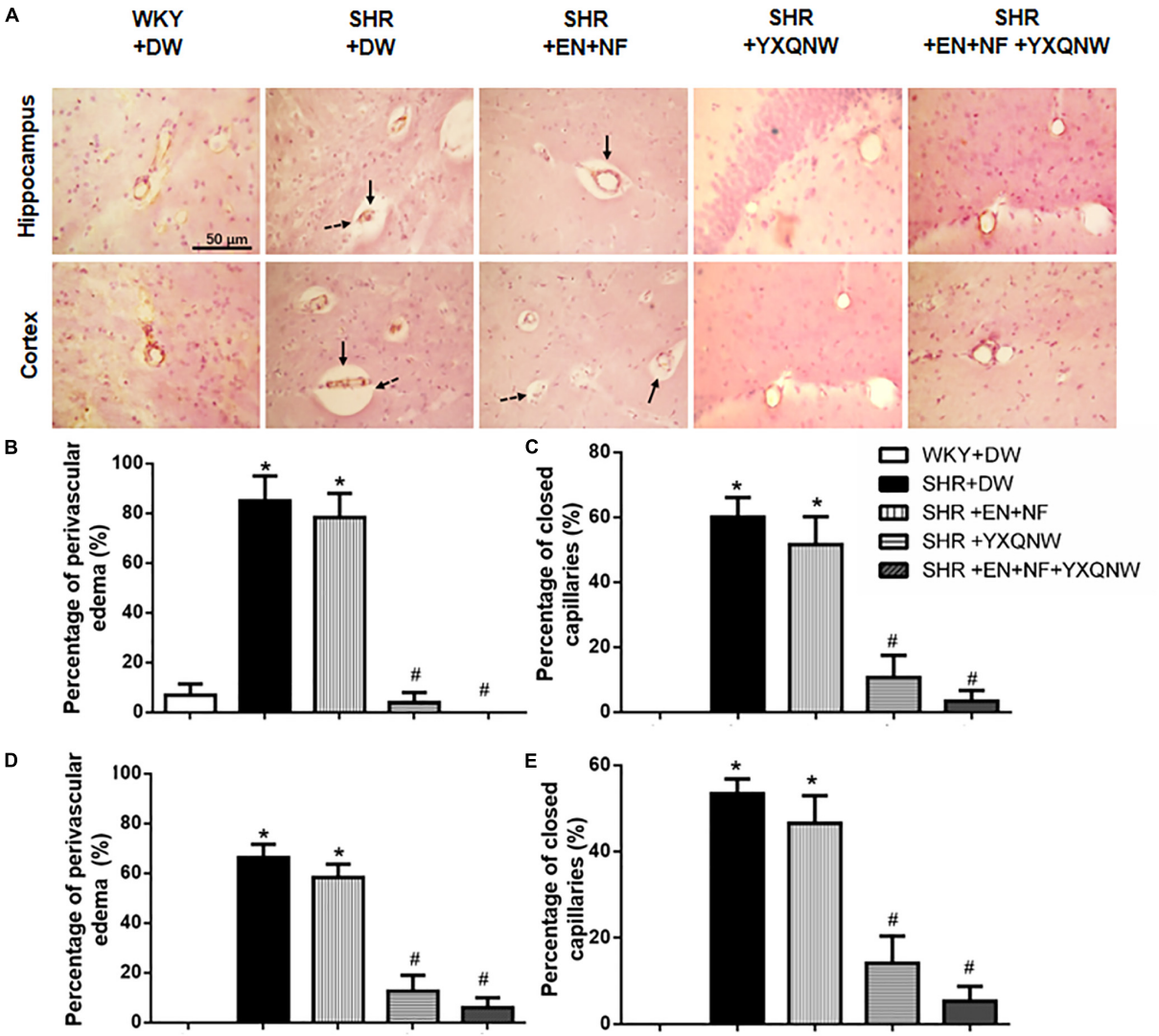


FIGURE 2 | YXQNW inhibits the perivascular edema and reduces the number of closed capillaries in the hippocampus and cortex of SHR. **(A)** Representative images in the region between CA1 to DG of hippocampus and region of cortex stained by immunohistochemistry staining for CD31 in all the groups. Dotted arrows stand for closed capillaries and solid arrows stand for blood vessels with perivascular edema. Bar = 50 μm. **(B)** The percentage of the capillaries with perivascular edema to the total number of capillaries in a region between CA1 and DG of hippocampus evaluated in five randomly selected micrographs for each animal. **(C)** The percentage of the closed capillaries to the total number of capillaries in hippocampus evaluated in five randomly selected micrographs for each animal. **(D)** The percentage of the capillaries with perivascular edema to the total number of capillaries in cortex evaluated in five randomly selected micrographs for each animal. **(E)** The percentage of the closed capillaries to the total number of capillaries in cortex evaluated in five randomly selected micrographs for each animal. $^{*}P < 0.05$ vs. control group, $^{\#}P < 0.05$ vs. SHR + DW group. $n = 20$.

YXQNW Protects BBB From Breakdown in SHR

The ameliorating effect of YXQNW on the perivascular edema suggests its potential to protect BBB. We thus assessed the effect of EN + NF, YXQNW, and their combination on BBB permeability by albumin leakage and EB dye extravasation at the right cerebral hemisphere of rats in various groups. As shown in **Figures 3A–C**, compared with the WKY + DW group (102.0 ± 5.95), albumin leakage in SHR + DW group was markedly increased (185.8 ± 7.68), which was not attenuated by EN + NF alone (187.1 ± 10.06) but by YXQNW and EN + NF + YXQNW treatment (128.3 ± 2.22 and 107.6 ± 4.06) (**Figures 3A,B**). Compared with the WKY + DW (0.17 ± 0.17), the leukocyte adhesion in SHR group increased significantly (4.33 ± 0.84), which was not attenuated by EN + NF (3.50 ± 0.76, $P > 0.05$). In contrast, YXQNW and EN + NF + YXQNW treatment attenuated the leukocyte adhesion significantly, reaching to 2.50 ± 0.43 and 1.00 ± 0.52, respectively (**Figures 3A,C**).

The amount of EB dye extravasation in the right cerebral hemisphere was markedly increased in the SHR group (4.79 ± 0.17) compared with the WKY group (2.39 ± 0.28)

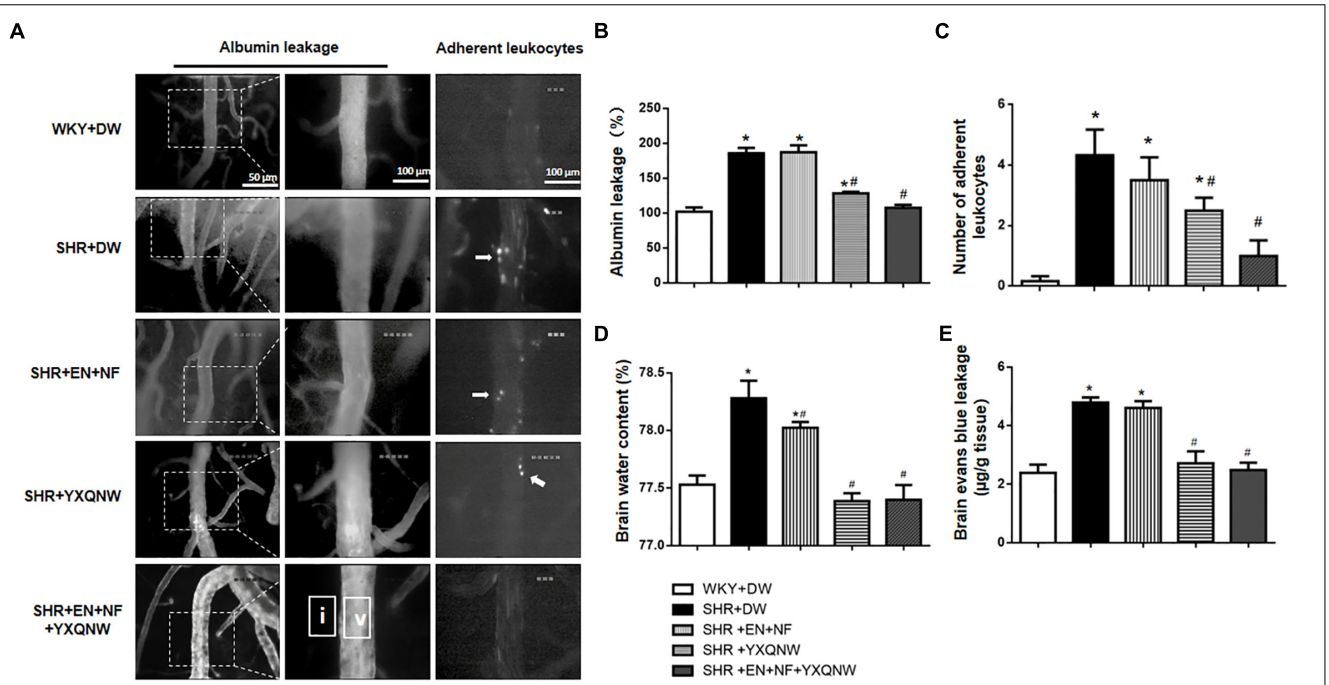


FIGURE 3 | YXQNW reduces venous albumin leakage, adherent leukocytes, Evans blue extravasation, and brain water content in SHR. **(A)** Representative images for albumin leakage from venules and adherent leukocytes in venules in all groups. Rectangles representing the areas for determination of fluorescence arrows stand for adherent leukocytes. Bar = 50 μm. v, cerebral venule; i, interstitial tissue. **(B)** Statistic analysis of albumin leakage. **(C)** Statistic analysis of adherent leukocytes. **(D)** The quantitative analysis of brain water content. **(E)** The quantitative analysis of Evans blue leakage. Values are the mean ± SEM. $^{*}P < 0.05$ vs. control group, $^{\#}P < 0.05$ vs. SHR + DW group.

(**Figure 3E**), which was not affected by EN + NF (4.60 ± 0.23, $P > 0.05$). Whereas, YXQNW and EN + NF + YXQNW treatment attenuated the EB dye extravasation significantly, reaching to 2.71 ± 0.41 and 2.48 ± 0.25, respectively (**Figure 3E**). Likewise, the brain water content varied among groups in a similar fashion (**Figure 3D**), pointing toward a conclusion that hypertension impairs cerebral microvessels leading to BBB hyperpermeability, which was attenuated by YXQNW but not by EN + NF.

YXQNW Protects the Neurons in CA1, CA2, CA3, and DG Regions of Hippocampus

To further specify the effect of YXQNW and EN + NF on the neurons of SHR, TUNEL and Nissl assays were performed for the hippocampus. **Figure 4** shows the representative images of Nissl staining in various groups. In the CA1, CA2, CA3, and DG regions of hippocampus, neurons of control group showed normal morphological features, while in SHR + DW group diverse neuronal damages such as scattered permutations and nuclear pyknosis occurred. Compared with SHR + DW group, YXQNW and EN + NF + YXQNW treatment effectively prevented the neuronal damages in SHR, while EN + NF did not show an obvious effect.

Figure 5 shows a large number of TUNEL-positive cells in the CA1 region and cortex region of SHR, which were hardly observed in the control group (0.00 ± 0.00). The high blood pressure-evoked increase in the number of TUNEL-positive cells in CA1 region [**Figures 5A(a1–e1),B**] (3.50 ± 0.65) and cortex region (5.50 ± 1.04) [**Figures 5A(a2–e2),C**] was significantly reduced in YXQNW-treated group (CA1: 0.50 ± 0.23, cortex: 4.25 ± 0.85, $P < 0.05$) and EN + NF + YXQNW-treated group (CA1: 0.50 ± 0.50, cortex: 0.50 ± 0.29, $P < 0.05$). Quantitative evaluation of TUNEL-positive cells revealed that EN + NF treatment reduced the number of TUNEL-positive cells in CA1 region as well, although less effective than YXQNW and EN + NF + YXQNW treatment (**Figure 5B**). Whereas, in cortex, the three treatments manifested differently as to the effect on the number of TUNEL-positive cells with EN + NF having no effect (6.00 ± 0.91, $P > 0.05$), while EN + NF + YXQNW being more effective than YXQNW alone (0.50 ± 0.29 vs. 4.25 ± 0.85, $P < 0.05$) (**Figure 5C**).

YXQNW Maintains the Integrity of Endothelial Cell Junctions

Endothelial cell TJ is an essential contributor to BBB. To gain insight into the rationale behind the role of YXQNW in maintaining BBB integrity, vascular endothelial cell TJ proteins claudin-5 and ZO-1 were examined for various groups by confocal microscopy (**Figure 6A**) revealing that claudin-5 localized between endothelial cells as continuous lines in control group. In SHR + DW group, these continuous distributions were disrupted apparently, becoming dotted lines, concomitant with reduction in immune staining, indicating a decrease in

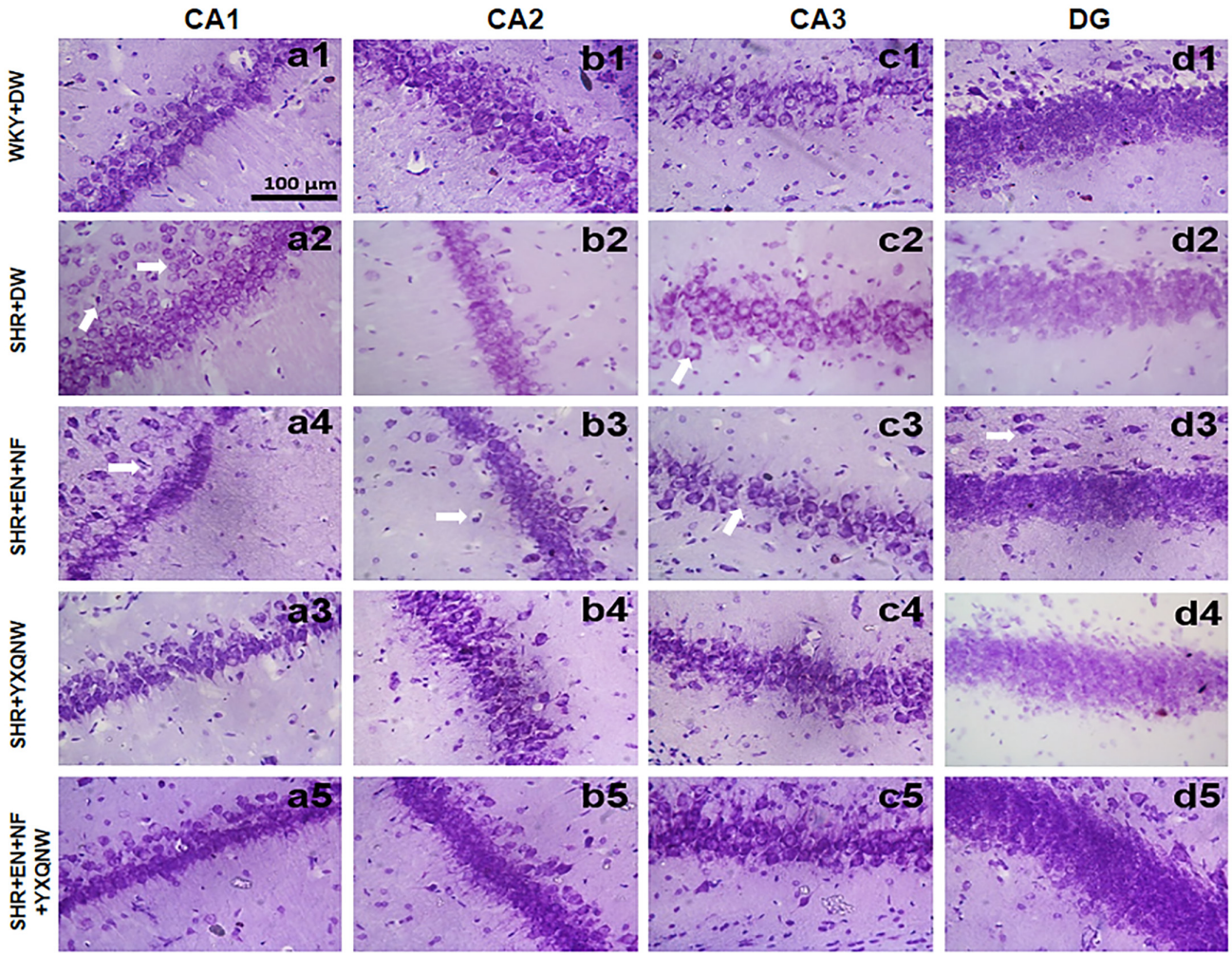


FIGURE 4 | YXQNW protects the neuron structure in CA1, CA2, CA3, and DG regions. Representative images of neuron structure in CA1, CA2, CA3, and DG regions in hippocampus of WKY + DW group **(a1–d1)**, SHR + DW group **(a2–d2)**, EN + NF group **(a3–d3)**, YXQNW group **(a4–d4)**, and EN + NF + YXQNW group **(a5–d5)**. Bar = 100 μm.

claudin-5 expression. This decrease was not restored by EN + NF treatment but alleviated evidently by YXQNW treatment and YXQNW combined with EN and NF treatment. These results were confirmed by Western blot (**Figure 6C**). Similar results were obtained for ZO-1 ($P < 0.05$, $n = 4$) (**Figures 6A,F**), JAM-1 ($P < 0.05$, $n = 4$) (**Figure 6D**), and occludin ($P < 0.05$, $n = 4$) (**Figure 6E**). These results indicated that YXQNW could alleviate the reduction in TJ proteins expression of SHR, which may account for the protective role of the YXQNW in BBB breakdown.

Western blot was used to analyze the expression of caveolin-1, another determinant of vascular permeability (**Figure 6B**), showing a marked increase in caveolin-1 protein level in the SHR + DW group compared with control group (1.71 ± 0.37 vs. 1.00 ± 0.00). This increase was not obviously attenuated by EN + NF treatment (1.35 ± 0.22), but protected by YXQNW treatment and EN + NF + YXQNW treatment with the later exhibiting a better effect (1.05 ± 0.15 and 0.90 ± 0.15, $P < 0.05$, $n = 6$), which may confirm the protective role of the drugs in BBB breakdown from transcellular pathways.

YXQNW Attenuates Energy Metabolism Disturbance

We next assessed the energy metabolism in different conditions, which is closely related to mitochondria function and plays a critical role in maintaining BBB integrity. ELISA analysis revealed a decrease in the content of Complexes I, II, and V in SHR compared with control group ($P < 0.05$, $n = 6$). Treatment with EN + NF + YXQNW attenuated this decrease, while either EN + NF or YXQW alone had no effect (**Figures 7A,B,D**, $P > 0.05$, $n = 6$). Meanwhile, there was no significant difference in the content of Complex IV between the five groups (**Figure 7C**). Correspondingly, ATP/ADP and ATP/AMP diminished in SHR, which was ameliorated by YXQNW alone and EN + NF + YXQNW (**Figures 7E,F**, $P < 0.05$, $n = 6$).

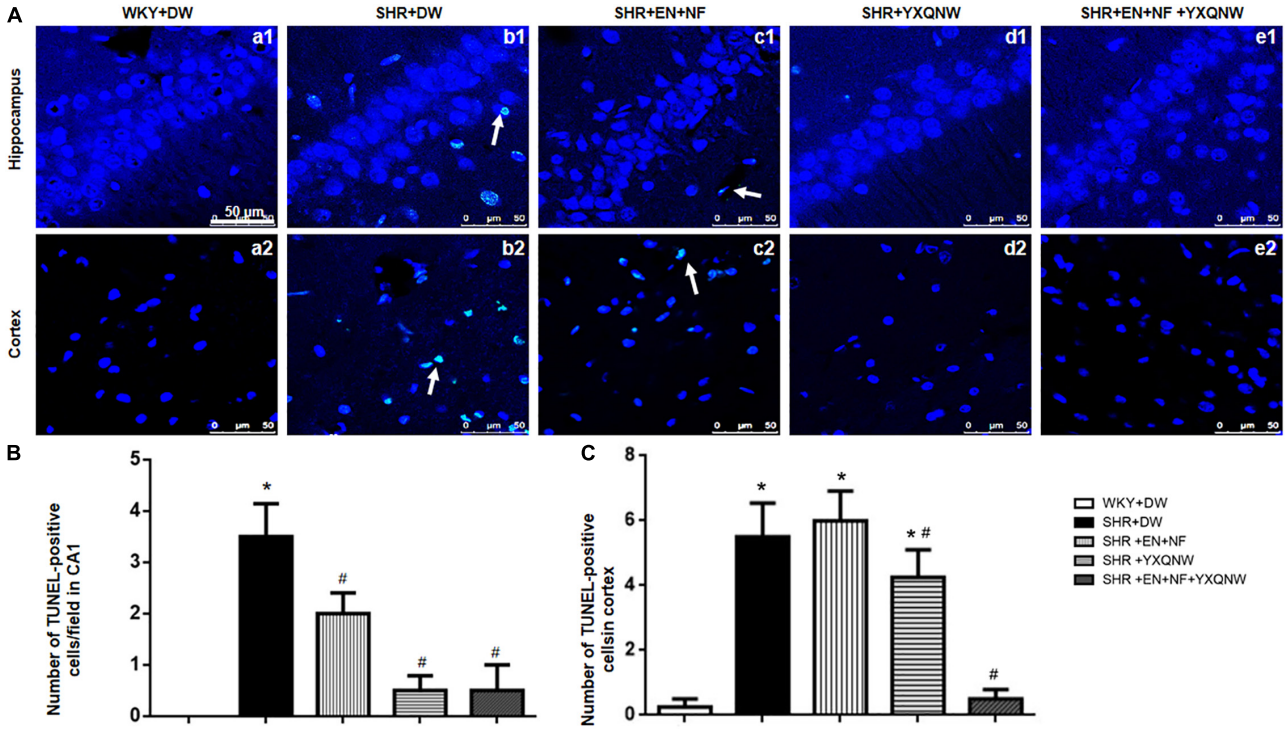


FIGURE 5 | YXQNW inhibits CA1 neuron death in hippocampus and cortex. **(A)** Representative images of neuron death in hippocampus CA1 and cortex of WKY + DW group **(a1,a2)**, SHR + DW group **(b1,b2)**, EN + NF group **(c1,c2)**, YXQNW group **(d1,d2)**, and EN + NF + YXQNW group **(e1,e2)**. White arrows indicate the localization of TUNEL-positive cells. Bar = 50 μm. **(B)** Statistic analysis of neuron death, the data were derived from five randomly selected micrographs in hippocampus for each animal. **(C)** Statistic analysis of neuron death evaluated in five randomly selected micrographs in cortex for each animal. The area of each micrograph selected was 2.1×10^4 μm^2. Values are the mean ± SEM. $^*P < 0.05$ vs. control group, $^{\#}P < 0.05$ vs. SHR + DW group. $n = 20$.

Western blot was further performed to assess the expression of ATP-α, ATP-β, and ATP-5D, the three subunits of Complex V, in different groups (**Figure 7G**). The result showed that all the three proteins decreased in SHR (**Figures 7H–J**, $P < 0.05$, $n = 6$), implying impairment of ATP synthases. This decrease was attenuated by treatment with EN + NF or/and YXQNW and the combination of the two with EN + NF + YXQNW being the most effective ($P < 0.05$, $n = 6$).

YXQNW Inhibits Src/MLCK/MLC Signaling Pathway

Activation of MLCK by phosphorylated Src kinase has been shown to lead to increased actin–myosin interaction and subsequently increased paracellular permeability (Birukov et al., 2001). We thus determined the expression of proteins involved in Src/MLCK/MLC signaling pathway by Western blot in different conditions (**Figure 8A**). The result shows that as compared with control, SHR exhibited a significant increase in the expression of MLCK (1.49 ± 0.25 vs. 1.00 ± 0.00), p-Src/T-Src (1.49 ± 0.25 vs. 1.00 ± 0.00), and p-MLC/T-MLC (2.42 ± 0.38 vs. 1.00 ± 0.00), suggesting an increased microvascular permeability via paracellular pathway. Treatment with EN + NF had no effect on the elevated expression of p-Src and p-MLC ($P > 0.05$, $n = 6$) (**Figures 8C,D**), even further enhanced the increase of MLCK (2.33 ± 0.37) (**Figure 8B**), suggesting ineffectiveness of EN + NF in modulating Src/MLCK/MLC signaling. On the other hand, YXQNW alone or its combination with EN + NF significantly ameliorated the increase in the expression of the three proteins (MLCK: 1.11 ± 0.12 and 1.19 ± 0.14, respectively; p-Src/T-Src: 1.44 ± 0.26 and 1.20 ± 0.15, respectively; and p-MLC/T-MLC: 0.95 ± 0.27 and 0.62 ± 0.05, respectively) (**Figures 8B–D**), highlighting the implication of Src/MLCK/MLC signaling in the protective effect of YXQNW on BBB breakdown in SHR.

DISCUSSION

The dysfunction of BBB in SHR has been known for >40 years (Hazama et al., 1975; Ueno et al., 2004). Consistent with these results, we observed in the present study an increased permeability of BBB in SHR, manifesting enhanced albumin leakage from cerebral venules and EB extravasation in the brain as well as increased brain water content. Importantly, this BBB breakdown cannot be prevented by treatment with EN plus NF, the two commonly used antihypertensive drugs, but rather protected by YXQNW. This result highlights YXQNW as a prophylaxis for the patients at risk of hypertensive encephalopathy.

As an animal model prone to BBB dysfunction, SHR has been used to explore the pathogenesis of BBB disruption during

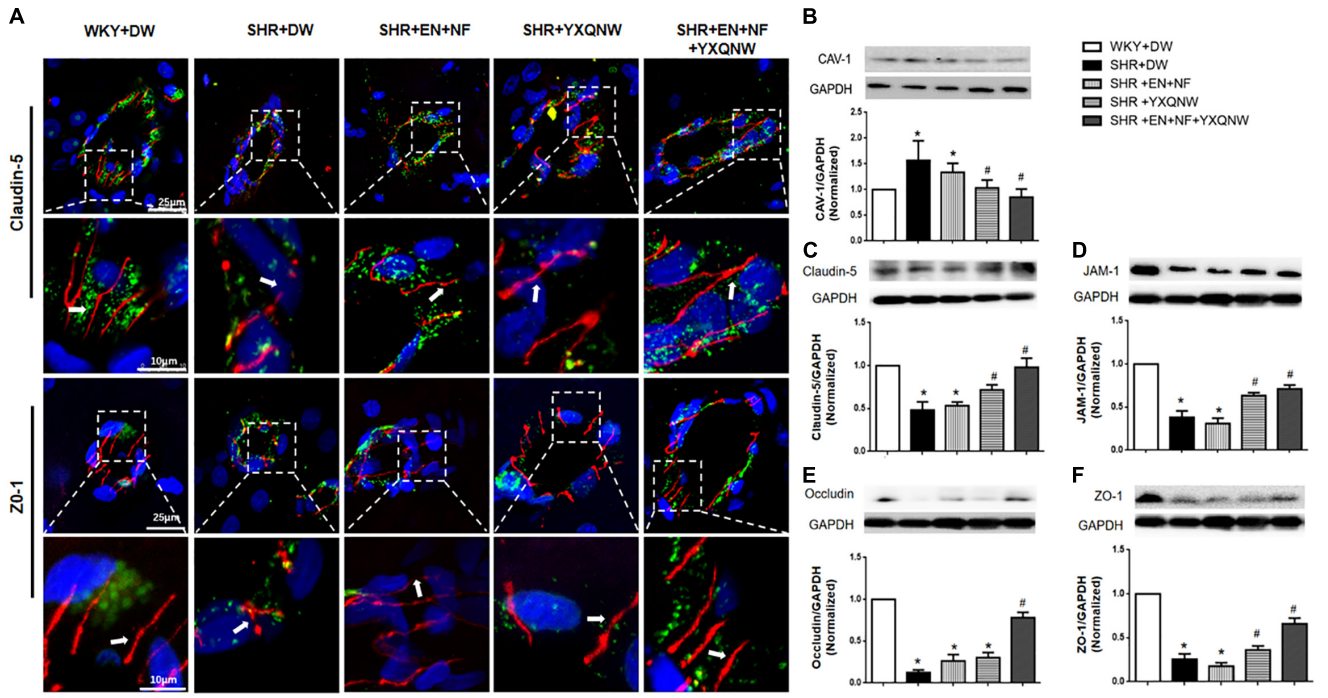


FIGURE 6 | YXQNW protects the decrease in TJ proteins and caveolin-1 expression. **(A)** Representative immunofluorescence confocal images of claudin-5 and ZO-1. Claudin-5 (red) and ZO-1 (red) localized at the peripheral of endothelial cells with marker vWF (green). Note the continuous distribution of claudin-5 and ZO-1 in cortical microvessels of control group. The disruption of claudin-5 and ZO-1 staining in SHR + DW was not reduced in the SHR + EN + NF group but markedly reduced in the YXQNW treatment group and EN + NF + YXQNW treatment group. White arrows indicate the localization of claudin-5 or ZO-1. **(B)** Representative Western blots and quantitative analysis of caveolin-1. **(C)** Representative Western blots and quantitative analysis of claudin-5. **(D)** Representative Western blots and quantitative analysis of JAM-1. **(E)** Representative Western blots and quantitative analysis of occludin. **(F)** Representative Western blots and quantitative analysis of ZO-1. Values are the mean ± SEM. $^{*}P < 0.05$ vs. control group, $^{\#}P < 0.05$ vs. SHR + DW group.

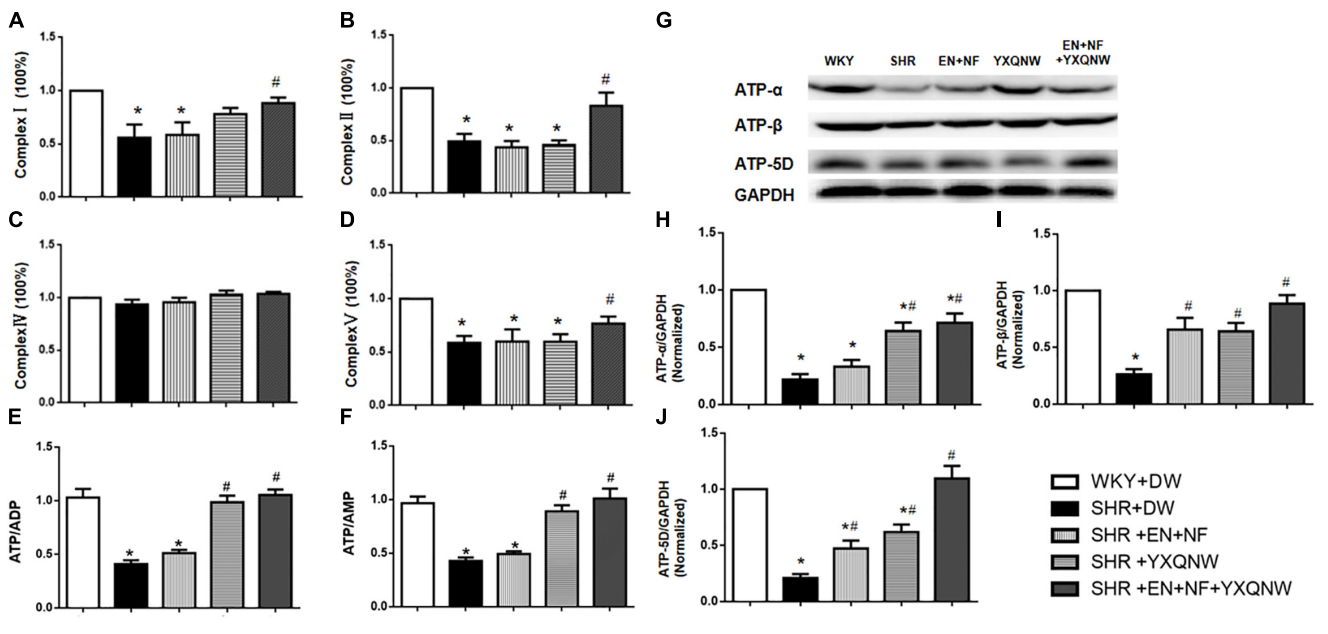


FIGURE 7 | YXQNW increases the expression of Complex I, Complex II, and Complex V and elevates the value of ATP/ADP, ATP/AMP, and the expression of ATP-α, ATP-β and ATP-5D in the cerebral cortex. **(A–D)** Statistical results from ELISA for Complex I, Complex II, Complex IV, and Complex V ($n = 6$), respectively. **(E,F)** Statistical results from ELISA for the value of ATP/ADP and ATP/AMP ($n = 6$). **(G)** Representative Western blots of ATP-α, ATP-β, and ATP-5D. **(H–J)** Quantitative analysis of ATP-α, ATP-β, and ATP-5D. $^{*}P < 0.05$ vs. control group, $^{\#}P < 0.05$ vs. SHR + DW group.

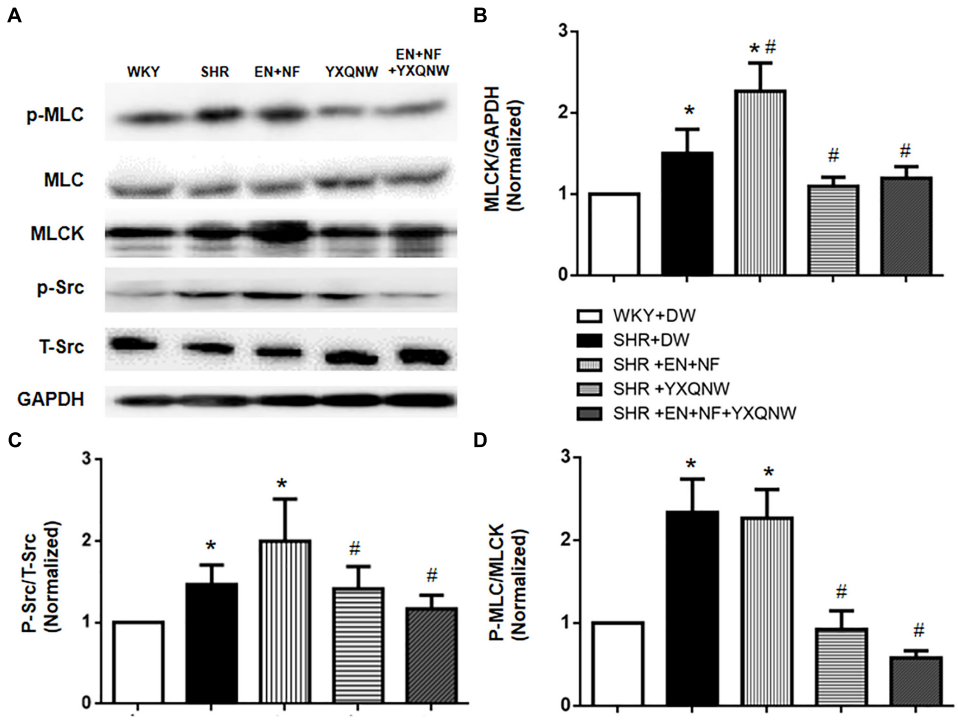


FIGURE 8 | YXQNW inhibits Src/MLCK/MLC signaling pathway of SHR. **(A)** Representative Western blots of p-Src, MLCK, and p-MLC. **(B–D)** Quantitative analysis of p-MLC, MLCK, and p-Src, respectively. Values are the mean ± SEM. $^{*}P < 0.05$ vs. control group, $^{\#}P < 0.05$ vs. SHR + DW group.

chronic hypertension (Seyed et al., 2012). Several mechanisms have been reported to mediate the hypertension-caused BBB disruption, including enhanced transendothelial cell transport (Tagami et al., 1983), structure change in TJ and altered distribution of glucose transporter-1 (Lippoldt et al., 2000), increased expression of AQP4 in the end feet of astrocytes (Ishida et al., 2006), and the like. The present study revealed that compared with WKY rats, SHR presented a decreased expression of TJ proteins and an increased expression of caveolin-1, the principal protein of caveolae. This result suggests that both paracellular and transcellular pathways are implicated in the BBB dysfunction of SHR. In line with the result of enhanced BBB permeability, the dysregulated expression of TJ proteins and caveolin-1 in SHR was attenuated by YXQNW but not by EN + NF. Interestingly, supplement of EN + NF potentiated the effect of YXQNW to relive the dysregulation of caveolin-1 and some of the TJ proteins, such as in the case of claudin-5, occludin, and ZO-1, implying that some coordination between YXQNW and antihypertensive drugs likely occurs.

The present study revealed an impaired energy metabolism in SHR, possibly due to sclerosis and spasm of the arteries in SHR brain which lead to insufficient perfusion, causing temporary brain tissue hypoxia (Garrido and Griendling, 2009) which impacts the structure and function of mitochondria. The impaired energy metabolism may result in mar functional cell skeleton, including dissembling of F-actin and improperly regulated myosin–actin interaction, since both of which are energy-dependent process (Hinshaw et al., 1993). It is worth noting that a normally functional cell skeleton is known to provide a support for the integrity of endothelial cell junctions and is thus involved in regulation of vascular permeability (Alexander et al., 2015). In the present study, YXQNW, but not EN + NF, restored the impaired energy metabolism in SHR, which at least partially contributes to the protective effect of YXQNW on BBB breakdown.

Increasing evidence indicates the importance of Src signaling in modulation of BBB. Src activation impacts interaction between myosin and actin filaments through a pathway involving MLCK and MLC, leading to dysregulation of cell junction proteins (Guerrero et al., 2004). In addition, Src activation evokes phosphorylation of caveolin-1 (Labrecque et al., 2004), which not only provokes *trans*-endothelial pathway but also causes degradation of junction proteins, collectively resulting in BBB breakdown. The present study observed an increase in p-Src, MLCK, and p-MLC in SHR, suggesting implication of this signaling in BBB hyperpermeability. The reason for the activation of Src in SHR is at present unknown. One likelihood is oxidative stress generated from disrupted respiratory chain as evidenced by downregulation of Complexes I, II, and V. Impressively, YXQNW, but not EN + NF, inhibited the activation of Src/MLCK/MLC-signaling pathway, suggesting involvement of this signaling in the protective effect of YXQNW on BBB breakdown in SHR. Nevertheless, more study is needed to explore the possible involvement of other mechanism in the BBB dysfunction in SHR and the role of YXQNW in the occasion concerned.

Contracted arteriole in hypertensive patients reduces the blood supply to the irrigated brain territory. In addition, following BBB breakdown, albumin leakage and perivascular edema occurs, which imposes pressure on microvessels leading to narrowing even closing of the vessels, as evidenced in our study. As a consequence, the neurons will be subjected to deprivation of oxygen and glucose, which provokes oxidative stress resulting in neuron apoptosis. As expected, we observed a significantly increased apoptotic neurons in SHR, which may probably underlie hypertensive dementia. Administration of EN + NF reduced the number of TUNEL-positive cells in CA1, but had no effect on that in cortex. On the contrary, administration of YXQNW diminished TUNEL-positive neurons in both CA1 and cortex significantly, suggesting broader effect of this medicine than that of EN + NF in prevention of hypertension-related encephalopathy.

As a compound Chinese medicine, YXQNQ consists of 11 herbs with each containing numerous bioactive ingredients. Identification of the ingredient(s) in YXQNW responsible for the effects observed in the present study is a huge task, which needs much more work in the future. Moreover, the present study did not evaluate the intravascular surface and intravascular water, which may affect the brain wet weight thus contributes to W/D. This issue needs to be investigated by further study. Nevertheless, this limitation does not influence the conclusion that BBB is impaired in SHR thanks to the other evidence such as albumin leakage from cerebral venules and EB extravasation.

CONCLUSION

In conclusion, the present study demonstrated the potential of YXQNW to attenuate BBB breakdown in SHR without interfering with the antihypertensive effect of EN + NF, which involves regulation of energy metabolism and Src/MLCK/MLC signaling. This result suggests YXQNW as an adjuvant management for hypertensive-adjective patients to prevent hypertensive encephalopathy.

DATA AVAILABILITY STATEMENT

All datasets generated for this study are included in the manuscript/supplementary files.

ETHICS STATEMENT

The experiment handling was approved by the Committee on the Ethics of Animal Experiments of Peking University Health Science Center (LA2017214).

AUTHOR CONTRIBUTIONS

Y-QJ performed the research, analyzed the data, and wrote the manuscript. PH and KS contributed to the animal experiments. LY contributed to the Nissl stain, immunohistochemistry, and immunofluorescence. C-SP and PH contributed to the Western blotting. QL contributed to the other experiments. J-YF revised the manuscript. Z-ZM and J-YH designed and funded the research, interpreted the data, and finally approved the submission of this manuscript. All authors read and agreed with the manuscript.

FUNDING

This work was supported by the State Key Laboratory of Core Technology in Innovative Chinese Medicine (20170034) and the National Natural Science Foundation of China Grant (81541009).

REFERENCES

Alexander, G.-P., Alí Francisco, C.-M., Martha, V.-A., Hilda, V.-R., and Michael, S. (2015). The role of actin-binding proteins in the control of endothelial barrier integrity. *Thromb. Haemost.* 113, 20–36. doi: 10.1160/TH14-04-0298

Birukov, K. G., Csortos, C., Marzilli, L., Dudek, S., Ma, S. F., Bresnick, A. R., et al. (2001). Differential regulation of alternatively spliced endothelial cell myosin light chain kinase isoforms by p60(Src). *J. Biol. Chem.* 276, 8567–8573. doi: 10.1074/jbc.M005270200

Chen, Q. F., Liu, Y. Y., Pan, C. S., Fan, J. Y., Yan, L., Hu, B. H., et al. (2018). Angioedema and hemorrhage after 4.5-hour tPA (tissue-type plasminogen activator) thrombolysis ameliorated by T541 via restoring brain microvascular integrity. *Stroke* 49, 2211–2219. doi: 10.1161/STROKEAHA.118.021754

Chrysant, S. G. (2007). The pathophysiologic role of the brain renin-angiotensin system in stroke protection: clinical implications. *J. Clin. Hypertens.* 9, 454–459. doi: 10.1111/j.1524-6175.2007.06602.x

Fan, Y., Yang, X., Tao, Y., Lan, L., Zheng, L., and Sun, J. (2015). Tight junction disruption of blood-brain barrier in white matter lesions in chronic hypertensive rats. *Neuroreport* 26, 1039–1043. doi: 10.1097/WNR.0000000000000464

Garrido, A. M., and Griendling, K. K. (2009). NADPH oxidases and angiotensin II receptor signaling. *Mol. Cell. Endocrinol.* 302, 148–158. doi: 10.1016/j.mce.2008.11.003

Go, A. S., Mozaffarian, D., Roger, V. L., Benjamin, E. J., Berry, J. D., Blaha, M. J., et al. (2014). Executive summary: heart disease and stroke statistics–2014 update: a report from the American heart association. *Circulation* 129, 399–410. doi: 10.1161/01.cir.0000442015.53336.12

Gu, Y. Y., Huang, P., Li, Q., Liu, Y. Y., Liu, G., Wang, Y. H., et al. (2018). YangXue qingnao wan and silibinin capsules, the two chinese medicines. *Front. Physiol.* 9:658. doi: 10.3389/fphys.2018.00658

Guerrero, J., Santibanez, J. F., Gonzalez, A., and Martinez, J. (2004). EGF receptor transactivation by urokinase receptor stimulus through a mechanism involving Src and matrix metalloproteinases. *Exp. Cell Res.* 292, 201–208. doi: 10.1016/j.yexcr.2003.08.011

Hazama, F., Amano, S., Haebara, H., and Okamoto, K. (1975). Changes in vascular permeability in stroke-prone spontaneously hypertensive rats studied with peroxidase as a tracer. *Acta. Pathol. JPN* 25, 565–574. doi: 10.1111/j.1440-1827.1975.tb01991.x

Heistad, D. D. (1984). Protection of the blood-brain barrier during acute and chronic hypertension. *Fed. Proc.* 43, 205–209.

Hinshaw, D. B., Burger, J. M., Miller, M. T., Adams, J. A., Beals, T. F., and Omann, G. M. (1993). ATP depletion induces an increase in the assembly of a labile pool of polymerized actin in endothelial cells. *Am. J. Physiol. Cell Physiol.* 264, C1171–C1179. doi: 10.1152/ajpcell.1993.264.5.C1171

Huang, P., Zhou, C. M., Qin, H., Liu, Y. Y., Hu, B. H., Chang, X., et al. (2012). Cerebralcare granule(R) attenuates blood-brain barrier disruption after middle

cerebral artery occlusion in rats. *Exp. Neurol.* 237, 453–463. doi: 10.1016/j.expneurol.2012.07.017

Ishida, H., Takemori, K., Dote, K., and Ito, H. (2006). Expression of glucose transporter-1 and aquaporin-4 in the cerebral cortex of stroke-prone spontaneously hypertensive rats in relation to the blood-brain barrier function. *Am. J. Hypertens.* 19, 33–39. doi: 10.1016/j.amjhyper.2005.06.023

Labrecque, L., Nyalendo, C., Langlois, S., Durocher, Y., Roghi, C., Murphy, G., et al. (2004). Src-mediated tyrosine phosphorylation of caveolin-1 induces its association with membrane type 1 matrix metalloproteinase. *J. Biol. Chem.* 279, 52132–52140. doi: 10.1074/jbc.M409617200

Li, Y., Li, Q., Pan, C.-S., Yan, L., Hu, B.-H., Liu, Y.-Y., et al. (2018). Bushen huoxue attenuates diabetes-induced cognitive impairment by improvement of cerebral microcirculation: involvement of RhoA/ROCK/moesin and Src signaling pathways. *Front. Physiol.* 9:527. doi: 10.3389/fphys.2018.00527

Lippoldt, A., Kniesel, U., Liebner, S., Kalbacher, H., Kirsch, T., Wolburg, H., et al. (2000). Structural alterations of tight junctions are associated with loss of polarity in stroke-prone spontaneously hypertensive rat blood-brain barrier endothelial cells. *Brain Res.* 885, 251–261. doi: 10.1016/s0006-8993(00)02954-1

Mamo, J. C. L., Lam, V., Giles, C., Coulson, S. H., Fimognari, N., Mooranian, A., et al. (2017). Antihypertensive agents do not prevent blood-brain barrier dysfunction and cognitive deficits in dietary-induced obese mice. *Int. J. Obes.* 41, 926–934. doi: 10.1038/ijo.2017.57

Marwick, T. H., Gillebert, T. C., Aurigemma, G., Chirinos, J., Derumeaux, G., Galderisi, M., et al. (2015). Recommendations on the use of echocardiography in adult hypertension: a report from the European Association of Cardiovascular Imaging (EACVI) and the American Society of Echocardiography (ASE) dagger. *Eur. Heart. J. Cardiovasc. Imaging* 16, 577–605. doi: 10.1093/ehjci/jev076

Seyed, K. T., Daniele, T., and Francesco, A. (2012). Spontaneously hypertensive rat as a model of vascular brain disorder: microanatomy, neurochemistry and behavior. *J. Neurol. Sci.* 322, 241–249. doi: 10.1016/j.jns.2012.05.047

Sun, K., Hu, Q., Zhou, C. M., Xu, X. S., Wang, F., Hu, B. H., et al. (2010). Cerebralcare granule, a Chinese herb compound preparation, improves cerebral microcirculatory disorder and hippocampal CA1 neuron injury in gerbils after ischemia-reperfusion. *J. Ethnopharmacol.* 130, 398–406. doi: 10.1016/j.jep.2010.05.030

Tagami, M., Kubota, A., Sunaga, T., Fujino, H., Maezawa, H., Kihara, M., et al. (1983). Increased transendothelial channel transport of cerebral capillary endothelium in stroke-prone SHR. *Stroke* 14, 591–596. doi: 10.1161/01.str.14.4.591

Tian, G. H., Sun, K., Huang, P., Zhou, C. M., Yao, H. J., Huo, Z. J., et al. (2013). Long-term stimulation with electroacupuncture at DU20 and ST36 rescues hippocampal neuron through attenuating cerebral blood flow in spontaneously hypertensive rats. *Evid. Based Complement. Alternat. Med.* 2013:482947. doi: 10.1155/2013/482947

Ueno, M., Sakamoto, H., Liao, Y. J., Onodera, M., Huang, C. L., Miyanaka, H., et al. (2004). Blood-brain barrier disruption in the hypothalamus of young adult spontaneously hypertensive rat. *Histochem. Cell Biol.* 122, 131–137.

Wang, F., Hu, Q., Chen, C. H., Xu, X. S., Zhou, C. M., Zhao, Y. F., et al. (2012). The protective effect of cerebralcare granule(R) on brain edema, cerebral microcirculatory disturbance, and neuron injury in a focal cerebral ischemia rat model. *Microcirculation* 19, 260–272. doi: 10.1111/j.1549-8719.2011.00155.x

Wang, Y., Zhang, R., Tao, C., Xu, Z., Chen, W., Wang, C., et al. (2018). Blood-brain barrier disruption and perivascular beta-amyloid accumulation in the brain of aged rats with spontaneous hypertension: evaluation with dynamic contrast-enhanced magnetic resonance imaging. *Korean J. Radiol.* 19, 498–507. doi: 10.3348/kjr.2018.19.3.498

Xu, X. S., Ma, Z. Z., Wang, F., Hu, B. H., Wang, C. S., Liu, Y. Y., et al. (2009). The antioxidant cerebralcare granule attenuates cerebral microcirculatory disturbance during ischemia-reperfusion injury. *Shock* 32, 201–209. doi: 10.1097/SHK.0b013e3181996d61

Xu, Y., Liu, Z., Song, X., Zhang, K., Li, X., Li, J., et al. (2015). Cerebralcare granule(R) attenuates cognitive impairment in rats continuously overexpressing microRNA-30e. *Mol. Med. Rep.* 12, 8032–8040. doi: 10.3892/mmr.2015.4469

Conflict of Interest: The authors declare that the research was conducted in the absence of any commercial or financial relationships that could be construed as a potential conflict of interest.

Copyright © 2019 Jiao, Huang, Yan, Sun, Pan, Li, Fan, Ma and Han. This is an open-access article distributed under the terms of the Creative Commons Attribution License (CC BY). The use, distribution or reproduction in other forums is permitted, provided the original author(s) and the copyright owner(s) are credited and that the original publication in this journal is cited, in accordance with accepted academic practice. No use, distribution or reproduction is permitted which does not comply with these terms.

frontiers in Physiology

SYSTEMATIC REVIEW
published: 16 October 2019
doi: 10.3389/fphys.2019.01292

Ginkgolide B for Myocardial Ischemia/Reperfusion Injury: A Preclinical Systematic Review and Meta-Analysis

Peng-Chong Zhu[1†], Qiang Tong[1†], Zhuang Zhuang[1], Zi-Hao Wang[1], Li-Hui Deng[1], Guo-qing Zheng[2] and Yan Wang[1*]*

[1] Department of Cardiology, The Second Affiliated Hospital and Yuying Children's Hospital of Wenzhou Medical University, Wenzhou, China, [2] Department of Neurology, The Second Affiliated Hospital and Yuying Children's Hospital of Wenzhou Medical University, Wenzhou, China

Ginkgolide B (GB) is an extract of dried Ginkgo biloba leaves and possesses various pharmacological activities in the cardiovascular system. Herein, we aim to assess the available preclinical evidence and possible mechanisms of GB for myocardial ischemia/reperfusion injury. The study quality score was assessed using the CAMARADES 10-item checklist. Rev-Man 5.3 software was used for data analyses. Nineteen studies with total 437 animals were included for analysis. Meta-analyses indicated that GB interventions significantly reduce myocardial infarct size and cardiac markers when compared with control ($P < 0.05$). The possible mechanisms via which GB exerts cardioprotective effects are mainly associated with anti-oxidation, anti-inflammation, anti-apoptosis, and improvement of energy metabolism. Our study indicates that GB might be a promising cardioprotective agent for myocardial ischemia/reperfusion injury and may contribute to future clinical trial design.

Keywords: Ginkgolide B, myocardial ischemia/reperfusion injury, possible mechanisms, preclinical evidence, meta-analysis

OPEN ACCESS

Edited by:
Qiaobing Huang,
Southern Medical University, China

Reviewed by:
Lin Yao,
Guangzhou University of Chinese Medicine, China
You Yun,
China Academy of Chinese Medical Sciences, China

***Correspondence:**
Guo-qing Zheng
gq_zheng@sohu.com
Yan Wang
wywzchina@sina.com

[†]These authors have contributed equally to this work

Specialty section:
This article was submitted to Vascular Physiology, a section of the journal Frontiers in Physiology

Received: *25 July 2019*
Accepted: *25 September 2019*
Published: *16 October 2019*

Citation:
Zhu P-C, Tong Q, Zhuang Z, Wang Z-H, Deng L-H, Zheng G and Wang Y (2019) Ginkgolide B for Myocardial Ischemia/Reperfusion Injury: A Preclinical Systematic Review and Meta-Analysis. Front. Physiol. 10:1292. doi: 10.3389/fphys.2019.01292

INTRODUCTION

Coronary heart disease (CHD) is the leading cause of death and disability globally (Ibanez et al., 2015). Acute myocardial infarction (AMI) is one critical clinical presentation of coronary artery disease (Yellon and Hausenloy, 2007). Early restoration of blood flow through thrombolysis or primary percutaneous coronary intervention has been proved to be the most effective method to rescue ischemic myocardium, reduce infarct size, and improve the clinical outcomes (Frank et al., 2012). However, the process of reperfusion paradoxically lead to myocardial ischemia/reperfusion (I/R) injury such as myocardial necrosis, stunning, heart failure, no-reflow and reperfusion arrhythmias (Binder et al., 2015), which would undermine the benefits of myocardial reperfusion (Minamino, 2012). Myocardial I/R injury is an intricate phenomenon involved in many factors, all conducing to the final damage inflicted on the cardiomyocyte (Bulluck et al., 2016). Over the past 3 decades, numerous therapeutic strategies, both pharmacologic and non-pharmacologic, have been proposed to ameliorate the myocardial I/R injury in animal experiments. However, the basic research yielded inconclusive results or failed to translate into the clinical setting efficiently (Eltzschig and Eckle, 2011). Hence, it is worthy to find a novel cardioprotective therapeutic intervention to prevent further tissue injury caused by reperfusion.

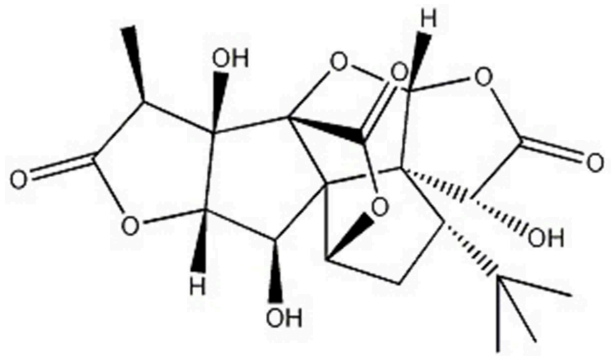


FIGURE 1 | Chemical structures of GB ($C_{20}H_{24}O_{10}$).

Ginkgo biloba L., known as "living fossil" in plant kingdom (Jacobs and Browner, 2000), its leaves were applied as a traditional Chinese medicine (TCM) for the management of cardiovascular disorders for hundreds of years because of its properties of promoting blood circulation to remove blood stasis (Zhang et al., 2016) and activating meridians to stop pain (Li et al., 2017). Ginkgolide B (GB) (**Figure 1**), an extract of dried Ginkgo biloba leaves, was discovered as a natural antagonist of platelet activating factor (PAF) with various biological and pharmacological functions, including anti-allergic (Bilia, 2002), anti-inflammation (Xia and Fang, 2007), and anti-oxidation (Maclennan et al., 2002). Thus, it was widely used for I/R diseases including AMI.

The animal research has its special primary purpose in improving the understanding of physiologic and pathologic processes (Briel et al., 2013). Systematic reviews of preclinical studies play an important role in healthcare practice which can help promote the translation of findings from animal studies to clinical trials rapidly and appropriately, and avoid unintended waste of time (Sandercock and Roberts, 2002). In addition, preclinical systematic review can contribute to illustrate mechanisms, synthesize the available evidence, support clinical decision-making, and improve the methodological quality of experiments and guide health policy (Roberts et al., 2002). Many animal studies have hitherto investigated the role of GB in myocardial I/R injury. However, the efficacy and mechanisms of GB for myocardial I/R injury have not been systematically appraised and summarized. In the present study, we performed a systematic review for these animal studies to assess the available preclinical evidence and possible mechanisms of GB in treating myocardial I/R injury.

METHODS

Data Sources and Search Strategy

The PRISMA checklist is available as supporting information (Stewart et al., 2015). We searched for animal studies of GB for myocardial I/R injury in Chinese National Knowledge Infrastructure (CNKI), EMBASE, PubMed, VIP information database, Web of Science, and Wanfang data Information Site published up to the end of April 2019. The following search phrases were used: "Yinxingneizhi B (MeSH Terms) OR Ginkgolide B (Title/Abstract)" AND "Myocardial infarction OR Myocardial ischemia OR Myocardial I/R". The references of the included articles cited were searched manually for the eligible studies.

Eligibility Criteria

Studies were included for analysis when they meet: (1) animal studies assessing the administration of GB for myocardial I/R model *in vivo* or *ex vivo* except cell studies, case reports, reviews, abstracts, and comments; (2) analyzed intervention received GB treatment merely; comparator intervention received vehicle or no treatment; (3) primary outcomes were myocardial infarction (MI) size, myocardial injury marker, ST-segment changes in electrocardiograms, or cardiac function indicators in cardiac ultrasound, while secondary outcomes were serum indices or protein levels relative to the mechanisms of GB in myocardial I/R injury. The studies compared with other TCM, administered other additional pharmacological treatment, without predetermined outcome index and without involving animal models of myocardial I/R injury were excluded.

Data Extraction

The following details were recorded: (1) first author's name and year of publication; (2) animal information, including species, gender, number, and weight; (3) methods for myocardial I/R model establishment, including I/R duration and coronary artery occluded; (4) method for anaesthetic induction; (5) the information of treatment, including time of intervention, dose, and route of administration; (6) the primary outcome measures, secondary outcome measures and its intergroup differences. Only the data of final test was collected when outcome measures were tested at different time points. The result of highest dose was extracted if various doses of drugs were used in the study. If some data were only expressed as graphs, we reached out to the authors for raw data. Measure numerical values by digital ruler software when no response was got from authors.

Risk of Bias in Individual Studies

Two authors independently evaluated the quality of study using the 10-point scoring scale (Macleod et al., 2004): A, peer-reviewed publication; B, statement of temperature control; C, random allocation to groups; D, allocation concealment; E, blinded assessment of outcome; F, use of anesthetic without significant intrinsic cardioprotective activity; G, appropriate animal model (aged, diabetic, or hypertensive); H, sample size calculation; I, compliance with animal welfare regulations; and J, statement of potential conflict of interests. Study selection, data extraction, and quality evaluation of studies were independently performed by two authors, and the disputes were discussed in group discussion.

Statistical Analysis

All outcome measures were treated as continuous data. Every outcome with at least 2 available studies was analyzed with RevMan V.5.3 software. Outcomes were presented as

Standardized mean difference (SMD) with 95% confidence interval (CI). Heterogeneity among the studies was evaluating using the I-square (I^2) statistics test. If $I^2 > 50\%$, a random effects model was applied; otherwise, a fixed effects model was applied. P-value <0.05 was considered significant. A forest plot was created to summarize the meta-analysis study results.

RESULTS

The initial search yielded a total of 213 studies. After excluding 137 irrelevant and duplicated studies, the full texts of 76 studies were screened. In the process, 57 studies were excluded according to the inclusion and exclusion criteria. Ultimately, 19 studies (Liebgott et al., 2000; Jiao et al., 2002; Rioufol et al., 2003; Billottet et al., 2005; Zhang et al., 2005, 2018; Hao et al., 2009, 2013, 2016; Zhao et al., 2014; Pei et al., 2015; Xiong and Wei, 2015; Bai et al., 2016; Cao et al., 2016; Hao and Dong, 2017; Meng, 2017; Zhuang et al., 2017; Chai et al., 2018; Yang et al., 2018) were selected. A detailed step of the selection process is shown in **Figure 2**.

Characteristics of Included Studies

Twelve Chinese studies (Zhang et al., 2005; Hao et al., 2013, 2016; Zhao et al., 2014; Xiong and Wei, 2015; Bai et al., 2016; Cao et al., 2016; Hao and Dong, 2017; Meng, 2017; Zhuang et al., 2017; Chai et al., 2018; Yang et al., 2018) and 7 English studies (Liebgott et al., 2000; Jiao et al., 2002; Rioufol et al., 2003; Billottet et al., 2005; Hao et al., 2009; Pei et al., 2015; Zhang et al., 2018) were published between 1996 and 2018. Male Sprague-Dawley rats (11 studies) (Hao et al., 2009, 2013, 2016; Xiong and Wei, 2015; Bai et al., 2016; Hao and Dong, 2017; Meng, 2017; Zhuang et al., 2017; Chai et al., 2018; Yang et al., 2018; Zhang et al., 2018), male/female Sprague-Dawley rats (2 studies) (Zhao et al., 2014; Cao et al., 2016), male Wistar rats (4 studies) (Liebgott et al., 2000; Jiao et al., 2002; Billottet et al., 2005; Pei et al., 2015), male/female Wistar rats (1 study) (Zhang et al., 2005), and male/female Farm pigs (1 study) (Rioufol et al., 2003)were utilized. Chloral hydrate was used in 4 studies (Zhao et al., 2014; Xiong and Wei, 2015; Yang et al., 2018; Zhang et al., 2018); pentobarbital sodium in 7 studies (Liebgott et al., 2000; Billottet et al., 2005; Hao et al., 2013, 2016; Pei et al., 2015; Cao et al., 2016; Hao and Dong, 2017); urethane in 6 studies (Jiao et al., 2002; Zhang et al., 2005; Bai et al., 2016; Meng, 2017; Zhuang et al., 2017; Chai et al., 2018); pentobarbitalin 2 studies (Rioufol et al., 2003; Hao et al., 2009) for anesthesia. Ligating the coronary artery was to induce the model of I/R, of which the left anterior descending coronary artery (LAD) was in 11 studies (Jiao et al., 2002; Rioufol et al., 2003; Pei et al., 2015; Xiong and Wei, 2015; Bai et al., 2016; Cao et al., 2016; Meng, 2017; Zhuang et al., 2017; Chai et al., 2018; Yang et al., 2018; Zhang et al., 2018). Others were established by the langendorff method (Liebgott et al., 2000; Billottet et al., 2005; Zhang et al., 2005; Hao et al., 2009, 2013, 2016; Zhao et al., 2014; Hao and Dong, 2017). MI size as outcome was reported in 9 studies (Jiao et al., 2002; Hao et al., 2009, 2016; Xiong and Wei, 2015; Bai et al., 2016; Cao et al., 2016; Meng, 2017; Zhuang

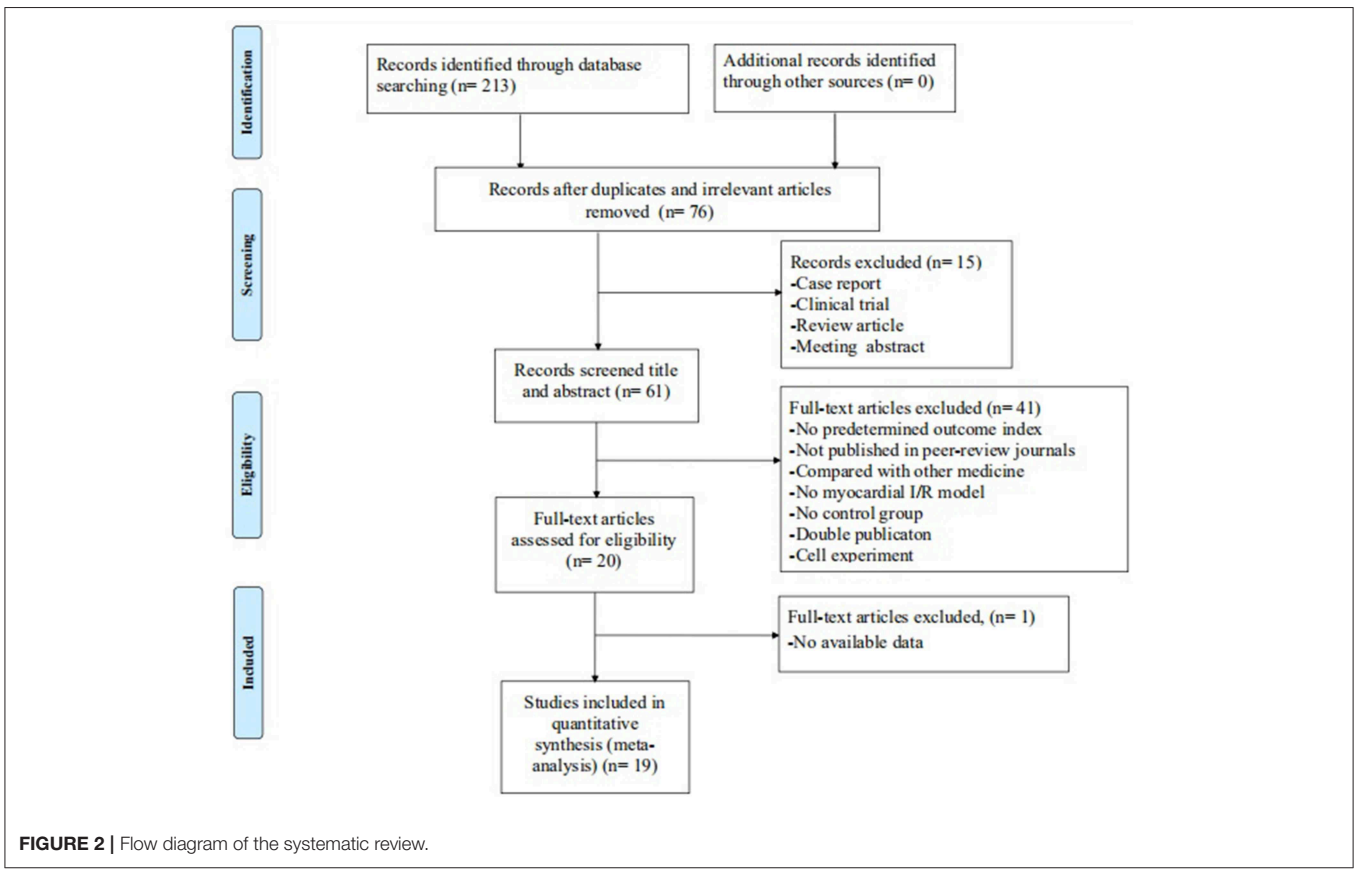


FIGURE 2 | Flow diagram of the systematic review.

TABLE 1 | Characteristics of the 19 included studies.

Study (years)	Species (Sex, *n* = experimental/ control group)	Weight	Model (method)	Anesthetic	Treatment group (method to GB)	Control group	Outcome index (time)	Intergroup differences
Zhuang et al., 2017 (1)	SD rats (male, 20/20)	220–260 g	Block LAD for 30 min then reperfusion	Urethane (650 mg/kg)	Intraperitoneal injection GB (60 mg/kg*d), once a day, for 7 days, after establishing model	Intraperitoneal injection isasteric normal saline, once a day, for 7 days, after establishing model	1. Infarct size (AAI/LVA) 2. Apoptosis index 3. Bcl-2 4. Bax 5. Caspase-3	1. $P < 0.01$ 2. $P < 0.01$ 3. $P < 0.01$ 4. $P < 0.01$ 5. $P < 0.01$
Xiong and Wei, 2015 (2)	SD rats (male, 20/20)	250–270 g	Block of LAD for 30 min then reperfusion for 48 h	7% chloral hydrate	Gavaged with GB (60 mg/kg*d), once a day, for 7 days, before establishing model	Gavaged with isasteric normal saline, once a day, for 7 days, before establishing model	1. Infarct size (AAI/LVA) 2. EF 3. FS 4. Bcl-2 5. Bax 6. p-ErK 7.p-JNK 8. p-p38MAPK	1. $P < 0.01$ 2. $P < 0.01$ 3. $P < 0.01$ 4. $P < 0.01$ 5. $P < 0.01$ 6. $P < 0.01$ 7. $P < 0.01$ 8. $P < 0.01$
Cao et al., 2016 (3)	SD rats (male/female, 10/10)	200–240 g	Block LAD for 30 min then reperfusion for 2 h	Pentobarbital sodium (45 mg/kg)	Tail intravenous injection GB (8 mg/kg), 1 h before establishing model	Tail intravenous injection isasteric normal saline, 1 h before establishing model	1. Infarct size (AAI/LVA) 2. CK 3. LDH 4. SOD 5. MDA	1. $P < 0.05$ 2. $P < 0.01$ 3. $P < 0.01$ 4. $P < 0.01$ 5. $P < 0.01$
Meng, 2017 (4)	SD rats (male, 20/20)	220–260 g	Block LAD for 30 min then reperfusion	Urethane (650 mg/kg)	Intraperitoneal injection GB (60 mg/kg*d), once a day, for 7 days, after establishing model	Intraperitoneal injection isasteric normal saline, once a day, for 7 days, after establishing model	1. Infarct size (AAI/LVA) 2. EF 3. FS 4. LVIDd 5. LVIDs 6. SV 7. Apoptosis index 8. AST 9. CK 10. LDH	1. $P<0.01$ 2. $P<0.01$ 3. $P<0.01$ 4. $P<0.01$ 5. $P<0.01$ 6. $P < 0.01$ 7. $P < 0.01$ 8. $P < 0.01$ 9. $P < 0.01$
Bai et al., 2016 (5)	SD rats (male, 20/20)	220–260 g	Block LAD for 30 min then reperfusion	Urethane (650 mg/kg)	Intraperitoneal injection GB (60 mg/d), once a day, for 7 days, after establishing model	Intraperitoneal injection isasteric normal saline, once a day, for 7 days, after establishing model	1. Infarct size (AAI/LVA) 2. Apoptosis index 3. SOD 4. GSH-Px 5. CAT 6. MDA 7. AST 8. CK 9. LDH 10. NF-kB	1. $P < 0.01$ 2. $P < 0.01$ 3. $P < 0.01$ 4. $P < 0.01$ 5. $P < 0.01$ 6. $P < 0.01$ 7. $P < 0.01$ 8. $P < 0.01$ 9. $P < 0.01$ 10. $P < 0.01$
Chai et al., 2018 (6)	SD rats (male, 20/20)	220–260 g	Block LAD for 30 min then reperfusion for 1 h	Urethane (1 g/kg)	Intraperitoneal injection GB (60 mg/kg*d), once a day, for 7 days, before establishing model	Intraperitoneal injection (18 mg/kg*d) normal saline, once a day, for 7 days, before establishing model	1. Arrhythmia score 2. SOD 3. GSH-Px 4. MDA	1. $P < 0.01$ 2. $P < 0.01$ 3. $P < 0.01$ 4. $P < 0.01$
Yang et al., 2018 (7)	SD rats (male, 7/7)	180–220 g	Block LAD for 30 min then reperfusion for 2 h	10% chloral hydrate	Intraperitoneal injected with GB (60 mg/kg), 30 min before establishing model	Intraperitoneal injection isasteric normal saline, 30 min before establishing model	1. LVSP 2. LVDP 3. +dP/dtmax 4. –dP/dtmax 5. Caspase-3	1. $P < 0.05$ 2. $P < 0.05$ 3. $P < 0.05$ 4. $P < 0.05$ 5. $P < 0.05$

(Continued)

TABLE 1 | Continued

Study (years)	Species (Sex, *n* = experimental/ control group)	Weight	Model (method)	Anesthetic	Treatment group (method to GB)	Control group	Outcome index (time)	Intergroup differences
Jiao et al., 2002 (8)	Wistar rats (male, 12/12)	250–300 g	Block LAD for 30 min then reperfusion for 3 h	Urethane (1 g/kg)	Intraperitoneal injection GB (5 mg/kg), 25 and 10 min before establishing model respectively	Intraperitoneal injection isasteric normal saline, 25 and 10 min before establishing model respectively	1. Infarct size (AAI/AAR) 2. LVSP 3. +dP/dtmax 4. –dP/dtmax 5. Apoptosis index	1. $P < 0.05$ 2. $P > 0.05$ 3. $P < 0.05$ 4. $P > 0.05$ 5. $P < 0.05$
Rioufol et al., 2003 (9)	Farm pigs (male/female, 6/7)	27–28 Kg	Block LAD for 10 min then reperfusion for 3 h	Pentobarbital (15 mg/kg)	Intravenous injection GB (0.3 mg/kg), 48 h and 24 h before establishing model	Intravenous injection isasteric normal saline, 48 h and 24 h before establishing model	1. HR 2. Mean arterial pressure 3. Segment shortening	1. $P > 0.05$ 2. $P > 0.05$ 3. $P > 0.05$
Pei et al., 2015 (10)	Wistar rats (male, 10/12)	280–400 g	Block LAD for 5 min then reperfusion for 10 min	pentobarbitalsodium (4.5 mg/kg)	Intravenous injection GB (15 mg/kg), 10 min before establishing model	Intravenous injection isasteric normal saline, 10 min before establishing model	1. LVSP 2. Arrhythmia score 3. +dP/dtmax 4. –dP/dtmax 5. LDH	1. $P < 0.01$ 2. $P < 0.01$ 3. $P < 0.01$ 4. $P < 0.01$ 5. $P < 0.05$
Hao et al., 2009 (11)	SD rats (male, 7/7)	220–250 g	Langendorff Model 30 min stabilization I/R (30 min/120 min)	Pentobarbital (150 mg/kg)	GB (10uM), for 10 min before ischemia	No treatment	1. Infarct size (AAI/LVA) 2. HR 3. LVSP 4. LVEDP 5. +dP/dtmax 6. –dP/dtmax 7. LDH 8. Bcl-2 9. Bax	1. $P < 0.05$ 2. $P < 0.01$ 3. $P > 0.05$ 4. $P > 0.05$ 5. $P < 0.05$ 6. $P < 0.05$ 7. $P < 0.05$ 8. $P > 0.05$ 9. $P > 0.05$
Hao and Dong, 2017 (12)	SD rats (male, 10/10)	350–500 g	Langendorff Model 30 min, I/R (30 min/60 min)	1% pentobarbital sodium	GB (10 μmol/L), first 10 min of reperfusion	No treatment	1. ΔLVP (LVSP -LVEDP) 2. +dP/dtmax 3. –dP/dtmax 4. LDH	1. $P < 0.05$ 2. $P < 0.05$ 3. $P < 0.05$ 4. $P < 0.05$
Hao et al., 2013 (13)	SD rats (male, 8/8)	200–250 g	Langendorff Model 30 min stabilization I/R (20 min/40 min)	1% pentobarbital sodium	GB (10 μmol/L), for 10 min before ischemia	No treatment	1. ΔLVP (LVSP -LVEDP) 2. +dP/dtmax 3. –dP/dtmax 4. HR 5. LDH 6. SOD	1. $P < 0.01$ 2. $P < 0.05$ 3. $P < 0.01$ 4. $P < 0.05$ 5. $P < 0.01$ 6. $P < 0.05$
Hao et al., 2016 (14)	SD rats (male, 10/10)	350–500 g	Langendorff Model 30 min stabilization I/R (30 min/90 min)	1% pentobarbital sodium	GB (10 μmol/L), first 10 min of reperfusion	No treatment	1. Infarct size (AAI/LVA) 2. LVSP 3. LVEDP 4. +dP/dtmax 5. –dP/dtmax 6. LDH 7. Bcl-2 8. Bax	1. $P < 0.05$ 2. $P > 0.05$ 3. $P < 0.05$ 4. $P < 0.05$ 5. $P < 0.05$ 6. $P < 0.01$ 7. $P < 0.05$ 8. $P < 0.05$

(Continued)

TABLE 1 | Continued

Study (years)	Species (Sex, *n* = experimental/ control group)	Weight	Model (method)	Anesthetic	Treatment group (method to GB)	Control group	Outcome index (time)	Intergroup differences
Liebgott et al., 2000 (15)	Wistar rats (male, 12/13)	300–350 g	Langendorff Model 30 min stabilization, low-flow ischemia/I/R (10 min/30 min/60 min)	Pentobarbital sodium (50 mg/kg)	GB (0.05 μg/ml), last 10 min of perfusion, entire period of low-flow ischemia and the first 10 min of reperfusion	No treatment	1. LVDP 2. LVEDP 3. RPP 4. LVdP/dt 5. CF	1. $P < 0.02$ 2. $P < 0.02$ 3. $P < 0.02$ 4. $P < 0.02$ 5. $P < 0.02$
Zhao et al., 2014 (16)	SD rats (male/female, 10/10)	200–250 g	Langendorff Model 30 min stabilization I/R (20 min/40 min)	10% chloral hydrate	GB (10 μmol/L), for 10 min before ischemia	No treatment	1. ΔLVP (LVSP -LVEDP) 2. +dP/dtmax 3. –dP/dtmax 4. LDH	1. $P < 0.01$ 2. $P < 0.05$ 3. $P < 0.01$ 4. $P < 0.01$
Zhang et al., 2005 (17)	Wistar rats (male/female, 8/8)	200–250 g	Langendorff Model 30 min stabilization, I/R (15 min/30 min)	20% Urethane (1.0 g/kg)	GB (10 μmol/L), for 10 min before ischemia	No treatment	1. Arrhythmia score 2. LDH 3. CK 4. SOD 5. MDA	1. $P < 0.01$ 2. $P < 0.05$ 3. $P < 0.05$ 4. $P < 0.05$ 5. $P < 0.01$
Billottet et al., 2005 (18)	Wistar rats (male, 12/12)	300–350 g	Langendorff Model 30 min stabilization, low-flow ischemia/I/R (20 min/20 min/60 min)	Pentobarbital sodium (50 mg/kg)	GB (0.05 μg/ml), last 10 min of perfusion, entire period of low-flow ischemia and the first 10 min of reperfusion	No treatment	1. LVDP 2. LVEDP 3. RPP 4. LVdP/dt 5. CF	1. $P < 0.05$ 2. $P < 0.05$ 3. $P < 0.05$ 4. $P < 0.05$ 5. $P < 0.05$
Zhang et al., 2018 (19)	SD rats (male, 8/8)	250–300 g	Block LAD for 40 min then reperfusion for 2 h	Chloral hydrate (300 mg/kg)	Intraperitoneal injection GB (32 mg/kg*d), once a day, for 7 days, before establishing model	Intraperitoneal injection isasteric normal saline, once a day, for 7 days, after establishing model	1. Infarct size (AAI/AAR) 2. histopathological scores 3. PMNs 4. TNF-α, 5. IL-6 6. MPO	1. $P < 0.05$ 2. $P < 0.05$ 3. $P < 0.05$ 4. $P < 0.05$ 5. $P < 0.05$ 6. $P < 0.05$

AAI, Area at infarct; AAR, area at risk; AST, aspartate transaminase; Bax, Bcl-2-Associated X; Bcl-2, B-cell lymphoma-2; CAT, catalase; CK, creatine kinase; EF, ejection fraction; ErK, extracellular signal-regulated kinase; FS, fractional shorting; GSH-Px, glutathione peroxidase; HR, heart rate; IL-6, interleukin-6; JNK, c-Jun N-terminal kinase; LAD, left anterior descending coronary artery; LVA, left ventricular area; LVDP, left ventricular developed pressure; LVEDP, left ventricular end diastolic pressure; LDH, lactate dehydrogenase; LVIDd, left ventricular internal diameter at end-diastole; LVIDs, left ventricular internal diameter at end-systole; LVSP, Left ventricular systolic pressure; MDA, malondialdehyde; MPO, myeloperoxidase; ±dp/dtmax, Maximal rate of the increase/decrease of left ventricular pressure; p38MAPK, p38 mitogen-activated protein kinase; NF-kB, Nuclear factor-kappa B; PMNs, polymorphonuclears; RPP, rate pressure pruduct; SOD, superoxide dismutase; SV, stroke volume; SD rats, Sprague-Dawley; TNF-α, tumor necrosis factor-α.

et al., 2017; Zhang et al., 2018); ejection fraction (EF) in 2 studies (Xiong and Wei, 2015; Meng, 2017), fractional shorting (FS) in 2 studies (Xiong and Wei, 2015; Meng, 2017); Maximal rate of the increase/decrease of left ventricular pressure (±dp/dtmax) in 8 studies (Jiao et al., 2002; Hao et al., 2009, 2013, 2016; Zhao et al., 2014; Pei et al., 2015; Hao and Dong, 2017; Yang et al., 2018); left ventricular developed pressure (LVDP) in 3 studies (Liebgott et al., 2000; Billottet et al., 2005; Yang et al., 2018); left ventricular end diastolic pressure (LVEDP) in 4 studies (Liebgott et al., 2000; Billottet et al., 2005; Hao et al., 2009, 2016); myocardial cell apoptosis index (AI) in 4 studies (Jiao et al., 2002; Bai et al., 2016; Meng, 2017; Zhuang et al., 2017); arrhythmia score in 3 studies (Zhang et al., 2005; Pei et al., 2015; Chai et al., 2018). Level of lactate dehydrogenase (LDH) was reported in 9 studies (Hao et al., 2009, 2013, 2016; Zhao et al., 2014; Pei et al., 2015; Bai et al., 2016; Cao et al., 2016; Hao and Dong, 2017; Meng, 2017); creatine kinase (CK) in 4 studies (Zhang et al., 2005; Bai et al., 2016; Cao et al., 2016; Meng, 2017) superoxide dismutase (SOD) in 5 studies (Zhang et al., 2005; Hao et al., 2013; Bai et al., 2016; Cao et al., 2016; Chai et al., 2018); malondialdehyde (MDA) in 4 studies (Zhang et al., 2005; Bai et al., 2016; Cao et al., 2016; Chai et al., 2018); glutathione peroxidase (GSH-Px) in 2 studies (Bai et al., 2016; Chai et al., 2018); caspase-3 in 2 studies (Zhuang et al., 2017; Yang et al., 2018); B-cell lymphoma-2 (Bcl-2) in 4 studies (Hao et al., 2009, 2016; Xiong and Wei, 2015; Zhuang et al., 2017) and Bcl-2-Associated X (Bax) in 4 studies (Hao et al., 2009, 2016; Xiong and Wei, 2015; Zhuang et al., 2017); aspartate transaminase (AST) in 2 studies (Bai et al., 2016; Meng, 2017). Nuclear factor-kappaB (NF-kB) was mentioned in 2 study (Bai et al., 2016; Zhang et al., 2018); p38-mitogen-activated protein kinase (p38-MAPK), extracellular signal-regulated kinase (ERK) and c-Jun N-terminal kinase (JNK) in 1 study (Xiong and Wei, 2015); coronary flow (CF) in 1 study (Billottet et al., 2005); segment shortening in 1 study (Rioufol et al., 2003), mean arterial pressure (MAP) in 1 study (Rioufol et al., 2003), and tumor necrosis factor-α (TNF-α) and interleukin-6 (IL-6) in 1 study (Zhang et al., 2018). The characteristics of selected study is provided in **Table 1**.

Study Quality

Detailed results of methodological quality are presented in **Table 2** and **Figure 3**. All studies were peer-reviewed. Use of anesthetic without significant intrinsic cardioprotective activity were all described. Eleven studies (Liebgott et al., 2000; Rioufol et al., 2003; Billottet et al., 2005; Hao et al., 2009; Pei et al., 2015; Xiong and Wei, 2015; Bai et al., 2016; Zhuang et al., 2017; Chai et al., 2018; Yang et al., 2018; Zhang et al., 2018) reported control of temperature. None of the studies discussed allocation concealment, blinded assessment of outcome and the sample size calculation. No study choose the appropriate animal model. Compliance with animal welfare regulations was stated in 12 studies (Liebgott et al., 2000; Rioufol et al., 2003; Billottet et al., 2005; Zhao et al., 2014; Pei et al., 2015; Xiong and Wei, 2015; Bai et al., 2016; Hao et al., 2016; Zhuang et al., 2017; Chai et al., 2018; Yang et al., 2018; Zhang et al., 2018) and statement of potential conflict of interests was declared in 2 studies (Pei et al., 2015; Zhang et al., 2018).

TABLE 2 | Risk of bias of the included studies.

Study	A	B	C	D	E	F	G	H	I	J	Total
Zhuang et al., 2017 (1)	+	+	+	−	−	+	−	−	+	−	5
Xiong and Wei, 2015 (2)	+	+	+	−	−	+	−	−	+	−	5
Cao et al., 2016 (3)	+	−	+	−	−	+	−	−	−	−	3
Meng, 2017 (4)	+	−	+	−	−	+	−	−	−	−	3
Bai et al., 2016 (5)	+	+	+	−	−	+	−	−	+	−	5
Chai et al., 2018 (6)	+	+	+	−	−	+	−	−	+	−	5
Yang et al., 2018 (7)	+	+	+	−	−	+	−	−	+	−	5
Jiao et al., 2002 (8)	+	−	+	−	−	+	−	−	+	−	3
Rioufol et al., 2003 (9)	+	+	+	−	−	+	−	−	+	−	5
Pei et al., 2015 (10)	+	+	+	−	−	+	−	−	+	+	6
Hao et al., 2009 (11)	+	+	+	−	−	+	−	−	+	−	4
Hao and Dong, 2017 (12)	+	−	+	−	−	+	−	−	+	−	3
Hao et al., 2013 (13)	+	−	+	−	−	+	−	−	+	−	3
Hao et al., 2016 (14)	+	−	+	−	−	+	−	−	+	−	4
Liebgott et al., 2000 (15)	+	+	+	−	−	+	−	−	+	−	5
Zhao et al., 2014 (16)	+	−	+	−	−	+	−	−	+	−	4
Zhang et al., 2005 (17)	+	−	+	−	−	+	−	−	+	−	3
Billottet et al., 2005 (18)	+	+	+	−	−	+	−	−	+	+	6
Zhang et al., 2018 (19)	+	+	+	−	−	+	−	−	+	−	5

Studies fulfilling the criteria of: A, peer reviewed publication; B, control of temperature; C, random allocation to treatment or control; D, blinded induction of model; E, blinded assessment of outcome; F, use of anesthetic without significant intrinsic cardioprotective activity; G, appropriate animal model (aged, diabetic, or hypertensive); H, sample size calculation; I, compliance with animal welfare regulations; J, statement of potential conflict of interests.

Effectiveness

Primary Outcome Measures

Myocardial infarction size

We divided the studies into two parts by different calculation methods: (1) Area at infarct/area at risk (AAI/AAR): meta-analysis of 3 studies (Jiao et al., 2002; Xiong and Wei, 2015; Zhang et al., 2018) indicated that MI size was significantly reduced using GB compared with control (SMD −3.66, 95% CI [−4.57 to −2.76], $P < 0.00001$; $I^2 = 24\%$) (**Figure 4**); (2) Area at infarct/left ventricular area (AAI/LVA): meta-analysis of 6 studies (Hao et al., 2009, 2016; Bai et al., 2016; Cao et al., 2016; Meng, 2017; Zhuang et al., 2017) indicated that MI size was significantly reduced by

using GB compared with control (SMD −2.52, 95% CI [−3.01 to −2.04], $P < 0.00001$; $I^2 = 89\%$). There was high statistical heterogeneity among comparison of MI size (AAI/LVA). We performed a sensitivity analysis, the result remained after excluding each of these studies. In addition, subgroup analysis is layered with the following groups: experimental model (*in vivo* or *ex vivo*), stage of GB administration (pre-treatment and post-treatment), and frequency of drug administration. GB prevented MI size more obviously at the model *in vivo* than the model *ex vivo* (SMD = −2.91 vs. SMD = −0.98, $P < 0.05$, **Figure 5A**). Groups with more times (≥5) of administration of GB showed a better outcome than that with fewer times (<5) (SMD = −4.13 vs. SMD = −1.23, $P < 0.05$, **Figure 5B**). Compared with giving GB after the model, the GB pre-treatment (before introducing the model) did not produce a better outcome (SMD = −1.37 vs. SMD = −3.00, $P < 0.05$, **Figure 5C**).

Cardiac function and the level of ST-segment elevation

GB was significant for improving EF and FS ($P < 0.05$) (Xiong and Wei, 2015; Meng, 2017); increasing +dp/dtmax and LVSP (Jiao et al., 2002; Hao et al., 2009, 2013, 2016; Zhao et al., 2014; Pei et al., 2015; Hao and Dong, 2017; Yang et al., 2018) in systolic function ($P < 0.05$); increasing –dp/dtmax (Jiao et al., 2002; Hao et al., 2009, 2013, 2016; Zhao et al., 2014; Pei et al., 2015; Hao and Dong, 2017; Yang et al., 2018) and LVDP (Liebgott et al., 2000; Billottet et al., 2005; Yang et al., 2018) ($P < 0.05$), and decreasing LVEDP (SMD−1.98, 95% CI [−2.53 to −1.42], $P < 0.00001$; $I^2 = 43\%$) (**Figure 6**) in diastolic function; decreasing the arrhythmia score (Zhang et al., 2005; Pei et al., 2015; Chai et al., 2018) ($P < 0.05$); and reducing the ST segment elevation (Chai et al., 2018) ($P < 0\ 05$), when compared with control.

Myocardial injury marker

Meta-analysis of 4 studies (Zhang et al., 2005; Bai et al., 2016; Cao et al., 2016; Meng, 2017) indicated GB was significant for decreasing the level of CK using (SMD −1.05, 95% CI [−1.49 to −0.61], $P < 0.00001$; $I^2 = 37\%$) (**Figure 7A**); and 2 studies (Bai et al., 2016; Meng, 2017) for decreasing the level of AST (SMD −1.92, 95% CI [−2.55 to −1.29], $P < 0.00001$; $I^2 = 0\%$) (**Figure 7B**) compared with control. Level of LDH was measured in 9 studies (Hao et al., 2009, 2013, 2016; Zhao et al., 2014; Pei et al., 2015; Bai et al., 2016; Cao et al., 2016; Hao and Dong, 2017; Meng, 2017), and all of them indicated GB was significant for reducing the level of LDH ($P < 0.05$) compared with control.

Secondary Outcome Measures

Four studies (Jiao et al., 2002; Bai et al., 2016; Meng, 2017; Zhuang et al., 2017) showed that GB-treated group was superior to the untreated group according to the reduced AI ($n = 56$, SMD −3.54, 95% CI [−4.17 to −2.92], $P< 0.00001$; $I^2 = 0\%$) (**Figure 8A**); 5 studies (Zhang et al., 2005; Hao et al., 2013; Bai et al., 2016; Cao et al., 2016; Chai et al., 2018) increasing SOD (SMD −2.23, 95% CI [1.77 to 2.69], $P < 0.00001$; $I^2 = 43\%$) (**Figure 8B**); 2 studies (Bai et al., 2016; Chai et al., 2018) increasing GSH-Px (SMD 1.89, 95% CI [1.35 to 2.43], $P < 0.00001$; $I^2 = 0\%$) (**Figure 8C**); 4 studies (Zhang et al., 2005; Bai et al., 2016; Cao et al., 2016; Chai et al., 2018) reducing MDA ($P < 0.05$); 2 studies (Zhuang et al., 2017; Yang et al., 2018) reducing caspase-3 ($P < 0.05$); 4 studies (Hao et al., 2009, 2016; Xiong and Wei, 2015; Zhuang et al., 2017) increasing the ratio of Bcl-2/Bax protein ($P < 0.05$); 1 study (Hao et al., 2016) reducing expression level of p-Akt ($P < 0.05$); 1 study (Chai et al., 2018) decreasing content of Ca^{2+} in myocardium ($P < 0.05$); 2 studies (Bai et al., 2016; Zhang et al., 2018) decreasing expression of NF-κB; 1 study (Xiong and Wei, 2015) decreasing the level of p-ErK, p-JNK, p-p38MAPK; 1 study (Zhang et al., 2018) suppressing PMNs infiltration ($P < 0.05$); and 1 study (Zhang et al., 2018) decreasing TNF-α and IL-6 ($P < 0.05$).

DISCUSSION

Summary of Evidence

In the present study, 19 studies with total 437 animals were included. GB exerted potential cardioprotective function, largely through antioxidant, anti-inflammation, anti-apoptosis and improvement of energy metabolism.

Possible Mechanism

In the early phase of reperfusion, the ischemic myocardium generates oxidative stress. Oxidative stress can increases the release of oxidative free radicals production such as ROS, RNS, and OH and decreases the ability of free radicals scavenging, which further leads to cardiomyocyte cell injury (Navarro-Yepes et al., 2014). The excessive production of oxidative free radicals in the cellular and subcellular levels peroxidates the lipid, opens the mitochondrial permeability transition pore and dysfunctions the sarcoplasmic reticulum, resulting in overloaded intracellular Ca^{2+} and damaged cell membrane (Hausenloy and Yellon, 2013). Therefore, decreasing the accumulation of oxygen free radicals is an important approach to protect against myocardial I/R injury. The present study showed that GB could increase the level of antioxidant enzymes such as SOD, GSH-Px and CAT, maintain the dynamic balance of oxygen free radicals formation, restrain trigger of lipid peroxidation, protect biomembranes' integrity and function, and decrease the release of MDA from mitochondria, thereby exerts cardioprotective effect in through antioxidation.

Myocardial I/R damages the myocardium through inflammatory response (Marchant et al., 2012). During the processes of I/R injury, NF-κB pathway (Wang et al., 2007), which is critical to the inflammation and apoptosis during various diseases, mediates the upregulated expression of various pro-inflammatory cytokines such as TNF-α, IL-6, and IL-1β (Ma et al., 2014). In addition, the upstream factors of NF-kB—mitogen-activated protein kinase (MAPK) signaling pathway, including p38 MAPK, ERK, and JNK, also participates in regulating the inflammation (Chung et al., 2012; Himaya et al., 2012). The present study showed that GB exerted anti-inflammatory effect via significantly inhibiting the expression of NF-κB proteins, reducing the level of phosphorylation of p38, Jnk, and Erk protein, and decreasing the expression of TNF-a and IL-6 compared with control.

Myocardial I/R sequentially induce the cardiomyocyte Ca^{2+} overload, oxidative stress, opening of the mitochondrial

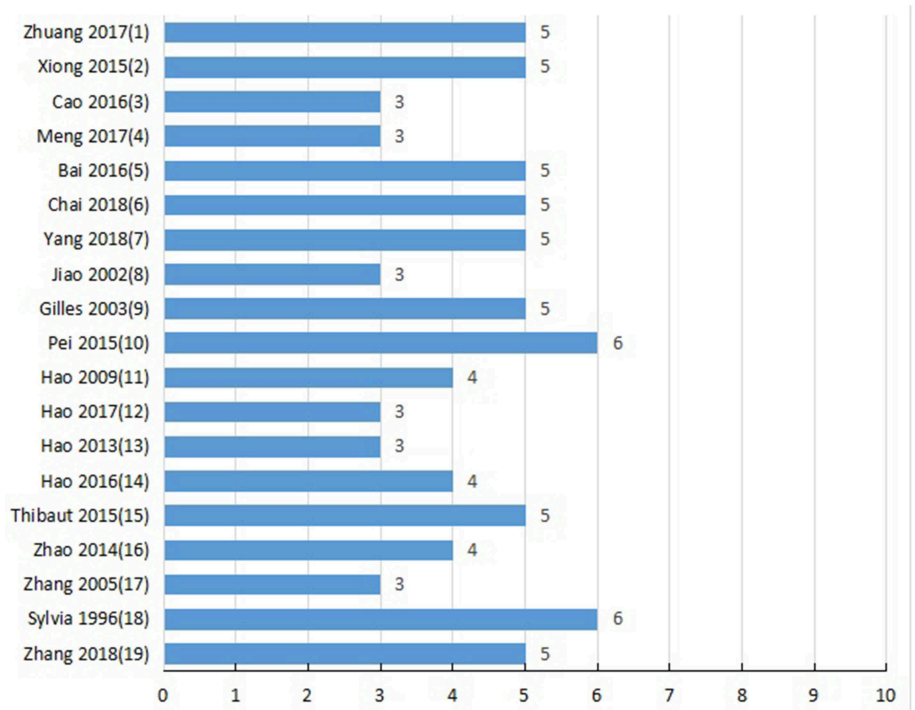


FIGURE 3 | Methodological quality for each study included.

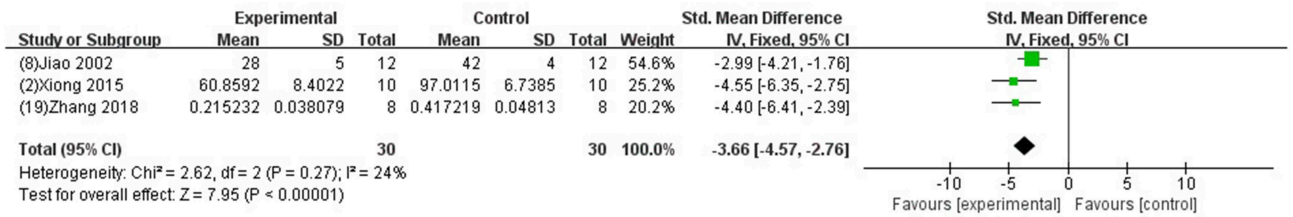


FIGURE 4 | Forest plot of animal studies investigating the effect of GB on myocardial infarction size (AAI/AAR) reduction.

permeability transition pore, mitochondrial membrane depolarization and uncoupling of oxidative phosphorylation, and ATP depletion and cell death (Hausenloy and Yellon, 2003; Murphy and Steenbergen, 2008). The present study found that GB could improve the activity of Na^+-K^+-ATPase and Ca^{2+}-Mg^{2+}-ATPase, decrease the content of Ca^{2+} in myocardium, protect mitochondrial respiratory activity, reduce the accumulation of free fatty acid, lactic acid, elevate the ratio of ATP/AMP, maintain the homeostasis, and improve amplitude of cardiomyocyte shortening by modulating cardiac Ca^{2+} regulatory proteins such as SERCA2a, phospholamban, and Na^+-Ca^{2+}exchanger.

Myocardial I/R injury resulted in cardiomyocyte apoptosis, which contributed to infarct size and ventricular dysfunction (Movassagh and Foo, 2008). The Bcl-2 family proteins were related to regulating the outer mitochondrial membrane (OMM) permeability. Increasing of OMM permeability caused by Bax could induce apoptosis, whereas decreasing the permeability caused by Bcl-2 could inhibit apoptosis (Ulgen et al., 2011). The present study indicated that GB could increase the expression of Bcl-2, decrease the expression of Bax, thus upregulate the ratio of Bcl-2/Bax to maintain the permeability of mitochondria, to inhibit activation of caspase-3, to inhibit the release of cytochrome C, to regulate intracellular free calcium concentration, and to reduce the activation and infiltration of macrophage, suggesting that GB may alleviate the myocardial I/R injury by anti-apoptosis. A summary of the cardioprotective mechanism of GB is provided in schematic (**Figure 9**).

Limitations

Firstly, only Chinese and English studies were included, potentially causing certain bias (Guyatt et al., 2011). Secondly, the methodological quality score was generally moderate. Items identified as the core standards of research design such as

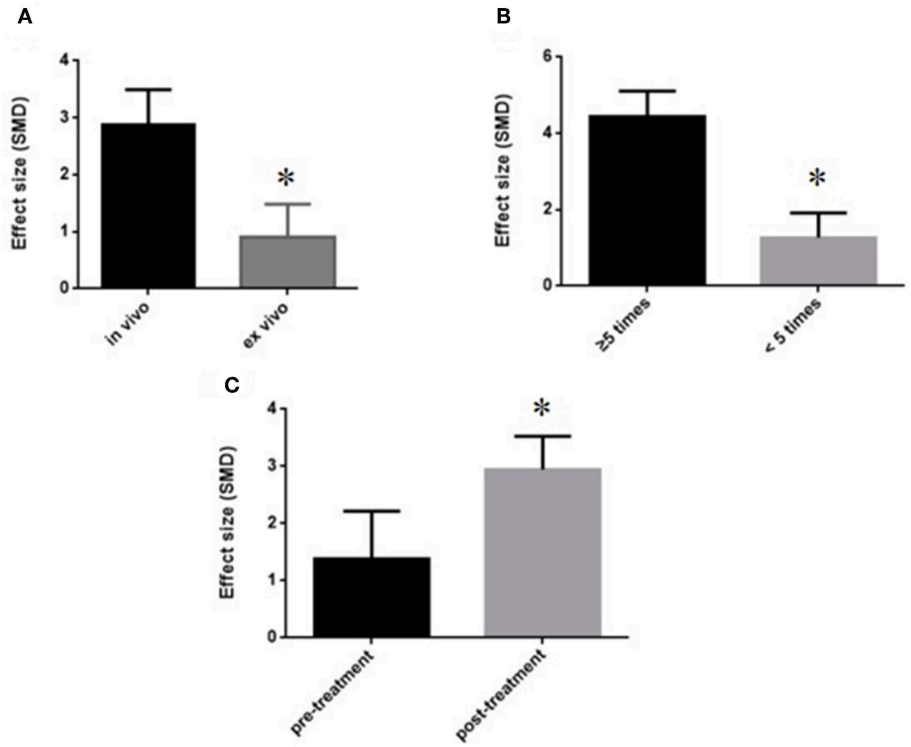


FIGURE 5 | Subgroup analyses of the myocardial infarct size (infarct area/left ventricular area). **(A)** Experimental model; **(B)** stage of GB administration; **(C)** frequency of drug administration. The magnitude of absolute value SMD reflected the effect size. *$P < 0.05$ vs. control groups.

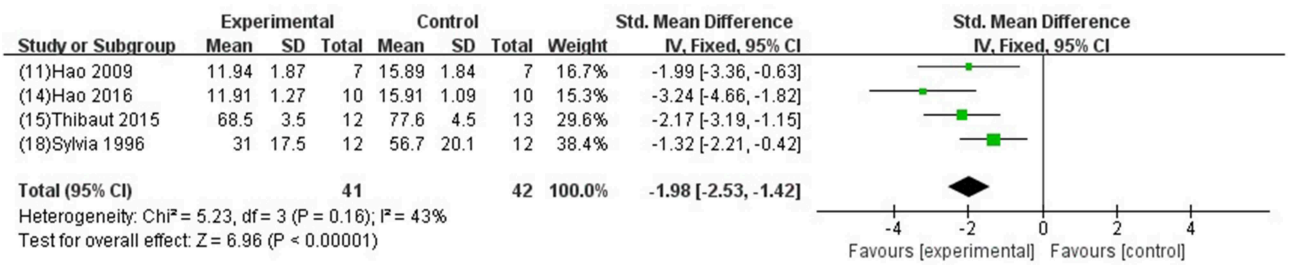


FIGURE 6 | Forest plot of animal studies investigating the effect of GB on LVEDP decrease.

allocation concealment, blinded assessment of outcome and the sample size calculation were failed to describe. The moderate methodological quality may affect the accuracy of the results (Landis et al., 2012; Macleod et al., 2015). Finally, 4 studies (Rioufol et al., 2003; Zhang et al., 2005; Zhao et al., 2014; Cao et al., 2016) used female animals. The response and sensitivity of experimental animals with the different gender to drugs and stimuli may be different, which could influence the final experimental results (Bae and Zhang, 2005).

Implications

MI size is strongly associated with progressive worsening of left ventricular function and congestive heart failure, and enhance the long-term morbidity and mortality. Therefore, MI size can be used in clinical studies as a substitute endpoint for clinical outcomes and as an important prognostic measure when caring for patients with AMI (Ndrepepa et al., 2017). Physicians are striving to reduce the MI size so as to improve the prognosis of patients (Begley and Ioannidis, 2015). In animal studies, MI size is the robust primary outcome that invariably used to evaluate the efficacy of various pharmacological or non-pharmacological strategies that prevent I/R injury (Zhou et al., 2018). In the present study, the results showed that GB could reduce the MI size, improve the diastolic and systolic function, decrease the level of CK, AST, and LDH, increase the level of GSH-Px. Thus, our study is valuable to the translational development.

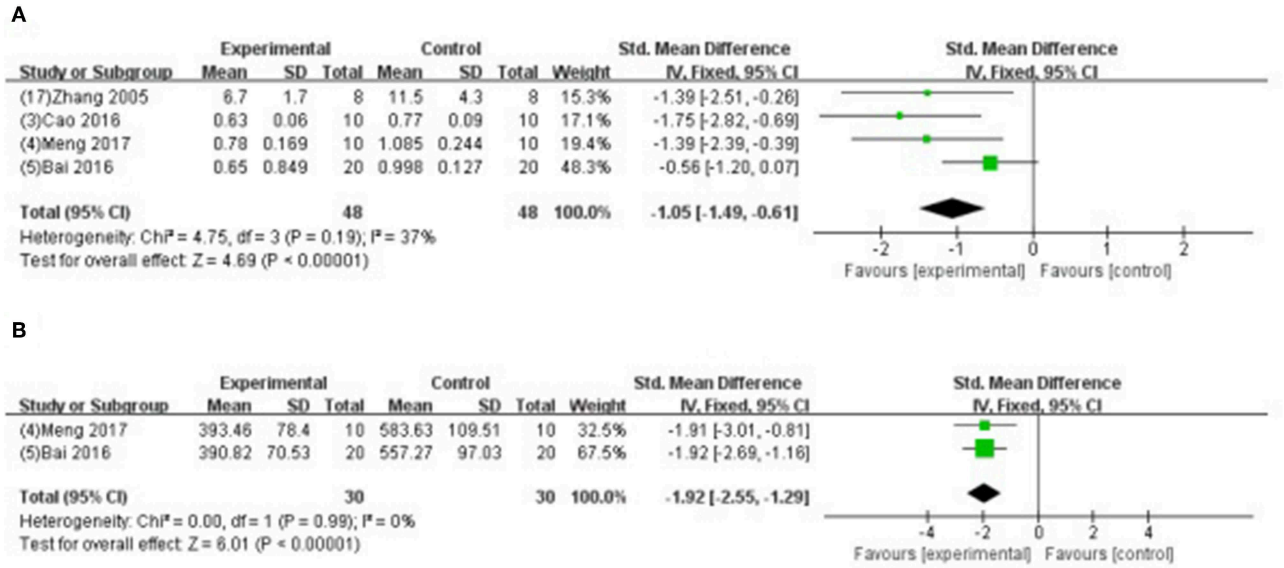


FIGURE 7 | (A) Forest plot of animal studies investigating the effect of GB on creatine kinase decrease. **(B)** Forest plot of animal studies investigating the effect of GB on aspartate transaminase decrease.

Animal studies are mainly targeted toward enriching our understanding of the mechanisms, etiology of human diseases, and forming the foundation on which future studies are built (Begley and Ioannidis, 2015). Accurate and complete reporting of animal studies is important to support the valid and reproducible research, while lower-quality reporting is related to deficiencies in experimental design that introduce bias and exaggerate effect sizes in the literature (Leung et al., 2018). The poor experimental design would restrain the translational development from animal studies into the clinical trials (Briel et al., 2013). The ARRIVE (Animals in Research: Reporting *In Vivo* Experiments) guidelines consist of a 20-item checklist published in 2010 with the aim of promoting the transparency and accuracy of animal research reporting, and of maximizing the availability and utility of information gained from every experiment (Gulin et al., 2015; Liu et al., 2016). In the present study, owing to the methodological quality, the results should be interpreted with caution. Thus, we proposed that further experiment design and reporting of the animal studies should refer to the ARRIVE guidelines (Kilkenny et al., 2010).

Inappropriate selection of the animal models could contribute to spurious or inconsistent results, as well as unnecessary animal use (Lecour et al., 2014). Given that animals with complications or risk factors such as ageing, diabetes and hypertension are close to the patients with myocardial infarction amalgamated with hypertension, hyperlipidemia, diabetes, insulin resistance, heart failure, altered coronary circulation and aging, we advise that further studies should use the appropriate animals instead of the young and healthy ones (Ferdinandy et al., 2014). These cardiovascular risks and comorbidities need to treat both short and long term, and contribute to the development of IR injury and complicate the therapy (Rossello and Yellon, 2016).

Animal models are often used to study the effectiveness of a drug or procedure and explore the mechanisms before proceeding to clinical trial (Roberts et al., 2002; Liao et al., 2012), which can be divided into *in vivo* and *ex vivo* models. The environment in which the *in vivo* myocardial infarction model located is exposed to normal humoral influences and neuronal regulation, and thus *in vivo* models can fully test the effect of the drug as an organic whole. However, many internal factors act as confounders, resulting in the deficiencies of the drug's effectiveness. In addition, the process of ligating the coronary artery and putting it back into the body needs high-tech requirements and high costs. In comparison, the isolated heart model with its broad spectrum of physiological, biochemical, and morphological measurements is a powerful *ex vivo* cardiovascular research tool that can be applied under numerous pathological condition (Skrzypiec-Spring et al., 2007; Liao et al., 2012). It possesses high-reproducibility, convenient operation, accurate results and time-saving due to the relatively simple process. Meanwhile, it is conducive to explore the mechanisms because various influencing factors can be strictly controlled easily. Compared with the cell models, the isolated heart model provides a more realistic correlation with the *in vivo* studies (Nahar et al., 2013). However, since the experimental environment of the *ex vivo* model can't fully simulate the internal environment, the results may not be comprehensive. According to the characteristics of animal models, *in vivo* experiments are mainly used to study the pharmacodynamics of pharmaceuticals, while the e*x vivo* experiments are more commonly contributed to explore mechanisms and physiological processes. This may explain the reason why the effect on infarct size *in vivo* heart

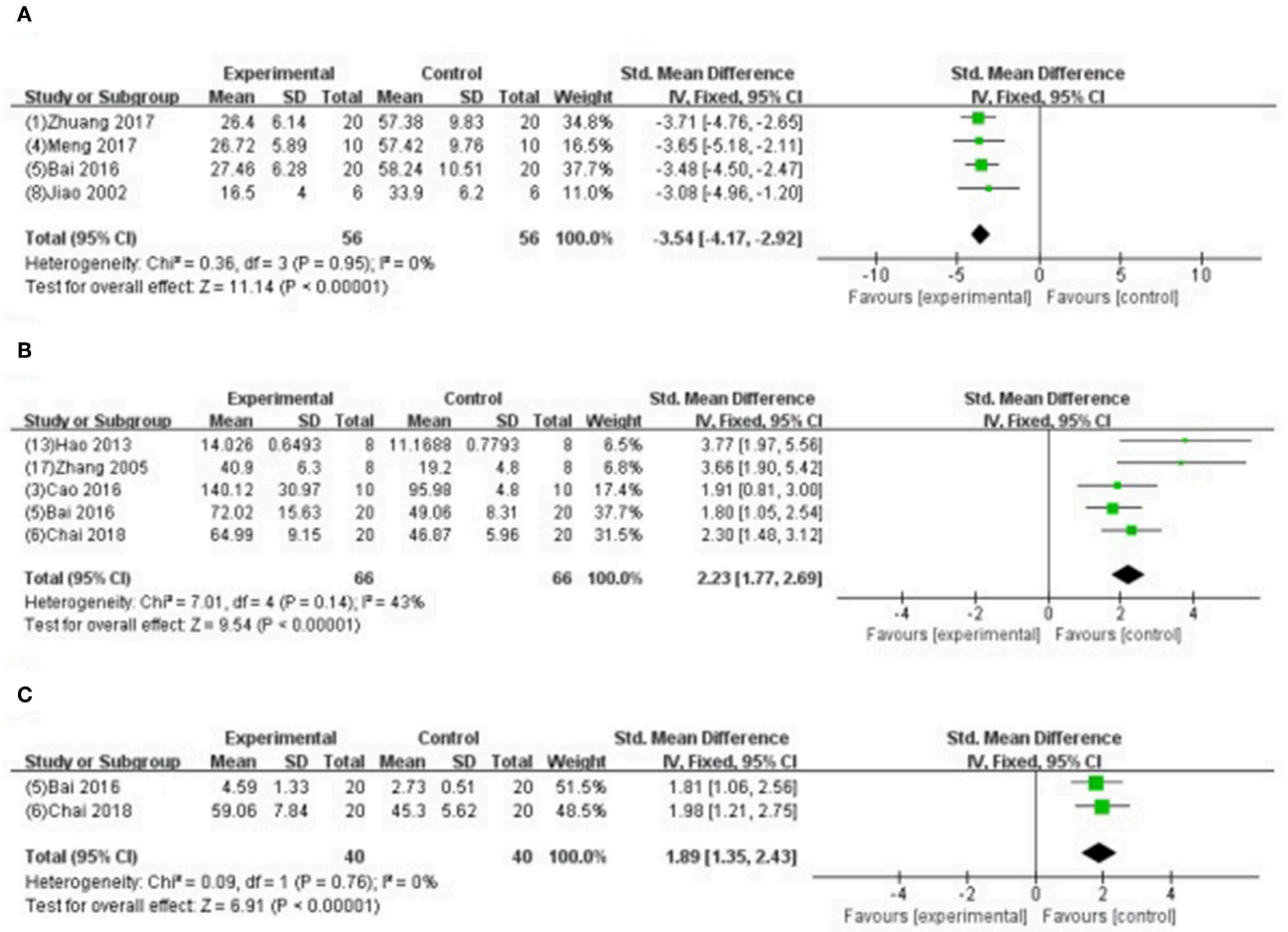


FIGURE 8 | (A) Forest plot of animal studies investigating the effect of GB onapoptosis index decrease. **(B)** Forest plot of animal studies investigating the effect of GB onsuperoxide dismutasedecrease. **(C)** Forest plot of animal studies investigating the effect of GB on glutathione peroxidase.

model (Bai et al., 2016; Cao et al., 2016; Meng, 2017; Zhuang et al., 2017) showed better effects compared with the isolated heart model in the present study (Hao et al., 2009, 2016). Future experiments can select different models for different experimental purposes. However, no single experimental model is sufficient to investigate of the mechanism and therapeutic effects of the drug simultaneously (Jiang et al., 2016). In order to test the drug research systematically and deeply, we strongly suggest to utilize two models that complement each other.

The group with more times (≥5) of drug administration (Bai et al., 2016; Meng, 2017; Zhuang et al., 2017) showed a better outcome than that with fewer times (<5) (Hao et al., 2009, 2016; Cao et al., 2016). The pharmacological effect of TCM comes from biologically active part or active chemical components, which demonstrate the preventive and therapeutic effects. The bioactive ingredients of TCM are very complex and totally different from that of modern western medicine. The research on a scientific theory about TCM's pharmacological effects and bioactive ingredients is limited (Huang et al., 2015). The bioavailability of active ingredients in TCM is low, and their affinity is weak (Yu and Lu, 2018). The effect of drug treatment is relatively slow, which requires a certain period of treatment. GB is a pure compound of the Ginkgo biloba leaves. In the present study, 3 studies (Bai et al., 2016; Meng, 2017; Zhuang et al., 2017) were administrated GB, qd, for 7 days, whereas other 3 studies (Hao et al., 2009, 2016; Cao et al., 2016) were administrated GB only 1 time. The drug concentration in the body increases proportionally when the dosage of the drug is administrated more times. Repeated administration of drugs would help to achieve and maintain the effective blood concentrations. Therefore, further studies administer GB for multiple times.

GB was an antagonist of PAF that inhibits platelet activation/aggregation via competitive binding to PAF receptor (Heinroth-Hoffmann et al., 1990). Owing to the slow onset time of herbal efficacy, administration of herbs before the induction of models was often used for herbal pharmacological

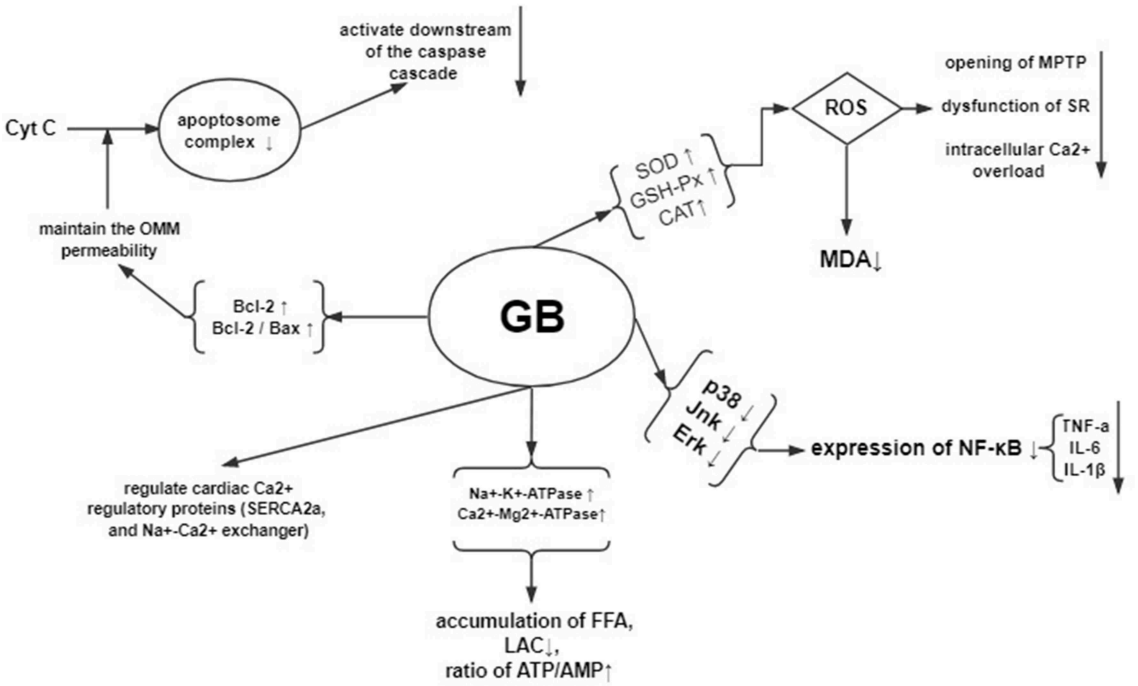


FIGURE 9 | Mechanisms of GB exerted cardioprotective effects in myocardial ischemia/reperfusion injury.

researches in order to reach the effective plasma concentration. The treatment post-model induction is more in line with clinical practice. Thus, it is more appropriate to study herbal pharmacology in both two different administrations. The results of present study showed that the efficacy in post-model induction group were better than that in the pre-model induction group, suggesting that the GB has fast onset time of decreasing platelet function directly via inhibiting the effect of PAF to alleviate myocardial I/R injury. Further study of this novel issue is needed.

Mechanisms underlying the pathogenesis of myocardial I/R injury are particularly complex, multifactorial and highly interconnected (Russo et al., 2017). The oxidative stress, apoptosis, energy metabolism disorder, and inflammation were described above. Other mechanisms such as Calcium paradox, pH paradox, metabolic modulation, Magnesium therapeutic, hypothermia, and autophagy, were also related to reperfusion injury. Based on the understanding of the pathophysiology of I/R injury, several advance non-pharmacological and pharmacological cardioprotective strategies were proposed to protect the ischemic myocardium in recent years. About non-pharmacological therapy, studies in animal models showed that ischemic pre-and post-conditioning, remote ischemic conditioning and hypothermia potentially stimulate the cardioprotective response. Meanwhile, different cardioprotective pharmacological agents have been confirmed in preclinical studies. These pharmacological agents include agonists of β-adrenoceptors (β-AR) or adenosine receptors, L-type voltage-dependent Ca^{2+} channels (VDCC) or mitochondrial Ca^{2+} uniporter (MCU) blockers, anti-platelet, modulators of NO biosynthesis or Na^{+}/Ca^{2+} exchanger (NCX), resveratrol, methylene blue and intestinal lipase inhibitors (Caricati-Neto et al., 2019). In the future, nanotechnology-guided drug delivery systems will become new direction (Minamino, 2012), and novel cardioprotective mechanisms of GB should be investigated.

Assessing the risk of bias of the individual studies is a key feature of a systematic review. The Cochrane risk of bias (RoB) Tool is developed by the Cochrane Collaboration to establish consistency and avoid discrepancies in assessing the methodological quality of RCTs (Hooijmans et al., 2014). Analogously, when conducting systematic review of preclinical studies, the main difference is the methodological quality assessment methods. Some checklists have been developed to evaluate the quality of *in vivo* animal intervention experiments (Hooijmans et al., 2014; Zhang et al., 2017), including the SYstematic Review Centre for Laboratory animal Experimentation (SYRCLE)'s RoB tool and the Collaborative Approach to Meta-Analysis and Review of Animal Data from Experimental Studies (CAMARADES) 10-item checklist. About *in vitro* studies, the ROB assessment can refer to 10-item scale developed by our group (Bao et al., 2018). However, there are no quality assessment tools for a systematical review of *ex vivo* studies. The 9 out of 10 items of CAMARADES checklist are involved in the process of *ex vivo* studies except an item of animal model. Therefore, it is appropriate that we choose the CAMARADES 10-item list to assess the quality of *ex vivo* studies. The *ex vivo* studies are commonly contributed to

explore mechanisms and physiological processes; however, many experimental did not choose animal models with comorbidities such as diabetes, hypertension, and atherosclerosis. When using the CAMARADES 10-item checklist to evaluate the quality of study, the point of appropriate animal model did not award that potentially caused bias accordingly. Thus, further *ex vivo* studies should choose appropriate models that make the results more accurate and comprehensive so as to improve efficiency in the design of study and promote the translation of findings from animal studies into clinic.

CONCLUSION

The present study demonstrated that GB could alleviate the myocardial I/R injury, mainly through the antioxidation, anti-inflammation, anti-apoptosis, and the improvement of energy metabolism.

DATA AVAILABILITY STATEMENT

The raw data supporting the conclusions of this manuscript will be made available by the authors, without undue reservation, to any qualified researcher.

AUTHOR CONTRIBUTIONS

YW, GZ, and P-CZ contributed to the study conception and design. P-CZ, QT, ZZ, Z-HW, and L-HD contributed to the acquisition, the analysis, and/or the interpretation of data. GZ and YW gave the final approval and contributed overall responsibility for this published work.

FUNDING

This work was supported by the grant of National Natural Science Foundation of China (81473491/81573750/81173395/H2902).

REFERENCES

Bae, S., and Zhang, L. (2005). Gender differences in cardioprotection against ischemia/reperfusion injury in adult rat hearts: focus on Akt and protein kinase C signaling. *J. Pharmacol. Exp. Ther.* 315, 1125–1135. doi: 10.1124/jpet.105.090803

Bai, Z. C., Chen, M. C., and Li, H. F. (2016). The effects of ginkgolide B on oxidative stress in rats with myocardial ischemia-reperfusion injury. *JETCM* 25, 1480–1483. doi: 10.3969/j.issn.1004-745X.2016.08.008

Bao, X. Y., Zheng, Q., Tong, Q., Zhu, P. C., Zhuang, Z., Zheng, G. Q., et al. (2018). Danshensu for myocardial ischemic injury: preclinical evidence and novel methodology of quality assessment tool. *Front. Pharmacol.* 9:1445. doi: 10.3389/fphar.2018.01445

Begley, C. G., and Ioannidis, J. P. (2015). Reproducibility in science: improving the standard for basic and preclinical research. *Circ. Res.* 116, 116–126. doi: 10.1161/CIRCRESAHA.114.303819

Bilia, A. R. (2002). *Ginkgo biloba* L. *Fitoterapia* 73, 276–279. doi: 10.1016/S0367-326X(02)00071-0

Billottet, L., Martel, S., Culcasi, M., Drieu, K., Carrupt, P.-A., and Pietri, S. (2005). Influence of lipophilicity and stereochemistry at the C7 position on the cardioprotective and antioxidant effect of ginkgolides during rat heart ischemia and reperfusion. *Drug Dev. Res.* 64, 157–171. doi: 10.1002/ddr.10424

Binder, A., Ali, A., Chawla, R., Aziz, H. A., Abbate, A., and Jovin, I. S. (2015). Myocardial protection from ischemia-reperfusion injury post coronary revascularization. *Expert Rev Cardiovasc Ther.* 13, 1045–1057. doi: 10.1586/14779072.2015.1070669

Briel, M., Muller, K. F., Meerpohl, J. J., Von Elm, E., Lang, B., Motschall, E., et al. (2013). Publication bias in animal research: a systematic review protocol. *Syst. Rev.* 2, 23. doi: 10.1186/2046-4053-2-23

Bulluck, H., Yellon, D. M., and Hausenloy, D. J. (2016). Reducing myocardial infarct size: challenges and future opportunities. *Heart* 102, 341–348. doi: 10.1136/heartjnl-2015-307855

Cao, J. P., Li, X., Ma, Y., Li, X., Ma, Y., Shu, J. L., et al. (2016). Study of protective effects of ginkgolide B on myocardial ischemia reperfusion injury in rats. *Prev. Treat. Cardio Cereb. Vasc. Dis.* 16, 8–10. doi: 10.3969/j.issn.1009-816x.2016.01.03

Caricati-Neto, A., Errante, P. R., and Menezes-Rodrigues, F. S. (2019). Recent advances in pharmacological and non-pharmacological strategies of cardioprotection. *Int. J. Mol. Sci.* 20:E4002. doi: 10.3390/ijms20164002

Chai, L. N., Du, R., and Zhang, Y. Y. (2018). Effects and mechnism of ginkgolide B on myocardial arrhythmia induced by myocardial ischemia – reperfusion. *JETCM* 27, 619–621. doi: 10.3969/j.issn.1004-745X.2018.04.016

Chung, J. W., Choi, R. J., Seo, E. K., Nam, J. W., Dong, M. S., Shin, E. M., et al. (2012). Anti-inflammatory effects of (Z)-ligustilide through suppression of mitogen-activated protein kinases and nuclear factor-κB activation pathways. *Arch. Pharm. Res.* 35, 723–732. doi: 10.1007/s12272-012-0417-z

Eltzschig, H. K., and Eckle, T. (2011). Ischemia and reperfusion–from mechanism to translation. *Nat. Med.* 17, 1391–1401. doi: 10.1038/nm.2507

Ferdinandy, P., Hausenloy, D. J., Heusch, G., Baxter, G. F., and Schulz, R. (2014). Interaction of risk factors, comorbidities, and comedications with ischemia/reperfusion injury and cardioprotection by preconditioning, postconditioning, and remote conditioning. *Pharmacol. Rev.* 66, 1142–1174. doi: 10.1124/pr.113.008300

Frank, A., Bonney, M., Bonney, S., Weitzel, L., Koeppen, M., and Eckle, T. (2012). Myocardial ischemia reperfusion injury: from basic science to clinical bedside. *Semin. Cardiothorac. Vasc. Anesth.* 16, 123–132. doi: 10.1177/1089253211436350

Gulin, J. E., Rocco, D. M., and Garcia-Bournissen, F. (2015). Quality of reporting and adherence to ARRIVE guidelines in animal studies for chagas disease preclinical drug research: a systematic review. *PLoS Negl. Trop. Dis.* 9:e0004194. doi: 10.1371/journal.pntd.0004194

Guyatt, G. H., Oxman, A. D., Montori, V., Vist, G., Kunz, R., Brozek, J., et al. (2011). GRADE guidelines: 5. Rating the quality of evidence–publication bias. *J. Clin. Epidemiol.* 64, 1277–1282. doi: 10.1016/j.jclinepi.2011.01.011

Hao, Y. L., and Dong, W. (2017). Combination of ginkgolide A and B in improving the cardiac function in aged rats with ischemia/reperfusion injury. *J. Qiqihar Univ. Med.* 38, 1863–1865. doi: 10.3969/j.issn.1002-1256.2017.16.002

Hao, Y. L., Jiang, Y. L., Wang, Y. W., Jiang, R., He, J., Yu, C., et al. (2013). Effects of combined treatment with ginkgolides B and C on rat cardiac function after ischemia/reperfusion injury. *Acta Acad. Med. Xuzhou* 33, 733–736.

Hao, Y. L., Sun, Y., Xu, C., Jiang, X., Sun, H., Wu, Q., et al. (2009). Improvement of contractile function in isolated cardiomyocytes from ischemia-reperfusion rats by ginkgolide B pretreatment. *J. Cardiovasc. Pharmacol.* 54, 3–9. doi: 10.1097/FJC.0b013e3181a91410

Hao, Y. L., Yang, Y., Wu, J. X., Peng, K., Zhang, C. P., Sun, H., et al. (2016). Improvement of contractile function of isolated hearts with ischemia-reperfusion injury of aged rats by ginkgolide B post-treatment. *Chin. J. New Drugs* 25, 2707–2713.

Hausenloy, D. J., and Yellon, D. M. (2003). The mitochondrial permeability transition pore: its fundamental role in mediating cell death during ischaemia and reperfusion. *J. Mol. Cell. Cardiol.* 35, 339–341. doi: 10.1016/S0022-2828(03)00043-9

Hausenloy, D. J., and Yellon, D. M. (2013). Myocardial ischemia-reperfusion injury: a neglected therapeutic target. *J. Clin. Invest.* 123, 92–100. doi: 10.1172/JCI62874

Heinroth-Hoffmann, I., Hauser, A., and Mest, H. J. (1990). Effects of platelet activating factor antagonists on arachidonic acid-induced platelet aggregation and TXA2 formation. *Prostaglandins Leukot. Essent. Fatty Acids* 41, 181–182. doi: 10.1016/0952-3278(90)90087-2

Himaya, S. W., Ryu, B., Qian, Z. J., and Kim, S. K. (2012). Paeonol from Hippocampus kuda Bleeler suppressed the neuro-inflammatory responses in vitro via NF- κB and MAPK signaling pathways. *Toxicol. In Vitro* 26, 878–887. doi: 10.1016/j.tiv.2012.04.022

Hooijmans, C. R., Rovers, M. M., De Vries, R. B., Leenaars, M., Ritskes-Hoitinga, M., and Langendam, M. W. (2014). SYRCLE's risk of bias tool for animal studies. *BMC Med. Res. Methodol.* 14:43. doi: 10.1186/1471-2288-14-43

Huang, Y., Zhao, Y., Liu, F., and Liu, S. (2015). Nano traditional Chinese medicine: current progresses and future challenges. *Curr. Drug Targets* 16, 1548–1562. doi: 10.2174/1389450116666150309122334

Ibanez, B., Heusch, G., Ovize, M., and Van De Werf, F. (2015). Evolving therapies for myocardial ischemia/reperfusion injury. *J. Am. Coll. Cardiol.* 65, 1454–1471. doi: 10.1016/j.jacc.2015.02.032

Jacobs, B. P., and Browner, W. S. (2000). *Ginkgo biloba*: a living fossil. *Am. J. Med.* 108, 341–342. doi: 10.1016/S0002-9343(00)00290-4

Jiang, D. S., Yi, X., Zhu, X. H., and Wei, X. (2016). Experimental *in vivo* and *ex vivo* models for the study of human aortic dissection: promises and challenges. *Am. J. Transl. Res.* 8, 5125–5140.

Jiao, X. Y., Luo, N., Zhi, J. M., and Zhao, R. R. (2002). Effects of exogenous platelet activating factor and its antagonist ginkgolide B on ischemia-reperfusion injury of myocardium in rats. *Chin. J. Pharmacol. Toxic.* 2, 81–87. doi: 10.3321/j.issn:1000-3002.2002.02.001

Kilkenny, C., Browne, W. J., Cuthill, I. C., Emerson, M., and Altman, D. G. (2010). Improving bioscience research reporting: the ARRIVE guidelines for reporting animal research. *J. Pharmacol. Pharmacother.* 1, 94–99. doi: 10.4103/0976-500X.72351

Landis, S. C., Amara, S. G., Asadullah, K., Austin, C. P., Blumenstein, R., Bradley, E. W., et al. (2012). A call for transparent reporting to optimize the predictive value of preclinical research. *Nature* 490, 187–191. doi: 10.1038/nature11556

Lecour, S., Botker, H. E., Condorelli, G., Davidson, S. M., Garcia-Dorado, D., Engel, F. B., et al. (2014). ESC working group cellular biology of the heart: position paper: improving the preclinical assessment of novel cardioprotective therapies. *Cardiovasc. Res.* 104, 399–411. doi: 10.1093/cvr/cvu225

Leung, V., Rousseau-Blass, F., Beauchamp, G., and Pang, D. S. J. (2018). ARRIVE has not ARRIVEd: support for the ARRIVE (Animal Research: Reporting of *in vivo* Experiments) guidelines does not improve the reporting quality of papers in animal welfare, analgesia or anesthesia. *PLoS ONE* 13:e0197882. doi: 10.1371/journal.pone.0197882

Li, S. J., Geng, J. L., Zhang, Y., Yang, N., Zhou, F., Akiye, J.Y., et al. (2017). Advances in pharmacological research of *Ginkgo biloba*. *Drug Eval. Res.* 40, 731–741. doi: 10.7501/j.issn.1674-6376.2017.06.002

Liao, R., Podesser, B. K., and Lim, C. C. (2012). The continuing evolution of the Langendorff and ejecting murine heart: new advances in cardiac phenotyping. *Am. J. Physiol. Heart Circ. Physiol.* 303, H156–H167. doi: 10.1152/ajpheart.00333.2012

Liebgott, T., Miollan, M., Berchadsky, Y., Drieu, K., Culcasi, M., and Pietri, S. (2000). Complementary cardioprotective effects of flavonoid metabolites and terpenoid constituents of *Ginkgo biloba* extract (EGb 761) during ischemia and reperfusion. *Basic Res. Cardiol.* 95, 368–377. doi: 10.1007/s003950070035

Liu, Y., Zhao, X., Mai, Y., Li, X., Wang, J., Chen, L., et al. (2016). Adherence to ARRIVE guidelines in Chinese journal reports on neoplasms in animals. *PLoS ONE* 11:e0154657. doi: 10.1371/journal.pone.0154657

Ma, L., Liu, H., Xie, Z., Yang, S., Xu, W., Hou, J., et al. (2014). Ginsenoside Rb3 protects cardiomyocytes against ischemia-reperfusion injury via the inhibition of JNK-mediated NF- κB pathway: a mouse cardiomyocyte model. *PLoS ONE* 9:e103628. doi: 10.1371/journal.pone.0103628

Maclennan, K. M., Darlington, C. L., and Smith, P. F. (2002). The CNS effects of *Ginkgo biloba* extracts and ginkgolide B. *Prog. Neurobiol.* 67, 235–257. doi: 10.1016/S0301-0082(02)00015-1

Macleod, M. R., Lawson McLean, A., Kyriakopoulou, A., Serghiou, S., De Wilde, A., Sherratt, N., et al. (2015). Risk of bias in reports of *in vivo* research: a focus for improvement. *PLoS Biol.* 13:e1002273. doi: 10.1371/journal.pbio.1002273

Macleod, M. R., O'collins, T., Howells, D. W., and Donnan, G. A. (2004). Pooling of animal experimental data reveals influence of study design and publication bias. *Stroke* 35, 1203–1208. doi: 10.1161/01.STR.0000125719.25853.20

Marchant, D. J., Boyd, J. H., Lin, D. C., Granville, D. J., Garmaroudi, F. S., and Mcmanus, B. M. (2012). Inflammation in myocardial diseases. *Circ. Res.* 110, 126–144. doi: 10.1161/CIRCRESAHA.111.243170

Meng, J. F. (2017). Protective effects of ginkgolide B on rats with myocardial ischemia reperfusion injury. *JETCM* 26, 1977–1979. doi: 10.3969/j.issn.1004-745X.2017.11.028

Minamino, T. (2012). Cardioprotection from ischemia/reperfusion injury: basic and translational research. *Circ. J.* 76, 1074–1082. doi: 10.1253/circj.CJ-12-0132

Movassagh, M., and Foo, R. S. (2008). Simplified apoptotic cascades. *Heart Fail. Rev.* 13, 111–119. doi: 10.1007/s10741-007-9070-x

Murphy, E., and Steenbergen, C. (2008). Mechanisms underlying acute protection from cardiac ischemia-reperfusion injury. *Physiol. Rev.* 88, 581–609. doi: 10.1152/physrev.00024.2007

Nahar, K., Gupta, N., Gauvin, R., Absar, S., Patel, B., Gupta, V., et al. (2013). In vitro, *in vivo* and *ex vivo* models for studying particle deposition and drug absorption of inhaled pharmaceuticals. *Eur. J. Pharm. Sci.* 49, 805–818. doi: 10.1016/j.ejps.2013.06.004

Navarro-Yepes, J., Burns, M., Anandhan, A., Khalimonchuk, O., Del Razo, L. M., Quintanilla-Vega, B., et al. (2014). Oxidative stress, redox signaling, and autophagy: cell death versus survival. *Antioxid. Redox Signal.* 21, 66–85. doi: 10.1089/ars.2014.5837

Ndrepepa, G., Colleran, R., and Kastrati, A. (2017). Reperfusion injury in ST-segment elevation myocardial infarction: the final frontier. *Coron. Artery Dis.* 28, 253–262. doi: 10.1097/MCA.0000000000000468

Pei, H. X., Hua, R., Guan, C. X., and Fang, X. (2015). Ginkgolide B reduces the degradation of membrane phospholipids to prevent ischemia/reperfusion myocardial injury in rats. *Pharmacology* 96, 233–239. doi: 10.1159/000438945

Rioufol, G., Pietri, S., Culcasi, M., Loufoua, J., Staat, P., Pop, C., et al. (2003). *Ginkgo biloba* extract EGb 761 attenuates myocardial stunning in the pig heart. *Basic Res. Cardiol.* 98, 59–68. doi: 10.1007/s00395-003-0380-4

Roberts, I., Kwan, I., Evans, P., and Haig, S. (2002). Does animal experimentation inform human healthcare? Observations from a systematic review of international animal experiments on fluid resuscitation. *BMJ* 324, 474–476. doi: 10.1136/bmj.324.7335.474

Rossello, X., and Yellon, D. M. (2016). Cardioprotection: the disconnect between bench and bedside. *Circulation* 134, 574–575. doi: 10.1161/CIRCULATIONAHA.116.022829

Russo, I., Penna, C., Musso, T., Popara, J., Alloatti, G., Cavalot, F., et al. (2017). Platelets, diabetes and myocardial ischemia/reperfusion injury. *Cardiovasc. Diabetol.* 16:71. doi: 10.1186/s12933-017-0550-6

Sandercock, P., and Roberts, I. (2002). Systematic reviews of animal experiments. *Lancet* 360:586. doi: 10.1016/S0140-6736(02)09812-4

Skrzypiec-Spring, M., Grotthus, B., Szelag, A., and Schulz, R. (2007). Isolated heart perfusion according to Langendorff—still viable in the new millennium. *J. Pharmacol. Toxicol. Methods* 55, 113–126. doi: 10.1016/j.vascn.2006.05.006

Stewart, L. A., Clarke, M., Rovers, M., Riley, R. D., Simmonds, M., Stewart, G., et al. (2015). Preferred reporting items for systematic review and meta-analyses of individual participant data: the PRISMA-IPD statement. *JAMA* 313, 1657–1665. doi: 10.1001/jama.2015.3656

Ulgen, B. O., Field, M. G., Qureshi, W., Knight, R. A., Stephanou, A., Latchman, D. S., et al. (2011). The role of minocycline in ischemia-reperfusion injury: a comprehensive review of an old drug with new implications. *Recent Pat. Cardiovasc. Drug Discov.* 6, 123–132. doi: 10.2174/157489011795933783

Wang, Q., Tang, X. N., and Yenari, M. A. (2007). inflammatory response in stroke. *J. Neuroimmunol.* 184, 53–68. doi: 10.1016/j.jneuroim.2006.11.014

Xia, S. H., and Fang, D. C. (2007). Pharmacological action and mechanisms of ginkgolide B. *Chin. Med. J.* 120, 922–928. doi: 10.1097/00029330-200705020-00013

Xiong, N., and Wei, S. (2015). Study on protection of ginkgolide B against myocardial ischemia-reperfusion injury and its mechanism. *Chin.*

J. Mod. Appl. Pharm. 32, 289–294. doi: 10.13748/j.cnki.issn1007-7693.2015.03.008

Yang, Y. H., Chen, C. Y., and Yuan, Z. P. (2018). Protective effect of ploygonati odorati rhizoma extract against mitochondrial damage and apoptosis in myocardial cells of myocardial ischemia-reperfusion injury in rats. *Chin. J. Exp. Tradit. Med. Formul.* 24, 136–140. doi: 10.13422/j.cnki.syfjx.20181626

Yellon, D. M., and Hausenloy, D. J. (2007). Myocardial reperfusion injury. *N. Engl. J. Med.* 357, 1121–1135. doi: 10.1056/NEJMra071667

Yu, S. Y., and Lu, Y. (2018). Discussion on action mechanisms of traditional Chinese medicine. *Chin. J. Pharmacol. Toxicol.* 32, 347–354. doi: 10.3867/j.issn.1000-3002.2018.05.001

Zhang, G. B., Chen, D. Y., Gui, C. Q., and Lu, X. H. (2005). Expermental study on protective effect of ginkgolide B on isolated rats' hearts with ischemia- reperfusion. *Chin. J. Tradit. Med. Sci. Technol.* 12, 92–94. doi: 10.3969/j.issn.1005-7072.2005.02.012

Zhang, H. F., Huang, L. B., Zhong, Y. B., Zhou, Q. H., Wang, H. L., Zheng, G. Q., et al. (2016). An overview of systematic reviews of *Ginkgo biloba* extracts for mild cognitive impairment and dementia. *Front. Aging Neurosci.* 8:276. doi: 10.3389/fnagi.2016.00276

Zhang, K. J., Zhu, J. Z., Bao, X. Y., Zheng, Q., Zheng, G. Q., and Wang, Y. (2017). Shexiang baoxin pills for coronary heart disease in animal models: preclinical evidence and promoting angiogenesis mechanism. *Front. Pharmacol.* 8:404. doi: 10.3389/fphar.2017.00404

Zhang, R., Xu, L., Zhang, D., Hu, B., Luo, Q., Han, D., et al. (2018). Cardioprotection of ginkgolide B on myocardialischemia/reperfusion-induced inflammatory injury via regulation of A20-NF- κB pathway. *Front. Immunol.* 9:2844. doi: 10.3389/fimmu.2018.02844

Zhao, T., Sheng, N., Su, Z. P., Wang, Q., and Ye, Y. (2014). Effects of ginkgolide B, ginkgolide C and their combined therapy on the cardiacfunction of rats withischemia/reperfusion injury. *Acta Acad. Med. Xuzhou.* 1, 18–21.

Zhou, H., Ma, Q., Zhu, P., Ren, J., Reiter, R. J., and Chen, Y. (2018). Protective role of melatonin in cardiac ischemia-reperfusion injury: from pathogenesis to targeted therapy. *J. Pineal Res.* 64:e12471. doi: 10.1111/jpi.12471

Zhuang, H. Y., Lv, J., Li, Y. L., and Shi, Y. T. (2017). Effects of ginkgolide B against apoptosis and expression of related proteins in myocardial cells of myocardial ischemia-reperfusion in rats. *Jiangsu J. Trad. Chin. Med.* 49, 81–84. doi: 10.3969/j.issn.1672-397X.2017.12.033

Conflict of Interest: The authors declare that the research was conducted in the absence of any commercial or financial relationships that could be construed as a potential conflict of interest.

Copyright © 2019 Zhu, Tong, Zhuang, Wang, Deng, Zheng and Wang. This is an open-access article distributed under the terms of the Creative Commons Attribution License (CC BY). The use, distribution or reproduction in other forums is permitted, provided the original author(s) and the copyright owner(s) are credited and that the original publication in this journal is cited, in accordance with accepted academic practice. No use, distribution or reproduction is permitted which does not comply with these terms.

frontiers in Pharmacology

ORIGINAL RESEARCH
published: 22 October 2019
doi: 10.3389/fphar.2019.01261

Screening for Potential Active Components of Fangji Huangqi Tang on the Treatment of Nephrotic Syndrome by Using Integrated Metabolomics Based on "Correlations Between Chemical and Metabolic Profiles"

Xiao Liu[1], Qi-Gang Zhou[2], Xiao-Chai Zhu[1], Li Xie[1] and Bao-Chang Cai[1]*

[1] School of Pharmacy, Nanjing University of Chinese Medicine, Nanjing, China, [2] School of Pharmacy, Nanjing Medical University, Nanjing, China

OPEN ACCESS

Edited by:
Jing-Yan Han,
Peking University, China

Reviewed by:
Aiping Lu,
Hong Kong Baptist University, Hong Kong
Yubo Li,
Tianjin University of Traditional Chinese Medicine, China

***Correspondence:**
Xiao Liu
liuxiao04_0@163.com

Specialty section:
This article was submitted to Ethnopharmacology, a section of the journal Frontiers in Pharmacology

Received: *24 April 2019*
Accepted: *30 September 2019*
Published: *22 October 2019*

Citation:
Liu X, Zhou Q-G, Zhu X-C, Xie L and Cai B-C (2019) Screening for Potential Active Components of Fangji Huangqi Tang on the Treatment of Nephrotic Syndrome by Using Integrated Metabolomics Based on "Correlations Between Chemical and Metabolic Profiles". Front. Pharmacol. 10:1261. doi: 10.3389/fphar.2019.01261

As for traditional Chinese medicine (TCM) prescription, what puzzled researchers most was how to select proper chemical markers to represent the whole pharmacological action system. In this paper, an integrated metabolomic method was presented for a systematic discovery of potential active components in Fangji Huangqi Tang (FHT), a well-known TCM prescription for nephrotic syndrome treatment, based on "correlations between chemical and metabolic profiles." Firstly, a metabolomics study was carried out to select representative biomarkers of nephrotic syndrome. Then, after drug administration, the dynamic process of serum composition was investigated by the ultra-high performance liquid chromatography coupled with electrospray ionization–quadrupole–time of flight–mass spectrometry (UHPLC-ESI-Q-TOF-MS) technique to detect the prototypes and related metabolites of relative components from FHT. Pearson correlation analysis was finally used to find out the correlations between the endogenous metabolic spectrums and the chemical serum spectrums. As a result, 17 biomarkers for nephrotic syndrome indication were identified, and the main metabolic pathways of their concern included linoleic acid metabolism; cyanoamino acid metabolism; alpha-linolenic acid metabolism; glycine, serine, and threonine metabolism; arachidonic acid metabolism; and glycerophospholipid metabolism. Meanwhile, active components in FHT for nephrotic syndrome treatment were screened out, including (+)-tetrandrine demethylation, fenfangjine G hydrogenation, tetrandrine, *N*-methylfangchinoline, tetrandrine demethylation, fangchinoline, glycyrrhetic acid, astragaloside II alcohol dehydration, atractylenolide III demethylation + hydrogenation, atractylenolide III demethylation + hydrogenation, and licoricone-*N*-acetylcysteine conjugation. This study demonstrated a promising way to elucidate the active chemical material basis of TCM prescription.

Keywords: Fangji Huangqi Tang, metabonomics, correlation analysis, nephrotic syndrome, marker

INTRODUCTION

Nephrotic syndrome is a common disease of the urinary system, which could be divided into primary and secondary types, with clinical manifestations such as proteinuria, hypoalbuminemia, edema, and hyperlipidemia. Due to its complicated pathogeny and various pathological types, treatment of nephrotic syndrome is very difficult in the clinic (Crawford and Gipson, 2017; Kang et al., 2017). Compared with modern drugs, traditional Chinese medicine (TCM) had some special advantages in treating nephrotic syndrome, especially in the aspects of reducing proteinuria and side effects of immunosuppressive drugs, as well as alleviating the complications of hypercoagulability or gastrointestinal mucosa edema (Wang and Wang, 2004; Nie, 2008; Wu et al., 2014). Furthermore, compared with hormone, TCM application to treatment of nephrotic syndrome is also a good way to avoid side effects and to reduce high recurrence rate of disease.

The most characteristic clinical manifestation of nephrotic syndrome is edema. According to the theory of Chinese medicine, the reason for edema could be concluded to Qi Xu, especially caused by deficient spleen or kidney functions. In other words, the disorder of the spleen or kidney is an important factor during nephrotic syndrome development. Fangji Huangqi Tang (FHT), a classic TCM prescription in Chinese clinical application for the treatment of chronic glomerulonephritis, is composed of the roots of four kinds of Chinese herbal medicines, namely, *Stephania tetrandra* S. Moore (FJ), *Astragalus membranaceus* Fisch. ex Bunge (HQ), *Atractylodes macrocephala* Koidz. (BZ), and *Glycyrrhiza uralensis* Fisch. ex DC. (GC). A large number of literatures indicated that FHT showed a significant effect on nephrotic syndrome (Chen et al., 2013; Zhang and Yu, 2015; Liu et al., 2019). However, underlying active components and modern therapeutic mechanisms of FHT for nephrotic syndrome are still unclear.

The curative and protective effects of TCM have already been widely and fully recognized through clinical practice for thousands of years in China. However, the detailed bioactive components and potential mechanisms for most of TCM remained poorly understood. People know that using a single index or a simple superposition way to explain the multi-herb synergistic characteristics of TCM would not be sensible. In recent years, papers on metabolomics of TCM began to appear (Zhou et al., 2016; Cui et al., 2017; Pang et al., 2018), including report on TCM metabonomics for nephrotic syndrome treatment, by which the protective effect of total flavonoids in *Astragali Radix* against adriamycin-induced nephropathy was proved using rats (Zhang et al., 2018). Metabolomics technology and biomarkers were used in these papers to screen out active or toxic substances in TCM. However, this kind of work was not too much by now, and how to assess the efficacy of herbal drugs in a metabolomic way quantitatively is to some extent a challenging problem. In this paper, a novel strategy based on metabonomics combined with spectrum–effect research was proposed for FHT active chemicals investigation. The core academic thought of metabonomics (Jové et al., 2014; Patel and Ahmed, 2014; Bjerrum et al., 2015) was integrated into a classical spectrum–effect relationship research method. The variational biological levels of biomarkers *in vivo* were regarded as the indicators to reflect the pathological and physiological changes of the organism under the actions of drugs, by which way the traditional spectrum–effect relationship was translated to the relationships between drug chemical spectrums and serum metabolic profiles. Actually, this action of translation would benefit the researchers with a better reproducibility of the experimental data obtained from chemical spectrum analyses, as well as a lower financial cost because of the absence of biochemical index assay. It was hoped that this newly developed method would clarify the most active chemicals in FHT to treat nephrotic syndrome. Also, the elucidation of FHT acting material bases would be an innovative way for modern research of TCM formulas.

MATERIALS AND METHODS

Chemicals and Reagents

Four component herbs of FHT were obtained as follows: *A. membranaceus* Fisch. ex Bunge (HQ) and *G. uralensis* Fisch. ex DC. (GC) were obtained from the Nanjing Haichang Chinese Medicine Group Corporation (Nanjing, China), and *S. tetrandra* S. Moore (FJ) and *A. macrocephala* Koidz. (BZ) were obtained from the Hebei Chinese Medicine Group Corporation (Hebei, China). These species were authenticated by Prof. Jianwei Chen (School of Pharmacy, Nanjing University of Chinese Medicine) for their botanical origin before use (**Supplementary Figures 1–4**). Voucher specimens (no. NZY-LIU-2019001 for FJ; no. NZY-LIU-2019002 for HQ; no. NZY-LIU-2019003 for BZ; and no. NZY-LIU-2019004 for GC) were deposited in the Herbarium of Traditional Chinese Medicine, School of Pharmacy, Nanjing University of Chinese Medicine, Nanjing, China. Acetonitrile and water were of LC-MS grade from Merck Company (Darmstadt, Germany). HPLC-grade methanol was purchased from ANPEL Scientific Instrument Co., Ltd. (Shanghai, China), as well as HPLC-grade formic acid with a purity of 99% (Anaqua Chemicals Supply, USA). All the other reagents were of analytical grade and obtained from the Nanjing Chemical Reagent Company (Nanjing, China).

Decoction Preparation

According to the original composition and preparation process recorded in "Jin-Gui-Yao-Lue," FHT was obtained following these procedures: dry herb pieces of *S. tetrandra* S. Moore (20 g), *A. membranaceus* Fisch. ex Bunge (25 g), *A. macrocephala* Koidz. (15 g), and *G. uralensis* Fisch. ex DC.(10 g) were mixed together in a certain ratio (4:5:3:2, *w*/*w*/*w*/*w*) and macerated in deionized water for 30 min before being decocted twice with boiling water (1:10, *w*/*v*, and 1:8, *w*/*v*, respectively), 20 min for each time. Then the solution was filtered through a two-layer mesh, combined and concentrated to a density of 1 g/ml for intragastric administration (*i.g.*).

The composition of FHT used in this paper was characterized by UHPLC-ESI-Q-TOF-MS chromatograms (Wang et al., 2015). Fangchinoline, atractylenolide I, tetrandrine, atractylenolide III,

calycosin-7-glucoside, liquiritigenin, isoliquiritigenin, liquiritin, isoliquiritin, and glycyrrhizin were tested as the dominating compounds for obvious representational significance during this work for a description of the composition of FHT. The typical total ion chromatogram (TIC) and extract ion chromatogram for 10 major compounds of FHT in positive ion mode were shown in **Supplementary Figure 5**, and the chemical structures of the 10 selected major compounds of FHT were given out in **Supplementary Figure 6**.

Animals and Drug Administration

Male Sprague-Dawley (SD) rats (n = 18), weighing 200–220 g, were supplied by the Slaccas Experiment Animal Company (Shanghai, China). Temperature and humidity conditions of the breeding environment were kept constant, with food and water provided *ad libitum*. All the rats were acclimated in the laboratory for at least 1 week prior to the experiment. Before testing, animals were fasted overnight with free access to water. All the animal experiments were carried out according to the Guidelines for the Care and Use of Laboratory Animals and were approved by the Animal Ethics Committee of Nanjing University of Chinese Medicine [approval number: ACU-13(20151120)].

Rats were randomly divided into a normal group (Group A, n = 6) and a model group (Group B, n = 12). A nephrotic syndrome model was prepared by giving rats injections of adriamycin (doxorubicin, 4 mg/kg) *via* the tail vein twice on the 1st and 14th days, respectively (Liu et al., 2019). The normal-group rats were injected with the same volume of saline instead. On the 0th (before injection) and 17th days after the first adriamycin injection, urine samples were collected from rats.

On the 22nd day, after the first adriamycin injection, all the rats in Group B were further randomly divided into an untreated model group (n = 6) and a test group (n = 6). The rats in the test group were administered with FHT at a dose of 14 g/kg (calculating by crude herb) for 5 weeks; meanwhile, the rats in the normal and model groups were given saline instead. Both FHT and saline were given to rats by gavage only once in 1 day. Blood samples (no more than 0.5 ml) of all these three groups of rats were collected from the orbital vein into tubes without being heparinized on 5th, 12th, 19th, 22nd, 23rd, 24th, 25th, 36th, 44th, 49th, 54th, and 57th days. The whole experiment period was 57 successive days.

Urinary protein excretion was determined by benzethonium chloride turbidimetric method using the urine samples within a period of 24 h in metabolic cages. Total cholesterol (TC), total triglyceride (TG), blood urea nitrogen (BUN), and cystatin C (Cys C) levels were measured by using commercially available kits based on colorimetric assays (Jian Cheng Biological Technology Co., LTD, Nanjing, China).

Sample Preparation

Blood samples were kept for 30 min under room temperature and then centrifuged to get a good separation at 4,000 rpm for 5 min. The supernatant was collected and stored at −80°C until analysis.

Spiked into centrifuge tubes was 0.1 ml of serum, which was and then mixed with 500 μl of methanol by vortex mixing for 30 s. The mixture was separated by centrifugation at 12,000 rpm for 5 min. The upper layer was then transferred to another tube and evaporated to dryness under nitrogen at 40°C. The residue was reconstituted with 100 μl of methanol, vortexed for 30 s, and centrifuged at 12,000 rpm for 3 min. Finally, 2 μl of the supernatant was used for UHPLC-ESI-Q-TOF-MS analysis.

Meanwhile, 15 plasma samples were randomly selected from real serum samples and were mixed together as quality control (QC) samples. These QC samples contained the most data of each group. They were analyzed to equilibrate the UHPLC-ESI-Q-TOF-MS system and to monitor the stability of this method. All these samples were maintained at 4°C during analysis.

UHPLC-ESI-Q-TOF-MS Conditions

For analysis of serum samples, an ekspert™ ultra LC 100-XL system coupled to hybrid quadrupole time-of-flight tandem mass spectrometry (LCMS-Triple TOF™ 5600, AB SCIEX, Foster City, CA) with an electrospray ionization (ESI) interface was used. The Analyst 1.6 software was installed for highly efficient data recording and processing.

Chromatographic separation was performed on a C_{18} reversed-phase UHPLC column (2.1 mm × 100 mm, 1.8 μm, Agilent). The column temperature was set at 30°C. The flow rate was 0.4 ml/min. The mobile phase consisted of (A) 0.1% formic acid in water and (B) acetonitrile. In order to obtain endogenous components with different polarities, the optimized gradient elution of metabonomics was set as follows: 0–15 min, 5–95% B; 15–16 min, 95% B; and 16–17 min, 95–5% B. At the same time, based on a previous study (Wang et al., 2015), the optimized gradient elution for FHT relative components detection in rat serum was as follows: 0–3 min, 17% B; 3–10 min, 17–70% B; 10–12 min, 70% B; 12–18 min, 70–80% B; 18–20 min, 80% B; 20–23 min, 80–100% B; 23–26 min, 100% B; 26–28 min, 100–17% B; and 28–30 min, 17% B.

The mass spectrometer was operated in positive ion modes. The following parameter settings were used: turbo spray temperature (TEM) of 550°C; declustering potential (DP) of 60 V; collision energy (CE) of 35 V; nebulizer gas (Gas 1) of 55 psi; heater gas (Gas 2) of 55 psi; and curtain gas of 35. Nitrogen was used as the nebulizer and auxiliary gas. TOF-MS and TOF-MS/MS were performed with the mass ranges of m/z 100–1,200 and 50–1,000, respectively. The experiments were running with a 200 ms accumulation time for TOF-MS and 80 ms accumulation time for TOF-MS/MS. Continuous recalibration was carried out every 3 h. In addition, dynamic background subtraction (DBS) and information-dependent acquisition (IDA) were applied to trigger acquisition of MS/MS for these constituents with extremely low signal levels.

Biomarker Screening and Identification

Raw data collected by the UHPLC-ESI-Q-TOF-MS system were imputed into the MarkerView™ software for principal component analysis (PCA). Before that, the alignment and normalization of the

chromatogram peaks were performed. The time range was 1–17 min, the scan range of quality was 100–1,000 *m/z*, the tolerance range of the mass number was 0.05, and the peak strength threshold was 100. The intensity of extracted ion was standardized by the total peak area method (normalized using total area sums). The samples collected on the 22nd day from the A and B groups were tested for screening differentiated endogenous metabolites. The identification of these selected biomarkers was accomplished by comparing the information from qualitative analysis and secondary mass spectrums and then confirmed by literatures as well as public databases including the Human Metabolome Database (HMDB), METLIN, and Small Molecular Pathway Database (SMPD). Furthermore, the identified metabolites were determined by a comparison with reference standards available in the lab. Also, the intensities of these selected biomarkers were detected and recorded.

Dynamic Detection of Serum Composition

Post-acquisition analyses were performed using the PeakView™ 1.2 software, which employed an extensive list of information of fragmentation in combination with the elemental compositions of the substrate molecules to generate a series of extracted ion chromatograms (XICs). The accurate mass and composition information for the precursor ions and fragment ions were quickly analyzed. Furthermore, the analyses of metabolites and prototype components were performed using the MetabolitePilot™ 1.5 programs containing a variety of functions such as predicted metabolites, generic peak finding, isotope pattern, and mass defect, based on a previous work (Wang et al., 2015).

Correlation Analysis Between Chemical and Metabolic Profiles

The basic idea of canonical correlation analysis (CCA) is to study the relationships between two sets of variations, as well as to determine the related degree. In this work, CCA was applied to find out the relationships between chemical and metabolic profiles. For each time point, the peak areas of relative components and their metabolites from FHT and the candidate biomarkers detected from rat serum samples were comprehensively calculated by using professional SPSS software for statistics (SPSS for Windows 17.0, SPSS Inc., USA).

RESULTS

Results of Plasma Metabonomics

Nephrotic Syndrome Modeling

The biomedical indexes of rats for nephrotic syndrome indication in the normal and model groups, such as urinary protein, TC, TG, BUN, and Cys C, were investigated firstly to determine whether the nephrotic syndrome model was constructed successfully. The results are shown in **Supplementary Table 1**. Compared with those in the normal group, 24 h urine protein, TC, TG, BUN, and Cys C levels in the model group were obviously elevated, which indicated that the nephrotic syndrome model was successfully induced.

The serum samples of rats in normal and model groups were monitored and supervised by the MarkerView™ software of AB SCIEX. The representative TICs of the serum samples from the normal group and model group in positive ion mode were shown in **Supplementary Figure 7**. The scores of rats in each group were obtained by PCA (**Figure 1**). The separation of the serum samples from model and normal groups was quite obvious. The spots of the model group distributed far from those of normal group. This result showed that the metabolism of rats in the model group was significantly altered. Through the analysis of the loading graph, the meaningful molecular weights of the endogenous molecules were found for each group (**Figure 2**). The results indicated that the intravenous injection of adriamycin could lead to kidney damage in rats and resulted in nephrotic syndrome.

Identification of Endogenous Metabolites

The potential biomarkers that made sense to grouping were finally found based on PCA score diagrams and loading diagrams. By comparing the possible biomarkers with the literatures and public online databases, 17 biomarkers in rat serum were preliminarily identified as shown in **Table 1**.

According to the results listed in **Table 1**, the endogenous components including L-3-cyanoalanine, alanylglycine, phosphoserine, *N*-acetyl-L-methionine, serinyl-proline, *N*-acetyl-L-phenylalanine, Lyso PE [0:0/22:1 (13Z)], Lyso PE [(6Z, 9Z, 12Z, 15Z)/0:0], PC (24:0), PC [22:4 (7Z, 10Z, 13Z, 16Z)/16:0], and PC [22:6 (4Z, 7Z, 10Z, 13Z, 16Z, 19Z, 19Z, 19Z)/18:1 (9Z)] in the nephrotic syndrome model group presented an upward trend. Meanwhile, allysine, 2-phenylglycine, L-homocysteic acid, methionyl-glycine, L-aspartyl-4-phosphate, and Lyso PC (P-16:0) in the nephrotic syndrome model group showed a downward trend. By comparing the changes of serum endogenous substances in the model group and the normal group, the significant increase or downregulation of these components was finally found. A relationship between endogenous components and nephrotic syndrome was discovered, which indicated that these endogenous metabolites could be used as characteristic biomarkers of nephrotic syndrome.

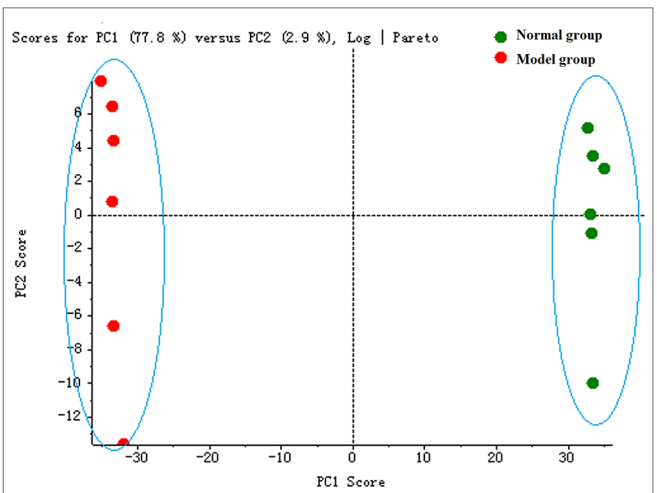


FIGURE 1 | The principal component analysis (PCA) score plot of rat serum samples between normal and model groups.

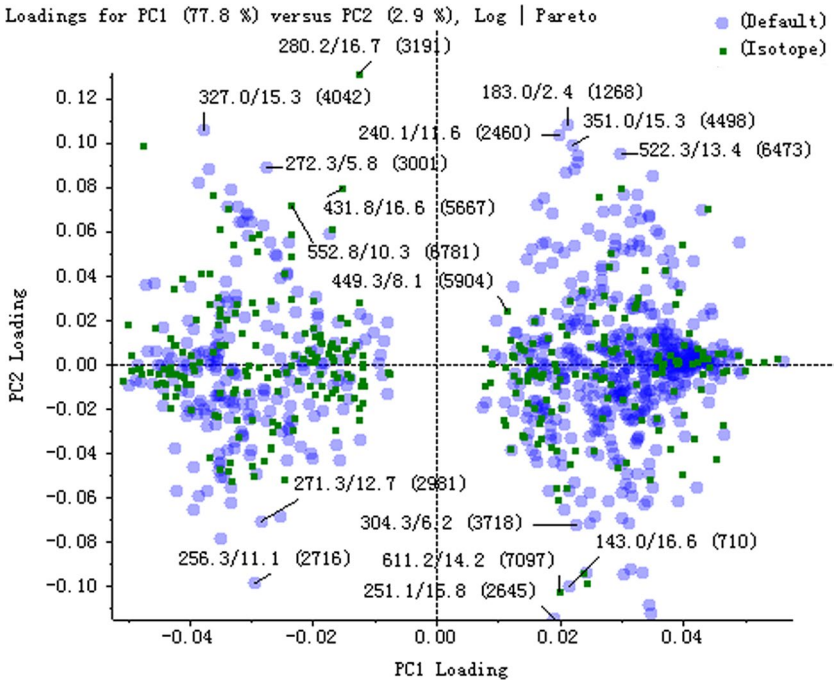


FIGURE 2 | The loading plot of principal component analysis (PCA) between normal and model groups in positive ion mode.

TABLE 1 | Results of potential biomarkers detected in rat serum.

No.	Extract mass	Formula	Adduct	Retention time	Mass error	Matching rate	Identification	Database ID	Trend
1	115.0225	$C_4H_6N_2O_2$	$[M+H]^+$	16.5	5.3	100%	L-3-Cyanoalanine	HMDB60245	Up
2	146.0590	$C_6H_{11}NO_3$	$[M+H]^+$	3.9	0.8	95%	Allysine	HMDB01263	Down
3	147.0493	$C_5H_{10}N_2O_3$	$[M+H]^+$	16.5	0.3	97%	Alanylglycine	HMDB06899	Up
4	152.0354	$C_8H_9NO_2$	$[M+H]^+$	16.5	4.6	99%	2-Phenylglycine	HMDB02210	Down
5	184.0259	$C_4H_9NO_5S$	$[M+H]^+$	16.6	7.5	100%	L-Homocysteic acid	HMDB02205	Down
6	185.9871	$C_3H_8NO_6P$	$[M+H]^+$	16.6	–2.2	100%	Phosphoserine	HMDB00272	Up
7	192.0642	$C_7H_{13}NO_3S$	$[M+H]^+$	2.5	3	95%	*N*-Acetyl-L-methionine	HMDB11745	Up
8	203.1056	$C_8H_{14}N_2O_4$	$[M+H]^+$	6.7	2.5	98%	Serinyl-proline	HMDB29047	Up
9	207.0860	$C_7H_{14}N_2O_3S$	$[M+H]^+$	4.1	–0.1	100%	Methionyl-glycine	HMDB28973	Down
10	208.0879	$C_{11}H_{13}NO_3$	$[M+H]^+$	4.1	6.7	100%	*N*-Acetyl-L-phenylalanine	HMDB00512	Up
11	214.0379	$C_4H_8NO_7P$	$[M+H]^+$	16.7	0.9	100%	L-Aspartyl-4-phosphate	HMDB12250	Down
12	480.3467	$C_{24}H_{50}NO_6P$	$[M+H]^+$	10.6	–0.1	95%	Lyso PC (P-16:0)	HMDB10407	Down
13	536.3723	$C_{27}H_{54}NO_7P$	$[M+H]^+$	10.2	1.3	100%	Lyso PE [0:0/22:1 (13Z)]	HMDB11491	Up
14	559.4400	$C_{35}H_{58}O_5$	$[M+H]^+$	8.4	0.7	100%	DG [14:1 (9Z)/18:4 (6Z, 9Z, 12Z, 15Z)/0:0]	HMDB07048	Up
15	608.4654	$C_{32}H_{66}NO_7P$	$[M+H]^+$	13.1	4.7	100%	Lyso PC (24:0)	HMDB10405	Up
16	810.6001	$C_{46}H_{84}NO_8P$	$[M+H]^+$	15.3	3.2	100%	PC [22:4 (7Z, 10Z, 13Z, 16Z)/16:0]	HMDB08626	Up
17	832.5862	$C_{48}H_{82}NO_8P$	$[M+H]^+$	15.4	1.7	100%	PC [22:6 (4Z, 7Z, 10Z, 13Z, 16Z, 19Z)/18:1 (9Z)]	HMDB08729	Up

Metabolic Pathway Analysis

Potential metabolic pathways of nephrotic syndrome were explored by imputing these 17 endogenous biomarkers listed in **Table 1** into MetaboAnalyst. Then, all the corresponding pathways were constructed according to *p* values given by pathway topology analysis (*x*-axis) (Xia and Wishart, 2011), with the most significant pathways colored in red (**Figure 3**).

In **Figure 3**, results showed that these 17 endogenous metabolites in rats involved in nephrotic syndrome were mainly related to six metabolic pathways. The six pathways included

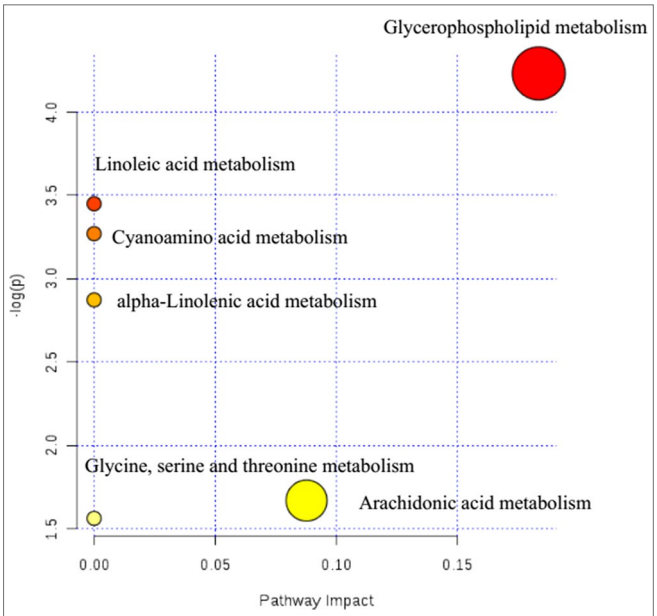


FIGURE 3 | Summary of pathway analysis of serum samples collected from nephrotic syndrome rats.

linoleic acid metabolism with an impact value of 0; cyanoamino acid metabolism with an impact value of 0; alpha-linolenic acid metabolism with an impact value of 0; glycine, serine, and threonine metabolism with an impact value of 0.087; arachidonic acid metabolism with an impact value of 0 and glycerophospholipid metabolism with an impact value of 0.183. It is suggested that the pathway of glycerophospholipid metabolism was the most important metabolic pathway for nephrotic syndrome formation, for the reason that the threshold of the impact value over 0.10 was commonly accepted as the most important metabolic pathway (Hoffmann et al., 2014). According to historical reports, lipid mediators, including eicosanoids, platelet-activating factor (PAF), and other chemotactic factors, have been proposed to contribute to leukocyte infiltration, mesangial proliferation, extracellular matrix protein production, vasoreactivity, and coagulation (Kees-Folts and Diamond, 1993). Further evidence of a relationship between PAF and the development of nephrotic syndrome was proven to be the marked elevation in plasma PAF-AH activity (Mimura et al., 1996).

Intensity-Time Variation of Biomarkers

In order to investigate the influence of FHT on the characteristic endogenous components, the rats with nephrotic syndrome

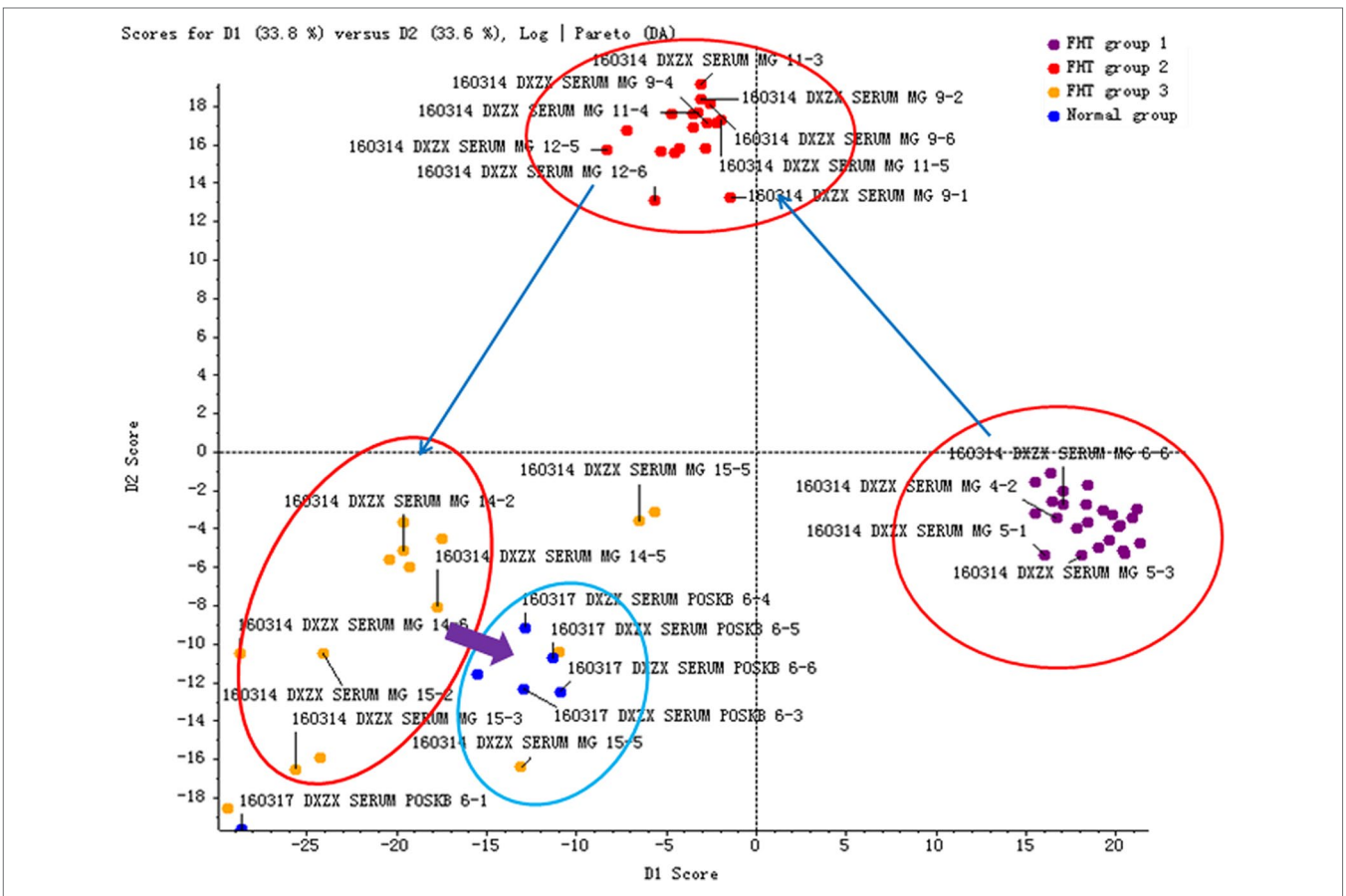


FIGURE 4 | Time-related trajectory of metabolite patterns of nephrotic syndrome rats after FHT administration (FHT group 1 stands for the serum samples collected in an early drug medication: 23rd day; FHT group 2 stands for the serum samples collected in midterm drug medication: 44th day; FHT group 3 stands for the serum samples collected in later period of drug medication: 57th day).

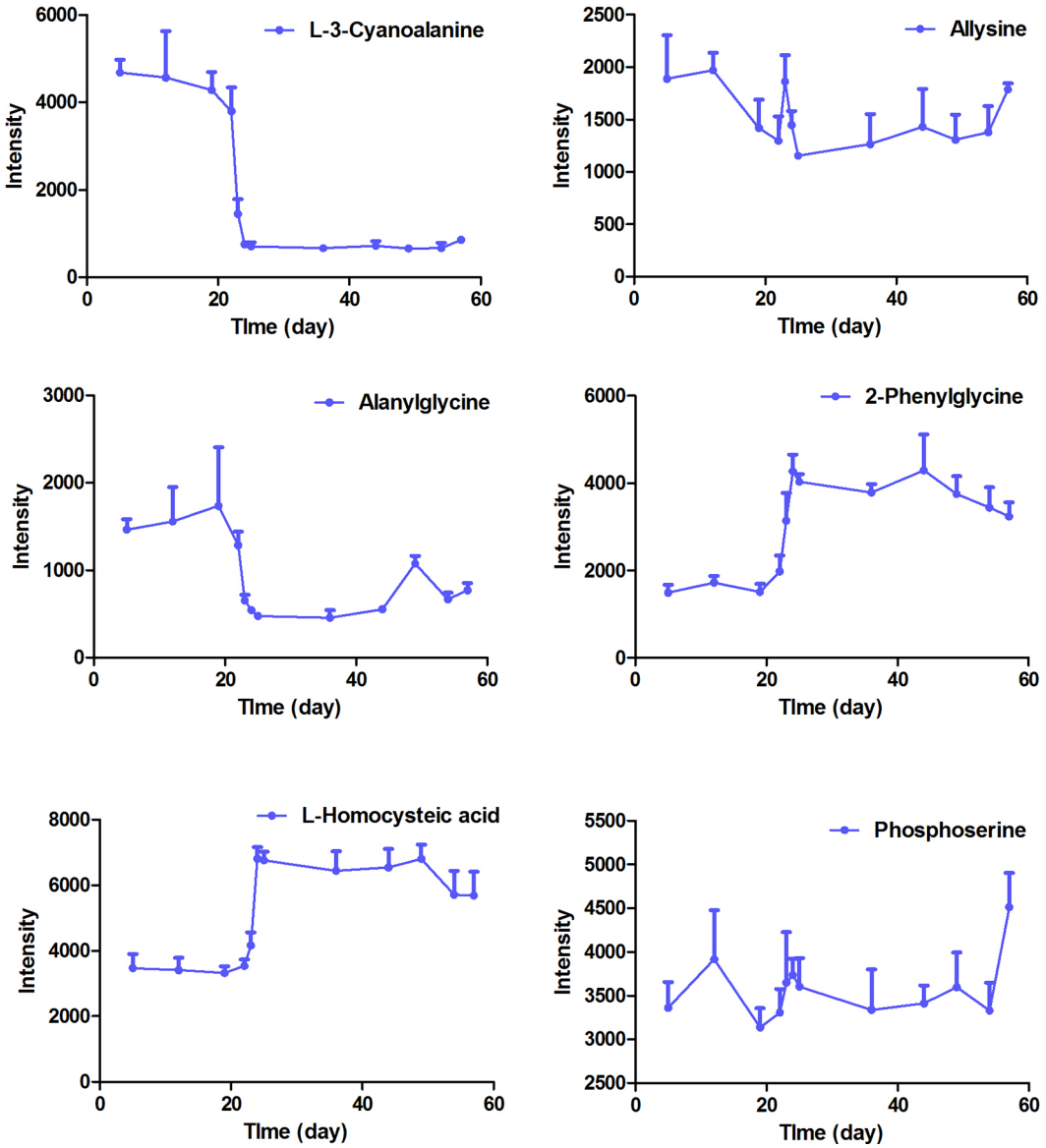


FIGURE 5 | The intensity-time variation profiles of endogenous markers, including L-3-cyanoalanine, allysine, alanylglycine, 2-phenylglycine, L-homocysteic acid, and phosphoserine.

were administrated with FHT once a day for 5 weeks. The blood samples of rats were collected at different time points. The intensity data of 17 endogenous biomarkers in the rat serum samples were extracted and analyzed by the PeakView™ software of AB SCIEX. The PCA score plot derived from the UHPLC-MS profiles of rat serum samples after FHT treatment in positive mode was shown in **Figure 4**. The plot shows a time-related trajectory of metabolite patterns at different time points after FHT treatment. And it can be seen that the metabolite pattern of rats was brought back to normal or near normal.

The intensity-time variations of endogenous biomarkers were shown in **Figures 5**–**7**. The endogenous biomarkers containing 2-phenylglycine, L-homocysteic acid, and L-aspartyl-4-phosphate in FHT group showed a tendency to increase, while others like L-3-cyanoalanine, alanylglycine, *N*-acetyl-L-methionine, methionyl-glycine, *N*-acetyl-L-phenylalanine, Lyso PE [0:0/22:1 (13Z)], DG [14:1 (9Z)/18:4 (6Z, 9Z, 12Z, 15Z)/0:0], Lyso PC (24:0), and PC [22:6 (4Z, 7Z, 10Z, 13Z, 16Z, 19Z)/18:1 (9Z)] in the test group showed a tendency to decrease. Lipid metabolism disorder is usually related to the occurrence and development of nephropathy. Lyso PE [0:0/22:1 (13Z)], DG [14:1 (9Z)/18:4 (6Z, 9Z, 12Z, 15Z)/0:0], Lyso PC (24:0), and PC [22:6 (4Z, 7Z, 10Z, 13Z, 16Z, 19Z, 19Z)/18:1 (9Z)] all belonged to low-density lipoprotein, which plays an important role in

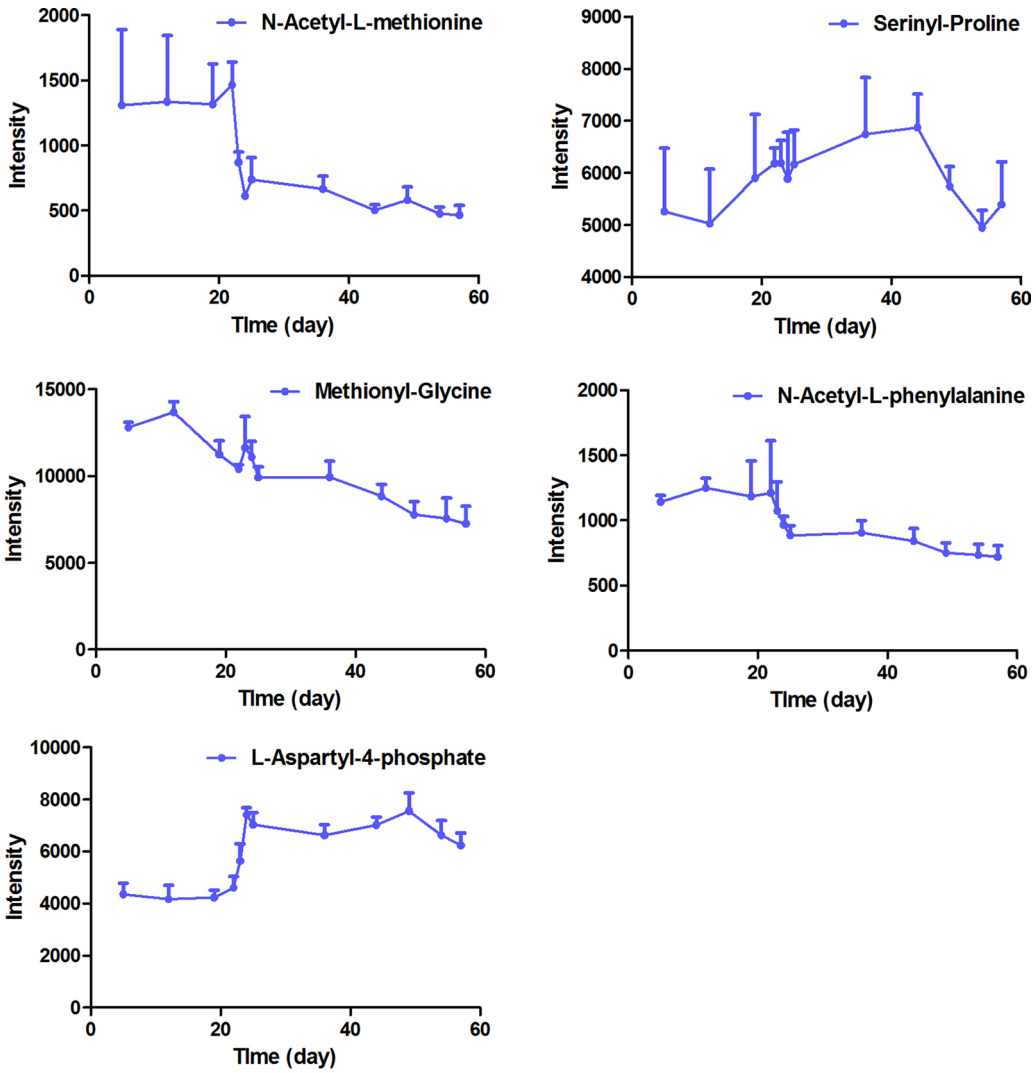


FIGURE 6 | The intensity-time variation profiles of endogenous markers, including acetyl-L-methionine, serinyl-proline, methionyl-glycine, *N*-acetyl-L-phenylalanine, and L-aspartyl-4-phosphate.

lipid metabolism (Gaits et al., 1997). In model and test groups, the intensity of low-density lipoprotein showed a certain trend of change, which was consistent with the literature report (Gaits et al., 1997). The results indicated that FHT could regulate these endogenous substances to a certain degree.

Dynamic Detection of FHT Relative Components

The FHT relative components in rat serum were identified by using the UHPLC-ESI-Q-TOF-MS technique based on high-resolution mass spectrometry of AB SCIEX Triple TOF™ 5600 and mass spectrum analysis software of PeakView™ based on the analysis of the chemical components in FHT developed at a previous stage; meanwhile, the metabolic pathway database in serum was established (Wang et al., 2015). In order to guarantee the accuracy of experimental results, the components in serum samples with an intensity less than 100 at various time points were dismissed. As a result, 43 components were selected to be involved in chemical spectrum–metabolic spectrum correlation analysis. The list of constituents in rat serum after oral administration of FHT by using the UHPLC-ESI-Q-TOF-MS method is shown in **Supplementary Table 2**. The typical ion chromatography spectrums of rat serum after being administered with FHT in positive and negative ion modes are shown in **Supplementary Figure 8**.

Correlation Discovery Between Chemical and Metabolic Spectrums

The typical correlation analysis method was adopted to find out the relationships between chemical spectrum and metabolic

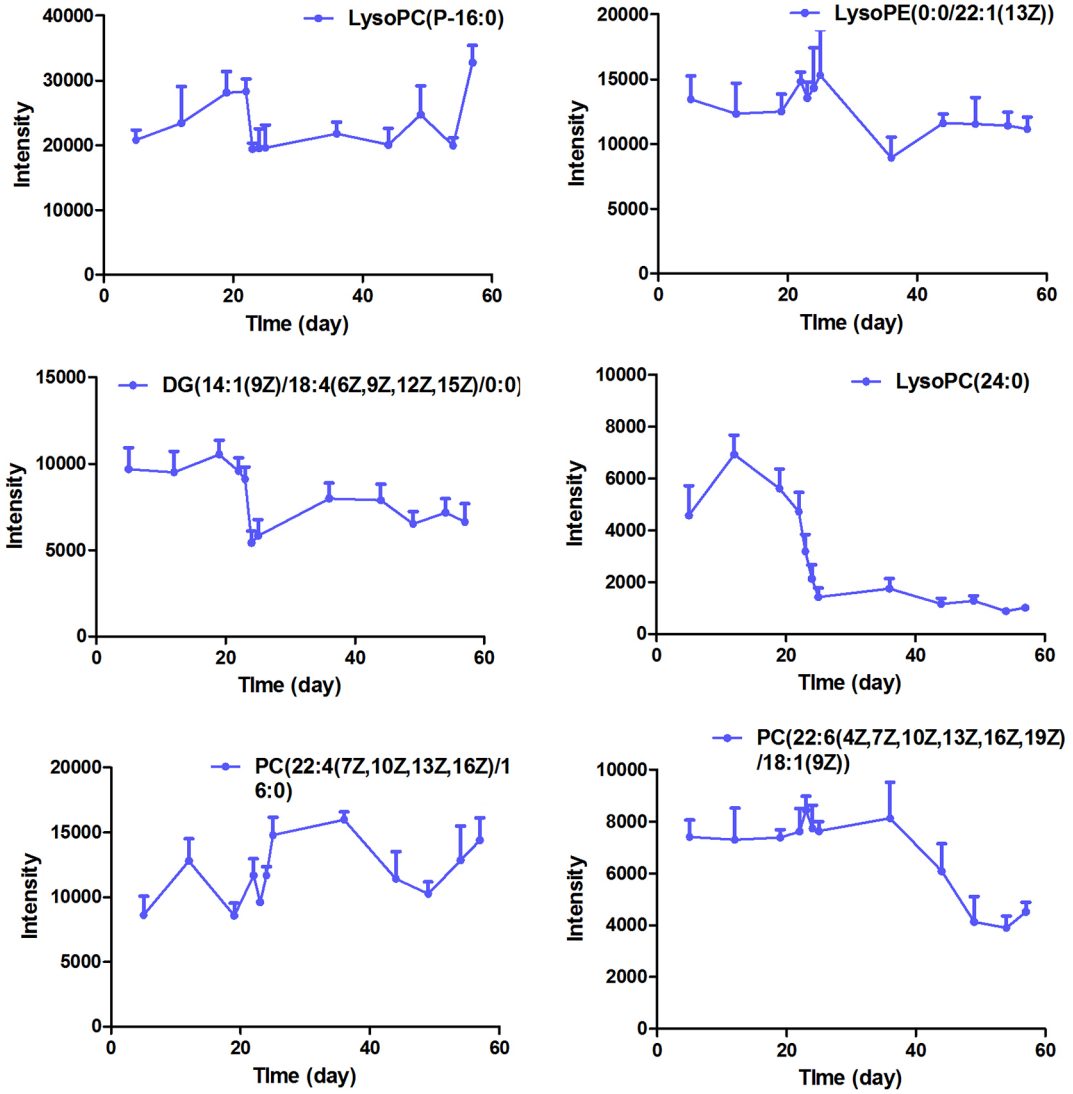


FIGURE 7 | The intensity-time variation profiles of endogenous markers, including Lyso PC (P-16:0), Lyso PE [0:0/22:1 (13Z)], DG [14:1 (9Z)/18:4 (6Z, 9Z, 12Z, 15Z)/0:0], Lyso PC (24:0), PC [22:4 (7Z, 10Z, 13Z, 16Z)/16:0], and PC [22:6 (4Z, 7Z, 10Z, 13Z, 16Z, 19Z)/18:1 (9Z)].

spectrum with the purpose of screening the potential active components in FHT. The relationships of 43 relative compounds found in FHT and endogenous components, including L-3-cyanoalanine, alanylglycine, 2-phenylglycine, L-homocysteic acid, *N*-acetyl-L-methionine, methionyl-glycine, *N*-acetyl-L-phenylalanine, L-aspartyl-4-phosphate, Lyso PE [0–0 draw/pay z (13)], DG [14:1 (z)/o (12z, z, 6z, 9, 15 z)/0–0], Lyso PC (24:0), and PC [22:6 (4Z, 7Z, 10Z, 13Z, 16Z, 19Z, 19Z)/18:1 (9Z)], under a series of time points were investigated based on a chemical–metabolic spectrum correlation analysis. The results are shown in **Figure 8** and **Supplementary Tables 3–8**, which suggested that there was a significant correlation between the intensity changes of alkaloid components and the response intensity of differential endogenous substances in rat serum after drug administration, such as (+)-tetrandrine demethylation, fenfangjine G hydrogenation, tetrandrine, *N*-methylfangchinoline, tetrandrine demethylation, and fangchinoline. The alkaloids are the main active components of *S. tetrandra* S. Moore. This phenomenon was consistent with the traditional Chinese medical theory that "the medicine as sovereign is the core of the whole prescription." At the same time, the study found that the alkaloids absorbed were transformed reciprocally through certain metabolic ways *in vivo*. It was speculated that these alkaloids and their metabolites worked efficiently by synergistic effect. In addition, the components of saponins were significantly correlated with the difference endogenous markers. The saponin compounds were derived from *A. membranaceus* (Fisch.) Bge—another medicine serving

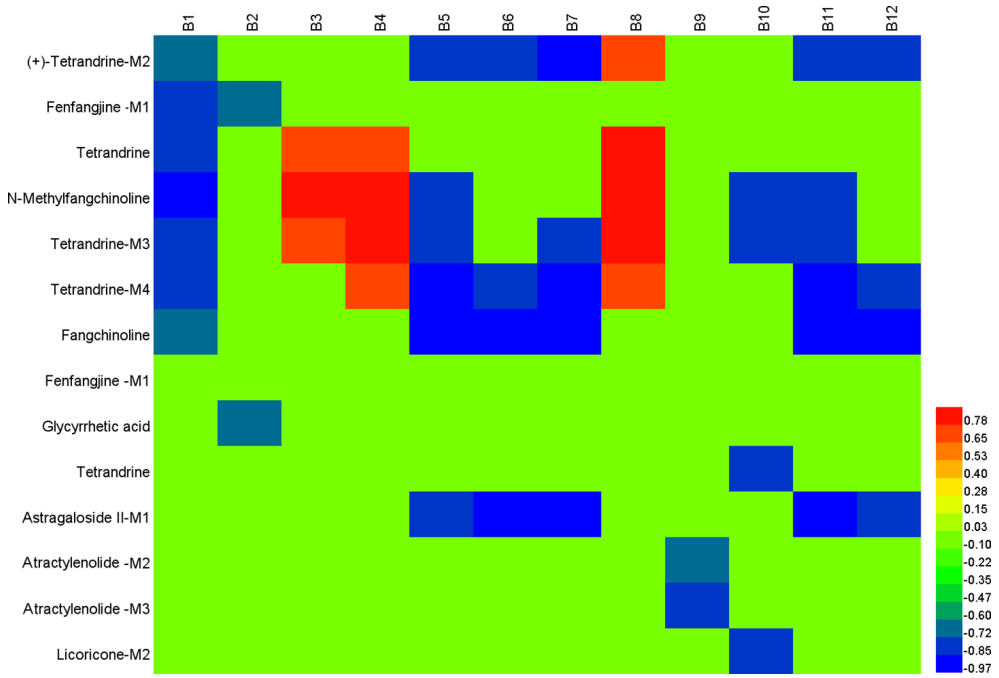


FIGURE 8 | Correlation analysis map between potential biomarkers and Fangji Huangqi Tang (FHT) relative chemical components based on Pearson correlation coefficient using a color scale from significantly negative correlation (blue) to significantly positive correlation (red). B1, L-3-cyanoalanine; B2, alanylglycine; B3, 2-phenylglycine; B4, L-homocysteic acid; B5, *N*-acetyl-L-methionine; B6, methionyl-glycine; B7, *N*-acetyl-L-phenylalanine; B8, L-aspartyl-4-phosphate; B9, Lyso PE [0–0 draw/pay z (13)]; B10, DG [14:1 (z)/o (12 z, z, 6z, 9, 15 z)/0–0]; B11, Lyso PC (24:0); B12, PC [22:6 (4Z, 7Z, 10Z, 13Z, 16Z, 19Z, 19Z)/18:1 (9Z)].

as sovereign in the whole prescription of FHT. Also, literatures already proved that saponins of *A. membranaceus* (Fisch.) Bge showed certain therapeutic effects on chronic renal disease (Yan et al., 2017; Zhou et al., 2017). Furthermore, the results of this work indicated that alkaloids and lactones in FHT could regulate lipid metabolism in rats. Lipid metabolism disorder was always believed to be an important pathological manifestation in the pathogenesis of nephrotic syndrome, because massive loss of proteinuria could result in lipid metabolism disorder. It was suggested that the alkaloids and lactones in FHT might treat nephrotic syndrome by the regulating lipid metabolism way in rats.

Active components in FHT for nephrotic syndrome treatment were screened out, including (+)-tetrandrine demethylation, fenfangjine G hydrogenation, tetrandrine, *N*-methylfangchinoline, tetrandrine demethylation, fangchinoline, glycyrrhetic acid, astragaloside II alcohol dehydration, atractylenolide III demethylation + hydrogenation, atractylenolide III demethylation + hydrogenation, and licoricone-*N*-acetylcysteine conjugation. From the results, we could see that they were prototypes as well as metabolites. Certainly, metabolites came from the corresponding prototypes. Tetrandrine, fenfangjine G, fangchinoline, glycyrrhetic acid, astragaloside II, atractylenolide III, and licoricone were finally found to be related to FHT efficacy on nephrotic syndrome treatment. Among them, tetrandrine, fenfangjine G, and fangchinoline came from *S. tetrandra* S. Moore (FJ); astragaloside II came from *A. membranaceus* Fisch. ex Bunge (HQ); atractylenolide III came from *A. macrocephala* Koidz. (BZ); and glycyrrhetic acid and licoricone came from *G. uralensis* Fisch. ex DC. (GC). According to our previous work, the quantities of these components in FHT were between 0.54 and 41.19 μg/ml (Wang et al., 2016), which are relatively high enough to be of sensible pharmacological relevance for herbal drugs. In all, chemical components in FHT, as well as their metabolites, were found to be the active materials for nephrotic syndrome treatment. These compounds were found to be involved in some metabolic pathways, including glycerophospholipid metabolism; linoleic acid metabolism; cyanoamino acid metabolism; alpha-linolenic acid metabolism; glycine, serine, and threonine metabolism; and arachidonic acid metabolism. For a long time, TCM was believed to exert pharmacological effects by multi-targets in multiforms. In this paper, prototypes of FHT relative components, as well as their metabolites, were found to be active substances for nephrotic syndrome treatment in rats by moderation effects in certain metabolic pathways, which proved supporting evidence for the speculation concerning the synergistic effect of the complex components in TCM.

CONCLUSION

In this paper, a synthetic strategy combining the UHPLC-ESI-Q-TOF-MS chemical profiling technique and the CCA statistical method was successfully applied to screen

out the potential active components in FHT for nephrotic syndrome treatment. Different from classical spectrum–effect relationship studies, the work in this paper concentrated on the relationships between drug relative chemical spectrums and serum biomarker profiles. It provided a meaningful reference mode to reveal the chemical material basis of complex TCM. The limitation of this work was that the specific ways for these components to exert their activities were not clearly explained. Further studies should be concentrated on the evaluation of the efficacy of these active components in FHT on the special pathways as well as their interactions.

DATA AVAILABILITY STATEMENT

The raw data supporting the conclusions of this manuscript will be made available by the authors, without undue reservation, to any qualified researcher.

ETHICS STATEMENT

All the animal experiments were carried out according to the Guidelines for the Care and Use of Laboratory Animals, and were approved by the Animal Ethics Committee of Nanjing University of Chinese Medicine [Approval number: ACU-13(20151120)].

AUTHOR CONTRIBUTIONS

XL, X-CZ, and LX carried out the studies, performed the statistical analysis, and wrote the manuscript. Q-GZ participated in the animal experiments. XL and B-CC designed the work and revised the manuscript. All the authors have read and approved the final version.

FUNDING

This work was financially supported by the National Natural Science Foundation of China (no. 81503207), Major Projects of Natural Science Foundation of Jiangsu Higher Education Institutions (no. 17KJA360006) and Jiangsu Province "333" project.

SUPPLEMENTARY MATERIAL

The Supplementary Material for this article can be found online at: https://www.frontiersin.org/articles/10.3389/fphar.2019.01261/full#supplementary-material

REFERENCES

Bjerrum, J. T., Wang, Y., Hao, F., Coskun, M., Ludwig, C., Günther, U., et al. (2015). Metabonomics of human fecal extracts characterize ulcerative colitis, Crohn's disease and healthy individuals. *Metabolomics* 11, 122–133. doi: 10.1007/s11306-014-0677-3

Chen, G. L., Liu, H. P., and Cheng, F. (2013). Fangjihuangqi tang improved lower urinary tract dysfunction in benign prostatic hyperplasia rats model. *J. Tradit. Chin. Med.* 33, 349–354. doi: 10.1016/S0254-6272(13)60177-6

Crawford, B. D., and Gipson, D. S. (2017). Improving the evidence for the management of childhood nephrotic syndrome. *Kidney Int.* 92, 21–23. doi: 10.1016/j.kint.2017.02.029

Cui, D. N., Wang, X., Chen, J. Q., Lv, B., Zhang, P., Zhang, W., et al. (2017). Quantitative evaluation of the compatibility effects of huangqin decoction on the treatment of irinotecan-induced gastrointestinal toxicity using untargeted metabolomics. *Front. Pharmacol.* 8, 211. doi: 10.3389/fphar.2017.00211

Gaits, F., Salles, J. P., and Chap, H. (1997). Dual effect of lysophosphatidic acid on proliferation of glomerular mesangial cells. *Kidney Int.* 51, 1022–1027. doi: 10.1038/ki.1997.143

Hoffmann, T., Krug, D., Hüttel, S., and Müller, R. (2014). Improving natural products identification through targeted LC-MS/MS in an untargeted secondary metabolomics workflow. *Anal. Chem.* 86, 10780–10788. doi: 10.1021/ac502805w

Jové, M., Portero-Otín, M., Naudí, A., Ferrer, I., and Pamplona, R. (2014). Metabolomics of human brain aging and age-related neurodegenerative diseases. *J. Neuropathol. Exp. Neurol.* 7, 640–657. doi: 10.1097/NEN.0000000000000091

Kang, H. G., Seo, H., Lim, J. H., Kim, J. I., Han, K. H., Park, H. W., et al. (2017). Markers of disease and steroid responsiveness in paediatric idiopathic nephrotic syndrome: whole-transcriptome sequencing of peripheral blood mononuclear cells. *J. Int. Med. Res.* 45, 948–963. doi: 10.1177/0300060516652762

Kees-Folts, D., and Diamond, J. R. (1993). Relationship between hyperlipidemia, lipid mediators, and progressive glomerulosclerosis in the nephrotic syndrome. *Am. J. Nephrol.* 13, 365–375. doi: 10.1159/000168651

Liu, X., Zhu, X. C., Xie, L., and Cai, B. C. (2019). Pharmacokinetic/pharmacodynamic modelling of effective components of Fangji Huangqi Tang for its treatment of nephrotic syndrome. *New J. Chem.* 43, 338–347. doi: 10.1039/C8NJ03040E

Mimura, K., Zhao, B., Muguruma, K., Frenkel, R. A., and Johnston, J. M. (1996). Changes in glycerophospholipid profile in experimental nephrotic syndrome. *Metabolism* 45, 822–826. doi: 10.1016/S0026-0495(96)90153-5

Nie, L. (2008). Clincal experience in TCM treatment of refractory nephrotic syndrome. *J. Tradit. Chin. Med.* 28, 46–48. doi: 10.1016/S0254-6272(08)60013-8

Pang, H. Q., Yue, S. J., Tang, Y. P., Chen, Y. Y., Tan, Y. J., Cao, Y. J., et al. (2018). Integrated metabolomics and network pharmacology approach to explain possible action mechanisms of Xin-Sheng-Hua granule for treating anemia. *Front Pharmacol.* 9, 165. doi: 10.3389/fphar.2018.00165

Patel, S., and Ahmed, S. (2014). Emerging field of metabolomics: Big promise forcancer biomarker identification and drug discovery. *J. Pharm. Biomed. Anal.* 22, 63–74. doi: 10.1016/j.jpba.2014.12.020

Wang, X. L., Liu, X., Xu, X. Y., Zhu, T. T., Shi, F., Qin, K. M., et al. (2015). Screening and identification of multiple constituents and their metabolites of Fangji Huangqi Tang in rats by ultra-high performance liquid chromatography coupled with quadrupole time-of-flight tandemmass spectrometry basing on coupling data processing techniques. *J. Chromatogr. B Analyt. Technol. Biomed. Life Sci.* 985, 14–28. doi: 10.1016/j.jchromb.2015.01.021

Wang, X. L., Liu, X., Zhu, T. T., and Cai, B. C. (2016). Development and validation of an UHPLC-QqQ-MS technique for simultaneous determination of ten bioactive components in Fangji Huangqi Tang. *J. Anal. Methods. Chem.* 2016, 1435106. doi: 10.1155/2016/1435106

Wang, W., and Wang, S. Q. (2004). Nephrotic syndrome and the TCM treatment. *J. Tradit. Chin. Med.* 24, 201–203.

Wu, J. B., Ye, S. F., Liang, C. L., Li, Y. C., Yu, Y. J., Lai, J. M., et al. (2014). Qi-Dan Fang ameliorates adriamycin-induced nephrotic syndrome rat model by enhancing renal function and inhibiting podocyte injury. *J. Ethnopharmacol.* 151, 1124–1132. doi: 10.1016/j.jep.2013.12.028

Xia, J., and Wishart, D. S. (2011). Web-based inference of biological patterns, functions and pathways from metabolomic data using MetaboAnalyst. *Nat. Protoc.* 6, 743–760. doi: 10.1038/nprot.2011.319

Yan, W., Xu, Y., Yuan, Y. H., Tian, L., Wang, Q., Xie, Y. Y., et al. (2017). Renoprotective mechanisms of Astragaloside IV in cisplatin-induced acute kidney injury. *Free Radic. Res.* 51, 669–683. doi: 10.1080/10715762.2017.1361532

Zhang, W. N., Li, A. P., Qi, Y. S., Qin, X. M., and Li, Z. Y. (2018). Metabolomics coupled with system pharmacology reveal the protective effect of

total flavonoids of Astragali Radix against adriamycin-induced rat nephropathy model. *J. Pharm. Biomed. Anal.* 158, 128–136. doi: 10.1016/j.jpba.2018.05.045

Zhang, J. J., and Yu, R. H. (2015). Treatment of focal segmental glomerular sclerosis by modified fangji huangqi decoction (Chinese characters: see text□): a case report of one patient. *Zhongguo Zhong Xi Yi Jie He Za Zhi* 35, 252–253.

Zhou, H. N., Zhang, P. J., Hou, Z. G., Xie, J. B., Wang, Y. M., Yang, B., et al. (2016). Research on the relationships between endogenous biomarkers and exogenous toxic substances of acute toxicity in radix aconiti. *Molecules* 21, 1623. doi: 10.3390/molecules21121623

Zhou, W., Chen, Y., and Zhang, X. Y. (2017). Astragaloside IV alleviates lipopolysaccharide-induced acute kidney injury through down-regulating cytokines, CCR5 and p-ERK, and elevating anti-oxidative ability. *Med. Sci. Monit.* 23, 1413–1420. doi: 10.12659/MSM.899618

Conflict of Interest: The authors declare that the research was conducted in the absence of any commercial or financial relationships that could be construed as a potential conflict of interest.

Copyright © 2019 Liu, Zhou, Zhu, Xie and Cai. This is an open-access article distributed under the terms of the Creative Commons Attribution License (CC BY). The use, distribution or reproduction in other forums is permitted, provided the original author(s) and the copyright owner(s) are credited and that the original publication in this journal is cited, in accordance with accepted academic practice. No use, distribution or reproduction is permitted which does not comply with these terms.

frontiers in Physiology

ORIGINAL RESEARCH
published: 25 October 2019
doi: 10.3389/fphys.2019.01320

Post-treatment With Qing-Ying-Tang, a Compound Chinese Medicine Relives Lipopolysaccharide-Induced Cerebral Microcirculation Disturbance in Mice

*Hao-Min Wang[1,2,3,4,5,6], Ping Huang[2,3,4,5,6†], Quan Li[2,3,4,5,6], Lu-Lu Yan[2,3,4,5,6], Kai Sun[2,3,4,5,6], Li Yan[2,3,4,5,6], Chun-Shui Pan[2,3,4,5,6], Xiao-Hong Wei[2,3,4,5,6], Yu-Ying Liu[2,3,4,5,6], Bai-He Hu[2,3,4,5,6], Chuan-She Wang[1,2,3,4,5,6], Jing-Yu Fan[2,3,4,5,6] and Jing-Yan Han[1,2,3,4,5,6]**

[1]Department of Integration of Chinese and Western Medicine, School of Basic Medical Sciences, Peking University, Beijing, China, [2]Tasly Microcirculation Research Center, Peking University Health Science Center, Beijing, China, [3]Key Laboratory of Microcirculation, State Administration of Traditional Chinese Medicine of the People's Republic of China, Beijing, China, [4]Key Laboratory of Stasis and Phlegm, State Administration of Traditional Chinese Medicine of the People's Republic of China, Beijing, China, [5]State Key Laboratory of Core Technology in Innovative Chinese Medicine, Beijing, China, [6]Beijing Microvascular Institute of Integration of Chinese and Western Medicine, Beijing, China

OPEN ACCESS

Edited by:
John D. Imig,
Medical College of Wisconsin,
United States

Reviewed by:
Keith David Rochfort,
Dublin City University, Ireland
Chunyu Niu,
Hebei North University, China

***Correspondence:**
Jing-Yan Han
hanjingyan@bjmu.edu.cn

†Co-first author

Specialty section:
This article was submitted to Vascular Physiology, a section of the journal Frontiers in Physiology

Received: 15 May 2019
Accepted: 01 October 2019
Published: 25 October 2019

Citation:
Wang H-M, Huang P, Li Q, Yan L-L, Sun K, Yan L, Pan C-S, Wei X-H, Liu Y-Y, Hu B-H, Wang C-S, Fan J-Y and Han J-Y (2019) Post-treatment With Qing-Ying-Tang, a Compound Chinese Medicine Relives Lipopolysaccharide-Induced Cerebral Microcirculation Disturbance in Mice. Front. Physiol. 10:1320. doi: 10.3389/fphys.2019.01320

Objective: Lipopolysaccharide (LPS) causes microvascular dysfunction, which is a key episode in the pathogenesis of endotoxemia. This work aimed to investigate the effect of Qing-Ying-Tang (QYT), a compound Chinese medicine in cerebral microcirculation disturbance and brain damage induced by LPS.

Methods: Male C57/BL6 mice were continuously transfused with LPS (7.5 mg/kg/h) through the left femoral vein for 2 h. QYT (14.3 g/kg) was given orally 2 h after LPS administration. The dynamics of cerebral microcirculation were evaluated by intravital microscopy. Brain tissue edema was assessed by brain water content and Evans Blue leakage. Cytokines in plasma and brain were evaluated by flow cytometry. Confocal microscopy and Western blot were applied to detect the expression of junction and adhesion proteins, and signaling proteins concerned in mouse brain tissue.

Results: Post-treatment with QYT significantly ameliorated LPS-induced leukocyte adhesion to microvascular wall and albumin leakage from cerebral venules and brain tissue edema, attenuated the increase of MCP-1, MIP-1α, IL-1α, IL-6, and VCAM-1 in brain tissue and the activation of NF-κB and expression of MMP-9 in brain. QYT ameliorated the downregulation of claudin-5, occludin, JAM-1, ZO-1, collagen IV as well as the expression and phosphorylation of VE-cadherin in mouse brain.

Conclusions: This study demonstrated that QYT protected cerebral microvascular barrier from disruption after LPS by acting on the transcellular pathway mediated by caveolae and paracellular pathway mediated by junction proteins. This result suggests QYT as a potential strategy to deal with endotoxemia.

Keywords: leukocyte, hyperpermeability, NF-κB, Src, tight junctions, caveolin-1

INTRODUCTION

Lipopolysaccharide (LPS) causes endotoxemia and sepsis, leading to multiple organ failure and infectious shock resulting in a range of disastrous sequels (Berger et al., 2017). Encephalopathy is a common manifestation of endotoxemia (Siami et al., 2008), with a mortality rate of 76.1%, of which the prognosis is mostly neurological dysfunction or persistent vegetative state (Tong et al., 2015). Despite application of fluid resuscitation, vasoactive medicines and glucocorticoid, dealing with endotoxemia remains a challenge for clinician.

LPS binds to toll like receptor 4 (TLR-4) (Tsukamoto et al., 2018) and activates nuclear transcription factor κB (NF-κB), causing the release of inflammatory factors and the expression of chemotactic molecules and adhesion molecules, promoting the recruitment of leukocytes in venules (Bienvenu and Granger, 1993; Khakpour et al., 2015), resulting in microvascular occlusion and tissue ischemia (Cohen, 2002). Reduced tissue perfusion stimulates the conversion of xanthine dehydrogenase to xanthine oxidase, which brings about a massive surge of free radicals, including superoxide, hydrogen peroxide, and hydroxyl radical (Jean-Baptiste, 2007). Free radicals can activate matrix metalloproteinases (MMPs) (Vanlaere and Libert, 2009) and induce the degradations of tight junctions (TJs), leading to brain blood barrier (BBB) breakdown (Coisne and Engelhardt, 2011). As a major component of BBB, endothelial permeability is regulated by transcellular pathway mediated by the caveolae and paracellular pathway mediated by endothelial cell junctions (Keaney and Campbell, 2015). LPS recognized by TLR4 activates Src family protein tyrosine kinases (Plociennikowska et al., 2015), which in turn induces NF-κB translocation or directly activates Rock kinase and myosin light chain kinase (MLCK) signaling that causes disruption of endothelial cell junctions (Clark et al., 2015) and impairs integrity of vascular basement membrane, resulting in hyperpermeability, hemorrhage and thrombosis (Mombouli and Vanhoutte, 1999), which eventually lead to multiple organ failure, septic shock and even death (Khakpour et al., 2015). Therefore, ameliorating microvascular hyperpermeability and edema is anticipated as an important treatment strategy.

Qing-Ying-Tang (QYT) is a traditional Chinese medicine formula consisting of nine different decoction pieces. Currently, QYT has been used in clinic in China to cope with various disorders, ranging from dermatological diseases to acute infectious diseases including endotoxemia (Zhang et al., 2009; Gao et al., 2014). Clinical trials have shown that QYT combined with Western medicine for the treatment of sepsis can not only quickly eliminate the clinical symptoms and decrease the occurrence of multiple organ dysfunction syndromes, but also reduce the incidence of complications (Ji et al., 2015). In addition, some other beneficial role of QYT has been reported in clinic, such as regulation of blood fat and humoral immunity in patients with thromboangiitis obliterans (Fu, 2005), curative effect for viral encephalitis patients, who are not sensitive to hormones and anti-inflammatory drugs (Dong, 2007), reduction of high fever after abdominal surgery (Feng and Xu, 2015). However, only limited study is available so far, mostly in Chinese, regarding the rationale behind the effect of QYT on endotoxemia. On the other hand, we have previously shown that catalpol, an ingredient of the QYT formula, can reduce LPS-caused mesenteric microvascular hyperpermeability and hemorrhage (Zhang et al., 2016). DLA (Li et al., 2012) and salvianolic acid B (Lin et al., 2013), the other two constituents of QYT, have been reported to improve LPS-induced mouse cerebral microcirculation and rat lung microcirculation disorders, respectively. In view of the findings above, we speculated that the effect of QYT on endotoxemia may implicate improvement of microvascular hyperpermeability. This study was designed to test this speculation.

MATERIALS AND METHODS

Animals

The animals used in the present study were C57/BL6 mice, male, with body weight of 18–22 g, which were purchased from Beijing Vital River Laboratory Animal Technology Company Limited (certificate no SCKX 2016-0011), and kept in an environment of temperature of 23 ± 2°C and relative humidity of 40 ± 5% with a 12-h light/dark cycle. The animals were fed with rodent food and water but underwent fasted for 12 h before experiment with allowing for access to water ad libitum. The experimental procedures were carried out as per the European commission guideline (2010/63/EU). All animals were handled based on the guidelines of the Peking University Animal Research Committee. The Committee on the Ethics of Animal Experiments of Peking University Health Science Center approved the surgical procedures and experimental protocol (LA2017-183).

Reagents

QYT granules were obtained from Guangdong Yi Fang Pharmaceutical Co Ltd. (Guangzhou, GD, China), which consist of *rhinoceros horn* (xijiao) [*buffalo horn* (shuiniujiao) instead] (32.7%), *rehmannia glutinosa* (shengdihuang) (6.4%), *scrophularia* (yuanshen) (9.8%), *bamboo leaf* (zhuyexin) (3.2%), *Ophiopogon japonicus* (maidong) (9.7%), *salvia miltiorrhiza* (danshen) (6.5%), *coptis* (huanglian) (5.4%), *honeysuckle* (jinyinhua) (9.8%), and *forsythia* (lianqiao) (6.5%). LPS, fluorescein isothiocynate (FITC)-conjugated bovine serum albumin (FITC-BSA), Cresyl violet acetate and Evans blue were from Sigma Chemical (St. Louis, MO, United States). Rhodamine 6G was purchased from Fluka Chemie AG (Buchs, Switzerland). Antibodies against occludin, JAM-1, ZO-1, cav-1, phosphor-cav-1, VE-cadherin, and GAPDH were obtained from Cell Signaling Technology (Beverly, MA, United States). Assay kit for cathepsin B and antibody against claudin-5 were purchased from Invitrogen Corporation (Camarillo, CA, United States). Antibodies against VCAM-1, NF-κB p65, phosphor-p65, p50, and TLR-4 were obtained from Santa Cruz Biotechnology (SantaCruz, CA, United States). Antibodies against ICAM-1, Src, phosphor-Src, CD18, CD68, Iba1, collagen IV, and MMP-9 were obtained from Abcam (Cambridge, United Kingdom).

Animal Grouping for Experiment

Five groups were set up in this study: (1) NS group, (2) NS + QYT group, (3) LPS 4 h group, (4) LPS 24 h group,

and (5) LPS + QYT group, 3 9 mice in each (see **Table 1** for detail). Animals were anesthetized using 2% pentobarbital sodium (60 mg/kg body weight, i.p.), and treated as follows. The mice in LPS 4 h group, LPS 24 h group and LPS + QYT group received an uninterrupted infusion of LPS solution in saline (7.5 mg/kg/h) for 2 h through left femoral vein, meanwhile, the animals in NS group and NS + QYT group received the same amount of vehicle the same way. Upon awaking from anesthesia, the mice were permitted to eat freely. Four hours thereafter, the mice in NS + QYT group and LPS + QYT group were orally administered with QYT (14.3 g/kg), while those in NS group, LPS 4 h group and LPS 24 h group received equal amount of NS in the same manner. The concentration of QYT used in this study was determined based on our preliminary experiment, as well as on the clinical dosage (Ji et al., 2015) that was converted to dosage in mice with minor modification.

Identification of Composition in Rat Plasma After Oral Administration of Qing-Ying-Tang

Two male Wistar rats, weighting around 250 g, received the granule of QYT (15 g/kg body weight) by gavage, and the blood collection was performed at 15 min, 30 min, 1 h, 2 h, 4 h, 6 h, 10 h, and 24 h after administration and frozen at −20°C until analysis. Twenty microliter plasma samples were added into 400 μl methanol. The samples were mixed for 1 min and then centrifuged at 13,000 rpm for 10 min. The supernatant was transferred to Waters Q-TOF/MS system for further analysis. Separation was conducted on a Waters T3 column (2.1 mm × 100 mm, 1.8 μm) at 35°C. The ultraviolet spectra were recorded at 203/254/280/330 nm. The flow rate was 0.3 ml/min. Mass spectrometry was carried out for full scan analysis in the mass range of m/z 50–1,500 in positive and negative ionization mode, respectively. Mode MS^E: the collision energy of dissociation was set from 20 to 60 eV. Mode MS/MS: the collision energy of dissociation was set at 20 eV.

Acute toxicity studies show that a maximum six times the experimental dose is still safe.

Assessment of Heart Parameters and Survival Rate

The mice were monitored for heart parameters including heart rate (HR), systolic blood pressure (SBP), and diastolic blood pressure (DBP) at baseline and 2, 4, and 24 h after LPS administration by using an oscillometric device (Softron BP-98E; Softron, Tokyo, Japan). The survival rate of animals was recorded over a period of 48 h.

Observation of Microcirculation Dynamics

Under anesthesia with 2% pentobarbital sodium (60 mg/kg body weight, i.p.), mice were subjected to intubation *via* the left femoral vein and grinding on left parietal bone using a hand-held drill (STRONG-90; Saeshin, Daegu, Korea) to reveal the cerebral cortical microvasculature. Venules with a diameter of 35–45 μm and a length of 200 μm were chose for study.

To assess adherent leukocytes, rhodamine 6G served as a fluorescence tracer to label leukocytes, which was administrated at 1.5 mg/kg body weight to mice through the femoral vein. Ten min thereafter, the cerebral microcirculation was probed by an upright intravital fluorescent microscope (BX51WT; Olympus, Tokyo, Japan) equipped with a CCD camera (USS-301; Uniq, Santa Clara, United States) using a helium-neon laser beam for illumination.

TABLE 1 | Number of animals for different experimental groups and various parameters.

	NS	NS + QYT	LPS 4 h	LPS 24 h	LPS + QYT	Total
HR, SBP, and DBP	10	10	10	10	10	50
Leukocyte adhesion	6	6	6	6	6	30
Albumin leakage						
MCP-1, GM-CSF, MIP-1α, TNF-α, IL-1α, IL-1β, and IL-6 in plasma and brain tissue homogenate	8	8	8	8	8	40
Cathepsin B activity in plasma and brain tissue homogenate						
Western blot assay						
Evans blue extravasation	6	6	6	6	6	30
Water content	6	6	6	6	6	30
Nissl stain, TUNEL stain, and immunofluorescence	3	3	3	3	3	15
Total	39	39	39	39	39	195

The animals used for albumin leakage were the same as those for detection of leukocyte adhesion. The animals used for detection of cathepsin B activity in plasma and brain tissue homogenate, and western blot were the same as those for detection of MCP-1, GM-CSF, MIP-1α, TNF-α, IL-1α, IL-1β, and IL-6 in plasma and brain tissue homogenate.

Venular images were acquired under irradiation at wavelength of 543 nm, and used for evaluation of adherent leukocytes, which were identified as cells that remained on the venular walls for more than 10 s (Kurose et al., 1994). The number of adherent leukocytes was scored at 0, 1, 2, 4, and 24 h after LPS infusion and expressed as the number per 200 μm of venule length.

To assess albumin leakage from venules, the mice received FITC-albumin (50 mg/kg) by infusion through femoral vein. Ten min thereafter, a super-sensitive CCD camera (USS-301; Uniq, Santa Clara, United States) was applied to acquire fluorescence signal at excitation wave length of 420–490 nm and emission wave length of 520 nm. The fluorescence intensities of FITC-albumin within the venules (Iv) and outside the venules (Ii) were evaluated by use of Image-Pro Plus 5.0 software, and Ii/Iv served as a measure of albumin leakage. The ratio of albumin leakage at a time point to that of the baseline was designated as the ratio of albumin leakage at that point (Zhang et al., 2016).

Determination of Cytokines Concentration in Plasma and Brain Tissue Homogenate

At 4 or 24 h after LPS challenge, the mice were killed and blood and brain tissue were gathered. The concentrations of MCP-1, GM-CSF, MIP-1α, TNF-α, IL-1α, IL-1β, and IL-6 in plasma and brain tissue were determined by flow cytometry using a BD cytometric bead array kit (BD Biosciences, San Jose, United States) (Zhao et al., 2012) according to the instruction of manufacture. Briefly, following anticoagulation with heparin (20 unit/ml), the blood was centrifuged at 1,300 g, 4°C for 10 min to separate plasma, in 50 μl of which bead was added in a proportion of 1:1 (v/v), and incubated at room temperature in dark for 1 h. Phycoerthrin-labeled antibody (50 μl) was then added and incubated for 2 h at room temperature followed washing with 1 ml washing buffer. Brain tissue was homogenized, centrifuged, and processed the same way. The mean fluorescence intensity of cytokines was assessed by flow cytometry (FACS Calibur; BD Biosciences, San Jose, United States), and the data were analyzed by the BD cytometric bead array analysis software (Zhang et al., 2014).

Frozen Sections

Frozen sections were prepared for histology. For this propose, mice under anesthesia were subjected to infusion through the left ventricle with normal saline (NS) followed by 4% paraformaldehyde in 0.1 M PBS for 40 min. Brains were collected and further fixed in 4% paraformaldehyde overnight. After infused in 30% sucrose at 4°C for 2 days, the samples were embedded in TissueTek OCT compound (Miles Inc., IN, United States), frozen in 2-methylbutane cooled in liquid-nitrogen. Coronal brain sections were prepared with a cryostat microtome (CM1900; Leica, Nussloch, Germany) at −20°C. After mounted and air-dried, the brain sections were stored at −20°C (Gu et al., 2018).

Nissl Staining

Nissl staining was conducted on the sections using cresyl violet acetate as reported (Gu et al., 2018). The result was evaluated with a light microscope (BX512DP70; Olympus, Tokyo, Japan).

Immunofluorescence Staining

Immunofluorescence staining was undertaken as routine. Specifically, after antigen retrieval and blocking of nonspecific binding, the following primary antibodies were applied to the sections: mouse anti-claudin-5 (1:50), mouse anti-occludin (1:50), rabbit anti-VCAM-1 (1:50), mouse anti-Iba1 (1:400), rabbit anti-CD68 (1:400), rabbit anti-CD18 (1:200), mouse anti-caveolin-1 (1:100), rabbit anti-collagen IV (1:100), and rabbit anti-vWF (1:200). Negative control was performed simultaneously to confirm the specificity of antibodies. After washed by PBS for three times, the specific binding was recognized by the following secondary antibodies: Dylight 488-labeled goat anti-rabbit IgG (1:100, KPL, Gaithersburg, MD, United States) and Dylight 549-labeled goat anti-mouse IgG (1:100, KPL, Gaithersburg, MD, United States). Hoechst 33342 (Molecular Probes) was applied to display the nuclei. The results were evaluated by use of a laser scanning confocal microscope (TCS SP8; Leica, Mannheim, Germany). For quantitative analysis, three sections were chose for each group and five fields were randomly selected in section. Analysis was done using Image -Pro Plus 5.0 software.

TUNEL Assay

Apoptotic neurons were detected by TUNEL assay using an *in situ* cell death detection kit (Roche, Basel, Switzerland) as per the instruction of the manufacturer. The results were evaluated using a laser scanning confocal microscope (TCS SP8; Leica, Mannheim, Germany).

Evans Blue Leakage and Brain Water Content

To delve into the BBB breakdown, Evans blue leakage in brain was first determined as previously described (Hu et al., 2009). In brief, mice received Evans blue dye (4% in NS, 3 ml/kg) by injection *via* the right femoral vein. Four h later, the animals were anesthetized with pentobarbital sodium (0.1 g/kg body weight, i.p.) and transcardially perfused with NS. Brains were taken out, homogenized in PBS and centrifuged at 2,000 × *g* for 15 min at 4°C. Then, 0.5 ml of the resultant supernatant was mixed with trichloroacetic acid in a proportion of 1:1 (v/v), incubated overnight and centrifugated at 2,000 × *g* for 15 min at 4°C. The supernatant was subjected to spectrophotometric quantification of leaked Evans blue dye at 620 nm. Brains water content was measured alike as described (Hu et al., 2011). For this, brains were removed from mice under anesthesia, weighed (wet weight) and then dried in an oven at 80°C for 72 h and weighed again (dry weight). The percentage of water content was calculated according the equation [(wet weight − dry weight)/wet weight] × 100% (Huang et al., 2012).

Determination of Cathepsin B Activity

At 4 or 24 h after LPS challenge, the mice were sacrificed and blood and brain tissue were taken. Cathepsin B activity was determined using an cathepsin B assay kit (Invitrogen

Corporation, Camarillo, CA, United States) according to the instruction of the manufacturer. The change in absorbance was measured spectrophotometrically at 460 nm for determination of Cathepsin B activity.

Western Blot

For western blot analysis, animals in NS and LPS groups were sacrificed at 4 and 24 h, respectively, while animals in NS + QYT and LPS + QYT groups were sacrificed at 24 h. Brains were removed and cerebral cortex were used for preparation of whole cell proteins by RIPA buffer. Protein samples were separated using a 10% Tris-HCl precast gel by electrophoresis (Bio-Rad Laboratories, Hercules, CA, United States) at 80 V for 120–150 min, transferred to polyvinylidene fluoride membranes. Following blocked with 3% skimmed milk in TBST the membranes were incubated overnight at 4°C with primary antibodies against ICAM-1 (1:2000), VCAM-1 (1:2,000), claudin-5 (1:200), occludin (1:1,000), JAM-1(1:1,000) and ZO-1 (1:1,000), VE-cadherin (1:1,000), caveolin-1 (1:1,000), p-caveolin-1 (1:500), MMP-9 (1:1,000), collagen IV (1:1,000), TLR-4 (1:400), Src (1:1,000), p-Src (1:500), NF-κB p65 (1:1,000), NF-κB p-p65 (1:500), NF-κB p50 (1:1,000), and GAPDH (1:4,000). After washed with TBST for three times, specific bindings were recognized with the respective horseradish peroxidase-conjugated secondary antibody (1:5,000, Santa Cruz Biotechnology, Santa Cruz, CA, United States) by incubation at room temperature for 60 min and revealed using enhanced chemiluminescence detection kit (Applygen Technologies, Beijing, China). Band intensities were quantified by densitometry and presented as mean area density using Quantity One image analyzer software (Bio-Rad; Richmond, CA, United States).

Data Analysis

Data analysis was carried out using one-way ANOVA or two-way ANOVA followed by Bonferroni test and expressed as mean ± SEM with a value of $p < 0.05$ being considered statistically significant.

RESULTS

A Total of 10 Compositions of Qing-Ying-Tang Are Found in Rat Plasma

A total of 10 compositions of QYT were revealed in rat plasma following oral administration. At each time point, the relative concentration of components in rat plasma (peak area/Σpeak area) × 100% was presented in **Figure 1**. Pharmacokinetic parameters, including like Tmax and T1/2, were calculated by the software PKSolveyh. The pharmacokinetic parameters of each compound were summarized in **Table 2**.

Qing-Ying-Tang Post-treatment Relieves the Vital Sign Depravation and Increases the Survival Rate After Lipopolysaccharide Stimulation

Figures 2A–C present respectively the results of the HR, SBP and DBP of the mice in different groups using a vital parameter monitor recorded at 0, 2, 4, and 24 h after LPS stimulation. As noticed, LPS stimulation resulted in a significant depravation of vital signs manifesting a decrease in HR 24 h after LPS challenge, and in SBP and DBP starting from 2 h after LPS till 24 h, which were all relieved by post-treatment with QYT. Moreover, the survival rate of the animals decreased significantly starting from 24 h after LPS administration, which was improved by QYT (**Figure 2D**).

Qing-Ying-Tang Decreases the Leukocytes Adhesion to Brain Venules and Ameliorates the Increased Expression of VCAM-1

To assess the role of QYT in the brain venule dysfunction after LPS challenge, the leukocyte adhesion to brain venules was examined. **Figure 3A** shows the images of brain venules which stand for what observed in various conditions at 0, 1, 2, 4,

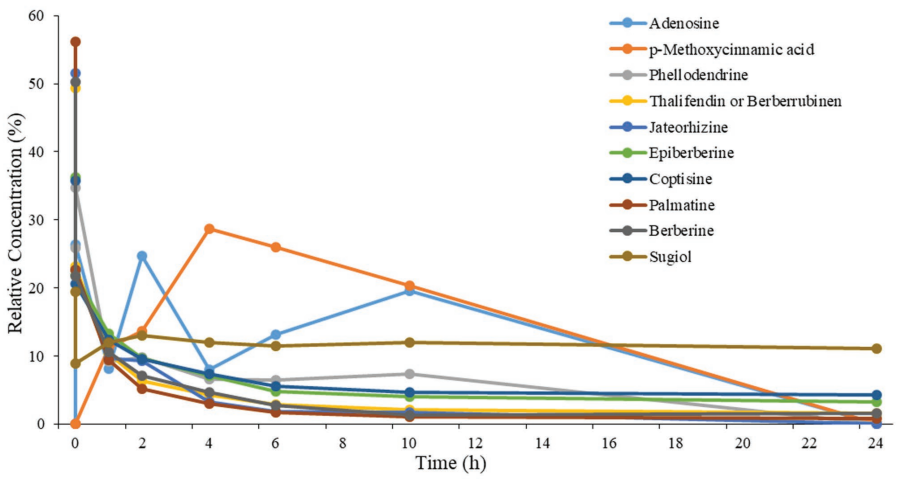


FIGURE 1 | Relative concentration-time profiles of the 10 components in plasma after oral administration of QYT to rats. $n = 2$.

and 24 h after LPS stimulation. Two hours after LPS instillation, the number of leukocytes adhering to venules increased significantly and did not recover at 24 h (**Figures 3A,C**). Post-treatment with QYT after LPS instillation can significantly reduce the number of leukocyte adhesion at 24 h (**Figures 3A,D**). A quantification of the number of adhering leukocytes in different groups confirmed the results (**Figure 3B**). VCAM-1 and ICAM-1 are critical adhesion molecules that recruit leukocytes to inflamed areas. Thus, the immunofluorescence staining of VCAM-1 was conducted, and the expression of VCAM-1 and ICAM-1 was assessed by western blot for mice brain from various groups. As noticed in **Figures 3C,D**, the expression of VCAM-1 increased in LPS group. This LPS-elevated VCAM-1 expression was relieved by QYT treatment; whereas, no significant difference in ICAM-1 was noticed among groups.

TABLE 2 | The pharmacokinetic parameters of 10 absorbed components in rat plasma after administration of the QYT.

Compound	T_{max} (h)	$T_{1/2}$ (h)
Adenosine	0.5	/
p-Methoxycinnamic acid	4	12.09
Phellodendrine	0.5	/
Thalifendin or berberrubinen	0.25	17.40
Jateorhizine	0.25	7.62
Epiberberine	0.25	22.03
Coptisine	0.25	31.74
Palmatine	0.25	11.99
Berberine	0.25	16.48
Sugiol	0.25	227.71*

*The absorption rates of alkaloids were relatively fast after the rats were administered with QYT. And the peak time of blood concentrations were within 15 min.*There may be error.*

Qing-Ying-Tang Diminishes the Pro-inflammatory Cytokine Concentration in Mice Brain Tissue After Lipopolysaccharide Challenge

To explore the effect of QYT on the inflammatory process elicited by LPS, the concentrations of MCP-1, GM-CSF, MIP-1α, TNF-α, IL-1α, IL-1β, and IL-6 in mice plasma and brain were examined. As shown in **Figure 4**, all pro-inflammatory factors but GM-CSF in bran tissue increased significantly at 4 h after LPS instillation, and recovered to different extent after 24 h of LPS instillation. Of notice, the LPS-elicited elevation in MCP-1, MIP-1α, IL-6, and IL-1α in brain tissue was decreased significantly by QYT, implying the potential of QYT to attenuate the inflammation process evoked by LPS. On the other hand, no effect of QYT on the level of proinflamatory cytokines in plasma was observed.

Qing-Ying-Tang Reduces the CD68 and CD18 Positive Cells and Modulates the Lipopolysaccharide-Induced Alternation of Src and NF-κB

CD68 and CD18-positive cells were evaluated in various conditions by immunofluorescence, and the results are displayed in **Figure 5A**. In comparison with NS (**Figures 5Aa,Ab**) groups, numerous CD68 and CD18-positive cells were found in LPS 4 h (**Figure 5Ad**) and LPS 24 h (**Figure 5Ae**) groups, hinting leukocyte infiltration in brain after LPS challenge. This LPS

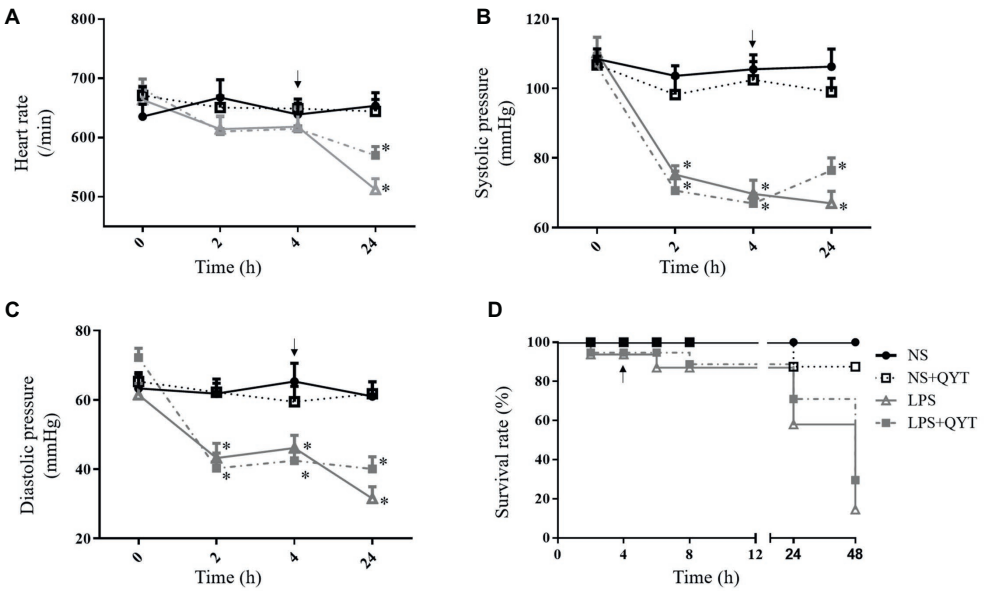


FIGURE 2 | The effect of QYT post-treatment on the physiological parameters in different groups. **(A)** HR. **(B)** SBP. **(C)** DBP. **(D)** Survival rate. Arrows indicate the time when QYT was administrated. Values are mean ± SEM. *$p < 0.05$ vs. NS group, $n = 10$.

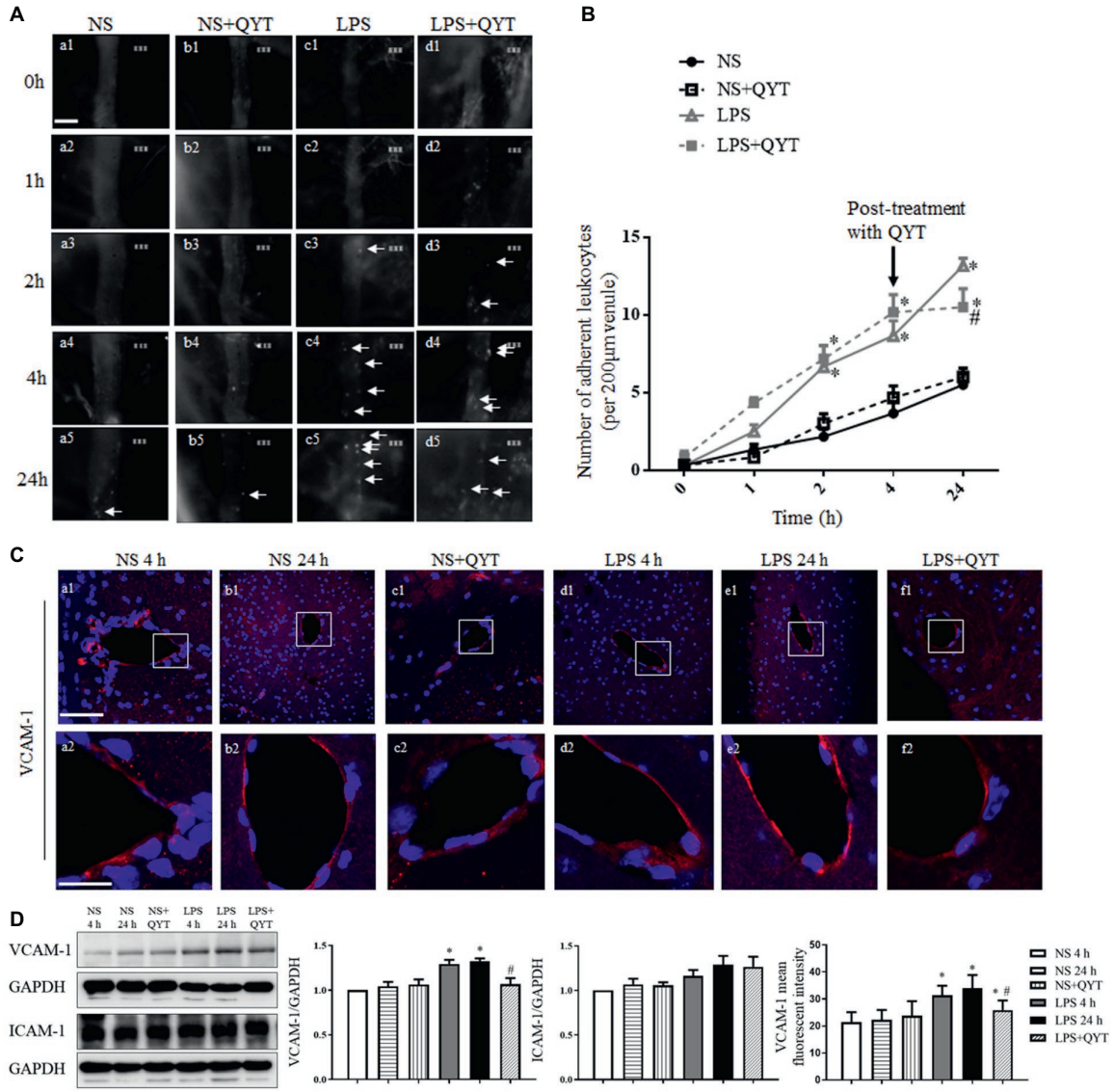


FIGURE 3 | QYT attenuates leukocytes adhesion to cerebral venules and protects the upregulation of VCAM-1 after LPS. **(A)** Representative images of leukocytes adherent to cerebral venules in different groups acquired at different times. Arrows refer to adherent leukocytes. Bar = 50 μm. **(B)** Statistic analysis of the number of leukocytes adhering to cerebral venules in various groups. Values are the mean ± SEM. $^{*}p < 0.05$ vs. NS group, $^{\#}p < 0.05$ vs. LPS group, $n = 6$. **(C)** The representative immunofluorescence images of VCAM-1 in different groups acquired by confocal microscope. Red color denotes VCAM-1 and blue color represents nuclei. The rectangle region in each picture **(a1-f1)** is magnified and shown below **(a2-f2)** correspondingly. Bars = 100 μm in **(a1-f1)**, Bars = 25 μm in **(a2-f2)**. **(D)** Representative western blot bands and quantitative analysis of VCAM-1 and ICAM-1, and statistic result of VCAM-1 fluorescent intensity. All the quantifications were conducted based on the data of four independent experiments with GAPDH as a loading control. Values are the mean ± SEM. $^{*}p < 0.05$ vs. NS group, $^{\#}p < 0.05$ vs. LPS 24 h group, $n = 4$ for western blot, $n = 3$ for immunostaining.

provoked leukocyte infiltration was relieved considerably by QYT treatment (**Figure 5Af**). To explore the signaling involved in the role of QYT, the expression of TLR-4 and Src and activation of NF-κB in brain tissue were determined by western blot. As noticed in **Figures 5B–H**, LPS challenge for 4 and 24 h led to an elevated expression of TLR-4 (**Figures 5B,C**), expression and phosphorylation of Src (**Figures 5B,D,E**), and activation of NF-κB (**Figures 5B,F–H**) in brain tissue. Post-treatment with QYT had no effect on the augmented expression of TLR-4 and p-Src by LPS, while attenuated the increased expression of Src and activation of NF-κB, implying involvement of these signaling in the beneficial effect of QYT.

Qing-Ying-Tang Relieves the Increase in Cerebral Vascular Permeability After Lipopolysaccharide

Cerebral vascular permeability was assessed in various groups by detecting the dynamics of FITC-labeled albumin leakage

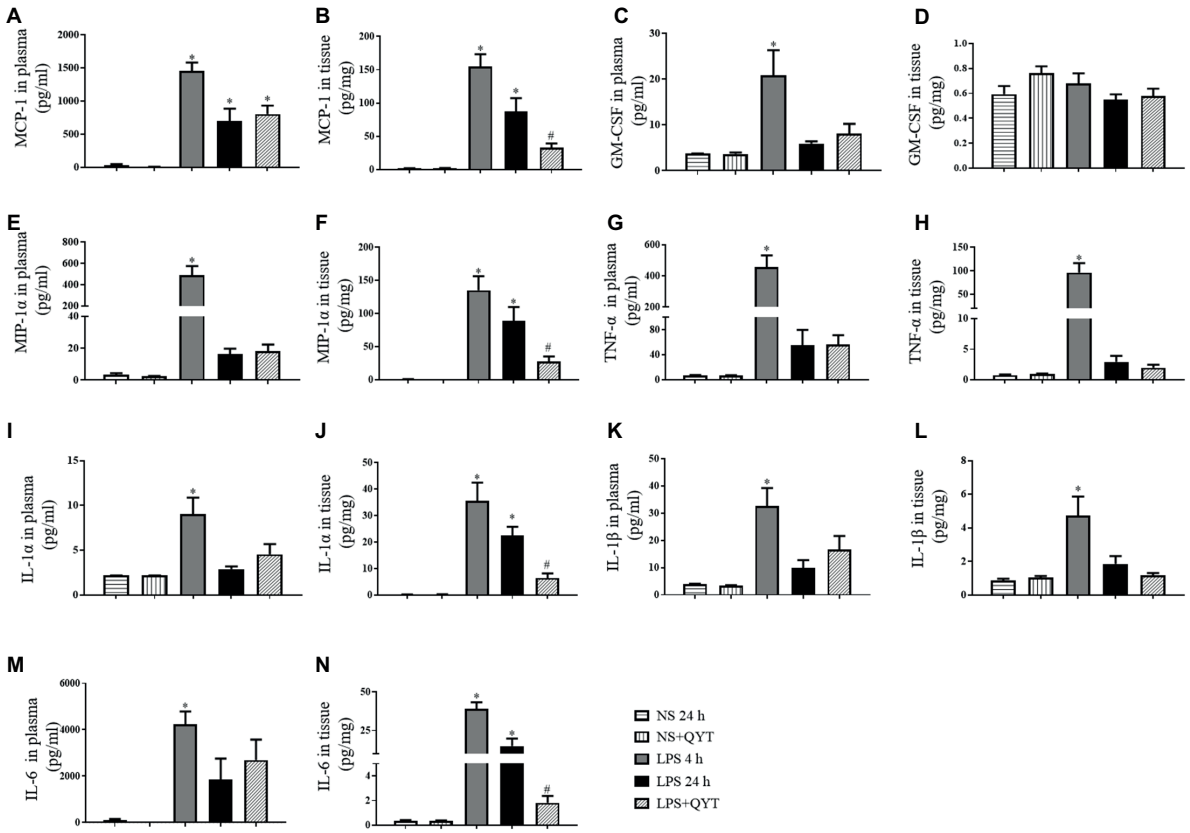


FIGURE 4 | Effect of QYT on the concentration of pro-inflammatory cytokine in mouse brain and plasma after LPS challenge. **(A)** The concentration of MCP-1 in plasma; **(B)** The concentration of MCP-1 in brain tissue. **(C)** The concentration of GM-CSF in plasma; **(D)** The concentration of GM-CSF in brain tissue. **(E)** The concentration of MIP-1α in plasma; **(F)** The concentration of MIP-1α in brain tissue. **(G)** The concentration of TNF-α in plasma; **(H)** The concentration of TNF-α mouse brain tissue. **(I)** The concentration of IL-1α in plasma; **(J)** The concentration of IL-1α in brain tissue. **(K)** The concentration of IL-1β in plasma; **(L)** The concentration of IL-1β in brain tissue. **(M)** The concentration of IL-6 in plasma; **(N)** The concentration of IL-6 in brain tissue. The cytokines were assessed by flow cytometry at 4 and 24 h after LPS stimulation, respectively. Values are the mean ± SEM. $^{*}p < 0.05$ vs. NS group, $^{\#}p < 0.05$ vs. LPS 24 h group, $n = 8$.

from cerebral venules. As shown in **Figure 6A**, fluorescence was observed in the venules and barely outside in NS and NS + QYT groups. In contrast, an obvious fluorescence was visible in perivascular areas in both LPS and LPS + QYT groups 1 h after LPS infusion (**Figures 6Ac2,Ad2**), which was further augmented in the LPS group at 2, 4, and 24 h (**Figures 6Ac3–Ac5**). Surprisingly, QYT post-treatment reduced albumin leakage even though microvascular permeability had increased (**Figure 6Ad5**). These results were further verified by a quantification of dynamics of albumin extravasation (**Figure 6B**).

Consistent with albumin leakage, Evans blue dye extravasated markedly in the brain of mice in LPS 24 h group compared with those in NS and NS + QYT groups. Post-treatment with QYT decreased the LPS-evoked extravasation of Evans blue dye significantly (**Figures 6C,D**). Meanwhile, QYT treatment significantly diminished the brain water content as compared with LPS 24 h group (**Figure 6E**). All in all, these results prove the capacity of QYT to relieve the LPS-provoked increment of BBB permeability.

Qing-Ying-Tang Alleviates Downregulation of Junction Proteins and Upregulation of Caveolae and Caveolin-1 in Endothelial Cells

To explore the reason for the amelioration effect of QYT on protecting BBB from breakdown, vascular endothelial TJ and AJ proteins were evaluated by confocal microscopy and western blot. Confocal microscopy showed claudin-5 as continuously intermediate lines between endothelial cells in NS and NS + QYT groups (**Figures 7Aa1,Aa2,Ab1,Ab2,Ac1,Ac2**). While in LPS 4 h and LPS 24 h groups (**Figures 7Ad1,Ad2, Ae1,Ae2**), these continuous distributions became interrupted, accompanying with a reduced immune staining, implying a lessened expression of claudin-5 in LPS stimulation groups. Importantly, this lessened expression was ameliorated by post-treatment with QYT (**Figures 7D,Af1,Af2**). Similar results were obtained alike by western blot (**Figures 7B,C**). Additionally, western blot found that the expression of other 3 components of TJs including occludin, JAM-1 and ZO-1, and the important component of AJs, VE-cadherin varied among groups in a similar manner (**Figures 7B,E–H**). These results indicated

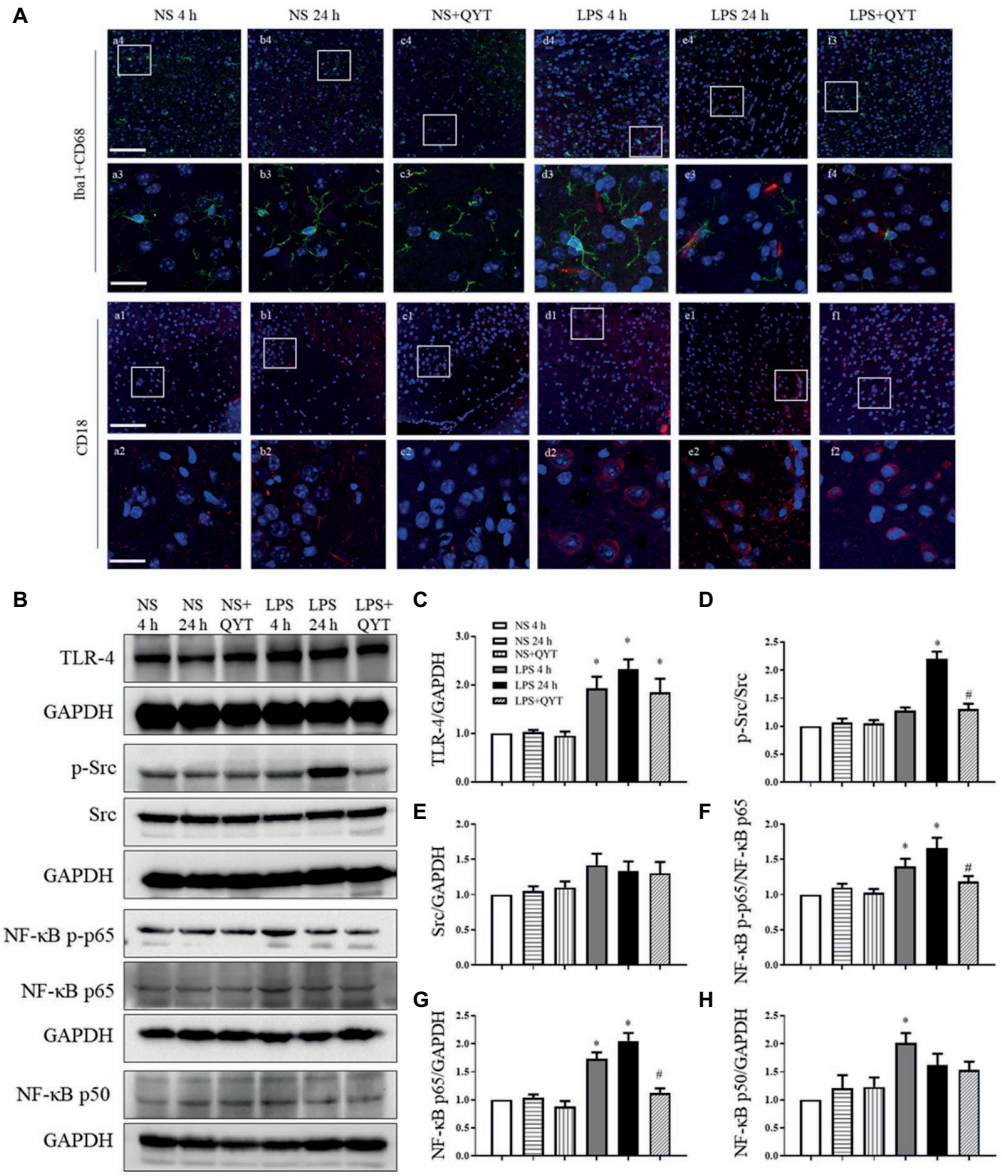


FIGURE 5 | QYT reduces the number of CD68 and CD18 positive cells and modulates the LPS-evoked change in Src and NF-κB. **(A)** Representative immunofluorescence confocal images of Iba1 co-labeling with CD68 and CD18 acquired by confocal microscope in different groups. Red color denotes CD68 **(a1-f1, a2-f2)** and CD18 **(a3-f3, a4-f4)**, green color denotes Iba1 **(a1-f1, a2-f2)** and blue color represents nuclei. The rectangle region in pictures numbered 1 and 3 are enlarged and presented below as picture numbered 2 and 4, correspondingly. Bars = 100 μm in **(a1-f1, a3-f3)**, Bars = 25 μm in **(a2-f2, a4-f4)**. **(B)** Representative western blot bands of TLR-4, p-Src, Src, and NF-κB (p-p65, p65, and p50) in different groups. Shown on the right side are the quantitative analysis of TLR-4 **(C)**, p-Src **(D)**, Src **(E)**, NF-κB [p-p65 **(F)**, p65 **(G)**, p50 **(H)**] in different groups, respectively. All the quantifications were conducted based on the data of four independent experiments with GAPDH as a loading control. Values are the mean ± SEM. $^{*}p < 0.05$ vs. NS group, $^{\#}p < 0.05$ vs. LPS 24 h group, $n = 4$.

that QYT attenuated the reduction in TJ and AJ expression induced by LPS, which may at least partly account for the role of QYT in protection of BBB from breakdown.

Caveolae are structures that mediate endothelial cell permeability by transcellular transport with cav-1 as the main component. In present study, confocal microscopy revealed no obvious change in the expression of cav-1 in brain among groups (**Figures 8A,E**). However, western blot showed an increased cav-1 phosphorylation in LPS 4 h and LPS 24 h groups (**Figures 8B,C**), while no difference in the cav-1 expression was observed among groups (**Figure 8D**). Noticeably, the LPS caused increment in cav-1 phosphorylation was blunted significantly by post-treatment with QYT (**Figure 8C**). These results suggested that QYT attenuates the BBB breakdown after LPS stimulation by intervention of both inter endothelial and transendothelial pathway.

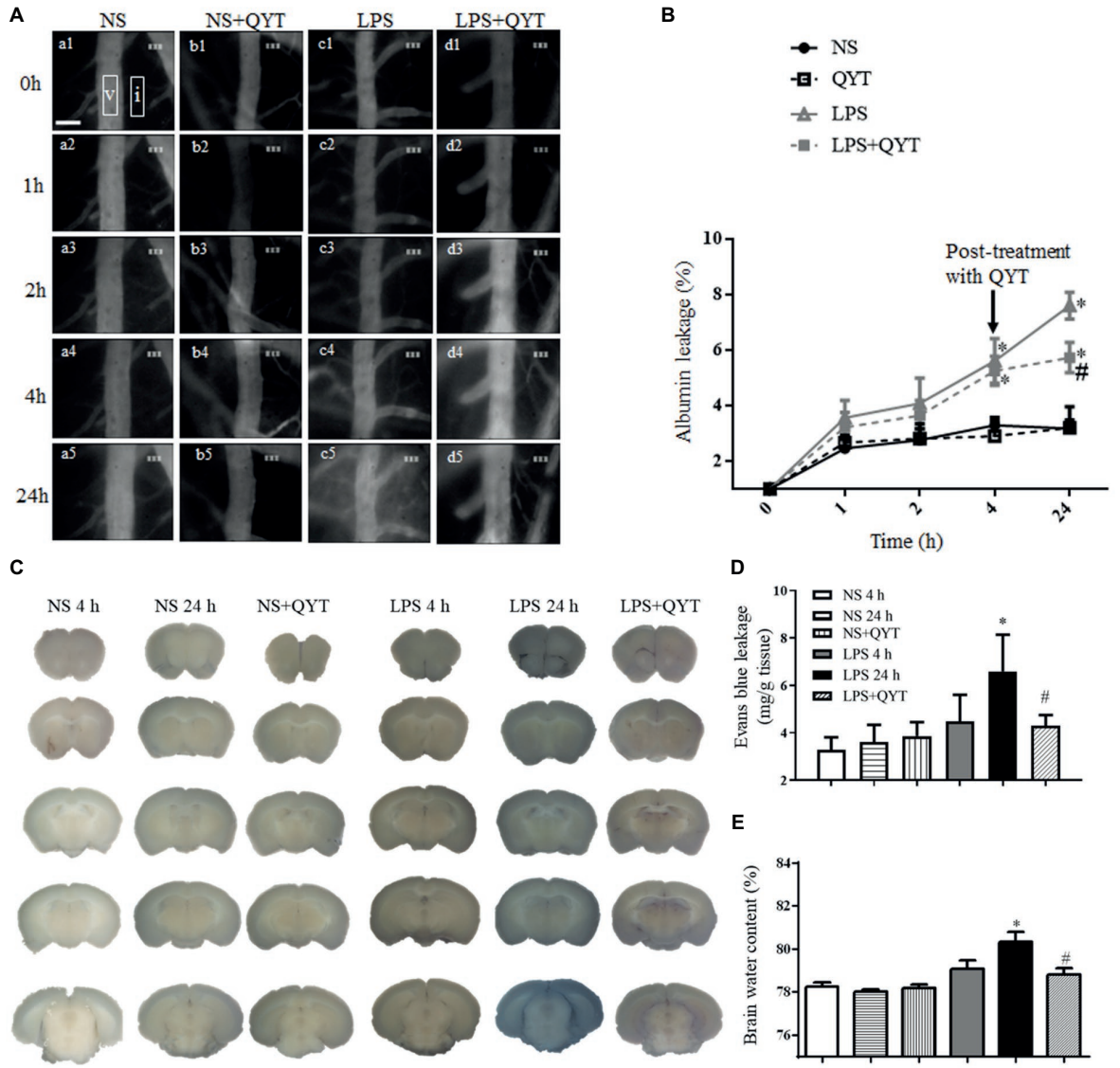


FIGURE 6 | QYT reduces albumin leakage, Evans blue extravasation, and brain water content. **(A)** Pictures representing FITC-albumin leaked from cerebral venules in different groups. Rectangles are the regions on which fluorescence intensity was determined. V, cerebral venule. I, interstitial tissue. Bar = 50 μm. **(B)** Time course of change in the albumin leakage from cerebral venules in various groups. Values are the mean ± SEM. $^{*}p < 0.05$ vs. NS group, $^{\#}p < 0.05$ vs. LPS group, $n = 6$. **(C)** Photos representing Evans blue leakage in the brains in different groups. **(D)** Quantification of Evans blue leakage. **(E)** Brain water content. Values are the mean ± SEM. $^{*}p < 0.05$ vs. NS group, $^{\#}p < 0.05$ vs. LPS 24 h group, $n = 6$.

Qing-Ying-Tang Relieves the Lipopolysaccharide-Evoked Damage of Collagen IV and Increased Expression of MMP-9 in Brain, Protects Cathepsin B Activation in Plasma and Brain

Collagen IV examined by confocal microscopy exhibited an continuous distribution around the endothelium in brain in NS and NS + QYT groups, while LPS instillation led to a discontinuity of collagen IV, which was relieved by treatment with QYT (**Figures 9A,D**). These results were proved by western blot (**Figures 9B,C**). The expression of MMP-9 was further assessed by western blot and the result showed that the contents of MMP-9 in brain tissue were apparently increased after LPS challenge, while post-treatment with QYT protected the LPS-induced increase in MMP-9 (**Figures 9B,E**). This result suggested involvement of inhibition of MMP-9 expression in the role of QYT in protecting microvascular basement membrane after LPS challenge. Cathepsin B has been known to cleave type IV collagen (Victor et al., 2011; Shoji et al., 2014; Tong et al., 2015) and participate in the regulation of BBB. The present study observed an increase in cathepsin B activation in plasma as well as in brain tissue of mice exposed to LPS, which was significantly repressed by QYT post-treatment (**Figures 9F,G**).

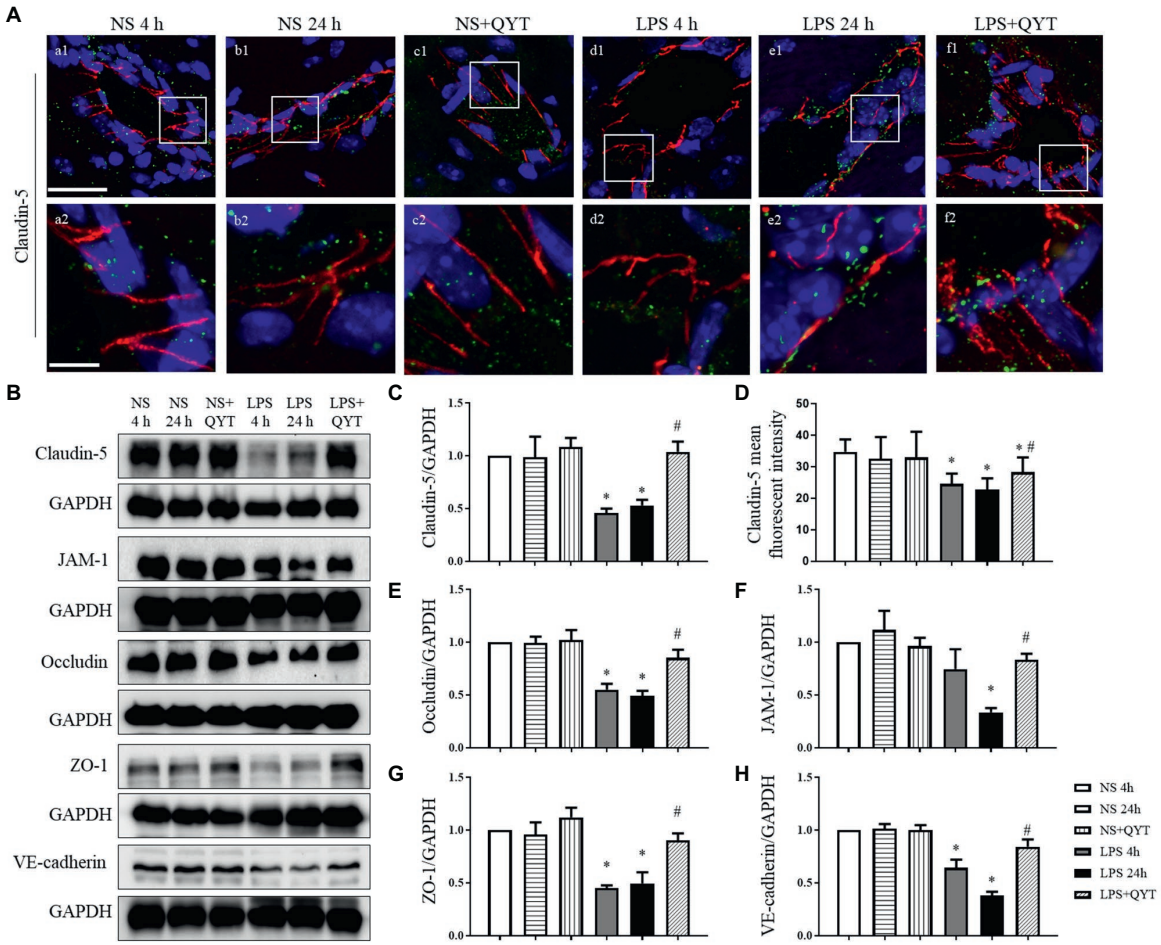


FIGURE 7 | QYT relieves the reduced expression of junction proteins in vascular endothelial cells. **(A)** The immunofluorescence confocal pictures showing claudin-5. Claudin-5 (red) localized at peripheral of the endothelial cells which were marked by VWF (green). Blue color shows nuclei. The rectangle region in each picture numbered 1 is magnified and shown below as pictures numbered 2, correspondingly. Bars = 50 μm in **(a1-f1)**, Bars = 7.5 μm in **(a2-f2)**. **(B)** Representative western blots of claudin-5, occludin, JAM-1, ZO-1 and VE-cadherin in different groups. Shown on the right side is the quantification of claudin-5 **(C)**, occludin **(E)**, JAM-1 **(F)**, ZO-1 **(G)**, VE-cadherin **(H)**, respectively. **(D)** The quantitative analysis of claudin-5 fluorescent intensity. All the quantifications were performed based on the data of four independent experiments and normalized to GAPDH, respectively. Values are the mean ± SEM. $^{*}p < 0.05$ vs. NS group, $^{\#}p < 0.05$ vs. LPS 24 h group, $n = 4$ for western blot, $n = 3$ for immunostaining.

Qing-Ying-Tang Protects Against the Neuronal Damage and Apoptosis Induced by Lipopolysaccharide

The effect of QYT post-treatment on neuron morphology in neocortex and CA1, CA2, CA3, and DG region of hippocampus after LPS stimulation was assessed by Nissl staining (**Figure 10**). Neurons of NS group (**Figures 10Aa,Ab**) exhibited normal features in morphology, while those in LPS 4 h and LPS 24 h groups showed a diversity of damages including cell swelling, nuclear contraction, and crush (**Figures 10Ac,Ad**). Post-treatment with QYT effectively prevented the neuronal damages induced by LPS (**Figure 10Ae**). TUNEL assay was carried out to assess neuron apoptosis after LPS stimulation, and the result found that a large number of TUNEL-positive cells was present in the cortex region of mice exposed to LPS (**Figures 10Bd,Be**), whereas TUNEL-positive cells were scarcely visible in NS and NS + QYT groups (**Figures 10Ba–Bc**). The number of TUNEL-positive cells was decreased in QYT post-treatment groups in comparison with LPS 24 h groups (**Figure 10Bf**).

DISCUSSION

Encephalopathy is one of the manifestations of endotoxemia. The present study demonstrates that post-treatment with QYT significantly attenuates the LPS-induced cerebral microcirculation disorders of mice, including decreased leukocyte adhesion and albumin efflux, along with a reduction of cytokines in brain tissue. Meanwhile, QYT treatment elevated HR and increased SBP and DBP, improved the hypodynamic status and survival rate of mice.

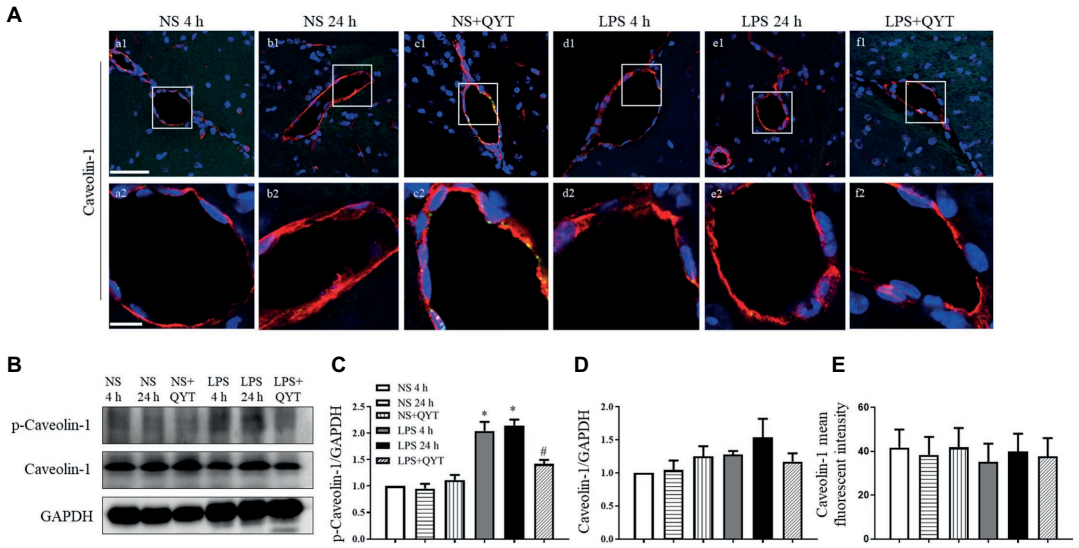


FIGURE 8 | QYT reduces the expression and phosphorylation of caveolin-1. **(A)** Representative immunofluorescence confocal photographs of caveolin-1 (red) in different groups, wherein nuclei are revealed by blue color. The rectangle region in each picture numbered 1 is magnified and shown below as picture numbered 2, correspondingly. Bars = 50 μm in **(a1-f1)**, Bars = 10 μm in **(a2-f2)**. **(B)** Representative western blots of p-caveolin-1 and caveolin-1. Shown on the right side is the quantification of p-caveolin-1/ caveolin-1 **(C)** and caveolin-1/GAPDH **(D)**. **(E)** Quantification of caveolin-1 fluorescent intensity. All the quantifications were conducted based on the data of four independent experiments and normalized to GAPDH, respectively. Values are the mean ± SEM. $^{*}p < 0.05$ vs. NS group, $^{\#}p < 0.05$ vs. LPS 24 h group, $n = 4$ for western blot, $n = 3$ for immunostaining.

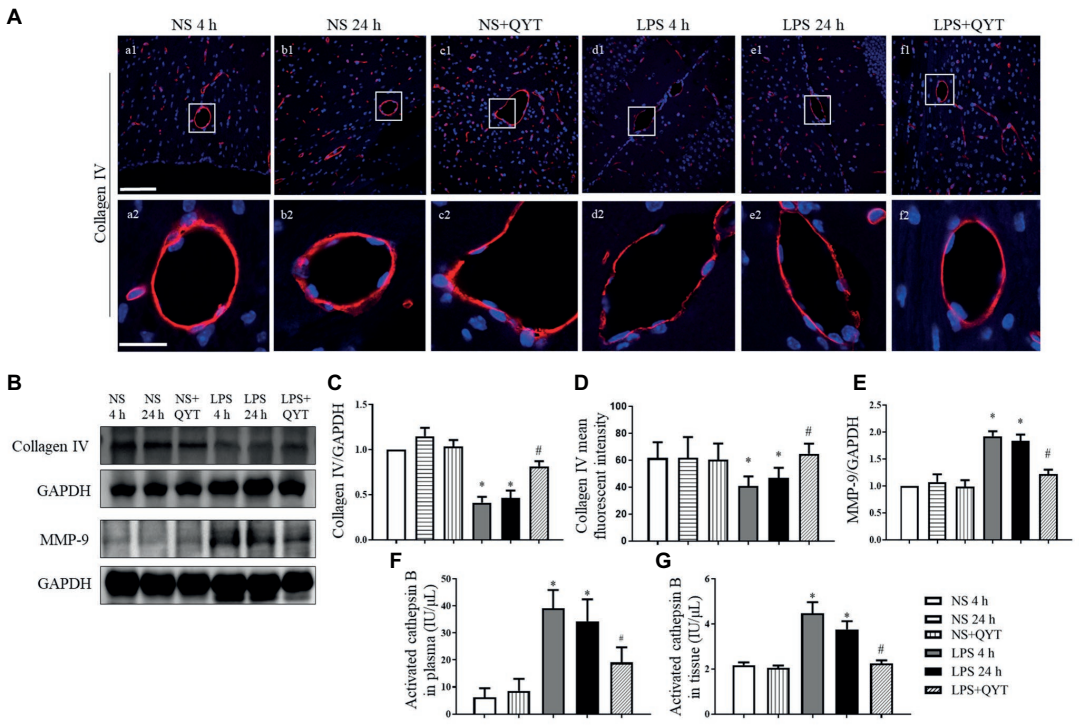


FIGURE 9 | The effect of QYT on LPS-caused alteration in collagen IV, MMP-9, and cathepsin B. **(A)** Representative immunofluorescence confocal photos of collagen IV (red), wherein blue color shows nuclei. The rectangle region in each picture numbered 1 is magnified and presented below as picture numbered 2. Bars = 100 μm in **(a1-f1)**, Bars = 25 μm in **(a2-f2)**. **(B)** Representative western blots of MMP-9 and collagen IV. Shown on the right side is the quantitative analysis of collagen IV **(C)** and MMP-9 **(E)**. Quantifications were conducted based on the data of four independent experiments using GAPDH as a loading control. **(D)** Quantitative analysis of collagen IV fluorescent intensity. **(F,G)** Quantitative analysis of activated cathepsin B in plasma **(F)** and in brain tissue **(G)** in various conditions. Values are the mean ± SEM. $^{*}p < 0.05$ vs. NS group, $^{\#}p < 0.05$ vs. LPS 24 h group, $n = 6$.

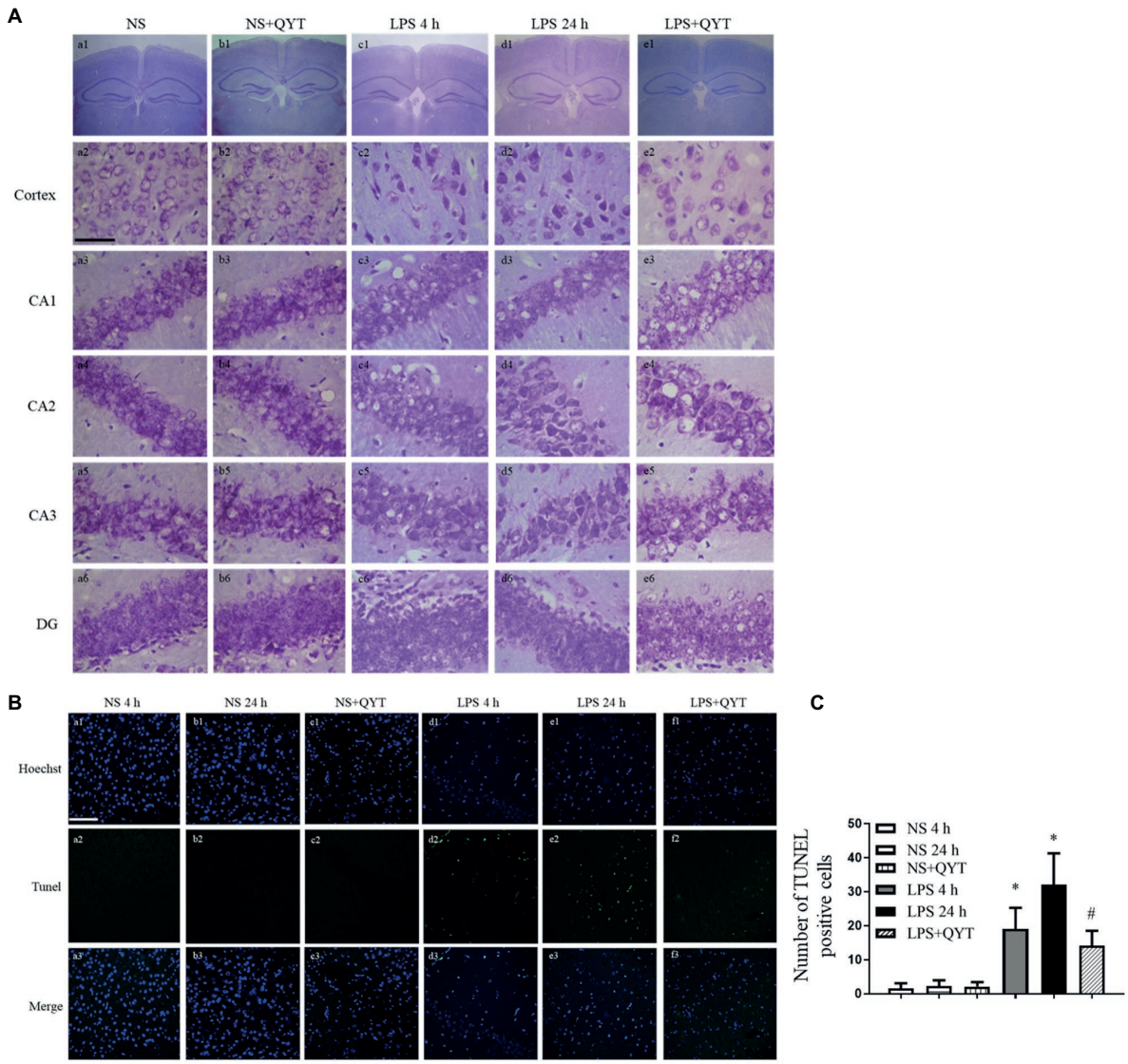


FIGURE 10 | QYT prevents the neuronal injury and apoptosis caused by LPS. **(A)** Brain neocortex and hippocampus sections are processed for Nissl staining. Bar = 50 μm. **(B)** Brain neocortex tissue sections are processed with TUNEL staining. Bar = 100 μm. **(C)** Quantitative analysis of TUNEL positive cells.

Cerebral microvascular exudation caused by LPS plays a pivotal role in pathogenesis of sepsis-associated encephalopathy which causes high brain pressure and edema, accounting for the occurrence of disturbed consciousness of sepsis (Coisne and Engelhardt, 2011; Tauber et al., 2017). Despite clinically commonly used hormone-supportive therapy, dehydration and antihypertensive approaches, the cerebral edema and disturbance of consciousness in sepsis have not been completely resolved. The present study demonstrates the beneficial role of QYT in LPS-induced cerebral microvascular hyperpermeability, as evidenced by the decrease in brain Evans blue exudation and brain water content, suggesting QYT as a potential therapy to counteract this threat.

Cerebral microvascular exudation is a consequence of breakdown of BBB, to which endothelium and basement membrane are major contributors (Abbott et al., 2010). In present study, LPS challenge impaired endothelial cells junctions by downregulation of tight junction proteins, increased caveolae by activation of caveolin-1, and damage on basement membrane by enhanced expression of MMP-9 and cathepsin B, which collectively led to BBB breakdown. Of notice, QYT treatment relieved all the changes after LPS, thus protected BBB from disintegrity. LPS-caused BBB breakdown is mediated through a range of signaling, including activation of multiple protein-tyrosine kinases, NF-κB activation and nuclear translocation, oxidative stress, and release of pro inflammatory cytokines, all initiating with binding of LPS to TLR-4 and taking place successively and coordinately (Gong et al., 2008; Kawai and Akira, 2011). It is at present unknown exactly which signaling (s) be implicated

in the observed effect of QYT. We have previously reported that catalpol, the active ingredient of Rehmannia glutinosa contained in QYT formula, can reduce LPS-induced mesenteric microvascular permeability and hemorrhage by regulating TLR-4 and Src signaling pathways (Zhang et al., 2016). DLA (Wang et al., 2009) and salvianolic acid B (Lin et al., 2013; Pan et al., 2015), the active constituents of Salvia, inhibits the degradation of I-κB, nuclear translocation of NF-κB and activation of Src kinase, inhibits the expression and phosphorylation of Cav-1 and degradation of ZO-1 and therefore protects from mesenteric and pulmonary microcirculation disorders in rat. However, the present study did not reveal the protective effect of QYT on Src activation, nor on TLR-4 expression, thus excluded the involvement of TLR-4 expression and Src signaling in the beneficial role of QYT in microvascular hyperpermeability after LPS. The reason for ineffectiveness of catalpol, DLA, and salvianolic acid B in inhibiting Src activation and TLR-4 expression in the present case is unknown. As to the mechanism for the protective effect of QYT on LPS- caused BBB breakdown, what is clear is that QYT prevented the increased activation of NF-κB after LPS. It is likely that it is the blocking the of NF-κB signaling by QYT that reduced the level of proinflammatory cytokines, protected the downregulation of junctions proteins, and upregulation of MMP-9 and adhesion molecules, thus improved cerebral microcirculation and protected BBB from breakdown after LPS.

QYT consists of nine different components, each of them contains numerous bioactive ingredients. The present study focused on the effect of QYT as a whole on the LPS-induced cerebral vascular hyperpermeability and its underlying mechanism. Much more work is required to elucidate the role of any individual ingredient in QYT in the effect observed.

CONCLUSION

This study demonstrated that post-treatment with QYT attenuated LPS-induced cerebral microcirculatory disorder, inhibiting leukocyte adhesion to microvessels, protecting microvascular hyperpermeability as evidenced by the decreased albumin exudation and brain edema, which is correlated with reduced proinflammatory cytokines level and increased expression of junctions proteins.

DATA AVAILABILITY STATEMENT

All datasets generated for this study are included in the article/ supplementary material.

AUTHOR CONTRIBUTIONS

H-MW undertook the research, analyzed the data, and wrote the manuscript. PH performed western blotting and analyzed the data of western blotting and immunostaining. QL contributed to the animal experiments. L-LY designed and performed pharmacokinetics and toxicity studies. KS contributed to the measurement of MCP-1, GM-CSF, MIP-1α, TNF-α, IL-1α, IL-1β, and IL-6 in plasma and brain tissue homogenate and the determination of HR, SBP, and DBP. L-LY contributed to the Nissl stain and immunofluorescence. C-SP contributed to the western blotting. Y-YL, C-SW, X-HW, and B-HH contributed to the other experiments. J-YF and PH revised the manuscript. J-YH designed and funded the research, interpreted the data, and finally approved the submission of this manuscript. All authors read and agreed with the manuscript.

FUNDING

This work was supported by the State Key Laboratory of Core Technology in Innovative Chinese Medicine Grant 20170034.

ACKNOWLEDGMENTS

The authors thank Jing Wu, Yue Chen, Jian-Ru Yang, Qi-Hua He for excellent technical assistance with the laser scanning confocal microscope operation. The work of pharmacokinetics was nicely supported by Chu Yang, Kong Jing from division of pharmacology and toxicology, Tasly Academy.

REFERENCES

Abbott, N. J., Patabendige, A. A., Dolman, D. E., Yusof, S. R., and Begley, D. J. (2010). Structure and function of the blood-brain barrier. *Neurobiol. Dis.* 37, 13–25. doi: 10.1016/j.nbd.2009.07.030

Berger, R. E., Rivers, E., and Levy, M. M. (2017). Management of septic shock. *N. Engl. J. Med.* 376, 2282–2285. doi: 10.1056/NEJMclde1705277

Bienvenu, K., and Granger, D. N. (1993). Molecular determinants of shear rate-dependent leukocyte adhesion in postcapillary venules. *Am. J. Phys.* 264, H1504–H1508. doi: 10.1152/ajpheart.1993.264.5.H1504

Clark, P. R., Kim, R. K., Pober, J. S., and Kluger, M. S. (2015). Tumor necrosis factor disrupts claudin-5 endothelial tight junction barriers in two distinct NF-kappaB-dependent phases. *PLoS One* 10:e0120075. doi: 10.1371/journal.pone.0120075

Cohen, J. (2002). The immunopathogenesis of sepsis. *Nature* 420, 885–891. doi: 10.1038/nature01326

Coisne, C., and Engelhardt, B. (2011). Tight junctions in brain barriers during central nervous system inflammation. *Antioxid. Redox Signal.* 15, 1285–1303. doi: 10.1089/ars.2011.3929

Dong, J. (2007). The application and development of QingYing decoction in "analysis of heat diseases". *Clin. J. Tradit. Chin. Med.* 19, 74–75. doi: 10.16448/j.cjtcm.2007.01.059

Feng, Y. H., and Xu, X. (2015). One case of treatment with Qingying decoction for high fever after total hysterectomy. *Global Tradit. Chin. Med.* 8, 729–730. doi: 10.3969/j.issn.1674-1749.2015.06.025

Fu, L. (2005). Regulating effect of modified Qingying decoction on blood lipid and body fluid immunity in patients with vascular occlusive angiitis. *J. Nanjing Univ. Tradit. Chin. Med.* 21, 360–362. doi: 10.14148/j.issn.1672-0482.2005.06.007

Gao, Z., Xu, J., Sun, D., Zhang, R., Liang, R., Wang, L., et al. (2014). Traditional Chinese medicine, Qing Ying Tang, ameliorates the severity of acute lung injury induced by severe acute pancreatitis in rats via the upregulation of aquaporin-1. *Exp. Ther. Med.* 8, 1819–1824. doi: 10.3892/etm.2014.1987

Gong, P., Angelini, D. J., Yang, S., Xia, G., Cross, A. S., Mann, D., et al. (2008). TLR4 signaling is coupled to SRC family kinase activation, tyrosine phosphorylation of zonula adherens proteins, and opening of the paracellular pathway in human lung microvascular endothelia. *J. Biol. Chem.* 283, 13437–13449. doi: 10.1074/jbc.M707986200

Gu, Y. Y., Huang, P., Li, Q., Liu, Y. Y., Liu, G., Wang, Y. H., et al. (2018). YangXue QingNao Wan and Silibinin capsules, the two Chinese medicines, attenuate cognitive impairment in aged LDLR (+/−) Golden Syrian hamsters involving protection of blood brain barrier. *Front. Physiol.* 9:658. doi: 10.3389/fphys.2018.00658

Hu, Q., Chen, C., Yan, J., Yang, X., Shi, X., Zhao, J., et al. (2009). Therapeutic application of gene silencing MMP-9 in a middle cerebral artery occlusion-induced focal ischemia rat model. *Exp. Neurol.* 216, 35–46. doi: 10.1016/j.expneurol.2008.11.007

Hu, Q., Ma, Q., Zhan, Y., He, Z., Tang, J., Zhou, C., et al. (2011). Isoflurane enhanced hemorrhagic transformation by impairing antioxidant enzymes in hyperglycemic rats with middle cerebral artery occlusion. *Stroke* 42, 1750–1756. doi: 10.1161/STROKEAHA.110.603142

Huang, P., Zhou, C. M., Qin, H., Liu, Y. Y., Hu, B. H., Chang, X., et al. (2012). Cerebralcare granule(R) attenuates blood-brain barrier disruption after middle cerebral artery occlusion in rats. *Exp. Neurol.* 237, 453–463. doi: 10.1016/j.expneurol.2012.07.017

Jean-Baptiste, E. (2007). Cellular mechanisms in sepsis. *J. Intensive Care Med.* 22, 63–72. doi: 10.1177/0885066606297123

Ji, G. R., He, M., Zhang, Z. C., and Li, L. (2015). Clinical observation of "Qingying decoction" combined with Western medicine in treating patients with sepsis. *Acta Univ. Tradit. Med. Sin. Pharmacol. Shanghai* 29, 27–29. doi: 10.16306/j.1008-861x.2015.04.008

Kawai, T., and Akira, S. (2011). Toll-like receptors and their crosstalk with other innate receptors in infection and immunity. *Immunity* 34, 637–650. doi: 10.1016/j.immuni.2011.05.006

Keaney, J., and Campbell, M. (2015). The dynamic blood-brain barrier. *FEBS J.* 282, 4067–4079. doi: 10.1111/febs.13412

Khakpour, S., Wilhelmsen, K., and Hellman, J. (2015). Vascular endothelial cell toll-like receptor pathways in sepsis. *Innate Immun.* 21, 827–846. doi: 10.1177/1753425915606525

Kurose, I., Wolf, R., Grisham, M. B., and Granger, D. N. (1994). Modulation of ischemia/reperfusion-induced microvascular dysfunction by nitric oxide. *Circ. Res.* 74, 376–382. doi: 10.1161/01.RES.74.3.376

Li, Y. J., Han, D., Xu, X. S., Liu, Y. Y., Sun, K., Fan, J. Y., et al. (2012). Protective effects of 3,4-dihydroxyphenyl lactic acid on lipopolysaccharide-induced cerebral microcirculatory disturbance in mice. *Clin. Hemorheol. Microcirc.* 50, 267–278. doi: 10.3233/CH-2011-1435

Lin, F., Liu, Y. Y., Xu, B., Sun, K., Wang, H. Y., Li, Q., et al. (2013). Salvianolic acid B protects from pulmonary microcirculation disturbance induced by lipopolysaccharide in rat. *Shock* 39, 317–325. doi: 10.1097/SHK.0b013e318283773e

Mombouli, J. V., and Vanhoutte, P. M. (1999). Endothelial dysfunction: from physiology to therapy. *J. Mol. Cell. Cardiol.* 31, 61–74. doi: 10.1006/jmcc.1998.0844

Pan, C. S., Liu, Y. H., Liu, Y. Y., Zhang, Y., He, K., Yang, X. Y., et al. (2015). Salvianolic acid B ameliorates lipopolysaccharide-induced albumin leakage from rat mesenteric venules through Src-regulated transcellular pathway and paracellular pathway. *PLoS One* 10:e0126640. doi: 10.1371/journal.pone.0146204

Plociennikowska, A., Hromada-Judycka, A., Borzecka, K., and Kwiatkowska, K. (2015). Co-operation of TLR4 and raft proteins in LPS-induced pro-inflammatory signaling. *Cell. Mol. Life Sci.* 72, 557–581. doi: 10.1007/s00018-014-1762-5

Shoji, A., Kabeya, M., Ishida, Y., Yanagida, A., Shibusawa, Y., and Sugawara, M. (2014). Evaluation of cathepsin B activity for degrading collagen IV using a surface plasmon resonance method and circular dichroism spectroscopy. *J. Pharm. Biomed. Anal.* 95, 47–53. doi: 10.1016/j.jpba.2014.02.009

Siami, S., Annane, D., and Sharshar, T. (2008). The encephalopathy in sepsis. *Crit. Care Clin.* 24, 67–82, viii. doi: 10.1016/j.ccc.2007.10.001

Tauber, S. C., Eiffert, H., Bruck, W., and Nau, R. (2017). Septic encephalopathy and septic encephalitis. *Expert Rev. Anti-Infect. Ther.* 15, 121–132. doi: 10.1080/14787210.2017.1265448

Tong, D. M., Zhou, Y. T., Wang, G. S., Chen, X. D., and Yang, T. H. (2015). Early prediction and outcome of septic encephalopathy in acute stroke patients with nosocomial coma. *J. Clin. Med. Res.* 7, 534–539. doi: 10.14740/jocmr2176w

Tsukamoto, H., Takeuchi, S., Kubota, K., Kobayashi, Y., Kozakai, S., Ukai, I., et al. (2018). Lipopolysaccharide (LPS)-binding protein stimulates CD14-dependent toll-like receptor 4 internalization and LPS-induced TBK1-IKK-IRF3 axis activation. *J. Biol. Chem.* 293, 10186–10201. doi: 10.1074/jbc.M117.796631

Vanlaere, I., and Libert, C. (2009). Matrix metalloproteinases as drug targets in infections caused by gram-negative bacteria and in septic shock. *Clin. Microbiol. Rev.* 22, 224–239. doi: 10.1128/CMR.00047-08

Victor, B. C., Anbalagan, A., Mohamed, M. M., Sloane, B. F., and Cavallo-Medved, D. (2011). Inhibition of cathepsin B activity attenuates extracellular matrix degradation and inflammatory breast cancer invasion. *Breast Cancer Res.* 13:R115. doi: 10.1186/bcr3058

Wang, F., Liu, Y. Y., Liu, L. Y., Zeng, Q. J., Wang, C. S., Sun, K., et al. (2009). The attenuation effect of 3,4-dihydroxy-phenyl lactic acid and salvianolic acid B on venular thrombosis induced in rat mesentery by photochemical reaction. *Clin. Hemorheol. Microcirc.* 42, 7–18. doi: 10.3233/CH-2009-1180

Zhang, B. G., Cheng, T. F., and Liu, Q. F. (2009). Efficiency and clinical application of QING-YING-TANG. *Chin. Tradit. Pat. Med.* 31, 1741–1744.

Zhang, Y. P., Pan, C. S., Yan, L., Liu, Y. Y., Hu, B. H., Chang, X., et al. (2016). Catalpol restores LPS-elicited rat microcirculation disorder by regulation of a network of signaling involving inhibition of TLR-4 and SRC. *Am. J. Physiol. Gastrointest. Liver Physiol.* 311, G1091–G1104. doi: 10.1152/ajpgi.00159.2016

Zhang, Y., Sun, K., Liu, Y. Y., Zhang, Y. P., Hu, B. H., Chang, X., et al. (2014). Ginsenoside Rb1 ameliorates lipopolysaccharide-induced albumin leakage from rat mesenteric venules by intervening in both trans- and paracellular pathway. *Am. J. Physiol. Gastrointest. Liver Physiol.* 306, G289–G300. doi: 10.1152/ajpgi.00168.2013

Zhao, H. P., Feng, J., Sun, K., Liu, Y. Y., Wei, X. H., Fan, J. Y., et al. (2012). Caffeic acid inhibits acute hyperhomocysteinemia-induced leukocyte rolling and adhesion in mouse cerebral venules. *Microcirculation* 19, 233–244. doi: 10.1111/j.1549-8719.2011.00151.x

Conflict of Interest: The authors declare that the research was conducted in the absence of any commercial or financial relationships that could be construed as a potential conflict of interest.

Copyright © 2019 Wang, Huang, Li, Yan, Sun, Yan, Pan, Wei, Liu, Hu, Wang, Fan and Han. This is an open-access article distributed under the terms of the Creative Commons Attribution License (CC BY). The use, distribution or reproduction in other forums is permitted, provided the original author(s) and the copyright owner(s) are credited and that the original publication in this journal is cited, in accordance with accepted academic practice. No use, distribution or reproduction is permitted which does not comply with these terms.

frontiers in Pharmacology

SYSTEMATIC REVIEW
published: 04 December 2019
doi: 10.3389/fphar.2019.01403

Efficacy and Safety of Ginkgo Leaf Extract and Dipyridamole Injection for Ischemic Stroke: A Systematic Review and Meta Analysis

Ping Xue[1], Zhuoya Ma[1] and Shuguang Liu[2]**

[1] Department of Neurology, Liaocheng People's Hospital, Liaocheng, China, [2] Department of Intensive Care Unit, Yanggu People's Hospital, Yanggu, China

OPEN ACCESS

Edited by:
Gerald A. Meininger,
University of Missouri,
United States

Reviewed by:
Ligia Salgueiro,
University of Coimbra,
Portugal
Michael Heinrich,
UCL School of Pharmacy,
United Kingdom

***Correspondence:**
Zhuoya Ma
zhuoyamane@163.com
Shuguang Liu
shuguanglem@163.com

Specialty section:
This article was submitted to Ethnopharmacology, a section of the journal Frontiers in Pharmacology

Received: 26 March 2019
Accepted: 04 November 2019
Published: 04 December 2019

Citation:
Xue P, Ma Z and Liu S (2019) Efficacy and Safety of Ginkgo Leaf Extract and Dipyridamole Injection for Ischemic Stroke: A Systematic Review and Meta Analysis. Front. Pharmacol. 10:1403. doi: 10.3389/fphar.2019.01403

Objective: Ginkgo leaf extract and dipyridamole injection (GDI), a kind of Chinese medicine preparation, has been considered as a promising supplementary treatment for ischemic stroke. The aim of this study was to systematically evaluate the clinical efficacy and safety of GDI mediated therapy for ischemic stroke.

Methods: PubMed, Cochrane Library, Medline, Embase, Web of Science, Wanfang database, Chinese Scientific Journal Database (VIP), China National Knowledge Infrastructure (CNKI) and Chinese Biological Medicine Database (CBM), were searched systematically for clinical trials of conventional treatments combined with GDI for ischemic stroke. The reported outcomes including overall response, hemorrheology and blood lipid indexes, and adverse events were systematically investigated.

Results: Data from thirty-nine trials including 3,182 ischemic stroke patients were involved. The results indicated that, compared with conventional treatments alone, the combination of conventional treatments with GDI obviously improved the overall response (odds ratio [OR] = 4.14, 95% confidence interval [CI] = 3.26–5.25, $P < 0.00001$), neurological status (National Institutes of Health Stroke Scale, OR = –3.13, 95% CI = –3.98 to –2.28, $P < 0.00001$) and activity of daily living (Barthel Index score, OR = 14.10, 95% CI = 9.51–18.68, $P < 0.00001$) of patients. Moreover, the hemorheology and blood lipids indexes of ischemic stroke patients were also significantly ameliorated after the combined therapy ($P < 0.01$). The frequency of adverse events did not differ significantly between the two groups ($P > 0.05$).

Conclusion: Evidence from the meta-analysis suggested that the combination of conventional treatments and GDI is safe and more effective in treating ischemic stroke than conventional treatments alone. Therefore, GDI mediated therapy could be recommended as an adjuvant treatment for ischemic stroke.

Keywords: ginkgo leaf extract and dipyridamole injection, traditional Chinese medicine, conventional treatments, ischemic stroke, meta-analysis

INTRODUCTION

Ischemia stroke is one of the common cerebrovascular diseases, and is a major cause of death and disability (Chen et al., 2019). It is characterized by the partial or complete loss of blood supply in part of the brain tissues, which account for about 80% of all stroke events (Chen et al., 2019). Ischemia results in reduced neuron number and interrupted neural axon network, and eventually resulting in the permanent loss of nerve tissue or disabled brain function (Xue et al., 2018). Over fifty million peoples are suffering ischemic stroke in the world, and nearly 50% of stroke survivors are left with disabling sequelae (Xue et al., 2018). Currently, the conventional therapy, including thrombolysis, controlling cerebral edema, neuroprotective agents, restoring blood supply to ischemic area, reducing blood viscosity, preventing and treating complications, controlling hypertension, etc. is the main clinical therapy for ischemia stroke (Ma et al., 2017; Chen et al., 2019). However, it functions mainly at the early stage of ischemia with a short time window, and therefore its clinical application is severely limited (Xue et al., 2018). Thus, the more effective agents for ischemia stroke patients are desirable.

Ginkgo extract is a Chinese traditional herb which made from the dried leaves of the *Ginkgo biloba* L (Ginkgoaceae) (Zeng et al., 2005), and has been widely applied as an effective complementary drug for brain disorder treatment in numerous hospitals of China. Ginkgo extract can protect the neurons against reactive oxygen species, regulates vasomotor, improves hemorheology and can also reduces infarction size by improving neurological function (Kampkotter et al., 2007; Nash and Shah, 2015; Tulsulkar et al., 2016; Liu et al., 2019). Zhang et al. (2018) demonstrated that ginkgo extract can inhibit astrocytic lipocalin-2 expression and alleviates neuro-inflammatory injury *via* the JAK2/STAT3 pathway after ischemic stroke. Ginkgo leaf extract and dipyridamole injection (GDI) is a compound preparation, which mainly consists of ginkgo flavone glycosides (24–25%), terpene lactones [ginkgolides (3.1%) and bilobalide (2.9%)] and dipyridamole (10%) (Zeng et al., 2005; Tan et al., 2018). Currently, several clinical trials indicated that conventional treatments combined with GDI exhibits more prominent therapeutic effects for ischemic stroke than conventional treatments alone (Wang et al., 2015; Li et al., 2017). However, the scientific evidence has not been systematically reviewed. Therefore, in this study, we conducted a meta-analysis to investigate the clinical efficacy and safety of GDI for ischemic stroke, in order to provide the best available evidence for clinical practice and further research planning on ischemia stroke treatment.

MATERIALS AND METHODS

Search Strategy and Selection Criteria

This systematic review and meta-analysis was performed following the PRISMA guidelines and Cochrane Handbook. Literatures were searched across nine electronic databases, including PubMed, Cochrane Library, Medline, Embase, Web of Science, Wanfang database, Chinese Scientific Journal Database (VIP), China National Knowledge Infrastructure (CNKI) and Chinese Biological Medicine Database (CBM), before December 2018, with key terms "ginkgo biloba" or "ginkgo leaf extract" or "ginkgo dipyridamolum" or "ginkgo leaf extract and dipyridamole injection" or "yinxingdamo injection" and "ischemic stroke" or "cerebral infarction" or "brain infarction" or "cerebral ischemia" or "brain ischemia," without language restriction (**Supplementary Table 1**). No language limits were applied.

Inclusion criteria: (1) Randomized controlled trials (RCTs) concerning ischemic stroke patients were included; (2) Research subjects (ischemic stroke patients) must meet WHO diagnostic criteria of ischemic stroke and exclude cerebral hemorrhage by brain computerized tomography (CT) or magnetic resonance imaging (MRI). (3) Articles involving more than 30 ischemic stroke patients; (4) There were no other medicines in combination with the conventional treatments in the experimental group, except for GDI, compared with the conventional treatments as a control; (5) Literatures comparing the clinical outcomes of conventional treatments plus GDI adjuvant therapy (experimental group) with conventional treatments alone (control group); (6) One or more outcome measures, including the overall response rate, neurological deficit score, serum level of CRP, hemorheology and blood lipid indexes, adverse events must be included in each study.

Exclusion criteria: (1) Studies not focus on GDI were excluded; (2) Inappropriate criteria in experimental or control group were excluded; (3) articles without sufficient available data were excluded; (4) Non-contrast articles, non-clinical studies, literature reviews, meta-analysis, meeting abstracts, case reports, repeated studies and experimental model researches were excluded.

Data Extraction and Quality Assessment

Data were extracted by two reviewers (PX and ZM) independently according to the same inclusion and exclusion criteria; disagreements were adjudicated by the third investigator (SL). The extracted characteristics comprised the following items: (a) first author's names; (b) years of publication; (c) number of cases; (d) patient ages; (e) intervening measure; (f) dosage of GDI; (g) duration of treatment and (h) study parameter types. The quality of included trials was evaluated according to Cochrane Handbook (Zeng et al., 2015).

Outcome Definition

Clinical responses include treatment efficacy and adverse events. Treatment efficacy was evaluated in terms of the overall response rate (ORR), National Institutes of Health Stroke Scale (NIHSS), Barthel Index (BI) score, hemorrheology and blood lipid indexes. The hemorrheology indexes covered the following indicators: whole blood viscosity (WBV), plasma viscosity (PV), whole blood high-shear viscosity (WBHSV), whole blood low-shear viscosity (WBLSV), and content of fibrinogen (FIB). The blood lipid indicators [Plasma total cholesterol (TC), triglycerides (TG), high density lipoprotein-cholesterol (HDL-C); low density lipoprotein-cholesterol (LDL-C)] and plasma C reactive protein (CRP) of ischemic stroke patients were determined and compared between the GDI and non-GDI groups. Adverse events including fever, fullness in head, allergy, hemorrhage, palpitation, nausea and vomiting were taken into assessment.

Statistical Analysis

Statistical analysis was performed using the Review Manager 5.3 (Cochrane Collaboration, Oxford, UK) and Stata 13.0 (Stata Corp., College Station, TX, USA). All data were expressed as odds ratio (OR) and 95% confidence intervals (CI), and $P < 0.05$ indicates difference with statistical significance. Heterogeneity among studies was estimated using the Cochran's Q statistic and I^2 tests, $I^2 > 50\%$ or $P < 0.1$ indicated a high statistical heterogeneity (Jackson et al., 2012). A fixed-effects model was used to pool the estimates when heterogeneity was absent ($I^2 < 50\%$). Otherwise, a random effects model was selected.

Publication bias was numerically examined by Begg's and Egger's tests and presented by funnel plots. If publication bias existed, we used the trim-and-fill method to adjust the pooled estimates of the potential unpublished studies in the meta-analysis, which were compared with the original pooled OR (Liang et al., 2017; Lin et al., 2018). Sensitivity analysis was conducted to investigate the influence of different GDI dosages, sample sizes and research types on clinical efficacy.

RESULTS

Search Results

A total of 2,152 articles were identified with initial retrieve. 1,709 papers were excluded due to duplication. After title and abstract review, 324 articles were further excluded because they were not clinical trials (n = 202) or were unrelated studies (n = 104) or were reviews and meta-analysis (n = 7) or were case report (n = 11), leaving 119 studies as potentially relevant. After detailed assessment of full texts, articles without control group (n = 14), publications with inappropriate criteria of experimental or control group (n = 34), trials with insufficient data (n = 15) and studies not focus on GDI (n = 17) were excluded. Finally, 39 trials (Tang et al., 2009; Wang et al., 2009; Li, 2010; Long et al., 2010; Huang and Yuan, 2010; Tian et al., 2010; Zhou et al., 2010; Chen et al., 2011; Yang, 2012; Wang, 2012; Lan, 2013; Ding, 2013; Lin and Lin, 2013; Tang, 2013; Fang, 2014; Huang et al., 2014; Jiang, 2014; Yang, 2014; Wang, 2014a; Wang, 2014b; Chu, 2015; Liu, 2015; Sun, 2015; Zeng, 2015; Chen, 2016; Cui, 2016; Fu et al., 2016; Zhou et al., 2016; Li, 2016; Li, 2017; Dai, 2017; Guo, 2017; Wei, 2017; Ai, 2017; Zhang, 2017; Wang, 2018; Yi et al., 2018; Zhang, 2018; Zheng et al., 2018) involving 3,182 ischemic stroke patients were included in this analysis (**Figure 1**).

Patient Characteristics

After selection, all included trials were performed in different medical centers of China. In total, 1,596 ischemic stroke patients were treated by conventional treatments in combination with GDI adjuvant therapy, while 1,589 patients were treated by conventional treatments alone. Detailed information of the involved studies and ischemic stroke patients is shown in **Table 1**. All included trials except one (Yang, 2014) clearly introduce the dosage of GDI. Twenty-two studies specifically describe the manufacturer of GDI and the remaining seventeen studies lacked clear description of production information (**Supplementary Table 2**). The compositions and concentrations of GDI in all included trials are the same (every 10ml GDI contained 9.0–11.0 mg total flavonoids and 3.6–4.4 mg dipyridamole). The Quality Standards of GDI in this study have been approved by Chinese State Food and Drug Administration (SFDA), and granted the Manufacturing Approve Number issued by Chinese SFDA. All pharmaceutical companies involved followed the quality processing procedure outlined in pharmacopeia.

Quality Assessment

The assessment of bias risk is shown in **Figure 2**. Thirty-four studies (Wang et al., 2009; Tang et al., 2009; Li, 2010; Huang and Yuan, 2010; Tian et al., 2010; Long et al., 2010; Zhou et al., 2010; Chen et al., 2011; Wang, 2012; Yang, 2012; Ding, 2013; Lin and Lin, 2013; Tang, 2013; Lan, 2013; Yang, 2014; Huang et al., 2014; Fang, 2014; Wang, 2014a; Wang, 2014b; Chu, 2015; Liu, 2015; Zeng, 2015; Cui, 2016; Fu et al., 2016; Li, 2016; Zhou et al., 2016; Chen, 2016; Zhang, 2017; Wei, 2017; Ai, 2017; Yi et al., 2018; Wang, 2018; Zhang, 2018; Zheng et al., 2018) were determined as low risk and the remaining five studies (Jiang, 2014; Sun, 2015; Dai, 2017; Guo, 2017; Li, 2017) were not true RCTs. All included trials did not provide clear description of performance and detection risks. The attrition risks of involved trials were low. Four trials (Huang and Yuan, 2010; Li, 2010; Ding, 2013; Chu, 2015) were considered as high reporting risk owing to lack of primary outcomes (ORR) and twenty-three studies (Tang et al., 2009; Zhou et al., 2010; Tian et al., 2010; Chen et al., 2011; Wang, 2012; Yang, 2012; Tang, 2013; Lin and Lin, 2013; Yang, 2014; Jiang, 2014; Fang, 2014; Fu et al., 2016; Li, 2016; Chen, 2016; Cui, 2016; Zhou et al., 2016; Ai, 2017; Dai, 2017; Wei, 2017; Zhang, 2018; Zheng et al., 2018; Wang, 2018; Yi et al., 2018) were considered as unclear reporting risk due to lack of safety assessment.

ORR Assessments

Thirty-five clinical trials (Wang et al., 2009; Tang et al., 2009; Tian et al., 2010; Long et al., 2010; Zhou et al., 2010; Chen et al., 2011; Yang, 2012; Wang, 2012; Lan, 2013; Tang, 2013; Lin and Lin, 2013; Huang et al., 2014; Jiang, 2014; Wang, 2014a; Wang, 2014b; Fang, 2014; Yang, 2014; Liu, 2015; Sun, 2015; Zeng, 2015; Chen, 2016; Cui, 2016; Li, 2016; Zhou et al., 2016; Fu et al., 2016; Dai, 2017; Guo, 2017; Li, 2017; Wei, 2017; Zhang, 2017; Ai, 2017; Wang, 2018; Yi et al., 2018; Zhang, 2018; Zheng et al., 2018) involving 2,792 cases compared the ORR between the two groups (**Figure 3**). Our pooled results showed that patients underwent combined therapy had significantly improved ORR (OR = 4.14, 95% CI = 3.26-5.25, $P < 0.00001$) compared with conventional treatments alone. There was no heterogeneity, and a fixed-effect model was used to carry out the meta-analysis.

NIHSS

Fourteen trials (Tian et al., 2010; Tang, 2013; Jiang, 2014; Yang, 2014; Chu, 2015; Sun, 2015; Chen, 2016; Fu et al., 2016; Li, 2016; Zhou et al., 2016; Zhang, 2017; Zhang, 2018; Yi et al., 2018; Wang, 2018) with 1,058 participants measured the neurological status according to the NIHSS (**Figure 4**). Results showed that the neurological status of ischemic oke patients received combined therapy was obviously improved compare to those treated by conventional treatments

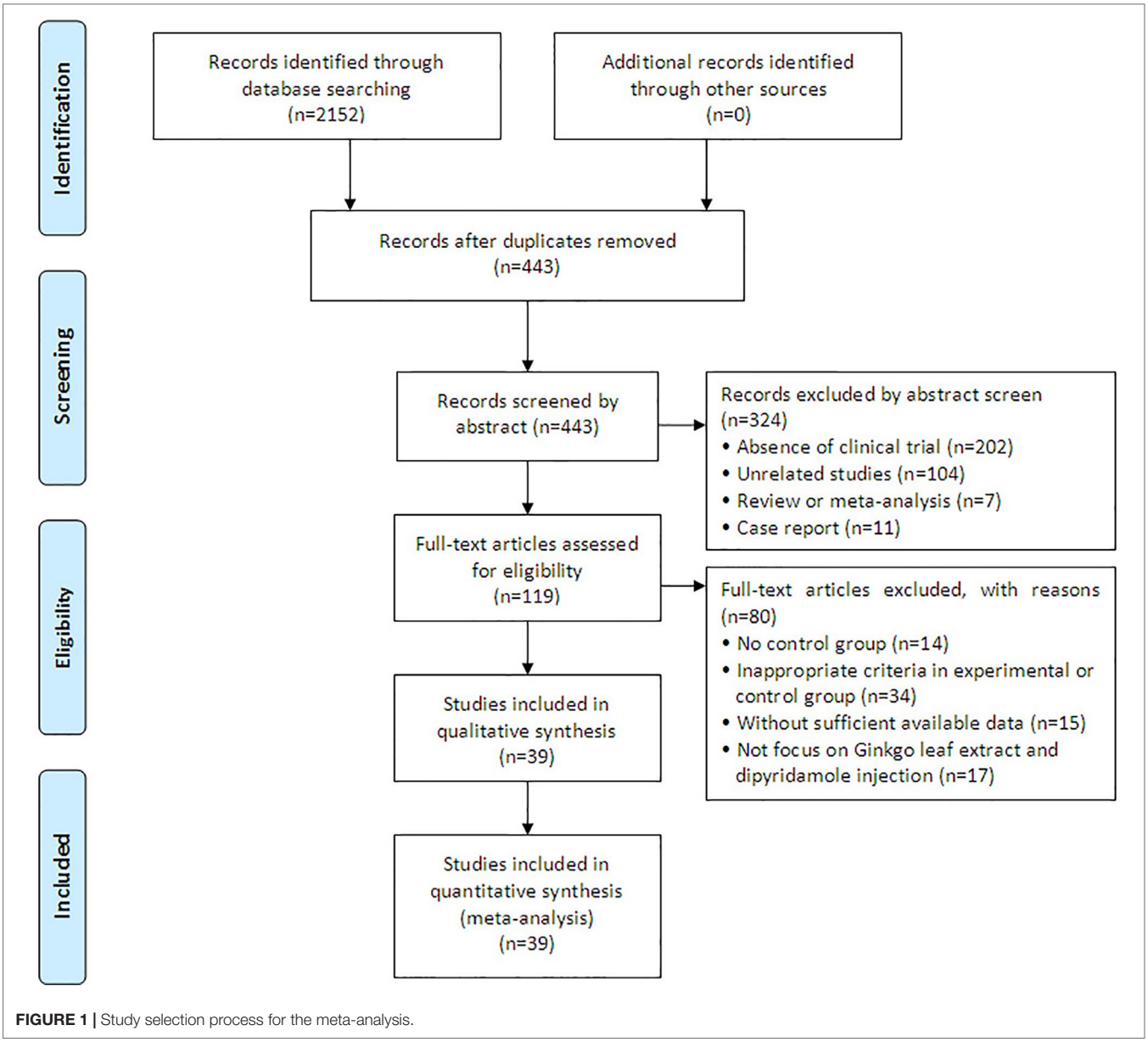


FIGURE 1 | Study selection process for the meta-analysis.

alone (OR = −3.13, 95% CI = −3.98 to −2.28, $P < 0.00001$). There was significant heterogeneity among the studies ($I^2 = 97\%$, $P < 0.00001$); therefore, a random-effects model was conducted to pool data and so any conclusions need to be made with caution.

Sensitivity Analysis Was Performed to Explore an Individual Study's Influence on the Pooled Results by Deleting One Single Study Each Time From Pooled Analysis. as **Supplementary Table 3** and **Supplementary Figure 1** Signified, the Results Revealed That No Individual Studies Significantly Affected the NIHSS, Which Indicated Statistically Robust Results.

BI Score

Three trials (Huang and Yuan, 2010; Fu et al., 2016; Zhang, 2018) involving 368 ischemic stroke patients evaluated the activity of daily living according to the BI Score. As shown in **Figure 5**, the BI Score of ischemic stroke patients in the combined group were significantly higher than that of the control group (OR = 14.10, 95% CI = 9.51–18.68, $P < 0.00001$). A P-value = 0.04 and I^2 = 69% indicated that there was significant heterogeneity among the studies; thus a random effect model was employed.

CRP Level

There were six studies (Wang et al., 2009; Li, 2010; Fang, 2014; Li, 2016; Chen, 2016; Zhang, 2018) involving 508 patients measured the level of CRP (**Supplementary Figure 2**). The pooled analysis showed that compared with the conventional treatments alone, combined with GDI could significantly reduce the serum CRP levels of ischemic stroke patients (OR = −2.36, 95% CI = −3.25

TABLE 1 | Clinical information from the eligible trials in the meta-analysis.

Included studies	Patients Con/Exp	Age (year)		Interview Measure (Exp/Con)	Conventional treatments	Dosage of GDI	Duration	Parameter types
		Con	Exp					
Ai DJ (2017)	34/34	–	–	CT+GDI vs CT	Ganglioside	20-30 ml/Day	–	ORR
Chen L (2011)	30/32	61 ± 5.87 (mean)	61 ± 5.32 (mean)	CT+GDI vs CT	–	20 ml/Day	14 days	ORR, BVI
Chen TH (2016)	31/31	58 ± 1.36 (mean)	59 ± 2.13 (mean)	CT+GDI vs CT	–	20 ml/Day	30 days	ORR, NIHSS, CRP
Chu WM (2015)	30/30	66.38 ± 7.57 (mean)	67.17 ± 5.34 (mean)	CT+GDI vs CT	–	30 ml/Day	14 days	NIHSS, BLI
Cui XF (2016)	35/35	–	–	CT+GDI vs CT	Ozagrel	40 ml/Day	28 days	ORR
Dai CM (2017)	50/50	–	–	CT+GDI vs CT	Aspirin	20 ml/Day	14 days	ORR
Ding HY (2013)	30/30	75.6 ± 5.3 (mean)	75.3 ± 5.1 (mean)	CT+GDI vs CT	Ganglioside	30 ml/Day	14 days	BVI, AE
Fang XW (2014)	50/50	–	–	CT+GDI vs CT	–	20 ml/Day	28 days	ORR, CRP
Fu DF (2016)	42/42	61.7 (mean)	61.5 (mean)	CT+GDI vs CT	–	20 ml/Day	14 days	ORR, NIHSS, BI
Guo ZX (2017)	33/35	60 (mean)	62 (mean)	CT+GDI vs CT	Ozagrel	20 ml/Day	14 days	ORR, AE
Huang SP (2010)	42/42	66.9 (mean)	67.8 (mean)	CT+GDI vs CT	–	40 ml/Day	–	BI
Huang WH (2014)	39/39	58.94 ± 5.28 (mean)	57.63 ± 5.73 (mean)	CT+GDI vs CT	Ozagrel	20 ml/Day	14 days	ORR, AE
Jiang X (2014)	50/50	–	–	CT+GDI vs CT	Aspirin	20 ml/Day	14 days	ORR, NIHSS, BVI
Lan BW (2013)	35/35	52.71 ± 3.35 (mean)	52.32 ± 3.11 (mean)	CT+GDI vs CT	Ozagrel	20 ml/Day	14 days	ORR, AE
Li CX (2010)	43/43	–	–	CT+GDI vs CT	–	20 ml/Day	14 days	CRP
Li GQ (2017)	43/43	–	–	CT+GDI vs CT	Edaravone	25 ml/Day	14 days	ORR, AE
Li NP (2016)	30/30	65.0 ± 7.5 (mean)	66.9 ± 6.8 (mean)	CT+GDI vs CT	–	20 ml/Day	14 days	ORR, NIHSS, CRP, BVI
Lin CD (2013)	32/32	–	–	CT+GDI vs CT	Cinepazide malete	20 ml/Day	28 days	ORR
Liu W (2015)	17/18	60.5 ± 0.5 (mean)	70.8 ± 0.8 (mean)	CT+GDI vs CT	Ozagrel	20 ml/Day	15 days	ORR, AE
Long XY (2010)	75/76	64.2 (median)	65.4 (median)	CT+GDI vs CT	Heparin	20 ml/Day	14 days	ORR, BVI, AE
Sun YF (2015)	38/41	65.7 ± 2.3 (mean)	64.3 ± 2.4 (mean)	CT+GDI vs CT	Edaravone	20 ml/Day	14 days	ORR, NIHSS, AE
Tang HM (2009)	45/45	–	–	CT+GDI vs CT	Aspirin	20 ml/Day	14 days	ORR, BVI
Tang XJ (2013)	39/39	–	–	CT+GDI vs CT	Aspirin	20 ml/Day	14 days	ORR, NIHSS, BVI
Tian XJ (2010)	33/34	66.4 (mean)	67.5 (mean)	CT+GDI vs CT	Fibrinolytic enzyme	20 ml/Day	14 days	ORR, NIHSS, BLI
Wang FF (2014)	30/30	52-65	50-62	CT+GDI vs CT	Ozagrel	20 ml/Day	14 days	ORR, AE
Wang JS (2009)	50/50	59 (median)	61 (median)	CT+GDI vs CT	Nimodipine	20 ml/Day	14 days	ORR, CRP, AE
Wang Q (2014)	60/60	–	–	CT+GDI vs CT	Aspirin	20 ml/Day	14 days	ORR, AE
Wang YH (2012)	59/60	60 ± 9.78 (mean)	59 ± 10.9 (mean)	CT+GDI vs CT	Aspirin	30 ml/Day	14 days	ORR
Wang ZG (2018)	18/18	65.63 ± 8.05 (mean)	65.17 ± 8.54 (mean)	CT+GDI vs CT	Ozagrel	20 ml/Day	14 days	ORR, NIHSS
Wei N (2017)	61/61	65.93 ± 5.52 (mean)	66.26 ± 5.47 (mean)	CT+GDI vs CT	Edaravone	10 ml/Day	14 days	ORR, BVI
Yang J (2012)	29/27	55.4 ± 17.6 (mean)	60.5 ± 16.4 (mean)	CT+GDI vs CT	–	30 ml/Day	15 days	ORR
Yang L (2014)	37/37	–	–	CT+GDI vs CT	Aspirin	–	14 days	ORR, NIHSS, BVI
Yi JT (2018)	45/45	54.12 ± 12.25 (mean)	53.74 ± 10.78 (mean)	CT+GDI vs CT	–	25 ml/Day	14 days	ORR, NIHSS, BVI
Zeng JW (2015)	27/28	58.9 ± 3.9 (mean)	59.5 ± 4.1 (mean)	CT+GDI vs CT	Ozagrel	20 ml/Day	14 days	ORR, AE
Zhang SY (2017)	45/45	60.12 ± 2.36 (mean)	60.13 ± 2.31 (mean)	CT+GDI vs CT	Ozagrel	30 ml/Day	14 days	ORR, NIHSS, BVI, AE
Zhang T (2018)	50/50	43.23 ± 1.34 (mean)	42.96 ± 1.48 (mean)	CT+GDI vs CT	–	30 ml/Day	14 days	ORR, NIHSS, CRP, BI
Zheng XH (2018)	50/50	64.1 ± 3.0 (mean)	68.2 ± 3.4 (mean)	CT+GDI vs CT	GM1	20 ml/Day	14 days	ORR, BLI
Zhou J (2016)	39/39	64.8 ± 11.1 (mean)	64.2 ± 11.2 (mean)	CT+GDI vs CT	Ozagrel	40 ml/Day	14 days	ORR, NIHSS
Zhou M (2010)	60/60	64.3 ± 7.9 (mean)	62.5 ± 6.8 (mean)	CT+GDI vs CT	–	20 ml/Day	14 days	ORR

Con, control group (conventional treatments alone group); Exp, experimental group (conventional treatments and GDI combined group). ORR, overall response rate; CT, conventional treatments; GDI, Ginkgo leaf extract and dipyridamole injection; GM1, monosialotetrahexosylganglioside; NIHSS, National Institutes of Health Stroke Scale; BI, Barthel Index score; BVI, Blood Viscosity Index; BLI, Blood lipid index; CPR, plasma C reactive protein; AE, adverse events.

to −1.48, $P < 0.00001$). There was statistical heterogeneity in CRP ($P < 0.00001$, $I^2 = 92\%$) according to the heterogeneity test. Therefore, the random effects model was used to pool this meta-analysis.

Hemorrheology Assessment

The hemorrheology of ischemic stroke patients was measured between GDI and non-GDI groups in eleven controlled studies (Tang et al., 2009; Long, et al., 2010; Chen, et al., 2011; Ding, 2013; Tang, 2013; Jiang, 2014; Yang, 2014; Li, 2016; Wei, 2017; Zhang, 2017; Yi et al., 2018) (**Supplementary Figure 3**). In this analysis, our results showed that the hemorrheology of ischemic stroke patients received combined therapy was significantly improved compare to those treated by conventional treatments alone, indicated by significantly reduced WBV (OR = −1.32, 95% CI = −1.40 to −1.24, $P < 0.00001$), PV (OR = −0.34, 95% CI = −0.51 to −0.17,

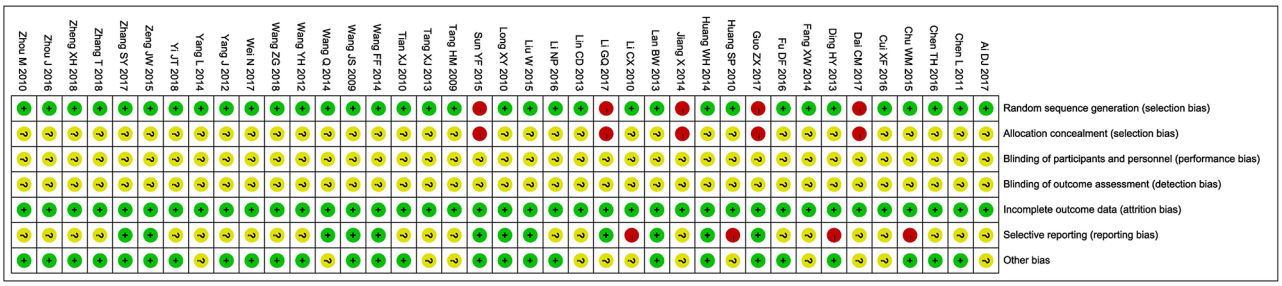


FIGURE 2 | Risk of bias summary: review of authors' judgments about each risk of bias item for included studies. Each color represents a different level of bias: red for high-risk, green for low-risk, and yellow for unclear-risk of bias.

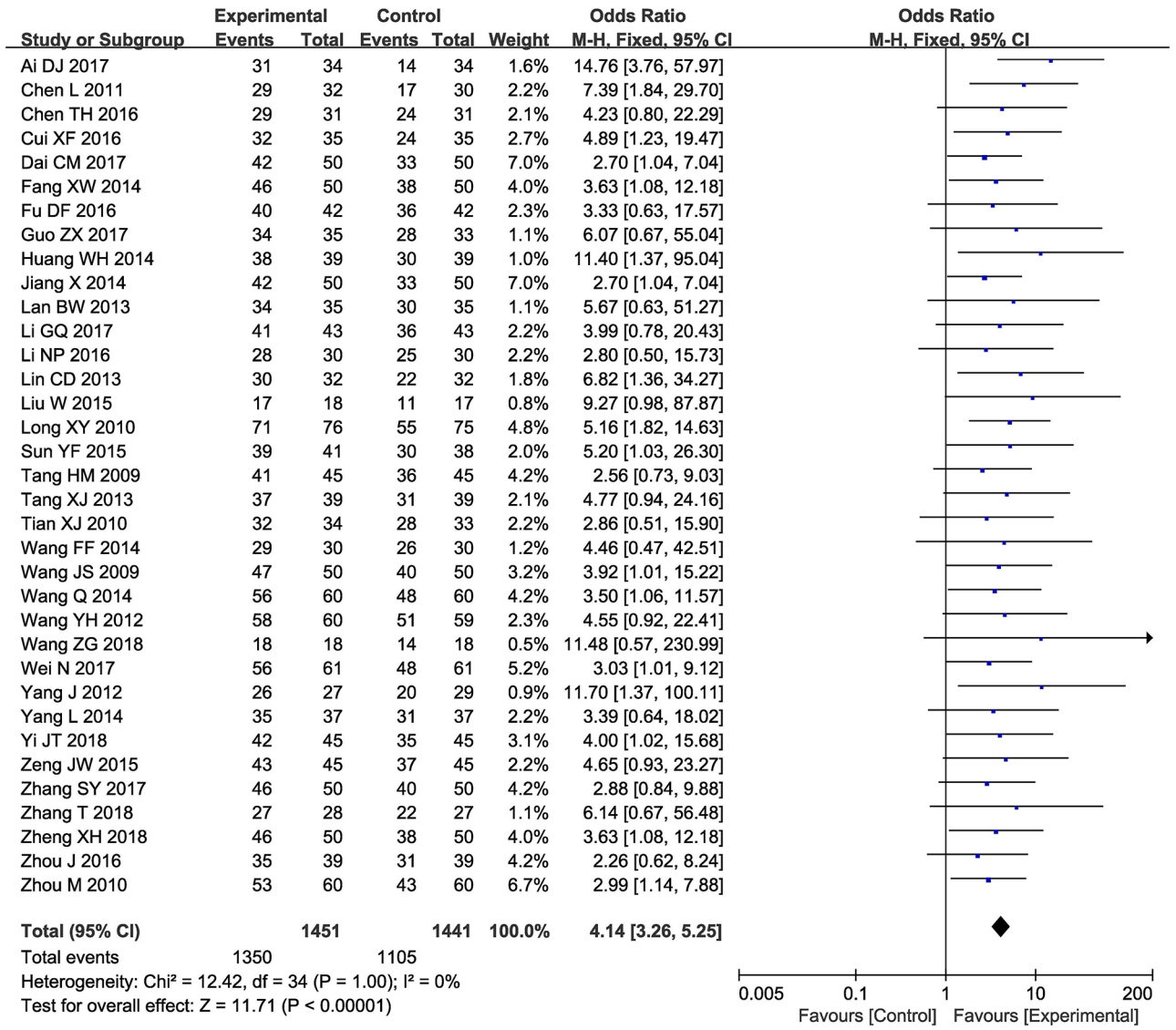


FIGURE 3 | Forest plot of the comparison of overall response rate (ORR) between the experimental and control group. Control group, conventional treatments alone group; Experimental group, conventional treatments and GDI combined group. GDI, Ginkgo leaf extract and dipyridamole injection. The fixed-effects meta-analysis model (Mantel-Haenszel method) was used.

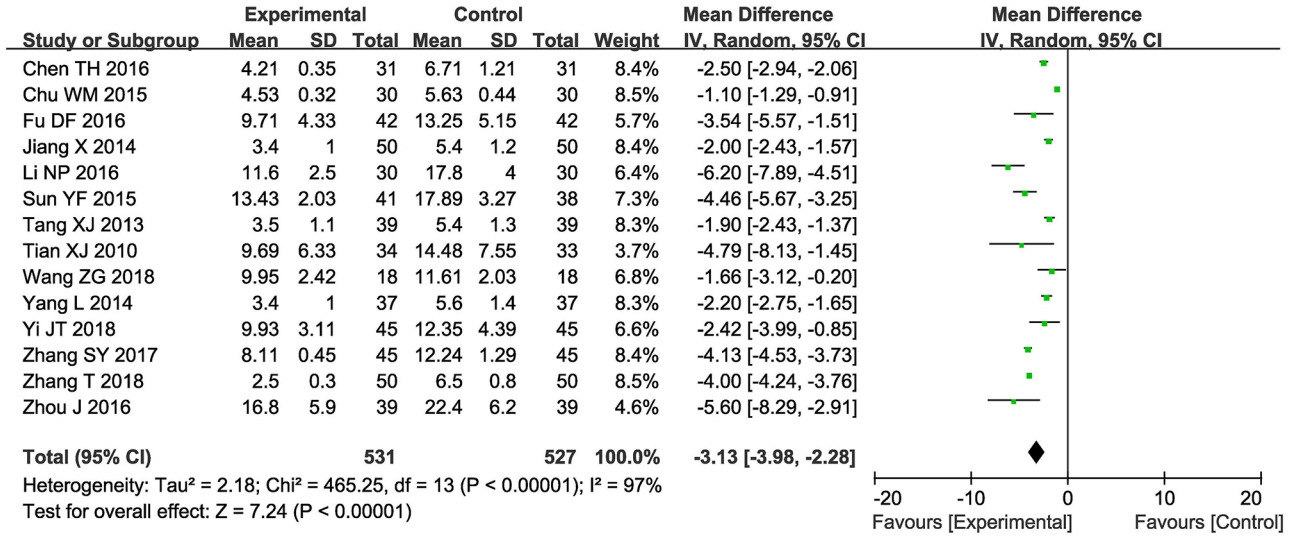


FIGURE 4 | Forest plot of the comparison of National Institutes of Health Stroke Scale (NIHSS) between the experimental and control group. Control group, conventional treatments alone group; Experimental group, conventional treatments and GDI combined group. GDI, Ginkgo leaf extract and dipyridamole injection. The random effects meta-analysis model (Inverse Variance method) was used.

$P < 0.0001$), WBHV (OR = −1.64, 95% CI = −2.39 to −0.89, $P < 0.0001$), WBLV (OR = −1.56, 95% CI = −2.33 to −0.79, $P < 0.0001$) and FIB (OR = −0.55, 95% CI = −1.43 to −0.34, $P = 0.002$). WBV ($P = 0.99$, $I^2 = 0\%$) was not heterogeneous among the studies, so fixed-effect model was used to analyzing its OR. Otherwise, random-effect model was used.

Blood Lipid Assessment

There were three studies (Tian et al., 2010; Chu 2015; Zheng et al., 2018) reported the amelioration of blood lipid after the treatment of GDI and conventional therapy (**Supplementary Figure 4**). The meta-analysis revealed that the blood lipid level of patients was significantly improved compared with the conventional treatments alone, indicated by obviously decreased levels of TC (OR = −0.65, 95% CI = −0.82 to −0.48, $P < 0.00001$), TG (OR = −0.86, 95% CI = −1.24 to −0.49, $P < 0.00001$) and LDL-C (OR = −0.97, 95% CI = −1.24 to −0.70, $P < 0.00001$), and significantly increased HDL-C levels (OR = 0.23, 95% CI = 0.12–0.33, $P < 0.0001$) in blood. HDL-C ($P = 0.68$, $I^2 = 0\%$) was not heterogeneous among the studies, so fixed-effect model was used to analyzing its OR. Otherwise, random-effect model was used.

Adverse Events Assessment

Thirteen trials (Wang et al., 2009; Long et al., 2010; Ding, 2013; Lan, 2013; Wang, 2014a; Wang, 2014b; Huang et al., 2014; Liu, 2015; Sun, 2015; Zeng, 2015; Li, 2017; Guo, 2017; Zhang, 2017) involving 1,052 ischemic stroke patients evaluated the safety of GDI mediated therapy. The most common side effects of GDI treatment were fever, fullness in head, allergy, hemorrhage, palpitation, nausea and vomiting which usually subsided after symptomatic treatment. No severe adverse event occurred during GDI treatment, and the occurrence of these adverse reactions in the two groups was similar (**Figure 6**, Total side effects: OR = 0.74, 95% CI = 0.51–1.09, $P = 0.13$; Fever: OR = 0.85, 95% CI = 0.30–2.39, $P = 0.75$; Fullness in head: OR = 0.84, 95% CI = 0.29–2.45, $P = 0.75$; Allergy: OR = 0.49, 95% CI = 0.17–1.42, $P = 0.19$; Hemorrhage: OR = 1.00, 95% CI = 0.25–4.08, $P = 1.00$; Palpitation: OR = 2.08, 95% CI = 0.50–8.61,

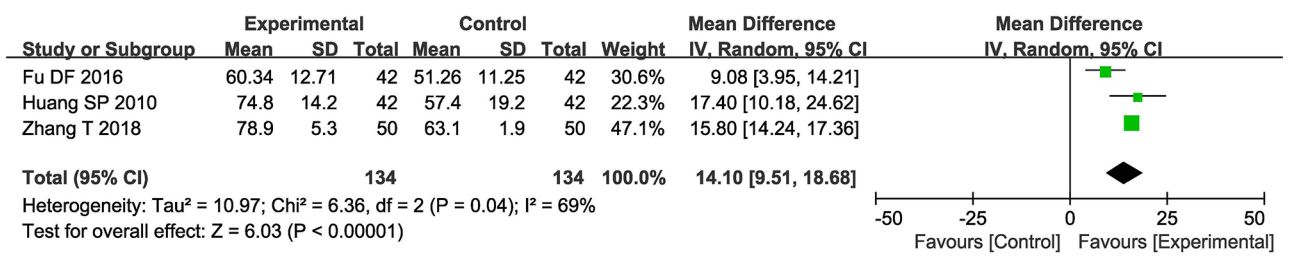


FIGURE 5 | Forest plot of the comparison of Barthel Index (BI) score between the experimental and control group. Control group, conventional treatments alone group; Experimental group, conventional treatments and GDI combined group. GDI, Ginkgo leaf extract and dipyridamole injection. The random effects meta-analysis model (Inverse Variance method) was used.

$P = 0.31$; Nausea and vomiting: OR = 1.00, 95% CI = 0.24–4.13, $P = 1.00$). Fixed-effect models were used to analyze OR rate because of low heterogeneity.

Publication Bias

Publication bias was assessed visually by funnel plots. As shown in **Figure 7**, the funnel plots were symmetrical in NIHSS and total adverse events (TAE), but were asymmetrical in ORR.

We further assessed publication bias by Begg's and Egger's regression tests, and ORR was found with bias (Begg = 0.001; Egger = 0.001). No significant publication bias for NIHSS (Begg = 0.584; Egger = 0.638) and total side effects (Begg = 0.855; Egger = 0.986) was observed in these analyses. To determine if the bias affect the pooled risk of ORR, we conducted trim and filled analysis. The adjusted OR indicated same trend with the result of the primary analysis (before: $P < 0.0001$, after: $P < 0.0001$), reflecting the reliability of our primary conclusions.

Sensitivity Analysis

We also conducted subgroup analysis to explore the source of heterogeneity in ORR, NIHSS and TAE with respect to GDI dosages, sample sizes and types of involved studies. As shown in **Table 2**, our analysis results showed that no significant difference was found between different dosages of GDI, sample sizes and study types in ORR and NIHSS. Moreover, our results showed that GDI may alleviate the TAE caused by routine treatments when its dosage not more than 20 ml/day.

DISCUSSION

Traditional Chinese medicine has been used to treat ischemic stroke in China during the past two thousand years. A survey in China showed that about 70% of doctors surveyed indicated that Chinese herb were effective complementary therapies for ischemic stroke (Zeng et al., 2005). GDI, a kind of Chinese medicine preparation, has been clinically applied as an effective adjuvant agent for reducing brain injuries, and enhancing functional recovery (Nash and Shah, 2015; Wang et al., 2015; Li et al., 2017). Even though there was statistical analysis of published literatures, a comprehensive and systematic evaluation of GDI for the treatment of ischemia stroke is still rare. In this analysis, we conducted a wide range of online search according strict inclusion and exclusion criteria, by which to provide an internationally accessible systematic review of the clinical efficacy and safety of GDI for the ischemia stroke.

The meta-analysis was carried out in thirty-five articles (Tang et al., 2009; Wang et al., 2009; Tian et al., 2010; Long et al., 2010; Zhou et al., 2010; Chen et al., 2011; Wang, 2012; Yang, 2012; Tang, 2013; Lan, 2013; Lin and Lin, 2013; Huang et al., 2014; Fang, 2014; Jiang, 2014; Wang, 2014a; Wang, 2014b; Yang, 2014; Liu, 2015; Zeng,

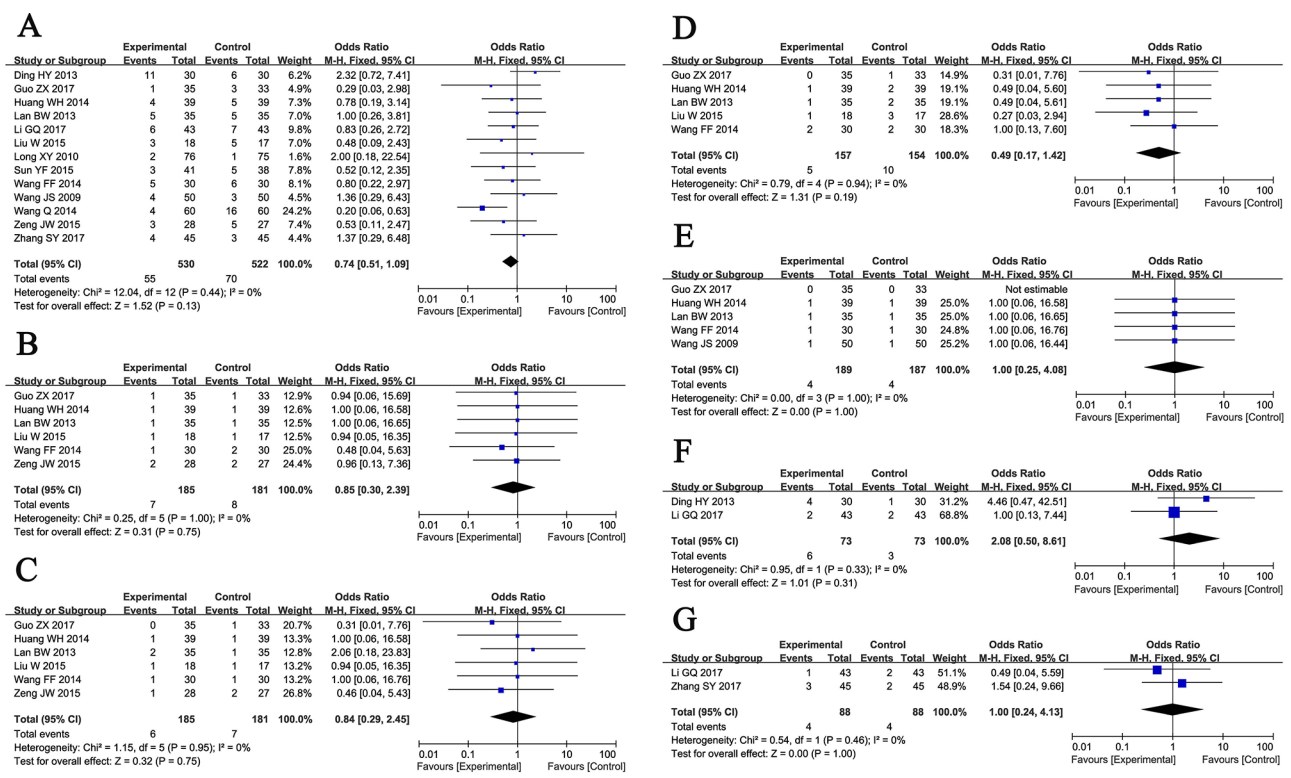


FIGURE 6 | Forest plot of the comparison of adverse effects including total adverse effects **(A)**, fever **(B)**, fullness in head **(C)**, allergy **(D)**, hemorrhage **(E)**, palpitation **(F)**, nausea and vomiting **(G)** between the experimental and control group. Control group, conventional treatments alone group; Experimental group, conventional treatments and GDI combined group; GDI, Ginkgo leaf extract and dipyridamole injection. The fixed-effects meta-analysis model (Mantel-Haenszel method) was used.

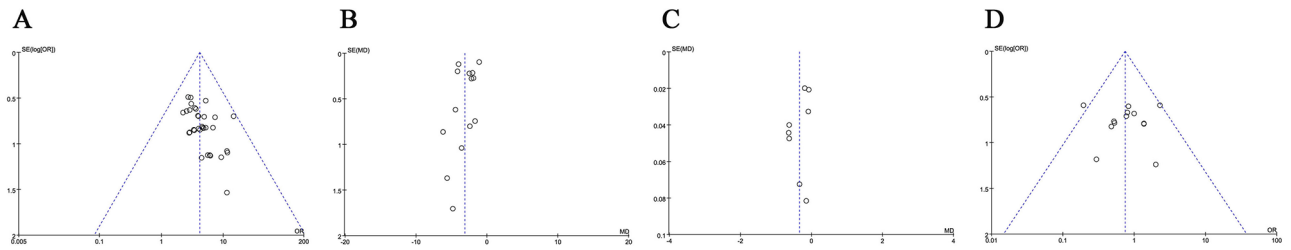


FIGURE 7 | Funnel plot of overall response rate (ORR, **A**), National Institutes of Health Stroke Scale (NIHSS, **B**), plasma viscosity (PV, **C**) and total adverse effects (TAE, **D**).

TABLE 2 | Subgroup analyses of ORR, NIHSS and TAE between the experimental and control group.

Parameter	Factors at study level	Analysis	Heterogeneity		Odds Ratio	95% CI	*P*-value
		Method	I^2 (%)	*P*-value	(OR)		
ORR	**Dosage of GDI**						
	20ml/day	Fixed	0	1.00	3.95	3.00–5.21	<0.00001
	>20ml/day	Fixed	0	0.71	4.83	2.97–7.87	<0.00001
	Study sample size						
	>80	Fixed	0	1.00	3.41	2.52–4.62	<0.00001
	<80	Fixed	0	0.99	5.53	3.75–8.14	<0.00001
	Type of control trials						
	RCTs	Fixed	0	1.00	4.34	3.34–5.64	<0.00001
	Non-RCTs	Fixed	0	0.91	3.30	1.89–5.77	<0.0001
NIHSS	**Dosage of GDI**						
	20ml/day	Fixed	83	<0.00001	–3.01	–3.77 to –2.25	<0.00001
	>20ml/day	Fixed	99	<0.00001	–3.32	–5.07 to –1.57	0.0002
	Study sample size						
	>80	Random	94	<0.00001	–3.26	–4.25 to –2.26	<0.00001
	<80	Random	93	<0.00001	–2.94	–3.79 to –2.09	<0.00001
	Type of control trials						
	RCTs	Random	98	<0.00001	–3.14	–4.11 to –**2**.18	<0.00001
	Non-RCTs	Random	93	0.0002	–3.16	–5.57 to –0.76 3	0.01
TAE	**Dosage of GDI**						
	20ml/day	Fixed	0	0.64	0.58	0.36–0.91	0.02
	>20ml/day	Fixed	0	0.48	1.40	0.68–2.87	0.36
	Study sample size						
	>80	Fixed	41	0.15	0.63	0.35–1.15	0.13
	<80	Fixed	0	0.66	0.83	0.51–1.37	0.46
	Type of control trials						
	RCTs	Fixed	19	0.27	0.78	0.51–1.20	0.26
	Non-RCTs	Fixed	0	0.71	0.61	0.26–1.42	0.25

GDI, Ginkgo leaf extract and dipyridamole injection; ORR, overall response rate; NIHSS, National Institutes of Health Stroke Scale; TAE, total adverse events; RCTs, randomized controlled trials.

2015; Sun, 2015; Chen, 2016; Li, 2016; Zhou et al., 2016; Cui, 2016; Fu et al., 2016; Wei, 2017; Guo, 2017; Ai, 2017; Zhang, 2017; Dai, 2017; Li, 2017; Wang, 2018; Yi et al., 2018; Zhang, 2018; Zheng et al., 2018) to evaluate the ORR. Compared with conventional treatments alone, GDI combined with conventional treatments was associated with obviously higher ORR. Moreover, the combination therapy also significantly improved the neurological status and activity of daily living of ischemic stroke patients. CRP has important value in the prediction, prevention and prognosis of ischemic stroke (Matsuo et al., 2016; Yu et al., 2019). Our analysis results showed that the CRP level of patients was obviously decreased after conventional treatments and GDI combined therapy. Moreover, hemorheology and blood lipids indexes of patients were also significantly ameliorated. All these results indicated that GDI can protect ischemic stroke from injury, which may be related with its action on regulating the blood viscosity and level of blood lipid.

Safety is the top priority of a therapeutic strategy, and also a key factor for their clinical application and further development. This analysis confirmed the safety of GDI in ischemic stroke treatment. The most common side effects during GDI therapy were fever, fullness in head, allergy, hemorrhage, palpitation, nausea, and vomiting, and all of them did not differ significantly between the two groups. Therefore, GDI is a safe auxiliary medicine for ischemic stroke.

The analysis on therapeutic effects may be influenced by several factors. We used three clinical variables (GDI dosages, sample sizes,

and research types) to interact with three outcome indicators (ORR, NIHSS, and TAE) and found that the TAE might be associated with GDI dosages. However, recent studies on the impact of these factors on the curative effect of GDI adjuvant therapy remain insufficient and further investigations such as biobliographic references that support this statement still should be performed.

There are some limitations in our analysis. As an important Chinese herb preparation, GDI was mainly applied in China, which may bring the unavoidable regional bias and subsequently influence the clinical application of GDI worldwide. In other countries such as America, India and Iran, *G. biloba* extract has also been used for acute ischemic stroke treatment and the prevention of cognitive decline (Garg et al., 1995; Dodge et al., 2008; Oskouei et al., 2013), but these studies were eventually excluded because they did not meet the inclusion criteria. We will keep following the updated researches on GDI mediated therapy for ischemic stroke in the world, and perform further systematical research on it. Moreover, several results showed significantly heterogeneity among the included trials, which may be due to the different ages of ischemic stroke patients and routine drug types. Therefore, the findings from our study should be dealt with some caution. Finally, a possible interaction between other drugs and ginkgo should be considered. However, our data were extracted from published papers and they did not provide sufficient information on this aspect. Therefore, based on currently available literatures, there are insufficient data to perform a statistical analysis to evaluate the correlation. We will keep paying close attention to this concern in our later studies

CONCLUSION

In summary, this meta-analysis indicated that GDI combined with conventional treatments was effective in treating ischemic stroke. Clinical application of GDI not only obviously enhanced the ORR of conventional treatments, but also effectively improved the blood viscosity and blood lipid level of ischemic stroke patients. However, because the low quality of some included trials increases risks and bias, the clinical efficacy and safety of GDI-mediate therapy for ischemic stroke still needs methodologically rigorous trials to verify.

DATA AVAILABILITY STATEMENT

All datasets generated for this study are included in the article/ **Supplementary Material**.

AUTHOR CONTRIBUTIONS

SL and ZM put forward this topic and designed this study. PX and ZM performed article screening, data collection and extraction, and manuscript writing. PX, ZM, and SL conducted the data analysis. SL polished the written English.

SUPPLEMENTARY MATERIAL

The Supplementary Material for this article can be found online at: https://www.frontiersin.org/articles/10.3389/fphar.2019.01403/full#supplementary-material

SUPPLEMENTARY FIGURE 1 | Sensitivity Analysis for National Institutes of Health Stroke Scale (NIHSS).

SUPPLEMENTARY FIGURE 2 | Forest plot of the comparison of plasma C reactive protein (CRP) between the experimental and control group. Control group, conventional treatments alone group; Experimental group, conventional treatments and GDI combined group. GDI, Ginkgo leaf extract and dipyridamole injection. The random effects meta-analysis model (Inverse Variance method) was used.

SUPPLEMENTARY FIGURE 3 | Forest plot of the comparison of the hemorrheology indexes including WBV **(A)**, PV **(B)**, WBHSV **(C)**, WBLSV **(D)** and FIB **(E)** between the experimental and control group. Control group, conventional treatments alone group; Experimental group, conventional treatments and GDI combined group. WBV, whole blood viscosity; PV, plasma viscosity; WBHSV, whole blood high-shear viscosity; WBLSV, whole blood low-shear viscosity; FIB, content of fibrinogen; GDI, Ginkgo leaf extract and dipyridamole injection.

SUPPLEMENTARY FIGURE 4 | Forest plot of the comparison of the blood lipid indexes including TC **(A)**, TG **(B)**, HDL-C **(C)** and LDL-C **(D)** between the experimental and control group. Control group, conventional treatments alone group; Experimental group, conventional treatments and GDI combined group. TC, plasma total cholesterol; TG, triglycerides; HDL-C, high density lipoprotein-cholesterol; LDL-C, low density lipoprotein-cholesterol; GDI, Ginkgo leaf extract and dipyridamole injection.

REFERENCES

Ai, D. J. (2017). Effective method and effect analysis of drug treatment for cerebral infarction sequela. *Med. Inform.* 30, 116–117. doi: 10.3969/j.issn.1006-1959.2017.05.074

Chen, L., Zhang, T. Z., and Li, M. L. (2011). Therapeutic effect observation of gingko dipyridamole for acute cerebral infarction. *Healthmust-Readmagazine* 9, 49.

Chen, Z., Xue, T., Huang, H., Xu, J., Shankar, S., Yu, H., et al. (2019). Efficacy and safety of sonothombolysis versus non-sonothombolysis in patients with acute ischemic stroke: a meta-analysis of randomized controlled trials. *PloS One* 14, e0210516. doi: 10.1371/journal.pone.0210516

Chen, T. H. (2016). Clinical observation of ginkgo leaf extract and dipyridamole injection in the treatment of type 2 diabetes patients with cerebral infarction. *Shenzhen J. Integr. Trad. Chin. West. Med.* 26, 27–28. doi: 10.16458/j.cnki.1007-0893.2016.18.013

Chu, W. M. (2015). Observation on efficacy of ginkgo leaf extract and dipyridamole injection in treatment of ischemic stroke patients. *China Trop. Med.* 15, 115–117. doi: 10.13604/j.cnki.46-1064/r.2015.01.041

Cui, X. F. (2016). Application effect analysis of gingko dipyridamole and ozagrel for the treatment of cerebral infarction. *Clin. Res.* 24, 103–104.

Dai, C. M. (2017). Effective observation of aspirin combined with gingko dipyridamole injection in the treatment of acute cerebral infarction. *China Health Care Nutrit.* 27, 104–105.

Ding, H. Y. (2013). Gingko dipyridamole injection combined with ganglioside for the treatment of 30 cases patients with acute cerebral infarction Shaanxi J. *Trad. Chin. Med.* 34, 288–289.

Dodge, H. H., Zitzelberger, T., Oken, B. S., Howieson, D., and Kaye, J. (2008). A randomized placebo-controlled trial of Ginkgo biloba for the prevention of cognitive decline. *Neurology* 70, 1809–1817. doi: 10.1212/01.wnl.0000303814.13509.db

Fang, X. W. (2014). Effect of ginkgo-dipyidamolum injection on CRP, IL-6 and sICAM-1 in the patients with type 2 diabetic with cerebral infraction. *J. Hunan Normal Univ. (Med. Sci.)* 11, 81–84.

Fu, D. F., Qiu, J., Yu, S. R., and Li, W. H. (2016). Clinical experience of gingko dipyridamole in treating 42 cases patients with acute cerebral infarction. *Stud. Trace Elem. Health* 33, 13–14.

Garg, R. K., Nag, D., and Agrawal, A. (1995). A double blind placebo controlled trial of ginkgo biloba extract in acute cerebral ischaemia. *J. Assoc. Physicians. India.* 43, 760–763.

Guo, Z. X. (2017). Clinical efficacy observation of gingko dipyridamole combined with Ozagrel injection in the treatment of cerebral infarction. *Med. Inform.* 30, 84–85. doi: 10.3969/j.issn.1006-1959.2017.12.052

Huang, S. P., and Yuan, D. Y. (2010). Curative effect observation of gingko dipyridamole injection and early rehabilitation therapy in treating 42 cases of patients with cerebral infarction. *Chin. J. Trad. Med. Sci. Tech.* 17, 63–64. doi: 10.3969/j.issn.1005-7072.2010.01.029

Huang, W. H., Qiu, Z. X., and Zeng, X. (2014). Clinical observation of gingko dipyridamole combined with Ozagrel injection in the treatment of cerebral infarction. *Shenzhen J. Integr. Trad. Chin. West. Med.* 24, 26–27.

Jackson, D., White, I. R., and Riley, R. D. (2012). Quantifying the impact of between-study heterogeneity in multivariate meta-analyses. *Stat. Med.* 31, 3805–3820. doi: 10.1002/sim.5453

Jiang, X. (2014). Discussion on clinical efficacy of gingko dipyridamole combined with aspirin in the treatment of acute cerebral infarction. *China Foreign Med. Treat.* 29, 144–146. doi: 10.3969/j.issn.1674-0742.2014.29.074

Kampkotter, A., Pielarski, T., Rohrig, R., Timpel, C., Chovolou, Y., and Watjen, W. (2007). The Ginkgo biloba extract EGb761 reduces stress sensitivity, ROS accumulation and expression of catalase and glutathione S-transferase 4 in Caenorhabditis elegans. *Pharmacol. Res.* 55, 139–147. doi: 10.1016/j.phrs.2006.11.006

Lan, B. W. (2013). Effective observation of gingko dipyridamole combined with ozagrel injection in the treatment of cerebral infarction. *Chin. J. Med. Guide* 15, 1477–1479. doi: 10.3969/j.issn.1009-0959.2013.09.061

Li, S., Zhang, X., Fang, Q., Zhou, J., Zhang, M., Wang, H., et al. (2017). Ginkgo biloba extract improved cognitive and neurological functions of acute ischaemic stroke: a randomised controlled trial. *Stroke Vasc. Neurol.* 2, 189–197. doi: 10.1136/svn-2017-000104

Li, C. X. (2010).Clinical analysis of gingko dipyridamole in the treatment of patients with massive cerebral infarction. *China Foreign Med. Treat.* 29, 123. doi: 10.3969/j.issn.1674-0742.2010.09.095

Li, N. P. (2016). Clinical observation on treating ACI with the Yinxing Damo decoction. *Clin. J. Chin. Med.* 8, 65–66. doi: 10.3969/j.issn.1674-7860.2016.26.035

Li, G. Q. (2017). Clinical efficacy investigation of edaravone combined with gingko dipyridamole in the treatment of acute cerebral infarction. *For All Health* 11, 178. doi: 10.3969/j.issn.1009-6019.2017.01.238

Liang, M., Chen, Q., Zhang, Y., He, L., Wang, J., Cai, Y., et al. (2017). Impact of diabetes on the risk of bedsore in patients undergoing surgery: an updated quantitative analysis of cohort studies. *Oncotarget* 8, 14516–14524. doi: 10.18632/oncotarget.14312

Lin, C. D., and Lin, C. S. (2013). Randomized parallel controlled study of Yinxing Damo injection combined with Kelinao in the treatment of acute cerebral infarction. *J. Pract. Trad. Chin. Inter. Med.* 27, 50–51. doi: 10.3969/j.issn.1671-7813.2013.06(s).26

Lin, L., Chu, H., Murad, M. H., Hong, C., Qu, Z., Cole, S. R., et al. (2018). Empirical Comparison of Publication Bias Tests in Meta-Analysis. *J. Gen. Intern. Med.* 33 (8), 1260–1267. doi: 10.1007/s11606-018-4425-7

Liu, Q., Jin, Z., Xu, Z., Yang, H., Li, L., Li, G., et al. (2019). Antioxidant effects of ginkgolides and bilobalide against cerebral ischemia injury by activating the Akt/Nrf2 pathway *in vitro* and *in vivo*. *Cell Stress Chaperones*. 24, 441–452. doi: 10.1007/s12192-019-00977-1

Liu, W. (2015). Effect analysis of Ozagrel and gingko dipyridamole in the treatment of acute cerebral infarction. *Contemp. Med. Forum.* 13, 270–271.

Long, X. Y., Jiang, M. C., Yin, L. P., and Lin, Y. H. (2010). Clinical analysis of low molecular weight heparin combined with gingko dipyridamole in the treatment of acute cerebral infarction. *Med. Inform.* 5, 487–489. doi: 10.3969/j.issn.1006-1959-c.2010.03.025

Ma, X., Yang, Y. X., Chen, N., Xie, Q., Wang, T., He, X., et al. (2017). Meta-Analysis for Clinical Evaluation of Xingnaojing Injection for the Treatment of Cerebral Infarction. *Front. Pharmacol.* 8, 485. doi: 10.3389/fphar.2017.00485

Matsuo, R., Ago, T., Hata, J., Wakisaka, Y., Kuroda, J., Kuwashiro, T., et al. (2016). Plasma C-Reactive Protein and Clinical Outcomes after Acute Ischemic Stroke: A Prospective Observational Study. *PloS One* 11, e0156790. doi: 10.1371/journal.pone.0156790

Nash, K. M., and Shah, Z. A. (2015).Current Perspectives on the Beneficial Role of Ginkgo biloba in Neurological and Cerebrovascular Disorders. *Integr. Med. Insights* 10, 1–9. doi: 10.4137/IMI.S25054

Oskouei, D. S., Rikhtegar, R., Hashemilar, M., Sadeghi-Bazargani, H., Sharifi-Bonab, M., Sadeghi-Hokmabadi, E., et al. (2013). The effect of Ginkgo biloba on functional outcome of patients with acute ischemic stroke: a double-blind, placebo-controlled, randomized clinical trial. *J. Stroke Cerebrovasc. Dis.* 22, e557–e563. doi: 10.1016/j.jstrokecerebrovasdis.2013.06.010

Sun, Y. F. (2015). Study on the clinical efficacy and safety of Yinxingdamo injection combined with edaravone in treatment of acute cerebral infarction. *China Foreign Med. Treat.* 34, 158–160. doi: 10.3969/j.issn.1674-0742.2015.28.065

Tan, D., Wu, J. R., Cui, Y. Y., Zhao, Y., Zhang, D., Liu, S., et al. (2018). Ginkgo Leaf Extract and Dipyridamole Injection as Adjuvant Treatment for Angina Pectoris: A Meta-Analysis of 41 Randomized Controlled Trials. *Chin. J. Integr. Med.* 24, 930–937. doi: 10.1007/s11655-018-2557-6

Tang, H. M., Tang, H. N., and Chen, X. (2009). Effective observation of aspirin combined with gingko dipyridamole injection in the treatment of acute cerebral infarction. *Chin. J. Misdiagnostics* 9, 8844–8845.

Tang, X. J. (2013). Curative effect observation of aspirin combined with gingko dipyridamole for patients with acute cerebral infarction. *Hebei Med. J.* 35, 1188–1189. doi: 10.3969/j.issn.1002-7386.2013.08.033

Tian, X. J., Hao, J., Ji, S. B., Wang, Y. M., Li, H. H., Xing, H. X., et al. (2010). Clinical analysis of gingko dipyridamole combined with fibrinolytic enzyme in the treatment of early cerebral infarction. *Lishizhen Med. Mater. Med. Res.* 21, 20183–20184. doi: 10.3969/j.issn.1008-0805.2010.08.112

Tulsulkar, J., Glueck, B., Hinds, T. D. Jr., and Shah, Z. A. (2016). Ginkgo biloba Extract Prevents Female Mice from Ischemic Brain Damage and the Mechanism Is Independent of the HO1/Wnt Pathway. *Transl. Stroke Res.* 7, 120–131. doi: 10.1007/s12975-015-0433-7

Wang, J. S., Xia, S. L., Li, Z. Z., and Li, X. C. (2009). Role of Ginkgo bilobate extract combined with nimodipine in the treatment of early cerebral infarction. *Chin. J. Ethnomed. Ethnopharm.* 18, 101–102. doi: 10.3969/j.issn.1007-8517.2009.15.070

Wang, L., Zhang, T., and Bai, K. (2015). [System evaluation on Ginkgo Biloba extract in the treatment of acute cerebral infarction]. *J. Cent. South Univ. (Med. Sci.)* 40, 1096–1102. doi: 10.11817/j.issn.1672-7347.2015.10.007

Wang, Y. H. (2012). Clinical effect observation of gingko dipyridamole combined with aspirin in the treatment of acute cerebral infarction. *China Health Care Nutrit.* 22, 2126. doi: 10.3969/j.issn.1004-7484(x).2012.07.455

Wang, F. F. (2014a). Clinical observation of gingko dipyridamole combined with Ozagrel injection in the treatment of advanced cerebral infarction. *For All Health* 8, 171–172. doi: 10.3969/j.issn.1009-6019.2014.12.227

Wang, Q. (2014b). Clinical efficacy observation of gingko dipyridamole combined with aspirin in the treatment of acute cerebral infarction. *China Prac. Med.* 9, 134–135.

Wang, Z. G. (2018). Clinical Study of gingko dipyridamole combined with Ozagrel intravenous drop in the treatment of cerebral infarction. *Health Guide* 31, 72. doi: 10.3969/j.issn.1006-6845.2018.31.065

Wei, N. (2017). Effect of Yinxingdamo injection and edaravone on the hemorheology and curative effect of patients with stroke. *Syst. Med.* 2, 33–36. doi: 10.19368/j.cnki.2096-1782.2017.06.033

Xue, P., Wang, M., and Yan, G. (2018). Mesenchymal stem cell transplantation as an effective treatment strategy for ischemic stroke in Asia: a meta-analysis of controlled trials. *Ther. Clin. Risk. Manage.* 14, 909–928. doi: 10.2147/TCRM.S161326

Yang, J. (2012). Clinical observation of gingko dipyridamole in the treatment of 56 cases of cerebral infarction. *J. Front. Med.* 2, 157–158. doi: 10.3969/j.issn.2095-1752.2012.12.148

Yang, L. (2014). Clinical efficacy of gingko dipyridamole combined with aspirin in the treatment of acute cerebral infarction. *For All Health* 8, 491.

Yi, J. T., Wang, C. P., and Jia, M. (2018). Effect of Ginkgo Biloba on fibrinolytic function and platelet parameters in patients with acute cerebral infarction. *Chin. J. Thromb. Hemostasis* 24, 1004–1006. doi: 10.3969/j.issn.1009-6213.2018.06.035

Yu, B., Yang, P., Xu, X., and Shao, L. (2019). C-reactive protein for predicting all-cause mortality in patients with acute ischemic stroke: a meta-analysis. *Biosci. Rep.* 39. doi: 10.1042/BSR20181135

Zeng, X., Liu, M., Yang, Y., Li, Y., and Asplund, K. (2005). Ginkgo biloba for acute ischaemic stroke. *Cochrane Database Syst. Rev.* 4, CD003691.

Zeng, X., Zhang, Y., Kwong, J. S., Zhang, C., Li, S., Sun, F., et al. (2015). The methodological quality assessment tools for preclinical and clinical studies, systematic review and meta-analysis, and clinical practice guideline: a systematic review. *J. Evid. Based Med.* 8, 2–10. doi: 10.1111/jebm.12141

Zeng, J. W. (2015). Efficacy and safety analysis of gingko dipyridamole adjuvant therapy for the treatment of cerebral infarction. *Mod. Diag. Treat.* 26, 94–95.

Zhang, Y., Liu, J., Yang, B., Zheng, Y., Yao, M., Sun, M., et al. (2018). Ginkgo biloba Extract Inhibits Astrocytic Lipocalin-2 Expression and Alleviates Neuroinflammatory Injury via the JAK2/STAT3 Pathway After Ischemic Brain Stroke. *Front. Pharmacol.* 9, 518. doi: 10.3389/fphar.2018.00518

Zhang, S. Y. (2017). Therapeutic effect observation and evaluation of gingko dipyridamole injection combined with Ozagrel on cerebral infarction. *Pract. Clin. J. Integr. Trad. Chin. West. Med.* 17, 42–43. doi: 10.13638/j.issn.1671-4040.2017.05.025

Zhang, T. (2018). Clinical study of Ginkgo Leaf Extract and Dipyridamole injection in the treatment of young and middle-aged patients with acute cerebral infarction. *China Mod. Med.* 25, 132–134. doi: 10.3969/j.issn.1674-4721.2018.01.041

Zheng, X. H., Zheng, X. D., Xiao, L., and Peng, K. J. (2018). Effect of gingko dipyridamole combined with monosialotetrahexosylganglioside on blood lipid level in patients with cerebral infarction. *Jiangxi Med. J.* 53, 144–146. doi: 10.3969/j.issn.1006-2238.2018.2.020

Zhou, M., Tong, L. G., and Feng, J. (2010). Effect observation of gingko dipyridamole injection on mild cognitive impairment after ischemic stroke. *J. Emerg. Trad. Chin. Med.* 19, 21–22. doi: 10.3969/j.issn.1004-745x.2010.01.013

Zhou, J., Xiong, J., and Huang, J. (2016). Curative effect analysis of gingko dipyridamole injection combined with Ozagrel intravenous drip in the treatment of cerebral infarction. *Shenzhen J. Integr. Trad. Chin. West. Med.* 26, 134–136. doi: 10.16458/j.cnki.1007-0893.2016.19.067

Conflict of Interest: The authors declare that the research was conducted in the absence of any commercial or financial relationships that could be construed as a potential conflict of interest.

Copyright © 2019 Xue, Ma and Liu. This is an open-access article distributed under the terms of the Creative Commons Attribution License (CC BY). The use, distribution or reproduction in other forums is permitted, provided the original author(s) and the copyright owner(s) are credited and that the original publication in this journal is cited, in accordance with accepted academic practice. No use, distribution or reproduction is permitted which does not comply with these terms.

frontiers in Physiology

ORIGINAL RESEARCH
published: 19 December 2019
doi: 10.3389/fphys.2019.01528

MRI Evaluation of Axonal Remodeling After Combination Treatment With Xiaoshuan Enteric-Coated Capsule and Enriched Environment in Rats After Ischemic Stroke

*Man-Zhong Li[1,2], Yu Zhan[1,2], Le Yang[1,2], Xue-Feng Feng[1,2], Hai-Yan Zou[1,2], Jian-Feng Lei[3], Ting Zhao[1,2], Lei Wang[1,2] and Hui Zhao[1,2]**

[1] School of Traditional Chinese Medicine, Capital Medical University, Beijing, China, [2] Beijing Key Lab of TCM Collateral Disease Theory Research, Beijing, China, [3] Medical Imaging Laboratory of Core Facility Center, Capital Medical University, Beijing, China

OPEN ACCESS

Edited by:
Jing-Yan Han,
Peking University, China

Reviewed by:
Alla B. Salmina,
Krasnoyarsk State Medical University named after Prof. V.F.Voino-Yasenetski, Russia
Yi Zhang,
Beijing University of Chinese Medicine, China

***Correspondence:**
Hui Zhao
zhaohuishouyi@sina.com

Specialty section:
This article was submitted to Vascular Physiology, a section of the journal Frontiers in Physiology

Received: *11 September 2019*
Accepted: *04 December 2019*
Published: *19 December 2019*

Citation:
Li M-Z, Zhan Y, Yang L, Feng X-F, Zou H-Y, Lei J-F, Zhao T, Wang L and Zhao H (2019) MRI Evaluation of Axonal Remodeling After Combination Treatment With Xiaoshuan Enteric-Coated Capsule and Enriched Environment in Rats After Ischemic Stroke. Front. Physiol. 10:1528. doi: 10.3389/fphys.2019.01528

Xiaoshuan enteric-coated capsule (XSEC) is a compound Chinese medicine widely used for the treatment of ischemic stroke. Enriched environment (EE) is a rehabilitative intervention designed to facilitate physical, cognitive, and social activity after brain injury. This study aimed to assess whether the XSEC and EE combination could provide synergistic efficacy in axonal remodeling compared to that with a single treatment after ischemic stroke using magnetic resonance imaging (MRI) followed by histological analysis. Rats were subjected to permanent middle cerebral artery occlusion and treated with XSEC and EE alone or in combination for 30 days. T2-weighted imaging and diffusion tensor imaging (DTI) were performed to examine the infarct volume and axonal remodeling, respectively. The co-localization of Ki67 with NG2 or CNPase was examined by immunofluorescence staining to assess oligodendrogenesis. The expressions of growth associated protein-43 (GAP-43) and growth inhibitors NogoA/Nogo receptor (NgR)/RhoA/Rho-associated kinase2 (ROCK2) were measured using western blot and qRT-PCR. The Morris water maze (MWM) was performed to evaluate the cognitive function. MRI and histological measurements indicated XSEC and EE individually benefited axonal reorganization after stroke. Notably, XSEC + EE decreased infarct volume compared with XSEC or EE monotherapy and increased ipsilateral residual volume compared with vehicle group. DTI showed XSEC + EE robustly increased fractional anisotropy while decreased axial diffusivity and radial diffusivity in the injured cortex, striatum, and external capsule. Meanwhile, diffusion tensor tractography revealed XSEC + EE elevated fiber density in the cortex and external capsule and increased fiber length in the striatum and external capsule compared with the monotherapies. These MRI measurements, confirmed by histology, showed that XSEC + EE promoted axonal restoration. Additionally, XSEC + EE amplified oligodendrogenesis, decreased the expressions

of NogoA/NgR/RhoA/ROCK2, and increased the expression of GAP-43 in the peri-infarct tissues. In parallel to these findings, rats treated with XSEC + EE exhibited higher cognitive recovery than those treated with XSEC or EE monotherapy, as evidenced by MWM test. Taken together, our data implicated that XSEC + EE exerted synergistic effects on alleviating atrophy and encouraging axonal reorganization partially by promoting oligodendrogenesis and overcoming intrinsic growth-inhibitory signaling, thereby facilitating higher cognitive recovery.

Keywords: ischemic stroke, *Xiaoshuan* enteric-coated capsule, enriched environment, magnetic resonance imaging, axonal remodeling

INTRODUCTION

Ischemic stroke is one of the most common causes of morbidity and mortality worldwide (Chen et al., 2014). Although stroke mortality has been declining with effective thrombolysis, a large proportion of stroke patients exhibit long-term disability (Zhang and Chopp, 2009). Ischemic stroke induces neuronal loss and elicits profound white matter injury, as characterized by demyelination and axonal injury, which is critical for poor neurological outcomes (Wang et al., 2016; Etherton et al., 2019). Thus, it comes as no surprise that many therapeutic approaches focusing on neuroprotection in rodent models of cerebral ischemia have failed in large clinical trials (Gladstone et al., 2002). Therefore, additional attention should be paid to protect the white matter and boost axonal remodeling that may provide long-term neurological benefits after an ischemic stroke.

Xiaoshuan enteric-coated capsule (XSEC) is a Chinese herb compound preparation derived from *Buyang Huanwu* Decoction (BYHWD), a classic traditional Chinese medicinal formula for the treatment of stroke in China for centuries (Hao et al., 2012). BYHWD has shown a convincing effect on neuroprotection and neuroregeneration in stroke patients and experimental stroke animal models (Hao et al., 2012; Zhao et al., 2012; Wei et al., 2013). In particular, it has been reported that BYHWD enhances axonal remodeling and functional recovery after spinal cord injury in rats (Chen et al., 2008) and facilitates axonal regeneration of injured peripheral nerves (Chang et al., 2016; Kim and Namgung, 2018), implicating that BYHWD has a growth-promoting activity on injured axons. However, the unstable quality and lack of uniform standards of BYHWD limits its clinical use. XSEC is a novel preparation of BYHWD approved by the China Food and Drug Administration for treating stroke-induced disabilities (drug permit document: Z20000025). Our previous study demonstrated that XSEC promotes neurovascular remodeling and improves neurological function after ischemic stroke in animal models (Zhang et al., 2016). However, the effects of XSEC on axonal remodeling after stroke have not been investigated.

In recent years, enriched environment (EE) has attracted a great deal of attention in stroke rehabilitation (Janssen et al., 2014; Livingston-Thomas et al., 2016). EE is an intervention designed to facilitate physical, cognitive, and social activity by the provision of equipment and organization in the environment. In particular, many studies have shown that EE promotes the expression of trophic factors and certain transmitters; improves synaptic and axonal plasticity accompanied with reorganization of neuronal networks in the remaining brain after brain injury; and leads to learning, memory, and sensorimotor recovery, either alone or in conjunction with other therapies (Zhang X. et al., 2017; Zhang et al., 2018). Given that EE as a rehabilitative intervention has the potential to augment endogenous regenerative processes and enhance functional recovery, the therapeutic effects of XSEC on post-ischemic remodeling may be augmented in combination with EE.

Magnetic resonance imaging (MRI) is a powerful means for non-invasively monitoring the structural and functional alterations of the brain (Jiang et al., 2010b). Although EE- or BYHWD-induced axonal plasticity and repair have been well-documented in histological studies, limited studies have reported using MRI to investigate the therapeutic effects of XSEC or EE monotherapy and combination therapy on axonal remodeling in cerebral ischemic rats. Accordingly, we non-invasively evaluated axonal abnormalities of ischemic brain in rats using MRI and specifically investigated the therapeutic effects of XSEC or EE monotherapy and combination therapy on axonal remodeling in cerebral ischemic rats.

Myelin is essential for axonal structure and function. Oligodendrocytes, myelin forming cells in the central nervous system (CNS), are highly vulnerable to ischemia injury (Zhang et al., 2013). Stroke acutely induces mature oligodendrocyte damage, leading to the disruption of axonal structure. Successful regeneration of oligodendrocytes is essential for remyelination after brain injuries. It has been previously demonstrated that cerebral ischemia can stimulate the proliferation of oligodendrocyte precursor cells (OPCs) in ischemic brain (Zhang et al., 2010; Franklin and Goldman, 2015). However, endogenous oligodendrogenesis in response to stroke is limited, and most of these OPCs fail to differentiate into mature oligodendrocytes to form myelin sheaths for sprouting axons following an ischemic stroke (Cafferty et al., 2008). Preclinical studies have shown that enhancement of endogenous oligodendrogenesis by cell- and pharmacological-based therapies is closely associated with the augmentation of sprouting axons in ischemic brain (Zhang et al., 2012; Ramos-Cejudo et al., 2015).

In addition to neuronal intrinsic capacity, axonal regeneration can be constrained by intrinsic myelin-associated neurite growth inhibitors. Among them, NogoA expressed by oligodendrocytes is a principal inhibitor for axonal regrowth in injured adult CNS.

NogoA and its receptor NgR appear to exert inhibitory effects on regenerative axonal extension by activating intracellular components, RhoA and its downstream target Rho-associated kinase2 (ROCK2) (Pernet and Schwab, 2012; Fujita and Yamashita, 2014). Therefore, manipulations that amplify stroke-induced oligodendrogenesis and counteract neurite growth inhibitors may enhance axonal regeneration and functional recovery (Otero-Ortega et al., 2017). Thus, the present study further examined whether the combination treatment could induce endogenous oligodendrogenesis and overcome the intrinsic axonal growth-inhibitory pathways NogoA/NgR and RhoA/ROCK2, thus, providing us with valuable insight into the beneficial effects of a combined therapeutic approach of XSEC and EE interventions on axonal remodeling after an ischemic stroke.

MATERIALS AND METHODS

Preparation of XSEC

XSEC (batch no: 20170706) was supplied by Sanmenxia Sinoway Pharmaceutical, Co., Ltd. (Henan, China). The processing of XSEC followed a strict quality control, and the main ingredients of XSEC were subjected to standardization in our previous study (Zhang et al., 2016). XSEC was dissolved in physiological saline to a concentration of 28 mg/mL before use. The dose of XSEC (140 mg/kg) used in this study was determined based on our previous study (Li et al., 2018b).

Housing Conditions

EE housing was 90 cm long × 75 cm wide × 50 cm high, with climbing ladders, chains, different shaped tubes, plastic tunnels, and small boxes to provide sensorimotor and cognitive stimulations. Objects were changed every 2 days. Additionally, EE provided enhanced social stimulations as a total of 8–10 rats were housed together (Jiang et al., 2016). The standard housing condition was 40 cm long × 30 cm wide × 20 cm high without objects mentioned in the EE housing, and animals were housed in sets of 3 per cage.

Animals and Experimental Design

Adult male Sprague–Dawley rats (aged 8 weeks and weighing 300–320 g) were purchased from Vital River Laboratory Animal Technology, Co., Ltd. (Beijing, China). Rats were housed in a temperature (23 ± 1°C) and humidity-controlled (55 ± 10%) environment with 12-h light–dark cycles. All experimental procedures were performed according to the National Institute of Health Guide for the Care and Use of Laboratory Animals and approved by the Capital Medical University Animal Ethics Committee (Permit number: AEEI-2018-052). Efforts were made to reduce the number of animals used and avoid their suffering wherever possible.

Focal cerebral ischemia was induced in rats by permanent occlusion of the middle cerebral artery (MCAO) as described previously (Longa et al., 1989). Briefly, the rats were anesthetized under isoflurane (5% for induction and 2% for maintenance) in N_2O/O_2 (70/30). The right common carotid artery (CCA), external carotid artery (ECA), and internal carotid artery (ICA) were exposed through a midline neck incision. A 4-0 monofilament nylon suture (Beijing Sunbio Biotech, Co., Ltd., China) was inserted through the right ECA and gently advanced into the lumen of the ICA to occlude the origin of the MCA. Rats showing no behavior deficits, including rotational asymmetry and dysfunctional limb placement, were excluded from the study (Ruscher et al., 2009).

Rats with successfully induced MCAO were randomly divided into four groups: (i) vehicle group, MCAO rats were treated with saline and housed in standard condition; (ii) EE group, MCAO rats were treated with saline and housed in the EE cage; (iii) XSEC group, MCAO rats were treated with XSEC and housed in standard condition; (iv) XSEC + EE group, MCAO rats were treated with XSEC and housed in the EE cage. Sham-operated rats that were subjected to the same surgical procedure but without occlusion of the MCA were grouped under the control group. Control rats were treated with saline and housed in standard condition. XSEC and XSEC + EE treated rats were intragastrically administered with XSEC once daily for 30 consecutive days starting at 24 h after MCAO. Rats in the control, vehicle, and EE groups were administered saline at 5 mL/kg in the same manner. EE and XSEC + EE treated rats were housed in EE cages at 8:00 PM each day and returned to the standard cages at 8 AM the following day for a period of 30 days after MCAO. The testing order of the animals was based on a random number list to avoid experimental bias during the tests (random was generated by: http://www.99cankao.com/numbers/random-number-generator.php).

In vivo Analysis by MRI and Diffusion Tensor Imaging

MRI measurements were performed on the 31st day after MCAO using a 7.0T animal MRI scanner (Bruker, PharmaScan, Germany). A total of 40 rats (8 rats per group) were used.

T2-weighted imaging (T2WI) was conducted using a fast spin-echo pulse sequence. Infarct tissues were determined from abnormal hyperintensity regions on T2 images (Chan et al., 2009). Infarct volume was calculated by multiplying the total infarct area measured on individual slices by the slice thickness (0.7 mm) (Liu et al., 2011). Similarly, hemispheric and ventricular volumes were obtained. Residual hemispheric volume was calculated by subtracting the infarct and ventricular volumes from the hemispheric volume (Plane et al., 2008). Data were expressed as the ratio of the ipsilateral residual hemispheric volume relative to the contralateral. 3D reconstruction of the infarct tissue was achieved by 3D Slicer software[1].

Diffusion tensor imaging (DTI) was performed with an axial single-shot spin echo-planar imaging sequence (Zhang et al., 2016). The directionally encoded color (DEC), fractional anisotropy (FA), axial diffusivity (AD), and radial diffusivity (RD) maps were reconstructed by Paravision version5.1 software (Bruker, Germany). Regions of interest (ROIs) were placed in the bilateral cortex, striatum, and external capsule on DTI parametric maps according to rat atlas (Paxinos and Watson, 1986).

[1]https://www.slicer.org/

Next, diffusion tensor tractography (DTT) was performed using the 3D Slicer software. The mean fiber length and fiber density of the bilateral cortex, striatum, and external capsule were obtained according to our previous study (Li et al., 2018a). All data were presented as the ratio of the ipsilateral value relative to the contralateral value. All analyses were performed in a blinded manner.

Tissue Processing

At the end of MRI scan, rats (n = 4 per group) were deeply anesthetized and perfused transcardially with 0.9% saline followed by 4% paraformaldehyde. The brains were removed and post-fixed in the same fixative at 4°C overnight. Brain blocks locating from −0.4 to 0.4 mm relative to the bregma were cut, processed, and embedded in paraffin. A series of 5 μm-thick coronal brain sections were sliced from the paraffin block for immunostaining. Peri-ischemic tissues of the remaining rats (n = 4 per group) were separated according to a previously described method (Ashwal et al., 1998) for qRT-PCR and western blot analysis to detect the expressions of axonal growth related molecules and axonal growth inhibitory molecules.

Histological Evaluation

Luxol fast blue (LFB) staining was performed as reported previously (Shi et al., 2010). Three microscopic fields from the peri-infarct cortex, striatum, external capsule, and their contralateral homologous areas were randomly selected. Data were expressed as the ipsilateral integrated optical density (IOD) relative to the contralateral IOD.

The proliferation of OPCs was detected by double-labeled immunostaining against Ki67 (a marker of proliferating cell) and NG2 (a marker of OPC), whereas Ki67 and CNPase (a marker for oligodendrocytes) double-labeled immunostaining was performed to determine newly matured oligodendrocytes as previously described (Zou et al., 2016). Briefly, sections were stained with primary antibodies against rabbit anti-Ki67 (Abcam; ab15580; 1:100) in combination with mouse anti-NG2 (Abcam; ab50009; 1:200) or mouse anti-CNPase (Abcam; ab6319; 1:300), followed by incubation in species- and isotype-appropriate Alexa Fluor 488 and 594 secondary antibodies. For quantitative analysis, the number of $Ki67^+/NG2^+$ and $Ki67^+/CNPase^+$ cells was estimated in three randomly selected microscopic regions from the peri-infarct cortex and striatum. Data were expressed by the average number of cells per mm^2. All images were visualized with a digital camera connected to an optical or fluorescence microscope and analyzed with NIS-Elements Basic Research Image Collection Analysis system (Nikon, Japan) by an investigator blind to the experimental groups.

qRT-PCR Analysis

Total RNA was extracted from the peri-infarct tissues using RNAprep pure Kit (for tissue) (Tiangen, DP431, Beijing, China), and cDNA was synthetized using FastQuant RT Kit (Tiangen, KR106, Beijing, China). RT-PCR was performed on a CFX Connect™ Real-Time PCR Detection System (Bio-Rad) using SuperReal PreMix Plus (Tiangen, FP205, Beijing, China). The primer sequences were as follows (forward and reverse, respectively): NG2, 5′-AGCCCATGGCC TTCACTATCAC-3′ and 5′-CCGGCCCTGAATCACTGTCTA-3′; CNPase, 5′-GGAGACATAGTGCCCGCAAAG-3′ and 5′-TTGCACTCGTGCAGCGTA-3′; growth associated protein-43 (GAP-43), 5′-CACCATGCTGTGCTGTATGAGAA-3′ and 5′-GTCCACGGAAGCTAGCCTGA-3′; NogoA, 5′-CTTGGTCA TGTGAACAGCACAATAA-3′ and 5′-CATTGAACAAGGCAC CAACGTAA-3′; NgR, 5′-TCCAGTCATGCCGAAATCTCAC-3′ and 5′-TGGTAGGGTCCACGACATGAAG-3′; RhoA, 5′-CA GCAAGGACCAGTTCCCAGA-3′ and 5′-AGCTGTGTCCCAT AAAGCCAACTC-3′; ROCK2, 5′-CTAACAGTCCGTGGGTGG TTCA-3′ and 5′-CTCAGGCACATCATAATTGCTCATC-3′; β-actin, 5′-GGAGATTACTGCCCTGGCTCCTA-3′ and 5′-GACTCATCGTACTCCTGCTTGCTG-3′. The reactive conditions were as follows: denaturing at 95°C for 15 min, followed by 40 cycles of 95°C for 10 s, 55°C for 31 s, and 72°C for 30 s. Data were presented as relative mRNA level according to the $2^{-\Delta\Delta Ct}$ method. Actin served as an internal standard.

Western Blot Analysis

Peri-ischemic tissues were homogenized in radioimmunoprecipitation assay (RIPA) buffer (Applygen, Beijing, China). Protein concentration was determined, and equal amounts of proteins (21 μg per lane) were separated on 10% sodium dodecyl sulfate (SDS)-polyacrylamide gels, and then transferred onto polyvinylidene difluoride membranes (Millipore, Billerica, MA, United States). Membranes were blocked with 5% non-fat milk for 1 h at room temperature and then incubated overnight at 4°C with the primary antibodies against the following proteins: NG2 (1:2000), CNPase (1:2000), GAP-43 (Epitomics, #2259-1, 1:5000), NogoA (Abcam; ab62024; 1:5000), NgR (Abcam; ab26291; 1:5000), RhoA (Abcam; ab68826; 1:20000), ROCK2 (Abcam; ab125025; 1:40000), and GAPDH (Neobioscience; NBL01c; 1:40000). After washing, the membranes were incubated with secondary horseradish peroxidase-labeled anti-rabbit (CWBIO; CW0103S; 1:20000) or anti-mouse (CWBIO; CW0102S; 1:20000) IgG. Immunoreactive bands were visualized using an enhanced chemiluminescent kit (Aspen Biotechnology, Hubei, China). The optical densities of the protein bands were measured using the ImageJ software. GAPDH served as a loading control.

Behavioral Study

A total of 50 rats (9–11 rats per group) were submitted to spatial learning and memory test in the Morris water maze (MWM) without undergoing MRI and histological studies at days 31–36 after MCAO (Jing et al., 2015). The reason was that a previous MRI study had demonstrated that rats who were subjected to short periods of training in the MWM show structural modifications and rapid changes in diffusion MRI indices (Blumenfeld-Katzir et al., 2011; Hofstetter and Assaf, 2017). Moreover, behavioral training and testing may increase the number of hippocampal neurons (Gould et al., 1999) and change the regional gray matter volume (Sumiyoshi et al., 2014).

The MWM consisted of a circular tank with a circular transparent platform (15 cm in diameter). The tank was filled with water (18–20°C) and divided into four virtual quadrants

(quadrants I, II, III, and IV). During spatial acquisition test, the platform was placed 1.5 cm below the water surface in the middle of quadrant I to serve as the goal. The animals received four trials a day for four consecutive days. For each trial, the rat was allowed to swim for 60 s to find the submerged platform. If the rat failed to locate the platform within 60 s, it was guided to the platform and left on it for 10 s. The path length taken by the animals to locate the platform was recorded and analyzed with a video tracking system (JLBehv-MWMG, Jiliang Software Technology, Co., Ltd., Shanghai). To assess spatial memory retention, the probe trial was performed 24 h after the last acquisition trial. The platform was removed from the maze, and the rats were allowed to swim for 30 s. The percentage of distance traveled by the rats in the trained quadrant (quadrant I) was calculated.

Following the probe trial, the animals were subjected to a platform-switched learning task to assess repeated reversal spatial learning and memory (Morris et al., 1982). Briefly, the hidden platform was placed in the center of quadrant II for the first trial, and moved to quadrant III or quadrant IV on the second and third trial, respectively. For each trial, the rats had 60 s to locate the hidden platform. The swimming track of rats to the new location was recorded, and the path length taken by the animals to locate the platform was analyzed. An experimenter blind to the group information performed data analysis.

Statistical Analysis

All data were expressed as mean ± standard error of the mean (SEM). Statistical analyses were performed using the SPSS 21.0 (SPSS, Inc., United States) software. Data from the MWM acquisition test were analyzed using two-way repeated measures ANOVA (between subject factor–treatment; within subject factor-time) with Bonferroni's *post hoc* test. Data from the probe trial, platform-switched test, MRI, and histological measurements were analyzed by one-way ANOVA, followed by Bonferroni's *post hoc* test. Significance was defined as $P < 0.05$.

RESULTS

Combination of XSEC and EE Therapy Reduced Infarct Volume and Alleviated Tissue Atrophy in MCAO Rats

T2WI was conducted to measure the infarct size on the 31st day after MCAO. Axial T2 images exhibited normal structure in the control rats. Abnormal hyperintense signals indicating tissue infarction were primarily detected in the ipsilateral cortex, striatum, and external capsule after MCAO (**Figures 1A,B**). Treating rats with XSEC + EE combination or XSEC alone significantly reduced the infarct volume compared with that in vehicle group ($P < 0.001$ or $P < 0.01$, **Figure 1C**). Notably, XSEC + EE combination produced a remarkable decrease in the infarct volume compared to XSEC ($P < 0.05$) or EE ($P < 0.001$) alone.

To determine chronic cerebral atrophy after MCAO, residual volume of the ipsilateral hemisphere was measured. When compared with the vehicle group, XSEC + EE robustly elevated the ratio of residual volume ($P < 0.05$), while XSEC or EE monotherapy showed no statistic differences on the ratio of residual volume (Vehicle, 0.4094 ± 0.0482; XSEC, 0.5615 ± 0.0478; EE, 0.4983 ± 0.0386; XSEC + EE, 0.7922 ± 0.0436, **Figure 1D**), indicating that the combined actions of XSEC and EE significantly alleviated atrophy of the ipsilateral hemisphere. Notably, XSEC + EE exhibited a slight increase in the ratio of residual volume compared to the XSEC or EE monotherapy groups, however, no statistical difference was detected.

Combination of XSEC and EE Therapy Alleviated Axonal Microstructural Damage in MCAO Rats Based on MRI Parameters

DTI was performed to examine microstructural changes in the axons on the 31st day after MCAO (**Figure 2A**). Significantly decreased relative FA but increased relative AD and RD were observed in the ipsilateral cortex, striatum, and external capsule of the vehicle rats compared with those in the control rats ($P < 0.01$ or $P < 0.001$, **Figure 2B**). XSEC and EE monotherapies and XSEC + EE combination profoundly increased the relative FA in the corresponding regions and decreased the relative AD and RD in the ipsilateral cortex and external capsule compared with those in the vehicle group ($P < 0.05$–0.001). In addition, rats treated with XSEC alone or XSEC + EE combination exhibited alleviated relative RD in the ipsilateral striatum compared with those in the vehicle rats ($P < 0.05$). In particular, increased relative FA in the ipsilateral cortex was observed with XSEC + EE combination compared to that with XSEC or EE monotherapy ($P < 0.05$). Notably, only XSEC + EE combination decreased the relative AD in the ipsilateral striatum compared with that in the vehicle group ($P < 0.05$).

Combination of XSEC and EE Therapy Facilitated Axonal Restoration in MCAO Rats

Diffusion tensor tractography was performed to detect the integrity and connectivity of the nerve fibers (**Figure 3A**). Quantitative data showed that the relative fiber length and fiber density reduced dramatically in the ipsilateral cortex, striatum, and external capsule of the vehicle rats in comparison with those in the control rats ($P < 0.001$, **Figure 3B**). XSEC or EE monotherapy and combination therapy significantly elevated the relative fiber length in the ipsilateral striatum and external capsule and increased the relative fiber density in the ipsilateral cortex and striatum compared with that in the vehicle group ($P < 0.05$–0.001). Furthermore, rats treated with XSEC + EE combination and EE monotherapy also exhibited increased relative fiber density in the ipsilateral external capsule compared with that in the vehicle rats ($P < 0.05$). In particular, XSEC + EE combination further resulted in higher fiber length in the ipsilateral striatum and external capsule and higher fiber density in the cortex and external capsule compared to that by XSEC or EE monotherapy ($P < 0.05$–0.01). Of note, only

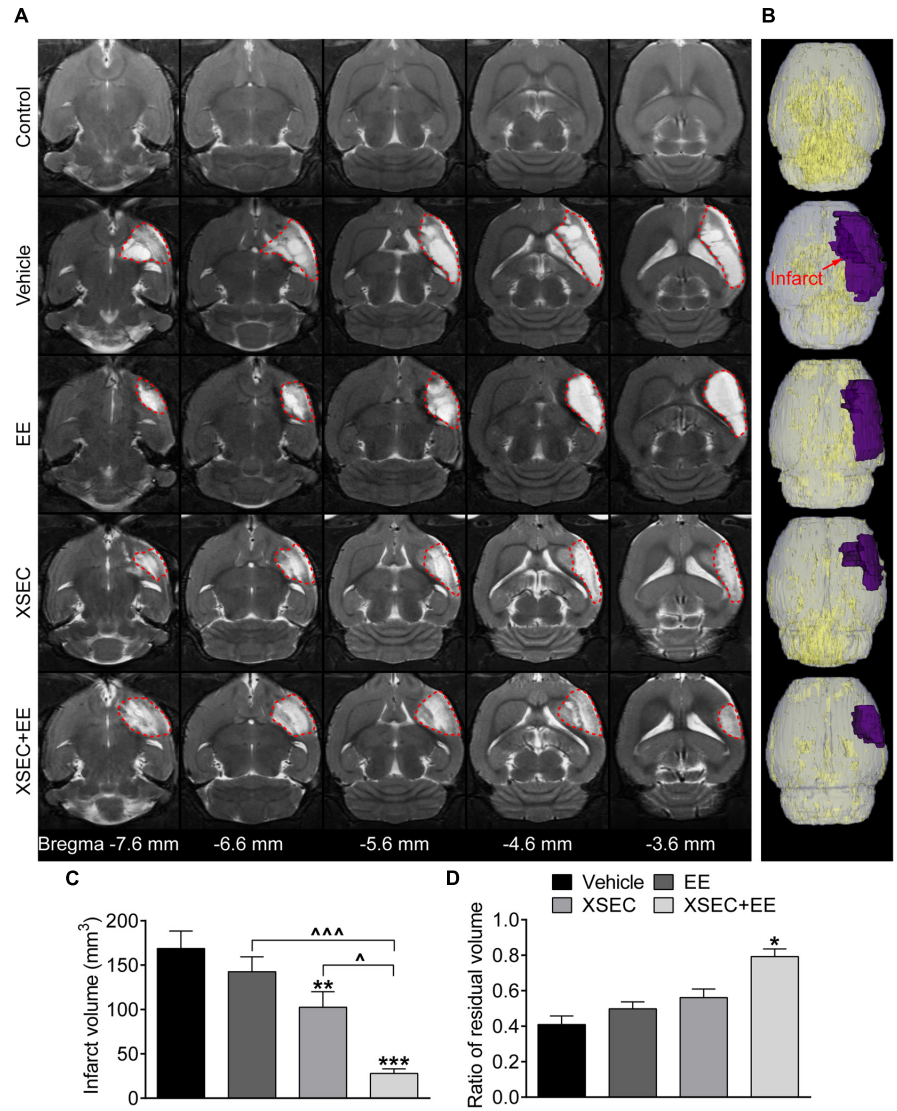


FIGURE 1 | Effect of XSEC or EE and their combination on the infarct volume in MCAO rats. **(A)** Representative axial T2 images (bregma –7.6 to –3.6 mm) obtained from various group rats on the 31st day after MCAO. The infarct tissues were surrounded by red dotted lines. **(B)** Typical 3D reconstruction images of ischemic lesion were acquired by 3D Slicer software (purple region indicated the infarction). **(C,D)** Quantitative analysis of the infarct volume and the ratio of residual volume, respectively (one-way ANOVA followed by Bonferroni's *post hoc* test, $n = 8$ per group). $^{*}P < 0.05$, $^{**}P < 0.01$, $^{***}P < 0.001$ vs. vehicle group. $^{\wedge}P < 0.05$, $^{\wedge\wedge\wedge}P < 0.001$ vs. XSEC + EE group.

XSEC + EE combination elevated the relative fiber length in the ipsilateral cortex compared with that in the vehicle group ($P < 0.001$).

Combination of XSEC and EE Therapy Preserved Myelinated Axons in MCAO Rats

Luxol fast blue staining was performed to detect myelinated axons (**Figure 4A**). For the vehicle rats, LFB staining showed marked cavitation areas and myelin loss in the axonal tracts in the ischemic cortex, striatum, and external capsule, suggesting that ischemia directly injures axons and the myelin structure. However, XSEC or EE monotherapy and combination markedly increased the relative IOD of LFB in the peri-infarct cortex, striatum, and external capsule compared with that in the vehicle group ($P < 0.001$, **Figure 4B**). It is noteworthy that XSEC + EE combination produced a significantly higher relative IOD of LFB in the peri-infarct cortex than that by EE monotherapy ($P < 0.01$).

Combination of XSEC and EE Therapy Enhanced OPCs Proliferation and Maturation in MCAO Rats

The proliferation of OPCs was detected by double-labeled immunostaining against Ki67 and NG2 (**Figures 5A,B,D**).

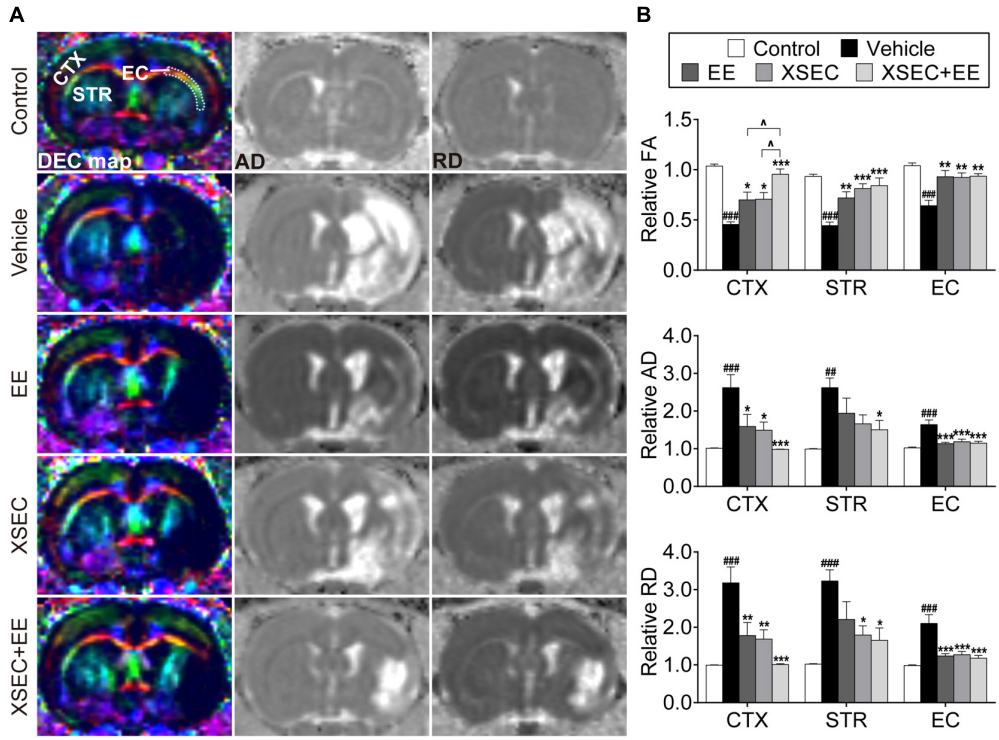


FIGURE 2 | Effect of XSEC or EE and their combination on the axonal microstructural changes in MCAO rats. **(A)** Representative DEC, AD, RD maps (bregma –0.6 mm) were obtained from various group rats on the 31st day after MCAO. ROIs of the cortex (CTX), striatum (STR), and external capsule (EC) were identified on the DEC map. **(B)** Quantitative analysis of the relative FA, AD, and RD in the ipsilateral cortex, striatum and external capsule (one-way ANOVA followed by Bonferroni's *post hoc* test, $n = 8$ per group). $^{\#\#}P < 0.01$, $^{\#\#\#}P < 0.001$ vs. control group. $^{*}P < 0.05$, $^{**}P < 0.01$, $^{***}P < 0.001$ vs. vehicle group. $^{\wedge}P < 0.05$ vs. XSEC + EE group.

XSEC and EE monotherapies and XSEC + EE combination all significantly increased the number of $Ki67^+/NG2^+$ cells in the peri-infarct cortex and striatum compared with those in the vehicle group ($P < 0.05$–$P < 0.001$, **Figure 5C**). Notably, combination treatment produced a considerably higher number of $Ki67^+/NG2^+$ cells in the peri-infarct cortex compared with that by XSEC or EE monotherapy ($P < 0.05$ or $P < 0.01$), suggesting that XSEC + EE combination facilitated OPCs proliferation.

Further, Ki67 and CNPase double-labeled immunostaining was performed to determine the maturation of OPCs (**Figures 5A,B,E**). Compared to the vehicle group, XSEC + EE combination and XSEC monotherapy both markedly increased the number of $Ki67^+/CNPase^+$ cells in the peri-infarct cortex and striatum ($P < 0.05$–0.001, **Figure 5C**), and a higher number of $Ki67^+/CNPase^+$ cells was detected in the peri-infarct striatum of EE-treated rats ($P < 0.05$). Notably, XSEC + EE combination enhanced the number of $Ki67^+/CNPase^+$ cells in the peri-infarct cortex, which was significantly higher compared to that by XSEC ($P < 0.01$) or EE monotherapy ($P < 0.05$). This result suggested that the XSEC + EE combination enhanced the generation of new myelinating oligodendrocytes.

Moreover, protein and mRNA levels of NG2 and CNPase were analyzed by western blot and qRT-PCR. XSEC + EE combination and XSEC monotherapy significantly elevated the mRNA level of CNPase and protein expression of NG2/CNPase compared with that in the vehicle group ($P < 0.05$ or $P < 0.01$, **Figures 5F,G**). Notably, only XSEC + EE combination increased NG2 mRNA level compared with that in the vehicle rats ($P < 0.05$). In addition, the combination treatment resulted in significantly upregulated protein expression of NG2 and mRNA level of CNPase compared with those by EE monotherapy ($P < 0.05$).

Combination of XSEC and EE Therapy Elevated Axonal Growth Marker and Suppressed Axonal Growth Inhibitors in MCAO Rats

GAP-43, a marker for axonal growth cones, was examined to evaluate axonal outgrowth (Sandelius et al., 2018). A significant decrease in the mRNA and protein expression of GAP-43 was observed in the vehicle rats compared with those in the control rats ($P < 0.05$–0.001, **Figures 6A,B**). However, XSEC monotherapy and XSEC + EE combination significantly upregulated GAP-43 mRNA and protein expression compared with those in the vehicle group ($P < 0.05$ or $P < 0.01$).

As axonal outgrowth could be hindered by intrinsic axonal growth inhibitory molecules, the expressions of NogoA,

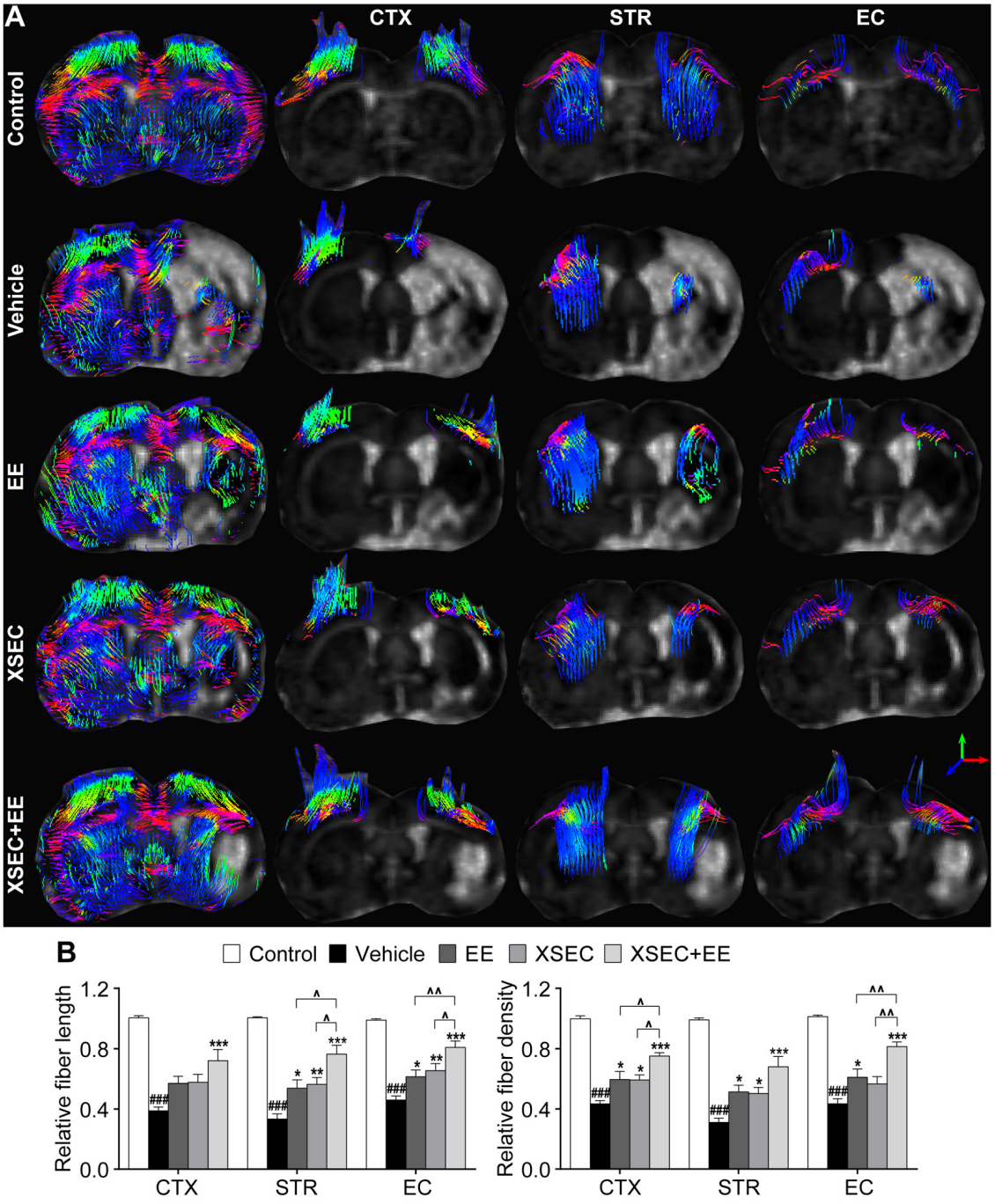


FIGURE 3 | Effect of XSEC or EE and their combination on the axonal restoration in MCAO rats. **(A)** Diffusion tensor tractography (DTT) of the brain at bregma –0.6 mm and the anatomical pathway of the cortex (CTX), striatum (STR), and external capsule (EC), respectively. **(B)** Quantitation of the relative fiber length and fiber density in the ipsilateral cortex, striatum and external capsule (one-way ANOVA followed by Bonferroni's *post hoc* test, $n = 8$ per group). $^{###}P < 0.001$ vs. control group. $^{*}P < 0.05$, $^{**}P < 0.01$, $^{***}P < 0.001$ vs. vehicle group. $^{\wedge}P < 0.05$, $^{\wedge\wedge}P < 0.01$ vs. XSEC + EE group.

NgR, RhoA, and ROCK2 were measured in the peri-infarct tissue. Compared to the control group, the expressions of NogoA/NgR protein and mRNA increased noticeably in the vehicle group ($P < 0.01$ or $P < 0.001$, **Figures 6C,D**). XSEC and EE monotherapies and XSEC + EE combination significantly downregulated NgR protein and NogoA/NgR mRNA expressions compared with those in the vehicle group ($P < 0.01$ or $P < 0.001$). Notably, XSEC + EE combination further attenuated NogoA protein expression compared with that in the vehicle group ($P < 0.05$).

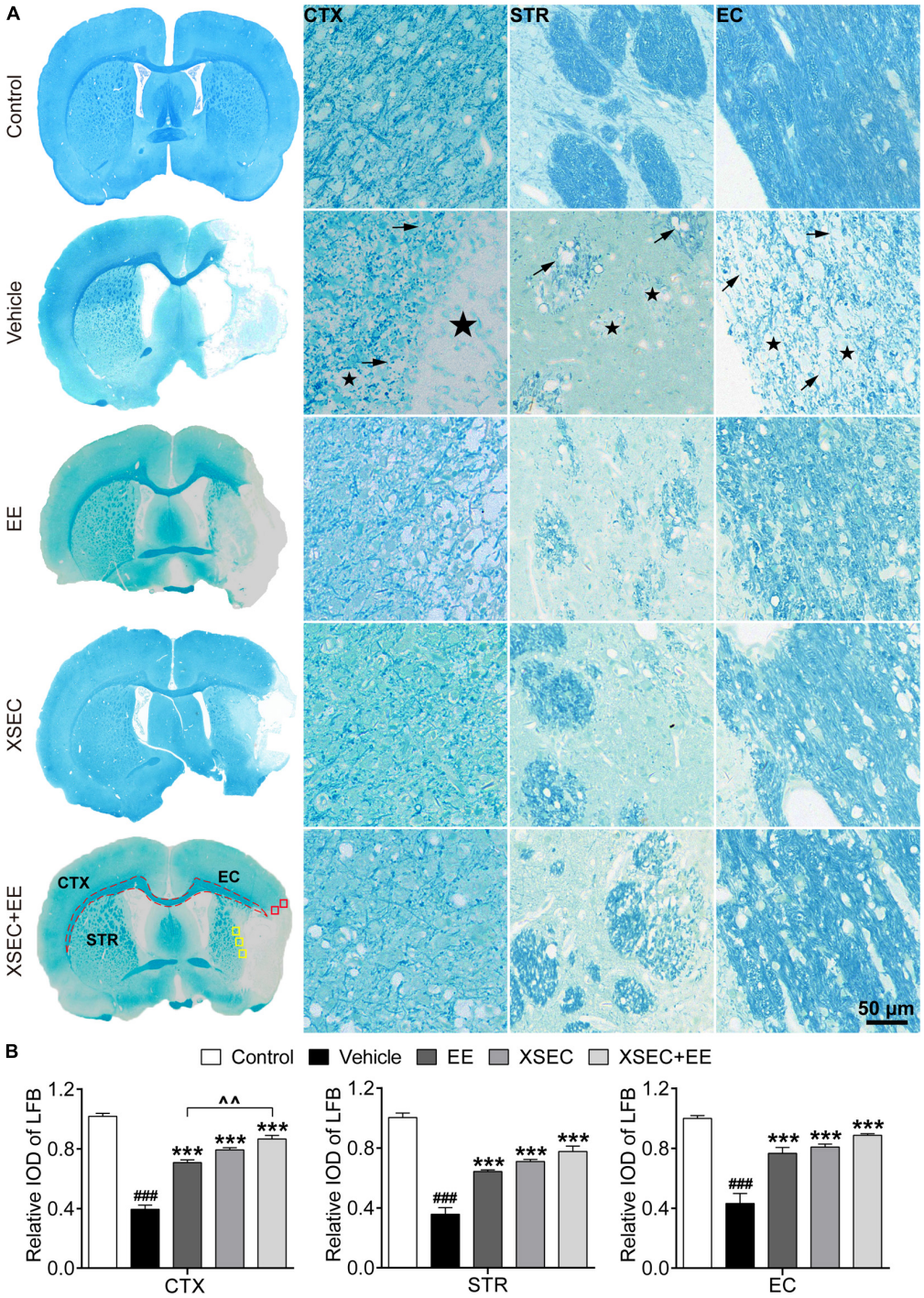


FIGURE 4 | Effect of XSEC or EE and their combination on the myelinated axons in MCAO rats. **(A)** Typical LFB staining photographs showing the alterations of myelin sheath in the ipsilateral cortex, striatum and external capsule. ROIs of the peri-infarct cortex (CTX, red boxes), striatum (STR, yellow boxes), and external capsule (EC, dashed line) were indicated in the representative LFB map from a XSEC + EE treated rat. Remarkable cavitation areas (stars) and partial loss of myelin sheaths (arrows) in the axonal tracts were observed. **(B)** Quantitative data of the relative IOD of LFB in the ipsilateral cortex, striatum and external capsule (one-way ANOVA followed by Bonferroni's *post hoc* test, $n = 4$ per group). $^{###}P < 0.001$ vs. control group. $^{***}P < 0.001$ vs. vehicle group. $^{\wedge\wedge}P < 0.01$ vs. XSEC + EE group.

Moreover, mRNA and protein levels of RhoA and ROCK2 were significantly downregulated by the combination treatment compared with that in the vehicle group ($P < 0.05$ or $P < 0.01$, **Figures 6E,F**). Moreover, rats treated with XSEC monotherapy showed reduced ROCK2 protein and mRNA levels, whereas EE-treated rats exhibited alleviated mRNA

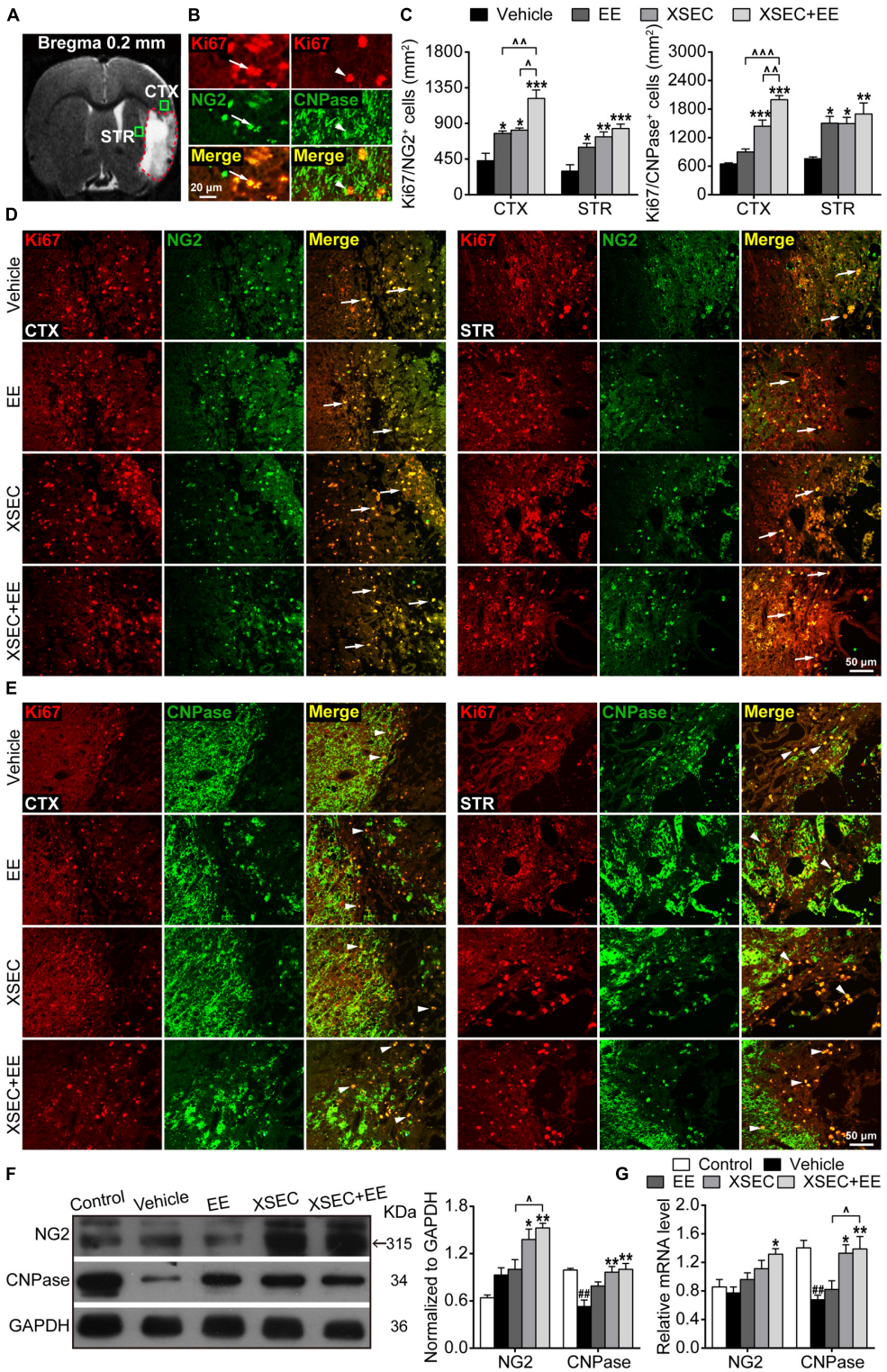


FIGURE 5 | Effect of XSEC or EE and their combination on oligodendrogenesis in MCAO rats. **(A)** A representative coronal T2WI image at the level of bregma 0.2 mm. Boxes indicated the peri-infarct cortex and striatum where images were taken. **(B)** Representative images showing the co-expressed cells of $Ki67^+/NG2^+$ and $Ki67^+/CNPase^+$. **(C)** Quantitative data of the number of $Ki67^+/NG2^+$ and $Ki67^+/CNPase^+$ co-expressed cells in the peri-infarct cortex and striatum. **(D,E)** Representative images of Ki67/NG2 and Ki67/CNPase double immunofluorescent staining in the peri-infarct cortex and striatum. **(F,G)** Quantitative analysis of the protein and mRNA level of NG2 and CNPase in the peri-infarct brain tissues, respectively (one-way ANOVA followed by Bonferroni's *post hoc* test, $n = 4$ per group). $^{\#\#}P < 0.01$ vs. control group. $^*P < 0.05$, $^{**}P < 0.01$, $^{***}P < 0.001$ vs. vehicle group. $^\wedge P < 0.05$, $^{\wedge\wedge}P < 0.01$, $^{\wedge\wedge\wedge}P < 0.001$ vs. XSEC + EE group.

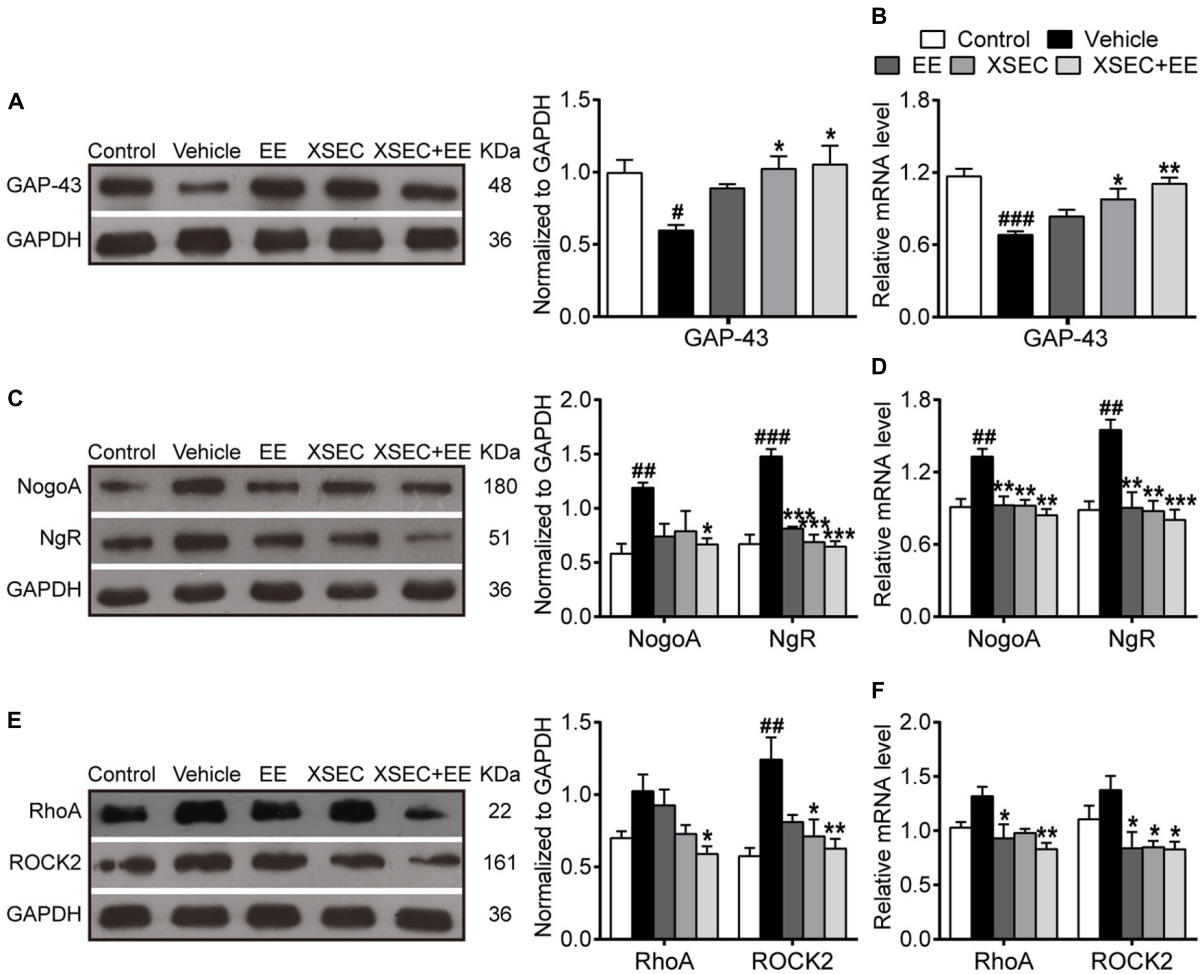


FIGURE 6 | Effect of XSEC or EE and their combination on the expressions of GAP-43, NogoA/NgR and RhoA/ROCK2 in MCAO rats. Quantitative analysis of the protein **(A,C,E)** and mRNA **(B,D,F)** levels of GAP-43, NogoA/NgR, and RhoA/ROCK2, respectively (one-way ANOVA followed by Bonferroni's *post hoc* test, $n = 4$ per group). $^{\#}P < 0.05$, $^{\#\#}P < 0.01$, $^{\#\#\#}P < 0.001$ vs. control group. $^{*}P < 0.05$, $^{**}P < 0.01$, $^{***}P < 0.001$ vs. vehicle group.

level of RhoA/ROCK2 compared with that in the vehicle rats ($P < 0.05$).

Combination of XSEC and EE Therapy Improved Cognitive Function in MCAO Rats

The MWM task was performed to assess the spatial learning and memory capacity of all rats. In the spatial acquisition test, repeated measures of ANOVA showed significant overall effects of time and treatment on the path length (time, $F_{(3,135)} = 46.098$, $P < 0.001$; treatment, $F_{(4,45)} = 7.847$, $P < 0.001$). These results indicated improved spatial learning over time in all testing rats, and the treated rats showed better learning acquisition than the vehicle rats. *Post hoc* analysis revealed that vehicle rats covered longer swimming distances to find the submerged platform on the 2nd and 3rd training day compared with that by the control rats ($P < 0.05$, **Figure 7B**), indicating impaired spatial learning after MCAO. Treatment with either EE monotherapy or XSEC + EE combination significantly reduced swimming distances by rats to locate the hidden platform on the 2nd and 3rd training day ($P < 0.05$–0.01). Moreover, XSEC-treated rats also traveled shorter swimming distances than vehicle rats on the 3rd training day ($P < 0.05$).

In the probe trial (**Figure 7A**), vehicle rats exhibited lower percentages of distance traveled in the target quadrant compared with that by the control rats ($P < 0.001$, **Figure 7C**), demonstrating that the memory retention capacity was reduced after MCAO. XSEC-, EE-, and XSEC + EE-treated rats displayed better memory retention, as evidenced by the significantly higher percentage of distance traveled in the target quadrant than the vehicle rats ($P < 0.05$ or $P < 0.001$).

In the platform-switched learning trial (**Figure 7D**), vehicle rats showed much longer swimming distances to find the location of the changed platform than those by the control rats ($P < 0.05$ or $P < 0.001$, **Figure 7E**). EE monotherapy and XSEC + EE combination rats exhibited a clear preference for the new target quadrant with much shorter swimming distances to locate the

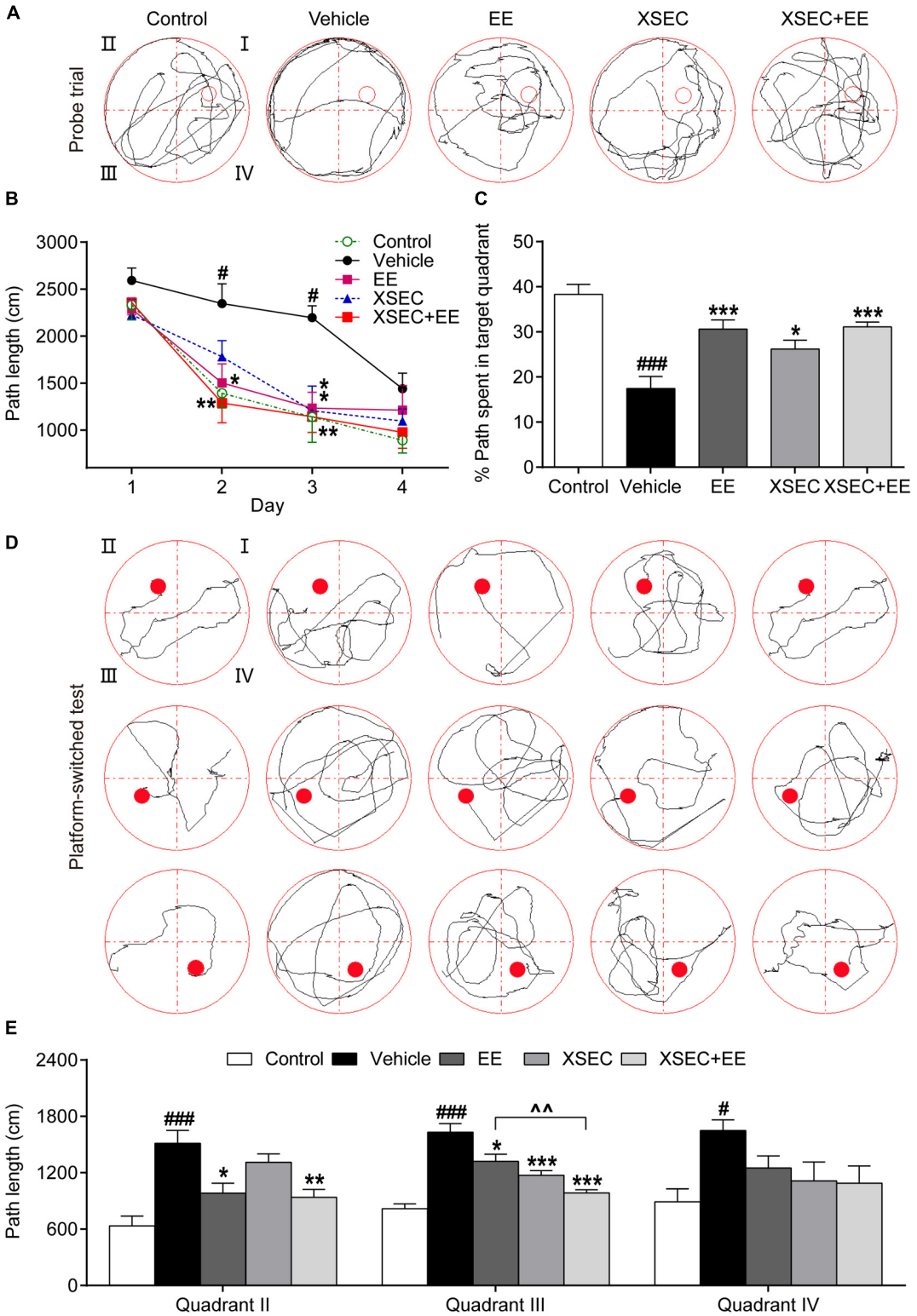


FIGURE 7 | Effect of XSEC or EE and their combination on spatial learning and memory in MCAO rats. **(A)** Swimming traces of the rats in the probe trial. **(B)** The path length taken by rats to find the submerged platform in the spatial acquisition trial (two-way ANOVA with repeated measures, n = 9–11 per group). **(C)** The percentage of swimming distances of rats spent in the target quadrant (quadrant I) during the probe trial. **(D)** Swimming traces of the rats in the platform-switched test. **(E)** The path length of the rats traveled to locate the platform in the platform-switched test (one-way ANOVA followed by Bonferroni's *post hoc* test for **C,E**, n = 9–11 per group). $^{\#}P < 0.05$, $^{\#\#\#}P < 0.001$ vs. control group. $^{*}P < 0.05$, $^{**}P < 0.01$, $^{***}P < 0.001$ vs. vehicle group. $^{\wedge\wedge}P < 0.01$ vs. XSEC + EE group.

switched platform in quadrants II and III compared to those by the vehicle rats ($P < 0.05$–0.001). XSEC-treated rats also showed shorter distances to find the platform in quadrant III compared to those by the vehicle rats ($P < 0.001$). Of note, rats treated with XSEC + EE combination traveled significantly shorter distances to find the platform than the EE-treated rats in quadrant III ($P < 0.01$).

DISCUSSION

Although several lines of evidence have demonstrated that XSEC and EE may independently promote brain plasticity and neurological recovery after an ischemic stroke (Nygren et al., 2006; Chen et al., 2015, 2017; Zhang et al., 2016), the efficacy of a combination of XSEC and EE on post-stroke axonal injury and remodeling still needed to be elucidated. Based on our MRI and histological methodologies, the present study demonstrated that the combined actions of XSEC and EE exerted synergistic effects on reducing cerebral atrophy, facilitating axonal remodeling, and improving spatial learning and memory in a permanent MCAO rat model accompanied with amplifying stroke-induced oligodendrogenesis and overcoming the intrinsic axonal growth inhibitory signals, which was beneficial to axonal outgrowth.

Magnetic resonance imaging can non-invasively monitor neuronal remodeling related to neurological outcome after brain injury (Jiang et al., 2010a). T2WI is a favorable tool to determine anatomical characteristics and pathological changes of the brain (Liu et al., 2011). In the present study, T2WI images showed that a large scale of infarction was located in the ipsilateral MCA territory in MCAO rats. XSEC individually decreased the infarct volume compared with that in vehicle group, and this effect was further boosted by the combined application of XSEC and EE. Notably, EE monotherapy did not produce beneficial effects in restoring brain infarct volume, which was in agreement with previous studies (Soderstrom et al., 2009; Xie et al., 2019). It should be also be noted that the combination treatment had an added beneficial effect as evidenced by significantly reduced atrophy of the ipsilateral hemisphere following an ischemic stroke, whereas the monotherapies showed no effect. This finding suggested that the combination treatment might provide additive benefits for reducing brain tissue loss in MCAO rats.

Axonal sprouting and regeneration are critical processes during brain repair after stroke injury and are related to improvements in neurologic deficits after a stroke (Ueno et al., 2012). DTI has been widely applied to non-invasively monitor microstructural alterations of the white matter and fiber-rich gray matter in animals and patients with ischemic stroke (Bai et al., 2015; Jung et al., 2017). Using this technique, we assessed the effects of XSEC and EE separately or in combination on axonal recovery. The most commonly applied parameter from DTI is FA. FA characterizes the density, distribution, and orientational coherence of the axons (Granziera et al., 2007). The other DTI-derived parameters AD and RD may be useful to elucidate the changes in axons and myelin, respectively (Aung et al., 2013). In the present study, decreased FA accompanied with increased AD and RD were identified in the cortex, striatum, and external capsule of the ischemic hemisphere in the vehicle rats. In general, a decrease in FA in the lesioned area represents demyelination and axonal degeneration (Tuor et al., 2014). Meanwhile, the phenomenon of increased AD has been attributed to structural breakdown of axons, whereas enhanced RD may result from widespread myelin degradation after stroke (Pitkonen et al., 2012). DTI data in this study indicated widespread loss of integrity of axons and myelin in a rat model of 30-days permanent MCAO. Notably, XSEC + EE combination displayed increased FA accompanied by reduced AD and RD in the cortex, striatum, and external capsule ipsilateral to the site of ischemic injury. In particular, FA of the combination treatment group remained significantly higher in the ipsilateral cortex compared to that in XSEC or EE monotherapy. The increased FA is positively associated with the reorganization of white matter, e.g., due to axonal remodeling (Wiesmann et al., 2017). The attenuation in AD and RD corresponds with axonal growth and myelination, respectively (Jiang et al., 2010a). Thus, DTI parameters presented here suggested that the combined intervention alleviated white matter lesions and facilitated axonal reorganization following an ischemic stroke. In correspondence with DTI results, DTT maps revealed that decreased axonal projections emanated from the ischemic striatum, cortex, and external capsule in the vehicle rats. However, XSEC + EE combination robustly elevated fiber density in the ischemic cortex and external capsule and increased fiber length in the striatum and external capsule compared to those with the monotherapies, suggesting an improvement in the fiber tract repair. These results were in agreement with the morphological study of myelin fibers by LFB staining. Histological results showed that ischemic rats treated with XSEC and EE combination had a significantly higher density of LFB positive axons in the perilesional brain regions compared with that in the vehicle rats. Based on the results of MRI and histopathological analysis, the present study demonstrated the better effect of XSEC + EE combination therapy on facilitating axonal remodeling. These findings highlighted the therapeutic potential of the combined action of XSEC and EE for long-term rehabilitation after an ischemic stroke.

Oligodendrogenesis plays a critical role in axonal reorganization after stroke. Although the repair capacity of the CNS is limited, regeneration of mature oligodendrocytes has been observed in the peri-infarct areas after stroke (Zhang et al., 2010; Franklin and Goldman, 2015). In this study, we found that MCAO rats exhibited an increase in the numbers of NG2-positive OPCs and newly generated CNPase-positive oligodendrocytes along the peri-infarct striatum and cortex, whereas they were not detected in the undamaged hemisphere of MCAO rats and intact brain of the control rats. Our results were consistent with previous reports indicating that a stroke increased oligodendrogenesis in the peri-infarct areas (Zhang et al., 2010; Ramos-Cejudo et al., 2015). Although far from being completely understood, accumulating evidences have suggested that a complex interaction of extrinsic and intrinsic cues from the ischemic microenvironment would impact the proliferation and differentiation of OPCs after a stroke (Moore et al., 2011; Zhang et al., 2013). Experimental evidences have indicated that

astrocyte-secreted factors could positively or negatively influence OPCs proliferation, differentiation, and survival during CNS injury and demyelination (Moore et al., 2011). For example, insulin-like growth factor-1 (IGF-1) secreted by astrocytes supports the proliferation of oligodendrocytes and generation of myelinating oligodendrocytes under conditions of brain injury (Chesik et al., 2008). Bone morphogenic proteins (BMPs) expressed by reactive astrocytes during adult CNS injury block the process of oligodendrocyte differentiation (See and Grinspan, 2009). Moreover, the M1-macrophages of microglial cells, dominating early after demyelination, support the proliferation and migration of OPCs, whereas the M2-dominant phenotype in demyelinated lesions is essential for efficient remyelination by promoting oligodendrocyte differentiation (Miron et al., 2013; Braun et al., 2016).

It should be noted that endogenous oligodendrogenesis in response to a stroke is limited. Although a stroke could induce the proliferation of OPCs, most of these OPCs fail to develop into mature oligodendrocytes, resulting in insufficient remyelination (Zhang et al., 2013). Therefore, understanding the molecular environment of injured cerebral tissue will help to understand endogenous oligodendrogenesis in response to stroke and thus, help in designing therapeutic approaches for the amplification of these cells, which may lead to efficient remyelination and axonal regeneration.

EE enhances newborn glial scar astroglia and NG2-positive OPCs in the post-ischemic neocortex, which may be beneficial for brain repair and post-stroke plasticity (Komitova et al., 2006). In parallel, the present study showed that XSEC and EE separately or in combination enhanced OPCs proliferation and increased the numbers of newly generated mature oligodendrocytes in the vicinity of the ischemic regions compared with that in the vehicle rats. Of note, XSEC + EE combination resulted in higher numbers of NG2-positive OPCs and CNPase-positive oligodendrocytes in the peri-infarct cortex compared with that by XSEC or EE monotherapy. Furthermore, the protein and mRNA levels of NG2 and CNPase increased significantly by XSEC + EE combination treatment. These results, along with the information obtained from DTI, DTT, and histopathological presentations, likely reflected that the combined application of XSEC and EE enhanced the production of OPCs and increased the number of newly generated oligodendrocytes, leading to substantial remyelination and increased myelinated axons in the peri-infarct regions. These may be important mechanisms for the beneficial effect of XSEC + EE combination.

Despite the requirement of intrinsic factors from regenerating axons, myelin-associated neurite growth inhibitors, as a potential mechanism, limit axonal regeneration and functional recovery after an ischemic stroke (Schwab and Strittmatter, 2014). Several studies have indicated that some specific neurite growth inhibitory factors enriched in myelin could limit axonal regeneration and functional recovery after an ischemic stroke (Kilic et al., 2010; Fujita and Yamashita, 2014). Among them, NogoA expressed by oligodendrocytes is a principal inhibitor for axonal regrowth in the injured CNS. NogoA binding to the NgR complex activates RhoA and its downstream target ROCK2, ultimately leading to axonal growth cone collapse and neurite outgrowth inhibition (Etienne-Manneville and Hall, 2002; Kilic et al., 2010; Fujita and Yamashita, 2014; Schwab and Strittmatter, 2014). Hence, strategies that aim at the inhibition of NogoA signaling can promote axonal regeneration and behavioral recovery (Pernet and Schwab, 2012). The present study demonstrated that XSEC + EE combination significantly lessened cerebral atrophy and induced axonal reorganization in perilesional brain regions. In light of this, we further explored whether the separate and combined actions of XSEC and EE could overcome the intrinsic axonal growth inhibitory pathways to facilitate axonal remodeling. According to the results of this study, XSEC or EE monotherapy was sufficient to counteract ischemic stroke-induced high expression of NgR protein and NogoA/NgR/ROCK2 mRNA. In particular, XSEC + EE combination markedly downregulated the protein expressions of NogoA and RhoA compared to that in the vehicle group. To further confirm that NogoA/NgR and RhoA/ROCK2 downregulation by XSEC and EE combination could promote axonal elongation, we assessed the axonal growth marker GAP-43, which was primarily localized in the axonal growth cone. Our current result revealed significantly reduced protein and mRNA levels of GAP-43 in vehicle-treated MCAO rats, whereas XSEC + EE combination remarkably enhanced protein and mRNA levels of GAP-43 compared to those in the vehicle group. The high level of GAP-43 is associated with axonal extension and cytoskeletal reorganization (Loncarevic-Vasiljkovic et al., 2009). Based on this, our data strongly suggested that XSEC + EE combination could enhance axonal regrowth by overcoming intrinsic growth inhibitory signals.

Axonal damage leads to persistent deficits with limited recovery of function (Kilic et al., 2010; Fujita and Yamashita, 2014). Promoting axonal reorganization is a primary contributor in cognitive function recovery during brain repair after stroke injury (Zatorre et al., 2012). In light of this, we investigated whether the enhancement in axonal remodeling by XSEC + EE combination might contribute to the improvement in learning and memory performance in the MWM task. Our results were consistent with previous reports and indicated that XSEC and EE monotherapies improved spatial reference learning and memory performance, as evaluated by the MWM test (Dahlqvist et al., 2004; Li et al., 2018b). Interestingly, the combined action of both permitted faster adaptation to a changed testing environment, as revealed in the platform-switched learning trial. In this task, rats must eliminate their initial learning and learn new information to find the repeatedly changing platform (Vorhees and Williams, 2006). Previous studies have supported that cortical and striatal dysfunction may be closely linked to specific reversal learning impairments (Kesner and Churchwell, 2011; Wei et al., 2011). With the information obtained from DTI analysis and histological evaluation, we demonstrated that XSEC + EE combination induced axonal reorganization and amplified oligodendrogenesis around peri-infarct tissues. These findings raised the interesting possibility that the faster adaptation to a changed testing environment by XSEC + EE combination treatment may be related to axonal remodeling in the peri-infarct regions.

There are several limitations in our study that should be mentioned. Firstly, the main anti-ischemic stroke components of XSEC needed to be further investigated. Based on the traditional documentation of BYHWD, XSEC is prepared from seven medicinal herbs, viz., *Astragalus membranaceus*, *Angelica sinensis*, *Paeonia lactiflora*, *Ligusticum chuanxiong*, *Prunus persica*, *Carthamus tinctorius*, and *Pheretima aspergillum*. All the herbs are recorded in the Chinese Pharmacopoeia. *In vivo* and *in vitro* experiments have confirmed that some of the active constituents isolated from these crude herbs have beneficial effects on preventing damage to the brain. *A. membranaceus* is the major component of XSEC. Many active compounds, such as astragaloside IV and calycosin-7-*O*-β-D-glucoside, derived from *A. membranaceus* possess a variety of biological activities, such as antioxidant, anti-apoptosis, and anti-inflammatory activities, that reverse ischemic injury (Fu et al., 2014; Li et al., 2017; Yin et al., 2019). In particular, astragaloside IV promotes hippocampal neurogenesis in the intact brain, and astragaloside VI induces proliferation of neural stem cells (NSCs) in the subventricular zone (SVZ) and peri-infarct cortex via activating the epidermal growth factor receptor (EGFR)/mitogen-activated protein kinase (MAPK) pathway after a stroke (Huang et al., 2018; Chen et al., 2019). Hydroxysafflor yellow A is a bioactive ingredient extracted from *C. tinctorius*. It has been reported that hydroxysafflor yellow A improves synaptic plasticity and cognitive function in cerebral ischemia-reperfused rats (Yu et al., 2018). A recent *in vitro* study reported that hydroxysafflor yellow A inhibited apoptosis and autophagy of NSCs via the p38 MAPK/MK2/Hsp27-78 signaling pathway (Li et al., 2019). Paeoniflorin, the main ingredient of *P. lactiflora*, possesses anti-inflammatory activity and improves regional cerebral blood flow and increases neurogenesis following cerebral ischemia (Zhang L.G. et al., 2017; Ko et al., 2018). Taken together, these findings suggested that XSEC exhibits neuroprotective and neurorestorative effects on stroke through multiple components aimed at multiple targets and mechanisms. Further studies on its active components to augment axonal regeneration after a stroke may be of great importance to elucidate the mechanistic basis on XSEC.

Secondly, the exact mechanism by which XSEC and EE restore brain structure and function is still unclear. Our previous study showed that XSEC + EE combination improved neurobehavioral performance by promoting focal neurogenesis and angiogenesis (Zhan et al., 2019). In this study, we further demonstrated that XSEC + EE combination conferred brain remodeling by promoting endogenous oligodendrogenesis and axonal reorganization and downregulating axonal growth inhibitory signaling, thereby improving neurological functional outcome after an ischemic stroke. These findings raised the interesting possibility that the beneficial effect of the combination treatment with XSEC and EE might be related to augmenting endogenous restorative mechanisms and improving global neural environment in the ischemic regions. Future investigations to elucidate the underlying molecular mechanisms that lead to facilitated rehabilitation with XSEC + EE combination treatment are necessary.

CONCLUSION

Taken together, our data implicated that XSEC + EE combination had synergistic effects in promoting endogenous brain remodeling by inducing oligodendrogenesis, increasing myelinated axons, and promoting axonal reorganization in the peri-infarct regions coupled with downregulating intrinsic axonal growth inhibitory signaling, thereby improving learning and memory function outcome after an ischemic stroke. This is an important result that should impact the future design of neurorestorative treatment to stimulate brain remodeling processes using multifactorial combination therapies.

DATA AVAILABILITY STATEMENT

The raw data supporting the conclusions of this article will be made available by the authors, without undue reservation, to any qualified researcher.

ETHICS STATEMENT

The animal study was reviewed and approved by the National Institutes of Health Guide for the Care and Use of Laboratory Animals Capital Medical University Animal Ethics Committee.

AUTHOR CONTRIBUTIONS

M-ZL performed qRT-PCR experiments, analyzed data, and drafted the manuscript. X-FF carried out animal experiments. TZ performed behavior tests. YZ contributed to immunostaining examination. LY conducted western blot detection. J-FL performed MRI experiments. H-YZ helped to analyze data. LW revised the manuscript. HZ designed the study, supervised the whole project and reviewed the manuscript.

FUNDING

This work was supported by the National Natural Science Foundation of China (Grant Nos. 81774381 and 81473745) and the Beijing Municipal Natural Science Foundation (Grant No. 7172034).

ACKNOWLEDGMENTS

We thank Zhong-Xin Xiao for his help in microscope imaging.

REFERENCES

Ashwal, S., Tone, B., Tian, H. R., Cole, D. J., and Pearce, W. J. (1998). Core and penumbral nitric oxide synthase activity during cerebral ischemia and reperfusion. *Stroke* 29, 1037–1046. doi: 10.1161/01.STR.29.5.1037

Aung, W. Y., Mar, S., and Benzinger, T. L. (2013). Diffusion tensor MRI as a biomarker in axonal and myelin damage. *Imaging Med.* 5, 427–440. doi: 10.2217/iim.13.49

Bai, Y. Y., Wang, L. S., Chang, D., Zhao, Z., Lu, C. Q., Wang, G. Z., et al. (2015). Synergistic effects of transplanted endothelial progenitor cells and RWJ 67657 in diabetic ischemic stroke models. *Stroke* 46, 1938–1946. doi: 10.1161/STROKEAHA.114.008495

Blumenfeld-Katzir, T., Pasternak, O., Dagan, M., and Assaf, Y. (2011). Diffusion MRI of structural brain plasticity induced by a learning and memory task. *PLoS One* 6:e20678. doi: 10.1371/journal.pone.0020678

Braun, R., Klein, R., Walter, H. L., Ohren, M., Freudenmacher, L., Getachew, K., et al. (2016). Transcranial direct current stimulation accelerates recovery of function, induces neurogenesis and recruits oligodendrocyte precursors in a rat model of stroke. *Exp. Neurol.* 279, 127–136. doi: 10.1016/j.expneurol.2016.02.018

Cafferty, W. B. J., Mcgee, A. W., and Strittmatter, S. M. (2008). Axonal growth therapeutics: regeneration or sprouting or plasticity? *Trends Neurosci.* 31, 215–220. doi: 10.1016/j.tins.2008.02.004

Chan, K. C., Khong, P. L., Lau, H. F., Cheung, P. T., and Wu, E. X. (2009). Late measures of microstructural alterations in severe neonatal hypoxic-ischemic encephalopathy by MR diffusion tensor imaging. *Int. J. Dev. Neurosci.* 27, 607–615. doi: 10.1016/j.ijdevneu.2009.05.012

Chang, I. A., Lim, H. D., Kim, K. J., Shin, H., and Namgung, U. (2016). Enhanced axonal regeneration of the injured sciatic nerve by administration of Buyang Huanwu decoction. *J. Ethnopharmacol.* 194, 626–634. doi: 10.1016/j.jep.2016.10.053

Chen, A., Wang, H., Zhang, J. W., Wu, X. Q., Liao, J., Li, H., et al. (2008). BYHWD rescues axotomized neurons and promotes functional recovery after spinal cord injury in rats. *J. Ethnopharmacol.* 117, 451–456. doi: 10.1016/j.jep.2008.02.029

Chen, H. J., Shen, Y. C., Shiao, Y. J., Liou, K. T., Hsu, W. H., Hsieh, P. H., et al. (2015). Multiplex brain proteomic analysis revealed the molecular therapeutic effects of Buyang Huanwu Decoction on cerebral ischemic stroke mice. *PLoS One* 10:e0140823. doi: 10.1371/journal.pone.0140823

Chen, J. L., Venkat, P., Zacharek, A., and Chopp, M. (2014). Neurorestorative therapy for stroke. *Front. Hum. Neurosci.* 8:382. doi: 10.3389/fnhum.2014.00382

Chen, X., Wu, H., Chen, H., Wang, Q., Xie, X. J., and Shen, J. (2019). Astragaloside VI promotes neural stem cell proliferation and enhances neurological function recovery in transient cerebral ischemic injury via activating EGFR/MAPK signaling cascades. *Mol. Neurobiol.* 56, 3053–3067. doi: 10.1007/s12035-018-1294-3

Chen, X. P., Zhang, X., Xue, L., Hao, C. Z., Liao, W. J., and Wan, Q. (2017). Treatment with enriched environment reduces neuronal apoptosis in the periinfarct cortex after cerebral ischemia/reperfusion injury. *Cell. Physiol. Biochem.* 41, 1445–1456. doi: 10.1159/000468368

Chesik, D., De Keyser, J., and Wilczak, N. (2008). Insulin-like growth factor system regulates oligodendroglial cell behavior: therapeutic potential in CNS. *J. Mol. Neurosci.* 35, 81–90. doi: 10.1007/s12031-008-9041-2

Dahlqvist, P., Ronnback, A., Bergstrom, S. A., Soderstrom, I., and Olsson, T. (2004). Environmental enrichment reverses learning impairment in the Morris water maze after focal cerebral ischemia in rats. *Eur. J. Neurosci.* 19, 2288–2298. doi: 10.1111/j.1460-9568.2004.03248.x

Etherton, M. R., Wu, O., Giese, A. K., Lauer, A., Boulouis, G., Mills, B., et al. (2019). White matter integrity and early outcomes after acute ischemic stroke. *Transl. Stroke Res.* 10, 630–638. doi: 10.1007/s12975-019-0689-4

Etienne-Manneville, S., and Hall, A. (2002). Rho GTPases in cell biology. *Nature* 420, 629–635. doi: 10.1038/nature01148

Franklin, R. J. M., and Goldman, S. A. (2015). Glia disease and repair - remyelination. *Cold Spring Harb. Perspect. Biol.* 7:a020594. doi: 10.1101/cshperspect.a020594

Fu, S., Gu, Y., Jiang, J. Q., Chen, X., Xu, M., Chen, X., et al. (2014). Calycosin-7-O-beta-D-glucoside regulates nitric oxide/caveolin-1/matrix metalloproteinases pathway and protects blood-brain barrier integrity in experimental cerebral ischemia-reperfusion injury. *J. Ethnopharmacol.* 155, 692–701. doi: 10.1016/j.jep.2014.06.015

Fujita, Y., and Yamashita, T. (2014). Axon growth inhibition by RhoA/ROCK in the central nervous system. *Front. Neurosci.* 8:338. doi: 10.3389/fnins.2014.00338

Gladstone, D. J., Black, S. E., and Hakim, A. M. (2002). Toward wisdom from failure - Lessons from neuroprotective stroke trials and new therapeutic directions. *Stroke* 33, 2123–2136. doi: 10.1161/01.STR.0000025518.34157.51

Gould, E., Beylin, A., Tanapat, P., Reeves, A., and Shors, T. J. (1999). Learning enhances adult neurogenesis in the hippocampal formation. *Nat. Neurosci.* 2, 260–265. doi: 10.1038/6365

Granziera, C., D'Arceuil, H., Zai, L., Magistretti, P. J., Sorensen, A. G., and de Crespigny, A. J. (2007). Long-term monitoring of post-stroke plasticity after transient cerebral ischemia in mice using in vivo and ex vivo diffusion tensor MRI. *Open Neuroimag. J.* 1, 10–17. doi: 10.2174/1874440000701010010

Hao, C. Z., Wu, F., Shen, J., Lu, L., Fu, D. L., Liao, W. J., et al. (2012). Clinical efficacy and safety of buyang huanwu decoction for acute ischemic stroke: a systematic review and meta-analysis of 19 randomized controlled trials. *Evid Based Complement. Alternat. Med.* 2012:630124. doi: 10.1155/2012/630124

Hofstetter, S., and Assaf, Y. (2017). The rapid development of structural plasticity through short water maze training: a DTI study. *Neuroimage* 155, 202–208. doi: 10.1016/j.neuroimage.2017.04.056

Huang, F., Lan, Y., Qin, L., Dong, H., Shi, H., Wu, H., et al. (2018). Astragaloside IV promotes adult neurogenesis in hippocampal dentate gyrus of mouse through CXCL1/CXCR2 signaling. *Molecules* 23:E2178. doi: 10.3390/molecules23092178

Janssen, H., Ada, L., Bernhardt, J., McElduff, P., Pollack, M., Nilsson, M., et al. (2014). An enriched environment increases activity in stroke patients undergoing rehabilitation in a mixed rehabilitation unit: a pilot non-randomized controlled trial. *Disabil. Rehabil.* 36, 255–262. doi: 10.3109/09638288.2013.788218

Jiang, C. Y., Yu, K. W., Wu, Y., Xie, H. Y., Liu, G., Wu, J. F., et al. (2016). Enriched environment enhances poststroke neurological function recovery on rat: involvement of p-ERK1/2. *J. Stroke Cerebrovasc.* 25, 1590–1598. doi: 10.1016/j.jstrokecerebrovasdis.2016.03.004

Jiang, Q., Zhang, Z. G., and Chopp, M. (2010a). MRI evaluation of white matter recovery after brain injury. *Stroke* 41, S112–S113. doi: 10.1161/STROKEAHA.110.595629

Jiang, Q., Zhang, Z. G., and Chopp, M. (2010b). MRI of stroke recovery. *Stroke* 41, 410–414. doi: 10.1161/STROKEAHA.109.568048

Jing, Z., Shi, C. Z., Zhu, L. H., Xiang, Y. H., Chen, P. H., Xiong, Z. L., et al. (2015). Chronic cerebral hypoperfusion induces vascular plasticity and hemodynamics but also neuronal degeneration and cognitive impairment. *J. Cereb. Blood Flow Metab.* 35, 1249–1259. doi: 10.1038/jcbfm.2015.55

Jung, W. B., Han, Y. H., Chung, J. J., Chae, S. Y., Lee, S. H., Im, G. H., et al. (2017). Spatiotemporal microstructural white matter changes in diffusion tensor imaging after transient focal ischemic stroke in rats. *NMR Biomed.* 30:e3704. doi: 10.1002/nbm.3704

Kesner, R. P., and Churchwell, J. C. (2011). An analysis of rat prefrontal cortex in mediating executive function. *Neurobiol. Learn. Mem.* 96, 417–431. doi: 10.1016/j.nlm.2011.07.002

Kilic, E., ElAli, A., Kilic, U., Guo, Z. Y., Ugur, M., Uslu, U., et al. (2010). Role of Nogo-A in neuronal survival in the reperfused ischemic brain. *J. Cereb. Blood Flow Metab.* 30, 969–984. doi: 10.1038/jcbfm.2009.268

Kim, K. J., and Namgung, U. (2018). Facilitating effects of Buyang Huanwu decoction on axonal regeneration after peripheral nerve transection. *J. Ethnopharmacol.* 213, 56–64. doi: 10.1016/j.jep.2017.10.036

Ko, C. H., Huang, C. P., Lin, Y. W., and Hsieh, C. L. (2018). Paeoniflorin has anti-inflammation and neurogenesis functions through nicotinic acetylcholine receptors in cerebral ischemia-reperfusion injury rats. *Iran. J. Basic Med. Sci.* 21, 1174–1178. doi: 10.22038/Ijbms.2018.30371.7322

Komitova, M., Perfilieva, E., Mattsson, B., Eriksson, P. S., and Johansson, B. B. (2006). Enriched environment after focal cortical ischemia enhances the generation of astroglia and NG2 positive polydendrocytes in adult rat neocortex. *Exp. Neurol.* 199, 113–121. doi: 10.1016/j.expneurol.2005.12.007

Li, H., Liu, Y., Wen, M., Zhao, F., Zhao, Z., Liu, Y., et al. (2019). Hydroxysafflor yellow A (HSYA) alleviates apoptosis and autophagy of neural stem cells induced by heat stress via p38 MAPK/MK2/Hsp27-78 signaling pathway. *Biomed. Pharmacother.* 114:108815. doi: 10.1016/j.biopha.2019.108815

Li, M., Li, H., Fang, F., Deng, X., and Ma, S. (2017). Astragaloside IV attenuates cognitive impairments induced by transient cerebral ischemia and reperfusion in mice via anti-inflammatory mechanisms. *Neurosci. Lett.* 639, 114–119. doi: 10.1016/j.neulet.2016.12.046

Li, M. Z., Zhang, Y., Zou, H. Y., Ouyang, J. Y., Zhan, Y., Yang, L., et al. (2018a). Investigation of *Ginkgo biloba* extract (EGb 761) promotes neurovascular restoration and axonal remodeling after embolic stroke in rat using magnetic resonance imaging and histopathological analysis. *Biomed. Pharmacother.* 103, 989–1001. doi: 10.1016/j.biopha.2018.04.125

Li, M. Z., Zhang, Y., Zou, H. Y., Wang, Y. L., Cheng, B. Y., Wang, L., et al. (2018b). Xiaoshuan enteric-coated capsule alleviates cognitive impairment by enhancing hippocampal glucose metabolism, hemodynamics and neuroplasticity of rat with chronic cerebral hypoperfusion. *Sci. Rep.* 8:7449. doi: 10.1038/s41598-018-25929-0

Liu, H. S., Shen, H., Harvey, B. K., Castillo, P., Lu, H. B., Yang, Y. H., et al. (2011). Post-treatment with amphetamine enhances reinnervation of the ipsilateral side cortex in stroke rats. *Neuroimage* 56, 280–289. doi: 10.1016/j.neuroimage.2011.02.049

Livingston-Thomas, J., Nelson, P., Karthikeyan, S., Antonescu, S., Jeffers, M. S., Marzolini, S., et al. (2016). Exercise and environmental enrichment as enablers of task-specific neuroplasticity and stroke recovery. *Neurotherapeutics* 13, 395–402. doi: 10.1007/s13311-016-0423-9

Loncarevic-Vasiljkovic, N., Pesic, V., Tanic, N., Milanovic, D., Popic, J., Kanazir, S., et al. (2009). Changes in markers of neuronal and glial plasticity after cortical injury induced by food restriction. *Exp. Neurol.* 220, 198–206. doi: 10.1016/j.expneurol.2009.08.024

Longa, E. Z., Weinstein, P. R., Carlson, S., and Cummins, R. (1989). Reversible middle cerebral artery occlusion without craniectomy in rats. *Stroke* 20, 84–91. doi: 10.1161/01.STR.20.1.84

Miron, V. E., Boyd, A., Zhao, J. W., Yuen, T. J., Ruckh, J. M., Shadrach, J. L., et al. (2013). M2 microglia and macrophages drive oligodendrocyte differentiation during CNS remyelination. *Nat. Neurosci.* 16, 1211–1275. doi: 10.1038/nn.3469

Moore, C. S., Abdullah, S. L., Brown, A., Arulpragasam, A., and Crocker, S. J. (2011). How factors secreted from astrocytes impact myelin repair. *J. Neurosci. Res.* 89, 13–21. doi: 10.1002/jnr.22482

Morris, R. G., Garrud, P., Rawlins, J. N., and O'Keefe, J. (1982). Place navigation impaired in rats with hippocampal lesions. *Nature* 297, 681–683. doi: 10.1038/297681a0

Nygren, J., Wieloch, T., Pesic, J., Brundin, P., and Deierborg, T. (2006). Enriched environment attenuates cell genesis in subventricular zone after focal ischemia in mice and decreases migration of newborn cells to the striatum. *Stroke* 37, 2824–2829. doi: 10.1161/01.STR.0000244769.39952.90

Otero-Ortega, L., Gomez-de Frutos, M. C., Laso-Garcia, F., Sanchez-Gonzalo, A., Martinez-Arroyo, A., Diez-Tejedor, E., et al. (2017). NogoA neutralization promotes axonal restoration after white matter injury in subcortical stroke. *Sci. Rep.* 7:9431. doi: 10.1038/s41598-017-09705-0

Paxinos, G., and Watson, C. (1986). *The Rat Brain in Stereotaxic Coordinates*. Sydney: Academic Press.

Pernet, V., and Schwab, M. E. (2012). The role of Nogo-A in axonal plasticity, regrowth and repair. *Cell Tissue Res.* 349, 97–104. doi: 10.1007/s00441-012-1432-6

Pitkonen, M., Abo-Ramadan, U., Marinkovic, I., Pedrono, E., Hasan, K. M., Strbian, D., et al. (2012). Long-term evolution of diffusion tensor indices after temporary experimental ischemic stroke in rats. *Brain Res.* 1445, 103–110. doi: 10.1016/j.brainres.2012.01.043

Plane, J. M., Whitney, J. T., Schallert, T., and Parent, J. M. (2008). Retinoic acid and environmental enrichment alter subventricular zone and striatal neurogenesis after stroke. *Exp. Neurol.* 214, 125–134. doi: 10.1016/j.expneurol.2008.08.006

Ramos-Cejudo, J., Gutierrez-Fernandez, M., Otero-Ortega, L., Rodriguez-Frutos, B., Fuentes, B., Vallejo-Cremades, M. T., et al. (2015). Brain-derived neurotrophic factor administration mediated oligodendrocyte differentiation and myelin formation in subcortical ischemic stroke. *Stroke* 46, 221–228. doi: 10.1161/STROKEAHA.114.006692

Ruscher, K., Johannesson, E., Brugiere, E., Erickson, A., Rickhag, M., and Wieloch, T. (2009). Enriched environment reduces apolipoprotein E (ApoE) in reactive astrocytes and attenuates inflammation of the peri-infarct tissue after experimental stroke. *J. Cereb. Blood Flow Metab.* 29, 1796–1805. doi: 10.1038/jcbfm.2009.96

Sandelius, A., Cullen, N. C., Kallen, A., Rosengren, L., Jensen, C., Kostanjevecki, V., et al. (2018). Transient increase in CSF GAP-43 concentration after ischemic stroke. *BMC Neurol.* 18:202. doi: 10.1186/s12883-018-1210-5

Schwab, M. E., and Strittmatter, S. M. (2014). Nogo limits neural plasticity and recovery from injury. *Curr. Opin. Neurobiol.* 27, 53–60. doi: 10.1016/j.conb.2014.02.011

See, J. M., and Grinspan, J. B. (2009). Sending mixed signals: bone morphogenetic protein in myelination and demyelination. *J. Neuropathol. Exp. Neurol.* 68, 595–604. doi: 10.1097/NEN.0b013e3181a66ad9

Shi, X. Z., Kang, Y. L., Hu, Q., Chen, C. H., Yang, L., Wang, K., et al. (2010). A long-term observation of olfactory ensheathing cells transplantation to repair white matter and functional recovery in a focal ischemia model in rat. *Brain Res.* 1317, 257–267. doi: 10.1016/j.brainres.2009.12.061

Soderstrom, I., Strand, M., Ingridsson, A. C., Nasic, S., and Olsson, T. (2009). 17 beta-estradiol and enriched environment accelerate cognitive recovery after focal brain ischemia. *Eur. J. Neurosci.* 29, 1215–1224. doi: 10.1111/j.1460-9568.2009.06662.x

Sumiyoshi, A., Taki, Y., Nonaka, H., Takeuchi, H., and Kawashima, R. (2014). Regional gray matter volume increases following 7 days of voluntary wheel running exercise: a longitudinal VBM study in rats. *Neuroimage* 98, 82–90. doi: 10.1016/j.neuroimage.2014.04.075

Tuor, U. I., Morgunov, M., Sule, M., Qiao, M., Clark, D., Rushforth, D., et al. (2014). Cellular correlates of longitudinal diffusion tensor imaging of axonal degeneration following hypoxic-ischemic cerebral infarction in neonatal rats. *Neuroimage Clin.* 6, 32–42. doi: 10.1016/j.nicl.2014.08.003

Ueno, Y., Chopp, M., Zhang, L., Buller, B., Liu, Z., Lehman, N. L., et al. (2012). Axonal outgrowth and dendritic plasticity in the cortical peri-infarct area after experimental stroke. *Stroke* 43, 2221–2228. doi: 10.1161/STROKEAHA.111.646224

Vorhees, C. V., and Williams, M. T. (2006). Morris water maze: procedures for assessing spatial and related forms of learning and memory. *Nat. Protoc.* 1, 848–858. doi: 10.1038/nprot.2006.116

Wang, Y., Liu, G., Hong, D. D., Chen, F. H., Ji, X. M., and Cao, G. D. (2016). White matter injury in ischemic stroke. *Prog. Neurobiol.* 141, 45–60. doi: 10.1016/j.pneurobio.2016.04.00

Wei, C. J., Singer, P., Coelho, J., Boison, D., Feldon, J., Yee, B. K., et al. (2011). Selective inactivation of adenosine A(2A) receptors in striatal neurons enhances working memory and reversal learning. *Learn. Mem.* 18, 459–474. doi: 10.1101/lm.2136011

Wei, R. L., Teng, H. J., Yin, B., Xu, Y., Du, Y., He, F. P., et al. (2013). A systematic review and meta-analysis of Buyang Huanwu Decoction in animal model of focal cerebral ischemia. *Evid. Based Complement. Alternat. Med.* 2013:138484. doi: 10.1155/2013/138484

Wiesmann, M., Zinnhardt, B., Reinhardt, D., Eligehausen, S., Wachsmuth, L., Hermann, S., et al. (2017). A specific dietary intervention to restore brain structure and function after ischemic stroke. *Theranostics* 7, 493–512. doi: 10.7150/thno.17559

Xie, H. Y., Yu, K. W., Zhou, N. Y., Shen, X. Y., Tian, S., Zhang, B., et al. (2019). Enriched environment elicits proangiogenic mechanisms after focal cerebral ischemia. *Transl. Stroke Res.* 10, 150–159. doi: 10.1007/s12975-018-0629-8

Yin, F., Zhou, H., Fang, Y., Li, C., He, Y., Yu, L., et al. (2019). Astragaloside IV alleviates ischemia reperfusion-induced apoptosis by inhibiting the activation of key factors in death receptor pathway and mitochondrial pathway. *J. Ethnopharmacol.* 248:112319. doi: 10.1016/j.jep.2019.112319

Yu, L., Duan, Y., Zhao, Z., He, W., Xia, M., Zhang, Q., et al. (2018). Hydroxysafflor yellow A (HSYA) improves learning and memory in cerebral ischemia reperfusion-injured rats via recovering synaptic plasticity in the hippocampus. *Front. Cell. Neurosci.* 12:371. doi: 10.3389/fncel.2018.00371

Zatorre, R. J., Fields, R. D., and Johansen-Berg, H. (2012). Plasticity in gray and white: neuroimaging changes in brain structure during learning. *Nat. Neurosci.* 15, 528–536. doi: 10.1038/nn.3045

Zhan, Y., Li, M. Z., Yang, L., Feng, X. F., Zhang, Q. X., Zhang, N., et al. (2019). An MRI study of neurovascular restorative after combination treatment with *Xiaoshuan* enteric-coated capsule and enriched environment in rats after stroke. *Front. Neurosci.* 13:701. doi: 10.3389/fnins.2019.00701

Zhang, J., Zou, H., Zhang, Q., Wang, L., Lei, J., Wang, Y., et al. (2016). Effects of *Xiaoshuan* enteric-coated capsule on neurovascular functions assessed by quantitative multiparametric MRI in a rat model of permanent cerebral

ischemia. *BMC Complement. Altern. Med.* 16:198. doi: 10.1186/s12906-016-1184-z

Zhang, L., Chopp, M., Zhang, R. L., Wang, L., Zhang, J., Wang, Y., et al. (2010). Erythropoietin amplifies stroke-induced oligodendrogenesis in the rat. *PLoS One* 5:e11016. doi: 10.1371/journal.pone.0011016

Zhang, L. G., Wang, L. J., Shen, Q. Q., Wang, H. F., Zhang, Y., Shi, C. G., et al. (2017). Paeoniflorin improves regional cerebral blood flow and suppresses inflammatory factors in the hippocampus of rats with vascular dementia. *Chin. J. Integr. Med.* 23, 696–702. doi: 10.1007/s11655-015-2124-3

Zhang, R. L., Chopp, M., Roberts, C., Wei, M., Wang, X. L., Liu, X. S., et al. (2012). Sildenafil enhances neurogenesis and oligodendrogenesis in ischemic brain of middle-aged mouse. *PLoS One* 7:e48141. doi: 10.1371/journal.pone.0048141

Zhang, R. L., Chopp, M., and Zhang, Z. G. (2013). Oligodendrogenesis after cerebral ischemia. *Front. Cell. Neurosci.* 7:201. doi: 10.3389/fncel.2013.00201

Zhang, X., Chen, X. P., Lin, J. B., Xiong, Y., Liao, W. J., and Wan, Q. (2017). Effect of enriched environment on angiogenesis and neurological functions in rats with focal cerebral ischemia. *Brain Res.* 1655, 176–185. doi: 10.1016/j.brainres.2016.11.001

Zhang, Y. J., Xu, D., Qi, H., Yuan, Y., Liu, H., Yao, S. L., et al. (2018). Enriched environment promotes post-stroke neurogenesis through NF-κB-mediated secretion of IL-17A from astrocytes. *Brain Res.* 1687, 20–31. doi: 10.1016/j.brainres.2018.02.030

Zhang, Z. G., and Chopp, M. (2009). Neurorestorative therapies for stroke: underlying mechanisms and translation to the clinic. *Lancet Neurol.* 8, 491–500. doi: 10.1016/S1474-4422(09)70061-4

Zhao, L. D., Wang, J. H., Jin, G. R., Zhao, Y., and Zhang, H. J. (2012). Neuroprotective effect of Buyang Huanwu Decoction against focal cerebral ischemia/reperfusion injury in rats - Time window and mechanism. *J. Ethnopharmacol.* 140, 339–344. doi: 10.1016/j.jep.2012.01.026

Zou, H. Y., Long, J. F., Zhang, Q. X., Zhao, H. Y., Bian, B. L., Wang, Y. L., et al. (2016). Induced cortical neurogenesis after focal cerebral ischemia - Three active components from Huang-Lian-Jie-Du decoction. *J. Ethnopharmacol.* 178, 115–124. doi: 10.1016/j.jep.2015.12.001

Conflict of Interest: The authors declare that the research was conducted in the absence of any commercial or financial relationships that could be construed as a potential conflict of interest.

Copyright © 2019 Li, Zhan, Yang, Feng, Zou, Lei, Zhao, Wang and Zhao. This is an open-access article distributed under the terms of the Creative Commons Attribution License (CC BY). The use, distribution or reproduction in other forums is permitted, provided the original author(s) and the copyright owner(s) are credited and that the original publication in this journal is cited, in accordance with accepted academic practice. No use, distribution or reproduction is permitted which does not comply with these terms.

frontiers in Pharmacology

REVIEW
published: 14 January 2020
doi: 10.3389/fphar.2019.01549

Saussureae Involucratae Herba (Snow Lotus): Review of Chemical Compositions and Pharmacological Properties

Guowei Gong[1†], Jing Huang[2†], Yang Yang[1], Baohui Qi[1], Guangyi Han[3], Yuzhong Zheng[4], Huan He[1], Kelvin Chan[5], Karl WK Tsim[6,7] and Tina TX Dong[6,7*]*

[1] Department of Biological Engineering, Zunyi Medical University, Zhuhai, China, [2] College of Environmental and Biological Engineering, Putian University, Putian, China, [3] Gansu Institute for Drug Control, Lanzhou, China, [4] Department of Biology, Hanshan Normal University, Chaozhou, China, [5] School of Pharmacy & Biomolecular Sciences, Liverpool John Moores University, Liverpool, United Kingdom, [6] Shenzhen Key Laboratory of Edible and Medicinal Bioresources, HKUST Shenzhen Research Institute, Shenzhen, China, [7] Division of Life Science and Center for Chinese Medicine, The Hong Kong University of Science and Technology, Hong Kong, Hong Kong

OPEN ACCESS

Edited by:
Jing-Yan Han,
Peking University, China

Reviewed by:
Ying Wang,
University of Macau, China
Hubiao Chen,
Hong Kong Baptist University, Hong Kong

***Correspondence:**
Kelvin Chan
k.k.chan@ljmu.ac.uk
Tina TX Dong
botina@ust.hk

[†]These authors have contributed equally to this work

Specialty section:
This article was submitted to Ethnopharmacology, a section of the journal Frontiers in Pharmacology

Received: *09 April 2019*
Accepted: *29 November 2019*
Published: *14 January 2020*

Citation:
Gong G, Huang J, Yang Y, Qi B, Han G, Zheng Y, He H, Chan K, Tsim KWK and Dong TTX (2020) Saussureae Involucratae Herba (Snow Lotus): Review of Chemical Compositions and Pharmacological Properties. Front. Pharmacol. 10:1549. doi: 10.3389/fphar.2019.01549

Saussureae Involucratae Herba is the dried ground part of *Saussurea involucrata* (Kar. et Kir.) Sch.-Bip, which is also named as "Snow lotus" and being used in traditional Uyghur and/or Chinese medicine. This rare herb can be found at 4,000 m elevation in western part of Tianshan Mountain, Xinjiang China. According to China Pharmacopoeia (2015), the major pharmaceutical values of "Snow lotus" (Xuě liánhuā in Chinese) are alleviating rheumatoid arthritis, accelerating blood circulation and mitigating other "cold" syndromes. Traditionally, the clinical application of "Snow lotus" includes the treatments in inflammation-associated disorder, blood circulation acceleration and heat and dampness elimination. Recent studies suggested that "Snow lotus" possessed therapeutic effects associating with anti-cancer, anti-oxidation, adipogenesis suppression and neuroprotection activities, which were proposed to be related with its bioactive constitutes, i.e. acacetin, hispidulin, and rutin. In the present review, we aim to summarize pharmacological effects and underlying cell signaling pathways of "Snow lotus" in treating various medical problems.

Keywords: Saussureae Involucratae Herba, traditional Chinese medicine, traditional Uyghur medicine, herbal medicine, Snow lotus

INTRODUCTION

The history of Traditional Uyghur medicine (TUM) spans over 2,500 years and is still being practiced today (Upur et al., 2011). Ghazi Bay recorded fennel, senna, salt and other 312 types of TUM herbs, as well as its therapeutic functions, in the book of "Ghazi Bay medicinal book", written in about 400 B.C. (Yishakejiang et al., 2005). The predominant concept of TUM is based on four unique elements of air, fire, water and soil, and each element is corresponding to specific humor, i.e. "phlegm", "blood", "yellow bile" and "black bile" (Shahabi et al., 2008). Uygur doctors believe that the occurrence of disease has close relationship with the destruction of temperament balance, which

results in abnormal body fluid disequilibrium. The mainstay of health is to keep right ratio and precise balance of humors based on their quality and quantity. Therefore, adjusting and balancing body fluids are the fundamental principle for disorder treatments according to the TUM theory. Indeed, traditional Chinese medicine (TCM) and TUM share abundant similarities, and the major responsibilities of TUM and/or TCM are modulating health conditions, promoting health and having therapeutic strategies for specific diseases or symptom treatments. Nowadays, traditional medicine is often referring to complementary or alternative medicine. In developing countries, e.g. Asian and African, up to 80% of the population consumes herbal decoction in meeting the primary health care needs. A massive of ancient literatures, including book and pharmacopoeia, have recorded the existence of TCM and/or TUM prescriptions and their beneficial functions, disease preventions and clinical applications (Packer et al., 2004). Nevertheless, the metabolites, pharmaceutical values and action mechanisms of these TCM and/or TUM in modulating human health are still behind veil. This review provides some detailed information and pharmaceutical values of TUM and/or TCM herbal materials in general, using "Snow lotus" as an example.

According to the China Pharmacopoeia (2015), "Snow lotus" is the dried ground part of *Saussurea involucrata* (Kar. et Kir.) Sch.-Bip (**Figure 1**), which is being used for inflammation-associated disorder treatments, such as rheumatoid arthritis, cancer, modulating lipid metabolism, and improving gynecological and reproductive problem, enhancing blood circulation and mitigation of other "cold" syndrome (Chik et al., 2015). The incidences of rheumatoid arthritis, gastric cancer and hepatic cancer are much less in Uygur population, as compared to other parts of China, probably have a close relationship with the common consumption of "Snow lotus" in Xinjiang area (Byambaragchaa et al., 2013; Yu et al., 2013; Chik et al., 2015; Wang et al., 2016). According to China Pharmacopeia (2015), the primary pharmaceutical values of "Snow lotus" is maintaining body homeostasis. **Figure 2** summarizes the possible functions of "Snow lotus". The major bioactive components exhibited the clinical functions were reported to be acacetin, hispidulin and rutin (Chik et al., 2015). The structures of these chemicals are presently shown in **Figure 3**. Most of the "Snow lotus"-concentrated herbal decoctions are capable of mitigating "cold" syndromes or diseases both in male and female. This materia medica is one of the major ingredients found within "Snow lotus" capsule being sold in China, which is aiming for dysmenorrhoea treatment. Moreover, the water decoction having "Snow lotus", *Lycii fructus* and *Angelica sinensis* Radix could promote the secretion of androgen, to enhance the sexual function for male patients, which therefore has been used for infertility treatment (Zhao, 1963).



FIGURE 1 | The pictures of Snow lotus. Saussureae Involucratae Herba is described in the HKCMMS Volume 8. http://www.cmd.gov.hk/hkcmms/vol8/pdf_e/Saussureae_Involucratae_Herba_v8_e.pdf.

BOTANICAL CLASSIFICATION

"Snow lotus" is a dicotyledonous plant, classified under Compositae. The commonly found "Snow lotus" is clustered into subgenus of *Amphilaena* and *Eriocovgne*. The subgenus of *Amphilaena* contains *S. involucrata, S. globosa,* S. *wettsteiniana,* S. *polycolea,* S. *uniflora,* S. *velutina,* S. *phaeantha,* S. *orgaadayi,* S. *tangutica,* S. *bracteata,* S. *erubescens,* S. *nigrescens,* S. *iodostegia,* S. *glandulosissima, and* S. *sikkimensi* (Chen et al., 2019). The subgenus of *Eriocovgne* includes *S. aster, S. glacialis, S. gnaphaloides, S. laniceps* and *S. medusa* (Zhai et al., 2009). However, *S. involucrata*, *S. laniceps*, and *S. medusa* are the most commonly used species in clinical applications (Yi et al., 2010).

The morphological features of *S. involucrata* show similarities with *S. laniceps* and *S. medusa* (Chen et al., 2014a). The microscopic characteristics, as determined by scanning electron microscopy (SEM), of these *Saussurea* species had been reported and identified: the pollen grains were the indicative markers showing their distinctive characteristics. The pollen grains of *S. laniceps* was sub-rounded, light yellow, covered with perforate and verruca warts. However, the pollen of *S. medusa* was bigger, and the outer surface was sculptured with dense spinules. *S. involucrata* had yellow pollen and wart on outer surface (Chen et al., 2014a). Recently, a new species of "Snow lotus", named as *S. bogedaensis*, has been explored and reported in the eastern part of Tianshan Mountain (Chen and Wang, 2018). The genetic analysis showed that *S. bogedaensis* and *S. involucrata* had a close relationship, which might suggest that these two plants are deriving from a common ancestor (Chen and Wang, 2018). Moreover, *S. bogedaensis* shares similar pharmaceutical values

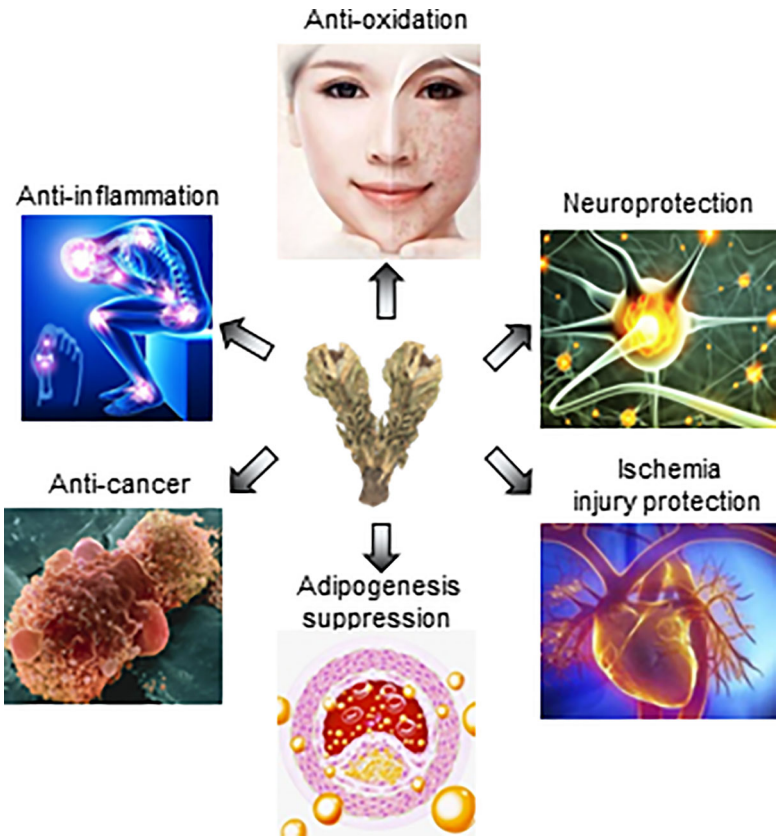


FIGURE 2 | The pharmaceutical values of Snow lotus. Saussureae Involucratae Herba possesses anti-oxidative functions, neuroprotective effects, anti-inflammatory-induced diseases, anti-cancer, anti-obesity and ischemia injury protective pharmaceutical values.

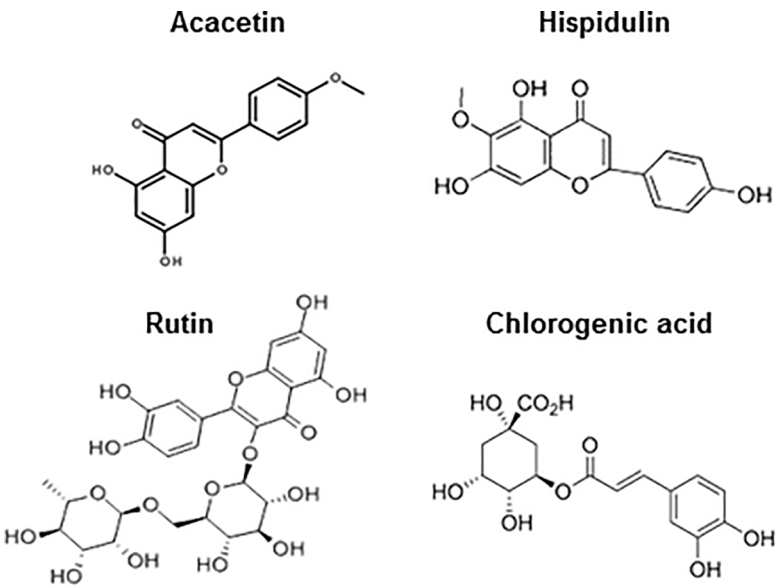


FIGURE 3 | Chemical structures of major bioactive components isolated from Snow lotus. The chemical structures of acacetin, hispidulin, rutin and chlorogenic acid are shown here.

with *S. involucrate*; hence, *S. bogedaensis* could act as an alternative to *S. involucrata* in clinical applications. Yi et al., 2010 conducted systematic experiments to demonstrate that *S. laniceps* was the most potent *Saussurea* species as the source of TCM, instead of *S. involucrata* or *S. medusa*.

BIOSYNTHESIS OF SECONDARY METABOLITES

The full-length gene encoding flavonoid-3-O-glucosyltransferase (3GT) (GenBank Accession No. JN092127), cloned from *S. involucrata,* was isolated and employed to search for the biosynthesis of plant secondary metabolites (**Figure 4**). The transcripts of 3GT members were detected massively in leaves and callus of *S. involucrata,* and which were able to catalyze the secondary glycosylation products by transferring activated sugar donors to acceptors. The 3GT gene of *S. involucrata* was constructed under the control of a cauliflower mosaic virus (CaMV) 35S promoter, and then the homologous transformation was done by an agrobacterium rihizogenes-mediated transformation system (**Figure 4**) (Tang et al., 2012). Thus, a transgenic *S. involucrata* having over expression of 3GT gene was generated. Two major transcriptional factors, i.e. anthocyanin pigment 1 (PAP1) and leaf color (Lc), involved in the phenylpropanoid pathways are proposed to contribute regulatory functions of the biosynthetic pathways (Qiu et al., 2013). In the genetic modified plant, *S. involucrata*, the over expressed PAP1 and Lc were able to accumulate purple pigments by the massive aggregation of anthocyanin (Qiu et al., 2013). In parallel, the increased augmentations of chlorogenic acid, syringin, cyanrine and rutin in the transgenic herbal material were able to increase its anti-oxidative functions, as measured by ABTS (2,2'-azinobis-3-ethylbenzotiazo-line-6-sulfonic acid) and FRAP (ferric reducing anti-oxidant power) (**Figure 5**) (Qiu et al., 2010).

FUNGUS AND HOST PLANT

Fungal growth on *S. involucrata* has been reported to play unique roles. Endophytic fungi, responsible for species diversity and keeping the host fitness, were isolated and identified by morphological and molecular methods from *S. involucrata*. The isolated fungi are classified into 14 taxa, and most of them are belonging to *Cylindrocarpon* sp. (Lv et al., 2010). Some of *S. involucrata* plants contain dark pigment that is named as dark septate endophytic (DSE) fungus (Lv et al., 2010). The most predominant DSE fungus was DSE-37, as determined by the DNA fragment of internal transcribed spacer regions. The results indicated that DSE-37 was congeneric to *Mycocentrospora* (Wu et al., 2010). After over one-month cultivation of *S. involucrata* in the present of DSE-37, fungal hyphae were branched and twisted together and finally formed "hyphae nets" in epidermal layers, which was proposed to be the positive effect of DSE-37 on the root development. Besides, the content of rutin was much concentrated in DSE-37 positive *S. involucrata* plants as compared to the control, indicating DSE-37 was one of

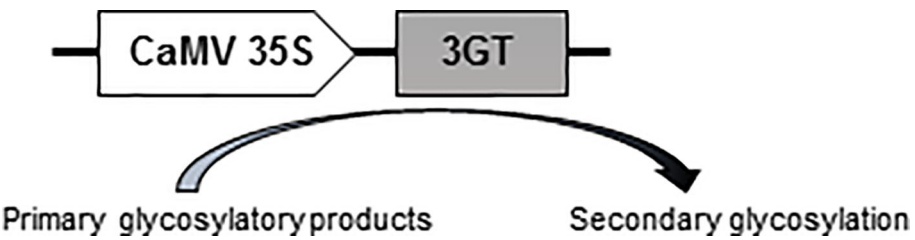


FIGURE 4 | Flow chart of secondary metabolites. The employment of 3GT was used in *S. involucrata* to catalyze the formation of primary glycosylatory metabolites.

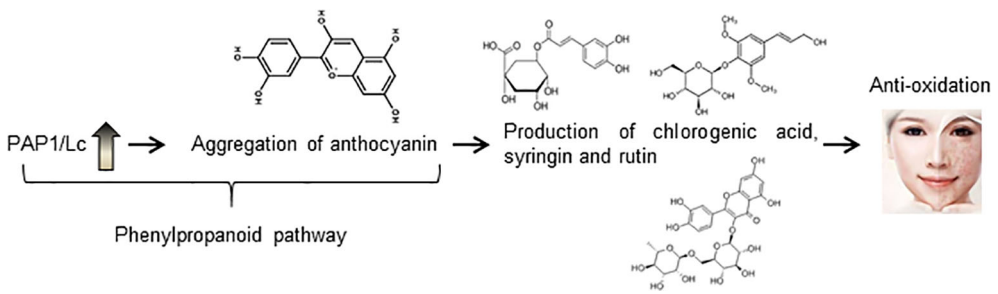


FIGURE 5 | Flow chart of phenylpropanoid pathways. PAP1/Lc up-regulates the biosynthetic pathway of anthocyanin, and which has the mentioned anti-oxidative functions.

indispensable constituents in supporting the development of "Snow lotus" (Wu et al., 2010).

BIOLOGICAL ACTIVITY OF "SNOW LOTUS"

Neuroprotection Effect

"Snow lotus" was found to have therapeutic effects against severe acute pancreatitis (SAP)-induced brain injury using *in vivo* tests. In SAP-induced rats, administration of the extract of "Snow lotus" decreased the mortality rate. In parallel, the serum levels of endothelin-1 (ET-1) and nitric oxide (NO) were significantly reduced, as compared to the control group (Wang et al., 2018). Meanwhile, the pathological changes in pancreas and brain were milder, as comparing to SAP-untreated rats. It is also found that PI3K/Akt signaling pathway was associated with development and progression of SAP-induced brain injury. The intraperitoneal injection of "Snow lotus" extract in SAP-treated rats induced the protein expression of PI3K/Akt (Wang et al., 2018), which should be an indication of therapeutic function of "Snow lotus" in brain damage (**Table 1**). In another investigation on "Snow lotus" extract using D-galactose-induced brain injury mice, promising therapeutic functions were observed. After 6-week of recovery with the herbal treatment in the injured mice, an enhancement of superoxide dismutase and glutathione peroxidase, as well as a decrease of lipid peroxidation, was revealed in the plasma (Yang et al., 2012). Furthermore, the ethyl acetate extract of "Snow lotus"-treated mice showed an improved behavioral performance in step-through passive avoidance task (Yang et al., 2012).

Acacetin, an o-methylated flavone from "Snow lotus" or other Asteraceae family (Zhao et al., 2016a), was shown to be a neuroprotective agent by suppression of depolarization-evoked glutamate release and cytosolic free Ca^{2+} concentration in the hippocampal nerve terminals, which was hypothesized to be prevented by Cav2.2 (N-type) and Cav2.1 (P/Q-type) channel blockers (Lin et al., 2014). Rutin was a predominant bioactive constituent found within "Snow lotus". Consumption of rutin was capable of alleviating the permanent bilateral common carotid artery occlusion (BCCAO) in rat model by revealing central cholinergic functions, oxidative stress-induced damages, inflammatory responses and neuronal damages in cerebral cortex and hippocampus (Qu et al., 2014). Besides, rutin was capable of modulating neurodegeneration by increasing production of neurotropic factors and attenuating rate of apoptosis (Na et al., 2014). The presence of rutin decreased the acrylamide-induced cytotoxicity, as well as the amount of malondialdehyde, as compared to the control group (Motamedshariaty et al., 2014).

Anti-epileptic functions of hispidulin have been proposed to be one of distinctive characteristics in "Snow lotus". This chemical was shown to suppress the release of glutamate, activated by a specific K^+ channel blocker 4-aminopyridine, and which restrained glutamate release from cortical synaptosome *via* presynaptic voltage-dependent Ca^{2+} entry and ERK/synapsin signaling blockage (Lin et al., 2012a). Treatment with hispidulin in cell cultures alleviated the bupivacaine-induced neurotoxicity cell injury *via* enhancing the activations of AMPK and GSK3β levels in mitochondrial membrane (Niu et al., 2014).

Ischemia/Reperfusion Injury Protection

Acacetin acts as a promising atrium-selective agent in treating atrial fibrillation. In human atrial myocytes, acacetin delayed rectifier K^+ current and transient outward K^+ current, as well as prolonging action potential. Besides, acacetin blocked the acetylcholine-activated K^+ current without affecting other cardiac currents (Li et al., 2008). The water-soluble pro-drug, acacetin phosphate, was reported to protect rats from ischemia/reperfusion injury (**Table 2**). Molecular analysis revealed that acacetin prevented the reduction of anti-oxidative kinases and

TABLE 1 | Summary of neuro-protection functions of "Snow lotus" and/or its major biochemical.

Models	Parameters measured	Active components	Reference
In vivo	ET-1 and NO content in serum	"Snow lotus" extract	Wang et al., 2018
In vivo	Behavioral test	Ethyl acetate extract of "Snow lotus"	Yang et al., 2012
In vivo	Cytosolic free Ca^{2+} concentration	Acacetin	Lin et al., 2014
In vivo/ in vitro	Oxidative stress-induced damage, inflammatory responses and neuronal	Rutin	Qu et al., 2014
In vivo	Malondialdehyde	Rutin	Motamedshariaty et al., 2014
In vivo	AMPK and GSK3β activations	Hispidulin	Niu et al., 2014
In vitro	Neurotropic factors production	Rutin	Na et al., 2014
In vitro	Glutamate activation	"Snow lotus" extract	Lin et al., 2012a

TABLE 2 | Summary of ischemia/reperfusion injury protection of "Snow lotus" and/or its major biochemical.

Models	Parameters measured	Active components	Reference
In vivo	Acetylcholine-activated K+ current	Acacetin	Li et al., 2008
In vivo	lipid peroxidation activation and infracts size	Rutin	Krishna et al., 2005; Annapurna et al., 2009; Ali et al., 2009
In vivo	cGMP, iNOS and 3-NT concentrations	Rutin	Korkmaz & Kolankaya, 2013
In vitro/ in vivo	ROS formation and pro-inflammatory cytokine concentration	Acacetin	Wu et al., 2018
In vitro	Cytokine levels	Acacetin	Liu et al., 2016

thioredoxin, and which therefore reduced the release of various inflammatory cytokines. The result of acacetin treatment was to suppress myocyte apoptosis, after induced by ischemia/reperfusion (Liu et al., 2016). In addition, acacetin having a concentration ranging from 0.3 to 3.0 μM was capable of declining cardiomyocyte apoptosis and reactive oxygen species (ROS) production by altering the ratio of Bax/Bcl-2 (Wu et al., 2018). Moreover, acacetin could induce the release of pro-inflammatory cytokines, e.g. TLR-4 and IL-6, in cultured H9C2 cells (Wu et al., 2018).

Rutin exhibits similar pharmaceutical functions as that of acacetin (Korkmaz & Kolankaya, 2013; Lv et al., 2018). The pre-treatment of rutin in rats dramatically attenuated cyclic guanosine monophosphate (cGMP) and NO level in serum and inhibited inducible nitric oxide synthase (iNOS) and 3-nitrotyrosine (3-NT) formation in kidney (Korkmaz and Kolankaya, 2013). In addition, the cardio-protective functions of rutin by revealing ischemia–reperfusion-induced myocardial infarction were also reported in rats (Krishna et al., 2005; Ali et al., 2009; Annapurna et al., 2009). The intake of rutin showed the cardio-protection by restraining infract size in normal and diabetic rats: the underling action mechanism was believed to trigger lipid peroxidation in myocardial tissues (Krishna et al., 2005; Ali et al., 2009; Annapurna et al., 2009).

Adipogenesis Suppression

In high-fat-diet-induced (HFD) obese mice, acacetin reduced body weight and visceral adipose tissue. In differentiated 3T3-L1 cells, applied acacetin increased the level of glycerol in culture medium and significantly inhibited lipid accumulation by Oil Red O staining. In addition, acacetin reduced the transcript and protein expressions of adipogenesis-related transcription factors, including the CCAAT/enhancer-binding protein in cultured adipocytes. In parallel, acacetin treatment increased sirtuin 1 expression and AMPK phosphorylation (Liou et al., 2017). Besides, acacetin was able to suppress the levels of inflammatory mediators, as well as levels of MAPK and NF-κB pathways, in cultured macrophages, as treated with differentiated media deriving from cultured 3T3-L1 adipocytes (Su et al., 2014a; Liou et al., 2017). In insulin-resistant adipocytes, acacetin treatment significantly reduced the levels of chemokines MCP-1 and CCL5 in these cells, as to restore the resistance (Liou et al., 2017).

Administration of rutin in mice could modulate obesity, fatty liver and insulin resistance by increasing energy-consuming gene expressions in brown adipose tissue, including Pgc1α and Dio2, *via* up-regulating mitochondrial size and mitochondrial DNA (mtDNA) content, as well as those mitochondrial biogenesis-related genes, i.e. peroxisome proliferator-activated receptor γ (PARPγ), coactivator-1α (PGC-1α) and nuclear respiratory factor-1 (NRF-1) (Gao et al., 2013; Seo et al., 2015). Furthermore, rutin also restricted the transcriptions of Srebp1c and Cd36, leading to a blockade of developing fatty liver (Gao et al., 2013). After oral administration of rutin in obese mice for 1 week, the rutin-treated group showed over 3-fold longer exhaustive swimming time than the blank control, and which, in parallel, significantly reduced the plasma content of lactic acid (**Table 3**). In rutin-treated mice, the rates of transcription and translation of PGC-1α gene were enhanced in their soleus muscle, and these changes were associated with increased endurance capacity (Su et al., 2014b).

Hispidulin, another major flavonoid in "Snow lotus", was shown to possess therapeutic potential in against dyslipidemia. In cultured HepG2 cells, hispidulin acted as an agonist of PPARα and regulated the downstream lipid-metabolizing enzymes, e.g. fatty-acid binding protein 1 and 2, acyl-CoA synthetase 1, carnitine palmitoyltransferase 1α, acetyl-CoA acetyltransferase 1, acyl-coenzyme A dehydrogenase 1 and HMG-CoA synthase 2. In dyslipidemic rat model, the treatment of hispidulin significantly reduced total serum cholesterol, triglyceride and low-density lipoprotein cholesterol, as well as increasing the serum level of high-density lipoprotein cholesterol (Wu and Xu, 2016).

Anti-Cancer Effect

The anti-cancer properties of "Snow lotus" have been documented. In SK-Hep1 human hepatocellular carcinoma cell line, the cell proliferation was significantly inhibited by the ethanol extract of "Snow lotus" (**Table 4**). This treatment also caused cell cycle arrest at G1-phase, inhibition of DNA synthesis and apoptosis induction *via* caspase 3 and 9 signaling. (Byambaragchaa et al., 2014). In addition, the ethanol extract of "Snow lotus" showed anti-metastatic property by inhibiting invasion and motility of cancer cells *via* activation of an inhibitor for matrix metalloproteinase-2/-9 (MMP-2/-9) (Byambaragchaa et al., 2013). The anti-neoplastic activity of different herbal extracts deriving from "Snow lotus" was shown in PC-3 prostate cancer cells, which included the herbal fractions by using extracting solvents of methanol, ethyl acetate, n-butanol and water. Among these extractives, the ethyl acetate extract showed the most promising effect in inhibiting cancer cell (Yu

TABLE 3 | Summary of adipogenesis suppression effects of "Snow lotus" and/or its major biochemical.

Models	Parameters measured	Active components	Reference
In vivo/in vitro	Body and visceral adipose tissue weight; AMPK phosphorylation, MCP-1 and CCL5 contents	Acacetin	Liou et al., 2017
In vivo/in vitro	mtDNA content; PARPγ, PGC-1α and NRF-1 transcriptional and translational effects	Rutin	Gao et al., 2013; Seo et al., 2015
In vivo/in vitro	Total serum cholesterol, triglyceride and low-density lipoprotein cholesterol and PPARα activations	Hispidulin	Wu and Xu, 2016
In vivo	Srebp1c and Cd36 levels	Rutin	Gao et al., 2013
In vivo	Exhaustive swimming time	Rutin	Su et al., 2014b
In vitro	Inactivation of MAPK and NF-κB pathways	Acacetin	Su et al., 2014a

TABLE 4 | Summary of anti-cancer functions of "Snow lotus" and/or its major biochemicals.

Models	Parameters measured	Active components	Reference
In vivo/ in vitro	Prolong the lifespan of xenograft nude mice	Rutin	Alonso-Castro et al., 2013; Chen et al., 2013
In vivo	Capillary-like tube formation and down regulation of VEGF expression	Acacetin	Liu et al., 2011; Bhat et al., 2013
In vivo	Suppressing PC-3 cancer and reducing EGFR activation in prostate cancer	"Snow lotus" extract	Way et al., 2010; Yu et al., 2013
In vitro	Cell invasion and motility	Rutin Acacetin Hispidulin	Pan et al., 2005; Araújo et al., 2011; Byambaragchaa et al., 2013; Yu et al., 2013; Kim H et al., 2014; Gao et al., 2014; Kim C et al., 2015
In vitro	Cell cycle, DNA synthesis	"Snow lotus" extract	Byambaragchaa et al., 2014
In vivo	Tumor size and SphK1	Hispidulin and rutin	Lin et al., 2012b; Gao et al., 2017

et al., 2013). More importantly, the ethyl acetate extract of "Snow lotus" markedly reduced the phosphorylation of epidermal growth factor receptor, one of the therapy targets for prostate cancer (Way et al., 2010).

Acacetin has been shown to induce apoptosis and suppress cell proliferation in gastric carcinoma, oral squamous carcinoma and prostate cancer cells (Pan et al., 2005; Kim H et al., 2014; Kim C et al., 2015). This chemical suppressed the growth of human umbilical vein endothelial cell and the formation of capillary-like tube (Bhat et al., 2013). Acacetin also blocked the phosphorylations of Stat-1 (Tyr701) and Stat-3 (Tyr705), as well as restrained the expression levels of pro-angiogenic factors, e.g. VEGF, eNOS, iNOS, MMP-2 and bFGF, in cancer cells (Bhat et al., 2013). Moreover, over-expression of HIF-1α or AKT inhibited acacetin-restraining VEGF protein level, demonstrating that AKT and HIF-1α could be the downstream key factors in suppressing VEGF expression in ovarian cancer cell (Liu et al., 2011).

Hispidulin is being considered as a potential compound in treating gastric cancer and hepatocellular carcinoma (Yu et al., 2013; Gao et al., 2014). The treatment of hispidulin in AGS human gastric adenocarcinoma cell line could reduce cyclooxygenase-2 (COX-2) expression while keeping a high expression of nonsteroidal-anti-inflammatory-drug-(NSAID-) activated gene-1 (NAG-1). NAG-1 is known to be associated with apoptosis, and the down regulation of this protein expression may promote tumorigenesis (**Table 4**). In NAG-1 constitutive expressed cells, the G1/S phase was arrested, as well as inducing cancer cell apoptosis: this outcome was proposed to be mediated by increased expression of Egr-1 and activated ERK1/2 signaling (Yu et al., 2013). In accordance to anti-cancer notion of hispidulin, Gao and co-workers (Gao et al., 2013) demonstrated that the hispidulin-triggered apoptosis in HepG2 cells could be mediated by the mitochondrial dysfunction, as well as the blockage of P13K/Akt pathway. Subsequently, they showed that hispidulin also prevented proliferation of acute myeloid leukemia cell and triggered cell death *via* an intrinsic mitochondrial pathway by restraining the extracellular matrix metalloproteinase inducer (Gao et al., 2016). Injection of hispidulin in xenograft nude mice in a dose-dependently inhibited tumor size and decreased SphK1 activity, as well as an increase of ceramide accumulation in tumor tissues (Gao et al., 2017).

Excessive anti-cancer functions of rutin have been reported. Rutin dramatically suppressed tumor size justifying anti-leukemic potential in xenograft nude mice (Lin et al., 2012b). Another *in vivo* study has shown that the rutin application reduced detrimental effects and relative organ weight in mice, and more importantly, the increment of mean survival time was observed (Alonso-Castro et al., 2013). *In vitro* study demonstrated the altered Bax/Bcl2 ratio in cultured LAN-5 cell after the treatment of rutin (Chen et al., 2013). Moreover, rutin was known to induce cancer cell apoptosis along with proliferation, angiogenesis and/or metastasis inhibition in colorectal cell lines (Araújo et al., 2011).

Anti-Inflammation

According to TCM and/or TUM, the extract of "Snow lotus" has been used as a therapeutic agent for inflammation and pain-related disorders. Recent studies have helped to reveal the signaling mechanism contributing in such pharmacological effects. Yi and co-workers had demonstrated that the ethanolic extract of "Snow lotus" possessed anti-inflammatory and anti-nociceptive functions in a mouse model of croton oil-induced ear edema (Yi et al., 2012). In parallel, the oral administration of "Snow lotus" extract was used to treat rats suffering from the collagen II (CII)-induced arthritis (Xu et al., 2016): the infiltration of inflammatory cell, synovial hyperplasia, swelling index and delaying joint destruction were found to be alleviated (**Table 5**). The serum levels of rheumatoid factor, cartilage oligomeric matrix protein (COMP), C-reactive protein and anti-CII IgG antibodies were significantly reduced. Moreover, the therapeutic effects on rheumatoid arthritis by alcohol and water extractives of "Snow lotus" were compared. The effect of ethanolic extract was more potent than that of water extract in treating rheumatoid arthritis in rat model. The ethanolic herbal extract significantly ameliorated rheumatoid arthritis severity, and the over productions of cytokines, e.g. TNF-α, IL-1β, and IL-6, were markedly attenuated in the serum of "Snow lotus" intake rats (Han et al., 2016). Yi and co-workers (2012) presented similar results in *in vitro* analysis of the ethanolic herbal extract: the application of extract in cultures suppressed ROS formation significantly, and the IC50 was 409.6 mg/L. Xiao and co-workers (2011) showed that application of "Snow lotus" extract on cultured macrophage could reduce the levels of PGE2 and NO from 294.9 ng/mL to

TABLE 5 | Summary of anti-inflammatory functions of "Snow lotus" and/or its major biochemical.

Models	Parameters measured	Active components	Reference
In vivo	Synovial hyperplasia, swelling index, joint destruction and serum cytokine levels	"Snow lotus" and rutin	Chen et al., 2014b; Xu et al., 2016; Han et al., 2016
In vivo	Eosinophil infiltration and goblet cell hyperplasia in lung tissue	"Snow lotus" extract	Huang and Liou, 2012
In vivo	ROS formation	Rutin	Guardia et al., 2001; Ostrakhovitch and Afanas'ev, 2001
In vivo	Skin rush and inflammation Epidermal hyperplasia and protein level	Rutin	Choi et al., 2014; Gęgotek et al., 2017

238.6 ng/mL and 6.61 ng/mL to 4.52 ng/mL, respectively. Another study illustrated the action of acacetin in mitigating airway hyper-responsiveness in asthmatic mice. The treatment of acacetin reduced the levels of chemokines and Th2-associated cytokines in asthmatic mice, and which effectively suppressed eosinophil infiltration and goblet cell hyperplasia in lung tissue (Huang and Liou, 2012).

The pre-treatment of rutin declined the lipopolysaccharide (LPS)-induced arterial blood gas exchange and neutrophils infiltration *in vivo*, and also restrained macrophage inflammatory protein-2 and MMP-9 secretion (Chen et al., 2014b). Significantly decrement in rheumatoid arthritis scores by restraining ROS formation were observed in the rutin-treated rats, and these findings were in line with the rat model of adjuvant arthritis. In addition, rutin inhibited the duplicate inflammatory phases, i.e. acute and chronic stages (Guardia et al., 2001; Ostrakhovitch and Afanas'ev, 2001). Besides, the skin care functions of rutin have been explored to demonstrate the pharmaceutical values of rutin on ultraviolet B (UVB)-induced inflammation *in vivo* (Choi et al., 2014). Pre-treatment and post-treatment of rutin with UVB declined epidermal hyperplasia and protein level in mice (Choi et al., 2014; Gęgotek et al., 2017). Furthermore, rutin suppressed UVB-induced expressions of COX-2 and iNOS through p38 MAP kinase and JNK inhibition.

Other Pharmaceutical Values

"Snow lotus" is classified as a "kidney-tonifying" in TCM practice, and which is being applied to treat osteoarthritis, articular cartilage injury and osteoporosis with a long history. In a herbal mixture having "Snow lotus" and three other "kidney-tonifying" TCMs, i.e. Astragali Radix, Salviac Miltiorhizae Radix & Rhzizoma and Epimedii Herba, is known to promote the proliferation and osteogenic differentiation of bone marrow-derived mesenchymal stem cells (BMSCs) (Cai et al., 2015). Rutin stimulated proliferation and differentiation of osteosarcoma MG-63 cells by analyzing the increase of cell viability, alkaline phosphatase (ALP), collagen type I and mineralization (Hyun et al., 2014). Similar pharmaceutical functions of rutin have been reported in rat calvarial osteoblast cells (Yang et al., 2006). Osteoclast growth, ROS formation and cytokine secretion were being restricted in the rutin-treated bone cultures (Kyung et al., 2008). Rutin also inhibited the ovariectomy-induced osteopenia in rats by accelerating the formation of osteoblast (Horcajada-Molteni et al., 2000). Hispidulin has estrogenic and anti-osteoporosis functions, and which could act as a promising medicine for osteoporosis modulation. The application of hispidulin in ovariectomy rat model could attenuate bone loss after 2 months of treatment (Zhou et al., 2014). In hispidulin-treated cultures, activated ALP activity was revealed in cultured MC3T3E1 cells, and additionally osteoclastic activity was suppressed in cultured RAW 264.7 cell *via* prohibiting RANKL-induced activation of JNK and p38 (Nepal et al., 2013).

CONCLUSION

The pharmaceutical functions of *S. involucrata (*a TUM and/or a TCM herbal material) and its key bioactive chemical ingredients, identified and isolated from this herb, were summarized and reviewed here. These known pharmaceutical properties include immune-modulation, anti-inflammation, adipogenesis inhibition, neuroprotection and ischemia injury protection. Due to its distinct habitat, the resource of "Snow lotus" is rather rare. The plant grows at over 4,000 m altitude in mountainous rocky environment under rather harsh climatic conditions. The plant takes over 8 years to mature before the harvest. Furthermore, over harvesting in China is destroying the growing environment and causing the damage of *S. involucrata* species quality. As a result, these are the major reasons for rarity of "Snow lotus" in the market. The cultivation of "Snow lotus" has been tried by the Xinjiang Technical Institute of Physics & Chemistry in China, the results showed that the harvest period could be shorten from 8 years to 2 years, and the major chemical contents were not decreased. Furthermore, the standard operating procedure of artificial cultivation of "Snow lotus" has been established today, and the cultivation has already extended to 4,000 m altitude. Besides, there are many "Snow lotus" products being available in current herbal market, including cosmeceuticals, food supplements and medications. Although there have been many studies and researches on "Snow lotus", future research can be carried out in two directions. Firstly, active components, morphological identification, pharmacological effects and metabolisms need to be explored based on the studies of *S. involucrat* and *S. laniceps* (Chen et al., 2014a; Fan et al., 2015; Chen et al., 2016; Yi et al., 2016; Chen et al., 2017). Secondly, in order to extract these active components as much as possible from "Snow lotus", the potential approaches to pre-treat the extracts could be considered, such as pre-soaking, liquid

ammonia pre-treatment and co-digestion (Zhao et al., 2016b; Hassan et al., 2017; Zhao et al., 2017a; Zhao et al., 2017b; Qiao et al., 2018). Innovative technology in these areas of research are urgently needed.

AUTHOR CONTRIBUTIONS

GG, KC, and KT wrote the main text. JH and TD had great contribution in second time revision, polishing manuscript and helping in revising figures.

FUNDING

Supported by Research Fund of Zunyi Medical University for the Doctoral Program (F-937), NNSF of Guangdong (2018A030307074), Science and Technology Planning Project of Guangdong (2014A020221058), China. Shenzhen Science and Technology Innovation Committee (JCYJ20160229205812004; ZDSYS201707281432317; JCYJ20170413173747440; JCYJ20180306174903174). Scientific Research and Innovation of Putian University (2018ZP03, 2018ZP08, 2018ZP07).

REFERENCES

Ali, M. S., Mudagal, M. P., and Goli, D. (2009). Cardioprotective effect of tetrahydrocurcumin and rutin on lipid peroxides and antioxidants in experimentally induced myocardial infarction in rats. *Pharmazie.* 64, 132–136

Alonso-Castro, A. J., Domínguez, F., and García-Carrancá, A. (2013). Rutin exerts antitumor effects on nude mice bearing SW480 tumor. *Arch. Med. Res.* 44, 346–351. doi: 10.1016/j.arcmed.2013.06.002

Annapurna, A., Reddy, C. S., Akondi, R. B., and Rao, S. R. (2009). Cardioprotective actions of two bioflavonoids, quercetin and rutin, in experimental myocardial infarction in both normal and streptozotocin-induced type I diabetic rats. *J. Pharm. Pharmacol.* 61, 1365–1374. doi: 10.1211/jpp/61.10.0014

Araújo, J. R., Gonçalves, P., and Martel, F. (2011). Chemopreventive effect of dietary polyphenols in colorectal cancer cell lines. *Nutr. Res.* 31, 77–87. doi: 10.1016/j.nutres.2011.01.006

Bhat, T. A., Nambiar, D., Tailor, D., Pal, A., Agarwal, R., and Singh, R. P. (2013). Acacetin inhibits *in vitro* and *in vivo* angiogenesis and down-regulates Stat signaling and VEGF expression. *Cancer Prev. Res. (Phila).* 6, 1128–1139. doi: 10.1158/1940-6207.CAPR-13-0209

Byambaragchaa, M., Dela Cruz, J., Yang, S. H., and Hwang, S. G. (2013). Anti-metastatic potential of ethanol extract of *Saussurea involucrata* against hepatic cancer *in vitro*. *Asian Pac J. Cancer Prev.* 14, 5397–5402. doi: 10.7314/apjcp.2013.14.9.5397

Byambaragchaa, M., Dela Cruz, J., Kh, A., and Hwang, S. G. (2014). Anti-cancer potential of an ethanol extract of *Saussurea involucrata* against hepatic cancer cells *in vitro*. *Asian Pac J. Cancer Prev.* 15, 7527–7532. doi: 10.7314/apjcp.2014.15.18.7527

Cai, B., Zhang, A. G., Zhang, X., Ge, W. J., Dai, G. D., Tan, X. L., et al. (2015). Promoting effects on proliferation and chondrogenic differentiation of bone marrow-derived mesenchymal stem cells by four "Kidney-Tonifying" traditional Chinese herbs. *BioMed. Res. Int.* 2015, 792161. doi: 10.1155/2015/792161

Chen, J., and Wang, Y. J. (2018). New *Saussurea* (Asteraceae) species from Bogeda Mountain, eastern Tianshan, China, and inference of its evolutionary history and medical usage. *PloS One* 13, e0199416. doi: 10.1371/journal.pone.0199416

Chen, Y. S., Hu, Q. H., Zhang, X., Zhu, Q., and Kong, L. D. (2013). Beneficial effect of rutin on oxonate-induced hyperuricemia and renal dysfunction in mice. *Pharmacology* 92, 75–83. doi: 10.1159/000351703

Chen, Q. L., Yi, T., Tang, Y. N., Wong, L. L., Huang, X. X., Zhao, Z. Z., et al. (2014a). Comparative authentication of three "Snow Lotus" herbs by macroscopic and microscopic features. *Microsc Res. Techniq.* 77, 631–641. doi: 10.1002/jemt.22381

Chen, W. Y., Huang, Y. C., Yang, M. L., Lee, C. Y., Chen, C. J., Yeh, C. H., et al. (2014b). Protective effect of rutin on LPS-induced acute lung injury *via* down-regulation of MIP-2 expression and MMP-9 activation through inhibition of Akt phosphorylation. *Int. Immunopharmacol.* 22, 409–413. doi: 10.1016/j.intimp.2014.07.026

Chen, Q. L., Chen, X.,. Y., Zhu, L., Chen, H. B., Ho, H. M., Yeung, W. P., et al. (2016). Review on *Saussurea laniceps*, a potent medicinal plant known as "snow lotus": botany, phytochemistry and bioactivities. *Phytochem. Rev.* 15, 537–565. doi: 10.1007/s11101-015-9452-y

Chen, Q. L., Zhu, L., Tang, Y. N., Kwan, H. Y., Zhao, Z. Z., Chen, H. B., et al. (2017). Comparative evaluation of chemical profiles of three representative "snow lotus" herbs by UPLC-DAD-QTOF-MS combined with principal component and hierarchical cluster analyses. *Drug Test Anal.* 9, 1105–1115. doi: 10.1002/dta.2123

Chen, J., Zhao, Y. B., Wang, Y. J., and Li, X. G. (2019). Identification of species and materia medica within *Saussurea* subg. *Amphilaena* based on DNA barcodes. *PeerJ.* 7, e6357. doi: 10.7717/peerj.6357

Chik, W. I., Zhu., L., Fan., L. L., Yi, T., Zhu, G. Y., Gou, X. J., et al. (2015). *Saussurea involucrata*: a review of the botany, phytochemistry and ethnopharmacology of a rare traditional herbal medicine. *J. Ethnopharmacol.* 172, 44–60. doi: 10.1016/j.jep.2015.06.033

Choi, K. S., Kundu, J. K., Chun, K. S., Na, H. K., and Surh, Y. J. (2014). Rutin inhibits UV-B radiation-induced expression of COX-2 and iNOS in hairless mouse skin: p38 MAP kinase and JNK as potential targets. *Arch. Biochem. Biophys.* 559, 38–45. doi: 10.1016/j.abb.2014.05.016

Fan, J. Y., Chen, H. B., Zhu, L., Chen, H. L., Zhao, Z. Z., and Yi, T. (2015). *Saussurea medusa*, source of the medicinal herb snow lotus: a review of its botany, phytochemistry, pharmacology and toxicology. *Phytochem. Rev.* 14, 353–366. doi: 10.1007/s11101-015-9408-2

Gęgotek, A., Bielawska, K., Biernack, M., Dobrzyńska, I., and Skrzydlewska, E. (2017). Time-dependent effect of rutin on skin fibroblasts membrane disruption following UV radiation. *Redox Biol.* 12, 733–744. doi: 10.1016/j.redox.2017.04.014

Gao, M., Ma, Y., and Liu, D. (2013). Rutin suppresses palmitic acids-triggered inflammation in macrophages and blocks high fat diet-induced obesity and fatty liver in mice. *Pharm. Res.* 30, 2940–2950. doi: 10.1007/s11095-013-1125-1

Gao, H., Wang, H., and Peng, J. (2014). Hispidulin induces apoptosis through mitochondrial dysfunction and inhibition of P13k/Akt signaling pathway in HepG2 cancer cells. *Cell Biochem. Biophys.* 69, 27–34. doi: 10.1007/s12013-013-9762-x

Gao, H., Liu, Y., Li, K., Wu, T., Peng, J., and Jing, F. (2016). Hispidulin induces mitochondrial apoptosis in acute myeloid leukemia cells by targeting extracellular matrix metalloproteinase inducer. *Am. J. Transl. Res.* 8, 1115–1132.

Gao, M., Gao, H., Han, M., Liu, K., Peng, J., and Han, Y. (2017). Hispidulin suppresses tumor growth and metastasis in renal cell carcinoma by modulating ceramide-sphingosine 1-phosphate rheostat. *Am. J. Cancer Res.* 7, 1501–1514.

Guardia, T., Rotelli, A. E., Juarez, A. O., and Pelzer, L. E. (2001). Anti-inflammatory properties of plant flavonoids. effects of rutin, quercetin and hesperidin on adjuvant arthritis in rat. *Farmaco.* 56, 683–687. doi: 10.1016/s0014-827x(01)01111-9

Han, X., Su, D., Xian, X., Zhou, M., Li, X., Huang, J., et al. (2016). Inhibitory effects of *Saussurea involucrata* (Kar. et Kir.) Sch. -Bip. on adjuvant arthritis in rats. *J. Ethnopharmacol.* 194, 228–235. doi: 10.1016/j.jep.2016.09.008

Hassan, M., Umar, M., Ding, W. M., Mehryar, E., and Zhao, C. (2017). Methane enhancement through co-digestion of chicken manure and oxidative cleaved wheat straw: Stability performance and kinetic modeling perspectives. *Energy.* 141, 2314–2320. doi: 10.1016/j.energy.2017.11.110

Horcajada-Molteni, M. N., Crespy, V., Coxam, V., Davicco, M. J., Rémésy, C., and Barlet, J. P. (2000). Rutin inhibits ovariectomy-induced osteopenia in rats. *J. Bone Miner Res.* 15, 2251–2258. doi: 10.1359/jbmr.2000.15.11.2251

Huang, W. C., and Liou, C. J. (2012). Dietary acacetin reduces airway hyper responsiveness and eosinophil infiltration by modulating eotaxin-1 and th2 cytokines in a mouse model of asthma. *Evid Based Complement Alternat Med.* 2012, 910520. doi: 10.1155/2012/910520

Hyun, H., Park, H., Jeong, J., Kim, J., Kim, H., Oh, H., et al. (2014). Effects of watercress containing rutin and rutin alone on the proliferation and osteogenic differentiation of human osteoblast-like MG-63 cells. *Korean J. Physiol. Pharmacol.* 18, 347–352. doi: 10.4196/kjpp.2014.18.4.347

Kim, H. R., Park, C. G., and Jung, J. Y. (2014). Acacetin (5,7-dihydroxy-4'-methoxyflavone) exhibits *in vitro* and *in vivo* anticancer activity through the

suppression of NF-kappaB/Akt signaling in prostate cancer cells. *Int. J. Mol. Med.* 33, 31–324. doi: 10.3892/ijmm.2013.1571

Kim, C. D., Cha, J. D., Li, S., and Cha, I. H. (2015). The mechanism of acacetin-induced apoptosis on oral squamous cell carcinoma. *Arch. Biol.* 60, 1283–1298. doi: 10.1016/j.archoralbio.2015.05.009

Korkmaz, A., and Kolankaya, D. (2013). Inhibiting inducible nitric oxide synthase with rutin reduces renal ischemia/reperfusion injury. *Can. J. Surg.* 56, 6–14. doi: 10.1503/cjs.004811

Krishna, K. M., Annapurna, A., Gopal, G. S., Chalam, C. R., Madan, K., Kumar, V. K., et al. (2005). Partial reversal by rutin and quercetin of impaired cardiac function in streptozotocin-induced diabetic rats. *Can. J. Physiol. Pharmacol.* 83, 343–355. doi: 10.1139/y05-009

Kyung, T., Lee, J., Shin, H., and Choi, H. (2008). Rutin inhibits osteoclast formation by decreasing reactive oxygen species and TNF-α by inhibiting activation of NF-κB. *Exp. Mol. Med.* 40, 52–58. doi: 10.3858/emm.2008.40.1.52

Li, G. R., Wang, H. B., Qin, G. W., Jin, M. W., Tang, Q., Sun, H. Y., et al. (2008). Acacetin, a natural flavone, selectively inhibits human atrial repolarization potassium currents and prevents atrial fibrillation in dogs. *Circulation.* 117, 2449–2457. doi: 10.1161/CIRCULATIONAHA.108.769554

Lin, T. Y., Lu, C. W., Wang, C. C., Lu, J. F., and Wang, S. J. (2012a). Hispidulin inhibits the release of glutamate in rat cerebrocortical nerve terminals. *Toxicol. Appl. Pharmacol.* 263, 233–243. doi: 10.1016/j.taap.2012.06.015

Lin, J. P., Yang, J. S., Lin, J. J., Lai, K. C., Lu, H. F., Ma, C. Y., et al. (2012b). Rutin inhibits human leukemia tumor growth in a murine xenograft model *in vivo*. *Environ. Toxicol.* 27, 480–484. doi: 10.1002/tox.20662

Lin, T. Y., Huang, W. J., Wu, C. C., Lu, C. W., and Wang, S. J. (2014). Acacetin inhibits glutamate release and prevents kainic acid-induced neurotoxicity in rats. *PloS One* 9, e88644. doi: 10.1371/journal.pone.0088644

Liou, C. J., Wu, S. J., Chen, L. C., Yeh, K. W., Chen, C. Y., and Huang, W. C. (2017). Acacetin from traditionally used *Saussurea involucrata* Kar. et Kir. suppressed adipogenesis in 3T3-L1 dipocytes and attenuated lipid accumulation in obese mice. *Front. Pharmacol.* 8, 589. doi: 10.3389/fphar.2017.00589

Liu, L. Z., Jing, Y., Jiang, L., Jiang, X., Jiang, Y., Rojanasakul, Y., et al. (2011). Acacetin inhibits VEGF expression, tumor angiogenesis and growth through AKT/HIF-1α pathway. *Biochem. Biophys. Res. Commun.* 413, 299–305. doi: 10.1016/j.bbrc.2011.08.091

Liu, H., Yang, L., Wu, H. J., Chen., K. H., Lin, F., Li, G., et al. (2016). Water-soluble acacetin prodrug confers significant cardioprotection against ischemia/reperfusion injury. *Sci. Rep.* 6, 36435. doi: 10.1038/srep36435

Lv, Y. L., Zhang, F. S., Chen, J., Cui, J. L., Xing, Y. M., Li, X. D., et al. (2010). Diversity and antimicrobial activity of endophytic fungi associated with the alpine plant *Saussurea involucrata*. *Biol. Pharm. Bull.* 33, 1300–1306. doi: 10.1248/bpb.33.1300

Lv, L., Yao, Y., Zhao, G., and Zhu, G. (2018). Rutin inhibits coronary heart disease through ERK1/2 and Akt signaling in a porcine model. *Exp. Ther. Med.* 15, 506–512. doi: 10.3892/etm.2017.5365

Motamedshariaty, V. S., Farzad, S. A., Nassiri-Asl, M., and Hosseinzadeh, H. (2014). Effects of rutin on acrylamide-induced neurotoxicity. *Daru.* 22, 27. doi: 10.1186/2008-2231-22-27

Na, J. Y., Kim, S., Song, K., and Kwon, J. (2014). Rutin alleviates prion peptide-induced cell death through inhibiting apoptotic pathway activation in dopaminergic neuronal cells. *Cell Mol. Neurobiol.* 34, 1071–1079. doi: 10.1007/s10571-014-0084-3

Nepal, M., Choi, H. J., and Choi, B. Y. (2013). Hispidulin attenuates bone resorption and osteoclastogenesis *via the* RANKL-induced NF-κB and NFATc1 pathways. *Eur. J. Pharmacol.* 715, 96–104. doi: 10.1016/j.ejphar.2013.06.002

Niu, X., Chen, J., Wang, P., Zhou, H., Li, S., and Zhang, M. (2014). The effects of hispidulin on bupivacaine-induced neurotoxicity: role of AMPK signaling pathway. *Cell Biochem. Biophys.* 70, 241–249. doi: 10.1007/s12013-014-9888-5

Ostrakhovitch, E. A., and Afanas'ev, I. B. (2001). Oxidative stress in rheumatoid arthritis leukocytes: suppression by rutin and other antioxidants and chelators. *Biochem. Pharmacol.* 62, 743–746. doi: 10.1016/s0006-2952(01)00707-9

Packer, L., Ong, C. N., and Halliwell, B. (2004). *Herbal and traditional medicine, molecular aspects of health* (New York: Marcel Dekker), 2.

Pan, M. H., Lai, C. S., Hsu, P. C., and Wang, Y. J. (2005). Acacetin induces apoptosis in human gastric carcinoma cells accompanied by activation of caspase cascades and production of reactive oxygen species. *J. Agric. Food Chem.* 53, 620–630. doi: 10.1021/jf048430m

Qiao, X. L., Zhao, C., Shao, Q. J., and Hassan, M. (2018). Structural characterization of corn stover lignin after hydrogen peroxide presoaking prior to ammonia fiber expansion pretreatment. *Energ Fuel.* 32, 6022–6030. doi: 10.1021/acs.energyfuels.8b00951

Qiu, J., Xue, X., Chen, F., Li, C., Bolat, N., Wang, X., et al. (2010). Quality evaluation of Snow Lotus (*Saussurea*): quantitative chemical analysis and antioxidant activity assessment. *Plant Cell Rep.* 29, 1325–1337. doi: 10.1007/s00299-010-0919-4

Qiu, J., Gao, F., Shen, G., Li, C., Han, X., Zhao, Q., et al. (2013). Metabolic engineering of the phenylpropanoid pathway enhances the antioxidant capacity of *Saussurea involucrata*. *PloS One* 8, e70665. doi: 10.1371/journal.pone.0070665

Qu, J., Zhou, Q., Du, Y., Zhang, W., Bai, M., Zhang, Z., et al. (2014). Rutin protects against cognitive deficits and brain damage in rats with chronic cerebral hypoperfusion. *Br. J. Pharmacol.* 171, 3702–3715. doi: 10.1111/bph.12725

Seo, S., Lee, M., Chang, E., Shin, Y., Oh, S., Kim, I., et al. (2015). Rutin increases muscle mitochondrial biogenesis with AMPK activation in high-fat diet-induced obese rats. *Nutrients.* 7, 8152–8169. doi: 10.3390/nu7095385

Shahabi, S., Hassan, Z. M., Mahdavi, M., Dezfouli, M., Torabi, R. M., and Naseri, M. (2008). Hot and cold matures and some parameters of neuroendocrine and immune systems in traditional Iranian medicine: a preliminary study. *J. Altern. Complement Med.* 14, 147–156. doi: 10.1089/acm.2007.0693

Su, K. Y., Yu, C. Y., Chen, Y. W., Huang, Y. T., Chen, C. T., Wu, H. F., et al. (2014a). Rutin, a flavonoid and principal component of *Saussurea involucrata*, attenuates physical fatigue in a forced swimming mouse model. *Int. J. Med. Sci.* 11, 528–537. doi: 10.7150/ijms.8220

Su, K. Y., Yu, C. Y., Chen, Y. P., Hua, K. F., and Chen, Y. L. (2014b). 3,4-Dihydroxytoluene, a metabolite of rutin, inhibits inflammatory responses in lipopolysaccharide-activated macrophages by reducing the activation of NF-κB signaling. *BMC Complement Altern. Med.* 14, 21. doi: 10.1186/1472-6882-14-21

Tang, Y., Yuan, H., and Qin, J. (2012). Identification and characterization of a flavonoid-3-O-glucosyltransferase gene from *Saussurea involucrata*. *Sheng Wu Gong Cheng Xue Bao.* 28, 705–714.

Upur, H., Yusup, A., Baudrimont, I., Umar, A., Berke, B., Yimit, D., et al. (2011). Inhibition of cell growth and cellular protein, DNA and RNA synthesis in human hepatoma (HepG2) cell by ethanol extract of abnormal Savda Munziq of traditional Uighur medicine. *Evid Based Complement Alternat Med.* 2011, 251424. doi: 10.1093/ecam/nen062

Wang, C., Ha, X., Li, W., Xu, P., Gu, Y., Wang, T., et al. (2016). Correlation of A2bAR and KLF4/KLF15 with obesity-dyslipidemia induced inflammation in Uygur population. *Mediators Inflamm.* 7015620. doi: 10.1155/2016/7015620

Wang, X., Chu, L., Liu, C., Wei, R., Xue, X., Xu, Y., et al. (2018). Therapeutic effects of *Saussurea involucrata* injection against severe acute pancreatitis-induced brain injury in rats. *BioMed. Pharmacother.* 100, 564–574. doi: 10.1016/j.biopha.2018.02.044

Way, T. D., Lee, J. C., Kuo, D. H., Fan, L. L., Huang, C. H., Lin, H. Y., et al. (2010). Inhibition of epidermal growth factor receptor signaling by *Saussurea involucrata*, a rare traditional Chinese medicinal herb, in human hormone-resistant prostate cancer PC-3 cells. *J. Agric. Food Chem.* 58, 3356–3365. doi: 10.1021/jf903793p

Wu, X., and Xu, J. (2016). New role of hispidulin in lipid metabolism: PPARα activator. *Lipids* 51, 1249–1257. doi: 10.1007/s11745-016-4200-7

Wu, L. Q., Lv, Y. L., Meng, Z. X., Chen, J., and Guo, S. X. (2010). The promoting role of an isolate of dark-septate fungus on its host plant *Saussurea involucrata* Kar. et Kir. *Mycorrhiza.* 20, 127–135. doi: 10.1007/s00572-009-0268-8

Wu, W. Y., Li, Y. D., Cui, Y. K., Wu, C., Hong, Y. X., Li, G., et al. (2018). The natural flavone acacetin confers cardiomyocyte protection against hypoxia/reoxygenation injury *via* AMPK-mediated activation of Nrf2 signaling pathway. *Front. Pharmacol.* 9, 497. doi: 10.3389/fphar.2018.00497

Xiao, W., Li, N., Bolati, M., Wang, X. J., Jia, X. G., and Zhao, Y. Q. (2011). Advances in studies on chemical components and pharmacological activities of Saussurea Involucratae Herba. *Drugs Clin.* 26, 344–348. doi: 10.1016/j.ejphar.2011.05.061

Xu, M., Guo, Q., Wang, S., Wang, N., Wei, L., and Wang, J. (2016). Anti-rheumatoid arthritic effects of *Saussurea involucrata* on type II collagen-induced arthritis in rats. *Food Funct.* 7, 763–770. doi: 10.1039/c5fo00603a

Yang, Y. J., Yang, Z. L., Wang, D. C., Xiao, X. C., and Li, P. (2006). Comparative study on effects of rutin and quercetin on metabolism in osteoblast cells. *Zhong Yao Cai.* 29, 467–470.

Yang, Y. C., Lin, H. Y., Su, K. Y., Chen, C. H., Yu, Y. L., Lin, C. C., et al. (2012). Rutin, a flavonoid that is a main component of *Saussurea involucrata,* attenuates the senescence effect in D-galactose aging mouse model. *Evid Based Complement Alternat Med.* 2012, 980276. doi: 10.1155/2012/980276

Yi, T., Lo, H., Zhao, Z., Yu, Z., Yang, Z., and Chen, H. (2012). Comparison of the chemical composition and pharmacological effects of the aqueous and ethanolic extracts from a Tibetan "Snow Lotus" (*Saussurea laniceps*) herb. *Molecules.* 17, 7183–7194. doi: 10.3390/molecules17067183

Yi, T., Zhao, Z. Z., Yu, Z. L., and Chen, H. B. (2010). Comparison of the anti-inflamatory and anti-nociceptive effects of three medical plants known as "Snow Lotus" herb in traditional Uighur and Tibetan medicines. *J. Ethnopharmacol.* 128, 405–411. doi: 10.1016/j.jep.2010.01.037

Yi, T., Zhu, L., Zhu, G. Y., Tang, Y. N., Xu, J., Fan, J. Y., et al. (2016). HSCCC-based strategy for preparative separation of *in vivo* metabolites after administration of an herbal medicine: *Saussurea laniceps*, a case study. *Sci. Rep.* 6, 33036. doi: 10.1038/srep33036

Yishakejiang, M., Abudureyimu, K., and Abulake, R. (2005). *China medical encyclopedia-Uyghur medicine volume, first ed* (Shanghai: Shanghai Science and Technology Press), pp: 7.

Yu, C. Y., Su, K. Y., Lee, P. L., Jhan, J. Y., Tsao, P. H., Chan, D. C., et al. (2013). Potential therapeutic role of hispidulin in gastric cancer through induction of apoptosis *via* NAG-1 signaling. *Evid Based Complement Alternat Med.* 2013, 518301. doi: 10.1155/2013/518301

Zhai, K. F., Wang, C., Gao, G. Z., Cao, W. G., Xu., L. S., and Xing, J. G. (2009). Advances in study on *Saussurea involucrate*. *Hubei Agric. Science.* 48, 2869–2873.

Zhao, C., Shao, Q. J., Ma, Z. Q., Li, B., and Zhao, X. J. (2016a). Physical and chemical characterizations of corn stalk resulting from hydrogen peroxide presoaking prior to ammonia fiber expansion pretreatment. *Ind. Crop Prod.* 83, 86–93. doi: 10.1016/j.indcrop.2015.12.018

Zhao, Y., Cai, L., Sui, Q., Lin, F., Jiang, W., Chen, J., et al. (2016b). Facile synthesis of acacetin and its derivatives. *Bioorg Med. Chem. Lett.* 26, 3577–3580. doi: 10.1016/j.bmcl.2016.06.018

Zhao, C., Cao, Y., Ma, Z. Q., and Shao, Q. J. (2017a). Optimization of liquid ammonia pretreatment conditions for maximizing sugar release from giant reed (*Arundo donax* L.). *Biomass Bioenerg.* 98, 61–69. doi: 10.1016/j.biombioe.2017.01.001

Zhao, C., Qiao, X. L., Cao, Y., and Shao, Q. J. (2017b). Application of hydrogen peroxide presoaking prior to ammonia fiber expansion pretreatment of energy crops. *Fuel.* 205, 184–191. doi: 10.1016/j.fuel.2017.05.073

Zhao, X. M. (1963). *Supplement to compendium of Materia Medica* (Beijing: People's Medical Publishing House), 249–251.

Zhou, R., Wang, Z., and Ma, C. (2014). Hispidulin exerts anti-osteoporotic activity in ovariectomized mice *via* activating AMPK signaling pathway. *Cell Biochem. Biophys.* 69, 311–317. doi: 10.1007/s12013-013-9800-8

Conflict of Interest: The authors declare that the research was conducted in the absence of any commercial or financial relationships that could be construed as a potential conflict of interest.

Copyright © 2020 Gong, Huang, Yang, Qi, Han, Zheng, He, Chan, Tsim and Dong. This is an open-access article distributed under the terms of the Creative Commons Attribution License (CC BY). The use, distribution or reproduction in other forums is permitted, provided the original author(s) and the copyright owner(s) are credited and that the original publication in this journal is cited, in accordance with accepted academic practice. No use, distribution or reproduction is permitted which does not comply with these terms.

frontiers in Pharmacology

ORIGINAL RESEARCH
published: 24 January 2020
doi: 10.3389/fphar.2019.01598

Comparative Pharmacokinetics of Hydrophilic Components in *Salvia miltiorrhiza Bge*. and *Carthamus tinctorius L.* in Rats That Underwent Cerebral Ischemia Reperfusion Using an HPLC-DAD Method

Xixi Zhao[1†], Li Yu[1†], Yulin Chen[1], Yu Wang[1], Haitong Wan[1] and Jiehong Yang[2*]*

[1] College of Life Science, Zhejiang Chinese Medical University, Hangzhou, China, [2] College of Basic Medical Sciences, Zhejiang Chinese Medical University, Hangzhou, China

OPEN ACCESS

Edited by:
Jing-Yan Han,
Peking University, China

Reviewed by:
Jianxin Chen,
Beijing University of Chinese Medicine, China
Wanying Wu,
Chinese Academy of Sciences, China

***Correspondence:**
Haitong Wan
whtong@126.com
Jiehong Yang
yjhong@zcmu.edu.cn

[†]These authors have contributed equally to this work

Specialty section:
This article was submitted to Ethnopharmacology, a section of the journal Frontiers in Pharmacology

Received: *05 June 2019*
Accepted: *10 December 2019*
Published: *24 January 2020*

Citation:
Zhao X, Yu L, Chen Y, Wang Y, Wan H and Yang J (2020) Comparative Pharmacokinetics of Hydrophilic Components in Salvia miltiorrhiza Bge. and Carthamus tinctorius L. in Rats That Underwent Cerebral Ischemia Reperfusion Using an HPLC-DAD Method. Front. Pharmacol. 10:1598. doi: 10.3389/fphar.2019.01598

Background: In China, the combination of herb *Salvia miltiorrhiza Bge.* (Danshen) and *Carthamus tinctorius L*. (Honghua) is an effective treatment for stroke. A previous study showed that the combination of four herbal components: danshensu (DSS), hydroxysafflor yellow A (HSYA), salvianolic acid A (SAA), and salvianolic acid B (SAB) was effective for treatment of cerebral ischemia-reperfusion (I/R) injury in rats. However, the pharmacokinetic characteristics of this formula require further investigation. The present study investigated the pharmacokinetic differences between each component of in two formulas in cerebral I/R injury rats. The influencing factors may affect the compatibility of components were analyzed.

Methods: Focal cerebral I/R was induced by middle cerebral artery occlusion (MCAO). Rats that underwent MCAO were randomly divided into two groups and administered treatments through the tail vein. Blood samples were collected at predetermined time points following administration. The concentrations of DSS, HSYA, SAB, and SAA in rat plasma were determined using HPLC-DAD, and the main pharmacokinetic parameters were calculated. Pharmacokinetic parameters were calculated using DAS 3.2.6 software and SPSS 23.0 statistical analysis software.

Results: Our results showed that DSS, HSYA, SAB, and SAA in MCAO model rats had statistically significant differences in two formulas. For DSS and SAA, pharmacokinetic parameters with statistically significant differences including $AUC_{(0-t)}$, $AUMC_{(0-t)}$, $MRT_{(0-t)}$, $VRT_{(0-t)}$, $t_{1/2z}$, V_z, CL_z, and C_{max} ($P < 0.01$). For HSYA, significant differences in the parameters including $AUC_{(0-t)}$, $AUMC_{(0-t)}$, $MRT_{(0-t)}$, $VRT_{(0-t)}$ ($P < 0.01$), CL_z and C_{max} ($P < 0.05$).

Conclusion: The difference in pharmacokinetic parameters in response to each component may have been due to differences in the dosages of the components (HSYA, SAA, SAB) and the compatibility of components. Meanwhile, there were many

influencing factors could affect the compatibility of components, such as the metabolism by CYP450 enzymes, plasma protein binding rates, and effects related to the blood-brain barrier (BBB). Moreover, our study provided new insights, such as choosing appropriate dosages of active components of traditional Chinese medicine (TCM) to aid in prevention and treatment of cerebral ischemic diseases. The method and results in this study could provide a foundation for future pharmacological studies of the active components in Danshen and Honghua.

Keywords: danshensu, hydroxysafflor yellow A, salvianolic acid A, salvianolic acid B, compatibility, middle cerebral artery occlusion, pharmacokinetics

INTRODUCTION

Ischemic stroke is a common cerebrovascular disease (CVD) and the most common cause of death worldwide (Lozano et al., 2012). It is characterized by sudden loss of blood circulation to an area of the brain, resulting in a corresponding loss of neurologic function (Donnan et al., 2008). It's the incidence of ischemic stroke is increasing with an aging population (Chen et al., 2017c). The global burden of ischemic strokes is nearly fourfold more common than hemorrhagic strokes (Kalaria et al., 2016). Cerebral ischemia-reperfusion (I/R) injury can occur during stroke treatment. This type of injury is of great concern because of the poor efficient medicine and clinical management.

"*Salvia miltiorrhiza Bge.* (Danshen)- *Carthamus tinctorius L.* (Honghua)" is a known herb pair used in ancient traditional Chinese medicine (TCM) prescriptions for ischemic stroke (Li et al., 2013). This herb pair has been used historically in China and other countries in Asia to treat cardiovascular and CVDs (Qin et al., 2009; Liu et al., 2011; Chen et al., 2017b; Zhang et al., 2017b). Danshensu (DSS), salvianolic acid A (SAA), and salvianolic acid B (SAB) are the main hydrophilic components of Danshen (**Figure 1**) (Li et al., 2018c). Hydroxysafflor yellow A (HSYA) is a bioactive component of the dried flower of Honghua (**Figure 1**) (Hui et al., 2018). Studies have shown that DSS, SAA, SAB, and HSYA have therapeutic effects on cardiovascular and CVDs, through anti-inflammatory, anti-oxidative activities, etc (Fan et al., 2017; Feng et al., 2017; Xu et al., 2017; Sun et al., 2018).

Our previous study showed that DSS, HSYA, SAB, and SAA in combination protected against cerebral I/R injury in rats by inhibiting the response of endoplasmic reticulum (ER) stress and inflammation (Chen et al., 2018). The previous results showed that the protective effects of the combination group four (CG4) and six (CG6) on cerebral I/R were more significant in nine dosage-changing combination groups (Chen et al., 2018). Compared with the model group, CG4 (formula was as follows: 30 mg/kg DSS + 2.5 mg/kg SAA + 16 mg/kg SAB + 8 mg/kg HSYA) and CG6 (formula was as follows: 30 mg/kg DSS + 10 mg/kg SAA + 8 mg/kg SAB+ 4 mg/kg HSYA) treatment displayed that the neurological deficit scores were significantly reduced in cerebral I/R model rats ($P < 0.05$). In terms of ER stress, CG4 and CG6 treatment displayed that the mRNA expression of GRP-78 ($P < 0.01$) was significantly increased and the mRNA expression of CHOP was significantly decreased ($P < 0.01$). Meanwhile, in terms of inflammation, CG4 and CG6 treatment displayed that the protein expression of NF-κB p65 and the mRNA expressions of nuclear factor-kB (NF-κB), tumor necrosis factor-α (TNF-α), and interleukin-6 (IL-6) were significantly decreased in the cerebral cortex ($P < 0.01$).

However, the pharmacokinetic characteristics of these two groups (CG4 and CG6) have not been characterized. Therefore, the present study evaluated the pharmacokinetic differences of each component in two formulas (CG4 and CG6) in rats that underwent cerebral I/R injury. We also analyzed the potential factors which could affect the compatibility of these active components.

MATERIALS AND METHODS

Chemicals and Reagents

Danshensu (DSS) (purity ≥98%, batch No. SZ201707038DSS), HSYA (purity ≥98%, Batch No. SZ201702005QA), SAB (purity ≥98%, Batch No. SZ201706003DB), and SAA (purity ≥98%, Batch No. SZ201706001DA) were purchased from Shizhou Biological Technology Co., Ltd (Nanjing, China) for use in plasma analysis. *p*-Hydroxybenzoic acid [internal standard (IS), purity ≥99%] was purchased from Guangfu Chemical Research Institute (Tianjin, China). Heparin sodium (Batch No. 2B010350) was purchased from Dingguochangsheng Biotechnology Co., Ltd (Beijing, China). HPLC grade methanol and acetonitrile were obtained from Tedia company. Pure water was supplied by a Millipore pure water system (Millipore, America).

Experimental Animals

Adult male Sprague–Dawley (SD) rats, weighing 280 ± 20 g, were obtained from the animal experiment center of Zhejiang Chinese Medical University (Certification No. SCXK 2014-0001). The animals were housed in an environmentally controlled room (temperature: 25 ± 2°C, humidity: 45 ± 5%) for at least 5 days prior to experimental procedures. The rats were fasted overnight with free access to water prior to experiments. Animal welfare and experimental procedures were strictly in accordance with the Regulation for the Administration of Affairs Concerning Experimental Animals (State Science and Technology

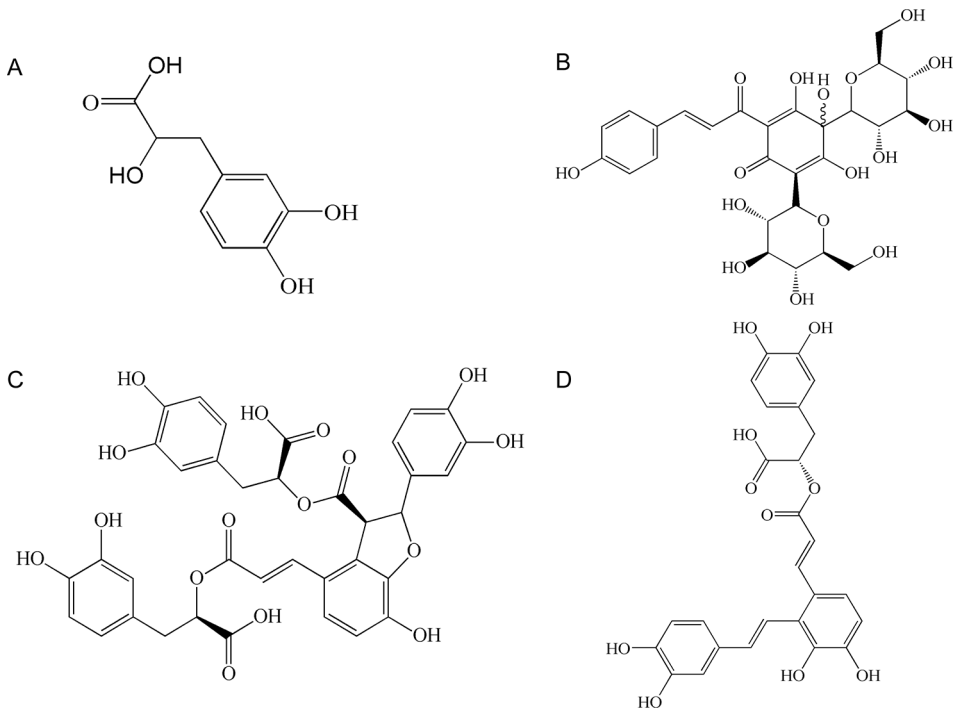


FIGURE 1 | The chemical structure of four components: **(A)** danshensu (DSS); **(B)** hydroxysafflor yellow A (HSYA); **(C)** salvianolic acid B (SAB); **(D)** salvianolic acid A (SAA).

Commission, 1988) and approved by the Animal Subjects Review Board of Zhejiang Chinese Medical University.

Focal Middle Cerebral Artery Occlusion

The MCAO model was implemented according to the method of Longa et al. (Longa et al., 1989). The rats were anesthetized with 10% chloral hydrate solution (0.3 ml/100 g) by intraperitoneal injection. An incision was made in the skin, and the right common carotid artery (CCA), the external carotid artery (ECA), and internal carotid artery (ICA) were isolated. The ECA and CCA were ligated, and a 0.26-mm polylysine-coated nylon monofilament was introduced into the right ICA through the CCA to occlude the middle cerebral artery (MCA) in the brain. After 1 hour of occlusion, the suture was withdrawn to allow reperfusion for 23 hours. A heating pad was used to maintain a core temperature of 37 ± 0.5°C during the surgery.

Pharmacokinetic Study

Rats that underwent MCAO were randomly assigned to the following two groups (n = 5 per group): CG4 (30 mg/kg DSS + 8 mg/kg HSYA + 16 mg/kg SAB + 2.5 mg/kg SAA) and CG6 (30 mg/kg DSS + 4 mg/kg HSYA + 8 mg/kg SAB + 10 mg/kg SAA). The drugs were prepared by 0.9% saline. After reperfusion for 23 hours following 1 hours of cerebral ischemia, each group was administered the drug formulas *via* the tail vein.

After intravenous injection, 0.5 ml of blood was collected from the jaw vein after 2, 5, 10, 15, 30, 45, 60, 90, 120,150, 180, and 240 minutes respectively. In addition, 18 μl of heparin sodium was added as an anticoagulant. After centrifugation at 4,000 rpm for 12 minutes, plasma samples were transferred to clean tubes and stored at −20°C until analysis.

Method Validation

Standard stock solutions of DSS, HSYA, SAB, and SAA were prepared in methanol at a concentration of 1 mg/ml. Six different concentrations of reference standard solution were prepared in 100 μl of blank rat plasma with appropriate volumes of the standard stock solution. The final concentrations in plasma were 1, 2, 8, 25, 50, and 100 μg/ml for DSS; 1, 2, 8, 15, 30, and 60 μg/ml for HSYA; 1, 2, 7.5, 30, 60, and 120 μg/ml for SAB; and 1, 2, 12.5, 50, 100, and 200 μg/ml for SAA.

p-Hydroxybenzoic acid was prepared as an IS in methanol at a concentration of 1 mg/ml solution. The IS solution was diluted tenfold (0.1 mg/ml) for experimental use.

These standard solutions were subjected to the entire analytical procedure to validate the linearity, accuracy, precision, recovery, and stability [quality control (QC)] of the method.

Plasma Sample Preparation

The plasma samples (100 μl) were mixed with 10% phosphoric acid (5 μl), 10 μl of IS solution, and 300 μl of methanol. The mixture was vortexed for 30 seconds and centrifuged at 12,000 rpm for 10 minutes at 4°C. After centrifugation, the supernatant was transferred to another tube, and the extract was evaporated to dryness under a gentle stream of nitrogen. The residue was

reconstituted with methanol:0.1% phosphoric acid (50:50, v/v), then centrifuged at 12,000 rpm for 10 minutes at 4°C. The supernatants were analyzed using HPLC after centrifugation.

Instrumentation and Chromatographic Conditions

Analysis was performed on an Agilent 1200 series HPLC system (including G1311A quaternary gradient pump, G1316A column temperature box, G1315D diode array detector, G1322A on-line degasser, and chemical workstation). Chromatographic separation was achieved using an Eclipse XDB-C18 (5 μm, 4.6 mm × 250 mm) analytical column at maintained at 30℃. The mobile phases were acetonitrile (mobile phase A) and 0.1% phosphoric acid (mobile phase B). The gradient elution procedure was as follows: 0–17 minutes, 9%–33% A; 17–24 minutes, 33%–40% A; and 24–31 minutes, 40%–9% A. The flow rate was 1 ml/min. The detector was set to dual-wavelength detection at 280 nm for DSS, SAB, and SAA, and 403 nm for HSYA. The injection volume was 20 μl.

Data Processing and Statistical Analysis

Pharmacokinetic parameters for DSS, HSYA, SAB, and SAA were calculated from the plasma concentration versus time data using Drug and Statistic Version 3.2.6 (DAS 3.2.6) software (the Mathematical Pharmacology Committee, Chinese Pharmacological Society, China). Experimental data and pharmacokinetic parameters were expressed as the mean ± standard deviation (SD). Variance analysis was using SPSS 23.0 statistical software.

RESULTS

Specificity

The chromatograms showed baseline separation of DSS, HSYA, SAB, SAA, and *p*-hydroxybenzoic acid without any interference from components of plasma (**Figure 2**).

Investigation of Linearity and Lower Limit of Detection

All analytes were linear across the ranges evaluated. In **Table 1**, *Y* was the peak-area ratio of the analytes to the IS and *X* was the plasma concentration of the analytes. The lower limit of detection (LLOD) was defined as the level at which the signal to noise ratio was 3. The LLOD for DSS, HSYA, SAB, and SAA were 0.14, 0.09, 0.21, and 0.1 μg/ml, respectively.

Accuracy and Precision

Intra-day precision was evaluated at five different times on the same day, and inter-day precision was evaluated on five different days in a week. The results were summarized in **Table 2**. The interday and intraday precisions values for DSS, HSYA, SAB, and SAA, expressed as percent relative standard deviations (%RSD), were less than 10% at each concentration. Accuracy, expressed as the percent relative error (%RE) was also less than 10% for each analyte at each concentration. These results indicated that the method was reliable and reproducible for biological sample analysis.

Recovery

Recovery is the measure of the ability to extract an analyte test samples. The recoveries of DSS, HSYA, SAB, and SAA from plasma are summarized in **Table 2**.

Stability

Control solutions of DSS, HSYA, SAB, and SAA at three different concentrations (**Table 2**) were spiked into blank rat plasma. The drug-containing plasma samples were frozen at −20°C, thawed three times, then pretreated, and injected onto the HPLC. The stability of the method for each sample was expressed as the relative standard deviation (%RSD). The results were 0.363, 0.310, and 0.923% for DSS; 0.471, 0.420, and 0.533% for HSYA; 1.496, 1.497, and 3.479% for SAB; and 0.165, 0.219, and 0.874% for SAA. The %RSD values obtained in the stability study were less than 10%. The results showed that the samples were stable after repeated freeze-thaw cycles.

Pharmacokinetics Study

The plasma concentration-time curve in rats with MCAO is shown in **Figure 3**, and the main pharmacokinetic parameters from non-compartmental model analysis are summarized in **Table 3**.

After injecting the two combined medications groups separately, DSS and SAA induced statistically significant differences in $AUC_{(0-t)}$, $AUMC_{(0-t)}$, $MRT_{(0-t)}$, $VRT_{(0-t)}$, $t_{1/2z}$, V_z, CL_z, and C_{max} (P <0.01). In addition, HSYA induced statistically significant differences in $AUC_{(0-t)}$, $AUMC_{(0-t)}$, $MRT_{(0-t)}$, $VRT_{(0-t)}$ (P <0.01), CL_z, and C_{max} (P <0.05). Although the mechanisms are unclear, differences were observed *in vivo* following intravenous administration.

DISCUSSION

In this study, an HPLC-DAD method for simultaneous determination of DSS, HSYA, SAB, and SAA in MCAO model rats was established. Methanol was chosen as the protein-precipitating solvent during sample pretreatment to improve the peak shapes of the analytes. The reliability of this analytical method was confirmed by validating the specificity, linearity, precision, recovery, and stability of the method. The method was used to analyze the relationship between plasma concentration and time.

Cerebrovascular disease (CVD) is a leading cause of morbidity and mortality worldwide (Mozaffarian et al., 2016). Ischemic cerebral vascular disease (ICVD) is the predominant form of CVD (Wan et al., 2015). Ischemic stroke is a serious threat to human health and is the most frequent cause of permanent disability in adults worldwide (Lozano et al., 2012). The pathophysiological processes in ischemic stroke are diverse, and include inflammation, apoptosis, oxidative stress, intracellular calcium overload, and destruction of the blood brain barrier (BBB) (Tobin et al., 2014; Li et al., 2016; Li et al., 2018a).

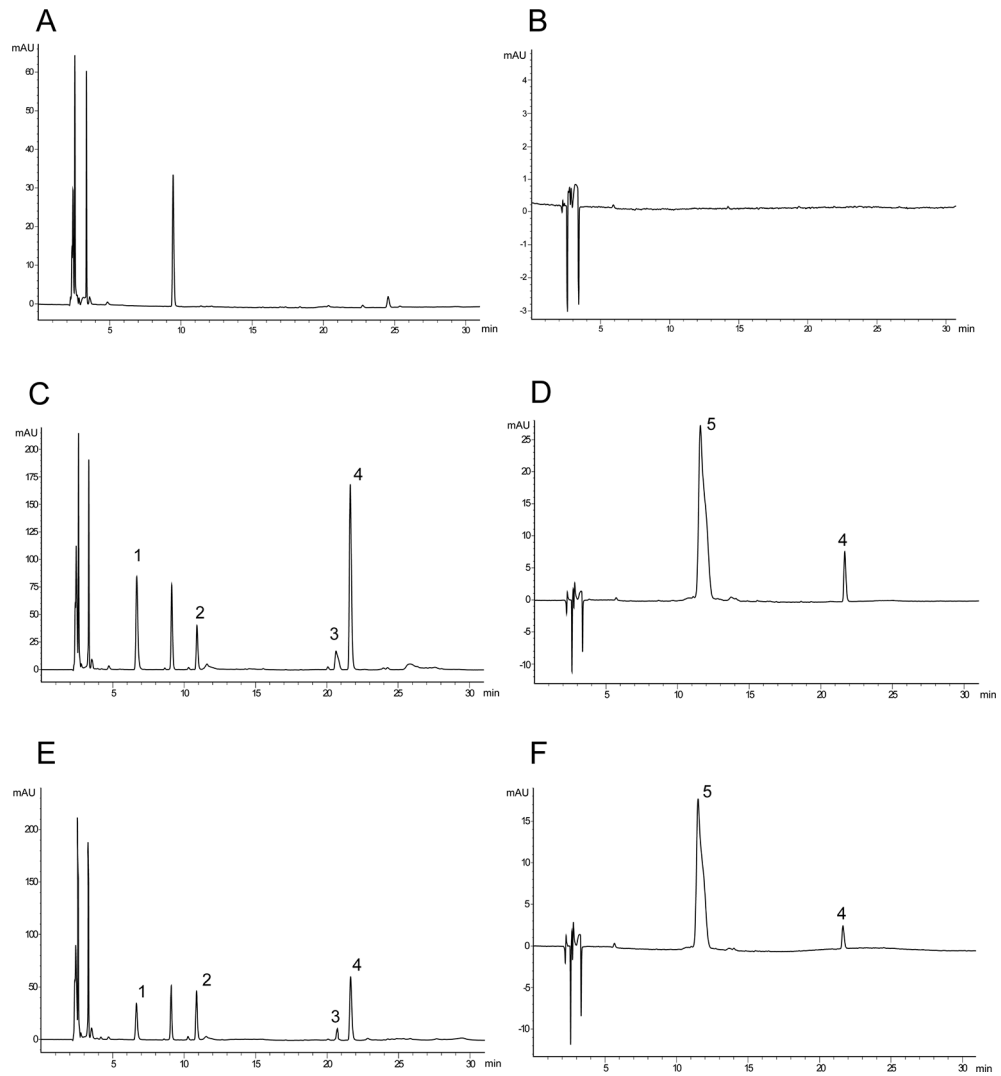


FIGURE 2 | Typical chromatograms of rat plasma. **(A)** Blank serum sample (280 nm); **(B)** blank serum sample (403 nm); **(C)** blank serum sample spiked with danshensu (DSS), hydroxysafflor yellow A (HSYA), salvianolic acid B (SAB), salvianolic acid A (SAA), and internal standard (IS) (280 nm); **(D)** blank serum sample spiked with HSYA and *p*-hydroxybenzoic acid (403 nm); **(E)** after 10 minutes of administration (280 nm); **(F)** after 10 minutes of administration (403 nm) (1: DSS; 2: *p*-hydroxybenzoic acid (IS); 3: SAB; 4: SAA; 5: HSYA).

TABLE 1 | Linearity for the analysis of danshensu (DSS), hydroxysafflor yellow A (HSYA), salvianolic acid B (SAB), and salvianolic acid A (SAA) under standard solutions.

Analyte	Calibration curve	Correlation coefficient (*r*)	Linearity(mg/L)
DSS	$Y = 0.0341X + 0.0506$	0.9956	1~100
HSYA	$Y = 0.0881X + 0.0472$	0.9975	1~60
SAB	$Y = 0.0113X + 0.0549$	0.998	1~120
SAA	$Y = 0.1226X + 0.0881$	0.9994	1~200

TCM herbs and their components have been widely used as therapeutic agents in China since ancient times (Sun et al., 2015). Danshen and Honghua, a well-known "herb pair," can stimulate blood circulation and dissipate blood stasis (Gao et al., 2016). The compositions of TCMs are very complex, and clinical effects often depend on composite effects of multiple components (Zhou et al., 2018). We previously showed that the combination of four herbal components in Danshen and Honghua protected against cerebral I/R injury in rats (Chen et al., 2018). Therefore, combinations of different classes of effective components with complementary mechanisms could result in improved therapeutic results.

TABLE 2 | Precisions and recoveries of each reference substance (n = 5).

Analyte	Concentration (mg/L)	Recovery (%, mean ± SD)	Intra-day		Inter-day	
			RSD (%)	RE (%)	RSD (%)	RE (%)
DSS	12.5	100.4 ± 0.1	0.9	–9.8	0.8	–6.9
	25	107.3 ± 0.1	0.4	1.9	0.4	–2.0
	50	109.3 ± 3.2	0.5	–3.3	0.4	0.4
HSYA	7.5	90.0 ± 0.1	0.9	–7.6	0.5	–4.0
	15	86.6 ± 0.2	0.4	–3.8	0.5	–6.5
	30	93.6 ± 0.8	0.5	–6.7	0.6	–3.3
SAB	15	128.3 ± 1.2	1.5	–6.9	5.4	8.1
	30	111.4 ± 0.8	0.5	7.7	4.3	–5.9
	60	67.5 ± 2.0	2.2	–8.2	1.6	–6.2
SAA	25	102.4 ± 0.1	0.4	–3.8	1.5	–3.7
	50	79.4 ± 0.3	0.5	–2.2	0.5	–5.3
	100	84.5 ± 2.1	0.6	–4.7	0.7	–2.6

Due to the severe symptoms and complications following strokes, the physiological status of patients can vary over time and between individuals. Pharmacokinetic studies to evaluate treatment of strokes are critical. This study was the first to investigate the effects of cerebral I/R on the pharmacokinetic compatibility for four herbal components. This was also the first study to compare the pharmacokinetic properties of these drugs in MCAO model rats. The pharmacokinetic parameters for DSS, HSYA, SAB, and SAA were significantly different in formulas of CG4 and CG6.

Compared with CG4, the pharmacokinetic parameters for DSS in CG6 showed that the exposure to DSS in plasma was significantly enhanced, the residence time was prolonged, and the clearance rate was reduced ($P < 0.01$). This result indicated that changes in the dosages of other components (HSYA, SAA, SAB) may have influenced the pharmacokinetics of DSS *in vivo* when the dosage of DSS was constant. Compared with CG4, the pharmacokinetic parameters for HSYA in CG6 showed that the absorption rate, the residence time, and the clearance rate were decreased. The opposite effect was observed for SAA. The results showed that increased SAA dosage resulted in increased $AUC_{(0-t)}$, $AUMC_{(0-t)}$, $MRT_{(0-t)}$, $VRT_{(0-t)}$, and C_{max} in CG6 compared to those in CG4 (**Table 3**). As shown in **Figure 3**, after administration, SAB was detected 2 minutes after administration. However, SAB was rapidly catabolized and was not detected 15 minutes after administration of CG6 formula. These results may have been due to lower sensitivity for, and lower dosages of, SAB (CG4: 16 mg/kg; CG6: 8 mg/kg). These results indicated that increasing or decreasing the dosage of a component impacted the pharmacokinetics of other components.

After reviewing the literature, we found that metabolic differences in the evaluated components may have been related to the compatibility of components. There are many influencing factors could affect the compatibility of components in addition to changes in the dosages of the components.

Cytochrome P450 (CYP450) enzymes are the main enzymes involved in human enzymatic metabolism (Tracy et al., 2016),

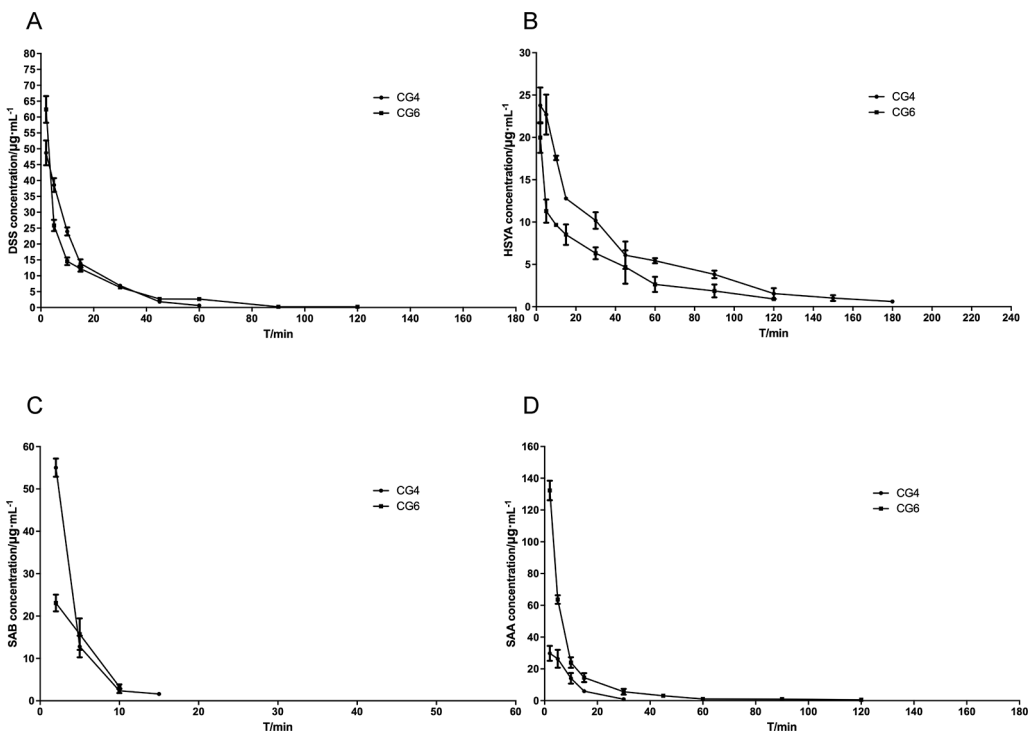


FIGURE 3 | Blood concentrating-time of components. **(A)** danshensu (DSS); **(B)** hydroxysafflor yellow A (HSYA); **(C)** salvianolic acid B (SAB); **(D)** salvianolic acid A (SAA).

TABLE 3 | Pharmacokinetic parameters of danshensu (DSS), hydroxysafflor yellow A (HSYA), salvianolic acid B (SAB), and salvianolic acid A (SAA) in different groups (n = 5).

Parameters	Unit	DSS		HSYA		SAB		SAA	
		CG4	CG6	CG4	CG6	CG4	CG6	CG4	CG6
$AUC_{(0-t)}$	mg/L*h	12.117 ± 0.075	13.164 ± 0.022**	16.206 ± 0.134	8.994 ± 0.159**	5.783 ± 0.27	/	5.816 ± 0.129	20.91 ± 0.048**
$AUMC_{(0-t)}$	h*h*mg/L	2.479 ± 0.062	4.453 ± 0.017**	11.633 ± 0.139	5.068 ± 0.125**	0.196 ± 0.05	/	0.688 ± 0.026	4.155 ± 0.028**
$MRT_{(0-t)}$	h	0.205 ± 0.019	0.338 ± 0.016**	0.718 ± 0.039	0.563 ± 0.081**	0.034 ± 0.031	/	0.118 ± 0.083	0.199 ± 0.029**
$VRT_{(0-t)}$	h^2	0.04 ± 0.016	0.211 ± 0.021**	0.456 ± 0.061	0.258 ± 0.076**	0.002 ± 0.001	/	0.009 ± 0.003	0.107 ± 0.015**
$t_{1/2z}$	h	0.17 ± 0.025	0.376 ± 0.072**	0.66 ± 0.192	0.535 ± 0.281	0.03 ± 0.011	/	0.085 ± 0.059	0.504 ± 0.013**
V_z	L/kg	0.599 ± 0.075	1.217 ± 0.015**	0.451 ± 0.12	0.318 ± 0.12	0.119 ± 0.043	/	0.052 ± 0.018	0.342 ± 0.057**
CL_z	L/h/kg	2.444 ± 0.032	2.242 ± 0.019**	0.476 ± 0.11	0.412 ± 0.098*	2.76 ± 0.135	/	0.422 ± 0.016	0.47 ± 0.032**
C_{max}	mg/L	48.721 ± 0.091	62.388 ± 0.12**	24.261 ± 0.137	19.978 ± 0.481*	55.031 ± 0.151	/	29.781 ± 0.047	132.347 ± 0.121**

*Values are given as mean ± SD of five rats. *: P < 0.05; **: P < 0.01; compared with CG4.*

and account for about 75% of drug metabolism in the human kidneys, liver, and intestines (Guengerich, 2008). Moreover, CYP450 enzymes are also key factors in drug interactions caused by the combination of TCM-TCM pairs and TCM-Western medicine pairs (Lu et al., 2015). Drug interactions that active or inhibit P450 enzymes can alter rates of P450-mediated metabolism (Tracy et al., 2016). A previous study showed that SAA can competitively inhibit CYP2C8 and partially inhibit CYP2J2 (Xu et al., 2018). DSS was shown to be a competitive inhibitor of CYP2C9 (Qiu et al., 2008). HSYA was shown to inhibit the activity of CYP1A2 and CYP2C11, and to increase the activity of CYP3A1 (Xu et al., 2014). Another report showed that injections that contain Danshen, or other formulations with high levels of tanshinones may lead to Danshen-drug interactions (Chen et al., 2017a). Therefore, if the two combination groups were to be administered separately, different pharmacokinetics may be observed due to altered rates of P450-mediated metabolism. These results agreed with our experimental results, which showed that the observed higher values of $AUC_{(0-t)}$ and C_{max} in CG6 than CG4 possibly resulted from decreased elimination of DSS (**Table 3**). And the slower metabolism of DSS in CG6 may be due to the rates of CYP450-mediated metabolism, which could be altered by the interaction of components. And the CL_z of HSYA in CG6 was significantly lower than that in CG4 (**Table 3**). So, the metabolic rates of CYP450 enzymes is one of the important factors that may influence the compatibility of components and the pharmacokinetic processes of them in two formulas in addition to changes in the dosage of components.

Plasma protein binding rate is associated with drug-drug interactions, which can affect the absorption, distribution, metabolism, and excretion of drugs *in vivo* (Bohnert and Gan, 2013). According to previous reports, DSS had a low plasma protein binding rate (Zhang et al., 2017a), and HSYA, SAB, and SAA had a high plasma protein binding rate (Jing et al., 2010; Wang et al., 2011; Chen et al., 2017a). Thus, in the process of drug metabolism, the loss rate of SAA, SAB, and HSYA were high. In pharmacokinetics, the distribution is described by the parameter V, the apparent volume of distribution. And low plasma binding usually means an extensive tissue distribution (Oie, 1986). These results agreed with our experimental results which showed that, compared with CG4, the parameter V_z for DSS in CG6 showed the more extensive distribution, while the dosage of DSS was constant ($P < 0.01$). In addition, the parameter V_z for HSYA in CG6 showed no significant difference while the dosage of HSYA was decreased, compared with CG4 ($P > 0.05$). These results indicated that intravenous injection of a formula containing these four components may affect the compatibility of components *in vivo* due to their different plasma protein binding rates, leading to different pharmacokinetic process of each component in two formulas.

Previous studies have shown that administration of either DSS, HSYA, SAB, or SAA resulted in distinct mechanisms of protection against cerebral I/R damage, such reduction of inflammation and oxidative stress (Sun et al., 2010; Fan et al., 2017; Xu et al., 2017). The BBB is a dynamic interface between the blood and the brain parenchyma (Sifat et al., 2017; Jiang et al., 2018). The ability of a drug to cross the BBB is a key factor in therapeutic efficacy. The disruption of the BBB by I/R has been shown to contribute to increased levels of SAA in the brains of I/R model rats (Feng et al., 2017). When damage occurs, SAA can reach the brain through the BBB and induce therapeutic effects in cerebral I/R model rats. In addition, studies have shown that HSYA can cross the BBB, resulting in downregulation of 12/15-lipoxygenase (12/15-LOX) and its metabolic products (Sun et al., 2012), and attenuation of occludin, claudin-5, and ZO-1 expressions, resulting in BBB permeability and improvement of tight junctions in MCAO mice (Lv and Fu, 2018). Meanwhile, DSS can readily permeate the BBB when normal rats were orally administered of Danshen extract (Zhang et al., 2011). Another study showed that SAB distributed rapidly to blood-rich tissues, such as the kidney (Li et al., 2018b). These findings indicated the pharmacokinetic differences of these four components in two formulas may result from the different effects of the components on the BBB.

CONCLUSION

In our study, an HPLC-DAD method for simultaneous determination of DSS, HSYA, SAB, and SAA in MCAO model rats was established. Comparison of the pharmacokinetic parameters of the four herbal components in different formulas in MCAO model rats showed that difference in pharmacokinetic

parameters may have been related to the changes in dosages of the components (HSYA, SAA, and SAB) and the compatibility of components. Meanwhile, there were many influencing factors could affect the compatibility of components, such as the metabolic rates of CYP450 enzymes, plasma protein binding rates and the effects of the components on the BBB. Furthermore, this study may provide guidance for evaluation of pharmacokinetic parameters and pharmacological effects of active components of TCMs in pathological states.

DATA AVAILABILITY STATEMENT

The datasets generated for this study are available on request to the corresponding authors.

ETHICS STATEMENT

Animal welfare and experimental procedures were strictly in accordance with the Regulation for the Administration of Affairs Concerning Experimental Animals (State Science and Technology Commission, 1988) and approved by the Animal Subjects Review Board of Zhejiang Chinese Medical University.

AUTHOR CONTRIBUTIONS

XZ, LY, HW, and JY participated in designing experiments, carried out the experiments in this study, prepared the first draft, and revising of this manuscript. YC performed the drug administration and blood sampling. YW participated in data analysis. All authors contributed to manuscript revision, read and approved the final manuscript.

FUNDING

This research was financially supported by the Natural Science Foundation of Zhejiang Province (No. LZ17H270001) and the National Natural Science Foundation of China (No. 81874366, 81803992, 81873226).

REFERENCES

Bohnert, T., and Gan, L. S. (2013). Plasma protein binding: from discovery to development. *J. Pharm. Sci.* 102 (9), 2953–2994. doi: 10.1002/jps.23614

Chen, F., Li, L., and Tian, D. D. (2017a). Salvia miltiorrhiza roots against cardiovascular disease: consideration of herb-drug interactions. *BioMed. Res. Int.* 2017, 1–12. doi: 10.1155/2017/9868694

Chen, L., Li, W. W., and Liu, C. H. (2017b). Neruroprotective effect of Salviamiltiorrhiza-Safflower on cerebral ischemia reperfusion injury in rats. *Pharmacol. Clin. Chin. Mater. Clin. Med.* 33, 161–166. doi: 10.13412/j.cnki.zyyl.2017.01.044

Chen, Z. D., Jiang, B., Ru, X. J., Sun, H. X., Sun, D. L., Liu, X. T., et al. (2017c). Mortality of stroke and its subtypes in china: results from a nationwide population-based survey. *Neuroepidemiology* 48, 95–102. doi: 10.1159/000477494

Chen, Y. L., Wan, H. T., Zhou, H. F., Yu, L., He, Y., Li, C., et al. (2018). Protective effects of Salvia miltiorrhiza and Carthamus tinctorius active ingredients in different compatibility on cerebral ischemia/reperfusion injury in rats. *Chin. Trad. Herb. Drugs* 49, 3875–3881. doi: 10.7501/j.issn.0253-2670.2018.16.022

Donnan, G. A., Fisher, M., Macleod, M., and Davis, S. M. (2008). Stroke. *Lancet* 371, 1612–1623. doi: 10.1016/S0140-6736(08)60694-7

Fan, Y., Luo, Q. P., Wei, J. J., Lin, R. H., Lin, L. L., Li, Y. K., et al. (2017). Mechanism of salvianolic acid B neuroprotection against ischemia/reperfusion induced cerebral injury. *Brain Res.* 1679, 125–133. doi: 10.1016/j.brainres.2017.11.027

Feng, S. Q., Aa, N., Geng, J. L., Huang, J. Q., Sun, R. B., Ge, C., et al. (2017). Pharmacokinetic and metabolomic analyses of the neuroprotective effects of salvianolic acid A in a rat ischemic stroke model. *Acta Pharmacol. Sin.* 38, 1435–1444. doi: 10.1038/aps.2017.114

Gao, L. N., Cui, Y. L., Yan, K., and Qiu, C. (2016). Advances in studies on compatibility of Salviae Miltiorrhizae Radix et Rhizoma and Carthamii Flos. *Chin. Trad. Herb. Drugs* 47, 671–679. doi: 10.7501/j.issn.0253-2670.2016.04.024a

Guengerich, F. P. (2008). Cytochrome p450 and chemical toxicology. *Chem. Res. Toxicol.* 21 (1), 70–83. doi: 10.1021/tx700079z

Hui, A., Wu, W. F., and Cheng, P. (2018). Hydroxysafflor yellow a: a promising therapeutic agent for a broad spectrum of diseases. *Evid. Based. Complement Alternat. Med.* 2018, 1–17. doi: 10.1155/2018/8259280

Jiang, X., Andjelkovic, A. V., Zhu, L., Yang, T., Bennett, M. V. L., Chen, J., et al. (2018). Blood-brain barrier dysfunction and recovery after ischemic stroke. *Prog. Neurobiol.* 163-164, 144–171. doi: 10.1016/j.pneurobio.2017.10.001

Jing, C. J., Chen, X. H., Liu, X., Bi, K. S., and Guo, D. A. (2010). Determination of the binding rate of rat plasma protein with salvianolic acid B. *Acta Pharm. Sin.* 45, 343–346. doi: 10.16438/j.0513-4870.2010.03.011

Kalaria, R. N., Akinyemi, R., and Ihara, M. (2016). Stroke injury, cognitive impairment and vascular dementia. *Biochim. Biophys. Acta* 1862, 915–925. doi: 10.1016/j.bbadis.2016.01.015

Li, S. J., Tang, Y. P., Shen, J., Li, J. P., Guo, J. M., and Duan, J. A. (2013). Research of Chinese medicine pairs (VII)——Salviae Miltiorrhizae Radix et Rhizoma-Carthami Flos. *Chin. J. Chin. Mater. Med.* 38, 4227–4231. doi: 10.4268/cjcmm20132408

Li, K., Ding, D., and Zhang, M. (2016). Neuroprotection of Osthole against cerebral ischemia/reperfusion injury through an anti-apoptotic pathway in rats. *Biol. Pharm. Bull.* 39, 336–342. doi: 10.1248/bpb.b15-00699

Li, P., Stetler, R. A., Leak, R. K., Shi, Y., Li, Y., Yu, W., et al. (2018a). Oxidative stress and DNA damage after cerebral ischemia: potential therapeutic targets to repair the genome and improve stroke recovery. *Neuropharmacology* 134, 208–217. doi: 10.1016/j.neuropharm.2017.11.011

Li, S., Xie, X. M., Li, D. X., Yu, Z. G., Tong, L., and Zhao, Y. L. (2018b). Simultaneous determination and tissue distribution studies of four phenolic acids in rat tissue by UFLC-MS/MS after intravenous administration of salvianolic acid for injection. *BioMed. Chromatogr.* 32 (3), e4128. doi: 10.1002/bmc.4128

Li, Z. M., Xu, S. W., and Liu, P. Q. (2018c). Salvia miltiorrhizaBurge (Danshen): a golden herbal medicine in cardiovascular therapeutics. *Acta Pharmacol. Sin.* 39 (5), 802–824. doi: 10.1038/aps.2017.193

Liu, J. G., Zhang, D. W., Li, J., Feng, J. T., Yang, X. P., Shi, D. Z., et al. (2011). Effects of Salvia miltiorrhiza and Carthamus tinctorius aqueous extracts and compatibility on rat myocardial ischemic reperfusion injury. *Chin. J. Chin. Mater. Med.* 36, 189–194. doi: 10.4268/cjcmm20110222

Longa, E. Z., Weinstein, P. R., Carlson, S., and Cummins, R. (1989). Reversible middle cerebral artery occlusion without craniectomy in rats. *Stroke.* 20, 84–91. doi: 10.1161/01.str.20.1.84

Lozano, R., Naghavi, M., Foreman, K., Lim, S., Shibuya, K., Aboyans, V., et al. (2012). Global and regional mortality from 235 causes of death for 20 age groups in 1990 and 2010: a systematic analysis for the global burden of disease study 2010. *Lancet* 380, 2095–2128. doi: 10.1016/s0140-6736(12)61728-0

Lu, T. L., Su, L. L., Ji, D., Gu, W., and Mao, C. Q. (2015). Interaction between CYP450 enzymes and metabolism of traditional Chinese medicine as well as enzyme activity assay. *Chin. J. Chin. Mater. Med.* 40 (18), 3524–3529. doi: 10.4268/cjcmm20151802

Lv, Y. N., and Fu, L. S. (2018). The potential mechanism for Hydroxysafflor yellow A attenuating blood-brain barrier dysfunction via tight junction signaling pathways excavated by an integrated serial affinity chromatography and shotgun proteomics analysis approach. *Neurochem. Int.* 112, 38–48. doi: 10.1016/j.neuint.2017.10.012

Mozaffarian, D., Benjamin, E. J., Go, A. S., Arnett, D. K., Blaha, M. J., Cushman, M., et al. (2016). Heart disease and stroke statistics-2016 update: a report from the american heart association. *Circulation.* 133, e38–e360. doi: 10.1161/CIR.0000000000000350

Oie, S. (1986). Drug distribution and binding. *J. Clin. Pharmacol.* 26 (8), 583–586. doi: 10.1002/j.1552-4604.1986.tb02953.x

Qin, F., Liu, Y. X., Zhao, H. W., Huang, X., Ren, P., and Zhu, Z. Y. (2009). Chinese medicinal formula Guan-Xin-Er-Hao protects the heart against oxidative stress induced by acute ischemic myocardial injury in rats. *Phytomedicine.* 16 (2-3), 215–221. doi: 10.1016/j.phymed.2008.08.005

Qiu, F. R., Zhang, R., Sun, J. G., A, J. Y., Hao, H. P., Peng, Y., et al. (2008). Inhibitory effects of seven components of danshen extract on catalytic activity of cytochrome P450 enzyme in human liver microsomes. *Drug Metab. Dispos.* 36 (7), 1308–1314. doi: 10.1124/dmd.108.021030

Sifat, A. E., Vaidya, B., and Abbruscato, T. J. (2017). Blood-brain barrier protection as a therapeutic strategy for acute ischemic stroke. *AAPS J.* 19 (4), 957–972. doi: 10.1208/s12248-017-0091-7

State Science and Technology Commission (1988). *Affairs Concerning Experimental Animals* (Beijing: Ministry of Science and Technology).

Sun, X., Wei, X. B., Qu, S. F., Zhao, Y. X., and Zhang, X. M. (2010). Hydroxysafflor Yellow A suppresses thrombin generation and inflammatory responses following focal cerebral ischemia-reperfusion in rats. *Bioorg. Med. Chem. Lett.* 20, 4120–4124. doi: 10.1016/j.bmcl.2010.05.076

Sun, L., Yang, L., Xu, Y. W., Liang, H., Han, J., Zhao, R. J., et al. (2012). Neuroprotection of hydroxysafflor yellow A in the transient focal ischemia: inhibition of protein oxidation/nitration, 12/15-lipoxygenase and blood-brain barrier disruption. *Brain Res.* 1473, 227–235. doi: 10.1016/j.brainres.2012.07.047

Sun, K., Fan, J. Y., and Han, J. Y. (2015). Ameliorating effects of traditional Chinese medicine preparation, Chinese materia medica and active compounds on ischemia/reperfusion-induced cerebral microcirculatory disturbances and neuron damage. *Acta Pharm. Sin. B.* 5 (1), 8–24. doi: 10.1016/j.apsb.2014.11.002

Sun, Y., Xu, D. P., Qin, Z., Wang, P. Y., Hu, B. H., Yu, J. G., et al. (2018). Protective cerebrovascular effects of hydroxysafflor yellow A (HSYA) on ischemic stroke. *Eur. J. Pharmacol.* 818, 604–609. doi: 10.1016/j.ejphar.2017.11.033

Tobin, M. K., Bonds, J. A., Minshall, R. D., Pelligrino, D. A., Testai, F. D., and Lazarov, O. (2014). Neurogenesis and inflammation after ischemic stroke: what is known and where we go from here. *J. Cereb. Blood Flow Metab.* 34 (10), 1573–1584. doi: 10.1038/jcbfm.2014.130

Tracy, T. S., Chaudhry, A. S., Prasad, B., Thummel, K. E., Schuetz, E. G., Zhong, X. B., et al. (2016). Interindividual variability in cytochrome P450-mediated drug metabolism. *Drug Metab. Dispos.* 44 (3), 343–351. doi: 10.1124/dmd.115.067900

Wan, L., Cheng, Y. F., Luo, Z. Y., Guo, H. B., Zhao, W. J., Gu, Q. L., et al. (2015). Neuroprotection, learning and memory improvement of a standardized extract from Renshen Shouwu against neuronal injury and vascular dementia in rats with brain ischemia. *J. Ethnopharmacol.* 165, 118–126. doi: 10.1016/j.jep.2015.02.027

Wang, J. M., Zou, T., Zhang, Y. Y., and Fan, N. (2011). Study on plasma protein binding rate of hydroxysafflor yellow A in Safflor yellow powder injection. *Chin. Trad. Pat. Med.* 33, 947–949. doi: 10.1016/0305-1978(94)90122-8

Xu, R. A., Xu, Z. S., and Ge, R. S. (2014). Effects of hydroxysafflor yellow A on the activity and mRNA expression of four CYP isozymes in rats. *J. Ethnopharmacol.* 151 (3), 1141–1146. doi: 10.1016/j.jep.2013.12.025

Xu, H., Liu, W. X., Liu, T. L., Su, N., Guo, C., Feng, X. N., et al. (2017). Synergistic neuroprotective effects of Danshensu and hydroxysafflor yellow A on cerebral ischemia-reperfusion injury in rats. *Oncotarget* 8, 115434–115443. doi: 10.18632/oncotarget.23272

Xu, M. J., Jiang, L. F., Wu, T., Chu, J. H., Wei, Y. D., Aa, J. Y., et al. (2018). Inhibitory effects of Danshen components on CYP2C8 and CYP2J2. *Chem. Biol. Interact.* 289, 15–22. doi: 10.1016/j.cbi.2018.04.011

Zhang, Y. J., Wu, L., Zhang, Q. L., Li, J., Yin, F. X., and Yuan, Y. (2011). Pharmacokinetics of phenolic compounds of Danshen extract in rat blood and brain by microdialysis sampling. *J. Ethnopharmacol.* 136 (1), 129–136. doi: 10.1016/j.jep.2011.04.023

Zhang, Q., Dai, G. L., Ju, W. Z., Guo, J. M., Sun, B. T., Zong, Y., et al. (2017a). Determination of binding rates of human plasma protein with seven bioactive components in Danhong injection. *Chin. Pharmacol. Bull.* 33, 712–718. doi: 10.3969/j.issn.1001-1978.2017.05.024

Zhang, X. H., Zheng, W., Wan, T. R., Ren, P., Wang, F. S., Ma, X. L., et al. (2017b). Danshen-Chuanxiong-Honghua ameliorates cerebral impairment and improves spatial cognitive deficits after transient focal ischemia and identification of active compounds. *Front. Pharmacol.* 8, 452. doi: 10.3389/fphar.2017.00452

Zhou, J., Li, M., Jin, W. F., Li, X. H., Fan, H. J., and Zhang, Y. Y. (2018). Pharmacokinetic study on protocatechuic aldehyde and hydroxysafflor yellow A of danhong injection in rats with Hyperlipidemia. *Pharmacology* 102, 154–160. doi: 10.1159/000491020

Conflict of Interest: The authors declare that the research was conducted in the absence of any commercial or financial relationships that could be construed as a potential conflict of interest.

Copyright © 2020 Zhao, Yu, Chen, Wang, Wan and Yang. This is an open-access article distributed under the terms of the Creative Commons Attribution License (CC BY). The use, distribution or reproduction in other forums is permitted, provided the original author(s) and the copyright owner(s) are credited and that the original publication in this journal is cited, in accordance with accepted academic practice. No use, distribution or reproduction is permitted which does not comply with these terms.

frontiers in Pharmacology

ORIGINAL RESEARCH
published: 17 March 2020
doi: 10.3389/fphar.2020.00236

Total Glycosides of *Cistanche deserticola* Promote Neurological Function Recovery by Inducing Neurovascular Regeneration *via* Nrf-2/Keap-1 Pathway in MCAO/R Rats

Fujiang Wang[1], *Ruiyan Li*[2], *Pengfei Tu*[1], *Jianping Chen*[3], *Kewu Zeng*[1]* *and Yong Jiang*[1]*

[1] State Key Laboratory of Natural and Biomimetic Drugs, School of Pharmaceutical Sciences, Peking University, Beijing, China, [2] Department of Pharmacology, Changzhi Medical College, Shanxi, China, [3] School of Chinese Medicine, The University of Hong Kong, Hong Kong, Hong Kong

OPEN ACCESS

Edited by:
Jing-Yan Han,
Peking University, China

Reviewed by:
Yumin Luo,
Capital Medical University, China
Jiangang Shen,
The University of Hong Kong, Hong Kong

***Correspondence:**
Kewu Zeng
ZKW@bjmu.edu.cn
Yong Jiang
yongjiang@bjmu.edu.cn

Specialty section:
This article was submitted to Ethnopharmacology, a section of the journal Frontiers in Pharmacology

Received: 25 July 2019
Accepted: 20 February 2020
Published: 17 March 2020

Citation:
Wang F, Li R, Tu P, Chen J, Zeng K and Jiang Y (2020) Total Glycosides of Cistanche deserticola Promote Neurological Function Recovery by Inducing Neurovascular Regeneration via Nrf-2/Keap-1 Pathway in MCAO/R Rats. Front. Pharmacol. 11:236. doi: 10.3389/fphar.2020.00236

Background: The traditional Chinese medicine *Cistanche deserticola* has been reported to be valid for cardiovascular and cerebrovascular diseases. However, its active components for the protection of ischemic stroke are not clear. We aimed to explore the active components of *C. deserticola* against ischemic stroke as well as its potential mechanisms.

Methods: We investigated the brain protective effects of extracts from *C. deserticola*, total glycosides (TGs), polysaccharides (PSs), and oligosaccharides (OSs) in a rat model of middle cerebral artery occlusion-reperfusion (MCAO/R). 2, 3, 5-Triphenyltetrazolium chloride (TTC) staining was used to assess the cerebral infarction volume, and Evans blue assay was adopted to assess the blood-brain barrier (BBB) permeability. Then, the expressions CD31, α-SMA, PDGFRβ, SYN, PSD95, MAP-2, ZO-1, claudin-5, occludin, Keap-1, and Nrf-2 were analyzed using western blotting or immunofluorescence, and the activities MDA, SOD, CAT, and GSH-Px were analyzed using kits.

Results: TGs treatment remarkably decreased neurological deficit scores and infarction volumes, promoted angiogenesis and neural remodeling, and effectively maintained blood-brain-barrier integrity compared with the model group. Furthermore, TGs significantly decreased MDA levels and increased antioxidant activities (SOD, CAT, and GSH-Px) in brains. Meanwhile, TGs remarkably downregulated Keap-1 expression and facilitated Nrf-2 nuclear translocation. On the contrary, no protective effects were observed for PSs and OSs groups.

Conclusion: TGs are the main active components of *C. deserticola* against MCAO/R-induced cerebral injury, and protection is mainly *via* the Nrf-2/Keap-1 pathway.

Keywords: *Cistanche deserticola*, cerebral injury, total glycosides, polysaccharides, oligosaccharides, Nrf-2/Keap-1 pathway

INTRODUCTION

Strokes are considered to be a major cause of death and disability in the world (Donnan et al., 2008). Nearly 87% of all stroke cases are triggered by ischemic stroke (Ovbiagele and Nguyen-Huynh, 2011). Currently, the most effective agent and the only FDA-approved drug used for ischemic stroke treatment is recombinant tissue plasminogen activator. However, a large amount of stroke patients fail to respond to this drug, owing to its narrow therapeutic time window and a serious risk of hemorrhagic complications (Lee et al., 2012; Schellinger and Kohrmann, 2014). A major challenge of thrombolytic treatment is ischemia/reperfusion (I/R) injury, which is considered as a main cause of brain injury and function destruction. Reperfusion after cerebral ischemia increases the risk of brain hemorrhage, while leading to neurovascular injury and producing excessive reactive oxygen species (ROS) which damage the blood-brain barrier (Alluri et al., 2015). A number of studies have confirmed that the disruption of the BBB is a major cause of the pathogenesis of ischemic stroke (Cao et al., 2016b).

The BBB consists mainly of endothelial cells, pericytes, astrocytes, neurons, and the basement membranes. The core components of the BBB are cerebral microvascular endothelial cells that are joined by tight junctions, thus restricting exogenous molecules into the brain. The pathological alterations of tight junctions—particularly occludin, claudin-5, and zonula occludens-1 (ZO-1)—significantly affect the BBB function during an ischemic stroke, especially barrier permeability (Liu et al., 2014; Hu et al., 2018; Liu et al., 2019). During I/R periods, excessive ROS is one of the main factors leading to the direct damage of brain neurons (Ding et al., 2014). ROS overproduction leads to the degradation of certain junctions and BBB disruption, which results in exogenous molecules entering into the brain through the BBB, leading to brain damage aggravation (Cheon et al., 2016; Zhang Q. Y. et al., 2017). Therefore, protection of the BBB by anti-oxidants has been regarded as a potential way to prevent reperfusion injury.

Besides the breakdown of the BBB, I/R can result in neurovascular injury and neuronal death (Jung et al., 2010). During a stroke, increased neuronal cell death may result from oxidative stress (Chi et al., 2018), and numerous studies have shown that ROS aggravates stroke severity and neurological damage (Kondo et al., 1997; Crack et al., 2001; Crack et al., 2006). Although clinical trials have not got satisfactory results, neuroprotection is still a promising strategy for treatment of acute ischemic stroke (Moretti et al., 2015). Thus, finding effective neuroprotection drugs to treat strokes is a benefit for stroke patients.

Traditional Chinese medicine (TCM) takes measures to intervene against the body's internal imbalance (Gaire, 2018). Owing to the complex pathogenesis of ischemic strokes, the multifactorial effect of TCM and their active constituents play a critical role in the treatment of strokes. *Cistanche deserticola* Y. C. Ma, widespread in arid or semi-arid areas throughout Mongolia and Northwest China, has been a widely used TCM herb for the treatment of various diseases such as forgetfulness and depression for more than 1,000 years in China. Modern pharmacological studies indicated that the crude extracts from *C. deserticola* showed multiple pharmacological activities, such as enhancing learning and memory function, neuroprotection, enhancing immunity, antioxidant, anti-aging, and antifatigue effects (Ko and Leung, 2007; Wang et al., 2012; Li et al., 2015). Chemical analysis of *C. deserticola* showed that its main constitutes include phenylethanoid glycosides, iridoid glycosides, polysaccharides and oligosaccharides (Jiang and Tu, 2009). However, the active components of *C. deserticola* for brain protection are not very clear.

The neuroprotective property of *C. deserticola* implies its therapeutic potential in cognitive-related illness such as stroke and depression, as well as Alzheimer's disease (Wang et al., 2017). However, research on the impact of *C. deserticola* on strokes, including its active components and action mechanisms, is very limited. In the current work, we explored the protective effect of three extracts from *C. deserticola*, total glycosides (TGs, phenylethanoid glycosides, and other glycosides), polysaccharides (PSs), and oligosaccharides (OSs) on cerebral I/R injuries. Our findings may contribute to the accurate clinical application of *C. deserticola* and provide a candidate agent for ischemic stroke therapy.

MATERIALS AND METHODS

Chemicals and Reagents

The stems of *Cistanche deserticola* were purchased from Alashan, Inner Mongolia, and identified by one of the authors (P.-F. Tu). TGs, PSs, and OSs were prepared according to our previously reported method (Gao et al., 2015). Quantitative analysis of TGs was performed by high-performance liquid chromatography (HPLC) as previously described (Li et al, 2019), and its chromatogram is shown in **Figure 1**. The main components of TGs are echinacoside, tubuloside A, acteoside, isoacteoside, and 2'-acetylacteoside; their contents are 163.05 mg/g, 4.125 mg/g, 41.66 mg/g, 22.655 mg/g, and 12.045 mg/g, respectively. The contents of PSs and OSs are 69.42% and 65.24%, respectively, as determined by HPLC and the phenol–sulfuric acid analysis, respectively (Zhang A. et al., 2018; Shi et al, 2019).

The standard references of echinacoside (A0282), tubuloside A (A0942), acteoside (A0280), isoacteoside (A0281), and 2'-acetylacteoside (A0943) were purchased from Chengdu Must Biotechnology (Sichuan, China). The purities of all standards are more than 98%. Nissl stain H&E kits were bought from Boster (Wuhan, China). Edaravone (T0407-1) was bought from Target Mol (Shanghai, China). Rabbit anti-rat MAP-2 (ab32454), Nrf-2 (ab31163), PDGFRβ (ab32570), Keap-1 (ab66620), and mouse anti-rat CD31 (ab24590) were purchased from Abcam Inc (Cambridge, MA, USA). Rabbit anti-rat Claudin5 (BS1069), ZO-1 (BS9802M), and Occludin (BS72035) were bought from Bioworld Technology (Nanjing, China). Cell Signaling Technology Inc. (Boston, MA, USA) was the source of rabbit anti-rat Synapsin-1 (SYN,5297T), PSD95 (3450T), α-Smooth Muscle Actin (α-SMA,19245T). GAPDH (HRP-60004) was purchased from Proteintech Group, Inc. (Chicago, USA).

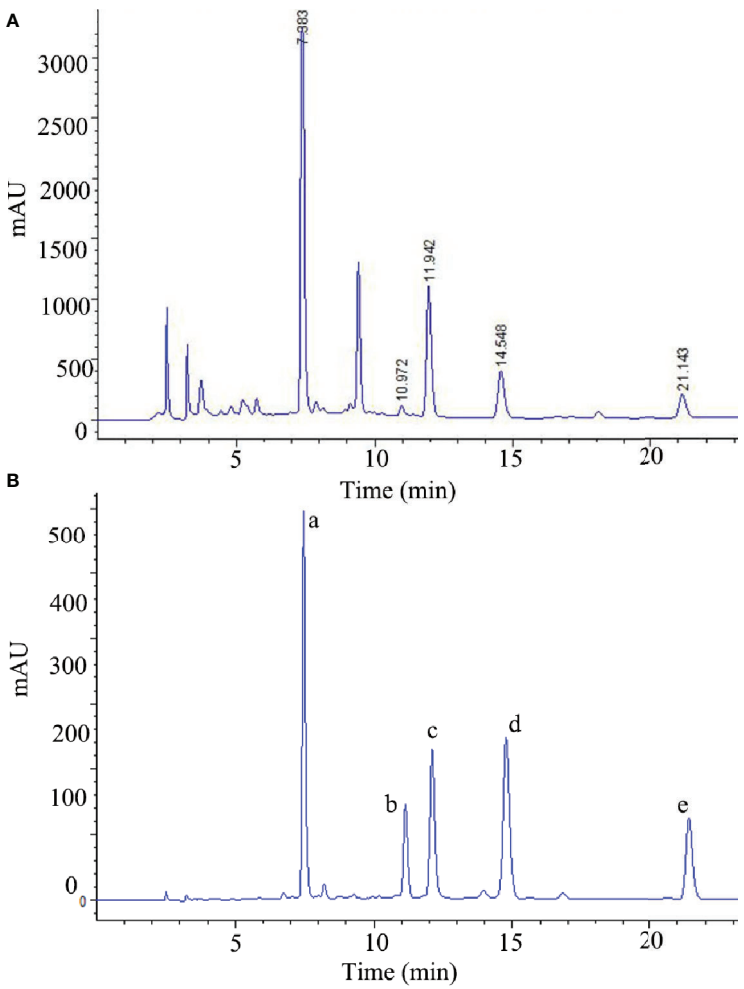


FIGURE 1 | The HPLC chromatograms of the TGs **(A)** and standard references **(B)**. (a) echinacoside, (b) tubuloside A, (c) acteoside, (d) isoacteoside, (e) 2'-acetylacteoside of TGs.

Secondary antibodies were supplied by Zhongshan Golden Bridge Biotechnology (Beijing, China). Hoechst 33258 was obtained from Beyotime (Jiangsu, China).

Animals

Sprague-Dawley rats (male, weighing 250–300g) were obtained from Vital River Laboratory Animal Technology (Beijing, China) and housed in an airconditioned room kept on a 12 h light/dark cycle. All animal experiments were performed in accordance with the animal research ARRIVE guidelines (Kilkenny et al., 2010; McGrath et al., 2010), and approved by the Institutional Animal Care and Use Committee of Peking University Health Science Center (LA2019123).

Animal Experimental Protocols

The rats were subjected to MCAO/R, as previously described (Wang et al., 2018). Briefly, the left common carotid artery (CCA), external carotid artery (ECA), and internal carotid artery (ICA) were exposed, and a 3-0 nylon monofilament suture was inserted from the ECA into the ICA until reaching the middle cerebral artery (MCA). After 1.5 h of MCA occlusion, reperfusion was simulated by removing the filament. During the surgical procedure, the body temperature of all rats was maintained at 37.0°C.

Drug Administration

The rats were randomly separated into six groups using the SPSS software version 22.0 as described (Jiang et al., 2014): normal group (NOR); model group (MOD); edaeavone group (positive drug, 6 mL/kg, EDI); TGs group (280 mg/kg, TGs); PSs group (280 mg/kg, PSs), and OSs group (280 mg/kg, OSs). TGs, PSs, and OSs were administrated ig once a day after MCAO/R for 14 days. The NOR and MOD groups were treated with normal saline. The animal numbers are shown in **Table 1**.

TABLE 1 | Number of animals for different experimental groups and various parameters at 14 d after administration.

Parameters	NOR	MOD	EDI	TGs	PSs	OSs	Total
Weight, mNSS	18	18	18	18	18	18	108
TTC	8	8	8	8	8	8	48
H&E,Nissl stain	5	5	5	5	5	5	30
Immunofluorescent	5	5	5	5	5	5	30
Total	36	36	36	36	36	36	216

Measurement of Weight and Modified Neurological Deficit Scores (mNSS)

Body weight was monitored on the 14th day using an ADVENTURE™ Digital Scale (OHAUS, New Jersey, USA). The mNSS was assessed according to the method described by FJ Wang (Wang et al., 2018), with minor revisions.

2, 3, 5-Triphenyltetrazolium Chloride (TTC) Staining

Infarct volume was measured as described previously (Wang et al., 2015). In brief, the brains were sectioned into seven equally spaced coronal blocks (2 mm). These sections were stained with 2% TTC (Coolaber, Beijing, China) at 37°C for 15 min. Infarct volume (%) = (ipsilateral ischemic hemisphere volume −contralateral ischemic hemisphere volume)/contralateral ischemic hemisphere volume × 100.

Nissl and H&E Staining

The rats were deeply anesthetized, and the whole brain was then rapidly removed from the skull and fixed using 4% paraformaldehyde and embedded in paraffin wax and sectioned into slice of 7 μm thickness. The sections were stained with Nissl and H&E. In this study, six random 200 × 200 μm fields were captured in each tissue specimen with a light microscope. The number of Nissl's bodies was counted with IPP software version 6.0 (Media Cybernetics, Bethesda, USA).

Evans Blue Assay

Rats were injected with 2% EB (Coolaber Science & Technology Co., LTD) after MCAO/R. Two hours later, the rats were anesthetized and the whole brain was then rapidly removed and homogenized in acetone. The supernatants were analyzed at 620 nm by an 800 TS absorbance reader (BioTek, USA).

Measurement of the Activities of Catalase (CAT), Superoxide Dismutase (SOD), Malondialdehyde (MDA), and Glutathione Peroxidase (GSH-Px)

All serum samples were centrifuged at 4,000 × rpm for 15 min at 4°C, and then analyzed to detect the activities of MDA, CAT, SOD, and GSH-Px following the manufacturer's instructions (Jiangsu Meimian industrial Co., Ltd, China).

Western Blotting Analysis

Brain tissues (100 mg) collected from each rat were homogenized and lysed in RIPA lysis buffer, and then analyzed to detect the protein concentration using a BCA kit (Beijing TransGen Biotech Co., Ltd.). Tissue total proteins were loaded on 10% SDS-PAGE gels and transferred onto a nitrocellulose membrane. The membrane was blocked using 5% skim milk, then incubated overnight with primary antibodies at 4°C. The membrane was then incubated with a secondary antibody. Western blot analysis was analyzed using Kodak Digital Imaging System (5200 Multi, Tanon, China).

Immunofluorescent Analysis

Immunofluorescence staining for CD31, α-SMA, ZO-1, claudin5, occludin, PDGFRβ, SYN, PSD95, MAP-2, Nrf-2 and Keap-1 were performed. Primary antibodies against Nrf-2, CD31, α-SMA, ZO-1, claudin5, occludin, PDGFRβ, SYN, PSD95, MAP-2 and Keap-1 were diluted to 1:200 and 1:100, respectively. The secondary antibodys of Alexa Flur 488 mouse anti-rabbit IgG and rhodamine (TRITC) goat anti-rabbit IgG were both diluted to 1:200. The nucleuses were stained by Hoechst 33258. Images were captured using Vectra® Polaris™ Automated Quantitative Pathology Imaging System (PerkinElmer, USA). The protein expression was analyzed using IPP software version 6.0.

Statistical Analysis

All data were described as mean ± SD. SPSS software version 22.0 was performed for statistical analysis. One-way ANOVA was used when comparing different groups. $P < 0.05$ was considered to be statistical difference.

RESULTS

TGs Increase Body Weight and Reduces Brain Damages in MCAO/R Rats

After 14 days of cure with TGs, PSs, Oss, and EDI, the body weights, neurological deficits and infarct volumes of I/R rats were evaluated. The results showed that the body weights in the MOD group were greatly decreased, while the decreased weights in TGs, PSs and EDI groups were obviously increased (**Figure 2A**). Neurological deficit scores were substantially lowered by EDI and TGs (**Figure 2B**). The brain slices in NOR group rats were deep red and there were no infarctions, while the rats of the MOD group showed a large ipsilateral cerebral infarction. After TGs treatment, the infarct volumes were significantly reduced

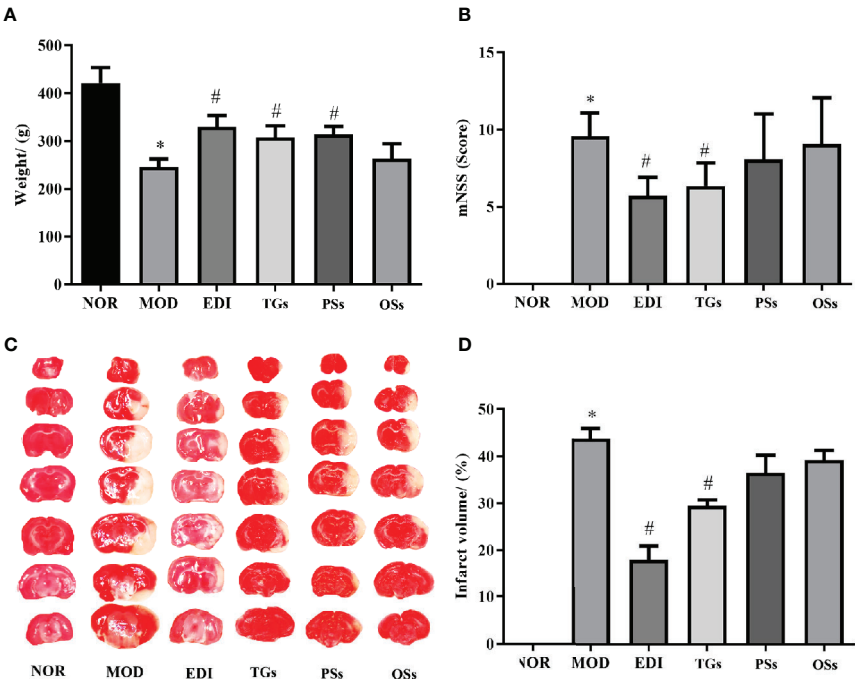


FIGURE 2 | TGs reduce the brain damage induced by transient focal cerebral ischemia. **(A)** TGs increase weight in the MCAO/R rats. **(B)** TGs decrease neurological deficit scores at 14 d post-MCAO/R. **(C, D)** Representative photographs of TTC-stained coronal brain sections show viable (red) and dead (white) tissues; TTC staining shows that the cerebral infarction areas in the TGs group are significantly smaller than those in the model group. $^{*}P < 0.05$ vs NOR. $^{\#}P < 0.05$ vs MOD.

(**Figures 2C, D**). The PSs and OSs treatment showed no obvious effect on the above indexes. The above data showed that TGs could markedly alleviate the I/R-induced cerebral injury, but PSs and OSs could not.

TGs Ameliorate Histopathological Damage in MCAO/R Rats

In order to determine some of the effects of TGs, PSs, and OSs treatment on histopathological damages, H&E staining was done to reveal pathological damage. The histomorphological structures of brains in the NOR group were arranged regularly. The morphology changes in the TGs groups were slighter than those in the MOD group. However, the PSs and OSs treatment groups showed no significant amelioration of the morphology changes (**Figure 3**).

TGs Attenuate Neuronal Injury After I/R-Induced Rats

Nissl staining showed the histopathological changes of neurons in the penumbra of ischemic area. As shown in **Figure 4**, the normal neurons had a clear nucleolus and intact structure. In the MOD group, the neurons had enlarged intercellular spaces. The nissl bodies were disappeared, shrunken and deep stained. However, these changes were rarely observed in the EDI, TGs, and PSs groups. These results illustrated that TGs and PSs could significantly attenuate ischemia/reperfusion-induced neuronal injury.

TGs Attenuate BBB Disruption After I/R-Treated Rats

Evans blue assay is a classical method for researching the change of BBB permeability. The experiment results showed that increased Evans blue was observed in the MOD group, while there was significantly decreased Evans blue in the TGs and EDI treated rats. Moreover, there was no significant difference between PSs and OSs therapy groups (**Figure 5**). These results suggested that TGs could significantly attenuate BBB disruption.

TGs Promote Angiogenesis in I/R Injured Rats

More recent studies show that angiogenesis plays a critical role in neurological functional recovery and prognostic outcome after acute ischemic stroke (Yuen et al., 2015). To evaluate effects of TGs, PSs, and OSs on angiogenesis, the CD31 and α-SMA were used to quantify the capillary numbers. Immunofluorescence staining showed that the MOD group caused a remarkable decrease in the expressions of CD31 (**Figures 6A, B**) and α-SMA (**Figures 6C, D**) in the penumbra of ischemic areas of I/R rats, in comparison with the normal rats. This result illustrated that I/R could cause the vascular damage in the cortex penumbra of ischemic hemispheres. However, the TGs and EDI treatment remarkably increased capillary density, angiogenesis, and arteriogenesis as indicated by increased expressions of CD31 and α-SMA. These results suggest that TGs could promote

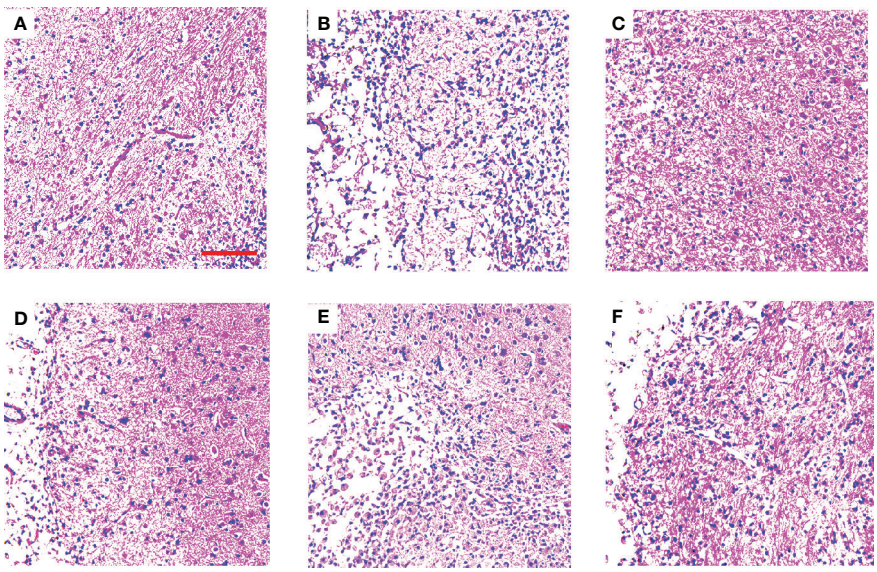


FIGURE 3 | TGs ameliorate histopathological damage in MCAO/R rats. HE staining of coronal sections in the penumbra of ischemic areas of NOR, MOD, EDI, TGs, PSs, and OSs groups at 14 d after I/R. The cell morphology in the MOD group is shrinkage, nuclear pyknosis, and vacuolization, while the cells in the TGs group are relatively normal and show less damage, compared with those in the MOD group. **(A–F)** are NOR, MOD, EDI, TGs, PSs, and OSs groups, respectively. Scale bar = 100 μm.

angiogenesis in the ischemic penumbra of I/R rats, but the PSs and OSs could not.

TGs Increase Expression of Tight Junction Proteins in I/R Injured Rats

BBB disruption can elevate brain water content and tissue swelling, leading to brain injury. Tight junction proteins are important structural components of the BBB (Tenreiro et al., 2016; Jiang et al., 2018). To test whether TGs, PSs, and OSs treatment after stroke might influence BBB integrity, the expressions of ZO-1, claudin-5, and occludin were performed by immunofluorescence analysis. The results indicated that the expressions of claudin-5, occludin, and ZO-1 were visibly decreased in the MOD group. However, they were substantially increased after 14 days of TGs administration. PSs and OSs groups showed no significant changes in these protein expressions (**Figure 7**). These data indicated that the TGs can regulate tight junction protein expressions and probably maintain BBB integrity after I/R injury.

TGs Increase Pericyte Coverage on Capillaries in I/R Injured Rats

Pericyte coverage on capillaries plays a critical role in maintaining BBB integrity (Armulik et al., 2010; Daneman et al., 2010). Thus, we tested whether pericyte coverage could be increased by TGs, PSs, and OSs treatment. Immunofluorescence intensity analysis results showed that both PDGFRβ and CD31 expressions were dramatically decreased in the MOD group. Administration of TGs to the I/R rats significantly recovered or even increased the expression intensities of the PDGFRβ and CD31, but no difference was observed in the PSs and OSs treatment groups (**Figure 8**). Thus, treatment of TGs could significantly increase pericyte coverage. These findings further confirmed that TGs can maintain the integrity of BBB after I/R.

TGs Promote Neural Remodeling in I/R Injured Rats

According to numerous studies, neurogenesis after a stroke can significantly improve functional recovery (Grefkes and Ward, 2014; Zhang et al., 2019). Synaptophysin (SYN), postsynaptic density 95 (PSD-95) proteins and microtubule-associated protein 2 (MAP-2) were used as markers to examine neuronal plasticity in the ischemic penumbra of the cortex. In order to assess the effects of TGs, PSs, and OSs treatment on neurogenesis in I/R injured rats, the immunofluorescence and western blot for SYN, PSD95 and MAP-2 expressions were performed. As shown in **Figures 9** and **10**, the SYN, PSD95 and MAP-2 expression levels in I/R rats after 14 days reperfusion decreased in comparison with the NOR rats, while the TGs and PSs cure could significantly up-regulate their expression levels. The OSs group had no significant change compared with the MOD group. The data indicated that the TGs and PSs cure was able to dramatically promote neural remodeling after I/R injury.

TGs Alter Nrf-2 and Keap-1 Expressions in I/R Injured Rats

Oxidative stress is a main pathogenic mechanism in I/R injury (Ya et al., 2018; Yu et al., 2018). The studies verified that Nrf-2 is a master regulator of antioxidative responses (Thompson et al., 2015). To investigate Nrf-2 and Keap-1 mediated oxidative responses after I/R injury, we evaluated the cytoplasmic

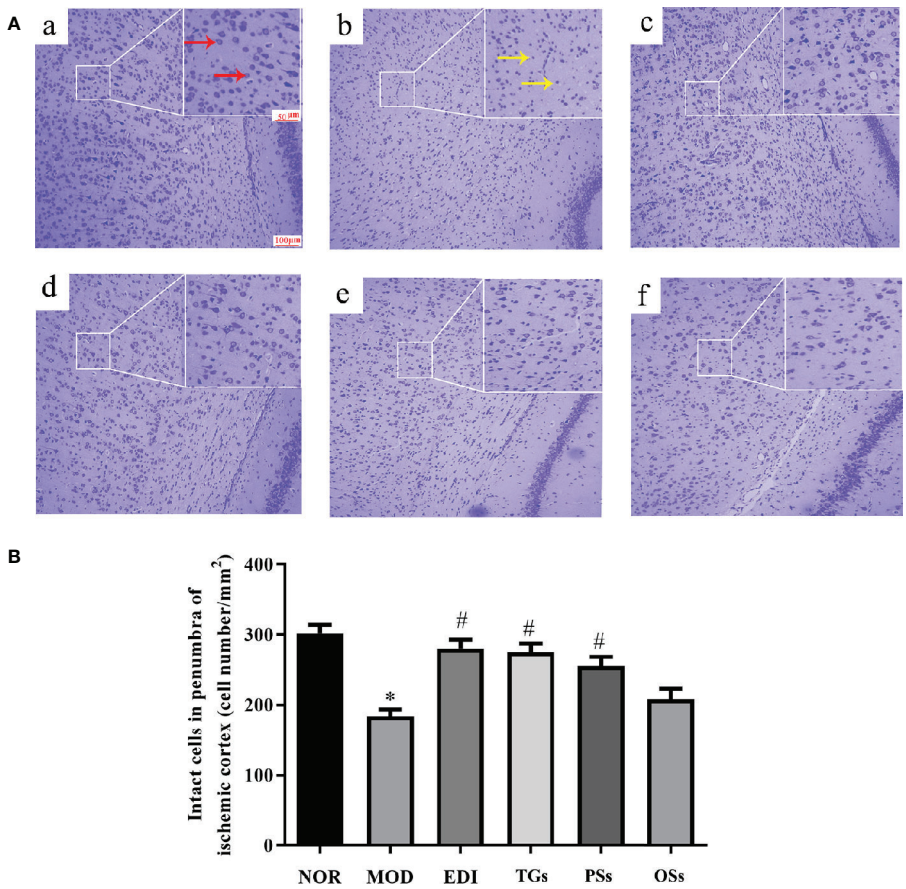


FIGURE 4 | TGs attenuate neuronal injury after I/R-treated rats. **(A)** Nissl staining in the penumbra of ischemic area of I/R rats. Normal neurons have normal morphology with clear nucleolus, abundant cytoplasm, and intact structure (red arrow). Abnormal neurons are shrunken and deep stained (yellow arrow), while a greater increase of intact cells is evident in the TGs group compared with the MOD group. a–f are NOR, MOD, EDI, TGs, PSs and OSs groups, respectively. **(B)** Quantitative analysis of intact cells in penumbra of ischemic area at 14 days after treatment. $^{*}P < 0.05$ vs NOR, $^{\#}P < 0.05$ vs MOD.

expression as well as nuclear translocation of Keap-1. Meanwhile, the expression of Nrf-2 in I/R injured rats brain tissues was also assayed (**Figures 10** and **11**). According to the immunofluorescence analysis, Nrf-2 was found to be mainly located at the cytoplasm in the NOR group. In the TGs group, the expression of Nrf-2 in cytoplasmic localization was downregulated, but upregulated in the nucleus, and a decreased Keap-1 expression was also observed. The data showed that the brain protection of TGs could be associated with the modulation of Nrf-2 and Keap-1.

TGs Attenuate Brain Tissue Oxidative Stress in I/R Injured Rats

In order to confirm the antioxidative effects of TGs, the activities of SOD, CAT, GSH-Px and MDA were evaluated in I/R injured rats. In **Figure 12**, the content of MDA was markedly increased in the MOD group, and at the same time the activities of SOD, CAT, and GSH-Px were decreased, compared to the normal rats. Conversely, TGs treatment led to a significant decrease in the content of MDA and increase in the activities of SOD, CAT and GSH-Px. These results further confirmed the antioxidation activity of TGs.

DISCUSSION

Many studies suggest that the TCM *C. deserticola* has extensive biological activities, e.g. enhancing the ability to learn, memory, and immunity (Dong et al., 2007; Jiang and Tu, 2009; Wang et al., 2017; Xia et al., 2018). However, the active components of *C. deserticola* for neuroprotection remain unclear. The current work aims to screen the active components from *C. deserticola* against ischemic stroke on the MCAO/R model. Three extracts from *C. deserticola* (TGs, PSs, and OSs) were used to evaluate their effects on MCAO/R rats, as well as possible mechanisms.

Stroke is a common acute cerebrovascular disease. Epidemiological studies show that stroke is more common in men than in women (Sealy-Jefferson et al., 2012; Guzik and

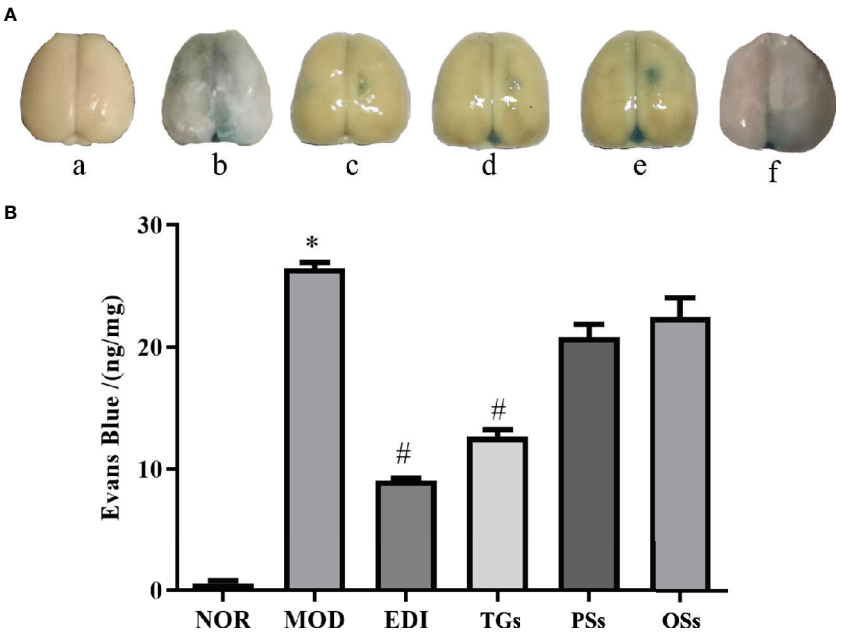


FIGURE 5 | TGs attenuate BBB disruption after I/R injury. **(A)** Representative pictures of Evans blue extravasation. a–f are NOR, MOD, EDI, TGs, PSs, and OSs groups, respectively. **(B)** Quantitative analysis of Evans blue extravasation from brain extracts at 14 days after treatment. $^{*}P < 0.05$ vs NOR, $^{\#}P < 0.05$ vs MOD.

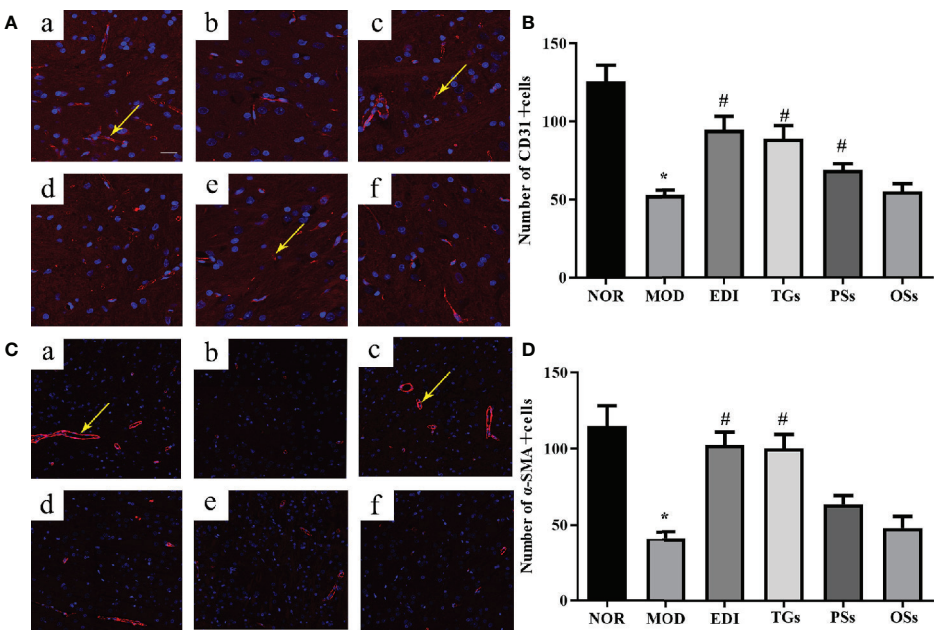


FIGURE 6 | TGs promote neovascularization in rats with cerebral I/R. Representative images obtained from the cortex penumbra of ischemic hemispheres. **(A, C)** Representative immunofluorescence images of CD31 and α-SMA in the I/R rats after treatment with TGs, PSs and OSs for 14 days, respectively. a–f are NOR, MOD, EDI, TGs, PSs, and OSs groups, respectively. **(B, D)** The bar graphs show the analysis of positive immunostaining of CD31 and α-SAM in the I/R rats at 14 days after treatment. $^{*}P < 0.05$ vs NOR, $^{\#}P < 0.05$ vs MOD. Scale bar in all panels = 100 μm.

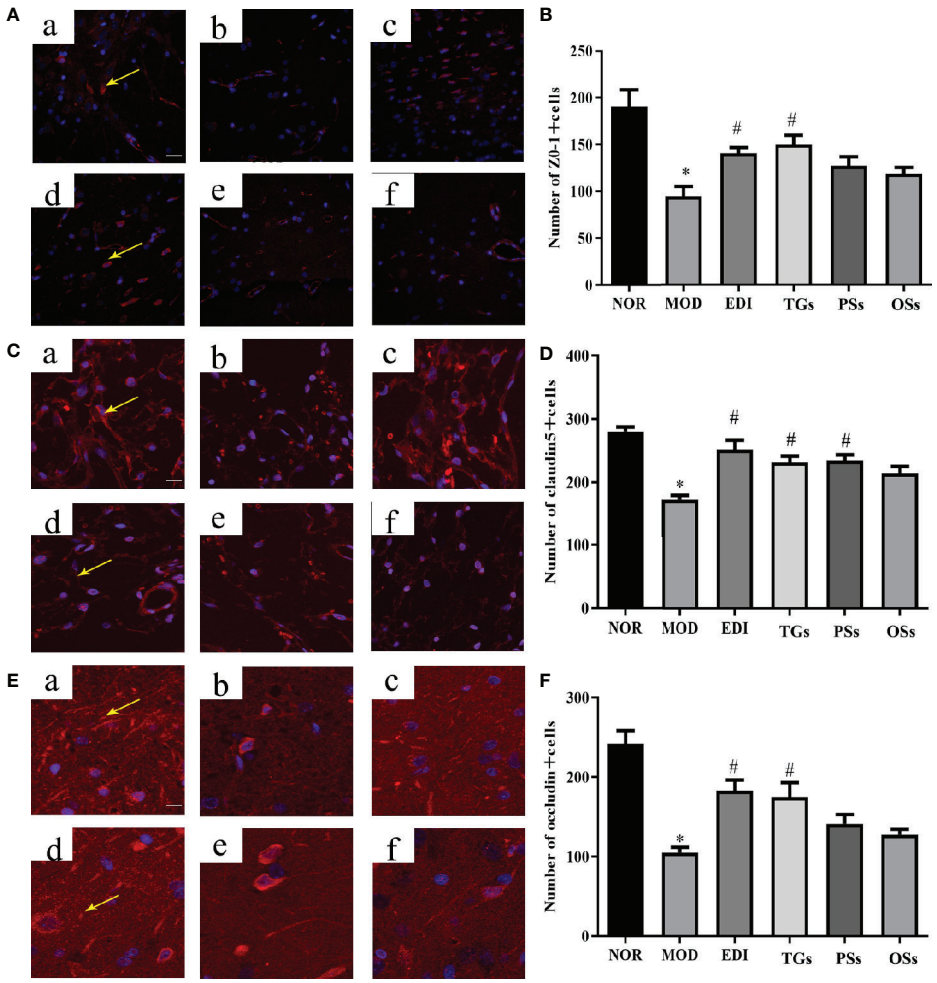


FIGURE 7 | TGs increase expression of tight junction proteins in MCAO/R rats. Representative images obtained from the cortex penumbra of ischemic hemispheres. **(A, C, E)** Protein expression levels of ZO-1, claudin5, and occludin were measured by immunofluorescence, respectively. **(B, D, F)** Statistical analysis of the numbers of ZO-1, claudin5, and occludin positive cells, respectively. a–f are NOR, MOD, EDI, TGs, PSs and OSs groups, respectively. $^{*}P < 0.05$ vs NOR, $^{\#}P < 0.05$ vs MOD. Scale bar = 50 μm.

Bushnell, 2017). Thus, in our experiment, male rats were adopted for the tests. Our results proved that I/R induction accelerated oxidative stress and infarct volume, breaking the BBB and leading to nerve and cerebrovascular injury. After screening, TGs were found to decrease infarct volume and promote neural remodeling and angiogenesis. Moreover, TGs were observed to maintain BBB integrity after I/R injury. On the contrary, PSs and OSs bring no significant alleviation to I/R injury. Thus, TGs are considered the major active fraction of *C. deserticola* for neuroprotection, potentially through promoting neural remodeling, angiogenesis and BBB integrity *via* activating Nrf-2/Keap-1 pathway.

Mounting evidence indicates that establishment of effective collateral circulation is significantly important for avoiding the formation of infarction and ischemic penumbra, and is a critical treatment at an early stage of ischemic stroke (ElAli, 2016; Iwasawa et al., 2016). The proliferation of vascular endothelial cells and smooth muscle cells after ischemic infarction determines the establishment of collateral circulation. However, the ischemia models have a common phenomenon—that is, oxidative stress widely existed in the brain microvasculature. Study data have displayed that a large number of antioxidants can disturb the function of the BBB and the properties of angiogenesis (Mentor and Fisher, 2017). CD31 and α-SMA are the markers of vascular endothelial cells as well as smooth muscle cells, respectively (Saboor et al., 2016). To investigate the effect on the above-mentioned cell proliferation of the extracts from *C. deserticola*, we examined the expressions of CD31 and α-SMA in the cerebral ischemic penumbra homogenate. Our data showed that TGs strikingly enhanced the expressions of CD31 and α-SMA. However, there was no significant differences for

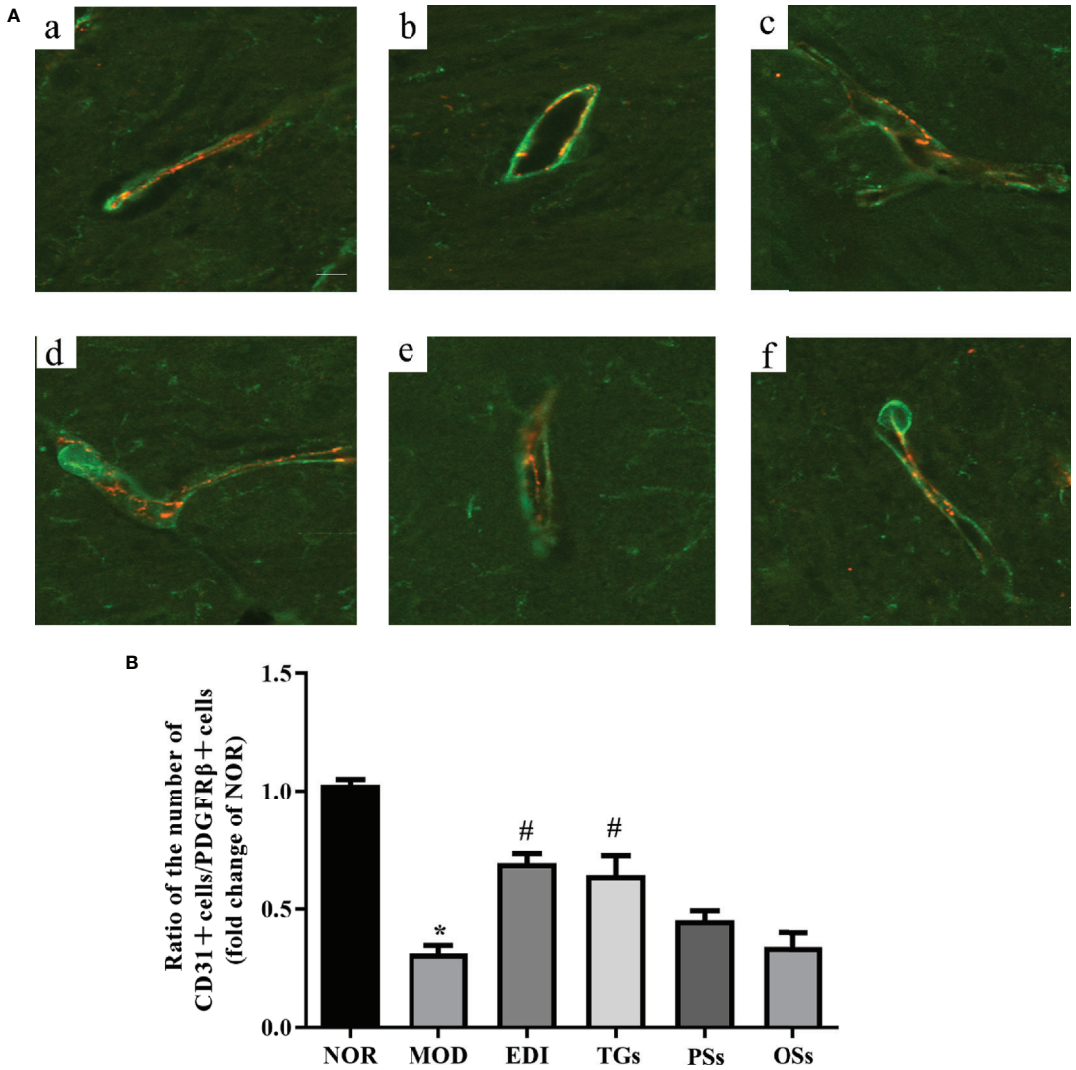


FIGURE 8 | TGs increases pericyte coverage on capillaries in I/R injury rats. Representative images obtained from the ischemic penumbra of cortex. **(A)** Representative immunofluorescence images of PDGFRβ (green) and CD31 (red) staining in the MCAO/R rats at 14 days after TGs, PSs and OSs treatment. a–f are NOR, MOD, EDI, TGs, PSs and OSs groups, respectively. **(B)** Ratio of CD31-positive cell numbers to the PDGFRβ-positive cell numbers in each tissue. $^{*}P < 0.05$ vs NOR, $^{\#}P < 0.05$ vs MOD. Scale bar in all panels = 20 μm.

PSs and OSs groups. Therefore, we deduced that TGs may reduce brain damage by promoting angiogenesis *via* increasing the expressions of CD31 and α-SMA, whereas PSs and OSs provided no such protection from brain damage. These results further confirmed that only TGs could prevent cerebral I/R injury.

Ischemic stroke can be thought as the result of cerebral ischemia caused by impairment in the neuronal plasticity or remodeling of brain areas. The majority of stroke patients suffer neurological deficits. Activating neurogenesis is a promising strategy for stroke patients to improve their neurological functions (Cramer and Chopp, 2000). Neurogenesis directly participates in neurological function recovery after brain I/R injury (Zhang et al., 2019). Previous research shows that TGs can improve the survival rate of hippocampal pyramidal cells and induce neurogenesis (Lian et al., 2017). Oxidative stress causes the loss of neurons during lots of diseases, such as Parkinson, stroke, and so on (Duan and Si, 2019; Singh et al., 2019). Nrf-2 transcribes lots of genes related to neuro-protection in their promoter region, mainly including SOD, MDA, CAT, and γ-glutamyl cysteine ligases, etc (Satoh et al., 2006). SYN, PSD-95, and MAP-2 proteins, which are associated closely with synaptic formation and neurotransmission, can be considered as markers of research neuronal plasticity in the ischemic penumbra region. After studying, we found that the cure with TGs could significantly increase the expressions of PSD95, SYN, and

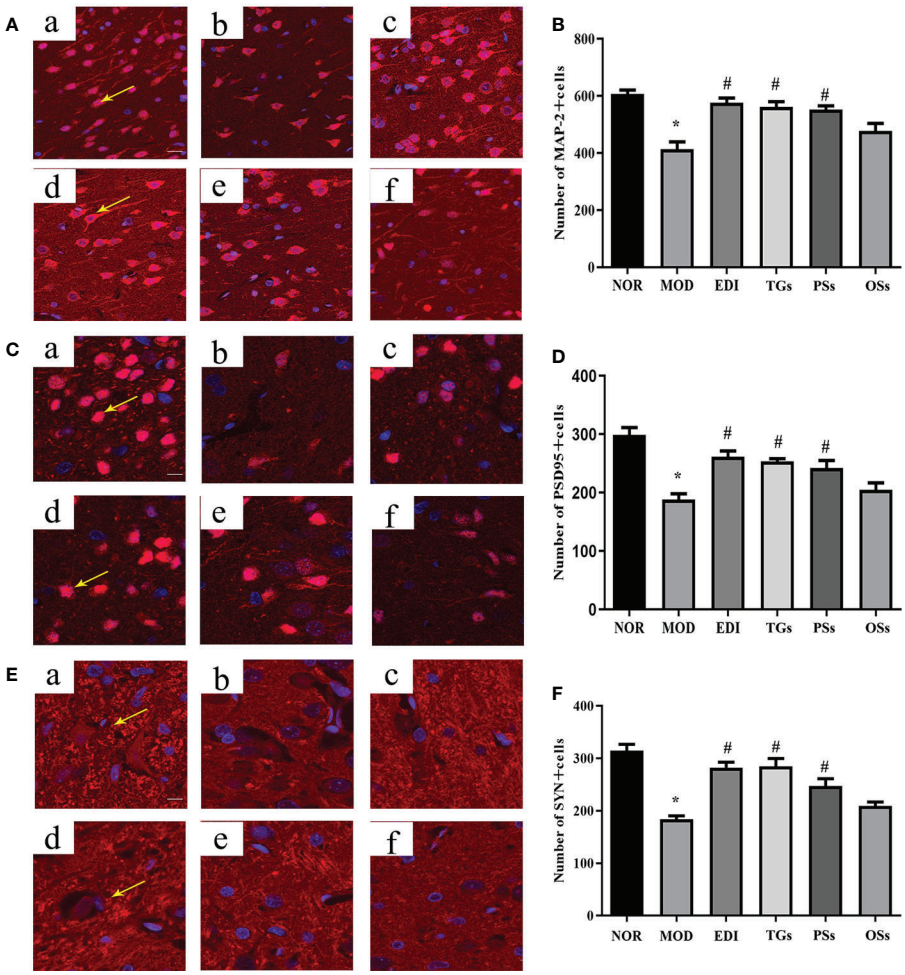


FIGURE 9 | TGs promote neural remodeling in I/R injury rats. Representative images obtained from the cortex penumbra of ischemic hemispheres. **(A, C, E)** Representative immunofluorescence images of MAP-2, PSD95 and SYN in the MCAO/R rats at 14 days after TGs, PSs and OSs treatment. **(B, D, F)** Statistical analysis of the numbers of MAP-2, PSD95 and SYN positive cells, respectively. a–f are NOR, MOD, EDI, TGs, PSs and OSs groups, respectively. $^{*}P < 0.05$ vs NOR, $^{\#}P < 0.05$ vs MOD. Scale bar in all panels = 50 μm.

MAP-2, indicating that the cerebral protection of TGs was correlated with the enhanced neuronal plasticity during I/R. However, it's a pity that there is no obvious difference for PSs as well as OSs groups. These results indicated that TGs could enhance neuroplasticity after cerebral I/R injury.

Imaging research into stroke patients showed that BBB dysfunction can be thought as a striking attribute of the peri-ischemic brain (Bang et al., 2007). The TJs, which are composed of cytoplasmic proteins, transmembrane proteins, and junction adhesion molecules between capillary endothelial cells, are very important in maintaining BBB integrity (Ye et al., 2019). Among them, ZO-1, claudin-5, and occludin are the most important proteins in TJs. Mounting evidence indicates that the increased permeability of BBB induced by ischemia generally correlates with the alterations of ZO-1, claudin-5, and occludin (Cao et al., 2016a; Page et al., 2016; Yu et al., 2017; Liu et al., 2018). In this work, the results demonstrated that although TGs could significantly increase the expressions of ZO-1, claudin-5, and occludin proteins in MCAO-induced brain tissues, neither PSs nor OSs did. The BBB consists of cerebral endothelial cells and is closely associated with pericytes (Nyul-Toth et al., 2016). Pericytes are vital to BBB integrity (Bell et al., 2010). Ischemic stroke triggers pericytes death and detachment from brain endothelial cells in the acute phase, thus destabilizing the microvasculature and altering BBB properties (Zechariah et al., 2013). Our data showed that TGs could increase pericyte coverage on capillaries and increase the expression levels of ZO-1, claudin-5 and occludin. These phenomena proved that TGs could effectively protect BBB integrity after cerebral I/R injury. In summary, TGs may attenuate cerebral

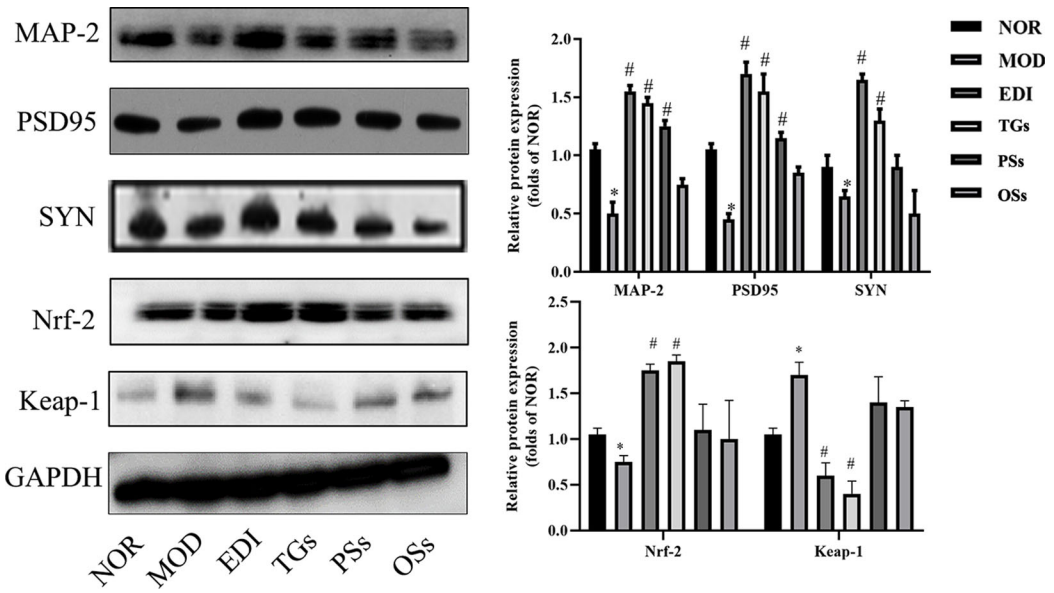


FIGURE 10 | TGs promote the expressions of MAP-2, PSD95, SYN and Nrf-2 and reduce the expression of Keap-1 in I/R-treated rats. *$P < 0.05$ vs NOR, #$P < 0.05$ vs MOD.

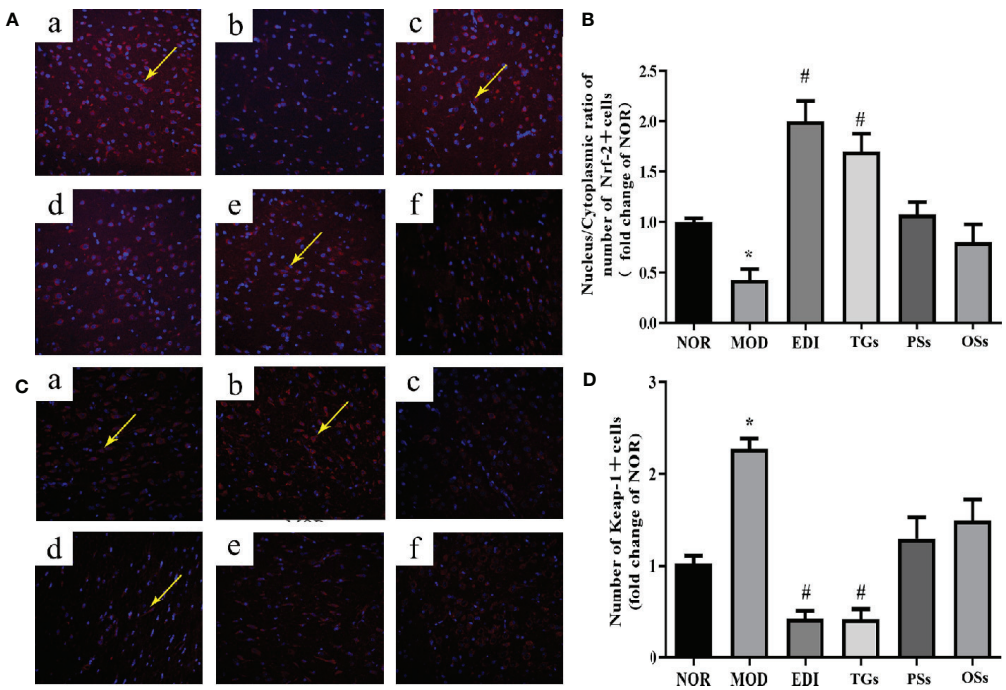


FIGURE 11 | TGs significantly decrease the expression of Keap-1 and facilitate the nuclear translocation of Nrf-2. Representative images obtained from the cortex penumbraof ischemic hemispheres. **(A)** Keap-1 dependent Nrf-2 nuclear translocation was observed in I/R rats brain tissue. **(C)** Keap1 degradation after TGs treatment to I/R rats braintissue. The analysis was carried out using immunofluorescence staining. af are NOR, MOD, EDI, TGs, PSs and OSs groups, respectively. **(B**, **D)** Bar graphs show aquantification of the nucleus/cytoplasmic ratio of Nrf-2 and the expression of Keap-1. *$P < 0.05$ vs NOR, #$P < 0.05$ vs MOD. Scale bar = 100 mm.

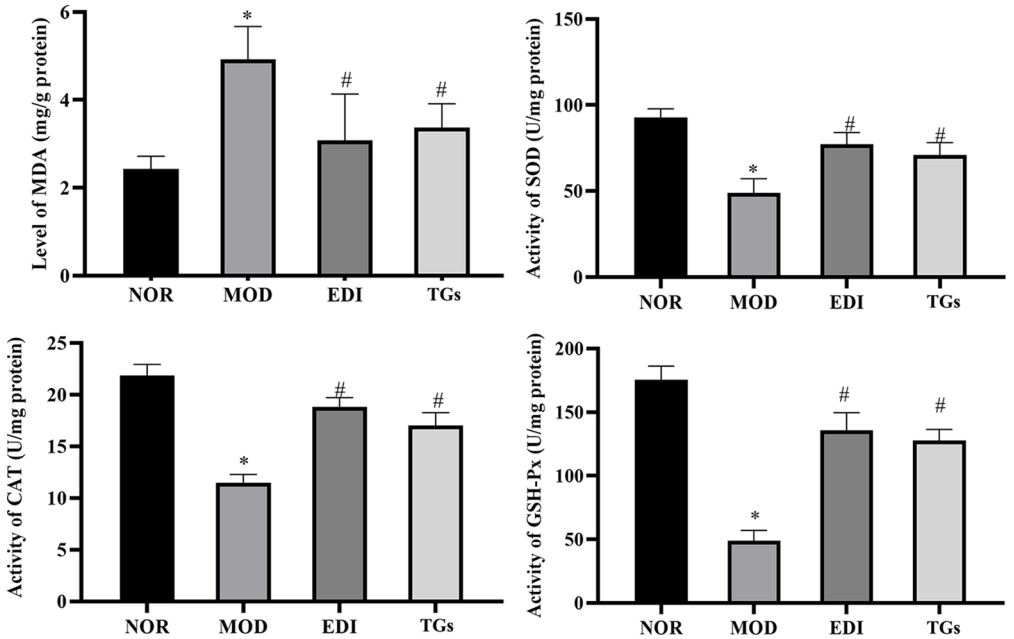


FIGURE 12 | TGs elevate the levels of SOD, CAT and GSH-Px and reduces the level of MDA in I/R-treated rats. The content of MDA increases in the brain tissue after I/Rinjury, along with the activities of SOD, CAT, and GSH-Px decrease. TGs treatment reverses these injury-induced changes. $^{*}P < 0.05$ vs NOR, $^{\#}P < 0.05$ vs MOD.

injury in multiple ways, such as promoting angiogenesis, improving neuronal plasticity, and maintaining the integrity of the BBB.

We then investigated the signaling pathway to explore the mechanism underlying the TGs brain protection. The process of I/R injury is multifactorial, and thus numerous mechanisms are involved in the pathogenesis. Oxidative stress is a fundamental risk factor contributing to I/R-induced brain injury (Suda et al., 2013), such as BBB structure damage, vascular endothelial dysfunction, and aggravation of ischemic neuronal injury (Xiong et al., 2015; Caglayan et al., 2019; Priestley et al., 2019). Thus, oxidative stress has become an attractive therapeutic target in I/R-induced brain injury. Phase 2 enzymes, which are mediated by nuclear factor E2-related factor-2 (Nrf-2), have been considered as an important means by which neurons protect themselves against oxidative stress (Suzuki and Yamamoto, 2015; Ya et al., 2018). Mounting evidences indicate that activation of Nrf-2 during I/R is a potential therapeutic target for neuroprotection (Ding et al., 2015; Zhang R. et al., 2017). Nrf-2, as an important regulator of endogenous antioxidant defense, mediates the level of heme oxygenase 1 (HO-1) and other antioxidant enzymes, such as NAD(P)H quinone oxidoreductase 1 (NQO1), SOD, CAT, GSH, and MDA (Siow et al., 2007; Ding et al., 2014). Moreover, Nrf-2 plays an important regulator role in angiogenesis. The present study shows that Nrf-2 can be significantly enhanced and activated in the process of vascular development (Wei et al., 2013).

As previously described (Jiang and Tu, 2009), TGs contain lots of bioactive compounds, for example echinacoside, tubuloside A, acteoside, isoacteoside and 2'-acetylacteoside, and some of them showed neuroprotective functions after cerebral I/R injury (Peng et al., 2016). Echinacoside has lots of pharmacological effects, such as antioxidation, anti-senescence, neuroprotection, anti-inflammation, promotion of cicatrization, hepatoprotection, promotion of bone formation and anti-tumor activities (Yu et al., 2016; Li et al., 2018; Zhang Y. et al., 2018; Ji et al., 2019; Xu et al., 2019). Recently, echinacoside has been identified as a potent antioxidant in the central nervous system (Lu et al., 2016). Echinacoside can cut down MDA content and improve the activities of SOD and GSH-Px in ischemia brain injury, and molecular docking analysis displayed that echinacoside may bind to Keap-1, leading to the Nrf-2 nuclear translocation (Li et al., 2018). The study of Xia showed that acteoside could decrease the infarct volume and brain water content to improve neurological deficits in MCAO/R rats through mitigating oxidative stress (Xia et al., 2018). Other studies have demonstrated that isoacteoside could increase the activities of cellular antioxidant enzymes, SOD and CAT in H_2O_2-treated V79-4 cells (Chae et al., 2005). Based on the above reports of the active compounds contained in TGs, it is possible to deduce that TGs could protect against ischemic stroke *via* the antioxidation pathways.

Li reported on the neuroprotective effects of phenylethanoid glycosides (PhGs) on H_2O_2-induced apoptosis on PC12 cells *via* the Nrf2/ARE pathway (Li et al., 2018). These PhGs significantly suppressed by triggering Nrf2 nuclear translocation and increasing expressions of HO-1, NQO1, glutamate cysteine ligase-catalytic subunit (GCLC), and glutamate-cysteine ligase modifier subunit (GCLM) (Li et al., 2018; Gong et al., 2019). Therefore, these findings suggest that the Nrf-2/ARE pathway plays a crucial role in

PhGs-mediated protective effects on neuronal cells. Similarly, in this study, we found that TGs could decrease the level of MDA and increase the levels of SOD, CAT, and GSH-Px in the I/R rats. Meanwhile, TGs could upregulate the Nrf2 expression in the nucleus, downregulate the corresponding expression in the cytoplasm, and significantly decrease the Keap-1 expression. Therefore, the Nrf-2/Keap-1 pathway may be involved in TGs-mediated neuroprotective effects. Further validation of this pathway would be performed *in vitro* cell culture with oxygen-glucose deprivation/reoxygenation injury models in the future. Moreover, *C. deserticola* extracts were administrated in our study for 14 days continuously. Since adult neurogenesis would affect the interpretation of neuroprotective effects during 14 days reperfusion, neurogenesis cannot be excluded in our current experiment design in exploring the neuroprotective effect of CTs. This is the limitation of our research.

In conclusion, it is the TGs from *C. deserticola* that can enhance angiogenesis and neurogenesis as well as maintain the integrity of the BBB in I/R injury rats, but not the PSs and OSs. The effects could be mediated by the activation of the Nrf-2/Keap-1 pathway.

DATA AVAILABILITY STATEMENT

The raw data supporting the conclusions of this article will be made available by the authors, without undue reservation, to any qualified researcher.

ETHICS STATEMENT

This work was carried out according to the Guidelines for Animal Experiments of Peking University. The study protocols were approved by the Institutional Animal Care and Use Committee at the Peking University Health Science Center (LA2019123).

AUTHOR CONTRIBUTIONS

YJ, KZ, and PT designed the research. FW performed the research. FW and RL analyzed the data. FW, RL, and JC wrote the manuscript and HPLC analysis. JC, KZ, YJ, and PT revised the manuscript.

FUNDING

This study was supported by the National Key Research and Development Project (2017YFC1702400, 2019YFC1711000), the National Natural Science Foundation of China (81773932), and the National Key Technology R&D Program "New Drug Innovation" of China (2018ZX09711001-008-003).

REFERENCES

Alluri, H., Anasooya Shaji, C., Davis, M. L., and Tharakan, B. (2015). Oxygen-glucose deprivation and reoxygenation as an in vitro ischemia-reperfusion injury model for studying blood-brain barrier dysfunction. *J. Vis. Exp.* 99, e52699. doi: 10.3791/52699

Armulik, A., Genove, G., Mae, M., Nisancioglu, M. H., Wallgard, E., Niaudet, C., et al. (2010). Pericytes regulate the blood-brain barrier. *Nature* 468 (7323), 557–561. doi: 10.1038/nature09522

Bang, O. Y., Buck, B. H., Saver, J. L., Alger, J. R., Yoon, S. R., Starkman, S., et al. (2007). Prediction of hemorrhagic transformation after recanalization therapy using T2*-permeability magnetic resonance imaging. *Ann. Neurol.* 62 (2), 170–176. doi: 10.1002/ana.21174

Bell, R. D., Winkler, E. A., Sagare, A. P., Singh, I., LaRue, B., Deane, R., et al. (2010). Pericytes control key neurovascular functions and neuronal phenotype in the adult brain and during brain aging. *Neuron* 68 (3), 409–427. doi: 10.1016/j.neuron.2010.09.043

Caglayan, B., Kilic, E., Dalay, A., Altunay, S., Tuzcu, M., Erten, F., et al. (2019). Allyl isothiocyanate attenuates oxidative stress and inflammation by modulating Nrf2/HO-1 and NF-kappaB pathways in traumatic brain injury in mice. *Mol. Biol. Rep.* 46 (1), 241–250. doi: 10.1007/s11033-018-4465-4

Cao, G., Jiang, N., Hu, Y., Zhang, Y., Wang, G., Yin, M., et al. (2016a). Ruscogenin attenuates cerebral ischemia-induced blood-brain barrier dysfunction by suppressing TXNIP/NLRP3 inflammasome activation and the MAPK pathway. *Int. J. Mol. Sci.* 17 (9), 1–17. doi: 10.3390/ijms17091418

Cao, G., Ye, X., Xu, Y., Yin, M., Chen, H., Kou, J., et al. (2016b). YiQiFuMai powder injection ameliorates blood-brain barrier dysfunction and brain edema after focal cerebral ischemia-reperfusion injury in mice. *Drug Des. Dev. Ther.* 10, 315–325. doi: 10.2147/dddt.S96818

Chae, S., Kim, J. S., Kang, K. A., Bu, H. D., Lee, Y., Seo, Y. R., et al. (2005). Antioxidant activity of isoacteoside from *Clerodendron trichotomum*. *J. Toxicol. Environ. Health A* 68 (5), 389–400. doi: 10.1080/15287390590900750

Cheon, S. Y., Cho, K. J., Kim, S. Y., Kam, E. H., Lee, J. E., and Koo, B. N. (2016). Blockade of apoptosis signal-regulating kinase 1 attenuates matrix metalloproteinase 9 activity in brain endothelial cells and the subsequent apoptosis in neurons after ischemic injury. *Front. Cell Neurosci.* 10, 213. doi: 10.3389/fncel.2016.00213

Chi, H., Chang, H. Y., and Sang, T. K. (2018). Neuronal cell death mechanisms in major neurodegenerative diseases. *Int. J. Mol. Sci.* 19 (10), 1–18. doi: 10.3390/ijms19103082

Crack, P. J., Taylor, J. M., Flentjar, N. J., de Haan, J., Hertzog, P., Iannello, R. C., et al. (2001). Increased infarct size and exacerbated apoptosis in the glutathione peroxidase-1 (Gpx-1) knockout mouse brain in response to ischemia/reperfusion injury. *J. Neurochem.* 78 (6), 1389–1399. doi: 10.1046/j.1471-4159.2001.00535.x

Crack, P. J., Taylor, J. M., Ali, U., Mansell, A., and Hertzog, P. J. (2006). Potential contribution of NF-kappaB in neuronal cell death in the glutathione peroxidase-1 knockout mouse in response to ischemia-reperfusion injury. *Stroke* 37 (6), 1533–1538. doi: 10.1161/01.Str.0000221708.17159.64

Cramer, S. C., and Chopp, M. (2000). Recovery recapitulates ontogeny. *Trends Neurosci.* 23 (6), 265–271. doi: 10.1016/s0166-2236(00)01562-9

Daneman, R., Zhou, L., Kebede, A. A., and Barres, B. A. (2010). Pericytes are required for blood-brain barrier integrity during embryogenesis. *Nature* 468 (7323), 562–566. doi: 10.1038/nature09513

Ding, Y., Chen, M., Wang, M., Wang, M., Zhang, T., Park, J., et al. (2014). Neuroprotection by acetyl-11-keto-beta-Boswellic acid, in ischemic brain injury involves the Nrf2/HO-1 defense pathway. *Sci. Rep.* 4, 7002. doi: 10.1038/srep07002

Ding, Y., Chen, M., Wang, M., Li, Y., and Wen, A. (2015). Posttreatment with 11-keto-beta-boswellic acid ameliorates cerebral ischemia-reperfusion injury: Nrf2/HO-1 pathway as a potential mechanism. *Mol. Neurobiol.* 52 (3), 1430–1439. doi: 10.1007/s12035-014-8929-9

Dong, Q., Yao, J., Fang, J. N., and Ding, K. (2007). Structural characterization and immunological activity of two cold-water extractable polysaccharides from

Cistanche deserticola Y. C. Ma. *Carbohydr. Res.* 342 (10), 1343–1349. doi: 10.1016/j.carres.2007.03.017

Donnan, G. A., Fisher, M., Macleod, M., and Davis, S. M. (2008). Stroke. *Lancet* 371 (9624), 1612–1623. doi: 10.1016/s0140-6736(08)60694-7

Duan, Q., and Si, E. (2019). MicroRNA-25 aggravates Abeta1-42-induced hippocampal neuron injury in Alzheimer's disease by downregulating KLF2 via the Nrf2 signaling pathway in a mouse model. *J. Cell Biochem.* 120 (9), 15891–15905. doi: 10.1002/jcb.28861

ElAli, A. (2016). The implication of neurovascular unit signaling in controlling the subtle balance between injury and repair following ischemic stroke. *Neural Regener. Res.* 11 (6), 914–915. doi: 10.4103/1673-5374.184485

Gaire, B. P. (2018). Herbal medicine in ischemic stroke: challenges and prospective. *Chin. J. Integr. Med.* 24 (4), 243–246. doi: 10.1007/s11655-018-2828-2

Gao, Y., Jiang, Y., Dai, F., Han, Z., Liu, H., Bao, Z., et al. (2015). Study on laxative constituents in *Cistanche deserticola* Y. C. Ma. *Mod. Chin. Med.* 17 (04), 19–22 +26. doi: 10.13313/j.issn.1673-4890.2015.4.003

Gong, X., Xu, Y., Ren, K., Bai, X., Zhang, C., and Li, M. (2019). Phenylethanoid glycosides from *Paraboea martinii* protect rat pheochromocytoma (PC12) cells from hydrogen peroxide-induced cell injury. *Biosci. Biotechnol. Biochem.* 83 (12), 2202–2212. doi: 10.1080/09168451.2019.1654359

Grefkes, C., and Ward, N. S. (2014). Cortical reorganization after stroke: how much and how functional? *Neuroscientist* 20 (1), 56–70. doi: 10.1177/1073858413491147

Guzik, A., and Bushnell, C. (2017). Stroke epidemiology and risk factor management. *Continuum (Minneap Minn)* 23 (1, Cerebrovascular Dis), 15–39. doi: 10.1212/con.0000000000000416

Hu, S., Wu, Y., Zhao, B., Hu, H., Zhu, B., Sun, Z., et al. (2018). *Panax notoginseng* Saponins protect cerebral microvascular endothelial cells against oxygen-glucose deprivation/reperfusion-induced barrier dysfunction via activation of PI3K/Akt/Nrf2 antioxidant signaling pathway. *Molecules* 23 (11), 1–17. doi: 10.3390/molecules23112781

Iwasawa, E., Ichijo, M., Ishibashi, S., and Yokota, T. (2016). Acute development of collateral circulation and therapeutic prospects in ischemic stroke. *Neural Regener. Res.* 11 (3), 368–371. doi: 10.4103/1673-5374.179033

Ji, S., Li, S., Zhao, X., Kang, N., Cao, K., Zhu, Y., et al. (2019). Protective role of phenylethanoid glycosides, Torenoside B and Savatiside A, in Alzheimer's disease. *Exp. Ther. Med.* 17 (5), 3755–3767. doi: 10.3892/etm.2019.7355

Jiang, Y., and Tu, P. F. (2009). Analysis of chemical constituents in *Cistanche* species. *J. Chromatogr. A* 1216 (11), 1970–1979. doi: 10.1016/j.chroma.2008.07.031

Jiang, T., Yu, J. T., Zhu, X. C., Wang, H. F., Tan, M. S., Cao, L., et al. (2014). Acute metformin preconditioning confers neuroprotection against focal cerebral ischaemia by pre-activation of AMPK-dependent autophagy. *Br. J. Pharmacol.* 171 (13), 3146–3157. doi: 10.1111/bph.12655

Jiang, X., Andjelkovic, A. V., Zhu, L., Yang, T., Bennett, M. V. L., Chen, J., et al. (2018). Blood-brain barrier dysfunction and recovery after ischemic stroke. *Prog. Neurobiol.* 163-164, 144–171. doi: 10.1016/j.pneurobio.2017.10.001

Jung, J. E., Kim, G. S., Chen, H., Maier, C. M., Narasimhan, P., Song, Y. S., et al. (2010). Reperfusion and neurovascular dysfunction in stroke: from basic mechanisms to potential strategies for neuroprotection. *Mol. Neurobiol.* 41 (2-3), 172–179. doi: 10.1007/s12035-010-8102-z

Kilkenny, C., Browne, W. J., Cuthill, I. C., Emerson, M., and Altman, D. G. (2010). Improving bioscience research reporting: the ARRIVE guidelines for reporting animal research. *PLoS Biol.* 8 (6), e1000412. doi: 10.1371/journal.pbio.1000412

Ko, K. M., and Leung, H. Y. (2007). Enhancement of ATP generation capacity, antioxidant activity and immunomodulatory activities by Chinese Yang and Yin tonifying herbs. *Chin. Med.* 2, 3. doi: 10.1186/1749-8546-2-3

Kondo, T., Reaume, A. G., Huang, T. T., Carlson, E., Murakami, K., Chen, S. F., et al. (1997). Reduction of CuZn-superoxide dismutase activity exacerbates neuronal cell injury and edema formation after transient focal cerebral ischemia. *J. Neurosci.* 17 (11), 4180–4189. doi: 10.1523/JNEUROSCI.17-11-04180

Lee, M., Saver, J. L., Alger, J. R., Hao, Q., Starkman, S., Ali, L. K., et al. (2012). Blood-brain barrier permeability derangements in posterior circulation ischemic stroke: frequency and relation to hemorrhagic transformation. *J. Neurol. Sci.* 313 (1-2), 142–146. doi: 10.1016/j.jns.2011.08.048

Li, N., Wang, J., Ma, J., Gu, Z., Jiang, C., Yu, L., et al. (2015). Neuroprotective effects of cistanches herba therapy on patients with moderate alzheimer's disease. *Evid Based Complement Altern. Med.* 2015, 103985. doi: 10.1155/2015/103985

Li, M., Xu, T., Zhou, F., Wang, M., Song, H., Xiao, X., et al. (2018). Neuroprotective effects of four phenylethanoid glycosides on H(2)O(2)-induced apoptosis on PC12 cells via the Nrf2/ARE pathway. *Int. J. Mol. Sci.* 19 (4), 1–17. doi: 10.3390/ijms19041135

Li, R., Zhao, M., Tu, P., and Jiang, Y. (2019). Simultaneous determination of five phenylethanoid glycosides in Cistanches Herba using quantitative analysis of multi-components by single marker. *J. Chin. Pharm. Sci.* 28 (08), 537–546. doi: 10.5246/jcps.2019.08.051

Lian, J., Wang, L., Zhao, F., Lin, S., Yan, X., Jia, J., et al. (2017). Effects of glycosides of cistanche on synaptic morphological plasticity in senescence accelerated mice. *J. Baotou Medl Coll.* 33 (08), 78–80. doi: 10.16833/j.cnki.jbmc.2017.08.036

Liu, Y., Wang, D., Wang, H., Qu, Y., Xiao, X., and Zhu, Y. (2014). The protective effect of HET0016 on brain edema and blood-brain barrier dysfunction after cerebral ischemia/reperfusion. *Brain Res.* 1544, 45–53. doi: 10.1016/j.brainres.2013.11.031

Liu, P., Zhang, R., Liu, D., Wang, J., Yuan, C., Zhao, X., et al. (2018). Time-course investigation of blood-brain barrier permeability and tight junction protein changes in a rat model of permanent focal ischemia. *J. Physiol. Sci.* 68 (2), 121–127. doi: 10.1007/s12576-016-0516-6

Liu, S., Chang, L., and Wei, C. (2019). The sonic hedgehog pathway mediates Tongxinluo capsule-induced protection against blood-brain barrier disruption after ischaemic stroke in mice. *Basic Clin. Pharmacol. Toxicol.* 124 (6), 660–669. doi: 10.1111/bcpt.13186

Lu, C. W., Lin, T. Y., Huang, S. K., and Wang, S. J. (2016). Echinacoside inhibits glutamate release by suppressing voltage-dependent Ca(2+) entry and protein kinase C in rat cerebrocortical nerve terminals. *Int. J. Mol. Sci.* 17 (7), 1–13. doi: 10.3390/ijms17071006

McGrath, J. C., Drummond, G. B., McLachlan, E. M., Kilkenny, C., and Wainwright, C. L. (2010). Guidelines for reporting experiments involving animals: the ARRIVE guidelines. *Br. J. Pharmacol.* 160 (7), 1573–1576. doi: 10.1111/j.1476-5381.2010.00873.x

Mentor, S., and Fisher, D. (2017). Aggressive antioxidant reductive stress impairs brain endothelial cell angiogenesis and blood brain barrier function. *Curr. Neurovasc Res.* 14 (1), 71–81. doi: 10.2174/1567202613666161129113950

Moretti, A., Ferrari, F., and Villa, R. F. (2015). Neuroprotection for ischaemic stroke: current status and challenges. *Pharmacol. Ther.* 146, 23–34. doi: 10.1016/j.pharmthera.2014.09.003

Nyul-Toth, A., Suciu, M., Molnar, J., Fazakas, C., Hasko, J., Herman, H., et al. (2016). Differences in the molecular structure of the blood-brain barrier in the cerebral cortex and white matter: an in silico, in vitro, and ex vivo study. *Am. J. Physiol. Heart Circ. Physiol.* 310 (11), H1702–H1714. doi: 10.1152/ajpheart.00774.2015

Ovbiagele, B., and Nguyen-Huynh, M. N. (2011). Stroke epidemiology: advancing our understanding of disease mechanism and therapy. *Neurotherapeutics* 8 (3), 319–329. doi: 10.1007/s13311-011-0053-1

Page, S., Munsell, A., and Al-Ahmad, A. J. (2016). Cerebral hypoxia/ischemia selectively disrupts tight junctions complexes in stem cell-derived human brain microvascular endothelial cells. *Fluids Barriers CNS* 13 (1), 16. doi: 10.1186/s12987-016-0042-1

Peng, F., Chen, J., Wang, X., Xu, C., Liu, T., and Xu, R. (2016). Changes in levels of phenylethanoid glycosides, antioxidant activity, and other quality traits in cistanche deserticola slices by steam processing. *Chem. Pharm. Bull. (Tokyo)* 64 (7), 1024–1030. doi: 10.1248/cpb.c16-00033

Priestley, J. R. C., Fink, K. E., McCord, J. M., and Lombard, J. H. (2019). NRF2 activation with protandim attenuates salt-induced vascular dysfunction and microvascular rarefaction. *Microcirculation*, 26 (7), e12575. doi: 10.1111/micc.12575

Saboor, F., Reckmann, A. N., Tomczyk, C. U., Peters, D. M., Weissmann, N., Kaschtanow, A., et al. (2016). Nestin-expressing vascular wall cells drive development of pulmonary hypertension. *Eur. Respir. J.* 47 (3), 876–888. doi: 10.1183/13993003.00574-2015

Satoh, T., Okamoto, S. I., Cui, J., Watanabe, Y., Furuta, K., Suzuki, M., et al. (2006). Activation of the Keap1/Nrf2 pathway for neuroprotection by electrophilic [correction of electrophillic] phase II inducers. *Proc. Natl. Acad. Sci. U. S. A.* 103 (3), 768–773. doi: 10.1073/pnas.0505723102

Schellinger, P. D., and Kohrmann, M. (2014). 4.5-hour time window for intravenous thrombolysis with recombinant tissue-type plasminogen activator is established firmly. *Stroke* 45 (3), 912–913. doi: 10.1161/strokeaha.113.002700

Sealy-Jefferson, S., Wing, J. J., Sanchez, B. N., Brown, D. L., Meurer, W. J., Smith, M. A., et al. (2012). Age- and ethnic-specific sex differences in stroke risk. *Gend Med.* 9 (2), 121–128. doi: 10.1016/j.genm.2012.02.002

Shi, Z., Wu, Y., Zhu, Y., Cui, Wang, M., Yin, H., et al. (2019). Quantitative determination of betaine, mannitol, fructose, glucose and sucrose in Cistanches Herba by HPLC-ELSD. *Mod. Chin. Med.* 32 (6), 1–11. doi: 10.13313/j.issn.1673-4890.20190320006

Singh, D., Reeta, K. H., Sharma, U., Jagannathan, N. R., Dinda, A. K., and Gupta, Y. K. (2019). Neuro-protective effect of monomethyl fumarate on ischemia reperfusion injury in rats: Role of Nrf2/HO1 pathway in peri-infarct region. *Neurochem. Int.* 126, 96–108. doi: 10.1016/j.neuint.2019.03.010

Siow, R. C., Ishii, T., and Mann, G. E. (2007). Modulation of antioxidant gene expression by 4-hydroxynonenal: atheroprotective role of the Nrf2/ARE transcription pathway. *Redox Rep.* 12 (1), 11–15. doi: 10.1179/135100007x162167

Suda, S., Katsura, K., Kanamaru, T., Saito, M., and Katayama, Y. (2013). Valproic acid attenuates ischemia-reperfusion injury in the rat brain through inhibition of oxidative stress and inflammation. *Eur. J. Pharmacol.* 707 (1-3), 26–31. doi: 10.1016/j.ejphar.2013.03.020

Suzuki, T., and Yamamoto, M. (2015). Molecular basis of the Keap1-Nrf2 system. *Free Radic. Biol. Med.* 88 (Pt B), 93–100. doi: 10.1016/j.freeradbiomed.2015.06.006

Tenreiro, M. M., Ferreira, R., Bernardino, L., and Brito, M. A. (2016). Cellular response of the blood-brain barrier to injury: Potential biomarkers and therapeutic targets for brain regeneration. *Neurobiol. Dis.* 91, 262–273. doi: 10.1016/j.nbd.2016.03.014

Thompson, J. W., Narayanan, S. V., Koronowski, K. B., Morris-Blanco, K., Dave, K. R., and Perez-Pinzon, M. A. (2015). Signaling pathways leading to ischemic mitochondrial neuroprotection. *J. Bioenerg. Biomembr.* 47 (1-2), 101–110. doi: 10.1007/s10863-014-9574-8

Wang, T., Zhang, X., and Xie, W. (2012). *Cistanche deserticola* Y. C. Ma, "Desert ginseng": a review. *Am. J. Chin. Med.* 40 (6), 1123–1141. doi: 10.1142/s0192415x12500838

Wang, X., Wang, S., Wang, J., Guo, H., Dong, Z., Chai, L., et al. (2015). Neuroprotective effect of xueshuantong for injection (lyophilized) in transient and permanent rat cerebral ischemia model. *Evid Based Complement Altern. Med.* 2015, 134685. doi: 10.1155/2015/134685

Wang, D., Wang, H., and Gu, L. (2017). The antidepressant and cognitive improvement activities of the traditional chinese herb cistanche. *Evid Based Complement Altern. Med.* 2017, 3925903. doi: 10.1155/2017/3925903

Wang, F. J., Wang, S. X., Chai, L. J., Zhang, Y., Guo, H., and Hu, L. M. (2018). Xueshuantong injection (lyophilized) combined with salvianolate lyophilized injection protects against focal cerebral ischemia/reperfusion injury in rats through attenuation of oxidative stress. *Acta Pharmacol. Sin.* 39 (6), 998–1011. doi: 10.1038/aps.2017.128

Wei, Y., Gong, J., Thimmulappa, R. K., Kosmider, B., Biswal, S., and Duh, E. J. (2013). Nrf2 acts cell-autonomously in endothelium to regulate tip cell formation and vascular branching. *Proc. Natl. Acad. Sci. U. S. A.* 110 (41), E3910–E3918. doi: 10.1073/pnas.1309276110

Xia, D., Zhang, Z., and Zhao, Y. (2018). Acteoside attenuates oxidative stress and neuronal apoptosis in rats with focal cerebral ischemia-reperfusion injury. *Biol. Pharm. Bull.* 41 (11), 1645–1651. doi: 10.1248/bpb.b18-00210

Xiong, W., MacColl Garfinkel, A. E., Li, Y., Benowitz, L. I., and Cepko, C. L. (2015). NRF2 promotes neuronal survival in neurodegeneration and acute nerve damage. *J. Clin. Invest.* 125 (4), 1433–1445. doi: 10.1172/jci79735

Xu, H. T., Zhang, C. G., He, Y. Q., Shi, S. S., Wang, Y. L., and Chou, G. X. (2019). Phenylethanoid glycosides from the *Schnabelia nepetifolia* (Benth.) P.D.Cantino promote the proliferation of osteoblasts. *Phytochemistry* 164, 111–121. doi: 10.1016/j.phytochem.2019.05.003

Ya, B. L., Liu, Q., Li, H. F., Cheng, H. J., Yu, T., Chen, L., et al. (2018). Uric acid protects against focal cerebral ischemia/reperfusion-induced oxidative stress via activating Nrf2 and regulating neurotrophic factor expression. *Oxid. Med. Cell Longev* 2018, 6069150. doi: 10.1155/2018/6069150

Ye, Z. Y., Xing, H. Y., Wang, B., Liu, M., and Lv, P. Y. (2019). DL-3-n-butylphthalide protects the blood-brain barrier against ischemia/hypoxia injury via upregulation of tight junction proteins. *Chin. Med. J. (Engl.)* 132 (11), 1344–1353. doi: 10.1097/cm9.0000000000000232

Yu, Q., Li, X., and Cao, X. (2016). Cardioprotective effects of phenylethanoid glycoside-rich extract from *Cistanche deserticola* in ischemia-reperfusion-induced myocardial infarction in rats. *Ann. Vasc. Surg.* 34, 234–242. doi: 10.1016/j.avsg.2016.04.002

Yu, N., Wang, Z., Chen, Y., Yang, J., Lu, X., Guo, Y., et al. (2017). The ameliorative effect of bloodletting puncture at hand twelve Jing-well points on cerebral edema induced by permanent middle cerebral ischemia via protecting the tight junctions of the blood-brain barrier. *BMC Complement Altern. Med.* 17 (1), 470. doi: 10.1186/s12906-017-1979-6

Yu, W., Gao, D., Jin, W., Liu, S., and Qi, S. (2018). Propofol prevents oxidative stress by decreasing the ischemic accumulation of succinate in focal cerebral ischemia-reperfusion injury. *Neurochem. Res.* 43 (2), 420–429. doi: 10.1007/s11064-017-2437-z

Yuen, C. M., Chung, S. Y., Tsai, T. H., Sung, P. H., Huang, T. H., Chen, Y. L., et al. (2015). Extracorporeal shock wave effectively attenuates brain infarct volume and improves neurological function in rat after acute ischemic stroke. *Am. J. Transl. Res.* 7 (6), 976–994.

Zechariah, A., ElAli, A., Doeppner, T. R., Jin, F., Hasan, M. R., Helfrich, I., et al. (2013). Vascular endothelial growth factor promotes pericyte coverage of brain capillaries, improves cerebral blood flow during subsequent focal cerebral ischemia, and preserves the metabolic penumbra. *Stroke* 44 (6), 1690–1697. doi: 10.1161/strokeaha.111.000240

Zhang, Q. Y., Wang, Z. J., Sun, D. M., Wang, Y., Xu, P., Wu, W. J., et al. (2017). Novel therapeutic tffects of teonurine on ischemic stroke: new mechanisms of BBB integrity. *Oxid. Med. Cell Longev* 2017, 7150376. doi: 10.1155/2017/7150376

Zhang, R., Xu, M., Wang, Y., Xie, F., Zhang, G., and Qin, X. (2017). Nrf2-a promising therapeutic target for defensing against oxidative stress in stroke. *Mol. Neurobiol.* 54 (8), 6006–6017. doi: 10.1007/s12035-016-0111-0

Zhang, A., Yang, X., Li, Q., Yang, Y., Zhao, G., Wang, B., et al. (2018). Immunostimulatory activity of water-extractable polysaccharides from *Cistanche deserticola* as a plant adjuvant in vitro and in vivo. *PLoS One* 13 (1), e0191356. doi: 10.1371/journal.pone.0191356

Zhang, Y., Wang, K., Chen, H., He, R., Cai, R., Li, J., et al. (2018). Anti-inflammatory lignans and phenylethanoid glycosides from the root of *Isodon ternifolius* (D.Don) Kudo. *Phytochemistry* 153, 36–47. doi: 10.1016/j.phytochem.2018.05.017

Zhang, K., Zhang, Q., Deng, J., Li, J., Li, J., Wen, L., et al. (2019). ALK5 signaling pathway mediates neurogenesis and functional recovery after cerebral ischemia/reperfusion in rats via Gadd45b. *Cell Death Dis.* 10 (5), 360. doi: 10.1038/s41419-019-1596-z

Conflict of Interest: The authors declare that the research was conducted in the absence of any commercial or financial relationships that could be construed as a potential conflict of interest.

The handling editor declared a shared affiliation, though no other collaboration, with the authors KZ, YJ, at time of review.

Copyright © 2020 Wang, Li, Tu, Chen, Zeng and Jiang. This is an open-access article distributed under the terms of the Creative Commons Attribution License (CC BY). The use, distribution or reproduction in other forums is permitted, provided the original author(s) and the copyright owner(s) are credited and that the original publication in this journal is cited, in accordance with accepted academic practice. No use, distribution or reproduction is permitted which does not comply with these terms.

frontiers in Pharmacology

ORIGINAL RESEARCH
published: 20 March 2020
doi: 10.3389/fphar.2020.00242

Different Processed Products of Curcumae Radix Regulate Pain-Related Substances in a Rat Model of Qi Stagnation and Blood Stasis

Zhimin Chen[1†], Lin Hu[1†], Yujiao Liao[1], Xi Zhang[1], Zhuo Yang[1,2], Changjiang Hu[1*] and Lingying Yu[1]*

[1] Chengdu University of Traditional Chinese Medicine, Chengdu, China, [2] Chengdu Women's and Children's Central Hospital, Chengdu, China

OPEN ACCESS

Edited by:
Anthony Booker,
University of Westminster,
United Kingdom

Reviewed by:
Karl Tsim,
Hong Kong University of Science and Technology, Hong Kong
Guang Chen,
Guang'anmen Hospital of China Academy of Chinese Medical Sciences, China

***Correspondence:**
Zhimin Chen
czm346578767@163.com
Changjiang Hu
hhccjj@hotmail.com

† These authors have contributed equally to this work

Specialty section:
This article was submitted to Ethnopharmacology, a section of the journal Frontiers in Pharmacology

Received: 19 August 2019
Accepted: 21 February 2020
Published: 20 March 2020

Citation:
Chen Z, Hu L, Liao Y, Zhang X, Yang Z, Hu C and Yu L (2020) Different Processed Products of Curcumae Radix Regulate Pain-Related Substances in a Rat Model of Qi Stagnation and Blood Stasis. Front. Pharmacol. 11:242. doi: 10.3389/fphar.2020.00242

Background: Curcumae blood Radix (Yujin) has been widely used to treat Qi stagnation and stasis in TCM. According to the Chinese Pharmacopoeia, the tuberous roots of *Curcuma longed* L. (i.e., Huangsiyujin, HSYJ) is one of the major species of Yujin. According to the processing theory of TCM, stir-frying HSYJ with vinegar might strengthen the effect of dispersing stagnated hepatoqi to relieve pain, and stir-frying HSYJ with wine might strengthen the effect of promoting blood circulation in order to remove blood stasis. However, the mechanism for the enhancement of clinical efficacy by processing is unclear.

Aim/Hypothesis: This study was aimed at evaluating the effect of different processed products of HSYJ on chemical constituents and pain-related substances to explore underlying mechanisms of HSYJ in treating pain caused by Qi stagnation and blood stasis.

Methods: The effects of different processing methods on the paste yield of water decoction were analyzed, and the content of the main constituents were detected by HPLC. A rat model of Qi stagnation and blood stasis was established by tail clamp stimulation combined with subcutaneous adrenaline injection. After treatment and intervention with HSYJ and its processed products, β-endorphin (β-EP) and 5-hydroxytryptamine (5-HT) were measured by ELISA, and the expression of c-fos was evaluated by immunohistochemistry.

Results: After stir-frying with vinegar or wine, the extract yield and curcumin content increased. Compared with model group, raw HSYJ could significantly improve the abnormality of 5-HT in plasma ($P < 0.05$) and β-EP in brain ($P < 0.01$). Stir-frying HSYJ with vinegar or wine could significantly improve the abnormality of 5-HT in plasma, β-EP in brain, and the expression of c-fos ($P < 0.01$). Stir-frying HSYJ with vinegar could also significantly increase the level of β-EP in plasma ($P < 0.05$).

Conclusion: These results showed that different processing methods have certain effects on the chemical constituents of HSYJ, mainly in increasing the decoction rate and curcumin content. HSYJ and its processed products can reduce 5-HT levels, increase β-EP levels, and inhibit the expression of c-fos in model rats. The effects of stir-frying HSYJ with vinegar on β-EP levels in plasma was superior to others.

Keywords: tuberous roots of *Curcuma longa* L. (i.e., Huangsiyujin, HSYJ), curcumins, β-endorphin (β-EP), 5-hydroxytryptamine (5-HT), c-fos

INTRODUCTION

Curcumae Radix (Yujin) is the dried root tuber of *Curcuma wenyujin* Y. H. Chen et C. Ling, *Curcuma longa* L., *Curcuma kwangsiensis* S. G. Lee et C. F. Liang, or *Curcuma phaeocaulis* Val. The drugs derived from the former two are known as "Wenyujin" and "Huangsiyujin," respectively, and the drugs derived from the others are known as "Guiyujin" and "Lüsiyujin," respectively, according to their different appearances. As one of the major species of Curcumae Radix, Huangsiyujin (HSYJ) is a well-known genuine traditional Chinese medicine in Sichuan. Its properties include activating blood, relieving pain, moving Qi, relieving depression, clearing the heart, cooling the blood, disinhibiting the gallbladder, and abating jaundice (Shiyuan, 2010; Chinese Pharmacopoeia Commission, 2015). It is widely used in Qi stagnation and blood stagnation syndrome (Tingmo, 2012). Modern pharmacological studies have shown that HSYJ has many functions, such as reducing inflammation (Jia et al., 2010; Chen-Xia et al., 2011), easing pain (Zhao et al., 2018), causing anti-thrombosis and anti-platelet aggregation (Jiang et al., 2015; Yongfeng, 2018), as well as being an antioxidant (Bengmark, 2006; Tuba and Ilhami, 2008), antidepressive, and cholagogue (Jiang et al., 2015).

The processing technology of Chinese herbal medicines is a traditional pharmaceutical technology based on the basic theory of TCM; this takes into consideration the differentiation of symptoms and the nature of drugs as well as the different requirements of dispensation and preparation. It is an important part of TCM, which has been accumulated and developed in clinical practice by TCM physicians. According to the processing theory of TCM, raw Yujin is good at relieving depression, by soothing the liver to regulate Qi, and relieving pain, by promoting blood circulation to remove blood stasis. Stir-frying with vinegar can concentrate the effects on liver meridian to strengthen the effect of dispersing stagnated hepatoqi to relieve pain; stir-frying with wine strengthens the effect of promoting blood circulation to remove blood stasis (Ye and Yuan, 2005; Administration, 2016).

In an earlier study, we found that HSYJ could increase the pain threshold, prolong latency of twisting, decrease writhing times, and influence hemorheology (Chen et al., 2019). Its processing mechanism, however, is not yet clear. This study was aimed at evaluating the effect of different processed products of HSYJ on chemical constituents and pain-related substances (β-EP, 5-HT, and c-fos protein expression) to explore the underlying processing mechanisms of HSYJ; the intention has been to provide reference for the further study, the development of Chinese patent medicine and clinical application of HSYJ.

MATERIALS AND METHODS

Chemicals and Reagents

The reference standards of curcumin, demethoxycurcumin, and bisdemethoxycurcumin (purity > 98%) were purchased from the National Institutes for Food and Drug Control (Beijing, China). Methanol and acetonitrile (Fisher, United States) were of high-performance liquid chromatography (HPLC) grade. Other reagents were of analytical purity. Water was glass distilled and filtered through a Milli-Q water purification system (Millipore, Bedford, MA, United States) prior to use.

Animals

SPF-grade Sprague-Dawley rats (200 ± 20 g) were obtained from Chengdu Dashuo Experimental Animal Co., Ltd. (Chengdu, China). Animals were housed in polypropylene cages and were sent to an animal room 5 days in advance for acclimatization (Chengdu University of Traditional Chinese Medicine, Chengdu, China). They were maintained under controlled conditions (a 12 h light-dark cycle at 22 ± 2°C) on a standard pellet diet and had free access to water. Animal experiments were approved by the Committee of Scientific Research and the Committee of Animal Care of Chengdu University of Traditional Chinese Medicine (Chengdu, China).

Medicinal Materials and Reagents

Medicinal materials were collected from the genuine producing areas and authenticated as the dried root tuber of *Curcuma longa* L. by Professor LI Min (Chengdu University of Traditional Chinese Medicine, Chengdu, China). The sample information is shown in **Table 1**.

Xuefu Zhuyu Pian (Lot:170409) was purchased from Weifang Zhongshi Pharmaceutical Co., Ltd. (Shandong, China). Epinephrine Hydrochloride Injection (Lot:170507) was purchased from Grand Pharma (China) Co., Ltd. (Wuhan, China).

TABLE 1 | Information of HSYJ samples.

No.	Production no	Place of Origin	Place of Purchase
H1	170701	Sichuan	Co.A
H2	17120804	Leshan (Sichuan)	Co.B
H3	XLS18030906	Qianwei (Sichuan)	Co.C

Processing Methods of HSYJ

Prepared slices of HSYJ was processed according to the Pharmacopeia of the People's Republic of China (Vision 2015) (Chinese Pharmacopoeia Commission, 2015) and the Standard for Processing of Traditional Chinese Medicine in Sichuan Province (Vision 2015) (Administration, 2016).

Raw HSYJ

Raw HSYJ was washed clean, moistened thoroughly, cut into slices, and dried.

Stir-Frying HSYJ With Vinegar

We took slices HSYJ, mixed them with a certain amount of rice vinegar evenly, moistened them thoroughly until the vinegar was absorbed completely, poured the drugs into a frying container, and fried them for 10 min (temperature 120–150°C) before we took them out and laid them down to cool. The amount used was 100 kg drugs with 15 kg vinegar. The vinegar was diluted with the same volume of water.

Stir-Frying HSYJ With Wine

We took slices HSYJ, mixed them with a certain amount of yellow wine evenly, moistened them thoroughly until the wine was absorbed completely, poured the drugs into a frying container, and fried them for 10 min (temperature 120–150°C) before we took them out and laid them down to cool. The amount used was 100 kg drugs with 10 kg wine. The wine was diluted with 1.5-fold water.

Preparation of Decoction

The decoction was prepared according to the Standard for Management of TCM Decocting Room in Medical Institutions and Technical Requirements for Quality Control and Standard Formulation of TCM Granules.

HSYJ and its processed products were boiled for 30 min after soaking for 30 min with nine times the amount of water before being filtered. The dregs were boiled twice with seven times the amount of water for 30 min each time, and they were then filtered and mixed with the previous filtrate. The mixed decoction was concentrated by vacuum concentration ($T \leq 50°C$). The dosage for rats was 0.9 $g \cdot kg^{-1}$ according to the conversion of human clinical dosage.

A positive drug was prepared by grinding up Xuefu Zhuyu Pian and dissolving this in water. The dosage given to the rat was 0.432 $g \cdot kg^{-1}$ according to the conversion of human clinical dosage.

Extraction Yield

We took 50 mL of decoction and put it in an evaporating dish that had been dried to a constant weight. We then steamed it in a water bath, dried it in an oven at 105°C for 3 h, and cooled it in a dryer for 30 min. We then weighed it quickly and precisely and calculated the extraction yield. The extraction yield (%) of the sample was calculated with the dried product.

Determination of Curcumins in Decoction

Sample Preparation

We took 50 mL of decoction and steamed it in a water bath ($T \leq 60°C$), dissolved it in methanol of a fixed volume of 10 mL. This was then shaken and filtered with a filter (0.45 μm pore size) prior to injection.

Analysis Condition of HPLC

HPLC determinations were performed by using a SHIMADZU LC-2030C instrument (Shimadzu Corporation, Japan) equipped with a DAD detector, an auto sampler, a column heater, and a SHIMADZU Shim-pack GIST C18 (250 mm × 4.6 mm, 5 μm) column. The mobile phase was acetonitrile-4% glacial acetic acid aqueous solution (48:52); the detection wavelength was 425 nm; the flow rate was 1 $mL \cdot min^{-1}$; and the column temperature was 30°C.

Trail Grouping and Animal Model Establishment

A total of 36 animals were randomly and equally divided into six groups (male and female in half): a control group (CG), model group (MG), Raw HSYJ group (SHG), Stir-frying HSYJ with vinegar group (CHG), Stir-frying HSYJ with wine group (JHG), and positive group (PoG). Except for the CG, the rest of the groups replicated the blood stasis model due to liver-Qi depression by the referenced methods (Shuzhi, 2014). When the model was finished, the animals were fasted for more than 12 h, but water was given normally. The samples were taken under anesthesia. The experimental procedure and dosing treatment plan are shown in **Figure 1**.

Determination of 5-HT and β-EP by ELISA

We collected plasma using heparin as an anticoagulant and centrifuged it for 5 min at 3,000 rpm. The samples were stored in aliquot at −20°C for later use. We avoided repeated freeze-thaw cycles. Rat brain tissue samples were rinsed with normal saline and stored at −20°C. At the time of detection, rat liver tissue samples were thawed in 37°C water and weighed to the appropriate amount of tissue, ground with nine times the normal saline, and centrifuged for 10 min at 3,000 rpm. The supernatant was removed and assayed immediately. Rat 5-Hydroxytryptamine (5-HT) in plasma was detected with 5-HT ELISA Kit (Lot: C0167140192, Cusabio Biotech Co., Ltd., Wuhan, China). Rat beta-endorphin (β-EP) in plasma and brain were detected with β-EP ELISA Kit (Lot: C0167180196, Cusabio Biotech Co., Ltd., Wuhan, China).

Immunohistochemistry Examination

The fixed brain was dehydrated by an automatic dehydrator before being embedded and sliced. The devoted slices were put in the dye vat and performed in 3% hydrogen peroxide (methanol and 30% H_2O_2 was 99:1) for 10 min at room temperature. Afterward, the slices were washed three times with PBS for 5 min each time. We then immersed them into 0.01M citrate

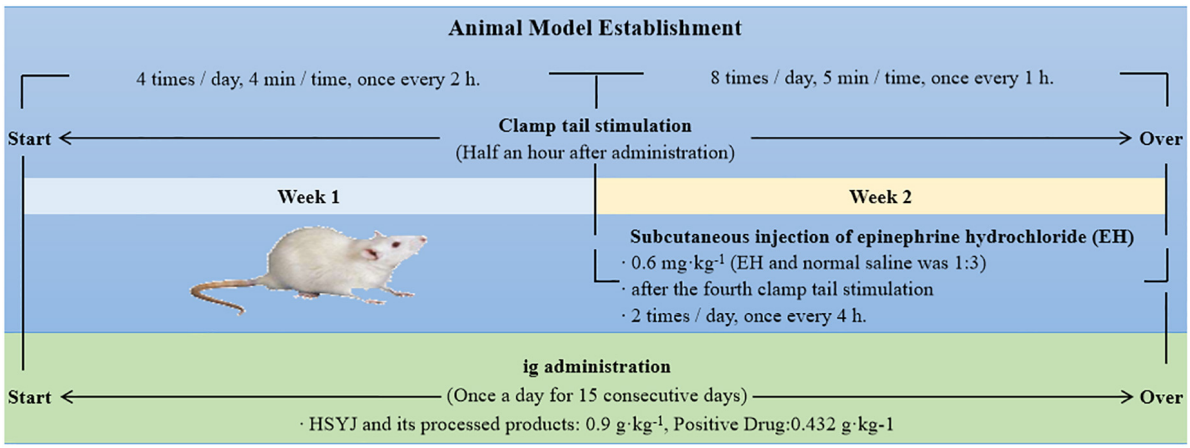


FIGURE 1 | Diagrammatic sketch of the experimental process.

buffer (PH 6.0), used high fire in a microwave oven to break off after boiling, and we repeated this one time after 5 min. After cooling, we washed them two times with PBS for 5 min each time. The slices were then incubated with normal goat serum (ZSGB-BIO, Beijing, China) at room temperature for 20 min. The sections were incubated with primary antibody for c-fos (rabbit polyclonal antibody, 1:100 dilution, Abcam, CA, United States) overnight at 4°C. The sections were then processed with the secondary antibody with goat anti-rabbit (ZSGB-BIO, Beijing, China) for 30 min at 37°C. We washed them three times with PBS for 5 min each time. Used DAB (ZSGB-BIO, Beijing, China) to develop color at room temperature, we controlled the reaction time under the microscope for 2 min and washed the sections with distilled water. Slices were slightly re-dyed with hematoxylin and sealed with neutral gum after dehydration and transparency.

Images were collected by a BA400Digital microscope (Motic China Group Co., Ltd.). The whole tissue was observed at 100 × magnification for each pathological section, and microscopic images were collected by selecting three fields of vision at 400 × magnification. Measured integrated optical density (IOD) and the area of all images by Image-Pro Plus 6.0 (Media Cybernetics, United States) and calculated mean density (MD) of each image.

Statistical Analysis

Statistical analyses were performed by repeating one-way analysis of variance (ANOVA), and this was followed by LSD's *post hoc* multiple-comparison test by using SPSS 19.0 software. The $P < 0.05$ was considered to represent statistical significance.

RESULTS

Extraction Yield and Curcumins

The extraction yield was significantly increased after being stir-fried with vinegar or wine, but there was no significant difference between the stir-frying HSYJ with vinegar and stir-frying HSYJ with wine, indicating that processing could increase the dissolution of chemical constituents (**Table 2**). **Figure 2** shows the chromatogram of HPLC was well separated. After stir-frying with vinegar or wine, it was able to increase the dissolution of curcumins in water. The results are shown in **Table 2**. Similarly, there is no regularity in the content difference between stir-frying HSYJ with vinegar and stir-frying HSYJ with wine. The curcumins of H2 stir-frying HSYJ with vinegar were, however, much higher than those stir-frying with wine, which may be the source of the mechanism behind enhancing the analgesic effect of stir-frying with vinegar.

TABLE 2 | Effects of different processing methods on the extraction yield and curcumins of HSYJ.

No.	Processing	Extraction Yield %	Bisdemethoxycurcumin (μg/g)	Demethoxycurcumin (μg/g)	Curcumin (μg/g)
H1	Raw HSYJ	13.83	1.237	2.460	7.344
	Stir-Frying With Vinegar	14.87	2.889	4.742	14.028
	Stir-Frying With Wine	14.43	3.048	5.293	15.689
H2	Raw HSYJ	9.99	0.162	–	–
	Stir-Frying With Vinegar	11.09	2.618	2.260	2.097
	Stir-Frying With Wine	11.64	0.403	0.334	0.104
H3	Raw HSYJ	9.02	2.386	8.594	30.128
	Stir-Frying With Vinegar	10.29	2.724	9.501	33.084
	Stir-Frying With Wine	10.12	3.051	9.889	33.907

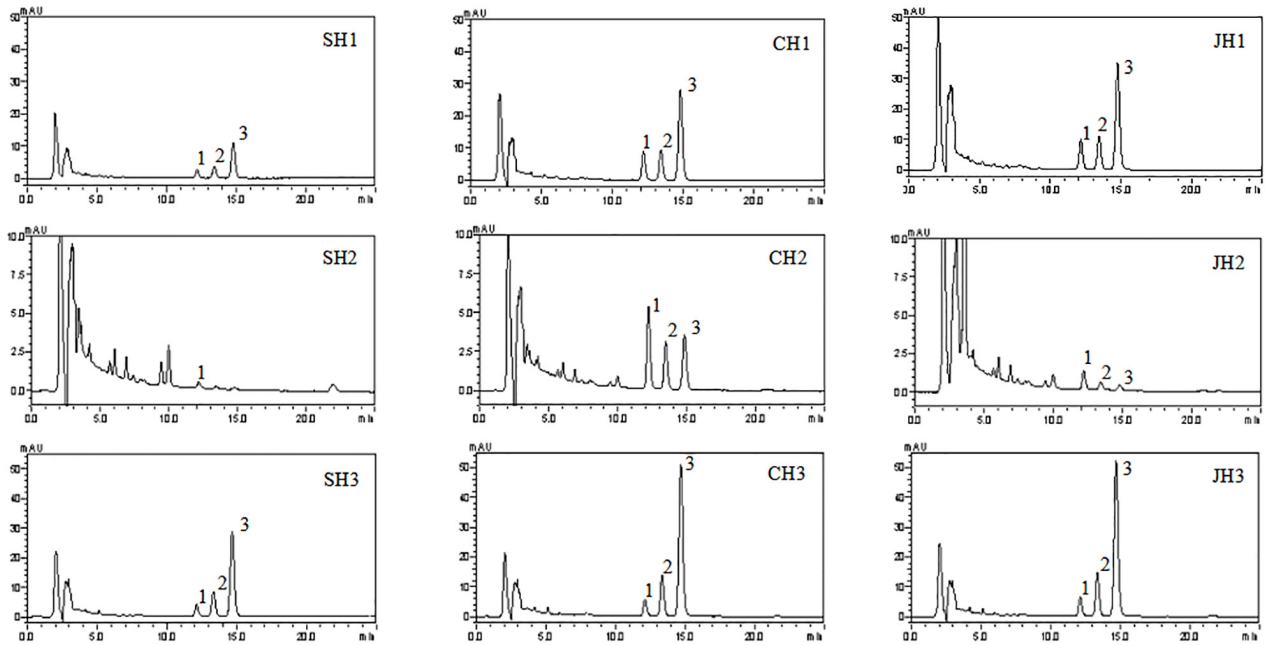


FIGURE 2 | The chromatogram of HSYJ and its processed products 3.2 5-HT Level.

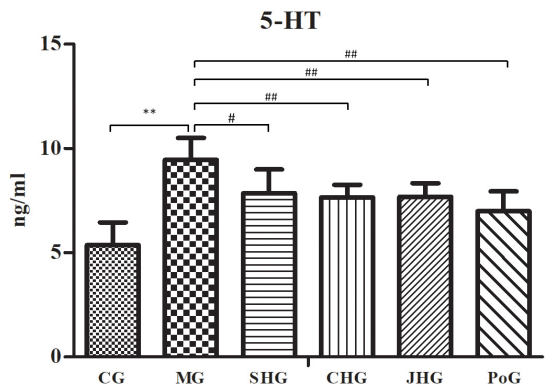


FIGURE 3 | 5-HT level in plasma analysis using ELISA (mean ± SD, $n = 6$). Results showed HSYJ and its processed products could significantly improve 5-HT abnormality in plasma of model rats. $^{*}P < 0.05$ and $^{**}P < 0.01$ vs. Control group; $^{\#}P < 0.05$ and $^{\#\#}P < 0.01$ vs. model group.

The results of changes to the 5-HT level are shown in **Figure 3**. Compared with the CG, the 5-HT level in plasma of MG was significantly increased ($P < 0.01$). After administration, HSYJ and its processed products could significantly improve 5-HT abnormality in plasma of model rats, but there was no difference between them.

β-EP Level

The results of the changes to the β-EP level in plasma and brain are shown in **Figure 4**. Compared with the CG, the level of β-EP in plasma and brain of MG decreased significantly ($P < 0.01$). As an analgesic substance, the decrease of β-EP may be the mechanism behind Qi stagnation and blood stasis, causing pain. After administration, HSYJ and its processed products could improve β-EP abnormality in plasma and brain of model rats. Compared with MG, the β-EP in brain of HSYJ and its processed products increased significantly, and CHG and JHG were higher than those of GG. There was a significant difference between SHG and JHG. The results showed that HSYJ could enhance the analgesic effect by increasing the release of β-EP. The levels of β-EP in brain of drug groups were higher than that in CG, which may be due to the large release of β-EP in the brain in order to inhibit body pain. However, only the level of β-EP in plasma of CHG increased significantly, suggesting that stir-frying with vinegar not only increased the release of β-EP in brain but also promoted its entry into blood.

C-fos Expression

The results of the expression of c-fos in the brain of rats are shown in **Figure 5**. Compared with the CG, MG was significantly increased ($P < 0.01$). The indicator of the pain response is such that, the stronger the expression of c-fos, the stronger the pain the body experiences (Huang et al., 2010). After administration, the expression of c-fos in CHG and JHG decreased significantly ($P < 0.01$), but there was no significant difference in SHG, which indicated that HSYJ could enhance the analgesic effect of the body by stir-frying with vinegar or wine. There was, however, no significant difference in the administration groups.

DISCUSSION

As a unique pharmaceutical technology in China, the processing technology of Chinese herbal medicines plays an important

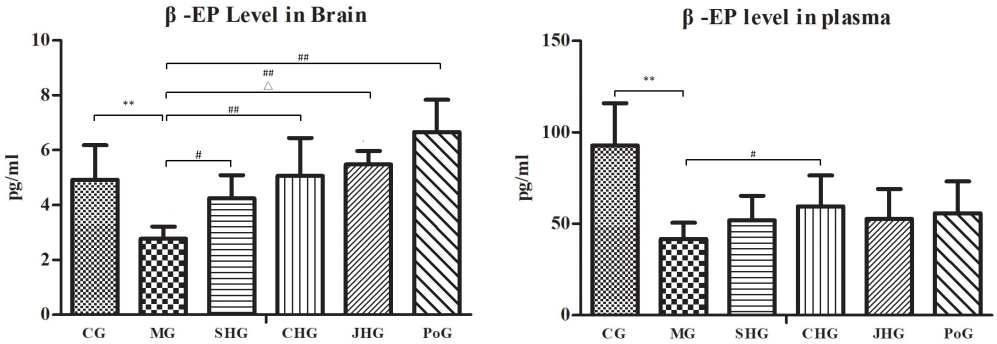


FIGURE 4 | β-EP level in plasma and brain analysis using ELISA (mean ± SD, $n = 6$). Results showed HSYJ and its processed products could improve β-EP abnormality in plasma and brain of model rats. CHG has a significant effect on β-EP in brain and plasma. SHG and JHG only have significant effect on β-EP in plasma, but there is a significant difference between JHG and SHG. $^{*}P < 0.05$ and $^{**}P < 0.01$ vs. Control group; $^{\#}P < 0.05$ and $^{\#\#}P < 0.01$ vs. model group. $^{\triangle}P < 0.05$ vs. SHG.

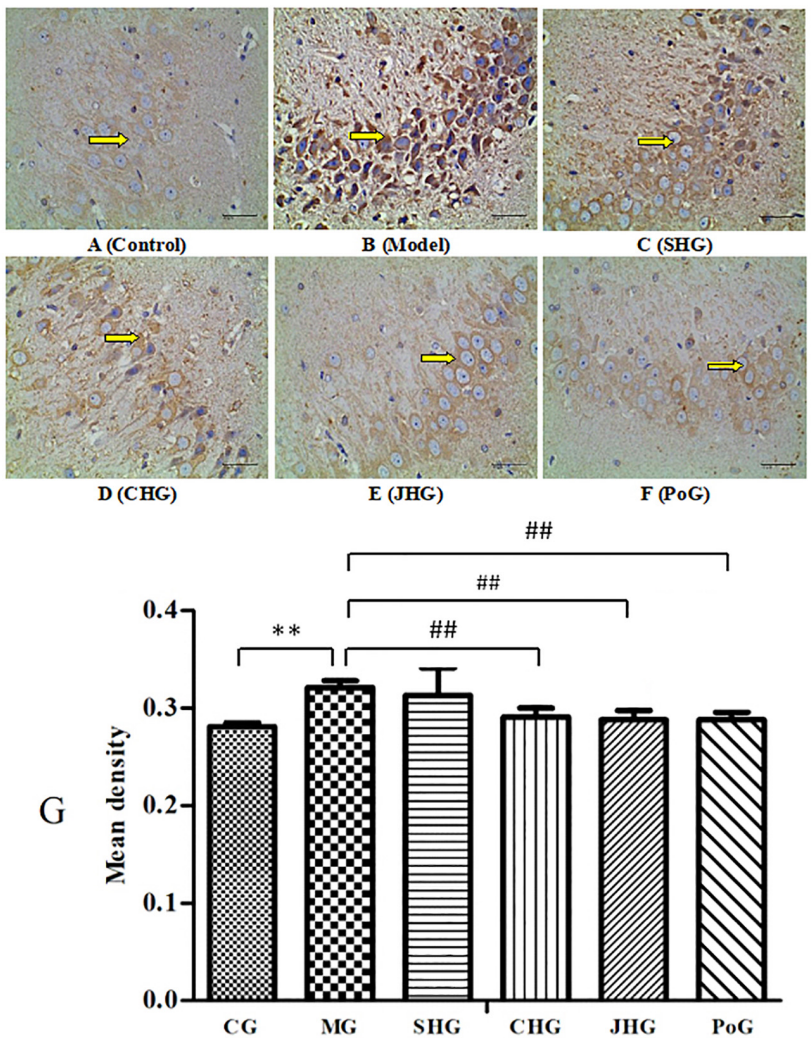


FIGURE 5 | Expression of c-fos in rat brain analysis using immunohistochemistry (400×). **(A)** Control group, **(B)** Model group, **(C)** SHG group, **(D)** CHG group, **(E)** JHG group, **(F)** Positive group of c-fos immunohistochemistry staining. Bars **(G)** represent the means ± SD of 6 rats per group. Results showed CHG and JHG could improve c-fos abnormality. $^{*}P < 0.05$ and $^{**}P < 0.01$ vs. Control group; $^{\#}P < 0.05$ and $^{\#\#}P < 0.01$ vs. model group. $^{\triangle}P < 0.05$ vs. SHG.

role in improving the clinical efficacy of traditional Chinese medicine. Physical and chemical changes of Chinese Materia Medica will occur in the course of processing, and the pharmacological effects will be changed because of these changes, thus resulting in different clinical significance. Huangsiyujin, as a common medicine for Qi stagnation and blood stasis in TCM clinic, has a variety of processed products. Their functions are also dissimilar. However, few scholars have studied the differences of chemical constituents and pharmacodynamics of different processed products of HSYJ.

Traditional Chinese medicine clinically uses decoctions as medicines. In a broad sense, the extraction yield of decoctions can be used as one of the indexes to evaluate the quality of prepared slices of Chinese crude drugs. Modern research showed (Liu et al., 2018) that volatile oil and curcumins are the main chemical constituents of HSYJ. This has also been confirmed in our previous studies (Chen et al., 2019). In this study, the extraction yield and curcumins of HSYJ and its processed products were determined. The results showed that the HSYJ stir-frying with wine or vinegar was beneficial to the dissolution of chemical constituents such as bisdemethoxycurcumin, demethoxycurcumin, and curcumin in water decoctions. This may be because the texture of HSYJ becomes loose after stir-frying, which is more conducive to the dissolution of its chemical constituents. In addition, after stir-frying with wine or vinegar, it may promote the transformation of components and increase solubility.

The theory of TCM argues that stagnation of Qi may bring about pain. 5-HT is a strong pain-inducing substance (Wang et al., 2017, 2018). The elevated level of 5-HT in model rats is consistent with the TCM theory that "the pain is caused by obstruction." β-EP, as one of the main bodies of endogenous opioid peptides, is produced by the hypothalamus and pituitary in vertebrates during exercise, excitement, pain, consumption of spicy food, and orgasm, and it resembles opiates in its ability to produce analgesia and a feeling of well-being (Chang-Hui and Shi-Jia, 2012; Zhang et al., 2016). Many studies have confirmed its analgesic effect, and it has become recognized as an inhibitory neurotransmitter to adjust pain (Qun et al., 2012; Du et al., 2016). The immediate early gene c-fos is frequently called the "third messenger" of the nucleus and is used to detect pathogenesis in central nervous system disorders. Under normal conditions, c-fos is present in the nucleus, but it is activated and transcribed to form mRNA in the cytoplasm and form fos proteins when the cells are subjected to various noxious stimuli (including pain, trauma, etc.) (Hongsheng and Liu, 2014). Now, a large number of studies have shown that the expression of c-fos can be interpreted as a sign of the excitement of painful neurons, and it is thus a useful tool for pain research (Huang et al., 2010; Hongsheng and Liu, 2014). Therefore, detection of β-EP and c-fos can determine whether there is pain neuron excitation in the rat body and can assess the body's feedback. The results show that the analgesic mechanism of HSYJ may be to regulate the release of 5-HT, increase the content of β-EP, especially the release of β-EP in brain tissue, and inhibit the transmission of nociceptive pain information by inhibiting the expression of c-fos proteins in order to finally achieve the analgesic effect. After stir-frying with vinegar or wine, the effect becomes enhanced. This may be due to the fact that stir-frying with vinegar might help to concentrate the effects on liver meridian to strengthen analgesic effect by dispersing stagnated hepatoqi, and stir-frying with wine might strengthen the effect of promoting blood circulation for removing blood stasis; the body's meridians become normal, and so the body does not feel pain or discomfort. This study provides reference for the further study, the development of Chinese patent medicine and clinical application of HSYJ. We will also continue to conduct in-depth research on its mechanism from other aspects.

CONCLUSION

This study indicated that different processing methods have certain effects on the chemical constituents of HSYJ, and this is achieved mainly through increasing the extraction yield and content of bisdemethoxycurcumin, demethoxycurcumin, and curcumin. Modern research showed that curcumin might play an analgesic role through a variety of mechanisms and alleviate different types of pain. HSYJ and its processed products may alleviate pain by regulating the release of 5-HT, increasing the content of β-EP and inhibiting the expression of c-fos. Stir-frying HSYJ with vinegar is more conducive to the release and blood entry of β-EP, thus enhancing the analgesic effect of the body, which is consistent with the traditional Chinese medicine theory of "stir-frying with vinegar into liver to strengthen the effect of dispersing stagnated hepatoqi to relieve pain."

DATA AVAILABILITY STATEMENT

The datasets generated for this study are available on request to the corresponding author.

ETHICS STATEMENT

This study was conducted in strict accordance with the recommendations of the Guidelines for the Care and Use of Laboratory Animals of the Ministry of Science and Technology of China. The protocol was approved by the Committee of Animal Care of Chengdu University of Traditional Chinese Medicine (Chengdu, China).

AUTHOR CONTRIBUTIONS

ZC overall responsibility for the manuscript. LH revised the manuscript and polished the language. YL, XZ, ZY, and LY performed the experiments. CH was involved in the design of the research.

FUNDING

The authors acknowledge financial supports from the National Project for Standardization of Chinese Materia Medica (No. ZYBZH-Y-SC-42), which was organized by the National Development and Reform Commission and State Administration of Traditional Chinese Medicine of the People's Republic of China.

REFERENCES

Administration, S. F. A. D. (2016). *Sichuansheng Zhongyao Yinpian Paozhi Guifan*. Chengdu: Sichuan Science and Technology Press.

Bengmark, S. (2006). Curcumin, an atoxic antioxidant and natural NFkappaB, cyclooxygenase-2, lipooxygenase, and inducible nitric oxide synthase inhibitor: a shield against acute and chronic diseases. *J. Parenter. Enteral Nutr.* 30, 45–51. doi: 10.1177/014860710603000145

Chang-Hui, L. I., and Shi-Jia, Y. U. (2012). Effects of Mudan particles on serum 5-HT and β-EP expressions in diabetic rats. *J. Tradit. Chin. Med. Univ. Hum.* 32, 25–27.

Chen, Z., Quan, L., Zhou, H., Zhao, Y., Chen, P., Hu, L., et al. (2019). Screening of active fractions from *Curcuma* longa radix isolated by HPLC and GC-MS for promotion of blood circulation and relief of pain. *J. Ethnopharmacol.* 234, 68–75. doi: 10.1016/j.jep.2018.09.035

Chen-Xia, H. U., Liu, G., Jia-Qi, H. E., and Yan-Wu, L. I. (2011). Effect of herbs of *Curcuma* genus on synovitis of experimental RA rats. *Chin. Arch. Tradit. Chin. Med.* 29, 95–97.

Chinese Pharmacopoeia Commission (2015). *Pharmacopoeia of the People's Republic of China*. Beijing: China Medical Science Press.

Du, J. Y., Liang, Y., Fang, J. F., Jiang, Y. L., Shao, X. M., He, X. F., et al. (2016). Effect of systemic injection of heterogenous and homogenous opioids on peripheral cellular immune response in rats with bone cancer pain: a comparative study. *Exp. Ther. Med.* 12, 2568–2576. doi: 10.3892/etm.2016.3647

Hongsheng, R., and Liu, S. (2014). Effect of Shentongzhuyu capsuleson c-fos,GFAP,andβ-EP in acetic acid induced pain model of mice. *Pharmacol. Clin. Chin. Mater. Med.* 30, 5–8.

Huang, X., Yang, J., Chang, J. K., and Dun, N. J. (2010). Amylin suppresses acetic acid-induced visceral pain and spinal c-fos expression in the mouse. *Neuroscience* 165, 1429–1438. doi: 10.1016/j.neuroscience.2009.11.063

Jia, S. H., Hong, W., Jia-Lin, Y. U., Wei, X. D., and Zhang, X. P. (2010). Protective effects of curcumin on neonatal rats with necrotizing enterocolitis. *Chin. J. Contemp. Pediatri.* 12, 132–136.

Jiang, H., Song, J., Yan, L. C., Deng, J. Q., and Zhao, J. N. (2015). Comparative study on pharmacological of different varieties of Radix Curcumae. *China J. Tradit. Chin. Med. Pharm.* 30, 4491–4494.

Liu, W. X., Wang, Z.-Y., Chong-jun, Z., Er-wen, L., Xin, L., Yi-han, Q., et al. (2018). Study on content and fingerprint of volatile oil from *Curcuma* longa radix. *Chin. Tradit. Herb. Drugs* 49, 5923–5928.

Qun, L., Xin, H., and Le-Qun, S. U. (2012). Study on the effects of Yuanhuzhitong formula on pain-related substances in formalin-induced pain model and dysmenorrhea rats. *Chin. J. Hosp. Pharm.* 32, 593–596.

Shiyuan, J. (2010). *Jin Shiyuan's Experience in Traditional Chinese Medicine Identification*. Beijing: China Press of Traditional Chinese Medicine.

Shuzhi, Q. (2014). *Study on the Biological Indexes of Erythrocyte Membrane of Three Activating Microcirculation and Removing Stasis Prescription to Qi Stagnation and Blood Stasis Model Rats*. Doctor dissertation, University of Chinese Medicine, Heilongjiang.

Tingmo, Z. (2012). *Clinical Pharmacology of TCM*. Shanghai: Shanghai Scientific and Technical Publishers.

Tuba, A., and Ilhami, G. I. (2008). Antioxidant and radical scavenging properties of curcumin. *Chem. Biol. Interact.* 174, 27–37. doi: 10.1016/j.cbi.2008.05.003

Wang, F., Li, G., Wang, Y., and Neurology, D. O. (2018). Mechanism of 5-hydroxytryptamine involved in migraine and its prospect. *J. Guangdong Pharm. Univ.* 145, 136–139.

Wang, J., Xiao, Y., Liang, X. X., Liu, H., Wang, Z. G., Meng, L., et al. (2017). Effect of Qiu's point on expressions of PGI2, TXA2 and 5-HT in rat model of renal colic. *China J. Modern Med.* 27, 35–39.

Ye, D., and Yuan, S. (2005). *Zhongyao Paozhixue Cidian*. Shanghai: Shanghai Scientific and Technical Publishers.

Yongfeng, Z. (2018). *Study on the Standardized Process and Pharmacodynamics of Curcuma Radix*. Chengdu: Chengdu University of Traditional Chinese Medicine.

Zhang, C., Franklin, T., and Sarkar, D. K. (2016). Inhibition of mammary cancer progression in fetal alcohol exposed rats by β-endorphin neurons. *Alcohol. Clin. Exp. Res.* 40, 134–140. doi: 10.1111/acer.12941

Zhao, Y. C. Z., Liang, Q., Haiting, Z., Wenbing, L., and Changjiang, H. (2018). Comparison of pharmacodynamics of 4 different source of *Curcumae* radix. *Asia Pac. Tradit. Med.* 14, 51–53.

Conflict of Interest: The authors declare that the research was conducted in the absence of any commercial or financial relationships that could be construed as a potential conflict of interest.

Copyright © 2020 Chen, Hu, Liao, Zhang, Yang, Hu and Yu. This is an open-access article distributed under the terms of the Creative Commons Attribution License (CC BY). The use, distribution or reproduction in other forums is permitted, provided the original author(s) and the copyright owner(s) are credited and that the original publication in this journal is cited, in accordance with accepted academic practice. No use, distribution or reproduction is permitted which does not comply with these terms.

frontiers in Physiology

ORIGINAL RESEARCH
published: 25 March 2020
doi: 10.3389/fphys.2020.00201

HuangqiGuizhiWuwu Decoction Prevents Vascular Dysfunction in Diabetes via Inhibition of Endothelial Arginase 1

Hong Cheng[1†], Tian Lu[1†], Jingya Wang[1], Yucen Xia[1], Xiaoshu Chai[2], Minyi Zhang[1], Yutong Yao[1], Na Zhou[1], Sisi Zhou[1], Xinyi Chen[1], Weiwei Su[3], Cunzhi Liu[4], Wei Yi[1], Yongjun Chen[1] and Lin Yao[1]**

[1] School of Pharmaceutical Sciences, South China Research Center for Acupuncture and Moxibustion, Guangzhou University of Chinese Medicine, Guangzhou, China, [2] Department of Oncology, Guangdong Provincial Hospital of Traditional Chinese Medicine, Guangzhou University of Chinese Medicine, Guangzhou, China, [3] Guangdong Key Laboratory of Plant Resources, School of Life Sciences, Sun Yat-sen University, Guangzhou, China, [4] Acupuncture Research Center, Beijing University of Chinese Medicine, Beijing, China

Hyperglycemia induces vascular endothelial dysfunction, which contributes to the development of vascular complication of diabetes. A classic prescription of traditional medicine, *HuangqiGuizhiWuwu* Decoction (HGWWD) has been used for the treatment of various cardiovascular and cerebrovascular diseases, which all are related with vascular pathology. The present study investigated the effect of HGWWD treatment in streptozocin (STZ)-induced vascular dysfunction in mouse models. *In vivo* studies were performed using wild type mice as well as arginase 1 knockout specific in endothelial cells (EC-A1$^{-/-}$) of control mice, diabetes mice and diabetes mice treated with HGWWD (60 g crude drugs/kg/d) for 2 weeks. For *in vitro* studies, aortic tissues were treated with mice serum containing HGWWD with or without adenoviral arginase 1 (Ad-A1) transduction in high glucose (HG) medium. We found that HGWWD treatment restored STZ-induced impaired mean velocity and pulsatility index of mouse left femoral arteries, aortic pulse wave velocity and vascular endothelial relaxation accompanied by elevated NO production in the aorta and plasma, as well as reduced endothelial arginase activity and aortic arginase 1 expression. The protective effect of HGWWD is reversed by an inhibitor of nitric oxide synthesis. Meanwhile, the preventive effect of serum containing HGWWD in endothelial vascular dysfunction is completely blocked by Ad-A1 transduction in HG incubated aortas. HGWWD treatment further improved endothelial vascular dysfunction in STZ induced EC-A1$^{-/-}$ mice. This study demonstrates that HGWWD improved STZ-induced vascular dysfunction through arginase 1 – NO signaling, specifically targeting endothelial arginase 1.

Keywords: *HuangqiGuizhiWuwu* decoction, arginase 1, nitric oxide, diabetic vascular dysfunction, endothelial-dependent vasorelaxation

OPEN ACCESS

Edited by:
Jing-Yan Han,
Peking University, China

Reviewed by:
Jingyan Han,
Boston University, United States
Michael S. Wolin,
New York Medical College, United States

***Correspondence:**
Yongjun Chen
ychen@gzucm.edu.cn;
chyj417@126.com
Lin Yao
Lyao526@gzucm.edu.cn

†These authors have contributed equally to this work

Specialty section:
This article was submitted to Vascular Physiology, a section of the journal Frontiers in Physiology

Received: *08 December 2019*
Accepted: *21 February 2020*
Published: *25 March 2020*

Citation:
Cheng H, Lu T, Wang J, Xia Y, Chai X, Zhang M, Yao Y, Zhou N, Zhou S, Chen X, Su W, Liu C, Yi W, Chen Y and Yao L (2020) HuangqiGuizhiWuwu Decoction Prevents Vascular Dysfunction in Diabetes via Inhibition of Endothelial Arginase 1. Front. Physiol. 11:201. doi: 10.3389/fphys.2020.00201

INTRODUCTION

The number of diabetes patients is expected to increase from 415 million in 2015 to 640 million by 2040 globally (Gao et al., 2016). Vascular complication of diabetes is one of the most serious manifestations of the disease (Rask-Madsen and King, 2013), and the leading cause for this condition is vascular dysfunction including impaired vascular endothelial vasodilation, reduced vascular compliance, and slowed blood flow (Shi and Vanhoutte, 2017). The most well-established clinical advances in the prevention of vascular complication include the control of glucose, cholesterol and blood pressure, which can slow the progression of diabetic microvascular pathology and reduce the risk of cardiovascular disease (Ong et al., 2008). However, the effect of the above-mentioned treatment on vascular dysfunction is not ideal (Grunberger, 2017; Ali et al., 2018). Therefore, there is an urgent need for the discovery and development of new drugs for the treatment of diabetic vascular complication.

Traditional Chinese medicine has long been involved in the treatment of cardiovascular diseases. *HuangqiGuizhiWuwu* Decoction (HGWWD), originated from "Synopsis of the Golden Chamber," is one of the main prescriptions for treating vascular disease in ancient China. Recent clinical evidence-based studies have shown that HGWWD has a positive therapeutic effect on various cardiovascular and cerebrovascular diseases. For example, HGWWD can improve cerebral blood flow in stroke patients and alleviate the subjective symptoms of diabetic peripheral neuropathy (Baiqing, 2015; Pang et al., 2016). Similarly, a recent study reported that HGWWD effectively treated lower extremity macroangiopathy in diabetic patients (Hu et al., 2018). However, the underlying mechanism behind the HGWWD prevention of diabetes-induced vascular complication is poorly understood.

Studies from diabetic mice models and human patients with cardiovascular disease have reported abnormal arginase activation in the vascular endothelium (Romero et al., 2008, 2012; Beleznai et al., 2011; Shemyakin et al., 2012). Arginase, a urea cycle enzyme, can reciprocally regulate nitric oxide (NO) production by nitric oxide synthase (NOS) through competition for their common substrate, L-arginine (Bhatta et al., 2017). There are two isoforms of arginases: arginase 1, located in the cytoplasm and arginase 2, largely present in the mitochondria. We and other previous research found that elevated vascular arginase activity, especially arginase 1, can impair normal vascular endothelial function in various cardiovascular disease models, for example, diabetes (Elms et al., 2013), atherosclerosis (Rabelo et al., 2015), hypertension (Toque et al., 2013), aging (Santhanam et al., 2007), coronary artery disease (Shemyakin et al., 2012), and ischemia-reperfusion (Jung et al., 2010). We recently reported that knocking out endothelial arginase 1 completely prevented obesity-induced vasculopathy, including endothelial-dependent dysfunction, arterial stiffening and vascular inflammation (Bhatta et al., 2017; Yao et al., 2017). All of these findings indicate that arginase 1, especially in endothelial cells, is a valuable target for the treatment of vascular disease.

In this study, we evaluated the therapeutic effect of HGWWD on diabetes-induced vascular dysfunction and investigated whether the ameliorative effect of HGWWD on diabetic vascular endothelial dysfunction is associated with endothelial arginase 1-NO signaling.

MATERIALS AND METHODS

Arginase1 knockout specific in endothelial cells mice (EC-A1$^{-/-}$) are obtained from Dr. W.R. Caldwell Laboratory (Augusta University, United States). As described previously (Bhatta et al., 2017), EC-A1$^{-/-}$ mice were generated by mice expressed Cre-Cadherin 5 (C57BL/6J × 129S1/SvImJ, Stock No. 017968, Jackson Laboratory) crossed with mice carrying floxed arginase 1 alleles (A1$^{loxp/loxp}$,C57BL/6J xB6.Cg-Thy1^{a},Stock No. 008817, Jackson Laboratory). Littermate A1$^{loxp/loxp}$ mice were used as control mice. C57BL/6J Wild type male mice (WT) were obtained from Jinan Peng Yue Experimental Animal Breeding Co., Ltd. (Jinan, China). All mice were housed under a 12 h light/dark cycle with *ad libitum* access to water and food. All experimental procedures in this study were performed according to Institutional Animal Care and Use Committee of Guangzhou University of Chinese Medicine (GZUCM). Diabetic mice were used in a model of streptozotocin (STZ, 50 mg/kg)-induced diabetes (Yao et al., 2013). After 8 weeks of diabetes progression, the mice from the Chinese formula treatment groups received *HuangqiGuizhiWuwu* Decoction (HGWWD) by daily gavage at different doses (60 g/kg/d of crude drugs) for another 2 weeks with or without co-treatment with L-Name (NOS inhibitor) (Anea et al., 2012). Blood glucose and body weight levels of each animal were measured at the first day, second, eighth, and tenth weeks of STZ injection. Both hemodynamic function and vascular wall function were assessed by ultrasound as previously described (Bhatta et al., 2015; Kenwright et al., 2015; Faita et al., 2018; Esfandiarei et al., 2019). Vascular endothelial function was measured by myograph as previously described (Yao et al., 2013). Vascular NO production was determined using the fluorescent NO indicator4, 5-diaminofluorescein diacetate (DAF-2 DA) (Yao et al., 2013). Arginase activity in aortic lysates or plasma samples was determined as previously described (Yao et al., 2013). The mRNA levels of arginase 1 and arginase 2 were measured by quantitative reverse transcription PCR (Q-PCR) as previously described (Bhatta et al., 2017). Data are shown as mean ± SEM. The number of experiments is indicated by "n." Statistical differences were determined using analysis of variance (ANOVA) followed by Tukey post-test. $P < 0.05$ were taken as significant. Detailed methods are provided in **Supplementary Material and Methods**.

RESULTS

HGWWD Treatment Prevents Diabetes-Induced Impairment of the Vascular System

The function of the vascular system can be regulated by both hemodynamic function and vascular wall function (Pugsley and Tabrizchi, 2000; Lee, 2013). In diabetes patients and animal models, abnormal characteristics of hemodynamic and vascular wall function have been reported *in vivo* studies by non-invasive ultrasonography (Cardoso et al., 2015; Faita et al., 2018; Chirinos et al., 2019; Kozera et al., 2019). In this study, we chose mean velocity (MV) to represent the kinetic energy of the blood flow, pulsatility index (PI) to evaluate the vascular resistance and pulse wave velocity (PWV) to predict vascular wall stiffness (Panaritis et al., 2005; Lee, 2013; Alman et al., 2018), which are commonly used in evaluating the function of vascular system. The effect of HGWWD on the function of vascular system is indirectly evaluated by these three parameters after 2 weeks of HGWWD treatment in diabetic mice (**Supplementary Figures S1, S2**). As shown in **Figures 1A–D**, STZ reduced the values of MV and increased PI values of left femoral arteries in mice, compared with control mice. We also found that the values of aortic PWV were elevated in STZ mice (**Figure 1D**). Furthermore, HGWWD administration improved values of MV, PI, and PWV caused by STZ injection (**Figures 1A–D**). To determine whether the effect of HGWWD happens through regulation of metabolic syndrome, we tested the change in blood glucose and body weight at different points in time (1st day, 2nd day, 8th week, and 10th week) after STZ injection, with and without HGWWD. Mice started to show a large increase in glucose levels and a reduction in body weight at 2 weeks after STZ injection. Unexpectedly, HGWWD did not alter glucose levels or body weight in mice with STZ (**Figures 1E,F**). Taken together, these results suggest that the protection that HGWWD provides against the impairment of both hemodynamic function and vascular wall function is not secondary to the improvement of blood glucose and body weight.

HGWWD Treatment Restores Diabetes-Induced Vascular Endothelial Dysfunction

The dysfunction of endothelium located in the flow-tissue interface is considered as the initiation of vascular disorder (Rahman et al., 2007), which contributes to atherosclerosis formation (Gimbrone and Garcia-Cardena, 2016), vascular inflammation (Yang et al., 2016) and vascular remodeling (Vandersmissen et al., 2015; Hao et al., 2019). We previously found that there is significant vascular impairment at 8 weeks in the STZ mouse model (Yao et al., 2013). To determine the effects of HGWWD on vascular endothelial dysfunction in diabetes, we analyzed the acetylcholine (Ach)-induced vasorelaxation response in aortas from control and STZ-induced mice with or without HGWWD. As shown in **Figures 2A–C**, STZ induction impaired vasorelaxation responded to Ach in aortas, presented by

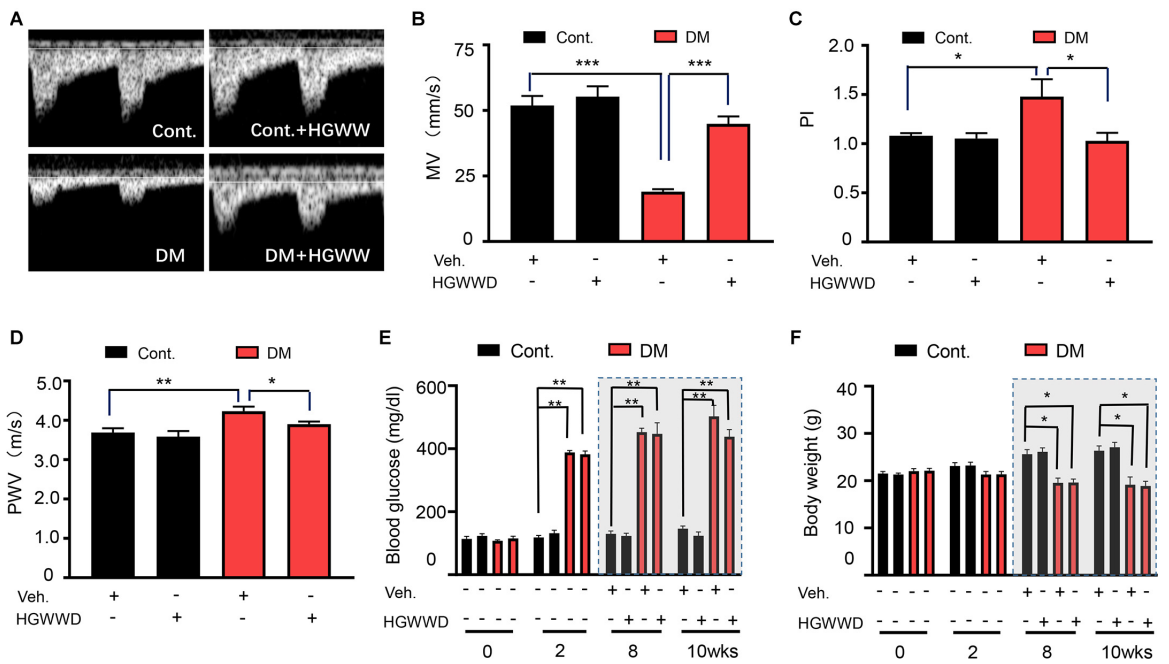


FIGURE 1 | HGWWD prevented the impairment of vascular system without altering blood glucose and body weight in STZ mice. **(A)** Representative images of Pulsed Doppler spectral waveform of left femoral arteries in mice. **(B–D)** The analysis of MV and PI of left femoral arteries and aortic PWV in mice by ultrasound. **(E)** Blood glucose level and **(F)** body weight at 0, 2nd, 8th, and 10th weeks of STZ injection with or without HGWWD treatment. MV, mean velocity; PI, pulsatility index; PWV, pulse wave velocity; STZ, streptozotocin; Cont., non-diabetic normal mice; DM, diabetic mice induced by STZ; HGWWD, *HuangqiGuizhiWuwu* Decoction. Values are presented as mean ± SEM, $^{*}P < 0.05$, $^{**}P < 0.01$, and $^{***}P < 0.001$, n = 6–8 mice/group.

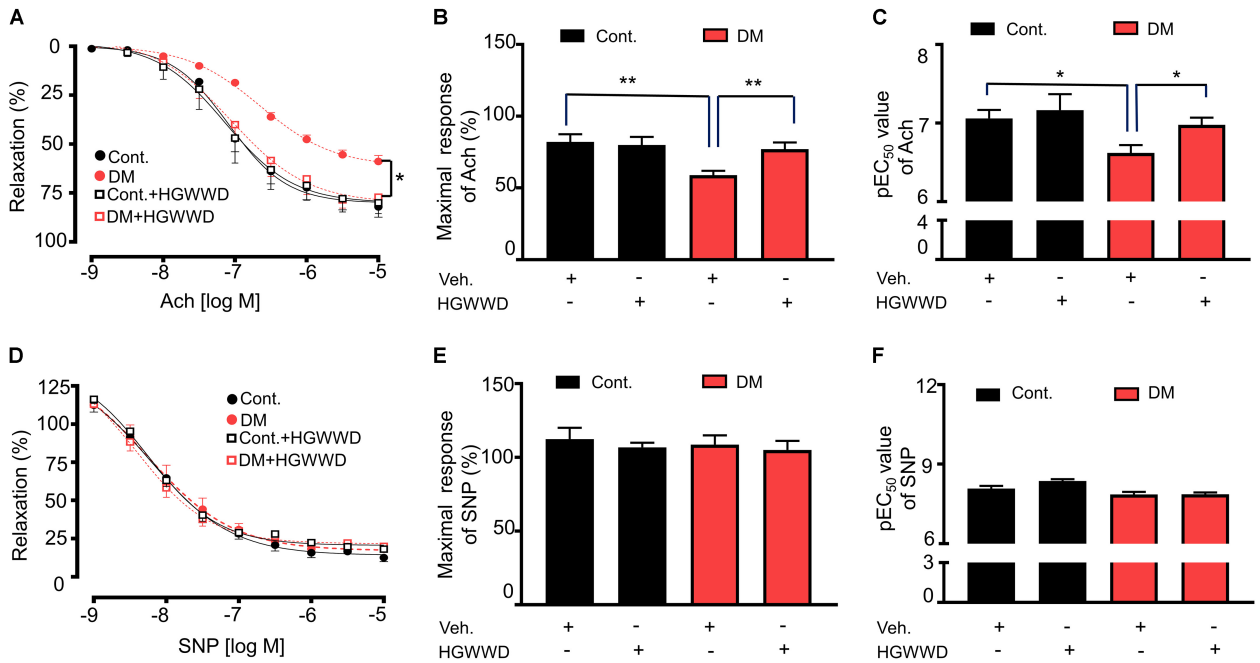


FIGURE 2 | HGWWD prevented STZ-induced decreased in endothelium-dependent vasorelaxation to Ach. **(A)** Effects of HGWWD presented in relaxation curve and **(B)** the value of maximal relaxation (E_{max}) and **(C)** pEC_{50} (the negative logarithm of EC_{50}) of Ach. **(D)** Effect of HGWWD in endothelium-independent vasorelaxation curve and **(E)** the value of E_{max} and **(F)** pEC_{50} of sodium nitroprusside (SNP). Values are presented as mean ± SEM, $^*P < 0.05$ and $^{**}P < 0.01$, n = 10–16 samples from 5 to 8 mice/group.

a decrease in the maximal relaxation (E_{max}) value and an increase in EC_{50} in response to Ach from diabetic mice compared with controls. Intriguingly, HGWWD restored deficits of endothelial-dependent vasorelaxation in diabetic mice. To determine whether smooth muscle function is involved in the effect of HGWWD, we measured endothelial-independent relaxation to the NO donor sodium nitroprusside (SNP). As **Figures 2D–F** shows, curves of SNP were normal in all groups. All of these data indicate that HGWWD prevented diabetic vascular endothelial dysfunction by targeting the vascular endothelium.

HGWWD Treatment Prevents Diabetes-Induced Vascular Endothelial Dysfunction Through NO Signaling

The ability of the endothelium to synthesize NO is a key indicator for predicting and evaluating vascular function (Behrendt and Ganz, 2002). To investigate whether the protection of HGWWD in vascular endothelial dysfunction is related to vascular NO production, first we determined the NO levels in the aortas by DAF-2 fluorescence intensity (indicator of available NO). As shown in **Figures 3A,B**, the intensity of DAF-2 fluorescence was significantly reduced in diabetic mice compared with control mice, and the reduction in NO production was reversed by HGWWT. To determine whether the effect of HGWWT on vascular endothelial dysfunction requires NO signaling, diabetic mice were co-treated with HGWWD and L-Name (NOS inhibitor). We found that L-Name remarkably abolished the potentiating effect of HGWWD in plasma NO bioavailability in diabetic mice (**Figure 3C**). To further test whether altered plasma NO levels by HGWWD are related to the promotion of vascular endothelial function, we examined the vascular relaxation in response to Ach. L-Name treatment blocked the protective effect of HGWWD in diabetes-induced endothelial dysfunction, shown by reduced E_{max} value and elevated EC_{50} in response to Ach (**Figures 3D–F**). All of these results indicate that HGWWD treatment improved diabetes-induced vascular endothelial dysfunction through NO signaling.

HGWWD Alleviates the Level of Endothelial Arginase Activation in Diabetic Aortas

To assess whether endothelial arginase activation is involved in the effects of HGWWD, arginase activity was analyzed in aortas and endothelial cells. The arginase activity in the endothelium was calculated by the subtraction of values for the endothelium denuded aortas from values of vascular tissues with an intact endothelial layer (Yao et al., 2013). As shown **Figures 4A–C**, arginase activity was largely enhanced in vascular endothelial cells of diabetic mice compared with non-diabetic, which was blocked by HGWWD. Consistently, HGWWD attenuated the increased arginase activity of the intact aortas as well. To identify which isoforms of arginase are important for the effect of HGWWD, we firstly determined the mRNA levels of arginase 1 and arginase 2 in aortas. HGWWD blunted the elevation of aortic arginase 1 mRNA levels induced by STZ (**Figure 4D**), but there was no difference in arginase 2 mRNA levels of all three groups

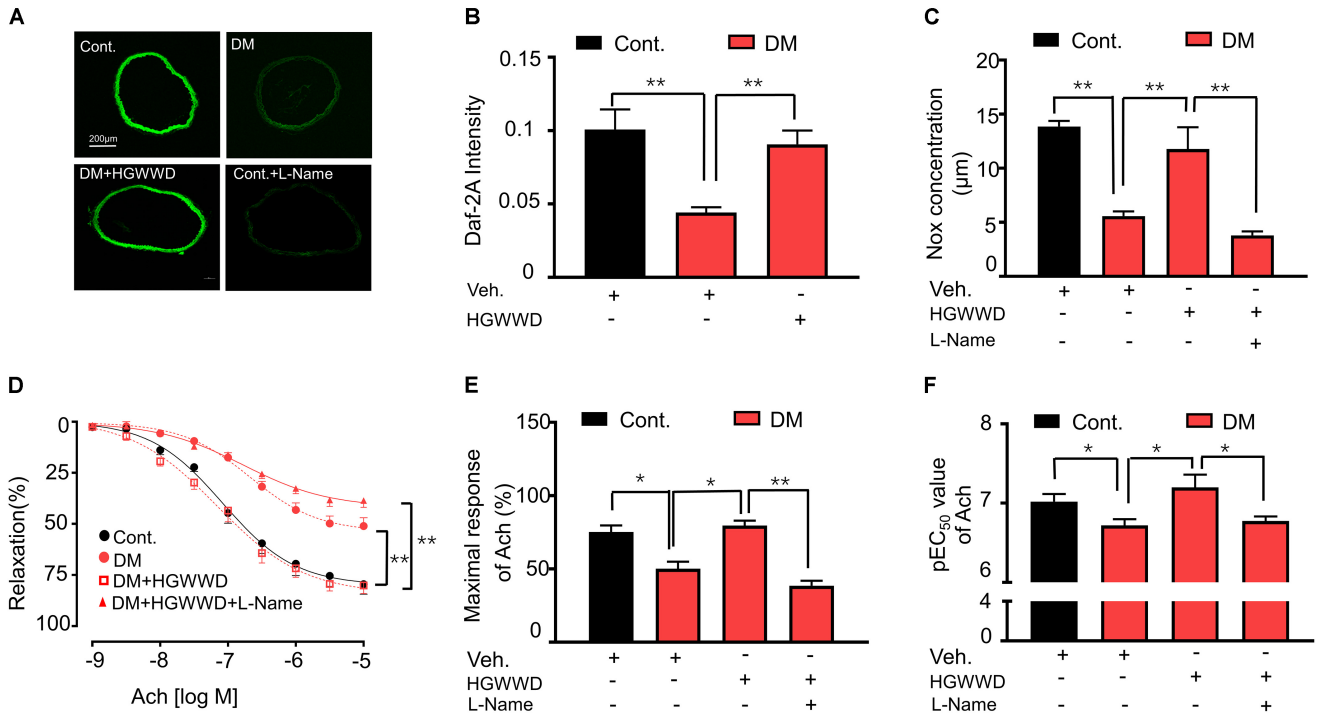


FIGURE 3 | The prevention of HGWWD in vascular endothelial dysfunction was blocked by the inhibition of nitric oxide production. **(A)** Representative images of 4, 5-diaminofluorescein diacetate (DAF-2 DA) in aortic rings from all groups, corrected for fluorescence in the presence of L-Name. **(B)** Fluorometric analysis of DAF2-DA loaded aortic rings. **(C)** Total NO bioavailability (NOx) levels in plasma. **(D)** endothelium-dependent vasorelaxation curve, **(E)** the value of E_{max} and **(F)** pEC_{50} of Ach from all groups. Values are presented as mean ± SEM, $^{*}P < 0.05$ and $^{**}P < 0.01$, n = 8–16 samples from 4 to 8 mice/group.

(**Figure 4E**). Similarly, western blot analysis showed that STZ caused the elevation of arginase 1 protein level in the aorta, which can be reduced by HGWWD treatment (**Figure 4F**). Together, these findings indicate that HGWWD prevented STZ from increasing arginase activity and arginase 1expression, especially in endothelial cells.

Arginase 1 Overexpression Reversed the Effect of HGWWD on HG-Induced Vascular Endothelial Dysfunction

We then determined whether reduced arginase 1 expression is the key mechanism for the HGWWD treatment by using adenoviral transduction to overexpress arginase 1 in isolated aortas (**Figure 5A**). As shown in **Figure 5B**, western blot analysis confirmed that arginase 1 expression was significantly increased in the aorta with arginase 1 transduction. To mimic hyperglycemia conditions, isolated aortas were exposed to Kreb's buffer containing normal glucose (NG) and high glucose (HG) *ex vivo*. Aortas incubated with HG for 24 h started to exhibit significant vascular endothelial dysfunction (**Supplementary Figure S3**). Predictably, overexpression of arginase 1 blocked the effect of HGWWD on the impairment of vascular E_{max} and EC_{50} values (**Figures 5C–E**). In contrast, vasorelaxant responses to SNP were not different among all the groups (**Figure 5F**). These data further support the idea that HGWWD prevents vascular endothelial dysfunction through reducing vascular arginase 1.

Arginase 1 in Endothelial Cells Is Critical for HGWWD on Vascular Endothelial Dysfunction

We next determined whether endothelial arginase 1is involved in the prevention of HGWWD on vascular endothelial dysfunction in STZ mice models. The mating strategy of endothelial-specific arginase 1 knockout (EC-A1$^{-/-}$) mice is shown in **Figure 6A**. Immunostaining evidence indicates that arginase 1 immunoreactivity was abolished inEC-A1$^{-/-}$ aortic sections (**Figure 6B**). In the STZ model, lack of arginase 1 in endothelial cells increased vascular E_{max} compared with aortas from littermate controls (A1$^{loxp\backslash loxp}$), but it did not alter the values of EC_{50} (**Figures 6C–E**). These results indicate that lost arginase 1 in endothelial cells attenuates STZ-caused vascular endothelial dysfunction. Interestingly, lacking endothelial arginase 1 cannot further increase the effect of HGWWD on improved vascular E_{max} or EC_{50} in STZ mice (**Figures 6C–E**). In contrast, the vasorelaxation curves of SNP were similar among all groups (**Figure 6F**). These data provide further support to the notion that HGWWD protects STZ-induced vascular endothelial dysfunction via endothelial arginase 1.

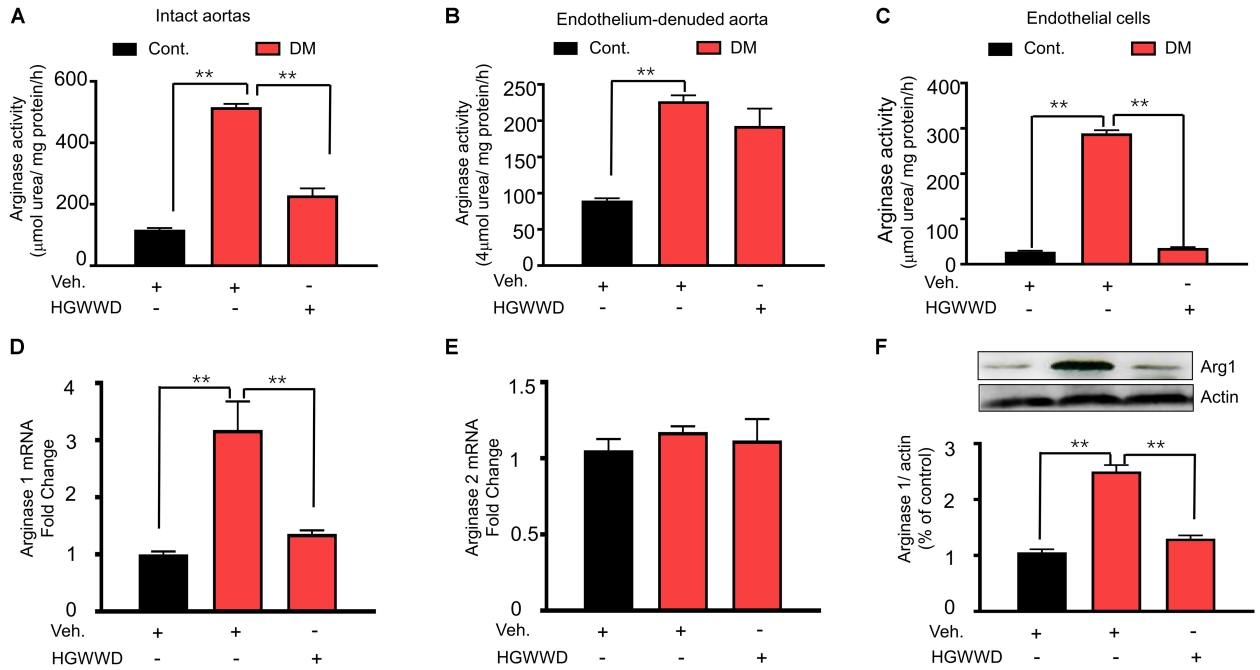


FIGURE 4 | HGWWD attenuated endothelial arginase activity and aortic arginase1 expression in STZ mice. The values of arginase activity in **(A)** intact aortas, **(B)** endothelium-denuded aortas and **(C)** endothelial cells of aortic tissues. The mRNA levels of **(D)** arginase 1 and **(E)** arginase 2 in aorta rings. **(F)** The expression of arginase 1 in aortic rings. Values are presented as mean ± SEM, $^{**}P < 0.01$, n = 8–12 samples from 4 to 6 mice/group.

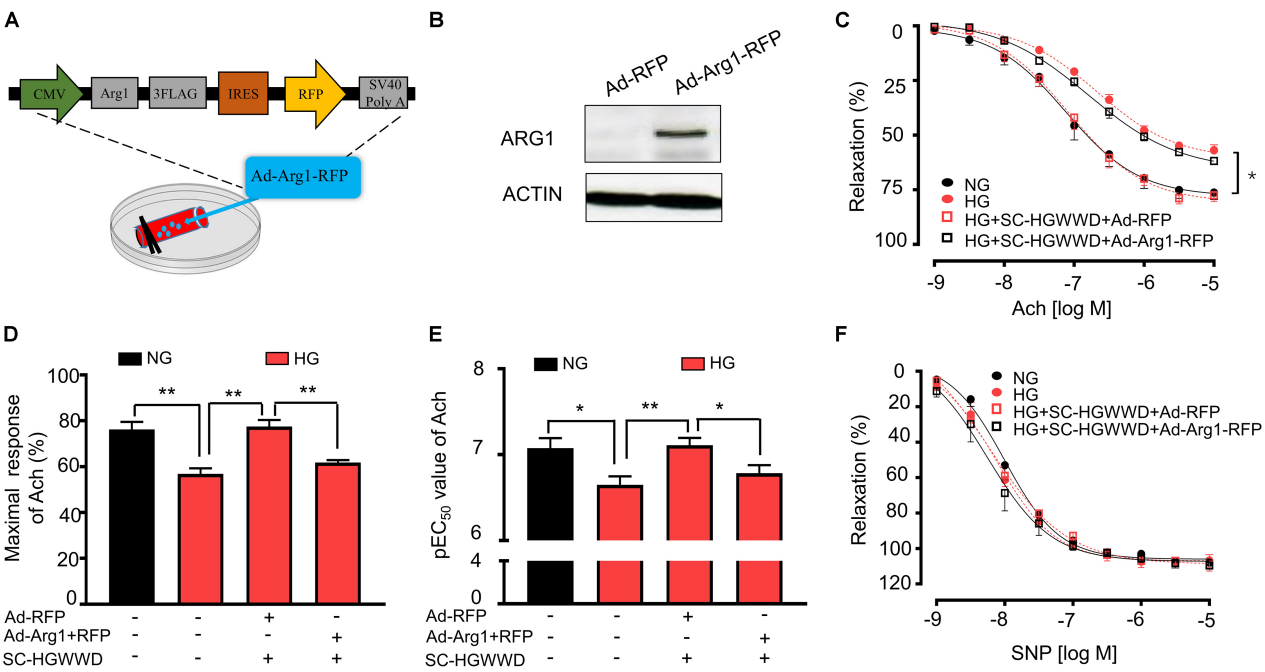


FIGURE 5 | The prevention of HGWWD in vascular endothelial dysfunction was blocked by over expression of arginse 1 in high-glucose (HG) – incubated aortas. **(A)** Illustration of aortic transduction with Ad-Arg1-RFP; **(B)** The arginase 1 expression in aortic tissues after Ad-RFP and Ad-Arg1-RFP groups, Ad-RFP serves as control; **(C)** Endothelium-dependent vasorelaxation curve and **(D)** the value of E_{max} and **(E)** pEC_{50} of Ach in NG, HG and HG + SC-HGWWD incubated aortas with or without ad-Arg1-RFP. **(F)** endothelium-independent vasorelaxation curve of SNP. Ad-Arg1-RFP: aortic transduction with adenoviral vector carrying wild type arginase 1 with red fluorescence protein; Ad-RFP, aortic transduction with adenovirus transduction in RFP adenoviral vector; NG, normalglucose; HG, high glucose; SC-HGWWD, Serum containing HGWWD. Values are presented as mean ± SEM, $^{*}P < 0.05$ and $^{**}P < 0.01$, n = 10–12 samples from 5 to 6 mice/group.

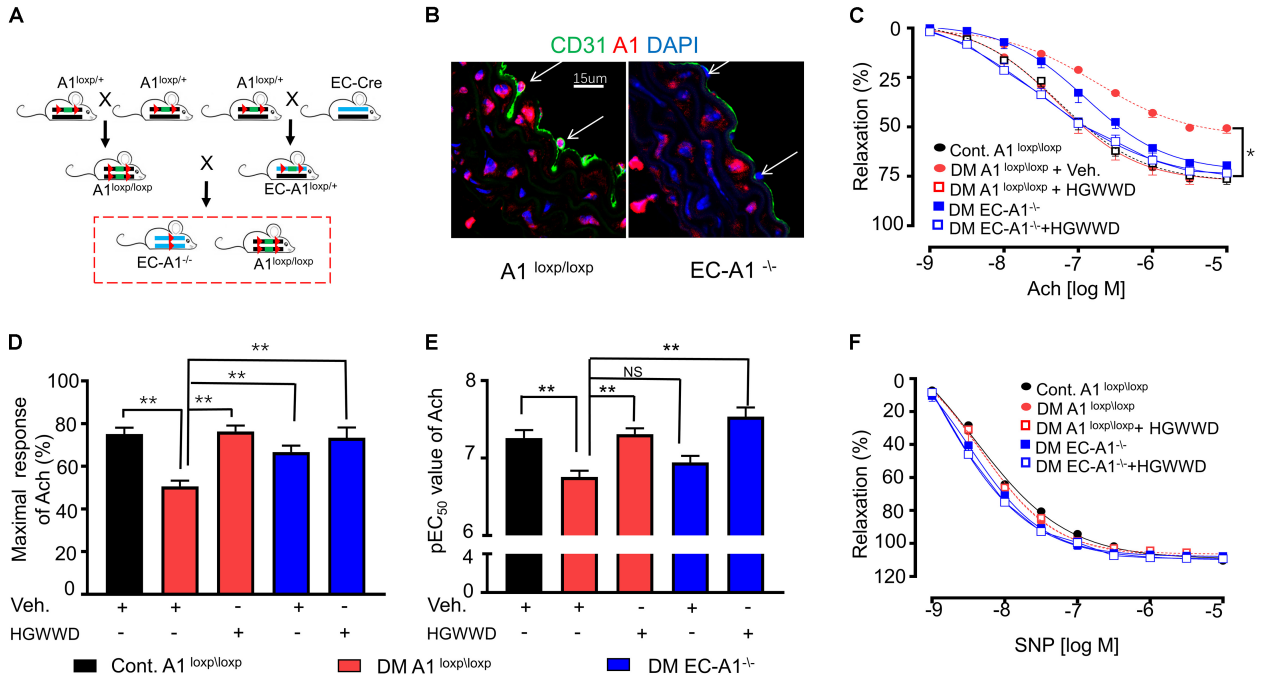


FIGURE 6 | HGWWD prevented STZ-induced vascular endothelial dysfunction through endothelial specific arginase 1. **(A)** The generation of arginase 1 deletion in endothelial cells (EC-A1$^{-\backslash -}$) mice; **(B)** Immunostaining in aortic sections of (EC-A1$^{-\backslash -}$ and its littermates (A1$^{loxp/loxp}$) mice of control by antibodies of endothelial marker (CD31) and arginase 1; **(C)** Endothelium-dependent relaxation curve; **(D)** the values of E_{max} and **(E)** pEC_{50} of Ach in mice of EC-A1$^{-\backslash -}$, A1$^{loxp/loxp}$, diabetes and diabetes treated with or without HGWWD treatment; **(F)** endothelium-independent vasorelaxation curve to SNP. Values are presented as mean ± SEM, $^{*}P < 0.05$ and $^{**}P < 0.01$, n = 10–12 samples from 5 to 6 mice/group.

DISCUSSION

In this study, we found that (1) treatment with HGWWD for 2 weeks protected against diabetes-induced impairment of both hemodynamic function and vascular wall function, but did not alter blood glucose levels and body weight in diabetic mice; (2) HGWWD prevented diabetes-caused vascular endothelial dysfunction through arginase 1-NO signaling; (3) endothelial arginase 1 is a critical target for the prevention of HGWWD on vascular endothelial dysfunction in diabetic models.

HGWWD is used in the treatment of various cardiovascular and cerebrovascular diseases, including diabetic lower extremity macroangiopathy (Hu et al., 2018), diabetic peripheral neuropathy (Liu et al., 2019), and stroke (Li, 2015). Similarly, we found that HGWWD significantly ameliorated vascular wall and hemodynamic dysfunction, especially endothelial dysfunction in STZ-induced mice (**Figures 1**, **2**), suggesting that HGWWD is effective in treating the disorder of vascular system caused by diabetes. Controlling blood glucose levels is one of the most common therapies for slowing the progress of vascular disease in diabetic patients (Zhang et al., 2019). However, our present study shows that HGWWD has no effect on blood glucose in diabetic mice (**Figures 1D,E**), which is supported by several clinical studies (Liu, 2005; Bian, 2010; Lu and You, 2010; Pang et al., 2016). One study reported that HGWWD can reduce the glucose levels of diabetic patients (Chen, 2019), but the reasons for this discrepancy are unclear. We speculate the different effects of HGWWD on blood glucose may be attributable to differences in dosage or duration of treatment. Nevertheless, this study provides evidence to support that this traditional Chinese formula can significantly attenuate vascular complications in diabetes patients.

In this study, we reported that HGWWD treatment significantly restored aortic vascular endothelial dysfunction through NO signaling (**Figure 3**). Abnormal NO levels have been reported in vascular pathological conditions (Bondonno et al., 2016), and intervention in NO signaling can effectively prevent various vascular disorders, including endothelial dysfunction, vascular inflammation and vascular stiffness (Bondonno et al., 2016; Batko et al., 2019; Chen et al., 2019). Furthermore, excessive arginase activation can down-regulate NO production by reducing NOS availability through competition for their common substrate L-arginine (Bhatta et al., 2017; Zhou et al., 2018). This notion is supported by our results showing that HGWWD decreased endothelial arginase activity and aortic arginase 1 expression in STZ mice (**Figure 4**). Moreover, overexpression of arginase 1 in the aorta can block the effect of HGWWD in diabetic mice (**Figure 5**) and the lack of endothelial arginase 1 cannot further improve the vascular endothelial function in the HGWWD-treated diabetic group (**Figure 6**). Thus, for the first time, we demonstrated that HGWWD prevented STZ-induced vascular dysfunction through arginase 1-NO signaling in vascular endothelial cells. Similarly,

some other traditional medicines treated the vascular pathology involved in mechanisms with regulating vascular endothelium dysfunction and NO production, including Yangxin Decoction (Li et al., 2011), Taohong Siwu Decoction (Zhang, 2014), Shixiao San (Wang X. et al., 2015), Ling-Yang-Gou-Teng-decoction (Zhao et al., 2018). Moreover, our previous study also found that Xiao-Shen-Formula prevented the impairment of renal microvascular remodeling via inhibiting arginase activation (An et al., 2018). Altogether, our study further confirms that endothelial Arginase-NO signaling is a valuable therapeutic target in the invention of vascular disease.

There is wide belief that traditional Chinese multi-component formulas act on multiple targets. Besides arginase 1-NO signaling in endothelial cells, our results revealed that there should be other mechanisms involved the effect of HGWWD on the protection of vascular impairment in the STZ model. We found that HGWWD has better effect in preventing vascular endothelial function of diabetes than knocking out endothelial arginase 1 alone (**Figure 6**). Furthermore, there are other pharmacological effects of HGWWD, including the reduction of oxidative stress levels in diabetic neuropathy and myocardial ischemia-reperfusion injury in rats (Qi et al., 2013; Wang Y.-C. et al., 2015; Zhang et al., 2017), and anti-inflammation in nephropathy mice or arthritis in rats (Huang et al., 2009; Li et al., 2016; Liu, 2017; Liu et al., 2018). It is conceivable that the findings of this paper could shed light on the pharmacological mechanisms of HGWWD treatment, particularly in targeting endothelial arginase 1.

DATA AVAILABILITY STATEMENT

The datasets generated for this study are available on request to the corresponding author.

ETHICS STATEMENT

The animal study was reviewed and approved by the Institutional Animal Care and Use Committee of Guangzhou University of Chinese Medicine (GZUCM).

AUTHOR CONTRIBUTIONS

LY, YC, WS, CL, and WY conceived and designed the protocol. HC, TL, JW, YX, XCha, MZ, YY, NZ, SZ, and XChe performed the experiments. LY, YC, HC, and TL analyzed the data. LY and YC wrote the manuscript. All the authors reviewed and approved the submitted version of the manuscript.

FUNDING

This work was supported, in part, by the National Natural Science Foundation of China (Grant Nos. 31600937 to LY, 81973948 to YC, and 31600843 to YX), National Key R&D Program of China (Grant No. 2019YFC1712105 to CL and YC), Guangdong Province Universities and Colleges Pearl River Scholar Funded Scheme (China, Grant 2016 A1-AFD018181Z3903 to YC), and Special Fund for Science and Technology Cultivation of Guangdong University Students in 2019 (China, Grant No. pdjh2019b0117).

SUPPLEMENTARY MATERIAL

The Supplementary Material for this article can be found online at: https://www.frontiersin.org/articles/10.3389/fphys.2020.00201/full#supplementary-material

FIGURE S1 | The experimental schedule of STZ model with HGWWD treatment. STZ, streptozotocin; HGWWD, *HuangqiGuizhiWuwu* Decoction; NO, nitric oxide.

FIGURE S2 | Schematic diagram of the measurement of mouse left femoral artery and aortic by ultrasound system. **(A)** Schematic diagram of mouse left femoral artery under the digital ultrasound platform. **(B)** The schematic diagram of mouse left femoral artery under the PW-mode combining with color flow Doppler imaging. **(C)** Schematic diagram of the analysis of peak systolic velocity (PSV)and end diastolic velocity (EDV) of mouse left femoral artery. **(D)** Schematic diagram of the analysis of mean velocity (MV) of mouse left femoral artery. **(E)** The schematic diagram of the measurement of pulse wave velocity (PWV). **(F)** The image of aorta under the M-mode. **(G)** Schematic diagram of the analysis of PWV under the enlarged image aortic vertical section from the part labeled by yellow dotted line.

FIGURE S3 | (A–C) Aortic endothelium-dependent relaxation curve, **(D)** maximal relaxation and **(E)** pEC_{50} of Ach in HG incubation for 12, 24, and 36 h. Values are presented as mean ± SEM, $^{*}P < 0.05$ and $^{**}P < 0.001$, $n = 10$ samples from 5 mice/group.

REFERENCES

Ali, S. R., Ozdemir, B. A., and Hinchliffe, R. J. (2018). Critical appraisal of the quality of evidence addressing the diagnosis, prognosis, and management of peripheral artery disease in patients with diabetic foot ulceration. *Eur. J. Vasc. Endovasc. Surg.* 56, 401–408. doi: 10.1016/j.ejvs.2018.05.009

Alman, A. C., Talton, J. W., Wadwa, R. P., Urbina, E. M., Dolan, L. M., Hamman, R. F., et al. (2018). Inflammation, adiposity, and progression of arterial stiffness in adolescents with type 1 diabetes: the SEARCH CVD Study. *J. Diabetes Complications* 32, 995–999. doi: 10.1016/j.jdiacomp.2018.08.004

An, X., Zhang, M., Zhou, S., Lu, T., Chen, Y., and Yao, L. (2018). Xiao-shen-formula, a traditional Chinese medicine, improves glomerular hyper-filtration in diabetic nephropathy via inhibiting arginase activation and heparanase expression. *Front. Physiol.* 9:1195. doi: 10.3389/fphys.2018.01195

Anea, C. B., Cheng, B., Sharma, S., Kumar, S., Caldwell, R. W., Yao, L., et al. (2012). Increased superoxide and endothelial NO synthase uncoupling in blood vessels of Bmal1-knockout mice. *Circ. Res.* 111, 1157–1165. doi: 10.1161/circresaha.111.261750

Baiqing (2015). Efficacy and effect of huangqi guizhi wuwu decoction on diabetic peripheral neuropathy. *Chin. Pat. Med.* 37, 962–964. doi: 10.1097/MD.0000000000016696

Batko, K., Krzanowski, M., Pietrzycka, A., Gajda, M., Dumnicka, P., Fedak, D., et al. (2019). Interplay of nitric oxide metabolites and markers of endothelial injury, inflammation and vascular disease in the spectrum of advanced chronic kidney disease. *Kardiol. Pol.* 78, 51–58. doi: 10.33963/kp.15065

Behrendt, D., and Ganz, P. (2002). Endothelial function. From vascular biology to clinical applications. *Am. J. Cardiol.* 90, 40L–48L. doi: 10.1016/s0002-9149(02)02963-6

Beleznai, T., Feher, A., Spielvogel, D., Lansman, S. L., and Bagi, Z. (2011). Arginase 1 contributes to diminished coronary arteriolar dilation in patients with diabetes. *Am. J. Physiol. Heart Circ. Physiol.* 300, H777–H783. doi: 10.1152/ajpheart.00831.2010

Bhatta, A., Yao, L., Toque, H. A., Shatanawi, A., Xu, Z., Caldwell, R. B., et al. (2015). Angiotensin II-induced arterial thickening, fibrosis and stiffening involves elevated arginase function. *PLoS One* 10:e0121727. doi: 10.1371/journal.pone.0121727

Bhatta, A., Yao, L., Xu, Z., Toque, H. A., Chen, J., Atawia, R. T., et al. (2017). Obesity-induced vascular dysfunction and arterial stiffening requires endothelial cell arginase 1. *Cardiovasc. Res.* 113, 1664–1676. doi: 10.1093/cvr/cvx164

Bian, X. (2010). *A Theoretical, Clinical and Experimental Study on the Treatment of Diabetic Peripheral Neuropathy by Jiawei Guizhi Wuwu Decoction*. Nanjing: Nanjing university of Chinese Medicine.

Bondonno, C. P., Croft, K. D., and Hodgson, J. M. (2016). Dietary nitrate, nitric oxide, and cardiovascular health. *Crit. Rev. Food Sci. Nutr.* 56, 2036–2052. doi: 10.1080/10408398.2013.811212

Cardoso, C. R., Moran, C. B., Marinho, F. S., Ferreira, M. T., and Salles, G. F. (2015). Increased aortic stiffness predicts future development and progression of peripheral neuropathy in patients with type 2 diabetes: the Rio de Janeiro Type 2 diabetes cohort study. *Diabetologia* 58, 2161–2168. doi: 10.1007/s00125-015-3658-9

Chen, Y. J., Wu, S. C., Wang, H. C., Wu, T. H., Yuan, S. F., Lu, T. T., et al. (2019). Activation of angiogenesis and wound healing in diabetic mice using NO-delivery dinitrosyl iron complexes. *Mol. Pharm.* 16, 4241–4251. doi: 10.1021/acs.molpharmaceut.9b00586

Chen, Z. (2019). Evaluation on the overall effect of huangqi guizhi wuwu decoction given to elderly patients with hip fracture with diabetes after surgery. *Med. Theory Pract.* 32, 2936–2938.

Chirinos, J. A., Bhattacharya, P., Kumar, A., Proto, E., Konda, P., Segers, P., et al. (2019). Impact of diabetes mellitus on ventricular structure, arterial stiffness, and pulsatile hemodynamics in heart failure with preserved ejection fraction. *J. Am. Heart Assoc.* 8:e011457. doi: 10.1161/jaha.118.011457

Elms, S. C., Toque, H. A., Rojas, M., Xu, Z., Caldwell, R. W., and Caldwell, R. B. (2013). The role of arginase I in diabetes-induced retinal vascular dysfunction in mouse and rat models of diabetes. *Diabetologia* 56, 654–662. doi: 10.1007/s00125-012-2789-5

Esfandiarei, M., Hoxha, B., Talley, N. A., Anderson, M. R., Alkhouli, M. F., Squire, M. A., et al. (2019). Beneficial effects of resveratrol and exercise training on cardiac and aortic function and structure in the 3xTg mouse model of Alzheimer's disease. *Drug Des. Devel. Ther.* 13, 1197–1211. doi: 10.2147/dddt.S196119

Faita, F., Di Lascio, N., Rossi, C., Kusmic, C., and Solini, A. (2018). Ultrasonographic characterization of the db/db mouse: an animal model of metabolic abnormalities. *J. Diabetes Res.* 2018:4561309. doi: 10.1155/2018/4561309

Gao, H. X., Regier, E. E., and Close, K. L. (2016). International diabetes federation world diabetes congress 2015. *J. Diabetes* 8, 300–302. doi: 10.1111/1753-0407.12377

Gimbrone, M. A. Jr., and Garcia-Cardena, G. (2016). Endothelial cell dysfunction and the pathobiology of atherosclerosis. *Circ. Res.* 118, 620–636. doi: 10.1161/circresaha.115.306301

Grunberger, G. (2017). Should side effects influence the selection of antidiabetic therapies in type 2 diabetes? *Curr. Diab. Rep.* 17:21. doi: 10.1007/s11892-017-0853-8

Hao, Y. M., Yuan, H. Q., Ren, Z., Qu, S. L., Liu, L. S., Dang, H., et al. (2019). Endothelial to mesenchymal transition in atherosclerotic vascular remodeling. *Clin. Chim. Acta* 490, 34–38. doi: 10.1016/j.cca.2018.12.018

Hu, H., Tian, W., Qin, Y., and Zhang, J. (2018). Clinical effect of huangqi guizhi wuwu decoction on diabetic vascular lesions in lower limbs. *Clin. Med. Res. Pract.* 3, 109–110. doi: 10.19347/j.cnki.2096-1413.201809053

Huang, X.-M., Zhang, Y., He, D., Zhang, L., Zheng, N.-J., Xie, L.-X., et al. (2009). An experimental study on the effect of dinghuang lotion on the expression of substance P in the skin of rats with chronic renal failure. *Chin. Sci. Technol. Tradit. Chin. Med.* 16, 97–98.

Jung, C., Gonon, A. T., Sjoquist, P. O., Lundberg, J. O., and Pernow, J. (2010). Arginase inhibition mediates cardioprotection during ischaemia-reperfusion. *Cardiovasc. Res.* 85, 147–154. doi: 10.1093/cvr/cvp303

Kenwright, D. A., Thomson, A. J., Hadoke, P. W., Anderson, T., Moran, C. M., Gray, G. A., et al. (2015). A protocol for improved measurement of arterial flow rate in preclinical ultrasound. *Ultrasound Int. Open* 1, E46–E52. doi: 10.1055/s-0035-1564268

Kozera, G. M., Neubauer-Geryk, J., Wolnik, B., Szczyrba, S., Wojczal, J., Nyka, W. M., et al. (2019). Cerebral and skin microcirculatory dysfunction in type 1 diabetes. *Postepy Dermatol. Alergol.* 36, 44–50. doi: 10.5114/ada.2018.81185

Lee, J. (2013). Image-based evaluation of vascular function and hemodynamics. *Pulse (Basel)* 1, 108–122. doi: 10.1159/000354110

Li, S., Dong, X., Zhu, L., and Zhang, Q. (2016). Effects of saponins in huangqi guizhi wuwu decoction on immune function suppression. *Henan Tradit. Chin. Med.* 36, 479–481. doi: 10.16367/j.issn.1003-5028.2016.03.0209

Li, Y. (2015). Observation on the effect of astragalus guizhi wuwu decoction on treating qi deficiency and blood stasis stroke. *Clin. Stud. Tradit. Chin. Med.* 7, 27–28. doi: 10.3969/j.issn.1674-7860.2015.13.012

Li, Y., Zhou, Y., Wang, Y., and Liu, Y. (2011). Effect of medicated serum of yangxin decoction on Smad4 mRNA expression in human umbilical vein endothelial cell injury model induced by H2O2. *New Chin. Med.* 43, 124–126. doi: 10.13457/j.cnki.jncm.2011.06.069

Liu, J. (2017). *Studied the Mechanism of Huangqi Guizhi wuwu Decoction on Rheumatoid Arthritis Based on the Yak-stat Signaling Pathway*. Shanxi: Shanxi university of traditional Chinese medicine.

Liu, J., Hong, G., Ji, C., and Zheng, X. (2019). Clinical value of astragalus guizhi wuwu decoction combined with mecobalamine tablets in the treatment of diabetic peripheral neuropathy. *Forum Basic Med.* 23, 1007–1009. doi: 10.19435/j.1672-1721.2019.07.074

Liu, Q. (2005). *Clinical Study on the Treatment of Type 2 Diabetic Peripheral Neuropathy by Jiawei Guizhi wuwu Decoction*. Sichuan: Chengdu university of traditional Chinese medicine.

Liu, W., Shi, L., Wan, Q., Wu, Y., Huang, D., and Gao, J. (2018). Explore the renal protective mechanism of huangqi guizhi wuwu decoction on IgA nephrotic mice based on NLRP3 inflammasome. *Chin. J. Tradit. Chin. Med.* 33, 1746–1751.

Lu, Y., and You, L. (2010). Clinical observation of astragalus guizhi wuwu decoction in the treatment of diabetic peripheral neuropathy. *Chin. Med. Emerg.* 19, 1297–1298.

Ong, K. L., Cheung, B. M., Wong, L. Y., Wat, N. M., Tan, K. C., and Lam, K. S. (2008). Prevalence, treatment, and control of diagnosed diabetes in the U.S. National Health and Nutrition Examination Survey 1999-2004. *Ann. Epidemiol.* 18, 222–229. doi: 10.1016/j.annepidem.2007.10.007

Panaritis, V., Kyriakidis, A. V., Pyrgioti, M., Raffo, L., Anagnostopoulou, E., Gourniezaki, G., et al. (2005). Pulsatility index of temporal and renal arteries as an early finding of arteriopathy in diabetic patients. *Ann. Vasc. Surg.* 19, 80–83. doi: 10.1007/s10016-004-0134-2

Pang, B., Zhao, T. Y., Zhao, L. H., Wan, F., Ye, R., Zhou, Q., et al. (2016). Huangqi guizhi wuwu decoction for treating diabetic peripheral neuropathy: a meta-analysis of 16 randomized controlled trials. *Neural. Regen. Res.* 11, 1347–1358. doi: 10.4103/1673-5374.189202

Pugsley, M. K., and Tabrizchi, R. (2000). The vascular system. An overview of structure and function. *J. Pharmacol. Toxicol. Methods* 44, 333–340. doi: 10.1016/s1056-8719(00)00125-8

Qi, F., Qiu, C. L., Zhu, L., Zhao, S., and Yang, X. L. (2013). Protective effect of huangqi guizhi wuwu decoction on diabetic rats induced by STZ. *Chin. J. Basic Med. Tradit. Chin. Med.* 19, 631–633.

Rabelo, L. A., Ferreira, F. O., Nunes-Souza, V., da Fonseca, L. J., and Goulart, M. O. (2015). Arginase as a critical prooxidant mediator in the binomial endothelial dysfunction-atherosclerosis. *Oxid. Med. Cell. Longev.* 2015:924860. doi: 10.1155/2015/924860

Rahman, S., Rahman, T., Ismail, A. A., and Rashid, A. R. (2007). Diabetes-associated macrovasculopathy: pathophysiology and pathogenesis. *Diabetes Obes. Metab.* 9, 767–780. doi: 10.1111/j.1463-1326.2006.00655.x

Rask-Madsen, C., and King, G. L. (2013). Vascular complications of diabetes: mechanisms of injury and protective factors. *Cell Metab.* 17, 20–33. doi: 10.1016/j.cmet.2012.11.012

Romero, M. J., Iddings, J. A., Platt, D. H., Ali, M. I., Cederbaum, S. D., Stepp, D. W., et al. (2012). Diabetes-induced vascular dysfunction involves arginase I. *Am. J. Physiol. Heart Circ. Physiol.* 302, H159–H166. doi: 10.1152/ajpheart.00774.2011

Romero, M. J., Platt, D. H., Tawfik, H. E., Labazi, M., El-Remessy, A. B., Bartoli, M., et al. (2008). Diabetes-induced coronary vascular dysfunction involves increased arginase activity. *Circ. Res.* 102, 95–102. doi: 10.1161/CIRCRESAHA.107.155028

Santhanam, L., Lim, H. K., Lim, H. K., Miriel, V., Brown, T., Patel, M., et al. (2007). Inducible NO synthase dependent S-nitrosylation and activation of arginase1 contribute to age-related endothelial dysfunction. *Circ. Res.* 101, 692–702. doi: 10.1161/circresaha.107.157727

Shemyakin, A., Kovamees, O., Rafnsson, A., Bohm, F., Svenarud, P., Settergren, M., et al. (2012). Arginase inhibition improves endothelial function in patients with coronary artery disease and type 2 diabetes mellitus. *Circulation* 126, 2943–2950. doi: 10.1161/circulationaha.112.140335

Shi, Y., and Vanhoutte, P. M. (2017). Macro- and microvascular endothelial dysfunction in diabetes. *J. Diabetes* 9, 434–449. doi: 10.1111/1753-0407.12521

Toque, H. A., Nunes, K. P., Rojas, M., Bhatta, A., Yao, L., Xu, Z., et al. (2013). Arginase 1 mediates increased blood pressure and contributes to vascular endothelial dysfunction in deoxycorticosterone acetate-salt hypertension. *Front. Immunol.* 4:219. doi: 10.3389/fimmu.2013.00219

Vandersmissen, I., Craps, S., Depypere, M., Coppiello, G., van Gastel, N., Maes, F., et al. (2015). Endothelial Msx1 transduces hemodynamic changes into an arteriogenic remodeling response. *J. Cell Biol.* 210, 1239–1256. doi: 10.1083/jcb.201502003

Wang, X., Zhang, R., Gu, L., Zhang, Y., Zhao, X., Bi, K., et al. (2015). Cell-based screening identifies the active ingredients from traditional Chinese medicine formula Shixiao San as the inhibitors of atherosclerotic endothelial dysfunction. *PLoS One* 10:e0116601. doi: 10.1371/journal.pone.0116601

Wang, Y.-C., Wu, Y., Ye, H.-Y., Jia, H.-Q., Xu, Y.-Z., Li, W.-W., et al. (2015). Protective effect of huangqi guizhi wuwu decoction on myocardial ischemia-reperfusion injury in rats. *Shanghai J. Tradit. Chin. Med.* 49, 80–83. doi: 10.16305/j.1007-1334.2015.10.026

Yang, X., Chang, Y., and Wei, W. (2016). Endothelial dysfunction and inflammation: immunity in rheumatoid arthritis. *Mediators Inflamm.* 2016:6813016. doi: 10.1155/2016/6813016

Yao, L., Bhatta, A., Xu, Z., Chen, J., Toque, H. A., Chen, Y., et al. (2017). Obesity-induced vascular inflammation involves elevated arginase activity. *Am. J. Physiol. Regul. Integr. Comp. Physiol.* 313, R560–R571. doi: 10.1152/ajpregu.00529.2016

Yao, L., Chandra, S., Toque, H. A., Bhatta, A., Rojas, M., Caldwell, R. B., et al. (2013). Prevention of diabetes-induced arginase activation and vascular dysfunction by Rho kinase (ROCK) knockout. *Cardiovasc. Res.* 97, 509–519. doi: 10.1093/cvr/cvs371

Zhang, B. (2014). Effect of drug serum containing taohong siwu decoction on expression of TNF- TNF, McP-1 and il-1 in human umbilical vein endothelial cells induced by LPS. *Liaoning J. Tradit. Chin. Med.* 41, 2280–2283. doi: 10.13192/j.issn.1000-1719.2014.11.004

Zhang, W.-W., Han, Y.-S., Wang, C., Fan, Y., and Tian, M. (2017). Effects of huangqi guizhi wuwu decoction on Trx and Txnip expression in peripheral nervous tissue of diabetic rats. *Chin. J. Tradit. Chin. Med.* 45, 57–59. doi: 10.19664/j.cnki.1002-2392.2017.04.016

Zhang, Z. Y., Miao, L. F., Qian, L. L., Wang, N., Qi, M. M., Zhang, Y. M., et al. (2019). Molecular mechanisms of glucose fluctuations on diabetic complications. *Front. Endocrinol. (Lausanne)* 10:640. doi: 10.3389/fendo.2019.00640

Zhao, X., Liu, J., Yang, S., Song, D., Wang, C., Chen, C., et al. (2018). Ling-Yang-Gou-Teng-decoction prevents vascular dementia through inhibiting oxidative stress induced neurovascular coupling dysfunction. *J. Ethnopharmacol.* 222, 229–238. doi: 10.1016/j.jep.2018.03.015

Zhou, Z., Mahdi, A., Tratsiakovich, Y., Zahoran, S., Kovamees, O., Nordin, F., et al. (2018). Erythrocytes from patients with type 2 diabetes induce endothelial dysfunction via arginase I. *J. Am. Coll. Cardiol.* 72, 769–780. doi: 10.1016/j.jacc.2018.05.052

Conflict of Interest: The authors declare that the research was conducted in the absence of any commercial or financial relationships that could be construed as a potential conflict of interest.

Copyright © 2020 Cheng, Lu, Wang, Xia, Chai, Zhang, Yao, Zhou, Zhou, Chen, Su, Liu, Yi, Chen and Yao. This is an open-access article distributed under the terms of the Creative Commons Attribution License (CC BY). The use, distribution or reproduction in other forums is permitted, provided the original author(s) and the copyright owner(s) are credited and that the original publication in this journal is cited, in accordance with accepted academic practice. No use, distribution or reproduction is permitted which does not comply with these terms.

frontiers in Physiology

ERRATUM
published: 20 January 2021
doi: 10.3389/fphys.2021.650179

Erratum: *HuangqiGuizhiWuwu* Decoction Prevents Vascular Dysfunction in Diabetes via Inhibition of Endothelial Arginase 1

*Frontiers Production Office**

Frontiers Media SA, Lausanne, Switzerland

Keywords: *HuangqiGuizhiWuwu* decoction, arginase 1, nitric oxide, diabetic vascular dysfunction, endothelial-dependent vasorelaxation

OPEN ACCESS

Approved by:
Frontiers Editorial Office, Frontiers Media SA, Switzerland

***Correspondence:**
Frontiers Production Office
production.office@frontiersin.org

Specialty section:
This article was submitted to Vascular Physiology, a section of the journal Frontiers in Physiology

Received: *06 January 2021*
Accepted: *06 January 2021*
Published: *20 January 2021*

Citation:
Frontiers Production Office (2021) Erratum: HuangqiGuizhiWuwu Decoction Prevents Vascular Dysfunction in Diabetes via Inhibition of Endothelial Arginase 1. Front. Physiol. 12:650179. doi: 10.3389/fphys.2021.650179

An Erratum on

***HuangqiGuizhiWuwu* Decoction Prevents Vascular Dysfunction in Diabetes via Inhibition of Endothelial Arginase 1**

by Cheng, H., Lu, T., Wang, J., Xia, Y., Chai, X., Zhang, M., et al. (2020). Front. Physiol. 11:201. doi: 10.3389/fphys.2020.00201

Due to a production error, there was a mistake in **Figure 1** as published. The wrong figure appeared. The corrected **Figure 1** appears below. The publisher apologizes for this mistake.

The original article has been updated.

Copyright © 2021 Frontiers Production Office. This is an open-access article distributed under the terms of the Creative Commons Attribution License (CC BY). The use, distribution or reproduction in other forums is permitted, provided the original author(s) and the copyright owner(s) are credited and that the original publication in this journal is cited, in accordance with accepted academic practice. No use, distribution or reproduction is permitted which does not comply with these terms.

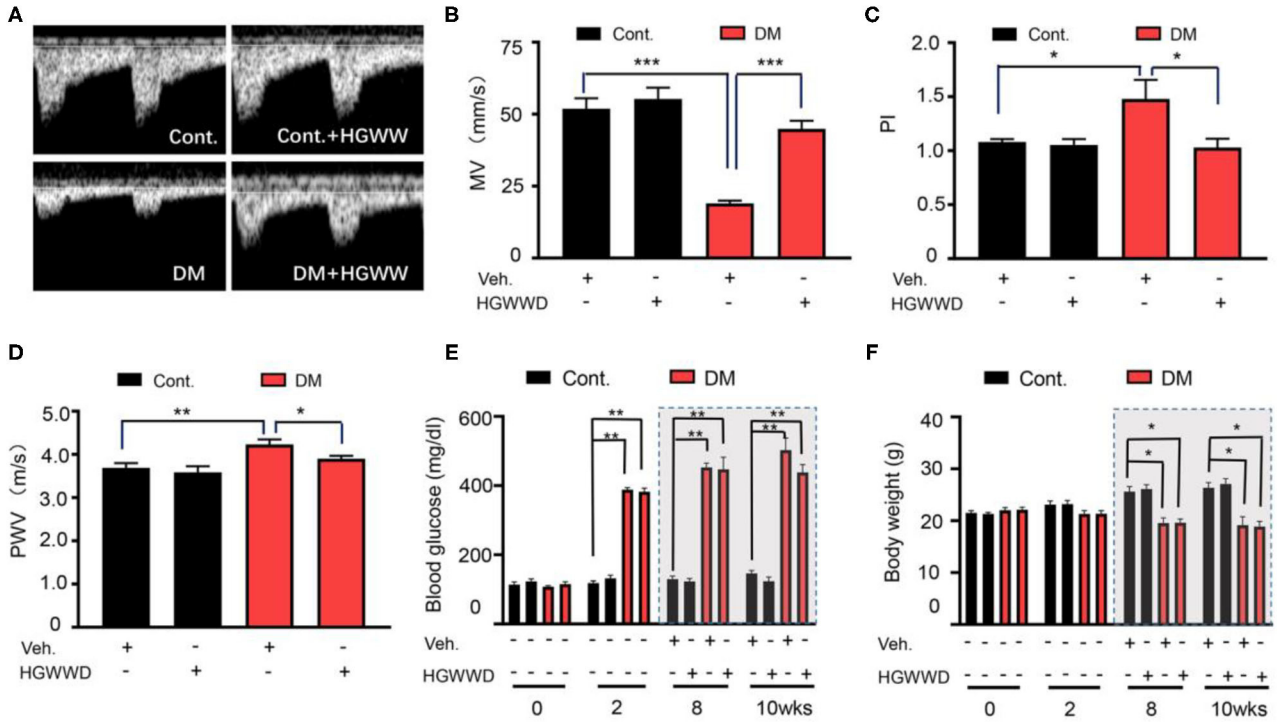


FIGURE 1 | HGWWD prevented the impairment of vascular system without altering blood glucose and body weight in STZ mice. **(A)** Representative images of Pulsed Doppler spectral waveform of left femoral arteries in mice. **(B–D)** The analysis of MV and PI of left femoral arteries and aortic PWV in mice by ultrasound. **(E)** Blood glucose level and **(F)** body weight at 0, 2nd, 8th, and 10th weeks of STZ injection with or without HGWWD treatment. MV, mean velocity; PI, pulsatility index; PWV, pulse wave velocity; STZ, streptozotocin; Cont., non-diabetic normal mice; DM, diabetic mice induced by STZ; HGWWD, *HuangqiGuizhiWuwu* Decoction. Values are presented as mean ± SEM, $^{*}P < 0.05$, $^{**}P < 0.01$, and $^{***}P < 0.001$, $n = 6$–8 mice/group.

frontiers in Pharmacology

ORIGINAL RESEARCH
published: 03 April 2020
doi: 10.3389/fphar.2020.00383

Zi Shen Huo Luo Formula Enhances the Therapeutic Effects of Angiotensin-Converting Enzyme Inhibitors on Hypertensive Left Ventricular Hypertrophy by Interfering With Aldosterone Breakthrough and Affecting Caveolin-1/Mineralocorticoid Receptor Colocalization and Downstream Extracellular Signal-Regulated Kinase Signaling

Xiaotong Song[1,2†], Yue Zhao[1†], Shijun Wang[1,2], Yuan Wang[1,2], Qian Chen[1,2], Haijun Zhao[1,2], Hua Wang[3], Sheng Tian[1,2], Huayun Yu[1,2] and Zhichun Wu[1,2*]*

[1] College of Traditional Chinese Medicine, Shandong University of Traditional Chinese Medicine, Jinan, China, [2] Shandong Co-innovation Center of Classic TCM Formula, Shandong Provincial Education Department, Jinan, China, [3] Department of Geriatric Medicine, Hospital Affiliated to Shandong University of Traditional Chinese Medicine, Jinan, China

Left ventricular hypertrophy (LVH) is an important characteristic of hypertensive heart disease. Renin-angiotensin system (RAS) blockers have been shown to be effective drugs for the reversal of LVH. Clinical and experimental studies have shown that Zi Shen Huo Luo Formula (ZSHLF) can improve the efficacy of perindopril in the treatment of hypertensive LVH, but its mechanism is unclear. This study aimed to investigate the possible mechanism to improve the efficacy of perindopril. First, we identified 23 compounds in ZSHLF by ultra performance liquid chromatography/tandem mass spectrometry (UPLC-MS/MS) analysis, among which ferulic acid, caffeic acid, vanillic acid, berberine, rutin, quercetin, kaempferol, stachydrine, and tiliroside have been reported to reduce blood pressure and exhibit cardioprotective effects. Second, we treated spontaneously hypertensive rats (SHRs) with perindopril and ZSHLF for 12 continuous weeks and found that chronic use of perindopril could increase the aldosterone (ALD) levels and cause aldosterone breakthrough (ABT). ZSHLF combined with perindopril reduced the ALD levels, interfered with ABT, decreased blood pressure, improved left ventricular diastolic dysfunction, and decreased the collagen volume fraction; these effects were superior to those of perindopril alone. In vitro experiments,

OPEN ACCESS

Edited by:
Jing-Yan Han,
Peking University, China

Reviewed by:
Bertram Pitt,
University of Michigan, United States
Tan Loh Teng Hern,
Guangdong University of Technology, China

***Correspondence:**
Huayun Yu
01000029@sdutcm.edu.cn
Zhichun Wu
wuzhichun@sdutcm.edu.cn

[†]These authors have contributed equally to this work

Specialty section:
This article was submitted to Ethnopharmacology, a section of the journal Frontiers in Pharmacology

Received: *07 January 2020*
Accepted: *12 March 2020*
Published: *03 April 2020*

Citation:
Song X, Zhao Y, Wang S, Wang Y, Chen Q, Zhao H, Wang H, Tian S, Yu H and Wu Z (2020) Zi Shen Huo Luo Formula Enhances the Therapeutic Effects of Angiotensin-Converting Enzyme Inhibitors on Hypertensive Left Ventricular Hypertrophy by Interfering With Aldosterone Breakthrough and Affecting Caveolin-1/Mineralocorticoid Receptor Colocalization and Downstream Extracellular Signal-Regulated Kinase Signaling. Front. Pharmacol. 11:383. doi: 10.3389/fphar.2020.00383

ALD-induced cardiomyocytes (H9c2 cells) and cardiac fibroblasts were treated with ZSHLF-containing serum, which suppressed ALD-induced cardiomyocyte hypertrophy and cardiac fibroblast proliferation, increased mineralocorticoid receptor (MR) and Cav-1 colocalization and decreased phosphorylated epidermal growth factor receptor (pEGFR) and phosphorylated extracellular signal-regulated kinase (pERK) protein expression the cells. In conclusion, ZSHLF can interfere with ABT and affect the pathological role of ALD by affecting MR and Cav-1 interactions and EGFR/ERK signaling pathway. These effects represent a possible mechanism by which ZSHLF improves the efficacy of angiotensin-converting enzyme inhibitors (ACEIs) in hypertensive LVH treatment. However, the major bioactive components or metabolites responsible for the effects and the implications of these findings in patients need further verification.

Keywords: hypertension, left ventricular hypertrophy, aldosterone breakthrough, Zi Shen Huo Luo formula, mineralocorticoid receptor, EGFR signaling pathway

INTRODUCTION

Left ventricular hypertrophy (LVH) is an important characteristic of hypertensive heart disease that mainly involves cardiomyocyte hypertrophy and fibrosis due to cardiac fibroblast proliferation. LVH is the inciting event of several adverse cardiovascular events, such as arrhythmia, heart failure, myocardial infarction, and even sudden death (Jekell et al., 2018; Slivnick and Lampert, 2019). Reversing hypertensive LVH and reducing the occurrence of cardiovascular complications and mortality are the focuses of clinical hypertension treatments (Xiong et al., 2013). Renin-angiotensin system (RAS) blockers, such as angiotensin-converting enzyme inhibitors (ACEIs) and angiotensin receptor blockers (ARBs), are applied clinically to manage pathological cardiac hypertrophy (Hellawell and Margulies, 2012). RAS blockers lower plasma aldosterone (ALD) levels at the beginning of treatment, but the ALD levels may return to or exceed the pretreatment values as the treatment time increases. This phenomenon is known as aldosterone breakthrough (ABT), and it may limit the beneficial effects of RAS blockers (Christ et al., 2004; Ubaid-Girioli et al., 2007). Furthermore, high ALD levels can cause pathological remodeling in the context of heart disease, fibrosis, and LVH (Takeda et al., 2000; Wynn, 2008; Chou et al., 2018), participating in the pathological progression of cardiovascular clinical events. ALD receptor antagonists, such as spironolactone and eplerenone, are commonly used in clinical practice. However, chronic use may cause adverse reactions (Toyonaga et al., 2011), limiting their application. Thus, strongly interfering with ABT and controlling the cardiac hypertrophy induced by elevated ALD are important strategies for improving the efficacy of RAS blockers and reducing the risk of cardiovascular risk events.

ALD-mediated fibrosis and detrimental cardiac remodeling are associated with mineralocorticoid receptor (MR) activation in the cardiovascular system; these events are mainly mediated by steroid receptors localized at the plasma membrane instead of by classic nuclear hormone receptors (Williams, 2013). There is evidence that the activation of ALD described above may involve interaction with caveolin-1 (Cav-1), which binds to MR and localizes to the cell membranes of cardiac cells, where it mediates intracellular events *via* cell surface receptors (Baudrand et al., 2014). Upon excessive ALD stimulation, MR is released from the membrane (Krug et al., 2011), after which it transactivates epidermal growth factor receptor (EGFR), activates MAPK and ERK1/2 (Ricchiuti et al., 2011; Dooley et al., 2012; Chen et al., 2013), and enters the nucleus to regulate the transcription of downstream signaling molecules and to promote cardiomyocyte hypertrophy and myocardial fibrosis (Navaneethan and Bravo, 2013).

Zi Shen Huo Luo Formula (ZSHLF), a traditional Chinese medicine (TCM) herbal formula, is composed of six crude drug materials. Previous studies have confirmed that ZSHLF combined with perindopril can improve the diastolic function of the left ventricle in spontaneously hypertensive rats (SHRs) and patients with hypertensive LVH (Wang and Gao, 2013; Yang et al., 2018). These results are consistent with the results of modern pharmacological studies reported in the literature, which indicate that herbal medicines in ZSHLF such as *Scrophularia ningpoensis* Hemsl., *Achyranthes bidentata* Bl., *Coptis chinensis* Franch., *Paeonia suffruticosa* Andr., *Leonurus japonicus* Houtt., and *Cinnamomum cassia* Presl. can lower blood pressure, inhibit cardiomyocyte hypertrophy and ventricular remodeling and have protective effects on the heart (Mhatre et al., 2009; Huang et al., 2012; Wojtyniak et al., 2013; Dan et al., 2016; Sobhani et al., 2017).

Although its effects are known, the chemical composition and pharmacological mechanism of ZSHLF are poorly understood. The present study aimed to identify the effects of ZSHLF treatment on ABT, the interaction between MR and Cav-1 in myocardial tissue and downstream EGFR signaling.

MATERIALS AND METHODS

Animals

Male 15-week-old SHRs (n=24, weighing 260–300 g), male 15-week-old Wistar-Kyoto (WKY) rats (n=8, weighing 280–320 g),

and male and female 6-week-old Sprague-Dawley (SD) rats (n=20, half male and half female, weighing 180–220 g) were provided by Vital River Laboratory Animal Technology Co., Ltd. (Beijing, China) and were maintained at the Animal Experimental Center of Shandong University of Traditional Chinese Medicine (Shandong, China). All rats were maintained in an environment with a controlled temperature (23–24 °C) and relative humidity (50–60%) and had free access to water and food. All experiments were conducted with the approval of the Institutional Animal Care and Use Committee and were in compliance with the Use and Care of Laboratory Animals guidelines.

Drug Materials

ZSHLF consists of six Chinese herbal medicines, including the dried roots of *Scrophularia ningpoensis* Hemsl. and *Achyranthes bidentata* Bl., the dried rhizome of *Coptis chinensis* Franch., the dried root cortex of *Paeonia suffruticosa* Andr., the dried aerial part of *Leonurus japonicus* Houtt., and the dried bark of *Cinnamomum cassia* Presl., at a fixed ratio of 20:15:12:12:20:3, respectively. These herbs were purchased from the Affiliated Hospital of Shandong University of Traditional Chinese Medicine (Shandong, China) and identified by Prof. H.Y. Liu. The details of the drug materials are given in **Supplementary Table 1**. The above drugs were macerated in eight volumes of distilled water for 60 min and decocted for 30 min. After filtration, the remaining drugs were added to six volumes of water and decocted for 20 min. The filtrates were mixed, concentrated to 8.2 g crude drug/ml and filtered through a 0.2 μm membrane. Perindopril (Servier Tianjin Pharmaceutical Co., Ltd., Tianjin, China) was dissolved in distilled water to make a suspension of 0.1 mg/ml before use and stored at 4 °C.

Preparation of ZSHLF-Containing Serum

Three days after adaptive breeding, the SD rats were randomly divided into blank control serum group and ZSHLF-containing serum group. The rats in the ZSHLF-containing serum group received ZSHLF intragastrically at a dose of 8.2 g/kg twice daily for 5 d. The rats in the blank control serum group were given equal volumes of normal saline (NS). The rats were starved for 12 h after the last administration of ZSHLF at a 1-day dosage. One hour after the last dose, blood was collected; the serum was separated, inactivated at 56 °C and filtered with a 0.22 μm membrane. The serum was frozen at −80 °C.

Chemical Composition Analysis of ZSHLF by UPLC-MS/MS

Ultra performance liquid chromatography/tandem mass spectrometry (UPLC-MS/MS) analysis was performed on a Thermo Fisher UltiMate 3000 RS [Thermo Fisher Scientific (China) Co., Ltd., China] system coupled to a Q-Exactive high-resolution mass spectrometer [Thermo Fisher Scientific (China) Co., Ltd., China]. Two microliters of sample solution was injected into a Thermo Hypersil GOLD column (100×2.1 mm, 1.9 μm). After optimizing the chromatographic conditions, the column temperature was adjusted to 35 °C, and the autosampler was conditioned at 10 °C. A 200 μl sample solution was injected into the system for analysis. The mobile phase consisted of 0.1% formic acid aqueous solution (A) and acetonitrile (B). A linear gradient elution was applied (0–5 min, 2–20% B; 5–10 min, 20–50% B; 10–15 min, 50–80% B; 15–25 min, 80–95% B; 25–30 min, 95–2% B) at a flow rate of 0.3 ml/min. Mass spectrometric detection was carried out with an electrospray ionization (ESI) interface set in positive or negative ionization mode.

Rat Grouping and Drug Administration

After 1 week of acclimation, 24 SHRs were randomly divided into three groups (n=8/group): SHR control group (SHR group), perindopril group (PEP group), combination of ZSHLF, and perindopril group (ZSHLF group). Eight WKY rats of the same age were used as the normal control group (WKY group). The ZSHLF group received 1 mg/kg/d perindopril in the morning and received 8.2 g/kg/d ZSHLF in the afternoon. The PEP group received the same dosage of perindopril in the morning and the same amount of NS in the afternoon. The SHR and WKY groups were orally fed the same volumes of NS twice daily. The rats were treated for 12 weeks.

Blood Pressure Measurement

After 0, 4, 8, and 12 weeks of treatment, the tail-cuff method was used to measure systolic blood pressure (SBP) and diastolic blood pressure (DBP) with a BP-2010A intelligent noninvasive blood pressure meter (Softron Beijing Biotechnology Co., Ltd., China). Each rat was placed in a heated tube (38 °C) for 10–15 min before measurement to raise its body temperature. Each group of rats was measured in parallel, and each rat was measured three times. The mean of the three readings was regarded as the value of that parameter for the animal.

Blood Collection and Serum ALD Detection

At weeks 0, 4, 8, and 12, rats were anesthetized with 4% isoflurane and maintained on 2% isoflurane, and blood samples were collected from the jugular vein. The blood samples were centrifuged at 3,500 r/min for 10 min to isolate serum. The serum ALD levels were measured with an enzyme-linked immunosorbent assay (ELISA).

Hemodynamic Recording and Tissue Specimens

After 12 weeks of treatment, rats were anesthetized by intraperitoneal injection of 7% chloral hydrate (3 ml/kg). A catheter connected to a pressure sensor was inserted into the right carotid artery and advanced into the left ventricle to measure hemodynamic parameters. After 5 min of stabilization, the left ventricular systolic pressure (LVSP), left ventricular end diastolic pressure (LVDP), and changes in the maximal rate of the pressure increase in the contract phase (+dp/dtmax) and the maximal rate of the pressure decrease in the diastole phase (−dp/dtmax) in the left ventricle were observed

and recorded with LabChart software. After hemodynamic recording, the myocardial tissues were cut from the apex and immediately washed with ice-cold phosphate buffer. The tissue samples were cut into two segments: one segment was immediately frozen in liquid nitrogen and stored at −80 °C until analysis, and the other segment was fixed in 4% paraformaldehyde (PFA) for Masson staining.

Masson Staining

The left ventricular apex tissues of rats were fixed with 4% PFA for 24 h, embedded in paraffin, and serially sliced to a thickness of 5 μm. The sections were stained with modified Masson's trichrome staining solution and observed under a light microscope. Image-Pro Plus 6.0 image analysis software was used to analyze and calculate the collagen volume fraction (CVF) with the following equation: CVF = (collagen area/total cardiac muscle area) ×100%.

Cell Culture and Treatment

The H9c2(2-1) cell line was purchased from the Cell Bank of Type Culture Collection of the Chinese Academy of Sciences (Shanghai, China), and the rat cardiac fibroblast (RCF) cell line was purchased from Procell Life Science & Technology Co., Ltd. (Wuhan, China). The H9c2 cells and RCFs were grown in DMEM (HyClone, USA) supplemented with 10% fetal bovine serum (FBS) and 1% penicillin/streptomycin in a humidified atmosphere of 5% CO_2 at 37°C. The cells were divided into the following groups: blank serum control group (BC group), model (ALD group), ALD+ZSHLF (ZSHLF group). The cells in the ZSHLF group were treated with various concentrations of ZSHLF-containing serum (5%, 10%, and 20%) for 2 h, while the cells in the BC group and ALD group were treated with 10% blank serum for 2 h. The cells in the ALD group and ZSHLF group were incubated with ALD for 30 min.

Cardiac Fibroblast Proliferation Assay

Cardiac fibroblast proliferation was analyzed using the Cell Counting Kit-8 (CCK-8) assay (CP002, Signalway Antibody, USA) according to the instructions. After RCFs were treated by different methods, the cells were resuspended in CCK-8 reagent and serum-free essential minimal medium at a volume ratio of 1:10. The cells were incubated for 1 h at 37°C in a 5% CO_2 incubator (ThermoForma3111). A microplate reader (MK3, Finnpipette) was used to measure the absorbance at 450 nm.

α-Actinin Immunofluorescence Labeling for Measurement of the Cell Surface Area

The surface areas of cardiomyocytes were measured by α-actinin immunofluorescence labeling. After treatment, H9c2 cells were washed with PBS, fixed in 4% PFA for 20 min and then blocked with goat serum for 1 h at room temperature. The H9c2 cells were then incubated with an anti-α-actinin antibody (1:60, AB50591, Abcam, UK) overnight at 4 °C. The cells were washed with PBS and incubated with secondary antibodies conjugated to FITC (bs-0346R-FITC, Beijing Solarbio Science & Technology Co., Ltd., Beijing, China) for 1 h in a dark, moist chamber. After washing three times with PBS, the cells were stained with DAPI (04002, Beijing Solarbio Science & Technology Co., Ltd., Beijing, China) for 10 min and examined under a fluorescence microscope (Olympus BX51). Then, the cells were observed and photographed under a 400× fluorescence microscope; five different fields of view were randomly selected for each group. The cell surface areas were analyzed using ImageJ software.

Immunofluorescence and Colocalization Analysis

After the cells were treated, fixed, and blocked with 10% goat serum, they were incubated overnight with an anti-MR antibody (1:60; rabbit polyclonal, AB64457, Abcam, UK) and an anti-Cav-1 antibody (1:60; mouse monoclonal, AB85491, Abcam, UK). The samples were then treated with FITC-conjugated anti-mouse IgG (1:500, ZF-0312-FITC, Zsbio, Beijing, China) and anti-rabbit IgG/RBITC (ZF-0316-RBITC, Zsbio, Beijing, China) secondary antibodies for 1 h at room temperature. The slides were observed and photographed under an Olympus IX73 fluorescence inverted microscope (IX73-DP80, Olympus Corporation, Tokyo, Japan). ImageJ software was used for colocalization analysis and indirect assessment of the sizes of the colocalized pixel areas with Pearson's correlation coefficient (Pearson's r) in each set of images.

Western Blot Analysis

Western blot analysis was performed on protein extracts of tissues and cells. The proteins were first resolved by 5% and 10% SDS-PAGE and electrotransferred onto PVDF membranes (Millipore, USA). After blocking, the membranes were incubated with primary antibodies overnight at 4 °C. The following primary antibodies were used: anti-EGFR antibody (1:1,200, rabbit monoclonal antibody, AB52894, Abcam, UK), anti-EGFR (phosphor Y1068) antibody (1:800, rabbit polyclonal antibody, AB5644, Abcam, UK), anti-ERK1+ERK2 antibody (1:1000, rabbit polyclonal antibody, AB17942, Abcam, UK), anti-phosphor-Erk1/2 (Thr202/Tyr204) antibody (1:600, rabbit monoclonal, 4370S, Cell Signaling Technology, Inc., USA), and anti-β-actin antibody (1:1000, rabbit polyclonal antibody, AB8227, Abcam, UK). Then, the membranes were incubated with a secondary antibody (1:3000, goat anti-rabbit Ig G, AB205718, Abcam, UK) at room temperature for 1 h before being incubated with an electrochemiluminescence reagent for 30 s to 2 min and exposed to Kodak film. The data are presented as the relative optical density (ROD, relative to β-actin) and were determined using ImageJ software.

Statistical Analysis

The Statistical Package for the Social Sciences (SPSS) 22.0 was used for statistical analysis. The data are expressed as the means ± standard deviations ($\bar{x} \pm s$). Statistical significance was determined by one-way ANOVA followed by Bonferroni's multiple comparison test. A value of $P < 0.05$ was considered to indicate statistical significance.

RESULTS

Identification of the Components of ZSHLF

UPLC-MS/MS analysis was utilized to reveal the chemical profile of ZSHLF and identify the components. Upon comparison of the MS data, 23 compounds were identified (1–23). These compounds accounted for most of the main peaks in the chromatogram and included different kinds of components, such as flavones (e.g., 12, 14, 18, and 19), phenolic acids (e.g., 11), triterpenoids (e.g., 6 and 21), and alkaloids (e.g., 4, 5, and 9) (**Figure 1** and **Table 1**).

ZSHLF Combined With Perindopril Effectively Lowered the Blood Pressure and Serum ALD Levels of SHRs

SBP and DBP were significantly higher in the SHR group than in the WKY group at each tested time point (**Supplementary Tables 2** and **3**, $P < 0.05$). Before treatment, no significant differences in SBP or DBP were found among the SHRs ($P > 0.05$). The SBP in each treatment group and the DBP in the ZSHLF group were lower than those in the SHR group at 4, 8, and 12 weeks ($P < 0.05$). Compared with that in the PEP group, the DBP in the ZSHLF group was lower at 4, 8, and 12 weeks ($P < 0.05$) (**Figures 2A, B**).

The serum ALD levels are shown in **Figure 2C**. Before and after treatment, the serum ALD levels in the SHR group were significantly higher than those in the WKY group (**Supplementary Table 4**, $P < 0.05$). Before treatment, no significant differences in serum ALD levels were found in the SHR group ($P > 0.05$). After 4 and 8 weeks of treatment, the serum ALD levels of the PEP and ZSHLF groups were significantly lower than those of the SHR group ($P < 0.05$). However, at 12 weeks, the serum ALD level of the PEP group was elevated nearly to the pretreatment value. The serum ALD level of the ZSHLF group remained low and was lower than those of the SHR and PEP groups ($P < 0.05$) (**Figure 2C**).

Effects of ZSHLF on Left Ventricular Diastolic Function in SHRs

As shown in **Figure 3**, compared with the WKY group, the other groups exhibited decreases in ± dp/dtmax and increases in LVDP (**Supplementary Table 5**, $P < 0.05$). No significant differences in LVSP, ± dp/dtmax, or LVDP were found between the PEP and SHR groups ($P > 0.05$). However, an obvious improvements in the hemodynamic parameters were observed in the ZSHLF group compared with the SHR group ($P < 0.05$). Furthermore, LVDP was significantly decreased and ± dp/dtmax was significantly increased in the ZSHLF group compared with the PEP group ($P < 0.05$).

ZSHLF Reduced Collagen Deposition and Inhibited the Progression of Myocardial Fibrosis in SHRs

As shown in **Figure 4**, Masson staining showed the presence of blue collagen fibers and red cardiomyocytes. In the WKY group, the myocardial fibers were neatly arranged, with few collagen fibers. In the SHR group, there was obvious myocardial fibrosis and significantly increased collagen composition. The cardiac CVF in the SHR group was significantly higher than that in the WKY group (**Supplementary Table 6**, $P < 0.05$). The CVF of the ZSHLF group was significantly lower than those of the SHR and PEP groups ($P < 0.05$).

ZSHLF-Containing Serum Inhibited ALD-Induced Cardiomyocyte Hypertrophy and Cardiac Fibroblast Proliferation

To investigate whether ZSHLF reduced cardiac hypertrophy caused by ALD *in vitro*, H9c2 cells were stimulated with ALD (10^{-9} mol/L). The cellular surface area was measured by α-actinin immunofluorescence staining, which showed that ALD-induced H9c2 cells were significantly enlarged (**Supplementary Table 7**, **Figure 5**). The cardiomyocytes

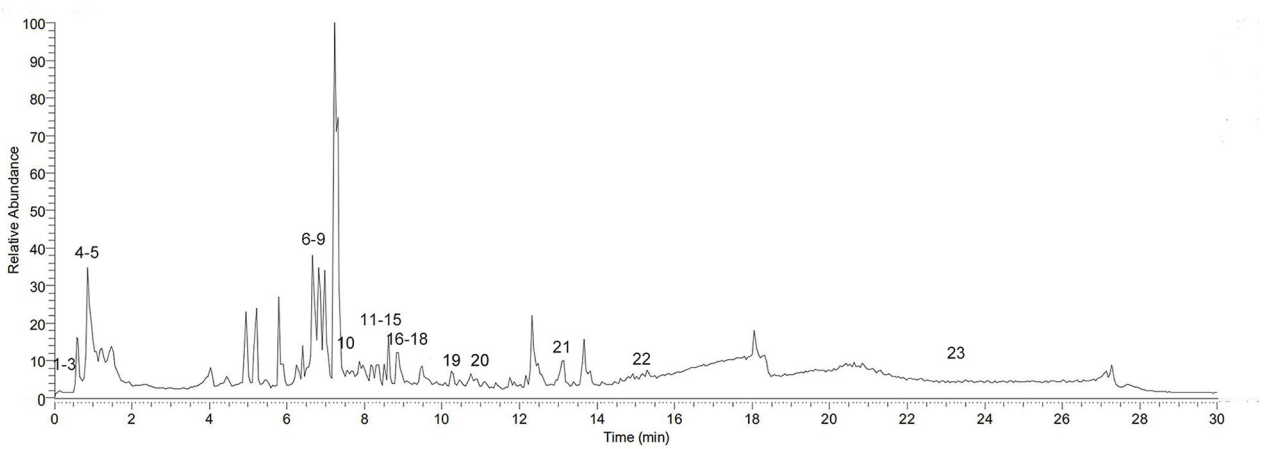


FIGURE 1 | Base peak ion (BPI) chromatogram of Zi Shen Huo Luo Formula (ZSHLF) in a positive ion flow diagram obtained by UPLC-MS/MS analysis.

TABLE 1 | Components of Zi Shen Huo Luo Formula (ZSHLF) identified by UPLC-MS/MS analysis.

Peak No.	t_R (min)	Measured $[M-H]^-$ (m/z)	Predicted $[M-H]^-$ (m/z)	△(ppm)	Formula	Identification	Derived from
1	0.23	278.1518	278.1517	0.3	$C_{16}H_{22}O_4$	Dibutyl phthalate	A
2	0.28	162.0681	162.0680	0.36	$C_{10}H_{10}O_2$	Methyl cinnamate	C
3	0.35	270.2559	270.2558	0.24	$C_{17}H_{34}O_2$	Methyl palmitate	A
4	0.85	117.0790	117.0792	−1.62	$C_5H_{11}O_2$	Betaine	A
5	0.89	143.0946	143.0945	0.96	$C_7H_{13}NO_2$	DL-Stachydrine	D
6	6.59	152.1201	152.1202	−0.90	$C_{10}H_{16}O$	D-(+)-Camphor	C
7	6.64	180.0423	180.0418	2.39	$C_9H_8O_4$	Caffeic acid	B
8	6.76	290.0790	290.0787	1.05	$C_{15}H_{14}O_6$	Catechin	F
9	6.78	335.1158	335.1148	2.85	$C_{20}H_{17}NO_4$	Berberine	E
10	7.60	152.0473	152.0474	−0.42	$C_8H_8O_3$	Vanillin	E
11	8.47	168.0423	168.0441	−11.02	$C_8H_8O_4$	Vanillic acid	B
12	8.52	302.0427	302.0425	0.65	$C_{15}H_{10}O_7$	Quercetin	A
13	8.52	464.0955	464.0953	0.31	$C_{21}H_{20}O_{12}$	Quercetin-β-D-glucoside	D
14	8.53	610.1534	610.1523	0.65	$C_{27}H_{30}O_{16}$	Rutin	A
15	8.65	194.0580	194.0580	−0.65	$C_{10}H_{10}O_4$	Ferulic acid	B
16	8.80	146.0368	146.0368	−0.04	$C_9H_6O_2$	Coumarin	C
17	8.93	220.1827	220.1826	0.70	$C_{15}H_{24}O$	(−)-Caryophyllene oxide	C
18	9.28	286.0477	286.0477	0.12	$C_{15}H_{10}O_6$	Kaempferol	A
19	10.41	188.1049	188.1035	7.5169	$C_9H_{16}O_4$	Azelaic acid	A, C
20	11.11	594.1373	594.1362	1.89	$C_{30}H_{26}O_{13}$	Tiliroside	D
21	13.18	270.0528	288.0629	1.42	$C_{15}H_{10}O_5$	Apigenin	D
22	15.19	278.1518	278.1517	0.36	$C_{16}H_{22}O_4$	Diisobutylphthalate	A
23	23.36	284.2715	284.2709	2.33	$C_{18}H_{36}O_2$	Stearic acid	A

A, root of Achyranthes bidentata Bl.; B, root of Scrophularia ningpoensis Hemsl.; C, bark of Cinnamomum cassia Presl.; D, aerial part of Leonurus japonicus Houtt.; E, rhizome of Coptis chinensis Franch.; and F, root cortex of Paeonia suffruticosa Andr.

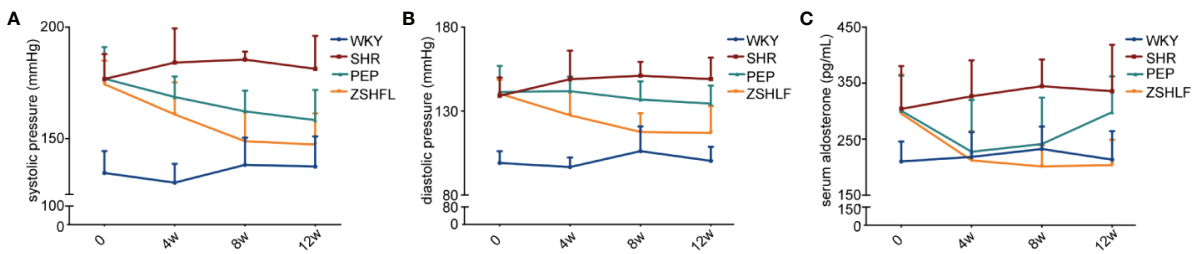


FIGURE 2 | Effect of Zi Shen Huo Luo Formula (ZSHLF) on blood pressure and serum aldosterone (ALD) levels in spontaneously hypertensive rat (SHRs). **(A)** Effect of ZSHLF on systolic pressure of rats in different groups at each time point. **(B)** Effect of ZSHLF on diastolic pressure in different groups at each time point. **(C)** Effect of ZSHLF on serum ALD levels in different groups at each time point. The data represent the mean ± standard deviation, $n = 8$.

surface area was significantly lower in the 10% and 20% ZSHLF groups than in the ALD group (**Figure 5B**, $P < 0.05$). There was no significant difference between the 10% and 20% ZSHLF groups ($P > 0.05$).

To investigate whether ZSHLF attenuates ALD-induced cardiac fibroblast proliferation *in vitro*, ALD was used to stimulate the proliferation of RCFs (10^{-7} mol/L). The cell viability of RCFs was assessed by CCK-8 assay after treatment. The results showed that cell viability was significantly higher in the ALD group than in the BC group (**Supplementary Table 7**, $P < 0.05$). After treatment with different concentrations of ZSHLF-containing serum, the cells in the ZSHLF serum-treated groups exhibited significantly lower viability than those in the ALD group ($P < 0.05$); furthermore, cell viability was lower in the 10% and 20% ZSHLF groups than in the 5% concentration group ($P < 0.05$). No significant differences were found between the 10% and 20% groups ($P > 0.05$).

Thus, ZSHLF-containing serum prevented ALD-induced cardiomyocyte hypertrophy and cardiac fibroblast proliferation. The 10% and 20% concentrations of medicated serum had good effects, and there was no significant difference between them. Therefore, the 10% concentration of medicated serum was selected for further study.

ZSHLF Increased Cav-1 and MR Colocalization in ALD-Induced H9c2 Cells and RCFs

To investigate the molecular mechanism by which ZSHLF affected ALD-induced cardiomyocyte hypertrophy and cardiac

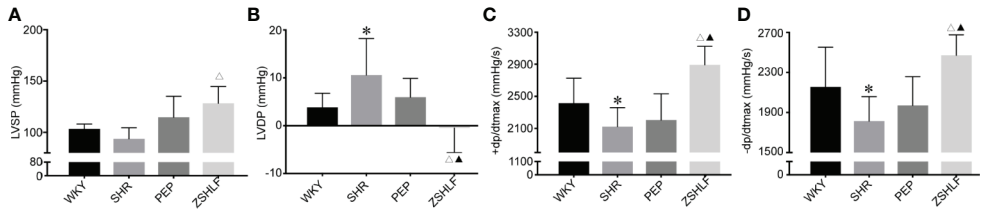


FIGURE 3 | Effects of Zi Shen Huo Luo Formula (ZSHLF) on hemodynamic parameters in spontaneously hypertensive rat (SHRs). **(A)** Left ventricular hypertrophy (LVSP) of each group. **(B)** Left ventricular end diastolic pressure (LVDP) of each group. **(C)** +dp/dtmax of each group. **(D)** –dp/dtmax of each group. The data represent the mean ± standard deviation, n=8. *P < 0.05 vs. the WKY group; △P < 0.05 vs. the SHR group; ▲P < 0.05 vs. the PEP group.

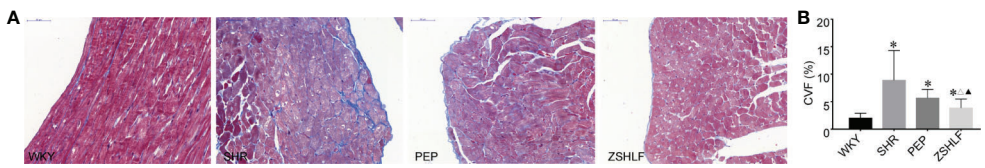


FIGURE 4 | Effects of Zi Shen Huo Luo Formula (ZSHLF) on the collagen fibers of spontaneously hypertensive rat (SHRs). **(A)** Effect of ZSHLF on Masson staining in each group. **(B)** Effect of ZSHLF on the CVF in each group. The data represent the mean ± standard deviation, n=3. *P < 0.05 vs. the WKY group; △P < 0.05 vs. the SHR group; ▲P < 0.05 vs. the PEP group.

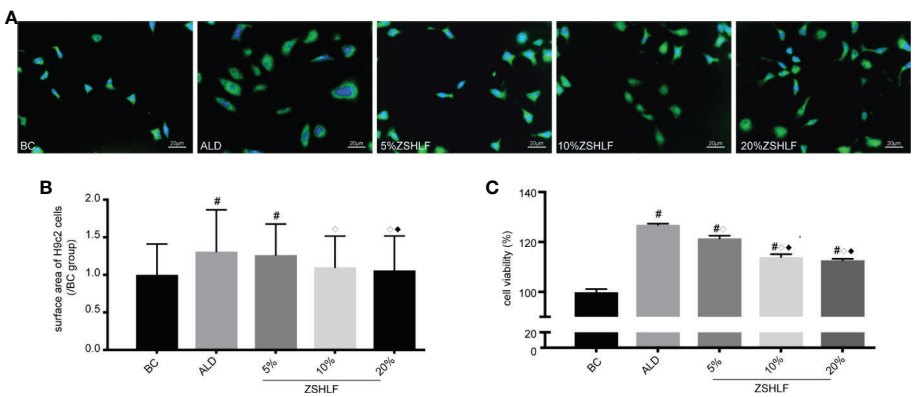


FIGURE 5 | Effects of various concentrations of Zi Shen Huo Luo Formula (ZSHLF)-containing serum on the sizes of H9c2 cells and the proliferation of rat cardiac fibroblasts (RCFs). **(A)** Immunofluorescence staining of α-actinin in cardiomyocytes in different groups at different concentrations. Immunofluorescence staining was observed at 400× magnification. **(B)** Effects of ZSHLF-containing serum on cardiomyocytes surface area (10–15 cells per field, 5 fields per group; the data represent the mean ± standard deviation). **(C)** Effects of ZSHLF-containing serum on the proliferation of cardiac fibroblasts (the data represent the mean ± standard deviation, n=3). #P < 0.05 vs. the BC group; ◇P < 0.05 vs. the ALD group; ◆P < 0.05 vs. the 5% ZSHLF group.

fibroblast proliferation, changes in Cav-1 and MR colocalization in H9c2 cells and RCFs were observed. As shown in **Figure 6**, ALD decreased Cav-1 and MR colocalization in H9c2 cells and RCFs. However, compared with ALD-induced cells, H9c2 cells pretreated with ZSHLF showed marked increases in Pearson's r for Cav-1 and MR colocalization (**Supplementary Table 8**, $P < 0.05$). Although Pearson's r of RCFs was higher than that of the ALD-induced cells, the difference was not significant ($P > 0.05$).

Effects of ZSHLF on the Protein Expression of EGFR and ERK in H9c2 Cells and RCFs

The western blot analysis results are shown in **Figure 7**; no significant differences in EGFR or ERK protein expression were found among the BC, ALD, and ZSHLF groups for H9c2 cells and RCFs (**Supplementary Tables 9** and **10**, $P > 0.05$). The protein expression levels of pEGFR and pERK in the two cell

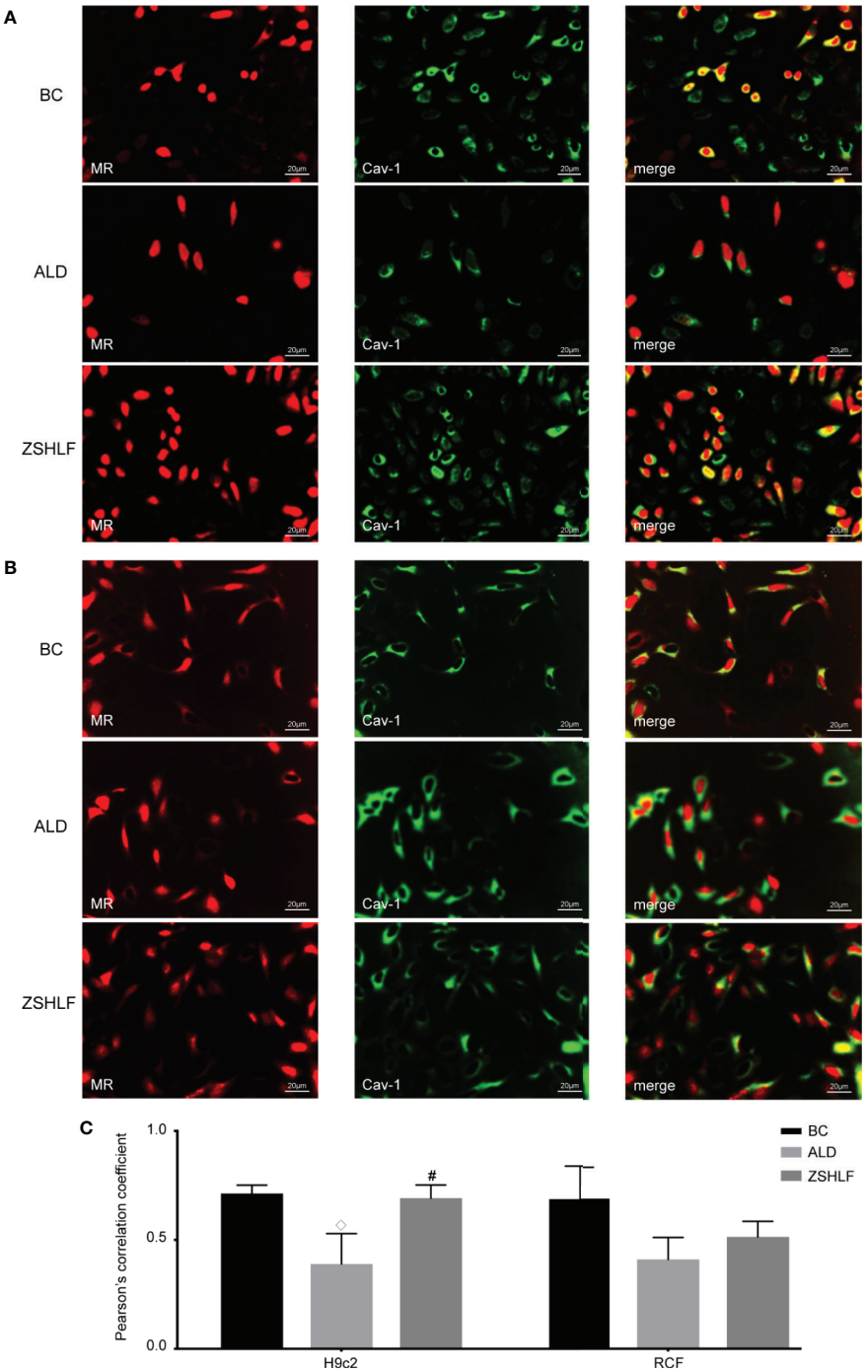


FIGURE 6 | Effects of Zi Shen Huo Luo Formula (ZSHLF) on caveolin-1 (Cav-1) and mineralocorticoid receptor (MR) colocalization in aldosterone (ALD)-induced H9c2 cells and rat cardiac fibroblasts (RCFs). **(A)** Immunofluorescence labeling of Cav-1 (green) and MR (red) in H9c2 cells. **(B)** Immunofluorescence labeling of Cav-1 (green) and MR (red) in RCFs. **(C)** Effect of ZSHLF on Pearson's r between Cav-1 and MR in H9c2 cells and RCFs. The data represent the mean ± standard deviation, n=3. $^{\#}P < 0.05$ vs. the BC group; $^{\diamond}P < 0.05$ vs. the ALD group.

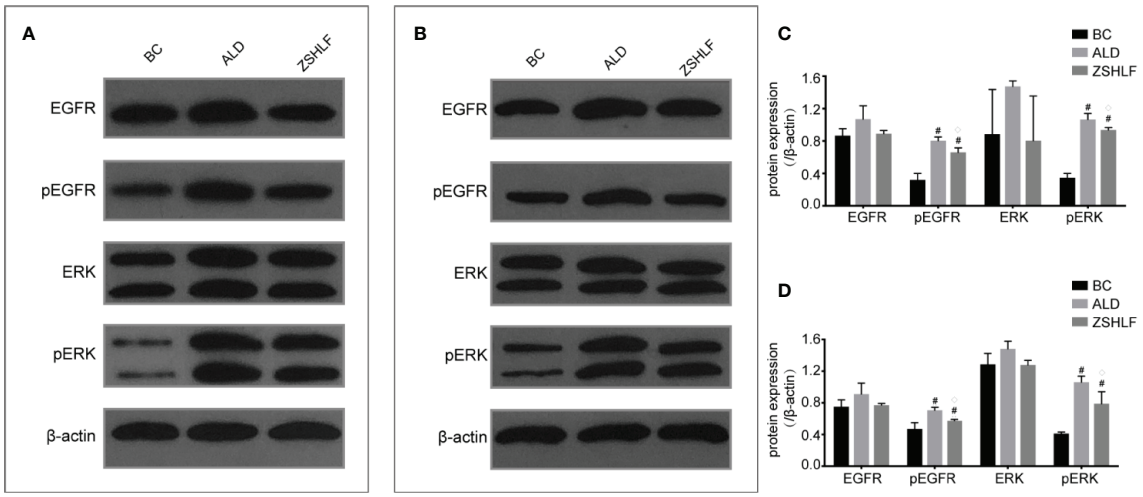


FIGURE 7 | Effects of Zi Shen Huo Luo Formula (ZSHLF) on the expression of EGFR, ERK, pEGFR, and pERK in H9c2 cells and rat cardiac fibroblasts (RCFs) in different groups as assessed by western blot analysis. **(A)** The protein expression of EGFR, pEGFR, ERK, and pERK in H9c2 cells was measured by western blot analysis. **(B)** The protein expression of EGFR, pEGFR, ERK, and pERK in RCFs was measured by western blot analysis. **(C)** Relative optical density (ROD) of EGFR, pEGFR, ERK, and pERK in H9c2 cells. **(D)** ROD of EGFR, pEGFR, ERK, and pERK in RCFs. The data represent the mean ± standard deviation, n=3. $^{\#}P < 0.05$ vs. the BC group; $^{\diamond}P < 0.05$ vs. the ALD group.

lines were significantly higher in the ALD and ZSHLF groups than in the BC group ($P < 0.05$). Furthermore, compared with ALD group, ZSHLF treatment inhibited pEGFR and pERK protein expression in the two cell lines ($P < 0.05$).

DISCUSSION

In this study, the chemical characteristics of the ZSHLF decoction were first characterized, and 23 compounds were identified by UPLC-MS/MS analysis. These findings, which can provide a basis for further screening of the active ingredients in ZSHLF. Then, the effects of ZSHLF with perindopril on ABT in the treatment of hypertensive LVH was investigated *in vivo*. All SHRs showed elevated serum ALD levels, myocardial diastolic dysfunction, and myocardial interstitial collagen fiber deposition. Perindopril reduced blood pressure and serum ALD levels, but the serum ALD levels rebounded after 12 weeks of treatment, representing the phenomenon was ABT; furthermore, perindopril could not effectively improve heart function or inhibit myocardial interstitial collagen fiber deposition. ZSHLF effectively controlled serum ALD levels, improved cardiac function and inhibited myocardial fibrosis, and the effects were better than those of perindopril alone. In vitro, ZSHLF-containing serum significantly inhibited ALD-induced cardiomyocyte hypertrophy and cardiac fibroblast proliferation. Taken together, our results suggest that ZSHLF can improve the efficacy of perindopril in the treatment of hypertensive LVH and that the effect may be related to interference with ABT and inhibition of ALD-induced pathological remodeling.

ZSHLF, a traditional Chinese compound formulated according to clinical experience, has been used clinically to treat hypertensive LVH for more than 10 years. Much evidence suggests that ZSHLF has many biological properties, including antihypertensive properties; for example, it improves hemorheology and cardiac function, and reverses LVH (Liu et al., 2013; Zhang et al., 2016; Lu et al., 2019; Mousavi et al., 2019; Yang and Lao, 2019).

We putatively identified 23 chemical compounds in ZSHLF by UPLC-MS/MS analysis. Among them, ferulic acid, caffeic acid and vanillic acid were identified to be derived from *Scrophulariae Radix*. These compounds have been reported to reduce blood pressure, improve cardiovascular structure and left ventricular function (Alam et al., 2013; Kumar et al., 2014) and exert cardioprotective effects (Agunloye et al., 2019). Berberine was found to be derived from *Coptidis Rhizoma*, which can effectively improve ventricular ejection fraction and heart function (Feng et al., 2019). Oleanolic acid, rutin, quercetin, and kaempferol were identified to have arisen from *Achyranthis Bidentatae Radix*. These compounds have been reported to have antihypertensive properties (Kaur and Muthuraman, 2016; Madlala et al., 2016; Marunaka et al., 2017) that inhibit cardiac hypertrophy and delay heart remodeling (Liao et al., 2015; Du et al., 2019). Both quercetin and rutin exhibit cardioprotective effects against isoprenaline-induced cardiac fibrosis in rats, and the mechanism may be related to inhibition of the RAS

(Li et al., 2013). Stachydrine and tiliroside were identified to originate from *Leonuri Herba*. These compounds have been reported to have antihypertensive properties (Silva et al., 2013) that improve cardiac hypertrophy and myocardial fibrosis (Zhao et al., 2017). Catechin was found to come from *Moutan Cortex*, which has antihypertensive properties that inhibit angiotensin-converting enzyme (He, 2017). In summary, previous studies have confirmed that the main active constituents of ZSHLF may play roles as antihypertensive, anti-myocardial fibrosis, and cardioprotective agents and may be part of the material basis for ZSHLF function. These finding also provide guidance for our subsequent definitive constituent analysis.

Experimental and clinical evidence indicates that protracted exposure to inappropriately elevated ALD levels causes significant changes in left ventricular structure and function (Catena et al., 2015). Although the use of ACEIs and ARBs may initially decrease plasma ALD levels, chronic therapy with these drugs may lead to ABT, in which ALD levels return to or exceed the baseline levels (Struthers and MacDonald, 2004). ABT is an important phenomenon in hypertensive patients treated with ACEIs or ARBs (Soberman and Weber, 2000). Excessive secretion of ALD for long periods of time is related to pathological remodeling of myocardial tissue (Young et al., 1994; Gilbert and Brown, 2010). Therefore, ALD blockade may have added value for factors other than blood pressure in the treatment of hypertension (Hargovan and Ferro, 2014). The results of this study showed that in the PEP group, serum ALD levels tended to decrease in the early phase of treatment but increased to levels near the pretreatment values later in treatment. The serum ALD levels in the ZSHLF group remained low and were lower than those in the SHR and PEP groups. These findings suggested that the ABT phenomenon occurred during the course of perindopril treatment and that ZSHLF could effectively limit the occurrence of ABT.

It has been conclusively shown that activation of MR in the cardiovascular system promotes tissue fibrosis and has negative consequences for cardiac function following cardiac events (Young and Rickard, 2015). Classically, MR belongs to the steroid receptor superfamily, and MR effects are ascribed to ligand-receptor binding and activation of gene transcription. However, MR effects may explain the association of ALD with detrimental myocardial remodeling; ALD activation is mainly mediated by steroid receptors localized at the plasma membrane instead of by classic nuclear hormone receptor interactions (Williams, 2013). Cav-1 is an important landmark structural protein of caveolae that binds to MR and restricts its translocation and EGFR transactivation, thereby negatively regulating EGFR signaling. Inappropriate ALD levels cause direct adverse effects *via* MR actions initiated in caveolae and lead to activation of protein kinase signaling cascades (Baudrand et al., 2014). Under high-level ALD stimulation, MR is released from the cell membrane, after which it transactivates EGFR, activates the MAPK/ERK signaling pathway through c-Src, and promotes cardiomyocyte hypertrophy and fibrosis (Krug et al., 2011; Dooley et al., 2012). MR activation on the cell membrane extends the pathological features of ALD and may be an essential way to promote cardiomyocyte hypertrophy and myocardial fibrosis (Krug et al., 2011; Bienvenu et al., 2012). The results of this study showed that ALD increased the surface areas of myocardial cells, promoted the proliferation of cardiac fibroblasts, reduced Cav-1 and MR colocalization in two cell lines, and upregulated the expression of pEGFR and pERK. ALD did not affect EGFR or ERK protein expression, suggesting that ALD-induced cardiomyocyte hypertrophy and cardiac fibroblast proliferation were associated with inhibition of the binding between Cav-1 and MR, as well as promoting EGFR phosphorylation activation. ZSHLF-containing serum increased Cav-1 and MR colocalization on the cell membranes of cardiomyocytes and reduced the protein expression of pEGFR and pERK. These effects represent a possible mechanism for the inhibition of myocardial hypertrophy and fibrosis induced by ALD.

We have also summarized existing problems and future study directions. Although we analyzed the original forms of the drug-derived components of the ZSHLF decoction and medicated serum, the specific biological components or metabolites were not determined. The literature has also confirmed the antihypertensive and antifibrotic effects of the medicinal components. It is not clear which component or combination of components is responsible for reducing ABT; the issue needs further clarification. Our study found that ZSHLF can effectively control ALD levels, but aldosterone release is regulated in various ways, and whether other mechanisms participate in the observed effects should be further studied. In addition, this study involved investigation and validation only in experimental studies; observation of and research on related clinical patients have not yet been performed. We plan to conduct further research on potential applications in patients.

CONCLUSIONS

In summary, the current findings suggest that ZSHLF could interfere with ABT and suppress ALD-induced cardiomyocyte hypertrophy and cardiac fibroblast proliferation by affecting MR and Cav-1 colocalization and the downstream EGFR signaling pathway. These effects may represent one of the mechanisms by which ZSHLF improves the efficacy of ACEIs in reversing hypertensive LVH.

DATA AVAILABILITY STATEMENT

All datasets generated for this study are included in the article/ **Supplementary Material**.

ETHICS STATEMENT

The animal study was reviewed and approved by Welfare Ethics Committee of Experimental Animals of Shandong University of Traditional Chinese Medicine.

AUTHOR CONTRIBUTIONS

ZW and HY conceived and designed the experiments. XS wrote the manuscript. YZ and QC participated in the animal experiments. HY and HW participated in the cell experiments. SW, YW, and HZ helped perform the analyses with constructive discussions. ST carried out the statistical analyses. All authors have read and approved the manuscript.

FUNDING

This work was supported by the National Natural Science Foundation of China (No. 81503539).

SUPPLEMENTARY MATERIAL

The Supplementary Material for this article can be found online at: https://www.frontiersin.org/articles/10.3389/fphar.2020.00383/full#supplementary-material

REFERENCES

Agunloye, O. M., Oboh, G., Ademiluyi, A. O., Ademosun, A. O., Akindahunsi, A. A., Oyagbemi, A. A., et al. (2019). Cardio-protective and antioxidant properties of caffeic acid and chlorogenic acid: Mechanistic role of angiotensin converting enzyme, cholinesterase and arginase activities in cyclosporine induced hypertensive rats. *BioMed. Pharmacother.* 109, 450–458. doi: 10.1016/j.biopha.2018.10.044

Alam, M. A., Sernia, C., and Brown, L. (2013). Ferulic acid improves cardiovascular and kidney structure and function in hypertensive rats. *J. Cardiovasc. Pharmacol.* 61 (3), 240–249. doi: 10.1097/FJC.0b013e31827cb600

Baudrand, R., Pojoga, L. H., Romero, J. R., and Williams, G. H. (2014). Aldosterone's mechanism of action: roles of lysine-specific demethylase 1, caveolin and striatin. *Curr. Opin. Nephrol. Hypertens.* 23 (1), 32–37. doi: 10.1097/01.mnh.0000436543.48391.e0

Bienvenu, L. A., Morgan, J., Rickard, A. J., Tesch, G. H., Cranston, G. A., Fletcher, E. K., et al. (2012). Macrophage mineralocorticoid receptor signaling plays a key role in aldosterone-independent cardiac fibrosis. *Endocrinology* 153 (7), 3416–3425. doi: 10.1210/en.2011-2098

Catena, C., Colussi, G., Brosolo, G., Novello, M., and Sechi, L. A. (2015). Aldosterone and Left Ventricular Remodeling. *Horm. Metab. Res.* 47 (13), 981–986. doi: 10.1055/s-0035-1565055

Chen, D., Chen, Z., Park, C., Centrella, M., McCarthy, T., Chen, L., et al. (2013). Aldosterone stimulates fibronectin synthesis in renal fibroblasts through mineralocorticoid receptor-dependent and independent mechanisms. *Gene* 531 (1), 23–30. doi: 10.1016/j.gene.2013.08.047

Chou, C. H., Hung, C. S., Liao, C. W., Wei, L. H., Chen, C. W., Shun, C. T., et al. (2018). IL-6 trans-signalling contributes to aldosterone-induced cardiac fibrosis. *Cardiovasc. Res.* 114 (5), 690–702. doi: 10.1093/cvr/cvy013

Christ, M., Grimm, W., and Maisch, B. (2004). [Significance of aldosterone antagonist therapy]. *Internist (Berl)* 45 (3), 347–354. doi: 10.1007/s00108-003-1087-1

Dan, H., Zhang, L., Qin, X., Peng, X., Wong, M., Tan, X., et al. (2016). Moutan cortex extract exerts protective effects in a rat model of cardiac ischemia/reperfusion. *Can. J. Physiol. Pharmacol.* 94 (3), 245–250. doi: 10.1139/cjpp-2015-0168

Dooley, R., Harvey, B. J., and Thomas, W. (2012). Non-genomic actions of aldosterone: from receptors and signals to membrane targets. *Mol. Cell Endocrinol.* 350 (2), 223–234. doi: 10.1016/j.mce.2011.07.019

Du, Y., Han, J., Zhang, H., Xu, J., Jiang, L., and Ge, W. (2019). Kaempferol Prevents Against Ang II-induced Cardiac Remodeling Through Attenuating Ang II-induced Inflammation and Oxidative Stress. *J. Cardiovasc. Pharmacol.* 74 (4), 326–335. doi: 10.1097/fjc.0000000000000713

Feng, X., Sureda, A., Jafari, S., Memariani, Z., Tewari, D., Annunziata, G., et al. (2019). Berberine in Cardiovascular and Metabolic Diseases: From Mechanisms to Therapeutics. *Theranostics* 9 (7), 1923–1951. doi: 10.7150/thno.30787

Gilbert, K. C., and Brown, N. J. (2010). Aldosterone and inflammation. *Curr. Opin. Endocrinol. Diabetes Obes* 17 (3), 199–204. doi: 10.1097/med.0b013e3283391989

Hargovan, M., and Ferro, A. (2014). Aldosterone synthase inhibitors in hypertension: current status and future possibilities. *JRSM Cardiovasc. Dis.* 3. doi: 10.1177/2048004014522440

He, J. (2017). Bioactivity-Guided Fractionation of Pine Needle Reveals Catechin as an Anti-hypertension Agent via Inhibiting Angiotensin-Converting Enzyme. *Sci. Rep.* 7 (1), 8867. doi: 10.1038/s41598-017-07748-x

Hellawell, J. L., and Margulies, K. B. (2012). Myocardial reverse remodeling. *Cardiovasc. Ther.* 30 (3), 172–181. doi: 10.1111/j.1755-5922.2010.00247.x

Huang, X. Y., Chen, C. X., Zhang, X. M., Liu, Y., Wu, X. M., and Li, Y. M. (2012). Effects of ethanolic extract from Radix Scrophulariae on ventricular remodeling in rats. *Phytomedicine* 19 (3-4), 193–205. doi: 10.1016/j.phymed.2011.09.079

Jekell, A., Nilsson, P. M., and Kahan, T. (2018). Treatment of Hypertensive Left Ventricular Hypertrophy. *Curr. Pharm. Des.* 24 (37), 4391–4396. doi: 10.2174/1381612825666181203092918

Kaur, S., and Muthuraman, A. (2016). Therapeutic evaluation of rutin in two-kidney one-clip model of renovascular hypertension in rat. *Life Sci.* 150, 89–94. doi: 10.1016/j.lfs.2016.02.080

Krug, A. W., Pojoga, L. H., Williams, G. H., and Adler, G. K. (2011). Cell membrane-associated mineralocorticoid receptors? New evidence. *Hypertension* 57 (6), 1019–1025. doi: 10.1161/hypertensionaha.110.159459

Kumar, S., Prahalathan, P., and Raja, B. (2014). Vanillic acid: a potential inhibitor of cardiac and aortic wall remodeling in l-NAME induced hypertension through upregulation of endothelial nitric oxide synthase. *Environ. Toxicol. Pharmacol.* 38 (2), 643–652. doi: 10.1016/j.etap.2014.07.011

Li, M., Jiang, Y., Jing, W., Sun, B., Miao, C., and Ren, L. (2013). Quercetin provides greater cardioprotective effect than its glycoside derivative rutin on isoproterenol-induced cardiac fibrosis in the rat. *Can. J. Physiol. Pharmacol.* 91 (11), 951–959. doi: 10.1139/cjpp-2012-0432

Liao, H. H., Zhang, N., Feng, H., Zhang, N., Ma, Z. G., Yang, Z., et al. (2015). Oleanolic acid alleviated pressure overload-induced cardiac remodeling. *Mol. Cell Biochem.* 409 (1-2), 145–154. doi: 10.1007/s11010-015-2520-1

Liu, X. H., Pan, L. L., Deng, H. Y., Xiong, Q. H., Wu, D., Huang, G. Y., et al. (2013). Leonurine (SCM-198) attenuates myocardial fibrotic response via inhibition of NADPH oxidase 4. *Free Radic. Biol. Med.* 54, 93–104. doi: 10.1016/j.freeradbiomed.2012.10.555

Lu, Y., Deng, Y., Liu, W., Jiang, M., and Bai, G. (2019). Searching for calcium antagonists for hypertension disease therapy from Moutan Cortex, using bioactivity integrated UHPLC-QTOF-MS. *Phytochem. Anal.* 30 (4), 456–463. doi: 10.1002/pca.2828

Madlala, H. P., Metzinger, T., van Heerden, F. R., Musabayane, C. T., Mubagwa, K., and Dessy, C. (2016). Vascular Endothelium-Dependent and Independent Actions of Oleanolic Acid and Its Synthetic Oleanane Derivatives as Possible Mechanisms for Hypotensive Effects. *PloS One* 11 (1), e0147395. doi: 10.1371/journal.pone.0147395

Marunaka, Y., Marunaka, R., Sun, H., Yamamoto, T., Kanamura, N., Inui, T., et al. (2017). Actions of Quercetin, a Polyphenol, on Blood Pressure. *Molecules* 22 (2), 209–. doi: 10.3390/molecules22020209

Mhatre, M., Tilak-Jain, J., De, S., and Devasagayam, T. P. (2009). Evaluation of the antioxidant activity of non-transformed and transformed pineapple: a comparative study. *Food Chem. Toxicol.* 47 (11), 2696–2702. doi: 10.1016/j.fct.2009.06.031

Mousavi, S. M., Karimi, E., Hajishafiee, M., Milajerdi, A., Amini, M. R., and Esmaillzadeh, A. (2019). Anti-hypertensive effects of cinnamon supplementation

in adults: A systematic review and dose-response Meta-analysis of randomized controlled trials. *Crit. Rev. Food Sci. Nutr.*, 1–11. doi: 10.1080/10408398.2019.1678012

Navaneethan, S. D., and Bravo, E. L. (2013). Aldosterone breakthrough during angiotensin receptor blocker use: more questions than answers? *Clin. J. Am. Soc. Nephrol.* 8 (10), 1637–1639. doi: 10.2215/cjn.07370713

Ricchiuti, V., Lapointe, N., Pojoga, L., Yao, T., Tran, L., Williams, G. H., et al. (2011). Dietary sodium intake regulates angiotensin II type 1, mineralocorticoid receptor, and associated signaling proteins in heart. *J. Endocrinol.* 211 (1), 47–54. doi: 10.1530/joe-10-0458

Silva, G. C., Pereira, A. C., Rezende, B. A., da Silva, J. P., Cruz, J. S., de Souza Mde, F., et al. (2013). Mechanism of the antihypertensive and vasorelaxant effects of the flavonoid tiliroside in resistance arteries. *Plant Med.* 79 (12), 1003–1008. doi: 10.1055/s-0032-1328765

Slivnick, J., and Lampert, B. C. (2019). Hypertension and Heart Failure. *Heart Fail Clin.* 15 (4), 531–541. doi: 10.1016/j.hfc.2019.06.007

Soberman, J. E., and Weber, K. T. (2000). Spironolactone in congestive heart failure. *Curr. Hypertens. Rep.* 2 (5), 451–456. doi: 10.1007/s11906-000-0027-x

Sobhani, Z., Nami, S. R., Emami, S. A., Sahebkar, A., and Javadi, B. (2017). Medicinal Plants Targeting Cardiovascular Diseases in View of Avicenna. *Curr. Pharm. Des.* 23 (17), 2428–2443. doi: 10.2174/1381612823666170215104101

Struthers, A. D., and MacDonald, T. M. (2004). Review of aldosterone- and angiotensin II-induced target organ damage and prevention. *Cardiovasc. Res.* 61 (4), 663–670. doi: 10.1016/j.cardiores.2003.11.037

Takeda, Y., Yoneda, T., Demura, M., Miyamori, I., and Mabuchi, H. (2000). Sodium-induced cardiac aldosterone synthesis causes cardiac hypertrophy. *Endocrinology* 141 (5), 1901–1904. doi: 10.1210/endo.141.5.7529

Toyonaga, J., Tsuruya, K., Ikeda, H., Noguchi, H., Yotsueda, H., Fujisaki, K., et al. (2011). Spironolactone inhibits hyperglycemia-induced podocyte injury by attenuating ROS production. *Nephrol. Dial Transplant.* 26 (8), 2475–2484. doi: 10.1093/ndt/gfq750

Ubaid-Girioli, S., Ferreira-Melo, S. E., Souza, L. A., Nogueira, E. A., Yugar-Toledo, J. C., Coca, A., et al. (2007). Aldosterone escape with diuretic or angiotensin-converting enzyme inhibitor/angiotensin II receptor blocker combination therapy in patients with mild to moderate hypertension. *J. Clin. Hypertens. (Greenwich)* 9 (10), 770–774. doi: 10.1111/j.1751-7176.2007.tb00091.x

Wang, H., and Gao, H. (2013). Clinical Study of Zishen Huoluo Decoction on Left Ventricular Hypertrophy in Hypertension. *Lishizhen Med. Mater Med. Res.* 24 (10), 2435–2436. doi: 10.3969/j.issn.1008-0805.2013.10.052

Williams, J. S. (2013). Evolving research in nongenomic actions of aldosterone. *Curr. Opin. Endocrinol. Diabetes Obes* 20 (3), 198–203. doi: 10.1097/MED.0b013e328360c200

Wojtyniak, K., Szymanski, M., and Matlawska, I. (2013). Leonurus cardiaca L. (motherwort): a review of its phytochemistry and pharmacology. *Phytother. Res.* 27 (8), 1115–1120. doi: 10.1002/ptr.4850

Wynn, T. A. (2008). Cellular and molecular mechanisms of fibrosis. *J. Pathol.* 214 (2), 199–210. doi: 10.1002/path.2277

Xiong, X., Yang, X., Liu, Y., Zhang, Y., Wang, P., and Wang, J. (2013). Chinese herbal formulas for treating hypertension in traditional Chinese medicine: perspective of modern science. *Hypertens. Res.* 36 (7), 570–579. doi: 10.1038/hr.2013.18

Yang, M., and Lao, L. (2019). Emerging Applications of Metabolomics in Traditional Chinese Medicine Treating Hypertension: Biomarkers, Pathways and More. *Front. Pharmacol.* 10, 158. doi: 10.3389/fphar.2019.00158

Yang, P., Yang, F., Zhao, Y., Shao, Z., Wang, M. J., Li, Y. X., et al. (2018). Effect of Zishen Huoluo Formular combined with perindopril on left ventricular hypertrophy in spontaneously hypertensive rats. *Chin. J. Gerontol* 38 (07), 1675–1678.

Young, M. J., and Rickard, A. J. (2015). Mineralocorticoid receptors in the heart: lessons from cell-selective transgenic animals. *J. Endocrinol.* 224 (1), R1–13. doi: 10.1530/joe-14-0471

Young, M., Fullerton, M., Dilley, R., and Funder, J. (1994). Mineralocorticoids, hypertension, and cardiac fibrosis. *J. Clin. Invest.* 93 (6), 2578–2583. doi: 10.1172/jci117269

Zhang, C. C., Gu, W. L., Wu, X. M., Li, Y. M., Chen, C. X., and Huang, X. Y. (2016). Active components from Radix Scrophulariae inhibits the ventricular remodeling induced by hypertension in rats. *Springerplus* 5, 358. doi: 10.1186/s40064-016-1985-z

Zhao, L., Wu, D., Sang, M., Xu, Y., Liu, Z., and Wu, Q. (2017). Stachydrine ameliorates isoproterenol-induced cardiac hypertrophy and fibrosis by suppressing inflammation and oxidative stress through inhibiting NF-kappaB and JAK/STAT signaling pathways in rats. *Int. Immunopharmacol* 48, 102–109. doi: 10.1016/j.intimp.2017.05.002

Conflict of Interest: The authors declare that the research was conducted in the absence of any commercial or financial relationships that could be construed as a potential conflict of interest.

Copyright © 2020 Song, Zhao, Wang, Wang, Chen, Zhao, Wang, Tian, Yu and Wu. This is an open-access article distributed under the terms of the Creative Commons Attribution License (CC BY). The use, distribution or reproduction in other forums is permitted, provided the original author(s) and the copyright owner(s) are credited and that the original publication in this journal is cited, in accordance with accepted academic practice. No use, distribution or reproduction is permitted which does not comply with these terms.

frontiers in Pharmacology

ORIGINAL RESEARCH
published: 21 April 2020
doi: 10.3389/fphar.2020.00458

Danqi Pill Protects Against Heart Failure Post-Acute Myocardial Infarction *via* HIF-1α/PGC-1α Mediated Glucose Metabolism Pathway

Qian Zhang[1†], Dongqing Guo[2†], Yuanyuan Wang[1†], Xiaoping Wang[2], Qiyan Wang[2], Yan Wu[3], Chun Li[4], Wei Wang[1*] and Yong Wang[1,2*]*

[1] School of Chinese Medicine, Beijing University of Chinese Medicine, Beijing, China, [2] The School of Life Sciences, Beijing University of Chinese Medicine, Beijing, China, [3] Institute of Chinese Medicine, Beijing University of Chinese Medicine, Beijing, China, [4] Modern Research Center for Traditional Chinese Medicine, Beijing University of Chinese Medicine, Beijing, China

OPEN ACCESS

Edited by:
Jing-Yan Han,
Peking University, China

Reviewed by:
Tan Loh Teng Hern,
Guangdong University of Technology, China
Jinming Zhang,
Chengdu University of Traditional Chinese Medicine, China

***Correspondence:**
Chun Li
lichun19850204@163.com
Wei Wang
wangwei26960@126.com
Yong Wang
doctor_wangyong@163.com

†These authors have contributed equally to this work

Specialty section:
This article was submitted to Ethnopharmacology, a section of the journal Frontiers in Pharmacology

Received: 15 December 2019
Accepted: 24 March 2020
Published: 21 April 2020

Citation:
Zhang Q, Guo D, Wang Y, Wang X, Wang Q, Wu Y, Li C, Wang W and Wang Y (2020) Danqi Pill Protects Against Heart Failure Post-Acute Myocardial Infarction via HIF-1α/PGC-1α Mediated Glucose Metabolism Pathway. Front. Pharmacol. 11:458. doi: 10.3389/fphar.2020.00458

Aim: Heart failure (HF) post-acute myocardial infarction (AMI) leads to a large number of hospitalizations and deaths worldwide. Danqi pill (DQP) is included in the 2015 national pharmacopoeia and widely applied in the treatment of HF in clinics in China. We examined whether DQP acted on glucose metabolism to protect against HF post-AMI *via* hypoxia inducible factor-1 alpha (HIF-1α)/peroxisome proliferator-activated receptor α co-activator (PGC-1α) pathway.

Methods and Results: In this study, left anterior descending (LAD) artery ligation induced HF post-AMI rats and oxygen-glucose deprivation-reperfusion (OGD/R)-induced H9C2 cell model were structured to explore the efficacy and mechanism of DQP. Here we showed that DQP protected the heart against ischemic damage as evidenced by improved cardiac functions and attenuated inflammatory infiltration. The expressions of critical proteins involved in glucose intake and transportation such as GLUT4 and PKM2 were up-regulated, while negative regulatory proteins involved in oxidative phosphorylation were attenuated in the treatment of DQP. Moreover, DQP up-regulated NRF1 and TFAM, promoted mitochondrial biogenesis and increased myocardial adenosine triphosphate (ATP) level. The protection effects of DQP were significantly compromised by HIF-1α siRNA, suggesting that HIF-1α signaling pathway was the potential target of DQP on HF post-AMI.

Conclusions: DQP exhibits the efficacy to improve myocardial glucose metabolism, mitochondrial oxidative phosphorylation and biogenesis by regulating HIF-1α/PGC-1α signaling pathway in HF post-AMI rats.

Keywords: Danqi Pill (DQP), heart failure (HF), acute myocardial infarction (AMI), glucose metabolism, HIF-1α/PGC-1α pathway

INTRODUCTION

Heart failure (HF) post-acute myocardial infarction (AMI) leads to a large number of hospitalizations and deaths worldwide (Ponikowski et al., 2016). Although the understanding of the mechanism of heart failure is deepening, new and different strategies for the treatment of HF are urgently needed.

Currently, one attractive approach for HF post-AMI treatment is to optimize myocardial substrate utilization (Torsten et al., 2013). Emerging evidence indicates that cardiomyocytes predominantly rely on glucose metabolism to produce ATP after AMI, which has higher energetic efficiency under ischemia (Nickel et al., 2013; Fillmore et al., 2014). Hence, focusing on glucose metabolism including glucose intake, transportation, and mitochondrial oxidation are extensively investigated (Diakos et al., 2016; Tuomainen and Tavi, 2017).

Due to hypoxia and ischemia after AMI, myocardial glucose intake and transportation were increased for compensatory ATP production (Brenner, 2018). Glucose transporter protein 4 (GLUT4), and pyruvate kinase M2 (PKM2) related to the myocardial glucose intake and metabolism pathway were activated (Szablewski, 2017; Williams et al., 2018). Furthermore, mitochondrial dysfunctions occur in the failing heart. The dysfunctions include impaired mitochondrial structure and electron transport chain components, inhibited oxidative phosphorylation, altered substrate utilization, increased ROS, and so on (Mori et al., 2012; Sang-Bing et al., 2013; Brown et al., 2017). Cardiac pyruvate dehydrogenase kinase 1 and 4 (PDK1 and PDK4) are downstream targets of peroxisome proliferator-activated receptor alpha (PPARα) (Czarnowska et al., 2016), which can phosphorylate and inhibit pyruvate dehydrogenase (PDH), the crucial enzyme catalyzing pyruvate to acetyl CoA to fuel mitochondrial TCA cycle (Fillmore and Lopaschuk, 2013). Uncoupling protein 2 (UCP2) is a mitochondrial proton carrier and functions in energy homeostasis (Akhmedov et al., 2015). Increased UCP2 provided channels for proton to transport into mitochondrial matrix, and then inhibited the ATP synthesis (Yang et al., 2018). Pecqueur C et al. show that UCP2 knocking-out cells preferentially utilize glucose metabolism instead of fatty acid oxidation (Pecqueur et al., 2008). Peroxisome proliferator-activated receptor co-activator α (PGC-1α) is a cofactor of PPARα transcription factors and their interaction regulates the expression of mitochondrial oxidation related genes (Scarpulla, 2011). PGC-1α also activates transcription factors nuclear respiratory factor 1 (NRF1) and mitochondrial transcription factor A (TFAM) to promote mitochondrial biogenesis and oxidation phosphorylation.

HIF-1α regulates the hypoxic response during an ischemic event (Sousa Fialho et al., 2018). HIF-1α is hydroxylated by prolyl hydroxylase 2 (PHD2) and the hydroxylated HIF-1α is easy to be degraded by ubiquitination proteasome pathway under normoxia (Wong et al., 2013). In hypoxia, accumulated HIF-1α is transported into the nucleus and form dimers with HIF-1β to regulated genes associated with glucose metabolism (Krishnan et al., 2009; Abud et al., 2012; Ambrose et al., 2014). This serves to increase intracellular glucose intake, augment glucose transportation, mitochondrial oxidative phosphorylation, and biogenesis (Hashmi and Al-Salam, 2012).

Danqi Pill (DQP) is a well-known Chinese patent medicine and used in treating coronary heart disease (Wang et al., 2016). However, the potential pharmacological mechanism of DQP on glucose metabolism remains unknown. Therefore, we examined whether DQP acted on glucose metabolism to protect against HF post-AMI *via* HIF-1α/PGC-1α pathway.

MATERIALS AND METHODS

Drugs

Danqi Pill (DQP) is composed of two Chinese herbs at a composition of 1:1 (*Salvia miltiorrhiza* and *Panax notoginseng*). And the manufacturer is Beijing Tongrentang Pharmacy Co., Ltd. (Z11020471). The fingerprint of DQP was performed by high-performance liquid chromatography (HPLC) (**Figure S1**). Trimetazidine dihydrochloride Tablets (TMZ) were purchased from Servier Pharmaceutical Co., Ltd. (Tianjin, China, No. 2008344)

Animals

Male Sprague-Dawley (SD) rats (220 g) were obtained from Beijing Vital River Laboratory Animal Technology Co., Ltd. Animal housing and experiments were under the guidelines for the Care and Use of laboratory animals (NIH), and the study ethically was approved by the Animal Care and Use Committee of Beijing University of Chinese Medicine. The acute myocardial infarction rat model was induced by left coronary artery anterior descending branch ligation as previously described (Wang et al., 2014). After the surgery, rats were randomly divided as sham, model, DQP-L (0.75 g/kg/day), DQP (1.5 g/kg/day), DQP-H (3.0 g/kg/day), and TMZ (6.3 mg/kg/day) group. Rats were treated with different drugs for 4 weeks.

Echocardiography

All rats were anaesthetized using 1% pentobarbital sodium and subjected to echocardiographic examination. Echocardiography (Vevo 2100, Visual Sonics, Canada) was performed to assess the cardiac function. Parasternal short-axis M-mode frames were recorded and related parameters included left ventricular internal dimension-systole (LVID;s), left ventricular internal dimension-diastole (LVID;d), ejection fraction (EF), and fractional shortening (FS).

Histological Examination

After 48 h fixing in the 4% paraformaldehyde, the myocardial tissues were embedded in paraffin and were sectioned at 5 μm thickness. Cardiac paraffin sections were stained with Hematoxylin-Eosin (HE) to evaluate the degree of inflammatory infiltration.

Measurement of Myocardial ATP Levels

The fresh cardiac samples and cell lysates were prepared following the manufacture's insturction of ATP assay kit (A095, Nanjing Jiancheng, China). ATP levels were detected and calculated in reference to the corresponding standard curves and were expressed as μmol/gprot.

PET/CT Examination

Rats were in abrosia for 12 h before PET/CT scan. An amount of ~1 mCi of ^{18}F-FDG was injected *via* the tail vein. After 20 min, PET-CT images were acquired (Inveon, Siemens Medical Solutions Knoxville, TN, United States). In our study, after being anesthetized with 1–1.5% isoflurane, the rats were placed in the supine position during PET/CT scanning and the acquisition time was 2~3 min per rats. Non-contrast-enhanced low-dose CT progressed by 30–80 kVp X-ray source.

Standardized uptake value (SUV) was calculated as follows: SUV=C/(D/M). C means activity concentration in the heart, D means injected dose, and M means body weight.

Immunostaining Assay

Deparaffinized myocardial tissues sections (5 μm) were blocked with 5% sheep serum for 1 h and incubated with anti-GLUT4 (1:500) overnight at 4°C. After incubated with a secondary antibody, the samples were stained with diaminobenzidine (DAB) and re-stained with hematoxylin.

Western Blotting Analysis of Protein Expressions

The proteins of heart tissues samples or H9C2 cells were extracted using RIPA lysis buffer containing a protease inhibitor. Protein samples were separated with 8%-10% sodium dodecyl sulfate polyacrylamide gel electrophoresis (SDS-PAGE) blots and then transferred to the PVDF membranes. These membranes were blocked with 5% non-fat milk for 1 h and then incubated with primary antibodies: anti-GLUT4 (#2213, CST, 1:2,000), anti-PKM2 (60268, Proteintech, 1:500), anti-NRF1 (12482-1, Proteintech, 1:500), anti-TFAM (22586-1, Proteintech, 1:500), anti-UCP2 (#89326s, CST, 1:200), anti-PDK4 (ab89295, Abcam, 1:1,000), anti-PDK1 (ab110025, Abcam, 1:1000), anti-PPARα (ab24509, Abcam, 1:2,000), anti-RXRα (#3085, CST, 1:1,000), anti-PGC-1α (ab54481, Abcam, 1:1,000), anti-HIF-1α (sc-10790, SANTA CRUZ, 1:500), anti-PHD2 (ab26058, Abcam, 1:1,000), anti-GAPDH (ab8245, Abcam, 1:5,000) at 4°C overnight. After three washes, the membranes were incubated with the secondary antibodies (goat anti-rabbit IgG 1:12,000 and goat anti-mouse IgG 1:5,000) for 1h. Proteins were detected using enhanced chemiluminescent (ECL) Plus Western blotting detection reagent (GE Healthcare, UK) by UVP BioImaging Systems (Bio-Rad, Hercules, CA, USA).

Cell Culture and OGD/R Model

H9C2 cells were cultured in Dulbecco's Modified Eagle Medium (DMEM) supplemented with 10% FBS and 1% penicillin/streptomycin under 5% CO_2. In OGD/R model, cells were incubated using earle's balanced salt solution and plated in a controlled hypoxic plastic chamber at 37°C for 8 h and then the cells were cultured in the normal medium and normoxia for 12 h. Cell viability was performed as previously described by CCK8 assay (Chang et al., 2017).

Small Interfering RNA (siRNA) Transfection

H9C2 cells were transfected HIF-1α siRNA (50 nmol/L) using lipofectamine 2000^{TM} (Invitrogen). The sequences of HIF-1α siRNA were 5′GCAUUGAAGUUAGAGUCAAdTd3′, 3′ UUGACUCUAACUUCAAUGCdTd5′, which were synthetized by Hanbio Biotechnology Co., Ltd. (Shanghai, China). After transfection, cells were randomly divided into control group, OGD/R group, OGD/R+DQP, OGD/R+HIF-1α siRNA+DQP, and OGD/R+HIF-1α siRNA treated group. The concentration of DQP on H9C2 cell was 400 μg/ml as described previously (Zhang et al., 2018).

Mitochondrial Membrane Potential (△Ψm)

ΔΨm was assessed using the JC-1 staining kit (Beyotime Biotechnology, Shanghai, China). H9C2 cells were incubated with JC-1 probe for 20 min at 37°C. Cells were washed for three times with PBS and observed by a laser confocal microscopy (Leica Microsystems GmbH). The green fluorescence (Ex = 514 nm, Em = 529 nm) was used for monomers detection and the red fluorescence (Ex = 585 nm, Em = 590 nm) was used for J-aggregates detection. Five randomly chosen fields were photographed. The fluorescence intensity was analysed using Image ProPlus software and the ratio of aggregates/monomers fluorescence intensity was calculated.

Statistical Analysis

Data was presented as mean ± SD. Analyses were performed by Graphpad 6 and SPSS 20.0 statistical software. One-way ANOVA were used to compare values between groups. P-value less than 0.05 was assumed to be statistical significance.

RESULTS

DQP Reduced Cardiac Dysfunctions and Increased the ATP Level in HF Post-AMI Rats

Rat cardiac functions were evaluated by echocardiography (**Figure 1A**). Compared with model group, DQP with different doses could up-regulate EF and FS values significantly. LVID;d in DQP with different doses and TMZ group were decreased significantly while LVID;s in the four groups had no statistical differences, suggesting that DQP with different doses and TMZ improved cardiac function mainly through decreasing end-diastolic ventricular dilatation (**Figure 1B**). Histological evaluation of HE staining exhibited that treatment with DQP in three doses and TMZ attenuated inflammatory cell infiltration

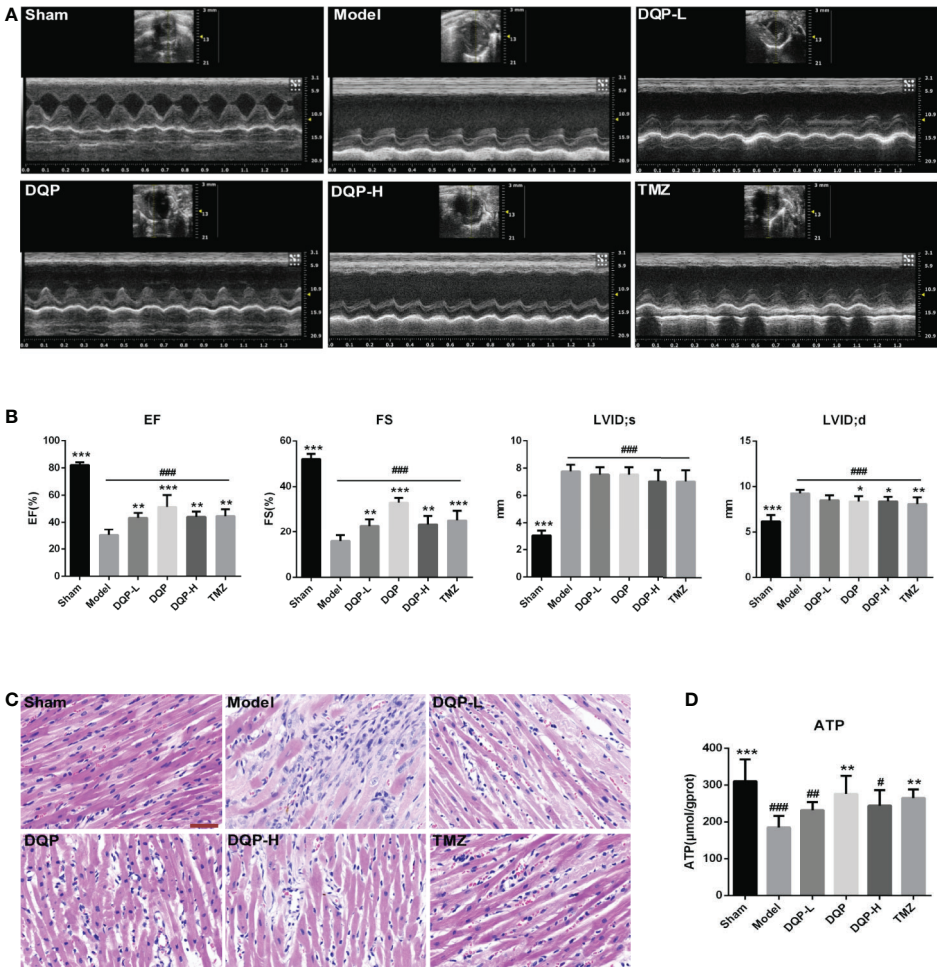


FIGURE 1 | Danqi Pill (DQP) in different doses reduced cardiac dysfunctions, inhibited inflammatory cell infiltration and increased adenosine triphosphate (ATP) production. **(A)** Representative echocardiograms in heart sections. **(B)** Echocardiography analyses of ejection fraction (EF), fractional shortening (FS), left ventricular internal dimension-diastole (LVID;d), and left ventricular internal dimension-systole (LVID;s). **(C)** Histological analyses of H&E staining. The scale bar is 50 μm. **(D)** Myocardial ATP levels in different groups. $^{\#}P < 0.05$, $^{\#\#}P < 0.01$, $^{\#\#\#}P<0.001$ compared with sham; $^{*}P < 0.05$, $^{**}P < 0.01$, $^{***}P < 0.001$ compared with model. N = 6 per group.

and edema of cardiomyocytes caused by ischemia (**Figure 1C**). Energy in the form of ATP is needed for the heart to fuel its contractile machinery and the ionic pumps that serve to regulate its function (Kadkhodayan et al., 2013). DQP and TMZ treatment increased myocardial ATP levels significantly (**Figure 1D**). These data implicate that DQP could rescue heart function in HF post-AMI rats.

DQP Promoted Cardiac Glucose Metabolism in HF Post-AMI Rats

It has been widely reported that substrate utilization change in the heart failure and metabolic therapy has attracted widespread attention (Stanley et al., 2005). Fatty acid oxidation is the main fuel source for normal cardiomyocytes, however it shifts to glucose metabolism in the process of HF (Brown et al., 2017). To elucidate the effects of DQP on glucose metabolism, PET/CT was firstly applied to assess the uptake of glucose located in myocardial tissue. PET/CT images exhibited that abnomal accumulation of ^{18}F-FDG in the heart of HF post-AMI rat, which may be caused by increased inflammatory response and glucose metabolism disorders (Aoyama et al., 2017; Wisenberg et al., 2019). DQP and TMZ could significantly reduce the accumulation of glucose in the rat heart (**Figure 2A**). GLUT4 is the main protein to assist glucose transport (Vargas et al., 2019), while PKM2 is the key enzyme involved in the glucose metabolism (Zhang et al., 2019). Therefore, we explored whether DQP influenced the expression of pivotal proteins involved in the glucose intake and metabolism. DQP treatment could promote GLUT4 and PKM2 expressions compared with HF post-AMI rats determined by Western blots (**Figure 2B**). Histological results also revealed that DQP and TMZ both increased the GLUT4 expression (**Figure 2C**).

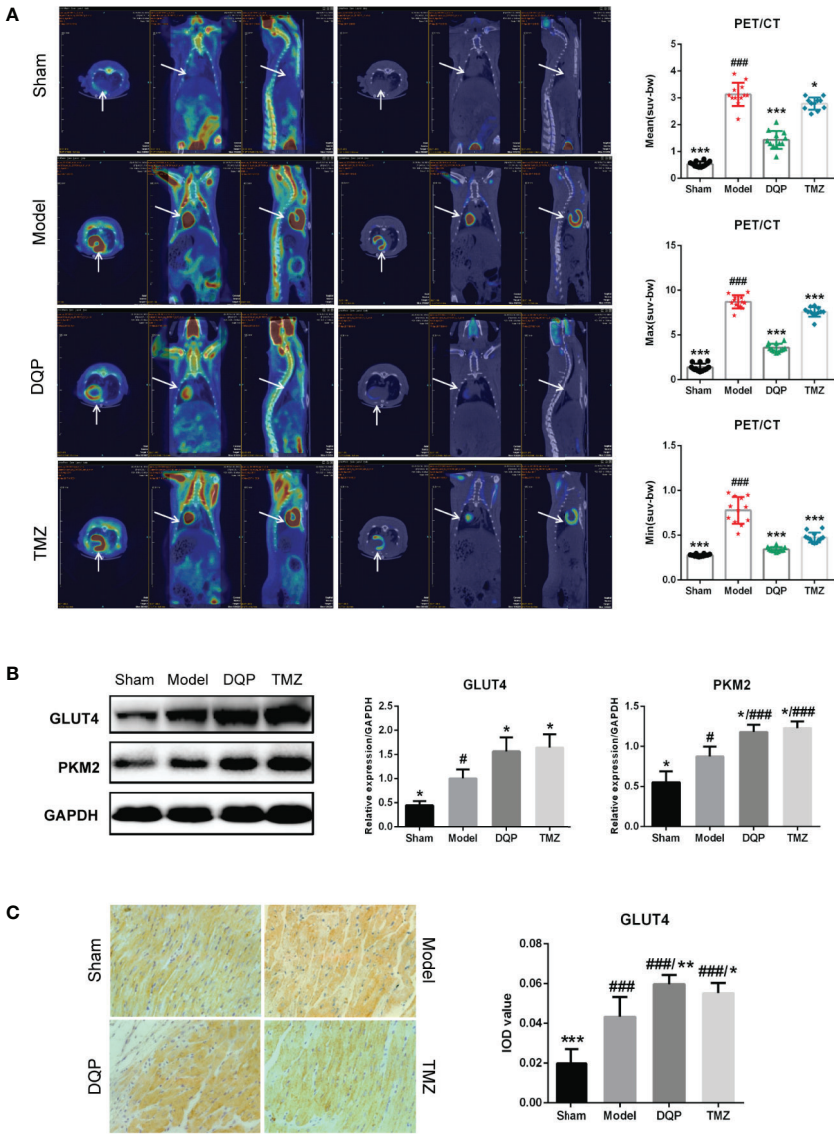


FIGURE 2 | Danqi Pill (DQP) promoted cardiac glucose metabolism in heart failure (HF) post-acute myocardial infarction (AMI) rats. **(A)** ^{18}F-FDG uptake detected by PET/CT in four groups. Quantitative analyses of mean, max, and min standardized uptake value (SUV). **(B)** Cardiac protein expressions of GLUT4 and PKM2 and densitometric analyses. **(C)** Immunostaining of GLUT4 in cardiac sections and quantification of GLUT4. Region of interest (ROI) = 12 per rat. $^{\#}P < 0.05$, $^{\#\#\#}P < 0.001$ compared with sham; $^{*}P < 0.05$, $^{**}P < 0.01$, $^{***}P < 0.001$ compared with model. N = 3 per group for western blotting. N = 6 per group for IHC.

DQP Promoted Glucose Metabolism by Activating Myocardial Mitochondrial Oxidation Pathway in HF Post-AMI Rats

The heart is a high energy consuming organ, which needs to consume a lot of ATP to maintain its contraction. In addition to fatty acid oxidation, glucose aerobic oxidation is another important energy source for the heart (van Bilsen et al., 2004). UCP2 and two subtypes of PDKs named as PDK4 and PDK1 were chosen to assess the ability of mitochondrial oxidative phosphorylation. As shown in **Figure 3A**, the expressions of PDK4, PDK1, and UCP2 in model group were significantly increased by 37.25%, 56.53% and 46.83% compared with the sham group. In DQP treated group compared with model group, expressions of PDK4, PDK1, and UCP2 were decreased respectively by 29.92%, 35.61%, and 30.34%. Then, we detected the proteins involved in the mitochondrial biogenesis including NRF1 and TFAM. DQP and TMZ treatment significantly promoted the protein production of NRF1 and TFAM (**Figure 3B**).

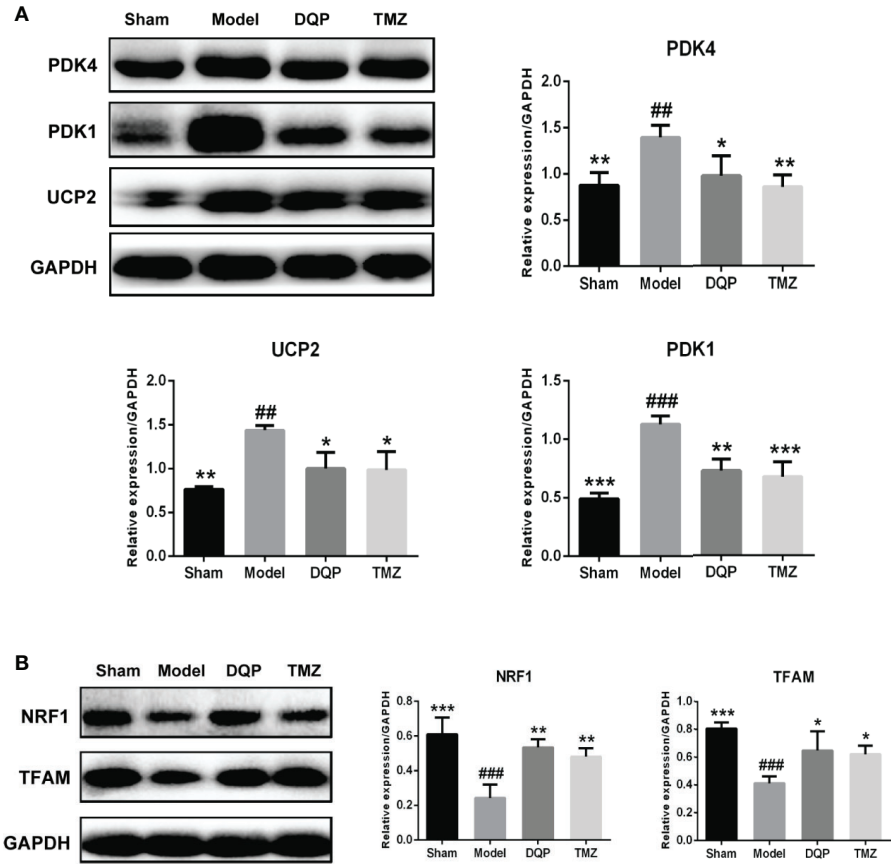


FIGURE 3 | Danqi Pill (DQP) promoted glucose metabolism by activating myocardial mitochondrial oxidation pathway in heart failure (HF) post-acute myocardial infarction (AMI) rats. **(A)** Western blot analysis the expressions of PDK4, PDK1, and UCP2 in all groups. **(B)** Western blot analysis the expressions of NRF1 and mitochondrial transcription factor A (TFAM) in all groups. Densitometric analysis was shown in the graph. GADPH was used as internal reference. $^{\#\#}P < 0.01$, $^{\#\#\#}P < 0.001$ compared with sham; $^{*}P < 0.05$, $^{**}P < 0.01$,$^{***}P < 0.001$ compared with model. N = 3 per group.

DQP Activated HIF-1α/PGC-1α Signaling Pathway in HF Post-AMI Rats

Extensive research indicates that PGC-1α interacts with other transcription factors, such as RXRα and PPARα to regulate the mitochondrial biogenesis and oxidative phosphorylation (Duncan, 2011; Wang et al., 2013). DQP treatment could increase PPARα, RXRα, and PGC-1α protein levels by 77.02%, 107.64%, and 90.53% compared with model rats, respectively (P<0.001). TMZ had similar effects as DQP, but the promotion effects of TMZ were milder than DQP (P<0.05, **Figure 4A**). HIF-1α plays a key role in hypoxia adaptation by promoting the expression of hypoxia inducible genes and participating in the specific response of tissue cells to hypoxia (Suzuki et al., 2017). DQP and TMZ treatment dramatically increased HIF-1α protein level in the heart of HF post-AMI rats, as determined by western blots. PHD2 acts as the primary rate-limiting HIF prolyl hydroxlase which affects transcriptional stability of HIF-1α (Flashman et al., 2010). DQP and TMZ could markedly downregulated the expressions of PHD2 respectively (**Figure 4B**).

DQP Protected Against OGD/R-Induced H9C2 Cells Injury *via* Regulating HIF-1α

To determine the role of HIF-1α on the protection of DQP in OGD/R-induced H9C2 cells, HIF-1α siRNA was applied. Immunoblots showed that OGD/R could induce HIF-1α production, whereas DQP treatment further promoted the increase of HIF-1α. In our study, siRNA was applied to interfere in HIF-1α expression, while DQP could increase HIF-1α level in H9C2 transfected with siRNA (**Figure 5A**). CCK-8 assay results demonstrated HIF-1α siRNA could suppress the facilitation of DQP in the proliferation of OGD/R H9C2 cells (**Figure 5B**). The assessment of mitochondrial transmembrane potential was performed by JC-1 probe. The findings showed that the ratio of aggregates/monomers increased in response to DQP, suggesting the $\triangle\Psi$m returned to normal. However, the

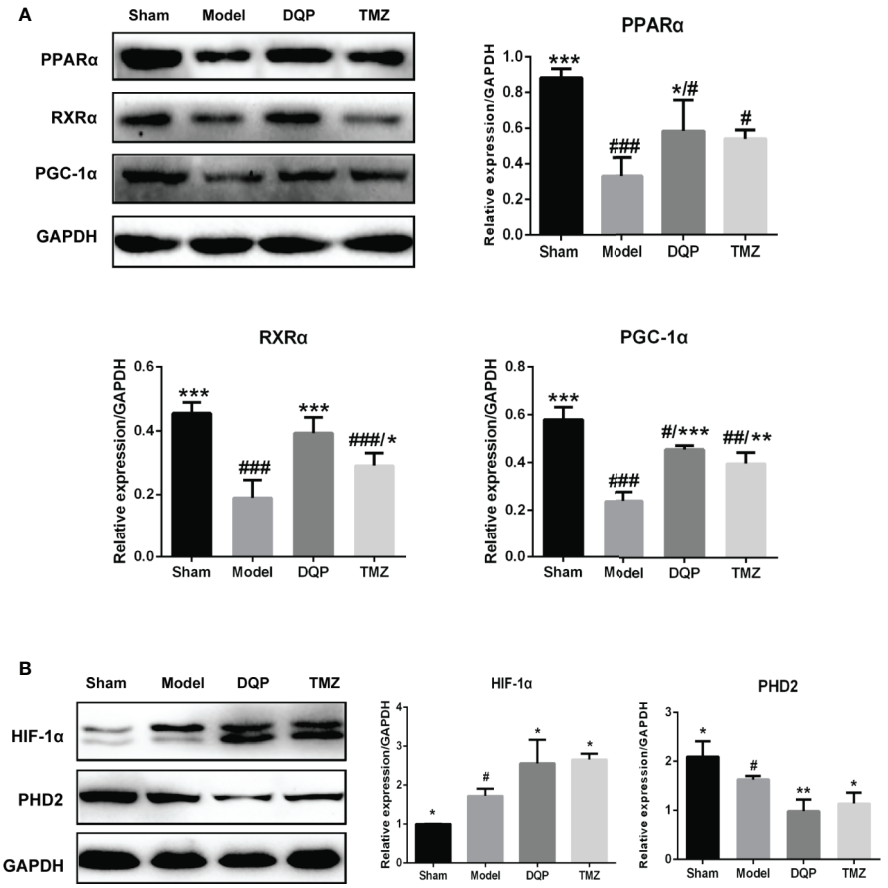


FIGURE 4 | Danqi Pill (DQP) activated HIF1α/PGC1α signaling pathway in heart failure (HF) post-acute myocardial infarction (AMI) rats. **(A)** Western blot analysis the expressions of PPARα, RXRα, and PGC-1α in the four groups. Densitometric analysis was showed. **(B)** Effects of DQP on expressions of HIF-1α and PHD2 in HF post-AMI Rats; WB bands and protein quantitative results of HIF-1α and PHD2 in heart tissues of rats. $^{\#}p < 0.05$, $^{\#\#}p < 0.01$, $^{\#\#\#}P < 0.001$ compared with sham; $^{*}P < 0.05$, $^{**}P < 0.01$, $^{***}P < 0.001$ compared with model. N =3 per group.

ratio decreased when using HIF-1α siRNA (**Figure 5C**). Intracellular ATP concentration also was examined in OGD/R-induced H9C2 cells. ATP level was up-regulated in response to DQP, while it was neutralized by using HIF-1α siRNA (**Figure 5D**). Overall, the protective mechanism of DQP was related to HIF-1α pathway.

DISCUSSION

In the current study, we investigated the pharmacological mechanisms of DQP on glucose metabolism *via* the HIF-1α/PGC-1α signaling pathway. The results indicated that: (1) DQP inhibited cardiac dysfunction and inflammatory infiltration, increased ATP levels in the HF post-AMI rats. (2) DQP improved glucose metabolism through myocardial glucose intake and transportation pathway in HF post-AMI rats. (3) DQP treatment promoted mitochondrial oxidation phosphorylation and mitochondrial biogenesis. (4) The protective effects of DQP were associated with HIF-1α/PGC-1α pathway.

Heart contractions require a great deal of ATP, which is mainly from myocardial fatty acid oxidation and glucose metabolism (Niemann et al., 2018). However, the failing heart predominantly relies on anaerobic glycolysis to produce ATP after AMI, and decreases the use of glucose oxidation metabolism (Karwi et al., 2018). In our previous study, DQP treatment increased local oxygen supply by inhibiting the damage of cardiomyocytes and promoting angiogenesis (Jiao et al., 2018), accompanying with the increasing lipid metabolism (Zhang et al., 2018). Increased angiogenesis and oxygen supply also promote glucose oxidation. The essential process of glucose aerobic oxidation is the glycolytic pathway in which GLUT4 and PKM2 play essential roles. The expressions of GLUT4 and PKM2 in ischemic myocardial tissue were promoted to ensure the energy supply after the intervention of DQP.

HIF-1α could increase myocardial glucose intake and transportation in order to continuously provide the compensatory energy supply by regulating myocardial GLUT4 and PKM2 genes expressions (Rees et al., 2015). HIF-1α also facilitates activation of PDK1 and PDK4 as well as UCP2 to

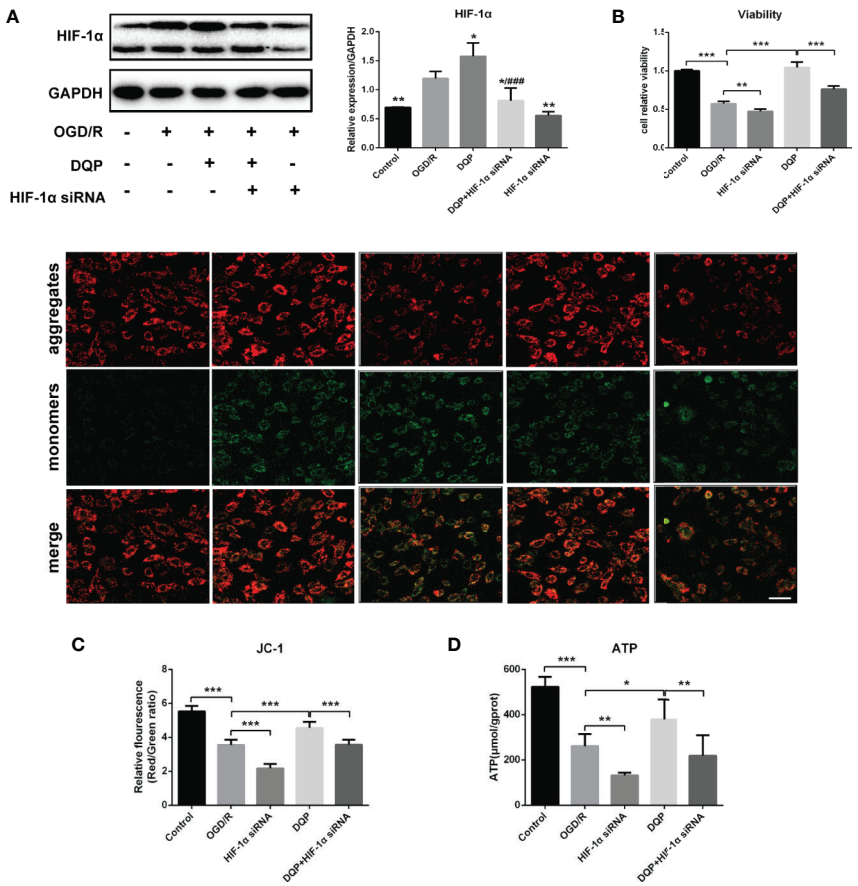


FIGURE 5 | Danqi Pill (DQP) protected against oxygen-glucose deprivation-reperfusion (OGD/R)-induced H9C2 cells injury *via* up-regulating HIF-1α. **(A)** Immunoblot of HIF-1α in H9C2 Cells. **(B)** HIF-1α small interfering RNA (siRNA) suppressed the facilitation of DQP in the proliferation of OGD/R H9C2 cells. **(C)** HIF-1α siRNA decreased mitochondrial membrane potential (△Ψm) with/without DQP treatment in OGD/R-induced H9C2 cells. △Ψm was measured by JC-1 probe (400 ×, Scale bar 100 μm). **(D)** Intracellular adenosine triphosphate (ATP) levels in H9C2 Cells. $^{*}P < 0.05$, $^{**}P < 0.01$, $^{***}P < 0.01$ compared with model; $^{\#\#\#}P < 0.001$ compared with DQP. N = 3 per group for WB and N=6 for the other experiments.

enhance the mitochondrial oxidative phosphorylation (Cunha-Oliveira et al., 2018). Moreover, NRF1 and TFAM play distinct roles in mitochondrial biogenesis (Yao et al., 2016) and the upregulation of NRF1 and TFAM promotes mitochondrial DNA synthesis in infarcted cardiac muscle (Sheeran and Pepe, 2017). Therefore, HIF-1α signaling pathway is activated in cardiomyocytes to produce continuous ATP in adaption to hypoxia, by shifting myocardial metabolism substrate to glucose intake and transportation (Karwi et al., 2018). The levels of PDK1, PDK4, and UCP2 were weakened in the failing heart with DQP treatment, suggesting that DQP functioned by promoting glucose intake, transportation and oxidative phosphorylation to produce more ATP. Moreover, DQP could upregulate NRF1 and TFAM to promote the mitochondrial biogenesis. The up-stream pathways involved in regulating myocardial mitochondrial oxidation, glucose intake and transportation were further investigated. DQP could promote the expressions of PPARα, RXRα, PGC-1α, and HIF-1α. To further identify the effect of DQP on HIF-1α, the oxygen-dependent regulatory hydroxylases PHD2, which manifested affinity and specificity for each HIF-1α forming a feedback loop suffered ischemia (He et al., 2018), was investigated. Consistently, DQP promoted HIF-1α expression and weakened PHD2 expression. Moreover, HIF-1α siRNA abolished the protective effect of DQP on energy metabolism demonstrating that DQP could partly activate the HIF-1α and exert myocardial protection through HIF-1α signaling pathway.

As the limitations of our study, the active components of DQP participated in regulating HIF-1α/PGC-1α mediated glucose metabolism pathway are still unknown. We will further explore the combination of active components and HIF-1 α targets in DQP, so as to explain the regulatory mechanism of DQP more systematically and comprehensively. Besides, we found that different ligation sites might lead to different effects on the cardiac function and more experiments need to be conducted to confirm it in the future study.

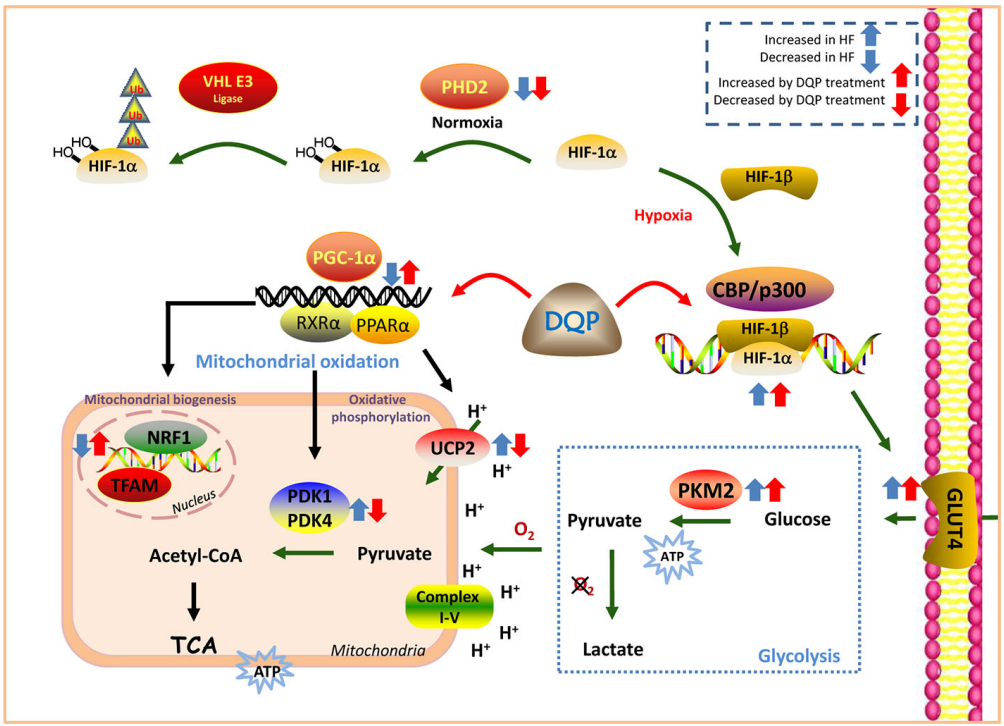


FIGURE 6 | Danqi Pill (DQP) targeted on HIF-1α/PGC-1α signaling pathway and finally elevated cardiac energy metabolism in the failing heart.

CONCLUSION

DQP has the efficacy to improve myocardial glucose intake, transportation and mitochondrial biogenesis and oxidative phosphorylation both *in vivo* and *in vitro*. The effects may be mediated by regulation of HIF-1α/PGC-1α signaling pathway (**Figure 6**).

DATA AVAILABILITY STATEMENT

All datasets generated for this study are included in the article/**Supplemental Material**.

ETHICS STATEMENT

The animal study was reviewed and approved by the Animal Care and Use Committee of Beijing University of Chinese Medicine.

AUTHOR CONTRIBUTIONS

CL, WW, and YoW conceived and designed the project. Each author has contributed significantly to the submitted work. QZ, DG, and YyW performed the research, analyzed the data, and drafted the manuscript. XW, QW, and YaW revised the manuscript. All authors read and approved the final manuscript.

FUNDING

This work was financially supported, in part, by grants from the National Natural Science Foundation of China (No. 81822049, 81673712, and 81673802), the New drug creation of Ministry of science and technology (No. 2019ZX09201004-001-011), the Fok Ying Tung Education Foundation (No. 151044), the Beijing Nova Program (Z171100001117028), and the Talent Young Scientist of China Association for Science and Technology (No. CACM-2017-QNRC2-C13, No. CACM-2018-QNRC2-C07).

SUPPLEMENTARY MATERIAL

The Supplementary Material for this article can be found online at: https://www.frontiersin.org/articles/10.3389/fphar.2020.00458/full#supplementary-material

REFERENCES

Abud, E. M., Maylor, J., Undem, C., Punjabi, A., Zaiman, A. L., Myers, A. C., et al. (2012). Digoxin inhibits development of hypoxic pulmonary hypertension in mice. *Proc. Natl. Acad. Sci. U. S. A.* 109, 1239–1244. doi: 10.1073/pnas.1120385109

Akhmedov, A. T., Rybin, V., and Marin-Garcia, J. (2015). Mitochondrial oxidative metabolism and uncoupling proteins in the failing heart. *Heart Failure Rev.* 20, 227–249. doi: 10.1007/s10741-014-9457-4

Ambrose, L. J., Abd-Jamil, A. H., Gomes, R. S., Carter, E. E., Carr, C. A., Clarke, K., et al. (2014). Investigating mitochondrial metabolism in contracting HL-1 cardiomyocytes following hypoxia and pharmacological HIF activation identifies HIF-dependent and independent mechanisms of regulation. *J. Cardiovasc. Pharmacol. Ther.* 19, 574–585. doi: 10.1177/1074248414524480

Aoyama, R., Takano, H., Kobayashi, Y., Kitamura, M., Asai, K., Amano, Y., et al. (2017). Evaluation of myocardial glucose metabolism in hypertrophic cardiomyopathy using 18F-fluorodeoxyglucose positron emission tomography. *PloS One* 12, e0188479. doi: 10.1371/journal.pone.0188479

Brenner, C. (2018). In depth understanding of adverse ventricular remodeling after acute myocardial infarction. *Int. J. Cardiol.* 257, 34. doi: 10.1016/j.ijcard.2017.12.080

Brown, D. A., Perry, J. B., Allen, M. E., Sabbah, H. N., Stauffer, B. L., Shaikh, S. R., et al. (2017). Expert consensus document: Mitochondrial function as a therapeutic target in heart failure. *Nat. Rev. Cardiol.* 14, 238–250. doi: 10.1038/nrcardio.2016.203

Chang, H., Li, C., Wang, Q., Lu, L., Zhang, Q., Zhang, Y., et al. (2017). QSKL protects against myocardial apoptosis on heart failure via PI3K/Akt-p53 signaling pathway. *Sci. Rep.* 7, 16986. doi: 10.1038/s41598-017-17163-x

Cunha-Oliveira, T., Ferreira, L. L., Coelho, A. R., Deus, C. M., and Oliveira, P. J. (2018). Doxorubicin triggers bioenergetic failure and p53 activation in mouse stem cell-derived cardiomyocytes. *Toxicol. Appl. Pharmacol.* 348, 1–13. doi: 10.1016/j.taap.2018.04.009

Czarnowska, E., Domal-Kwiatkowska, D., Reichman-Warmusz, E., Bierla, J. B., Sowinska, A., Ratajska, A., et al. (2016). The Correlation of PPARalpha Activity and Cardiomyocyte Metabolism and Structure in Idiopathic Dilated Cardiomyopathy during Heart Failure Progression. *PPAR Res.* 2016, 7508026. doi: 10.1155/2016/7508026

Diakos, N. A., Navankasattusas, S., Abel, E. D., Rutter, J., Mccreath, L., Ferrin, P., et al. (2016). Evidence of Glycolysis Up-Regulation andPyruvate Mitochondrial Oxidation Mismatch During Mechanical Unloading ofthe Failing Human Heart : Implications for Cardiac Reloading and Conditioning. *JACC Basic Trans. Sci.* 1, 432–444. doi: 10.1016/j.jacbts.2016.06.009

Duncan, J. G. (2011). Peroxisome proliferator activated receptor-alpha (PPARalpha) and PPAR gamma coactivator-1alpha (PGC-1alpha) regulation of cardiac metabolism in diabetes. *Pediatr. Cardiol.* 32, 323–328. doi: 10.1007/s00246-011-9889-8

Fillmore, N., and Lopaschuk, G. D. (2013). Targeting mitochondrial oxidative metabolism as an approach to treat heart failure. *Biochim. Biophys. Acta* 1833, 857–865. doi: 10.1016/j.bbamcr.2012.08.014

Fillmore, N., Mori, J., and Lopaschuk, G. D. (2014). Mitochondrial fatty acid oxidation alterations in heart failure, ischaemic heart disease and diabetic cardiomyopathy. *Br. J. Pharmacol.* 171, 2080–2090. doi: 10.1111/bph.12475

Flashman, E., Hoffart, L. M., Hamed, R. B., Bollinger, J. M.Jr., Krebs, C., and Schofield, C. (2010). Evidence for the slow reaction of hypoxia-inducible factor prolyl hydroxylase 2 with oxygen. *FEBS J.* 277, 4089–4099. doi: 10.1111/j.1742-4658.2010.07804.x

Hashmi, S., and Al-Salam, S. (2012). Hypoxia-inducible factor-1 alpha in the heart: a double agent? *Cardiol. Rev.* 20, 268–273. doi: 10.1097/CRD.0b013e31826287f6

He, X., Zeng, H., Roman, R. J., and Chen, J. X. (2018). Inhibition of prolyl hydroxylases alters cell metabolism and reverses pre-existing diastolic dysfunction in mice. *Int. J. Cardiol.* 272, 281–287. doi: 10.1016/j.ijcard.2018.08.065

Jiao, S., Tang, B., Wang, Y., Li, C., Zeng, Z., Cui, L., et al. (2018). Pro-angiogenic Role of Danqi Pill Through Activating Fatty Acids Oxidation Pathway Against Coronary Artery Disease. *Front. Pharmacol.* 9, 1414. doi: 10.3389/fphar.2018.01414

Kadkhodayan, A., Coggan, A. R., and Peterson, L. R. (2013). A "PET" area of interest: myocardial metabolism in human systolic heart failure. *Heart Failure Rev.* 18, 567–574. doi: 10.1007/s10741-012-9360-9

Karwi, Q. G., Uddin, G. M., Ho, K. L., and Lopaschuk, G. D. (2018). Loss of Metabolic Flexibility in the Failing Heart. *Front. Cardiovasc. Med.* 5, 68. doi: 10.3389/fcvm.2018.00068

Krishnan, J., Suter, M., Windak, R., Krebs, T., Felley, A., Montessuit, C., et al. (2009). Activation of a HIF1alpha-PPARgamma axis underlies the integration of glycolytic and lipid anabolic pathways in pathologic cardiac hypertrophy. *Cell Metab.* 9, 512–524. doi: 10.1016/j.cmet.2009.05.005

Mori, J., Basu, R., McLean, B. A., Das, S. K., Zhang, L., Patel, V. B., et al. (2012). Agonist-induced hypertrophy and diastolic dysfunction are associated with selective reduction in glucose oxidation: a metabolic contribution to heart failure with normal ejection fraction. *Circ. Heart Failure* 5, 493–503. doi: 10.1161/CIRCHEARTFAILURE.112.966705

Nickel, A., Löffler, J., and Maack, C. (2013). Myocardial energetics in heart failure. *Basic Res. Cardiol.* 108, 358. doi: 10.1007/s00395-013-0358-9

Niemann, B., Schwarzer, M., and Rohrbach, S. (2018). Heart and Mitochondria: Pathophysiology and Implications for Cardiac Surgeons. *Thoracic Cardiovasc. Surgeon* 66, 11–19. doi: 10.1055/s-0037-1615263

Pecqueur, C., Bui, T., Gelly, C., Hauchard, J., Barbot, C., Bouillaud, F., et al. (2008). Uncoupling protein-2 controls proliferation by promoting fatty acid oxidation and limiting glycolysis-derived pyruvate utilization. *FASEB J.* 22, 9–18. doi: 10.1096/fj.07-8945com

Ponikowski, P., Voors, A. A., Anker, S. D., Bueno, H., Cleland, J. G. F., Coats, A. J. S., et al. (2016). 2016 ESC Guidelines for the diagnosis and treatment of acute and chronic heart failure. *Eur. J. Heart Failure* 18, 2129. doi: 10.1016/j.rec.2016.11.005

Rees, M. L., Subramaniam, J., Li, Y., Hamilton, D. J., Frazier, O. H., and Taegtmeyer, H. (2015). A PKM2 signature in the failing heart. *Biochem. Biophys. Res. Commun.* 459, 430–436. doi: 10.1016/j.bbrc.2015.02.122

Sang-Bing, O., Hall, A. R., and Hausenloy, D. J. (2013). Mitochondrial dynamics in cardiovascular health and disease. *Antioxidants Redox Sign.* 19, 400–414. doi: 10.1089/ars.2012.4777

Scarpulla, R. C. (2011). Metabolic control of mitochondrial biogenesis through the PGC-1 family regulatory network. *Biochim. Biophys. Acta* 1813, 1269–1278. doi: 10.1016/j.bbamcr.2010.09.019

Sheeran, F. L., and Pepe, S. (2017). Mitochondrial Bioenergetics and Dysfunction in Failing Heart. *Adv. Exp. Med. Biol.* 982, 65–80. doi: 10.1007/978-3-319-55330-6_4

Sousa Fialho, M. D. L., Abd Jamil, A. H., Stannard, G. A., and Heather, L. C. (2018). Hypoxia-inducible factor 1 signalling, metabolism and its therapeutic potential in cardiovascular disease. *Biochim. Biophys. Acta Mol. Basis Dis.* 1865 (4), 831–843. doi: 10.1016/j.bbadis.2018.09.024.

Stanley, W. C., Recchia, F. A., and Lopaschuk, G. D. (2005). Myocardial substrate metabolism in the normal and failing heart. *Physiol. Rev.* 85, 1093–1129. doi: 10.1152/physrev.00006.2004

Suzuki, N., Gradin, K., Poellinger, L., and Yamamoto, M. (2017). Regulation of hypoxia-inducible gene expression after HIF activation. *Exp. Cell Res.* 356, 182–186. doi: 10.1016/j.yexcr.2017.03.013

Szablewski, L. (2017). Glucose transporters in healthy heart and in cardiac disease. *Int. J. Cardiol.* 230, 70–75. doi: 10.1016/j.ijcard.2016.12.083

Torsten, D., Tien Dung, N., and E Dale, A. (2013). Cardiac metabolism in heart failure: implications beyond ATP production. *Circ. Res.* 113, 709–724. doi: 10.1161/CIRCRESAHA.113.300376

Tuomainen, T., and Tavi, P. (2017). The role of cardiac energy metabolism in cardiac hypertrophy and failure. *Exp. Cell Res.* 360 (1), 12–18. doi: 10.1016/j.yexcr.2017.03.052

van Bilsen, M., Smeets, P. J., Gilde, A. J., and van der Vusse, G. J. (2004). Metabolic remodelling of the failing heart: the cardiac burn-out syndrome? *Cardiovasc. Res.* 61, 218–226. doi: 10.1016/j.cardiores.2003.11.014

Vargas, E., Podder, V., and Carrillo Sepulveda, M. A. (2019). *Physiology, Glucose Transporter Type 4 (GLUT4), StatPearls* (Treasure Island (FL): StatPearls Publishing LLC.).

Wang, R., Li, J. J., Diao, S., Kwak, Y. D., Liu, L., Zhi, L., et al. (2013). Metabolic stress modulates Alzheimer's beta-secretase gene transcription via SIRT1-PPARgamma-PGC-1 in neurons. *Cell Metab.* 17, 685–694. doi: 10.1016/j.cmet.2013.03.016

Wang, Y., Li, C., Liu, Z., Shi, T., Wang, Q., Li, D., et al. (2014). DanQi Pill protects against heart failure through the arachidonic acid metabolism pathway by attenuating different cyclooxygenases and leukotrienes B4. *BMC Complement. Altern. Med.* 14, 67. doi: 10.1186/1472-6882-14-67

Wang, Q., Li, C., Zhang, Q., Wang, Y., Shi, T., Lu, L., et al. (2016). The effect of Chinese herbs and its effective components on coronary heart disease through

PPARs-PGC1alpha pathway. *BMC Complement. Altern. Med.* 16, 514. doi: 10.1186/s12906-016-1496-z

Williams, A. L., Khadka, V., Tang, M., Avelar, A., Schunke, K. J., Menor, M., et al. (2018). HIF1 mediates a switch in pyruvate kinase isoforms after myocardial infarction. *Physiol. Genomics* 50, 479–494. doi: 10.1152/physiolgenomics.00130.2017

Wisenberg, G., Thiessen, J. D., Pavlovsky, W., Butler, J., Wilk, B., and Prato, F. S. (2019). Same day comparison of PET/CT and PET/MR in patients with cardiac sarcoidosis. *J. Nuclear Cardiol.* doi: 10.1007/s12350-018-01578-8

Wong, B. W., Kuchnio, A., Bruning, U., and Carmeliet, P. (2013). Emerging novel functions of the oxygen-sensing prolyl hydroxylase domain enzymes. *Trends Biochem. Sci.* 38, 3–11. doi: 10.1016/j.tibs.2012.10.004

Yang, C., Zhao, D., Liu, G., Zheng, H., Yang, H., Yang, S., et al. (2018). Atorvastatin Attenuates Metabolic Remodeling in Ischemic Myocardium through the Downregulation of UCP2 Expression. *Int. J. Med. Sci.* 15, 517–527. doi: 10.7150/ijms.22454

Yao, K., Zhang, W. W., Yao, L., Yang, S., Nie, W., and Huang, F. (2016). Carvedilol promotes mitochondrial biogenesis by regulating the PGC-1/TFAM pathway in human umbilical vein endothelial cells (HUVECs). *Biochem. Biophys. Res. Commun.* 470, 961–966. doi: 10.1016/j.bbrc.2016.01.089

Zhang, Q., Shao, M., Zhang, X., Wang, Q., Guo, D., Yang, X., et al. (2018). The Effect of Chinese Medicine on Lipid and Glucose Metabolism in Acute Myocardial Infarction Through PPARgamma Pathway. *Front. Pharmacol.* 9, 1209. doi: 10.3389/fphar.2018.01209

Zhang, Z., Deng, X., Liu, Y., Liu, Y., Sun, L., and Chen, F. (2019). PKM2, function and expression and regulation. *Cell Biosci.* 9, 52. doi: 10.1186/s13578-019-0317-8

Conflict of Interest: The authors declare that the research was conducted in the absence of any commercial or financial relationships that could be construed as a potential conflict of interest.

Copyright © 2020 Zhang, Guo, Wang, Wang, Wang, Wu, Li, Wang and Wang. This is an open-access article distributed under the terms of the Creative Commons Attribution License (CC BY). The use, distribution or reproduction in other forums is permitted, provided the original author(s) and the copyright owner(s) are credited and that the original publication in this journal is cited, in accordance with accepted academic practice. No use, distribution or reproduction is permitted which does not comply with these terms.

frontiers in Pharmacology

ORIGINAL RESEARCH
published: 08 May 2020
doi: 10.3389/fphar.2020.00651

Non-Targeted Metabolomic Profiling of Coronary Heart Disease Patients With Taohong Siwu Decoction Treatment

*Tianqi Tao[1], Tao He[1], Huimin Mao[1], Xudong Wu[2] and Xiuhua Liu[1]**

[1] Department of Pathophysiology, Chinese PLA General Hospital, Beijing, China, [2] Outpatient Department, Chinese PLA General Hospital, Beijing, China

Traditional Chinese medicine is one of the complementary and alternative therapies to improve the prognosis of coronary heart disease (CHD). Taohong Siwu Decoction (THSWD), a classical traditional Chinese medication that promotes blood circulation, is clinically beneficial in CHD. However, the underlying mechanism of THSWD is still unclear. To comprehensively understand the material foundation of the "blood", it is significantly important to study the differential metabolites involved in the treatment of CHD with Chinese medicinal herb promoting blood circulation in TCM theory. Hence, this study investigated the metabolic profiles of the serum in CHD patients to determine the differential metabolites between the THSWD group and the placebo group. Eleven CHD patients were recruited and divided into two groups randomly and double-blindly. Serum samples were determined by performing non-targeted ultra-performance liquid chromatography with tandem mass spectrometry-based metabolomics. Pearson's correlation analysis was used to assess the association between identified metabolites and clinical serum indexes of CHD. Based on the result, a total of 513 metabolites were found in the serum of CHD patients, of which 27, involved in 29 metabolic pathways, were significantly different between the two groups. Among the differential metabolites, THSWD upregulated succinylcarnitine in fatty acid metabolism and 5′-methylthioadenosine in cysteine and methionine metabolism compared with the placebo group. However, THSWD downregulated pelargonic acid, involved in FA metabolism; succinate, involved in the tricarboxylic acid cycle; gluconic acid, gluconolactone, and D-glucose, involved in pentose phosphate pathway; glycerophosphocholine, involved in glycerophospholipid metabolism; 8,9-dihydroxyeicosatrienoic acid (8,9-DiHETrE), L-lysine, *N*-acetyl-L-aspartic acid, *N*-alpha-acetyl-L-asparagine, hippurate, indoxyl sulfate, and 3-ureidopropionate involved in amino acid metabolism compared with the placebo group. Moreover, succinylcarnitine, pelargonic acid, succinate, D-glucose, gluconic acid, L-lysine, *N*-alpha-acetyl-L-asparagine, 5′-methylthioadenosine, indoxyl sulfate, 8,9-DiHETrE, and 3-ureidopropionate were associated with total cholesterol or low-density lipoprotein. Succinylcarnitine, pelargonic acid, gluconolactone, *N*-acetyl-L-aspartic acid, *N*-alpha-acetyl-L-asparagine, hippurate, and 5′-methylthioadenosine were associated with

OPEN ACCESS

Edited by:
Jing-Yan Han,
Peking University, China

Reviewed by:
Ping Li,
China Pharmaceutical University, China
Vivekananda Mandal,
Guru Ghasidas Vishwavidyalaya, India

***Correspondence:**
Xiuhua Liu
xiuhualiu98@163.com

Specialty section:
This article was submitted to Ethnopharmacology, a section of the journal Frontiers in Pharmacology

Received: *25 December 2019*
Accepted: *22 April 2020*
Published: *08 May 2020*

Citation:
Tao T, He T, Mao H, Wu X and Liu X (2020) Non-Targeted Metabolomic Profiling of Coronary Heart Disease Patients With Taohong Siwu Decoction Treatment. Front. Pharmacol. 11:651. doi: 10.3389/fphar.2020.00651

activated partial thromboplastin time. Our findings indicated that glycerophosphocholine, 8,9-DiHETrE, 5′-methylthioadenosine, hippurate, indoxyl sulfate, and 3-ureidopropionate might constitute the partial material foundation of the "blood" in CHD patients treated with THSWD.

Keywords: metabolomics, coronary heart disease, Taohong Siwu decoction, UPLC-MS/MS, randomized double-blind trial

INTRODUCTION

Coronary heart disease (CHD) is characterized by high morbidity and mortality, which contributes to cardiovascular diseases being the leading cause of death globally (Neumann et al., 2019). Therefore, it is crucial to concentrate on more effective treatment of CHD. In recent years, traditional Chinese medicine (TCM) has been considered a safe and effective alternative therapy in the treatment of CHD. TCM combined with Western medicine can be widely applied in CHD treatment. According to TCM theory, the blood is the mother of Qi, which means the blood is the carrier of Qi and governs nutrition to Qi. CHD with blood stasis syndrome is a common type of CHD; hence, promoting blood circulation and removing blood stasis in TCM theory are critical in CHD treatment (Xiong et al., 2015). Taohong Siwu Decoction (THSWD), originated from the "Golden Mirror of Medicine (Yizong Jinjian)" in Qing Dynasty, is commonly prescribed to promote blood circulation and remove blood stasis. It is composed of the following Chinese medicinal herbs: Tao Ren, Dang Gui, Chuan Xiong, Hong Hua, Chi Shao, and Sheng Di. According to the previous studies, THSWD improves angina symptoms, reduces blood lipids, and promotes anticoagulation (Ma et al., 2018; Tao et al., 2019). Other reports confirmed that THSWD improved microcirculation, protected the endothelial cells, and decreased the level of inflammatory factors (Liu et al., 2013). Although THSWD has beneficial effects on CHD treatment, its underlying mechanism is still unclear.

CHD is a complex metabolic disorder caused by coronary artery atherosclerosis, which leads to myocardial ischemia, infarction, or even heart failure. Metabolic abnormality had a critical role in CHD progression. Fatty acid (FA) oxidation is limited and the utilization of glucose catabolism increases in myocardial ischemia, which may eventually lead to the reduction of energy generation (Peterzan et al., 2017). Meanwhile, several accessory pathways of glucose metabolism such as the pentose phosphate pathway (PPP) are activated (Doenst et al., 2013). According to studies utilizing the acute blood stasis rat model and CHD patients with blood stasis syndrome, it is found that amino acid and lipid metabolites may be the partial material foundation of the "blood" in TCM theory (Hao et al., 2018; Zhao et al., 2019). Therefore, it is significantly important to study the differential metabolites to comprehensively understand the mechanism of Chinese medicinal herb promoting blood circulation in TCM theory.

Metabolomics (metabonomics) is considered an advanced systematic biological technique involved in the early screening, diagnosis, and prognosis of diseases by qualitatively and quantitatively analyzing low-molecular-weight metabolites (Shah et al., 2012). The most commonly used techniques of metabolomics mainly include high-resolution nuclear magnetic resonance spectroscopy and mass spectrometry (MS). MS is most commonly performed in conjunction with chromatography and is divided into gas chromatography-MS and liquid chromatography-MS (LC-MS). Among them, LC-MS is characterized by higher resolution and higher speed, which is appropriate to detect more complex samples in metabolomic studies. In this study, we used a non-targeted ultra-performance liquid chromatography with tandem mass spectrometry (UPLC-MS/MS) to study the differential low-molecular-weight metabolites in the serum of CHD patients before and after THSWD and placebo granules treatment to investigate the partial material foundation of the "blood".

MATERIALS AND METHODS

Recruitment and Study Design

Eleven CHD patients were recruited in the Outpatient Department of the Chinese People's Liberation Army (PLA) General Hospital from March 2017 to November 2017 in our study. CHD patients were treated according to the American College of Cardiology/American Heart Association (ACC/AHA) guidelines in 2014 (Fihn et al., 2014). Based on their routine Western medicine, five and six patients were treated with placebo granules for 12 weeks, and THSWD granules for 12 weeks, respectively. Demographic data were collected before the treatment, and clinical serum indexes were collected before and after the treatment. Placebo granules and THSWD granules were prepared from the China Resources Sanjiu Medical & Pharmaceutical Company (Shenzhen, China) according to the standard guidelines. Placebo granules were mainly composed of caramel (4 g) and maltodextrin (1000 g). The botanical compositions of THSWD granules are shown in **Table 1**, and the chemical compositions mainly consisted of verbascoside, ferulic acid, paeoniflorin, amygdalin, and hydroxysafflor yellow A, as indicated by the high-performance liquid chromatography (HPLC) profile of the extract performed by the manufacturer (**Figure 1**). The chemical structures of them were shown in **Figure 2**. The concentrations of the components in the three batches of THSWD samples detected by the manufacturer were listed in **Table 2**. The mean mass fractions of verbascoside, ferulic acid, paeoniflorin, amygdalin, and hydroxysafflor yellow A were 0.1003, 0.0280, 0.2792, 0.4790,

TABLE 1 | Botanical compositions of Taohong Siwu Decoction.

Herb (Local Name)	Medicinal Parts	Amount in Application (g)
Prunus persica (L.) Batsch (Tao Ren)	Seed	12.5
Angelica sinensis (Oliv.) Diels (Dang Gui)	Root	9.375
Conioselinum anthriscoides "Chuanxiong" (Chuan Xiong)	Root	4.688
Carthamus tinctorius L. (Hong Hua)	Flower	9.375
Paeonia lactiflora Pall. (Chi Shao)	Root	6.25
Rehmannia glutinosa (Gaertn.) DC. (Sheng Di)	Root	9.375

All components in THSWD granules were validated using http://mpns.kew.org/mpns-portal/?_ga=1.111763972.1427522246.1459077346.

and 0.3323 mg/g, respectively. Quality control (QC) of the pharmaceutical process was conducted in accordance with the Pharmaceutical Production Quality Management Standards (2015 edition). This study was approved by the Ethics Review Committee of the Chinese PLA General Hospital (No. S2015-048-01) and registered on the website of the Chinese Clinical Trial Registry (www.chictr.org.cn [Registration Number: ChiCTR-IOR-15006989]).

The inclusion criteria for the diagnosis of CHD were as follows: patients younger than 75 years and patients who met the stable CHD diagnostic criteria issued by the ACC/AHA guidelines in 2014. Patients were treated with routine medicine according to the established guidelines, and the original treatment was maintained during the study. Complications were treated according to the relevant guidelines. Patients with the following characteristics were excluded in the study: patients with severe liver or kidney dysfunction, uncontrolled blood pressure, severe chronic heart failure, severe arrhythmia, cardiac infarction or cardiac pacemaker, diabetes mellitus, hemorrhagic diseases, malignant tumors, autoimmune diseases, and hematological or psychiatric diseases, pregnant or lactating women, and patients who may manifest a possible anaphylactic reaction to the research drugs' components.

Randomization, Control, and Double-Blinding

This was a double-blind, randomized, and placebo-controlled clinical trial. Participants were randomly grouped by researchers using the Statistical Analysis System statistical software according to a random number table. Drugs were coded and packaged by random numbers. The blind bottom could not be disassembled during the trial. All of the participants, staff, and researchers were blinded to the treatment group allocation.

Sample Collection and Pre-treatment

Eleven participants fasted overnight, and 4 ml of peripheral venous blood was collected in the next morning and subsequently stored in a freezer at −80°C. Once the analysis was performed, the blood was thawed, and subsequently coagulated for 30 min at 4°C and centrifuged at 3000×*g* for 15 min. We added 400 µl of pre-chilled methanol to 100 µl serum supernatant; subsequently, the mixture was shaken for 15 s, incubated at −80°C for 1 h, and centrifuged at 13,400×*g* for 20

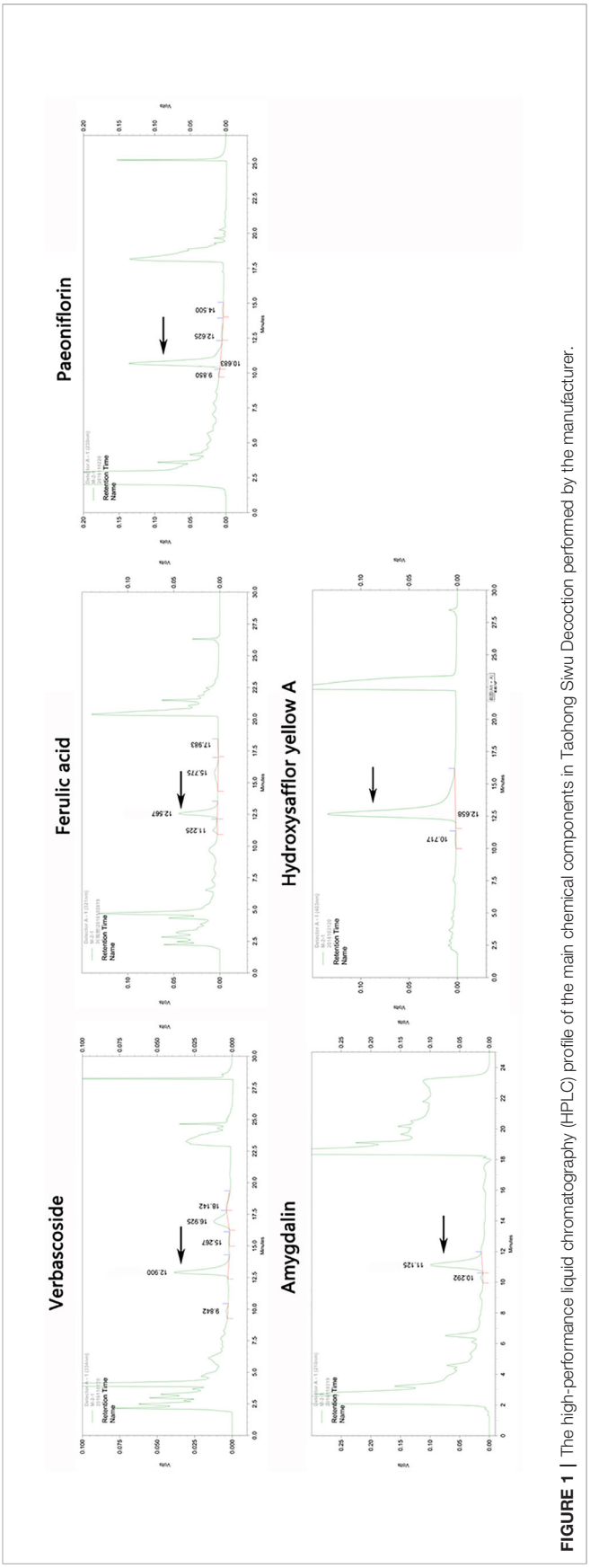


FIGURE 1 | The high-performance liquid chromatography (HPLC) profile of the main chemical components in Taohong Siwu Decoction performed by the manufacturer.

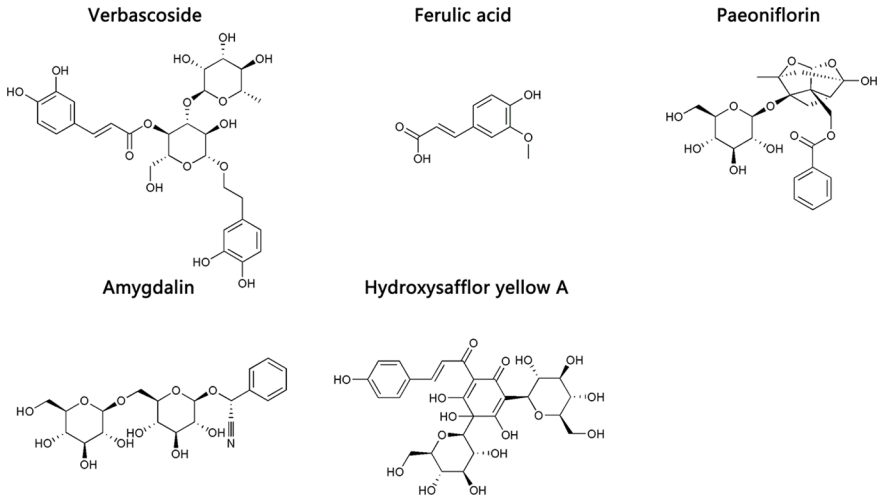


FIGURE 2 | The chemical structures of the main chemical components of Taohong Siwu Decoction.

TABLE 2 | Concentrations of the index components of Taohong Siwu Decoction (n = 3).

Lot Number	Mass fraction ($mg \cdot g^{-1}$)				
	Verbascoside	**Ferulic Acid**	**Paeoniflorin**	**Amygdalin**	**Hydroxysafflor Yellow A**
2016101801	0.0636	0.0181	0.2226	0.3731	0.2247
2016101802	0.1025	0.0281	0.1925	0.4401	0.3763
2016101803	0.1348	0.0376	0.4224	0.6239	0.3958
Mean	0.1003	0.0280	0.2792	0.4790	0.3323

min at 4°C. The supernatant was dried before storage at −80°C. A pooled QC sample solution was prepared by combining equal volumes of the serum from each sample. Once one QC sample ended, the instrumental stability was controlled during the batch process (Li et al., 2018).

Non-targeted Ultra-Performance Liquid Chromatography-Mass Spectrometry (MS)/MS Analysis and Metabolite Identification

Samples were detected by performing non-targeted UPLC-MS/MS using an Ultimate 3000 UHPLC (Dionex) system combined with a Thermo Q-Exactive (Orbitrap) mass spectrometer (Thermo Fisher Scientific, San Jose, CA, USA). Data identifications were performed using a Trace Finder. First, based on the endogenous MS database, metabolites were identified by accurate masses. Subsequently, the metabolites were identified at the MS/MS level using in-house MS/MS library, which was built using chemical standards. The matching confidence of experimental MS/MS spectra with MS/MS in the library was evaluated using library score. Normally, the metabolites with library score >30 were considered as MS/MS confirmed (Tang et al., 2016). The MS/MS spectra of representative metabolites were shown in the **Supplementary Figure**. A 0.25-min retention time deviation was applied, and the mass shifts of the primary and secondary identifications were 10 and 15 ppm, respectively (Ning et al., 2018).

Data Processing

Multivariate statistical analysis was performed using the SIMCA 14.0 software. Unsupervised principal component analysis (PCA) was used to assess the quality, homogeneity, outlier identification, and dominating trends of the group separation inherent in the data set. A supervised orthogonal partial least squares discriminant analysis (OPLS-DA) was applied to determine the differences between the classes and to identify the differential metabolites. Variable Importance in the Projection (VIP) value was generated using the OPLS-DA model, and the quality of the multivariate statistical analysis model was evaluated using R^2X and Q^2. Student's *t*-test was also used to determine the differences in metabolites between the two groups. Subsequently, the internal metabolite MS/MS database was used to identify metabolites by matching accurate quality and MS/MS spectra. MetaboAnalyst 4.0 (http://www.

metaboanalyst.ca/) and Pearson's correlation analysis were used to show the heat map of the differential metabolites and predict the metabolic pathways (Chong et al., 2018).

Statistical Analysis

The Statistical Package for the Social Sciences version 17.0 (Chicago, IL, USA) was used for statistical analysis. Student's *t*-test was performed for two-group comparisons on baseline characteristics and serum indexes before and after the treatment. Moreover, one-way analysis of variance was used to analyze the homogeneity of variance. Furthermore, values are presented as mean ± standard deviation. $P < 0.05$ was considered statistically significant.

RESULTS

Clinical Characteristics

In our study, 11 CHD patients were divided into two groups randomly and double-blindly: five patients were treated with placebo granules, and six patients were treated with THSWD granules for 12 weeks. The baseline characteristics and serum indexes of the participants were shown in **Table 3**, which included gender, age, body mass index (BMI), blood pressure, heart rate, 5 kinds of blood routine indexes (including red blood cell, hemoglobin, white blood cell, neutrophil, and platelet), 10 kinds of biochemical indexes [including alanine aminotransferase, aspartate aminotransferase, serum creatinine, blood urea nitrogen, uric acid, triglyceride, total cholesterol (TC), low-density lipoprotein (LDL), high-density lipoprotein, and fasting glucose], and 4 kinds of coagulation parameters [including prothrombin time, activated partial thromboplastin time (APTT), fibrinogen, and thrombin time]. The average ages of the CHD patients in the placebo group and THSWD group were 55.60 ± 6.47 years and 59.83 ± 7.39 years, and the average BMIs in the placebo group and THSWD group were 25.55 ± 5.26 and 25.49 ± 2.79 kg/m^2. The levels of TC and LDL were higher while that of APTT was lower in the THSWD group compared with the placebo group before the treatment ($P < 0.05$), while all values were within the normal ranges. However, there was no significant difference between the THSWD group and the placebo group in serum clinical indicators after the treatment ($P > 0.05$, **Table 4**), suggesting that THSWD granule treatment reversed the changes of the serum clinical indicators before treatment. It indicated that after THSWD granule treatment, levels of TC and LDL decreased while the level of the APTT increased in the THSWD group compared with the placebo group.

TABLE 3 | Baseline characteristics of patients.

	Placebo (n = 5)	THSW (n = 6)	P
Gender (F/M)	1/4	3/3	0.545
Age, year	55.60 ± 6.47	59.83 ± 7.39	0.344
BMI, kg/m^2	25.55 ± 5.26	25.49 ± 2.79	0.983
SBP, mm Hg	121.60 ± 16.70	132.33 ± 12.36	0.251
DBP, mm Hg	83.60 ± 9.94	77.67 ± 8.98	0.325
Heart rate, beats/min	70.40 ± 6.07	67.50 ± 7.53	0.506
RBC,×10^{12}/L	4.71 ± 0.15	4.65 ± 0.54	0.805
HGB, g/L	140.40 ± 7.57	141.33 ± 18.10	0.912
WBC,×10^9/L	6.06 ± 1.98	6.64 ± 1.02	0.544
NE, %	63.60 ± 9.72	58.92 ± 9.20	0.433
PLT,×10^9/L	225.80 ± 43.34	219.67 ± 28.40	0.784
AST, U/L	22.38 ± 2.00	21.02 ± 5.72	0.604
ALT, U/L	25.60 ± 8.61	27.98 ± 19.50	0.807
SCr, μmol/L	75.98 ± 14.73	68.33 ± 18.87	0.480
BUN, mmol/L	5.05 ± 0.86	5.43 ± 1.01	0.524
UA, μmol/L	338.14 ± 87.40	365.48 ± 70.43	0.579
TG, mmol/L	1.97 ± 1.39	1.49 ± 0.60	0.465
TC, mmol/L	2.90 ± 1.43	4.73 ± 0.64*	0.020
HDL, mmol/L	1.30 ± 0.47	1.19 ± 0.29	0.631
LDL, mmol/L	1.96 ± 0.49	2.96 ± 0.31*	0.003
Glu, mmol/L	4.98 ± 0.56	5.42 ± 0.44	0.180
PT, s	13.12 ± 0.55	12.35 ± 0.83	0.112
APTT, s	37.42 ± 1.72	33.55 ± 2.50*	0.017
FIB, g/L	2.83 ± 0.34	2.80 ± 0.48	0.902
TT, s	16.42 ± 0.66	17.58 ± 2.92	0.409

Values are mean ± SD.

**P < 0.05 vs. the placebo group.*

BMI, body mass index; SBP, systolic blood pressure; DBP, diastolic blood pressure; RBC, red blood cell; HGB, hemoglobin; WBC, white blood cell; NE, neutrophil; PLT, platelet; AST, aspartate aminotransferase; ALT, alanine aminotransferase; SCr, serum creatinine; BUN, blood urea nitrogen; UA, uric acid; TG, triglyceride; TC, total cholesterol; HDL, high-density lipoprotein; LDL, low-density lipoprotein; Glu, glucose; PT, prothrombin time; APTT, activated partial thromboplastin time; FIB, fibrinogen; TT, thrombin time.

Analysis of Quality Control Samples

To investigate the partial material foundation of the "blood", we detected serum metabolomics of CHD patients treated with THSWD by performing non-targeted LC-MS/MS analysis. We selected five serum samples in the placebo group and six serum samples in the THSWD group for metabolomic analysis at

TABLE 4 | Clinical characteristics of patients after treatment.

	Placebo (n = 5)	THSW (n = 6)	P
RBC,×10^{12}/L	5.00 ± 0.22	4.87 ± 0.49	0.573
HGB, g/L	149.00 ± 9.62	147.00 ± 15.09	0.804
WBC,×10^9/L	5.48 ± 1.42	6.45 ± 1.46	0.296
NE, %	61.70 ± 8.84	56.38 ± 6.37	0.276
PLT,×10^9/L	215.60 ± 48.24	217.83 ± 41.83	0.936
AST, U/L	22.70 ± 2.42	23.02 ± 8.65	0.939
ALT, U/L	24.82 ± 4.86	32.52 ± 24.80	0.515
SCr, μmol/L	77.70 ± 13.12	69.00 ± 16.43	0.365
BUN, mmol/L	4.75 ± 1.22	5.16 ± 1.15	0.583
UA, μmol/L	343.46 ± 107.60	316.40 ± 67.91	0.623
TG, mmol/L	1.40 ± 1.05	1.19 ± 0.44	0.650
TC, mmol/L	4.15 ± 0.39	4.82 ± 1.33	0.307
HDL, mmol/L	1.48 ± 0.53	1.21 ± 0.29	0.297
LDL, mmol/L	2.32 ± 0.50	3.20 ± 0.94	0.095
Glu, mmol/L	4.91 ± 0.53	5.27 ± 0.44	0.256
PT, s	12.90 ± 0.45	12.68 ± 0.40	0.419
APTT, s	37.24 ± 2.72	35.47 ± 3.20	0.354
FIB, g/L	2.98 ± 0.16	3.24 ± 0.26	0.092
TT, s	16.52 ± 0.93	16.52 ± 1.03	0.996

*Values are mean ± SD. *P < 0.05 vs. the placebo group.*

BMI, body mass index; SBP, systolic blood pressure; DBP, diastolic blood pressure; RBC, red blood cell; HGB, hemoglobin; WBC, white blood cell; NE, neutrophil; PLT, platelet; AST, aspartate aminotransferase; ALT, alanine aminotransferase; SCr, serum creatinine; BUN, blood urea nitrogen; UA, uric acid; TG, triglyceride; TC, total cholesterol; HDL, high-density lipoprotein; LDL, low-density lipoprotein; Glu, glucose; PT, prothrombin time; APTT, activated partial thromboplastin time; FIB, fibrinogen; TT, thrombin time.

random. Our study used a customized database and non-targeted metabolomic methods to analyze the data. Furthermore, we identified hundreds of compounds from data collection to data analysis of clear compounds based on the established Orbitrap workflow. Therefore, a total of 513 metabolites were conformed in the samples before and after treatment, which were identified with known MS/MS information. The detailed information of 513 identified metabolites including compound name, electrospray ionization mode, mass, and retention time were shown in the **Supplementary Table**.

Serum Metabolomics and Pathway Analysis

A total of 513 metabolites were identified in our study, and these metabolites were imported into the SIMCA-P software for PCA. The result of PCA showed that there was no significant difference between the two groups ($P > 0.05$). We subsequently performed the analysis using the two- or three-dimensional orthogonal partial least-squares discriminant method obtained in an OPLS-DA score chart (**Figure 3**). It showed a significant difference between the THSWD group and the placebo group ($R^2X = 70.5\%$, $Q^2 = 57.9\%$). However, there was no statistically significant difference between the two groups after treatment, suggesting that there were some differences in the baseline level of differential metabolites, affecting the overall comparison results between the groups after treatment.

Considering the screening of identified metabolites under the conditions of VIP > 1 and $P < 0.05$, it was found that there were 24 kinds of differential metabolites in the THSWD group and the placebo group before the treatment ($P < 0.05$, VIP > 1), and the differences were not observed after 12 weeks of treatment. Additionally, there were three differential metabolites in the THSWD group and the placebo group after treatment ($P < 0.05$) with no statistically significant difference before treatment, suggesting that the treatment of THSWD also changed the level of other three differential metabolites, revealing that THSWD treatment changed a total of 27 differential metabolites (**Figure 4**, **Tables 5** and **6**).

The result of the heat map showed a total of 24 differential metabolites between the THSWD group and the placebo group before treatment (**Figure 4A**, **Table 5**). Before treatment, levels of the 18 differential metabolites in the THSWD group were higher compared with that of the placebo group. Biliverdin (fold change [FC] = 1.93, FC in the THSWD/placebo groups), and propionylcarnitine (FC = 1.83) were obtained by electrospray ionization-positive (ESI+) mode. Threonic acid (FC = 1.45), succinate (FC = 1.38), sulfate (FC = 1.79), L-lysine (FC = 1.77), *N*-acetyl-L-aspartic acid (FC = 1.60), *N*-alpha-acetyl-L-asparagine (FC = 1.48), bilirubin (FC = 1.58), indoxyl sulfate (FC = 2.69), gluconic acid (FC = 1.60), pelargonic acid (FC = 1.43), 3-ureidopropionate (3-UPA) (FC = 1.41), D-glucose (FC = 1.43), hippurate (FC = 4.27), 8,9-dihydroxyeicosatrienoic acid (8,9-DiHETrE) (FC = 1.59), 2-furoic acid (FC = 1.53), and gluconolactone (FC = 1.47) were obtained by electrospray ionization-negative (ESI–) mode. However, there was no significant difference among the above 18 metabolites after THSWD treatment for 12 weeks, suggesting that THSWD treatment downregulated these 18 metabolites. In the THSWD group before treatment, levels of the six differential metabolites were lower compared with that of the placebo group. Succinylcarnitine (FC = 0.66), phosphorylcholine (FC = 0.71), 5′-methylthioadenosine (5′-MTA) (FC = 0.60), and 2-pyrrolidinone (FC = 0.68) were obtained by ESI+ mode. Myristic acid (FC = 0.72) and leukotriene A4 (FC = 0.86) were obtained by ESI– mode. However, there was no significant difference among the above six metabolites after THSWD treatment, suggesting that THSWD treatment upregulated these six metabolites.

The analysis of another three metabolites showed no difference between the two groups before the treatment, but there was significant difference after the treatment (**Figure 4B**, **Table 6**). The results showed that in the THSWD group, glycerophosphocholine (FC = 0.67) was downregulated, and *N*-acetyl-L-lysine (FC = 1.21) and *N*-acetylglutamic acid (FC = 1.14) were upregulated.

Considering software analysis and prediction, we found that the 27 differential metabolites associated with THSWD were involved in 29 metabolic pathways. The metabolic pathways closely associated with energy metabolism included FA metabolism, glycolysis or gluconeogenesis, citrate cycle (tricarboxylic acid [TCA] cycle), and PPP. Amino acid metabolism included phenylalanine metabolism; beta-alanine metabolism; alanine, aspartate, and glutamate metabolism; lysine biosynthesis; lysine degradation; cysteine and methionine metabolism; tyrosine metabolism; and arginine and proline metabolism. Additionally, it also included glycerophospholipid metabolism, arachidonic acid metabolism, biotin metabolism, sulfur metabolism, ether lipid metabolism, pantothenate and coenzyme A (CoA) biosynthesis, porphyrin and chlorophyll metabolism, propanoate metabolism, butanoate metabolism, galactose metabolism, ascorbate and aldarate metabolism, glyoxylate and dicarboxylate metabolism, starch and sucrose metabolism, pyrimidine metabolism, aminoacyl-transfer ribonucleic acid biosynthesis, amino sugar and nucleotide sugar metabolism, and purine metabolism (**Figure 5**, **Table 7**).

The correlation analysis between the 27 differential metabolites and differential serum clinical indexes (TC, LDL, and APTT) was shown by a Pearson's correlation heat map (**Figure 6**). Among them, pelargonic acid ($P = 0.008$, R = 0.749), D-glucose ($P = 0.017$, R = 0.697), succinate ($P = 0.004$, R = 0.788), L-lysine ($P = 0.022$, R = 0.679), *N*-alpha-acetyl-L-asparagine ($P = 0.001$, R = 0.840), indoxyl sulfate ($P = 0.029$, R = 0.653), 8,9-DiHETrE ($P = 0.010$, R = 0.737), and 3-UPA ($P = 0.035$, R = 0.636) were positively associated with TC. Succinylcarnitine ($P = 0.003$, R = −0.801) and 5′-MTA ($P = 0.003$, R = −0.802) were negatively associated with LDL. Pelargonic acid ($P = 0.027$, R = 0.662), gluconic acid ($P = 0.020$, R = 0.685), L-lysine ($P = 0.026$, R = 0.664), *N*-alpha-acetyl-L-asparagine ($P = 0.031$, R = 0.648), and indoxyl sulfate ($P = 0.009$, R = 0.742) were positively associated with LDL. Succinylcarnitine ($P = 0.005$, R = 0.781) and 5′-MTA ($P = 0.034$, R = 0.639) were positively associated

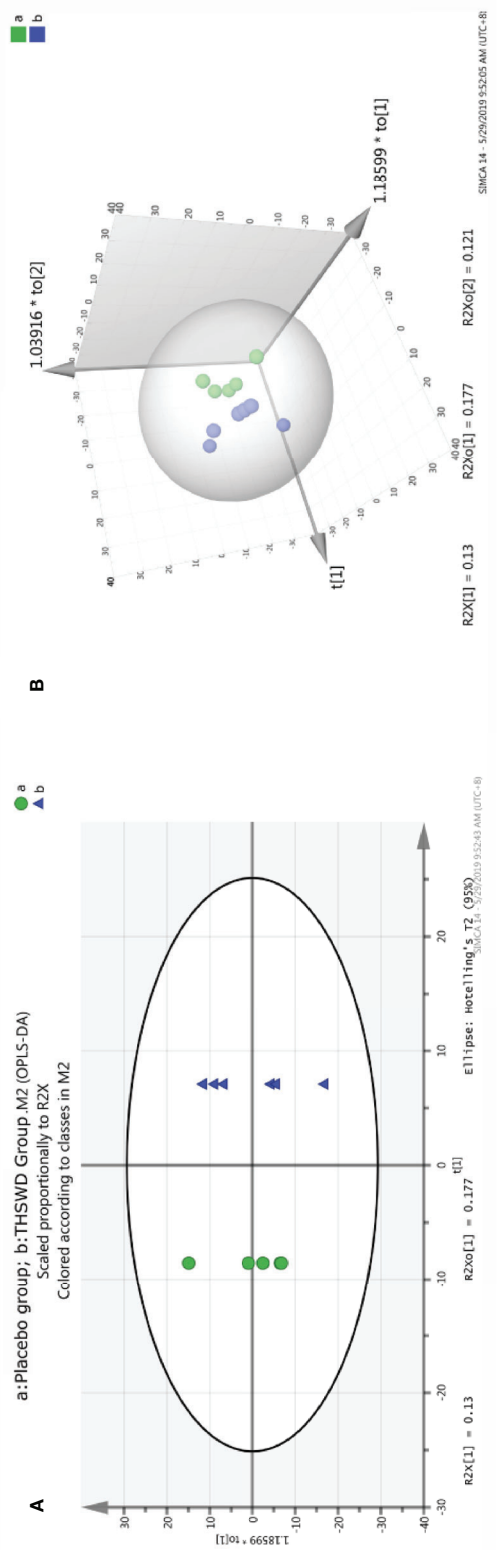


FIGURE 3 | The orthogonal partial least structures discriminant analysis (OPLS-DA) score plots compared the placebo group **(A)** with the THSWD group **(B)**. The placebo group is shown in green color, and the THSWD group is shown in blue color. A: the two-dimensional graph of the OPLS-DA score plots. B: the three-dimensional graph of the OPLS-DA score plots.

with APTT. Pelargonic acid (P = 0.010, R = −0.734), gluconolactone (P = 0.028, R=−0.658), *N*-acetyl-L-aspartic acid (P = 0.042, R = −0.620), *N*-alpha-acetyl-L-asparagine (P = 0.018, R = −0.694), and hippurate (P = 0.003, R=−0.800) were negatively associated with APTT.

DISCUSSION

Metabolic abnormality caused by myocardial ischemia plays a key role in the occurrence, development, and prognosis of CHD (Doenst et al., 2013). A combination of Western medicine and TCM is considered a safe and effective treatment for CHD. THSWD is a classical traditional Chinese medication that has a significant therapeutic effect on CHD by promoting blood circulation according to TCM theory. However, the underlying mechanism of THSWD on promoting blood circulation and removing blood stasis is unclear. Recent studies demonstrated that blood stasis was mainly associated with amino acid metabolism and lipid metabolism, suggesting that amino acid and lipid metabolites are associated with the "blood" in the TCM theory (Hao et al., 2018; Zhao et al., 2019). In this study, the non-targeted metabolomic analysis was used to detect the low-molecular-weight metabolites in CHD patients with THSWD and placebo granules treatment, and 513 kinds of metabolites were found. A total of 27 differential low-molecular-weight metabolites involved in 29 metabolic pathways were detected between the THSWD group and the placebo group. Among them, some metabolites play an important role on CHD. Succinylcarnitine in fatty acid metabolism and 5′-MTA in cysteine and methionine metabolism were increased in the THSWD group compared with the placebo group. However, pelargonic acid, involved in FA metabolism; succinate, involved in TCA cycle; gluconic acid, gluconolactone, and D-glucose, involved in PPP; glycerophosphocholine, involved in glycerophospholipid metabolism; 8,9-DiHETrE, involved in arachidonic acid metabolism; L-lysine, involved in lysine biosynthesis and degradation; *N*-acetyl-L-aspartic acid and *N*-alpha-acetyl-L-asparagine, involved in alanine, aspartate, and glutamate metabolism; hippurate, involved in phenylalanine metabolism; indoxyl sulfate, involved in tryptophan metabolism; and 3-UPA, involved in beta-alanine metabolism, were decreased in the THSWD group compared with the placebo group. Moreover, succinylcarnitine, pelargonic acid, succinate, D-glucose, gluconic acid, L-lysine, *N*-alpha-acetyl-L-asparagine, 5′-MTA, indoxyl sulfate, 8,9-DiHETrE, and 3-UPA were associated with TC or LDL. Succinylcarnitine, pelargonic acid, gluconolactone, *N*-acetyl-L-aspartic acid, *N*-alpha-acetyl-L-asparagine, hippurate, and 5′-MTA were associated with APTT. Our findings indicated that the low-molecular-weight metabolites might be associated with the anticoagulant and lipid-lowering effects of THSWD and constitute the partial material foundation of the "blood" in TCM theory.

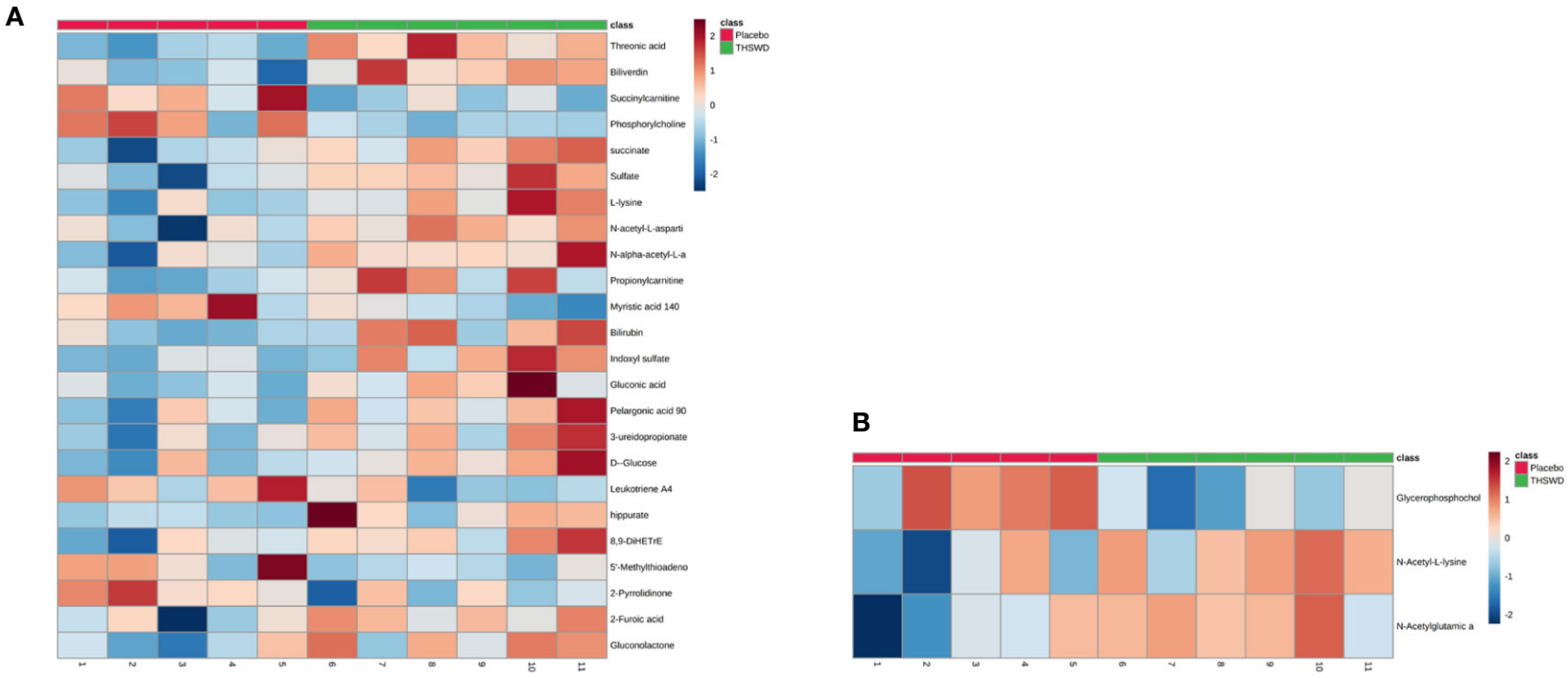


FIGURE 4 | The 27 differential metabolites in the two groups are shown in the heat map using MetaboAnalyst 4.0 (**A**: 24 differential metabolites between the THSWD group and the placebo group before treatment; **B**: 3 differential metabolites between the THSWD group and the placebo group after treatment). The row represents the metabolites, and the column represents the individual samples. The deeper the color, the greater the difference in metabolites. Red bands indicate upregulated metabolites, and blue bands indicate downregulated metabolites in the two groups.

TABLE 5 | Differential metabolites between the THSWD group and the placebo group before treatment from UPLC-MS/MS analysis.

Differential metabolites	ESI mode	Mass (m/z)	Mass Shift (ppm)	MS/MS confirmed	RT (min)	VIP	P	FC (THSWD/placebo)
Threonic acid	neg	135.0299	-0.848793939	Yes	0.90	2.40042	0.00058	1.45
Biliverdin	pos	583.25511	-0.460942063	Yes	1.89	2.09742	0.007122	1.93
Succinylcarnitine	pos	262.12906	-2.25525746	Yes	9.46	2.07186	0.008251	0.66
Phosphorylcholine	pos	184.07332	-1.733257937	Yes	5.83	2.05796	0.008941	0.71
succinate	neg	117.01881	4.12066833	Yes	0.88	2.01993	0.011028	1.38
Sulfate	neg	96.9601	-0.4768798	Yes	0.87	1.99716	0.012423	1.79
L-lysine	neg	145.09773	3.31739348	Yes	1.02	1.93366	0.017102	1.77
N-acetyl-L-aspartic acid	neg	174.04027	3.13659881	Yes	0.88	1.89204	0.020726	1.60
N-alpha-acetyl-L-asparagine	neg	173.05626	2.43054742	No	18.92	1.87169	0.022759	1.48
Propionylcarnitine	pos	218.13868	-0.3028414	Yes	7.16	1.85991	0.023979	1.83
Myristic acid (14:0)	neg	227.20111	2.41737985	No	11.91	1.8426	0.025752	0.72
Bilirubin	neg	583.25621	0.49360338	No	10.55	1.82541	0.027776	1.58
Indoxyl sulfate	neg	212.00178	2.70346738	Yes	6.18	1.7993	0.030837	2.69
Gluconic acid	neg	195.0505	1.95042561	Yes	0.90	1.7919	0.031714	1.60
Pelargonic acid (9:0)	neg	157.1234	-0.3713829	No	8.78	1.77715	0.033688	1.43
3-ureidopropionate	neg	131.04569	3.22608662	No	0.93	1.75349	0.03689	1.41
D-(+)-Glucose	neg	179.05611	-0.2205941	No	1.00	1.7372	0.03926	1.43
Leukotriene A4	neg	317.21222	2.07733691	No	13.11	1.73305	0.039865	0.86
Hippurate	neg	178.05097	-0.0956546	Yes	4.85	1.71272	0.04291	4.27
8,9-DiHETrE	neg	337.23843	–7.429894	No	12.89	1.71191	0.043078	1.59
5′-Methylthioadenosine	pos	298.09736	8.90499169	No	11.32	1.69579	0.045691	0.60
2-Pyrrolidinone	pos	86.06004	0.77251831	Yes	1.40	1.69382	0.045915	0.68
2-Furoic acid	neg	111.00876	–0.369243	No	0.87	1.68541	0.047254	1.53
Gluconolactone	neg	177.03994	2.33424636	No	0.89	1.68089	0.047968	1.47

THSWD, Taohong Siwu Decoction; ESI, electrospray ionization; RT, retention time; VIP, variable importance in the projection; P, probability; FC, fold change; Pos, positive; Neg, negative.

Lipid metabolism

Fatty Acid Metabolism

FA oxidation plays a critical role in myocardial energy generation. FAs are esterified to fatty acyl-CoA in the cytosol by carnitine palmitoyl transferase I (CPT I) located in the outer mitochondrial membrane. Long-chain acylcarnitine is subsequently transported into the mitochondrial matrix and converted back to long-chain acyl-CoA by CPT II. Acyl-CoA subsequently enters β-oxidation, generating acetyl-CoA (Peterzan et al., 2017). In this study, it was found for the first time that the serum level of succinylcarnitine in the THSWD group was lower compared with that of the placebo group before treatment, but there was no significant difference between the two groups after treatment with THSWD and placebo granules, suggesting that THSWD upregulated the succinylcarnitine level and promoted the β-oxidation of FAs. Further study showed that succinylcarnitine had a positive association with APTT and a negative association with LDL, illustrating that succinylcarnitine might be associated with the anticoagulant and lipid-lowering effects of THSWD.

Pelargonic acid, a type of medium-chain saturated FAs, provides free FAs for β-oxidation. A pilot study found that pelargonic acid was associated with the future onset of CHD in patients with type 2 diabetes by non-targeted metabolomic analysis (Omori et al., 2019). In our study, the serum level of pelargonic acid in the THSWD group was higher than that in the placebo group before treatment. However, after treatment, the changes in pelargonic acid were reversed, suggesting that THSWD may decrease the serum level of pelargonic acid by promoting the β-oxidation of FAs. Furthermore, it was found for the first time through correlation analysis that pelargonic acid was negatively associated with APTT, and positively associated with LDL and TC, suggesting that pelargonic acid might be related to the anticoagulation and lipid-lowering effects of THSWD.

Glycerophospholipid Metabolism

Phospholipids are involved in several pathophysiological process of CHD such as apoptosis, autophagy, proliferation, and inflammation. Phosphatidylcholine (PC) is one of the most important phospholipids in eukaryotic cells (Kosmas et al., 2018). LysoPC is the main component of ox-LDL. In the process of LDL oxidation, the level of lysoPC increases, and lysoPC is involved in the pathophysiological process of coronary atherosclerosis (Boyanovsky and Webb, 2009; Senn et al., 2012). Basak et al. found that lysoPC was better upregulated in the plasma of CHD patients than that of controls using LC-MS analysis (Basak et al., 2015). Glycerophosphocholine is produced by lysoPC. According to Hao et al.'s acute blood stasis rat model used to detect plasma metabolomics, the plasma level of glycerophosphocholine increased due to acute blood stasis (Hao et al., 2018). Our study showed that THSWD granule treatment downregulated glycerophosphocholine, suggesting that THSWD may alleviate coronary atherosclerosis and the symptoms of blood stasis by downregulating glycerophosphocholine.

Arachidonic Acid Metabolism

8,9-DiHETrE is a cytochrome P450 eicosanoid that is involved in the regulation of vascular tension, cardiac contractility, cell proliferation, and inflammation. The decrease of 8,9-DiHETrE indicates the limitation of the inflammation regulated by arachidonic acid. A recent cross-sectional study confirmed that

TABLE 6 | Differential metabolites between the THSWD group and the placebo group after treatment from UPLC-MS/MS analysis.

Differential metabolites	ESI mode	Mass (m/z)	Mass Shift (ppm)	MS/MS confirmed	RT (min)	P	FC (THSWD/placebo)
Glycerophosphocholine	pos	258.1101	−0.5460471	Yes	10.39	0.01205	0.67
N-acetyl-L-lysine	pos	189.12337	0.24395569	Yes	9.83	0.030883	1.21
N-acetylglutamic acid	neg	188.05645	−0.1722251	No	0.88	0.033159	1.14

THSWD, Taohong Siwu Decoction; ESI, electrospray ionization; RT, retention time; P, probability; FC, fold change; Pos, positive; Neg, negative.

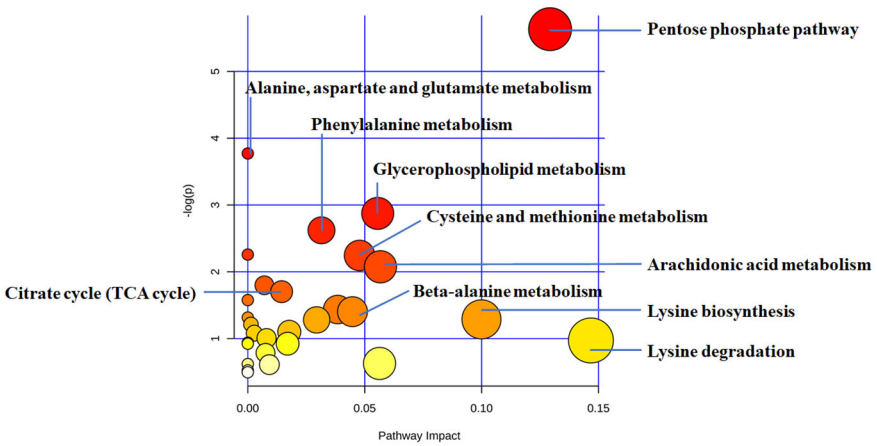


FIGURE 5 | The disturbed metabolic pathways showed differential metabolites between the THSWD group and the placebo group by MetaboAnalyst 4.0 software. Node radius was based on pathway impact values. Node color was based on *P* value.

8,9-DiHETrE was significantly associated with cardiovascular events; with every 1 nmol/L increase in the concentrations of 8,9-DiHETrE, the odds of acute coronary syndrome (ACS) increased by 454 times, suggesting that 8,9-DiHETrE is the most significant predictor of ACS (Caligiuri et al., 2017; Solati and Ravandi, 2019). In this study, we found that the serum level of 8,9-DiHETrE in the THSWD group before treatment was higher than that in the placebo group, but there was no significant difference in 8,9-DiHETrE after the treatment between the THSWD group and the placebo group, indicating that THSWD may downregulate the serum level of 8,9-DiHETrE and arachidonic acid metabolism-mediated inflammation. Additionally, we initially found that 8,9-DiHETrE was positively associated with TC by correlation analysis, illustrating that THSWD might also reduce the serum level of TC by decreasing 8,9-DiHETrE level.

Glucose Metabolism

The utilization of FAs and glucose is closely co-regulated in myocardial metabolism. The oxidation of FAs or glucose may directly inhibit the utilization of another, which is called "Randle cycle" (Randle, 1998). In myocardial ischemia, the oxidation of FAs is decreased, while glucose metabolism is increased in cardiomyocytes.

Tricarboxylic Acid Cycle

Pyruvate, generated through glycolysis, enters the mitochondrial matrix and undergoes oxidation to acetyl-CoA by the multienzyme complex pyruvate dehydrogenase. Subsequently, acetyl-CoA enters the TCA cycle and produced adenosine triphosphate (ATP). Succinate is the intermediate product of the tricarboxylic acid cycle. The formation of succinate is the only step to directly produce high-energy phosphate bond in the tricarboxylic acid cycle, which belongs to the substrate-level phosphorylation reaction. The succinate in the tricarboxylic acid cycle of the THSWD group was better up-regulated than that of the placebo group before treatment, but there was no statistically significant difference between the two groups after treatment, suggesting that the succinate was down-regulated after the treatment of THSWD. Combined with the changes in FA metabolism-related molecules, it suggests that glucose metabolism is inhibited and the intermediate product of the TAC cycle decreases due to the upregulation of FA metabolism. THSWD promoted energy generation with the increase of fatty acid metabolism and the decrease of glucose metabolism. Further correlation analysis showed that succinate was positively associated with TC, suggesting that THSWD could downregulated cholesterol level by reducing succinate level.

Pentose Phosphate Pathway

Glucose-6-phosphate is also possibly involved in PPP. PPP is an essential source of nicotinamide adenine dinucleotide phosphate (NADPH), which regulates oxidative stress and lipid synthesis and complement. In myocardial ischemia, the PPP is upregulated (Doenst et al., 2013). In this study, we found that levels of gluconic acid, gluconolactone, and D-glucose involved in PPP

were higher than those in the placebo group before THSWD treatment, but there was no significant difference after treatment, suggesting that THSWD downregulates the levels of gluconic acid, gluconolactone, and D-glucose involved in PPP. Combined with the differential metabolites' change in FA metabolism and the TCA cycle, it suggests that the upregulation of energy generation might inhibit PPP pathway. Furthermore, by performing correlation analysis, it was found for the first time that there was a negative association between gluconolactone and APTT; gluconic acid was positively associated with LDL; and there was a positive association between D-glucose and TC, suggesting that these three metabolites involved in PPP were also associated with the anticoagulant and lipid-lowering effects of THSWD.

Amino Acid Metabolism

Previous studies have found that blood stasis is associated with amino acid metabolism, as shown by the decrease of tryptophan and the increase of tyrosine in the blood stasis group compared with the control group, suggesting that the "blood" in the theory of Qi and the blood in TCM are closely associated with amino acid metabolism (Hao et al., 2018; Zhao et al., 2019). Fan et al. revealed that plasma metabolomic profiles in patients with different types of CHD by performing liquid chromatography-quadrupole time-of-flight MS, and found that levels of the amino acid metabolites, such as tryptophan, arginine, and leucine, increased with CHD progression (Fan et al., 2016). However, based on a mini-swine model of progressive chronic heart failure, metabolomic analysis of ischemic tissue and plasma in the model group revealed a significant decrease of alanine and glycine involved in amino acid metabolism as compared with controls (Wang et al., 2013). For the first time, we found that THSWD downregulated L-lysine, *N*-acetyl-L-aspartic acid, and *N*-alpha-acetyl-L-asparagine, but upregulated *N*-acetyl-L-lysine, and *N*-acetylglutamic acid, suggesting that THSWD regulated amino acid metabolism. We also found that *N*-acetyl-L-aspartic acid and *N*-alpha-acetyl-L-asparagine were negatively associated with APTT. L-lysine and *N*-alpha-acetyl-L-asparagine was positively associated with TC and LDL. The results indicated that THSWD might play a critical role in lipid reduction and anticoagulation by regulating amino acid metabolism. The following small molecular metabolites may be closely associated with the mechanism of THSWD in the treatment of CHD.

TABLE 7 | Differential metabolic pathway between the THSWD group and the placebo group.

Pathway Name	Match Status	Match Metabolites
Pentose phosphate pathway	3/32	Gluconic acid; Gluconolactone; D-glucose
Alanine, aspartate, and glutamate metabolism	2/24	N-acetyl-L-aspartic acid; Succinic acid
Glycerophospholipid metabolism	2/39	Phosphorylcholine; Glycerophosphocholine
Phenylalanine metabolism	2/45	Hippuric acid; Succinic acid
Biotin metabolism	1/11	L-lysine
Cysteine and methionine metabolism	2/56	5′-Methylthioadenosine; Sulfate
Arachidonic acid metabolism	2/62	Leukotriene A4; 8,9-DiHETrE
Sulfur metabolism	1/18	Sulfate
Citrate cycle (TCA cycle)	1/20	Succinic acid
Ether lipid metabolism	1/23	Glycerophosphocholine
Pantothenate and CoA biosynthesis	1/27	Ureidopropionic acid
beta-Alanine metabolism	1/28	Ureidopropionic acid
Glycolysis or gluconeogenesis	1/31	D-Glucose
Lysine biosynthesis	1/32	L-Lysine
Porphyrin and chlorophyll metabolism	2/104	Biliverdin; Bilirubin
Propanoate metabolism	1/35	Succinic acid
Butanoate metabolism	1/40	Succinic acid
Galactose metabolism	1/41	D-Glucose
Ascorbate and aldarate metabolism	1/45	Threonic acid
Lysine degradation	1/47	L-lysine
Fatty acid biosynthesis	1/49	Myristic acid
Glyoxylate and dicarboxylate metabolism	1/50	Succinic acid
Starch and sucrose metabolism	1/50	D-Glucose
Pyrimidine metabolism	1/60	Ureidopropionic acid
Aminoacyl-tRNA biosynthesis	1/75	L-Lysine
Tyrosine metabolism	1/76	Succinic acid
Arginine and proline metabolism	1/77	N-Acetyl-L-alanine
Amino sugar and nucleotide sugar metabolism	1/88	D-Glucose
Purine metabolism	1/92	Sulfate

5′-MTA, a nucleoside produced by S-adenosylmethionine during the synthesis of polyamines, is previously considered to inhibit tumor cell proliferation, invasion and apoptosis, and to regulate the inflammatory microenvironment of the tumor. Another study indicated that 5′-MTA pre-treatment significantly alleviated liver ischemia/reperfusion injury by inhibiting inflammatory response following liver transplantation *in vivo*, with the inhibition of NF-κB and MAPK signal pathway (Tang et al., 2014). We found that the level of 5′-MTA involved in cysteine and methionine metabolism was lower in the THSWD group than that in the placebo group before treatment; however, there was no significant difference in 5′-MTA level between the two groups after treatment, suggesting that THSWD upregulated the serum level of 5′-MTA. Further correlation analysis showed that 5′-MTA was positively associated with APTT and negatively associated with LDL, suggesting that 5′-MTA might be associated with the anticoagulation and lipid-lowering effect of THSWD.

Hippurate is a protein-bound uremic retention solute, which is significantly increased in the serum of patients with chronic renal failure (Vanholder et al., 2003). Previous studies found that hippurate levels in the serum were positively associated with diastolic blood pressure and echocardiographic indexes such as end-diastolic interventricular septal thickness, suggesting that hippurate can be considered as a new biomarker of the left ventricular overload (Yu et al., 2018). Additionally, other studies reported that hippurate causes endothelial dysfunction and oxidative stress by an increase in mitoROS *via* mitochondrial fission (Huang et al., 2018). We found that the level of hippurate in the THSWD group was higher than that in the placebo group before treatment, but there was no significant difference between the two groups after treatment, suggesting that THSWD decreases

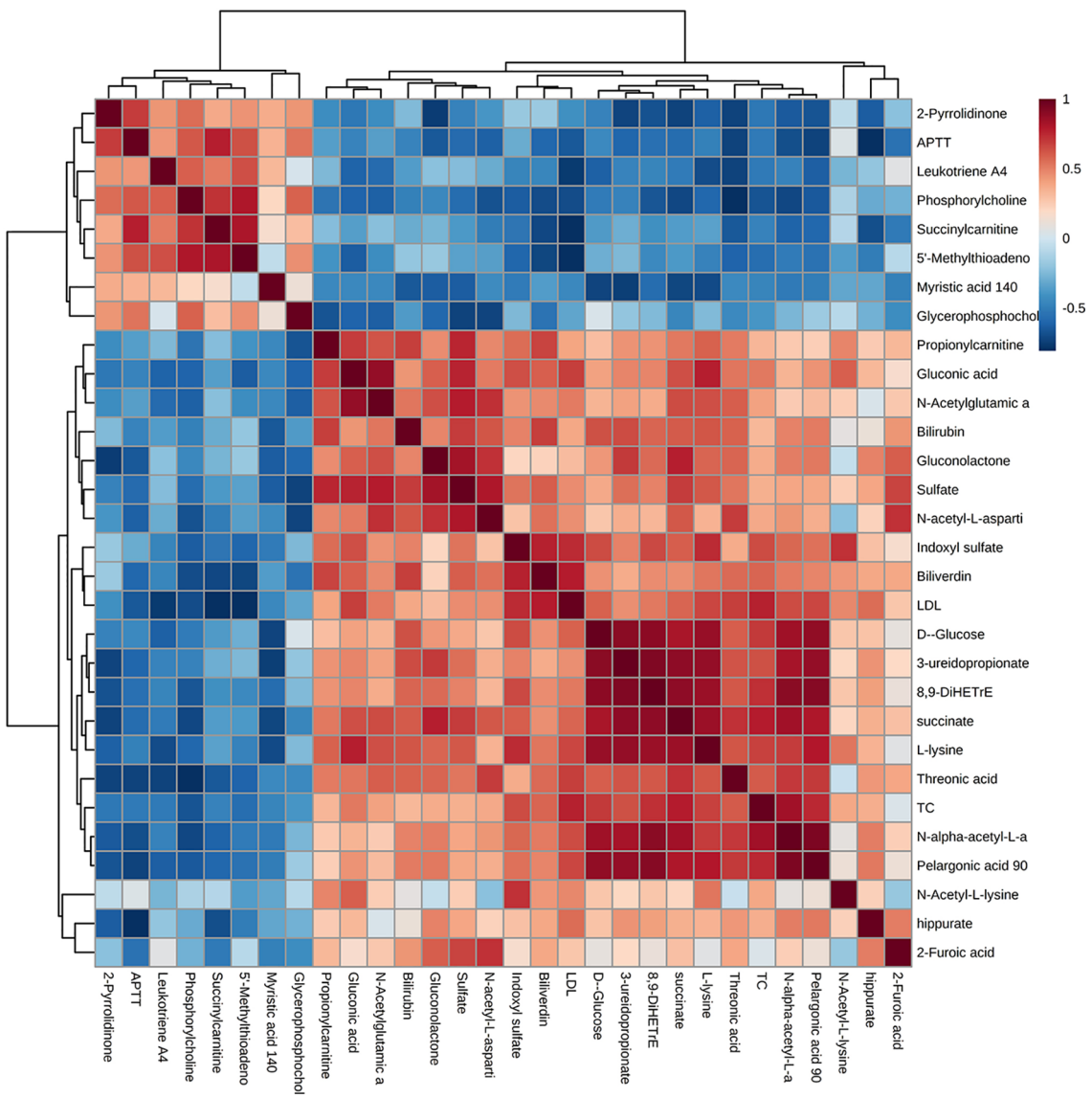


FIGURE 6 | A Pearson's correlation heat map of the serum metabolites and clinical parameters. Greater intensities of brown and blue indicate higher positive or negative correlations, respectively.

the serum level of hippurate. Furthermore, it was found for the first time through correlation analysis that hippurate was negatively associated with APTT, suggesting that hippurate might be associated with the anticoagulant effect of THSWD.

Indoxyl sulfate is also a protein-bound uremic toxin generated by tryptophan metabolism *via* the gut microbiota. A recent study found that indoxyl sulfate activated oxidative stress by regulating multiple NADPH oxidase-mediated redox signaling pathways and aggravated the progress of cardiovascular diseases such as chronic heart failure, arrhythmia, and CHD (Gao and Liu, 2017). Other studies prospectively assessed the all-cause mortality of 351 patients undergoing percutaneous revascularization for CHD or peripheral artery disease and found that the highest mortality rate was observed in the high indoxyl sulfate and low albumin group, suggesting that a higher indoxyl sulfate level add potentiating effects on lower albumin as a prognostic factor for cardiovascular disease (Watanabe et al., 2019). This study found that the level of indoxyl sulfate in the THSWD group was higher than that in the placebo group before treatment, but there was no significant difference between the two groups after treatment, suggesting that the level of indoxyl sulfate could be decreased after THSWD treatment. Further correlation analysis showed for the first time that indoxyl sulfate was positively associated with LDL and TC, suggesting that indoxyl sulfate might be associated with the lipid-lowering effect of THSWD.

3-UPA is a physiological metabolite produced by pyrimidine degradation that is involved in β-alanine metabolism. Other studies reported that 3-UPA acts as an endogenous neurotoxin

by inhibiting mitochondrial energy metabolism. In cultured chick neurons, 3-UPA induced the increase of reactive oxygen species and intracellular calcium concentrations. 3-UPA also inhibited complex V activity in a single respiratory chain, but it did not affect the mitochondrial FA oxidation (Kölker et al., 2001). This study found that before the treatment the serum level of 3-UPA in the THSWD group was higher than that in the placebo group, but there was no significant difference in 3-UPA after treatment, suggesting that THSWD could downregulate the level of 3-UPA. Moreover, it was found for the first time that 3-UPA was positively associated with TC, suggesting that 3-UPA might be also associated with the lipid-lowering effect of THSWD.

Limitation

Our study has some limitations. First, a small number of participants were selected in our study, which might be the reason for the statistically significant difference of metabolites between the two groups before the treatment. Second, the metabolomics itself has some limitations. A single instrument to detect all metabolites in a single analysis is not available. In the study of CHD-related metabolomics, the number of metabolites identified in serum was usually less than in cells or tissues, and the detected serum metabolites might originate from non-myocardial tissues. Moreover, the use of metabolic drugs and the excretion of liver and kidney affect the serum level of metabolites, increasing the uncertainty of applying metabolomics to the clinical detection of CHD.

CONCLUSION

In conclusion, THSWD promoted energy generation by upregulating FA metabolism and downregulating glucose metabolism. THSWD also downregulated glycerophospholipid metabolism and arachidonic acid metabolism, and was involved in amino acid metabolism. This was the first study to confirm the changes of serum metabolomics in CHD patients after the treatment of THSWD. It is revealed that small molecular metabolites such as glycerophosphocholine, 8,9-DiHETrE, 5′-MTA, hippurate, indoxyl sulfate, and 3-UPA may be the potential targets of THSWD for anticoagulation and lipid reduction, and the material foundation of the "blood" to promote blood circulation in CHD treatment.

DATA AVAILABILITY STATEMENT

The datasets generated for this study are available on request to the corresponding author.

ETHICS STATEMENT

The studies involving human participants were reviewed and approved by the Ethics Review Committee of the Chinese PLA General Hospital (No. S2015-048-01). The patients/participants provided their written informed consent to participate in this study.

AUTHOR CONTRIBUTIONS

XL conceived, designed, and supervised the clinical trial and experiments, and contributed to manuscript revision. TT performed the trial and statistical analysis, and drafted the manuscript. TH and HM co-performed the trial. XW co-supervised the clinical trial. All authors read and approved the submitted version.

FUNDING

This work was supported by the National Natural Science Foundation of China (No. 31971049) and the National Basic Research Program of China (No. 2015CB554402, 2015CB554405).

SUPPLEMENTARY MATERIAL

The Supplementary Material for this article can be found online at: https://www.frontiersin.org/articles/10.3389/fphar.2020.00651/full#supplementary-material

SUPPLEMENTARY FIGURE | The representative MS/MS spectra of six significant metabolites (succinylcarnitine, glycerophosphocholine, succinate, hippurate, indoxyl sulfate, gluconic acid). A: The MS/MS spectra of the serum sample; B. The MS/MS spectra in the in-house library.

SUPPLEMENTARY TABLE | The detail data of 513 identified metabolites.

REFERENCES

Basak, T., Varshney, S., Hamid, Z., Ghosh, S., Seth, S., and Sengupta, S. (2015). Identification of metabolic markers in coronary artery disease using an untargeted LC-MS based metabolomic approach. *J. Proteomics.* 127, 169–177. doi: 10.1016/j.jprot.2015.03.011

Boyanovsky, B. B., and Webb, N. R. (2009). Biology of secretory phospholipase A2. *Cardiovasc. Drugs Ther.* 23, 61–72. doi: 10.1007/s10557-008-6134-7

Caligiuri, S. P. B., Aukema, H. M., Ravandi, A., Lavallée, R., Guzman, R., and Pierce, G. N. (2017). Specific plasma oxylipins increase the odds of cardiovascular and cerebrovascular events in patients with peripheral artery disease. *Can. J. Physiol. Pharmacol.* 95, 961–968. doi: 10.1139/cjpp-2016-0615

Chong, J., Soufan, O., Li, C., Caraus, I., Li, S., Bourque, G., et al. (2018). MetaboAnalyst 4.0: towards more transparent and integrative metabolomics analysis. *Nucleic Acids Res.* 46, W486–W494. doi: 10.1093/nar/gky310

Doenst, T., Nguyen, T. D., and Abel, E. D. (2013). Cardiac metabolism in heart failure-implications beyond ATP production. *Circ. Res.* 113, 709–724. doi: 10.1161/CIRCRESAHA.113.300376

Fan, Y., Li, Y., Chen, Y., Zhao, Y. J., Liu, L. W., Li, J., et al. (2016). Comprehensive Metabolomic Characterization of Coronary Artery Diseases. *J. Am. Coll. Cardiol.* 68, 1281–1293. doi: 10.1016/j.jacc.2016.06.044

Fihn, S. D., Blankenship, J. C., Alexander, K. P., Bittl, J. A., Byrne, J. G., Fletcher, B. J., et al. (2014). 2014 ACC/AHA/AATS/PCNA/SCAI/STS focused update of the guideline for the diagnosis and management of patients with stable

ischemic heart disease: a report of the American College of Cardiology/American Heart Association Task Force on Practice Guidelines, and the American Association for Thoracic Surgery, Preventive Cardiovascular Nurses Association, Society for Cardiovascular Angiography and Interventions, and Society of Thoracic Surgeons. *Circulation.* 130, 1749–1767. doi: 10.1161/CIR.0000000000000095

Gao, H., and Liu, S. (2017). Role of uremic toxin indoxyl sulfate in the progression of cardiovascular disease. *Life Sci.* 185, 23–29. doi: 10.1016/j.lfs.2017.07.027

Hao, M., De, J., Li, L., Su, L., Gu, W., Gu, L., et al. (2018). Mechanism of curcuma wenyujin rhizoma on acute blood stasis in rats based on a UPLC-Q/TOF-MS metabolomics and network approach. *Molecules* 24 (1), E82. doi: 10.3390/molecules24010082

Huang, M., Wei, R., Wang, Y., Su, T., Li, P., and Chen, X. (2018). The uremic toxin hippurate promotes endothelial dysfunction via the activation of Drp1-mediated mitochondrial fission. *Redox Biol.* 16, 303–313. doi: 10.1016/j.redox.2018.03.010

Kölker, S., Okun, J. G., Hörster, F., Assmann, B., Ahlemeyer, B., Kohlmüller, D., et al. (2001). 3-Ureidopropionate contributes to the neuropathology of 3-ureidopropionase deficiency and severe propionic aciduria: a hypothesis. *J. Neurosci. Res.* 66, 666–673. doi: 10.1002/jnr.10012

Kosmas, C. E., Martinez, I., Sourlas, A., Bouza, K. V., Campos, F. N., Torres, V., et al. (2018). High-density lipoprotein (HDL) functionality and its relevance to atherosclerotic cardiovascular disease. *Drugs Context.* 7, 212525. doi: 10.7573/dic.212525. eCollection 2018.

Li, Z. J., Chen, W., Jiang, H., Li, X. Y., Zhu, S. N., and Liu, X. H. (2018). Effects of postoperative parenteral nutrition enhanced by multivitamin on metabolic phenotype in postoperative gastric cancer patients. *Mol. Nutr. Food Res.* 62, e1700757. doi: 10.1002/mnfr.201700757

Liu, Z. Q., Yin, D. K., Han, L., Li, B. K., and Peng, D. Y. (2013). Protective effect of medicated serum prepared with Taohong Siwu Decoction on hydrogen peroxide-induced human umbilical vein endothelial cells. *Zhongguo Zhong Yao Za Zhi.* 38, 402–406.

Ma, Q., Li, P. L., Hua, Y. L., Ji, P., Yao, W. L., Zhang, X. S., et al. (2018). Effects of Tao-Hong-Si-Wu decoction on acute blood stasis in rats based on a LC-Q/TOF-MS metabolomics and network approach. *Biomed. Chromatogr.* 32 (4). doi: 10.1002/bmc.4144

Neumann, F. J., Sousa-Uva, M., Ahlsson, A., Alfonso, F., Banning, A. P., Benedetto, U., et al. (2019). 2018 ESC/EACTS guidelines on myocardial revascularization. *Eur. Heart J.* 40, 87–165. doi: 10.1093/eurheartj/ehy394

Ning, P., Zheng, Y., Luo, Q., Liu, X., Kang, Y., Zhang, Y., et al. (2018). Metabolic profiles in community-acquired pneumonia: developing assessment tools for disease severity. *Crit. Care* 22, 130. doi: 10.1186/s13054-018-2049-2

Omori, K., Katakami, N., Yamamoto, Y., Ninomiya, H., Takahara, M., Matsuoka, T. A., et al. (2019). Identification of metabolites associated with onset of CAD in diabetic patients using CE-MS Analysis: A pilot study. *J. Atheroscler. Thromb.* 26, 233–245. doi: 10.5551/jat.42945

Peterzan, M. A., Lygate, C. A., Neubauer, S., and Rider, O. J. (2017). Metabolic remodeling in hypertrophied and failing myocardium: a review. *Am. J. Physiol. Heart Circ. Physiol.* 313, H597–H616. doi: 10.1152/ajpheart.00731

Randle, P. J. (1998). Regulatory interactions between lipids and carbohydrates: The glucose fatty acid cycle after 35 years. *Diabetes Metab. Rev.* 14, 263–283. doi: 10.1002/(sici)1099-0895(199812)14:4<263::aid-dmr233>3.0.co;2-c

Senn, T., Hazen, S. L., and Tang, W. H. (2012). Translating metabolomics to cardiovascular biomarkers. *Prog. Cardiovasc. Dis.* 55, 70–76. doi: 10.1016/j.pcad.2012.06.004

Shah, S. H., Kraus, W. E., and Newgard, C. B. (2012). Metabolomic profiling for the identification of novel biomarkers and mechanisms related to common cardiovascular diseases: form and function. *Circulation* 126, 1110–1120. doi: 10.1161/CIRCULATIONAHA.111.060368

Solati, Z., and Ravandi, A. (2019). Lipidomics of bioactive lipids in acute coronary syndromes. *Int. J. Mol. Sci.* 20, pii: E1051. doi: 10.3390/ijms20051051

Tang, Y., Zhang, W., Zhang, Y., Wang, W., Yao, F., Yan, J., et al. (2014). 5′-Methylthioadenosine attenuates ischemia reperfusion injury after liver transplantation in rats. *Inflammation* 37, 1366–1373. doi: 10.1007/s10753-014-9861-x

Tang, H., Wang, X., Xu, L., Ran, X., Li, X., Chen, L., et al. (2016). Establishment of local searching methods for orbitrap-based high throughput metabolomics analysis. *Talanta.* 156-157, 163–171. doi: 10.1016/j.talanta.2016.04.051

Tao, T. Q., Mao, H. M., Xia, L., and Liu, X. H. (2019). Efficacy and Safety Evaluation of Taohong Siwu Decoction for Patients with Angina Pectoris: A Meta-Analysis of Randomized Controlled Trials. *Chin. J. Integr. Med.* doi: 10.1007/s11655-019-3028-4

Vanholder, R., De Smet, R., Glorieux, G., Argilés, A., Baurmeister, U., Brunet, P., et al. (2003). Review on uremic toxins: classification, concentration, and interindividual variability. *Kidney Int.* 63, 1934–1943. doi: 10.1046/j.1523-1755.2003.00924.x

Wang, Y., Li, C., Chuo, W., Liu, Z., Ouyang, Y., Li, D., et al. (2013). Integrated proteomic and metabolomic analysis reveals the NADH-mediated TCA cycle and energy metabolism disorders based on a new model of chronic progressive heart failure. *Mol. Biosyst.* 9, 3135–3145. doi: 10.1039/c3mb70263d

Watanabe, I., Tatebe, J., Fujii, T., Noike, R., Saito, D., Koike, H., et al. (2019). Prognostic Significance of Serum Indoxyl Sulfate and Albumin for Patients with Cardiovascular Disease. *Int. Heart J.* 60, 129–135. doi: 10.1536/ihj.18-116

Xiong, X. J., Wang, Z., and Wang, J. (2015). Innovative strategy in treating angina pectoris with Chinese patent medicines by promoting blood circulation and removing blood stasis: experience from combination therapy in Chinese medicine. *Curr. Vasc. Pharmacol.* 13, 540–553. doi: 10.2174/1570161112666141014153735

Yu, T. H., Tang, W. H., Lu, Y. C., Wang, C. P., Hung, W. C., Wu, C. C., et al. (2018). Association between hippuric acid and left ventricular hypertrophy in maintenance hemodialysis patients. *Clin. Chim. Acta* 484, 47–51. doi: 10.1016/j.cca.2018.05.022

Zhao, L. L., Qiu, X. J., Wang, W. B., Li, R. M., and Wang, D. S. (2019). NMR Metabolomics and Random Forests Models to Identify Potential Plasma Biomarkers of Blood Stasis Syndrome With Coronary Heart Disease Patients. *Front. Physiol.* 10, 1109. doi: 10.3389/fphys.2019.01109

Conflict of Interest: The authors declare that the research was conducted in the absence of any commercial or financial relationships that could be construed as a potential conflict of interest.

Copyright © 2020 Tao, He, Mao, Wu and Liu. This is an open-access article distributed under the terms of the Creative Commons Attribution License (CC BY). The use, distribution or reproduction in other forums is permitted, provided the original author(s) and the copyright owner(s) are credited and that the original publication in this journal is cited, in accordance with accepted academic practice. No use, distribution or reproduction is permitted which does not comply with these terms.

frontiers in Physiology

REVIEW
published: 19 May 2020
doi: 10.3389/fphys.2020.00433

Targeting Myeloperoxidase (MPO) Mediated Oxidative Stress and Inflammation for Reducing Brain Ischemia Injury: Potential Application of Natural Compounds

Shuang Chen[1†], Hansen Chen[1,2†], Qiaohui Du[1] and Jiangang Shen[1,2]*

[1] School of Chinese Medicine, The University of Hong Kong, Pok Fu Lam, Hong Kong, [2] Shenzhen Institute of Research and Innovation, The University of Hong Kong, Shenzhen, China

Oxidative stress and inflammation are two critical pathological processes of cerebral ischemia-reperfusion injury. Myeloperoxidase (MPO) is a critical inflammatory enzyme and therapeutic target triggering both oxidative stress and neuroinflammation in the pathological process of cerebral ischemia-reperfusion injury. MPO is presented in infiltrated neutrophils, activated microglial cells, neurons, and astrocytes in the ischemic brain. Activation of MPO can catalyze the reaction of chloride and H_2O_2 to produce HOCl. MPO also mediates oxidative stress by promoting the production of reactive oxygen species (ROS) and reactive nitrogen species (RNS), modulating the polarization and inflammation-related signaling pathways in microglia and neutrophils. MPO can be a therapeutic target for attenuating oxidative damage and neuroinflammation in ischemic stroke. Targeting MPO with inhibitors or gene deficiency significantly reduced brain infarction and improved neurological outcomes. This article discusses the important roles of MPO in mediating oxidative stress and neuroinflammation during cerebral ischemia-reperfusion injury and reviews the current understanding of the underlying mechanisms. Furthermore, we summarize the active compounds from medicinal herbs with potential as MPO inhibitors for anti-oxidative stress and anti-inflammation to attenuate cerebral ischemia-reperfusion injury, and as adjunct therapeutic agents for extending the window of thrombolytic treatment. We highlight that targeting MPO could be a promising strategy for alleviating ischemic brain injury, which merits further translational study.

Keywords: ischemic stroke, myeloperoxidase, natural compound, neuroinflammation, oxidative stress

OPEN ACCESS

Edited by:
Jing-Yan Han,
Peking University, China

Reviewed by:
Stefano Tarantini,
University of Oklahoma Health Sciences Center, United States
Ke-Wu Zeng,
Peking University, China

***Correspondence:**
Jiangang Shen
shenjg@hkucc.hku.hk

† These authors have contributed equally to this work

Specialty section:
This article was submitted to Vascular Physiology, a section of the journal Frontiers in Physiology

Received: *20 January 2020*
Accepted: *08 April 2020*
Published: *19 May 2020*

Citation:
Chen S, Chen H, Du Q and Shen J (2020) Targeting Myeloperoxidase (MPO) Mediated Oxidative Stress and Inflammation for Reducing Brain Ischemia Injury: Potential Application of Natural Compounds. Front. Physiol. 11:433. doi: 10.3389/fphys.2020.00433

INTRODUCTION

Stroke is a major human disease burden leading to death and life-long disability. Tissue plasminogen activator (t-PA) is the only therapeutic drug for ischemic stroke approved by the US Food and Drug Administration (FDA). However, t-PA has a restricted time window of 4.5 h, and delayed t-PA infusion increases the risk of hemorrhagic transformation and carries high mortality (Wardlaw et al., 2012). Delayed t-PA infusion mediates cerebral ischemia-reperfusion injury. Thus,

it is important to develop novel therapy or/and combination agents for thrombolytic therapy to prevent and attenuate cerebral ischemia-reperfusion injury in ischemic stroke treatment.

The brain has a large oxygen consumption due to high a metabolic rate, and the sudden arrest of oxygen triggers oxidative stress, which plays an important role in mediating cerebral ischemia-reperfusion injury (Allen and Bayraktutan, 2009; Rodrigo et al., 2013). Recanalization with delayed thrombolytic treatment further produces reactive oxygen/nitrogen species (ROS/RNS) such as superoxide ($O2^-$), hydrogen peroxide (H_2O_2), hypochlorous acid (HOCl), nitric oxide (NO), and peroxynitrite ($ONOO^-$). Antioxidant therapies such as edaravone, NXY-059, and allopurinol improved outcomes of acute ischemic stroke patients (Lees et al., 2006; Muir et al., 2008; Nakase et al., 2011). Many other antioxidants also have the potential to reduce cerebral ischemia injury. For example, nicotinamide adenine dinucleotide (NAD +) is a crucial player in modulating cellular energy metabolism and oxidative damage (Kiss et al., 2019a,b). Cellular NAD + level was significantly decreased during cerebral ischemia/reperfusion injury and exogenous NAD + supplementation prevented oxidative stress and increased the production of ATP, subsequently reducing cerebral ischemia/reperfusion injury (Ying et al., 2007; Huang Q. et al., 2018). Recently, the roles of RNS, including nitrogen monoxide, nitrogen dioxide, and peroxynitrite, etc., have drawn significant attention from the scientific community. RNS could activate multiple cellular signaling pathways involved in the BBB disruption, infarction enlargement and apoptotic cell death in cerebral ischemia-reperfusion injury (Chen et al., 2013). Matrix metalloproteinase (MMP), a classic proteolytic enzyme, is one of the critical molecular targets of RNS in mediating neuroinflammation and hemorrhagic transformation during cerebral ischemia-reperfusion injury (Gasche et al., 1999; Yang Y. et al., 2007; Jickling et al., 2014; Vandooren et al., 2014). MMP-9 is a plasma biomarker for monitoring brain damage and predicting hemorrhagic transformation in ischemic stroke with thrombolytic treatment (Ramos-Fernandez et al., 2011). *N*G-nitro-*L*-arginine methyl ester (*L*-NAME), a non-selective NOS inhibitor, attenuated the BBB disruption through inhibiting MMP-9 activity in an experimental ischemic stroke animal model (Gursoy-Ozdemir et al., 2004). For decades, we have made great efforts to explore the roles of RNS in mediating BBB disruption and brain injury, and seeking therapeutic targets for drug discovery to attenuate cerebral ischemia-reperfusion injury (Shen et al., 2006; Liu et al., 2009; Gu et al., 2012; Chen et al., 2013 ,2019; Chen H. et al., 2018; Chen H.S. et al., 2015; Fu et al., 2014; Gong et al., 2015; Feng et al., 2018a,b). With the short lifetime of ROS and RNS, it is an extremely challenging task to directly detect ROS/RNS in viable systems. To resolve the problems, we have successfully developed several fluorescent probes with high specificity and sensitivity, and applied the probes to detect peroxynitrite and hypochlorous acid in ischemic stroke rat models (Peng et al., 2014, 2016; Bai et al., 2020). We found that the RNS production aggravates the BBB disruption and brain damage in cerebral ischemia-reperfusion injury through modulating caveolin-1 and MMPs, and targeting RNS/caveolin-1/MMPs signaling cascades could be an important therapeutic strategy to attenuate cerebral ischemia-reperfusion injury (Chen H.S. et al., 2015, Chen H. et al., 2018; Chen H.S. et al., 2018). Treatment of peroxynitrite scavengers attenuated the BBB damage, neuronal cell death and hemorrhagic transformation in different experimental ischemic stroke models (Xu et al., 2013; Chen H. et al., 2018; Chen et al., 2019). In our recent review articles, we highlight peroxynitrite as a therapeutic target for ischemic stroke (Chen et al., 2013, 2016; Chen H.S. et al., 2018).

Inflammatory factors play crucial roles in cerebral ischemia-reperfusion injury. At the early stage of cerebral ischemia, the activation of glial cells and infiltration of leukocytes in the injured tissue produced great amounts of pro-inflammatory factors such as TNF-α and IL-1β, contributing to BBB damage and hemorrhagic transformation (Jayaraj et al., 2019; Yang C. et al., 2019). The infiltrated neutrophils produced inflammatory factors and aggravated cerebral ischemia-reperfusion injury (Anrather and Iadecola, 2016). Furthermore, reactive and proliferative astrocytes can also disrupt neurovascular cell balance and form a neuroinflammatory environment that is harmful to neurogenesis (Popa-Wagner et al., 2019). Inflammatory factors can activate MMPs, disrupt BBB integrity and worsen brain damage (Rosell et al., 2008; Jickling et al., 2015). The cross-talk between oxidative stress and neuroinflammation in ischemic stroke has been extensively studied (Collino et al., 2006; Chehaibi et al., 2016; Reiche et al., 2019; Yang Q. et al., 2019; Zhou F. et al., 2019). ROS activates various inflammatory factors for inducing neural cell death, disrupting the integrity of the BBB and enlarging the infarct volume (Crack and Taylor, 2005; Chen H.S. et al., 2018). The production of ROS could aggravate inflammatory responses of the peripheral immunological system and central nervous system by inducing the activation of adhesion molecules and promoting immunocyte infiltration (Granger and Kvietys, 2015; Mizuma and Yenari, 2017; Chen H.S. et al., 2018; Sun et al., 2018). The cross-talk and interaction of ROS/RNS and inflammatory factors could be a critical pathological mechanism and therapeutic target in cerebral ischemia-reperfusion injury. In this review article, we focus on the roles of critical neuroinflammatory enzyme myeloperoxidase (MPO) in mediating oxidative stress and neuroinflammation in cerebral ischemia-reperfusion injury, and summarize recent progress made in bioactive compounds from medicinal plants with antioxidant and anti-inflammation effects for ischemic stroke treatment.

ROLES OF MPO IN ISCHEMIC BRAIN INJURY BY MEDIATING INFLAMMATION AND OXIDATIVE STRESS

As a heme-containing peroxidase, MPO is highly expressed in multiple inflammatory cells, including neutrophils, activated microglia, monocytes/macrophage, as well as astrocytes and neurons (Nagra et al., 1997; Green et al., 2004; Forghani et al., 2015; Yu et al., 2016). MPO genetic variability appears to increase the risk of ischemic stroke (Manso et al., 2011) and MPO polymorphisms could be associated with the severity of

brain damage and functional outcomes (Hoy et al., 2003). The increased MPO activity was reported in both experimental stroke animal models and ischemic stroke patients (Barone et al., 1991; Cojocaru et al., 2010; Kong et al., 2014; Jin et al., 2018). The MPO activity in the ischemic cortex was increased early at 6 h of ischemia onset, peaked at day 5, and gradually returned to basal level at day 15 in both transient middle cerebral artery occlusion (tMCAO) and permanent MCAO (pMCAO) animal models (Barone et al., 1995). Interestingly, tMCAO had a significantly higher MPO level in the ischemic cortex than the pMCAO model after stroke onset (Barone et al., 1995), indicating that reperfusion could aggravate the activation of MPO for neuroinflammation. The penumbra area had higher MPO expression than the core (Horvath et al., 2018). With the survival of neural cells in the penumbra, this discovery raises the potential therapeutic value to prevent further loss of neural cells in the ischemic brain. Clinical studies yield similar results to animal experiments. The increase of MPO level in plasma was associated with the severity of ischemic brain damage in ischemic stroke patients (Palm et al., 2018; Tziomalos et al., 2019). A functional MRI study reported the positive correlation between MPO expression and infarct volume in ischemic stroke rat brains (Breckwoldt et al., 2008).

The neutrophil activation and degranulation appear to be important mediators for MPO induction and the source of MPO in plasma (Tay et al., 2015). MPO activity derived from neutrophils was peaked at day 1–3 of stroke onset, whereas MPO from the macrophage/microglia at day 5–7 (Breckwoldt et al., 2008). Neutrophil inhibitory factor (rNIF) was revealed to reduce neutrophil infiltration and infarct size in the ischemic brain (Barone et al., 1995). Neutrophil depletion by using an anti-neutrophil monoclonal antibody (RP3) completely inhibited MPO activity, attenuated brain edema and reduced brain infarction in the ischemic brain after 24 h of reperfusion (Matsuo et al., 1994). Thus, neutrophil-mediated MPO activation contributes to inflammation and the severity of brain damage during ischemic stroke.

Myeloperoxidase activation also plays crucial roles in oxidative damage in ischemic stroke. N-acetyl lysyltyro sylcysteine amide (KYC, an MPO inhibitor) attenuated oxidative and nitrative damage in the cortex of ischemic core (Yu et al., 2016). Hypochlorous acid (HOCl) is a crucial cytotoxic factor contributing to the MPO-mediated oxidative injury in ischemic stroke. Activated MPO induces HOCl production *via* catalyzing the reaction of chloride and H_2O_2 to induce chlorinative stress (Weiss et al., 1982; Marquez and Dunford, 1994; Yap et al., 2007). HOCl has high diffusivity and oxidative activity to react with lipids, proteins and DNA (Schraufstatter et al., 1990; Prutz, 1996; Panasenko, 1997; Hawkins et al., 2003; Pattison et al., 2003). Activated phagocytes produce HOCl and recruit inflammatory cells to ischemic brain regions, subsequently mediating the BBB damage (Ullen et al., 2013). Of note, HOCl itself can exacerbate oxidative stress, promote the translocation of p67(phox) and p47(phox) of NAD(P)H oxidase and mediate the production of superoxide, peroxynitrite and oxidized eNOS dimer in endothelial cells (Xu et al., 2006). Genetic deletion or pharmacological intervention with MPO inhibitors decreased inflammatory cell recruitment, reduced infarct volume, protected the BBB integrity, attenuated neurological deficit and improved survival rates in rodent ischemic stroke model (Forghani et al., 2015; Yu et al., 2016; Kim et al., 2019). The MPO inhibition with 4-aminobenzoic acid hydrazide (ABAH) or MPO deficiency may create a protective environment that decreases inflammatory cell recruitment and increases survival factors to improve functional outcome (Kim et al., 2019). Of note, the MPO inhibitor was more effective when treated at the subacute phase than the acute phase (Forghani et al., 2015). The robust protection of the MPO inhibitor at the subacute phase was consistent with the delayed peak of MPO expression in the ischemic brain (Barone et al., 1995; Breckwoldt et al., 2008). These studies indicate that the MPO-mediated inflammation at the subacute phase could be a critical underlying mechanism contributing to inflammatory brain damage in ischemic stroke. Importantly, MPO inhibition may represent a promising therapeutic target for stroke therapy, particularly even days after the stroke has occurred. Given the reality that most stroke patients cannot make the golden therapeutic window for thrombolysis, further investigations in this aspect may create a novel therapeutic window for improving the outcome of ischemic stroke by reducing the MPO-mediated inflammation and oxidative injury practically. Therefore, the MPO-mediated oxidative stress and neuroinflammation could be critical therapeutic targets for reducing ischemic brain injury.

Furthermore, the MPO-mediated inflammation affects post-stroke neurogenesis. Treatment of 4-ABAH promoted neurogenesis, and induced proliferation of astrocytes in the subventricular zone (SVZ), striatum and cortex (Kim et al., 2016). MPO knockout mice had increased cell proliferation and improved neurological outcomes in post-ischemic stroke rats (Kim et al., 2016). MPO inhibitor KYC decreased the pro-inflammatory M1 microglial cells and N1 neutrophils, increased the proliferation and differentiation of neuronal stem cells in the ischemic cortex, and protected the exogenous neural stem cells in the ischemic brain (Yu et al., 2018). Therefore, MPO exerts its roles in mediating oxidative stress and inflammation and affects adult neurogenesis in the post-stroke brain.

The MPO-mediated neuroinflammation involves multiple cellular mediators and signaling pathways. PI3K/AKT signaling is one of the cellular signaling pathways in the MPO-mediated inflammation during ischemic brain injury. LY294002, a PI3K/AKT inhibitor, abolished the effects of 5-LOX inhibitor Zileuton on inhibiting MPO activity in ischemic brain injury (Tu et al., 2016). LY294002 eliminated the neuroprotective effects of repetitive ischemic preconditioning and its underlying mechanisms could be related to regulating MPO activity (Tu et al., 2015). Except for PI3K/Akt pathway, ADAMTS13 (a disintegrin and metalloprotease with thrombospondin type I repeats-13) can inhibit MPO activity by inactivating the hyperactive ultra-large von Willebrand factor (ULVWF). The MPO activity was enhanced in ADAMTS13-deficient mice but was reduced in VWF-deficient mice under focal cerebral ischemia (Khan et al., 2012). In addition, E-selectin deficient mice showed the reduction of MPO expression in the ischemic brain, possibly *via* reducing the neutrophil infiltration (Ma et al., 2012). PARP

also regulates neutrophil infiltration and MPO activity. The PARP inhibitor 3-aminobenzamide (3-AB) largely decreased MPO activity in the ischemic brain (Couturier et al., 2003). Therefore, MPO can be modulated by multiple cellular signaling mechanisms, and MPO is one of the inflammatory factors contributing to the pathology of ischemic stroke through a complex interaction with different cellular signaling molecules, which remains to be further elucidated.

MPO ACTIVATION AND THROMBOLYSIS-INDUCED ISCHEMIC BRAIN INJURY

Inflammatory factors mediate hemorrhage transformation in ischemic stroke with delayed t-PA treatment. Anti-leukocyte adhesion antibody (anti-CD18) significantly decreased the neurological deficit in a rat ischemic stroke model with t-PA treatment, indicating the potential of targeting leukocytes to extend the therapeutic window of t-PA (Barone et al., 1995). The t-PA treatment increased the MPO level in the plasma of ischemic stroke patients within 1 h (Dominguez et al., 2010). Notably, MPO activation can trigger oxidative stress and nitrosative stress in the ischemic brain by forming the chlorotyrosine and nitrotyrosine (Yu et al., 2016). We recently reported that nitrotyrosine was associated with MMPs activation, BBB disruption and hemorrhage transformation in ischemic stroke with delayed t-PA treatment (Chen H.S. et al., 2015; Chen H. et al., 2018). The MPO-mediated nitrosative stress could be a potential player in mediating hemorrhagic transformation in ischemic stroke with the delayed t-PA treatment. Notably, treatment of taurine, a HOCl scavenger, reduced the rates of hemorrhage transformation in experimental ischemic stroke animal model with delayed t-PA treatment (Guan et al., 2011). Hence, the production of HOCl might be a crucial cytotoxic factor in the MPO-mediated oxidative injury and inflammation. Inhibition of MPO-HOCl is a potential therapeutic strategy to minimize hemorrhage transformation, which warrants further investigation.

In summary, recent progress indicates that the study on the MPO-mediated oxidative injury and inflammation not only brings novel insight into understanding the molecular pathology of ischemic brain injury but also represents a promising strategy for drug discovery to target MPO for improving stroke outcome.

MEDICINAL HERBAL COMPOUNDS WITH THE MPO-INHIBITING ACTIVITY SHOWING ANTIOXIDANT, ANTI-INFLAMMATION, AND NEUROPROTECTIVE EFFECTS

Traditional herbal medicine is an important source for drug discovery due to its long history in clinical practice. Recent studies identified many active compounds with the bioactivities of inhibiting MPO activity, which can be potentially used to attenuate cerebral ischemia-reperfusion injury. Herein, we summarize representative active compounds in the following session. The chemical structures of the compounds refer to **Figure 1**.

FLAVONOIDS

Bioflavonoids are well-known antioxidants with neuroprotective properties. Quercetin is a representative flavonoid compound widely existed in medicinal herbs, including Ginkgo biloba leaves and others (Wu X.J. et al., 2019). Quercetin revealed its bioactivities of anti-oxidation, anti-tumor, anti-inflammatory, anti-platelet aggregation, etc. (Mosawy et al., 2013; Li Y. et al., 2016; Chen Z. et al., 2018; Wu L. et al., 2019). Treatment of quercetin (30, 50 mg/kg) attenuated neuronal cell death and reduced infarct size in both global and focal cerebral ischemia animal models (Ahmad et al., 2011; Annapurna et al., 2013; Park et al., 2018). Quercetin inhibited MPO activity and reduced oxidative stress-mediated neural damage in ischemic brain tissues (Annapurna et al., 2013). Rutin is another common and wild distributed flavonoid extracted from medicinal plants, such as Mulberry (Morus alba L.) (Zhao et al., 2015). Pre-treatment with rutin for 21 days (25 mg/kg, daily) significantly attenuated brain damage through up-regulating antioxidant enzymes and inhibiting oxidative stress (Khan et al., 2009). Rutin also revealed to inhibit MMP-9 activity and reduce BBB disruption (Jang et al., 2014). Interestingly, its neuroprotective and antioxidant effects are related to inhibiting MPO activity (Annapurna et al., 2013).

Eriodictyol is widely distributed in fruits and vegetables, and isolated from the Chinese herb Dracocephalum rupestre. Oral administration of eriodictyol (1, 2, 4 mg/kg) exhibited inhibitory effects on MPO expression and inflammation in a permanent ischemic stroke rat model. Eriodictyol treatment down-regulated the expression of TNF-α and iNOS in the ischemic cortex, decreased infarct size, improved motor function, and attenuated the memory deficit in permanent ischemic stroke rats (Ferreira Ede et al., 2016). Eriodictyol-7-O-glucoside (30 mg/kg), also showed neuroprotective effects against cerebral ischemic injury through activating the antioxidant signaling nuclear factor erythroid-2-related factor 2/antioxidant response element (Nrf2/ARE) (Jing et al., 2013).

Isorhamnetin is a typical flavonoid extracted from *Hippophae rhamnoides* (Li et al., 2015). Treatment of isorhamnetin (5 mg/kg) suppressed MPO activity, attenuated oxidative/nitrosative stress, inhibited inflammatory factors (IL-1β, IL-6, and TNF-α), preserved tight junction proteins and protected the BBB integrity in the acute ischemic stroke model (Zhao et al., 2016). The anti-inflammation and anti-oxidative bioactivities of isorhamnetin were also found in the *in vitro* cultured brain microvascular endothelial cells under oxygen and glucose deprivation (OGD) condition (Li W. et al., 2016).

Biochanin A, an O-methylated natural isoflavonoid, mainly exists in red clover, chickpea or other legumes. Biochanin A revealed various pharmacological functions, including

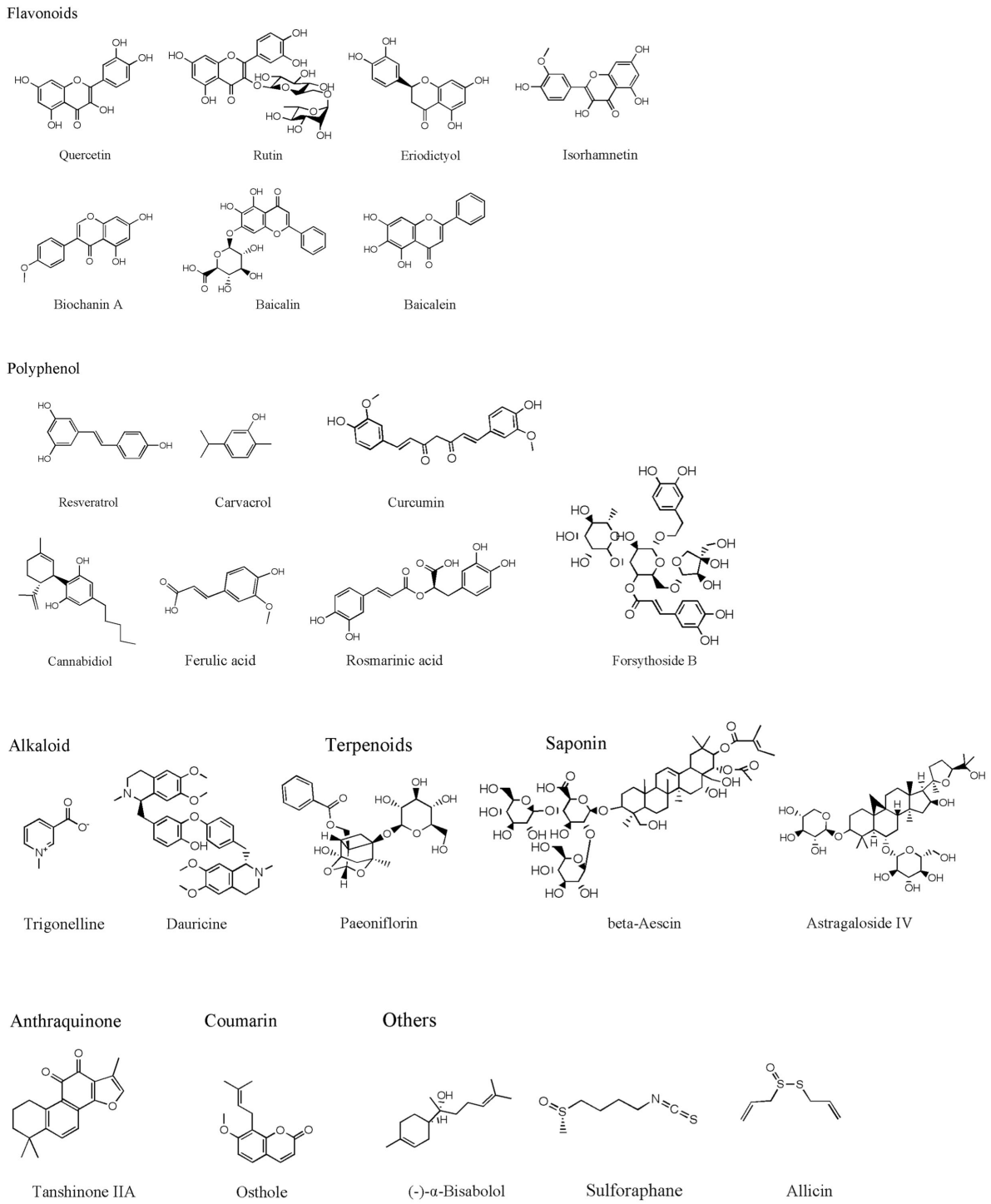


FIGURE 1 | The chemical structures of the natural compounds.

antioxidation, anti-inflammation and anti-tumorigenesis (Mishra et al., 2008; Liu et al., 2016; Guo et al., 2019). Biochanin A suppressed the activity of MPO and down-regulated the expression of IL-1β and TNF-α in acute ischemic brain injury. Treatment with biochanin A (10, 20, 40 mg/kg) significantly improved neurological outcomes, reduced infarct volume and brain edema in post-ischemic brain injury (Wang et al., 2015).

Baicalin and its aglycon baicalein are flavonoids extracted from *Scutellaria baicalensis*, a medicinal plant. Both baicalin and baicalein revealed their neuroprotective effects against cerebral

ischemia-reperfusion injury and the underlying mechanisms were related to their anti-oxidative stress, anti-apoptotic, anti-inflammation and anti-excitotoxicity properties (Tu et al., 2009, 2011a,b; Cui et al., 2010; Xue et al., 2010; Li H.Y. et al., 2012; Li et al., 2017; Liang et al., 2017; Yang et al., 2019). Baicalin (30, 100 mg/kg) and baicalein (50 mg/kg) showed to inhibit the MPO activity in the ischemic brain injury (Hwang et al., 2002; Tu et al., 2009). Our recent studies suggest that baicalin reduced infarct size, minimized the BBB damage and hemorrhage transformation in the experimental ischemic stroke model with delayed t-PA treatment. The underlying mechanisms could be attributed to the direct peroxynitrite-scavenging property (Xu et al., 2013; Chen H. et al., 2018).

POLYPHENOL

Resveratrol is a polyphenolic compound with a terpenoid structure, mainly found in plants such as grapes, peanuts, mulberry and knotweed. Resveratrol has been used for aging-related diseases such as cancer, cardiovascular diseases and stroke (Liu et al., 2013, 2018; Dou et al., 2019; Zhou X. et al., 2019). Resveratrol treatment (50 mg/kg) has potent anti-oxidative stress and anti-inflammatory properties and has neuroprotective effects against acute ischemic brain injury (Dou et al., 2019). The neuroprotective mechanisms involve multiple molecular targets such as MMP-9 (Pandey et al., 2015; Wei et al., 2015), NMDA receptor-mediated ERK-CREB signaling pathway (Li W. et al., 2016), JAK2/STAT3 pathway (Hou et al., 2018), neurotransmitters and neuromodulators, excitatory neurotransmitter glutamates, aspartate and neuromodulator d-Serine, etc. (Li et al., 2010). The inhibitory effects of resveratrol on MPO activity contributed to its neuroprotective effects (Fang et al., 2015; Lei and Chen, 2018; Lei et al., 2019). Furthermore, resveratrol had the capacity to cross BBB (Wang et al., 2002) and fusogenic liposomes could enhance the delivering efficiency of resveratrol across the BBB (Wiedenhoeft et al., 2019). Carvacrol is a monoterpene phenol and an isomer of thymol commonly found in many aromatic plants including *Origanum dictamnus, Origanum vulgare*, and *Origanum majorana*. Carvacrol treatment attenuated neuronal apoptosis, reduced infarct size and improved the neurological outcomes in both adult focal ischemic stroke model and neonatal cerebral hypoxic-ischemic model (Yu et al., 2012; Chen W. et al., 2015). Furthermore, carvacrol (10, 20, 40 mg/kg) dose-dependently down-regulated the MPO activity and the expressions of iNOS and COX-2 in the ischemic brain (Li Y. et al., 2016).

Curcumin is a polyphenol in the curry spice turmeric. In ancient Chinese and Indian medicine, curcumin was used to treat various diseases. Curcumin has multiple molecular targets, including transcription factors, growth factors and their receptors (Kunnumakkara et al., 2017). Curcumin has revealed its anti-inflammatory, antioxidant, anti-tumor and cardiovascular protective properties (Menon and Sudheer, 2007; Jiang et al., 2017; Kunnumakkara et al., 2017). The neuroprotective effects of curcumin treatment (150, 200 mg/kg) are related to inhibiting leukocyte infiltration, regulating microglia/macrophage polarization and inflammatory factors production, and inhibiting autophagy against cerebral ischemia-reperfusion injury (Liu et al., 2017; Huang L. et al., 2018; Bavarsad et al., 2019). The neuroprotective effects of curcumin are related to inhibition of TLR2/4-NF-κB signaling pathway and reduction of MPO activity in the ischemic brain (Tu et al., 2014).

Cannabidiol (CBD) isolated from *Cannabis sativa L. (Cannabaceae)* (Brand and Zhao, 2017) was reported to increase the cortex blood flow *via* the serotonergic 5-hydroxytryptamine 1A receptor-dependent mechanism (Mishima et al., 2005). CBD treatment (3 mg/kg) attenuated neuroinflammation through inhibiting MPO and HMGB1 in the ischemic brain (Hayakawa et al., 2008). A systematic review supported the neuroprotective effects of CBD in ischemic stroke treatment (England et al., 2015). The neuroprotective mechanisms were also related to inhibition of inflammatory factors NF-κB and tumor necrosis factor receptor 1 (TNFR1) (Khaksar and Bigdeli, 2017).

Angelica sinen-sis (Oliv.) Diels (AS) and *Ligusticum chuanxiong Hort. (LC)* are medicinal herbs used for stroke treatment for centuries in China. Ferulic acid (FA) is a bioactive ingredient of AS and LC. FA has revealed to scavenge superoxide radicals and restore vasodilation in spontaneously hypertensive rats (Suzuki et al., 2007). FA treatment at 100 mg/kg at the beginning of the MCAO stroke model effectively reduced infarct size and improved neurological deficits. The underlying mechanisms were related to inhibiting ICAM-1 and NF-κB, and reducing the infiltrations of the MPO immune-reactive cells (Cheng et al., 2008). Rosmarinic acid (RA) is a natural phenolic compound isolated from Chinese herb *Salvia miltiorrhiza* (Wu et al., 2015). RA treatment (50 mg/kg) inhibited HMGB1 expression and NF-κB activation, reduced the BBB permeability, decreased infarct size and alleviated neurological deficits in cerebral ischemia-reperfusion injury (Luan et al., 2013). The inhibitory effects of RA on MPO contributed to its neuroprotective effects against ischemic brain injury (Fonteles et al., 2016).

Forsythoside B is an anti-inflammatory compound extracted from the leave of *Lamiophlomis rotata Kudo*. Even delayed administration of forsythoside B at 5 h after reperfusion had a neuroprotective effect. Forsythoside B at the dosage of 20 mg/kg attenuated brain infarct size, brain edema, and BBB permeability through inhibiting MPO activity and NF-κB expression against cerebral ischemia/reperfusion injury (Jiang et al., 2010).

ALKALOIDS

Alkaloids are nitrogen-containing alkaline compounds from medicinal herbs. Trigonelline and dauricine are representative alkaloid with the MPO inhibitory effects. Intraperitoneal injection of trigonelline (100 mg/kg), a plant alkaloid from fenugreek seeds, inhibited MPO expression, improved the neurological outcomes and alleviated infarct size in ischemic stroke animal models (Pravalika et al., 2019). Dauricine is a BBB permeable bisbenzyl isoquinoline alkaloid extracted from *menispermum dauricum DC* root. Dauricine treatment at 5 or 10 mg/kg revealed its neuroprotective effects and the underlying

mechanisms were associated with the suppression of TNF-α, IL-1β, and ICAM-1 expression and inhibition of PMNs infiltration (Yang X.Y. et al., 2007).

TERPENOIDS

Paeoniflorin is a natural component derived from *Paeonia lactiflora Pall* and has anti-inflammatory properties. Intravenous injection of paeoniflorin (10,15, 20 mg/kg) at 10 min before or 30 min after MCAO effectively reduced infarct size and ameliorated the neurological deficit via inhibiting PMN infiltration and down-regulating inflammatory factors including TNF-α, IL-1β, and ICAM-1 (Tang N.Y. et al., 2010).

SAPONINS

Saponins are widely distributed in various plant species. As the active components in many medicinal herbs, saponins possess diverse biological activities, such as anti-inflammatory, anti-oxidative stress and neuroprotective effects (Guclu-Ustundag and Mazza, 2007). β-Aescin is a main bioactive compound isolated from *Aesculus hippocastanum*, a commonly used medicinal herb for vascular disorders in Traditional Chinese Medicine. Aescin has anti-inflammatory, anti-edema and anti-oxidation effects (Cheng et al., 2016; Gallelli, 2019). Pretreatment of β-Aescin (15, 30, 60 mg/kg) for 7 days significantly inhibited the MPO activity, reduced the neutrophils migration, lessened infarct sizes, ameliorated neurological deficit in the rat model of MCAO cerebral ischemia-reperfusion injury (Hu et al., 2004). Astragaloside IV, a major component of *Astragalus membranaceus*, showed its anti-inflammatory property in the focal cerebral ischemia-reperfusion rat model. Treatment of Astragaloside IV (10, 20 mg/kg) at the onset of ischemia or at 12 h after the reperfusion significantly alleviated infarct volume and neurological deficit. The underlying mechanisms could be related to inhibiting MPO, TNF-α, IL-1β, NF-κB expression and neutrophil adhesion (Li M. et al., 2012).

POLYSACCHARIDES

Fucoidan is a sulfated polysaccharide mainly exited in brown algae and brown seaweed. Treatment with fucoidan (80, 160 mg/kg) inhibited MPO activity and inflammation-associated cytokines such as IL-1, IL-6, TNF-α, and attenuated cerebral ischemia-reperfusion injury (Che et al., 2017).

ANTHRAQUINONE

Tanshinone IIA is a key bioactive compound in *Salvia miltiorrhiza*, a commonly used medicinal herb for cardiovascular and cerebral vascular diseases. Tanshinone IIA had neuroprotective effects against focal cerebral I/R injury, and its underlying mechanisms were considered to inhibit the expression of NF-κB, MMP-9 and HMGB1 (Liu et al., 2010; Tang C. et al., 2010). Meanwhile, Tanshinone IIA (25 mg/kg) also revealed to inhibit MPO activity, attenuate macrophage migration inhibitory factor, TNF-α and IL-6, and ameliorate BBB permeability and neurological dysfunction (Chen et al., 2012).

COUMARIN

Osthole, a natural coumarin derivative, is a bioactive compound from many medicinal herbs such as *Angelica pubescens, Cnidium monnieri*, and *Peucedanum ostruthium*. Osthole was reported to improve chronic cerebral hypoperfusion induced cognitive deficits and neuronal damage in the hippocampus (Ji et al., 2010). Osthole revealed its bioactivities of inhibiting MPO, MMP-9, IL-1β, and IL-8 for the neuroprotective effects against cerebral ischemic injury (Chao et al., 2010; Mao et al., 2011).

OTHER COMPOUNDS

Other compounds, like (-)-α-bisabolol, sulforaphane, and allicin, also have anti-inflammation effects on inhibiting inflammatory cytokines, including TNF-α, IL-1β, and IL-6. Those compounds are considered as potential candidates for adjuvant therapy against cerebral ischemia-reperfusion injury. For example, (-)-α-bisabolol is an unsaturated sesquiterpene alcohol existed in a variety of plants, such as *Matricaria chamomilla, Salvia runcinata* and *Myoporum crassifolium*. (-)-α-bisabolol has anti-inflammatory, antioxidant and anti-apoptotic activities (Sampaio et al., 2016). (-)-α-bisabolol (200 mg/kg) showed its neuroprotective effects on reducing infarct size and neurological deficits in a permanent MCAO animal model via inhibiting MPO, TNF-α and iNOS (Fernandes et al., 2019). Sulforaphane, an isothiocyanate occurring in cruciferous vegetables, transcriptionally up-regulated the genes controlling aerobic cells and inhibited oxidative stress and inflammation (Zhang et al., 1992). Intraperitoneally treatment with sulforaphane (10 mg/kg) at the onset of reperfusion dramatically ameliorated infarct volume, alleviated neurological deficit, and decreased neutrophils infiltration in ischemic brain injury. Sulforaphane also down-regulated the expressions of cleaved caspase-1, IL-1β, and IL-18 and inhibited the activation of NLRP3 inflammasome (Yu et al., 2017). Allicin is a major active compound in garlic. Allicin has anti-inflammatory, anti-fungal, antioxidant and anti-tumoral activities (Hunter et al., 2005; Chan et al., 2014; Zhou et al., 2014). Allicin treatment (50 mg/kg) revealed to reduce TNF-α level and MPO activity, ameliorated infarct size, alleviated brain edema and improved the neurological score in the experimental MCAO ischemic stroke rat models (Zhang et al., 2015).

PERSPECTIVES

Targeting MPO and cellular signaling cascades could be a therapeutic strategy to decrease infarct size and improve the neurological outcomes in ischemic stroke treatment (**Table 1**). As an inflammatory enzyme, MPO activation results in HOCl production, increases pro-inflammatory cytokine and mediates protein nitration (Nussbaum et al., 2013). MPO is also a highly versatile oxidative enzyme and participates in the pathological process of oxidative and nitrosative stress (Davies et al., 2008). The crosstalk of oxidative stress and inflammation could amplify brain damage in cerebral ischemia-reperfusion injury. The inhibition of MPO could reach two goals for antioxidant and anti-inflammation simultaneously. Importantly, MPO could be an important molecular target for ischemic stroke treatment practically that allows for a broad intervention time window (Kim et al., 2018). Thus, MPO inhibitors have translational values as therapeutic candidates for improving the outcomes of ischemic stroke treatment.

Both oxidative stress and inflammation are crucial pathological mechanisms in the BBB damage and hemorrhagic transformation in ischemic stroke with delayed t-PA treatment. The increased MPO in the plasma was found in ischemic stroke patients after receiving t-PA treatment (Dominguez et al., 2010). Treatment of MPO inhibitor KYC restored the BBB function in experimental autoimmune encephalomyelitis mice (Zhang et al., 2016), showing its potential to prevent inflammatory factors-mediated BBB damage. Thus, MPO-mediated HOCl production could be a crucial target for promoting anti-oxidative stress and anti-inflammation and preventing hemorrhagic transformation. Developing MPO inhibitors is a promising strategy for expending the golden therapeutic window for t-PA treatment.

Compounds from medicinal herbs are important sources for drug discovery. Many of them already show their potential as drug candidates for ischemic stroke treatment. We provide MPO inhibitory compounds in **Table 2**. Although many studies provide exciting results about the bioactivities of those compounds on MPO inhibition and neuroprotection in different experimental model systems, we should note that most of the studies only examine the activity and expression of MPO in the ischemic brain *in vivo*. It remains unknown whether those compounds have direct and specific actions of binding MPO or lead molecular modifications to MPO. Since most of the compounds exert antioxidant effects (**Table 2**), the antioxidant effects would, in turn, inhibit MPO activity in the ischemic brain. It is valuable to examine whether these compounds could directly inhibit MPO or not. On the other hand, the pharmacological effects of those natural compounds may also be due to modulating multiple targets and signaling pathways in the ischemic brain, rather than just a single target (Chen et al., 2017). The one-compound-multi-target pattern may allow for inhibiting MPO activity as well as other inflammatory factors. Furthermore, we would remark that those neuroprotective compounds may serve to reduce the complications of delayed t-PA treatment and extend the therapeutic time window of t-PA. Studies seldomly provide information on pharmacokinetic and pharmacodynamic

TABLE 1 | Intervention of inhibiting MPO for protecting ischemic stroke injury.

Treatment agent	Direct target	Experimental Model	Treatment time point and path	Dosage	Molecules Changes	Major Results	References
4-ABAH	MPO	tMCAO (I 30 min/R 21 day) (Mice)	Daily injections starting on day 2 after MCAO, continuing to day 21. I.P.	40 mg/kg	MPO	Infarct Volume, Neurological deficit, Survival	Forghani et al., 2015
N-acetyl lysyltyrosylcysteine amide (KYC)	MPO	tMCAO (I 30 min/R 3 day) (Mice)	1 h after reperfusion. I.P.	10 mg/kg	NIMP-R14, p53, nNOS, MPO, NO_2Tyr, 4-HNE	Neurological deficit, Infarct volume, BBB permeability	Yu et al., 2016
4-ABAH	MPO	tMCAO (I 30 min/R 7 day) (Mice)	Daily injections starting on day 2, continuing to day 7 after MCAO. I.P.	40 mg/kg	Hsp70, p-Akt, p53	Neuronal death, Grid walk, Adhesive	Kim et al., 2019
4-ABAH	MPO	tMCAO (I 30 min/R 7 day) (Mice)	at 8 h after the stroke and then twice daily up to day 7. I.P.	40 mg/kg	BDNF, p-CREB, AcH3	Cell proliferation	Kim et al., 2016
N-acetyl lysyltyrosylcysteine amide (KYC)	MPO	tMCAO (I 30 min/R 7 day) (Mice)	starting from 1 h, continuing to 7 days after MCAO. I.P.	10 mg/kg	SOX2, NO_2Tyr, ClTyr	Neurological deficit, brain atrophy, apoptosis	Yu et al., 2018
		tMCAO (I 30 min/R 3 day) (Mice)	starting from 1 h, continuing to 3 days after MCAO. I.P.	10 mg/kg	HMGB1, RAGE, NF-kB, ClTyr, NO_2Tyr, β-catenin	Apoptosis	

TABLE 2 | Natural compound inhibiting MPO for protecting ischemic stroke injury.

Compound	Representative sources	Experimental model	Treatment time point and path	Dosage	targets	Major results	References
Quercetin	Ruta graveolens L.	Global cerebral ischemia (I 30 min/R 4 h)	10 min before reperfusion (not given)	50 mg/kg	MDA, MPO, SOD, CAT	infarct volume	Annapurna et al., 2013
Rutin	Ruta graveolens L.	Global cerebral ischemia (I 30 min/R 4 h)	10 min before reperfusion (not given)	10 mg/kg	MDA, MPO, SOD, CAT	infarct volume	Annapurna et al., 2013
Eriodictyol	Dracocephalum rupestre and citrus fruits	pMCAO	30 mins before and 2 h after pMCAO and lasting for 5 days. I.G.	4 mg/kg	MPO, TNF-α, iNOS	neurological deficit, infarct volume, Open-field test, Y-maze test, Passive avoidance test	Ferreira Ede et al., 2016
Isorhamnetin	Hippophae rhamnoides L., Oenanthe javanica and Ginkgo biloba L.,	tMCAO (I 1 h/R 48 h)	Onset and 24 h of reperfusion. I.P.	5 mg/kg	Caspase-3, occluding, ZO-1, claudin-5, AQP4, MDA, iNOS, Nrf2, HO-1, 3-NT, NMDA NR1, MPO, TNF-α, IL-1β, IL-6	neurological deficit, infarct volume, brain edema, BBB permeability	Zhao et al., 2016
Biochanin A	red clover, chickpea or other legumes	tMCAO (I 2 h/R 24 h)	Lasting for 14 days before MCAO. I.P.	20, 40 mg/kg	MPO, TNF-α, IL-1β, p38	neurological deficit, infarct volume, brain edema,	Wang et al., 2015
Baicalin	Scutellaria baicalensis Georgi	pMCAO (24 h)	2 and 12 h after MCAO. I.P.	30, 100 mg/kg	MPO, iNOS, COX-2, Caspase-3	neurological deficit, infarct volume	Tu et al., 2009
Baicalein	Scutellariae radix	tMCAO (I 2 h/R 22 h)	promptly prior to and 2 h after the reperfusion	50 mg/kg	MPO	infarct volume	Hwang et al., 2002
Resveratrol	grapes, cranberries and peanuts	pMCAO (24 h)	Onset of MCAO. I.P.	100 mg/kg	IL-1β, TNF-α, COX2, MPO, Akt	neurological deficit, brain edema	Lei and Chen, 2018
Resveratrol	grapes, cranberries and peanuts	pMCAO (24 h)	2 h after MCAO. I.P.	100 mg/kg	MPO, TLR4, NF-κB, p65, COX-2, MMP-9, TNF-α, IL-1β	neurological deficit, infarct volume, brain edema, BBB permeability	Lei et al., 2019
Resveratrol	grapes, cranberries and peanuts	tMCAO (I 2 h/R 24 h)	starting at 3 h after reperfusion and lasting for 4 days. I.P.	30 mg/kg	Caspase-3, Bcl2, Bax, MPO, TNF-α	neurological deficit, infarct volume, brain edema	Fang et al., 2015
Carvacrol	Lamiaceae	tMCAO (I 2 h/R 24 h)	1 and 12 h after the onset of MCAO. I.P.	10, 20, 40 mg/kg	MPO, TNF-α, IL-1β, iNOS, COX-2, SOD, MDA, NF-κB p65	Not detected	Li Y. et al., 2016
Curcumin	Curcuma aromatica Salisb.	pMCAO (24 h)	2 and 12 h after MCAO. I.P.	10, 50 mg/kg	MPO, TLR2, TLR4, NF-κB p65, TNF-α, IL-1β	neurological deficit, infarct volume, brain edema, Neutrophil Infiltration	Tu et al., 2014
Cannabidiol	Marijuana	tMCAO (I 4 h/R 24 h)	immediately before and 3 h after MCAO. I.P.	3 mg/kg	MPO, HMGB1	neurological deficit, infarct volume, Rota-rod test	Hayakawa et al., 2008
Allicin	garlic	tMCAO (I 1.5 h/R 24 h)	3 h after reperfusion daily for five consecutive days. I.P.	50 mg/kg	MPO, Caspase-3, TNF-α	neurological deficit, infarct volume, brain edema	Zhang et al., 2015

(Continued)

TABLE 2 | Continued

Compound	Representative sources	Experimental model	Treatment time point and path	Dosage	Targets	Major results	References
Ferulic acid	Angelica sinensis and Ligusticum chuanxiong	tMCAO (I 1.5 h/R 24 h)	Onset of MCAO, I.V.	100 mg/kg	ICAM-1, MPO, NF-κB	neurological deficit, infarct volume	Cheng et al., 2008
Ferulic acid	Angelica sinensis and Ligusticum chuanxiong	tMCAO (I 1.5 h/R 2 h)	Onset of MCAO, I.V.	100 mg/kg	ICAM-1, MPO, NF-κB	Not detected	Cheng et al., 2008
Rosmarinic acid	Rosmarinus officinalis	pMCAO	30 mins before and 1 h after pMCAO and lasting for 5 days. I.P.	20 mg/kg	MPO, SYP, BDNF	neurological deficit, infarct volume, Open-field test, Y-maze test, Object recognition test, Water maze test	Fonteles et al., 2016
Forsythoside B	Lamiophlomis rotata Kudo	tMCAO (I 1 h/R 23 h)	3, 5, 7 h after reperfusion. I.V.	20 mg/kg	NF-κB, IκB-α, MPO	neurological deficit, infarct volume, brain edema, BBB permeability	Jiang et al., 2010
Trigonelline	Fenugreek seeds	tMCAO (I 1.5 h/R 24 h)	30 min before MCAO, or immediately after MCAO or 1 h post MCAO. I.P.	100 mg/kg	MPO, GSH, MDA, Nitrite	neurological deficit, infarct volume	Pravalika et al., 2019
Dauricine	Menispermum dauricum DC	tMCAO (I 1 h/R 24 h)	1 h after MCAO. I.P.	5, 10 mg/kg	MPO, ICAM-1, TNF-α, IL-1β	Polymorphic neutrophils Infiltration	Yang X.Y. et al., 2007
Paeoniflorin	paeonia lactiflora Pall	tMCAO (I 1.5 h/R 24 h)	10 min before MCAO. I.V	20 mg/kg	MPO, TNF-α, IL-1β, ED1, ICAM-1, Apoptosis	neurological deficit, infarct volume	Tang N.Y. et al., 2010
β -Aescin	Aesculus hippocastanum	tMCAO (I 2 h/R 24 h)	Lasting for 7 days before MCAO. I.P.	60 mg/kg	ICAM-1, E-selectin, MPO	neurological deficit, infarct volume, Neutrophil Infiltration	Hu et al., 2004
Astragaloside IV	astragalus membranaceus	tMCAO (I 1.5 h/R 24 h)	immediately and 12 h after the onset of reperfusion. I.P.	10, 20 mg/kg	MPO, TNF-α, IL-1β, ICAM-1, NF-κB	neurological deficit, infarct volume	Li M. et al., 2012
Fucoidan	brown algae	tMCAO (I 2h/R24 h)	7 days before MCAO, I.P.	80, 160 mg/kg	IL-1β, IL-6, MPO, TNF-α, MDA, SOD, p-53, Bax, Bcl2, p-ERK, JNK, p38	neurological deficit, infarct volume	Che et al., 2017
Tanshinone IIA	Danshen	tMCAO (I 2 h/R 24 h)	10 min after MCAO, I.P.	25 mg/kg	MPO, MIF, TNF-α, IL-6	neurological deficit, infarct volume, brain edema	Chen et al., 2012
Osthole	Angelica pubescens, Cnidium monnieri and Peucedanum ostruthium	tMCAO (I 2 h/R 24 h)	30 min before MCAO, I.P.	20, 40 mg/kg	MDA, GSH, MPO, IL-1β, IL-8	neurological deficit, infarct volume, brain edema	Chao et al., 2010
(−)-α -bisabolol	Matricaria chamomilla	pMCAO	1 day before and 1 h after pMCAO and lasting for 5 days. I.G.	200 mg/kg	MPO, TNF-α, iNOS	neurological deficit, infarct volume, Open-field test, Y-maze test, Passive avoidance test, Object recognition test, Morris water maze	Fernandes et al., 2019
Sulforaphane	cruciferous vegetables	tMCAO (I 1 h/R 24 h)	the beginning of reperfusion	5, 10 mg/kg	MPO, Caspase-1, IL-1β, IL-18, NLRP3	neurological deficit, infarct volume, neutrophils Infiltration	Yu et al., 2017

parameters when the pharmacological studies were performed to explore the neuroprotection of a selected compound. For the translational study, we should also pay specific attention to the pharmacokinetics and pharmacodynamics of those compounds and the toxicological evaluation for further development as therapeutic agents. Moreover, the potential interactions of those compounds with t-PA should be examined before being used as combination therapy.

CONCLUSION

In conclusion, MPO plays a vital role in mediating cerebral ischemia-reperfusion injury *via* mediating oxidative stress and neuroinflammation. Targeting MPO with natural compounds could be a promising strategy for treating ischemic stroke.

AUTHOR CONTRIBUTIONS

JS contributed as the senior author and the principal investigator (PI) of this study and refined the study. SC and HC wrote the first draft of the manuscript and contributed to the overall design. QD drew the structures of compounds. All authors read, critically reviewed, and approved the final manuscript.

FUNDING

This work was supported by the Hong Kong General Research Fund (GRF Nos. 17102915 and 17118717), the Research Grants Council, the Hong Kong SAR and Health and Medical Research Fund, the Hong Kong SAR (No. 13142901). The AoE/P-705/16 Areas of Excellence Scheme, RGC, The Hong Kong SAR; SIRI/04/04/2015/06 Shenzhen Basic Research Plan Project.

REFERENCES

Ahmad, A., Khan, M. M., Hoda, M. N., Raza, S. S., Khan, M. B., Javed, H., et al. (2011). Quercetin protects against oxidative stress associated damages in a rat model of transient focal cerebral ischemia and reperfusion. *Neurochem. Res.* 36, 1360–1371. doi: 10.1007/s11064-011-0458-6

Allen, C. L., and Bayraktutan, U. (2009). Oxidative stress and its role in the pathogenesis of ischaemic stroke. *Int. J. Stroke* 4, 461–470. doi: 10.1111/j.1747-4949.2009.00387.x

Annapurna, A., Ansari, M. A., and Manjunath, P. M. (2013). Partial role of multiple pathways in infarct size limiting effect of quercetin and rutin against cerebral ischemia-reperfusion injury in rats. *Eur. Rev. Med. Pharmacol. Sci.* 17, 491–500.

Anrather, J., and Iadecola, C. (2016). Inflammation and stroke: an overview. *Neurotherapeutics* 13, 661–670.

Bai, X., Yang, B., Chen, H., Shen, J. G. -, and Yang, D. (2020). HKOCl-4: a rhodol-based yellow fluorescent probe for detection of hypochlorous acid in living cells and tissues. *Organ. Chem. Front*.

Barone, F. C., Hillegass, L. M., Price, W. J., White, R. F., Lee, E. V., Feuerstein, G. Z., et al. (1991). Polymorphonuclear leukocyte infiltration into cerebral focal ischemic tissue: myeloperoxidase activity assay and histologic verification. *J. Neurosci. Res.* 29, 336–345. doi: 10.1002/jnr.490290309

Barone, F. C., Hillegass, L. M., Tzimas, M. N., Schmidt, D. B., Foley, J. J., White, R. F., et al. (1995). Time-related changes in myeloperoxidase activity and leukotriene B4 receptor binding reflect leukocyte influx in cerebral focal stroke. *Mol. Chem. Neuropathol.* 24, 13–30. doi: 10.1007/bf03160109

Bavarsad, K., Barreto, G. E., Hadjzadeh, M. A., and Sahebkar, A. (2019). Protective effects of curcumin against ischemia-reperfusion injury in the nervous system. *Mol. Neurobiol.* 56, 1391–1404. doi: 10.1007/s12035-018-1169-7

Brand, E. J., and Zhao, Z. (2017). Cannabis in chinese medicine: are some traditional indications referenced in ancient literature related to cannabinoids? *Front. Pharmacol.* 8:108. doi: 10.3389/fphar.2017.00108

Breckwoldt, M. O., Chen, J. W., Stangenberg, L., Aikawa, E., Rodriguez, E., Qiu, S., et al. (2008). Tracking the inflammatory response in stroke in vivo by sensing the enzyme myeloperoxidase. *Proc. Natl. Acad. Sci. U.S.A.* 105, 18584–18589. doi: 10.1073/pnas.0803945105

Chan, J. Y., Tsui, H. T., Chung, I. Y., Chan, R. Y., Kwan, Y. W., and Chan, S. W. (2014). Allicin protects rat cardiomyoblasts (H9c2 cells) from hydrogen peroxide-induced oxidative injury through inhibiting the generation of intracellular reactive oxygen species. *Int. J. Food Sci. Nutr.* 65, 868–873. doi: 10.3109/09637486.2014.925428

Chao, X., Zhou, J., Chen, T., Liu, W., Dong, W., Qu, Y., et al. (2010). Neuroprotective effect of osthole against acute ischemic stroke on middle cerebral ischemia occlusion in rats. *Brain Res.* 1363, 206–211. doi: 10.1016/j.brainres.2010.09.052

Che, N., Ma, Y., and Xin, Y. (2017). Protective role of fucoidan in cerebral ischemia-reperfusion injury through inhibition of MAPK signaling pathway. *Biomol. Ther. (Seoul)* 25, 272–278. doi: 10.4062/biomolther.2016.098

Chehaibi, K., Trabelsi, I., Mahdouani, K., and Slimane, M. N. (2016). Correlation of oxidative stress parameters and inflammatory markers in ischemic stroke patients. *J. Stroke Cerebrovasc. Dis.* 25, 2585–2593. doi: 10.1016/j.jstrokecerebrovasdis.2016.06.042

Chen, H., Guan, B., Chen, X., Chen, X., Li, C., Qiu, J., et al. (2018). Baicalin attenuates blood-brain barrier disruption and hemorrhagic transformation and improves neurological outcome in ischemic stroke rats with delayed t-PA treatment: involvement of ONOO(-)-MMP-9 pathway. *Transl. Stroke Res.* 9, 515–529. doi: 10.1007/s12975-017-0598-3

Chen, H. S., Chen, X., Li, W. T., and Shen, J. G. (2018). Targeting RNS/caveolin-1/MMP signaling cascades to protect against cerebral ischemia-reperfusion injuries: potential application for drug discovery. *Acta Pharmacol. Sin.* 39, 669–682. doi: 10.1038/aps.2018.27

Chen, Z., Yuan, Q., Xu, G., Chen, H., Lei, H., and Su, J. (2018). Effects of quercetin on proliferation and H(2)O(2)-induced apoptosis of intestinal porcine enterocyte cells. *Molecules* 23:2012. doi: 10.3390/molecules23082012

Chen, H., Guan, B., and Shen, J. (2016). Targeting ONOO-/HMGB1/MMP-9 signaling cascades: potential for drug development from chinese medicine to attenuate ischemic brain injury and hemorrhagic transformation induced by thrombolytic treatment. *Integr. Med. Int.* 3, 32–52.

Chen, H., Guan, B., Wang, B., Pu, H., Bai, X., Chen, X., et al. (2019). Glycyrrhizin prevents hemorrhagic transformation and improves neurological outcome in ischemic stroke with delayed thrombolysis through targeting peroxynitrite-mediated hmgb1 signaling. *Transl Stroke Res.* [Epub ahead of print]. doi: 10.1007/s12975-019-00772-1

Chen, H. S., Chen, X. M., Feng, J. H., Liu, K. J., Qi, S. H., and Shen, J. G. (2015). Peroxynitrite decomposition catalyst reduces delayed thrombolysis-induced hemorrhagic transformation in ischemia-reperfused rat brains. *CNS Neurosci. Ther.* 21, 585–590. doi: 10.1111/cns.12406

Chen, W., Xu, B., Xiao, A., Liu, L., Fang, X., Liu, R., et al. (2015). TRPM7 inhibitor carvacrol protects brain from neonatal hypoxic-ischemic injury. *Mol. Brain* 8:11. doi: 10.1186/s13041-015-0102-5

Chen, H. S., Qi, S. H., and Shen, J. G. (2017). One-compound-multi-target: combination prospect of natural compounds with thrombolytic therapy in acute ischemic stroke. *Curr. Neuropharmacol.* 15, 134–156. doi: 10.2174/1570159x14666160620102055

Chen, X. M., Chen, H. S., Xu, M. J., and Shen, J. G. (2013). Targeting reactive nitrogen species: a promising therapeutic strategy for cerebral ischemia-reperfusion injury. *Acta Pharmacol. Sin.* 34, 67–77. doi: 10.1038/aps.2012.82

Chen, Y., Wu, X., Yu, S., Lin, X., Wu, J., Li, L., et al. (2012). Neuroprotection of tanshinone IIA against cerebral ischemia/reperfusion injury through inhibition

of macrophage migration inhibitory factor in rats. *PLoS ONE* 7:e40165. doi: 10.1371/journal.pone.0040165

Cheng, C. Y., Ho, T. Y., Lee, E. J., Su, S. Y., Tang, N. Y., and Hsieh, C. L. (2008). Ferulic acid reduces cerebral infarct through its antioxidative and anti-inflammatory effects following transient focal cerebral ischemia in rats. *Am. J. Chin. Med.* 36, 1105–1119. doi: 10.1142/S0192415X08006570

Cheng, P., Kuang, F., and Ju, G. (2016). Aescin reduces oxidative stress and provides neuroprotection in experimental traumatic spinal cord injury. *Free Radic. Biol. Med.* 99, 405–417. doi: 10.1016/j.freeradbiomed.2016.09.002

Cojocaru, I. M., Cojocaru, M., Iliescu, I., Botnaru, L., Gurban, C. V., Sfrijan, F., et al. (2010). Plasma myeloperoxidase levels in patients with acute ischemic stroke. *Rom. J. Int. Med.* 48, 101–104.

Collino, M., Aragno, M., Mastrocola, R., Benetti, E., Gallicchio, M., Dianzani, C., et al. (2006). Oxidative stress and inflammatory response evoked by transient cerebral ischemia/reperfusion: effects of the PPAR-α agonist WY14643. *Free Radic. Biol. Med.* 41, 579–589. doi: 10.1016/j.freeradbiomed.2006.04.030

Couturier, J. Y., Ding-Zhou, L., Croci, N., Plotkine, M., and Margaill, I. (2003). 3-Aminobenzamide reduces brain infarction and neutrophil infiltration after transient focal cerebral ischemia in mice. *Exp. Neurol.* 184, 973–980. doi: 10.1016/S0014-4886(03)00367-4

Crack, P. J., and Taylor, J. M. (2005). Reactive oxygen species and the modulation of stroke. *Free Radic. Biol. Med.* 38, 1433–1444. doi: 10.1016/j.freeradbiomed.2005.01.019

Cui, L., Zhang, X., Yang, R., Liu, L., Wang, L., Li, M., et al. (2010). Baicalein is neuroprotective in rat MCAO model: role of 12/15-lipoxygenase, mitogen-activated protein kinase and cytosolic phospholipase A2. *Pharmacol. Biochem. Behav.* 96, 469–475. doi: 10.1016/j.pbb.2010.07.007

Davies, M. J., Hawkins, C. L., Pattison, D. I., and Rees, M. D. (2008). Mammalian heme peroxidases: from molecular mechanisms to health implications. *Antioxid. Redox. Signal.* 10, 1199–1234. doi: 10.1089/ars.2007.1927

Dominguez, C., Delgado, P., Vilches, A., Martin-Gallan, P., Ribo, M., Santamarina, E., et al. (2010). Oxidative stress after thrombolysis-induced reperfusion in human stroke. *Stroke* 41, 653–660. doi: 10.1161/STROKEAHA.109.571935

Dou, Z., Rong, X., Zhao, E., Zhang, L., and Lv, Y. (2019). Neuroprotection of resveratrol against focal cerebral ischemia/reperfusion injury in mice through a mechanism targeting gut-brain axis. *Cell Mol. Neurobiol.* 39, 883–898. doi: 10.1007/s10571-019-00687-3

England, T. J., Hind, W. H., Rasid, N. A., and O'Sullivan, S. E. (2015). Cannabinoids in experimental stroke: a systematic review and meta-analysis. *J. Cereb. Blood Flow Metab.* 35, 348–358. doi: 10.1038/jcbfm.2014.218

Fang, L., Gao, H., Zhang, W., Zhang, W., and Wang, Y. (2015). Resveratrol alleviates nerve injury after cerebral ischemia and reperfusion in mice by inhibiting inflammation and apoptosis. *Int. J. Clin. Exp. Med.* 8, 3219–3226.

Feng, J., Chen, X., Guan, B., Li, C., Qiu, J., and Shen, J. (2018a). Inhibition of peroxynitrite-induced mitophagy activation attenuates cerebral ischemia-reperfusion injury. *Mol. Neurobiol.* 55, 6369–6386. doi: 10.1007/s12035-017-0859-x

Feng, J., Chen, X., Lu, S., Li, W., Yang, D., Su, W., et al. (2018b). Naringin attenuates cerebral ischemia-reperfusion injury through inhibiting peroxynitrite-mediated mitophagy activation. *Mol. Neurobiol.* 55, 9029–9042. doi: 10.1007/s12035-018-1027-7

Fernandes, M. Y. D., Carmo, M., Fonteles, A. A., Neves, J. C. S., Silva, A., Pereira, J. F., et al. (2019). (-)-alpha-bisabolol prevents neuronal damage and memory deficits through reduction of proinflammatory markers induced by permanent focal cerebral ischemia in mice. *Eur. J. Pharmacol.* 842, 270–280. doi: 10.1016/j.ejphar.2018.09.036

Ferreira Ede, O., Fernandes, M. Y., Lima, N. M., Neves, K. R., Carmo, M. R., Lima, F. A., et al. (2016). Neuroinflammatory response to experimental stroke is inhibited by eriodictyol. *Behav. Brain Res.* 312, 321–332. doi: 10.1016/j.bbr.2016.06.046

Fonteles, A. A., de Souza, C. M., de Sousa Neves, J. C., Menezes, A. P., Santos do Carmo, M. R., Fernandes, F. D., et al. (2016). Rosmarinic acid prevents against memory deficits in ischemic mice. *Behav. Brain Res.* 297, 91–103. doi: 10.1016/j.bbr.2015.09.029

Forghani, R., Kim, H. J., Wojtkiewicz, G. R., Bure, L., Wu, Y., Hayase, M., et al. (2015). Myeloperoxidase propagates damage and is a potential therapeutic target for subacute stroke. *J. Cereb. Blood Flow Metab.* 35, 485–493. doi: 10.1038/jcbfm.2014.222

Fu, S., Gu, Y., Jiang, J. Q., Chen, X., Xu, M., Chen, X., et al. (2014). Calycosin-7-O-beta-D-glucoside regulates nitric oxide /caveolin-1/matrix metalloproteinases pathway and protects blood-brain barrier integrity in experimental cerebral ischemia-reperfusion injury. *J. Ethnopharmacol.* 155, 692–701. doi: 10.1016/j.jep.2014.06.015

Gallelli, L. (2019). Escin: a review of its anti-edematous, anti-inflammatory, and venotonic properties. *Drug Des. Dev. Ther.* 13, 3425–3437. doi: 10.2147/DDDT.S207720

Gasche, Y., Fujimura, M., Morita-Fujimura, Y., Copin, J. C., Kawase, M., Massengale, J., et al. (1999). Early appearance of activated matrix metalloproteinase-9 after focal cerebral ischemia in mice: a possible role in blood-brain barrier dysfunction. *J. Cereb. Blood Flow Metab.* 19, 1020–1028. doi: 10.1097/00004647-199909000-00010

Gong, J., Sun, F., Li, Y., Zhou, X., Duan, Z., Duan, F., et al. (2015). *Momordica charantia* polysaccharides could protect against cerebral ischemia/reperfusion injury through inhibiting oxidative stress mediated c-Jun N-terminal kinase 3 signaling pathway. *Neuropharmacology* 91, 123–134. doi: 10.1016/j.neuropharm.2014.11.020

Granger, D. N., and Kvietys, P. R. (2015). Reperfusion injury and reactive oxygen species: the evolution of a concept. *Redox Biol.* 6, 524–551. doi: 10.1016/j.redox.2015.08.020

Green, P. S., Mendez, A. J., Jacob, J. S., Crowley, J. R., Growdon, W., Hyman, B. T., et al. (2004). Neuronal expression of myeloperoxidase is increased in Alzheimer's disease. *J. Neurochem.* 90, 724–733. doi: 10.1111/j.1471-4159.2004.02527.x

Gu, Y., Zheng, G., Xu, M., Li, Y., Chen, X., Zhu, W., et al. (2012). Caveolin-1 regulates nitric oxide-mediated matrix metalloproteinases activity and blood-brain barrier permeability in focal cerebral ischemia and reperfusion injury. *J. Neurochem.* 120, 147–156. doi: 10.1111/j.1471-4159.2011.07542.x

Guan, W., Zhao, Y., and Xu, C. (2011). A Combined treatment with taurine and intra-arterial thrombolysis in an embolic model of stroke in rats: increased neuroprotective efficacy and extended therapeutic time window. *Transl. Stroke Res.*2, 80–91. doi: 10.1007/s12975-010-0050-4

Guclu-Ustundag, O., and Mazza, G. (2007). Saponins: properties, applications and processing. *Crit. Rev. Food Sci. Nutr.* 47, 231–258.

Guo, M., Lu, H., Qin, J., Qu, S., Wang, W., Guo, Y., et al. (2019). Biochanin a provides neuroprotection against cerebral ischemia/reperfusion injury by Nrf2-mediated inhibition of oxidative stress and inflammation signaling pathway in rats. *Med. Sci. Monit.* 25, 8975–8983. doi: 10.12659/MSM.918665

Gursoy-Ozdemir, Y., Can, A., and Dalkara, T. (2004). Reperfusion-induced oxidative/nitrative injury to neurovascular unit after focal cerebral ischemia. *Stroke* 35, 1449–1453. doi: 10.1161/01.STR.0000126044.83777.f4

Hawkins, C. L., Pattison, D. I., and Davies, M. J. (2003). Hypochlorite-induced oxidation of amino acids, peptides and proteins. *Amino Acids* 25, 259–274. doi: 10.1007/s00726-003-0016-x

Hayakawa, K., Mishima, K., Irie, K., Hazekawa, M., Mishima, S., Fujioka, M., et al. (2008). Cannabidiol prevents a post-ischemic injury progressively induced by cerebral ischemia via a high-mobility group box1-inhibiting mechanism. *Neuropharmacology* 55, 1280–1286. doi: 10.1016/j.neuropharm.2008.06.040

Horvath, E., Hutanu, A., Chiriac, L., Dobreanu, M., Oradan, A., and Nagy, E. E. (2018). Ischemic damage and early inflammatory infiltration are different in the core and penumbra lesions of rat brain after transient focal cerebral ischemia. *J. Neuroimmunol.* 324, 35–42. doi: 10.1016/j.jneuroim.2018.08.002

Hou, Y., Wang, K., Wan, W., Cheng, Y., Pu, X., and Ye, X. (2018). Resveratrol provides neuroprotection by regulating the JAK2/STAT3/PI3K/AKT/mTOR pathway after stroke in rats. *Genes Dis.* 5, 245–255. doi: 10.1016/j.gendis.2018.06.001

Hoy, A., Leininger-Muller, B., Poirier, O., Siest, G., Gautier, M., Elbaz, A., et al. (2003). Myeloperoxidase polymorphisms in brain infarction. Association with infarct size and functional outcome. *Atherosclerosis* 167, 223–230. doi: 10.1016/s0021-9150(02)00041-2

Hu, X. M., Zhang, Y., and Zeng, F. D. (2004). Effects of sodium beta-aescin on expression of adhesion molecules and migration of neutrophils after middle cerebral artery occlusion in rats. *Acta Pharmacol. Sin.* 25, 869–875.

Huang, L., Chen, C., Zhang, X., Li, X., Chen, Z., Yang, C., et al. (2018). Neuroprotective effect of curcumin against cerebral ischemia-reperfusion via mediating autophagy and inflammation. *J. Mol. Neurosci.* 64, 129–139. doi: 10.1007/s12031-017-1006-x

Huang, Q., Sun, M., Li, M., Zhang, D., Han, F., Wu, J. C., et al. (2018). Combination of NAD(+) and NADPH offers greater neuroprotection in ischemic stroke models by relieving metabolic stress. *Mol. Neurobiol.* 55, 6063–6075. doi: 10.1007/s12035-017-0809-7

Hunter, R., Caira, M., and Stellenboom, N. (2005). Thiolsulfinate allicin from garlic: inspiration for a new antimicrobial agent. *Ann. N. Y. Acad. Sci.* 1056, 234–241. doi: 10.1196/annals.1352.011

Hwang, Y. S., Shin, C. Y., Huh, Y., and Ryu, J. H. (2002). Hwangryun-Hae-Dok-tang (Huanglian-Jie-Du-Tang) extract and its constituents reduce ischemia-reperfusion brain injury and neutrophil infiltration in rats. *Life Sci.* 71, 2105–2117. doi: 10.1016/s0024-3205(02)01920-3

Jang, J. W., Lee, J. K., Hur, H., Kim, T. W., Joo, S. P., and Piao, M. S. (2014). Rutin improves functional outcome via reducing the elevated matrix metalloproteinase-9 level in a photothrombotic focal ischemic model of rats. *J. Neurol. Sci.* 339, 75–80. doi: 10.1016/j.jns.2014.01.024

Jayaraj, R. L., Azimullah, S., Beiram, R., Jalal, F. Y., and Rosenberg, G. A. (2019). Neuroinflammation: friend and foe for ischemic stroke. *J. Neuroinflamm.* 16:142. doi: 10.1186/s12974-019-1516-2

Ji, H. J., Hu, J. F., Wang, Y. H., Chen, X. Y., Zhou, R., and Chen, N. H. (2010). Osthole improves chronic cerebral hypoperfusion induced cognitive deficits and neuronal damage in hippocampus. *Eur. J. Pharmacol.* 636, 96–101. doi: 10.1016/j.ejphar.2010.03.038

Jiang, S., Han, J., Li, T., Xin, Z., Ma, Z., Di, W., et al. (2017). Curcumin as a potential protective compound against cardiac diseases. *Pharmacol. Res.* 119, 373–383. doi: 10.1016/j.phrs.2017.03.001

Jiang, W. L., Tian, J. W., Fu, F. H., Zhu, H. B., and Hou, J. (2010). Neuroprotective efficacy and therapeutic window of Forsythoside B: in a rat model of cerebral ischemia and reperfusion injury. *Eur. J. Pharmacol.* 640, 75–81. doi: 10.1016/j.ejphar.2010.04.055

Jickling, G. C., Liu, D., Ander, B. P., Stamova, B., Zhan, X., and Sharp, F. R. (2015). Targeting neutrophils in ischemic stroke: translational insights from experimental studies. *J. Cereb. Blood Flow Metab.* 35, 888–901. doi: 10.1038/jcbfm.2015.45

Jickling, G. C., Liu, D., Stamova, B., Ander, B. P., Zhan, X., Lu, A., et al. (2014). Hemorrhagic transformation after ischemic stroke in animals and humans. *J. Cereb. Blood Flow Metabol.* 34, 185–199. doi: 10.1038/jcbfm.2013.203

Jin, Y., Wei, F., Dai, X., Qi, M., and Ma, Y. (2018). Anti-inflammatory effect of 4-methylcyclopentadecanone in rats submitted to ischemic stroke. *Fundam. Clin. Pharmacol.* 32, 270–278. doi: 10.1111/fcp.12348

Jing, X., Ren, D., Wei, X., Shi, H., Zhang, X., Perez, R. G., et al. (2013). Eriodictyol-7-O-glucoside activates Nrf2 and protects against cerebral ischemic injury. *Toxicol. Appl. Pharmacol.* 273, 672–679.

Khaksar, S., and Bigdeli, M. R. (2017). Correlation between cannabidiol-induced reduction of infarct volume and inflammatory factors expression in ischemic stroke model. *Basic Clin. Neurosci.* 8, 139–146. doi: 10.18869/nirp.bcn.8.2.139

Khan, M. M., Ahmad, A., Ishrat, T., Khuwaja, G., Srivastawa, P., Khan, M. B., et al. (2009). Rutin protects the neural damage induced by transient focal ischemia in rats. *Brain Res.* 1292, 123–135. doi: 10.1016/j.brainres.2009.07.026

Khan, M. M., Motto, D. G., Lentz, S. R., and Chauhan, A. K. (2012). ADAMTS13 reduces VWF-mediated acute inflammation following focal cerebral ischemia in mice. *J. Thromb. Haemost.* 10, 1665–1671. doi: 10.1111/j.1538-7836.2012.04822.x

Kim, H., Wei, Y., Lee, J. Y., Wu, Y., Zheng, Y., Moskowitz, M. A., et al. (2016). Myeloperoxidase inhibition increases neurogenesis after ischemic stroke. *J. Pharmacol. Exp. Ther.* 359, 262–272. doi: 10.1124/jpet.116.235127

Kim, H. J., Wei, Y., Wojtkiewicz, G. R., Lee, J. Y., Moskowitz, M. A., and Chen, J. W. (2018). Reducing myeloperoxidase activity decreases inflammation and increases cellular protection in ischemic stroke. *J. Cereb. Blood Flow Metab.* doi: 10.1177/0271678X18771978

Kim, H. J., Wei, Y., Wojtkiewicz, G. R., Lee, J. Y., Moskowitz, M. A., and Chen, J. W. (2019). Reducing myeloperoxidase activity decreases inflammation and increases cellular protection in ischemic stroke. *J. Cereb. Blood Flow Metab.* 39, 1864–1877. doi: 10.1177/0271678X18771978

Kiss, T., Balasubramanian, P., Valcarcel-Ares, M. N., Tarantini, S., Yabluchanskiy, A., Csipo, T., et al. (2019a). Nicotinamide mononucleotide (NMN) treatment attenuates oxidative stress and rescues angiogenic capacity in aged cerebromicrovascular endothelial cells: a potential mechanism for the prevention of vascular cognitive impairment. *Geroscience* 41, 619–630. doi: 10.1007/s11357-019-00074-2

Kiss, T., Giles, C. B., Tarantini, S., Yabluchanskiy, A., Balasubramanian, P., Gautam, T., et al. (2019b). Nicotinamide mononucleotide (NMN) supplementation promotes anti-aging miRNA expression profile in the aorta of aged mice, predicting epigenetic rejuvenation and anti-atherogenic effects. *Geroscience* 41, 419–439. doi: 10.1007/s11357-019-00095-x

Kong, L. L., Wang, Z. Y., Han, N., Zhuang, X. M., Wang, Z. Z., Li, H., et al. (2014). Neutralization of chemokine-like factor 1, a novel C-C chemokine, protects against focal cerebral ischemia by inhibiting neutrophil infiltration via MAPK pathways in rats. *J. Neuroinflamm.* 11, 112. doi: 10.1186/1742-2094-11-112

Kunnumakkara, A. B., Bordoloi, D., Harsha, C., Banik, K., Gupta, S. C., and Aggarwal, B. B. (2017). Curcumin mediates anticancer effects by modulating multiple cell signaling pathways. *Clin. Sci. (Lond.)* 131, 1781–1799. doi: 10.1042/CS20160935

Lees, K. R., Zivin, J. A., Ashwood, T., Davalos, A., Davis, S. M., Diener, H. C., et al. (2006). NXY-059 for acute ischemic stroke. *N. Engl. J. Med.* 354, 588–600.

Lei, J., and Chen, Q. (2018). Resveratrol attenuates brain damage in permanent focal cerebral ischemia via activation of PI3K/Akt signaling pathway in rats. *Neurol. Res.* 40, 1014–1020. doi: 10.1080/01616412.2018.1509826

Lei, J. R., Tu, X. K., Wang, Y., Tu, D. W., and Shi, S. S. (2019). Resveratrol downregulates the TLR4 signaling pathway to reduce brain damage in a rat model of focal cerebral ischemia. *Exp. Ther. Med.* 17, 3215–3221. doi: 10.3892/etm.2019.7324

Li, C., Yan, Z., Yang, J., Chen, H., Li, H., Jiang, Y., et al. (2010). Neuroprotective effects of resveratrol on ischemic injury mediated by modulating the release of neurotransmitter and neuromodulator in rats. *Neurochem. Int.* 56, 495–500. doi: 10.1016/j.neuint.2009.12.009

Li, H. Y., Yuan, Z. Y., Wang, Y. G., Wan, H. J., Hu, J., Chai, Y. S., et al. (2012). Role of baicalin in regulating Toll-like receptor 2/4 after ischemic neuronal injury. *Chin. Med. J.* 125, 1586–1593.

Li, M., Qu, Y. Z., Zhao, Z. W., Wu, S. X., Liu, Y. Y., Wei, X. Y., et al. (2012). Astragaloside IV protects against focal cerebral ischemia/reperfusion injury correlating to suppression of neutrophils adhesion-related molecules. *Neurochem. Int.* 60, 458–465. doi: 10.1016/j.neuint.2012.01.026

Li, Q., Ren, F. Q., Yang, C. L., Zhou, L. M., Liu, Y. Y., Xiao, J., et al. (2015). Anti-proliferation effects of isorhamnetin on lung cancer cells in vitro and in vivo. *Asian Pac. J. Cancer Prev.* 16, 3035–3042. doi: 10.7314/apjcp.2015.16.7.3035

Li, S., Sun, X., Xu, L., Sun, R., Ma, Z., Deng, X., et al. (2017). Baicalin attenuates in vivo and in vitro hyperglycemia-exacerbated ischemia/reperfusion injury by regulating mitochondrial function in a manner dependent on AMPK. *Eur. J. Pharmacol.* 815, 118–126. doi: 10.1016/j.ejphar.2017.07.041

Li, W., Chen, Z., Yan, M., He, P., Chen, Z., and Dai, H. (2016a). The protective role of isorhamnetin on human brain microvascular endothelial cells from cytotoxicity induced by methylglyoxal and oxygen-glucose deprivation. *J. Neurochem.* 136, 651–659. doi: 10.1111/jnc.13436

Li, Y., Yao, J., Han, C., Yang, J., Chaudhry, M. T., Wang, S., et al. (2016b). Quercetin. *Inflamm. Immun. Nutr.* 8:167.

Li, Z., Fang, F., Wang, Y., and Wang, L. (2016a). Resveratrol protects CA1 neurons against focal cerebral ischemic reperfusion-induced damage via the ERK-CREB signaling pathway in rats. *Pharmacol. Biochem. Behav.* 14, 21–27. doi: 10.1016/j.pbb.2016.04.007

Li, Z., Hua, C., Pan, X., Fu, X., and Wu, W. (2016b). Carvacrol exerts neuroprotective effects via suppression of the inflammatory response in middle cerebral artery occlusion rats. *Inflammation* 39, 1566–1572. doi: 10.1007/s10753-016-0392-5

Liang, W., Huang, X., and Chen, W. (2017). The effects of baicalin and baicalein on cerebral ischemia: a review. *Aging Dis.* 8, 850–867. doi: 10.14336/AD.2017.0829

Liu, L., Zhang, X., Wang, L., Yang, R., Cui, L., Li, M., et al. (2010). The neuroprotective effects of Tanshinone IIA are associated with induced nuclear translocation of TORC1 and upregulated expression of TORC1, pCREB and BDNF in the acute stage of ischemic stroke. *Brain Res. Bull.* 82, 228–233. doi: 10.1016/j.brainresbull.2010.04.005

Liu, M., Yin, Y., Ye, X., Zeng, M., Zhao, Q., Keefe, D. L., et al. (2013). Resveratrol protects against age-associated infertility in mice. *Hum. Reprod.* 28, 707–717. doi: 10.1093/humrep/des437

Liu, W., Hendren, J., Qin, X. J., Shen, J., and Liu, K. J. (2009). Normobaric hyperoxia attenuates early blood-brain barrier disruption by inhibiting MMP-9-mediated occludin degradation in focal cerebral ischemia. *J. Neurochem.* 108, 811–820. doi: 10.1111/j.1471-4159.2008.05821.x

Liu, X., Wang, T., Liu, X., Cai, L., Qi, J., Zhang, P., et al. (2016). Biochanin A protects lipopolysaccharide/D-galactosamine-induced acute liver injury in mice by activating the Nrf2 pathway and inhibiting NLRP3 inflammasome activation. *Int. Immunopharmacol.* 38, 324–331. doi: 10.1016/j.intimp.2016.06.009

Liu, Y., Tong, L., Luo, Y., Li, X., Chen, G., and Wang, Y. (2018). Resveratrol inhibits the proliferation and induces the apoptosis in ovarian cancer cells via inhibiting glycolysis and targeting AMPK/mTOR signaling pathway. *J. Cell. Biochem.* 119, 6162–6172. doi: 10.1002/jcb.26822

Liu, Z., Ran, Y., Huang, S., Wen, S., Zhang, W., Liu, X., et al. (2017). Curcumin protects against ischemic stroke by titrating microglia/macrophage polarization. *Front. Aging Neurosci.* 9:233. doi: 10.3389/fnagi.2017.00233

Luan, H., Kan, Z., Xu, Y., Lv, C., and Jiang, W. (2013). Rosmarinic acid protects against experimental diabetes with cerebral ischemia: relation to inflammation response. *J. Neuroinflamm.*10:28. doi: 10.1186/1742-2094-10-28

Ma, X. J., Cheng, J. W., Zhang, J., Liu, A. J., Liu, W., Guo, W., et al. (2012). E-selectin deficiency attenuates brain ischemia in mice. *CNS Neurosci. Ther.* 18, 903–908. doi: 10.1111/cns.12000

Manso, H., Krug, T., Sobral, J., Albergaria, I., Gaspar, G., Ferro, J. M., et al. (2011). Variants in the inflammatory IL6 and MPO genes modulate stroke susceptibility through main effects and gene-gene interactions. *J. Cereb. Blood Flow Metab.* 31, 1751–1759. doi: 10.1038/jcbfm.2011.27

Mao, X., Yin, W., Liu, M., Ye, M., Liu, P., Liu, J., et al. (2011). Osthole, a natural coumarin, improves neurobehavioral functions and reduces infarct volume and matrix metalloproteinase-9 activity after transient focal cerebral ischemia in rats. *Brain Res.* 1385, 275–280. doi: 10.1016/j.brainres.2011.02.015

Marquez, L. A., and Dunford, H. B. (1994). Chlorination of taurine by myeloperoxidase. Kinetic evidence for an enzyme-bound intermediate. *J. Biol. Chem.* 269, 7950–7956.

Matsuo, Y., Onodera, H., Shiga, Y., Nakamura, M., Ninomiya, M., Kihara, T., et al. (1994). Correlation between myeloperoxidase-quantified neutrophil accumulation and ischemic brain injury in the rat. Effects of neutrophil depletion. *Stroke* 25, 1469–1475. doi: 10.1161/01.str.25.7.1469

Menon, V. P., and Sudheer, A. R. (2007). Antioxidant and anti-inflammatory properties of curcumin. *Adv. Exp. Med. Biol.* 595, 105–125.

Mishima, K., Hayakawa, K., Abe, K., Ikeda, T., Egashira, N., Iwasaki, K., et al. (2005). Cannabidiol prevents cerebral infarction via a serotonergic 5-hydroxytryptamine1A receptor-dependent mechanism. *Stroke* 36, 1077–1082. doi: 10.1161/01.STR.0000163083.59201.34

Mishra, P., Kale, R. K., and Kar, A. (2008). Chemoprevention of mammary tumorigenesis and chemomodulation of the antioxidative enzymes and peroxidative damage in prepubertal Sprague Dawley rats by Biochanin A. *Mol. Cell. Biochem.* 312, 1–9. doi: 10.1007/s11010-008-9714-8

Mizuma, A., and Yenari, M. A. (2017). Anti-inflammatory targets for the treatment of reperfusion injury in stroke. *Front. Neurol.* 8:467. doi: 10.3389/fneur.2017.00467

Mosawy, S., Jackson, D. E., Woodman, O. L., and Linden, M. D. (2013). Inhibition of platelet-mediated arterial thrombosis and platelet granule exocytosis by 3',4'-dihydroxyflavonol and quercetin. *Platelets* 24, 594–604. doi: 10.3109/09537104.2012.749396

Muir, S. W., Harrow, C., Dawson, J., Lees, K. R., Weir, C. J., Sattar, N., et al. (2008). Allopurinol use yields potentially beneficial effects on inflammatory indices in those with recent ischemic stroke: a randomized, double-blind, placebo-controlled trial. *Stroke* 39, 3303–3307. doi: 10.1161/STROKEAHA.108.519793

Nagra, R. M., Becher, B., Tourtellotte, W. W., Antel, J. P., Gold, D., Paladino, T., et al. (1997). Immunohistochemical and genetic evidence of myeloperoxidase involvement in multiple sclerosis. *J. Neuroimmunol.* 78, 97–107. doi: 10.1016/s0165-5728(97)00089-1

Nakase, T., Yoshioka, S., and Suzuki, A. (2011). Free radical scavenger, edaravone, reduces the lesion size of lacunar infarction in human brain ischemic stroke. *BMC Neurol.* 11:39. doi: 10.1186/1471-2377-11-39

Nussbaum, C., Klinke, A., Adam, M., Baldus, S., and Sperandio, M. (2013). Myeloperoxidase: a leukocyte-derived protagonist of inflammation and cardiovascular disease. *Antioxid. Redox. Signal.* 18, 692–713. doi: 10.1089/ars.2012.4783

Palm, F., Pussinen, P. J., Safer, A., Tervahartiala, T., Sorsa, T., Urbanek, C., et al. (2018). Serum matrix metalloproteinase-8, tissue inhibitor of metalloproteinase and myeloperoxidase in ischemic stroke. *Atherosclerosis* 271, 9–14. doi: 10.1016/j.atherosclerosis.2018.02.012

Panasenko, O. M. (1997). The mechanism of the hypochlorite-induced lipid peroxidation. *Biofactors* 6, 181–190. doi: 10.1002/biof.5520060212

Pandey, A. K., Bhattacharya, P., Shukla, S. C., Paul, S., and Patnaik, R. (2015). Resveratrol inhibits matrix metalloproteinases to attenuate neuronal damage in cerebral ischemia: a molecular docking study exploring possible neuroprotection. *Neural Regener. Res.* 10, 568–575. doi: 10.4103/1673-5374.278561

Park, D. J., Shah, F. A., and Koh, P. O. (2018). Quercetin attenuates neuronal cells damage in a middle cerebral artery occlusion animal model. *J. Vet. Med. Sci.* 80, 676–683. doi: 10.1292/jvms.17-0693

Pattison, D. I., Hawkins, C. L., and Davies, M. J. (2003). Hypochlorous acid-mediated oxidation of lipid components and antioxidants present in low-density lipoproteins: absolute rate constants, product analysis, and computational modeling. *Chem. Res. Toxicol.* 16, 439–449. doi: 10.1021/tx025670s

Peng, T., Chen, X., Gao, L., Zhang, T., Wang, W., Shen, J., et al. (2016). A rationally designed rhodamine-based fluorescent probe for molecular imaging of peroxynitrite in live cells and tissues. *Chem. Sci.* 7, 5407–5413. doi: 10.1039/c6sc00012f

Peng, T., Wong, N. K., Chen, X., Chan, Y. K., Sun, Z., Hu, J. J., et al. (2014). Molecular imaging of peroxynitrite with HKGreen-4 in live cells and tissues. *J. Am. Chem. Soc.* 136, 11728–11734. doi: 10.1021/jacs.7b13132

Popa-Wagner, A., Hermann, D., and Gresita, A. (2019). Genetic conversion of proliferative astroglia into neurons after cerebral ischemia: a new therapeutic tool for the aged brain? *Geroscience* 41, 363–368. doi: 10.1007/s11357-019-00136-5

Pravalika, K., Sarmah, D., Kaur, H., Vats, K., Saraf, J., Wanve, M., et al. (2019). Trigonelline therapy confers neuroprotection by reduced glutathione mediated myeloperoxidase expression in animal model of ischemic stroke. *Life Sci.* 216, 49–58. doi: 10.1016/j.lfs.2018.11.014

Prutz, W. A. (1996). Hypochlorous acid interactions with thiols, nucleotides DNA, and other biological substrates. *Arch. Biochem. Biophys.* 332, 110–120. doi: 10.1006/abbi.1996.0322

Ramos-Fernandez, M., Bellolio, M. F., and Stead, L. G. (2011). Matrix metalloproteinase-9 as a marker for acute ischemic stroke: a systematic review. *J. Stroke Cerebrovasc. Dis.* 20, 47–54. doi: 10.1016/j.jstrokecerebrovasdis.2009.10.008

Reiche, E. M. V., Gelinksi, J. R., Alfieri, D. F., Flauzino, T., Lehmann, M. F., de Araujo, M. C. M., et al. (2019). Immune-inflammatory, oxidative stress and biochemical biomarkers predict short-term acute ischemic stroke death. *Metab. Brain Dis.* 34, 789–804. doi: 10.1007/s11011-019-00403-6

Rodrigo, R., Fernández-Gajardo, R., Gutiérrez, R., Manuel Matamala, J., Carrasco, R., Miranda-Merchak, A., et al. (2013). Oxidative stress and pathophysiology of ischemic stroke: novel therapeutic opportunities. *CNS Neurol. Disord. Drug Targets* 12, 698–714. doi: 10.2174/18715273113120500015

Rosell, A., Cuadrado, E., Ortega-Aznar, A., Hernandez-Guillamon, M., Lo, E. H., and Montaner, J. (2008). MMP-9-positive neutrophil infiltration is associated to blood-brain barrier breakdown and basal lamina type IV collagen degradation during hemorrhagic transformation after human ischemic stroke. *Stroke* 39, 1121–1126. doi: 10.1161/STROKEAHA.107.500868

Sampaio, T. L., Menezes, R. R., da Costa, M. F., Meneses, G. C., Arrieta, M. C., Chaves Filho, A. J., et al. (2016). Nephroprotective effects of (-)-alpha-bisabolol against ischemic-reperfusion acute kidney injury. *Phytomedicine* 23, 1843–1852. doi: 10.1016/j.phymed.2016.11.008

Schraufstatter, I. U., Browne, K., Harris, A., Hyslop, P. A., Jackson, J. H., Quehenberger, O., et al. (1990). Mechanisms of hypochlorite injury of target cells. *J. Clin. Invest.* 85, 554–562. doi: 10.1172/JCI114472

Shen, J., Ma, S., Chan, P., Lee, W., Fung, P. C., Cheung, R. T., et al. (2006). Nitric oxide down-regulates caveolin-1 expression in rat brains during focal cerebral ischemia and reperfusion injury. *J. Neurochem.* 96, 1078–1089. doi: 10.1111/j.1471-4159.2005.03589.x

Sun, M. S., Jin, H., Sun, X., Huang, S., Zhang, F. L., Guo, Z. N., et al. (2018). Free radical damage in ischemia-reperfusion injury: an obstacle in acute ischemic stroke after revascularization therapy. *Oxid. Med. Cell Longev.* 2018, 3804979. doi: 10.1155/2018/3804979

Suzuki, A., Yamamoto, M., Jokura, H., Fujii, A., Tokimitsu, I., Hase, T., et al. (2007). Ferulic acid restores endothelium-dependent vasodilation in aortas of spontaneously hypertensive rats. *Am. J. Hypertens.* 20, 508–513. doi: 10.1016/j.amjhyper.2006.11.008

Tang, C., Xue, H., Bai, C., Fu, R., and Wu, A. (2010). The effects of Tanshinone IIA on blood-brain barrier and brain edema after transient middle cerebral artery occlusion in rats. *Phytomedicine* 17, 1145–1149. doi: 10.1016/j.phymed.2010.03.017

Tang, N. Y., Liu, C. H., Hsieh, C. T., and Hsieh, C. L. (2010). The anti-inflammatory effect of paeoniflorin on cerebral infarction induced by ischemia-reperfusion injury in Sprague-Dawley rats. *Am. J. Chin. Med.* 38, 51–64. doi: 10.1142/S0192415X10007786

Tay, A., Tamam, Y., Yokus, B., Ustundag, M., and Orak, M. (2015). Serum myeloperoxidase levels in predicting the severity of stroke and mortality in acute ischemic stroke patients. *Eur. Rev. Med. Pharmacol. Sci.* 19, 1983–1988.

Tu, X. K., Yang, W. Z., Chen, J. P., Chen, Y., Chen, Q., Chen, P. P., et al. (2015). Repetitive ischemic preconditioning attenuates inflammatory reaction and brain damage after focal cerebral ischemia in rats: involvement of PI3K/Akt and ERK1/2 signaling pathway. *J. Mol. Neurosci.* 55, 912–922. doi: 10.1007/s12031-014-0446-9

Tu, X. K., Yang, W. Z., Chen, J. P., Chen, Y., Ouyang, L. Q., Xu, Y. C., et al. (2014). Curcumin inhibits TLR2/4-NF-kappaB signaling pathway and attenuates brain damage in permanent focal cerebral ischemia in rats. *Inflammation* 37, 1544–1551. doi: 10.1007/s10753-014-9881-6

Tu, X. K., Yang, W. Z., Liang, R. S., Shi, S. S., Chen, J. P., Chen, C. M., et al. (2011a). Effect of baicalin on matrix metalloproteinase-9 expression and blood-brain barrier permeability following focal cerebral ischemia in rats. *Neurochem. Res.* 36, 2022–2028. doi: 10.1007/s11064-011-0526-y

Tu, X. K., Yang, W. Z., Shi, S. S., Chen, Y., Wang, C. H., Chen, C. M., et al. (2011b). Baicalin inhibits TLR2/4 signaling pathway in rat brain following permanent cerebral ischemia. *Inflammation* 34, 463–470. doi: 10.1007/s10753-010-9254-8

Tu, X. K., Yang, W. Z., Shi, S. S., Wang, C. H., and Chen, C. M. (2009). Neuroprotective effect of baicalin in a rat model of permanent focal cerebral ischemia. *Neurochem. Res.* 34, 1626–1634. doi: 10.1007/s11064-009-9953-4

Tu, X. K., Zhang, H. B., Shi, S. S., Liang, R. S., Wang, C. H., Chen, C. M., et al. (2016). 5-LOX inhibitor zileuton reduces inflammatory reaction and ischemic brain damage through the activation of PI3K/Akt signaling pathway. *Neurochem. Res.* 41, 2779–2787. doi: 10.1007/s11064-016-1994-x

Tziomalos, K., Katrini, K., Papagianni, M., Christou, K., Gkolfinopoulou, C., Angelopoulou, S. M., et al. (2019). Impaired antioxidative activity of high-density lipoprotein is associated with more severe acute ischemic stroke. *Metabolism* 98, 49–52. doi: 10.1016/j.metabol.2019.06.004

Ullen, A., Singewald, E., Konya, V., Fauler, G., Reicher, H., Nusshold, C., et al. (2013). Myeloperoxidase-derived oxidants induce blood-brain barrier dysfunction in vitro and in vivo. *PLoS ONE* 8:e64034. doi: 10.1371/journal.pone.0064034

Vandooren, J., Van Damme, J., and Opdenakker, G. (2014). On the structure and functions of gelatinase B/matrix metalloproteinase-9 in neuroinflammation. *Prog. Brain Res.* 214, 193–206. doi: 10.1016/B978-0-444-63486-3.00009-8

Wang, Q., Xu, J., Rottinghaus, G. E., Simonyi, A., Lubahn, D., Sun, G. Y., et al. (2002). Resveratrol protects against global cerebral ischemic injury in gerbils. *Brain Res.* 958, 439–447. doi: 10.1016/s0006-8993(02)03543-6

Wang, W., Tang, L., Li, Y., and Wang, Y. (2015). Biochanin A protects against focal cerebral ischemia/reperfusion in rats via inhibition of p38-mediated inflammatory responses. *J. Neurol. Sci.* 348, 121–125. doi: 10.1016/j.jns.2014.11.018

Wardlaw, J. M., Murray, V., Berge, E., Del Zoppo, G., Sandercock, P., Lindley, R. L., et al. (2012). Recombinant tissue plasminogen activator for acute ischaemic stroke: an updated systematic review and meta-analysis. *Lancet* 379, 2364–2372. doi: 10.1016/S0140-6736(12)60738-7

Wei, H., Wang, S., Zhen, L., Yang, Q., Wu, Z., Lei, X., et al. (2015). Resveratrol attenuates the blood-brain barrier dysfunction by regulation of the MMP-9/TIMP-1 balance after cerebral ischemia reperfusion in rats. *J. Mol. Neurosci. MN* 55, 872–879. doi: 10.1007/s12031-014-0441-1

Weiss, S. J., Klein, R., Slivka, A., and Wei, M. (1982). Chlorination of taurine by human neutrophils. Evidence for hypochlorous acid generation. *J. Clin. Invest.* 70, 598–607. doi: 10.1172/jci110652

Wiedenhoeft, T., Tarantini, S., Nyul-Toth, A., Yabluchanskiy, A., Csipo, T., Balasubramanian, P., et al. (2019). Fusogenic liposomes effectively deliver resveratrol to the cerebral microcirculation and improve endothelium-dependent neurovascular coupling responses in aged mice. *Geroscience* 41, 711–725. doi: 10.1007/s11357-019-00102-1

Wu, C. F., Hong, C., Klauck, S. M., Lin, Y. L., and Efferth, T. (2015). Molecular mechanisms of rosmarinic acid from Salvia miltiorrhiza in acute lymphoblastic leukemia cells. *J. Ethnopharmacol.* 176, 55–68. doi: 10.1016/j.jep.2015.10.020

Wu, L., Li, J., Liu, T., Li, S., Feng, J., Yu, Q., et al. (2019). Quercetin shows anti-tumor effect in hepatocellular carcinoma LM3 cells by abrogating JAK2/STAT3 signaling pathway. *Cancer Med.* 8, 4806–4820. doi: 10.1002/cam4.2388

Wu, X. J., Zhou, X. B., Chen, C., and Mao, W. (2019). Systematic investigation of quercetin for treating cardiovascular disease based on network pharmacology. *Comb. Chem. High. Throughput. Screen* 22, 411–420. doi: 10.2174/1386207322666190717124507

Xu, J., Xie, Z., Reece, R., Pimental, D., and Zou, M. H. (2006). Uncoupling of endothelial nitric oxidase synthase by hypochlorous acid: role of NAD(P)H oxidase-derived superoxide and peroxynitrite. *Arterioscler. Thromb. Vasc. Biol.* 26, 2688–2695. doi: 10.1161/01.ATV.0000249394.94588.82

Xu, M., Chen, X., Gu, Y., Peng, T., Yang, D., Chang, R. C., et al. (2013). Baicalin can scavenge peroxynitrite and ameliorate endogenous peroxynitrite-mediated neurotoxicity in cerebral ischemia-reperfusion injury. *J. Ethnopharmacol.* 150, 116–124. doi: 10.1016/j.jep.2013.08.020

Xue, X., Qu, X. J., Yang, Y., Sheng, X. H., Cheng, F., Jiang, E. N., et al. (2010). Baicalin attenuates focal cerebral ischemic reperfusion injury through inhibition of nuclear factor kappaB p65 activation. *Biochem. Biophys. Res. Commun.* 403, 398–404. doi: 10.1016/j.bbrc.2010.11.042

Yang, C., Hawkins, K. E., Dore, S., and Candelario-Jalil, E. (2019). Neuroinflammatory mechanisms of blood-brain barrier damage in ischemic stroke. *Am. J. Physiol. Cell Physiol.* 316, C135–C153. doi: 10.1152/ajpcell.00136.2018

Yang, Q., Huang, Q., Hu, Z., and Tang, X. (2019). Potential neuroprotective treatment of stroke: targeting excitotoxicity. *Oxidat. Stress Inflamm. Front. Neurosci.* 13:1036. doi: 10.3389/fnins.2019.01036

Yang, S., Wang, H., Yang, Y., Wang, R., Wang, Y., Wu, C., et al. (2019). Baicalein administered in the subacute phase ameliorates ischemia-reperfusion-induced brain injury by reducing neuroinflammation and neuronal damage. *Biomed. Pharmacother.* 117:109102. doi: 10.1016/j.biopha.2019.109102

Yang, X. Y., Jiang, S. Q., Zhang, L., Liu, Q. N., and Gong, P. L. (2007). Inhibitory effect of dauricine on inflammatory process following focal cerebral ischemia/reperfusion in rats. *Am. J. Chin. Med.* 35, 477–486. doi: 10.1142/S0192415X07004990

Yang, Y., Estrada, E. Y., Thompson, J. F., Liu, W., and Rosenberg, G. A. (2007). Matrix metalloproteinase-mediated disruption of tight junction proteins in cerebral vessels is reversed by synthetic matrix metalloproteinase inhibitor in focal ischemia in rat. *J. Cereb. Blood Flow Metab.* 27, 697–709. doi: 10.1038/sj.jcbfm.9600375

Yap, Y. W., Whiteman, M., and Cheung, N. S. (2007). Chlorinative stress: an under appreciated mediator of neurodegeneration? *Cell Signal.* 19, 219–228. doi: 10.1016/j.cellsig.2006.06.013

Ying, W., Wei, G., Wang, D., Wang, Q., Tang, X., Shi, J., et al. (2007). Intranasal administration with NAD+ profoundly decreases brain injury in a rat model of transient focal ischemia. *Front. Biosci.* 12:2728–2734. doi: 10.2741/2267 doi: 10.2741/2267

Yu, C., He, Q., Zheng, J., Li, L. Y., Hou, Y. H., and Song, F. Z. (2017). Sulforaphane improves outcomes and slows cerebral ischemic/reperfusion injury via inhibition of NLRP3 inflammasome activation in rats. *Int. Immunopharmacol.* 45, 74–78. doi: 10.1016/j.intimp.2017.01.034

Yu, G., Liang, Y., Huang, Z., Jones, D. W., Pritchard, K. A. Jr., et al. (2016). Inhibition of myeloperoxidase oxidant production by N-acetyl lysyltyrosylcysteine amide reduces brain damage in a murine model of stroke. *J. Neuroinflamm.* 13, 119. doi: 10.1186/s12974-016-0639-y

Yu, G., Liang, Y., Zheng, S., and Zhang, H. (2018). Inhibition of myeloperoxidase by N-Acetyl lysyltyrosylcysteine amide reduces oxidative stress-mediated

inflammation. neuronal damage, and neural stem cell injury in a murine model of stroke. *J. Pharmacol. Exp. Ther.* 364, 311–322. doi: 10.1124/jpet.117.245688

Yu, H., Zhang, Z. L., Chen, J., Pei, A., Hua, F., Qian, X., et al. (2012). Carvacrol, a food-additive, provides neuroprotection on focal cerebral ischemia/reperfusion injury in mice. *PLoS ONE* 7:e33584. doi: 10.1371/journal.pone.0033584 doi: 10.1371/journal.pone.0033584

Zhang, B., Li, F., Zhao, W., Li, J., Li, Q., and Wang, W. (2015). Protective effects of allicin against ischemic stroke in a rat model of middle cerebral artery occlusion. *Mol. Med. Rep.* 12, 3734–3738. doi: 10.3892/mmr.2015.3883

Zhang, H., Ray, A., Miller, N. M., Hartwig, D., Pritchard, K. A., and Dittel, B. N. (2016). Inhibition of myeloperoxidase at the peak of experimental autoimmune encephalomyelitis restores blood-brain barrier integrity and ameliorates disease severity. *J. Neurochem.* 136, 826–836. doi: 10.1111/jnc.13426

Zhang, Y., Talalay, P., Cho, C. G., and Posner, G. H. (1992). A major inducer of anticarcinogenic protective enzymes from broccoli: isolation and elucidation of structure. *Proc. Natl. Acad. Sci. U.S.A.* 89, 2399–2403. doi: 10.1073/pnas.89.6.2399

Zhao, J. J., Song, J. Q., Pan, S. Y., and Wang, K. (2016). Treatment with isorhamnetin protects the brain against ischemic injury in mice. *Neurochem. Res.* 41, 1939–1948. doi: 10.1007/s11064-016-1904-2

Zhao, S., Park, C. H., Li, X., Kim, Y. B., Yang, J., Sung, G. B., et al. (2015). Accumulation of rutin and betulinic acid and expression of phenylpropanoid and triterpenoid biosynthetic genes in mulberry (*Morus alba* L.). *J. Agric. Food Chem.* 63, 8622–8630. doi: 10.1021/acs.jafc.5b03221

Zhou, F., Wang, M., Ju, J., Wang, Y., Liu, Z., Zhao, X., et al. (2019). Schizandrin A protects against cerebral ischemia-reperfusion injury by suppressing inflammation and oxidative stress and regulating the AMPK/Nrf2 pathway regulation. *Am. J. Transl. Res.* 11, 199–209.

Zhou, X., Yang, J., Zhou, M., Zhang, Y., Liu, Y., Hou, P., et al. (2019). Resveratrol attenuates endothelial oxidative injury by inducing autophagy via the activation of transcription factor EB. *Nutr. Metab. (Lond.)* 16, 42. doi: 10.1186/s12986-019-0371-6

Zhou, Y. F., Li, W. T., Han, H. C., Gao, D. K., He, X. S., Li, L., et al. (2014). Allicin protects rat cortical neurons against mechanical trauma injury by regulating nitric oxide synthase pathways. *Brain Res. Bull.* 100, 14–21. doi: 10.1016/j.brainresbull.2013.10.013

Conflict of Interest: The authors declare that the research was conducted in the absence of any commercial or financial relationships that could be construed as a potential conflict of interest.

Copyright © 2020 Chen, Chen, Du and Shen. This is an open-access article distributed under the terms of the Creative Commons Attribution License (CC BY). The use, distribution or reproduction in other forums is permitted, provided the original author(s) and the copyright owner(s) are credited and that the original publication in this journal is cited, in accordance with accepted academic practice. No use, distribution or reproduction is permitted which does not comply with these terms.

frontiers in Pharmacology

ORIGINAL RESEARCH
published: 18 June 2020
doi: 10.3389/fphar.2020.00887

Clinical and Economic Evaluation of Salvianolate Injection for Coronary Heart Disease: A Retrospective Study Based on National Health Insurance Data in China

Lisong Yang[1†], Xiaolan Chen[2,3†], Carolina Oi Lam Ung[1], He Zhu[2], Hao Hu[1] and Sheng Han[2*]*

[1] State Key Laboratory of Quality Research in Chinese Medicine, Institute of Chinese Medical Sciences, University of Macau, Macau, Macau, [2] International Research Center for Medicinal Administration, Peking University, Beijing, China, [3] School of Physics and Telecommunication Engineering, South China Normal University, Guangzhou, China

OPEN ACCESS

Edited by:
Jing-Yan Han,
Peking University, China

Reviewed by:
Yi Wang,
Zhejiang University, China
Liming Lu,
Guangzhou University of Chinese Medicine, China

****Correspondence:***
Hao Hu
haohu@um.edu.mo
Sheng Han
hansheng@bjmu.edu.cn

[†]These authors share first authorship

Specialty section:
This article was submitted to Ethnopharmacology, a section of the journal Frontiers in Pharmacology

Received: *20 December 2019*
Accepted: *29 May 2020*
Published: *18 June 2020*

Citation:
Yang L, Chen X, Oi Lam Ung C, Zhu H, Hu H and Han S (2020) Clinical and Economic Evaluation of Salvianolate Injection for Coronary Heart Disease: A Retrospective Study Based on National Health Insurance Data in China. Front. Pharmacol. 11:887. doi: 10.3389/fphar.2020.00887

Objective: The study aimed to conduct clinical and economic evaluation of salvianolate injection for patients with coronary heart disease (CHD) in comparison to Danhong injection and alprostadil injection.

Method: This was a retrospective study using National Health Insurance Data about inpatients diagnosed with CHD in China in 2015 who met the inclusion criteria. The recruited patients were divided into two samples: surgery and non-surgery. The exposed group received salvianolate injection, while the control group received either alprostadil injection or Danhong injection. The medical cost per hospitalization, hospitalization duration, and the rehospitalization rates were used as outcome indicators. Heterogeneity was processed according to disease stratification. Propensity score matching and multivariate analysis were used for statistical analysis to control potential confounding factors.

Results: The hospitalization duration of salvianolate injection group was significantly ($P < 0.05$) shorter than that of Danhong injection group in the non-surgery sample. The hospitalization duration of salvianolate injection group was significantly ($P < 0.05$) shorter than those of alprostadil injection group in both surgery and non-surgery samples. In the non-surgery sample, the medical cost per hospitalization of salvianolate injection group was significantly ($P < 0.05$) lower than that of alprostadil injection group. However, there were no statistical differences of rehospitalization rates in salvianolate injection group versus alprostadil injection group or salvianolate injection group versus Danhong injection group in both surgery and non-surgery samples.

Conclusion: Salvianolate injection showed advantages in reducing hospitalization duration for inpatients with CHD when comparing with alprostadil injection and Danhong injection. The results of this real-world study can help to inform clinical practice for CHD patients.

Keywords: salviaolate injection, coronary heart disease, clinical evaluation, economic evaluation, Danhong injection, alprostadil injection

INTRODUCTION

Coronary atherosclerotic heart disease is a heart disease caused by myocardial ischemia, hypoxia, or necrosis. Its underlying cause is that coronary atherosclerosis causes stenosis, spasm, or obstruction of the coronary lumen. They are collectively referred as coronary heart disease (CHD) or coronary artery disease, called CHD for short (Chen, 2013). In recent years, the morbidity and prevalence rate of coronary disease in China has been increasing significantly, especially the young people's death of coronary disease gets more and more attention (Wan et al., 2012; Xu et al., 2018). According to the research data of the Lancet in 2013, the death rate of CHD in China increased by 31.6% from 1990 to 2010, and CHD rose from the seventh place to the second place in the list of causes of premature death in China (Yang et al., 2013). CHD can affect the quality of life of patients severely, for example, the incidence of sudden death in people with a record of CHD attack is 4 or 6 times higher than that in the general population (Klootwijk and Hamm, 1999). With the trend of patients being young, the possibility of disability in patients with CHD is also significantly increased. At the same time, all kinds of medical costs of CHD are enormous because of a long course, a low cure rate, and a high recurrence rate. In China, the average cost of interventional therapy for CHD is about 40,000 to 60,000 CNY per time, and the cost of coronary artery bypass grafting is about 40,000 to 100,000 CNY (Liu, 2008).

Salvia miltiorrhiza and its compound preparations have the effect of improving blood flow, activating blood circulation to dissipate blood stasis (Zhou et al., 2005; Wang and Xuan, 2008). Known as Danshen, they have been used in China for a long history with a wide variety and a large amount of consumption. They are extensively used in the treatment of cardiovascular diseases, such as CHD, angina pectoris, hyperlipidemia, and acute ischemic stroke (Walden and Tomlinson, 2011). In Japan, the United States, and some European countries, products of Salvia miltiorrhiza also can be obtained.

Traditional Chinese medicine injections (TCMIs) are produced from herbals using modern techniques and have been widely used in the clinic in China (China PC, 2015). Salvianolate injection is one of the most extensive prescription drugs used in the treatment of cardiovascular disease since it was launched in 2005 in China. Some TCMIs may contain multiple unknown compounds, but the components of salvianolate injection were clarified, which may lead to less severe anaphylaxis. Some clinical trials and systematic evaluations have confirmed that salvianolate injection can substantially improve the clinical symptoms of patients with CHD (Sun, 2014; Liu et al., 2016; Li, 2016), and can reduce the angina attacks with functional safety, low incidence of adverse drug reactions (Li and Huang, 2016; Feng et al., 2016; He et al., 2016; Zhang et al., 2016), which shows that salvianolate injection is well tolerated in the general population (Yan et al., 2017).

However, there are few clinical and economic evaluations of salvianolate injection in real-world practice. Some retrospective studies had compared salvianolate injection with other salvia miltiorrhiza injections (Li and Yin, 2010; Yu and Yan, 2012; Shi et al., 2014). Nevertheless, in clinical practice, doctors tend to choose drugs on consideration of patients' actual conditions. Therefore, to evaluate the clinical and economic effects of specific Chinese medicine products must consider realistic comparator drugs (Tian and Xie, 2010). In current literature, the evaluation of curative effect and economic benefit of the salvianolate injection with the comparison of other Chinese medicine products and chemical drugs for CHD patients in the real clinical environment is still lacking (Dong et al., 2018).

In current clinic practice, Danhong injection is a useful clinical medication for CHD and angina. It has a good curative effect with little adverse reaction (Zheng and Luo, 2013; Sun and Xie, 2014; Li et al., 2018). Besides, alprostadil injection can significantly improve myocardial microcirculatory disturbance and hemorheological disorder in patients with CHD, which is also used for CHD in the current clinic (Huang et al., 2017). However, in the literature, there are few comparative economic and clinical evaluation of Chinese patent medicine and chemical medicine in the treatment of CHD.

Therefore, this study aimed to conduct clinical and economic evaluation of salvianolate injection for patients with CHD in comparison to Danhong injection and alprostadil injection. It is expected that the findings can provide evidence for clinical treatment for CHD.

METHODS

Composition Information

On 25th May 2015, salvianolate injection was approved by the State Food and Drug Administration (SFDA) of China as a new drug (Batch Number: Z20050247-49). First authorized on 4th June 2007 to the Shanghai Green Valley Pharmaceutical Co, Ltd to manufacture, salvianolate injection was renewed on 15th July 2016 by SFDA.

Botanical

The species was named as Salvia miltiorrhiza Bunge (Family: Lamiaceae Martinov, Genus: Salvia L.), which is accepted by the Kew Medicinal plant names service, and its native range is Central & S. China to Vietnam (Kew, 2020). First published in Enum. Pl. China Bor.: 50 (1833), Salvia miltiorrhiza Bunge (Bge.) was cited by a lot of medicinal references such as Pharmacopoeia of China (2015), British Pharmacopoeia 2015, Vol. 4 (2014), U.S. Pharmacopoeia USP 39 (2016), and U.S. FDA Substance Registration System (2016) (British Pharmacopoeia Commission, 2015; China PC, 2015; United States Pharmacopeial Convention, 2016; U.S. FDA, 2016).

Chemical

Salvianolate injection is a traditional Chinese medicine injection identified by the SFDA, containing major homologues such as salvianolic acid B (≥85%), rosemary acid (≥10.1%), and lithospermic acid (≥1.9%).

Since the early 1930s, China has begun to study the chemical composition of salvia miltiorrhiza. However, these early studies focused on lipophilic compounds (Zhou et al., 2005). With the support of the Chinese Academy of Sciences and the Ministry of Science and Technology of PRC, the Shanghai Institute of Materia Medica found that the water-soluble active ingredients of salvia miltiorrhiza existed in the form of salts. Through active screening and pharmacological studies, it was found that active compounds are mainly salvianolic acid B and homologs, such as rosemary acid, lithospermic acid, dansensu, salvianolic acid B, tanshinone IIA, and dimethyl lithospermate (Chan et al., 2004; Kang et al., 2004; Li et al., 2009), among which salvianolic acid B had the strongest pharmacological effect. It was also clarified that salvianolic acid B was the most important active ingredients of salvia miltiorrhiza in the treatment of cardiovascular diseases. A method for extracting and purifying chemical constituents from salvia miltiorrhiza by ethanol extraction method was well established, related technologies have been approved as Chinese patents and United States patents.

Target Population and Data Source

The target population of this study is CHD patients who were followed up from the first inpatient treatment in 2015 to December 31, 2015. The data was collected from the National Urban Basic Medical Insurance Database at the China Medical Insurance Research Association. China Medical Insurance Research Association is a national, semi-official organization that is directly managed by the National Healthcare Security Administration of China. With the official support of the National Healthcare Security Administration of China, China Medical Insurance Research Association establishes and maintains the National Urban Basic Medical Insurance Database that regularly and systematically collects the reimbursement data of social insurance from all the provincial governments in China (China Medical Insurance Research Association). Therefore, the National Urban Basic Medical Insurance Database at the China Medical Insurance Research Association is one of the most reliable databases for retrospective study in China.

The specific inclusion criteria of the patients are:

1. Patient who diagnosed with CHD for the first time before September 30, 2015;
2. CHD was the principal diagnosis (identification terms: angina pectoris, CHD, coronary artery, atherosclerosis, cardiac or myocardial infarction, ICD-10 code: I20-I25) when discharged from inpatient department and frequency of visits occurred before September 30, 2015.

The specific exclusion criteria of the patients are:

1. Patients who younger than or equal to 18 years old;
2. Patients with malignant tumors or schizophrenic patients or patients on dialysis.

Treatment and Grouping

All patients were divided into exposed group and control group. The exposed group was hospitalized with salvianolate injection, and the control group was treated with Danhong injection or alprostadil injection. The outcomes of salvianolate injection and Danhong injection, salvianolate injection, and alprostadil injection were compared.

- Salvianolate Injection Group
  The principal diagnosis during hospitalization was CHD and was prescribed salvianolate injection while alprostadil injection and other traditional Chinese medicine injections of blood-activating and stasis-dissolving are not prescribed.
- Danhong Injection Group
  The principal diagnosis during hospitalization was CHD and was prescribed Danhong injection while alprostadil injection and other traditional Chinese medicine injections of blood-activating and stasis-dissolving are not prescribed.
- Alprostadil Injection Group
  The principal diagnosis during hospitalization was CHD and was prescribed alprostadil injection while other traditional Chinese medicine injections of blood-activating and stasis-dissolving are not prescribed.

Study Perspective and Cost

This study chose a perspective of medical insurance payer. All the costs were only based on the reimbursement records of medical insurance. Compared with the medical record data at hospitals, the insurance claim data in China has few risk and cost parameters. Therefore, this study focused on the medical costs per hospitalization because this data is most reliable data to reflect the economic effectiveness of treatments.

Outcomes

The outcome indicators of this study include medical cost per hospitalization, hospitalization duration, 10d re-hospitalization rate, 30d re-hospitalization rate, and 90d re-hospitalization rate. Their definitions are listed below:

- 10d Rehospitalization Rate: refers to the proportion of inpatients with CHD who re-hospitalized within 10 days of the total number of hospitalized patients in this group after the first hospitalization. (If there are more than one readmission for CHD, counted as rehospitalization)
- 30d Rehospitalization Rate: refers to the proportion of inpatients with CHD who re-hospitalized within 30 days of the total number of hospitalized patients in this group after the first hospitalization. (If there are more than one readmission for CHD, counted as rehospitalization)
- 90d Rehospitalization Rate: refers to the proportion of inpatients with CHD who re-hospitalized within 90 days of the total number of hospitalized patients in this group after the first hospitalization. (If there are more than one readmission for CHD, counted as rehospitalization)

Bias and Elimination

The primary bias of this study was the selection bias. Thus, the Propensity Score Matching (PSM) method was used to control the confounding factors and reduce the impact of confounding factors on the intervention effect estimation.

In this study, the surgery sample was covariate based on age, gender, region, level of medical institution, whether combined with stroke, whether nitrate esters are prescribed (ATC code: XC01DA), whether nitrate esters are prescribed (ATC code: XB01AD), whether percutaneous coronary intervention (PCI) or coronary artery bypass grafting (CABG) was used. The matching ratio is 1:1, and the caliper value is 0.05. Furthermore, the non-surgery sample was covariate based on age, gender, region, level of medical institution, whether combined with stroke, whether nitrate esters are prescribed (ATC code: XC01DA), whether nitrate esters are prescribed (ATC code: XB01AD). The matching ratio is 1:1, and the caliper value is 0.05.

Heterogeneity

In order to avoid or reduce the impact of disease severity on the results, stratified analysis was adopted in this study to divide the population of CHD patients into surgery sample and non-surgery sample according to whether they had received surgery during hospitalization, and the difference of outcome indicators between the exposure group and the two control groups was analyzed in each sample.

Statistical Analysis

Descriptive analysis: measurement data are described by mean ± standard deviation (x ± s) or median and quartile, and enumeration data are described by frequency and rate.

Single factor analysis: For measurement data, the indicators of exposure group and control group were compared, T-test was used to compare the indicators between the exposed group and the control group which obeyed the normal distribution, Wilcoxon rank sum test was used to compare the two groups of indicators that did not obey the normal distribution. For enumeration data, Chi-square test was used. For all the above, $P < 0.05$ was considered statistically significant.

Multiple-factor analysis: Multivariate linear regression model was used for the dependent variable of hospitalization cost per hospitalization and hospitalization duration. If the dependent variable did not obey normal distribution, then run a natural logarithmic transformation. If the variance was not homogeneous, then do robust regression adjustment.

RESULTS

In this study, 2,473 patients with CHD who met the inclusion and exclusion criteria were included, including 541 patients in the surgery sample and 1,932 patients in the non-surgery sample. The flowchart of sampling and grouping are summarized in **Figure 1**.

Baseline Characteristics of the Total Sample

The difference between the surgery sample and the non-surgery sample is statistically significant in the following variables: age, gender, level of medical institutions, regional distribution, whether comorbid with high blood pressure or heart failure or diabetes, whether combine medication with beta blockers or nitrate esters or angiotensin converting enzyme inhibitors (ACEI) or angiotensin receptor blockers (ARB) or antiplatelet/thrombolytic/anticoagulant or lipid-regulating drugs.

Among them, the age of the non-surgery sample is slightly higher than that of the surgery sample. There are more males in the surgery sample than in the non-surgery sample. The surgery

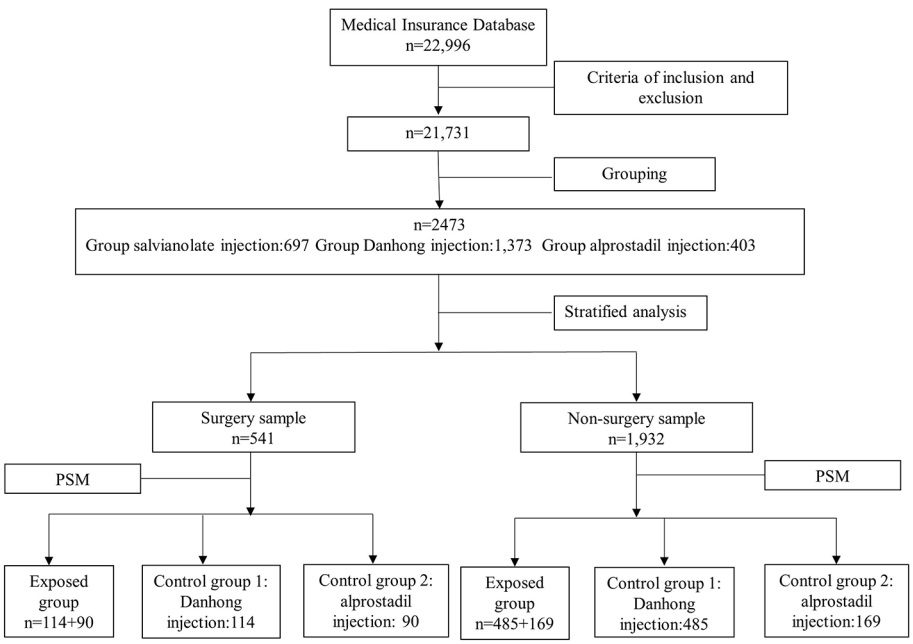


FIGURE 1 | Flowchart of sampling and grouping. The unit in the figure is per person.

sample mainly distributes in tertiary hospitals and eastern region, while the non-surgery sample mainly distributes in secondary and grass-roots hospitals and central and western region. The proportion of patients with high blood pressure, heart failure, and diabetes in the surgery sample was higher than that in the non-surgery sample, and the proportion of patients with drugs combined in the surgery sample was higher than that in the non-surgery sample except for calcium channel blockers. Among the hospitalized patients with CHD, 170 patients had undergone CHD related surgery (PCI/CABG), accounting for 6.9% (as shown in **Table 1**).

Surgery Sample: Salvianolate Injection and Danhong Injection

Baseline Characterization

After stratified analysis and PSM, 114 pairs of matched patients were obtained. In the surgery sample, the salvianolate injection group and the Danhong injection group were all 114 patients. There were statistically significant differences in the distribution of beta blockers and ACEI or ARB drugs between the two groups. The differences between the two groups were not statistically significant in the following variables: age, gender, level of medical institutions, regional distribution, whether comorbid with other diseases, whether combine medication with other drugs and whether had undergone CHD related surgery (as shown in **Table 2**).

Single-Factor Analysis of Outcome Indicators

In the surgery sample, between the salvianolate injection group and Danhong injection group, there were no significant differences in hospitalization duration, 10d rehospitalization rate, 30d rehospitalization rate, 90d rehospitalization rate, and the medical cost per hospitalization (as shown in **Table 3**).

Multi-Factor Analysis of Outcome Indicators

For multiple linear regression models to control potential confounding factors such as age, gender, medical institution level, and comorbidities, in the surgery sample, there was no significant difference between two groups in terms of hospitalization duration.

Surgery Sample: Salvianolate Injection and Alprostadil Injection

Baseline Characterization

After stratification analysis and PSM, 90 pairs of matched pairs were obtained. Among the surgery sample, 90 patients were in the salvianolate injection group and alprostadil injection group.

TABLE 1 | Overall baseline characteristics of hospitalized patients with CHD.

Variable	Total		Surgery sample		Non-surgery sample		Z/χ^2	*P*
	(N = 2473)		(N = 541)		(N = 1932)			
	N	%	N	%	N	%		
Age, P_{50} (P_{25}-P_{75})	68 (60–76)		67 (60–74)		68 (60–77)		2.39	0.0168
Gender							56.14	<0.001
Male	1225	49.5	345	63.8	880	45.6		
Female	1248	50.5	196	36.2	1052	54.5		
Level of medical institutions							206.46	<0.001
Tertiary hospital	1006	40.7	359	66.4	647	33.5		
Secondary hospital	1022	41.3	157	29.0	865	44.8		
Primary hospital	445	18.0	25	4.6	420	21.7		
Region							52.21	<0.001
Eastern region	1046	42.3	301	55.6	745	38.6		
Central region	1187	48.0	192	35.5	995	51.5		
Western region	240	9.7	48	8.9	192	9.9		
Comorbidity								
High blood pressure	700	28.3	205	37.9	495	25.6	31.36	<0.001
Heart failure	163	6.6	50	9.2	113	5.9	7.90	0.0050
Atrial fibrillation	50	2.0	7	1.3	43	2.2	1.85	0.1735
Heart valve disease	9	0.4	4	0.7	5	0.3	2.69	0.1009
Stroke	181	7.3	43	8.0	138	7.1	0.40	0.5250
Pulmonary embolism	6	0.2	0	0.0	6	0.3	1.68	0.1944
COPD	38	1.5	8	1.5	30	1.6	0.02	0.9015
chronic nephrosis	27	1.1	8	1.5	19	1.0	0.96	0.3271
Diabetes	643	26.0	215	39.7	428	22.2	67.95	0.0001
Drug combination								
Beta blockers	1182	47.8	342	63.2	840	43.5	65.99	0.0001
Nitrate esters	1932	78.1	506	93.5	1426	73.8	96.18	0.0001
ACEI or ARB	1141	46.1	307	56.8	834	43.2	31.36	0.0001
Calcium antagonist	922	37.3	199	36.8	723	37.4	0.07	0.7860
Antiplatelet/thrombolytic/anticoagulant	1428	57.7	476	88.0	952	49.3	259.55	0.0001
Lipid regulating agents	1817	73.5	473	87.4	1344	69.6	69.21	0.0001
Related surgery of CHD								
PCI/CABG	170	6.9	170	31.4				

TABLE 2 | Baseline characteristics of salvianolate injection group and Danhong injection group in the surgery sample.

Variable	Total (N = 228)		Salvianolate injection group (N = 114)		Danhong injection group (N = 114)		Z/χ^2	*P*
	N	%	N	%	N	%		
Age, P_{50} (P_{25}-P_{75})	65 (59–72)		65 (59–72)		65 (60–72)		–0.27	0.7870
Gender							1.97	0.1601
Male	152	66.7	81	71.1	71	62.3		
Female	76	33.3	33	29.0	43	37.7		
Level of medical Institutions							0.02	0.9895
Tertiary hospital	151	66.2	76	66.7	75	65.8		
Secondary hospital	69	30.3	34	29.8	35	30.7		
Primary hospital	8	3.5	4	3.5	4	3.5		
Region							0.24	0.8873
Eastern region	102	44.7	52	45.6	50	43.9		
Central region	106	46.5	53	46.5	53	46.5		
Western region	20	8.8	9	7.9	11	9.7		
Comorbidity								
High blood pressure	76	33.3	38	33.3	38	33.3	0.00	1.0000
Heart failure	20	8.8	9	7.9	11	9.7	0.22	0.6396
Atrial fibrillation	2	0.9	1	0.9	1	0.9	0.00	1.0000
Heart valve disease	1	0.4	1	0.9	0	0.0	1.00	0.3162
Stroke	14	6.1	6	5.3	8	7.0	0.30	0.5811
Pulmonary embolism	0	0.0	0	0.0	0	0.0		\
COPD	2	0.9	1	0.9	1	0.9	0.00	1.0000
Chronic nephrosis	2	0.9	2	1.8	0	0.0	2.02	0.1555
Diabetes	74	32.5	38	33.3	36	31.6	0.08	0.7773
Drug combination								
Beta blockers	141	61.8	63	55.3	78	68.4	4.18	0.0409
Nitrate esters	209	91.7	108	94.7	101	88.6	2.81	0.0935
ACEI or ARB	114	50.0	49	43.0	65	57.0	4.49	0.0341
Calcium antagonist	80	35.1	36	31.6	44	38.6	1.23	0.2669
Antiplatelet/thrombolytic/anticoagulant	202	88.6	103	90.4	99	86.8	0.69	0.4046
Lipid regulating agents	200	87.7	99	86.8	101	88.6	0.16	0.6865
Related surgery of CHD	69	30.3	37	32.5	32	28.1	0.52	0.4710

There was a statistically significant difference in the distribution of nitrate esters in the two groups. At the same time, there was no statistically significant difference in the distribution of age, gender, medical institution level, region, comorbidities, other drug combination, and whether or not CHD-related surgery was performed (as shown in **Table 4**).

Single-Factor Analysis of Outcome Indicators

In the surgery sample, average days per hospitalization in the salvianolate injection group was slightly lower than that in the alprostadil group, and the difference was statistically significant ($P < 0.05$). There was no significant difference in the 10d rehospitalization rate, 30d rehospitalization rate, 90d rehospitalization rate, and medical cost per hospitalization between the two groups (as shown in **Table 5**).

Multi-Factor Analysis of Outcome Indicators

Multiple linear regression models were applied to control potential confounding factors such as age, gender, medical institution level, and comorbidities. In the surgery sample, the average hospitalization days in the salvianolate injection group was 0.805 times as long as that in the alprostadil injection group, which means less than that in the alprostadil injection group, and the difference was statistically significant ($P = 0.023$).

TABLE 3 | Comparison of outcomes of salvianolate injection group and Danhong injection group in the surgery sample.

Variable	Total (N = 228)			Salvianolate injection group (N = 114)			Danhong injection group (N = 114)			Z/χ^2	*P*
	P_{50}	P_{25}	P_{75}	P_{50}	P_{25}	P_{75}	P_{50}	P_{25}	P_{75}		
Average days of per hospital stay	10	7	12	9	6	11	10	7	13	1.77	0.0766
10d rehospitalization rate, n (%)		3 (1.3)			0 (0.0)			3 (2.6)		3.04	0.0812
30d rehospitalization rate, n (%)		9 (4.0)			4 (3.5)			5 (4.4)		0.12	0.7338
90d rehospitalization rate, n (%)		20 (8.8)			13 (11.4)			7 (6.1)		1.97	0.1601
Medical costs per hospitalization	13170.3	8465.4	42342.5	12900.5	8208.5	42611.6	13578.2	8591.1	42073.4	0.41	0.6784

TABLE 4 | Baseline characteristics of the salvianolate injection group and the alprostadil injection group in the surgery sample.

Variable	Total (N = 180)		Salvianolate injection group (N = 90)		Alprostadil injection group (N = 90)		Z/χ^2	*P*
	N	%	N	%	N	%		
Age, P_{50} (P_{25}-P_{75})	66 (59–72)		64 (59–72)		68 (59–73)		0.59	0.5535
Gender							0.37	0.5428
Male	108	60.0	52	57.8	56	62.2		
Female	72	40.0	38	42.2	34	37.8		
Level of medical institutions							0.03	0.9852
Tertiary hospital	133	73.9	66	73.3	67	74.4		
Secondary hospital	45	25.0	23	25.6	22	24.4		
Primary hospital	2	1.1	1	1.1	1	1.1		
Region							2.67	0.2636
Eastern region	108	60.0	54	60.0	54	60.0		
Central region	54	30.0	30	33.3	24	26.7		
Western region	18	10.0	6	6.7	12	13.3		
Comorbidity							0.02	0.8793
High blood pressure	73	40.6	36	40.0	37	41.1		
Heart failure	21	11.7	10	11.1	11	12.2	0.05	0.8164
Atrial fibrillation	2	1.1	1	1.1	1	1.1	0.00	1.0000
Heart valve disease	1	0.6	0	0.0	1	1.1	1.01	0.3160
Stroke	16	8.9	8	8.9	8	8.9	0.00	1.0000
Pulmonary embolism	0	0.0	0	0.0	0	0.0		\
COPD	0	0.0	0	0.0	0	0.0		\
Chronic nephrosis	5	2.8	2	2.2	3	3.3	0.21	0.6501
Diabetes	72	40.0	36	40.0	36	40.0	0.00	1.0000
Drug combination								
Beta blockers	112	62.2	53	58.9	59	65.6	0.85	0.3563
Nitrate esters	174	96.7	84	93.3	90	100.0	6.21	0.0127
ACEI or ARB	96	53.3	45	50.0	51	56.7	0.80	0.3700
Calcium antagonist	64	35.6	27	30.0	37	41.1	2.42	0.1194
Antiplatelet/thrombolytic/anticoagulant	166	92.2	81	90.0	85	94.4	1.24	0.2656
Lipid regulating agents	160	88.9	82	91.1	78	86.7	0.90	0.3428
Related surgery of CHD	41	22.8	23	25.6	18	20.0	0.79	0.3742

Non-Surgery Sample: Salvianolate Injection and Danhong Injection

Baseline Characterization

After stratification analysis and PSM, 485 pairs of matched pairs were obtained. Among the surgery sample, 485 patients were in the salvianolate injection group and Danhong injection group. There was a statistically significant difference in the distribution of whether comorbid with pulmonary embolism in the two groups. At the same time, there was no statistically significant difference in the distribution of age, gender, medical institution level, region, other comorbidities, drug combination (as shown in **Table 6**).

Single-Factor Analysis of Outcome Indicators

In the non-surgical group, the average hospitalization duration in the salvianolate injection group was 9.2 ± 4.5 d, lower than that in the Danhong injection group (9.8 ± 4.8 d), and the difference was statistically significant ($P < 0.05$) (as shown in **Table 7**).

Multi-Factor Analysis of Outcome Indicators

Multiple linear regression models were used to control potential confounding factors such as age, gender, medical institution level, and comorbidities. There was no statistical difference ($P = 0.199$) in the days of hospitalization between the salvianolate group and the Danhong injection group in the non-surgery sample.

TABLE 5 | Comparison of outcomes between the salvianolate injection group and the alprostadil injection group in the surgery sample.

Variable	Total (N = 180)			Salvianolate injection group (N = 90)			Alprostadil injection group (N = 90)			Z/χ^2	*P*
	P_{50}	P_{25}	P_{75}	P_{50}	P_{25}	P_{75}	P_{50}	P_{25}	P_{75}		
Average days of per hospital stay	9	7	13	9	6	11	10	7	14	2.07	0.0389
10d rehospitalization rate, n (%)		0 (0.0)			0 (0.0)			0 (0.0)		\	
30d rehospitalization rate, n (%)		5 (2.8)			3 (3.3)			2 (2.2)		0.21	0.6501
90d rehospitalization rate, n (%)		19 (10.6)			10 (11.1)			9 (10.0)		0.06	0.8083
Medical cost per hospitalization	13542.4	8570.3	39148.7	12348.1	8047.8	45162.2	14167.3	10071.7	35914.0	0.89	0.3744

Non-Surgery Sample: Salvianolate Injection and Alprostadil Injection

Baseline Characterization

After stratification analysis and PSM, 169 pairs of matched pairs were obtained. Among the surgery sample, 169 patients were in the salvianolate injection group and alprostadil injection group. There was a statistically significant difference in the distribution of region, whether combined drugs with nitrate esters or antiplatelet/thrombolytic/anticoagulation, ACEI or ARB or calcium channel blockers between the two groups. At the same time, there was no statistically significant difference in the distribution of age, gender, medical institution level, region, comorbidities, other combined drugs that did not mentioned above (as shown in **Table 8**).

Single-Factor Analysis of Outcome Indicators

In the non-surgery sample, medical cost per hospitalization in the salvianolate injection group was lower than that in the alprostadil group. Moreover, the days of hospitalization at a time in the salvianolate injection group was slightly lower than

TABLE 6 | Baseline characteristics of the salvianolate injection group and Danhong injection group in the non-surgery sample.

Variable	Total		Salvianolate injection group		Danhong injection group		Z/χ^2	*P*
	(N = 970)		(N = 485)		(N = 485)			
	N	%	N	%	N	%		
Age, P_{50} (P_{25}-P_{75})	67 (59–76)		68 (60–76)		67 (59–76)		–0.96	0.3393
Gender							0.50	0.4783
Male	443	45.7	216	44.5	227	46.8		
Female	527	54.3	269	55.5	258	53.2		
Level of medical institutions							0.04	0.9800
Tertiary hospital	435	44.9	219	45.2	216	44.5		
Secondary hospital	440	45.4	219	45.2	221	45.6		
Primary hospital	95	9.8	47	9.7	48	9.9		
Region							2.47	0.2903
Eastern region	374	38.6	176	36.3	198	40.8		
Central region	516	53.2	265	54.6	251	51.8		
Western region	80	8.3	44	9.1	36	7.4		
Comorbidity								
High blood pressure	224	23.1	120	24.7	104	21.4	1.49	0.2228
Heart failure	56	5.8	33	6.8	23	4.7	1.90	0.1686
Atrial fibrillation	22	2.3	9	1.9	13	2.7	0.74	0.3883
Heart valve disease	1	0.1	0	0.0	1	0.2	1.00	0.3171
Stroke	50	5.2	29	6.0	21	4.3	1.35	0.2454
Pulmonary embolism	4	0.4	0	0.0	4	0.8	4.02	0.0451
COPD	7	0.7	2	0.4	5	1.0	1.30	0.2551
Chronic nephrosis	12	1.2	7	1.4	5	1.0	0.34	0.5613
Diabetes	200	20.6	100	20.6	100	20.6	0.00	1.0000
Drug combination								
Beta blockers	437	45.1	215	44.3	222	45.8	0.20	0.6515
Nitrate esters	696	71.8	336	69.3	360	74.2	2.93	0.0870
ACEI or ARB	434	44.7	219	45.2	215	44.3	0.07	0.7962
Calcium antagonist	347	35.8	185	38.1	162	33.4	2.37	0.1234
Antiplatelet/thrombolytic/anticoagulant	473	48.8	229	47.2	244	50.3	0.93	0.3353
Lipid regulating agents	725	74.7	373	76.9	352	72.6	2.41	0.1207

TABLE 7 | Comparison of the outcomes of the salvianolate injection group and the Danhong injection group in the non-surgery sample.

Variable	Total			Salvianolate injection group			Danhong injection group			Z/χ^2	*P*
	(N = 970)			(N = 485)			(N = 485)				
	P_{50}	P_{25}	P_{75}	P_{50}	P_{25}	P_{75}	P_{50}	P_{25}	P_{75}		
Average days of per hospital stay	9	7	12	9	7	11	9	7	12	2.12	0.0340
10d rehospitalization rate, n (%)		10 (1.0)			6 (1.2)			4 (0.8)		0.40	0.5249
30d rehospitalization rate, n (%)		22 (2.3)			13 (2.7)			9 (1.9)		0.74	0.3883
90d rehospitalization rate, n (%)		74 (7.6)			32 (6.6)			42 (8.7)		1.46	0.2265
Medical costs per hospitalization	6113.4	4514.9	9104.3	6056.7	4805.2	9038.0	6160.8	4119.0	9184.8	–1.75	0.0794

that in the alprostadil group, and the difference was statistically significant ($P < 0.05$) (as shown in **Table 9**).

Multi-Factor Analysis of Outcome Indicators

Multiple linear regression models were used to control potential confounding factors such as age, gender, medical institution level, and comorbidities. In the non-surgery sample, the days of per hospitalization of salvianolate injection group were 0.827 times that of the alprostadil group, which was lower than that of the alprostadil group, and the difference was statistically significant ($P = 0.011$). And in the non-surgery sample, the average hospitalization cost of the salvianolate injection group was 0.810 times that of the alprostadil group, which was lower than the alprostadil group, and the difference was statistically significant.

DISCUSSION

This study focused on the clinical and economic evaluation of salvianolate injection, comparing with alprostadil injection and Danhong injection, which are commonly used in the treatment of CHD (Li and Tang, 2006; Li and Wang, 2009). In this study,

TABLE 8 | Baseline characteristics of salvianolate injection group and alprostadil injection group in the non-surgery sample.

Variable	Total (N = 338)		Salvianolate injection group (N = 169)		Alprostadil injection group (N = 169)		Z/χ^2	P
	N	%	N	%	N	%		
Age, P_{50} (P_{25}-P_{75})	69 (62–78)		70 (61–79)		69 (63–78)		–0.38	0.7045
Gender							2.68	0.1019
Male	157	46.5	71	42.0	86	50.9		
Female	181	53.6	98	58.0	83	49.1		
Level of medical institutions							3.18	0.2043
Tertiary hospital	212	62.7	113	66.9	99	58.6		
Secondary hospital	104	30.8	48	28.4	56	33.1		
Primary hospital	22	6.5	8	4.7	14	8.3		
Region							9.68	0.0079
Eastern region	204	60.4	104	61.5	100	59.2		
Central region	115	34.0	62	36.7	53	31.4		
Western region	19	5.6	3	1.8	16	9.5		
Comorbidity								
High blood pressure	113	33.4	51	30.2	62	36.7	1.61	0.2047
Heart failure	31	9.2	19	11.2	12	7.1	1.74	0.1871
Atrial fibrillation	12	3.6	5	3.0	7	4.1	0.35	0.5566
Heart valve disease	1	0.3	0	0.0	1	0.6	1.00	0.3166
Stroke	18	5.3	8	4.7	10	5.9	0.23	0.6280
Pulmonary embolism		0.0		0.0		0.0		
COPD	3	0.9	0	0.0	3	1.8	3.03	0.0819
Chronic nephrosis	3	0.9	1	0.6	2	1.2	0.34	0.5620
Diabetes	100	29.6	43	25.4	57	33.7	2.78	0.0952
Drug combination								
Beta blockers	178	52.7	87	51.5	91	53.9	0.19	0.6630
Nitrate esters	282	83.4	113	66.9	169	100.0	67.12	<0.0001
ACEI or ARB	178	52.7	80	47.3	98	58.0	3.85	0.0499
Calcium antagonist	154	45.6	68	40.2	86	50.9	3.86	0.0493
Antiplatelet/thrombolytic/anticoagulant	210	62.1	91	53.9	119	70.4	9.86	0.0017
Lipid regulating agents	269	79.6	136	80.5	133	78.7	0.16	0.6856

TABLE 9 | Comparison of outcomes between the salvianolate injection group and the alprostadil injection group in the non-surgery sample.

Variable	Total (N = 338)			Salvianolate injection group (N = 169)			Alprostadil injection group (N = 169)			Z/χ^2	P
	P_{50}	P_{25}	P_{75}	P_{50}	P_{25}	P_{75}	P_{50}	P_{25}	P_{75}		
Average days of per hospital stay	10	7	14	9	7	12	10	8	14	2.48	0.0130
10d rehospitalization rate, n (%)		5 (1.5)			4 (2.4)			1 (0.6)		1.83	0.1765
30d rehospitalization rate, n (%)		9 (2.7)			6 (3.6)			3 (1.8)		1.03	0.3108
90d rehospitalization rate, n (%)		27 (8.0)			13 (7.7)			14 (8.3)		0.04	0.8410
Medical costs per hospitalization	8472.3	5629.2	11734.7	7718.7	5425.5	10616.4	9462.4	6037.9	12762.7	2.84	0.0045

we compared the two drugs with salvianolate injection through clinical and economic evaluation outcome indicators such as medical cost of hospitalization, days of hospital stay, and rehospitalization rate (Miao et al., 2006), to evaluate the drug economy and effectiveness of salvianolate injection in the real world. Because the data were not from controlled clinical trials, but from the real-world data, it can provide evidence for the effectiveness and economic effects (Yu and Yan, 2012). As real-world data can provide instructive information for clinical practice (Makady et al., 2017), the results of this study can provide a certain reference for the clinical practice of CHD.

However, real-world data also has certain defects and is prone to selection bias (Dimick and Livingston, 2010). Therefore, stratified analysis and PSM were used to reduce the impact of confounding factors on intervention effect estimation. The baseline situation between the study groups was more balanced and comparable than before (Pourhoseingholi et al., 2012). After PSM, stratified analysis, and multi-factor analysis, this study generated some significant findings that are worth further discussion as below.

Regarding hospitalization duration, it found that the hospitalization duration of salvianolate injection group was significantly shorter than that of Danhong injection group in the non-surgery sample. The hospitalization duration of salvianolate injection group was significantly shorter than those of alprostadil injection group in both surgery and non-surgery samples. Past research found that salvianolate injection was most frequently combined with clopidogrel and isosorbide dinitrate, and such combination showed higher clinical effectiveness as compared with other drug combinations (Chang et al., 2013). In particular, compared with conventional treatment for the treatment of CHD, the combination of salvianolate injection and conventional treatment was associated with a reduction in hospital stay (Dong et al., 2018). All of these findings show that clinical application of salvianolate injection has comparative advantages in reducing hospitalization stay of CHD patients.

Regarding medical cost per hospitalization, this study just found that the medical cost per hospitalization of salvianolate injection group was significantly ($P < 0.05$) lower than that of alprostadil injection group in the non-surgery sample. As for CHD patients, surgery often accounts for most of the medical cost of hospitalization. Therefore, application of salvianolate injection can only show its economic advantages for CHD inpatients in non-surgery group when compared with alprostadil injection.

For rehospitalization rates, it found no significantly statistical differences in salvianolate injection group vs. alprostadil injection group or salvianolate injection group vs. Danhong injection group in both surgery and non-surgery samples. It has been indicated that the risk factors for rehabilitation of CHD patients can be much related to body composition (Chen et al., 2017). Such kind of results implies that drug therapies for CHD treatment needs more patient-centered exploration.

This study has several strengths. Firstly, this study was based on real-world data. By using real-world data, the clinical and economic evaluation of salvianolate injection for CHD was conducted, which can better show the actual clinical practice. Secondly, the data of this study was collected from the National Urban Basic Medical Insurance Database, which covered the whole nation, so the findings have more generalizing significance for CHD treatment. Thirdly, Peng et al. mentioned in their previous study of cost-consequence analysis of salvianolate injection for the treatment of CHD that their study did not stratify the severity of CHD due to the limitation of the original medical record (Dong et al., 2018). Therefore, this study considered the severity of the patient's disease on the results. Subgroups were carried out to analyze the injection of salvianolate and the other two contrast drugs in the surgery sample and the non-surgery sample, respectively, to make the results more authentic and reliable.

However, at the same time, there were some limitations, which are worth improving in future research. Firstly, since this study was a retrospective study, and the baseline variables provided were limited, potential confounders were difficult to control. Although stratified analysis and PSM were used, the interference of confounders and the selective bias cannot be eliminated entirely. Secondly, although the data of this study came from the National Urban Basic Medical Insurance Database, the sample size that met the rigor enrollment and medication conditions was relatively small, which led to the failure of multi-factor analysis of part of the rehospitalization rate. Thirdly, the data source in this study is unable to provide sufficient economic and effectiveness indicators due to its data limitations, which may lead to some bias to some extent. The prospective design of cost-effectiveness analysis is suggested for future evaluation of salvianolate injection.

CONCLUSION

Salvianolate injection showed advantages in reducing hospitalization duration for inpatients with CHD when comparing with alprostadil injection and Danhong injection. The results of this real-world study can help to inform prescription practice for CHD patients. More prospective investigation can be employed in future studies on the effectiveness of salvianolate injection.

DATA AVAILABILITY STATEMENT

The raw data supporting the conclusions of this article will be made available by the authors, without undue reservation, to any qualified researcher.

ETHICS STATEMENT

The studies involving human participants were reviewed and approved by: The research was reviewed and approved by the Ethics Committee of Peking University (71603008). Written informed consent for participation was not required for this

study in accordance with the national legislation and the institutional requirements.

AUTHOR CONTRIBUTIONS

HH and SH designed the study. XC and HZ performed the statistical analysis. LY and XC wrote the first draft of the manuscript. SH and HZ gave conceptual advice. LY and HH revised the final draft. All authors contributed to the article and approved the submitted version.

ACKNOWLEDGMENTS

The authors gratefully acknowledge the support from the researchers of Peking University and the University of Macau.

REFERENCES

British Pharmacopoeia Commission. (2015). *British Pharmacopoeia 2015* Vol. 4 (London: The Stationery Office). Available at: http://www.pharmacopoeia.gov.uk/.

Chan, K., Chui, S. H., Wong, D. Y., Ha, W. Y., Chan, C. L., and Wong, R. N. (2004). Protective effects of danshensu from the aqueous extract of Salvia miltiorrhiza (Danshen) against homocysteine-induced endothelial dysfunction. *Life Sci.* 75, 3157–3171. doi: 10.1016/j.lfs.2004.06.010

Chang, Y. P., Zhang, H., Xie, Y. M., Zeng, X. B., Hu, J., and Zhuang, Y. (2013). Analysis of salvianolate injection combined with usual drugs in treatment of coronary heart disease in real world. *China J. Chin. Mater. Med.* 38 (18), 3186–3189. (in Chinese). doi: CNKI:SUN:ZGZY.0.2013-18-035

Chen, A., Horwich, T., and Nardoni, N. (2017). The effect of body composition on cardiovascular outcomes in cardiac rehabilitation patients with coronary heart disease. *J. Am. Coll. Cardiol.* 21; 69 (11 Supplement), 1846. doi: 10.1016/S0735-1097(17)35235-X

Chen, Y. (2013). Application of β-blockers in the treatment of coronary atherosclerotic heart disease. *Chin. J. Hypertension* 10, 922–925. (in Chinese). doi: CNKI:SUN:ZGGZ.0.2013-10-01

China Medical Insurance Research Association. http://www.chira.org.cn.

China PC (2015). *Pharmacopoeia of the People"s Republic of China, 2015 edition* (Beijing: China Medical Science and Technology Press), 292 p.

Dimick, J. B., and Livingston, E. H. (2010). Comparing treatments using observational study designs: what can we do about selection bias? *Arch. Surg.* 10, 927. doi: 10.1001/archsurg.2010.223

Dong, P., Hu, H., Guan, X., Ung, C. O., Shi, L., Han, S., et al. (2018). Cost-consequence analysis of salvianolate injection for the treatment of coronary heart disease. *Chin. Med.* 13 (1), 28. doi: 10.1186/s13020-018-0185-x

Feng, L., Zhou, Y., and Li, L. (2016). Comparison of efficacy and safety of salvianolate injection and salvia miltiorrhiza injection in the treatment of coronary heart disease. *J. Liaoning Univ. Tradit. Chin. Med.* 11, 183–185. (in Chinese). doi: 10.13194/j.issn.1673-842x.2016.11.057

He, X., Lvy, S., and Guo, Y. (2016). Clinical effect and safety of salvia miltiorrhiza polyphenols in treatment of coronary atherosclerotic heart disease. *Chin. J. Clin. Pharmacol.* 2, 105–107. (in Chinese). doi: 110.13699/j.cnki.1001-6821.2016.02.003

Huang, J., Wang, D., and Shi, H. (2017). Therapeutic effect of alprostadil on improving myocardial microcirculatory disturbance and hemorheology in patients with coronary heart disease. *Chin. J. Cardiovasc. Rehabil. Med.* 2, 199–202. doi: CNKI:SUN:JXUY.0.2015-29-144

Kang, D. G., Oh, H., Sohn, E. J., Hur, T. Y., Lee, K. C., Kim, K. J., et al. (2004). Lithospermic acid B isolated from Salvia miltiorrhiza ameliorates ischemia/reperfusion-induced renal injury in rats. *Life Sci.* 75 (15), 1801–1816. doi: 10.1016/j.lfs.2004.02.034

Kew, R. B. (2020). *Medicinal Plant Names Services*, Royal Botanic Gardens, Kew. Available at: https://mpns.science.kew.org/mpns-portal/plantDetail?plantId=183206&query=Salvia+miltiorrhiza+Bunge+&filter=&fuzzy=false&nameType=all&dbs=wcs.

Klootwijk, P., and Hamm, C. (1999). Acute coronary syndromes: diagnosis. *Lancet* 353: Suppl 2 (18), S10–S15. doi: 10.1016/S0140-6736(99)90235-0

Li, S., and Huang, S. (2016). Salvianolate in treatment of angina pectoris. *J. Changchun Univ. Chin. Med.* 4, 755–756. (in Chinese). doi: 10.13463/j.cnki.cczyy.2016.04.033

Li, Y., and Tang, J. (2006). Advances in pharmacological research of alprostadil. *J. Military Surgeon Southwest China* 6, 79–81. (in Chinese). doi: CNKI:SUN:JYXN.0.2006-06-050

Li, X., and Wang, Z. (2009). Advances in the efficacy and safety of alprostadil in the treatment of heart failure. *Chin. J. Misdiagn.* 9, 4553–4554. (in Chinese).

Li, X., and Yin, T. (2010). Clinic effect of salvianolate injection on patients with coronary heart diseases. *China J. Modern Med.* 4, 619–621. (in Chinese). doi: CNKI:SUN:ZXDY.0.2010-04-043

Li, Y. G., Song, L., Liu, M., and Wang, Z. T. (2009). Advancement in analysis of Salviae miltiorrhizae Radix et Rhizoma (Danshen). *J. Chromatogr. A* 1216 (11), 1941–1953. doi: 10.1016/j.chroma.2008.12.032

Li, H., Lin, X., and Liu, Q. (2018). Curative effect of Danhong injection on the clinical symptoms, adverse reactions and electrocardiogram of angina pectoris of coronary heart disease. *Int. J. Clin. Exp. Med.* 2, 910–915.

Li, F. (2016). Clinical observation of salvianolate injection combined with western medicine for patients with unstable angina pectoris. *J. New Chin. Med.* 10, 16–18. (in Chinese). doi: 10.13457/j.cnki.jncm.2016.10.007

Liu, Y., Yan, Y., and Zhai, S. (2016). Salvianolate for treatment of angina: An overview of systematic reviews. *Chin. J. Clin. Pharmacol.* 06, 560–562. (in Chinese). doi: 10.13699/j.cnki.1001-6821.2016.06.026

Liu, X. (2008). Progress in epidemiology of coronary heart disease and disease burden. *Chin. J. Cardiol.* 06, 573–576. (in Chinese). doi: 10.3321/j.issn:0253-3758.2008.06.026

Makady, A., ten Ham, R., and de Boer, A. (2017). Policies for use of real-world data in health technology assessment (HTA): a comparative study of six HTA agencies. *Value Health* 4, 520–532. doi: 10.1016/j.jval.2016.12.003

Miao, Y., Gao, Z., and Fengqin, X. U. (2006). Clinical observation on Salvianolate for the treatment of angina pectoris in coronary heart disease with heart-blood stagnation syndrome. *Tradit. Chin. Drug Res. Clin. Pharmacol.* 1, 2. (in Chinese).

Pourhoseingholi, M. A., Baghestani, A. R., and Vahedi, M. (2012). How to control confounding effects by statistical analysis. *Gastroenterol. Hepatol. Bed Bench* 2, 79.

Shi, Y., Yan, H., and Sun, S. (2014). Two kinds of radix salviae miltiorrhizae injection for angina pectoris: a systematic review and pharmacoeconomics analysis. *Chin. J. Evidence-Based Med.* 3, 287–291. (in Chinese). doi: 10.7507/1672-2531.20140050

Sun, W., and Xie, C. (2014). Clinical observation on Danhong injection in treating coronary heart disease angina pectoris. *Western J. Tradit. Chin. Med.* 3, 5–6. (in Chinese). doi: 10.3969/j.issn.1004-6852.2014.03.002

Sun, X. (2014). Salvia miltiorrhiza polyphenols acid salt and Danhong injection in treatment of elderly unstable angina pectoris. *J. Liaoning Univ. Tradit. Chin. Med.* 9, 182–183. (in Chinese). doi: 10.13194/j.issn.1673-842x.2014.09.063

Tian, F., and Xie, Y. (2010). Real-world study: a potential new approach to effectiveness evaluation of traditional Chinese medicine interventions. *J. Chin. Integr. Med.* 4, 301–306. (in Chinese). doi: 10.3736/jcim20100401

U.S. FDA (2016). *United States Food and Drug Administration Substance Registration System*, FDA's Global Substance Registration System. Available at: https://www.fda.gov/industry/fda-resources-data-standards/fdas-global-substance-registration-system.

United States Pharmacopeial Convention (2016). *The United States Pharmacopeia USP 39. The National Formulary NF 34* (Rockville: United States Pharmacopeial Convention). Available at: http://www.usp.org/about-usp.

Walden, R., and Tomlinson, B. (2011). "Cardiovascular Disease," in *Herbal medicine: biomolecular and clinical aspects*. Eds. I. F. Benzie, S. Wachtel-Galor, I. F. F. Benzie and S. Wachtel-Galor (Boca Raton (FL): CRC Press/Taylor & Francis), 375–405.

Wan, H., Li, Y., and Liu, J. (2012). The epidemiology of out-of-hospital deaths due to acute coronary events in young Beijing adults. *Chin. J. Internal Med.* 4, 274–278. (in Chinese). doi: 10.3760/cma.j.issn.0578-1426.2012.04.008

Wang, Y., and Xuan, L. (2008). Demonstration achievements of modernization of traditional Chinese medicine – research and development of salvianolate and salvianolate for injection. *Bull. Chin. Acad. Sci.* 5, 377–380. (in Chinese). doi: CNKI:SUN:KYYX.0.2005-05-008

Xu, F., Jiang, W., and Huang, L. (2018). Epidemiological study on pre-hospital death of acute coronary heart disease in residents aged 25~45 years in Wuhan city. *Pract. Prevent. Med.* 5, 592–593. (in Chinese). doi: CNKI:SUN:SYYY.0.2018-05-022

Yan, Y. Y., Yang, Y. H., Wang, W. W., Pan, Y. T., Zhan, S. Y., Sun, M. Y., et al. (2017). Post-Marketing Safety Surveillance of the Salvia Miltiorrhiza Depside Salt for Infusion: A Real World Study. *PloS One* 12 (1), e0170182. doi: 10.1371/journal.pone.0170182

Yang, G., Wang, Y., and Zeng, Y. (2013). Rapid health transition in China, 1990–2010: findings from the Global Burden of Disease Study 2010. *Lancet* 381, 1987–2015. doi: 10.1016/S0140-6736(13)61097-1

Yu, F., and Yan, S. (2012). Cost-effectiveness analysis of three traditional Chinese medicine injections for treating coronary heart disease and angina pectoris. *Tianjin Pharm.* 2, 53–4, 61. (in Chinese). doi: CNKI:SUN:TJYA.0.2012-02-024

Zhang, Y., Qin, Z., and Liu, J. (2016). Pharmacoeconomic study of 4 salvia miltiorrhiza preparations in the treatment of coronary heart disease and angina pectoris. *Chongqing Yi Xue* 8, 1081–1083. (in Chinese). doi: 10.3969/j.issn.1671-8348.2016.08.026

Zheng, H., and Luo, P. (2013). Clinical study of Danhong injection in treating angina pectoris of coronary heart disease. *Hebei Med.* 6, 936–938. (in Chinese). doi: CNKI:SUN:HCYX.0.2013-06-053

Zhou, L., Zuo, Z., and Chow, M. S. (2005). Danshen: an overview of its chemistry, pharmacology, pharmacokinetics, and clinical use. *J. Clin. Pharmacol.* 45, 1345–1359. doi: 10.1177/0091270005282630

Conflict of Interest: The authors declare that the research was conducted in the absence of any commercial or financial relationships that could be construed as a potential conflict of interest.

The handling editor declared a shared affiliation, though no other collaboration with several of the authors XC, HZ, SH, at the time of the review.

Copyright © 2020 Yang, Chen, Oi Lam Ung, Zhu, Hu and Han. This is an open-access article distributed under the terms of the Creative Commons Attribution License (CC BY). The use, distribution or reproduction in other forums is permitted, provided the original author(s) and the copyright owner(s) are credited and that the original publication in this journal is cited, in accordance with accepted academic practice. No use, distribution or reproduction is permitted which does not comply with these terms.

frontiers in Pharmacology

ORIGINAL RESEARCH
published: 14 July 2020
doi: 10.3389/fphar.2020.01045

Shexiang Baoxin Pill, a Traditional Chinese Herbal Formula, Rescues the Cognitive Impairments in APP/PS1 Transgenic Mice

Wei-Hui Hu[1,2,3†], Shing-Hung Mak[1,2†], Zhong-Yu Zheng[1,2], Ying-Jie Xia[1,2], Miranda Li Xu[1,2], Ran Duan[1,2,3], Tina Ting-Xia Dong[1,2,3], Shao-Ping Li[4], Chang-Sen Zhan[5,6], Xiao-Hui Shang[5,6] and Karl Wah-Keung Tsim[1,2,3]*

[1] Shenzhen Key Laboratory of Edible and Medicinal Bioresources, HKUST Shenzhen Research Institute, Shenzhen, China, [2] Division of Life Science and Center for Chinese Medicine and State Key Laboratory of Molecular Neuroscience, The Hong Kong University of Science and Technology, Hong Kong, Hong Kong, [3] Joint Laboratory of Guangdong Province and Hong Kong Region on Marine Bioresource Conservation and Exploitation, College of Marine Sciences, South China Agricultural University, Guangzhou, China, [4] Institute of Chinese Medical Sciences, University of Macau, Macau, Macau, [5] Shanghai Engineering Research Center for Innovation of Solid Preparation of TCM, Shanghai, China, [6] Shanghai Hutchison Pharmaceuticals Ltd., Shanghai, China

OPEN ACCESS

Edited by:
Qiaobing Huang,
Southern Medical University, China

Reviewed by:
Bing-Xing Pan,
Nanchang University, China
Wenda Xue,
Nanjing University of Chinese Medicine, China

***Correspondence:**
Karl Wah-Keung Tsim
botsim@ust.hk

[†]These authors have contributed equally to this work

Specialty section:
This article was submitted to Ethnopharmacology, a section of the journal Frontiers in Pharmacology

Received: *28 April 2020*
Accepted: *26 June 2020*
Published: *14 July 2020*

Citation:
Hu W-H, Mak S-H, Zheng Z-Y, Xia Y-J, Xu ML, Duan R, Dong TT-X, Li S-P, Zhan C-S, Shang X-H and Tsim KW-K (2020) Shexiang Baoxin Pill, a Traditional Chinese Herbal Formula, Rescues the Cognitive Impairments in APP/PS1 Transgenic Mice. Front. Pharmacol. 11:1045. doi: 10.3389/fphar.2020.01045

Background: Shexiang Baoxin Pill (SBP), a formulated traditional Chinese medicine (TCM), has been widely used to treat cardiovascular diseases for years. This herbal mixture has been shown to promote differentiation of cultured neuronal cells. Here, we aimed to investigate the effects of SBP in attenuating cognitive impairment in APP/PS1 transgenic mice.

Methods: Ethanol and water extracts of SBP, denoted as SBP_{EtOH} and SBP_{water}, were standardized and applied onto cultured rat pheochromocytoma PC12 cells. The potential effect of SBP_{EtOH} extract in attenuating the cognitive impairments in APP/PS1 transgenic mice was shown by following lines of evidence: (i) inhibition of Aβ fibril formation, (ii) suppression of secretions of cytokines, and (iii) improvement of behavioral tests by Morris water maze.

Results: SBP_{water} and SBP_{EtOH} inhibited the formation of β-amyloid fibrils and protected the Aβ-induced cytotoxicity in cultured PC12 cells. In APP/PS1 transgenic mice, the treatment of SBP_{EtOH} inhibited expressions of NO, NOS, AChE, as well as aggregation of Aβ. Besides, the levels of pro-inflammatory cytokines were suppressed by SBP treatment in the transgenic mice. Importantly, the behavioral tests by Morris Water maze indicated that SBP attenuated cognitive impairments in APP/PS1 transgenic mice.

Conclusion: The current result has supported the notion that SPB might ameliorate the cognitive impairment through multiple targets, suggesting that SBP could be considered as a promising anti-AD agent.

Keywords: Shexiang Baoxin Pill, Chinese medicine, acetylcholinesterase, neuroprotective, cognitive enhancing effect, Alzheimer's disease

INTRODUCTION

Alzheimer's disease (AD), characterized by dramatically declined of learning and memory, is the most common form of dementia affecting elderly population (Desgranges et al., 1998; Francis et al., 1999). The exact causes of AD remain unclear; however, the role of β-amyloid (Aβ) in the brain has been proposed to play key role in the pathological progress (Guidi et al., 2006). Fibrillar aggregate of Aβ is main constituent of plaques being found in AD patient's brain, and therefore which has been considered as one of important causative events during AD pathogenesis (Chen et al., 2000; Goldsworthy and Vallence, 2013; Hampel, 2013). Under this scenario, drugs having inhibitory effects on formation of Aβ fibrils and Aβ fibril-mediated neurotoxicity, therefore, may possess therapeutic values for AD.

Traditional Chinese medicine (TCM) has been extensively used for treatment of various diseases in Asian countries for thousand years. Having a long historical usage, TCM has been proved to be effective and safe, especially in treating chronic diseases associated with aging (Gao et al., 2008; Yang et al., 2011). **S**hexiang **B**aoxin **P**ill (SBP), a herbal formula deriving from TCM theory, has been widely used for treatment of cardiovascular problems for many years (Yan et al., 2006). There are seven medicinal constituents in SBP, i.e. Moschus, Bovis Calculus Artifactus, Ginseng Radix et Rhizoma, Styrax, Cinnamomi Cortex, Borneolum Syntheticum, and Bufonis Venenum. SBP is being recorded in 2015 edition of Chinese Pharmacopoeia. Being on the market for years, the efficacy of SBP is well recognized for its rapid and effective action in resolving cardiovascular problems (Lu et al., 2018). In addition, several lines of evidence have indicated that SBP is effective to treat stable angina pectoris and chest pain, as caused by coronary heart disease (Hong et al., 2006; Yan et al., 2006; He et al., 2009; Tian et al., 2011). Besides, the potential therapeutic effects of SBP in treating other diseases, including early hypertensive renal injury and mental depression have been proposed (Chen et al., 2008; Zhao et al., 2018).

In neuronal culture, the application of SBP was shown to promote differentiation as well as the expressions of those neuronal biomarkers, and this action was mediated by activating cAMP/PKA protein kinase A (PKA) and cAMP responsive element binding protein (CREB) signaling pathways (Xu et al., 2019). This *in vivo* study therefore suggested the possible application of SBP in treating neurological disorders. Here, we are aiming to further extend the anti-AD function of SBP by using mouse model. The APP/PS1 transgenic mouse, a commonly used mouse model for AD analysis, was treated with the intake of SBP, and the behavioral and biochemical changes in these mice were determined.

MATERIALS AND METHODS

Chemical and Medicinal Materials

A single batch of SBP and seven herbal materials or extracts were used here, i.e. Ginseng Radix et Rhizoma (supplied as the dried 75% ethanol extract of *Panax ginseng* root and rhizome, having more than 0.27% ginsenoside Re and ginsenoside Rg_1 and ginsenoside Rb_1 not less than 0.18% by weight, as defined by Chinese Pharmacopoeia; voucher #190603), Moschus (the dried secretion of musk sac of adult male *Moschus berezovskii*, *M. sifanicus*, or *M. moschiferus;* muscone is the main ingredient in Moschus; voucher #2017YR072), Cinnamomi Cortex (the dried stem bark of *Cinnamomum cassia*; voucher #180601), Bovis Calculus Artifactus (prepared with powder of cholic acid, cow bile, taurine, bilirubin, cholesterol, hyodeoxycholic acid, and trace elements; voucher #180511), Styrax (the acaroid resin obtained from the trunk of *Liquidambar orientalis* having over 5% cinnamic acid by weight, dissolved in ethanol; voucher #H2018050305). Borneolum Syntheticum (the synthetic crystal containing mainly borneol not less than 55% by weight, dissolved in ethanol; voucher #180602), and Bufonis Venenum (the dried secretion of *Bufo bufo* gargarizans or *Bufo melanostitus*; voucher #171102). The herbal materials, as well as SBP extracts, were provided by Shanghai Hutchison Pharmaceuticals Company (Shanghai, China). The batch number of SBP was 181006, and the preparation of SBP was performed following Chinese Pharmacopeia 2015. The same batches of SBP used for experiments were stored in Shanghai Hutchison Pharmaceuticals Ltd. The chemical composition of SBP was analyzed by HPLC previously (Xu et al., 2019; Yang et al., 2019). The herbal materials were authenticated morphologically and chemically with referring to Chinese Pharmacopeia 2015. The voucher species were stored at Center for Chinese Medicine at Hong Kong University of Science and Technology (voucher #181202). Dulbecco's modified Eagle's medium (DMEM) and fetal bovine serum (FBS) were from Invitrogen (Carlsbad, CA). Dimethyl sulfoxide (DMSO) and donepezil were from Sigma (St. Louis, MO). Purified synthetic $A\beta_{1-42}$ was from GL Biochem (Shanghai, China). The following antibodies Aβ, Bcl-2, Bax, and GAPDH were purchased from Abcam (Danvers, MA). The commercially available sandwich enzyme-linked immunosorbent assay (ELISA) kits of IL-6 and TNF-α were bought from cell signaling technology (Danvers, MA).

The preparation of water (SBP_{water}) or 95% ethanol (SBP_{EtOH}) extract of SBP was fully described previously (Xu et al., 2019). In brief, 20 g powders of SBP, Bovis Calculus Artifactus, Moschus, Bufonis Venenum, and Cinnamomi Cortex were sequentially sonicated twice in water or 95% ethanol at a proportion of 1:8 (w/v; 160 ml) and 1:6 (w/v; 120 ml) for 30 min each time at 37°C. Total extracts were combined. After dried under vacuum, they were stored at −80°C. The extract of SBP_{water} was dissolved in H_2O; while SBP_{EtOH} extract, extracts of Borneolum Syntheticum (synthetic having >55% bornel) and Ginseng Radix et Rhizoma were solubilized in dimethylsulfoxide (DMSO). Styrax solution was prepared with DMSO at a ratio of 1:100 (v:v). The extraction was in accord to preparative protocol of SBP (Chinese Pharmacopeia 2015). Stock solutions were at 100 mg/ml, stored at −20°C.

HPLC Fingerprint

One gram of SBP_{water} or SBP_{EtOH} was dissolved in 10 ml EtOH. The extract was filtered, and the supernatant was collected for chemical analysis (Gao et al., 2008; Xu et al., 2019). The analysis was performed with an Agilent HPLC 1200 system (Agilent,

Abbreviations: SBP, Shexiang Baoxin Pill; TCM, traditional Chinese medicine; AD, Alzheimer's disease; DMEM, Dulbecco's modified Eagle's medium; HRP, horse reddish peroxidase; NO, nitric oxide; NOS, nitric oxide synthase; AChE, acetylcholinesterase.

Waldbronn, Germany), equipped with a binary pump, a degasser, an auto sampler, a thermostatic column compartment, and a diode array detector (DAD). The samples were analyzed by using a PLATISIL C_{18} column (4.6 mm × 250 mm, 5 μm i.d.). Acetonitrile (A) and 0.03% phosphoric acid solution (B) were used as the mobile phase according to pre-set gradient program: 0–25 min, linear gradient 15–40% (A), 85–60% (B); 25–55 min, linear gradient 40–75% (A), 60–25% (B); 55–65 min, linear gradient 75–100% (A), 25–0% (B); 65–75 min, 100% (A). The column temperature was 25°C; the injection volume was at 10 μl; the flow rate was set at 0.8 ml/min; and the wavelength was 280 nm.

Cell Culture and Drug Treatment

PC12 cell line (CRL-1721), derived from rat adrenal medulla, was obtained from American Type Culture Collection (Manassas, VA). The cells were cultured in DMEM, supplemented with 6% horse serum and fetal bovine serum, 100 μg/ml streptomycin, and 100 units/ml penicillin in a humidified CO_2 (7.5%) incubator at 37°C. In drug treatment, PC12 cells were under serum starvation for 3 h in DMEM containing 1% fetal bovine serum and horse serum. After serum starvation, cells were treated with herbal extract for 48 h. Cell viability assay was used to determine a safe concentration range (0–500 μg/ml) of herbal extract, at which the extracts exerted no effect on cell proliferation or death. The water extracts of SBP, Ginseng extract, and Borneolum Syntheticum solution were used at 500 μg/ml; ethanol extracts and Styrax solution were used at 100 μg/m;. Cell viability was determined by MTT assay. In brief, cells were plated in 96-well plate at a density of 10,000 cells/well for 24 h and treated with drugs for 48 h. Then, 10 μl MTT solution, at a concentration of 5 mg/ml, was added into each well, incubated for another 3 h at 37°C. Using a microplate reader (Thermo Fisher Scientific, Waltham, MA), the absorbance was measured at 570 nm (Lam et al., 2016; Lam et al., 2017).

Preparation of $A\beta_{1\text{-}42}$

Preparation of $A\beta_{1\text{-}42}$ peptide was performed as previously reported (Yang et al., 2005). Briefly, to obtain monomeric $A\beta_{1\text{-}42}$, the lyophilized $A\beta_{1\text{-}42}$ was dissolved in 100% 1,1,1,3,3,3-hexafluoro-2-propanal (HFIP) and sonicated in a water bath for 10 min. Then, the $A\beta_{1\text{-}42}$ solution was subsequently stored in small aliquots at −80°C. Prior to use, the HFIP-treated monomeric $A\beta_{1\text{-}42}$ was immediately dried in the fume hood and dissolved in sterilized distilled water at a stocking concentration of 1 mM.

ThT Fluorescence Assay

The amounts of $A\beta_{1\text{-}42}$ fibrils resulting from aggregation of monomeric $A\beta_{1\text{-}42}$ were determined by Thioflavine T (ThT) assay, in which the fluorescence intensity represented the degree of $A\beta_{1\text{-}42}$ fibril formation (Yang et al., 2005; Kroth et al., 2012). $A\beta_{1\text{-}42}$ was diluted to 10 μM in PBS in brown microtube in the presence or absence of curcumin (30 μM), SBP extracts or other herbal extracts, and then which was incubated at 37°C for 6 days without agitation. Ten μl of $A\beta_{1\text{-}42}$ solution was mixed with 90 μl of 5 μM ThT in PBS, and the fluorescence intensity was measured at excitation and emission wavelength of 435 and 488 nm, respectively, with application of 96-well black plate.

MTT Assay

Cell viability was measured by MTT assay (Li et al., 2007; Choi et al., 2010). In brief, 24 h after cell seeding, the culture medium was replaced with FBS-free medium, and then $A\beta_{1\text{-}42}$ samples (15 μM) (co-incubated with or without curcumin, SBP extracts and herbal extracts at 37°C for 6 days) were added to the cultures. Forty-eight hours after incubation, 10 μl MTT, at a concentration of 5 mg/ml in PBS, was added into each well, and the cells were incubated for another 4 h. The formed formazan crystals were dissolved in DMSO, and the absorbance was determined using a microplate reader with wavelength at 570 nm.

Animal Treatment

The APP/PS1 transgenic mice and B6C3 wild type mice (all male) were obtained from Hangzhou Hibio company (Hangzhou, China). The mice were housed at two to three animals per cage under a 12 h light/dark cycle, and they were fed with standard food and water. The experimental protocols were approved by Animal Ethics Committee (Permit Number: HB1808021) and under the guidelines of "Principles of Laboratory Animal Care" (NIH publication No. 80-23, revised 1996) and Institutional Animal Care and Use Committees protocol (HBFM3.68-2015.). Five-month-old APP/PS1 transgenic mice were randomly divided into five groups: the model group, donepezil (2 mg/kg/day), SBP_{EtOH} (95% ethanol extract of SBP) low-dosage group (22.5 mg/kg/day), SBP_{EtOH} high-dosage group (45 mg/kg/day). Age-matched male wild-type (WT) B6C3 mice were used as the control group (n = 6). In the APP/PS1 mice model group and WT mice group, the mice were injected with corresponding volume of saline. Donepezil, dissolved in saline, and the SBP solution (2% DMSO, 6% cremophor EL, 92% NaCl) were administered intra-gastrically once per day. Drug treatment lasted for 60 days.

Morris Water Maze Test

Morris water maze test was performed, as described previously (Xian et al., 2014). The experimental apparatus composed of a blank circular water tank, and the diameter and height of the water tank was 100 and 35 cm, respectively. The depth of water (23 ± 1°C) in the tank was ~15.5 cm, and by adding ink, it was rendered opaque. The maze was divided into four equal quadrants by four poles along the perimeter of pool. A platform, of which the diameter was 4.5 cm and the height was 14.5 cm, was submerged about 1 cm below the water surface and set at the middle of one quadrant. The pool was placed in a test room, and there were various visual cues needed, e.g. lamps, pictures, etc. Twenty-four hours prior to the spatial training, the mice suffered four pre-training sessions as followed: the mice was placed on the platform for 20 s, given a 30 s free swim, and then assisted to the platform, where it was permitted to have a rest for another 20 s. Spatial training to find the platform hidden in the water maze was performed consecutively for 4 days. Each day, the mice was put in water in face of the pool wall at one of three randomized

starting positions, of which they did not contain the platform. The mice were allowed 60 s to catch the platform and given 20 s to stay on it. Animals failing to find the platform in a period of 60 s were manually guided to the platform and given 20 s to stay. The escape latency for finding the submerged platform was regarded as 60 s. Four trials were performed for each mouse per day, and the inter-trial interval lasted for 60 s. The escape latency to the submerged platform of each trial was recorded, and the average value of 4 trials was analyzed. Twenty-four hours after the final time of spatial training, the probe test was performed by removing the platform and giving each mouse to swim freely for 60 s. The time that each mouse spent swimming in the target quadrant, where the platform was once hidden previously, and the number of times (frequency) that it crossed over the platform site were recorded.

Histochemistry

Mice were anesthetized with chloral hydrate (100 mg/kg) 24 h after performing the behavioral test, and then the mice were perfused with ice-cold saline. The brains were dissected into two parts: one was frozen at −80°C for protein analysis and western blotting; the other was being fixation in 4% paraformaldehyde (pH 7.4) at 4°C overnight for immunohistochemistry. In sectioning, the fixed brains were successively dehydrated in ethanol, embedded in paraffin, and cut into 4 μm-thick sections. The sections were treated with 0.01 M sodium citrate for 15 min at 95°C and incubated with 3% H_2O_2 for 8 min. The sections were then reacted with primary rabbit antibody against Aβ (rabbit polyclonal, 1:100, Abcam) at 4°C, followed by interaction with horseradish peroxidase-conjugated goat anti-rabbit secondary antibody (1:200, Abcam), and finally visualized with diaminobenzidine tetrahydrochloride. The expression of Aβ was analyzed using Image-Pro Plus software. Five sections were randomly selected from each mouse.

Morphological Analysis

After fixation, the brain tissues were successively dehydrated in 80, 90, 95, and 100% ethanol. The tissues were embedded in paraffin for 5 h. The paraformaldehyde/paraffin-embedded samples were then sectioned to 4-μM thickness and mounted on microscope slides. The hematoxylin stain was used to dip the sections, and after that, slides were washed with water until the sections became blue. Next, the sections were immersed in eosin staining solution for 3–5 min and then washed with water again, until there was no floating color on the slides. After dehydration, the slides were fixed with neutral glue. Neuronal counts, located in the hippocampus, were performed under a microscope. The nucleus was blue, the cytoplasm was pink, and the red blood cells were bright red. Counts were performed in five to six adjacent fields, and all data are represented as number of neurons under each observation field.

Determination of Biomarkers

For determination of levels of NO, NOS, and AChE, 0.1 g of brain tissue was homogenized using 0.9 ml of pre-cold saline. After reacted on ice for 15 min, the homogenate was centrifuged at 2,500 rpm/min for 10 min at 4°C, and the supernatants were used to measure the levels of NO, NOS, and AChE with application of corresponding kits according to the manufacturer's instructions. To measure the level of NO, 300 μl homogenate was reacted with reagents in a NO kit (A013-2-1, Jiancheng Bio, Nanjing, China). After standing for 10 min, the mixture was centrifuged at 3,500 rpm/min for 15 min, and 150 μl supernatant was used to determine NO level with wavelength set at 550 nm. The wavelength to determine the level of NOS was set at 530 nm (A014-2, Jiancheng Bio), and the level of AChE was determined at the wavelength of 412 nm (A024-1-1, Jiancheng Bio). For the measurement of cytokines in mice, the blood was collected from the removal of eyeballs under anesthesia. After standing for 1 h at 37°C, the blood was centrifuged at 3,500 rpm/min for 10 min, and the serum was obtained. The serum was further used to determine the levels of IL-6 and TNF-α by using commercially available sandwich enzyme-linked immunosorbent assay (ELISA) kits (Invitrogen, Carlsbad, CA), following the manufacturer's manual.

RT-PCR Analysis

Total RNA of the hippocampus and cortex was extracted using RNazol following the manufacturer's instructions (Takara, Dalian, China): the concentration of RNA was determined spectrophotometrically at 260 nm. The quality of RNA was further assessed by the ratio of absorbance at 260 and 280 nm. The values of A260/A280 from 1.9 to 2.1 were considered as reasonable. Total RNA (1.5 μg) was applied to synthesize cDNA using HiScript-II Q RT SuperMix for qPCR kit (Vazyme Biotech, Nanjing, China) following the manufacturer's manual, and RT-PCR was performed using reagents and protocols from ChamQ SYBR Color qPCR Master Mix kit (Vazyme Biotech). The sequences of primers were shown: 5'-GCC TCC TCT CCT ACT TCG G-3′ (sense primer, S) and 5′-TCA GCC CAT CTT CTT CCA G-3′ (antisense primer, AS) for Bax; 5′- AAA CCC TCC ATC CTG TCC-3′ (S) and 5′-TCC TAA ACC CTG CTT CCC-3′ (AS) for murine Bcl-2; 5′-GAA GCA GGC ATC TGA GGG-3′ (S) and 5′-AAG GTG GAA GAG TGG GAG TT-3′(AS) for murine GAPDH. The relative expressions of Bax and Bcl-2 mRNA were normalized to the amount of GAPDH in the same cDNA following the relative quantification method ($2^{-\Delta\Delta CT}$ method).

Western Blotting

Protein extracts were extracted from frozen brain tissues using Nuclear and Cytosolic Protein Extraction kit (Chemicon, Temecula, CA), and protein concentrations were measured using the BCA protein assay kit based on protocol provided by the manufacturer. The protein samples were electrophoresed by sodium dodecyl sulfate-polyacrylamide gel electrophoresis (SDS-PAGE) for 3 h at 80 V, and then separated proteins were transferred onto polyvinylidene fluoride (PVDF) membranes. Next, the membranes were blocked with 5% (w/v) non-fat milk in TBS-T (Tris-buffer saline containing 0.1% Tween-20) at room temperature for 1 h. After blocking, the membranes were incubated at 4°C overnight with appropriate amounts of primary antibodies against Aβ, Bax, Bcl-2 (1:1,000, Abcam, Danvers, MA), and GAPDH (1:5,000, Abcam). Then, the membrane was rinsed with TBS-T three times, 5 mins per each time, and probed with horseradish peroxidase conjugated secondary antibody at room temperature for

2 h. To prove equal loading of samples, the membranes were incubated with monoclonal antibody GAPDH. Finally, the protein bands were visualized using the ECL Western blotting detection reagents (Amersham Biosciences, Buckinghamshire). The intensity of each band was analyzed with application of Image J software (NIH Image, Bethesda, MD).

Statistics Analysis

Statistical tests were performed using one-way analysis of variance (ANOVA); differences from basal or control values were classified as * $p < 0.05$; ** $p < 0.01$; *** $p < 0.001$.

RESULTS

SBP Inhibits Aβ$_{1-42}$ Fibrils and Protects Cell Damage

Previous records suggested that SBP_{water} and SBP_{EtOH} extracts were rather effective in triggering differentiation of cultured PC12 cells (Xu et al., 2019), and thus both of the extracts were subjected for further analyzed. The HPLC chromatogram of SBP_{water} and SBP_{EtOH} and 12 major peaks were identified (**Supplementary Figure 1**). The chemical information of non-volatile constituents in SBP was shown characteristically in the chromatogram, and the authenticated 12 peaks were precisely confirmed by comparison with known chemical standards, as reported previously (**Supplementary Figure 1;** Xu et al., 2019). The demonstrated HPLC chromatogram, as well as its chemical composition, could be used as fingerprint of SBP and other herbal extracts for quality control purpose, as to ensure the repeatability of biochemical experiments.

To evaluate the ability of each herbal extract (i.e. curcumin, $SBP_{EtOH,}$ or SBP_{water} and other seven individual herbal materials) in suppressing formation of Aβ$_{1-42}$ fibrils, the monomeric Aβ$_{1-42}$ was incubated with curcumin (a positive control), SBP_{water} or SBP_{EtOH} or other seven individual herbal extracts at 37°C for 6 consecutive days, as such allowing Aβ$_{1-42}$ to age. As shown in **Figure 1A**, neither water extract of Bovis Calculus nor 95% ethanol extracts of Borneolum Syntheticum and Styrax showed effect on formation of Aβ$_{1-42}$ fibrils. In contrast, SBP_{water}, SBP_{EtOH}, Bufonis Venenum extract, Cortex Cinnamomi extract, Moschus and Ginseng Radix et Rhizoma extract, and ethanol extract of Bovis Calculus, significantly suppressed Aβ$_{1-42}$ fibril formation with decreasing level of ThT fluorescence. The ethanol extracts of SBP, Bovis Calculus, Bufonis Venenum, Cortex Cinnamomi, and Moschus demonstrated strong capability in inhibiting formation of Aβ$_{1-42}$ fibrils than their water extracts (**Figure 1A**). The ethanol extract of SBP and Moschus showed better efficacy in suppressing Aβ$_{1-42}$ fibril formation. Curcumin, as a positive control, decreased the fluorescence intensity significantly, consistent with previous studies (Ono et al., 2004; Yang et al., 2005).

To determine toxicity of Aβ$_{1-42}$ aggregate being aged with drugs, Aβ$_{1-42}$ was incubated with curcumin, SBP_{EtOH} or SBP_{water} or other seven individual herbal extracts at 37°C for 6 days, and then which were used to treat cultured PC12 cells for 48 h. The treatment with Aβ$_{1-42}$ fibrils significantly decreased cell viability by ~60%

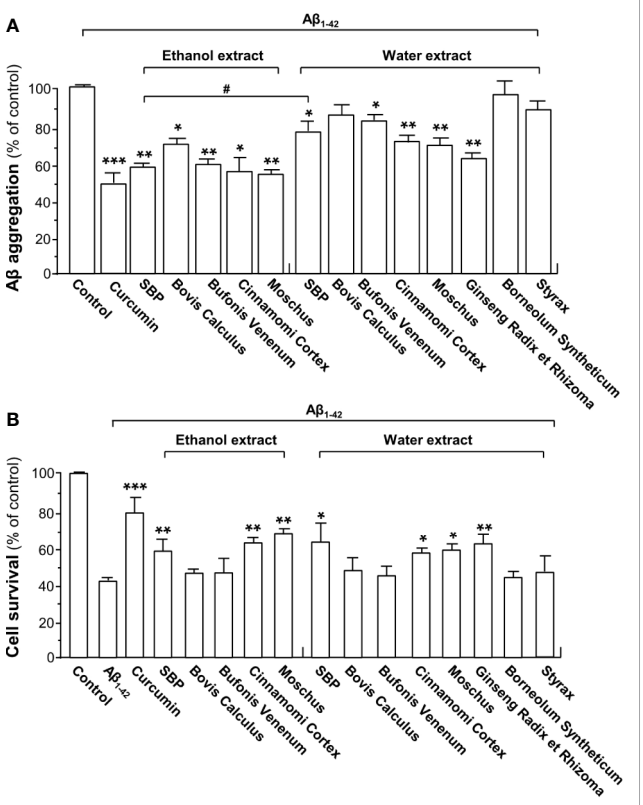


FIGURE 1 | SBP suppresses Aβ fibril formation and attenuated Aβ-induced toxicity in PC12 cells. **(A)** HFIP-reconstituted Aβ monomers (10 μM) were incubated at 37°C for 6 days with or without drugs (i.e. curcumin, SBP_{EtOH} or SBP_{water}, and other seven individual herbal materials). SBP_{EtOH}, ethanol extracts of various herbal materials, and Styrax solution were used at 100 μg/ml; and SBP_{water}, water extracts of various herbal materials, solutions of Ginseng Radix et Rhizoma extract and Borneolum Syntheticum were used at 500 μg/ml. Curcumin at 30 μM served as a positive control. The extent of Aβ aggregation was determined using ThT fluorescence assay. Data are expressed as Mean ± SEM of the percentage of control (no drug treatment), where $n = 4$; $p < 0.05$ (*); $p < 0.01$ (**); $p < 0.001$ (***) *vs* control group. $p < 0.05$ ($^{\#}$) *vs* SBP_{EtOH} group. **(B)** Inhibition of cytotoxicity in PC12 cells by drug-modified Aβ$_{1-42}$ aggregates. Aβ$_{1-42}$ (15 μM) was incubated at 37°C for 6 days in the presence or absence of drugs (i.e. curcumin, SBP_{EtOH} or SBP_{water}, and other seven individual herbal materials), and then treated to PC12 cells for 48 h. The doses were in (A). MTT assay was performed to determine the cell viability. Data are expressed as Mean ± SEM of the percentage of control (untreated culture), where $n = 4$; $p < 0.05$ (*); $p < 0.01$ (**); $p < 0.001$ (***) *vs* Aβ$_{1-42}$-treated group.

(**Figure 1B**). In comparison to Aβ$_{1-42}$ fibril, Aβ$_{1-42}$ having incubation with SBP_{water}, SBP_{EtOH}, extracts of Cortex Cinnamomi, Moschus, and Ginseng Radix et Rhizoma showed less toxicity to cultured PC12 cells, similar to that of curcumin. As compared to the water extract, the ethanol extract of Bufonis Venenum demonstrated significant effect in relieving Aβ$_{1-42}$-induced cell toxicity (**Figure 1B**). In contrast, the water extracts of Bovis Calculus, Bufonis Venenum, Borneolum Syntheticum, and Styrax were unable to protect the Aβ$_{1-42}$-induced cell toxicity (**Figure 1B**). The SBP-protected cell death against Aβ fibrils

probably due to the ability of herbal extract in reducing the fibrilization. In terms of dose and efficacy, SBP_{EtOH} extract showed better response as compared to that of SBP_{water} extract, and therefore SBP_{EtOH} was chosen for animal study.

SBP Rescues Behavioral Impairment

The experimental protocol for treatment with SBP_{EtOH} extract in mice was shown in **Figure 2A**. The behavioral test was performed in 56 days after the daily intake of herbal extract/drug. Mice were sacrificed at day 60 for biochemical analysis. Morris water maze was employed to reveal the dysfunction of spatial learning and memory. The shortened escape latency was found in the control mice during successive days of training; but which was not found in APP/PS1 transgenic mice, suggesting the establishment of behavioral model **(Figure 2B)**. The performance of drug-treated mice was improved through the training (Day 57–Day 59). The escape latency in APP/PS1 transgenic mice was higher than that of control group (non-transgenic; wild type), suggesting the transgenic mice took relatively longer time to find the hidden platform. As compared to model group, the treatment of SBP at high dose in APP/PS1 transgenic mice significantly shortened the mean latency to find the platform by ~50% from the Day 58 onward **(Figure 2B)**. In addition, treatment of donepezil significantly reduced the mean latency after Day 58. The low dose of SBP however did not decrease the mean latency, significantly. In addition, total distance traveled, swim velocity, and time near wall during the training period were measured (**Figures 2C–E**). As demonstrated, the treatment of donepezil significantly reduced the total distance of the swimming-tracking path **(Figure 2C),** as well as the time near the wall spent in target quadrant **(Figure 2D)**. In comparison with model group, the treatment of SBP at low and high doses in APP/PS1 transgenic mice obviously decreased the total distance of the swimming-tracking path **(Figure 2C)** and the time near the wall spent in target quadrant after Day 58 **(Figure 2D)**. Donepezil treatment significantly reduced the total distance and the time near the wall after Day 57. However, there was no significant difference between SBP-treated groups and model group in terms of swim velocity **(Figure 2E)**.

In the probe test, the distance, the time spent in target quadrant and the number of target crossings of mouse in Morris water maze were significantly reduced in APP/PS1 transgenic mice, as compared to the wild type mice **(Figures 3A–D)**. The mice having treatment of SBP, at low and high doses, induced an increase in the distance, the time spent in the target quadrant, and the number of target crossings, as compared to the model group. In addition, the mice having SBP treatment at high dose demonstrated a significant difference in the probe test **(Figures 3A–D)**. Donepezil, a positive control, significantly increased the distance and the time spent in target quadrant, as well as the number of target crossings of the transgenic mice. The high dose of SBP demonstrated better effect in increasing the number of target crossings than that of donepezil-treated group.

SBP Rescues Pathological Changes in APP/PS1 Mice

After behavioral analysis, the mouse was scarified, and the cross-section of brain was subjected to immunohistochemical studies. Two specific

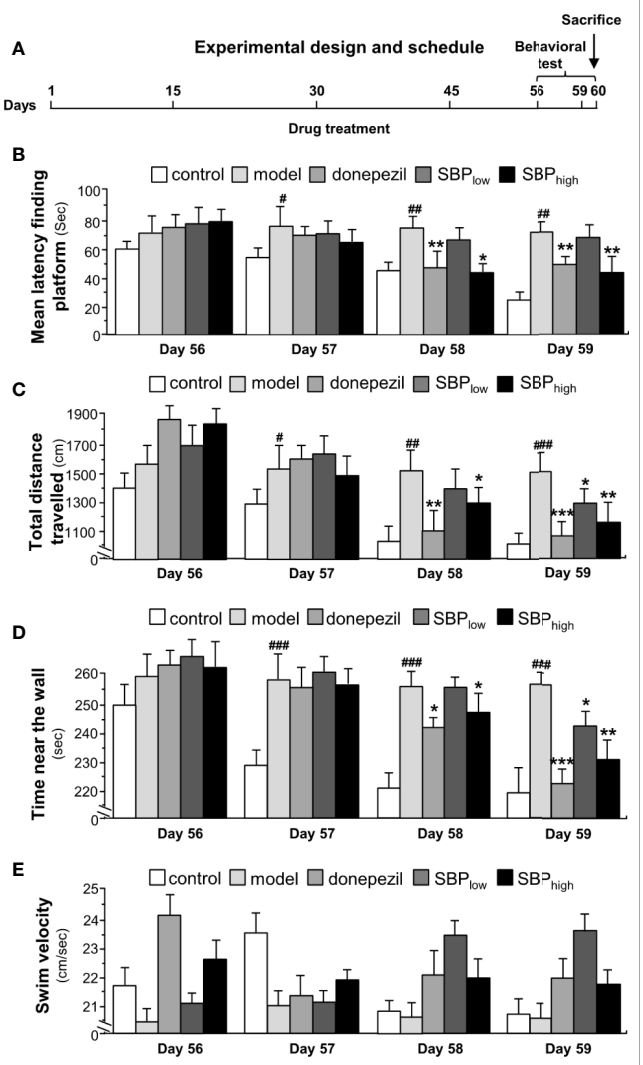


FIGURE 2 | The schedule of animal experiment. **(A)** The APP/PS1 transgenic mice and B6C3 wild type mice (all male at 5-month-old) were fed with standard food and water. The transgenic mice were randomly divided into five groups, i.e. model group, donepezil (2 mg/kg/day), SBP_{EtOH} (95% ethanol extract of SBP) low-dosage group (22.5 mg/kg/day), SBP_{EtOH} high-dosage group (45 mg/kg/day). Age-matched male wild-type (WT) B6C3 mice were used as control group (n = 6). In APP/PS1 mice model group and wild type mice group, the mice were injected with the corresponding volume of saline. Donepezil, dissolved in saline, and the SBP extract (2% DMSO, 6% cremophor EL, 92% NaCl) were administered intra-gastrically once per day starting on Day 1. Drug treatment lasted for 60 days. Behavioral test was started on Day 56. **(B)** The treatment of mice with herbal extracts were according to the protocol in Figure 2A. The latency to find a hidden platform during 4 consecutive days of training was determined in Morris water maze. **(C)** The total distance of swimming-tracking path during 4 consecutive days of training was determined. **(D)** The time near the wall spent in target quadrant (southeast, where the platform was placed during the training phase) during 4 consecutive days of training was determined. **(E)** The swim velocity during 4 consecutive days of training was determined. Values were expressed as mean ± SEM, where n = 6; $p < 0.05$ ($^{\#}$); $p < 0.01$ ($^{\#\#}$); $p < 0.001$ ($^{\#\#\#}$) *vs* control group. $^{*}p < 0.05$; $^{**}p < 0.01$; $^{***}p < 0.001$ *vs* model group.

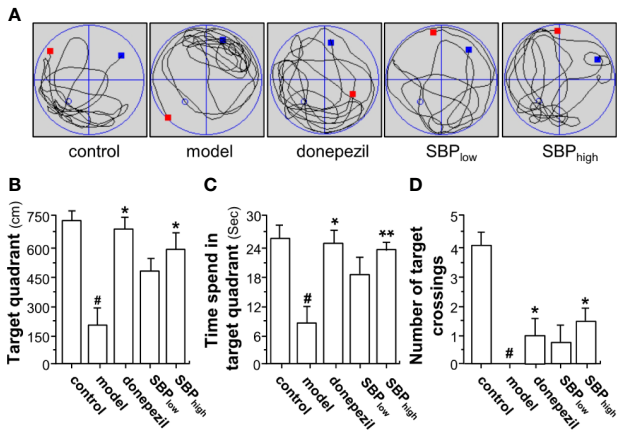


FIGURE 3 | SBP rescues memory deficits in APP/PS1 transgenic mice. **(A)** The treatment of mice with herbal extracts were according to the protocol in **Figure 2**. The typical swimming-tracking path on the fifth probe trial day was determined. The red square represents the place where the animal is being placed at the beginning of water maze test. The blue square represents the place where the animal is stopped at the end of water maze test. The blue circle represents the place where the platform is placed before water maze test. **(B)** the distance in target quadrant (southeast, where the platform had been placed during the training phase) in the probe trial (swimming 60 s without platform) was determined. **(C)** the time spent in the target quadrant was determined. **(D)** the number of target crossings in the target quadrant was determined. Values were expressed as mean ± SEM, where $n = 6$; $p < 0.05$ ($^{\#}$) *vs* control group. $^{*}p < 0.05$; $^{**}p < 0.01$ *vs* model group.

areas of the section, cerebral cortex and hippocampus, were chosen for analysis (**Supplementary Figure 2**). Immunohistochemistry revealed the robust identification of Aβ in cerebral cortex of the transgenic mice (**Figure 4**). APP/PS1 mice showed high level of Aβ plaque in cerebral cortex, as compared to that of control group. Donepezil decreased Aβ plaque by ~90% in APP/PS1 mice, as compared to model group (**Figure 4**). In parallel, the treatments of SBP, at low and high doses, inhibited formation of Aβ plaque by ~40 and ~60%, respectively, in the mouse brain: both doses were significant, as compared to control (**Figure 4**).

In addition, the effect of SBP on nuclear pyknosis of neurons in hippocampus of the transgenic mice was analyzed. The number of neurons suffering from nuclear pyknosis in APP/PS1 transgenic mice increased by ~13 folds, as compared to the mice in control group (**Figure 5**). SBP administration, at low and high doses, significantly decreased the number of neurons suffering from nuclear pyknosis to 4–5 folds of control mice, i.e. a reduction of over 2 folds from model group (**Figure 5**). Comparing to mice in model group, donepezil could attenuate the neurons experiencing nuclear pyknosis to ~3 folds of control.

The suppressive effects of SBP on protein levels of indicative biomarkers of AD mouse brain, i.e. NO, NOS, and AChE, were investigated. As shown in **Figure 6**, when compared to control group, protein levels of NO, NOS, and AChE in the brain of APP/PS1 transgenic mice were significantly elevated, at least over 2 folds. On the other hand, the treatment of SBP significantly reduced the expressions of NO, NOS, and AChE, as compared with the model group, i.e. un-treated APP/PS1 mice. The treatment of SBP at high

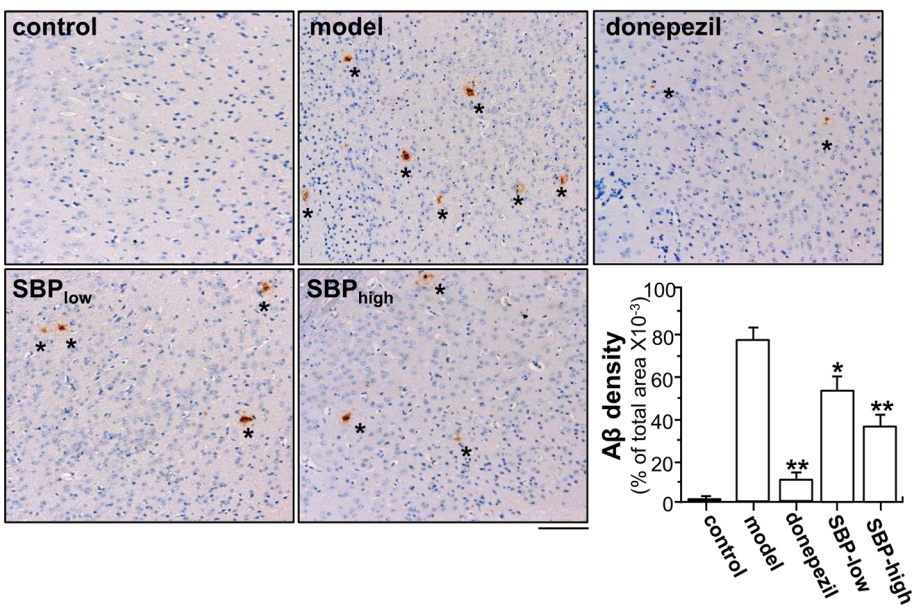


FIGURE 4 | SBP reduces Aβ expression in brain tissue. Brain tissues from drug-treated mice were collected from mice as described in **Figure 2**. Brain tissues were immuno-stained with anti-Aβ antibody. The cerebral cortex was selected for analysis, as indicated **Supplementary Figure 2**. Taupe area (star) represented the antibody staining. ImageJ software was used to do the quantification of Aβ plaque area. The control group was untreated wild type mice. Data are in Mean ± SEM of the Aβ density in terms of percentage of total area per view, where $n = 6$; $p < 0.05$ (*); $p < 0.01$ (**) *vs* model group. Bar = 100 μm.

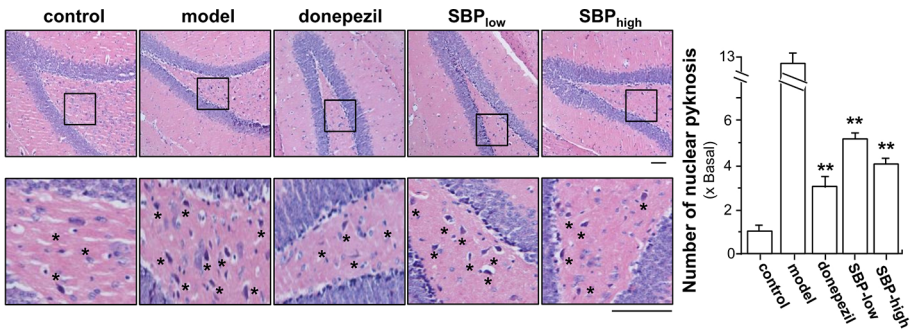


FIGURE 5 | SBP protects neurons from nuclear pyknosis in APP/PS1 transgenic mice. Brain tissues from drug-treated mice were collected from mice as described in **Figure 2**. The hippocampus was selected for analysis, as indicated **Supplementary Figure 2**. Brain tissues were collected and cut into sections at 4 μM thick. The sections were stained with hematoxylin and eosin stains. Typical pictures focusing the hippocampus were shown, in which the nucleus was blue, the cytoplasm was pink, and the red blood cells were bright red (left panel). The number of neurons having nuclear pyknosis (denoted as star for some but not all, for clarity) was determined under light microscope using Image proplus program (right panel). Results are expressed as the fold of change as compared to control (X Basal; untreated wild type mice), where the control was set as 1, Mean ± SEM, where $n = 6$; $p < 0.01$ (**) *vs* model group. Bar = 50 μm.

dose decreased the levels of NO, NOS, and AChE by ~70, ~50, and 40%, respectively. In addition, the treatment with donepezil reduced the protein levels of NO, NOS, and AChE (**Figure 6**). Moreover, we further examined the expressions of IL-6 and TNF-α in the mouse serum by performing an ELISA assay. In serum of APP/PS1 mice, the levels of IL-6 and TNF-α were increased at least by 2 folds (**Figure 6**). In addition, the inflammatory cytokine was determined in the SBP-treated mice. The treatment of SBP, at both low and high doses, was able to suppress the up-regulated cytokines in APP/PS1 mice (**Figure 6**). Similar to that of SBP, donepezil was able to decrease the expressions of IL-6 and TNF-α.

SBP Exerts Neuroprotective Effects *via* Anti-Apoptotic Pathway

To determine the possible anti-apoptotic signaling of SBP in neuroprotection, RT-PCR and western blotting assay were performed to determine expression of apoptotic genes. In APP/PS1 mice, the mRNA expression of Bax was increased by ~4 folds, as compared to wild type mice; while the mRNA level of Bcl-2 was decreased by ~90% (**Figure 7A**). In SBP-treated APP/PS1 mice, the expression of Bax was significantly reduced under a high dose of SBP intake, almost back to control level (**Figure 7A**). On the other hand, SBP treatment increased the mRNA level of Bcl-2 at both doses of SBP. As expected, the treatment with donepezil significantly altered the mRNA expressions of Bax and Bcl-2. The protein expressions of Bax and Bcl-2 demonstrated similar trends in western blotting analysis. In the brain of APP/PS1 mice, the expression levels of Aβ and Bax were increased markedly over 3 folds (**Figure 7B**). The treatment of SBP (high dose) in the transgenic mice significantly decreased the protein levels of Aβ and Bax almost back to the control. In parallel, the reduced Bcl-2 protein in APP/PS1 mice was restored by SBP (high dose) almost back to control level **(Figure 7B)**. Similarly, donepezil significantly decreased the ratio of Bax/Bcl-2. These results suggested the function of SBP in protecting neuron could be mediated by an anti-apoptotic pathway.

DISCUSSION

Very limited effective drugs are available for treatment of AD, and the current used single-targeted anti-AD drugs might only offer symptom relieving effects. The major reason could be that AD is caused by multiple factors; thus, safe and effective multi-functional anti-AD drug should be urgently needed (Scheltens et al., 2016). Amongst those multi-components of Chinse herbal medicine, SBP is a well-known herbal mixture being sold in the current herbal market for years. This herbal mixture is mainly used in treating cardiovascular diseases (Yan et al., 2006; Lu et al., 2018). Here, we are proposing another possible application of SBP in treating neurodegenerative diseases. In cultured neuronal cells, we have reported that SBP could induce neuro-differentiation, as well as cell protection, *via* activation of cAMP-PKA pathway (Xu et al., 2019). Our hypothesis of SBP as a new and promising anti-AD drug is supported by different lines of evidence. First, SBP exhibited neurite-outgrowth promoting activity in cultured neuronal cells, as reported previously (Xu et al., 2019). Second, SBP reduced Aβ aggregation, as well as the Aβ-induced neurotoxicity cultured cells. Third, SBP reduced amyloid deposition, as well as reduced expressions of NO, NOS, AChE in the brain. Several lines of evidence support the involvement of neuroinflammation playing a substantial role in development of neuropathological changes in AD patients (Rogers et al., 1988; Griffin et al., 1989). Reports have suggested that the anti-inflammatory treatments for inflammation-related diseases, such as rheumatoid arthritis, could show protective effects against AD development, i.e. up to 50% reduction in the risk of developing AD among those patients taking non-steroidal anti-inflammatory drugs (Rich et al., 1995). Having this notion, the anti-inflammatory effects of SBP could be accounted for anti-AD function in ours model, at least part of that. As demonstrated here, SBP suppressed production of inflammatory factors (IL-6 and TNFα) in serum of APP/PS1 transgenic mice. Last, SBP improved cognitive impairment of APP/PS1 transgenic mice. Under this scenario, SBP could be an excellent choice for AD treatment, or even as preventing agent. For a good reason, SBP has been on herbal

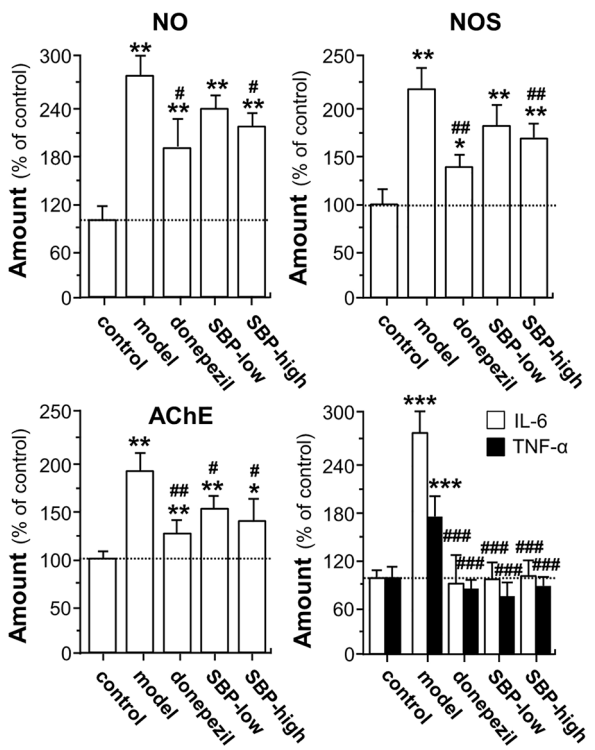


FIGURE 6 | SBP promotes expressions of NO, NOS, AChE, and cytokine in APP/PS1 transgenic mice. Treatment of mice was as described in **Figure 2**. For determination of levels of NO, NOS, and AChE, 0.1 g of brain tissue was homogenized using 0.9 ml of pre-cold saline. After reacted on ice for 15 min, the homogenate was centrifuged at 2,500 rpm/min for 10 min at 4°C, and the supernatants were used to measure the levels of NO, NOS, and AChE with application of corresponding kits according to the manufacturer's instructions. Blood was collected for the measurement of the amounts of IL-6 and TNF-α. The blood was centrifuged at 3,500 rpm/min for 10 min, and the serum was obtained by discarding the precipitant. The levels of IL-6 and TNF-α in the serum was further determined using commercially available ELISA kits. Data are expressed as Mean ± SEM of the percentage of change as compared with control (untreated wild type mice), where $n = 6$; $p < 0.05$ (*); $p < 0.01$ (**); $p < 0.001$ (***) *vs* control group. $p < 0.05$ (#); $p < 0.01$ (##); $p < 0.001$ (###) *vs* model group.

market for years, and millions of people have taken this herbal mixture during the years, which therefore guarantees its safety.

In the past decade, the over production and accumulation of Aβ in the brain have been hypothesized to play a crucial role in pathological cascades of AD. The *in vitro* data have indicated that SBP prevented Aβ-induced neurotoxicity by inhibiting the fibrilization process. In recent target for drug screening, drug having ability to reduce deposition and neurotoxicity of Aβ in brain could be potential anti-AD agents; however, few of them have achieved the final success (Wharton et al., 2012; Egan et al., 2019). One of the obstacles is that the drug candidates have shown promising positive results in *in vitro* model but not in *in vivo* model. The animal model of AD is not a straightforward issue, and several such disease models have been proposed. APP/PS1 transgenic mouse is one the most popular animal models to mimic the cognitive impairment of AD patients. APP/PS1 transgenic mouse, bearing double mutations on the genes of APP and PSEN1, develops amyloid plaque in neocortex at ~6 weeks of age and amyloid deposits in hippocampus at ~5 months (Lok et al., 2013). Moreover, APP/PS1 transgenic mouse exhibits cognitive impairments, and which can be examined by behavioral assays. SBP, a possible anti-AD candidate, processes activities in both *in vitro* and *in vivo* models, supporting its further exploration.

The development of AD is believed to be caused by multiple factors, and single-targeted drug is only offering limited symptom-relieve effect but not restore or delay the pathological progress. Having multiple-targeted therapeutic strategy therefore could provide synergy in treating the complex neurodegenerative disease. FDA has not approved new anti-AD drug since 2001, except a combination of AChE inhibitor and NMDA receptor antagonist in 2014. Many anti-AD drugs targeting various proteins are failed during the clinical trial because of its efficacy. Thus, a new direction to develop AD drug is in urgent need, and therefore the drug candidate having multi-functional target is a common approach. These candidates with disease-modifying potential may delay or reverse the pathological progress of AD. In accordance to this notion, TCM is effective and safe for treatment of many diseases (Gao et al., 2008; Jiang et al., 2013). Indeed, SBP is a herbal mixture, which is having multiple functions, including promotion of neurogenesis and neuroprotection, through regulating different therapeutic targets. The results of biochemical assays in APP/PS1 transgenic mice have supported our hypothesis. The elevated expressions of Aβ, NO, and NOS in the brain of APP/PS1 transgenic mice were effectively reduced by SBP. In addition, AChE, an enzyme target for several anti-AD drugs, was reduced by SBP, suggesting the cholinergic transmission might be enhanced. To account the efficacy of SBP in AD mice, the individual ingredients of SBP have been proposed to play role in the brain functions. SBP composes of eight herbal extracts, many of them are being applied in clinics for brain protection. For example, Moschus and Borneolum Synthcticum, known as a drug-pair in TCM, are known to treat cerebral stroke (Xiang et al., 2012). Moreover, the components from ginseng have been shown to have neuroprotective effects by suppressing the ROS formation and mitochondrial bioenergetics (Huang et al., 2019). Ginsenoside Re exerted anti-inflammatory effects by suppressing the formation of nitric oxide and attenuating the NF-κB signaling in the LPS-induced microglial cell (Wu et al., 2007). In parallel, ginsenoside Rg1 decreased the level of $A\beta_{1\text{-}42}$ by upregulating the expressions of PPARγ and insulin-degrading enzyme in hippocampus of a rat model of AD, demonstrating ginsenoside Rg1 has potential as a therapeutic agent for AD treatment (Quan et al., 2013). Thus, ginsenoside Re and ginsenoside Rg1 may contribute a lot to anti-inflammatory and neuroprotective effects of SBP, as demonstrated here. Supporting this notion, the major components of SBP, e.g. ginsenoside Re, ginsenoside Rg1 and cinnamic acid, could penetrate the blood-brain barrier (Jana et al., 2013; Zhao et al., 2018). Moreover, SBP regulated the expressions of mRNA and protein of apoptotic signaling proteins, e.g. Bcl-2 and Bax. In addition to the previous studies, SBP improved the cognitive impairment of

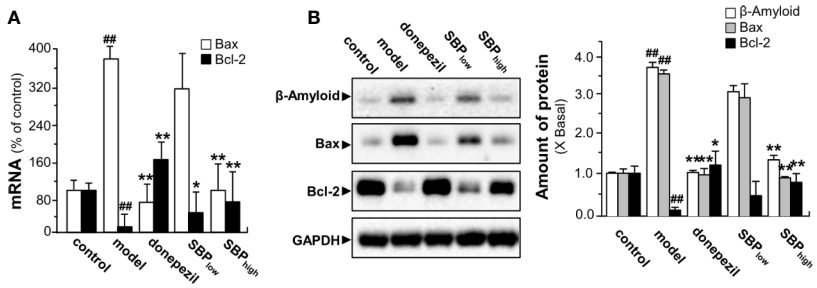


FIGURE 7 | SBP promotes neuroprotective effects *via* anti-apoptotic pathway. Treatment of mice was as described in **Figure 2**. **(A)** Effects of SBP on the mRNA expressions of Bax and Bcl-2 in the brains in APP/PS1 transgenic mice. Data are expressed as Mean ± SEM of the percentage of change (up or down regulated) as compared with control (untreated wild type mice), where $n = 6$; $p < 0.01$ ($^{\#\#}$) *vs* control group; $p < 0.05$ (*); $p < 0.01$ (**) model group. **(B)** Expression of β-Amyloid (~87 kDa), Bax (~21 kDa), and Bcl-2 (~26 kDa) in brain tissues of drug-treated mice (left panel). Expression of GAPDH (~36 kDa) served as a control. Quantitation of protein expression is shown (right panel). Results are expressed as the fold of change as compared to control (X Basal; untreated wild type mice), where the control was set as 1, Mean ± SEM, where $p < 0.01$ ($^{\#\#}$) *vs* control group; $n = 4$; $p < 0.05$ (*); $p < 0.01$ (**) *vs* model group.

APP/PS1 transgenic mice possibly through neuroprotection, enhancement of cholinergic signal transmission and promote neurogenesis. This notion will be worth to be further verified in more animal models associated with AD.

Drug repositioning or drug repurposing is one of the effective strategies to revisit the existent drugs for novel clinical application. The drug intake by patients might interact and regulate variety of targets, including receptors and kinases. The un-intended interaction between drug and non-therapeutic targets might produce unwanted side effects; however, some side effects, produced by the "off-target," might be useful to treat other diseases. There are many successful examples of drug repositioning. Sildenafil, commercially known as Viagra, is a well-known example for drug repositioning. Considering that multiple-targeted is one of the characteristics of TCMs, it is reasonable to explore additional therapeutic benefits of TCMs. In this connection, SBP, known in current herbal market, might be potential candidate for drug repositioning. In fact, several studies have tried to demonstrate additional therapeutic effects of SBP. Moreover, the safety and adverse effects of the old drug have been clearly studied. Thus, drug repositioning might greatly reduce the cost and period in drug development process. Our findings have not only indicated that SBP might be a promising candidate as an anti-AD agent, but also shed the light on the strategy of TCM repositioning.

CONCLUSION

We provided several lines of evidence to suggest that SBP could inhibit Aβ fibril formation, and the SBP-treated Aβ aggregates were of lower toxicity to neurons, as supported by increase in cell viability. Most encouragingly, the results in our present study demonstrated that SBP could significantly ameliorate the learning and memory impairments, reduce the area of Aβ plaque, suppress secretions of cytokines, and exert anti-apoptotic effects in APP/PS1 transgenic mice model of AD. Our findings extend the knowledge of mechanistic action of SBP in improving the memory impairments of AD, and which support SBP is worthy of further development into pharmaceutical medicines for AD treatment.

DATA AVAILABILITY STATEMENT

The raw data supporting the conclusions of this article will be made available by the authors, without undue reservation.

ETHICS STATEMENT

The animal study was reviewed and approved by Animal Ethics Committee (Permit Number: HB1808021).

AUTHOR CONTRIBUTIONS

W-HH and S-HM performed the experiments. Z-YZ and Y-JX prepared and analyzed the water and ethanol extracts of SBP. MX, RD, and TT-XD performed the HPLC fingerprint analysis and supplied the materials. S-PL, C-SZ, and X-HS designed and analyzed the data. TT-XD and KW-KT organized and supervised the study. All authors contributed to the article and approved the submitted version.

FUNDING

This study was supported by Chinese Association of Integrated Traditional and Western Medicine-SHPL Research Fund No. 2018001, Shenzhen Science and Technology Innovation Committee (ZDSYS201707281432317; JCYJ20170413173747440; JCYJ 20180306174903174), China Post-doctoral Science Foundation (2019M653087), Zhongshan Municipal Bureau of Science and Technology (ZSST20SC03); Guangzhou Science and

Technology Committee Research Grant (GZSTI16SC02; GZSTI17SC02); Hong Kong RGC Theme-based Research Scheme (T13-605/18-W); Hong Kong Innovation Technology Fund (UIM/340, UIM/385, ITS/500/18FP; TCPD/17-9); TUYF19SC02, PD18SC01, and HMRF18SC06.

SUPPLEMENTARY MATERIAL

The Supplementary Material for this article can be found online at: https://www.frontiersin.org/articles/10.3389/fphar.2020.01045/full#supplementary-material

SUPPLEMENTARY FIGURE 1 | HPLC fingerprint of SBP extracts. The chromatographic separation method, both ethanol and water extracts of SBP, i.e. SBPEtOH and SBPwater, was shown in materials and methods section. The identifies of peaks of HPLC fingerprints of SBPEtOH and SBPwater are: (1) benzoic acid from Styrax; (2) cinnamic acid from Styrax and Cinnamomi Cortex; (3) cinnamaldehyde from Styrax and Cinnamomi Cortex; (4) cinobufagin from Bufonis Venenum; (5) recibufogenin from Bufonis Venenum; (6) ethyl cinnamate from Styrax; (7) benzyl benzoate from Styrax; (8) benzyl cinnamate from Styrax; (9) phenethyl cinnamate from Styrax; (10) cinnamyl cinnamate from Styrax; (11) unknown from Styrax; and (12) unknown from Styrax. A typical profile was shown, where n = 4. The SBP extracts, as well as the extracts of various herbs, being used here were same as the one being used in our previous report (Xu et al., 2019).

SUPPLEMENTARY FIGURE 2 | Schematic sketch of mouse brain section. An outline of mouse cross-section showing the brain regions for histochemical analysis. The blue triangle represents the selected cerebral cortex for identification of Aβ plaque, as in **Figure 4**. The red star represents the selected hippocampus for identification of nuclear pyknosis of neurons, as in **Figure 5**. Bar = 1 mm.

REFERENCES

Chen, G., Chen, K. S., Knox, J., Inglis, J., Bernard, A., Martin, S. J., et al. (2000). A learning deficit related to age and b-amyloid plaques in a mouse model of Alzheimer's disease. *Nature* 408, 975–979. doi: 10.1038/35050103

Chen, W., Zhong, S., Wang, J., Dong, J., Wang, X., and Wang, J. (2008). Effect of heart-protecting musk pill on expression of bcl-2, caspase-3 in cerebral ischemia reperfusion injury in rats. *J. Emerg. Tradit. Chin. Med.* 17, 1421–1446.

Choi, R. C. Y., Zhu, J. T. T., Leung, K. W., Chu, G. K. Y., Xie, H. Q. H., Chen, V. P., et al. (2010). A flavonol glycoside, isolated from roots of *Panax notoginseng*, reduces amyloid-b-induced neurotoxicity in cultured neurons: signaling transduction and drug development for Alzheimer's disease. *J. Alzheimer Dis.* 19, 795–811. doi: 10.3233/JAD-2010-1293

Desgranges, B., Baron, J. C., Sayette, V., Petit-Taboue, M. C., Benali, K., Landeau, B., et al. (1998). The neural substrates of memory systems impairment in Alzheimer's disease. A PET study of resting brain glucose utilization. *Brain* 121, 611–631. doi: 10.1093/brain/121.4.611

Egan, M. F., Kost, J., Voss, T., Mukai, Y., Aisen, P. S., Cummings, J. L., et al. (2019). Randomized trial of verubecestat for prodromal Alzheimer's disease. *N. Engl. J. Med.* 380, 1408–1420. doi: 10.1056/NEJMoa1812840

Francis, P. T., Palmer, A. M., Snape, M., and Wilcock, G. K. (1999). The cholinergic hypothesis of Alzheimer's disease: a review of progress. Journal of Neurology. *Neurosurg. Psychiatry* 66, 137–147. doi: 10.1136/jnnp.66.2.137

Gao, Q. T., Cheung, J. K. H., Choi, R. C. Y., Cheung, A. W. H., Li, J., Jiang, Z. Y., et al. (2008). A Chinese herbal decoction prepared from Radix Astragali and Radix Angelicae Sinensis induces the expression of erythropoietin in cultured Hep3B cells. *Planta Med.* 74, 392–395. doi: 10.1055/s-2008-1034322

Goldsworthy, M. R., and Vallence, A. M. (2013). The role of beta-amyloid in Alzheimer's disease-related neurodegeneration. *J. Neurosci.* 33, 12910–12911. doi: 10.1523/JNEUROSCI.2252-13.2013

Griffin, W. S., Stanley, L. C., Ling, C., White, L., MacLeod, V., and Perrot, L. J. (1989). Brain interleukin 1 and S-100 immunoreactivity are elevated in down syndrome and Alzheimer disease. *Proc. Natl. Acad. Sci. U.S.A.* 86, 7611–7615. doi: 10.1073/pnas.86.19.7611

Guidi, I., Galimberti, D., Lonati, S., Novembrino, C., Bamonti, F., Tiriticco, M., et al. (2006). Oxidative imbalance in patients with mild cognitive impairment and Alzheimer's disease. *Neurobiol. Aging* 27, 262–269. doi: 10.1016/j.neurobiolaging.2005.01.001

Hampel, H. (2013). Amyloid-beta and cognition in aging and Alzheimer's disease: molecular and neurophysiological mechanisms. *J. Alzheimers Dis.* 33 (Suppl 1), S79–S86. doi: 10.3233/JAD-2012-129003

He, B. L., Guo, H., Yang, G. B., and Chen, Y. X. (2009). Clinical observation of Shexiangbaoxin pills in treating 72 cases of coronary. *Chin. Mod. Med.* 16, 66–67.

Hong, Y. D., Wu, H., and Zhao, P. (2006). Effects of Shexiang Baoxin Pill on carotid atheromatous plaque. *Zhongguo Zhong Xi Yi Jie He Za Zhi* 26, 780–783.

Huang, Y., Kwan, K. K. L., Leung, K. W., Yao, P., Wang, H. Y., Dong, T. T. X., et al. (2019). Ginseng extracts modulate mitochondrial bioenergetics of live cardiomyoblasts: a functional comparison of different extraction solvents. *J. Ginseng Res.* 43, 517–526. doi: 10.1016/j.jgr.2018.02.002

Jana, A., Modi, K. K., Roy, A., Anderson, J. A., Breemen, R. B., and Pahan, K. (2013). Up-regulation of neurotrophic factors by cinnamon and its metabolite sodium benzoate: therapeutic implications for neurodegenerative disorders. *J. Neuroimmune Pharmacol.* 8, 739–755. doi: 10.1007/s11481-013-9447-7

Jiang, M., Zhang, C., Cao, H., Chan, K., and Lu, A. (2013). The role of Chinese medicine in the treatment of chronic diseases in China. *Planta Med.* 77, 873–881. doi: 10.1055/s-0030-1270983

Kroth, H., Ansaloni, A., Varisco, Y., Jan, A., Sreenivasachary, N., Rezaei-Ghaleh, N., et al. (2012). Discovery and structure activity relationship of small molecule inhibitors of toxic betaamyloid-42 fibril formation. *J. Biol. Chem.* 287, 34786–34800. doi: 10.1074/jbc.M112.357665

Lam, K. Y. C., Chen, J., Lam, C. T., Wu, Q., Yao, P., Dong, T. T., et al. (2016). Asarone from Acori Tatarinowii Rhizoma potentiates the nerve growth factor-induced neuronal differentiation in cultured PC12 cells: a signaling mediated by protein kinase A. *PLoS One* 11, e0163337. doi: 10.1371/journal.pone.0163337

Lam, K. Y. C., Huang, Y., Yao, P., Wang, H., Dong, T. T. X., Zhou, Z., et al. (2017). Comparative study of different Acorus species in potentiating neuronal differentiation in cultured PC12 cells. *Phytother. Res.* 31, 1757–1764. doi: 10.1002/ptr.5904

Li, W. M., Kan, K. K., Carlier, P. R., Pang, Y. P., and Han, Y. F. (2007). East meets West in the search for Alzheimer's therapeutics—novel dimeric inhibitors from tacrine and huperzine A. *Curr. Alzheimer Res.* 4, 386–396. doi: 10.2174/156720507781788918

Lok, K., Zhao, H., Shen, H., Wang, Z., Gao, X., Zhao, W., et al. (2013). Characterization of the APP/PS1 mouse model of Alzheimer's disease in senescence accelerated background. *Neurosci. Lett.* 557, 84–89. doi: 10.1016/j.neulet.2013.10.051

Lu, L., Sun, X., Chen, C., Qin, Y., and Guo, X. (2018). Shexiang Baoxin Pill, derived from the traditional Chinese medicine, provides protective roles against cardiovascular diseases. *Front. Pharmacol.* 9, 1161. doi: 10.3389/fphar.2018.01161

Ono, K., Hasegawa, K., Naiki, H., and Yamada, M. (2004). Curcumin has potent anti-amyloidogenic effects for Alzheimer's beta-amyloid fibrils *in vitro*. *J. Neurosci. Res.* 75, 742–750. doi: 10.1002/jnr.20025

Quan, Q. K., Wang, J., Li, X., and Wang, Y. (2013). Ginsenoside Rg1 decreases $A\beta_{1-42}$ level by upregulating PPARγ and IDE expression in the hippocampus of a rat model of Alzheimer's disease. *PloS One* 8, e59155. doi: 10.1371/journal.pone.0059155

Rich, J. B., Rasmusson, D. X., Folstein, M. F., Carson, K. A., Kawas, C., and Brandt, J. (1995). Nonsteroidal anti-inflammatory drugs in Alzheimer's disease. *Neurology* 45, 51–55. doi: 10.1212/WNL.45.1.51

Rogers, J., Luber-Narod, J., Styren, S. D., and Civin, W. H. (1988). Expression of immune system-associated antigens by cells of the human central nervous system: relationship to the pathology of Alzheimer's disease. *Neurobiol. Aging* 9, 339–349. doi: 10.1016/S0197-4580(88)80079-4

Scheltens, P., Blennow, K., Breteler, M. M., de Strooper, B., Frisoni, G. B., Salloway , S., et al. (2016). Frontiers in probing Alzheimer's disease

biomarkers with fluorescent small molecules. *Alzheimer's Dis. Lancet* 388, 505–517. doi: 10.1016/S0140-6736(15)01124-1

Tian, D., Ling, S., Chen, G., Li, Y., Liu, J., Ferid, M., et al. (2011). Hypertensive nephropathy treatment by heart-protecting musk pill: a study of anti-inflammatory therapy for target organ damage of hypertension. *Int. J. Gen. Med.* 4, 131–139. doi: 10.2147/IJGM.S15235

Wharton, W., Stein, J. H., Korcarz, C., Sachs, J., Olson, S. R., Zetterberg, H., et al. (2012). The effects of ramipril in individuals at risk for Alzheimer's disease: results of a pilot clinical trial. *J. Alzheimers Dis.* 32, 147–156. doi: 10.3233/JAD-2012-120763

Wu, C. F., Bi, X. L., Yang, J. Y., Zhan, J. Y., Dong, Y. X., Wang, J. H., et al. (2007). Differential effects of ginsenosides on NO and TNF-alpha production by LPS-activated N9 microglia. *Int. Immunopharmacol.* 7, 313–320. doi: 10.1016/j.intimp.2006.04.021

Xian, Y. F., Mao, Q. Q., Wu, J. C., Su, Z. R., Chen, J. N., Lai, X. P., et al. (2014). Isorhynchophylline treatment improves the β-amyloid-induced cognitive impairment in rats via inhibition of neuronal apoptosis and tau protein hyperphosphorylation. *J. Alzheimers Dis.* 39, 331–346. doi: 10.3233/JAD-131457

Xiang, L., Jiang, P., Zhan, C., Chen, Z., Liu, X., Huang, X., et al. (2012). The serum metabolomic study of intervention effects of the traditional Chinese medicine Shexiang Baoxin Pill and a multi-component medicine polypill in the treatment of myocardial infarction in rats. *Mol. Biosyst.* 8, 2434–2442. doi: 10.1039/c2mb25172h

Xu, M. L., Zheng, Z. Y., Xia, Y. J., Liu, E. Y. L., Chan, S. K., Hu, W. H., et al. (2019). Shexiang Baoxin Pill, a formulated Chinese herbal mixture, induces neuronal differentiation of PC12 cells: a signaling triggered by activation of protein kinase A. *Front. Pharmacol.* 10, 1130. doi: 10.3389/fphar.2019.01130

Yan, S. K., Zhang, W. D., Liu, R. H., and Zhan, Y. C. (2006). Chemical fingerprinting of Shexiang Baoxin Pill and simultaneous determination of its major constituents by HPLC with evaporative light scattering detection and electrospray mass spectrometric detection. *Chem. Pharm. Bull. (Tokyo)* 54, 1058–1062. doi: 10.1248/cpb.54.1058

Yang, F., Lim, G. P., Begum, A. N., Ubeda, O. J., Simmons, M. R., and Ambegaokar, S. S. (2005). Curcumin inhibits formation of amyloid beta oligomers and fibrils, binds plaques, and reduces amyloid *in vivo*. *J. Biol. Chem.* 280, 5892–5901. doi: 10.1074/jbc.M404751200

Yang, X. X., Zhang, X. X., Chang, R. M., Wang, Y. W., and Li, X. N. (2011). Simultaneous quantification of five major active components in capsules of the traditional Chinese medicine 'Shu-Jin-Zhi-Tong' by high performance liquid chromatography. *J. Pharm. Anal.* 1, 284–290. doi: 10.1016/j.jpha.2011.08.002

Yang, L. Q., Li, R. Y., Yang, X. Y., Cui, Q. F., Wang, F. Y., Lin, G. Q., et al. (2019). Co-administration of Shexiang Baoxin Pill and chemotherapy drugs potentiated cancer therapy by vascular-promoting strategy. *Front. Pharmacol.* 10, 565. doi: 10.3389/fphar.2019.00565

Zhao, Y. N., Shao, X., Ouyang, L. F., Chen, L., and Gu, L. (2018). Qualitative detection of ginsenosides in brain tissues after oral administration of high-purity ginseng total saponins by using polyclonal antibody against ginsenosides. *Chin. J. Nat. Med.* 16, 175–183. doi: 10.1016/S1875-5364(18)30045-1

Conflict of Interest: The two authors, C-SZ and X-HS, are employed by the following companies: Shanghai Hutchison Pharmaceuticals Ltd. and Shanghai Engineering Research Center for Innovation of Solid Preparation of TCM.

The remaining authors declare that the research was conducted in the absence of any commercial or financial relationships that could be construed as a potential conflict of interest.

Copyright © 2020 Hu, Mak, Zheng, Xia, Xu, Duan, Dong, Li, Zhan, Shang and Tsim. This is an open-access article distributed under the terms of the Creative Commons Attribution License (CC BY). The use, distribution or reproduction in other forums is permitted, provided the original author(s) and the copyright owner(s) are credited and that the original publication in this journal is cited, in accordance with accepted academic practice. No use, distribution or reproduction is permitted which does not comply with these terms.

frontiers in Physiology

ORIGINAL RESEARCH
published: 17 July 2020
doi: 10.3389/fphys.2020.00805

Qiliqiangxin Capsules Optimize Cardiac Metabolism Flexibility in Rats With Heart Failure After Myocardial Infarction

*Wenkun Cheng, Lei Wang, Tao Yang, Aiming Wu, Baofu Wang, Tong Li, Ziwen Lu, Jingjing Yang, Yang Li, Yangyang Jiang, Xiaoxiao Wu, Hui Meng and Mingjing Zhao**

Key Laboratory of Chinese Internal Medicine of Ministry of Education and Beijing, Dongzhimen Hospital, Beijing University of Chinese Medicine, Beijing, China

Metabolic modulation is a promising therapy for ischemic heart disease and heart failure. This study aimed to clarify the regional modulatory effect of Qiliqiangxin capsules (QLQX), a traditional Chinese medicine, on cardiac metabolic phenotypes. Sprague–Dawley rats underwent left anterior descending coronary artery ligation and were treated with QLQX and enalapril. Striking global left ventricular dysfunction and left ventricular remodeling were significantly improved by QLQX. In addition to the posterior wall, QLQX also had a unique beneficial effect on the anterior wall subject to a severe oxygen deficit. Cardiac tissues in the border and remote areas were separated for detection. QLQX enhanced the cardiac ^{18}F-fluorodeoxyglucose uptake and the levels and translocation of glucose transport 4 (GLUT4) in the border area. Meanwhile, it also suppressed glucose transport 1 (GLUT1) in both areas, indicating that QLQX encouraged border myocytes to use more glucose in a GLUT4-dependent manner. It was inferred that QLQX promoted a shift from glucose oxidation to anaerobic glycolysis in the border area by the augmentation of phosphorylated pyruvate dehydrogenase, pyruvate dehydrogenase kinases 4, and lactic dehydrogenase A. QLQX also upregulated the protein expression of fatty acid translocase and carnitine palmitoyl transferase-1 in the remote area to possibly normalize fatty acid (FA) uptake and oxidation similar to that in healthy hearts. QLQX protected global viable cardiomyocytes and promoted metabolic flexibility by modulating metabolic proteins regionally, indicating its potential for driving the border myocardium into an anaerobic glycolytic pathway against hypoxia injuries and urging the remote myocardium to oxidize FA to maximize energy production.

Keywords: metabolic flexibility, heart failure, Qiliqiangxin capsules, metabolic modulation, border area, remote area

OPEN ACCESS

Edited by:
Jing-Yan Han,
Peking University, China

Reviewed by:
Maria Pia Gallo,
University of Turin, Italy
Mara Brancaccio,
University of Turin, Italy

***Correspondence:**
Mingjing Zhao
mjgx2004@163.com

Specialty section:
This article was submitted to Vascular Physiology, a section of the journal Frontiers in Physiology

Received: *18 December 2019*
Accepted: *17 June 2020*
Published: *17 July 2020*

Citation:
Cheng W, Wang L, Yang T, Wu A, Wang B, Li T, Lu Z, Yang J, Li Y, Jiang Y, Wu X, Meng H and Zhao M (2020) Qiliqiangxin Capsules Optimize Cardiac Metabolism Flexibility in Rats With Heart Failure After Myocardial Infarction. Front. Physiol. 11:805. doi: 10.3389/fphys.2020.00805

INTRODUCTION

Ischemic heart disease and chronic heart failure (HF) remain major causes of mortality worldwide despite advances made dramatically in therapeutic approaches on neurohormones and devices (Lytvyn et al., 2017). "Metabolic modulation" proved to be a promising pharmacological strategy by optimizing cardiac substrate preference given that substrate perturbations might underlie contractile dysfunction and left ventricular (LV) remodeling (Noordali et al., 2018; Birkenfeld et al., 2019). However, only few metabolic regulators are available in the clinic, accounting for insufficient evidence. Healthy adult hearts prefer fatty acids (FA) as the predominant energy source for 60–90%

of adenosine triphophate (ATP) production (Kolwicz et al., 2013). Of importance is that "metabolic flexibility" empowers a normal heart to switch between FA and other alternative substrates, including glucose, ketone bodies, and amino acids, depending on alterations in physiological conditions, thus ensuring continuous contractility (Gupta and Houston, 2017; Bertero and Maack, 2018). It is generally considered that the failing heart prefers glucose over FA, eliciting a current therapeutic paradigm that increasing glucose oxidation (or depressing FA utilization) is cardioprotective as glucose expends less oxygen for ATP generation (Liao et al., 2002; Li et al., 2016). Unexpectedly, either increasing glucose uptake by specific overexpression of GLUT1 in the murine heart (Yan et al., 2009) or depriving FA acutely using acipimox (Wolf et al., 2016) deteriorates cardiac metabolic inflexibility and functional failure. In addition, high fat feeding to increase FA oxidation (FAO) improves LV function in rats with myocardial infarction (MI) (Berthiaume et al., 2012). Hence, whether to further promote glucose utilization or normalize substrate to FA still remains unresolved (Lionetti et al., 2011). Currently, agents that stimulate glucose or FA might be tested further as they induce inflexibility. It is cautiously concluded that promoting metabolic extremes, either preference or inhibition for any one substrate, makes the heart further lose its flexibility and become vulnerable to adverse injuries under stressors. FA and glucose metabolism are both indispensable, and recovering substrate flexibility is a more desirable target for long-term metabolic modulation.

Recently, region-dependent LV remodeling after MI invoked great interest for its potential to detect more sensitive variables for prognosis and treatment (Torres et al., 2018; van Duijvenboden et al., 2019). According to the proximal–distal axis, the infarcted myocardium is divided into an infarcted area, a border area (adjacent to scar; hypoperfused), and a remote area (distal to scar; perfused) (van Duijvenboden et al., 2019). A series of studies confined the border area to be a discrete zone with hallmarks of unique structural (Sharov et al., 1997), mechanical (Torres et al., 2018), and transcriptional properties (van Duijvenboden et al., 2019) distinct from the remote myocardium. Importantly, metabolic remodeling post-MI is also identified as spatial non-uniformity. The transcriptome and regulatory profiles of mitochondrial oxidative phosphorylation and FAO and glucose metabolism were more perturbed in the border area than in remote areas (Rosenblatt-Velin et al., 2001; van Duijvenboden et al., 2019). It was proposed that the regional modulation of cardiac substrate utilization, that is, selecting the appropriate ones for distinct areas based on their local microenvironment, is a promising target for motivating metabolic flexibility.

Qiliqiangxin capsules (QLQX), a listed traditional Chinese medicine comprising 11 herbs, were approved by the China Food and Drug Administration in 2004. Its main components include Astragali Radix, Ginseng Radix et Rhizoma, Aconiti Lateralis Radix Preparata, Salvia Miltiorrhiza Radix et Rhizoma, Alismatis Rhizoma, Descuraunia Semen, Cinnamomi Ramulus, Carthami Flos, Periplocae Cortex, Polygonati Odorati Rhizoma, and Citri Reticulatae Pericarpium (Li et al., 2013; Zhang et al., 2019). The favorable efficacy of QLQX in HF therapy has been confirmed by a multicentral large-scale clinical trial (Li et al., 2013; Tang and Huang, 2013) and several lab experiments (Tao et al., 2015; Liang et al., 2016; Han et al., 2018). Interestingly, QLQX has a multi-target enhancing effect on cardiac FAO, glucose oxidation, and glycolysis (Shen et al., 2017; Wang et al., 2017, 2018), implying that QLQX might modulate substrate utilization by promoting metabolic flexibility. Thus, this study was designed to ascertain whether QLQX enabled the border and remote myocardium to choose individual optimal metabolic phenotype for improving global energetic efficiency. Glucose utilization was observed by positron emission tomography (PET), and changes in a range of metabolic enzymes were detected in both border and remote areas post-MI.

MATERIALS AND METHODS

HF Model After MI in Rats

Male Sprague–Dawley rats (230–250 g) were obtained from Beijing Vital River Laboratory Animal Technology Co., Ltd. [Animal license number: SCXK (Beijing) 2016-0006]. HF after MI was induced surgically in rats by left anterior descending coronary artery (LAD) ligation as described previously (Wu et al., 2013; Yang et al., 2019). Briefly, following anesthesia with sodium pentobarbital (40 mg/kg intraperitoneally) and intubation, a lateral thoracotomy was carried out to access the heart. The LAD occlusion was located between the pulmonary cone and the left atrial appendage 2–3 mm from the origin, using a 5–0 proline suture. The animals were maintained for 60 days after the surgery in a 12:12 h light–dark cycle at 24°C ± 1°C and a humidity of 60 ± 10% with *ad libitum* access to standard chow and water. Following the ligation or sham operation, the surviving rats were randomly assigned to four groups: sham group (sham, $n = 8$), model group (MI, $n = 8$), QLQX group (MI + QLQX, $n = 8$), and enalapril group (MI + enalapril, $n = 8$). All experimental procedures were approved by the Animal Care and Use Committee of Beijing University of Chinese Medicine and conformed with laboratory animal management and use regulations.

Drug and Interventions

Qiliqiangxin capsules (A20170820) were purchased from Shijiazhuang Yiling Pharmaceutical Co., Ltd. (Shijiazhuang, Hebei, China). The high reproducibility of QLQX was clarified by a fingerprint analysis, which exhibited a high similarity of 10 batches ranging from 0.978 to 1.000 (Zhang J. et al., 2013). Previous chemical analysis of QLQX, which was obtained from the same supplier and had the same batch number with QLQX in this study, identified the profile and concentrations of stable active ingredients (Fan et al., 2019). Enalapril was obtained from Yangzijiang Pharmaceutical Group Jiangsu Pharmaceutical Co., Ltd. (Taizhou, Jiangsu, China) as the positive control. Both the drug powder of Qiliqiangxin capsules and enalapril were dissolved in distilled water. From the second day after the surgery, Qiliqiangxin capsules and enalapril were administered for 60 days at doses of 0.514 g/(kg . d) and 2.857 mg/(kg . d), respectively (equivalent to 10 times the clinical dose), by gavage

once a day. An equal volume of distilled water was administered to the sham and MI groups.

Echocardiography

Transthoracic echocardiography was performed non-invasively 60 days after the surgery to assess LV structure and function using a Vevo 2100 high-resolution imaging system equipped with a 15-MHz transducer (VisualSonics, Toronto, Canada). Two-dimensional, M-mode parasternal echocardiograms from the long-axis view were captured for determining the ejection fraction (EF), fractional shortening (FS), LV end-systolic, and end-diastolic internal diameters (LVIDs and LVIDd), LV end-systolic and end-diastolic volumes (LVESV and LVEDV), LV end-systolic and end-diastolic anterior wall thicknesses (LVAWs and LVAWd), and LV end-systolic and end-diastolic posterior wall thicknesses (LVPWs and LVPWd).

Positron Emission Tomography

Regional myocardial utilization of glucose was determined by ^{18}F-fluorodeoxyglucose (^{18}F-FDG)-PET using a Micro PET/computed tomography (CT) scanner (Inveon, Siemens, TN, United States). ^{18}F-FDG, a glucose analog radiotracer (radiochemical purity > 95%), was synthesized by HTA Co., Ltd. (Beijing, China). Following fasting for 15–19 h prior to imaging, the rats were subjected to FDG administration as a bolus intravenous injection via the tail vein with the mean activities of approximately 1.0 mCi. All *in vivo* imaging experiments were carried out under inhalation anesthesia using isoflurane (induced with 4% and maintained with 1.5–2% concentration). The animal was then positioned prone on the scanner bed with the heart centered in the field of view. A 10-min separate CT acquisition was performed for anatomical reference before PET scanning at 80 kV, 500 μA, and 260-ms exposure time with a thickness of 0.22 mm. Then, a static 15-min PET scan was initiated 60 min after FDG injection. The CT data were reconstructed using a cone beam Feldkamp reconstruction algorithm (COBRA) method, and PET images were reconstructed using a three-dimensional ordered subset expectation maximization (OSEM3D)/maximum *a posteriori* (MAP) algorithm (2/18 iterations) with the matrix size of 128 × 128 voxels and the requested resolution of 1.5 mm. The ^{18}F-FDG uptake of LV myocardial segments was analyzed in the Inveon Research Workplace and quantified as a standardized uptake value (SUV). The PET images were re-angulated to typical heart short-axis and horizontal and vertical long-axis views and the regions of interest (ROI) were defined to the infarcted border area and the remote area (Tao et al., 2015; Zhang et al., 2018).

Western Blot Analysis

Myocardial tissues in both the infarcted border area and remote area were homogenized in radio immunoprecipitation assay (RIPA) lysis buffer (Applygen Technologies, Beijing, China) for total cell protein extraction, followed by protein quantification using a bicinchoninic acid (BCA) protein assay kit (Applygen Technologies, Beijing, China). Equal amounts of proteins (50 μg) were separated on a 4–12% gradient sodium dodecyl sulfate polyacrylamide gel electrophoresis (SDS-PAGE) gel and transferred onto nitrocellulose membranes in the transfer buffer. The membranes were probed with primary antibodies diluted in 5% w/v non-fat milk/Tris-buffered saline-Tween overnight at 4°C and then incubated for 1 h with appropriate horseradish peroxidase (HRP)-conjugated secondary antibodies (diluted 1:5000, Boster Biological Technology, Wuhan, China) at room temperature. The primary antibodies against glucose transporter 4 (GLUT4, 1:2000 dilution), glucose transporter 1 (GLUT1, 1:10,000 dilution), pyruvate dehydrogenase (PDH, 1:5000 dilution), phosphorylated PDH (p-PDH, 1:5000 dilution), pyruvate dehydrogenase kinase 4 (PDK4, 1:2000 dilution), lactate dehydrogenase A (LDHA, 1:1000 dilution), fatty acid translocase (FAT/CD36, 1:500 dilution), and carnitine palmitoyl transferase-1 (CPT-1, 1:500 dilution) were all from Abcam (Cambridge, United Kingdom). Glyceraldehyde-3-phosphate dehydrogenase (GAPDH) (1:5000 dilution, Applygen Technologies) was measured as a loading control. Finally, proteins were visualized with an enhanced chemiluminescence kit (Beyotime Biotechnology, Jiangsu, China) and quantified using ImageJ.

Histopathologic Staining

Cardiac tissue specimens embedded in paraffin were cut into 3-μm-thick transverse sections, mounted on glass slides and stained with hematoxylin and eosin (H&E) to assess cardiomyocyte morphology. Immunohistochemical analysis and immunofluorescence microscopy were also performed. Immunohistochemical staining was performed to determine several important metabolic proteins in the border and remote areas. The slides were submerged in citrate solution (pH 6.0) for heat-mediated antigen retrieval and incubated with 3% hydrogen peroxide (H_2O_2) to block endogenous peroxidase. After blocking with non-immune goat serum, the slices were incubated with primary antibodies raised against GLUT1 (diluted 1:500), GLUT4 (diluted 1:800), LDHA (diluted 1:1500), and CD36 (diluted 1:200) overnight at 4°C, followed by incubation with an HRP-conjugated goat anti-rabbit immunoglobulin G (IgG) secondary antibody at 37°C for 30 min. The staining was then developed with a diaminobenzidine (DAB) detection kit (ZSGB-BIO, Beijing, China). Immunofluorescence staining was carried out to observe the subcellular localization of GLUT4 and GLUT1. After permeabilization with 0.1% Triton X-100 in phosphate-buffered saline (PBS), the specimens were stained with primary antibodies against GLUT4 (diluted 1:500) and GLUT1 (diluted 1:500) overnight at 4°C and a subsequent Dylight 649-conjugated goat anti-rabbit IgG secondary antibody (Abbkine Scientific Co., Ltd., Wuhan, China) at a dilution of 1:500 for 1 h at room temperature. The slides were mounted using a fluorescent mounting medium containing 4,6-diamidino-2-phenylindole (DAPI), and the images were acquired with a Leica TCS SP8X confocal microscope (Leica, Wetzlar, Germany). Leica confocal software was employed to quantify the fluorescence intensity of sarcolemma and cytosol. The results were presented as the ratio of the expression levels of GLUTs.

Determination of Lactate, Na^+/K^+-ATPase, and Ca^{2+}-ATPase

The lactate content and the activities of Na^+/K^+-ATPase and Ca^{2+}-ATPase in the border-area myocardium were determined

with a lactate assay kit, an Na^+/K^+-ATPase assay kit, and a Ca^{2+}-ATPase assay kit, respectively (Nanjing Jiancheng Bioengineering Institute, Nanjing, China). The procedures were conducted in accordance with the kit instructions strictly.

Statistical Analysis

All data were presented as the means ± standard deviation (SD). Overall variables with normal distribution were analyzed using the Shapiro–Wilk test of normality. A one-way analysis of variance was conducted for comparisons of multiple groups, followed by pairwise comparisons with the least significant difference *post-hoc* testing or with Tamhane' T2 otherwise. The difference between mean SUVs in the border and remote areas was analyzed using a paired *t*-test. Analyses were performed with IBM SPSS Statistics 20. A *P*-value less than 0.05 was considered statistically significant.

RESULTS

Qiliqiangxin Improved Cardiac Function and Structure in Rats With HF

The cardiac function and structural changes in HF rats were measured with echocardiography and H&E staining. Significant decreases in EF and FS were noted in rats with MI 8 weeks after infarction, accompanied by much higher LVIDs, LVIDd, LVESV, and LVEDV as well as lower LVAWs, LVAWd, LVPWs, and LVPWd. In response to drug treatment, QLQX ameliorated impaired EF and FS post-MI and prevented LV remodeling by reducing the diameters and volumes. Enalapril mainly improved cavity dilatation but had minimal effect on the values of EF and FS. Besides, QLQX recovered both thinned LV anterior wall and posterior wall induced by MI, but enalapril only thickened the posterior wall (**Figure 1A**). Consistently, the morphological assessment showed that the MI group was characterized by a moderate disarrangement in the remote-area myocardium, which was rescued by both QLQX and enalapril. Also, marked necrosis of myofibrils, inflammatory infiltration, and interstitial fibrosis in the border area was relieved by only QLQX (**Figure 1B**).

Qiliqiangxin Optimized the Glucose Metabolism in the Remote- and Border-Area Myocardia in Rats With HF

Glucose metabolism in the myocardium was assessed using ^{18}F-FDG PET/CT. The fasted sham rats showed a minimal cardiac ^{18}F-FDG uptake in the remote and border areas. In comparison, a substantial uptake of ^{18}F-FDG in the border area and a slight increase in the remote area were induced after MI. In the border area, a rather higher ^{18}F-FDG uptake than that in rats with MI was observed in the QLQX and enalapril groups according to the mean and maximum (max) SUV with a consistent trend followed in minimum (min) SUV. However, in the remote area, the ^{18}F-FDG uptake was moderately elevated by QLQX, and enalapril might exert a more obvious promoting effect primarily indicated in min SUV. The comparisons of mean SUV between the two areas in each group showed no regional difference in the sham groups, but the ^{18}F-FDG uptake in the border area was much higher than that in the remote area in the MI, QLQX, and enalapril groups (**Figure 2**).

Qiliqiangxin Regulated GLUT1 and GLUT4 in the Remote- and Border-Area Myocardia in Rats With HF

To further verify metabolic changes shown in the results of ^{18}F-FDG PET, the total cell protein expression levels of GLUT4 and GLUT1 contributing to glucose uptake in the heart were determined by Western blot and immunohistochemical analyses. The results showed that MI led to a significant attenuation of insulin-sensitive GLUT4 but augmentation of insulin-insensitive GLUT1 in the border and remote areas. Following the treatment with QLQX and enalapril, the protein content of GLUT4 remained unchanged in the remote area but increased in the border area (**Figures 3A,B**), concomitant with a great suppressive effect on GLUT1 in both areas (**Figures 3D,E**). Subsequently, trafficking of the two glucose transporter isoforms was detected by immunofluorescence staining. The ratio of sarcolemmal and cytosolic GLUT4 in either remote or border area was dampened by MI; the ratio in the border myocardium showed significant increments in the treated groups (**Figure 3C**). However, MI stimulated the ratio of GLUT1 localized in the sarcolemma to that in the cytoplasm in both areas, which obviously reduced in response to QLQX and enalapril, but had no significant effect in the enalapril group in the remote area (**Figure 3F**).

Qiliqiangxin Affected the Glucose Oxidation Proteins in the Remote- and Border-Area Myocardia in Rats With HF

PDH, the rate-limiting enzyme of glucose oxidation, is inactivated via phosphorylation by specific PDH kinase (Stanley et al., 2005). Western blot analysis of the total-PDH (t-PDH) and phospho-PDH protein (p-PDH) expression in cardiac tissues helped in figuring out the glucose oxidation changes in all groups. Decreased phosphorylation of PDH, t-PDH expression (despite no statistical difference in the remote area), and ratio of p-PDH/t-PDH in both areas were found in the MI group. However, only the reduction of phospho-PDH, t-PDH, and p-PDH/t-PDH ratio in the border area rather than in the remote area was upregulated by QLQX and enalapril (**Figures 4A,B**). Consistently, cardiac expression of PDK4, the predominant PDH kinase isoform in the heart, was significantly suppressed in the MI group in both areas, and treatment with QLQX induced PDK4 only in the border area (**Figure 4C**).

Qiliqiangxin Modulated LDHA Expression in the Remote- and Border-Area Myocardia in Rats With HF

Western blot and immunochemistry examinations of LDHA were performed to further determine the glycolytic process in all

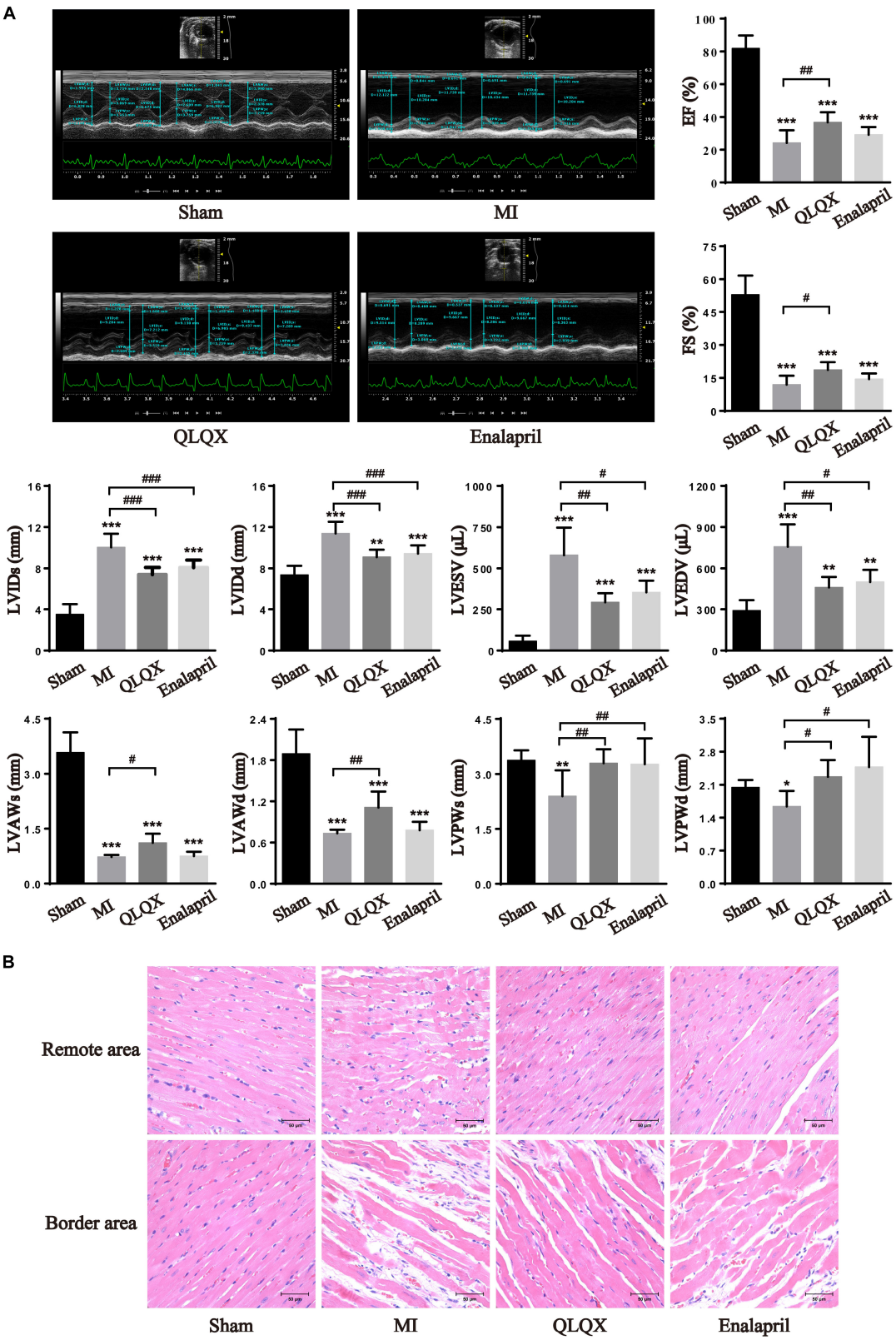


FIGURE 1 | Continued

FIGURE 1 | QLQX improved cardiac structure and function 8 weeks after MI. **(A)** Echocardiography parameters in all groups (n = 8 per group). EF: sham: 81.85 ± 7.90%; MI: 24.21 ± 7.68%; QLQX: 36.73 ± 6.16%; enalapril: 29.16 ± 4.65%. FS: sham: 53.00 ± 8.71%; MI: 12.00 ± 4.01%; QLQX: 18.65 ± 3.49%; enalapril: 14.45 ± 2.55%. LVIDs: sham: 3.52 ± 0.98 mm; MI: 10.04 ± 1.31 mm; QLQX: 7.40 ± 0.69 mm; enalapril: 8.07 ± 0.73 mm. LVIDd: sham: 7.37 ± 0.88 mm; MI: 11.39 ± 1.14 mm; QLQX: 9.09 ± 0.71 mm; enalapril: 9.44 ± 0.80 mm. LVESV: sham: 57.11 ± 33.07 μL; MI: 580.07 ± 167.32 μL; QLQX: 292.39 ± 57.34 μL; enalapril: 354.87 ± 70.37 μL. LVEDV: sham: 291.60 ± 74.64 μL; MI: 757.30 ± 162.17 μL; QLQX: 464.14 ± 75.98 μL; enalapril: 500.73 ± 89.07 μL. LVAWs: sham: 3.58 ± 0.55 mm; MI: 0.72 ± 0.05 mm; QLQX: 1.12 ± 0.25 mm; enalapril: 0.74 ± 0.13 mm. LVAWd: sham: 1.89 ± 0.35 mm; MI: 0.73 ± 0.05 mm; QLQX: 1.11 ± 0.23 mm; enalapril: 0.78 ± 0.12 mm. LVPWs: sham: 3.37 ± 0.27 mm; MI: 2.39 ± 0.70 mm; QLQX: 3.29 ± 0.38 mm; enalapril: 3.27 ± 0.71 mm. LVPWd: sham: 2.04 ± 0.16 mm; MI: 1.64 ± 0.33 mm; QLQX: 2.27 ± 0.36 mm; enalapril: 2.48 ± 0.64 mm. **(B)** H&E staining of heart tissues in the remote area and border area. Values are means ± SD. $^{*}P < 0.05$, $^{**}P < 0.01$, $^{***}P < 0.001$ vs. the sham group; $^{\#}P < 0.05$, $^{\#\#}P < 0.01$, $^{\#\#\#}P < 0.001$ vs. the MI group.

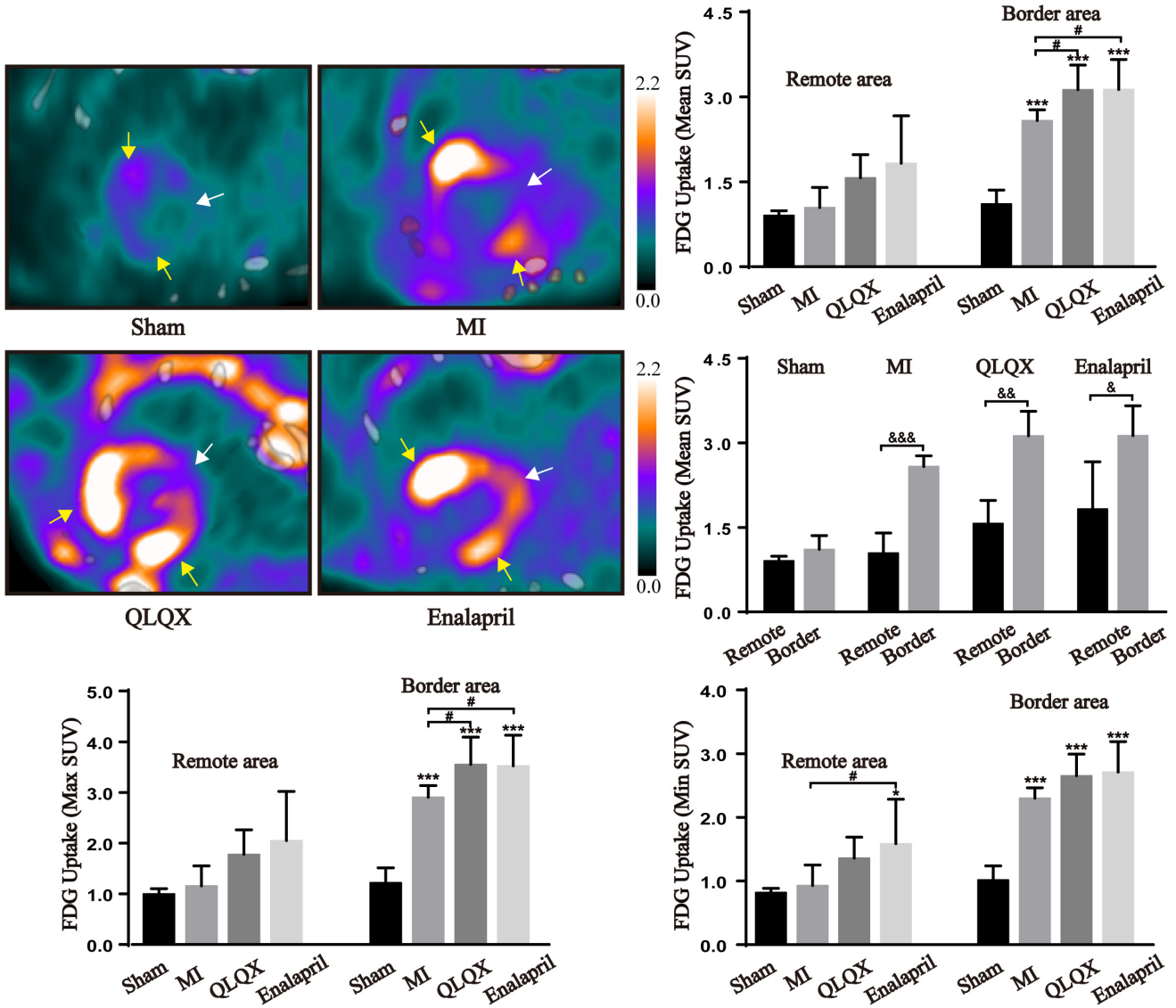


FIGURE 2 | QLQX optimized the cardiac glucose metabolism 8 weeks after MI. The representative cardiac images of ^{18}F-FDG PET/CT in all groups (remote area: white arrows; border area: yellow arrows) and the mean SUV, max SUV, and min SUV of ^{18}F-FDG in the remote area (sham: 0.91 ± 0.08, 1.00 ± 0.10, and 0.82 ± 0.06, respectively, MI: 1.04 ± 0.36, 1.16 ± 0.40, and 0.93 ± 0.32, respectively, QLQX: 1.57 ± 0.41, 1.78 ± 0.48, and 1.36 ± 0.33, respectively, enalapril: 1.83 ± 0.84, 2.05 ± 0.97, and 1.58 ± 0.70, respectively) and in the border area (sham: 1.11 ± 0.25, 1.22 ± 0.29, and 1.02 ± 0.22, respectively, MI: 2.58 ± 0.19, 2.91 ± 0.23, and 2.30 ± 0.16, respectively, QLQX: 3.13 ± 0.44, 3.55 ± 0.54, and 2.65 ± 0.34, respectively, enalapril: 3.13 ± 0.53, 3.52 ± 0.61, and 2.71 ± 0.48, respectively) myocardium (n = 5 per group). Values are means ± SD. $^{*}P < 0.05$, $^{***}P < 0.001$ vs. the sham group; $^{\#}P < 0.05$ vs. the MI group; $^{\&}P < 0.05$, $^{\&\&}P < 0.01$, $^{\&\&\&}P < 0.001$ vs. the remote area.

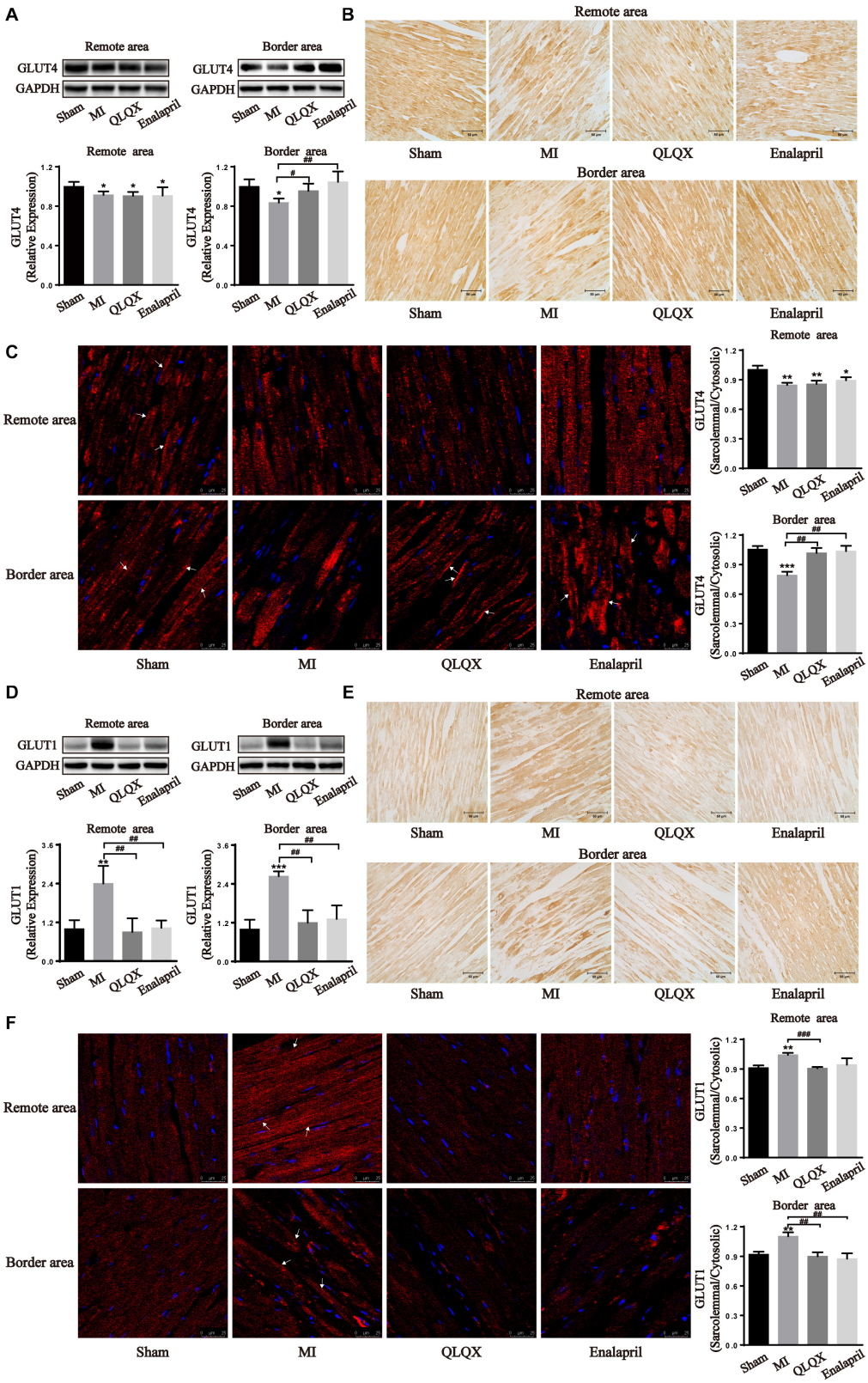


FIGURE 3 | Continued

FIGURE 3 | Effects of QLQX on glucose uptake transporters in infarcted hearts. **(A,D)** Western blot analysis of GLUT4 and GLUT1 protein expression in the remote area and border area (n = 3 or 4 per group). GLUT4: remote area: sham: 1.00 ± 0.04, MI: 0.91 ± 0.03, QLQX: 0.91 ± 0.04, enalapril: 0.91 ± 0.09; border area: sham: 1.00 ± 0.07, MI: 0.84 ± 0.04, QLQX: 0.96 ± 0.07, enalapril: 1.05 ± 0.11. GLUT1: remote area: sham: 1.00 ± 0.27, MI: 2.40 ± 0.55, QLQX: 0.90 ± 0.42, enalapril: 1.03 ± 0.23; border area: sham: 1.00 ± 0.29, MI: 2.64 ± 0.15, QLQX: 1.20 ± 0.39, enalapril: 1.32 ± 0.42. **(B,E)** Immunochemical staining of GLUT4 and GLUT1 in the remote and border areas. **(C,F)** Ratio of sarcolemmal to cytosolic expression of GLUT4 and GLUT1 and respective images of immunofluorescence confocal microscopy (indicated with arrows) in remote and border areas (n = 4 per group). GLUT4: remote area: sham: 1.00 ± 0.04, MI: 0.85 ± 0.02, QLQX: 0.86 ± 0.03, enalapril: 0.89 ± 0.03; border area: sham: 1.06 ± 0.03, MI: 0.79 ± 0.04, QLQX: 1.02 ± 0.05, enalapril: 1.04 ± 0.05. GLUT1: remote area: sham: 0.91 ± 0.02, MI: 1.04 ± 0.02, QLQX: 0.91 ± 0.01, enalapril: 0.94 ± 0.06; border area: sham: 0.92 ± 0.03, MI: 1.10 ± 0.04, QLQX: 0.90 ± 0.04, enalapril: 0.88 ± 0.05. **(B,E)** Immunochemical staining of GLUT4 and GLUT1 in the remote and border areas. Values are means ± SD. $^{*}P < 0.05$, $^{**}P < 0.01$, $^{***}P < 0.001$ vs. the sham group; $^{\#}P < 0.05$, $^{\#\#}P < 0.01$, $^{\#\#\#}P < 0.001$ vs. the MI group.

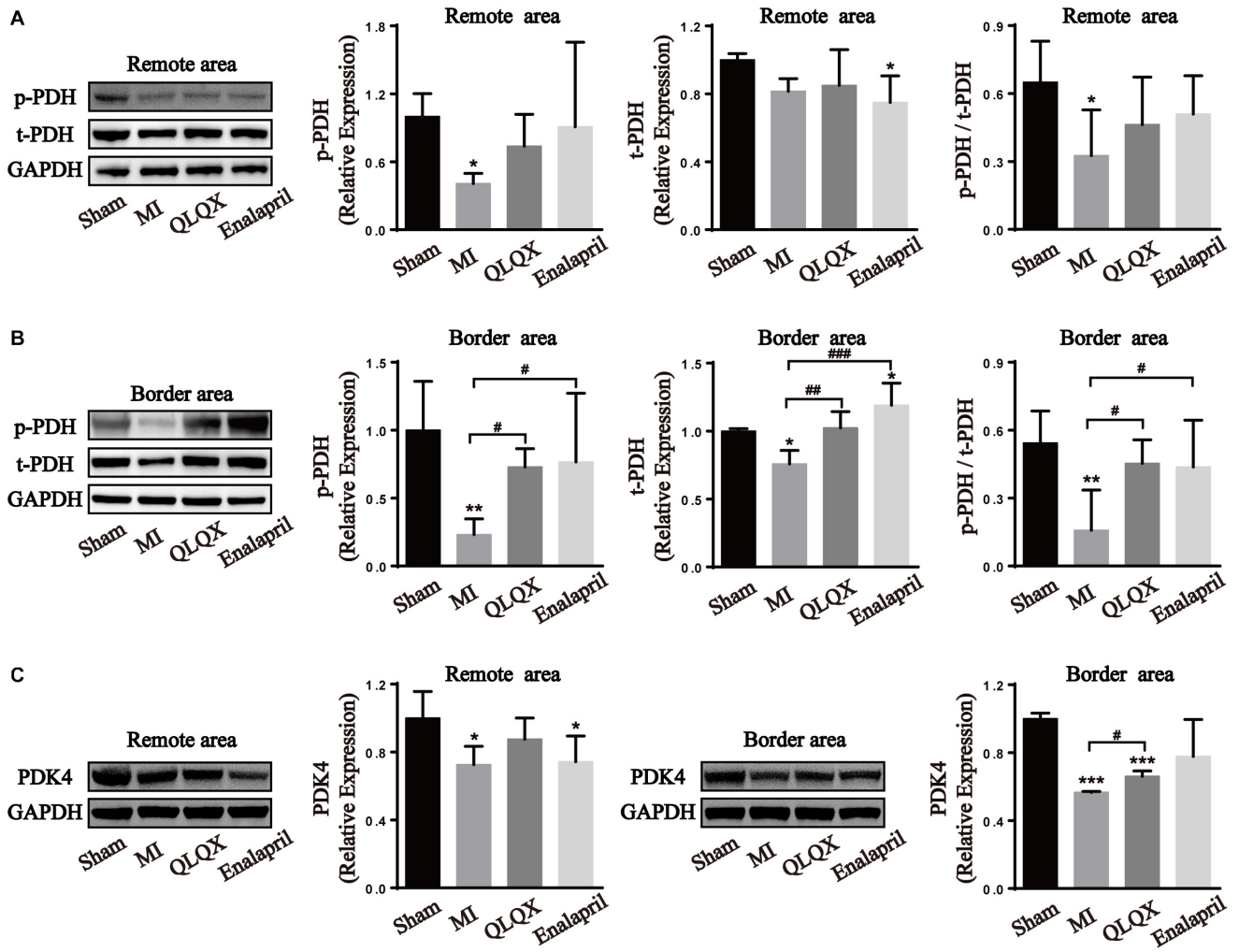


FIGURE 4 | Effects of QLQX on glucose oxidation enzymes in infarcted hearts. **(A)** Cardiac level of p-PDH, t-PDH, and the ratio of p-PDH to t-PDH in the remote area (n = 4 per group). Sham: 1.00 ± 0.20, 1.00 ± 0.04, and 0.65 ± 0.18, respectively, MI: 0.41 ± 0.09, 0.82 ± 0.07, and 0.33 ± 0.20, respectively, QLQX: 0.74 ± 0.28, 0.85 ± 0.21, and 0.46 ± 0.21, respectively, enalapril: 0.91 ± 0.75, 0.75 ± 0.16, and 0.51 ± 0.17, respectively. **(B)** Cardiac level of p-PDH, t-PDH, and the ratio of p-PDH to t-PDH in the border area (n = 4 per group). Sham: 1.00 ± 0.36, 1.00 ± 0.02, and 0.54 ± 0.14, respectively, MI: 0.23 ± 0.12, 0.76 ± 0.10, and 0.16 ± 0.18, respectively, QLQX: 0.73 ± 0.14, 1.02 ± 0.12, and 0.45 ± 0.10, respectively, enalapril: 0.77 ± 0.50, 1.19 ± 0.16, and 0.44 ± 0.21, respectively. **(C)** Western blot analysis of PDK4 in remote and border areas (n = 4 per group). Remote area: sham: 1.00 ± 0.16; MI: 0.73 ± 0.11; QLQX: 0.88 ± 0.12; enalapril: 0.74 ± 0.15. Border area: sham: 1.00 ± 0.03; MI: 0.57 ± 0.01; QLQX: 0.66 ± 0.03; enalapril: 0.78 ± 0.22. Values are means ± SD. $^{*}P < 0.05$, $^{**}P < 0.01$, $^{***}P < 0.001$ vs. the sham group;$^{\#}P < 0.05$, $^{\#\#}P < 0.01$, $^{\#\#\#}P < 0.001$ vs. the MI group.

groups. The results show that infarcted hearts were characterized by a marked decline in LDHA protein expression in the remote and border areas. LDHA content was induced in the border area but remained unchanged in the remote area by QLQX treatment. Meanwhile, LDHA in neither the border area nor in the remote area was influenced by enalapril (**Figures 5A,B**).

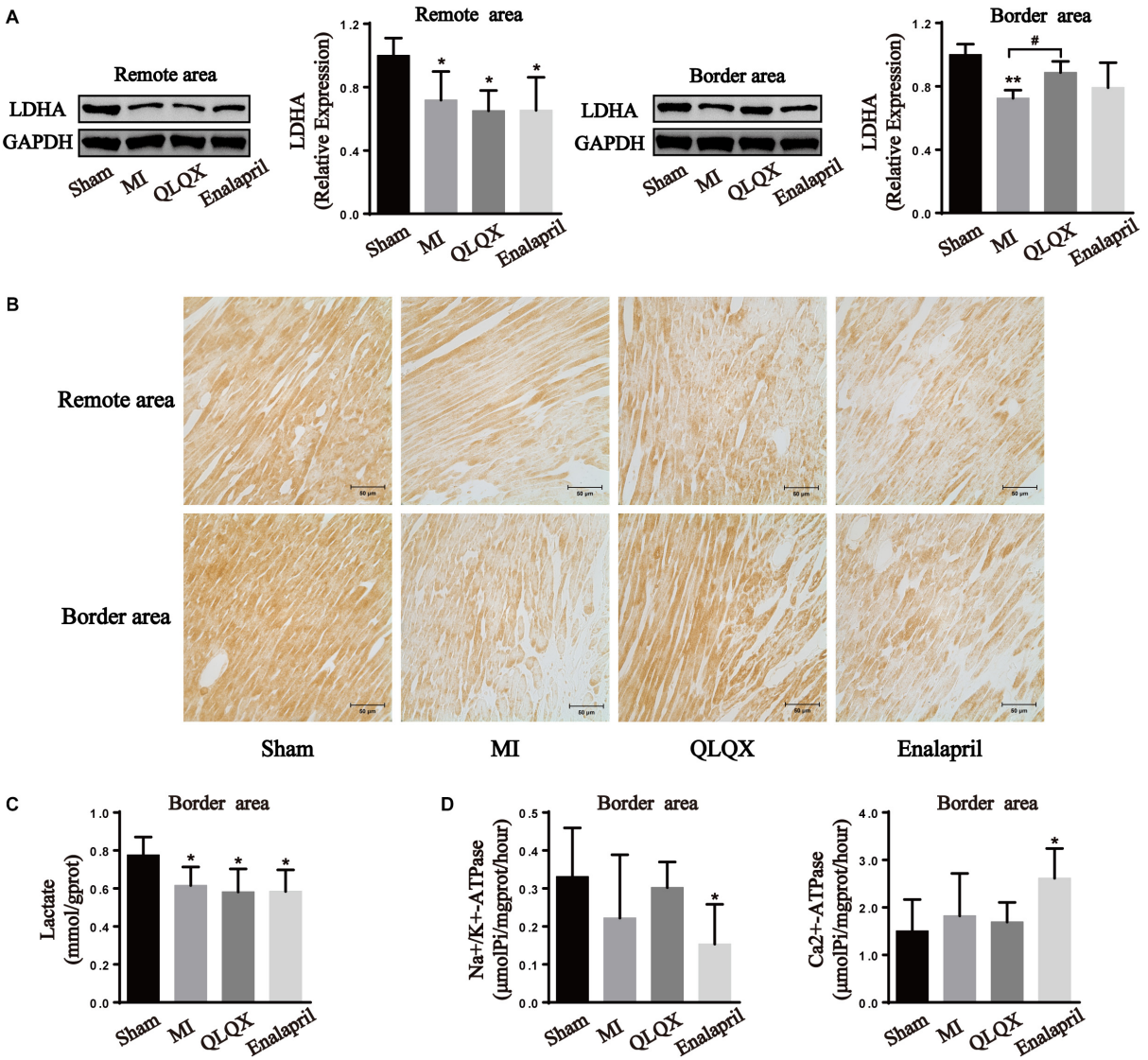


FIGURE 5 | Effects of QLQX on anaerobic glycolytic enzymes in infarcted hearts. **(A)** Western blot analysis of LDHA protein expression in remote and border areas (n = 4 per group). Remote area: sham: 1.00 ± 0.11; MI: 0.72 ± 0.18; QLQX: 0.65 ± 0.13; enalapril: 0.65 ± 0.21. Border area: sham: 1.00 ± 0.07; MI: 0.72 ± 0.05; QLQX: 0.89 ± 0.07; enalapril: 0.79 ± 0.16. **(B)** Immunochemical staining of LDHA in the remote and border areas. **(C)** Contents of lactate in the border area (n = 6–8 per group). Sham: 0.78 ± 0.10; MI: 0.62 ± 0.10; QLQX: 0.58 ± 0.12; enalapril: 0.58 ± 0.11. **(D)** Activity of Na^+/K^+-ATPase and Ca^{2+}-ATPase in the border area (n = 6–8 per group). Na^+/K^+-ATPase: sham: 0.33 ± 0.13; MI: 0.22 ± 0.17; QLQX: 0.30 ± 0.07; enalapril: 0.15 ± 0.10. Ca^{2+}-ATPase: sham: 1.50 ± 0.67; MI: 1.82 ± 0.89; QLQX: 1.70 ± 0.41; enalapril: 2.61 ± 0.63. Values are means ± SD. $^*P < 0.05$, $^{**}P < 0.01$ vs. the sham group; $^{\#}P < 0.05$ vs. the MI group.

Qiliqiangxin Did Not Adversely Affect Lactate Production and Ionic Homeostasis in the Border-Area Myocardium in Rats With HF

The results show that the content of lactate in the border-area cardiac tissue decreased in the MI group, but QLQX and enalapril had no effect on the content (**Figure 5C**). A downward trend was noted for Na^+/K^+-ATPase of the infarcted heart. QLQX did not show obvious effects on the content, whereas the Na^+/K^+-ATPase activity was significantly lower in the enalapril group than in the sham rats. Meanwhile, no significant differences were observed in the Ca^{2+}-ATPase of the sham, MI, and QLQX groups, and enalapril elevated cardiac Ca^{2+}-ATPase activity exceeding that in the sham group (**Figures 5C,D**).

Qiliqiangxin Influenced FA Metabolism Proteins in the Remote- and Border-Area Myocardia in Rats With HF

Moreover, the two proteins promoting FA metabolism were also determined. The infarcted heart showed a great reduction in the protein expression of CD36, a marker of FA uptake, and CPT-1, a marker of FA mitochondrial oxidation. QLQX

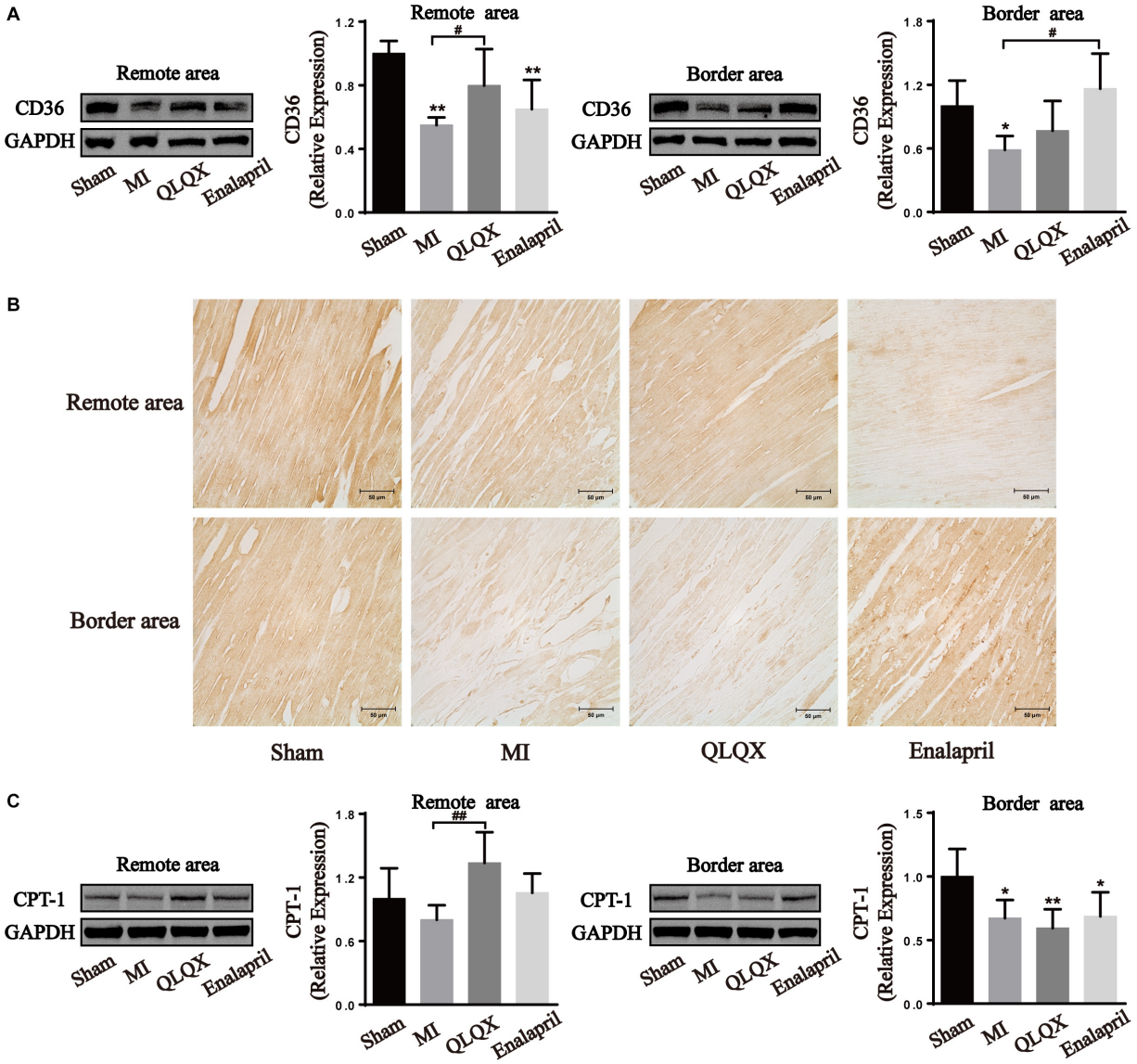


FIGURE 6 | The effects of QLQX on fatty acid uptake and oxidation proteins in failing infarcted hearts. **(A)** Western blot analysis of CD36 protein expression in remote and border areas (n = 4 per group). Remote area: sham: 1.00 ± 0.08; MI: 0.55 ± 0.05; QLQX: 0.80 ± 0.23; enalapril: 0.65 ± 0.18. Border area: sham: 1.00 ± 0.24; MI: 0.59 ± 0.13; QLQX: 0.77 ± 0.28; enalapril: 1.16 ± 0.33. **(B)** Immunochemical staining of CD36 in remote and border areas. **(C)** Western blot analysis of CPT-1 in remote and border areas (n = 4 per group). Remote area: sham: 1.00 ± 0.29; MI: 0.80 ± 0.14; QLQX: 1.34 ± 0.29; enalapril: 1.06 ± 0.18. Border area: sham: 1.00 ± 0.22; MI: 0.67 ± 0.14; QLQX: 0.59 ± 0.15; enalapril: 0.69 ± 0.19. Values are means ± SD. $^{*}P < 0.05$, $^{**}P < 0.01$ vs. the sham group; $^{\#}P < 0.05$, $^{\#\#}P < 0.01$ vs. the MI group.

significantly increased the expression level of CD36 and CPT-1 in the remote-area myocardium, but no difference between QLQX group and MI group was detectable in the border area. Enalapril appeared to upregulate only the CD36 expression in the border area (**Figure 6**).

DISCUSSION

Myocardial metabolic deterioration is the intrinsic hallmark of ischemic heart disease and HF, supporting the intriguing therapeutic perspectives of metabolic modulators (Doehner et al., 2014). However, the current pharmaceutical interventions aiming at energy substrates are worth further discussion considering their preference for a specific fuel at the expense of metabolic flexibility (Peterzan et al., 2017). Flexibility modulation is believed to be a more accurate target despite barely matched therapy. After MI, the injured ventricle undergoes a spatial heterogeneity in structural, mechanical, and metabolic remodeling response to a pathological environment (Sharov et al., 1997; Torres et al., 2018; van Duijvenboden et al., 2019). Hence, compelling distinct zones preferring the same substrate seem to

compromise the substrate flexibility. It may be better to treat the infarcted heart by separating it into two sections: the border area and the remote area.

QLQX has been proven to have a great potential as a promising metabolic modulator as it can regulate cardiac glucose and FA metabolism simultaneously by upregulating a large number of enzymes, including GLUT4, GLUT1, CD36, and so forth in different pathological models (Shen et al., 2017; Wang et al., 2017, 2018). This multi-targeting regulation might depend on the multiple components identified in QLQX, encompassing ginsenoside Rb1, astragaloside, salvianolic acid A, and so forth (Zhang et al., 2019). Most of these components have demonstrated an ability to target energy metabolism (Dong et al., 2017; Zheng et al., 2017; Cui et al., 2018). Enalapril is a classic medication for HF, which blocks the renin–angiotensin–aldosterone system (Yusuf et al., 1991). It is widely believed that enalapril predominantly aims at alleviating ventricular remodeling. However, the fact that enalapril lessens cardiac workload and energy demands provides indirect evidence for its metabolism-modulating properties (Gupta and Houston, 2017). Recently, angiotensin II has been clarified to induce a pronounced elevation in the levels of GLUT1 and a suppression of FAO enzymes, CD36, CPT-1, and so forth (Pellieux et al., 2006, 2009), directly highlighting that enalapril might also be a metabolic regulator. So, with enalapril as the control intervention, the results further reveal that QLQX enabled border and remote cardiomyocytes to metabolize different substrates according to the pathological conditions to fulfill energy demands in both areas and ultimately improve LV dysfunction and LV remodeling throughout the heart.

QLQX Protected Global LV Function and Structure

The echocardiography data from this study confirmed that a stable contractile dysfunction and LV dilatation occurred in the rat model of MI induced by LAD ligation for 8 weeks, consistent with previous results (Tao et al., 2015). QLQX could profoundly elevate the LV function. Both QLQX and enalapril alleviated cardiac dilatation (LVIDs, LVIDd, LVESV, and LVEDV). In the infarcted heart, LVAW and LVPW reduced, indicating an ongoing loss of viable myocardium, which originated from LVAW and progressively extended to LVPW. Both LVAW and LVPW were elevated by QLQX, whereas only LVPW was enhanced by enalapril. LVAW anatomically resembles the infarct and border areas, and LVPW equals the remote area. The results demonstrate that the myocardium in the border area was potentially salvageable and not only cells in the distal region, QLQX was also confirmed to preserve the survival cardiomyocytes closet to the scar. The morphological assessments support this conclusion.

QLQX Augmented Myocardial Glucose Uptake in the Border Area

An infarcted heart is commonly assumed to undergo a shift from FAO to glucose metabolism. Animal micro PET/CT has helped obtain the region-specific properties of myocardial glucose uptake. In line with other studies (Rosenblatt-Velin et al., 2001; Zhang et al., 2018), it has been observed that MI aroused a striking increase in glucose uptake, primarily distributed in the border area. QLQX and enalapril predominately evoked a stronger glucose entry into border cardiomyocytes but only exerted moderate effects on remote cells. The comparison of the mean SUV in the border and remote areas provided evidence that QLQX treatment favored regional differences in glucose uptake. The aforementioned glucose uptake alternations might be related to the regulation of glucose transporters. The two isoforms in human hearts, GLUT4 and GLUT1, facilitate glucose transport into cardiomyocytes by trafficking from the cytoplasm to the sarcolemma (Zhang L. et al., 2013). In the present study, GLUT4 protein expression appeared lower, whereas GLUT1 expression markedly increased throughout the infarcted heart. In addition, the ratio of sarcolemmal to cytosolic contents of GLUT4 also significantly decreased in both areas, suggesting a weakened translocation. However, the trafficking of GLUT1 was notably stimulated, indicating that MI led to a glucose uptake increase, yet in a GLUT1-dependent manner. GLUT4 is insulin dependent and serves as the major isoform in the adult myocardium, and the insulin-insensitive GLUT1 predominates in fetal hearts (Tran and Wang, 2019). The transition from GLUT4 to GLUT1 has been found in ischemic and failed myocardia previously; nevertheless, the mechanism remains unknown (Remondino et al., 2000; Rosenblatt-Velin et al., 2001). In the context of HF, insulin resistance weakens GLUT4 availability (Karwi et al., 2019). Therefore, GLUT1 expression may increase to compensate. QLQX and enalapril did not modify GLUT4 in the remote area but upregulated GLUT4 content and translocation in the border area significantly. In addition, QLQX downregulated GLUT1 in the entire myocardium, and so did enalapril, probably because angiotensin II might be an underlying activator of GLUT1 (Rosenblatt-Velin et al., 2001). The observations implied that QLQX and enalapril promoted glucose uptake in the border area in a GLUT4-dependent manner.

Compared with FA, glucose is considered more oxygen effective because it consumes less oxygen to produce the same amount of ATP (Peterzan et al., 2017), making it a preferred fuel to enhance cardiac efficiency under oxygen-limited conditions. However, long-term FAO deficiency cannot be totally compensated by glucose metabolism (van Bilsen et al., 2009). Hence, the modulation of QLQX to further stimulate glucose uptake only in the border area, which is injured more severely due to oxygen deprivation, may help in protecting against hypoxic damage without excessive glucose burden in the remote area.

QLQX Might Switch Metabolic Pathways From Glucose Oxidation to Glycolysis in the Border Area

Glucose is metabolized via oxidation under normoxic conditions alternatively via anaerobic glycolysis in oxygen deficits (Gupta and Houston, 2017). Pyruvate derived from glucose is converted

into acetyl-CoA for aerobic respiration by PDH which is inhibited when phosphorylated by PDH kinases, or it is converted into lactate and toward the anaerobic glycolytic pathway by LDH (Heggermont et al., 2016). Consistent with the changes in glucose utilization shown in PET, remarkable reductions in p-PDH expression and ratio of p-PDH/t-PDH in both border and remote areas were detected as indicative of a global enhancement in the glucose oxidative process. Concomitantly, QLQX and enalapril might prevent cardiomyocytes in the border area preferring excessive glucose oxidation, but they maintained, to some extent, the augmented glucose oxidation in the remote area, which was indicated by its promoting effect on the phosphorylation of PDH only in the border area. The concordant PDK4 changes further explained the distinct modulation of PDH in both areas with QLQX.

It is expected that an uncoupling between glycolysis and glucose oxidation and augmentation of anaerobic process are induced in HF (Lopaschuk, 2017). However, the present study argues an obvious absence of LDHA in both remote and border areas indicating glycolytic dysfunction. Similar results show that cardiomyocytes in the MI border zone failed to upregulate glycolysis-related genes and revert to glycolysis resembling the neonatal metabolic phenotype (van Duijvenboden et al., 2019). Further, the activity of LDH in the myocardium declined in a 6-week MI rat model, suggesting abnormal anaerobic energy generation (Afanasiev et al., 2014). QLQX exhibited a regional effect again in that it elevated the declined LDHA expression in the border area but not in the remote area. It seems that enalapril did not play a regulatory role in LDHA expression in the two areas. The lactate content and the activity of Na^+/K^+-ATPase and Ca^{2+}-ATPase were detected to further confirm whether QLQX could cause intracellular acidosis and disturb ion homeostasis in the border area attributed to its promoting effect on glycolysis. It became evident that the lactate production in the border myocardium of rats with MI was declined, which was consistent with the debilitated LDH expression. In a similar case, the cardiac release of purines and lactate decreased in rats with MI 8 weeks after infarction, indicating attenuated sensitivity to chronic ischemia of the infarcted myocardium (Kalkman et al., 1996). QLQX did not increase the lactate level, and the uncoupling of LDHA expression and lactate level in the QLQX group might be due to the conducive clearance of myocardial lactic acid by the active ingredients, such as ginsenoside and astragaloside (Chen et al., 2006; Yang et al., 2017). Consequently, disordered Na^+/K^+-ATPase and Ca^{2+}-ATPase caused by intracellular acidosis was not observed in the MI and QLQX groups. Collectively, QLQX could enhance glycolysis without deteriorating lactate production and ionic homeostasis in the border area.

Taken together, it appears that QLQX drives the infarcted heart to use different glucose metabolic pathways in discrete zones via modulating key enzymes, that is, partially keeping oxidizing glucose within the remote area while transiting oxidation to anaerobic glycolysis in the border area. To save the extremely hypoxic myocytes closest to the necrosis, the shift to anaerobic metabolism may be required for rapid energy generation without using much oxygen (Abdurrachim et al., 2015). On the contrary, for the myocardium away from the scar with better perfusion, not suppressing increased glucose oxidation contributes to less accumulation of protons and lactate from glycolysis. This advantage in terms of metabolic regulation distinguishes QLQX from enalapril. Hence, it protects the myocardium in both hypoxia-injured anterior and posterior walls.

QLQX Might Enhance FA Metabolism in the Remote Area

A dramatic decrease in FAO has been observed in HF probably due to either mitochondrial capacity abnormalities (Murphy and Hartley, 2018) or compromised FAO enzymes. In keeping with this, the present findings confirm reduced expression of CD36, a transporter involved in FA uptake, and CPT-1, which assists in FA entry into mitochondria throughout the myocardium. Further, a potential regional property of QLQX regulation on FAO was noted, which preserved the reduced CD36 and CPT-1 protein contents in the border myocytes but had a strong promoting effect on these two proteins in the remote myocardium. Reversely, enalapril only upregulated the CD36 protein expression in the border area.

FA is often discarded owing to its high oxygen consumption and potential lipotoxicity when modulating cardiac substrates in HF (Heggermont et al., 2016). However, increasing glucose by irreversibly removing FA may not be possible (He et al., 2012; Nakatani et al., 2013), and enhancing FA preference may be an alternative phenotype to restore cardiac energetics and function (Kaimoto et al., 2017). Considering that FA produces approximately three times the ATP per molecule compared with glucose (Peterzan et al., 2017), FA seems to be more efficient when oxygen is not limited in HF. Thus, stimulating FAO in the remote area may maximize energy synthesis to ensure effective functioning of myocytes. Conversely, maintaining FA utilization at a low level in the border area could avoid exacerbating hypoxic and lipotoxic injuries to the myocardium. The effects of QLQX on CD36 and CPT-1 indicate that it might exert a benign regulatory effect on cardiac FA metabolism although it requires further exploration. Enalapril has the potential to improve FA metabolism probably because angiotensin II exerts a strong suppressing effect on FAO and related genes. However, in the present study, enalapril seemed to augment only FA uptake transporter rather than the expression of FAO enzymes in the border area, implying that it was ineffective in anterior wall damage.

It is speculated that the regional metabolic regulatory advantage of QLQX might be a comprehensive outcome of its multicomponent and multi-target features. First, various components exert different regulatory effects on FAO and glycolysis. Ginsenosides, Astragaloside IV, and salsolinol, which were extracted from Ginseng Radix, Astragali Radix, and Aconiti Lateralis Radix Praeparata, in QLQX have been proven to upregulate myocardial FAO in HF (Kong et al., 2018; Tang et al., 2018; Chen et al., 2019; Wen et al., 2019). Salsolinol also could enhance glycolysis capacity, but salvianolic acid B, extracted from another herb in QLQX, inhibits cardiac

glycolysis (Xu et al., 2011). It is worth noting that Astragaloside IV reduces anaerobic glycolysis in the failing heart (Dong et al., 2017), but Astragali Radix itself could increase LDH expression level in human cardiomyocytes (Wang et al., 1979), suggesting other bioactive components of Astragali Radix at work in promoting glycolysis. Second, multiple components work cooperatively. A higher salvianolic acid B concentration was found in the cardiac ischemic area than in the non-ischemic area (Xu et al., 2011). Hence, it was inferred that the distribution of other ingredients in cardiac distinct areas might also be inhomogeneous. Additionally, the regulatory effect on targets of some components also seems to have obvious regional properties in the MI heart exemplified by the effect on energy disorder induced by MI. Radix Aconiti Lateralis Preparata extract predominately optimized the distribution patterns of energy metabolism–related molecules in the non-infarct zone (Wu et al., 2019). Therefore, under different pathological conditions, the distribution of pathological targets in remote and border areas might be dissimilar, which may induce specific active ingredients to reach different regions to exert their effects.

CONCLUSION

In conclusion, the observations confirmed that HF did result in a shift from FAO to glucose oxidation. For better accommodation with each microenvironment and energy demands, it is possible that QLQX could encourage the border myocardium (anterior wall) to favor anaerobic glycolysis but facilitate the remote area (posterior wall) to rely more on FA metabolism by regulating respective key enzymes, probably due to its multi-target effect. This region-dependent performance reserves metabolism flexibility to ensure energy efficiency, and a decrease in the levels of toxic intermediates in the distinct area concurrently. Despite the promising findings, the exact mechanism by which QLQX optimizes cardiac substrates regionally has yet to be determined. In addition, this study only focused on the regional issue; the metabolic modulation of QLQX in different-stage HF needs further investigation.

DATA AVAILABILITY STATEMENT

All datasets generated for this study are included in the article/supplementary material.

ETHICS STATEMENT

The animal study was reviewed and approved by the Animal Care and Use Committee of the Beijing University of Chinese Medicine.

AUTHOR CONTRIBUTIONS

WC was responsible for the experiment conduction, data analyses, and manuscript writing. LW, TY, and AW assisted in performing the animal experiments. BW, TL, and ZL contributed to the PET/CT examinations and analysis. JY and YL participated in the manuscript revision. YJ, XW, and HM offered help in the immunostaining and data analysis. MZ conceived and designed this study, supervised and wrote the manuscript, and provided expertise and continuous guidance as well as necessary reagents and equipment. All authors contributed to the article and approved the submitted version.

FUNDING

This study was funded by the National Natural Science Foundation of China (Grant No. 81541075) and the Beijing Municipal Natural Science Foundation Key Project (Grant No. 7161008).

ACKNOWLEDGMENTS

We would like to thank the financial support from the National Natural Science Foundation of China and the Beijing Municipal Natural Science Foundation.

REFERENCES

Abdurrachim, D., Luiken, J. J., Nicolay, K., Glatz, J. F., Prompers, J. J., and Nabben, M. (2015). Good and bad consequences of altered fatty acid metabolism in heart failure: evidence from mouse models. *Cardiovasc. Res.* 106, 194–205. doi: 10.1093/cvr/cvv105

Afanasiev, S. A., Egorova, M. V., Kondratyeva, D. S., Batalov, R. E., and Popov, S. V. (2014). Comparative analysis of changes of myocardial angiogenesis and energy metabolism in postinfarction and diabetic damage of rat heart. *J. Diabetes Res.* 2014:827896. doi: 10.1155/2014/827896

Bertero, E., and Maack, C. (2018). Metabolic remodelling in heart failure. *Nat. Rev. Cardiol.* 15, 457–470. doi: 10.1038/s41569-018-0044-6

Berthiaume, J. M., Young, M. E., Chen, X., McElfresh, T. A., Yu, X., and Chandler, M. P. (2012). Normalizing the metabolic phenotype after myocardial infarction: impact of subchronic high fat feeding. *J. Mol. Cell Cardiol.* 53, 125–133. doi: 10.1016/j.yjmcc.2012.04.005

Birkenfeld, A. L., Jordan, J., Dworak, M., Merkel, T., and Burnstock, G. (2019). Myocardial metabolism in heart failure: purinergic signalling and other metabolic concepts. *Pharmacol. Ther.* 194, 132–144. doi: 10.1016/j.pharmthera.2018.08.015

Chen, X., Wang, Q., Shao, M., Ma, L., Guo, D., Wu, Y., et al. (2019). Ginsenoside Rb3 regulates energy metabolism and apoptosis in cardiomyocytes via activating PPARalpha pathway. *Biomed. Pharmacother.* 120:109487. doi: 10.1016/j.biopha.2019.109487

Chen, X. J., Meng, D., Feng, L., Bian, Y. Y., Li, P., Yang, D., et al. (2006). Protective effect of astragalosides on myocardial injury by isoproterenol in SD rats. *Am. J. Chin. Med.* 34, 1015–1025. doi: 10.1142/s0192415x0600448x

Cui, Y. C., Yan, L., Pan, C. S., Hu, B. H., Chang, X., Fan, J. Y., et al. (2018). The contribution of different components in QiShenYiQi Pills(R) to its potential to modulate energy metabolism in protection of ischemic myocardial injury. *Front. Physiol.* 9:389. doi: 10.3389/fphys.2018.00389

Doehner, W., Frenneaux, M., and Anker, S. D. (2014). Metabolic impairment in heart failure: the myocardial and systemic perspective. *J. Am. Coll. Cardiol.* 64, 1388–1400. doi: 10.1016/j.jacc.2014.04.083

Dong, Z., Zhao, P., Xu, M., Zhang, C., Guo, W., Chen, H., et al. (2017). Astragaloside IV alleviates heart failure via activating PPARalpha to switch

glycolysis to fatty acid beta-oxidation. *Sci. Rep.* 7:2691. doi: 10.1038/s41598-017-02360-5

Fan, C., Tang, X., Ye, M., Zhu, G., Dai, Y., Yao, Z., et al. (2019). Qi-Li-Qiang-Xin alleviates isoproterenol-induced myocardial injury by inhibiting excessive autophagy via activating AKT/mTOR pathway. *Front. Pharmacol.* 10:1329. doi: 10.3389/fphar.2019.01329

Gupta, A., and Houston, B. (2017). A comprehensive review of the bioenergetics of fatty acid and glucose metabolism in the healthy and failing heart in nondiabetic condition. *Heart Fail Rev.* 22, 825–842. doi: 10.1007/s10741-017-9623-6

Han, A., Lu, Y., Zheng, Q., Zhang, J., Zhao, Y., Zhao, M., et al. (2018). Qiliqiangxin attenuates cardiac remodeling via inhibition of TGF-beta1/Smad3 and NF-kappaB signaling pathways in a rat model of myocardial infarction. *Cell Physiol. Biochem.* 45, 1797–1806. doi: 10.1159/000487871

He, L., Kim, T., Long, Q., Liu, J., Wang, P., Zhou, Y., et al. (2012). Carnitine palmitoyltransferase-1b deficiency aggravates pressure overload-induced cardiac hypertrophy caused by lipotoxicity. *Circulation* 126, 1705–1716. doi: 10.1161/circulationaha.111.075978

Heggermont, W. A., Papageorgiou, A. P., Heymans, S., and van Bilsen, M. (2016). Metabolic support for the heart: complementary therapy for heart failure? *Eur. J. Heart Fail.* 18, 1420–1429. doi: 10.1002/ejhf.678

Kaimoto, S., Hoshino, A., Ariyoshi, M., Okawa, Y., Tateishi, S., Ono, K., et al. (2017). Activation of PPAR-alpha in the early stage of heart failure maintained myocardial function and energetics in pressure-overload heart failure. *Am. J. Physiol. Heart Circ. Physiol.* 312, H305–H313. doi: 10.1152/ajpheart.00553.2016

Kalkman, E. A., Saxena, P. R., and Schoemaker, R. G. (1996). Sensitivity to ischemia of chronically infarcted rat hearts; effects of long-term captopril treatment. *Eur. J. Pharmacol.* 298, 121–128. doi: 10.1016/0014-2999(95)00784-9

Karwi, Q. G., Zhang, L., Wagg, C. S., Wang, W., Ghandi, M., Thai, D., et al. (2019). Targeting the glucagon receptor improves cardiac function and enhances insulin sensitivity following a myocardial infarction. *Cardiovasc. Diabetol.* 18:1. doi: 10.1186/s12933-019-0806-4

Kolwicz, S. C. Jr., Purohit, S., and Tian, R. (2013). Cardiac metabolism and its interactions with contraction, growth, and survival of cardiomyocytes. *Circ. Res.* 113, 603–616. doi: 10.1161/circresaha.113.302095

Kong, H. L., Hou, A. J., Liu, N. N., Chen, B. H., Dai, S. N., and Huang, H. T. (2018). The effects of ginsenoside Rb1 on fatty acid beta-oxidation, mediated by AMPK, in the failing heart. *Iran. J. Basic Med. Sci.* 21, 731–737. doi: 10.22038/ijbms.2018.24002.6016

Li, X., Liu, Y., Ma, H., Guan, Y., Cao, Y., Tian, Y., et al. (2016). Enhancement of glucose metabolism via PGC-1alpha participates in the cardioprotection of chronic intermittent hypobaric hypoxia. *Front. Physiol.* 7:219. doi: 10.3389/fphys.2016.00219

Li, X., Zhang, J., Huang, J., Ma, A., Yang, J., Li, W., et al. (2013). A multicenter, randomized, double-blind, parallel-group, placebo-controlled study of the effects of qili qiangxin capsules in patients with chronic heart failure. *J. Am. Coll. Cardiol.* 62, 1065–1072. doi: 10.1016/j.jacc.2013.05.035

Liang, T., Zhang, Y., Yin, S., Gan, T., An, T., Zhang, R., et al. (2016). Cardio-protecteffect of qiliqiangxin capsule on left ventricular remodeling, dysfunction and apoptosis in heart failure rats after chronic myocardial infarction. *Am. J. Transl. Res.* 8, 2047–2058.

Liao, R., Jain, M., Cui, L., D'Agostino, J., Aiello, F., Luptak, I., et al. (2002). Cardiac-specific overexpression of GLUT1 prevents the development of heart failure attributable to pressure overload in mice. *Circulation* 106, 2125–2131. doi: 10.1161/01.cir.0000034049.61181.f3

Lionetti, V., Stanley, W. C., and Recchia, F. A. (2011). Modulating fatty acid oxidation in heart failure. *Cardiovasc. Res.* 90, 202–209. doi: 10.1093/cvr/cvr038

Lopaschuk, G. D. (2017). Metabolic modulators in heart disease: past, present, and future. *Can. J. Cardiol.* 33, 838–849. doi: 10.1016/j.cjca.2016.12.013

Lytvyn, Y., Bjornstad, P., Udell, J. A., Lovshin, J. A., and Cherney, D. Z. I. (2017). Sodium glucose cotransporter-2 inhibition in heart failure: potential mechanisms, clinical applications, and summary of clinical trials. *Circulation* 136, 1643–1658. doi: 10.1161/CIRCULATIONAHA.117.030012

Murphy, M. P., and Hartley, R. C. (2018). Mitochondria as a therapeutic target for common pathologies. *Nat. Rev. Drug Discov.* 17, 865–886. doi: 10.1038/nrd.2018.174

Nakatani, K., Masuda, D., Oka, T., Okada, T., Kawase, R., Nakaoka, H., et al. (2013). Pressure overload induces hypertrophy and impaired cardiac function in long-chain fatty acid transporter CD36 knockout mice. *Circulation* 128:A12900.

Noordali, H., Loudon, B. L., Frenneaux, M. P., and Madhani, M. (2018). Cardiac metabolism – a promising therapeutic target for heart failure. *Pharmacol. Ther.* 182, 95–114. doi: 10.1016/j.pharmthera.2017.08.001

Pellieux, C., Aasum, E., Larsen, T. S., Montessuit, C., Papageorgiou, I., Pedrazzini, T., et al. (2006). Overexpression of angiotensinogen in the myocardium induces downregulation of the fatty acid oxidation pathway. *J. Mol. Cell Cardiol.* 41, 459–466. doi: 10.1016/j.yjmcc.2006.06.004

Pellieux, C., Montessuit, C., Papageorgiou, I., and Lerch, R. (2009). Angiotensin II downregulates the fatty acid oxidation pathway in adult rat cardiomyocytes via release of tumour necrosis factor-alpha. *Cardiovasc. Res.* 82, 341–350. doi: 10.1093/cvr/cvp004

Peterzan, M. A., Lygate, C. A., Neubauer, S., and Rider, O. J. (2017). Metabolic remodeling in hypertrophied and failing myocardium: a review. *Am. J. Physiol. Heart. Circ. Physiol.* 313, H597–H616. doi: 10.1152/ajpheart.00731.2016

Remondino, A., Rosenblatt-Velin, N., Montessuit, C., Tardy, I., Papageorgiou, I., Dorsaz, P. A., et al. (2000). Altered expression of proteins of metabolic regulation during remodeling of the left ventricle after myocardial infarction. *J. Mol. Cell Cardiol.* 32, 2025–2034. doi: 10.1006/jmcc.2000.1234

Rosenblatt-Velin, N., Montessuit, C., Papageorgiou, I., Terrand, J., and Lerch, R. (2001). Postinfarction heart failure in rats is associated with upregulation of GLUT-1 and downregulation of genes of fatty acid metabolism. *Cardiovasc. Res.* 52, 407–416. doi: 10.1016/s0008-6363(01)00393-5

Sharov, V. G., Sabbah, H. N., Ali, A. S., Shimoyama, H., Lesch, M., and Goldstein, S. (1997). Abnormalities of cardiocytes in regions bordering fibrous scars of dogs with heart failure. *Int. J. Cardiol.* 60, 273–279. doi: 10.1016/s0167-5273(97)00117-4

Shen, S., Jiang, H., Bei, Y., Zhang, J., Zhang, H., Zhu, H., et al. (2017). Qiliqiangxin attenuates adverse cardiac remodeling after myocardial infarction in ovariectomized mice via activation of PPARgamma. *Cell Physiol. Biochem.* 42, 876–888. doi: 10.1159/000478641

Stanley, W. C., Recchia, F. A., and Lopaschuk, G. D. (2005). Myocardial substrate metabolism in the normal and failing heart. *Physiol. Rev.* 85, 1093–1129. doi: 10.1152/physrev.00006.2004

Tang, B., Zhang, J. G., Tan, H. Y., and Wei, X. Q. (2018). Astragaloside IV inhibits ventricular remodeling and improves fatty acid utilization in rats with chronic heart failure. *Biosci. Rep.* 38:BSR20171036. doi: 10.1042/BSR20171036

Tang, W. H. W., and Huang, Y. (2013). Cardiotonic modulation in heart failure: insights from traditional Chinese medicine. *J. Am. Coll. Cardiol.* 62, 1073–1074. doi: 10.1016/j.jacc.2013.05.028

Tao, L., Shen, S., Fu, S., Fang, H., Wang, X., Das, S., et al. (2015). Traditional chinese medication qiliqiangxin attenuates cardiac remodeling after acute myocardial infarction in mice. *Sci. Rep.* 5:8374. doi: 10.1038/srep08374

Torres, W. M., Jacobs, J., Doviak, H., Barlow, S. C., Zile, M. R., Shazly, T., et al. (2018). Regional and temporal changes in left ventricular strain and stiffness in a porcine model of myocardial infarction. *Am. J. Physiol. Heart Circ. Physiol.* 315, H958–H967. doi: 10.1152/ajpheart.00279.2018

Tran, D. H., and Wang, Z. V. (2019). Glucose metabolism in cardiac hypertrophy and heart failure. *J. Am. Heart Assoc.* 8:e012673. doi: 10.1161/jaha.119.012673

van Bilsen, M., van Nieuwenhoven, F. A., and van der Vusse, G. J. (2009). Metabolic remodelling of the failing heart: beneficial or detrimental? *Cardiovasc. Res.* 81, 420–428. doi: 10.1093/cvr/cvn282

van Duijvenboden, K., de Bakker, D. E. M., Man, J. C. K., Janssen, R., Gunthel, M., Hill, M. C., et al. (2019). Conserved NPPB+ border zone switches from MEF2- to AP-1-driven gene program. *Circulation* 140, 864–879. doi: 10.1161/circulationaha.118.038944

Wang, B. Z., Yang, M. G., Pang, L., and Yu, Z. J. (1979). [Effect of Hong-Hua (Flos Carthami) on the extent of myocardial ischemia in the different infarct zones following coronary occlusion in the dog (author's transl)]. *Yao Xue Xue Bao* 14, 474–479.

Wang, J., Li, Z., Wang, Y., Zhang, J., Zhao, W., Fu, M., et al. (2017). Qiliqiangxin enhances cardiac glucose metabolism and improves diastolic function in spontaneously hypertensive rats. *Evid. Based Complement Alternat. Med.* 2017:3197320. doi: 10.1155/2017/3197320

Wang, Y., Han, X., Fu, M., Wang, J., Song, Y., Liu, Y., et al. (2018). Qiliqiangxin attenuates hypoxia-induced injury in primary rat cardiac microvascular endothelial cells via promoting HIF-1alpha-dependent glycolysis. *J. Cell Mol. Med.* 22, 2791–2803. doi: 10.1111/jcmm.13572

Wen, J., Zhang, L., Liu, H., Wang, J., Li, J., Yang, Y., et al. (2019). Salsolinol attenuates doxorubicin-induced chronic heart failure in rats and improves mitochondrial function in H9c2 cardiomyocytes. *Front. Pharmacol.* 10:1135. doi: 10.3389/fphar.2019.01135

Wolf, P., Winhofer, Y., Krssak, M., Smajis, S., Harreiter, J., Kosi-Trebotic, L., et al. (2016). Suppression of plasma free fatty acids reduces myocardial lipid content and systolic function in type 2 diabetes. *Nutr. Metab. Cardiovasc. Dis.* 26, 387–392. doi: 10.1016/j.numecd.2016.03.012

Wu, A., Zhai, J., Zhang, D., Lou, L., Zhu, H., Gao, Y., et al. (2013). Effect of wenxin granule on ventricular remodeling and myocardial apoptosis in rats with myocardial infarction. *Evid. Based Complement Alternat. Med.* 2013:967986. doi: 10.1155/2013/967986

Wu, H., Liu, X., Gao, Z. Y., Dai, Z. F., Lin, M., Tian, F., et al. (2019). Anti-myocardial infarction effects of radix aconiti lateralis preparata extracts and their influence on small molecules in the heart using matrix-assisted laser desorption/ionization-mass spectrometry imaging. *Int. J. Mol. Sci.* 20:4837. doi: 10.3390/ijms20194837

Xu, L., Deng, Y., Feng, L., Li, D., Chen, X., Ma, C., et al. (2011). Cardio-protection of salvianolic acid B through inhibition of apoptosis network. *PLoS One* 6:e24036. doi: 10.1371/journal.pone.0024036

Yan, J., Young, M. E., Cui, L., Lopaschuk, G. D., Liao, R., and Tian, R. (2009). Increased glucose uptake and oxidation in mouse hearts prevent high fatty acid oxidation but cause cardiac dysfunction in diet-induced obesity. *Circulation* 119, 2818–2828. doi: 10.1161/circulationaha.108.832915

Yang, T., Lu, Z., Wang, L., Zhao, Y., Nie, B., Xu, Q., et al. (2019). Dynamic changes in brain glucose metabolism and neuronal structure in rats with heart failure. *Neuroscience* 424, 34–44. doi: 10.1016/j.neuroscience.2019.10.008

Yang, Y. L., Li, J., Liu, K., Zhang, L., Liu, Q., Liu, B., et al. (2017). Ginsenoside Rg5 increases cardiomyocyte resistance to ischemic injury through regulation of mitochondrial hexokinase-II and dynamin-related protein 1. *Cell Death Dis.* 8:e2625. doi: 10.1038/cddis.2017.43

Yusuf, S., Pitt, B., Davis, C. E., Hood, W. B., and Cohn, J. N. (1991). Effect of enalapril on survival in patients with reduced left ventricular ejection fractions and congestive heart failure. *N. Engl. J. Med.* 325, 293–302. doi: 10.1056/nejm199108013250501

Zhang, J., Wei, C., Wang, H., Tang, S., Jia, Z., Wang, L., et al. (2013). Protective effect of qiliqiangxin capsule on energy metabolism and myocardial mitochondria in pressure overload heart failure rats. *Evid. Based Complement Alternat. Med.* 2013:378298. doi: 10.1155/2013/378298

Zhang, L., Jaswal, J. S., Ussher, J. R., Sankaralingam, S., Wagg, C., Zaugg, M., et al. (2013). Cardiac insulin-resistance and decreased mitochondrial energy production precede the development of systolic heart failure after pressure-overload hypertrophy. *Circ. Heart Fail.* 6, 1039–1048. doi: 10.1161/circheartfailure.112.000228

Zhang, Q., Shao, M., Zhang, X., Wang, Q., Guo, D., Yang, X., et al. (2018). The effect of chinese medicine on lipid and glucose metabolism in acute myocardial infarction through PPARgamma pathway. *Front. Pharmacol.* 9:1209. doi: 10.3389/fphar.2018.01209

Zhang, Y., Zhu, M., Zhang, F., Zhang, S., Du, W., and Xiao, X. (2019). Integrating pharmacokinetics study, network analysis, and experimental validation to uncover the mechanism of qiliqiangxin capsule against chronic heart failure. *Front. Pharmacol.* 10:1046. doi: 10.3389/fphar.2019.01046

Zheng, X., Wang, S., Zou, X., Jing, Y., Yang, R., Li, S., et al. (2017). Ginsenoside Rb1 improves cardiac function and remodeling in heart failure. *Exp. Anim.* 66, 217–228. doi: 10.1538/expanim.16-0121

Conflict of Interest: The authors declare that the research was conducted in the absence of any commercial or financial relationships that could be construed as a potential conflict of interest.

Copyright © 2020 Cheng, Wang, Yang, Wu, Wang, Li, Lu, Yang, Li, Jiang, Wu, Meng and Zhao. This is an open-access article distributed under the terms of the Creative Commons Attribution License (CC BY). The use, distribution or reproduction in other forums is permitted, provided the original author(s) and the copyright owner(s) are credited and that the original publication in this journal is cited, in accordance with accepted academic practice. No use, distribution or reproduction is permitted which does not comply with these terms.

frontiers in Pharmacology

ORIGINAL RESEARCH
published: 24 July 2020
doi: 10.3389/fphar.2020.01053

Evaluation of Long-Time Decoction-Detoxicated *Hei-Shun-Pian* (Processed *Aconitum carmichaeli* Debeaux Lateral Root With Peel) for Its Acute Toxicity and Therapeutic Effect on Mono-Iodoacetate Induced Osteoarthritis

Lei Zhang[1†], Ting Li[2†], Rongrong Wang[3†], Jiaan Xu[3], Li Zhou[4], Li Yan[3], Zhengyan Hu[5], Hongwen Li[6], Fucun Liu[7], Wenxi Du[4], Peijian Tong[1], Huiling Wu[2*], Shanxing Zhang[4], Letian Shan[4*] and Thomas Efferth[8]*

[1] School of Biological and Chemical Engineering, Zhejiang University of Science and Technology, Hangzhou, China, [2] The First Affiliated Hospital, Zhejiang University School of Medicine, Hangzhou, China, [3] College of Pharmacy, Zhejiang Chinese Medical University, Hangzhou, China, [4] The First Affiliated Hospital, Zhejiang Chinese Medical University, Hangzhou, China, [5] Department of Physicochemistry and Toxicology, Center for Disease Control and Prevention of Zhejiang Province, Hangzhou, China, [6] Experimental and Training Center, Zhejiang Pharmaceutical College, Ningbo, China, [7] Department of Orthopaedics, Changzheng Hospital, Second Military Medical University, Shanghai, China, [8] Department of Pharmaceutical Biology, Institute of Pharmacy and Biochemistry, Johannes Gutenberg University, Mainz, Germany

Background: As a degenerative joint disease with severe cartilage destruction and pain, osteoarthritis (OA) has no satisfactory therapy to date. In traditional Chinese medicine (TCM), *Aconitum carmichaeli* Debeaux derived *Hei-shun-pian* (*Hsp*) has been developed for joint pain treatment. However, it causes adverse events in OA patients. Long-time decoction has been traditionally applied to reduce the aconite toxicity of *Hsp* and other aconite herbs, but its detoxifying effect is uncertain.

Methods: *Hsp* was extracted with dilute decoction times (30, 60, and 120 min) and evaluated by toxicological, chemical, pharmacological assays. Acute toxicity assay and chemical analysis were employed to determine the toxicity and chemoprofile of *Hsp* extracts, respectively. Since the detoxified *Hsp* (d*Hsp*) was defined, its therapeutic effect was evaluated by using an OA rat model induced by monosodium iodoacetate. d*Hsp* at 14 g/kg was orally administered for 28 days, and the pain assessments (mechanical withdrawal threshold and thermal withdrawal latency) and histopathological analyses (HE and safranin-O staining) were performed. Real-time PCR (qPCR) was applied to determine the molecular actions of d*Hsp* on cartilage tissue and on chondrocytes. MTT assay was conducted to evaluate the effect of d*Hsp* on the cell viability of chondrocytes. The cellular and molecular assays were also conducted to analyze the functions of chemical components in d*Hsp*.

OPEN ACCESS

Edited by:
Jing-Yan Han,
Peking University, China

Reviewed by:
Jinming Zhang,
Chengdu University of Traditional Chinese Medicine, China
Subhalakshmi Ghosh,
Independent Researcher, Kolkata, India

***Correspondence:**
Wenxi Du
purpleraineer@163.com
Huiling Wu
zywhl@zju.edu.cn
Letian Shan
letian.shan@foxmail.com

†These authors have contributed equally to this work

Specialty section:
This article was submitted to Ethnopharmacology, a section of the journal Frontiers in Pharmacology

Received: *08 January 2020*
Accepted: *29 June 2020*
Published: *24 July 2020*

Citation:
Zhang L, Li T, Wang R, Xu J, Zhou L, Yan L, Hu Z, Li H, Liu F, Du W, Tong P, Wu H, Zhang S, Shan L and Efferth T (2020) Evaluation of Long-Time Decoction-Detoxicated Hei-Shun-Pian (Processed Aconitum carmichaeli Debeaux Lateral Root With Peel) for Its Acute Toxicity and Therapeutic Effect on Mono-Iodoacetate Induced Osteoarthritis. Front. Pharmacol. 11:1053. doi: 10.3389/fphar.2020.01053

Results: The chemoprofile result showed that the contents of toxic alkaloids (aconitine, mesaconitine, and hypaconitine) were decreased but that of non-toxic alkaloids (benzoylaconitine, benzoylmesaconitine, and benzoylhypaconitine) were increased with increasing decoction time. Acute toxicity assay showed that only *Hsp* extract with 120 min decoction was non-toxic within the therapeutic dose range. Thus, it was defined as d*Hsp* for further experiment. In OA experiment, d*Hsp* significantly attenuated joint pain and prevented articular degeneration from MIA attack. qPCR data showed that d*Hsp* restored the abnormal expressions of *Col10*, *Mmp2*, *Sox5*, *Adamts4/5/9*, and up-regulated *Col2* expression in rat cartilage. *In vitro*, d*Hsp*-containing serum significantly proliferated rat chondrocytes and regulated the gene expressions of *Col2*, *Mmp1*, *Adamts9*, and *Aggrecan* in a similar way as the *in vivo* data. Moreover, aconitine, mesaconitine, and hypaconitine exerted cytotoxic effects on chondrocytes, while benzoylaconitine and benzoylhypaconitine except benzoylmesaconitine exhibited similar molecular actions to d*Hsp*, indicating contributions of benzoylaconitine and benzoylhypaconitine to d*Hsp*.

Conclusions: This study defined d*Hsp* and demonstrated d*Hsp* as a potential analgesic and disease modifying agent against OA with molecular actions on the suppression of chondrocyte hypertrophy and extracellular matrix degradation, providing a promising TCM candidate for OA therapy.

Keywords: *Aconitum carmichaeli*, traditional Chinese medicine, osteoarthritis, monosodium iodoacetate, pain behaviour, analgesia

INTRODUCTION

Osteoarthritis (OA) is a progressive joint disease characterized by cartilage degradation, sclerosis of subchondral bone and osteophyte formation, resulting in chronic joint pain, joint stiffness, and disability. OA is the main cause of lower extremity disability around the globe, with hip and knee OA accounting for 17 million years lived with disability or 2.2% of all-cause years lived with disability (O'Neill et al., 2018). The incidence and severity of OA in women are higher than that in men. It is estimated that the lifetime risk of knee OA is about 40% in men and 47% in women (Johnson and Hunter, 2014). Even worse, due to the aging of the global population and the aggravation of obesity, the incidence of OA is getting higher and is expected to double by the year 2020 (Johnson and Hunter, 2014; Mandl, 2019). Current OA treatments are mostly targeting the symptomatic relief of pain and inflammation for joint function improvement. However, none of them can modify the OA progression, and their therapeutic outcomes are often associated with incomplete relief and side effects (Bijlsma et al., 2011). Therefore, development of novel anti-OA therapeutics is still sorely needed.

The lateral root of *Aconitum carmichaeli* Debx (family Ranunculaceae), named *Fu-zi* in China, is a widely used traditional Chinese medicine (TCM) with cardiotonic, analgesic, and anti-inflammatory activities. It was originally described by the earliest Pharmacopeia of China, "*Shennong Materia Medica*" (24–220 AD). However, *Fu-zi* is highly toxic, and diester-diterpenoid alkaloids (DDAs) such as aconitine, mesaconitine and hypaconitine are its main toxic components (He et al., 2017). These components can cause toxic side effects on the cardiovascular, nervous, respiratory and digestive systems, which can be mainly manifested as arrhythmia, hypotension, hypothermia, respiratory depression, muscle paralysis and central nervous dysfunction, and may even lead to death in severe cases (Chan, 2009). These side effects limited the clinical application of *Fu-zi*. Traditionally, processing methods have been developed for reduction of *Fu-zi*'s toxicity prior to prescription (China Pharmacopeia Committee, 2015). *Hei-shun-pian* (*Hsp*) is such a processed product that has been widely used as a principal herb in TCM formulas for treatment of joint pain, including *Gan-cao Fu-zi Tang* and *Fu-zi Tang* (Huang, 2013). Modern clinical studies have reported the therapeutic effects of those formulas on knee OA (Deng, 2008). Recently, we also reported in a clinical trial that *Fu-zi Tang* effectively alleviated knee pain and improved life quality of patients with mild to moderate knee OA (Liu et al., 2016). Nevertheless, adverse events still occurred with *Fu-zi Tang* treatment in those patients, indicating that *Hsp* remained toxic. It is well known that long-time decoction is a traditional and useful processing method for detoxifying aconite toxicity, resulting in derivatization of non-toxic alkaloids (benzoylaconitine, benzoylmesaconitine, and benzoylhypaconitine) from toxic

Abbreviations: DDAs, diester-diterpenoid alkaloids; d*Hsp*, detoxicated *Hsp*; DMSO, dimethyl sulfoxide; ECM, extracellular matrix; FBS, fetal bovine serum; HE, hematoxylin and eosin; *Hsp*, *Hei-shun-pian*; IMDM, Iscove's modified Dulbecco's medium; LSD, least significant difference; MIA, mono-iodoacetate; MWT, mechanical withdrawal threshold; OA, osteoarthritis; PCR, real time polymerase chain reaction; SO, safranin-O; TCM, traditional Chinese medicine; TWL, thermal withdrawal latency.

alkaloids (Tong et al., 2013). However, there is no standard procedure to optimize detoxification, resulting in potential risks for patients. To evaluate the traditional detoxifying effect on *Hsp* and to explore, whether or not the long-time decocted *Hsp* remains therapeutically effective, we conducted acute toxicity assay and chemical analysis to determine the detoxicated *Hsp* (d*Hsp*) and then employed an OA rat model to evaluate the therapeutic effect of d*Hsp*. Afterwards, the molecular actions of d*Hsp* on cartilage tissue and chondrocytes were clarified by real time PCR. This is the first report regarding the development and evaluation of d*Hsp*.

MATERIALS AND METHODS

Preparation of *Hsp* Extracts

Hei-shun-pian, a processed product of the lateral root of *Aconitum carmichaeli* Debx (Ranunculaceae) was harvested from Jiangyou (Sichuan, China) and authenticated by the authors (voucher specimen No. 081102). Detoxifying processing was applied in accordance with the procedure described in our previous report (Tong et al., 2013). The specific steps are as follows: The materials were powdered and evenly divided into three samples. Each sample was soaked in 10-fold water for 30 min, followed by boiling and decocting for 30 min, 60 min, and 120 min, respectively. Then, the water extract of each sample was collected after filtration, and 8-fold the amount of water was added to each residue, which is the same as the above procedure to decoct again, and to combine the first-stage extracts with the second-stage extracts of each sample. Finally, each supernatant was concentrated by rotary evaporation and freeze-dried to powder for storage and diluted into 1.0 g/ml for use. The extracts with 30 min decoction, 60 min decoction, 120 min decoction were labeled as *Hsp*-30, *Hsp*-60, and *Hsp*-120, respectively.

Chemicals and Reagents

Standard substances (HPLC grade) of aconitine (98.01% of purity, batch number: MUST-19110905), mesaconitine (99.14% of purity, batch number: MUST-19111311) and hypaconitine (99.09% of purity, batch number: MUST-19080210), benzoylaconitine (99.44% of purity, batch number: MUST-19103010), benzoylmesaconitine (99.66% of purity, batch number: MUST-19032807), and benzoylhypaconitine (99.46% of purity, batch number: MUST-20022710) were purchased from Chengdu Must Bioscience and Technology CO., LTD (Chengdu, China). Methanol and acetonitrile were of HPLC grade (Tedia, Fairfield, USA). Ammonium acetate and tetrahydrofuran were of analytical grade. Mono-iodoacetate (MIA) was purchased from Sigma (St. Louis, MO, United States). Iscove's modified Dulbecco's medium (IMDM), fetal bovine serum (FBS) and 0.25% trypsin were obtained from Gibco (Thermo Fisher Scientific, Inc., Waltham, MA, United States). 3-(4, 5-Dimethylthiazol-2-yl)-2,5-diphenyltetrazolium bromide (MTT) and dimethyl sulfoxide (DMSO) were obtained from Sigma-Aldrich (Taufkirchen, Germany). TRIzol reagent was purchased from Thermo Fisher Scientific Inc. The real time polymerase chain reaction (PCR) kit was purchased from Takara Biotechnology Co., Ltd. (Dalian, China). All antibodies were purchased from Cell Signaling Technology, Inc. (Danvers, MA, United States).

Animals and Cell Line

Male SD rats (180–220 g) and Kunming mice with both sexes (18–22 g) were purchased from Shanghai Laboratory Animal Center of Chinese Academy of Sciences (Grade SPF II Certificate No. SCXK2017-0005) and housed in ventilated cages at 22 ± 1°C under a 12/12 h light/dark cycle with water and food *ad libitum*. Primary chondrocyte was isolated from the rat articular cartilage and cultured as previously described (Wang et al., 2013).

Chemical Analysis

HPLC analysis was performed on an Agilent 1260 Infinity HPLC system (Agilent Technologies, CA, United States). Chromatographic separation was carried out on a Hypersil BDS C_{18} column (250×4.6 mm, 5 μm) (Dalian Elite Analytical Instrument Co., Ltd) at 30°C. The mobile phase consisted of 0.1 mol/l ammonium acetate solution and acetonitrile-tetrahydrofuran (100:50, v/v) with a flow rate of 1.0 ml/min. The elution gradient was started at 85% ammonium acetate solution, followed by decreasing the ammonium acetate solution to 74% within 40 min, subsequently, the mobile phase was switched to 85% ammonium acetate again for 45 min. The sample injection volume was 10 μl, and the detection wavelength was 235 nm. The standard substances of aconitine, mesaconitine and hypaconitine were dissolved in methanol to obtain working standard solutions. The data was analyzed to identify and quantify the aconitine, mesaconitine, and hypaconitine in *Hsp*-30, *Hsp*-60, and *Hsp*-120 extracts by two-point external standard method.

The UPLC-MS analysis was performed on an Acquity UPLC system (Waters, MA, USA) equipped with a Xevo TQ-S triple quadrupoleelectrospray ionization (ESI) MS (Waters, MA, USA) operated in positive ESI-mode. Chromatographic separation was carried out on an Acquity BEH C_{18} column (100 mm × 2.1 mm, particle size 1.7 μm) maintained at 40°C. The mobile phase consisted of 5 mM ammonium formate solution (0.1% formic acid) and methyl alcohol (55:45, v/v) with a flow rate of 0.4 ml/min. The sample injection volume was 5 μl. The standard substances of benzoylaconitine, benzoylmesaconitine and benzoylhypaconitine were dissolved in methyl alcohol to obtain working standard solutions. The data was analyzed to identify and quantify the benzoylaconitine, benzoylmesaconitine, and benzoylhypaconitine in *Hsp*-30, *Hsp*-60, and *Hsp*-120 extracts.

Acute Toxicity Assay

Male and female Kunming mice were randomly divided into 16 groups with 8 animals each (4 male and 4 female). Before oral administration, all mice were fasted for 12 h with water *ad libitum*. Each five groups were orally given one type of detoxicated *Hsp* (*Hsp*-30, *Hsp*-60, or *Hsp*-120) in doses of 40, 60, 80, 100, 120 g/kg, respectively. The control group received an equal volume of water. After a single administration, the animals were observed closely during first 24 h and were kept under

observation up to 14 days. The mortality of each group was observed. As an index for acute toxicity, LD_{50} with associated 95% confidence limits (CL) was determined by the Bliss's method.

Therapeutic Evaluation

A total of 30 rats were used for therapeutic evaluation of d*Hsp*. All rats were randomly and equally divided into three groups: NC as normal control group, OA as model group, and OA+d*Hsp* as d*Hsp* treated OA group. The OA and OA+d*Hsp* groups were intra-articularly injected with 50 μl of 20 mg/ml MIA through the patella ligament of rat knees using a 100 μl microliter syringe to establish the OA model, while NC group was treated with 50 μl of saline in a same way. Besides the MIA injection, rats in OA+d*Hsp* group were simultaneously treated with oral administration of 14 g/kg d*Hsp*, while OA and NC group were given the equal volume of saline, respectively. The treatment lasted for 28 days, and the pain-related mechanical withdrawal threshold (MWT) and thermal withdrawal latency (TWL) were tested after the last treatment. In addition, the serum of rats from NC group and OA+d*Hsp* group were collected to obtain blank serum and d*Hsp*-containing serum for *in vitro* experiment. Finally, all the animals were sacrificed under anesthesia, and the knee joints were taken immediately for histopathological and real time PCR assay.

Pain-Related Behavioral Observation

The TWL and MWT were measured by a Plantar Test apparatus (UgoBasile, Italy) and the von Frey test, respectively. The rats were placed in a transparent plastic box at room temperature (25 ± 2) °C. After the rats were quiet (stop combing hair and exploring activities), the cross mark on the tester was placed in the center of the left rear sole of the rats, and the instrument was opened away from the foot pad. Each rat was measured three times. In order to prevent the rats from being scalded by thermal radiation, the upper limit of time and temperature was set as 20 s and 35°C, respectively. For testing the mechanical pain threshold, the von Frey needle of the instrument was used to press the plantar surface of the left and right hind paws of each rat about three times. The rats showed rapid withdrawal of claws and licking of claws as the positive reaction of each test.

Histopathological Observation

The rat joints on one side were dissected immediately after sacrifice and fixed in 4% paraformaldehyde for 48 h, followed by decalcification with 5% hydrochloric acid for 96 h. After paraffin embedding, samples were sectioned (4~5 μm) and stained with HE (hematoxylin and eosin) and SO (safranin-O) using routine process. The HE stained slides were photographed under the microscope. According to Mankin's scoring system, statistical grading was carried out in the range of 0–13 points through double-blind observation.

Cell Viability Assay

The chondrocyte viability was determined by MTT assay. The 2nd generation of chondrocytes were seeded on 96-well plates at a density of 5×10^3 cells/well in 200 ml medium for 24 h, and treated with d*Hsp*-containing serum at 2.5, 5, 10, 15% for 24, 48, and 72 h and then treated with aconitine, mesaconitine, hypaconitine, benzoylaconitine, benzoylmesaconitine, and benzoylhypaconitine at dose ranges according to their concentrations in *Hsp*-120. A total of 20 ml MTT solution (5.0 mg/ml) was added to each well and incubated at 37°C for 4 h. 150 ml DMSO was subsequently added to each well to dissolve the formazan crystals and the optical density (OD) value was measured at 490 nm with a microplate reader (Bio-Rad Laboratories, Inc., Hercules, CA, United States). Proliferative rate (%) = (d*Hsp*-treated OD/untreated OD) ×100.

Real-Time PCR (qPCR)

qPCR assay was performed to test the relative mRNA expression of OA-related genes of rat joints obtained from the animal experiment and chondrocytes by using an ABI QuantStudio™ 7 Flex Real-Time PCR System (Applied Biosystems; Thermo Fisher Scientific, Inc.). An aliquot of chondrocytes were pre-treated with TNF-α (10 ng/ml) for 6 h, and then treated with d*Hsp*-containing serum (15%) for 24 h. Another aliquot of chondrocytes were treated with benzoylaconitine, benzoylmesaconitine and benzoylhypaconitine for 24 h at doses corresponding to their concentrations in *Hsp*-120. Total RNA was extracted from cartilage tissue or chondrocytes using TRIzol reagent and reverse transcription was performed to produce cDNA. The final PCR reaction system was 20.0 μl, comprising 10.0 μl SYBR® Premix Ex Taq II (Tli RnaseH Plus), 0.8 μl PCR Forward Primer, 0.8 μl PCR Reverse Primer, 2.0 μl template cDNA, 0.4 μl ROX Reference Dye, and 6.0 μl ddH_2O. The qPCR reaction conditions were as follows: 95°C for 30 s for initial denaturation, followed by 40 cycles of denaturation at 95°C for 5 s, annealing at 60°C for 34 s, and extension at 72°C for 40 s. At the end of each reaction, melting curve analysis was performed. *β-actin* was used as the reference gene and the $2^{-\Delta\Delta CT}$ method was used to analyze the relative mRNA expressions (**Table 1**).

Statistical Analysis

Data were expressed as mean ± SD and subjected to one-way ANOVA, followed by Fisher's least significant difference (LSD) comparison. All analyses were performed using an updated version of DPS software (Tang and Feng, 2007).

RESULTS

Chemoprofiles of *Hsp* Extracts

The HPLC chromatogram comparison of toxic components in *Hsp*-30, *Hsp*-60, and *Hsp*-120 extracts were shown in **Figures 1A–C**. The retention time of aconitine, mesaconitine, and hypaconitine in all samples were 21.091 – 22.092 min, 11.162 – 11.816 min, and 44.705 – 47.280 min, respectively. There were no remarkable chromatographic differences in the peak time of *Hsp* samples with different decocting times. Nevertheless, upon decoction with water, the peak height of each compound decreased gradually in a time-dependent manner, and the peak of aconitine was even found disappeared after 120 min decoction. The concentrations of three toxic components in

TABLE 1 | Primer sequences used for real-time PCR (qPCR) analysis.

Gene	Forward primer	Reverse primer
β-actin	5′-CCCGCGAGTACAACCTTCT-3′	5′-CGTCATCCATGGCGAACT-3′
Col2	5′-CTCAAGTCGCTGAACAACCA-3′	5′-GTCTCCGCTCTTCCACTCTG-3′
Aggrecan	5′-GCAGACATTGATGAGTGCCTC-3′	5′-CTCACACAGGTCCCCTCTGT-3′
Col10	5′-GATCATGGAGCTCACGGAAAA-3′	5′-CCGTTCGATTCCGCATTG-3′
Mmp1	5′-GGTGTGGTGTCTCACAGCTT-3′	5′-CGCTTTTCAACTTGCCTCCC-3′
Mmp2	5′-GATACCCCTTTGACGGTAAGGA-3′	5′-CCTTCTCCCAAGGTCCATAGC-3′
Sox5	5′-GGGGAGACAGATGGAGAGGT-3′	5′-GTGAGGCTTGTTGGGAAAAC-3′
Adamts9	5′-TACAGGCAAAGGCTGGTCTC-3′	5′-CTCAGGTAGCAGGGATGGAC-3′
Adamts5	5′-TGGAGTGTGTGGAGGGGATA-3′	5′-CGGACTTTTATGTGGGTTGC-3′
Adamts4	5′-TTCGCTGAGTAGATTCGTGGAG-3′	5′-TGAGTCGTTCGGAGGGTTTAG-3′

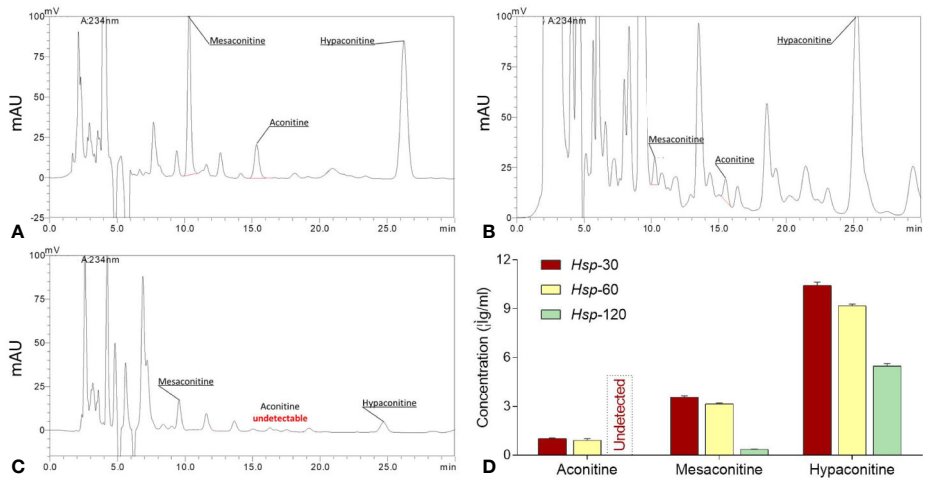


FIGURE 1 | HPLC chromatograms of *Hsp*-30 **(A)**, *Hsp*-60 **(B)**, and *Hsp*-120 **(C)**, and concentrations of aconitine, mesaconitine, and hypaconitine in *Hsp*-30, *Hsp*-60, and *Hsp*-120 **(D)**.

Hsp-30, *Hsp*-60, and *Hsp*-120 are shown in **Figure 1D**. The highest concentrations were found in *Hsp*-30, which attained 1.04 ± 0.03 μg/g for aconitine, 3.57 ± 0.07 μg/g for mesaconitine, 10.44 ± 0.20 μg/g for hypaconitine. Upon decoction with water, a stepwise decrease of each concentration was observed in different *Hsp* extracts with increasing decoction time. Especially when the decoction time attained 120 min, the concentrations of the three compounds reached the lowest level with undetected aconitine, 0.37 ± 0.01 μg/g of mesaconitine, and 5.47 ± 0.16 μg/g of hypaconitine. Thus, *Hsp*-120 was selected as d*Hsp* for the following animal experiment.

UPLC-MS was applied to identify and quantify the non-toxic derivatives of aconitines in *Hsp*-30, *Hsp*-60, and *Hsp*-120. As shown in **Figure 2**, benzoylaconitine, benzoylmesaconitine, and benzoylhypaconitine were all present in *Hsp*-30, *Hsp*-60, and *Hsp*-120, while their concentrations were increased with increasing decoction time. For example, benzoylaconitine was increased from 38.33 ± 0.44 μg/g in *Hsp*-30 to 58.08 ± 0.25 μg/g in *Hsp*-120, benzoylmesaconitine was increased from 197.20 ± 0.25 μg/g in *Hsp*-30 to 279.56 ± 0.36 μg/g in *Hsp*-120, and benzoylhypaconitine was increased from 44.90 ± 0.05 μg/g in *Hsp*-30 to 87.86 ± 0.09 μg/g in *Hsp*-120.

Acute Toxicity of *Hsp* Extracts

Our preliminary experiment found a rational dose range of d*Hsp* being 40 to 120 g/kg for the acute toxicity test, since 120 g/kg almost reached the maximum saturated solubility. As shown in **Figure 3**, within 24 h, the death was initiated by *Hsp*-30 at 80 g/kg and *Hsp*-60 at 100 g/kg with mortalities of 37.5% and 12.5%, respectively. At the end, the mice exposed to *Hsp*-30 at 120 g/kg were all dead with LD_{50} of 81.1 (68.0 to 96.8) k/kg, indicating a concentration-dependent and time-dependent manner of toxicity. *Hsp*-60 showed lesser acute toxicity than *Hsp*-30, which caused final mortality of 37.5% at 120 g/kg. However, no death occurred under the treatment of *Hsp*-120 within the dose and time ranges, indicating a certain safety of *Hsp*-120.

In Vivo Anti-OA Effect of d*Hsp*

MWT and TWL, respectively, reflect two behavioral responses: mechanical hyperalgesia and thermal hyperalgesia. As shown in **Figure 4A**, MWT and TWL were significantly decreased with OA modeling (both $P < 0.05$ versus NC group), while the abnormal levels were significantly restored by d*Hsp* after 28 days treatment (both $P < 0.01$ versus OA group). Histopathological results with HE and SO staining are shown

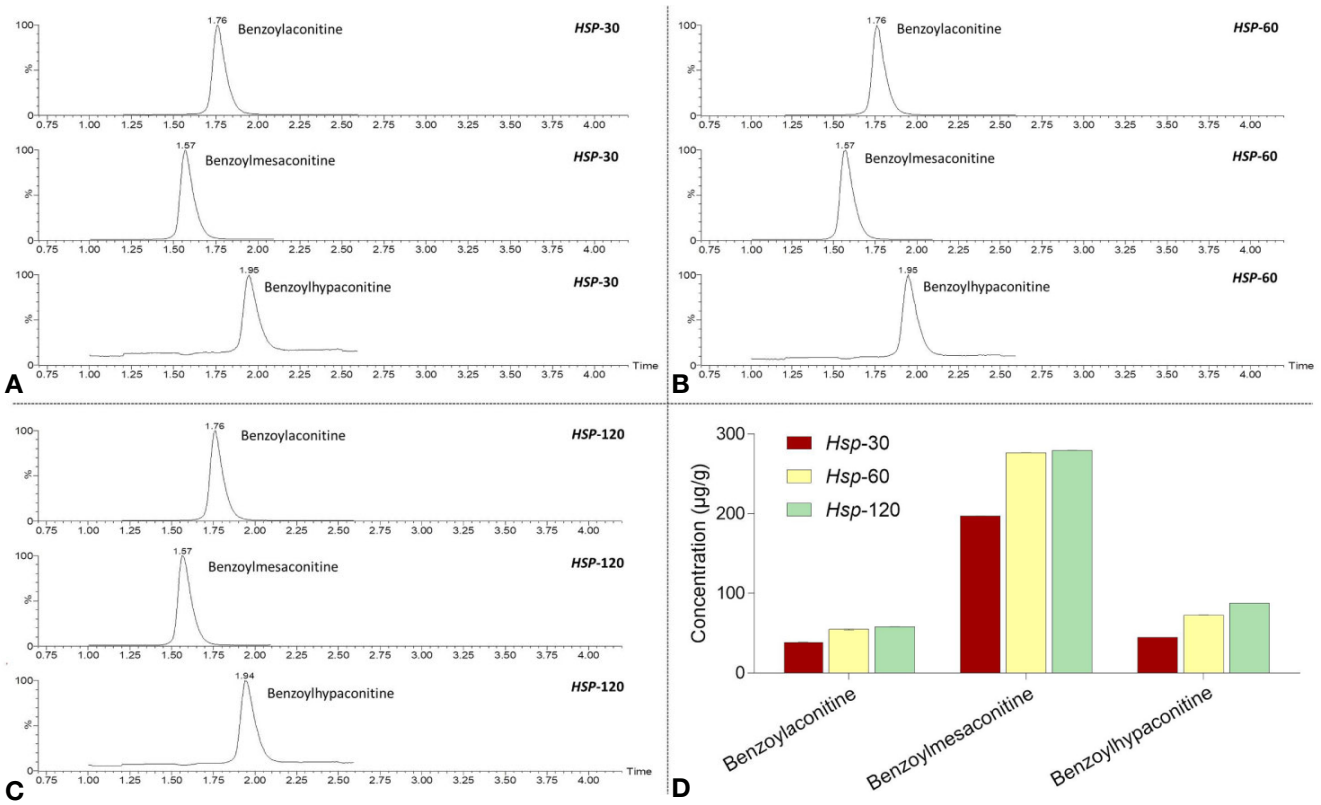


FIGURE 2 | UPLC-MS chromatograms of *Hsp*-30 **(A)**, *Hsp*-60 **(B)**, and *Hsp*-120 **(C)**, and concentrations of benzoylaconitine, benzoylmesaconitine, and benzoylhypaconitine in *Hsp*-30, *Hsp*-60, and *Hsp*-120 **(D)**.

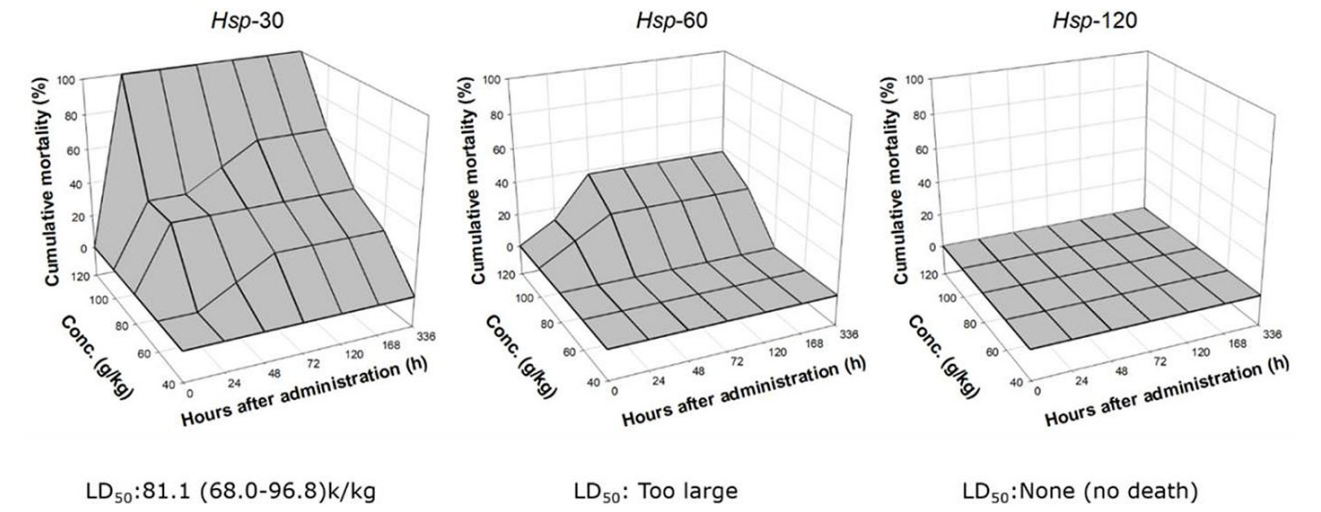


FIGURE 3 | Cumulative mortalities of mice after oral administration of *Hsp*-30, *Hsp*-60, and *Hsp*-120 (g/kg) with LD_{50} value and associated 95% confidence limits.

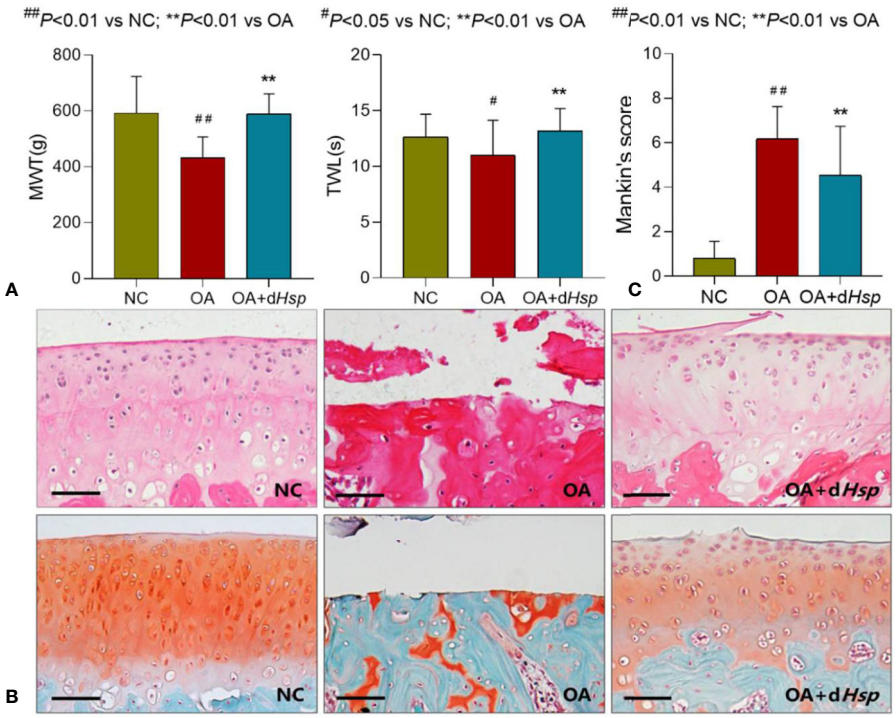


FIGURE 4 | (A) MWT (g), TWL (s) results of the left and right hind paws of rats tested after final d*Hsp* treatment (28 d); **(B)** Histopathological observation (HE and Safranin-O staining); **(C)** Mankin's scoring of rat knee joints at day 28 after d*Hsp* treatment. Values are presented as mean ± SD. $^{\#}P < 0.05$ vs. NC group; $^{\#\#}P<0.01$ vs. NC group; $^{**}P<0.01$ vs. OA group. Scale bar = 100 μm.

in **Figure 4B**. Severe cartilage damage, characterized by loss of chondrocytes and disorganization of extracelluar matrix, was observed in the OA group with significant increase of Mankin's score (**Figure 4C**, $P < 0.01$ versus NC group). As expected, the damaged phenotype was obviously relieved by d*Hsp* treatment with significant decrease of Mankin's score (**Figure 4C**, $P < 0.01$ versus OA group), in which the chondrocytes and extracelluar matrix were protected.

Molecular Actions of d*Hsp* on Cartilage

The molecular actions of d*Hsp* on the expression of OA-related genes in cartilage tissue were determined using qPCR assay. As shown in **Figure 5A**, MIA significantly up-regulated the expressions of *Col10*, *Mmp2*, *Sox5*, and *Adamts4/5/9*, as compared with that of NC group (all $P < 0.01$). After treatment of d*Hsp*, the abnormal expressions of those genes were significantly restored as compared with that of OA group (all $P < 0.05$ or 0.01). There was no obvious difference of *Col2* expression among all groups ($P > 0.05$).

Cellular and Molecular Actions of d*Hsp*-Containing Serum on Chondrocytes

To mimic the *in vivo* behavior of d*Hsp*, d*Hsp*-containing serum was applied for *in vitro* experiments. The proliferative effect of d*Hsp*-containing serum on chondrocytes was assessed by MTT assay. As shown in **Figure 5B**, d*Hsp*-containing serum at concentration range from 2.5% to 15% significantly increased cell viability of chondrocytes. The proliferative rate was increased from 0.3% to 10.2% after 24 h treatment, from 2.3% to 16.4% after 48 h treatment, and from 5.2% to 40.0% after 72 h treatment. It indicated that d*Hsp*-containing serum induced proliferation of chondrocytes in concentration-dependent and time-dependent manner.

The molecular actions of d*Hsp*-containing serum on the expression of OA related genes in chondrocytes were determined by qPCR assay. The rat primary chondrocytes were pretreated with TNF-α to induce inflammatory response for mimicking the pathological condition of OA. As shown in **Figure 5C**, TNF-α significantly down-regulated the mRNA expression of *Aggrecan* and up-regulated the mRNA expressions of *Mmp1* and *Adamts9*, as compared with that of NC group (all $P < 0.01$). After 24 h treatment of d*Hsp*-containing serum, the abnormal expressions of those genes were all restored toward the normal levels, as compared with that of TNF-α group (all $P < 0.05$ except for *Adamts9*). Similar to the *in vivo* result, there was no obvious difference of *Col2* expression between NC and TNF-α groups ($P > 0.05$). Nevertheless, after 24 h treatment of d*Hsp*-containing serum, the *Col2* expression was significantly up-regulated as compared with that of TNF-α group ($P < 0.05$).

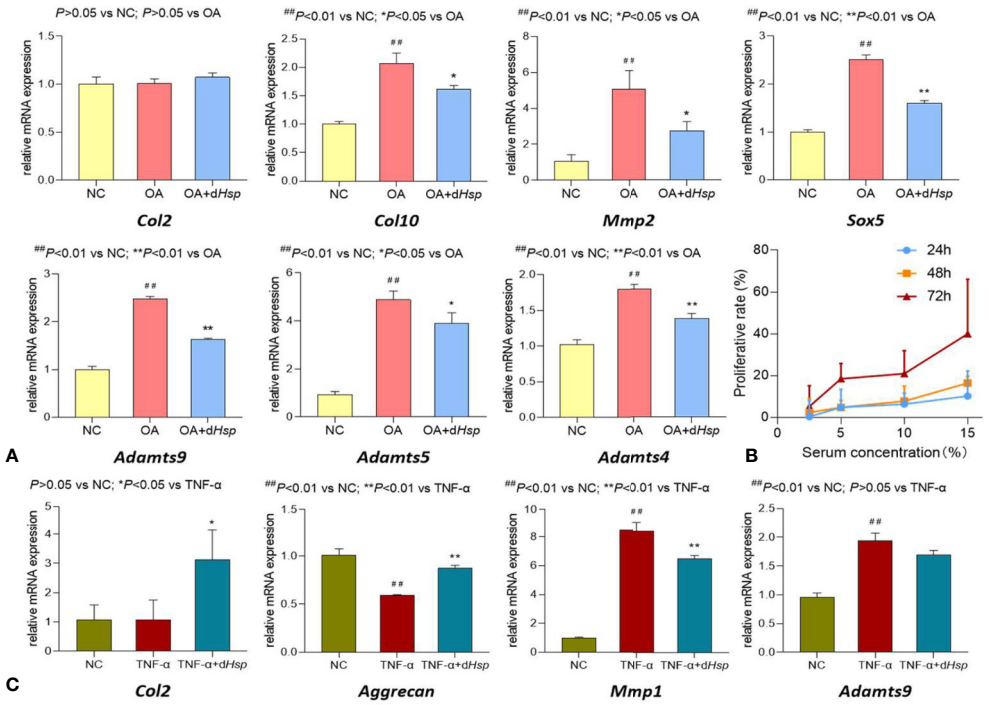


FIGURE 5 | (A) Relative mRNA expressions of OA-related genes in cartilage tissue after oral administration of saline (NC group), saline (OA group), and 14 g/kg d*Hsp* (OA+ d*Hsp* group). **(B)** Cell viability of chondrocytes treated with d*Hsp*-containing serum for 24, 48, and 72 h. **(C)** Relative mRNA expressions of target genes in chondrocytes treated with TNF-α or TNF-α plus d*Hsp*-containing serum for 24 h. Values are presented as mean ± SD. ##P<0.01 vs. NC group; *P<0.05 or **P<0.01 vs. TNF-α group.

Cellular and Molecular Actions of d*Hsp*-Contained Compounds on Chondrocytes

To further explore the potential mechanism of d*Hsp* on OA, cellular and molecular effects of d*Hsp*-contained alkaloids on chondrocytes were studied. MTT assay was conducted to evaluate the effect of aconitine, mesaconitine, hypaconitine, benzoylaconitine, benzoylmesaconitine, and benzoylhypaconitine on chondrocytes. For evaluating the contribution of each compound to d*Hsp*, the dose range for each compound was selected in accordance with their concentrations in d*Hsp*. For example, 5, 10, and 20 μg/ml were used as low, middle and high doses for aconitine, mesaconitine, hypaconitine, since the highest concentration of toxic aconitine in d*Hsp* was 5.47 ± 0.16 μg/ml (hypaconitine). Moreover, 30, 60, and 120 μg/ml were used as low, middle and high doses for benzoylaconitine, 140, 280, and 560 μg/ml were used as low, middle and high doses for benzoylmesaconitine, and 45, 90, and 180 μg/ml were used as low, middle and high doses for benzoylhypaconitine, in which their middle doses were similar to their concentrations in d*Hsp*.

As shown in **Figure 6A**, after 24 h treatment, aconitine, mesaconitine, and hypaconitine exerted significant inhibitory effects on chondrocytes at their dose ranges (all $P < 0.01$), indicating cytotoxicity of these compounds against chondrocytes. Besides, benzoylaconitine and benzoylhypaconitine at their dose ranges had non-toxic effect on chondrocytes, while benzoylmesaconitine at high dose exerted significant inhibitory effect ($P < 0.01$), suggesting that these compounds at their dose ranges, except benzoylmesaconitine at high dose, may contribute to the therapeutic effect of d*Hsp*. Thus, these three compounds were selected for the following qPCR assay. As shown in **Figure 6B**, as compared with control group, benzoylaconitine at middle dose significantly down-regulated the expressions of *Adamts4* and *Adamts5* with slight down-regulatory effect on *Col10* and *Adamts9*, while benzoylhypaconitine at middle dose significantly down-regulated the expressions of *Col10*, *Adamts4*, *Adamts5*, and *Adamts9*, suggesting these compounds as therapeutic components of d*Hsp*. However, benzoylmesaconitine at middle dose significantly up-regulated the expressions of *Adamts4*, *Adamts5*, and *Adamts9* with slight up-regulatory effect on *Col10*, indicating a negative contribution of this compound to d*Hsp*.

DISCUSSION

Joint impairment-associated pain is the key clinical feature of OA, mainly caused by synovial neurogenic inflammation and subchondral nerve damage (Neogi et al., 2016). With the onset of joint impairment, pain occurs and progressively disables the joint capacity and movement in OA patients. Thus, it is very important to reach pain relief during OA therapy and to employ specific preclinical model of OA that can be used to evaluate not only disease-modifying effects but also analgesic activity. MIA-induced rat model is a minimally invasive, rapidly developed, and reproducible OA model, which causes histomorphological

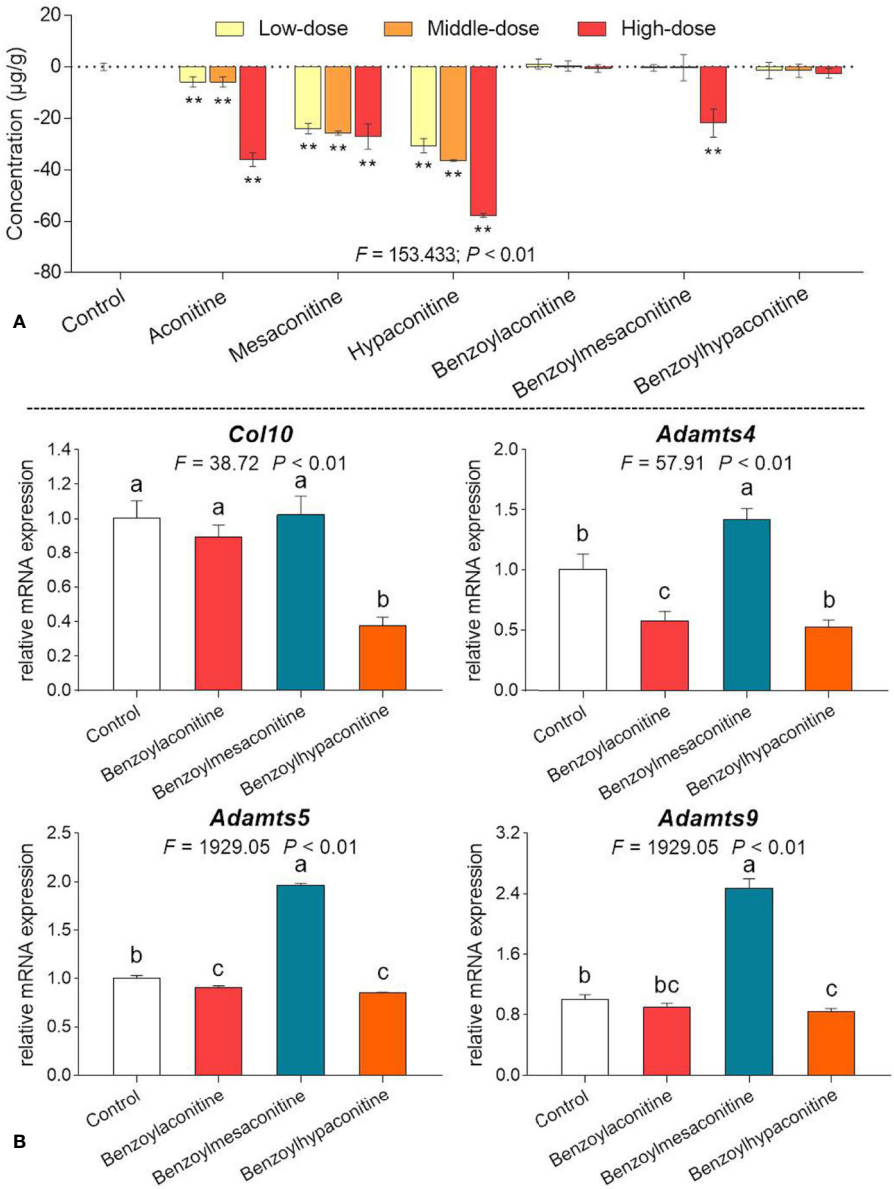


FIGURE 6 | Cell viability of chondrocytes with treatments of aconitine, mesaconitine, hypaconitine, benzoylaconitine, benzoylmesaconitine, and benzoylhypaconitine **(A)** and relative mRNA expressions of OA-related genes in chondrocytes with treatments of benzoylaconitine, benzoylmesaconitine, and benzoylhypaconitine **(B)**. Values are presented as mean ± SD. By means of LSD multiple comparisons, data with same lowercase letter indicate no significant difference between each other, while data with different letters indicate significant difference with each other. **P<0.01 vs. control group.

and functional joint impairment as well as pain behavior similar to human OA (Pitcher et al., 2016). MIA injected in articular cavity disrupts cartilage glycolysis and chondrocyte metabolism by inhibition of glyceraldehye-3-phosphate dehydrogenase, thereby inducing chondrocyte death, cartilage destruction and subchondral bone exposure (Lampropoulou-Adamidou et al., 2014). Subchondral bone is abundantly innervated and could potentially be a source of OA pain (Philpott et al., 2017). In addition, the severity of OA progression in this model can be controlled by MIA in a dose-dependent manner, therefore, the model of OA induced by MIA has become one of the most popular models to research the pain course and intervention effect of OA (Ogbonna et al., 2013; Chin et al., 2019).

As a commonly used TCM product, *Hsp* has attracted much attention for its therapeutic efficacy. However, it remains potentially toxic to patients (Liu et al., 2016). Long-time decoction is a traditional and rational method for detoxifying *Hsp*, the principle of which is that acetyl group at C_8 and benzoyl

group at C_{14} of DDAs are hydrolyzed under the action of water and heat, thereby reducing its content to obtain less toxic monoester-diterpenoid alkaloids and non-toxic non-esterified diterpenoid alkaloids (Yang et al., 2018). Up to now, it remains uncertain, how long time should be used and what effect it has. Previously, by means of long-time (120 min) decoction, we successfully removed the acute toxicity of *Bai-fu-pian* (*Bfp*), another kind of *Fu-zi*, and demonstrated unaltered therapeutic efficacy of detoxified *Bfp* (d*Bfp*) on rheumatoid arthritis (Tong et al., 2013). It suggests that 120 min decoction might be effective in detoxifying *Hsp*. Considering the difference between *Bfp* (with no peel) and *Hsp* (with peel) as well as the more common use of *Hsp* in clinic, it is necessary to demonstrate whether long-time (120 min) decoction is also effective in detoxifying *Hsp* without alteration of therapeutic efficacy. Therefore, this study extracted *Hsp* with gradient decoction times (30, 60, and 120 min) and studied their acute toxicity and chemoprofiles. The results showed that, with increasing decocting time, the toxicity and concentrations of toxic alkaloids of *Hsp* were time-dependently decreased and the concentration of non-toxic alkaloid derivatives increased (**Figures 1–3**). *Hsp* with 120 min decoction was found to contain minimal levels of toxic components (**Figure 1**) and maximal levels of non-toxic derivatives (**Figure 2**). Also, it was non-toxic within the maximal dose range (**Figure 3**). In fact, 120 min is the upper time limit for the decoction, since more than 120 min would be too long to be practical. Thus, we defined the 120 min decocted *Hsp* as detoxicated *Hsp* (d*Hsp*). Afterwards, an animal model of OA was employed to evaluate the therapeutic effect of d*Hsp*. After 28 day treatment, the analgesic effect of d*Hsp* was determined by assessments of mechanical and thermal sensitivity (**Figure 4A**). Meanwhile, the histopathological evidence combined with Mankin's grading analysis exhibited the chondroprotective effect of d*Hsp*. To further clarify the molecular actions of d*Hsp*, qPCR assay was conducted on both cartilage and chondrocytes. d*Hsp* significantly restored the abnormal expressions of *Col10*, *Mmp2*, *Sox5*, and *Adamts4/5/9* and up-regulated the *Col2* expression in damaged cartilage tissue. It also significantly restored the abnormal expressions of *Aggrecan*, *Mmp1* and *Adamts9* and up-regulated the *Col2* expression in TNF-α treated chondrocytes (**Figures 5A, C**). Moreover, the results of MTT assay showed that d*Hsp* significantly increased the cell viability of chondrocytes (**Figure 5B**). Further cellular and molecular assays showed that, among the six alkaloid components of *Hsp*, toxic alkaloids (aconitine, mesaconitine, and hypaconitine) were cytotoxic to chondrocytes, while benzoylaconitine and benzoylhypaconitine exhibited molecular actions similar to d*Hsp* (**Figure 6**). The result suggests that benzoylaconitine and benzoylhypaconitine are therapeutic components of d*Hsp*, which give positive contribution to the anti-OA effect of d*Hsp*.

The destruction of cartilage in the process of OA is closely related to the degradation of cartilage extracellular matrix (ECM) (Guilak et al., 2018). The ECM of cartilage is mainly composed of collagens and proteoglycan. Col2 is the main collagen in the ECM and plays an important role in the metabolism and stability of cartilage. Col10 is another collagen existing rarely in the healthy cartilage but mainly in the degenerative cartilage. It is highly expressed by hypertrophic chondrocytes as a marker of hypertrophic regeneration. In sections of human osteoarthritic cartilage, Col10 was found around hypertrophic chondrocyte clusters in the deep zone close to tidemark (He et al., 2019). Besides the collagens, aggrecan, known as a cartilage-specific proteoglycan core protein, is another crucial component of cartilage ECM (Hu et al., 2019). In the OA state, aggrecan was significantly degraded in the cartilage, and the expression of aggrecan was inversely related to the OA progression (Eid et al., 2006). In contrary, MMPs and ADAMTSs are enzymes positively related to the OA progression, which can destroy the integrity and function of cartilage by hydrolyzing the ECM (Malemud, 2019). Of these, MMP1 exerts the strongest degradation effect on Col2 as a collagenase produced by synovial cells (Mehana et al., 2019). MMP2, known as gelatinase A, is also an important factor in the pathogenesis of OA (Zeng et al., 2015). Among the members of ADAMTSs, ADAMTS9, ADAMTS 5 and ADAMTS 4 have been shown to greatly induce degradation of cartilage aggrecan and fibrosis of collagen, resulting in the loss of cartilage compression strength and eventual occurrence of OA (J. Bondeson et al., 2008; Ohtsuki et al., 2019). Sox5 acts as a transcription factor associated with chondrogenesis. It is a highly expressed in synovium with inflammation, and the degree of cartilage destruction can be significantly reversed when the expression of Sox5 is silenced (Feng et al., 2016). In this study, we found that the molecular actions of d*Hsp* were mediated by the regulation of gene expressions of *Col2*, *Aggrecan*, *Col10*, *Mmp1*, *Mmp2*, *Adamts4/5/9*, and *Sox5* in cartilage tissue and chondrocytes, suggesting a mechanism of d*Hsp* in association with the inhibition of ECM degradation and chondrocyte hypertrophy.

CONCLUSIONS

This is the first study reported that d*Hsp* has anti-OA effect independent of its toxicity, which provides a safe candidate for TCM formulation in OA therapy. So far, there are two issues warranting further investigation. Firstly, d*Hsp* has not completely reversed the OA histopathological changes in this study, since many chondrocytes remained lost on the cartilage. It might be due to the excessive severity of our MIA model. More OA models with moderate severity are needed for further evaluation the d*Hsp*'s effect. Secondly, although the representative alkaloids in d*Hsp* have been analyzed by this study, the roles of other components in d*Hsp* remain unclear and need to be explored in future.

DATA AVAILABILITY STATEMENT

The datasets generated during and/or analysed during the current study are available from the corresponding author on reasonable request..

ETHICS STATEMENT

The animal study was reviewed and approved by the Medical Norms and Ethics Committee of Zhejiang Chinese Medical University.

AUTHOR CONTRIBUTIONS

LZha performed and funded the main work for revision; TL contributed to the main work of this study. RW performed the chemical analysis and wrote the paper. JX performed the MTT and qPCR assays for revision. LZho and LY contributed to the molecular experiment. ZH performed the UPLC-MS assay. HL participated in cellular experiments. FL contributed to the design of this study. WD and HW designed and funded this study. LS designed this study and finalized the data analysis. PT provided research ideas. SZ participated in the data analysis. TE improved the experimental design and the writing of this paper. All authors contributed to the article and approved the submitted version.

FUNDING

This study was supported by the National Natural Science Foundation of China (Grant No. 81774331, 81873049, 81804125), the Zhejiang Provincial Natural Science Foundation of China (Grant No. LY18H270004), the Zhejiang Provincial Science and Technology Project of Traditional Chinese Medicine of China (Grant No. 2016ZZ011), the Zhejiang Provincial Key Construction University Superiority Characteristic Discipline (Traditional Chinese Pharmacology) Opening Foundation of China (Grant No. ZYX2018006), and the Ningbo Natural Science Foundation (2014A610277).

REFERENCES

Bijlsma, J. W. J., Berenbaum, F., and Lafeber, F. P. J. G. (2011). Osteoarthritis: an update with relevance for clinical practice. *Lancet* 377 (9783), 2115–2126. doi: 10.1016/s0140-6736(11)60243-2

Bondeson, J., Wainwright, S., Hughes, C., and Caterson, B. (2008). The regulation of the ADAMTS4 and ADAMTS5 aggrecanases in osteoarthritis: a review. *Clin. Exp. Rheumatol.* 26, 139–145.

Chan, T. Y. (2009). Aconite poisoning. *Clin. Toxicol. (Phila)* 47 (4), 279–285. doi: 10.1080/15563650902904407

Chin, K. Y., Wong, S. K., Japar Sidik, F. Z., Abdul Hamid, J., Abas, N. H., Mohd Ramli, E. S., et al. (2019). The Effects of Annatto Tocotrienol Supplementation on Cartilage and Subchondral Bone in an Animal Model of Osteoarthritis Induced by Monosodium Iodoacetate. *Int. J. Environ. Res. Public Health* 16 (16), 2897. doi: 10.3390/ijerph16162897

China Pharmacopeia Committee (2015). *Pharmacopeia of the People's Republic of China (The First Division)* (Beijing: China Chemical Industry Press), 191.

Deng, W. (2008). Clinical research on Gancao Fuzi decoction in treating osteoarthritis of knee joint. *J. Chin. Med. Mater.* 31 (07), 1107–1110. doi: 10.13863/j.issn1001-4454.2008.07.007

Eid, K., Thornhill, T. S., and Glowacki, J. (2006). Chondrocyte gene expression in osteoarthritis: Correlation with disease severity. *J. Orthop. Res.* 24 (5), 1062–1068. doi: 10.1002/jor.20137

Feng, X., Shi, Y., Xu, L., Peng, Q., Wang, F., Wang, X., et al. (2016). Modulation of IL-6 induced RANKL expression in arthritic synovium by a transcription factor SOX5. *Sci. Rep.* 6, 32001. doi: 10.1038/srep32001

Guilak, F., Nims, R. J., Dicks, A., Wu, C. L., and Meulenbelt, I. (2018). Osteoarthritis as a disease of the cartilage pericellular matrix. *Matrix Biol.* 71–72, 40–50. doi: 10.1016/j.matbio.2018.05.008

He, F., Wang, C. J., Xie, Y., Cheng, C. S., Liu, Z. Q., Liu, L., et al. (2017). Simultaneous quantification of nine aconitum alkaloids in Aconiti Lateralis Radix Praeparata and related products using UHPLC-QQQ-MS/MS. *Sci. Rep.* 7 (1), 13023. doi: 10.1038/s41598-017-13499-6

He, Y., Manon-Jensen, T., Arendt-Nielsen, L., Petersen, K. K., Christiansen, T., Samuels, J., et al. (2019). Potential diagnostic value of a type X collagen neo-epitope biomarker for knee osteoarthritis. *Osteoarthritis Cartilage* 27 (4), 611–620. doi: 10.1016/j.joca.2019.01.001

Hu, N., Gong, X., Yin, S., Li, Q., Chen, H., Li, Y., et al. (2019). Saxagliptin suppresses degradation of type II collagen and aggrecan in primary human chondrocytes: a therapeutic implication in osteoarthritis. *Artif. Cells Nanomed. Biotechnol.* 47 (1), 3239–3245. doi: 10.1080/21691401.2019.1647223

Huang, H. (2013). Shanghan Zabing Lun. *Clin. J. Tradit. Chin. Med.* 02, 38.

Johnson, V. L., and Hunter, D. J. (2014). The epidemiology of osteoarthritis. *Best Pract. Res. Clin. Rheumatol.* 28 (1), 5–15. doi: 10.1016/j.berh.2014.01.004

Lampropoulou-Adamidou, K., Lelovas, P., Karadimas, E. V., Liakou, C., Triantafillopoulos, I. K., Dontas, I., et al. (2014). Useful animal models for the research of osteoarthritis. *Eur. J. Orthop. Surg. Traumatol.* 24 (3), 263–271. doi: 10.1007/s00590-013-1205-2

Liu, F., Shan, L., Tong, P., Zou, J., and Xiao, L. (2016). Clinical study on Fuzi Tang for treatment of mild-to-moderate knee osteoarthritis with Cold-dampness stagnation syndrome. *J. Tradit. Chin. Orthoped. Traumatol.* 28 (01), 10–13.

Malemud, C. J. (2019). Inhibition of MMPs and ADAM/ADAMTS. *Biochem. Pharmacol.* 165, 33–40. doi: 10.1016/j.bcp.2019.02.033

Mandl, L. A. (2019). Osteoarthritis year in review 2018: clinical. *Osteoarthritis Cartilage* 27 (3), 359–364. doi: 10.1016/j.joca.2018.11.001

Mehana, E. E., Khafaga, A. F., and El-Blehi, S. S. (2019). The role of matrix metalloproteinases in osteoarthritis pathogenesis: An updated review. *Life Sci.* 234, 116786. doi: 10.1016/j.lfs.2019.116786

Neogi, T., Guermazi, A., Roemer, F., Nevitt, M. C., Scholz, J., Arendt-Nielsen, L., et al. (2016). Association of Joint Inflammation With Pain Sensitization in Knee Osteoarthritis: The Multicenter Osteoarthritis Study. *Arthritis Rheumatol.* 68 (3), 654–661. doi: 10.1002/art.39488

O'Neill, T. W., McCabe, P. S., and McBeth, J. (2018). Update on the epidemiology, risk factors and disease outcomes of osteoarthritis. *Best Pract. Res. Clin. Rheumatol.* 32 (2), 312–326. doi: 10.1016/j.berh.2018.10.007

Ogbonna, A. C., Clark, A. K., Gentry, C., Hobbs, C., and Malcangio, M. (2013). Pain-like behaviour and spinal changes in the monosodium iodoacetate model of osteoarthritis in C57Bl/6 mice. *Eur. J. Pain* 17 (4), 514–526. doi: 10.1002/j.1532-2149.2012.00223.x

Ohtsuki, T., Shinaoka, A., Kumagishi-Shinaoka, K., Asano, K., Hatipoglu, O. F., Inagaki, J., et al. (2019). Mechanical strain attenuates cytokine-induced ADAMTS9 expression via transient receptor potential vanilloid type 1. *Exp. Cell Res.* 383 (2), 111556. doi: 10.1016/j.yexcr.2019.111556

Philpott, H. T., O'Brien, M., and McDougall, J. J. (2017). Attenuation of early phase inflammation by cannabidiol prevents pain and nerve damage in rat osteoarthritis. *Pain* 158 (12), 2442–2451. doi: 10.1097/j.pain.0000000000001052

Pitcher, T., Sousa-Valente, J., and Malcangio, M. (2016). The Monoiodoacetate Model of Osteoarthritis Pain in the Mouse. *J. Vis. Exp.* (111), 53746. doi: 10.3791/53746

Tang, Q. Y., and Feng, M. G. (2007). DPS data processing system experimental design, statistical analysis and data mining. *Beijing Sci. Press*. pp. 43–80.

Tong, P., Wu, C., Wang, X., Hu, H., Jin, H., Li, C., et al. (2013). Development and assessment of a complete-detoxication strategy for Fuzi (lateral root of Aconitum carmichaeli) and its application in rheumatoid arthritis therapy. *J. Ethnopharmacol.* 146 (2), 562–571. doi: 10.1016/j.jep.2013.01.025

Wang, J., Zhu, X., Liu, L., Shi, X., Yin, L., Zhang, Y., et al. (2013). Effects of strontium on collagen content and expression of related genes in rat chondrocytes cultured in vitro. *Biol. Trace Elem. Res.* 153 (1-3), 212–219. doi: 10.1007/s12011-013-9640-9

Yang, M., Ji, X., and Zuo, Z. (2018). Relationships between the Toxicities of Radix Aconiti Lateralis Preparata (Fuzi) and the Toxicokinetics of Its Main Diester-Diterpenoid Alkaloids. *Toxins (Basel)* 10 (10), 391. doi: 10.3390/toxins10100391

Zeng, G. Q., Chen, A. B., Li, W., Song, J. H., and Gao, C. Y. (2015). High MMP-1, MMP-2, and MMP-9 protein levels in osteoarthritis. *Genet. Mol. Res.* 14 (4), 14811–14822. doi: 10.4238/2015.November.18.46

Conflict of Interest : The authors declare that the research was conducted in the absence of any commercial or financial relationships that could be construed as a potential conflict of interest.

Copyright © 2020 Zhang, Li, Wang, Xu, Zhou, Yan, Hu, Li, Liu, Du, Tong, Wu, Zhang, Shan and Efferth. This is an open-access article distributed under the terms of the Creative Commons Attribution License (CC BY). The use, distribution or reproduction in other forums is permitted, provided the original author(s) and the copyright owner(s) are credited and that the original publication in this journal is cited, in accordance with accepted academic practice. No use, distribution or reproduction is permitted which does not comply with these terms.

frontiers in Physiology

ORIGINAL RESEARCH
published: 26 August 2020
doi: 10.3389/fphys.2020.00734

Antihypertensive and Antifibrosis Effects of Acupuncture at PC6 Acupoints in Spontaneously Hypertensive Rats and the Underlying Mechanisms

Juan-Juan Xin, Qiu-Fu Dai, Feng-Yan Lu, Yu-Xue Zhao, Qun Liu, Jing-Jing Cui, Dong-Sheng Xu, Wan-Zhu Bai, Xiang-Hong Jing, Jun-Hong Gao and Xiao-Chun Yu**

Institute of Acupuncture and Moxibustion, China Academy of Chinese Medical Sciences, Beijing, China

Long-term hypertension can lead to both structural and functional impairments of the myocardium. Reversing left ventricular (LV) myocardial fibrosis has been considered as a key goal for curing chronic hypertension and has been a hot field of research in recent years. The aim of the present work is to investigate the effect of electroacupuncture (EA) at PC6 on hypertension-induced myocardial fibrosis in spontaneously hypertensive rats (SHRs). Thirty SHRs were randomized into model, SHR + EA, and SHR + Sham EA groups with WKY rats as a normal control. EA was applied once a day for 8 consecutive weeks. The cardiac fibrosis as well as the underlying mechanisms were investigated. After 8 weeks of EA treatment at PC6, the enhanced myocardial fibrosis in SHRs was characterized by an increased ratio of left ventricular mass index (LVMI), collagen volume fraction (CVF), and elevated content of hydroxyproline (Hyp) as well as the upregulated expression of collagen I and collagen III in myocardium tissue of SHRs. All these abnormal alterations in the SHR + EA group were significantly lower compared to the model group. In addition, EA at PC6 significantly improved the pathological changes of myocardial morphology. Meanwhile, the increased levels of angiotensin II (Ang II) and tumor necrosis factor-α (TNFα) and expression of transforming growth factor β1 (TGF-β1), connective tissue growth factor (CTGF), matrix metalloproteinase (MMP)-2, and MMP-9 in the serum or heart tissue of SHRs were also markedly diminished by EA. These results suggest that EA at bilateral PC6 could ameliorate cardiac fibrosis in SHRs, which might be mediated by the regulation of the Ang II – TGF-β_1 pathway.

Keywords: electroacupuncture, spontaneously hypertensive rats, myocardial fibrosis, angiotensin II, TGF-β_1, TNF-α

OPEN ACCESS

Edited by:
Jing-Yan Han,
Peking University, China

Reviewed by:
Klaus-Dieter Schlüter,
University of Giessen, Germany
Sushil Kumar Mahata,
VA San Diego Healthcare System, United States

****Correspondence:***
Jun-Hong Gao
drjunhonggao@aliyun.com
Xiao-Chun Yu
yuxc@mail.cintcm.ac.cn

Specialty section:
This article was submitted to Vascular Physiology, a section of the journal Frontiers in Physiology

Received: *09 December 2019*
Accepted: *08 June 2020*
Published: *26 August 2020*

Citation:
Xin J-J, Dai Q-F, Lu F-Y, Zhao Y-X, Liu Q, Cui J-J, Xu D-S, Bai W-Z, Jing X-H, Gao J-H and Yu X-C (2020) Antihypertensive and Antifibrosis Effects of Acupuncture at PC6 Acupoints in Spontaneously Hypertensive Rats and the Underlying Mechanisms. Front. Physiol. 11:734. doi: 10.3389/fphys.2020.00734

INTRODUCTION

Hypertension is a prevalent cardiovascular disorder that affects more than one billion people worldwide. Prolonged elevated blood pressure often leads to cardiac hypertrophic and myocardial fibrotic alterations, which are determinant for the development of heart failure, myocardial infarction, and stroke (Lewington et al., 2016). Therefore, the pathological progress from

hypertension to cardiac hypertrophy and myocardial fibrosis becomes the pivotal issue to address and turns to be a great challenge in clinical management (Diez, 2014). Herein, myocardial fibrosis is known to occur in patients with left ventricular hypertrophy (LVH) caused by persistently elevated blood pressure (Varo et al., 2000) and contributes critically to an increased risk of adverse cardiac events (Zile et al., 2015). It is mainly characterized by excessive accumulation of extracellular matrix (ECM) in the myocardium (Berk et al., 2007) and is deemed as an indicator of mortality in patients with failing myocardium (Lopez et al., 2015). Therefore, reversing or alleviating cardiac fibrosis by adequate blood pressure control would be a major therapeutic goal for patients to avoid the occurrence of heart failure.

Increasing evidence has suggested that both exaggerated collagen (type I and type III) synthesis and inadequate collagen degradation result in the accumulation of ventricular collagen (Varo et al., 2000) in the remodeling fibrotic interstitium of heart (Azevedo et al., 2016). In addition, the rate-limiting step in the extracellular degradation of collagen is the catalytic cleavage associated with the balance between MMPs and their inhibitors (Berk et al., 2007). The myocardial fibrosis can be myocyte death, inflammation, enhanced workload, or hypertrophy and is often aggravated by the renin-angiotensin system (RAS), cytokines (TNF-α), growth factors (such as TGF-β1 and CTGF), and matricellular proteins. Extensive evidence implicates that neuro-hormonal pathways play crucial roles in the pathogenesis of cardiac fibrosis, in which the function of angiotensin II (Ang II) has been highly emphasized due to its direct actions (Wu et al., 2002) and indirect contribution through TGF-β_1 (Chung et al., 2014). TGF-β_1 is ubiquitously expressed in the cardiovascular system (Biernacka et al., 2011), which can trigger the differentiation of cardiac fibroblasts to activated myofibroblasts and may directly participate in promoting cardiac fibrosis in experimental models (Dobaczewski et al., 2011) as well as in fibrotic human hearts (Mancini et al., 2018). In addition, TNF-α has been shown to regulate TGFβ isoforms by decreasing collagen synthesis in cardiac fibroblasts (Sivasubramanian et al., 2001) and increase MMP expression by reducing synthesis of inhibitors of metalloproteinases (Sun et al., 2007). To date, considerable progress has been made in antifibrotic activities of established drugs and novel compounds, including Ang-II pathway inhibitors (De Mello and Specht, 2006), TGF-β pathway inhibitors (Tank et al., 2014), and matrix metalloproteinase inhibitors (Spinale, 2007). Although these interventions may lead to a partial recovery of contractile function via a process known as "reverse remodeling" and thereby delay the progression toward heart failure (Gourdie et al., 2016), the individual and societal costs of heart diseases linked to fibrosis are staggering (Kohl and Gourdie, 2014). Notably, previous clinical studies have revealed that acupuncture is a stand-alone or adjunctive therapy in blood pressure control and treatment of various cardiovascular illnesses (Li et al., 2015). It has been demonstrated that Ang II (Shi et al., 2017), cytokines (TNF-α) (Murakami et al., 2019), growth factors (such as TGF-β_1 and CTGF) (Murakami et al., 2019), and matricellular proteins (Lin et al., 2016) could be modulated by EA treatment. However, the definitive mechanisms underlying antihypertensive and antifibrosis responses of EA are still unclear.

Increasing experimental and clinical studies show that EA at the PC6 acupoint produces therapeutic effects on the treatment of cardiovascular diseases (Li et al., 2015; Shi et al., 2017). Our previous work demonstrates the beneficial role of ACE, AT1R, and AT2R against hypertension-induced cardiac hypertrophy by EA applied at the bilateral PC6 acupoints (Xin et al., 2017). In the present study, using spontaneously hypertensive rats (SHRs), we sought to investigate EA's effect on the synthesis and deposition of collagen stimulated by profibrotic factors so as to explore the antifibrosis effects of acupuncture and its underlying mechanisms. Specifically, the possible roles of the AngII-TGFβ_1 pathway in the mediation of the inhibitory effects of EA (8 weeks) on hypertension and myocardial fibrosis were investigated in our present study.

MATERIALS AND METHODS

Animal Preparation

Thirty-six male SHRs at the age of 12 weeks and 12 male Wistar-Kyoto (WKY) rats of the same age, weighing 240–270 g, were obtained from Vital River Laboratories (Certificate NO. SCXK 2012–0001, Beijing, China). The rats were housed in cages at 24 ± 1°C and humidity of 50 ± 5% under a 12-h light/dark cycle and received standard diet and water *ad libitum*. The study was carried out adhering to guidelines provided by National Institutes of Health for the Care and Use of Laboratory Animals and all efforts were made to minimize suffering of animals.

Animal Grouping and Electroacupuncture Treatment

The rats were randomly divided into four groups: WKY group (n = 12), SHR group (n = 12), SHR + EA group (n = 12), and SHR + Sham group (n = 12). Under isoflurane inhalation anesthesia, the animals in the SHR + EA group were subjected to electroacupuncture treatment at bilateral Neiguan acupoints (PC6, located on the lateral of the lower 1/6 of the forearm between the adius and ulna). Sterilized disposable stainless steel needles (0.3 × 15 mm, Global brand, Suzhou, China) were penetrated 2 mm into the subcutis beneath the acupoints and connected with a Han's Acupoint and Nerve Stimulator (Model HANS-200A, Ji Sheng Medical Technology Co., Ltd., Nanjing, China). Electrical stimulation (2/15 Hz, 1 mA) proceeded for 30 min per day for a period of 8 weeks (Li et al., 2010). In the SHR + Sham group, needles were inserted in the superficial layer of PC6 with no electrical stimulation applied.

Blood Pressure Measurement

Under a conscious condition, the systolic blood pressure (SBP) was recorded by using a CODA Mouse & Rat Tail-Cuff Blood Pressure System (Kent Scientific Co., Torrington, CT, United States). The measurement was conducted once every week at 9–11 am in a quiet room. Before starting measurements,

the CODA cover was lifted and the animal's tail temperature measured by pointing the infrared thermometer at the tail's base. Following a 10 min warm-up period, 10 preliminary cycles were performed to allow the rats to adjust to the inflating cuff. The blood pressure of each rat was tested three consecutive times to calculate the mean value.

Assessment of Left Ventricular Mass Index

Six rats in each group were decapitated after 8 weeks of EA treatment; rat hearts were removed and washed with 4°C normal saline. After drying with filter paper, left ventricles were dissected and weighed to calculate left ventricular mass index (LVMI), which was defined as the ratio of left ventricular (LV) weight to body weight (mg/g).

Van Gieson Staining

Three rats in each group were anesthetized by 10% urethane and transcardially perfused with 250 mL of 0.9% saline immediately followed by 300 mL of 4% paraformaldehyde in 0.1 M phosphate-buffered solution (PB, pH 7.4). The LV section was cut off transversely at the mid-ventricular level for paraffin sectioning (Chen et al., 2012). The myocardial sections (5 μm) were deparaffinized and rehydrated and stained with Van Gieson according to Brilla's (Brilla et al., 1991) methods. In the Van Gieson–stained sections, myocardial cells were stained yellow while collagen was stained light red. The images were captured by a digital camera connected to a microscope (Pannoramic MIDI/250, 3D HISTECH, Hungary). Five randomly selected microscopic fields of each section were analyzed for collagen deposition using the Pannoramic viewer (Quant center, 3D HISTECH, Hungary), which was expressed as collagen volume fraction (CVF), the percentage of the area stained light red for collagen to the total area of each microscopic field. The CVF of each rat represents the mean of five randomly selected microscopic fields, which were measured to represent the development of myocardial fibrosis.

Hydroxyproline Content Assay

Hydroxyproline was assayed using the chloramine T assay (Jia et al., 2010). The apex of the left ventricle was defatted and lysed. Then, the sample was centrifuged at 3000 rpm for 10 min. After centrifugation, the supernatant was mixed with fresh chloramine T for 10 min, followed by mixture with Ehrlich's reagent at 75°C for 20 min. After samples were cooled, optical density was read at 550 nm with a spectrophotometer that was adjusted by a blank. The blank was prepared by the same procedure but without cardiac tissues in the reaction mixture. Hydroxyproline concentration, expressed as micrograms per milligram of dry heart weight, was then calculated as described before (Zhai et al., 2008).

Tissue Preparation and Immunohistochemical Staining

After 8 weeks of EA treatment, three rats in each group were anesthetized by 10% urethane and transcardially perfused with 250 mL of 0.9% saline immediately followed by 300 mL of 4% paraformaldehyde in 0.1 M phosphate-buffered solution (PB, pH 7.4). After perfusion, the LV tissue at the mid-ventricular level was dissected out from the heart and stored in 25% sucrose PB at 4°C. A series of LV sections from rats in each group were cut at a thickness of 20 μm on a cryostat (Thermo, Microm International FSE, Germany) and divided into three groups for the three sections. The sequentially mounted slides were prepared for their respective types of fluorescent immunohistochemical and histochemical staining. Primary antibodies, including mouse monoclonal anti-TGF-β1 antibody (1:250, Abcam, Hong Kong), rabbit polyclonal anti-collagen III antibody (1:100, Abcam), rabbit polyclonal anti-CTGF antibody (1:100, Abcam), and mouse monoclonal anti-collagen I antibody (1:100, Abcam) were used in this study. Goat antimouse Alexa Fluor 488 or 594 secondary antibody (1:500, Molecular Probes, Eugene, OR, United States) and goat antirabbit Alexa Fluor 488 or 594 secondary antibody (1:500; Molecular Probes) were used to visualize the corresponding primary antibodies. Additionally, Alexa Fluor 488 phalloidin (1:1000, Molecular Probes) and 4′, 6-diamidino-2-phenylindole (DAPI, 1:40,000; Molecular Probes) were applied for counterstaining. The three groups of tissue sections were treated with fluorescent immunohistochemical and histochemical stains to examine the relationship of (1) Collagen I and Collagen III, (2) TGF-β_1 and myocardial structure, and (3) CTGF and myocardial structure. The staining methods are as follows. After a brief washing in 0.1 M PB (pH 7.4), tissue sections were incubated in a 0.1 M PB (pH 7.4) containing 3% normal goat serum and 0.5% Triton X-100 for 30 min for blocking non-specific binding. To examine the correlation between Collagen I and Collagen III, the sections were transferred to mouse monoclonal anti-collagen I antibody (1:100, Abcam) and rabbit polyclonal anti-collagen III antibody (1:100, Abcam) to incubate overnight at 4°C. We used a similar procedure in the immunohistochemical staining to examine the correlation between TGF-β_1 and myocardial structure as well as CTGF and myocardial structure. After incubating with blocking solution, primary mouse monoclonal anti-TGF-β1 antibody (1:250, Abcam, Hong Kong) and rabbit polyclonal anti-CTGF antibody (1:100, Abcam) were simultaneously added onto the sections for incubation overnight at 4°C. On the following day, after washing five times with 0.1 M PB, sections were exposed to goat antimouse Alexa Fluor 594 secondary antibody (1:500; Molecular Probes, Eugene, OR, United States), followed by Alexa Fluor 488 phalloidin (1:1000; Molecular Probes). After 2 h of incubation, sections were washed five times with 0.1 M PB and stained with DAPI for 5 min. After washing, the sections were coverslipped with 50% glycerin. All immunohistochemistry for each staining combination was performed at the same time to ensure the consistency of staining. During the staining process, the sections were kept inside a black container at room temperature. Samples were recorded with a confocal imaging system (FV1200, Olympus, Japan) and analyzed using the Olympus Image Processing Software. Final images were processed with Adobe photoshop CS5 and Adobe illustrator CS5 (Adobe Systems, San Jose, CA, United States).

Enzyme-Linked Immunosorbent Assay of Ang II in Heart Tissue and TNF-αin the Serum

Six rats in each group were decapitated after 8 weeks of EA treatment; meanwhile, the blood and LV tissues were collected and centrifuged for reserve. Concentrations of Ang II in heart tissue and TNF-α in the serum were measured by ELISA following the manufacturer's protocol (R&D, Minneapolis, MN, United States).

Western Blotting

Heart tissues were lysed in RIPA buffer containing phosphatase and protease inhibitors (Roche Complete, Roche Diagnostics, Mannheim, Germany). The protein concentration in the supernatant was determined using the BCA method with a bovine serum albumin standard. An equal amount of total protein was subjected to SDS-PAGE and blotted on a NC membrane (Millipore, Billerica, MA, United States). The blots were blocked with 5% defatted milk powder in Tris-buffered saline (TBS) buffer and then incubated with the respective primary antibodies (mouse anti-collagen I 1:500, Abcam, United Kingdom; rabbit anti-collagen III 1:500, Abcam, United Kingdom; mouse anti-TGF-β_1 1:1000, Abcam, United Kingdom; rabbit anti-CTGF 1:1000, Abcam, United Kingdom; mouse anti-MMP2 1:2000, mouse anti-MMP9 1:500, Abcam, United Kingdom; mouse anti-glyceraldehyde-3-phosphate dehydrogenase (GAPDH) 1:20,000, TDY Biotech Co., Ltd., Beijing, China) overnight at 4°C. The membrane was washed with TBS and incubated with horseradish peroxidase-conjugated goat antimouse or rabbit IgG (1:10,000; TDY Biotech Co., Ltd., Beijing, China) for 40 min at room temperature. The targeted proteins were detected by using an enhanced chemiluminescence system (Millipore, Billerica, MA, United States). The quantification of band intensity was carried out using Image-Pro Plus software. Band densities were normalized to individual GAPDH internal control.

RNA Extraction and Quantitative Real-Time PCR

Total RNA was isolated from LV tissues of rats (approximately 100 mg) using an Ultrapure RNA Kit (CWbio, Co., Ltd., Cat#CW0581) and reverse transcribed into cDNA using a

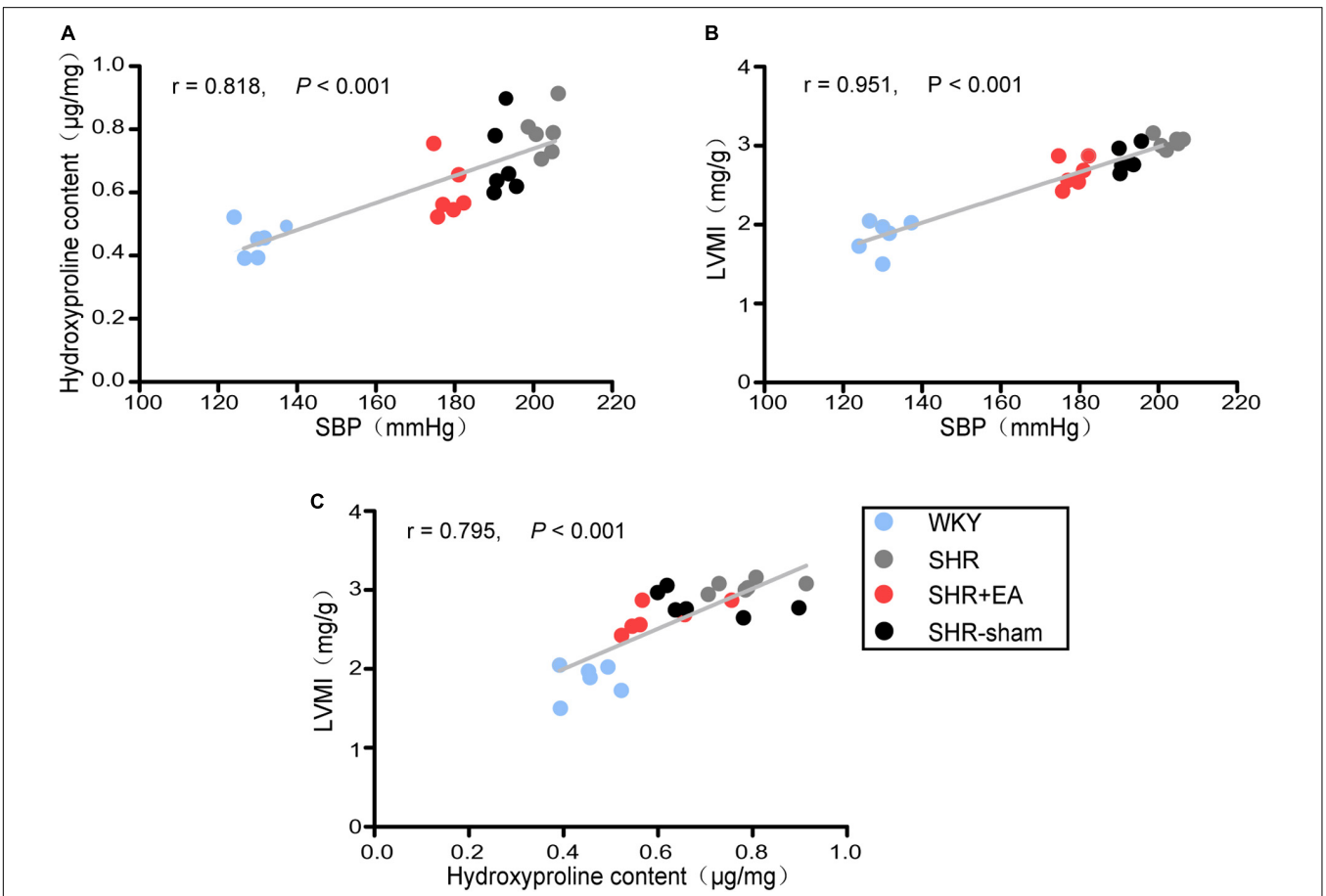


FIGURE 1 | Correlation analysis in WKY rats and SHRs. Systolic blood pressure (SBP) was measured by the tail-cuff method after 8 weeks of EA treatment. The left ventricles were harvested for various analyses. The relationship of hydroxyproline (Hyp) content with SBP, left ventricular mass index (LVMI) with SBP, and LVMI with hydroxyproline content is shown in **(A)**, **(B)**, and **(C)**, respectively (n = 6 each group).

PrimeScript™ RT Reagent Kit with gDNA Eraser (TaKaRa, Co., Ltd., Cat# RR047B) according to the manufacturer's instructions. Real-time PCR reactions were carried out using the SYBR® Premix Ex Taq™ II (Tli RNaseH Plus), ROX plus (TaKaRa, Co., Ltd., Cat# RR82LR) in an ABI 7500 thermal cycler (Thermo Fisher Scientific, Inc.). The amplification was performed as follows: 1 cycle of 95°C for 30 s and 45 cycles of 95°C for 5 s and 60°C for 40 s. Primers and probes were verified as operating at similar efficiencies. The levels of GAPDH expression were measured in all samples to normalize gene expression for sample-to-sample differences in RNA input, RNA quality, and reverse transcription efficiency. The fold differences in mRNA expression levels between samples were calculated using the 2-ΔΔ Ct relative quantification method. The primer sequences (Invitrogen Co., Ltd., Beijing, China) are as follows (forward and reverse, 5′-3′):

GAPDH, CCTTCCGTGTTCCTACCCC (forward) and GCCCAGGATGCCCTTTAGTG (reverse);
TNF-α, GGGCAGGTCTACTTTGGAGTCATTG (forward) and GGGCTCTGAGGAGTAGACGATAAAG (reverse);
TGF-β1, GAGAGCCCTGGATACCAACTACTGC (forward) and CAACCCAGGTCCTTCCTAAAGTCAA (reverse);
CTGF, GGGAAATGCTGTGAGGAGTGG (forward) and GCAGTTGGCTCGCATCATAGTT (reverse).

Statistical Analysis

All data are expressed as mean ± standard deviation (SD). Statistical analysis was performed using one-way analysis of variance (ANOVA) followed by Tukey's *post hoc* test or a repeated-measures ANOVA with the Bonferroni *post hoc* test for multiple comparisons. Changes of blood pressure in the same group were compared statistically by a paired *t* test. A probability of less than 0.05 was considered to be statistically significant.

RESULTS

EA Alleviates Cardiac Fibrosis via Suppressing Elevated Blood Pressure in SHR

To access the cardiac fibrotic alteration following prolonged elevated blood pressure, the SBP, LVMI, and level of hydroxyproline in cardiac tissue were examined at 21 weeks, and their reciprocal correlations are presented in **Figure 1**. Our data shows that, compared to WKY rats, the LVMI and hydroxyproline level were significantly higher in SHRs and had positive correlations with the increased SBP ($P < 0.001$, **Figures 1A,B**), suggesting the development of cardiac fibrosis was likely to be attributed to enhanced blood pressure. The LVMI was correlated with the hydroxyproline content ($P < 0.001$, **Figure 1C**), suggesting that reduced cardiac interstitial fibrosis contributes to the decreased LVMI by 8 weeks EA at PC6 in SHRs. Notably, 8 weeks EA treatment remarkably lowered the elevated SBP as well as the increased LVMI and hydroxyproline level in SHRs while no obvious changes were found in the SHR-Sham group.

Ameliorating Effects of EA on Myocardial Fibrosis in SHRs

EA Reduced the Accumulation of Collagen and the Level of Hydroxyproline in Myocardial Tissue of SHR

The fibrotic alteration in myocardial tissue was assessed by Van Gieson staining. As shown in **Figure 2A**, there was

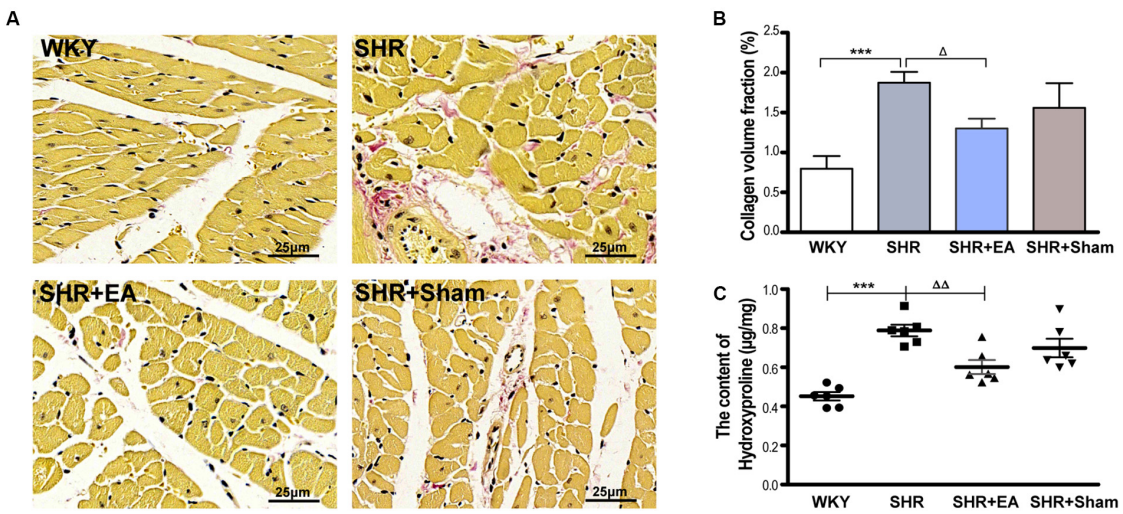


FIGURE 2 | Effect of EA treatment on cardiac interstitial fibrosis in SHR. The tissue was taken after 8 weeks of EA treatment from SHR or at the same time course from WKY, and stained by Van Gieson staining. **(A)** Representative micrographs of cardiac collagen in the interstitial space of the left ventricle, which were ameliorated by EA treatment (bar = 25 μm). **(B)** Quantitative analysis of collagen volume fraction (CVF) by Van Gieson staining in myocardial tissues. ***$P < 0.001$ vs. WKY; $^{\Delta}P < 0.05$ vs. SHR ($n = 3$ each group). **(C)** The hydroxyproline content (Hyp, μg/mg) was estimated after 8 weeks of EA treatment. ***$P < 0.001$ vs. WKY; $^{\Delta\Delta}P < 0.01$ vs. SHR ($n = 6$ each group).

excessive collagenic fiber hyperplasia in SHRs as characterized by enlarged, fractured, and disarranged myocardial fibers as well as hyperchromasia of light red cell components. As compared with SHR, these pathological damages were markedly restored in the SHR + EA group but showed less improvement in SHR + Sham group. Meanwhile, the CVF and level of Hyp in cardiac interstitial tissue were significantly increased in SHRs (**Figures 2B,C**, $P < 0.001$), which were attenuated by EA treatment (**Figures 2B,C**, $P < 0.05$, $P < 0.01$) rather than by sham EA. These results implied that EA at PC6 was effective in attenuating the myocardial fibrosis in SHRs.

EA Lowered the Expression of Col I and Col III in Myocardial Tissue of SHR

Based on immunostaining results (**Figure 3A**) and quantitative analysis (**Figures 3B,C**), as compared with WKY, the expression of Col I and Col III in the cardiac interstitial tissue of SHR were significantly increased, suggesting the excessive deposition of the collagen and sign of myocardial fibrosis. However, as compared with SHR, the expression of Col I and Col III were reduced in the SHR + EA group ($P < 0.001$) rather than the SHR + Sham group. These results show that EA at PC6 attenuated myocardial fibrosis in SHR via downregulating the local expression of Col I and Col III.

Involvement of Ang II, TGF-β_1 in the EA-Induced Antihypertensive and Antifibrosis Effects

Ang II, which has a great vasoconstrictive effect, plays an important role in myocardial interstitial fibrosis through TGF-β1. An enzyme-linked immunosorbent assay showed that the levels of Ang II in SHRs were significantly higher than WKY, in heart tissue (**Figure 4D**, $P < 0.001$). However, EA was effective in reducing the content of Ang II in SHRs (**Figure 4D**, $P < 0.001$), which might mediate the inhibitory effects of EA on myocardial hypertension and myocardial fibrosis. Immunofluorescent staining of myocardial tissue revealed that the fluorescence intensity of TGF-β_1 in SHR was significantly higher than WKY (**Figure 4A**), which was consistent with the quantitative outcomes derived from Western blotting and real-time PCR tests, showing that the local expression of TGF-β_1 was increased in SHRs (**Figures 4B,C**, $P < 0.001$). Notably, 8-week EA

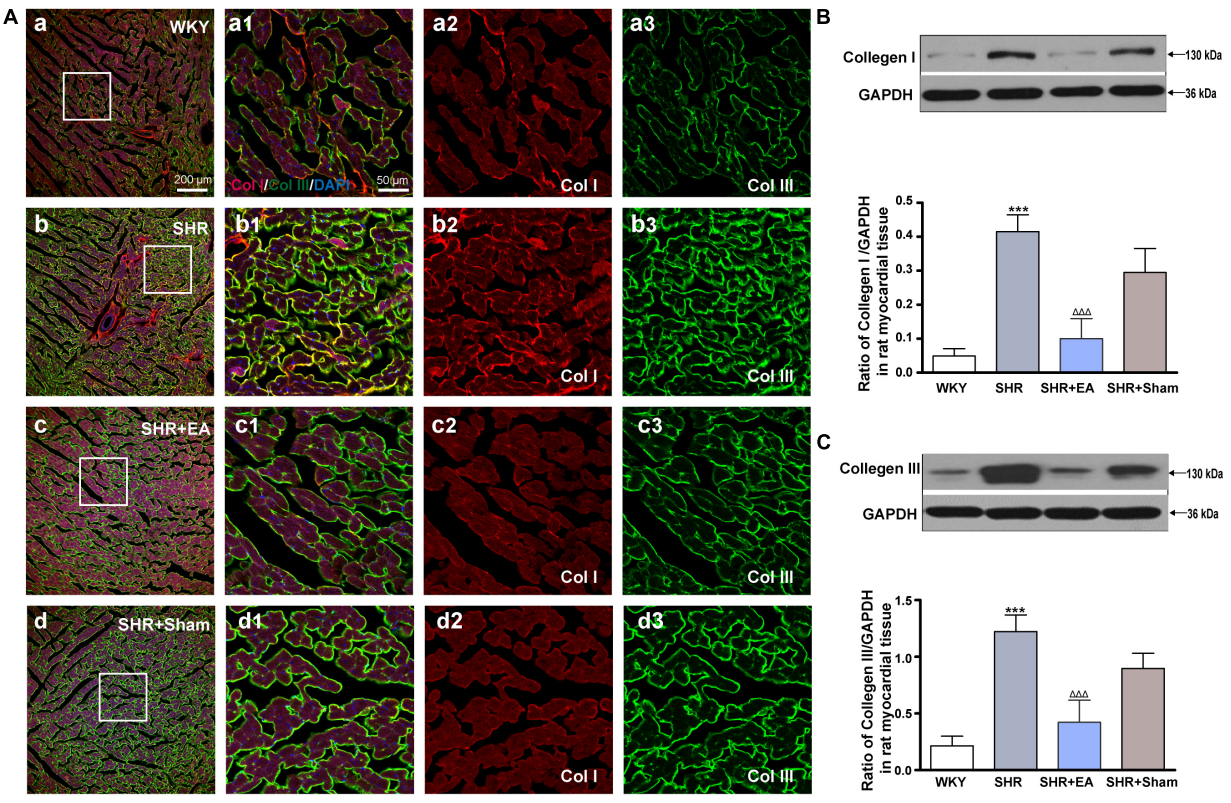


FIGURE 3 | Effect of EA treatment on Collagen I and Collagen III deposition in the left ventricle myocardium. Spontaneously hypertensive rats (SHRs) were treated with EA for 8 weeks. **(A)** The SHR and WKY rats' left ventricles were harvested for fluorescent immunohistochemical staining with Collagen I (red), Collagen III (green), and DAPI (blue). **(a–d)** Interstitial fibrosis in SHR myocardium documented by accumulation of fibrillary collagen I and collagen III. **(a1–d1)** The magnified photos from the areas of the boxes in **(a–d)**, respectively, showing the Collagen I and Collagen III in detail. **(a2–a3,b2–b3,c2–c3,d2–d3)** represent the tryptase **(a2–d2)** and phalloidin **(a3–d3)** distribution in **(a1–d1)**, respectively. Scale bar for **(a–d)** is shown in **(a)** (bar = 200 μm), for **(a1–a3,b1–b3,c1–c3)** shown in **(a1)** (bar = 50 μm). Western blotting analysis of Collagen I **(B)** and Collagen III **(C)** protein in left ventricular myocardium after 8 weeks of EA treatment. $^{***}P < 0.001$ vs. WKY; $^{\Delta\Delta\Delta}P < 0.001$ vs. SHR ($n = 3$ each group).

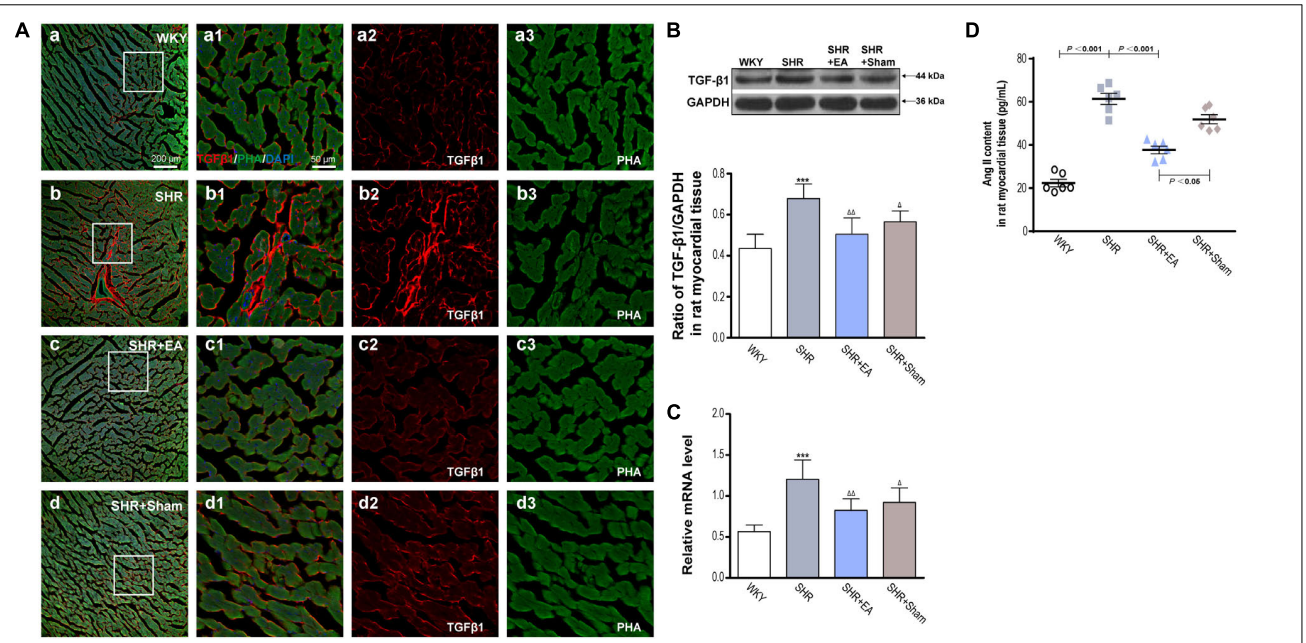


FIGURE 4 | Effect of EA treatment on TGF-β_1 deposition in the left ventricle myocardium. Spontaneously hypertensive rats (SHRs) were treated with EA for 8 weeks. **(A)** The SHR and WKY rats' left ventricles were harvested for fluorescent immunohistochemical staining and histochemical staining with TGF-β_1 (red), phalloidin (PHA, green), and DAPI (blue). **(a–d)** Fibrosis of the myocardium of SHRs and WKY rats as revealed by TGF-β_1 (red) accumulation. **(a1–d1)** The magnified photos from the areas of the boxes in **(a–d)**, respectively, showing the TGF-β_1 and myocardial structure in detail. **(a2-a3,b2-b3,c2-c3,d2-d3)** represent the TGF-β_1 **(a2–d2)** and phalloidin **(a3–d3)** distribution in **(a1–d1)**, respectively. Scale bar for **(a–d)** is shown in **(a)** (bar = 200 μm), for **(a1-a3,b1-b3,c1-c3)** shown in **(a1)** (bar = 50 μm). Western blotting analysis of TGF-β_1 **(B)** protein and real-time PCR analysis of TGF-β_1 **(C)** mRNA in left ventricular myocardium after 8 weeks of EA treatment. ***$P < 0.001$ vs. WKY; $^{\Delta}P < 0.05$, $^{\Delta\Delta}P < 0.01$ vs. SHR ($n = 3$ each group). **(D)** The concentration of TNF-αin myocardium measured by ELISA after 8 weeks of EA treatment ($n = 6$ each group).

treatment mildly attenuated the level of TGF-β1 in the SHR + EA group (**Figures 4B,C**, $P < 0.01$). In addition, both fluorescence intensity and protein expression of TGF-β_1 were also slightly reduced in the SHR+Sham group (**Figures 4B,C**, $P < 0.05$). These results show that EA attenuated hypertension and myocardial fibrosis via downregulating the expression of Ang II and TGF-β_1.

Effects of EA at PC6 on the Expression of CTGF in Myocardial Tissue of SHR

Fluorescent immunohistochemical staining and histochemical staining revealed that the fluorescence intensity of CTGF in SHR was significantly higher than in WKY (**Figure 5A**). As compared with WKY, both Western blotting and real-time PCR revealed that local expression of CTGF was significantly increased in myocardial tissue of SHRs (**Figures 5B,C**, $P < 0.01$, $P < 0.001$), which were attenuated in the SHR + EA group (**Figures 5B,C**, $P < 0.01$, $P < 0.05$). These results showed that EA attenuated hypertension and myocardial fibrosis via downregulating the expression of CTGF.

Involvement of TNF-α, MMP-2, and MMP-9 in the EA-Induced Antihypertensive and Antifibrosis Effects

Enzyme-linked immunosorbent assay and real-time PCR showed that the local expression of TNF-α in SHR was significantly higher than in WKY in both serum and heart tissue (**Figures 6A,B**, $P < 0.001$). In addition, Western blotting revealed that local expression of MMP-9 in SHR was markedly lower than in WKY (**Figure 6D**, $P < 0.001$), whereas MMP-2 showed no difference among three groups (**Figure 6C**), and the expression of MMP-9 showed no difference between the SHR and SHR + Sham groups (**Figure 6D**). Notably, EA was effective in reversing the expression patterns of TNF-α and MMP-9 in SHR ($P < 0.01$, $P < 0.001$), which might mediate the inhibitory effects of EA on myocardial hypertension and myocardial fibrosis.

DISCUSSION

Long-term hypertension is a common pathophysiologic condition in cardiac remodeling and plays a critical role in the pathogenesis of fibrotic cardiomyopathy in patients with primarily or genetically caused enhancement of blood pressure (Berk et al., 2007). Our previous results suggest that (Xin et al., 2017) the blood pressure of SHR from 13 to 21 weeks of age were sustained in the range of 170–200 mmHg and remained on an increasing trend with age while 8-week EA at PC6 was effective in lowering all phases of blood pressure in SHR rats. Therefore, MF induced by long-term hypertension is more likely to happen in SHRs of that age, which is suitable for the observation of the pathological process of hypertension-myocardial fibrosis in the present study (**Figure 7**).

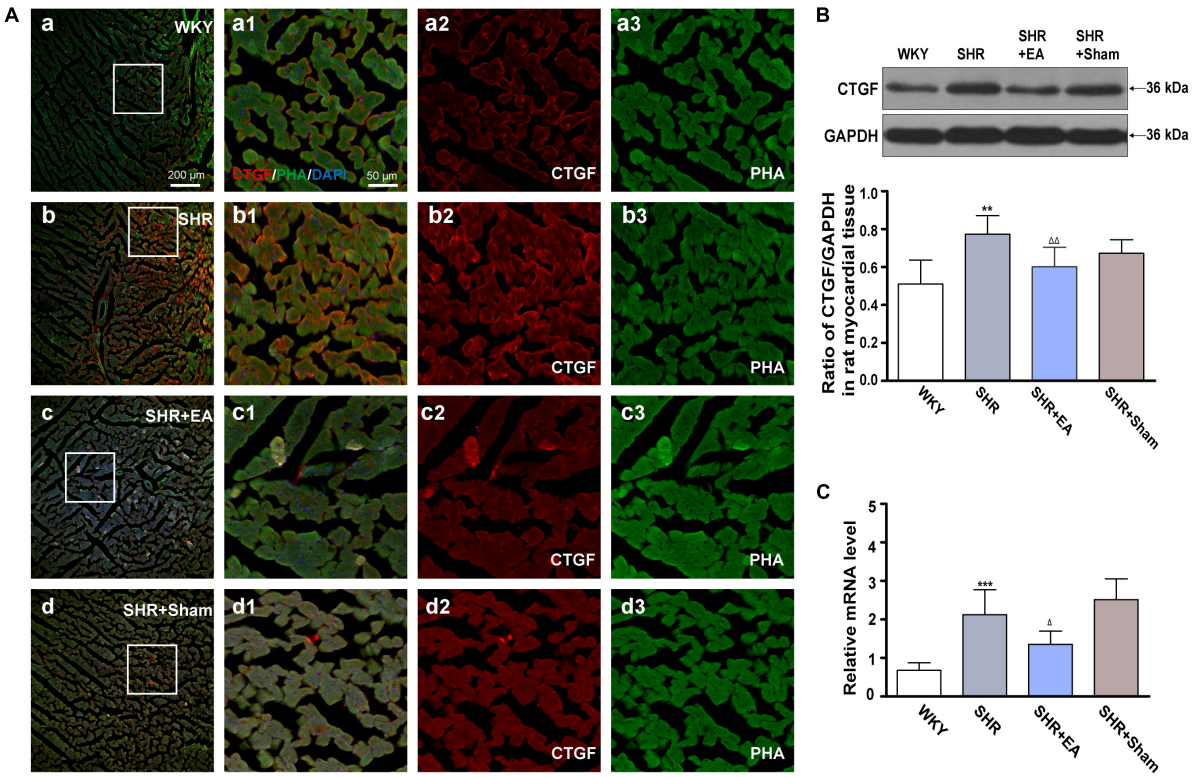


FIGURE 5 | Effect of EA treatment on CTGF deposition in the left ventricle myocardium. Spontaneously hypertensive rats (SHRs) were treated with EA for 8 weeks. **(A)** The SHR and WKY rats' left ventricles were harvested for fluorescent immunohistochemical staining and histochemical staining with CTGF (red), phalloidin (PHA, green), and DAPI (blue). **(a–d)** Fibrosis of the myocardium of SHR and WKY rats as revealed by TGF-β_1 (red) accumulation. **(a1–d1)** The magnified photos from the areas of the boxes in **(a–d)**, respectively, showing the CTGF and myocardial structure in detail. **(a2-a3,b2-b3,c2-c3,d2-d3)** represent the CTGF **(a2–d2)** and phalloidin **(a3–d3)** distribution in **(a1–d1)**, respectively. Scale bar for **(a–d)** is shown in **(a)** (bar = 200 μm), for **(a1-a3,b1-b3,c1-c3)** shown in **(a1)** (bar = 50 μm). Western blotting analysis of CTGF **(B)** protein and real-time PCR analysis of CTGF **(C)** mRNA in left ventricular myocardium after 8 weeks of EA treatment. $^{**}P < 0.01$, $^{***}P < 0.001$ vs. WKY; $^{\Delta}P < 0.05$, $^{\Delta\Delta}P < 0.01$ vs. SHR ($n = 3$ each group).

Cardiac interstitial fibrosis, which is characterized by the collagen-based matrix network, contributes to both systolic and diastolic dysfunction in numerous cardiac pathophysiologic conditions (Kong et al., 2014). Collagen type I make up approximately 85% of total myocardial collagen while collagen type III accounts for about 11% of the total in the heart (Kania et al., 2009). It was also found that the abnormally increased content and out-of-proportion two different kinds of collagen could reflex the pathological alteration of MF in the hypertensive condition.

In the present study, we investigated the antifibrosis effects of EA at PC6 in SHRs and its underlying mechanisms. Our result is in alignment with previous reports (Wang et al., 2017; Chiang et al., 2018) showing that, as compared with WKY controls, the collagen fiber proliferated obviously, and the CVF and Hyp as well as the expression of Col I and Col III in cardiac interstitial tissue were significantly increased in SHRs, which indicated the pathological manifestations of MF. Of note is that the degeneration and structure disturbance of the myocardium were improved by 8 weeks of EA treatment.

It has been suggested that acupuncture at certain acupoints exerts antihypertensive effects, ameliorating heart damage induced by hypertension (Li et al., 2012a). PC6 is effective to improve cardiac function and is a benefit for treating various cardiovascular disorders including hypertension (Xin et al., 2017) and myocardial ischemia (Shi et al., 2017), which is attributed to its anatomical basis, segmental mechanisms (Li and Longhurst, 2010), and modulation on endocrine networks (Li et al., 2012b). In the last decades, several studies have focused on the neurophysiological bases of the effects of PC6 stimulation on cardiovascular mechanisms. Our previous study demonstrates that 8-week EA at PC6 was effective in lowering SBP in SHRs. In the present study, we showed that the Hyp content was positively correlated with the SBP. The LVMI was also positively correlated with the SBP. These results suggest that the reduction of blood pressure by EA at PC6 may contribute to its attenuation of cardiac fibrosis.

Ang II, through the ANG II type 1 receptor (AT1R) (Varo et al., 2000), causes vasoconstriction and elevated blood pressure and plays a causal role in myocardial interstitial fibrosis (Wu et al., 2002). More importantly, Ang II is also downstream of TGF-β_1 to facilitate that pathological course (Shyu, 2017). TGF-β1 is a fibrogenic cytokine that may directly trigger the differentiation of cardiac fibroblasts to activated

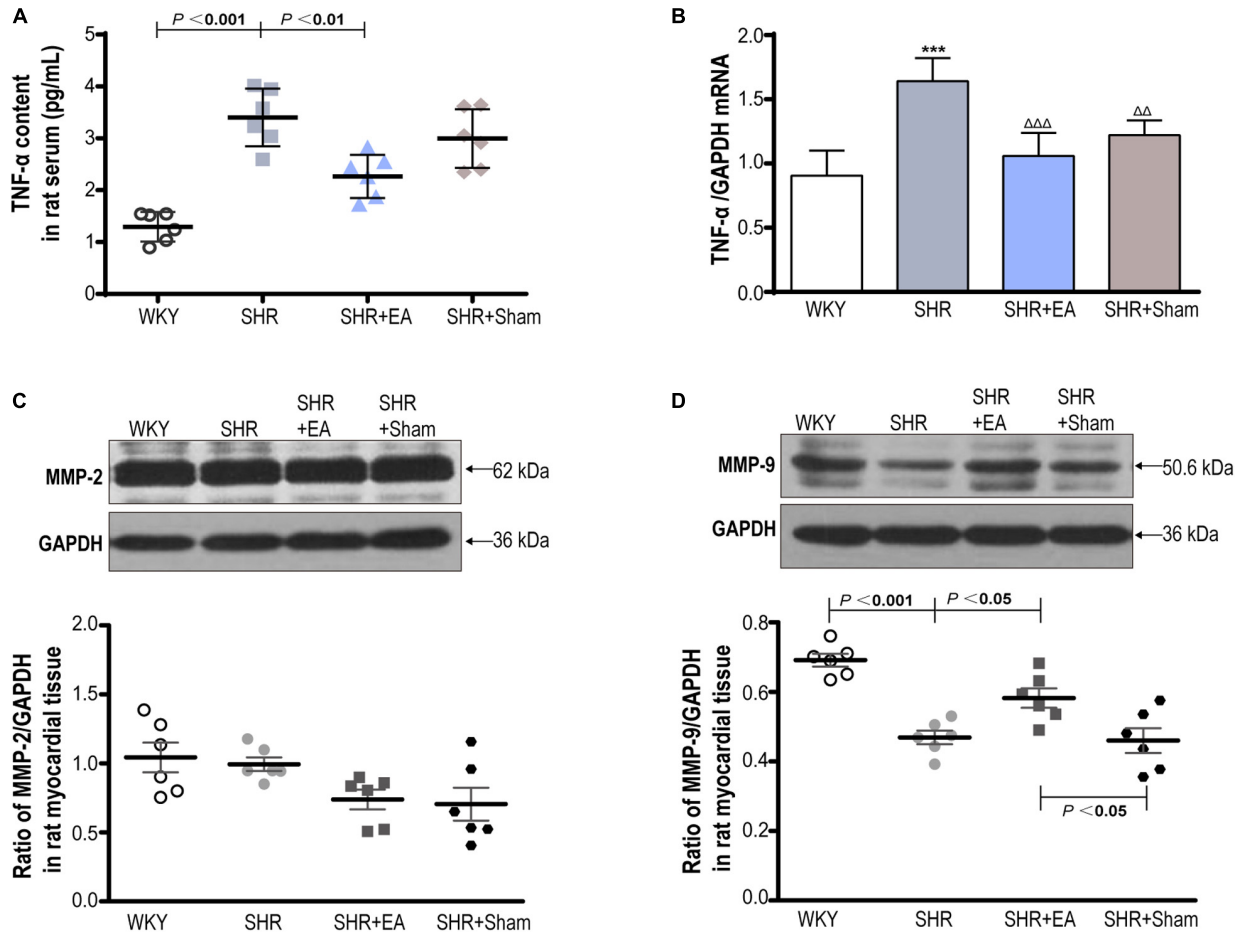


FIGURE 6 | The roles of TNF-α, MMP-2, and MMP-9 in the cardiac protective effects of EA on SHR. The concentration of TNF-αin serum **(A)** measured by ELISA and heart tissue **(B)** measured by real-time PCR after 8 weeks of EA treatment. Western blotting analysis of MMP-2 **(C)** and MMP-9 **(D)** protein in left ventricular myocardium after 8 weeks of EA treatment. ***$P < 0.001$ vs. WKY; $^{\Delta\Delta}P < 0.01$, $^{\Delta\Delta\Delta}P < 0.001$ vs. SHR ($n = 6$ each group).

myofibroblasts to encode fibrillary collagen (Dobaczewski et al., 2011) and participate in the transition from stable hypertrophy to heart failure (Lim and Zhu, 2006). Meanwhile, it was also found that CTGF, as a downstream mediator of TGF-β_1, also has a great effect on fibroblasts induced by TGF-β_1 (Varghese et al., 2017) and significantly upregulated in human heart failure and the myocardial fibrosis–associated animal model (Koshman et al., 2013). In addition, TNF-α, as a proinflammatory cytokine, promotes collagen deposition in fibrotic myocardium myocardia and ECM accumulation by affecting MMP expression and activity, which can lead to myocardial fibrosis (Leask, 2015). It has been shown that TNF-α suppressed the TGFβ_1/Smad signaling pathway through its key effector molecule NF-kB, which activates the inhibitory Smad7 (Kassiri et al., 2009), making these two cytokines combined closely. It was also found that the co-cross-talk of them can enhance fibrotic change in TNF-α overexpressing animals and may involve fibroblast-mast cell interactions (Zhang et al., 2011). Furthermore, by searching the database, we can easily find that, in the pressure overload model of heart disease, MMP2-deficient mice showed reduced myocardial hypertrophy and fibrosis (Matsusaka et al., 2006) while MMP9 deficiency partially improved myocardial hypertrophy and fibrosis following pressure overload (Heymans et al., 2005). Overall, the Ang II-TGF-β_1 pathway mediates the major pathophysiology of cardiac fibrosis, including cardiac fibroblast migration, proliferation, and collagen production (Chung et al., 2014).

Clinical studies suggest that antifibrotic activities of established drugs and compounds include Ang II inhibitors (De Mello and Specht, 2006) and TGF-β inhibitors as well as matrix metalloproteinase inhibitors (Spinale, 2007). Furthermore, aspirin, a non-selective epoxidase inhibitor, is becoming more and more popular in the clinic, and it can improve cardiac fibrosis by reducing the expression of TNF- α (Wu et al., 2012). However, the effective therapeutic strategies are still limited (Zile and Brutsaert, 2002). Therefore, developing new and effective approaches with minimum side effects to target cardiac disease processes linked to fibroblast function is an established therapeutic goal.

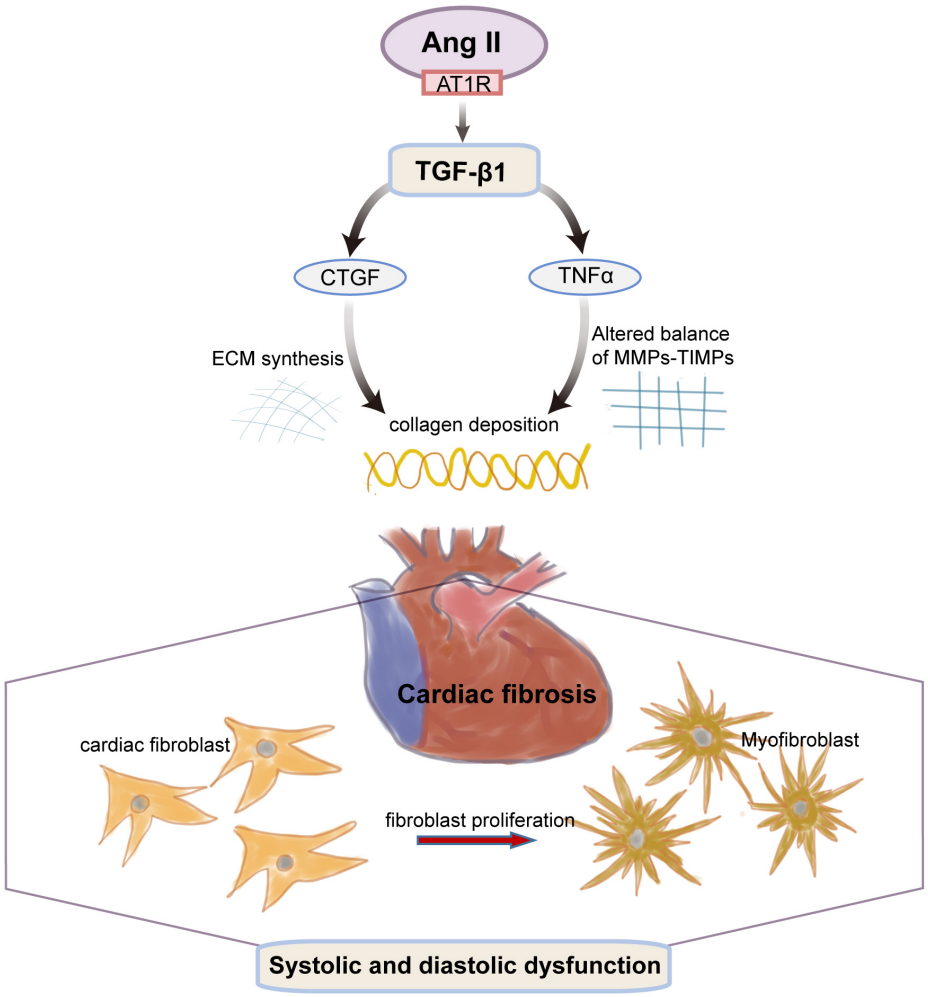


FIGURE 7 | The transition of fibroblasts to myofibroblasts is an early event in hypertension-induced myocardial fibrosis. Cardiac fibroblasts can produce a number of active substances (such as Ang II, TGF-β_1, CTGF, TNFα), which change the collagen deposition due to both a stiffening of the ECM synthesis and an altered balance of MMPs and their inhibitors (TIMP). The altered molecular and cellular events of the cardiac myocytes collectively result in progressive cardiac dysfunction.

Previous studies from our lab and from other researchers uncovered the promising effects of acupuncture at PC6 on blood pressure control and heart protection (Huang et al., 2014; Gao et al., 2015; Xin et al., 2017). Remarkably, our previous work has endeavored the influential role of Angiotensin-converting enzyme (ACE), AT1R, and AngII type 2 receptor (AT2R) on the pathological progression from hypertension to cardiovascular remodeling in SHR by EA treatment. It has been demonstrated that acupuncture at PC6 is effective for protecting the myocardium from chronic ischemic injury by decreasing the serous Ang II concentration (Shi et al., 2017). EA was effective in regulating the levels of TNFα in animal models of ulcerative colitis and zymosan-induced acute arthritis (Park and Namgung, 2018). Additionally, acupuncture at "Quchi" (LI 11) and "Zusanli" (ST 36) probably intervenes in the process of renal interstitial fibrosis by reducing synthesis of kidney type I, type III collagen and restraining expression of TGF-β1 (Chen et al., 2013). However, there's no evidence showing whether or not the Ang II-TGF-β1 pathway is involved in mediating the EA-induced antihypertensive and antifibrosis effects yet. The present study demonstrates that the levels of Ang II in SHRs were significantly higher than WKY in heart tissue. However, EA was effective in reducing the content of Ang II in SHRs. With fluorescent immunohistochemical staining and histochemical staining, Western blotting assay, and real-time PCR, we found that, in the SHR + EA group, the enhanced TGF-β_1 and CTGF were attenuated after 8 weeks of EA treatment, suggesting their involvements in the mediation of the EA's antihypertensive and antifibrosis effects on SHR.

On the other hand, enzyme-linked immunosorbent assay and real-time PCR, respectively, showed that, in the SHR + EA group, the elevated levels and local expression of TNF-α were significantly reduced in both serum and heart tissue. In addition, Western blotting revealed that EA was effective in reversing the expression patterns of MMP-9 in SHR, indicating their

involvement in the mediation of the EA's antihypertensive and antifibrosis effects on SHRs.

CONCLUSION

Collectively, the results of present study suggest that 8 weeks of EA at PC6 inhibited myocardial fibrosis in SHRs, which might be mediated by downregulation of an enhanced Ang II -TGF-β1-CTGF/TNF-α pathway as well as upregulation of the diminished expression of MMP-9. Moreover, targeting the Ang II-TGF-β1 pathway by EA treatment could slow down fibrogenic heart disease process and may provide a promising therapeutic approach that could potentially lead to a less invasive and possibly more effective treatment in cardiovascular disorders caused by hypertension-induced myocardial fibrosis.

DATA AVAILABILITY STATEMENT

The raw data supporting the conclusions of this article will be made available by the authors, without undue reservation, to any qualified researcher.

ETHICS STATEMENT

The animal study was reviewed and approved by the Committee on the Use and Care of Experimental Animals of Institute of Acupuncture and Moxibustion, China Academy of Chinese Medical Sciences.

AUTHOR CONTRIBUTIONS

The experiments were done by J-JX, J-HG, Q-FD, F-YL, Y-XZ, QL, J-JC, and D-SX. W-ZB and X-HJ provided advice on the statistical analyses and data interpretation. J-JX and X-CY drafted and finalized the manuscript. J-HG and X-CY were responsible for the conception, design, and supuervision of the implementation of the study. All authors contributed to the article and approved the submitted version.

FUNDING

This work was supported by the National Natural Science Foundation of China (Nos. 81804211, 81674089, and 81774439).

REFERENCES

Azevedo, P. S., Polegato, B. F., Minicucci, M. F., Paiva, S. A., and Zornoff, L. A. (2016). Cardiac remodeling: concepts, clinical impact, pathophysiological mechanisms and pharmacologic treatment. *Arq. Bras. Cardiol.* 106, 62–69.

Berk, B. C., Fujiwara, K., and Lehoux, S. (2007). ECM remodeling in hypertensive heart disease. *J. Clin. Invest.* 117, 568–575. doi: 10.1172/jci31044

Biernacka, A., Dobaczewski, M., and Frangogiannis, N. G. (2011). TGF-beta signaling in fibrosis. *Growth Fact.* 29, 196–202.

Brilla, C. G., Janicki, J. S., and Weber, K. T. (1991). Cardioreparative effects of lisinopril in rats with genetic hypertension and left ventricular hypertrophy. *Circulation* 83, 1771–1779. doi: 10.1161/01.cir.83.5.1771

Chen, Y., Wu, X., Yu, S., Fauzee, N. J., Wu, J., Li, L., et al. (2012). Neuroprotective capabilities of Tanshinone IIA against cerebral ischemia/reperfusion injury via anti-apoptotic pathway in rats. *Biol. Pharm. Bull.* 35, 164–170. doi: 10.1248/bpb.35.164

Chen, Z. J., Qu, Y., Zhang, L. D., Liu, Y., Wang, S. S., and Gu, L. Y. (2013). [Effects of acupuncture on kidney morphological structure and expression of TGF-beta1 mRNA in rats with spontaneous hypertension]. *Zhongguo Zhen Jiu* 33, 824–828.

Chiang, J. T., Badrealam, K. F., Shibu, M. A., Cheng, S. F., Shen, C. Y., Chang, C. F., et al. (2018). Anti-Apoptosis and anti-fibrosis effects of eriobotrya japonica in spontaneously hypertensive rat hearts. *Int J Mol Sci.* 19:1638. doi: 10.3390/ijms19061638

Chung, C. C., Kao, Y. H., Liou, J. P., and Chen, Y. J. (2014). Curcumin suppress cardiac fibroblasts activities by regulating proliferation, migration, and the extracellular matrix. *Acta Cardiol Sin.* 30, 474–482.

De Mello, W. C., and Specht, P. (2006). Chronic blockade of angiotensin II AT1-receptors increased cell-to-cell communication, reduced fibrosis and improved impulse propagation in the failing heart. *J. Renin Angiotensin Aldosterone Syst.* 7, 201–205. doi: 10.3317/jraas.2006.038

Diez, J. (2014). Arterial hypertension in patients with heart failure. *Heart Fail. Clin.* 10, 233–242. doi: 10.1016/j.hfc.2013.12.004

Dobaczewski, M., Chen, W., and Frangogiannis, N. G. (2011). Transforming growth factor (TGF)-beta signaling in cardiac remodeling. *J. Mol. Cell Cardiol.* 51, 600–606. doi: 10.1016/j.yjmcc.2010.10.033

Gao, J., Zhao, Y., Wang, Y., Xin, J., Cui, J., Ma, S., et al. (2015). Anti-arrhythmic effect of acupuncture pretreatment in the rats subjected to simulative global ischemia and reperfusion–involvement of intracellular Ca2+ and connexin 43. *BMC Complement Altern. Med.* 15:5. doi: 10.1186/s12906-015-0521-y

Gourdie, R. G., Dimmeler, S., and Kohl, P. (2016). Novel therapeutic strategies targeting fibroblasts and fibrosis in heart disease. *Nat. Rev. Drug Discov.* 15, 620–638. doi: 10.1038/nrd.2016.89

Heymans, S., Lupu, F., Terclavers, S., Vanwetswinkel, B., Herbert, J. M., Baker, A., et al. (2005). Loss or inhibition of uPA or MMP-9 attenuates LV remodeling and dysfunction after acute pressure overload in mice. *Am. J. Pathol.* 166, 15–25. doi: 10.1016/s0002-9440(10)62228-6

Huang, Y., Lu, S. F., Hu, C. J., Fu, S. P., Shen, W. X., Liu, W. X., et al. (2014). Electro-acupuncture at Neiguan pretreatment alters genome-wide gene expressions and protects rat myocardium against ischemia-reperfusion. *Molecules* 19, 16158–16178. doi: 10.3390/molecules191016158

Jia, H., Chen, X. L., Chen, C., Hu, Y. Y., and Yun, X. J. (2010). [Baicalin prevents the up-regulation of connective tissue growth factor in fibrotic lungs of rats]. *Sheng Li Xue Bao.* 62, 535–540.

Kania, G., Blyszczuk, P., and Eriksson, U. (2009). Mechanisms of cardiac fibrosis in inflammatory heart disease. *Trends Cardiovasc. Med.* 19, 247–252. doi: 10.1016/j.tcm.2010.02.005

Kassiri, Z., Defamie, V., Hariri, M., Oudit, G. Y., Anthwal, S., Dawood, F., et al. (2009). Simultaneous transforming growth factor beta-tumor necrosis factor activation and cross-talk cause aberrant remodeling response and myocardial fibrosis in Timp3-deficient heart. *J. Biol. Chem.* 284, 29893–29904. doi: 10.1074/jbc.m109.028449

Kohl, P., and Gourdie, R. G. (2014). Fibroblast-myocyte electrotonic coupling: does it occur in native cardiac tissue. *J. Mol. Cell Cardiol.* 70, 37–46. doi: 10.1016/j.yjmcc.2013.12.024

Kong, P., Christia, P., and Frangogiannis, N. G. (2014). The pathogenesis of cardiac fibrosis. *Cell Mol. Life Sci.* 71, 549–574.

Koshman, Y. E., Patel, N., Chu, M., Iyengar, R., Kim, T., Ersahin, C., et al. (2013). Regulation of connective tissue growth factor gene expression and fibrosis in human heart failure. *J. Card Fail.* 19, 283–294. doi: 10.1016/j.cardfail.2013.01.013

Leask, A. (2015). Getting to the heart of the matter: new insights into cardiac fibrosis. *Circ. Res.* 116, 1269–1276. doi: 10.1161/circresaha.116.305381

Lewington, S., Lacey, B., Clarke, R., Guo, Y., Kong, X. L., Yang, L., et al. (2016). The burden of hypertension and associated risk for cardiovascular mortality in China. *JAMA Intern. Med.* 176, 524–532.

Li, J., Li, J., Chen, Z., Liang, F., Wu, S., and Wang, H. (2012a). The influence of PC6 on cardiovascular disorders: a review of central neural mechanisms. *Acupunct. Med.* 30, 47–50. doi: 10.1136/acupmed-2011-010060

Li, J., Li, J., Liang, F., Hong, Y., Wu, S., Tang, H., et al. (2012b). Electroacupuncture at PC6 (Neiguan) improves extracellular signal-regulated kinase signaling pathways through the regulation of neuroendocrine cytokines in myocardial hypertrophic rats. *Evid. Based Complement. Alternat. Med.* 2012, 792820.

Li, P., and Longhurst, J. C. (2010). Neural mechanism of electroacupuncture's hypotensive effects. *Auton. Neurosci.* 157, 24–30. doi: 10.1016/j.autneu.2010.03.015

Li, P., Shibata, R., Maruyama, S., Kondo, M., Ohashi, K., Ouchi, N., et al. (2010). Fenofibrate promotes ischemia-induced revascularization through the adiponectin-dependent pathway. *Am. J. Physiol. Endocrinol. Metab.* 299, E560–E566.

Li, P., Tjen-A-Looi, S. C., Cheng, L., Liu, D., Painovich, J., Vinjamury, S., et al. (2015). Long-lasting reduction of blood pressure by electroacupuncture in patients with hypertension: randomized controlled trial. *Med. Acupunct.* 27, 253–266. doi: 10.1089/acu.2015.1106

Lim, H., and Zhu, Y. Z. (2006). Role of transforming growth factor-beta in the progression of heart failure. *Cell. Mol. Life Sci.* 63, 2584–2596.

Lin, R., Yu, K., Li, X., Tao, J., Lin, Y., Zhao, C., et al. (2016). Electroacupuncture ameliorates post-stroke learning and memory through minimizing ultrastructural brain damage and inhibiting the expression of MMP-2 and MMP-9 in cerebral ischemia-reperfusion injured rats. *Mol. Med. Rep.* 14, 225–233. doi: 10.3892/mmr.2016.5227

Lopez, B., Gonzalez, A., Ravassa, S., Beaumont, J., Moreno, M. U., San José, G., et al. (2015). Circulating biomarkers of myocardial fibrosis: the need for a reappraisal. *J. Am. Coll. Cardiol.* 65, 2449–2456.

Mancini, D., Monteagudo, J., Suarez-Farinas, M., Bander, J., Varshney, R., Gonzalez, J., et al. (2018). New methodologies to accurately assess circulating active transforming growth factor-beta1 levels: implications for evaluating heart failure and the impact of left ventricular assist devices. *Transl. Res.* 192, 15–29. doi: 10.1016/j.trsl.2017.10.006

Matsusaka, H., Ide, T., Matsushima, S., Ikeuchi, M., Kubota, T., Sunagawa, K., et al. (2006). Targeted deletion of matrix metalloproteinase 2 ameliorates myocardial remodeling in mice with chronic pressure overload. *Hypertension* 47, 711–717. doi: 10.1161/01.hyp.0000208840.30778.00

Murakami, H., Li, S., Foreman, R., Yin, J., Hirai, T., and Jdz, C. (2019). Ameliorating effects of electroacupuncture on dysmotility, inflammation, and pain mediated via the autonomic mechanism in a rat model of postoperative ileus. *J. Neurogastroenterol. Motil.* 25, 286–299. doi: 10.5056/jnm18094

Park, J. Y., and Namgung, U. (2018). Electroacupuncture therapy in inflammation regulation: current perspectives. *J. Inflamm. Res.* 11, 227–237. doi: 10.2147/jir.s141198

Shi, L., Fang, J., Zhao, J., Liu, G., Zhao, Q., Zhang, J., et al. (2017). Comparison of the therapeutic effects of acupuncture at PC6 and ST36 for chronic myocardial ischemia. *Evid. Based Complement. Alternat. Med.* 2017:7358059.

Shyu, K. G. (2017). The role of endoglin in myocardial fibrosis. *Acta Cardiol. Sin.* 33, 461–467.

Sivasubramanian, N., Coker, M. L., Kurrelmeyer, K. M., MacLellan, W. R., DeMayo, F. J., Spinale, F. G., et al. (2001). Left ventricular remodeling in transgenic mice with cardiac restricted overexpression of tumor necrosis factor. *Circulation* 104, 826–831. doi: 10.1161/hc3401.093154

Spinale, F. G. (2007). Myocardial matrix remodeling and the matrix metalloproteinases: influence on cardiac form and function. *Physiol. Rev.* 87, 1285–1342. doi: 10.1152/physrev.00012.2007

Sun, M., Chen, M., Dawood, F., Zurawska, U., Li, J. Y., Parker, T., et al. (2007). Tumor necrosis factor-alpha mediates cardiac remodeling and ventricular dysfunction after pressure overload state. *Circulation* 115, 1398–1407. doi: 10.1161/circulationaha.106.643585

Tank, J., Lindner, D., Wang, X., Stroux, A., Gilke, L., Gast, M., et al. (2014). Single-target RNA interference for the blockade of multiple interacting proinflammatory and profibrotic pathways in cardiac fibroblasts. *J. Mol. Cell Cardiol.* 66, 141–156. doi: 10.1016/j.yjmcc.2013.11.004

Varghese, S., Braggio, D. A., Gillespie, J., Toland, A. E., Pollock, R., Mayerson, J., et al. (2017). TGF-beta and CTGF are mitogenic output mediators of Wnt/beta-Catenin signaling in desmoid fibromatosis. *Appl. Immunohistochem. Mol. Morphol.* 25, 559–565. doi: 10.1097/pai.0000000000000340

Varo, N., Iraburu, M. J., Varela, M., Lopez, B., Etayo, J. C., and Diez, J. (2000). Chronic AT(1) blockade stimulates extracellular collagen type I degradation and reverses myocardial fibrosis in spontaneously hypertensive rats. *Hypertension* 35, 1197–1202. doi: 10.1161/01.hyp.35.6.1197

Wang, H., Zhang, X., Yu, P., Zhou, Q., Zhang, J., Zhang, H., et al. (2017). Traditional Chinese medication qiliqiangxin protects against cardiac remodeling and dysfunction in spontaneously hypertensive rats. *Int. J. Med. Sci.* 14, 506–514. doi: 10.7150/ijms.18142

Wu, L., Iwai, M., Nakagami, H., Chen, R., Suzuki, J., Akishita, M., et al. (2002). Effect of angiotensin II type 1 receptor blockade on cardiac remodeling in angiotensin II type 2 receptor null mice. *Arterioscler. Thromb. Vasc. Biol.* 22, 49–54. doi: 10.1161/hq0102.102277

Wu, R., Yin, D., Sadekova, N., Deschepper, C. F., de Champlain, J., and Girouard, H. (2012). Protective effects of aspirin from cardiac hypertrophy and oxidative stress in cardiomyopathic hamsters. *Oxid. Med. Cell Longev.* 2012, 761710.

Xin, J. J., Gao, J. H., Wang, Y. Y., Lu, F. Y., Zhao, Y. X., Jing, X. H., et al. (2017). Antihypertensive and antihypertrophic effects of acupuncture at PC6 acupoints in spontaneously hypertensive rats and the underlying mechanisms. *Evid. Based Complement. Alternat. Med.* 2017:9708094.

Zhai, Y., Gao, X., Wu, Q., Peng, L., Lin, J., and Zuo, Z. (2008). Fluvastatin decreases cardiac fibrosis possibly through regulation of TGF-beta(1)/Smad 7 expression in the spontaneously hypertensive rats. *Eur. J. Pharmacol.* 587, 196–203. doi: 10.1016/j.ejphar.2008.03.006

Zhang, W., Chancey, A. L., Tzeng, H. P., Zhou, Z., Lavine, K. J., Gao, F., et al. (2011). The development of myocardial fibrosis in transgenic mice with targeted overexpression of tumor necrosis factor requires mast cell-fibroblast interactions. *Circulation* 124, 2106–2116. doi: 10.1161/circulationaha.111.052399

Zile, M. R., Baicu, C. F., Ikonomidis, J. S., Stroud, R. E., Nietert, P. J., Bradshaw, A. D., et al. (2015). Myocardial stiffness in patients with heart failure and a preserved ejection fraction: contributions of collagen and titin. *Circulation* 131, 1247–1259. doi: 10.1161/circulationaha.114.013215

Zile, M. R., and Brutsaert, D. L. (2002). New concepts in diastolic dysfunction and diastolic heart failure: part II: causal mechanisms and treatment. *Circulation* 105, 1503–1508. doi: 10.1161/hc1202.105290

Conflict of Interest: The authors declare that the research was conducted in the absence of any commercial or financial relationships that could be construed as a potential conflict of interest.

Copyright © 2020 Xin, Dai, Lu, Zhao, Liu, Cui, Xu, Bai, Jing, Gao and Yu. This is an open-access article distributed under the terms of the Creative Commons Attribution License (CC BY). The use, distribution or reproduction in other forums is permitted, provided the original author(s) and the copyright owner(s) are credited and that the original publication in this journal is cited, in accordance with accepted academic practice. No use, distribution or reproduction is permitted which does not comply with these terms.

frontiers in Pharmacology

ORIGINAL RESEARCH
published: 17 September 2020
doi: 10.3389/fphar.2020.01083

Astragaloside IV Derivative (LS-102) Alleviated Myocardial Ischemia Reperfusion Injury by Inhibiting Drp1^{Ser616} Phosphorylation-Mediated Mitochondrial Fission

Li Chen[1,2], Xiao-Yi Chen[1], Qian-Long Wang[1], Si-Jin Yang[2], Hua Zhou[1], Li-Sheng Ding[3], Lin-Sen Qing[3] and Pei Luo[1]**

[1] State Key Laboratories for Quality Research in Chinese Medicines, Macau University of Science and Technology, Macau, China, [2] Department of Cardiac Encephalopathy, Traditional Chinese Medicine Hospital Affiliated to Southwest Medical University, Luzhou, China, [3] Chengdu Institute of Biology, Chinese Academy of Sciences, Chengdu, China

OPEN ACCESS

Edited by:
Gerald A. Meininger,
University of Missouri, United States

Reviewed by:
Maria Luisa Del Moral,
University of Jaén, Spain
Suresh Kumar Mohankumar,
JSS College of Pharmacy, India

***Correspondence:**
Lin-Sen Qing
qingls@cib.ac.cn
Pei Luo
pluo@must.edu.mo

Specialty section:
This article was submitted to Ethnopharmacology, a section of the journal Frontiers in Pharmacology

Received: 28 April 2020
Accepted: 02 July 2020
Published: 17 September 2020

Citation:
Chen L, Chen X-Y, Wang Q-L, Yang S-J, Zhou H, Ding L-S, Qing L-S and Luo P (2020) Astragaloside IV Derivative (LS-102) Alleviated Myocardial Ischemia Reperfusion Injury by Inhibiting Drp1^{Ser616} Phosphorylation-Mediated Mitochondrial Fission. Front. Pharmacol. 11:1083. doi: 10.3389/fphar.2020.01083

Our previous studies showed that Astragaloside IV derivative (LS-102) exhibited potent protective function against ischemia reperfusion (I/R) injury, but little is known about the mechanisms. Mitochondrial fission regulated by dynamin-related protein1 (Drp1) is a newly recognized determinant of mitochondrial function. This study aimed to investigate the protection of LS-102 on mitochondrial structure and function by regulating the activity of Drp1 using models of H9c2 cardiomyocyte injury induced by hypoxia-reperfusion (H/R), and rat heart injury induced by I/R. The results showed that LS-102 significantly decreased apoptosis, levels of ROS, CK, LDH, and calcium, upregulating MMP, and the Bax/Bcl-2 ratio in cardiomyocytes during I/R injury. Furthermore, LS-102 prevented I/R-induced mitochondrial fission by decreasing Drp1's mitochondrial localization through decreasing the phosphorylation of Drp1 at Ser616 (Drp1^{Ser616}) and increasing the phosphorylation of Drp1 at Ser637 (Drp1^{Ser637}) in H9c2 cells. Importantly, we also robustly confirmed Drp1^{Ser616} as a novel GSK-3β phosphorylation site. GSK-3β-mediated phosphorylation at Drp1^{Ser616} may be associated with mitochondrial fission during I/R of cardiomyocytes. In conclusion, LS-102 exerts cardio protection against I/R-induced injury by inhibiting mitochondrial fission via blocking GSK-3β-mediated phosphorylation at Ser616 of Drp1.

Keywords: astragalosidic acid, myocardial ischemia reperfusion, mitochondrial fission, GSK-3β, Drp1 phosphorylation

INTRODUCTION

Ischemic heart disease (IHD) is one of the biggest killers in the world (Nowbar et al., 2019). Early reperfusion therapy is now standard treatment for patients with acute myocardial infarction. However, myocardial ischemia reperfusion (I/R) further aggravates cell apoptosis, inflammation, and the production of reactive oxygen species (ROS) and calcium, which can lead to heart

conditions (Dominguez-Rodriguez et al., 2014). How to alleviate I/R injury is a key subject for the treatment of IHD (Jennings, 2013).

The study investigated mitochondrial dysfunction is a key factor of pathogenesis, examining whether the mitochondrial function is based on the stabilization of the mitochondrial membrane structure (Turer and Hill, 2010). Recent studies have highlighted that an imbalance of mitochondrial dynamics plays a role in the pathological process of disease (Kuzmicic et al., 2011). During I/R, massive fission of mitochondria causes damaged to the function and structure of mitochondria (Sharp et al., 2014). Concomitantly, the mPTP of myocardial mitochondria is opened and then cytochrome c release. Dynamin-related protein1 (Drp1) is the predominant molecular mediator of mitochondrial fission, which is recruited to fission sites on the mitochondrial outer membrane and initiates mitochondrial fission. Drp1-mediated mitochondrial fission not only aggravates mitochondrial dysfunction but also leads to cell death (Hu et al., 2017). Inhibiting the activity of Drp1 is a therapeutic target to reduce I/R-induced injury (Tao et al., 2018).

Dynamin-related protein1 activity is modulated by posttranslational modifications including phosphorylation, ubiquitination, sumoylation, S-nitrosylation, and so on. Phosphorylation of Drp1 plays a crucial role in Drp1 activity regulation (Jahani-Asl and Slack, 2007). Most studies show that ser616 phosphorylation promotes the translocation of Drp1 to the mitochondrial outer membrane, However, Ser637 phosphorylation reverses this process (Taguchi et al., 2007). Glycogen synthase kinase-3β (GSK-3β), a serine/threonine protein kinase, plays a critical role in mitochondrial bioenergetics, mitochondrial permeability, mitochondrial motility, and mitochondrial apoptosis. Recently, mounting evidence shows that GSK-3β can control cell fate by regulating mitochondrial morphology (Gomez et al., 2008). Previous studies have indicated that GSK-3β interacted with Drp1 in yeast and mammals (Hong et al., 1998; Chen et al., 2000). The activated GSK-3β increases Drp1 GTPase activity to cause mitochondrial fragmentation in the pathogenesis of Alzheimer's disease (AD; Yan et al., 2015). Furthermore, it is unclear whether GSK-3β can contribute to mitochondrial fragmentation in the pathogenesis of I/R through Drp1-dependent mechanisms.

Astragali Radix, which is commonly used in traditional Chinses medicine, has been included in the Chinese Pharmacopeia (Chinese Pharmacopoeia Commission, 2015). Studies have shown that Astragali Radix has pharmacological effects on cardiovascular diseases and immune regulation (Sun et al., 2019). Astragaloside IV (AS-IV), the major pharmacologically active ingredient of Astragali Radix, protects the internal organs from physical damage by exerting antioxidant, anti-inflammatory, and anti-apoptotic properties (Ren et al., 2013). Previous studies have demonstrated that AS-IV has a potent protective effect on I/R injury by activating the PI3K/Akt/GSK-3β pathway (Zhao et al., 2012). Astragalosidic acid (LS-102) is a new water-soluble derivative of astragaloside IV that has been synthesized by our team (Qing et al., 2019). However, the principle of the cardioprotective properties of LS-102 through mitochondrial dynamics in I/R injury has not been investigated. **Figure 1A** shows the structure of this new compound. In this study, two well-established models of I/R on SD rats and H9c2 cells were used to investigate the effect of LS-102 on mitochondrial dysfunction and the dynamics of cardiomyocytes.

MATERIALS AND METHODS

Animals and Experimental Design

Male Sprague-Dawley rats (180–220 g) were purchased from the Laboratory Animal Services Center, of the Chinese University of Hong Kong (Hong Kong). The animals were cultured with a standard diet in accordance with the Institutional Guidelines and Animal Ordinance, in the stable environment of an animal room of a specific pathogen-free (SPF) laboratory (12 h light/dark cycle, 40–50% humidity at 20–23°C). Sixty rats were randomized into six groups (n = 10), respectively as follows: Sham, I/R, Verapamil, Low LS-102, Mid LS-102, and High LS-102. Distilled water at 8 ml/kg was administered intragastrically as a vehicle in Sham and I/R groups. LS-102 was dissolved in distilled water and administered intragastrically at 2.5, 5 and 10 mg/kg 30 min before LAD ligation. Verapamil as a positive control was given intravenously at 0.2 mg/kg 30 min before LAD ligation (**Figure 1B**). LY294002 (0.25 mg/kg, s.c. Sigma, St. Louis, MO, United States) or Akt inhibitor IV (4 mg/kg, s.c. Sigma, St. Louis, MO, United States) was given immediately after the oral administration of LS-102 (10 mg/kg). Thus, fifty rats were randomized into five groups (n = 10), respectively as follows: Sham, I/R, LS-102, LY294002+ LS-102, and Akt inhibitor IV+ LS-102. Out of 10 rats in each group, 6 were used for ventricular function and infarct size measurement and 4 rats for western blot analysis (**Figure 1B**).

Myocardial I/R Injury Rat Model

The rat tests were performed according to the previous description with our modifications (Buerke et al., 1995). In brief, rats were anesthetized with pentobarbital sodium (i.p., 70 mg/kg body weight) and underwent endotracheal intubation and mechanical ventilation. After thoracotomy, rats were operated on, using an open-chest left anterior descending (LAD) coronary artery ligation, 30 min after ischemia, and then 90 min after reperfusion. The sham group rats were subjected to all the procedures except that the LAD ligation was not tightened. The vehicle or drugs were administered 30 min before ischemia via single oral administration. The right carotid artery was isolated and a Millar catheter (Millar Instruments, Inc., Houston, TX, United States) was inserted into the right carotid artery. Using a Power Lab (AD Instruments Pty Ltd., Castle Hill, Australia), mean arterial pressure (MAP) was recorded from the Millar catheter. An electrocardiogram (ECG) in lead II was recorded through needle electrodes attached to the limbs. The heart rate and ST-segment elevation were calculated off-line.

TTC and H&E Staining

Hearts were washed with ice-cold PBS after excising and then weighed. The infarct size of the whole left ventricle

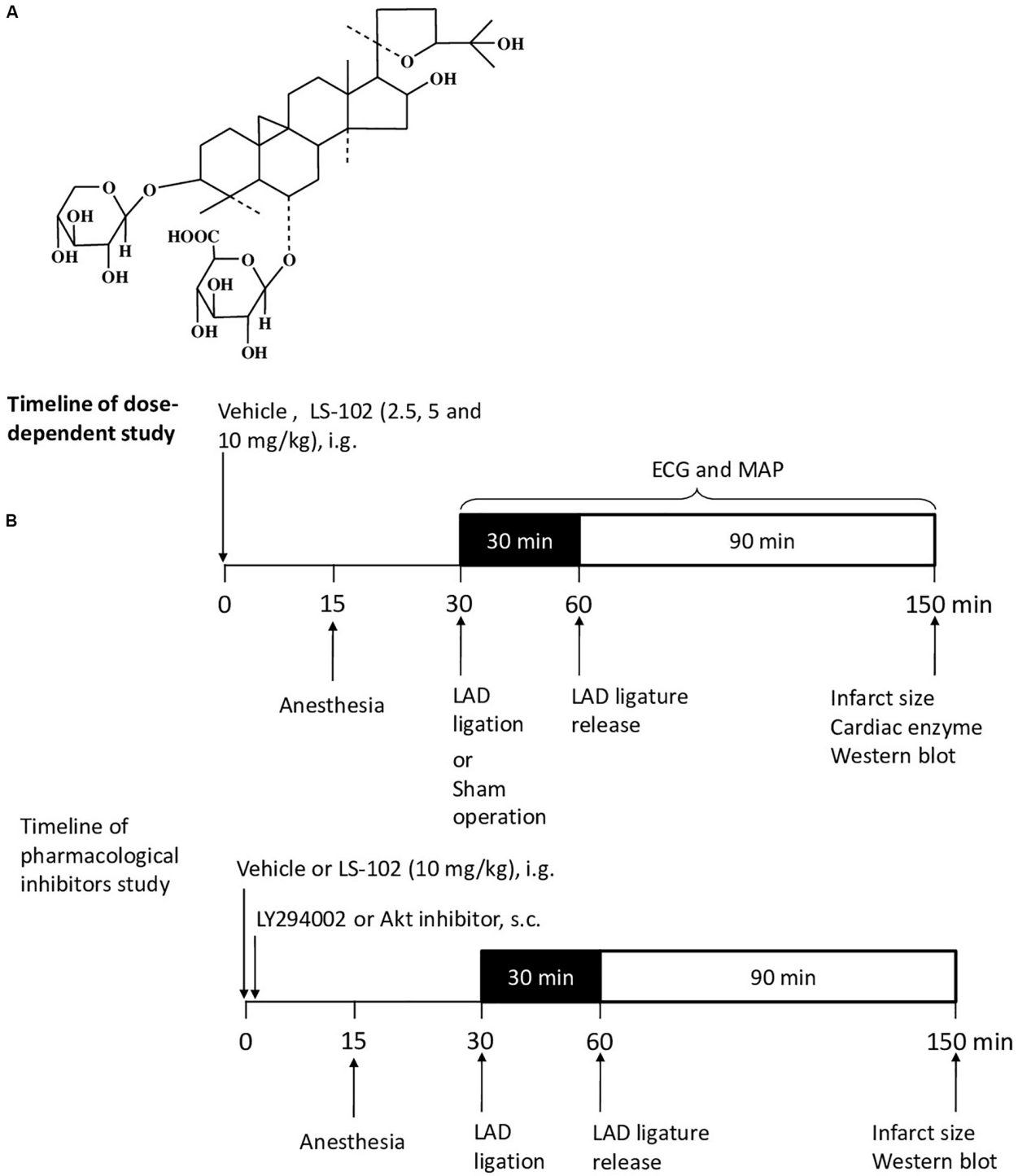


FIGURE 1 | Outline of the experimental protocol to assess the cardioprotective effect of LS-102 on the model of myocardial I/R-induced rat injury. **(A)** Molecular structure of LS-102. **(B)** Protocols of dose-dependent study and pharmacological inhibitors study. Rats were pretreated with vehicle or LS-102, followed by 30 min of ischemia and then 90 min of reperfusion. Rat hearts were collected for TTC and H&E staining, the rat serum samples were also collected to detect the activities of CK and LDH.

was determined using 2,3,5-triphenyltetrazolium as described previously (Zhou et al., 2011). The left ventricle was sliced into transverse sections of five 2–3-mm-thick and then stained in 1% TTC solution in PBS. Images of the stained sections were captured by leica DFC480. The Infarct area of each slice was measured using planimetry method and Image J software. The

histological changes in the heart tissue of the ischemic penumbra part in different groups were observed by H&E staining. Each heart was sectioned into a transverse (coronal) of four equal sections and then fixed directly in 10% buffered formalin in a cassette. Sections were dehydrated in increasing concentrations of ethanol, then cleared with xylene and embedded in paraffin, and then prepared for 3 μm sections.

Cell Culture and *in vitro* Cardiomyocyte Model of H/R

The H9c2 cells (CRL1446, ATCC, United States) were cultured in Dulbecco's Modified Eagle Medium (DMEM), supplemented with 10% fetal bovine serum (FBS) and 1% v/v penicillin/streptomycin (Gibco, Oklahoma, United States). Then the cells were seeded in tissue-culture dishes at 37°C with 5% humidified atmosphere CO_2. LS-102 synthesized by our team was dissolved in Dimethyl sulfoxide (DMSO) and stored as 50 μM store solution at −20°C. H9c2 cells were cultured in saturated glucose-free DMEM and exposed to Whitley H35 Hypoxystation (0.1% O_2, 5% CO_2, and 94.9% N_2) at 37°C for 12 h (hypoxia period) to induce hypoxia/reoxygenation (H/R) injury. Subsequently, the cells were cultured in DMEM supplemented with 10% FBS under normoxia (21% O_2) for 2 h (reoxygenation period).

Cell Viability and Mitochondrial Viability

The cell viability was detected by the method of 3-(4,5-dimethylthiazol-2-yl)-2,5-diphenyltetrazolium bromide (MTT, Molecular Probes, United States). A Multi-Mode Detection Platform (SpectraMax Paradigm, Molecular Devices, United States) was used to detect the absorbance at 570/650 nm. The mitochondrial viability assay kit (Abcam, United States) was used to observe the mitochondrial viability according to the manufacturer's recommendations. The fluorescence intensity was detected at 590 or 550 nm to the direction of excitation by using the Multi-Mode Detection Platform.

Lactate Dehydrogenase Activity, Intracellular Creatine Kinase Activity, Superoxide Dismutase (SOD) Activity, and ATP Content Assay

After treatment, the supernatant medium was collected to measure lactate dehydrogenase (LDH) activity using commercial assay kits (Beyotime Institute of Biotechnology, Beijing, China) according to the manufacturer's recommendations. An absorbance of 450/660 nm was calculated by a Multi-Mode Detection Platform. According to the manufacturers' respective protocols, the treated cells were collected using the creatine kinase (CK) test kit (Biovision, CA, United States) and the superoxide dismutase (SOD) test kit (Beijing Beiyang Institute of Biotechnology, China) to detect CK and SOD activities. An absorbance of 450 nm was evaluated by a Multi-Mode Detection Platform. 1×10^4 H9c2 cells/well were seeded in the dark 96-well plate. After treatment, a luminescent ATP detection assay kit (Abcam, Cambridge, United Kingdom) was employed to detect the ATP level according to the manual.

Apoptosis Analysis With a Flow Cytometer

Cell apoptosis was detected using FITC Annexin V Apoptosis Detection Kit (BD, Franklin Lakes, NJ, United States) according to the manufacturer's recommendations. Briefly, H9c2 cells were cultured in a six-well plate. After H/R treatment, cells were collected and washed three times with PBS and then suspended in 1× binding buffer containing FITC-labeled Annexin V and propidium iodide (BD, Franklin Lakes, NJ, United States) in dark at room temperature. The fluorescence intensity was examined by BD FACSAria III (BD Biosciences, Franklin Lakes, NJ, United States). The intensity of each group (1×10^4 cells) was calculated as representation. Apoptosis of each group was analyzed by Flow J software.

Evaluation of Oxygen Cellular Oxygen Consumption Rate

Seahorse XF8 device (Seahorse Bioscience, United States) was used to measure the oxygen consumption rate (OCR). Briefly, cells (5000 cells/well) were cultured in the XFp cell culture plates. After experiencing H/R, cells were incubated in the 37°C non-CO_2 incubator with 180 μl assay medium (XF Base Medium, 5.5 mM glucose, 1 mM pyruvate, and 2 mM L-glutamine, pH 7.4) according to the manufacturers' recommendations. The sensor cartridge of the XFp analyzer was calibrated for 24 h in the non-CO_2 incubator at 37°C. During the sensor calibration, the OCR of cells was normalized for total protein/well.

ROS, Calcium and Mitochondrial Membrane Potential (MMP) Determination

The CM-H2DCFDA dye, Fluo-4 AM calcium dye (Molecular Probes, United States), and JC-1 dye (Molecular Probes, United States) were employed to assess ROS, calcium, and MMP, respectively. The fluorescent images of calcium and JC-1 were captured by a confocal microscope. H9c2 cells (1×10^4/well) were seeded in μ-Slide 8-well glass bottom plates. Cells were labeled by Fluo-4 AM or JC-1 probe for 30 min after LS102 treatment according to the manufacturer's protocols. The fluorescent intensity of images was analyzed by using the Image J software and a randomly captured method was used to make sure there were three fields per group. The fluorescence intensity of calcium, ROS were detected by the flow cytometer. All cells in the 6-well plates were collected and then suspended in a pre-warmed DMEM buffer containing CM-H2DCFDA or Fluo-4 AM calcium dye. Each group (1×10^4 cells) intensity was calculated as representation.

Quantification of Mitochondrial Length and Fragmentation

The method of mitochondrial image quantification is the same as before (Dong et al., 2016). Cells were cultured in the μ-Slide 8-well glass bottom plate. The cells were stained by 50 nM MitoView Red (GeneCopoeia, United States) after treatment at 37°C for 30 min according to the manufacturer's

recommendations. Mitochondrial morphological and structural changes were observed by a confocal microscope. The six categories of the mitochondria length are as followed: 0–1 μm, 1–2 μm, 2–3 μm, 3–4 μm, 4–5 μm, >5 μm), and the fragmentation of mitochondria confirmed as 0–1 μm (Jahani-Asl and Slack, 2007). The percentage of the 0–1 μm mitochondria was calculated by dividing the number of 0–1 μm mitochondria with the number of total mitochondria.

Immunocytochemistry Analysis

H9c2 cells were seeded into a μ-Slide 8-well glass bottom plate at a total number of 5000 per well. After treatment, cells were first washed with PBST (0.1% Tween 20 to PBS) 3 times and then fixed with ice-cold 100% methanol for 15 min. Secondly, cells were permeabilized with 1% Triton X-100 for 20 min at room temperature. Thirdly, cells were blocked with 1% BSA/PBST buffer for 1 h and then incubated with a primary antibody of anti-Drp1 and anti-GSK-3β (1:100, Cell Signaling Technology, United States) overnight at 4 °C. Then, cells were incubated with Alexa Fluor 488-conjugated (green) and Fluor 555-conjugated (red) secondary antibody (1: 200, Cell Signaling Technology, United States) at room temperature for 2 h. DAPI (1X, Invitrogen, United States) was stained in the final step. The immunofluorescence images were captured by a confocal microscope.

Western Blot Analysis and Co-immunoprecipitation

Cells were lysed with ice-cold RIPA buffer (Cell Signaling, MA, United States) for 20 min after washing twice with ice-cold PBS. Then the cell lysates were collected and centrifuged at 12,000 *g* for 15 min at 4°C. Equal amounts of denatured protein were separated by 8, 10, or 12% SDS-PAGE gels, and then transferred onto polyvinylidene difluoride (PVDF) membranes (Millipore Corporation, Billerica, MA, United States). After being blocked with 5% (w/v) BSA for 1 h at room temperature, the PVDF membrane was incubated with primary antibodies of anti-Drp1, anti-p-Drp1(phospho S616), anti-PI3K, anti- p-PI3K and anti-caspase3 (1:500, Cell Signaling Technology, United States); anti-p-Drp1(phospho S637) antibody (1:500, Abcam, United States); anti-GSK-3β, anti-p-GSK-3β, anti-cytochrome c, anti-Bcl-2, and anti-Bax antibodies (1:1000, Cell Signaling Technology, United States); anti-Akt and anti-p-Akt (Ser473) antibodies (1:200, Santa Cruz Biotechnology, United States); α-tubulin (1:2000, Abcam, United States) at 4°C overnight. They were then washed with PBS-T three times and subsequently hybridized with peroxidase-conjugated secondary antibodies (1:1000, Beyotime Institute of Biotechnology, Beijing, China) for 1–2 h at room temperature. Finally, the PVDF membrane was washed with PBS-T three times and was scanned by an Amersham Imager 600 (STATE of LOUISIANA, United States). β-tubulin was used to normalize the target protein expression. Proteins were denatured by heating at 100°C for 10 min in the loading buffer (contain Tris-HCl, SDS, bromophenol blue, glycerol, and β-mercaptoethanol).

An immunoprecipitation kit (Sangon Biotech, Shanghai, China) was used to detect Drp1 binding to GSK-3β, according to the manufacturers' recommendation. The supernatant was incubated overnight at 4°C with anti-GSK-3β antibody, and then protein A agarose beads for another 2 h at room temperature. After that, the protein A agarose beads were washed six times with the 1 × IP buffer and once with the 0.1 × IP buffer. The beads were boiled in loading buffer for western blot. The PVDF membrane was incubated overnight at 4°C with the anti-Drp1 antibody.

Statistical Analysis

All data were analyzed via GraphPad Prism 5.0 (GraphPad Software Inc, San Diego, CA, United States) and expressed as means ± SEM. Using the method of one-way analysis of variance (ANOVA) with multiple comparisons to analyze the difference between 3 or more groups. Differences were considered statistically significant at *P*-values of $P < 0.05$.

RESULTS

Protective Effect of LS-102 on I/R Injury *in vivo*

The measurement of myocardial infarct size is an important parameter to evaluate I/R-induced myocardial injury. Myocardial infarct size (%) was estimated by using TTC staining. Three dosages of LS-102 (2.5, 5, and 10 mg/kg) were tested in rats subjected to 30 min LAD ligation followed by 90 min reperfusion. As shown in **Figures 2A,B**, the myocardial infarct size in the I/R group was 13.2 ± 1.4%, with a significant increase ($P < 0.01$) when compared with the Sham group. In those that were given an oral dosage 30 min before the acute ischemia, LS-102 exhibited significant protection to rat hearts against I/R injury in a dose-dependent manner to a significant degree. In the I/R group, the serum levels of CK-MB and LDH were significantly higher than those in the sham group ($P < 0.01$). Compared with the I/R group, 5 or 10 mg/kg LS-102 treatment significantly inhibited the elevation of CK-MB or LDH activities induced by acute I/R injury (**Figure 2C**). A comparison between the sham and I/R group revealed histologic changes of hearts, including coagulative necrosis, neutrophil polymorphs infiltration, interstitial hypercellularity, and abundant signs of hemorrhage (**Figure 2D**). The cardiomyocytes in the infarct section of LV appear deeply eosinophilic with loss of the cross striation and disappearance of the nuclei. Oral administration with LS-102 at 5 or 10 mg/kg significantly reduced the necrosis of cardiomyocytes with prominent interstitial edema and inhibited the RBCs accumulation in the interstitial spaces with neutrophil polymorphs infiltration, which confirmed that LS-102 could alleviate the myocardial damage due to I/R (**Figure 2E**).

In our experiments, the change of ST-segment elevation, arrhythmia, and hemodynamic were investigated after I/R in rats. As shown in **Table 1**, the amplitude of ST-segment and heart rate were recorded and used as the indicators of changes in ischemic electrocardiograph. After coronary artery occlusion, the ST-segment markedly upregulated to 0.23 ± 0.12 mV, after ischemia compared to baseline ($P < 0.05$).

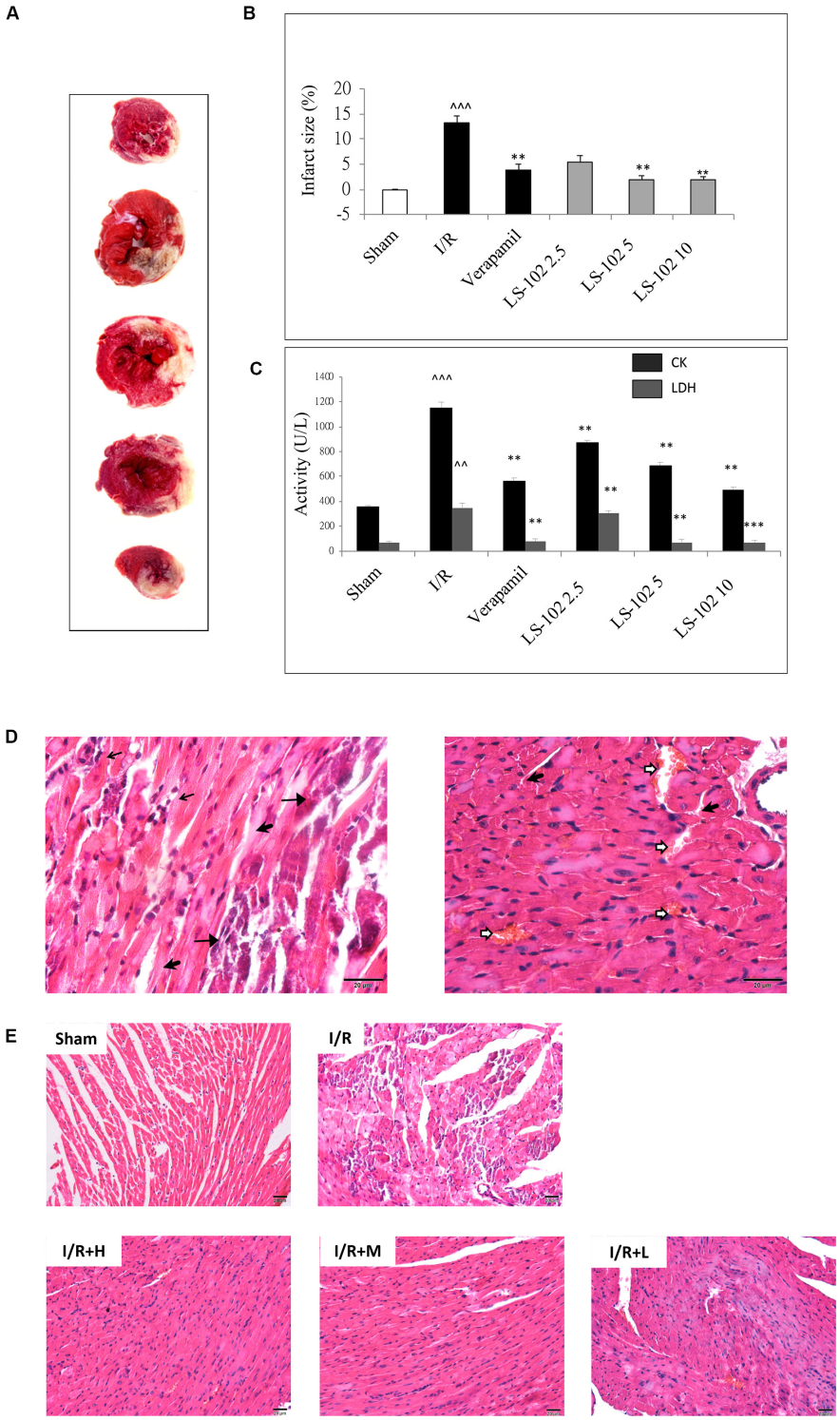


FIGURE 2 | Oral-administration of LS-102 exhibited a dose-dependent relationship of cardioprotective effect in rat heart. **(A)** Representative image of TTC staining sections of the left ventricle. The viable tissue was stained as red area and the unstained pale areas were presumed to be infarcted tissue. **(B)** Bar chart of infarct size (%). **(C)** The activities of CK and LDH in serum were detected. **(D)** Representative high power views of I/R myocardial tissue slice showing neutrophil polymorphs flooding the infarcted area (thin arrow), infarcted cardiomyocytes appearing deeply eosinophilic with loss of cross striations (arrow head), prominent interstitial edema (thick arrow), RBCs in the interstitial spaces (open arrow). **(E)** Illustration of H&E staining of the myocardial tissue in different groups (200 × magnification). Sham and I/R, distilled water 8ml/kg; LS-102 2.5, LS-102 2.5 mg/kg; LS-102 5, LS-102 5 mg/kg; LS-102 10, LS-102 10 mg/kg. Data are shown as mean ± SEM, n = 8–10/group. $^{\wedge\wedge}P < 0.001$, $^{\wedge}P < 0.01$, vs. Sham group, $^{***}P < 0.001$, $^{**}P < 0.01$ vs. I/R group.

TABLE 1 | Effect of LS-102 on heart about the hemodynamic parameters.

Groups	Baseline			Ischemia			Reperfusion		
	HR (beat/min)	MAP (mmHg)	ST height (mV)	HR (beat/min)	MAP (mmHg)	ST height (mV)	HR (beat/min)	MAP (mmHg)	ST height (mV)
Sham	389 ± 25	112 ± 5	0.03 ± 0.02	395 ± 15	120 ± 12	0.05 ± 0.06	381 ± 27	112 ± 5	0.02 ± 0.04
I/R	394 ± 24	121 ± 9	0.05 ± 0.04	435 ± 23*	101 ± 14	0.23 ± 0.12*	388 ± 29	99 ± 15**	0.11 ± 0.08
I/R+L **2.5**	412 ± 19	127 ± 14	0.06 ± 0.03	446 ± 20*	100 ± 11	0.13 ± 0.09	399 ± 22	101 ± 14*	0.08 ± 0.05
I/R+M **5**	397 ± 27	127 ± 11	0.04 ± 0.03	414 ± 24	114 ± 9	0.05 ± 0.03	388 ± 36	116 ± 19	0.08 ± 0.09
I/R+H **10**	401 ± 20	111 ± 8	0.06 ± 0.04	420 ± 32	125 ± 4	0.04 ± 0.05	400 ± 33	122 ± 10	0.08 ± 0.09

*The data showed the heart rate (HR), mean arterial pressure (MAP) and ST height of II lead ECG at the after 10 min of ischemia, and then 90 min of reperfusion. Values were expressed as mean ± SEM of 10 hearts from each group. Hearts underwent 30 min of ischemia and followed by 90 min of reperfusion. *P < 0.05 vs. the baseline of the same group. **P < 0.01 vs. the baseline of the same group.*

Oral-treatment with LS-102 at three dosages (2.5, 5, and 10 mg/kg) markedly diminished the ST-segment elevation. Heart rate increased after ischemia in the I/R group compared to the Sham group. The heart rate decreased and was significantly inhibited after LS-102 (5 or 10 mg/kg) treatment. There was also a significantly decreased MAP in the I/R group at 90 min after reperfusion compared to the baseline. Rats treated with 5 or 10 mg/kg of LS-102 did not appear to the significant and gradual drop in MAP during the process of the I/R. Arrhythmia can be characterized by the appearance of ventricular premature beats (repeated appearance number > 3, VPB); bigeminy/trigeminy (BG/TG); ventricular tachycardia/ventricular fibrillation (appearance of bizarre, irregular; random waveform; and wandering baseline. There were no identifiable QRS complexes or P waves, VT/VF)(Garcia and Miller, 2003). The above phenomenon was investigated by II lead ECG analysis (**Table 2**). Compared with sham operation group, marked arrhythmia was detected (VPB, 100%; BG/TG, 75%; VT/VF, 88%) in the I/R group ($P < 0.01$; $P < 0.01$ respectively). LS-102 treatment at high dose 10 mg/kg reduced the incidence of arrhythmia ((VPB, 30% vs. 100%, $P < 0.05$; BG/TG, 0% vs. 75%, $P < 0.01$; VT/VF, 10% vs. 88%, $P < 0.01$). The above data suggested that the effect of LS-102 exerted potent protective effects against acute I/R injury in rat hearts.

TABLE 2 | Effect of LS-102 on the incidence of cardiac arrhythmias in the rat.

Groups	Incidence (%)		
	VPB	BG/TG	VT/VF
Sham	0(0/10)	0(0/10)	0(0/10)
I/R	100(8/8)^	75(6/8)^	88(7/8)^
I/R+L **2.5**	89(8/9)	56(5/9)	78(7/9)
I/R+M **5**	20(2/10)*	20(2/10)	30(3/10)
I/R+H **10**	30(3/10)*	0(0/10)**	10(1/10)**

*VPB, ventricular premature beats; BG/TG, bigeminy/trigeminy; VT/VF, ventricular tachycardia/ventricular fibrillation. Numerals in parentheses represented numbers of arrhythmia hearts/number of total hearts. Values are expressed as mean ± SEM of 8–10 hearts from each group. Hearts underwent 30 min of ischemia and followed by 90 min of reperfusion. ^P < 0.01, vs Sham group; *P < 0.05, **P < 0.01, vs I/R group (χ^2 test).*

Oral-Administration of LS-102 Activated PI3K/Akt Pathways *in vivo*

Previous studies have indicated that the activation of PI3K/Akt pathways has cardioprotective effects and several pharmacological agents exert the cardioprotective effects by regulating the phosphorylation of PI3K and Akt. In our study, phosphorylation of PI3K at Tyr 458 and phosphorylation of Akt at Ser 473 were investigated by Western blot analysis in the myocardium after I/R. Compared with the Sham group, the I/R group markedly down-regulated the phosphorylation of PI3K and Akt (**Figures 3A,B**). We have observed that LS-102 treatment (5 and 10 mg/kg) activated the expression of PI3K and Akt, which might lead to reducing cardiomyocyte apoptosis, thereby protecting myocardium from I/R-induced injury. Furthermore, we examined whether the cardioprotective effect of LS-102 is abolished by pharmacological blockage of PI3K/Akt pathways. The results (**Figure 3C**) demonstrated that the simultaneous administration of PI3K inhibitor LY294002 or Akt inhibitor IV abolished the infarct size reduction effect of LS-102, as evidenced by an infarct size comparable to that of the I/R group. The results of the present study showed that LS-102 significantly enhanced the expression of pro-survival PI3K/Akt, thereby conferring myocardial protection. To understand further the exact molecular mechanisms involved in the I/R-induced cardio protection, LS-102 were carried out *in vitro* in this study.

LS-102 Attenuates Cardiomyocyte Death Induced by H/R *in vitro*

We used a well-established H/R model that caused cardiomyocyte death to investigate the protective effect of LS-102. Pretreated with LS-102 (0.3125, 0.625, and 1.25 μM) for 24 h, H9c2 cells were exposed to hypoxia (0.1% O_2, 5% CO_2, and 94.9% N_2), with saturated glucose-free DMEM at 37°C for 12 h, and then 2 h reoxygenation with culture medium. H/R significantly decreased the cell viability compared with the Normal group ($P < 0.001$). LS-102 increased cardiomyocyte survival after H/R damage in a dose-dependent manner (**Figure 4A**). The cytotoxicity of LS-102 in H9c2 cells was also examined under normoxia. LS-102 at the concentration of 1.25–20 μM did not lead to cellular cytotoxicity or proliferation in H9c2 cells (**Figure 4B**). Compared with the H/R group, the inhibitory effect of LS-102 on LDH and CK activities was in a dose-dependent manner (**Figure 4C**). In the

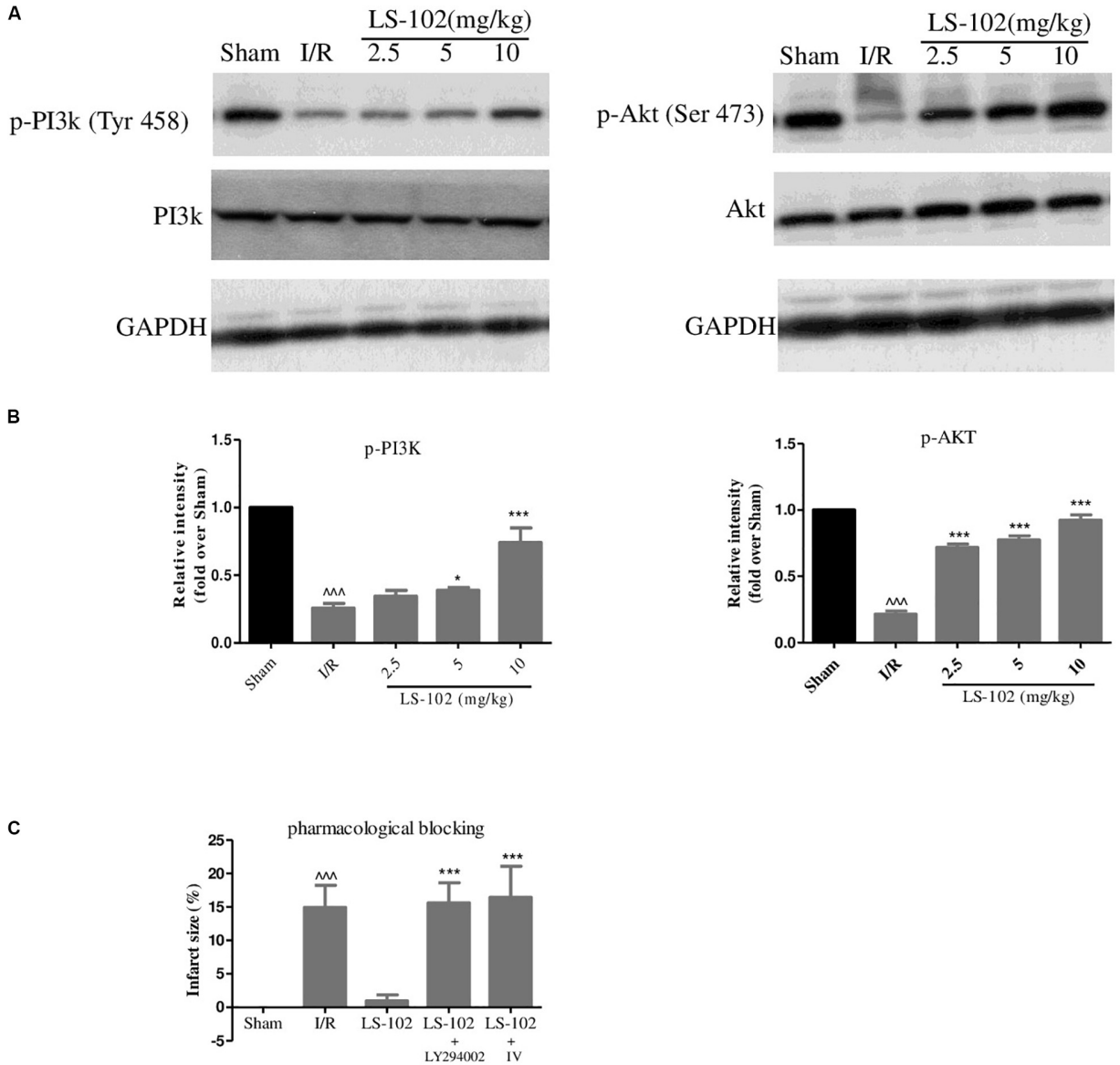


FIGURE 3 | Effect of LS-102 on the PI3K/ Akt signaling in rat heart. **(A)** Representative Western blot of total and phosphorylated PI3K and Akt. **(B)** Quantitative analysis of band intensity, values are expressed as mean ± S.E.M. of 4 hearts from each group. **(C)** Infarct size of a rat after the pharmacological blockage of PI3K and Akt. Sham and I/R, distilled water 8 ml/kg; LS-102, LS-102 10 mg/kg; LS-102+LY294002, LS-102 10 mg/kg+ PI3K inhibitor LY294002 0.25 mg/kg; LS-102+ IV, LS-102 10 mg/kg+Akt inhibitor IV 4mg/kg. Vehicle or LS-102 was given to rats 30 min before LAD ligation. Pharmacological inhibitors were given immediately after the administration of LS-102. Values are mean ± SEM of six rats from each group. ^^^$P < 0.001$, vs Sham group; *$P < 0.05$, ***$P < 0.001$, vs I/R group.

Normal group, cells were spindle-like and mostly arranged in parallel. Underwent H/R, cells were irregularly shrunk, rounded, and arranged in disorder. Treatment of LS-102 at 1.25 μM reduced disorderly arrangement and mostly restored the spindle-shaped morphology (**Figure 4D**).

Next, we examined the effects of LS-102 on apoptosis of H9c2 cells, which were analyzed by flow cytometry. As shown in **Figure 4E**, flow cytometric analysis demonstrated that the apoptotic cells including early apoptotic (Annexin V-FITC+/PI-) and late apoptotic cells (Annexin V-FITC+/PI+) were significantly upregulated in H/R group. LS-102 significantly reduced the percentage of apoptotic cells in a dose-dependent manner. When the treatment concentrations increased, the percentage of apoptotic cells decreased from 26.08% (H/R) to 13.61% (1.25 μM). The effects of LS-102 on caspase-3, Bax, and Bcl-2 protein expression in H9c2 cells were shown in **Figure 4F**. The imbalance of Bcl-2 and Bax protein expression after H/R is one of the major mechanisms underlying the cardiac apoptotic process. H/R led to significant decrease in Bcl-2/Bax expression from 1.00 (Normal) to 0.6362 ± 0.0868 (H/R) ($P < 0.001$). Cells treated with LS-102 significantly increased Bcl-2/Bax expression from 0.6362 ± 0.0868(H/R) to 0.909 ± 0.1(1.25 μM) ($P < 0.01$).

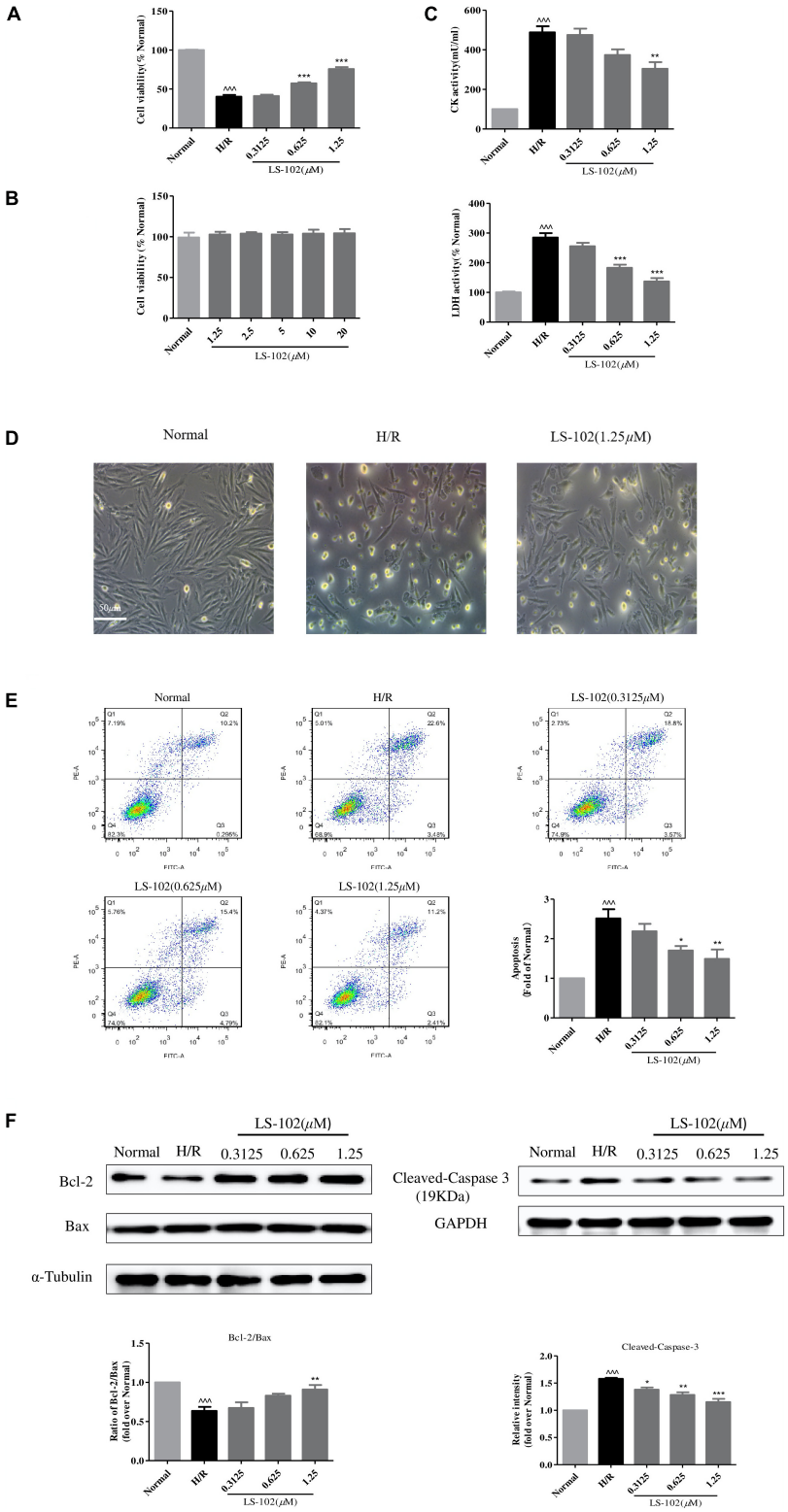


FIGURE 4 | Effects of LS-102 on cell survival after H/R in H9c2 cells. **(A)** Effect of LS-102 on cell viability. **(B)** Cytotoxicity of LS-102 in H9c2 cells under normoxia condition. **(C)** Effects of LS-102 on CK and LDH activities in serum. **(D)** Representative DIC images of H9c2 cells. **(E)** Effect of LS-102 on H/R-induced H9c2 cell apoptosis. Flow cytometry was used to detect apoptotic cells which were calculated the sum of the Q2 and Q3 quadrant. **(F)** Using western blot analysis to determine the protein expression of Bcl-2, Bax, and Cleaved-Caspase-3. The ratio of Bcl-2 to Bax was calculated and normalized to the Normal group. Values are means ± SEM of three or four independent experiments. ~~$P < 0.001$ vs. Normal group. *$P < 0.05$, **$P < 0.01$ and ***$P < 0.001$ vs. H/R group.

Furthermore, LS-102 significantly inhibited cleaved-caspase-3 expression in a dose-dependent manner and with a maximal decrease of 1.073578 at 1.25 μM ($P < 0.001$).

LS-102 Ameliorated Mitochondrial Dysfunction Induced by H/R *in vitro*

The effect of pre-treatment of LS-102 on mitochondrial function after H/R is shown in **Figure 5**. Mitochondrial viability, ATP production, and SOD activity were reduced in H/R compared to the Normal group ($P < 0.001$, $P < 0.001$, and $P < 0.01$, respectively). Our result was indicative of the significant improvement of mitochondrial viability, ATP production, and SOD activity by LS-102 in a dose-dependent manner (**Figure 5A**). We also assessed mitochondrial respiration by detecting the rate of oxygen consumption. The oxygen consumption rate of H9c2 changed evidently in H/R group (**Figure 5B**). After LS-102 treatment, OCR (Basal), OCR (Maximal), ATP, and Spare capacity were significantly increased ($P < 0.001$ vs. H/R group, **Figure 5B**).

Next, we explored the changes in MMP calculated by the ratio of red to green fluorescence. The intensity of the red fluorescent signal decreased in H/R after treatment LS-102(1.25 μM) in H9c2 cells. The intensity of the red fluorescent signal increased (**Figure 5C**). That indicated LS-102 enhanced MMP compared to the H/R ($P < 0.01$). Subsequently, we detected the release of cytochrome c by Western blot. A significant increase of cytochrome c in H9c2 cells exposed to H/R was observed (**Figure 5D**). In the presence of LS-102 treatment, the release of cytochrome c significantly reduced compared to the H/R group ($P < 0.01$). Furthermore, intracellular Ca^{2+} and ROS were significantly increased more than 2 times approximately after H/R ($P < 0.001$, $P < 0.001$, vs. Normal, respectively, **Figures 5E,F**). LS-102 treatment significantly suppressed intracellular Ca^{2+} and ROS production in a dose-dependent manner (**Figures 5E,F**).

LS-102 Regulated the Mitochondrial Dynamics by Inhibiting Drp1-Dependent Mitochondrial Fission

The effect of LS-102 on mitochondrial dynamics after H/R is shown in **Figure 6**. H9c2 cells were stained with Mitotracker Red CM-H_2 Ros to visualize the mitochondria. In the Normal group, mitochondria exhibited a tubular or thread-like structure, distributed uniformly throughout the cytoplasm (**Figure 6A**). Mitochondria were severely damaged after H/R, and the morphology changed into a small, vesicular, punctiform structure, accumulating in the perinuclear area. Both pre-treatment of LS-102 at 1.25 μM and GSK-3β inhibitor AR-A014418 at 10 μM significantly alleviated mitochondrial fragmentation and partly restored the mitochondria of rod-shape and net-like structure.

Quantitative analysis of frequency distribution and changes in the average mitochondrial length indicated that H/R significantly affected mitochondrial distribution and reduced mitochondrial length. The percentage of 0–1 μm exceeded 70%, indicating the frequency distribution of mitochondrial length among

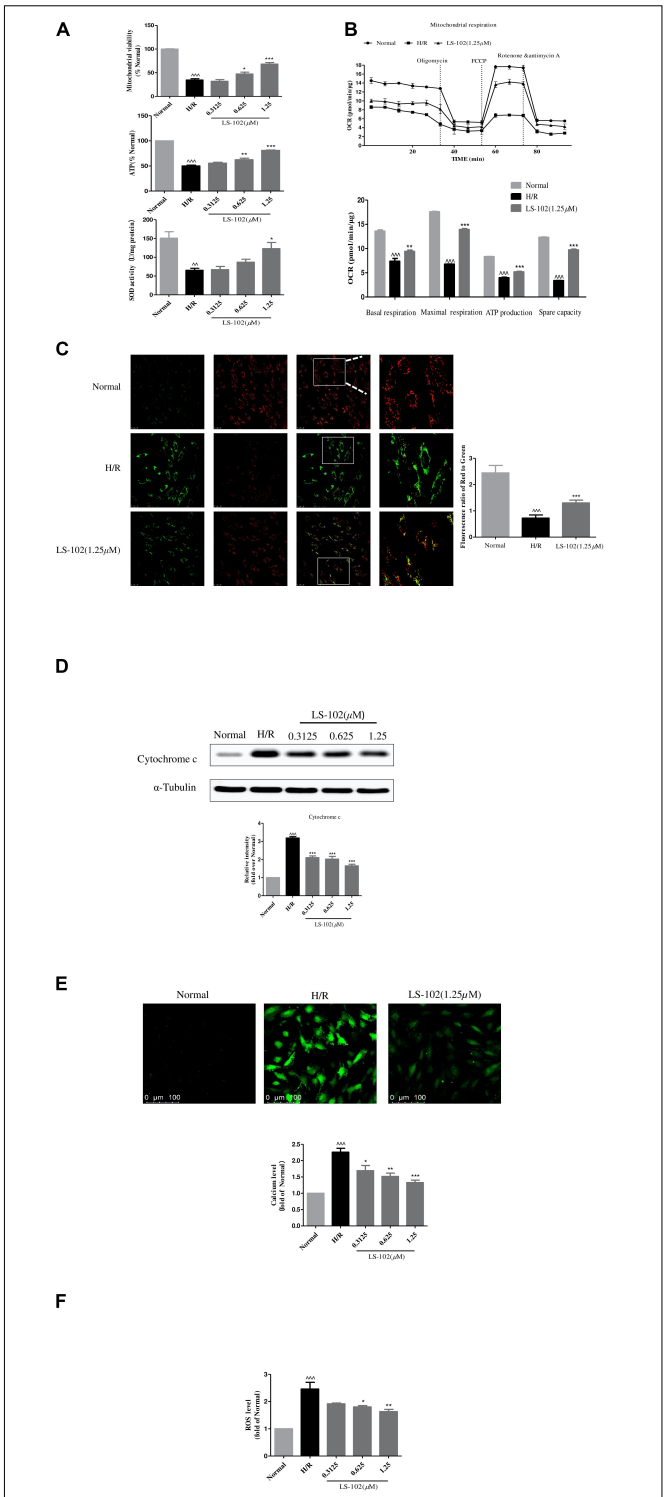


FIGURE 5 | Effects of LS-102 on the mitochondrial dysfunction induced by H/R in H9c2 cells. **(A)** Effect of LS-102 on mitochondrial viability, the content of ATP, and SOD activity. **(B)** The Seahorse XFp Extracellular Flux Analyzer was used to evaluate the effect of LS-102 on oxygen consumption rate (OCR). **(C)** Representative images of JC-1 fluorescent dye stained the mitochondrial membrane potential captured by confocal microscopy with ×40 objective (Olympus). Using the fluorescence microplate assay to calculate the *(Continued)*

FIGURE 5 | Continued
red/green ratio. **(D)** The protein of cytochrome c was detected by Western blot. **(E)** Representative images of Fluo-4AM stained calcium captured by confocal microscopy with ×20 objective (Olympus). The relative mean of the calcium fluorescence intensity was analyzed by flow cytometry. **(F)** The content of the ROS labeled H2DCFDA probe was analyzed by flow cytometry. The values were the means ± SEM of three or four independent experiments. ˆˆ$P < 0.01$, ˆˆˆ$P < 0.001$ vs. Normal group. *$P < 0.05$, **$P < 0.01$, and ***$P < 0.001$ vs. H/R group.

the H/R group (**Figure 6B**). LS-102 treatment significantly decreased the percentage of fragmented mitochondria to 36.34%. As a key regulator of mitochondrial fission, Drp1 is assembled into a spiral ring structure on the mitochondria to promote mitochondrial fission. Therefore, we conducted quantitative analysis of the diffusion and distribution of Drp1 in mitochondria. The analysis showed that H/R induced Drp1 translocation to mitochondria via immunofluorescence images. Treatment with LS-102 (1.25 μM) significantly lowered the level of Drp1 protein on the mitochondria ($P < 0.001$ vs. H/R group, **Figures 6C,D**). Previous studies have shown that the phosphorylation sites of Drp1 at Ser616 and Ser637 are closely related with Drp1 assemble to the mitochondrion (Jahani-Asl and Slack, 2007; Nishihara et al., 2007). As shown in **Figure 6E**, phosphorylation of Drp1^{Ser616} (p-Drp1^{Ser616}) and dephosphorylation of Drp1^{Ser637}(p-Drp1^{Ser637}) were significantly up-regulated (compared to the H/R group; $P < 0.001$). In addition, LS-102 treatment significantly decreased p-Drp1^{Ser616} and increased p-Drp1^{Ser637} levels in a dose-dependent manner, when compared with the H/R group ($P < 0.001$ vs. H/R group, **Figure 6E**). We further investigated the underlying upstream molecular mechanisms for regulation phosphorylation of Drp1.

One kinase, GSK-3β, can regulate the mPTP or cell death under the condition of oxidative stress. The inhibition of GSK-3β effectively enhances cell vitality and anti-oxidative ability. It has to date not been reported whether, during H/R, GSK-3β contributes to the process of Drp1-dependent mitochondrial fission. In our research, the inhibition activity of GSK-3β significantly downregulated the levels of phosphorylated Drp1^{Ser616} detected (compared to the H/R group, $P < 0.001$), but the level of p-Drp1^{Ser637} expression remained unchanged, as shown in **Figure 6F**. GSK-3β is not only a kinase but also an anchoring protein (Harwood, 2001). We used immunofluorescence and a Co-immunoprecipitation (Co-IP) assay to confirm the interaction between Drp1 and GSK-3β protein. We found that the co-localization of Drp1 with GSK-3β upregulated in the H/R group, which was attenuated by pre-treatment of LS-102 (**Figures 6G,H**). Consistently, the result of Co-IP further proved that GSK-3β can bind Drp1. In the H/R group, we found Drp1 in GSK-3β-IP elutes from H9c2 cells. LS-102 treatment decreased the binding of Drp1 to GSK-3β compared to the H/R group ($P < 0.001$, **Figures 6I,J**). All the evidence indicates that GSK-3β can bind to phosphorylate Drp1 resulting in mitochondrial fragmentation in the model of H/R-induced H9c2 cells. LS-102 can block GSK-3β-mediated

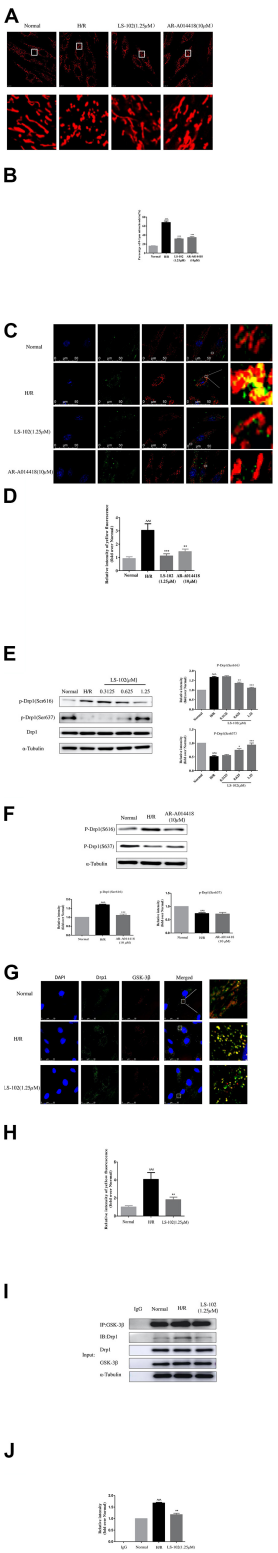


FIGURE 6 | Effects of LS-102 on Drp1-dependent mitochondrial fission induced by H/R in H9c2 cells. **(A)** Representative images showing MitoTracker Red CM-H2Ros staining (MitoROS; red) were captured by confocal microscopy with ×40 objective (Olympus). **(B)** Bar graph showing the
(Continued)

FIGURE 6 | Continued
percentage of fragmented mitochondria (mitochondrial length of less than 1 μm). **(C)** Co-localization analysis of Drp1 on mitochondria using a confocal microscope with ×40 objective (Olympus). H9c2 cells were stained with MitoROS (red), anti-Drp1 antibody (green). Nucleus was trained with DAPI (blue). The yellow dots indicated Drp1(green) on the mitochondria (red) location. **(D)** Qualitative analysis of colocalization by Image J software. **(E)** Phosphorylation of Drp1 was detected by Western blot analysis and incubated with anti-phospho-Drp1(Ser637) or anti-phospho-Drp1(Ser637) antibodies, the loading control was α-Tubulin. **(F)** The protein expression of p-Drp1^{Ser616} and p-Drp1^{Ser637} after treatment of GSK-3β inhibitor AR-A014418 were determined by Western blot. **(G)** Co-localization analysis of Drp1 (green) with GSK-3β (red) were captured by confocal microscopy with × 40 objective (Olympus). **(H)** Bar chart showing yellow fluorescence intensity. **(I,J)** The protein expression of Drp1 with GSK-3β was examined by Co-immunoprecipitation (Co-IP) assay and Western blot. The relative densities of immunoreactive bands were quantified over α-Tubulin using image J software. Values are the means ± SEM of three or four independent experiments. ˜$P < 0.05$, ˜˜$P < 0.001$ vs. Normal group. *$P < 0.05$, **$P < 0.01$ and ***$P < 0.001$ vs. H/R group.

Drp1 phosphorylation and decrease the co-localization of Drp1 with GSK-3β.

LS-102 Exerted Cardio Protection Against H/R Injury by Aactivating PI3K/Akt Pathways

This study has proved that GSK-3β acts as upstream signaling of Drp1 to induce mitochondrial fragmentation in H/R. Previous studies have shown that ischemic preconditioning enhances the phosphorylation and decreases the activity of GSK-3β by PI3K/Akt signal pathway. To validate the mechanisms of the underlying protective effect of LS-102, the protein expression of p-PI3K, PI3K, Akt, p-Akt, p-GSK-3β(Ser9), and GSK-3β were examined. As shown in **Figure 7A**, H/R-induced phosphorylation of PI3K, Akt, and GSK-3β decreased without influencing the total PI3K, Akt, and GSK-3β. Pre-treatment of LS-102 (0.3125, 0.625, and 1.25 μM) significantly increased the phosphorylation of PI3K, Akt, and GSK-3β in a dose-dependent manner ($P < 0.001$, vs. H/R). In addition, the protective effect of LS-102 was blocked by the PI3K inhibitor LY294002. LY294002, which abrogated the protective effects of LS-102 and could increase cell and mitochondrial viability, and decrease the release of cytochrome c (**Figures 7B,C**). All data has suggested that LS-102 increased cardiomyocyte survival in H/R by improving the mitochondria function and inhibiting Drp1-dependent mitochondrial fission via regulating the PI3K/Akt/GSK-3β pathway.

DISCUSSION

This study is the first to prove that LS-102 exerted a powerful protective effect on I/R-induced myocardium injury, decreasing oxidative stress and apoptosis. The mechanism of cardio protection was related to the PI3K/Akt signaling pathway *in vivo* and *vitro* (**Figure 8**). Recently, growing evidence has indicated that maintaining the balance of mitochondrial dynamics is a potential novel therapeutic target in I/R-induced injury. We also demonstrated that LS-102 effectively prevented mitochondrial fission by decreasing Drp1 phosphorylation at Ser616 and increasing Drp1 phosphorylation at Ser637 to maintain the integrity of mitochondrial structure and function. We discovered that the Drp1 protein was involved in the downstream signaling pathway of GSK-3β, which mediated mitochondrial fragmentation by modulating Drp1^{Ser616} phosphorylation during I/R of cardiomyocytes. Therefore, PI3K/Akt/GSK-3β signaling pathway regulates cell viability and apoptosis, at least in part, depending on the GSK-3β/Drp1-mediated balance of mitochondrial dynamics.

Astragaloside IV has been widely used for treating cardiovascular diseases. Despite its efficacy and safety, AS-IV has a major problem of low bioavailability. To change this limitation, our team synthesized a new water-soluble compound LS-102. In previous research, we found that the relative bioavailability of LS-102 was twice that of AS-IV (Zhang et al., 2017; Qing et al., 2019). After conducting this research, we further elucidated the impact of LS-102 on the myocardial I/R injury to provide evidence for future clinical applications. In animal models, our results showed that LS-102 preserved LV function, attenuated the incidence of arrhythmia, reduced infarct size, and decreased the release of CK, LDH via activating the PI3K/Akt signaling pathway. Additionally, the PI3K or Akt pharmacological inhibitor abrogated the protective effects of LS-102. It is essential for the dynamic balance of mitochondrial structure and function to maintain a functional heart as a response and adaptation to metabolic or environmental stresses (Yellon and Hausenloy, 2007; Walters et al., 2012; Kloner, 2017; Forte et al., 2020; Ghosh et al., 2020; Oh et al., 2020; Tong et al., 2020). We found that LS-102 significantly enhanced the survival rate of H9c2 cardiomyocytes by modulating mitochondria in the model of H/R-induced H9c2 cell injury. LS-102 increased mitochondrial viability, OCR, and ATP content. Meanwhile, LS-102 reduced free radical injury by decreasing ROS production, calcium overload, and increasing the activity of SOD. We also detected the influence of LS-102 on mitochondrial-related apoptosis pathways. LS-102 prevented the mitochondrial apoptosis pathway by stabilizing MMP, inhibiting the release of cytochrome c, decreasing the ratio of Bax/Bcl-2, and inhibiting the cleavage of Caspase-3. The protective effects of LS-102 are mainly attributed to the activation of the PI3K/Akt signaling pathway. Moreover, the PI3K inhibitor (LY294002) abolished the effect of LS-102 on H/R-induced cardiomyocytes, mitochondrial viability, and the release of cytochrome c, which was further confirmed it.

Mitochondrial fission can be described as mitochondrial dynamics, that play essential roles in maintaining mitochondrial homeostasis. Drp1-dependent mitochondrial excessive fission cause mitochondrial fragmentation, ROS production, depolarization of the MMP, the release of cytochrome c, and the susceptibility of cell apoptosis, which is a key player in the pathogenesis of I/R (James et al., 2003; Karbowski et al., 2004; Lee et al., 2004; Hamacher-Brady et al., 2006; Ong et al., 2010; Sharp et al., 2014). Reports from *in vitro* and *in vivo* studies have shown that pharmacologic or genetic inactivation of Drp1 intervention can prevent mitochondrial fission in myocardial I/R injury models (Ong et al., 2010; Disatnik et al., 2013; Sharp et al., 2014;

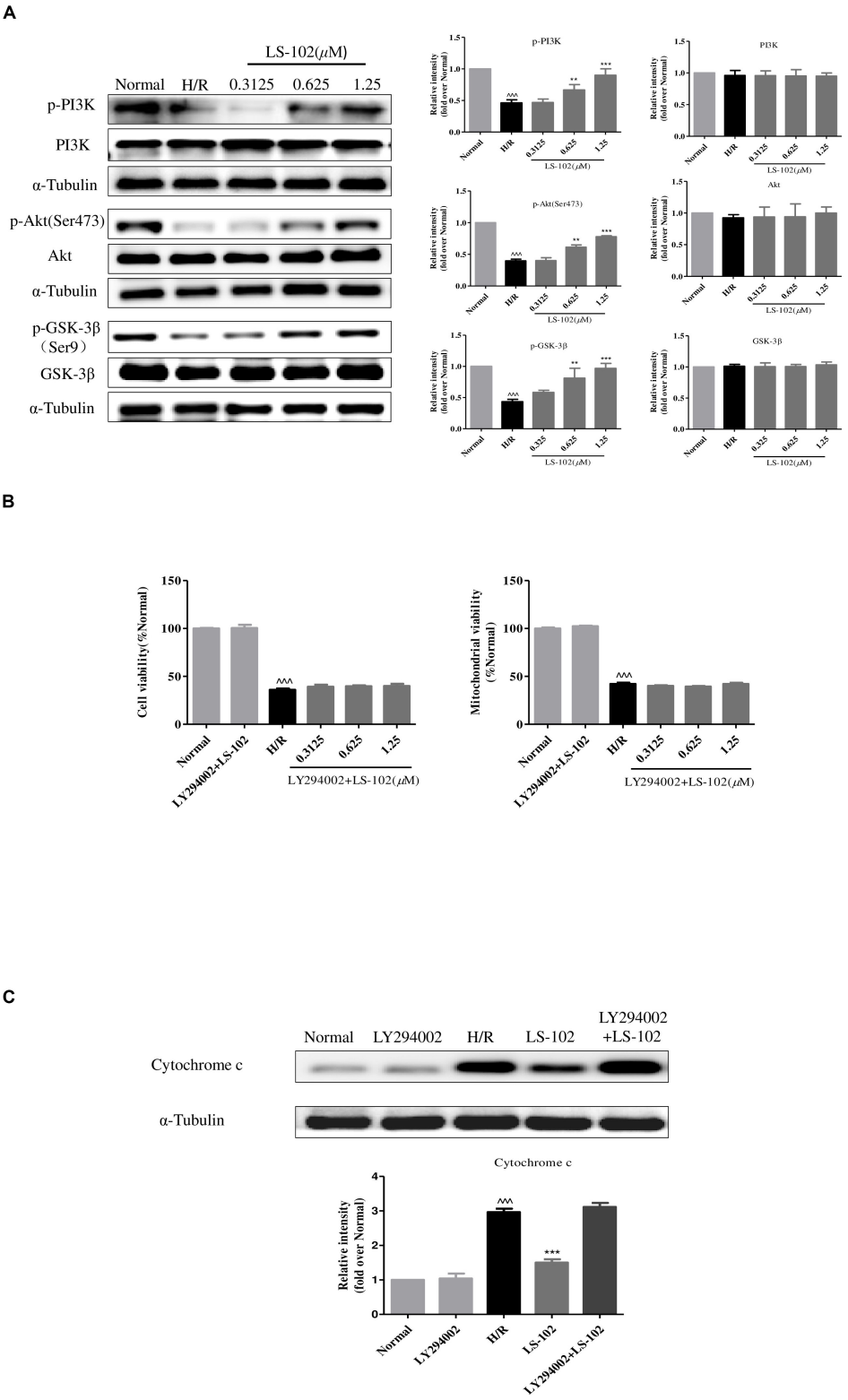


FIGURE 7 | Effect of LS-102 on PI3K/Akt/GSK-3β pathway of H9c2 cells exposed to H/R. **(A)** The protein expression of PI3K, p-PI3K, Akt, p-Akt, GSK-3β, and p-GSK-3β was analyzed by Western blot. **(B,C)** PI3K inhibitor LY294002 (10 μM) altered the effect of LS-102 on cell viability, mitochondrial viability, and the cytochrome c release after H/R in H9c2 cells. Values were the means ± SEM of three independent experiments in H9c2 cells after H/R. ^^$P < 0.001$ vs. Normal group. **$P < 0.01$ and ***$P < 0.001$ vs. H/R group.

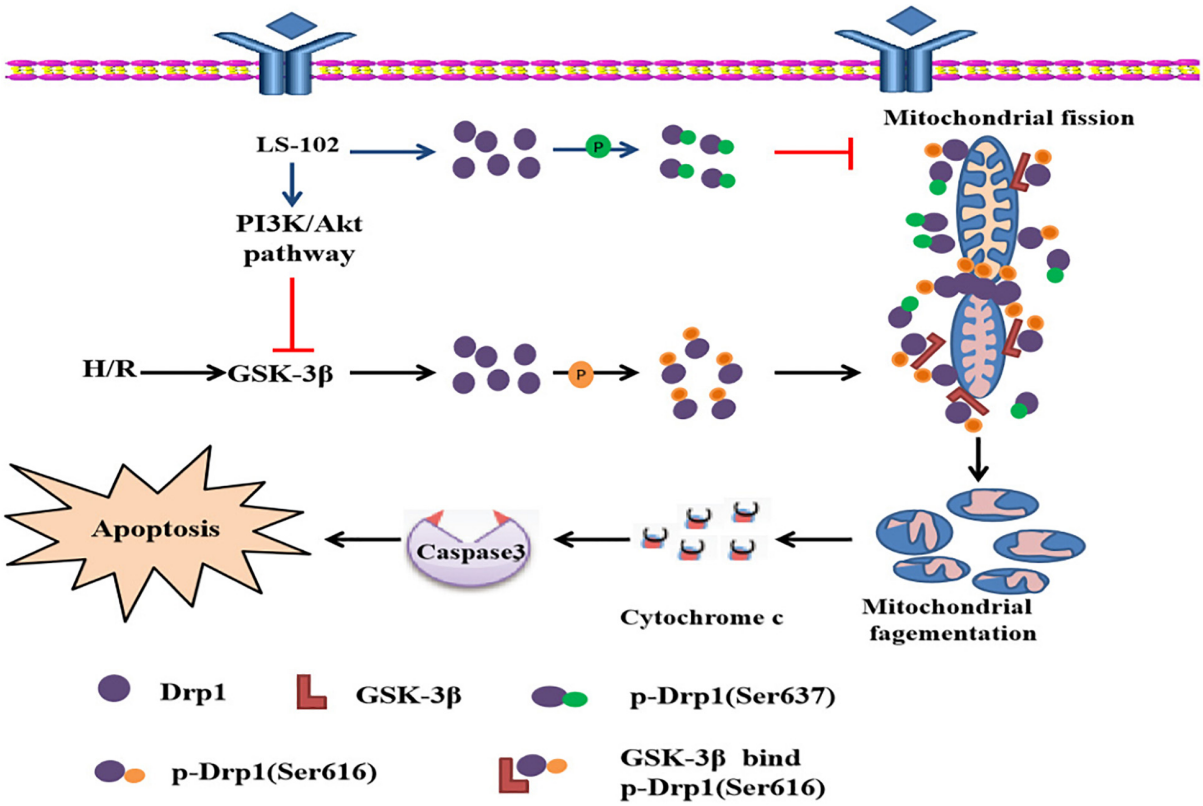


FIGURE 8 | Possiblemechanism of the cardioprotective effect of LS-102 in injury of H/R.

Maneechote et al., 2018). As far as we know, there is currently limited research about traditional Chinese medicine and the ability of these alternative drugs to regulate mitochondrial dynamics. In the present study, we observed that mitochondrial morphologies were changed into fragment or punctiform and the length of mitochondria was short compared with the normal mitochondria after H/R. These results were in agreement with our previous experimental and theoretical results (Dong et al., 2016). While LS-102 increased the length of mitochondrial and preserved mitochondrial morphologies and structure, LS-102 resisted and H/R-triggered the mitochondrial dynamic abnormality by preventing mitochondrial fragmentation. Although inhibition of the activity of Drp1, by Mdivi-1, or Drp1 siRNA, or TH or FK506 can preserve mitochondrial networking and ultrastructure to protect the heart, it can also have severe side effects or toxicity. LS-102 as natural products not only have less toxicity or side effects but they also keep a balance in the mitochondrial dynamic by decreasing the activity of Drp1. LS-102 provides us with a great source for screening new compounds in inhibition of the Drp1 activity.

Drp1-dependent mitochondrial fission is the primary reason to cause excessive mitochondrial fragmentation, which is regulated by Drp1. The activity of Drp1 GTPase enzyme and the ability of Drp1 mitochondrial translocation are mainly associated with the phosphorylation sites of Drp1 (Otera et al., 2013). It has been proven that Drp1 has many phosphorylation sites including serine 585 (Ser585), 616 (Ser616), 637 (Ser637), 656 (Ser656), and 693 (Ser693) (Cribbs and Strack, 2007; Cereghetti et al., 2008; Chou et al., 2012; Li and Li, 2015). Interestingly, Drp1 phosphorylation has opposing functional and morphological effects on different serine residues. Upregulated Drp1 activity and stimulated Drp1 mitochondrial translocation could be alerted via inhibition of PKCε and Ser637 dephosphorylation by activation of calcineurin or activation of Cdk1 and PKCδ during I/R (Cribbs and Strack, 2007).

In our study, we observed that Drp1 phosphorylation both at Ser616 and dephosphorylation at Ser637 elevated in H9c2 cells of H/R. Phosphorylation at Drp1 pSer616 site and dephosphorylation of Drp1 at Ser 637 site made Drp1 translocate to mitochondria and induced mitochondrial degeneration/fragmentation, which could be reversed by LS-102, as it prevented Drp1-dependent mitochondrial fission and balanced mitochondrial dynamics to maintain the integrity of mitochondrial structure and function. Meanwhile, we also proved that LS-102 exerted cardio protection via activation of the PI3K/Akt/GSK-3β signaling pathway. In H/R-induced mitochondrial dysfunction, these results indicate that GSK-3β could be an upstream signaling mechanism for increasing the activity of Drp1.

Current evidence suggests that GSK-3β is involved in mitochondrial dysfunction-mediated cell apoptosis. Inhibition of GSK-3β activity has been implicated as a cardioprotective

mechanism in I/R injury (Linseman et al., 2004; Watcharasit et al., 2008). Initially, Hong et al. (1998) demonstrated that GSK-3β interacted with the C-terminal GED domain of Drp1 in yeast and mammals (Hong et al., 1998; Chen et al., 2000). In a separate study of 2013, Chou et al. confirmed that GSK3β-mediated phosphorylation at the Ser693 site induced prolongation of mitochondrial morphology and presented an anti-apoptotic effect on H_2O_2-induced apoptosis (Chou et al., 2012). In addition to regulating the phosphorylation of Drp1 translocation to mitochondria, GSK-3β can also up-regulate the expression of Drp1. Wu et al. (2013) also found that GSK-3β facilitated cell death via the upregulation of Drp1 expression and mitochondrial fission (Wu et al., 2013). There is evidence that I/R induced GSK-3β activation (Zhai et al., 2011). However, little is known about the relationship between GSK-3β and mitochondrial fragmentation in H9c2 cells during H/R injury. In this study, we found that the GSK-3β inhibitor (AR-A014418) prevented H/R-induced Drp1 translocation to mitochondria and mitochondrial fragmentation. Furthermore, the inhibition of GSK-3β activity successfully prevented Drp1 phosphorylation at Ser616 in H9c2 cells. These results are the first to discover that GSK-3β-induced phosphorylation at Ser616 may be associated with mitochondrial fragmentation and correlated with weakened resistance to injury.

In 2017, Zhou et al. (2017) showed that increasing the Drp1 binding to GSK-3β might be an important factor in mPTP opening after cerebral I/R injury. In our study, we extend these findings and proved that GSK-3β bound Drp1 increased mitochondrial fragmentation, using Co-IP method. GSK-3β is one of the targets underlying I/R induced mitochondrial abnormalities and medication for GSK-3β-induced Drp1 phosphorylation may be the new target for the treatment of I/R injury. Interestingly, LS-102 not only blocked GSK-3β-mediated Drp1 phosphorylation but also decreased co-localization of Drp1 with GSK-3β. LS-102 prevented Drp1-mediated mitochondrial fission, partly because it blocked GSK-3β-induced Drp1 phosphorylation and exerted protective effects against I/R injury.

CONCLUSION

This study had outlined evidence that LS-102 is affected by ischemia-reperfusion both *in vivo* and *in vitro*, providing acute protection to the heart. Firstly, LS102 effectively protected the degree and scope of I/R induced injury in rats by reducing infarct size, the incidence of arrhythmia, the activity of CK, LDH, and preserving the LV function. Importantly, mitochondrial dysfunction is a key feature of ischemia reperfusion. Our study discovered that the LS-102 treatment ameliorated oxidative stress, apoptosis, and imbalance of mitochondrial dynamic, at least in part, associated with the PI3K/Akt signaling pathway in vivo and vitro. Moreover, this protection is related to the fact that it inhibits mitochondrial fission and maintains the integrity of mitochondrial structure and function. It requires inhibiting the phosphorylation of Drp1 via the activation of the GSK-3β pathway, thus it may provide a new pharmacological approach for the future development of therapeutic strategies.

ETHICS STATEMENT

The animal study was reviewed and approved by State Key Laboratories for Quality Research in Chinese Medicines, Macau University of Science and Technology.

AUTHOR CONTRIBUTIONS

PL and L-SQ designed the study and obtained the financial support. LC, X-YC, and Q-LW performed the experiments. LC wrote the manuscript. HZ and S-JY carried out the data analysis. LC, L-SD, and X-YC critically reviewed the manuscript. All authors read, discussed, and accepted the manuscript.

FUNDING

This research was financially supported by the Macao Science and Technology Development Fund (0157/2019/A3 to to PL) and the West Light Foundation of Chinese Academy of Sciences (No. 2018XBZG_XBQNXZ_A_005 to L-SQ). The content is solely the responsibility of the authors. The funders had no role in study design, data collection, and analysis, the decision to publish, or preparation of the manuscript.

REFERENCES

Buerke, M., Murohara, T., and Lefer, A. M. (1995). Cardioprotective effects of a C1 esterase inhibitor in myocardial ischemia and reperfusion. *Circulation* 91, 393–402. doi: 10.1161/01.cir.91.2.393

Cereghetti, G. M., Stangherlin, A., Martins de Brito, O., Chang, C. R., Blackstone, C., Bernardi, P., et al. (2008). Dephosphorylation by calcineurin regulates translocation of Drp1 to mitochondria. *Proc. Natl. Acad. Sci. U S A* 105, 15803–15808. doi: 10.1073/pnas.0808249105

Chen, C. H., Hwang, S. L., Howng, S. L., Chou, C. K., and Hong, Y. R. (2000). Three rat brain alternative splicing dynamin-like protein variants: interaction with the glycogen synthase kinase 3beta and action as a substrate. *Biochem. Biophys. Res. Commun.* 268, 893–898. doi: 10.1006/bbrc.2000.2197

Chinese Pharmacopoeia Commission. (2015). *Chinese Pharmacopoeia (2015 Ed.)*. Beijing: China Medical Science Press, 302–303.

Chou, C. H., Lin, C. C., Yang, M. C., Wei, C. C., Liao, H. D., Lin, R. C., et al. (2012). GSK3beta-mediated Drp1 phosphorylation induced elongated mitochondrial morphology against oxidative stress. *PLoS One* 7:e49112. doi: 10.1371/journal.pone.0049112

Cribbs, J. T., and Strack, S. (2007). Reversible phosphorylation of Drp1 by cyclic AMP-dependent protein kinase and calcineurin regulates mitochondrial fission and cell death. *EMBO Rep.* 8, 939–944. doi: 10.1038/sj.embor.7401062

Disatnik, M. H., Ferreira, J. C., Campos, J. C., Gomes, K. S., Dourado, P. M., Qi, X., et al. (2013). Acute inhibition of excessive mitochondrial fission after myocardial infarction prevents long-term cardiac dysfunction. *J. Am. Heart Assoc.* 2:e000461. doi: 10.1161/jaha.113.000461

Dominguez-Rodriguez, A., Abreu-Gonzalez, P., and Reiter, R. J. (2014). Cardioprotection and pharmacological therapies in acute myocardial

infarction: Challenges in the current era. *World J. Cardiol.* 6, 100–106. doi: 10.4330/wjc.v6.i3.100

Dong, G., Chen, T., Ren, X., Zhang, Z., Huang, W., Liu, L., et al. (2016). Rg1 prevents myocardial hypoxia/reoxygenation injury by regulating mitochondrial dynamics imbalance via modulation of glutamate dehydrogenase and mitofusin 2. *Mitochondrion* 26, 7–18. doi: 10.1016/j.mito.2015.11.003

Forte, M., Schirone, L., Ameri, P., Basso, C., Catalucci, D., Modica, J., et al. (2020). The role of mitochondrial dynamics in cardiovascular diseases. *Br. J. Pharmacol.* 17, 257–261. doi: 10.1111/bph.15068

Garcia, T. B., and Miller, G. (2003). Arrhythmia recognition. *JEMS* 28, 24–27.

Ghosh, R., Vinod, V., Symons, J. D., and Boudina, S. (2020). Protein and Mitochondria Quality Control Mechanisms and Cardiac Aging. *Cells* 9, 933. doi: 10.3390/cells9040933

Gomez, L., Paillard, M., Thibault, H., Derumeaux, G., and Ovize, M. (2008). Inhibition of GSK3beta by postconditioning is required to prevent opening of the mitochondrial permeability transition pore during reperfusion. *Circulation* 117, 2761–2768. doi: 10.1161/circulationaha.107.755066

Hamacher-Brady, A., Brady, N. R., and Gottlieb, R. A. (2006). Enhancing macroautophagy protects against ischemia/reperfusion injury in cardiac myocytes. *J. Biol. Chem.* 281, 29776–29787. doi: 10.1074/jbc.M603783200

Harwood, A. J. (2001). Regulation of GSK-3: a cellular multiprocessor. *Cell* 105, 821–824. doi: 10.1016/s0092-8674(01)00412-3

Hong, Y. R., Chen, C. H., Cheng, D. S., Howng, S. L., and Chow, C. C. (1998). Human dynamin-like protein interacts with the glycogen synthase kinase 3beta. *Biochem. Biophys. Res. Commun.* 249, 697–703. doi: 10.1006/bbrc.1998.9253

Hu, C., Huang, Y., and Li, L. (2017). Drp1-Dependent Mitochondrial Fission Plays Critical Roles in Physiological and Pathological Progresses in Mammals. *Int. J. Mol. Sci.* 18:144. doi: 10.3390/ijms18010144

Jahani-Asl, A., and Slack, R. S. (2007). The phosphorylation state of Drp1 determines cell fate. *EMBO Rep.* 8, 912–913. doi: 10.1038/sj.embor.7401077

James, D. I., Parone, P. A., Mattenberger, Y., and Martinou, J. C. (2003). hFis1, a novel component of the mammalian mitochondrial fission machinery. *J. Biol. Chem.* 278, 36373–36379. doi: 10.1074/jbc.M303758200

Jennings, R. B. (2013). Historical perspective on the pathology of myocardial ischemia/reperfusion injury. *Circ. Res.* 113, 428–438. doi: 10.1161/circresaha.113.300987

Karbowski, M., Arnoult, D., Chen, H., Chan, D. C., Smith, C. L., and Youle, R. J. (2004). Quantitation of mitochondrial dynamics by photolabeling of individual organelles shows that mitochondrial fusion is blocked during the Bax activation phase of apoptosis. *J. Cell Biol.* 164, 493–499. doi: 10.1083/jcb.200309082

Kloner, R. A. (2017). Mitochondrial Protective Agents for Ischemia/Reperfusion Injury. *Circ. Cardiovasc. Interv.* 10:e005805. doi: 10.1161/circinterventions.117.005805

Kuzmicic, J., Del Campo, A., López-Crisosto, C., Morales, P. E., Pennanen, C., Bravo-Sagua, R., et al. (2011). Mitochondrial dynamics: a potential new therapeutic target for heart failure. *Revista Española de Cardiol.* 64, 916–923. doi: 10.1016/j.rec.2011.05.022

Lee, Y. J., Jeong, S. Y., Karbowski, M., Smith, C. L., and Youle, R. J. (2004). Roles of the mammalian mitochondrial fission and fusion mediators Fis1. Drp1, and Opa1 in apoptosis. *Mol. Biol. Cell* 15, 5001–5011. doi: 10.1091/mbc.e04-04-0294

Li, C. Y., and Li, Y. G. (2015). Cardiac Sympathetic Nerve Sprouting and Susceptibility to Ventricular Arrhythmias after Myocardial Infarction. *Cardiol. Res. Pract.* 2015:698368. doi: 10.1155/2015/698368

Linseman, D. A., Butts, B. D., Precht, T. A., Phelps, R. A., Le, S. S., Laessig, T. A., et al. (2004). Glycogen synthase kinase-3beta phosphorylates Bax and promotes its mitochondrial localization during neuronal apoptosis. *J. Neurosci.* 24, 9993–10002. doi: 10.1523/jneurosci.2057-04.2004

Maneechote, C., Palee, S., Kerdphoo, S., Jaiwongkam, T., Chattipakorn, S. C., and Chattipakorn, N. (2018). Differential temporal inhibition of mitochondrial fission by Mdivi-1 exerts effective cardioprotection in cardiac ischemia/reperfusion injury. *Clin. Sci.* 132, 1669–1683. doi: 10.1042/cs20180510

Nishihara, M., Miura, T., Miki, T., Tanno, M., Yano, T., Naitoh, K., et al. (2007). Modulation of the mitochondrial permeability transition pore complex in GSK-3beta-mediated myocardial protection. *J. Mole. Cell. Cardiol.* 43, 564–570. doi: 10.1016/j.yjmcc.2007.08.010

Nowbar, A. N., Gitto, M., Howard, J. P., Francis, D. P., and Al-Lamee, R. (2019). Mortality from ischemic heart disease: Analysis of data from the World Health Organization and coronary artery disease risk factors From NCD Risk Factor Collaboration. *Circul. Cardiovascul. Q. Outcom.* 12:e005375.

Oh, C. M., Ryu, D., Cho, S., and Jang, Y. (2020). Mitochondrial Quality Control in the Heart: New Drug Targets for Cardiovascular Disease. *Korean Circ. J.* 50, 395–405. doi: 10.4070/kcj.2019.0416

Ong, S. B., Subrayan, S., Lim, S. Y., Yellon, D. M., Davidson, S. M., and Hausenloy, D. J. (2010). Inhibiting mitochondrial fission protects the heart against ischemia/reperfusion injury. *Circulation* 121, 2012–2022. doi: 10.1161/circulationaha.109.906610

Otera, H., Ishihara, N., and Mihara, K. (2013). New insights into the function and regulation of mitochondrial fission. *Biochim. Biophys. Acta* 1833, 1256–1268. doi: 10.1016/j.bbamcr.2013.02.002

Qing, L.-S., Chen, T.-B., Sun, W.-X., Chen, L., Luo, P., Zhang, Z.-F., et al. (2019). Pharmacokinetics comparison, intestinal absorption and acute toxicity assessment of a novel water-soluble astragaloside IV derivative (astragalosidic acid, LS-102). *Eur. J. Drug Metabol. Pharmacokinet.* 44, 251–259. doi: 10.1007/s13318-018-0515-5

Ren, S., Zhang, H., Mu, Y., Sun, M., and Liu, P. (2013). Pharmacological effects of Astragaloside IV: a literature review. *J. Tradit. Chin. Med.* 33, 413–416. doi: 10.1016/s0254-6272(13)60189-2

Sharp, W. W., Fang, Y. H., Han, M., Zhang, H. J., Hong, Z., Banathy, A., et al. (2014). Dynamin-related protein 1 (Drp1)-mediated diastolic dysfunction in myocardial ischemia-reperfusion injury: therapeutic benefits of Drp1 inhibition to reduce mitochondrial fission. *Faseb. J.* 28, 316–326. doi: 10.1096/fj.12-226225

Sun, W.-X., Zhang, Z.-F., Xie, J., He, Y., Cheng, Y., Ding, L.-S., et al. (2019). Determination of a astragaloside IV derivative LS-102 in plasma by ultra-performance liquid chromatography-tandem mass spectrometry in dog plasma and its application in a pharmacokinetic study. *Phytomedicine* 53, 243–251. doi: 10.1016/j.phymed.2018.09.019

Taguchi, N., Ishihara, N., Jofuku, A., Oka, T., and Mihara, K. (2007). Mitotic phosphorylation of dynamin-related GTPase Drp1 participates in mitochondrial fission. *J. Biol. Chem.* 282, 11521–11529. doi: 10.1074/jbc.m607279200

Tao, A., Xu, X., Kvietys, P., Kao, R., Martin, C., and Rui, T. (2018). Experimental diabetes mellitus exacerbates ischemia/reperfusion-induced myocardial injury by promoting mitochondrial fission: Role of down-regulation of myocardial Sirt1 and subsequent Akt/Drp1 interaction. *Int. J. Biochem. Cell Biol.* 105, 94–103. doi: 10.1016/j.biocel.2018.10.011

Tong, M., Zablocki, D., and Sadoshima, J. (2020). The role of Drp1 in mitophagy and cell death in the heart. *J. Mole. Cell. Cardiol.* 142, 138–145. doi: 10.1016/j.yjmcc.2020.04.015

Turer, A. T., and Hill, J. A. (2010). Pathogenesis of myocardial ischemia-reperfusion injury and rationale for therapy. *Am. J. Cardiol.* 106, 360–368. doi: 10.1016/j.amjcard.2010.03.032

Walters, A. M., Porter, G. A. Jr., and Brookes, P. S. (2012). Mitochondria as a drug target in ischemic heart disease and cardiomyopathy. *Circ. Res.* 111, 1222–1236. doi: 10.1161/circresaha.112.265660

Watcharasit, P., Thiantanawat, A., and Satayavivad, J. (2008). GSK3 promotes arsenite-induced apoptosis via facilitation of mitochondria disruption. *J. Appl. Toxicol.* 28, 466–474. doi: 10.1002/jat.1296

Wu, J. H., Zhang, S. H., Gao, F. J., Lei, Y., Chen, X. Y., Gao, F., et al. (2013). RNAi screening identifies GSK3β as a regulator of DRP1 and the neuroprotection of lithium chloride against elevated pressure involved in downregulation of DRP1. *Neurosci. Lett.* 554, 99–104. doi: 10.1016/j.neulet.2013.08.057

Yan, J., Liu, X. H., Han, M. Z., Wang, Y. M., Sun, X. L., Yu, N., et al. (2015). Blockage of GSK3β-mediated Drp1 phosphorylation provides neuroprotection in neuronal and mouse models of Alzheimer's disease. *Neurobiol. Aging* 36, 211–227. doi: 10.1016/j.neurobiolaging.2014.08.005

Yellon, D. M., and Hausenloy, D. J. (2007). Myocardial reperfusion injury. *N. Engl. J. Med.* 357, 1121–1135. doi: 10.1056/NEJMra071667

Zhai, P., Sciarretta, S., Galeotti, J., Volpe, M., and Sadoshima, J. (2011). Differential roles of GSK-3β during myocardial ischemia and ischemia/reperfusion. *Circ. Res.* 109, 502–511. doi: 10.1161/circresaha.111.249532

Zhang, Z.-F., Chen, L., Ding, L.-S., Liu, L., Zhou, H., Luo, P., et al. (2017). O14 Determination of DQ-798 in rat plasma by UHPLC-MS/MS and its application to a pharmacokinetic study. *Biochem. Pharmacol.* 139:114. doi: 10.1016/j.bcp.2017.06.079

Zhao, J., Yang, P., Li, F., Tao, L., Ding, H., Rui, Y., et al. (2012). Therapeutic effects of astragaloside IV on myocardial injuries: multi-target identification and network analysis. *PLoS One* 7:e44938. doi: 10.1371/journal.pone.0044938

Zhou, H., Hou, S. Z., Luo, P., Zeng, B., Wang, J. R., Wong, Y. F., et al. (2011). Ginseng protects rodent hearts from acute myocardial ischemia-reperfusion injury through GR/ER-activated RISK pathway in an endothelial NOS-dependent mechanism. *J. Ethnopharmacol.* 135, 287–298. doi: 10.1016/j.jep.2011.03.015

Zhou, X., Wang, H. Y., Wu, B., Cheng, C. Y., Xiao, W., Wang, Z. Z., et al. (2017). Ginkgolide K attenuates neuronal injury after ischemic stroke by inhibiting mitochondrial fission and GSK-3β-dependent increases in mitochondrial membrane permeability. *Oncotarget* 8, 44682–44693. doi: 10.18632/oncotarget.17967

Conflict of Interest: The authors declare that the research was conducted in the absence of any commercial or financial relationships that could be construed as a potential conflict of interest.

Copyright © 2020 Chen, Chen, Wang, Yang, Zhou, Ding, Qing and Luo. This is an open-access article distributed under the terms of the Creative Commons Attribution License (CC BY). The use, distribution or reproduction in other forums is permitted, provided the original author(s) and the copyright owner(s) are credited and that the original publication in this journal is cited, in accordance with accepted academic practice. No use, distribution or reproduction is permitted which does not comply with these terms.

frontiers in Physiology

ORIGINAL RESEARCH
published: 08 March 2021
doi: 10.3389/fphys.2021.525145

The Ameliorating Effects of Bushen Huatan Granules and Kunling Wan on Polycystic Ovary Syndrome Induced by Dehydroepiandrosterone in Rats

Yang Xu[1,2,3†], Chun-Shui Pan[3,4,5†], Quan Li[3,4,5], Hao-Lin Zhang[1,2], Li Yan[3,4,5], Gulinigaer Anwaier[3,6], Xiao-Yi Wang[3,6], Lu-Lu Yan[3,4,5], Jing-Yu Fan[3,4,5], Dong Li[1,2] and Jing-Yan Han[2,3,4,5,6,7*]*

[1] Department of Traditional Chinese Medicine, Peking University Third Hospital, Beijing, China, [2] Department of Integration of Chinese and Western Medicine, Peking University Health Science Center, Beijing, China, [3] Tasly Microcirculation Research Center, Peking University Health Science Center, Beijing, China, [4] Key Laboratory of Stasis and Phlegm, State Administration of Traditional Chinese Medicine, Beijing, China, [5] State Key Laboratory of Core Technology in Innovative Chinese Medicine, Tianjin, China, [6] Department of Integration of Chinese and Western Medicine, School of Basic Medical Sciences, Peking University, Beijing, China, [7] Academy of Integration of Chinese and Western Medicine, Peking University Health Science Center, Beijing, China

OPEN ACCESS

Edited by:
Zhongkui Hong,
University of South Dakota,
United States

Reviewed by:
Jianbo Wu,
Southwest Medical University, China
Haiping Zhao,
Capital Medical University, China

***Correspondence:**
Dong Li
lidong6512@sina.com
Jing-Yan Han
hanjingyan@bjmu.edu.cn

[†] These authors have contributed equally to this work

Specialty section:
This article was submitted to Vascular Physiology, a section of the journal Frontiers in Physiology

Received: 08 January 2020
Accepted: 12 February 2021
Published: 08 March 2021

Citation:
Xu Y, Pan C-S, Li Q, Zhang H-L, Yan L, Anwaier G, Wang X-Y, Yan L-L, Fan J-Y, Li D and Han J-Y (2021) The Ameliorating Effects of Bushen Huatan Granules and Kunling Wan on Polycystic Ovary Syndrome Induced by Dehydroepiandrosterone in Rats. Front. Physiol. 12:525145. doi: 10.3389/fphys.2021.525145

Aim: To investigate the effects of Bushen Huatan Granules (BHG) and Kunling Wan (KW), the two Chinese medicines, on the regulation of polycystic ovary syndrome (PCOS) and their underlying mechanisms.

Materials and Methods: PCOS rat model was established by subcutaneous injection of dehydroepiandrosterone (DHEA) (6 mg/100 g/day) for 20 days, followed by treatment with BHG (0.75, 1.49, and 2.99 g/kg) or KW (0.46, 0.91, and 1.82 g/kg) by gavage for 4 weeks. Estrous cycle was detected by vaginal smears. Follicles development was assessed by histology. Levels of testosterone and insulin in serum were tested by ELISA. Apoptosis of Granulosa cells (GCs) was evaluated by terminal deoxynucleotidyl transferase-mediated dUTP-biotin nick end-labeling staining. Pathways associated with apoptosis were detected with western blot. Pregnancy outcome was also assessed. GCs were pre-treated with 10^{-5} M testosterone *in vitro* for 24 h, then incubated with serum from rats receiving BHG (1.49 g/kg) or KW (1.82 g/kg). The parameters concerning apoptosis, mitochondrial function and endoplasmic reticulum stress were assessed.

Results: Post-treatment with either BHG or KW ameliorated DHEA-induced irregular estrous cycles, follicles development abnormalities, increase of testosterone and insulin in serum, and the apoptosis of GCs. Post-treatment with BHG decreased the expression of cleaved caspase-9/caspase 9, release of cytochrome C from mitochondria, and mitochondria reactive oxygen species production, increased activities of complex I, II, IV of ovarian tissue. Post-treatment with KW decreased the levels of caspase-12, GRP78, C/EBP homologous protein, phosphorylation of IRE-I, x-box-binding protein 1s, as well as phosphorylation of proline-rich receptor-like protein kinase, phosphorylation

of eukaryotic translation initiation factor 2α and ATF4 of ovarian tissue and GCs. Both BHG and KW ameliorated pregnancy outcome.

Conclusion: This study demonstrated BHG or KW as a potential strategy for treatment of PCOS induced by DHEA, and suggested that the beneficial role of the two medicines were mediated by different pathway with the effect of BHG being correlated with the regulation of mitochondria, while the effect of KW being attributable to protection of endoplasmic reticulum stress.

Keywords: granulosa cells, apoptosis, mitochondria, endoplasmic reticulum stress, traditional Chinese medicine

INTRODUCTION

Polycystic ovary syndrome (PCOS) is one of the most common endocrine and metabolic disorders characterized by hyperandrogenism, chronic anovulation and polycystic ovaries, which affects 5–20% of women at reproductive age worldwide (Eser et al., 2017; Yao et al., 2017; Zhong et al., 2018). PCOS accounts for about 70% of anovulatory infertility cases, affecting about 5.6% of women in China (Wu et al., 2015; Li et al., 2019). However, the pathogenesis and etiology of PCOS remain unclear (Wei et al., 2017).

Granulosa cells (GCs) play a crucial role in the growth and development of oocytes and ovarian follicles by providing a suitable microenvironment for them. Bidirectional communication between an oocyte and GCs via regulatory factors is the foundation of follicular growth (Nakamura et al., 2015; Murase et al., 2018). Therefore, dysfunction of GCs has been regarded as one of the key factors that affect the follicles development relevant to PCOS (Matsuda et al., 2012). Apoptosis of GCs in the PCOS patients and PCOS-like animals is noticed in previous studies (Wu et al., 2017; Zheng et al., 2017; Fu et al., 2018; Lima et al., 2018). A feature of PCOS is excessive androgen secretion (Chen et al., 2009), while excessive androgen was reported to promote the development of PCOS by inducing apoptosis and death of GCs (Lim et al., 2017a,b). Previous studies have shown that excessive androgen induced follicular development abnormalities, which promotes preantral follicle growth but suppresses later stages of follicular development (Jonard and Dewailly, 2004; Lee et al., 2018; Azhary et al., 2019). In spite of these findings, the signaling pathways that mediate androgen-induced apoptosis in GCs in PCOS have not been fully identified, which impedes the development of treatment of PCOS (Su et al., 2017; Elkady, 2019).

The standard treatment for PCOS in clinic are selective estrogen receptor modulators clomiphene (Beck et al., 2005), aromatase inhibitors (Casper and Mitwally, 2006) and gonadotropin (Hughes et al., 2000). However, these hormone regulators also have side effects affecting metabolic function and increasing the risk of multiple pregnancies and ovarian hyperstimulation syndrome (Tummon et al., 2005). In addition, there are still some patients who have poor response to ovulation induction therapy and some are still unable to be pregnant after ovulation (Palomba et al., 2006).

Traditional Chinese medicine is widely used in the treatment of PCOS in China. Bushen Huatan Granules (BHG) is an empirical prescription for PCOS, consisting of 10 compositions (**Supplementary Material 1**), which improves PCOS symptoms and pregnancy outcome in clinic. Kunling Wan (KW) is a standardized Chinese patent medicine for treatment of gynecopathy including PCOS, which consists of 31 compositions (**Supplementary Material 2**). Our previous study showed that KW has a great efficacy on infertility (Lv et al., 2019). Despite effectiveness of the two medicines in practice, the underlying mechanisms are not explored as yet.

The present study aimed to investigate the effect of BHG and KW, respectively, on the regulation of PCOS and pregnancy outcome induced by dehydroepiandrosterone (DHEA) in rat and their protective effect on the apoptosis of GCs and signaling pathways involved.

MATERIALS AND METHODS

Animals

Sprague Dawley (SD) rats of female, 3-week-old, 50 ± 5 g and male, 10-week-old, 350 ± 20 g were obtained from the Animals Center of Peking University Health Science Center with the certificate number SYXK 2016-0041. The rats were kept in an environment with ambient temperature of 24 ± 1°C and relative humidity of 50 ± 1% with a 12−h light/dark cycle. All animals were fed with standard rat chow and had free access to water and food. The study was carried out in line with the United Kingdom Animal Scientific Procedures Act 1986 and the EU Directive 2010/63/EU for animal experiments. All animals were handled based on the guidelines of the Peking University Animal Research Committee. The Committee on the Ethics of Animal Experiments of Peking

Abbreviations: ATF4/6: activating transcription factor 4/6; Bax: Bcl-2 associated X protein; Bcl-2: B-cell lymphoma-2; BHG: Bushen Huatan Granules; caspase-3/9/8/12: cysteinyl aspartate specific proteinase-3/9/8/12; CHOP: C/EBP homologous protein; COX4i1: cytochrome C oxidase subunit 4 isoform 1; DHEA: dehydroepiandrosterone; eIF2α: eukaryotic translation initiation factor 2α; ER stress: endoplasmic reticulum stress; GRP78: glucose-regulated protein 78; HE: hematoxylin and eosin; IR: insulin resistance; IRE1: inositol-requiring enzyme 1; KW: Kunling Wan; NS: normal saline; PCOS: polycystic ovary syndrome; PERK: proline-rich receptor-like protein kinase; p-eIF2α: phosphorylation-eukaryotic translation initiation factor 2α; p-IRE1: phosphorylation-inositol-requiring enzyme 1; p-PERK: phosphorylation-proline-rich receptor-like protein kinase; ROS: reactive oxygen species; TUNEL: terminal deoxynucleotidyl transferase-mediated dUTP-biotin nick end-labeling; XBP1s: x-box-binding protein 1s.

University Health Science Center approved the experimental protocol (LA2016314).

Reagents

Bushen Huatan Granules was supplied by Guangdong Yi Fang Pharmaceutical Co., Ltd. (Guangzhou, GD, China), which consists of 10 compositions (**Supplementary Materials 1**). KW (approval number: Z21021219, batch number 20180843) was obtained from Tasly Pharmaceutical Co., Ltd. (Fuxing, LN, China), which consists of 31 compositions (**Supplementary Materials 2**). DHEA was from Cayman Chemical (Ann Arbor, MI, United States). Testosterone was purchased from Wako Pure Chemical Industries (Osaka, Japan). GCs were from Fengmao Technology Co. (Beijing, China). Cell counting kit-8 (CCK-8) was purchased from Beyotime Biotechnology (Shanghai, China). Antibodies against cleaved caspase-9, caspase-8, caspase-12, glucose-regulated protein 78 (GRP78), ATF6, inositol-requiring enzyme 1 (IRE1) and phospho-IRE1 were purchased from Abcam (Cambridge, United Kingdom). Antibodies against Bcl-2 associated X protein (Bax), Bcl-2: B-cell lymphoma-2 (Bcl-2), cleaved caspase-3, caspase-3, caspase-9, cytochrome C, ATF4, x-box-binding protein 1s (XBP1s), proline-rich receptor-like protein kinase (PERK), phospho-PERK, eukaryotic translation initiation factor 2α (eIF2α), phospho-eIF2α, and C/EBP homologous protein (CHOP) were purchased from Cell Signaling Technology (Beverly, MA, United States). Antibody against cytochrome C oxidase subunit 4 isoform 1 (COX4i1) was obtained from Invitrogen Corporation (Camarillo, CA, United States).

Experiment Protocols

The PCOS model was established as previously reported (Roy et al., 1962). For this, female SD rats were subcutaneously injected daily with DHEA (6 mg/100 g body weight, dissolved in 0.1 mL sesame oil) for 20 consecutive days in the DHEA group. Animals in Control received sesame oil alone the same way. Starting from the 11th day of modeling, estrus cycle was determined every day by vaginal smear. After modeling, blood samples were taken from retroorbital venous plexuses. The animals in DHEA that exhibited disordered estrous cycles and higher level of testosterone than that in Control were either scarified as the group DHEA (3 weeks), or randomly divided into seven groups: DHEA (7 weeks) group, DHEA + BHG (0.75 g/kg), DHEA + BHG (1.49 g/kg), DHEA + BHK (2.99 g/kg), DHEA + KW (0.46 g/kg), DHEA + KW (0.91 g/kg), and DHEA + KW (1.82 g/kg). Rats in the DHEA + BHG groups and DHEA + KW groups were successively administrated daily, respectively, with BHG and KW at the dose indicated by gavage for 28 days. Both KW and BHG were dissolved in normal saline (NS). The doses of the drugs used in the present study were converted from their clinical dosage with low, medium and high dose being half, equivalent and twice of the clinical human dose, respectively, which showed no toxicity for the animals (**Supplementary Material 4**). Rats in the Control and DHEA (7 weeks) groups were given with NS (10 mL/kg) alone the same way. The number of rats used to determine each parameter in each group is detailed in **Table 1**.

TABLE 1 | The number of animals used for assessment of various parameters in each group.

Control	DHEA (3 weeks)	DHEA (7 weeks)	DHEA + BHG (0.75 g/kg)	DHEA + BHG (1.49 g/kg)	DHEA + BHG (2.99 g/kg)	DHEA + KW (0.46 g/kg)	DHEA + KW (0.91 g/kg)		Total
Observation of estrous cycle15	–	15	15	15	15	15	15	15	120
HE staining(3)	3	(3)	(3)	(3)	(3)	(3)	(3)	(3)	3, (24)
Testosterone and insulin in serum(6)	6	(6)	(6)	(6)	(6)	(6)	(6)	(6)	6, (48)
TUNEL staining(3)	(3)	(3)	(3)	(3)	(3)	(3)	(3)	(3)	(27)
MitoSOX(3)	(3)	(3)	(3)	(3)	(3)	(3)	(3)	(3)	(27)
Mitochondrial respiratory chain complexes activities8	8	8	8	8	8	8	8	8	72
Western blot(8)	(8)	(8)	(8)	(8)	(8)	(8)	(8)	(8)	(72)
Pregnancy outcome20	–	18	10	10	9	8	10	10	95
Total43	17	41	33	33	32	31	33	33	296

Numbers in brackets represent the number of the animals used in the respective experiment, and these animals were among those denoted above by the numbers free of brackets.

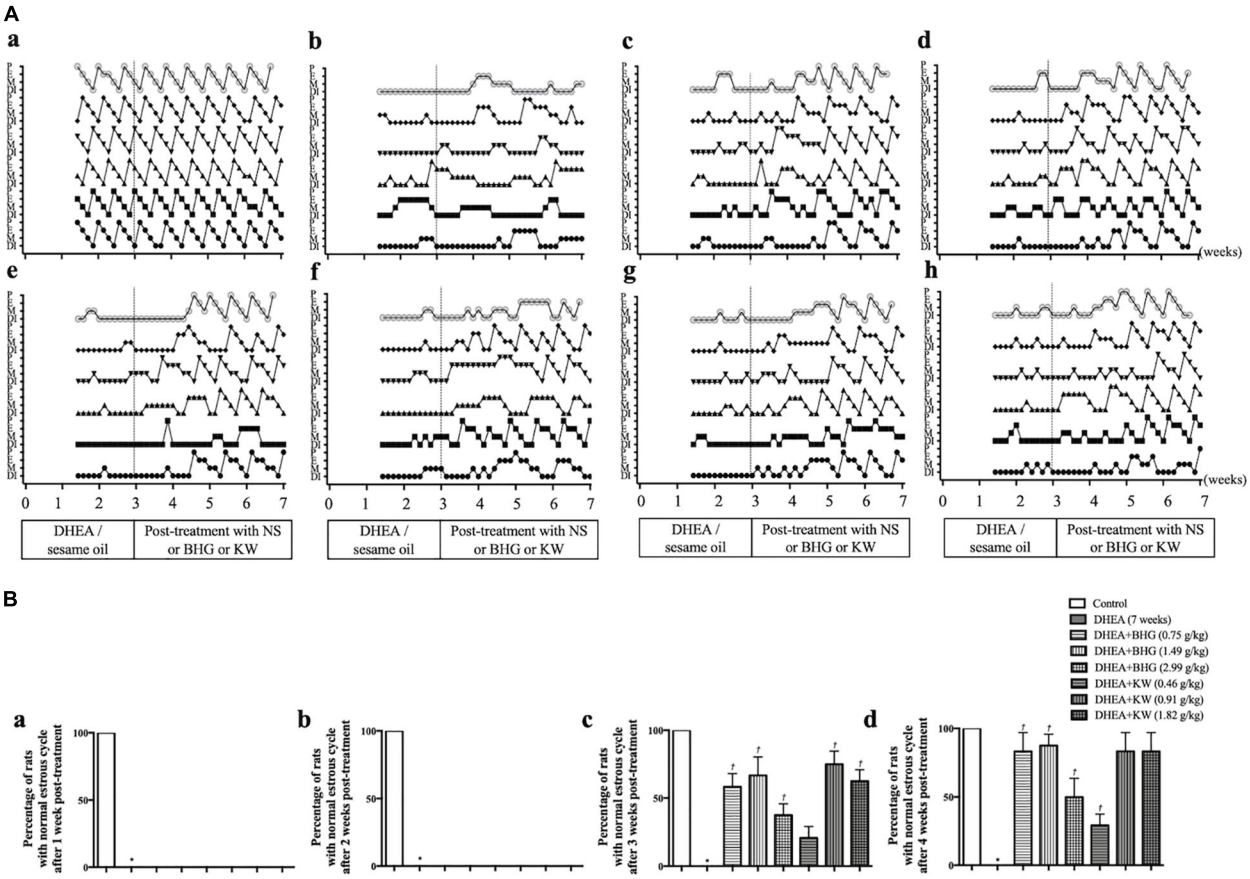


FIGURE 1 | Effect of post-treatment with BHG or KW on rat estrous cycle. **(A)** Representative depictions illustrating the changes of estrous cycle in Control **(a)**, DHEA (7 weeks) **(b)**, DHEA + BHG (0.75 g/kg) **(c)**, DHEA + BHG (1.49 g/kg) **(d)**, DHEA + BHG (2.99 g/kg) **(e)**, DHEA + KW (0.46 g/kg) **(f)**, DHEA + KW (0.91 g/kg) **(g)**, and DHEA + KW (1.82 g/kg) **(h)** group, respectively. P, preoestrus; E, estrus; M, metaoestrus; DI, diestrus. **(B)** Statistical result of the percentage of rats with normal estrous cycle after treatment with BHG or KW for 1, 2, 3, and 4 weeks. Results are presented as mean ± SEM. $^{*}P < 0.05$ vs. Control group; $^{\dagger}P < 0.05$ vs. DHEA (7 weeks) group, $n = 15$.

To investigate the ameliorating effects of BHG and KW on infertility of PCOS, some female rats were caged after 28-days-administration of drugs with males at a ratio of 1:1 overnight and checked for vaginal plugs the next morning. Successful mating was confirmed by the presence of vaginal plugs. The pregnant rats were cared until natural delivery. Numbers of mated and delivered rats as well as pups were counted.

Cell Culture and Treatment

Granulosa cells were cultured in DMEM (Invitrogen, Grand Island, NY, United States) containing 10% fetal bovine serum, at 37°C in a humidified incubator with 95% air-5% CO_2. GCs were pre-treated with 10^{-5} M testosterone for 24 h, then incubated for further 6 h in the presence of the serum from rats receiving BHG (1.49 g/kg) or KW (1.82 g/kg) and the parameters of interest were assessed.

Cell Viability Assay

Cell counting kit-8 assay was performed to detect the viabilities of GCs. For this, CCK-8 solution (10 μl) was added to each well, and the plates were incubated for 1 h at 37°C in moist box. The absorbance of each well at 450 nm was measured using Micro-Plate Reader (Bio-Rad, Hercules, CA, United States). Cell viability was quantified using average absorbance × 100%.

Ovary Index and Histological Evaluation of Ovarian

Ovaries were harvested from rats under anesthesia by intramuscular injection with 20% urethane. The ovary index (ovary wet weight/body weight) was determined and expressed as mg/g. Ovaries were fixed in 4% paraformaldehyde for 48 h and processed for paraffin sections as routine. Ten successive sections of 5 μm with an interval of 50 μm between each were collected from each ovary and stained with hematoxylin and eosin (HE), on which the follicles were classified and counted under a light microscope (BX512DP70; Olympus, Tokyo, Japan). The follicles at different development stages were defined as follows: primordial follicle, an oocyte surrounded by a layer of flat GCs; primary follicle, an oocyte surrounded by a layer of cubic GCs; secondary follicle, an oocyte surrounded by more

TABLE 2 | Number and percentage of the follicles in different development stages and corpus luteum.

	Control		DHEA (3 weeks)		DHEA (7 weeks)		DHEA + BHG (0.75 g/kg)		DHEA + BHG (1.49 g/kg)		DHEA + BHG (2.99 g/kg)		DHEA + KW (0.46 g/kg)		DHEA + KW (0.91 g/kg)		DHEA + KW (1.82 g/kg)	
	Number	Percentage	Number	Percentage	Number	Percentage	Number	Percentage	Number	Percentage	Number	Percentage	Number	Percentage	Number	Percentage	Number	Percentage
Primordial follicle	183.67 ± 6.27	48.23 ± 0.8	142.67 ± 13.13	39.33 ± 1.45*	144 ± 0.8	42 ± 1.73*	151.33 ± 9.86	43.67 ± 0.88	162.67 ± 10.78	43.17 ± 0.60	140.67 ± 8.63	39.67 ± 0.67	147.67 ± 5.84	38.67 ± 0.88	148.67 ± 9.29	40 ± 0.58	156.33 ± 9.74	42 ± 0.58
Primary follicle	118 ± 3.28	31.03 ± 0.32	134.33 ± 4.8	37.2 ± 0.71*	119.33 ± 5.76	34.67 ± 0.33*	107.67 ± 7.28	31.13 ± 1.07#†	109.33 ± 4.4	29 ± 0.58#†	113.67 ± 7.98	32 ± 0.58#	121.33 ± 7.11	31.67 ± 0.48#	118 ± 6.6	31.73 ± 0.48#	113 ± 7.06	30.4 ± 0.70#†
Secondary follicle	18.67 ± 1.21	4.93 ± 0.23	22.33 ± 1.29	6.23 ± 0.18	21 ± 2.08	6.13 ± 0.37	18 ± 0.72	5.17 ± 0.22	22.67 ± 2.01	6.03 ± 0.26	17.67 ± 2.06	5.03 ± 0.26	20 ± 0.39	5.19 ± 0.24	18.67 ± 0.75	5.07 ± 0.18	21.67 ± 0.99	5.79 ± 0.27
Antral follicle	48.67 ± 2.43	12.8 ± 0.42	31.67 ± 1.82	8.77 ± 0.12*	30 ± 1.78	8.73 ± 0.15*	42.67 ± 1.38	12.33 ± 0.44#†	49.67 ± 5.33	13.17 ± 1.17#†	43.67 ± 4.90	12.38 ± 0.61#†	45 ± 0.43	11.67 ± 0.35#†	45.67 ± 3.2	12.27 ± 0.15#†	49.33 ± 3.08	13.27 ± 0.37#†
Cystic follicle	5.67 ± 0.19	1.45 ± 0.03	24.67 ± 1	6.8 ± 0.42*	24.33 ± 1.62	7.07 ± 0.29*	16 ± 1.21	4.6 ± 0.1#†	16.33 ± 1.76	4.3 ± 0.25#†	18.33 ± 2.09	5.2 ± 0.36†	20 ± 1.45	5.2 ± 0.36†	17.33 ± 2.1	4.6 ± 0.23#†	18 ± 2.2	4.9 ± 0.38#†
Total count	380.67 ± 6.74		361.67 ± 19.77		344 ± 15.72		346.67 ± 18.59		376.67 ± 20		355 ± 22.14		382.67 ± 14.75		372.33 ± 26.6		371.67 ± 20.92	
Corpus luteum	68.67 ± 1.76		26.67 ± 0.88*		23 ± 1.15*		48 ± 1.73#†		49 ± 2.4#†		39.33 ± 2.4#†		48.67 ± 1.67#†		47.67 ± 4.26#†		40.33 ± 1.86#†	

*Statistical result of the number and percentage of the follicles in different development stages and corpus luteum in various groups. Results are presented as mean ± SE. *P < 0.05 vs. Control group; #P < 0.05 vs. DHEA (3 weeks) group; †P < 0.05 vs. DHEA (7 weeks) group, n = 15.*

than two layers of granular cells without follicular cavity; antral follicle, an oocyte with one or multiple follicular cavities and multiple layers of granular cells as well as cumulus GC layer. Nuclei was visible in oocyte; cystic follicle, a big cavity with a thin layer of granular cells and obvious theca cells without oocyte; corpus luteum, gland-like structure enriched in blood vessels.

Determination of Body Weight, Fasting Blood Glucose, HOMA Index, Testosterone and Insulin

The blood of rat was collected at the end of the study from the abdominal aorta or orbital vein. Serum samples were obtained by centrifugation at 2054 *g* for 20 min at 4°C and stored at −80°C before analysis. The levels of testosterone and insulin in serum were tested by using ELISA kits (Abcam, Cambridge, United Kingdom) in accordance with the manufacturer's instructions. Fasting Blood Glucose and HOMA Index were tested as routine.

Terminal Deoxynucleotidyl Transferase-Mediated dUTP-Biotin Nick End-Labeling Staining

Terminal deoxynucleotidyl transferase-mediated dUTP-biotin nick end-labeling (TUNEL) staining was performed on paraffin sections of rat ovary with a TUNEL kit (Roche, Basel, Switzerland) in accordance with the manufacturers protocol. Nuclei were stained with Hoechst 33342 (Invitrogen, Camarillo, CA, United States). TUNEL positive cells were counted on randomly selected five fields in each section, under a laser scanning confocal microscope (TCS SP8; Leica, Mannheim, Germany), one sections from each animal. The average was calculated and presented as cell number per field.

Quantification of ROS Production in Mitochondria of Ovarian Tissue

To assess reactive oxygen species (ROS) production, ovarian sections were incubated for 15 min at 37°C in the dark with MitoSOX-Red (Invitrogen, Camarillo, CA, United States), a fluorochrome specific for superoxide produced in mitochondria. Nuclei were stained with Hoechst 33342. Images were grasped by using a confocal microscopy (TCS SP8; Leica, Mannheim, Germany). For quantitative analysis, three sections were chosen in each group and five fields were randomly selected per section. Analysis was conducted by using Image-Pro Plus 6.0 software (Media Cybernetics, Bethesda, MD, United States).

Determination of Activities of Mitochondrial Respiratory Chain Complexes

The ovarian tissue was harvested and immediately frozen in liquid nitrogen and stored at −80°C till use. GCs were washed with PBS for three times and stored at −80°C till use. In accordance with the manufacturer's protocol, mitochondrial respiratory chain Complex I, Complex II, and Complex IV activities in tissues and GCs were measured using ELISA kits

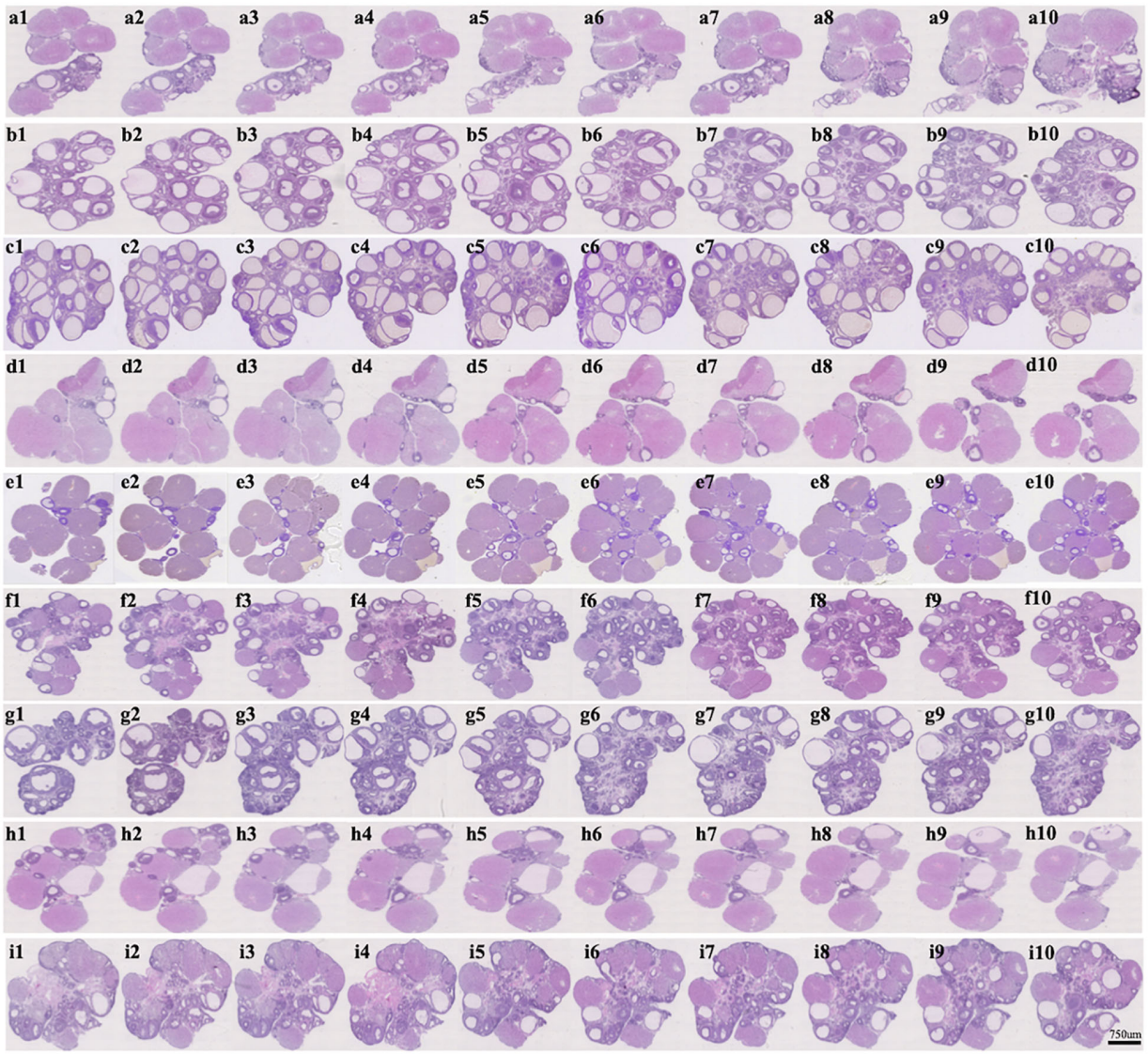


FIGURE 2 | Effect of post-treatment with BHG or KW on histology of the ovarian tissue. Representative images of 10 continuous HE staining sections of rat ovarian tissue in Control **(a1–a10)**, DHEA (3 weeks) **(b1–b10)**, DHEA (7 weeks) **(c1–c10)**, DHEA + BHG (0.75 g/kg) **(d1–d10)**, DHEA + BHG (1.49 g/kg) **(e1–e10)**, DHEA + BHG (2.99 g/kg) **(f1–f10)**, DHEA + KW (0.46 g/kg) **(g1–g10)**, DHEA + KW (0.91 g/kg) **(h1–h10)**, and DHEA + KW (1.82 g/kg) **(i1–i10)** group, respectively.

(Abcam, Cambridge, United Kingdom). Briefly, samples were homogenized, pelleted and adjusted to 5.5 mg/ml, subjected to detergent extraction and centrifugation for 20 min at 16,000 *g* (for Complex I), 12 000 g (for Complex II), and 24,127*g* (for Complex IV), followed by loading supernatant on plate and incubation for 3 h. Following washing for three times, optical density was measured after addition of assay solution.

Western Blot Assay

Rats under anesthesia were sacrificed at the end of the experiment, the ovarian tissue was harvested and immediately frozen in liquid nitrogen and stored at −80°C till use. The whole protein of the tissues and GCs were homogenized in RIPA lysis buffer with protease inhibitor (Applygen Technologies, Beijing, China). The isolation of cytoplasmic and mitochondrial proteins in tissues and GCs was completed according to the Mitochondrial Isolation kit instructions (Abcam, Cambridge, United Kingdom). Protein samples were separated by sodium dodecyl sulfate−polyacrylamide gel electrophoresis and transferred to polyvinylidene fluoride membrane. Blots were blocked with 5% fat-free milk or bovine serum albumin according to the antibody supplier's recommendation in Tris−buffered saline Tween, and membranes were incubated over night at 4°C with primary antibodies against Bax (1:1000), Bcl-2 (1:1000), cleaved caspase-3 (1:1000), caspase-3 (1:2000), cleaved caspase-9 (1:1000), caspase-9 (1:1000), caspase-8 (1:6000), caspase-12 (1:1000), cytochrome C (1:1000), COX4i1

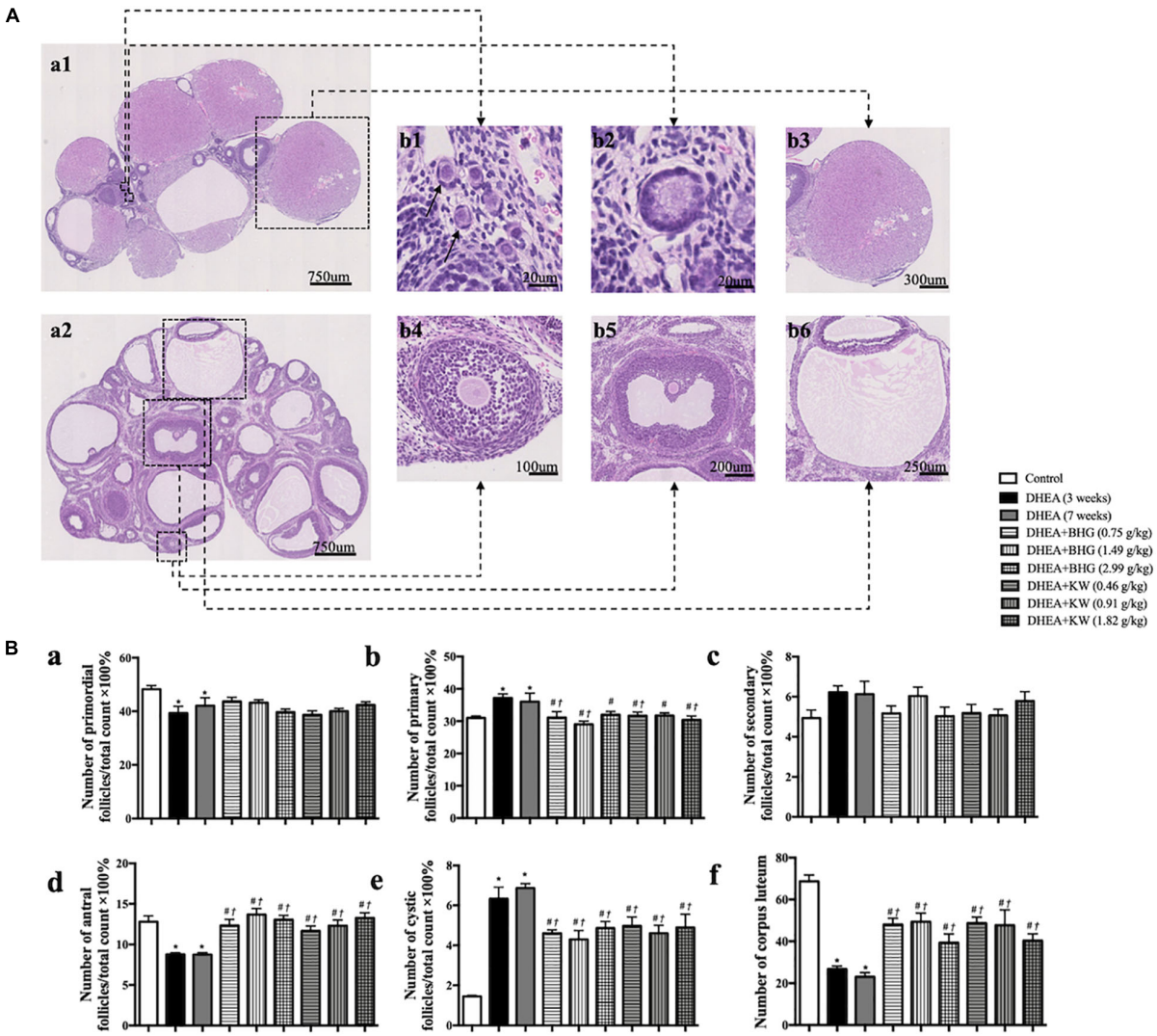


FIGURE 3 | Effect of post-treatment with BHG or KW on follicle development of the ovary. **(A)** Representative HE stained images of rat ovarian tissue **(a1, a2)**. Shown on right side are the representative images of primordial follicle **(b1)**, primary follicle **(b2)**, secondary follicle **(b4)**, antral follicle **(b5)**, cystic follicle **(b6)**, and corpus luteum **(b3)**, respectively. **(B)** Statistical result of the percentage of the follicles in different development stages and the number of corpus luteum in various groups. Results are presented as mean ± SEM. $^{*}P < 0.05$ vs. Control group; $^{\#}P < 0.05$ vs. DHEA (3 weeks) group; $^{\dagger}P < 0.05$ vs. DHEA (7 weeks) group, $n = 15$.

(1:1000), GRP78 (1:1000), CHOP (1:1000), ATF6 (1:1000), IRE1 (1:1000) and phospho-IRE1 (1:1000), XBP1s (1:1000), PERK (1:1000), phospho-PERK (1:1000), eIF2α(1:1000), phospho-eIF2α (1:1000), and ATF4 (1:1000) and GAPDH (1:5000). After washed with TBST for three times, the membranes were incubated with secondary antibody (1:5000) for 1 h at room temperature and washed again by TBST for three times. GAPDH was used as a loading control for cytoplasmic proteins, and COX4i1 was used as a loading control for mitochondria proteins. Enhanced Chemiluminescence Detection Kit (Applygen Technologies, Beijing, China) was used for revealing the bands. Band intensities were quantified by densitometry and presented as mean area density using Quantity One image analyzer software (Bio-Rad; Richmond, CA, United States).

Data Analysis

Statistical significances between groups were determined using one-way ANOVA with Bonferroni test. Data were expressed as mean ± SEM with $P < 0.05$ considered statistically significant.

RESULTS

BHG and KW, Respectively, Ameliorates Rat Estrous Cycle Dysfunction Induced by DHEA

The estrous cycles of rats were examined from the 11th day of modeling to the day the rats were killed. Representative records of estrous cycles of different groups are illustrated in **Figure 1A**.

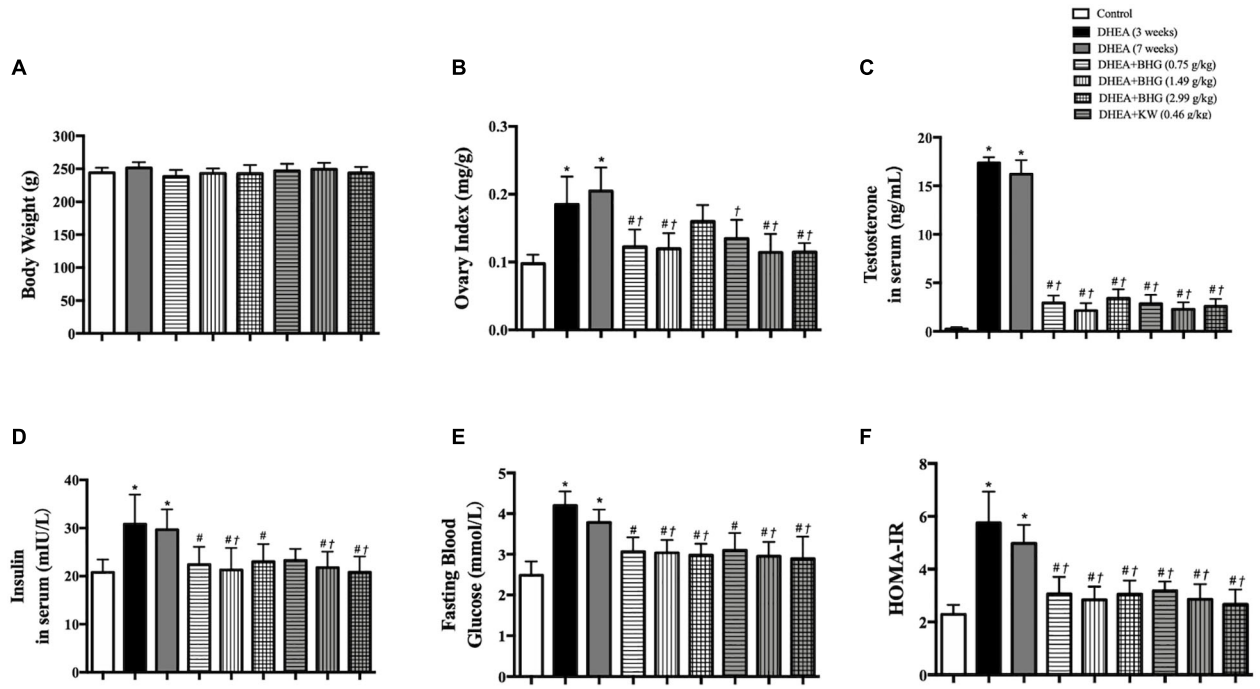


FIGURE 4 | Effect of post-treatment with BHG or KW on ovary index (ovary wet weight/body weight), the level of testosterone and insulin in rat serum and metabolism disorder. **(A)** The body weight in different group. **(B)** Ovary index (mg/g) of various groups. **(C)** Testosterone level in serum in various groups. **(D)** Insulin level in serum in various groups. **(E)** Fasting blood glucose in various groups. **(F)** HOMA index in various groups. Results are presented as mean ± SEM. $^{*}P < 0.05$ vs. Control group; $^{\#}P < 0.05$ vs. DHEA (3 weeks) group; $^{\dagger}P < 0.05$ vs. DHEA (7 weeks) group, $n = 15$ for testosterone level, $n = 8$ for others.

All rats in the Control group (**Figure 1Aa**) had normal estrous cycles. DHEA induced irregular estrous cycles, which persisted till the end of the study, if not intervened (**Figure 1Ab**). Post-treatment with BHG (0.75, 1.49, and 2.99 g/kg) or KW (0.46, 0.91, and 1.82 g/kg) all recovered the irregular estrous cycles form the third week of the administration (**Figure 1Ac–h**). **Figure 1B** and **Table 2** are the statistical results of the percentage of rats with normal estrous cycles after treatment with BHG or KW in different groups, which further confirmed the results of the estrous cycles records.

BHG and KW, Respectively, Ameliorates DHEA-Induced Follicles Development Abnormalities and Reduced Cystic Follicles Formation

The representative histological images from different groups are presented in **Figure 2**, which shows that the numbers of cystic follicles were significantly increased in DHEA (3 weeks) group (**Figure 2b**) and DHEA (7 weeks) group (**Figure 2c**) compared with the Control group (**Figure 2a**). Obviously, post-treatment with BHG (0.75, 1.49, and 2.99 g/kg) or KW (0.46, 0.91, and 1.82 g/kg) all reduced the number of cystic follicles to varying degree (**Figure 2d–i**). **Figure 3A** is the representative images of follicles at different developmental stages and corpus luteum. **Figure 3B** and **Table 2** are the percentage and number of the different follicles and corpus luteum in different groups, demonstrating that the percentage of primary follicles in DHEA (3 weeks) group and DHEA (7 weeks) group was increased, which was ameliorated by BHG and KW. In DHEA (3 weeks) group and DHEA (7 weeks) group, the percentage of antral follicles and the number of corpus luteum both significantly decreased, while the percentage of cystic follicles significantly increased. These results suggest that DHEA promotes early follicular growth and suppresses late follicular development. Post-treatment with BHG (0.75, 1.49, and 2.99 g/kg) or KW (0.46, 0.91, and 1.82 g/kg) all relieved abnormalities mentioned above, indicating the ameliorating effect of BHG and KW on follicles development abnormalities and cystic follicles formation.

BHG and KW, Respectively, Relieves DHEA-Induced Increase in Ovary Index, Testosterone in Serum and Metabolism Disorder

In line with the follicles development abnormalities and increased cystic follicles formation, DHEA, though had no effect on body weight (**Figure 4A**), also increased the ovary index as compared with Control group, while treatment with BHG (0.75 and 1.49 g/kg) and KW (0.46, 0.91, and 1.82 g/kg) both relieved this alteration (**Figure 4B**). Testosterone increased immediately after modeling and lasted until the end of the experiment if not interfered. The increased level of testosterone was prevented by treatment with BHG and KW at all doses (**Figure 4C**). Similarly,

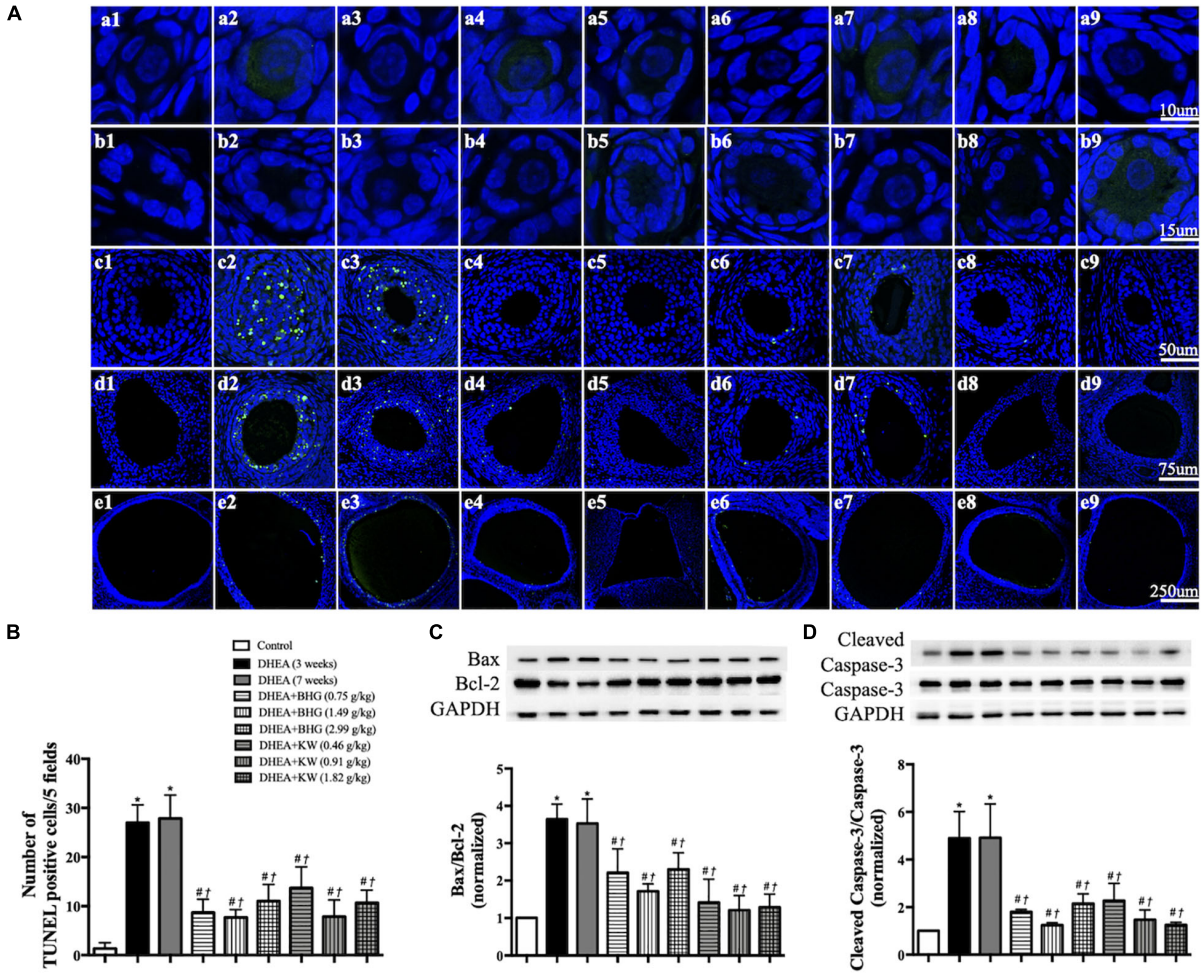


FIGURE 5 | Effect of post-treatment with BHG or KW on apoptosis of granulosa cells in ovarian tissue. **(A)** Representative TUNEL stained images of primordial follicle **(a)**, primary follicle **(b)**, secondary follicle **(c)**, antral follicle **(d)**, and cystic follicle **(e)** in Control **(1)**, DHEA (3 weeks) **(2)**, DHEA (7 weeks) **(3)**, DHEA + BHG (0.75 g/kg) **(4)**, DHEA + BHG (1.49 g/kg) **(5)**, DHEA + BHG (2.99 g/kg) **(6)**, DHEA + KW (0.46 g/kg) **(7)**, DHEA + KW (0.91 g/kg) **(8)**, and DHEA + KW (1.82 g/kg) **(9)**, group respectively. TUNEL positive cells are stained green. **(B)** Statistical result of the number of TUNEL positive cells per five fields in different groups. **(C)** Western blot for the expression of Bax to Bcl-2 in different groups with the quantification of Bax/Bcl-2 showing below. **(D)** Western blot for the expression of cleaved caspase-3 and caspase-3 in different groups with the quantification of cleaved caspase-3/caspase-3 showing below. Results are presented as mean ± SEM. $^{*}P < 0.05$ vs. Control group; $^{\#}P < 0.05$ vs. DHEA (3 weeks) group; $^{\dagger}P < 0.05$ vs. DHEA (7 weeks) group, $n = 3$ for TUNEL staining, $n = 8$ for western blot.

the level of insulin in serum (**Figure 4D**), fasting blood glucose (**Figure 4E**), and HOMA index (**Figure 4F**) increased after modeling and lasted for 4 weeks until the rats were scarified. These increases were prevented by treatment with BHG and KW.

BHG and KW, Respectively, Reduces the Apoptosis of Granulosa Cells Induced by DHEA

We next performed TUNEL staining on ovarian sections from various groups (**Figure 5A**). Apoptotic GCs were not noticed in Control group, but observed obviously in secondary follicle (**Figure 5A**, c2, c3), antral follicle (**Figure 5A**, d2, d3) and cystic follicle (**Figure 5A**, e2, e3) in DHEA (3 weeks) group and DHEA (7 weeks) group. The treatment with BHG and KW at all doses prevented the apoptosis in all type of follicles after DHEA (**Figure 5A**, c4 through 9, d4 through 9 and e4 through 9). These results were confirmed by statistical analysis (**Figure 5B**). Assessment by western blot provided further support for the results above, with the ratios of Bax to Bcl-2 and cleaved caspase-3 to caspase-3 varying among groups in a similar fashion as the TUNEL positive cells did (**Figures 5C,D**).

BHG and KW, Respectively, Decreases the Apoptosis Through Different Pathways

To explore the signaling pathways implicated in the role of the two drugs in attenuating the apoptosis of GCs after DHEA, western blots were carried out to assess the expression of cleaved caspase-9, caspase-9, caspase-8, and caspase-12 in ovarian tissue from various groups. As shown in **Figures 6A–C**, compared with

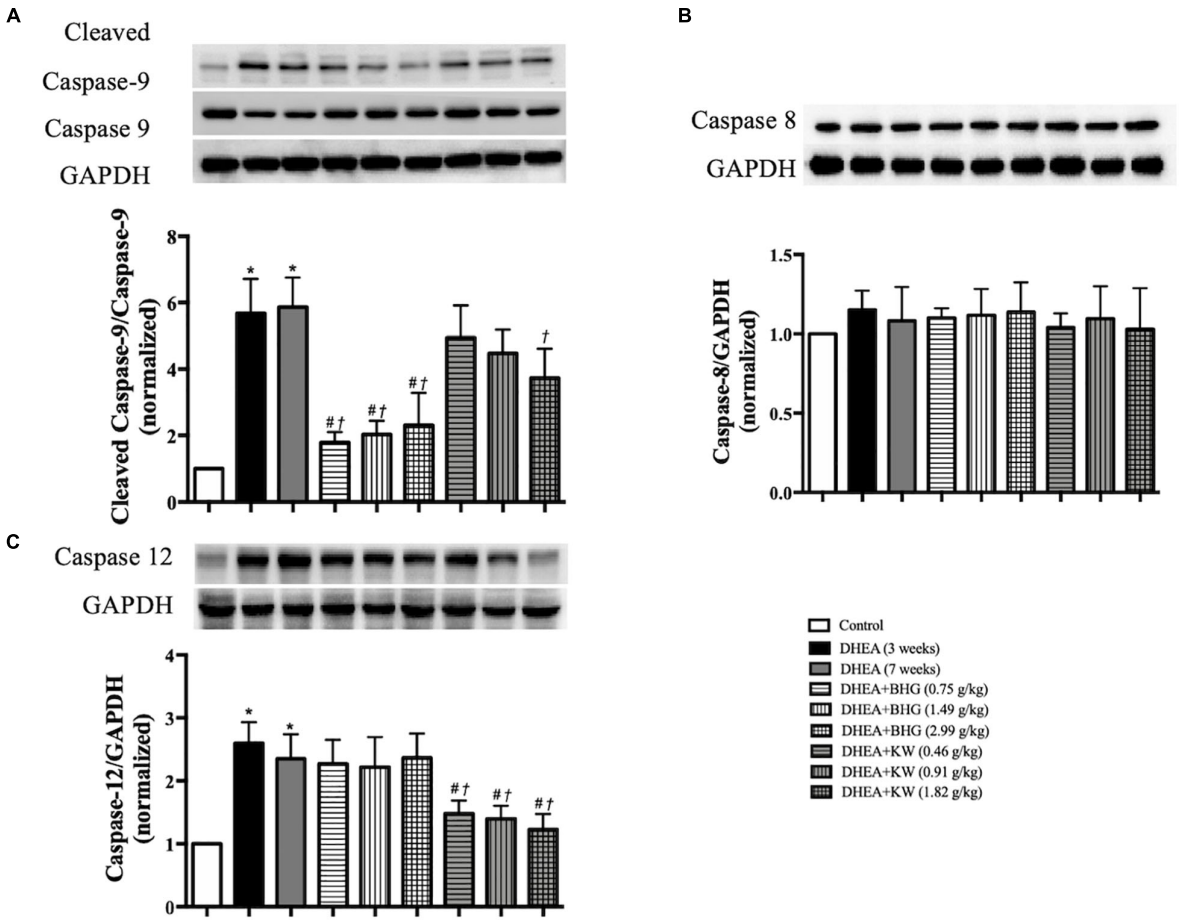


FIGURE 6 | Effect of post-treatment with BHG or KW on the apoptosis pathways. **(A)** Western blot for the expression of cleaved caspase-9 to caspase-9 in different groups with the quantification of cleaved caspase-9/caspase-9 showing below. **(B)** Western blot for the expression of caspase-8 in different groups with the quantification of caspase-8 showing below. **(C)** Western blot for the expression of caspase-12 in different groups with the quantification of caspase-12 showing below. Results are presented as mean ± SEM. $^{*}P < 0.05$ vs. Control group; $^{\#}P < 0.05$ vs. DHEA (3 weeks) group; $^{\dagger}P < 0.05$ vs. DHEA (7 weeks) group, $n = 8$.

the Control group, expression of the ratio of cleaved caspase-9 to caspase-9 and caspase-12 significantly increased in the DHEA (3 weeks) group and DHEA (7 weeks) group, while the expression of caspase-8 did not vary significantly among groups, indicating that the mitochondrial-dependent and endoplasmic reticulum (ER) stress pathways, but not death receptor-dependent pathway, were involved in the DHEA-induced GCs apoptosis. The increase in the expression of the ratio of cleaved caspase-9 to caspase-9 was significantly reduced by BHG, but not KW, at all the three doses tested. On the other hand, the increase in the expression of caspase-12 was significantly reduced by KW, but not BHG, at all the three doses. The results suggest that BHG and KW protected the DHEA-induced apoptosis, respectively, through different pathway.

BHG Attenuates the Dysfunctional Mitochondria After DHEA

The signaling pathway involved in the protective effect of BHG on apoptosis suggests occurrence of dysfunction of mitochondria in response to DHEA. To verify this inference, we first tested the cytochrome C release from mitochondria to cytosol by western blot in different groups, since one of the manifestations of dysfunctional mitochondria is open of mitochondrial permeability transition pore (mPTP). As shown in **Figure 7A**, the expression of cytochrome C in DHEA (3 weeks) group and DHEA (7 weeks) group increased in the cytosol fraction, compared to the mitochondrial fraction, indicating release of cytochrome C from the mitochondria into the cytosol. This change was protected by BHG, but not by KW. Release of mitochondrial cytochrome C into the cytosol is a known feature of the mitochondrial-dependent pathway of apoptosis (Allagnat et al., 2013). Dysfunctional mitochondria may manifest malregulated respiratory chain and oxidative stress alike. We thus tested mitochondrial ROS production in different groups with the MitoSOX probe. The production of ROS in mitochondria increased in DHEA (3 weeks) group and DHEA (7 weeks) group, which was reduced by BHG but not KW (**Figures 7B,C**). We next detected the activities of mitochondrial complex I (**Figure 7D**), II (**Figure 7E**), and

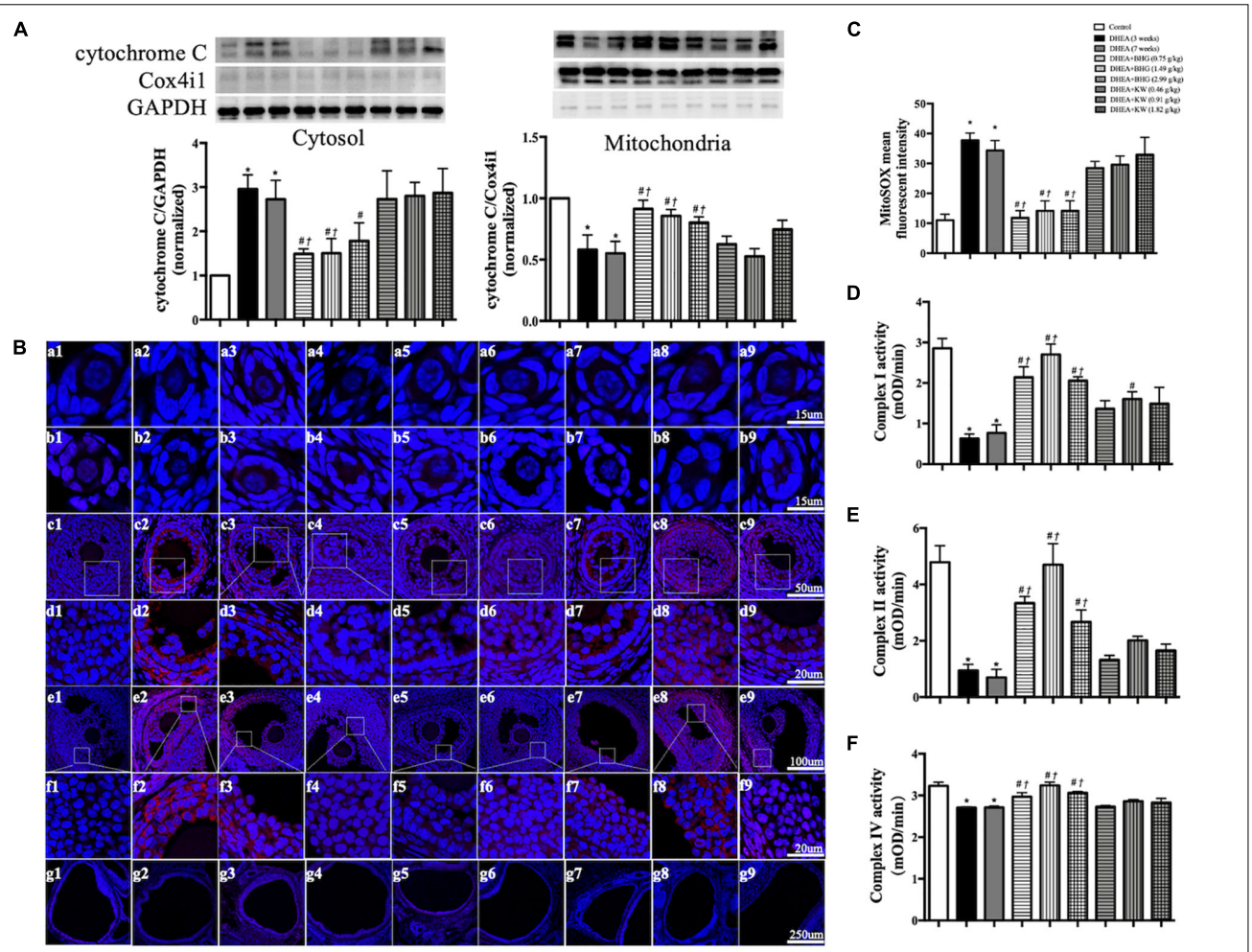


FIGURE 7 | Effect of BHG post-treatment on the dysfunction in mitochondria. **(A)** Representative immunoblot images of cytochrome C in cytosol and mitochondria with the quantification of cytochrome C/GAPDH and cytochrome C/Cox4i1 showing below. GAPDH and Cox4i1 were used as loading control for cytosolic and mitochondrial protein, respectively. **(B)** Representative confocal images of MitoSOX staining (red) for mitochondrial ROS production. Shown are primordial follicle **(a)**, primary follicle **(b)**, secondary follicle **(c)**, enlarged images of secondary follicle **(d)**, antral follicle **(e)**, enlarged images of antral follicle **(f)**, and cystic follicle **(g)** in Control **(1)**, DHEA (3 weeks) **(2)**, DHEA (7 weeks) **(3)**, DHEA + BHG (0.75 g/kg) **(4)**, DHEA + BHG (1.49 g/kg) **(5)**, DHEA + BHG (2.99 g/kg) **(6)**, DHEA + KW (0.46 g/kg) **(7)**, DHEA + KW (0.91 g/kg) **(8)**, and DHEA + KW (1.82 g/kg) **(9)** group, respectively. Nuclei are stained in blue. **(C)** Quantification of MitoSOX mean fluorescent intensity in different group. **(D–F)** Statistical results of complex I, II, IV activities of ovarian tissue from different groups tested by ELISA. Results are presented as mean ± SEM. $^{*}P < 0.05$ vs. Control group; $^{\#}P < 0.05$ vs. DHEA (3 weeks) group; $^{\dagger}P < 0.05$ vs. DHEA (7 weeks) group, $n = 3$ for MitoSOX staining, $n = 8$ for western blot and complex activity analysis.

IV (**Figure 7F**), and found that all of the mitochondrial complexes activities detected showed a significant decrease in DHEA (3 weeks) group and DHEA (7 weeks) group, and were ameliorated by post-treatment of BHG at all doses but not KW. These findings suggested that DHEA challenge impaired mitochondria thus initiated mitochondrial-dependent apoptotic signaling pathway, which was ameliorated by BHG post-treatment.

KW Relieves the ER Stress After DHEA Stimulation

Increase in the expression of caspase-12 following DHEA stimulation is indicative of ER stress. To further bear out this assumption and examine the role of KW in DHEA-caused ER stress, we tested the expression of GRP78 and CHOP, two marker proteins for the ER stress level. As shown in **Figures 8A,B**, compared with the Control group, DHEA (3 weeks) group and DHEA (7 weeks) group showed increased expression of GRP78 and CHOP, which was protected by post-treatment of KW at all doses but not BHG. We next examined by western blot which of the three ER stress sensors (ATF6, IRE1, and PERK) mediated the apoptosis of GCs. As shown in **Figure 8C**, the expression of ATF6 did not differ obviously among groups. In contrast, the ratio of phospho-IRE1 to IRE1 and XBP1s expression were upregulated significantly after modeling, which lasted until the end of the experiment if not interfered. After treatment of KW at all doses, the expression of phospho-IRE1

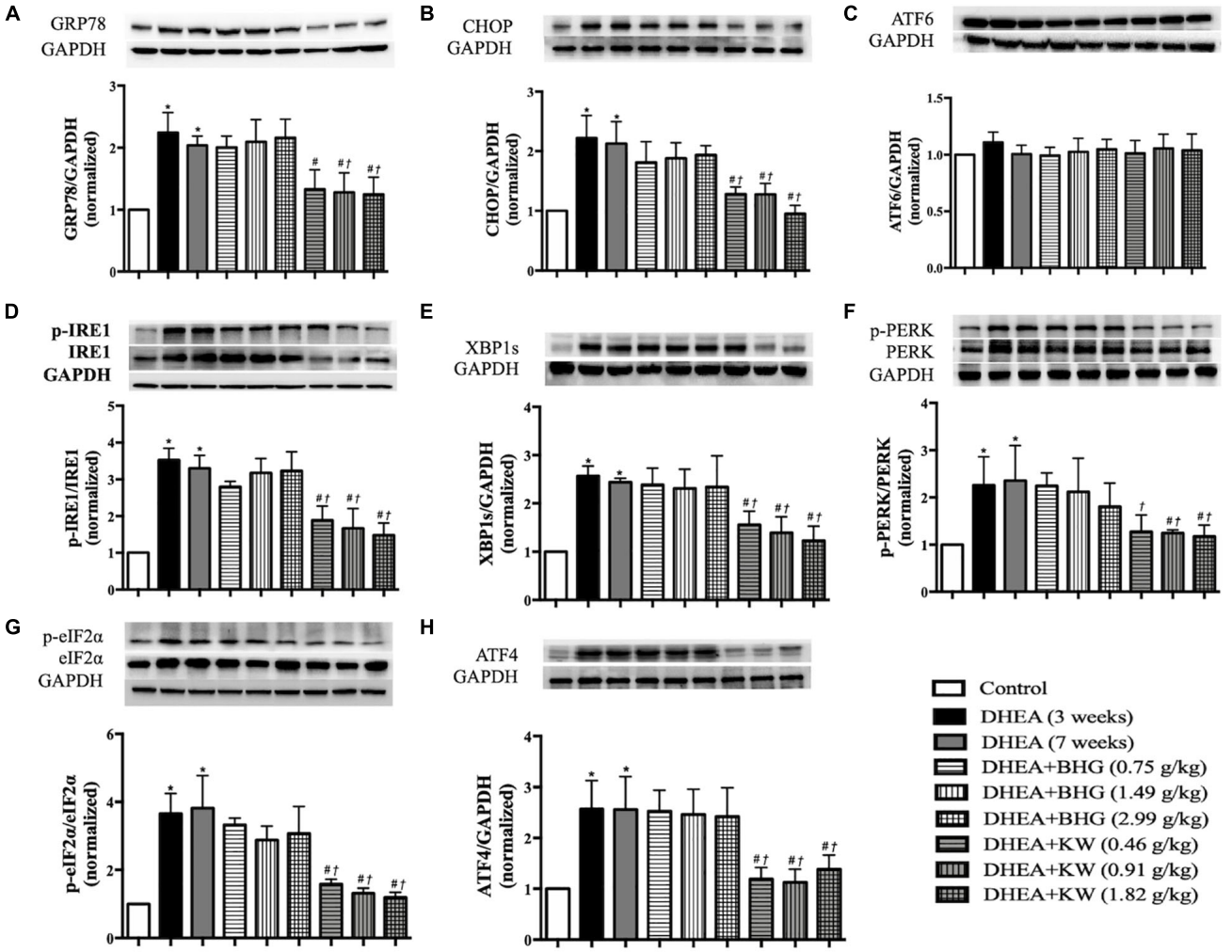


FIGURE 8 | Effect of KW post-treatment on ER stress. **(A–H)** Presented are the representative western blotting images of GRP78, CHOP, ATF6, phosphorylation-inositol-requiring enzyme 1(p-IRE1), IRE1, XBP1s, phosphorylation-proline-rich receptor-like protein kinase (p-PERK), PERK, phosphorylation-eukaryotic translation initiation factor 2α (p-eIF2α), eIF2α, and ATF4 with the quantification showing below. Results are presented as mean ± SEM. $^{*}P < 0.05$ vs. Control group; $^{\#}P < 0.05$ vs. DHEA (3 weeks) group; $^{\dagger}P < 0.05$ vs. DHEA (7 weeks) group, $n = 8$ for western blot.

TABLE 3 | Effects of BHG and KW, respectively, on pregnancy outcome in rats.

Groups	Examined	Percentage of mated number of rats (%)	Percentage of delivered number of rats (%)	Number of pups
Control	20	17 (85.0)	11 (64.7)	10.36 ± 0.64
DHEA (7 weeks)	18	7 (38.9)	2 (28.6)	4.50 ± 0.50*
DHEA + BHG (0.75 g/kg)	10	8 (80.0)	3 (37.5)	9.33 ± 0.88†
DHEA + BHG (1.49 g/kg)	10	9 (90.0)	5 (55.6)	9.8 ± 1.07†
DHEA + BHG (2.99 g/kg)	9	7 (77.8)	3 (42.9)	8.33 ± 1.20†
DHEA + KW (0.46 g/kg)	8	7 (87.5)	4 (57.1)	8.75 ± 1.25†
DHEA + KW(0.91 g/kg)	10	8 (80.0)	4 (50.0)	9.5 ± 1.76†
DHEA + KW (1.82 g/kg)	10	9 (90.0)	5 (55.6)	10.6 ± 1.08†

*Statistics result of pregnancy outcome in different groups. Results are presented as mean ± SEM. *P < 0.05 vs. Control group; †P < 0.05 vs. DHEA (7 weeks) group.*

to IRE1 and XBP1s was significantly decreased (**Figures 8D,E**). The ratio of phospho-PERK to PERK, phospho-eIF2α to eIF2α, and ATF4 expression varied among groups in a similar manner (**Figures 8F–H**). The results suggested it is the IRE1-XBP1s and PERK-eIF2α-ATF4, but not ATF6, that were involved in the DHEA-induced ER stress, which were ameliorated by KW post-treatment. Whereas BHG did not show effect on this signaling.

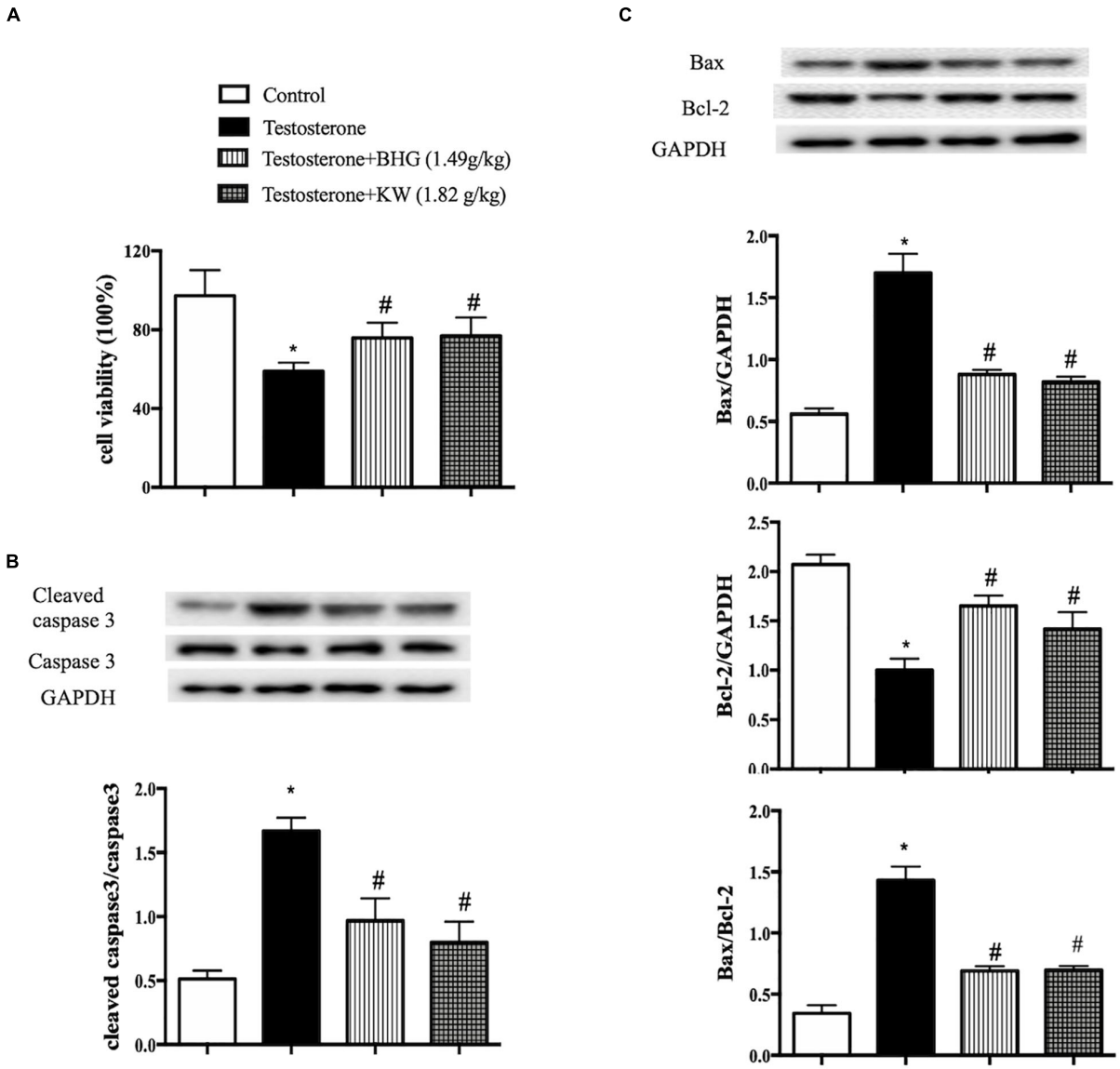


FIGURE 9 | Effect of post-treatment with BHG or KW on the cell viability and apoptosis of GCs induced by testosterone. **(A)** CCK-8 detection for GCs viability in different groups. **(B)** Western blot for the expression of cleaved caspase-3 and caspase-3 in different groups with the quantification of cleaved caspase-3/caspase-3 showing below. **(C)** Western blot for the expression of Bax, Bcl-2 in different groups with the quantification showing below. Results are presented as mean ± SEM. $^{*}P < 0.05$ vs. Control group; $^{\#}P < 0.05$ vs. Testosterone group, $n = 6$ for CCK-8, $n = 3$ for western blot. Testosterone + BHG (1.49 g/kg) denotes the cells treated with serum from animals receiving BHG at 1.49 g/kg, Testosterone + KW (1.82 g/kg) denotes the cells treated with serum from animals receiving KW at 1.82 g/kg.

BHG and KW, Respectively, Improves Pregnancy Outcome of DHEA-Induced PCOS

Polycystic ovary syndrome is one of the most common causes of female infertility, and approximately 74% of PCOS patients are infertile (Li et al., 2017, 2019). We investigated the ameliorating effect of BHG and KW, respectively, on pregnancy outcome of the DHEA-induced PCOS rats. Results showed that the percentage of delivered number of rats obviously decreased in the DHEA (7 weeks) group, while BHG and KW, respectively, improved the delivered rate. Compared with the Control group, the number of pups significantly reduced in the DHEA (7 weeks) group and improved significantly after post-treatment of BHG and KW (**Table 3**).

BHG and KW Ameliorates the GCs Viability and Reduces the Apoptosis of GCs Induced by Testosterone

The findings in PCOS model were verified *in vivo* in GCs. For this purpose, we first detected the effects of BHG and KW on viability and apoptosis of GCs induced by testosterone. As compared with control group, testosterone markedly decreased viability, while

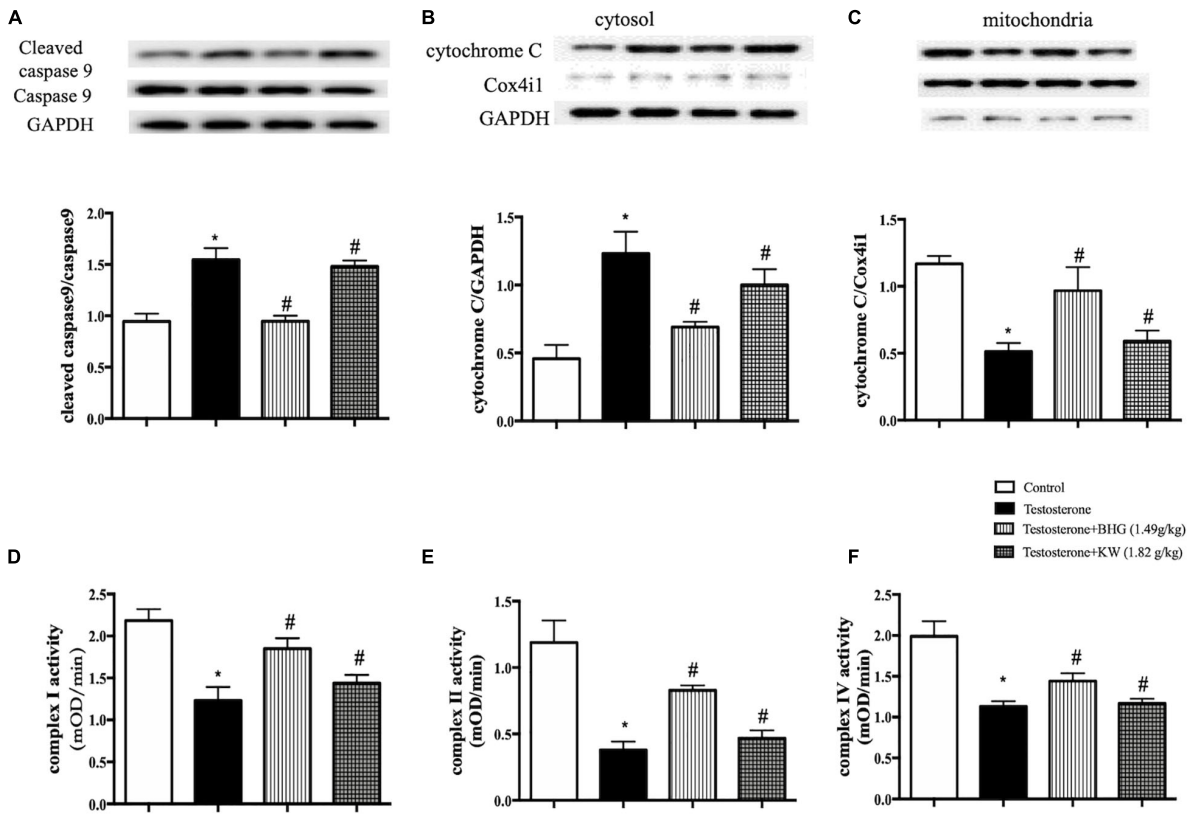


FIGURE 10 | Effect of BHG on the dysfunction in mitochondria of GCs induced by testosterone. **(A)** Western blot for the expression of cleaved caspase-9 and caspase-9 in different groups with the quantification of cleaved caspase-9/caspase-9 showing below. **(B)** Representative western blot images of cytochrome C in cytosol form various groups with quantification showing below. **(C)** Representative western blot images of cytochrome C in mitochondria from various groups with the quantification showing below. GAPDH and Cox4i1 were used as loading control for cytosolic and mitochondrial protein, respectively. **(D–F)** Statistical results of complex I, II, IV activities of GCs from different groups tested by ELISA. Results are presented as mean ± SEM. $^{*}P < 0.05$ vs. Control group; $^{\#}P < 0.05$ vs. Testosterone group, $n = 3$ for western blot and $n = 6$ for complex activity analysis. Testosterone + BHG (1.49 g/kg) denotes the cells treated with serum from animals receiving BHG at 1.49 g/kg, Testosterone + KW (1.82 g/kg) denotes the cells treated with serum from animals receiving KW at 1.82 g/kg.

both BHG and KW ameliorated GCs viability significantly after testosterone (**Figure 9A**). Western blot assessment showed that testosterone increased the ratios of cleaved caspase-3/caspase-3 and Bax/Bcl-2, elevated the level of Bax and decreased the level of Bcl-2 in GCs, while both BHG and KW ameliorated these alterations (**Figures 9B,C**).

BHG Decreases the Apoptosis Through Attenuating the Dysfunctional Mitochondria of GCs Induced by Testosterone

Western blots were carried out to assess the expression of cleaved caspase-9 and caspase-9 to explore the signaling pathways implicated in the apoptosis of GCs induced by testosterone. The results showed that testosterone induced the increase of cleaved caspase-9/caspase 9 in GCs. The increase ratio of cleaved caspase-9/caspase 9 was significantly reduced by BHG, but not KW (**Figure 10A**), indicating involvement of ameliorating dysfunctional mitochondria in the effect of BHG on apoptosis after testosterone. We next tested the function of mitochondria in different groups. As shown in **Figures 10B,C**, compared with the Control, the expression of cytochrome C in testosterone group increased in the cytosol fraction, but decreased in mitochondrial fraction, indicating release of cytochrome C from the mitochondria into the cytosol. BHG ameliorated this alteration, while KW had no effect. We next detected the activities of mitochondrial complex I, II, and IV and found that all of the mitochondrial complexes activities detected showed a significant decrease in testosterone group, which were ameliorated by BHG, but not by KW (**Figures 10D–F**). These findings suggested that BHG ameliorated the mitochondrial-dependent apoptotic signaling pathway induced by testosterone whereas KW did not show effect on this signaling.

KW Decreases the Apoptosis Through Relieving the ER Stress of GCs Induced by Testosterone

Caspase-12, GRP78, and CHOP are indicative proteins for ER stress. As shown in **Figure 11A**, testosterone increased

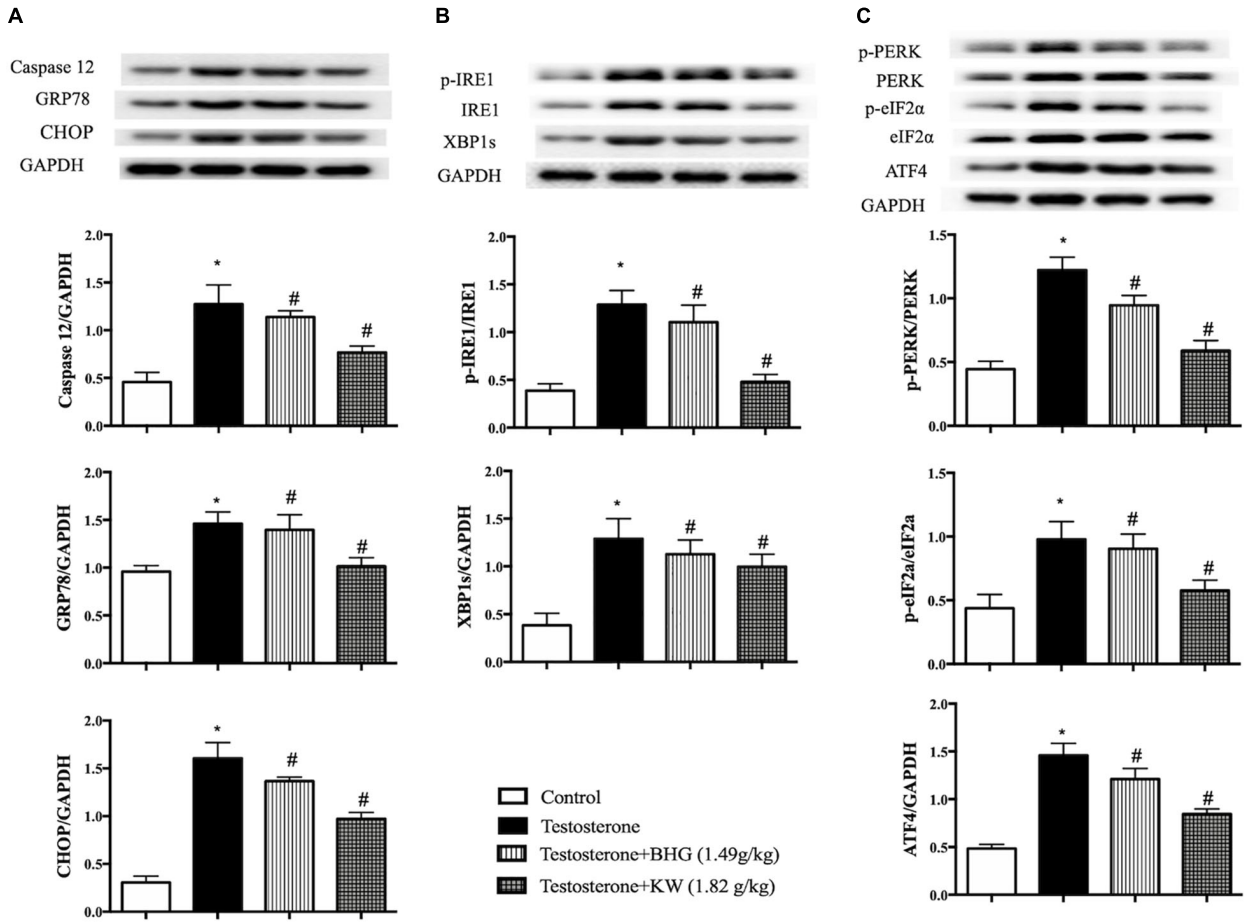


FIGURE 11 | Effect of KW on ER stress in GCs induced by testosterone. **(A)** Presented are the representative western blotting images of caspase-12, GRP78, CHOP with the quantification showing below; **(B)** presented are the representative western blotting images of p-IRE1, IRE1, XBP1s; **(C)** presented are the representative western blotting images of p-PERK, PERK, p-eIF2α, eIF2α, and ATF4 with the quantification showing below. Results are presented as mean ± SEM. $^{*}P < 0.05$ vs. Control group; $^{\#}P < 0.05$ vs. Testosterone group, $n = 3$ for western blot. Testosterone + BHG (1.49 g/kg) denotes the cells treated with serum from animals receiving BHG at 1.49 g/kg, Testosterone + KW (1.82 g/kg) denotes the cells treated with serum from animals receiving KW at 1.82 g/kg.

the expression of caspase-12, GRP78, and CHOP, which was decreased by KW, but not by BHG. We next examined ER stress sensors IRE1 and PERK in different group of GCs. Western blot assay showed that the ratios of phospho-IRE1/IRE1, phospho-PERK/PERK, phospho-eIF2α/eIF2α, and the level of ATF4 expression were increased by testosterone stimulation, which were all ameliorated by KW but not BHG (**Figures 11B,C**), indicating that KW ameliorated the ER stress-dependent apoptotic signaling pathway induced by testosterone whereas, BHG did not show effect on this signaling.

DISCUSSION

The present study demonstrated that BHG and KW ameliorated DHEA-induced PCOS symptoms such as irregular estrous cycles, polycystic ovary and high levels of testosterone and insulin in serum. Particularly, treatment with BHG and KW both improved the outcome of pregnancy, increased number of pups. These results verified the efficiency of BHG and KW in treatment of PCOS in clinic.

Increasing studies in PCOS patients and DHEA-induced PCOS animal model indicates apoptosis of GCs as one of the main manifestations of PCOS, which is involved in the dysfunction of GCs (Sun et al., 2017; Takahashi et al., 2017; Zhao et al., 2018), and emerges as a target for improvement of PCOS symptoms (Chang et al., 2013; Lim et al., 2017b; Lima et al., 2018). However, the signaling pathways implicated in apoptosis of GCs of PCOS have not been fully elucidated. Consistent with previous reports, the present study revealed a prominently increased apoptosis in GCs in rats in response to DHEA stimulation. Furthermore, signaling protein analysis found that the apoptosis in GCs after DHEA was mediated by mitochondria- and ER stress-dependent pathways, but without involvement of death receptor-dependent pathway. This result implies that mitochondria and ER were impaired in GCs of PCOS, as confirmed by the findings that DHEA caused an increase in cytochrome C release from mitochondria and a dysfunction of

mitochondria respiratory chain, as well as an upregulated ER stress protein. The dysfunctional mitochondria and ER stress may also account for the oxidative stress after DHEA observed in the present study, which is in line with the observations of others in patients (Devine et al., 2012; Karuputhula et al., 2013; Meng et al., 2013; Wang et al., 2019). Interestingly, we observed that both BHG and KW may attenuate the apoptosis in GCs after DHEA stimulation, but via different pathway with BHG targeting mitochondria-dependent apoptotic pathway while KW targeting ER stress-dependent apoptotic pathway. The findings in PCOS model was verified by *in vitro* study using GCs. This result shows that although BHG and KW are both effective in treatment of PCOS, but the underling mechanism likely differs from each other. More importantly, this finding provides clue for development of novel management to deal with PCOS.

In physiological condition, testosterone originates approximately equally from ovaries and adrenal grand. In ovaries, DHEA, the intermediate metabolite, transforms to androstenedione in theca cells, which is in part metabolized to testosterone in theca cells while remainder is converted to estrone in GCs (Rosenfield and Ehrmann, 2016). It is predicable that DHEA administration results in an increase in testosterone in plasma, as the case in present study, since the source for synthesis of testosterone has increased. On the other hand, we observed an increased apoptosis of GCs after DHEA, which is likely to contribute in part to the increase in DHEA-caused elevation of testosterone, as the apoptotic GCs protect androstenedione from converting to estrone thus increase the source for synthesis of testosterone. This notion is testified by the fact that BHG and KW attenuated the apoptosis in GCs, meanwhile, decreased the level of testosterone. This result is in accordance with a recent report showing that dysfunction of GCs may contribute to excessive secretion of androgen and abnormal follicles formation (Xu et al., 2011), and further documents the importance of apoptosis of GCs in the development of PCOS. Our *in vitro* experiment showed that testosterone decreased the GCs viability and increased the GCs apoptosis, both BHG and KW are effective in ameliorating the alterations of GCs induced by testosterone via different anti-apoptotic pathway.

The present study revealed that BHG and KW treatment protected insulin form increase in PCOS, this is likely attributable to their ability to decrease the level of testosterone, since hyperandrogen has been reported to induce hyperinsulinemia through the regulation of adiponectin, tumor necrosis factor, interleukin-6, leptin, and other factors (Escobar-Morreale, 2018).

In the present study, we tested three different doses for each medicine with the middle one being the equivalent human dose in clinic. For most parameters examined, no significant dose-dependent effect was observed for either medicine. This result may imply that the two medicines have a larger dose tolerance in term of the endpoints examined. However, it should be very careful to extrapolate this result to clinic, since high dose may exhibit some adverse side effect, as suggested by the fact that BHG at high dose seemed less effective at least for some parameters tested, and the morphology of ovarian tissue exposed to BHG at low and medium dose seemed to be better than that to BHG at high dose. Moreover, both drugs contain dozens of components. Another limitation of the present work is that no study is performed to explore the effective compound (s) responsible for the effect observed, although some compositions of both drugs were detected in the plasma after administration (**Supplementary Material 3**).

In summary, the present study demonstrated the efficiency of BHG and KW in treatment of PCOS in rat induced by DHEA, this effect is likely associated with attenuation of GCs apoptosis protecting testosterone from increase. BHG and KW exerted protective effect on GCs apoptosis via different pathway with BHG interfering in mitochondria-dependent apoptotic pathway while KW targeting ER stress-dependent apoptotic pathway.

PERSPECTIVE

Polycystic ovary syndrome accounts for about 70% of anovulatory infertility cases. BHG and KW are currently used in China to cope with PCOS with efficiency, however, the underlying mechanisms remain unknown. The present study confirmed the effect of the two medicines in treatment of rat PCOS model induced by DHEA and found that both medicines exhibit potential to attenuate GC apoptosis but via different pathway with BHG targeting mitochondria-dependent apoptotic pathway while KW targeting ER stress-dependent apoptotic pathway. This potential may contribute to downregulation of testosterone thus relieve the PCOS. These results provide scientific basis for the use of the two medicines in practice and promote their application. The finding that GC apoptosis in PCOS implicated mitochondria- and ER-stress dependent apoptotic pathways without involvement of death receptor-dependent apoptotic pathway offered clue for searching novel option to fight against PCOS.

DATA AVAILABILITY STATEMENT

All datasets generated for this study are included in the article/**Supplementary Material**.

ETHICS STATEMENT

The animal study was reviewed and approved by the Committee on the Ethics of Animal Experiments of Peking University Health Science Center.

AUTHOR CONTRIBUTIONS

YX and C-SP performed the experiments, analyzed the data, and wrote the manuscript. QL provided scientific guidance and oversight. H-LZ contributed to the animal experiments. LY contributed to confocal imaging. GA participated in western blot assay of GCs experiments. X-YW and L-LY participated in the preparation of sample for LC-MS analysis. J-YF and J-YH revised the manuscript. DL and J-YH supervised the research and provided key research directions. All authors read and agreed with the final article.

ACKNOWLEDGMENTS

The work of pharmacokinetics was nicely supported by Yang Chu, Jing Kong for LC-MS analysis from Tasly Academy.

SUPPLEMENTARY MATERIAL

The Supplementary Material for this article can be found online at: https://www.frontiersin.org/articles/10.3389/fphys.2021.525145/full#supplementary-material

REFERENCES

Allagnat, F., Klee, P., Cardozo, A. K., Meda, P., and Haefliger, J. A. (2013). Connexin36 contributes to INS-1E cells survival through modulation of cytokine-induced oxidative stress, ER stress and AMPK activity. *Cell Death Differ.* 20, 1742–1752. doi: 10.1038/cdd.2013.134

Azhary, J. M. K., Harada, M., Takahashi, N., Nose, E., Kunitomi, C., Koike, H., et al. (2019). Endoplasmic reticulum stress activated by androgen enhances apoptosis of Granulosa cells via induction of death receptor 5 in PCOS. *Endocrinology* 160, 119–132. doi: 10.1210/en.2018-00675

Beck, J. I., Boothroyd, C., Proctor, M., Farquhar, C., and Hughes, E. (2005). Oral anti-oestrogens and medical adjuncts for subfertility associated with anovulation. *Cochrane Database Syst Rev.* 25:Cd002249. doi: 10.1002/14651858.CD002249.pub2

Casper, R. F., and Mitwally, M. F. (2006). Review: aromatase inhibitors for ovulation induction. *J. Clin. Endocrinol. Metab.* 91, 760–771. doi: 10.1210/jc.2005-1923

Chang, C., Lee, S. O., Wang, R. S., Yeh, S., and Chang, T. M. (2013). Androgen Receptor (AR) physiological roles in male and female reproductive systems: lessons learned from ar-knockout mice lacking AR in selective cells. *Biol. Reprod.* 89:21. doi: 10.1095/biolreprod.113.109132

Chen, C., Wickenheisser, J., Ewens, K. G., Ankener, W., Legro, R. S., Dunaif, A., et al. (2009). PDE8A genetic variation, polycystic ovary syndrome and androgen levels in women. *Mol. Hum. Reprod.* 15, 459–469. doi: 10.1093/molehr/gap035

Devine, P. J., Perreault, S. D., and Luderer, U. (2012). Roles of reactive oxygen species and antioxidants in ovarian toxicity. *Biol. Reprod.* 86:27. doi: 10.1095/biolreprod.111.095224

Elkady, A. I. (2019). Targeting prostate cancer cell proliferation, stemness and metastatic potential using *Costus speciosus* derived phytochemicals. *Am. J. Transl. Res.* 11, 2550–2569.

Escobar-Morreale, H. F. (2018). Polycystic ovary syndrome: definition, aetiology, diagnosis and treatment. *Nat. Rev. Endocrinol.* 14, 270–284. doi: 10.1038/nrendo.2018.24

Eser, A., Erpolat, S., Kaygusuz, I., Balci, H., and Kosus, A. (2017). Investigation of *Demodex folliculorum* frequency in patients with polycystic ovary syndrome. *Ann. Bras. Dermatol.* 92, 807–810. doi: 10.1590/abd1806-4841.20176043

Fu, X., He, Y., Wang, X., Peng, D., Chen, X., Li, X., et al. (2018). MicroRNA-16 promotes ovarian Granulosa cell proliferation and suppresses apoptosis through targeting PDCD4 in polycystic ovarian syndrome. *Cell Physiol. Biochem.* 48, 670–682. doi: 10.1159/000491894

Hughes, E., Collins, J., and Vandekerckhove, P. (2000). Gonadotrophin-releasing hormone analogue as an adjunct to gonadotropin therapy for clomiphene-resistant polycystic ovarian syndrome. *Cochrane Database Syst. Rev.* 2000:Cd000097.

Jonard, S., and Dewailly, D. (2004). The follicular excess in polycystic ovaries, due to intra-ovarian hyperandrogenism, may be the main culprit for the follicular arrest. *Hum. Reprod. Update* 10, 107–117. doi: 10.1093/humupd/dmh010

Karuputhula, N. B., Chattopadhyay, R., Chakravarty, B., and Chaudhury, K. (2013). Oxidative status in Granulosa cells of infertile women undergoing IVF. *Syst. Biol. Reprod. Med.* 59, 91–98. doi: 10.3109/19396368.2012.743197

Lee, Y. H., Yang, H., Lee, S. R., Kwon, S. W., Hong, E. J., and Lee, H. W. (2018). Welsh onion root (*Allium fistulosum*) restores ovarian functions from Letrozole induced-polycystic ovary syndrome. *Nutrients* 10:1430. doi: 10.3390/nu10101430

Li, J., Xie, L. M., Song, J. L., Yau, L. F., Mi, J. N., Zhang, C. R., et al. (2019). Alterations of sphingolipid metabolism in different types of polycystic ovary syndrome. *Sci. Rep.* 9:3204. doi: 10.1038/s41598-019-38944-6

Li, Y., Deng, B., Ouyang, N., Yuan, P., Zheng, L., and Wang, W. (2017). Telomere length is short in PCOS and oral contraceptive does not affect the telomerase activity in Granulosa cells of patients with PCOS. *J. Assist. Reprod. Genet.* 34, 849–859. doi: 10.1007/s10815-017-0929-z

Lim, J. J., Han, C. Y., Lee, D. R., and Tsang, B. K. (2017a). Ring finger protein 6 mediates androgen-induced Granulosa cell proliferation and follicle growth via modulation of androgen receptor signaling. *Endocrinology* 158, 993–1004. doi: 10.1210/en.2016-1866

Lim, J. J., Lima, P. D. A., Salehi, R., Lee, D. R., and Tsang, B. K. (2017b). Regulation of androgen receptor signaling by ubiquitination during folliculogenesis and its possible dysregulation in polycystic ovarian syndrome. *Sci. Rep.* 7:10272. doi: 10.1038/s41598-017-09880-0

Lima, P. D. A., Nivet, A. L., Wang, Q., Chen, Y. A., Leader, A., Cheung, A., et al. (2018). Polycystic ovary syndrome: possible involvement of androgen-induced, chemerin-mediated ovarian recruitment of monocytes/macrophages. *Biol. Reprod.* 99, 838–852. doi: 10.1093/biolre/ioy096

Lv, B. Y., Sun, H. Y., Li, Q., Zhang, H. L., Pan, C. S., Yan, L., et al. (2019). The ameliorating effects of Bushen Tiaoxue granules and kunling wan on impaired angiogenesis and endometrial receptivity in rats following controlled ovarian hyperstimulation. *Microcirculation* 17:e12581. doi: 10.1111/micc.12581

Matsuda, F., Inoue, N., Manabe, N., and Ohkura, S. (2012). Follicular growth and atresia in mammalian ovaries: regulation by survival and death of granulosa cells. *J. Reprod. Dev.* 58, 44–50. doi: 10.1262/jrd.2011-012

Meng, Y., Qian, Y., Gao, L., Cai, L. B., Cui, Y. G., and Liu, J. Y. (2013). Downregulated expression of Peroxiredoxin 4 in Granulosa cells from polycystic ovary syndrome. *PLoS One* 8:e0076460. doi: 10.1371/journal.pone.0076460

Murase, T., Iwase, A., Komatsu, K., Bayasula, N. T., Osuka, S., Takikawa, S., et al. (2018). Follicle dynamics: visualization and analysis of follicle growth and maturation using murine ovarian tissue culture. *J. Assist. Reprod. Genet.* 35, 339–343. doi: 10.1007/s10815-017-1073-5

Nakamura, T., Iwase, A., Bayasula, B., Nagatomo, Y., Kondo, M., Nakahara, T., et al. (2015). CYP51A1 induced by growth differentiation factor 9 and follicle-stimulating hormone in Granulosa cells is a possible predictor for unfertilization. *Reprod. Sci.* 22, 377–384. doi: 10.1177/1933719114529375

Palomba, S., Russo, T., Orio, F. Jr., Falbo, A., Manguso, F., Sammartino, A., et al. (2006). Uterine effects of clomiphene citrate in women with polycystic ovary syndrome: a prospective controlled study. *Hum. Reprod.* 21, 2823–2829. doi: 10.1093/humrep/del267

Rosenfield, R. L., and Ehrmann, D. A. (2016). The Pathogenesis of polycystic ovary syndrome (PCOS): the hypothesis of PCOS as functional ovarian hyperandrogenism revisited. *Endocr. Rev.* 37, 467–520. doi: 10.1210/er.2015-1104

Roy, S., Mahesh, V. B., and Greenblatt, R. B. (1962). Effect of dehydroepiandrosterone and delta4-androstenedione on the reproductive organs of female rats: production of cystic changes in the ovary. *Nature* 196, 42–43. doi: 10.1038/196042a0

Su, L., Suyila, Q., Yang, L., Li, H., Xi, Y., and Su, X. (2017). Bax is involved in the anticancer activity of Velcade in colorectal cancer. *Exp. Ther. Med.* 14, 3179–3183. doi: 10.3892/etm.2017.4857

Sun, H. Y., Li, Q., Liu, Y. Y., Wei, X. H., Pan, C. S., Fan, J. Y., et al. (2017). Xiao-Yao-San, a Chinese medicine formula, ameliorates chronic unpredictable mild stress induced polycystic ovary in rat. *Front. Physiol.* 8:729. doi: 10.3389/fphys.2017.00729

Takahashi, N., Harada, M., Hirota, Y., Nose, E., Azhary, J. M., Koike, H., et al. (2017). Activation of endoplasmic reticulum stress in Granulosa cells from patients with polycystic ovary syndrome contributes to ovarian fibrosis. *Sci. Rep.* 7:10824. doi: 10.1038/s41598-017-11252-7

Tummon, I., Gavrilova-Jordan, L., Allemand, M. C., and Session, D. (2005). Polycystic ovaries and ovarian hyperstimulation syndrome: a systematic review*. *Acta Obstet. Gynecol. Scand.* 84, 611–616. doi: 10.1080/j.0001-6349.2005.00788.x

Wang, T., Zhang, J., Hu, M., Zhang, Y., Cui, P., Li, X., et al. (2019). Differential expression patterns of Glycolytic enzymes and mitochondria-dependent apoptosis in PCOS patients with endometrial hyperplasia, an early hallmark of endometrial cancer, in vivo and the impact of metformin In Vitro. *Int. J. Biol. Sci.* 15, 714–725. doi: 10.7150/ijbs.31425

Wei, D., Xie, J., Yin, B., Hao, H., Song, X., Liu, Q., et al. (2017). Significantly lengthened telomere in granulosa cells from women with polycystic ovarian syndrome (PCOS). *J. Assist. Reprod. Genet.* 34, 861–866. doi: 10.1007/s10815-017-0945-z

Wu, H., Yu, K., and Yang, Z. (2015). Associations between TNF-alpha and interleukin gene polymorphisms with polycystic ovary syndrome risk: a systematic review and meta-analysis. *J. Assist. Reprod. Genet.* 32, 625–634. doi: 10.1007/s10815-015-0449-7

Wu, X. Q., Wang, Y. Q., Xu, S. M., Liu, J. F., Bi, X. Y., Wang, Z. Q., et al. (2017). The WNT/beta-catenin signaling pathway may be involved in granulosa cell apoptosis from patients with PCOS in North China. *J. Gynecol. Obstet. Hum. Reprod.* 46, 93–99. doi: 10.1016/j.jgyn.2015.08.013

Xu, S., Linher-Melville, K., Yang, B. B., Wu, D., and Li, J. (2011). Micro-RNA378 (miR-378) regulates ovarian estradiol production by targeting aromatase. *Endocrinology* 152, 3941–3951. doi: 10.1210/en.2011-1147

Yao, K., Bian, C., and Zhao, X. (2017). Association of polycystic ovary syndrome with metabolic syndrome and gestational diabetes: aggravated complication of pregnancy. *Exp. Ther. Med.* 14, 1271–1276. doi: 10.3892/etm.2017.4642

Zhao, J., Xu, J., Wang, W., Zhao, H., Liu, H., Liu, X., et al. (2018). Long non-coding RNA LINC-01572:28 inhibits Granulosa cell growth via a decrease in p27 (Kip1) degradation in patients with polycystic ovary syndrome. *EBio Med.* 36, 526–538. doi: 10.1016/j.ebiom.2018.09.043

Zheng, Q., Li, Y., Zhang, D., Cui, X., Dai, K., Yang, Y., et al. (2017). ANP promotes proliferation and inhibits apoptosis of ovarian Granulosa cells by NPRA/PGRMC1/EGFR complex and improves ovary functions of PCOS rats. *Cell Death Dis.* 8, e3145. doi: 10.1038/cddis.2017.494

Zhong, Z., Li, F., Li, Y., Qin, S., Wen, C., Fu, Y., et al. (2018). Inhibition of microRNA-19b promotes ovarian Granulosa cell proliferation by targeting IGF-1 in polycystic ovary syndrome. *Mol. Med. Rep.* 17, 4889–4898. doi: 10.3892/mmr.2018.8463

Conflict of Interest: The authors declare that the research was conducted in the absence of any commercial or financial relationships that could be construed as a potential conflict of interest.

Copyright © 2021 Xu, Pan, Li, Zhang, Yan, Anwaier, Wang, Yan, Fan, Li and Han. This is an open-access article distributed under the terms of the Creative Commons Attribution License (CC BY). The use, distribution or reproduction in other forums is permitted, provided the original author(s) and the copyright owner(s) are credited and that the original publication in this journal is cited, in accordance with accepted academic practice. No use, distribution or reproduction is permitted which does not comply with these terms.

Advantages of publishing in Frontiers

OPEN ACCESS
Articles are free to read for greatest visibility and readership

FAST PUBLICATION
Around 90 days from submission to decision

HIGH QUALITY PEER-REVIEW
Rigorous, collaborative, and constructive peer-review

TRANSPARENT PEER-REVIEW
Editors and reviewers acknowledged by name on published articles

Frontiers
Avenue du Tribunal-Fédéral 34
1005 Lausanne | Switzerland

Visit us: www.frontiersin.org
Contact us: .frontiersin.org/about/contact

REPRODUCIBILITY OF RESEARCH
Support open data and methods to enhance research reproducibility

DIGITAL PUBLISHING
Articles designed for optimal readership across devices

FOLLOW US
@frontiersin

IMPACT METRICS
Advanced article metrics track visibility across digital media

EXTENSIVE PROMOTION
Marketing and promotion of impactful research

LOOP RESEARCH NETWORK
Our network increases your article's readership